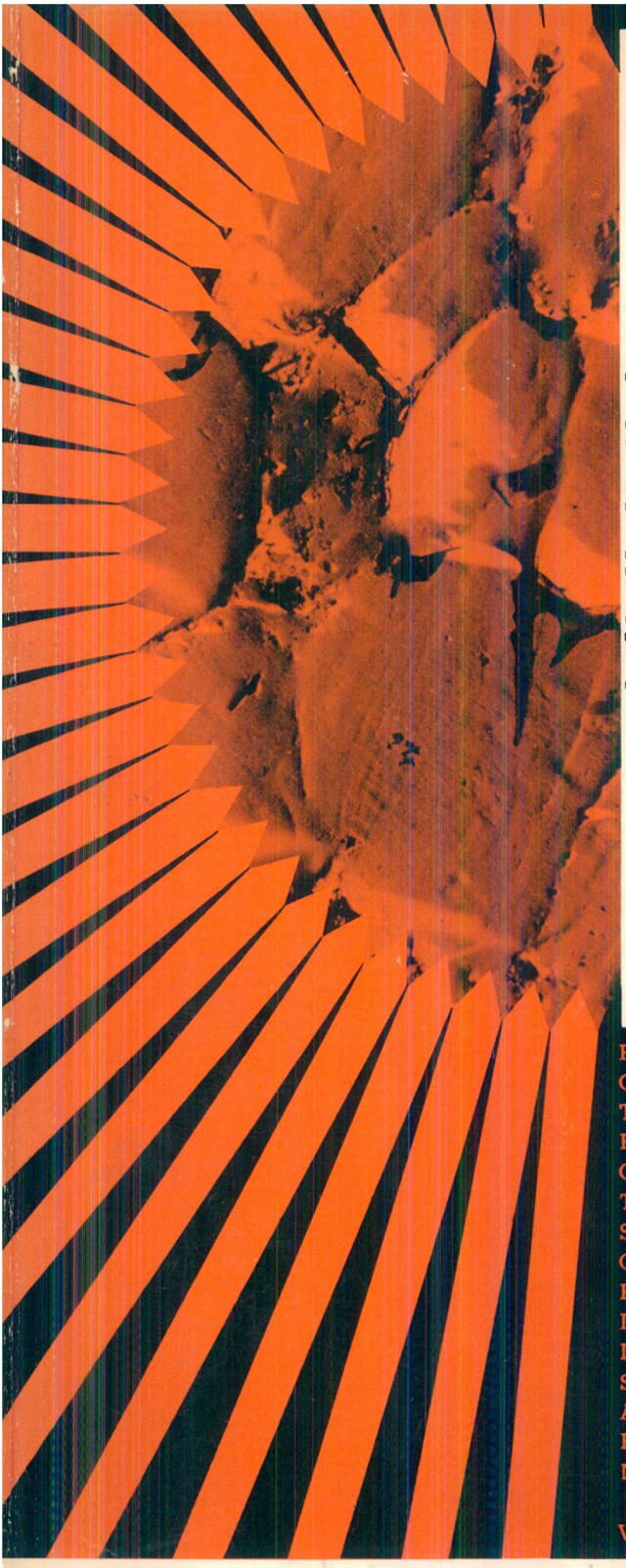


RADIATION DAMAGE IN REACTOR MATERIALS

PART OF THE PROCEEDINGS OF THE SYMPOSIUM ON RADIATION DAMAGE IN SOLIDS AND REACTOR MATERIALS

VENICE, 7-11 MAY 1962

SECTION FRANÇAISE

INTERNATIONAL ATOMIC ENERGY AGENCY, VIENNA, 1963

RADIATION DAMAGE IN REACTOR MATERIALS

The following States are Members of the International Atomic Energy Agency:

AFGHANISTAN
ALBANIA
ARGENTINA
AUSTRALIA
AUSTRIA
BELGIUM
BOLIVIA
BRAZIL
BULGARIA
BURMA
BYELORUSSIAN SOVIET SOCIALIST REPUBLIC
CAMBODIA
CANADA
CEYLON
CHILE
CHINA
COLOMBIA
CONGO (LÉOPOLDVILLE)
CUBA
CZECHOSLOVAK SOCIALIST REPUBLIC
DENMARK
DOMINICAN REPUBLIC
ECUADOR
EL SALVADOR
ETHIOPIA
FINLAND
FRANCE
FEDERAL REPUBLIC OF GERMANY
GHANA
GREECE
GUATEMALA
HAITI
HOLY SEE
HONDURAS
HUNGARY
ICELAND
INDIA
INDONESIA
IRAN
IRAQ
ISRAEL
ITALY
JAPAN
REPUBLIC OF KOREA
LEBANON
LIBERIA
LUXEMBOURG
MALI
MEXICO
MONACO
MOROCCO
NETHERLANDS
NEW ZEALAND
NICARAGUA
NORWAY
PAKISTAN
PARAGUAY
PERU
PHILIPPINES
POLAND
PORTUGAL
ROMANIA
SAUDI ARABIA
SENEGAL
SOUTH AFRICA
SPAIN
SUDAN
SWEDEN
SWITZERLAND
SYRIAN ARAB REPUBLIC
THAILAND
TUNISIA
TURKEY
UKRAINIAN SOVIET SOCIALIST REPUBLIC
UNION OF SOVIET SOCIALIST REPUBLICS
UNITED ARAB REPUBLIC
UNITED KINGDOM OF GREAT BRITAIN AND NORTHERN IRELAND
UNITED STATES OF AMERICA
URUGUAY
VENEZUELA
VIET-NAM
YUGOSLAVIA

The Agency's Statute was approved on 23 October 1956 by the Conference on the Statute of the IAEA held at United Nations Headquarters, New York; it entered into force on 29 July 1957. The Headquarters of the Agency are situated in Vienna. Its principal objective is "to accelerate and enlarge the contribution of atomic energy to peace, health and prosperity throughout the world".

Printed by the IAEA in Austria
August 1963

PROCEEDINGS SERIES

RADIATION DAMAGE

IN REACTOR MATERIALS

PART OF THE PROCEEDINGS OF THE SYMPOSIUM
ON RADIATION DAMAGE IN SOLIDS AND REACTOR MATERIALS
HELD BY THE INTERNATIONAL ATOMIC ENERGY AGENCY
AT THE FONDAZIONE CINI,
S. GIORGIO MAGGIORE, VENICE, 7 - 11 MAY 1962

INTERNATIONAL ATOMIC ENERGY AGENCY
VIENNA, 1963

RADIATION DAMAGE IN REACTOR MATERIALS, IAEA, VIENNA, 1963
STI/PUB/56a

FOREWORD

Radiation damage has presented a new design parameter for the selection of materials to be used in fuel and cladding elements, moderators, structural components and pressure vessels in nuclear reactors. The severe and novel requirements for certain optimum combinations of physical and nuclear properties have emphasized the need for a better understanding of the basic mechanisms of radiation damage. This knowledge is not only essential for progress in the field of nuclear energy, but has direct applications to space technology and semi-conductor research as well. The IAEA, as part of its programme of promoting nuclear technology, therefore convened the Symposium on Radiation Damage in Solids and Reactor Materials, 7 - 11 May 1962. At the invitation of, and with generous material assistance from, the Government of Italy, the Symposium was held at Venice.

The Symposium was primarily concerned with the investigation of the fundamental processes of radiation that underlie the behaviour of metals, alloys and ceramics that are actually useful or potentially useful reactor materials. Two sessions were devoted to studies of irradiation effects on simple metals, as these effects are easiest to interpret. Other topics included general theory, alloys, fissionable and moderator materials and special experimental techniques for radiation damage studies. The properties influenced by irradiation which were of main concern were those of primary importance to the behaviour of solids as reactor materials (e. g. dimensional stability, phase transformation, radiation hardening, fracture, fission-gas escape from uranium and its compounds). Other properties, such as optical, electrical and magnetic properties, and effects on semiconductors, ionic and other non-metallic crystals are also of interest in that these studies can increase our knowledge of the mechanism of radiation damage in solids and provide a tool for investigation into the physics of the solid state by offering a means of introducing controlled radiation damage. The subjects of corrosion and radiation chemistry were excluded.

The Symposium was attended by 220 participants from 24 Member States and one international organization. Of the 78 papers before the Symposium, 35 on radiation damage in solids generally and 3 on reactor materials were presented and discussed in full, while 35 papers formed the background for five panel discussions, which were introduced by five survey papers.

The present volume contains the survey papers and panel discussions on radiation damage in reactor materials, the 27 papers that formed the background to these discussions, and the 3 papers on this subject which were presented and discussed in full. With the three volumes published in 1962 and early 1963 under the title Radiation Damage in Solids, the present volume completes the proceedings of the Venice Symposium.

The Agency's thanks are particularly due to Dr. W. E. Roake and Mr. H.M. Mattys, of Hanford Laboratories, and to Professor J.H.W. Simmons, of Harwell, for kindly undertaking to edit the text of the panel discussions.

EDITORIAL NOTE

The papers and discussions incorporated in the proceedings published by the International Atomic Energy Agency are edited by the Agency's editorial staff to the extent considered necessary for the reader's assistance. The views expressed and the general style adopted remain, however, the responsibility of the named authors or participants.

For the sake of speed of publication the present Proceedings have been printed by composition typing and photo-offset lithography. Within the limitations imposed by this method, every effort has been made to maintain a high editorial standard; in particular, the units and symbols employed are to the fullest practicable extent those standardized or recommended by the competent international scientific bodies.

The affiliations of authors are those given at the time of nomination.

The use in these Proceedings of particular designations of countries or territories does not imply any judgment by the Agency as to the legal status of such countries or territories, of their authorities and institutions or of the delimitation of their boundaries.

The mention of specific companies or of their products or brand-names does not imply any endorsement or recommendation on the part of the International Atomic Energy Agency.

CONTENTS

A. RADIATION DAMAGE IN FISSIONABLE MATERIALS

1. Review of papers and panel discussion 3
(Reviewer and Moderator: A. Herpin)
2. Full text of papers:

Annealing kinetics of the quenched-in resistance of alpha-uranium 15
B. D. Sharma and K. Tangri

Внутреннее трение в уране 27
В. Е. Иванов и Б. И. Шаповал

The self-irradiation of plutonium and its delta alloys 35
C. E. Olsen, R. O. Elliott and T. A. Sandenaw

The cracking of irradiated uranium 59
R. G. Bellamy

Etude de la diffusion et de la précipitation des gaz rares dans les métaux 71
M. G. Brebec, V. Lévy, J. Leteurtre et Y. Adda

Swelling of uranium 95
B. A. Loomis

Dimensional stability of uranium under irradiation 109
J. H. Gittus, V. W. Eldred, A. Stuttard, G. Slattery and F. Chatterley

The effect of irradiation temperature and fission rate on the radiation stability of the uranium – 10 wt. % molybdenum alloy 133
A. A. Shoudy, W. E. McHugh and M. A. Silliman

Quelques résultats d'irradiation sur les combustibles envisagés pour « Rapsodie » 163
J.-P. Mustelier

B. RADIATION DAMAGE IN CERAMIC NUCLEAR FUEL

1. Review of papers and panel discussion 187
(Reviewer and Moderator: W. E. Roake)
2. Full text of papers:

Irradiation effects in fissile oxides and carbides at low and high burn-up levels 219
B. R. T. Frost, B. T. Bradbury and L. B. Griffiths

The low-temperature irradiation behaviour of cast uranium carbide 241
B. G. Childs, A. Ogilvie, J. C. Ruckman and J. L. Whitton

Effet de l'irradiation dans EL. 3 sur les alliages uranium-carbone de composition voisine de UC préparés par frittage-réaction sous charge 275
A. Accary, R. Darras et R. Caillat

Irradiation behaviour of uranium carbide fuels 287
D. I. Sinizer, B. A. Webb and S. Berger

Effects of high burn-up on oxide ceramic fuels 319
M. L. Bleiberg, R. M. Berman and B. Lustman

Irradiation alteration of uranium dioxide 429
W. E. Roake

Irradiation experiments with fuel suspensions 459
M. E. A. Hermans, H. S. G. Slooten and R. G. Sowden

C. RADIATION DAMAGE IN GRAPHITE

1. Review of papers and panel discussion:
Recent progress in the study of radiation damage in graphite 475
J. H. W. Simmons
Panel discussion 492
(Moderator: J. H. W. Simmons)
2. Full text of papers:

Etude comparative des effets des neutrons rapides sur le graphite monocristallin et le graphite nucléaire 499
J. Blons, G. Perriot et G. Tourand
Irradiations neutroniques à 78°K de graphites polycristallins 509
L. Bochirol, E. Bonjour et L. Weil
Mesures de paramètres de graphite industriel irradié dans l'azote liquide 523
M. Pluchery
An effect of flux level and flux spectrum on the accumulation of damage in reactor-irradiated graphite 531
H. Bridge, B.S. Gray, B. T. Kelly and H. Sørensen
Irradiation damage in graphite 553
W. N. Reynolds and P. A. Thrower
A model of radiation damage in graphite 565
T. Iwata and H. Suzuki
Radiation effects in carbons and graphites 581
H. H. Yoshikawa, E. M. Woodruff, J. M. Davidson, J. W. Helm and R. E. Nightingale
The behaviour of various graphites under neutron irradiation 593
E. Fitzer and O. Vohler
Comparison of irradiation damage in artificial and natural graphite at different irradiation temperatures 651
R. Gain
Evolution des propriétés physiques de graphites sous l'effet d'irradiations et de recuits successifs 663
J. Rappeneau, A. Fillâtre, G. Micaud et M. Quetier
The effect of heavy-particle bombardment on Wigner-energy storage in graphite 685
A. Willis and R. Penninckx

D. RADIATION DAMAGE IN BERYLLIUM OXIDE

Radiation damage in BeO 693
G. W. Keilholtz, J. E. Lee, Jr., R. P. Shields and W. E. Browning, Jr.
Comportement de l'oxyde de béryllium fritté irradié par des neutrons 703
J. Elston
Radiation effects in sintered BeO bodies of several compositions 725
C. G. Collins

Chairmen of Sessions and Secretariat of the Symposium 747
List of Participants 749
Author Index 761

A. RADIATION DAMAGE IN FISSIONABLE MATERIALS

1. Review of papers and panel discussion

(Part of Session 5)

RADIATION DAMAGE IN FISSIONABLE MATERIALS: REVIEW OF PAPERS AND PANEL DISCUSSION

Moderator: A. HERPIN

A. HERPIN: C'est une situation assez difficile que de commencer dans cette série de tables rondes qui est organisée, car on ne sait pas tellement bien encore quelle méthode marchera le mieux pour que la discussion soit la plus animée possible et la plus fructueuse possible. C'est un problème, par conséquent, qui est particulièrement difficile pour celui que nous appelons, nous, un animateur et que, je crois, les anglo-saxons appellent un modérateur. C'est d'autant plus difficile quand il s'agit, comme aujourd'hui, d'un animateur qui n'est pas particulièrement spécialiste de la question qu'il aura besoin d'animer, ce qui lui donnera probablement l'occasion, au cours de cette séance, de poser quelques questions tout à fait naïves qui, j'espère, pourront peut-être animer un peu la discussion. La méthode que je me suis permis d'utiliser aujourd'hui va consister à faire non pas un exposé d'ensemble pour débuter, suivi d'une discussion d'ensemble, mais plutôt à faire un papier d'ensemble qui sera entrecoupé par des discussions sur les différents papiers qui seront présentés, lorsqu'ils trouveront naturellement leur place dans mon exposé. Je pense que ceci doit vous permettre d'avoir une discussion peut-être un peu moins ingrate qu'une discussion d'environ trois quarts d'heure d'affilée, qui risquérait de lasser l'auditoire.

Nous devons nous occuper aujourd'hui des propriétés des matières fissiles irradiées. Les matières fissiles généralement utilisées sont l'uranium-235 et le plutonium. En pratique, nous nous occuperons aujourd'hui uniquement de l'uranium métallique éventuellement enrichi, soit en uranium-235, soit en plutonium. Certains éléments peuvent être ajoutés pour former des alliages qui sont plus stables au cours de l'irradiation, car finalement le problème que nous allons rencontrer d'un bout à l'autre de cet exposé sera la possibilité d'utiliser les meilleures formes possibles, du point de vue physique, de ces matières fissiles, de manière à ce qu'au cours de l'irradiation elles puissent subir des taux de combustion suffisamment élevés sans conduire à des dommages géométriques par trop importants, qui pourraient entraîner un mauvais fonctionnement dans la pile. Par conséquent le problème ainsi défini reste celui de la résistance de ces alliages aux effets d'irradiation. Cette résistance va naturellement dépendre de paramètres physiques de l'uranium et, plus exactement, de l'alliage que nous allons utiliser, en particulier de ses propriétés mécaniques à chaud ou à froid, propriétés qui d'ailleurs ne seront pas discutées ici puisqu'il n'y a aucun papier sur ceci, et l'évolution de ces propriétés sous irradiation. C'est là un problème difficile dans l'uranium, infiniment plus difficile que pour les autres métaux irradiés: les propriétés physiques de l'uranium changent d'une manière beaucoup plus forte au cours de l'irradiation que celles des autres matières. Ces propriétés de résistance sont également liées à la structure cristalline. Cette structure cristalline, pour l'uranium alpha, est fortement anisotrope. Par conséquent les propriétés, la tenue des matériaux fissiles en pile, va dépendre très fortement de la grosseur des grains et également de l'orientation de ces grains. Comment déterminer ces paramètres – grosseur des

grains, orientation des grains? Il y a évidemment la méthode classique de la métallographie par laquelle on peut réussir à déterminer la grosseur et l'orientation. Il y a également, en ce qui concerne la recherche de cette orientation, les méthodes traditionnelles, utilisées depuis très longtemps, des rayons X. C'est une méthode qui est généralement fort difficile en pratique parce que fort longue, l'uranium étant un matériau qui se prête relativement mal à l'étude par la diffraction des rayons X. Une méthode plus nouvelle, qui a été utilisée depuis quelques années seulement, est l'étude des matériaux fissiles, en particulier de l'uranium, au moyen de la diffraction des neutrons. C'est une technique infiniment plus commode parce que, alors que les rayons X ne permettent d'examiner qu'une petite partie de la matière – la pénétration des rayons X étant très faible – les neutrons, grâce à une pénétration beaucoup plus grande, permettent d'examiner des éléments massifs et de déterminer les orientations des cristallites et le degré d'orientation des cristallites dans un barreau étiré par exemple. En plus de cette structure cristallographique il existe également d'autres facteurs extrêmement importants qui sont les structures physiques de la matière avec laquelle on veut faire des éléments combustibles. Cette structure physique est malheureusement assez souvent mal connue. Il s'agirait de savoir quelle est la quantité de dislocations. On a depuis quelques années observé une dislocation dans l'uranium; on a pu dans certains cas mesurer des densités de dislocation, mais malgré tout, ceci n'a pu être fait que dans des cas assez rares. Il y a également des défauts ponctuels, qui sont essentiellement des lacunes dans l'uranium. D'autres défauts sont les macles de l'uranium qui sont fréquentes. D'autres encore sont les fautes d'empilement – qui ne sont pas autre chose que des macles moins régulières – mais dont je crois que l'existence, à l'heure actuelle, n'a pas encore été mise en evidence. Malheureusement, cette structure physique ne peut être atteinte que par les procédés auxquels j'ai fait allusion tout à l'heure, qui sont la microscopie, qui a permis l'évaluation des dislocations et aussi par des mesures macroscopiques telles que des mesures mécaniques ou des mesures de conductibilité électrique. Il est généralement fort difficile de connaître, de relier les propriétés mécaniques avec la structure physique de la matière: je pense que nous pouvons être persuadés, depuis deux jours que nous entendons des exposés sur ce sujet, que nous n'avons pas encore trouvé de loi parfaitement rigoureuse. La conductibilité électrique est une méthode probablement un peu plus simple pour l'étude de ces défauts ponctuels. Ceci est valable pour une substance fissile qui serait pure; malheureusement, les substances que l'on utilise dans les réacteurs atomiques contiennent un assez grand nombre d'impuretés et les propriétés de l'uranium non irradié devront dépendre très fortement de la pureté et également – d'une manière qu'il est difficile de prévoir – de l'état dans lequel se trouvent les impuretés: ces impuretés peuvent être dissoutes dans le réseau ou au contraire peuvent être présentes à l'état de précipité par exemple selon les joints de grains. Par conséquent, on peut penser que cette étude de l'uranium ou des matières fissiles, d'une manière plus générale, non irradiées est un excellent préliminaire, malheureusement encore inachevé, à l'étude de la matière fissile irradiée. Nous avons déjà aujourd'hui dans cette conférence plusieurs exposés qui correspondent à des études de ces matières fissiles avant leur irradiation. Tout d'abord nous en avons un concernant des ex-

périences sur la cinétique du recuit de l'uranium alpha trempé; il s'agit d'un exposé de Messieurs Sharma et Tangri, Inde*. Malheureusement les auteurs ne sont pas là. Nous avons aussi un papier soviétique de Messieurs Ivanov et Chapokhval*. Malheureusement également ces deux auteurs ne sont pas là. Je pense que nous pouvons quand même les mettre en discussion aujourd'hui, bien que le problème soit un peu difficile en ce qui concerne le papier soviétique pour lequel je n'ai reçu que très tardivement un exemplaire en langue russe, ce qui m'a empêché de le lire d'une manière un peu détaillée; tout ce que nous pouvons faire, je crois, c'est nous contenter du résumé, heureusement assez long. Les auteurs commencent par exposer une nouvelle méthode de détermination du frottement interne dans les métaux dans laquelle, au lieu d'utiliser des oscillations forcées, on utilise des pulsations périodiques. Je crois que, d'après le résumé, il est à peu près impossible de savoir exactement quelle était la méthode qu'ils ont utilisée. Ils ont appliqué leur nouvelle méthode, dans un domaine d'amplitude suffisante pour que les valeurs de ce frottement interne ne dépendent pas de l'amplitude, à l'étude de l'uranium dans une gamme de températures comprises entre 20 et 500°. Ils ont observé un maximum de frottement interne à 250°. Ils semblaient d'abord avoir attribué ce résultat à une hydruration possible de l'uranium et, ayant pris des précautions pour réellement retirer le maximum d'hydrure d'uranium de leur échantillon, ils ont observé qu'il leur restait encore un effet notable qu'ils ont attribué à des tensions internes. Est-ce qu'on est réellement sûr que cette déshydruration avait été complète? C'était la question, je crois, qu'on aurait pu leur poser. Il est extrêmement difficile de retirer tout l'hydrogène de l'uranium. Il y a évidemment quelques procédés physiques pour savoir s'il reste de l'hydrure d'uranium. Je crois que l'un des procédés que nous avons étudié en France et qui est assez sensible, c'est l'étude des propriétés magnétiques – l'hydrure d'uranium présente un point de curie à basse température, ce qui permet, dès qu'il y a des traces d'hydrure d'uranium, de déceler un moment magnétique permanent. Je ne sais pas si nous devons discuter ce papier. En ce qui concerne le papier de Messieurs Sharma et Tangri, nous avons un texte plus complet. Par conséquent, je crois que je vais simplement résumer très rapidement ce qu'ils ont étudié. Ils ont fait des expériences sur des fines lamelles qu'ils ont refroidies très rapidement ce qui leur a donné une vitesse de trempe assez grande, et ils ont mesuré les variations de résistivité électrique due à l'existence des lacunes. Ils ont cherché comment cette résistivité électrique pouvait être guérie et ils ont pu proposer un mécanisme de la guérison à température ordinaire. En ce qui concerne la guérison à plus basse température, il semble bien qu'ils aient trouvé quelques difficultés. Je crois qu'une des questions qu'on aurait pu leur poser, c'est de savoir quel était l'état de pureté de leurs échantillons, et quelle est l'influence des impuretés sur leurs mesures, car on sait très bien que dans ce cas on peut avoir des effets qui varient très notablement – nous en avons entendu parler déjà longuement†. En l'absence des auteurs nous n'engagerons pas de discussion. Ces différentes communications avaient trait à de l'uranium non irradié. Si, au contraire, nous considérons le plutonium, dans le fond, il

† Voir Radiation Damage in Solids I, AIEA, Vienne (1962), partie B « Pure Metals ».

* For full text, see section A.2.

n'existe pas de plutonium totalement non irradié puisque le plutonium lui-même est radioactif, donne une activité α susceptible de créer des dommages avant sa mise en pile, et c'est de ce problème que traitait le papier qui est présenté, je crois, ici par M. Elliott.

Short presentation by R. O. Elliott of

OLSEN, C.E., ELLIOTT, R.O. and SANDENAW, T.A.: The self-irradiation of plutonium and its delta alloys*

F. SEBILLEAU: Je voudrais apporter à la discussion quelques résultats que nous avons obtenus à Fontenay-aux-Roses en étudiant le pouvoir thermoélectrique du plutonium à basse température et qui montre une évidence indirecte de l'existence d'une septième forme allotropique du plutonium, ainsi que l'a suggéré le Dr. Elliott. Nous avons fait des cyclages thermiques de plutonium entre la température de l'hélium liquide et la température ordinaire, et nous avons observé que le pouvoir thermoélectrique montre une hystérésis très importante au cours de ce cyclage. D'autre part, un maintien d'une dizaine d'heures à la température de l'hélium liquide a montré que le pouvoir thermoélectrique ne donnait aucune variation. Ceci s'interprète très bien en supposant l'existence de deux phases, l'une au-dessous de 50°K, l'autre au-dessus, avec une transformation très étalée dans les températures et une transformation très paresseuse.

R.O. ELLIOTT: Yes, that is very good. I have only explained the newest evidence from the self-irradiation experiments; in addition, there is a thermal expansion anomaly near 50°C. Anomalies have been reported in the specific heat. The data that is being accumulated indicate that there is indeed a seventh allotropic form, which of course makes this element completely unique. No other element approaches this large number of allotropes.

Mr. A. HERPIN: Nous allons passer maintenant aux effets de l'irradiation sur les matériaux fissiles en pile. Ce sont essentiellement l'effet de gonflement et l'effet de croissance. Ces deux effets proviennent de la nature même du phénomène de fission, phénomène qui donne aux fragments de fission une énorme énergie dissipée, dans le solide sur un parcours relativement court – d'une dizaine de microns –. Ceci conduit par conséquent à une région extrêmement perturbée que l'on a appelée une pointe de fission. Cette pointe de fission est une zone cylindrique où on peut distinguer deux parties: la première partie, la partie centrale, est passée d'un état extrêmement désordonné à un état partiellement réordonné. C'est une zone où il existe de fortes perturbations. La partie externe est simplement perturbée par les dislocations et les fautes d'empilement consécutives à l'énorme variation de volume qu'il y a eu localement au moment de la fission. Cette pointe de fission est responsable du gonflement, de la croissance de l'uranium, croissance qui fait qu'un monocristal d'uranium après irradiation a vu sa direction 0-1-0 s'accroître et la direction 1-0-0 au contraire décroître au point de vue dimensionnel. De très nombreuses expériences ont été faites sur ce gonflement. Malheureusement, nous n'avons pas aujourd'hui de papier

* See section A.2 for full text of these papers.

concernant directement le gonflement en tant que phénomène élémentaire. Je voudrais simplement signaler le grand nombre de théories qui ont été proposées pour expliquer ce phénomène de croissance. Ces théories sont basées, les unes sur une diffusion anisotrope des lacunes après l'irradiation ou au cours de l'irradiation, les autres sur un fluage anisotrope au cours de l'irradiation elle-même, au moment de la formation de la pointe de fission. D'autres théories, plus récentes, proposent l'existence de boucles de dislocation qui seraient différentes suivant les plans cristallographiques devant lesquels elles sont placées. Ce sont les théories qui ont été élaborées en Grande-Bretagne par Westmancott, Martin et Hudson. Malheureusement, je pense que nous ne pouvons pas en discuter puisqu'il n'y a aucun papier correspondant à ceci et c'est infiniment dommage de ne pas parler d'une question qui est aussi intéressante. Ceux-ci sont les effets principaux. Je reviendrai tout à l'heure sur les effets de gonflement. Par contre, il existe d'autres effets qui sont les effets moins spécifiques tels que l'accélération du fluage sous irradiation et le durcissement consécutif à l'irradiation. En effet, l'accélération du fluage sous irradiation est un phénomène assez général dans l'étude des métaux irradiés, ce qu'on peut expliquer assez facilement par le grand nombre de défauts créés et la grande agitation des atomes au moment de l'irradiation. Quant au durcissement, il est simplement dû au fait que les dislocations peuvent se trouver bloquées par les défauts créés. Donc, ceux-ci sont des phénomènes extrêmement importants mais qui ne sont pas particuliers à l'uranium. Malgré tout, il existe un phénomène qui découle de cet effet de durcissement, c'est la fissuration. En effet, les barreaux utilisés dans un réacteur atomique sont soumis non seulement aux effets d'irradiation, mais aussi à des cycles thermiques qui font que la matière tend à se dilater et se contracter au cours du temps. Etant donné que l'uranium est très anisotrope, cette dilatation va faire apparaître des tensions très fortes entre les grains différemment orientés et ces tensions peuvent aboutir à la formation de fissures d'autant plus importantes que les cycles thermiques auront été plus importants. Nous avons maintenant, je crois, la possibilité de mettre en discussion la communication de M. Bellamy sur la fissuration de l'uranium irradié.

Short presentation by R. G. Bellamy of

BELLAMY, R. G., The cracking of irradiated uranium*

A. HERPIN: Le deuxième effet qui est caractéristique de l'irradiation des substances fissiles, c'est le gonflement dû à l'existence de produits de fission. Ces produits de fission qui demeurent dans la matière fissile sont soit des matières solides qui sont relativement solubles dans le métal, soit au contraire des substances très peu solubles qui sont les substances gazeuses telles que, essentiellement, le xénon et le krypton. Les premières, les matières solubles, vont produire une variation de la densité, parfaitement régulière et pratiquement indépendante de la température – environ 3% de variation de densité par pourcentage de taux de combustion. Au contraire, lorsqu'il s'agit de gaz peu solubles ou même pratiquement insolubles,

* For full text, see section A. 2

les atomes de ces gaz vont se loger où ils pourront, où ils trouveront de la place, à savoir essentiellement vers des lacunes et vers des dislocations. Malheureusement l'existence de ces lacunes et de ces dislocations va dépendre de l'histoire précédente de l'uranium, des traitements mécaniques ou thermiques qui ont pu donner naissance à ces lacunes et à ces dislocations. Si nous sommes à basse température, ces lacunes sont peu mobiles, par conséquent on peut supposer que les atomes de ce gaz vont rester dispersés dans la matrice du métal. Si, au contraire, la température devient plus grande, la diffusion des lacunes emportant leurs atomes de gaz rare provoquera leur rassemblement et conduira à la formation de bulles, qui vont provoquer également une diminution de la densité de l'échantillon d'uranium. Par conséquent, si l'on veut bien comprendre la formation de ces bulles, il est bon a priori de connaître le mécanisme de la diffusion. On peut faire l'expérience sur de l'uranium non irradié en essayant de dissoudre un gaz rare dans un métal non irradié et en mesurant la diffusion de ce gaz. Le travail que Mlle Lévy va présenter concerne ce sujet.

Short presentation by Miss V. Lévy of

BREBEC, M. G., LÉVY, V., LETEURTRE, J., QUERE, Y. et ADDA, Y.,: Etude de la diffusion et de la précipitation des gaz rares dans les métaux*

Short presentation by B. A. Loomis of

LOOMIS, B. A.: Swelling of uranium*

J. LEHMANN: Je voudrais faire une comparaison entre les résultats du Dr. Loomis sur le swelling obtenu par recuit de l'uranium irradié et les résultats que nous avons obtenus par recuit de l'alliage uranium-molybdène à 1% en poids après une irradiation jusqu'à 10 000 MWj/t dans un réacteur EL 3. Dans le cas de l'alliage uranium-molybdène, la mesure de densité après irradiation montre un accroissement de volume de 3%, ce qui correspond au volume des produits de fission solides pour un taux de combustion de 10 000 MWj/t. Donc, il n'y a pas de swelling. Des traitements thermiques à 450, 500 et 550° n'ont apporté qu'une variation de volume négligeable, ce qui est en accord avec les résultats du Dr. Loomis. Des traitements thermiques dans le haut de la phase alpha au-dessus de 550° apportent dans les deux cas un accroissement de volume. Toutefois, cet accroissement de volume est beaucoup plus important dans le cas de l'uranium que dans le cas de l'alliage uranium-molybdène. Il est de 8 à 18% après un burn-up de 0,3% sur la courbe du Dr. Loomis et il est seulement de $2\frac{1}{2}$% après un burn-up de 1% sur l'alliage uranium-molybdène. Le fait d'obtenir un acroissement de volume par chauffage du métal irradié est en désaccord avec ce qui a été observé par certains auteurs anglais, et en particulier par Pugh. Ces auteurs pensent que la croissance des bulles est contrôlée uniquement par la tension superficielle, celle-ci étant indé-

* For full text, see section A. 2

pendante de la température dans la zone 450-650°. Il ne s'ensuit donc aucun swelling au cours du recuit. Nos résultats et ceux du Dr. Loomis montrent au contraire une dépendance du swelling vis-à-vis de la température, ce qui semble correspondre à une corrélation entre le swelling et le fluage. Cette corrélation a été observée également par Bentley, de Atomics International, dans un certain nombre de matériaux. On peut expliquer les différences très importantes dans l'accroissement de volume des deux matériaux à 600° par les différences de leurs caractéristiques mécaniques. L'alliage uranium-molybdène a une résistance au fluage hors pile de 5 à 10 fois celle de l'uranium à 600° et une limite élastique environ trois fois supérieure. De plus, dans le cas du travail du Dr. Loomis il y a une recristallisation de l'uranium en grains très fins à 600°, ce qui abaisserait encore la résistance au fluage. A ce propos, je voudrais demander au Dr. Loomis à quoi est due cette recristallisation. Est-ce que c'est la conséquence de l'écrouissage apporté par l'irradiation? La comparaison des courbes de swelling obtenues par traitement dans les domaines bêta et gamma montre un bon accord entre l'uranium et l'alliage uranium-molybdène et le brusque accroissement de volume en phase gamma peut s'expliquer par le très fort accroissement du coefficient de diffusion du krypton dans l'uranium en phase gamma, tel qu'il a été déterminé dans le papier de Mlle Lévy et d'Adda.

B. A. LOOMIS: In addition to our experiments on uranium we have also studied the swelling of uranium alloys, including those containing up to 10 wt. % molybdenum. The general effect we observed with some molybdenum alloys that were included in these experiments was that for the most part the metallic elements added to the high-purity uranium caused the specimens to swell much more. Carbon, on the other hand, seemed to lower the swelling of uranium. I'm speaking of carbon content up to 1100 ppm. In answer to your question about the uranium recrystallization, let me say that the irradiated specimens appeared highly deformed and when heated to a recrystallization temperature large bubbles were formed on the grain boundaries. We see a large number of small pores and we're not sure of the interpretation. There are about ten pores per square centimetre. They have a diameter of about 0.02 - 0.06 μm. After recrystallization, when large bubbles were formed at grain boundaries, we did not see small pores within the recrystallized grains. This may indicate that the krypton and the xenon are diffusing to the grain boundaries.

A.A. SHOUDY: I would like to ask Dr. Loomis how he relates the out-of-pile swelling with in-pile swelling. Or doesn't he intend to do this?

B.A. LOOMIS: I would be very sceptical about extrapolating out-of-pile to in-pile behaviour. I think the Hanford Laboratories people intend to do this but I would consider it very fortuitous if there were some correlation.

A.A. SHOUDY: I would also like to ask whether you measured fission-gas release during heating.

B.A. LOOMIS: Yes, we did. The measurements were all negative. We did not observe any krypton or xenon release from the specimens. However this may have been due to the insensitivity of our apparatus. I would estimate that only a very small quantity of gas would be released.

E.D. HYAM: I was interested to see in Dr. Loomis's paper that he found small features rather like small bubbles in unirradiated uranium which had been cathodically vacuum-etched. We too have found this and they have all

the appearance of gas bubbles about 200-500 Å in diameter and we have also observed similar effects in unirradiated uranium. We do not know what causes this effect nor are we sure whether there is any way of modifying this effect by changing the etching technique. But it does seem as if cathodic vacuum etching might not be the best way of looking at very small gas bubbles of this order of size - 500 Å and below. We have found that simply fracturing irradiated uranium is in many respects a satisfactory alternative because the cleavage surfaces reveal the bubble distributions within the grains and the inter-granular surfaces reveal the distribution on grain boundaries.

The second point I wanted to make is that it is likely that there will be some contribution to the total swelling in these specimens due to stress-induced growth of gas bubbles, which is diffused into the grain boundaries. This phenomenon of stress-induced bubble growth was demonstrated in the paper we presented yesterday *, in the case of helium in irradiated beryllium. In the case of irradiated uranium the operative stresses would be generated by thermal cycling. The process would operate at temperatures sufficiently high in the alpha range to produce appreciable diffusion of vacancies at the top part of the cycle. Since cracks have not developed to any great extent in Dr. Loomis's specimens one would not really expect that the contribution to swelling by this effect would be very great, but one does wonder whether smaller swellings might be obtained if the annealing treatments were so arranged that each specimen has only one anneal. If I may take this business of stress-induced growth just one step further, the slide ** shows an example of it in a specimen of uranium - 0.5 at.% chromium which was irradiated to 2000 MWd/t at a temperature of 530°C. During the irradiation it had rather severe thermal cycling – about 70 cycles from the nominal irradiation temperature of 530°C down to about 150°C. At any rate, this specimen and a number of others like it developed pronounced grain boundary cracking and change of void along the grain boundaries. This particular specimen had identity decrease of about 4 - 3.5%. I'm afraid the slide isn't very clear, but you're looking now at a room-temperature impact fracture of this specimen. It is broken along a grain boundary and you're looking down on to the grain boundary surface. That surface is covered with small holes. There is a complete size distribution from spherical holes of about 300 or 400 Å in diameter up to sizes about 2 μm in diameter. The larger voids, over about perhaps 0.2 μm in size, are crystallographic in shape. They are polyhedra and are all oriented in the same way. The structure is very similar, indeed, to the other structures that we showed yesterday in helium bubbles and growth voids in beryllium.

One sees immediately the application to the paper by Bellamy +, because these voids grow under the inter-granular stresses. They spread sideways and form fissures, extending over the grain surfaces, which can be quite narrow. We consider that this stress-induced growth is another mode of crack formation which can operate at the top end of a thermal cycle.

B.A. LOOMIS: We observed no cracking in specimens annealed below

---

* HYAM, E.D. and SUMNER, G., "Irradiation damage to beryllium", Radiation Damage in Solids I, IAEA, Vienna (1962) 323-332

** Not included in the proceedings.

\+ BELLAMY, R.G., "The cracking of irradiated uranium", these Proceedings, section A. 2.

650°C. However in the specimen that we annealed at 650°C, which should have been in the alpha phase, we did observe considerable cracking and we attributed this to the fact that the alpha rate of transformation was lowered because of the fission products in the material. In the specimen that was annealed at 650°C, the structure appeared very similar to specimens annealed at higher temperatures in the beta phase. Its density decreased in a similar manner. Concerning the small pores that you see in the irradiated material, we have tried several different techniques – chemical etching, polishing, and then we also tried cathodic etching and various combinations of these. We always found approximately the same number of 200 - 600-μm pores. I am not sure what the interpretation of them is. They seem to be very real.

E.D. HYAM: May I add one more relevant comment on this point? We always notice that these tiny pores have got rather long shadow tails on them. One wonders whether one isn't observing tunneling down dislocations. This may account for the reason why one always gets these features, because one would attack such a structural feature both by cathodic vacuum etching and by chemical method.

B.A. LOOMIS: We do not observe these long tails that you speak of. However, I do see quite a bit of structure in addition to the small pores. The structure is very much smaller than the 200 - 600-μm pores and the smaller structure seems to be joined, that is, linking the 200 - 600-μm pores. I agree with you that fracturing specimens and looking at them without doing any chemical etching or polishing was probably the best procedure for studying these samples.

A. HERPIN: Pour l'instant, nous avons envisagé très rapidement – trop rapidement – les différents effets qui pouvaient se produire dans les matériaux fissiles. Nous avons en somme détaillé les différents phénomènes en considérant tout d'abord le gonflement puis la fissuration, et puis maintenant ce que nous voudrions savoir c'est ce qui se passe dans un combustible réellement mis dans un réacteur, réellement utilisé, et savoir comment il va se comporter. Il ne s'agira jamais d'uranium pur comme nous en avons entendu parler jusqu'à présent, mais d'alliage d'uranium, d'uranium plus ou moins stabilisé, je crois en l'occurrence avec de l'aluminium, du fer ou du chrome en petite quantité qui forment en quelque sorte des zones de pré-précipitation à l'intérieur de l'uranium, qui permettent de localiser un certain nombre de défauts et d'en abaisser la mobilité qui les rend extrêmement néfastes à haute température. Dans cette perspective, nous avons le papier de M. Gittus.

Short presentation by J. Gittus of

GITTUS, J.H., ELDRED, V.W., STUTTARD, A., SLATTERY, G. and CHATTERLEY, F.: Dimensional stability of uranium under irradiation *

Short presentation by A.E. Shoudy of

SHOUDY, A.A., McHUGH, W.E. and SILLIMAN, M.A.: The effect of irradiation temperature and fission rate on the radiation stability of uranium - 10 wt.% molybdenum alloy *

* For full text, see section A.2

Short presentation by J. P. Mustelier of

MUSTELIER, J. P.: Quelques résultats d'irradiation sur les combustibles envisagés pour «Rapsodie»*

A. T. CHURCHMAN: I would like to hear if Mr. Mustelier or his French colleagues can explain why the addition of plutonium destroys the swelling resistance of the uranium - 10% molybdenum alloy and at what plutonium level this effect develops.

Mme. Lehmann cast doubt on the effectiveness of surface tension restraint in the U-Mo alloys and suggested that creep strength was more appropriate. Does the plutonium reduce the creep strength of the alloy?

Greenwood, of Berkeley, England, has shown that, in the case of reactor uranium, if one takes into account the entropy of solution of the fission gases as well as the heat of solution, then there is a finite solubility of the gases in the γ-phase. The large gas bubbles will then grow at the expense of the smaller ones, giving breakaway swelling. For an excursion of T °C into the γ-phase for t sec, the equilibrium bubble radius is given by

$$r^2 \sim Dt \exp(\Delta Sr/k)\exp(-H/kT),$$

where k = the Boltzmann constant, D = diffusion coefficient of rare gases in the γ-phase, ΔSr = entropy of solution of rare gases in γ, and H = heat of solution of rare gases in the γ-phase.

An alternative explanation to that of Mme. Lehmann is that molybdenum additions and uranium so alter the fission-gas diffusion coefficient that the bubbles cannot grow by resolution. Further addition of plutonium may restore the original gas diffusion coefficient.

J. P. MUSTELIER: Malheureusement, je crois qu'il est bien difficile de répondre à ces questions. Je pense que des mesures seraient nécessaires pour mettre en évidence les paramètres que M. Churchman invoque.

* For full text, see section A. 2

A. RADIATION DAMAGE IN FISSIONABLE MATERIALS

2. Full text of papers

ANNEALING KINETICS OF THE QUENCHED-IN RESISTANCE OF ALPHA-URANIUM

B. D. SHARMA AND K. TANGRI
METALLURGY DIVISION, ATOMIC ENERGY ESTABLISHMENT,
BOMBAY, TROMBAY, INDIA

Abstract — Résumé — Аннотация — Resumen

ANNEALING KINETICS OF THE QUENCHED-IN RESISTANCE OF ALPHA-URANIUM. Results of investigations on the "quenched-in" residual resistivity of high-purity alpha-uranium are reported. Experiments were carried out on thin strips of alpha-uranium quenched from within the alpha-range with a high cooling rate. The decay of resistance at liquid-nitrogen and room temperatures has been measured.

From the calculations of activation energies for these recovery processes, it is seen that recovery at room temperature is primarily due to annealing of lattice vacancies and vacancy-impurity complexes. Low-temperature recovery, however, could not be explained by current theories of the quenched-in defects. This behaviour can possibly be attributed to the migration of some of the impurities, which are likely to be pinned into interstitial holes during quenching.

CINÉTIQUE DE LA SUPPRESSION PAR RECUIT DE LA RÉSISTANCE QUE L'URANIUM ALPHA ACQUIERT AU MOMENT DE SA TREMPE. Les auteurs donnent les résultats de leurs recherches sur la résistivité résiduelle acquise par de l'uranium alpha très pur au moment de sa trempe. Ils ont fait les expériences sur de fines lamelles d'uranium alpha, trempé à une température ne dépassant pas celle à laquelle l'uranium alpha n'est plus stable, et refroidi très rapidement. Ils ont mesuré la décroissance de la résistance à la température de l'azote liquide et à la température ambiante.

D'après les calculs effectués sur les énergies d'activation de ces processus de «guérison», on constate que la «guérison» à la température ambiante est principalement due à l'élimination par recuit des lacunes de réseau et des complexes lacune-impureté. Mais la «guérison» à basse température ne peut pas être expliquée par la théorie courante des défauts provoqués par la trempe. Ce comportement pourrait être attribué à la migration de certaines des impuretés, qui viendraient se loger dans les cavités interstitielles au moment de la trempe.

КИНЕТИКА ОТЖИГА ЗАКАЛЕННОГО СОПРОТИВЛЕНИЯ АЛЬФА-УРАНА. Сообщаются результаты исследований относительно "закаленного" остаточного удельного сопротивления альфа-урана высокой чистоты. Эксперименты выполнялись на тонких стержнях альфа-урана, закаленного в пределах альфа-пробега при высокой скорости охлаждения. Было измерено уменьшение сопротивления в жидком азоте и при комнатной температуре.

Из расчетов энергии активации для этих процессов восстановления видно, что восстановление при комнатной температуре происходит главным образом благодаря отжигу вакансий в решетке и комплексов вакансий-загрязнений. Низкая температура восстановления, однако, не может быть объяснена современными теориями закаленных дефектов. Это поведение, по-видимому, можно отнести к миграции некоторых загрязнений, которые, вероятно, могут во время отжига оседать в междоузлиях.

CINETICA DEL RECOCIDO DE REGENERACIÓN DE LA RESISTENCIA ELÉCTRICA EN EL URANIO ALFA TEMPLADO. Los autores comunican los resultados de sus investigaciones sobre la resistividad residual observada en el uranio alfa, de elevada pureza, después de un tratamiento de templado. Efectuaron sus experimentos con tiras delgadas de uranio alfa, templadas en el intervalo alfa, por enfriamiento rápido. Determinaron la disminución de la resistencia a la temperatura del nitrógeno líquido y a temperatura ambiente.

Del cálculo de las energías de activación correspondientes a estos procesos de regeneración se deduce que la regeneración a temperatura ambiente se debe en primer término al recocido de vacantes del reticulado y de complejos vacante-impureza. En cambio, la regeneración a baja temperatura no puede explicarse con ayuda de las teorías actualmente aceptadas sobre los defectos fijados mediante el enfriamiento. Este comportamiento debe atribuirse más bien a la migración de algunas de las impurezas que probablemente se localizan en los huecos intersticiales durante el templado.

1. INTRODUCTION

The quenched-in residual resistivity of metals has frequently been employed [1, 2] for studying the kinetics of their point defects, such as the lattice vacancies. These latter are of great significance in considerations of radiation damage in metals. The migrations of these defects to the sinks result in a decay of the residual-resistivity values. Considerable insight into the nature and stability of these defects can be obtained [3] from their activation-energy values of formation and migration. Whereas the energy of formation is calculated from the initial quenched-in resistance, the values for migration can be estimated by a careful analysis of the residual-resistance decay rates. Further, it has been shown [4] that, in impure metals, the impurity atoms act as traps for the vacancies in transit to the sinks and thus considerably influence the vacancy decay-rates. The activation-energy values also change due to the formation of impurity-vacancy complexes.

The present work was undertaken in order to study the influence of impurity atoms on the annealing kinetics of the quenched-in resistance of high-purity alpha-uranium. Some interesting inferences have been made regarding the dispersion of the impurity atoms during fast quenching. The residual-resistivity decay observed in these experiments has been discussed on the basis of the probable segregation of impurity atoms and their interactions with the lattice vacancies.

2. EXPERIMENTAL PROCEDURE

2. 1. Specimen preparation

The specimens for these investigations were prepared from high purity uranium*. As the quenching rate is a significant factor in the freezing-in of the lattice vacancies, the specimens were in the form of thin strips of approximate dimensions 6 cm × 0.06 cm × 0.05 cm. The strips were prepared by hot-rolling (600°C) uranium rods to an appropriate size and then further reducing them on emery paper. Fine grain size (37 μm) was considered essential to avoid the formation of micro-cracks during quenching. These specimens were annealed at 600°C for 15 min to remove any strains introduced during preparation.

2. 2. Quenching technique

Since the accuracy of the experiments on the quenched-in lattice defects depends entirely on their non-equilibrium super-saturation values, fast cooling-rates are always considered essential for such studies. In the present investigations the high-temperature quenching of the specimens was carried out in a specially designed vacuum tube-furnace wherein quenching rates as high as 10 000°C/s could be achieved by rushing in ice cold water.

---

* The main impurities were (in ppm by weight): Al ≃ 128; C ≃ 108; Zn ≃ 22; Ca ≃ 15.

To avoid the formation of lattice defects with short range interactions, the quenching temperature was kept within the alpha-uranium range only.

2.3. Resistivity measurements

The quenched specimens were quickly removed from the furnace tube, electro-polished and set on a specially designed mount. This was then transferred to a liquid-nitrogen flask for the resistivity measurements. The maximum time taken for this process was six minutes.

The changes in the residual resistivity of the specimens were measured using a standard potentiometer method; the accuracy for the potential drop measurements was 10^{-6} V. The current in the circuit was determined by measuring the potential drop across a standard one-ohm resistor in series with the specimen. A well-annealed uranium specimen was used as a dummy and the potential drop across it was compared with that across the quenched specimen to allow for any temperature changes in the liquid-nitrogen bath.

3. RESULTS

3.1. Quenched-in residual resistivity of alpha-uranium

The quenched-in residual resistivity ($\Delta\rho_{0i}$) of the uranium specimens was found to increase with increasing quenching-temperature (T_Q) over the range 490 to 640°C. The increase in the residual resistivity could be represented by an equation of the type,

$$\Delta\rho_{0i} = A \exp\left(-\frac{E}{kT}\right), \tag{1}$$

where E is the activation energy and A is a constant. Fig. 1 shows the straight line relationship obtained by plotting $\ln(100 \times \Delta\rho_{0i}/\rho_0)$ against $1/T_Q$; $\rho_0 = 8.861\,\mu\Omega$cm was the initial resistivity of the pre-quenched specimens at the liquid nitrogen temperature. The values of E and A, as evaluated from the graph (Fig. 1), were found to be 0.646 eV and 2.383 $\mu\Omega$cm respectively.

3.2. Recovery of the residual resistivity of quenched alpha-uranium specimens at 77 and 303°K

The recovery of the residual resistivity of the quenched alpha-uranium specimens was examined at 77°K and room temperature (303°K). For results on the resistivity decay at 77°K, the quenched specimens were kept immersed in the liquid nitrogen. The recovery at 303°K was observed by exposing the specimen to room temperature for regular time intervals and transferring it to the liquid nitrogen flask for the resistivity measurements.

The fractional decay of the residual resistivity at 77°K for specimens quenched from 763, 873 and 913°K has been plotted in Fig. 2a as a function of time. It was observed that all the recovery at 77°K of the residual resist-

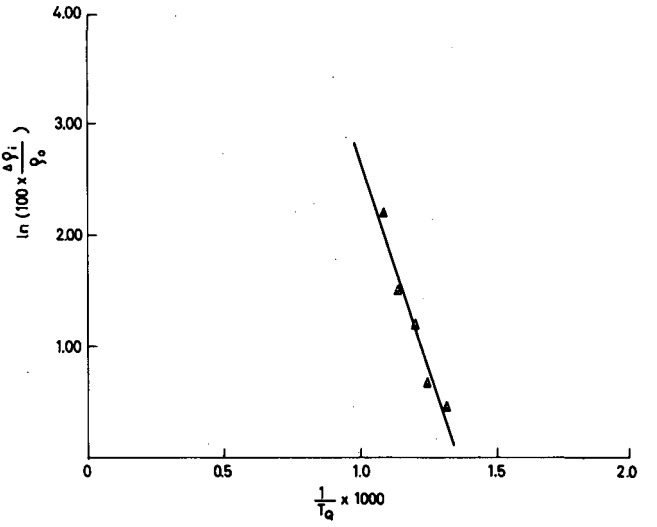


Fig. 1

The graph of $\ln(100 \times \Delta\rho_{0i}/\rho_0)$ plotted as a function of $1/T_Q$

ivity, which was only a fraction of the initial value, occurred over a short period, about 60 min. It was further noted that the initial decay was faster for specimens quenched from higher temperatures. The final resistivity-recoveries for specimens quenched from 763, 873 and 913°K were found to be 18, 21 and 35% of the initial value in each case respectively.

The changes in the residual resistivity of the specimens annealed at room temperature (303°K) have been plotted in Fig. 2b. Curves 1 and 2 are the resistivity decay curves for specimens quenched from 833 and 913°K respectively. The resistivity decay was much faster for these than for the specimens whose recovery was examined at 77°K. All the recovery occurred in about 30 min and was 37 and 42.5% of the initial values quenched-in from 833 and 903°K respectively.

The recovery of the quenched-in resistivity of a pha-uranium at 303°K was found to occur in two stages (see curve 3, Fig. 2b). Part 'AB' of the curve shows the fractional recovery occurring over about 50 min at 77°K for a specimen quenched from 873°K and part 'BC' represents the further recovery observed for the same specimen on annealing now at room temperature. These curves also show the temperature dependence of the processes responsible for the resistivity decay.

3.3. Activation energy values for the quenched-in resistivity decay of alpha-uranium at 77 and 303°K.

The activation energy for the residual-resistivity decay both at 77°K and room temperature (303°K) were evaluated on the basic assumption that the resistivity decay followed the annealing kinetics of the point defects.

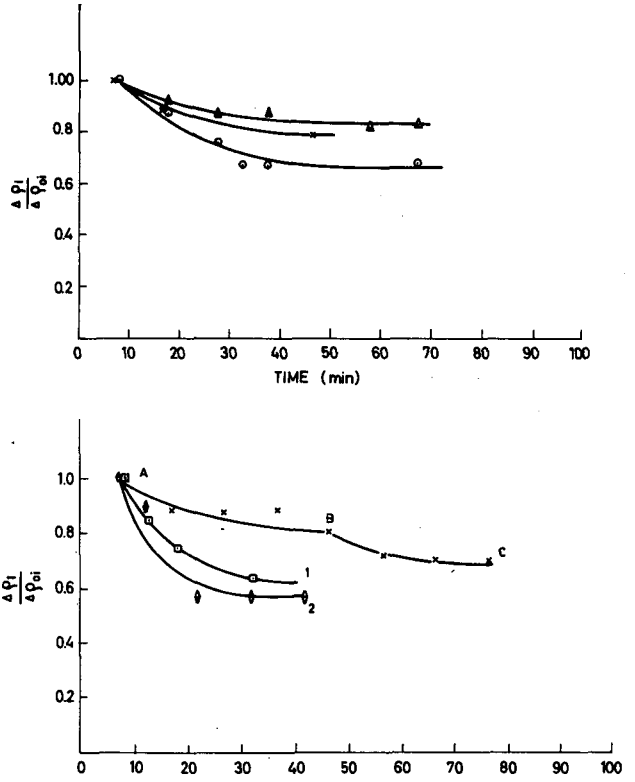


Fig. 2

The fractional decay of the residual resistivity at 77°K plotted as a function of time

△ × ⊙ ⊡ ▽ ◇ } specimen for which T_Q = { 763°K, 873°K, 913°K, 833°K, 873°K, 903°K }

Assuming that the resistivity decay followed the first-order kinetics of point-defect migration, its decay rate is represented by an equation,

$$\frac{\partial}{\partial t}(\Delta \rho_i) = -(\Delta \rho_i) z \nu \exp[-E_M/kT] \qquad (2)$$

where $\Delta \rho_i$, z, ν, E_M, and T represent the residual resistivity at any instant, the co-ordination number, the atomic frequency, the activation energy for resistivity decay and the annealing temperature respectively. The activation energy (E_M) can be calculated by integrating Eq. (2) and plotting

$\ln(\Delta\rho_i)$ against time. The slope of the straight line graph is given by $z\nu \exp(-E_M/kT)$. The value of the co-ordination number (z) depends upon the nature of the defect. In the present case the values of z were taken as 5 and 4 for the decays at 77 and 303°K respectively; the reasons are discussed later.

Fig. 3a shows the straight line graph obtained by plotting $\ln(\Delta\rho_i)$ against time for the resistivity decay at 77°K. Putting $\nu = 4\times10^{12}$ c/s, the activation energies for resistivity decay were found to be 0.218 ± 0.012 eV for the specimens quenched from 763 and 873°K. In the case of the specimen quenched from 913°K all points did not fall on the same straight line. The activation energy was, therefore, found to vary from 0.218 for the mean graph 'AB'

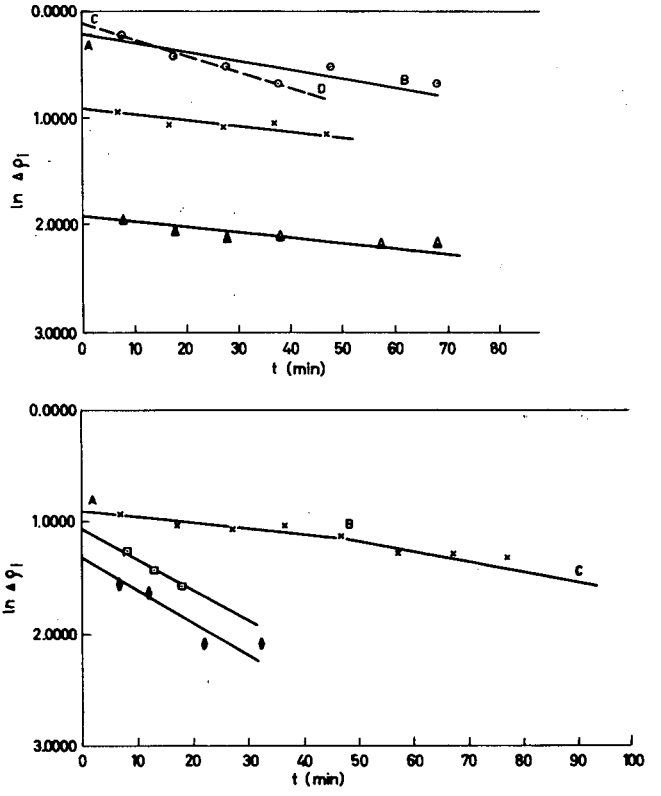


Fig. 3

The graph of ln $\Delta\rho_i$ (residual resistivity) plotted as a function of time (t). (data in 'a' relates to Fig. 2a; data in 'b' relates to Fig. 2b)

△ × ⊙ ⊡ ▽ ◇ } specimen for which T_Q = { 763°K, 873°K, 913°K, 833°K, 873°K, 903°K

to 0.210 eV for the graph 'CD' representing the initial (fast) stage of the decay (Fig. 2a).

In order to evaluate the activation energy for the resistivity decay at room temperature, Eq. (2) was modified to

$$\frac{\partial}{\partial t}(\Delta\rho_i) = -(\Delta\rho_i)\frac{z\nu}{c} \cdot \exp\left[\frac{E_M + B}{kt}\right] \tag{3}$$

to account for the effect of the high concentration (c) of impurities. B represents the binding energy for the formation of an impurity-vacancy complex. Values of $(E_M + B)$, which were calculated from the slopes of the lines drawn in Fig. 3b, for $\nu = 10^{13}$ c/s, were found to be 0.9809 ± 0.012 and 0.9919 ± 0.012 eV for the specimens quenched from 833 and 903°K respectively. For the specimen quenched from 873°K and annealed in two separate stages, the value was found to be 1.003 eV.

4. DISCUSSION

4.1. Quenched-in resistivity

According to the present theoretical concepts the quenched-in resistivity of the metals at low temperatures is attributed to the freezing-in of the supersaturation of thermal vacancies which subsequently act as scattering centres for conduction electrons. The number of these lattice vacancies per unit volume quenched-in from a temperature (T_Q) is given by

$$n = N \exp(-E_f/kT_a), \tag{4}$$

where N is the atomic density and E_f is the activation energy for the formation of a thermal vacancy.

The value of E_f for any metal is, using the simplest approximation, equal to its cohesive energy or the heat of sublimation. This approximation, however, always gives an overestimated value. A better value of E_f for uranium has been obtained using the elastic distortion model given by BROOKS [5]. In this case the energy of the formation of a vacancy is considered as equivalent to the elastic energy involved in creating a new spherical surface equal to the atomic volume within the metal. The total elastic energy involved in the process is given by,

$$E_{el} = 4\pi r_s^2 \gamma^2 \left[\frac{1}{2G r_s + \gamma}\right] \tag{5}$$

where r_s is the radius of the spherical surface, γ is the surface energy of a close-packed plane and G is the modulus of rigidity of the metal.

To determine E_f for uranium, the value of γ for a close-packed plane is calculated by distributing the sublimation energy of a uranium atom into

different planes in proportion to their bond-order values. The total bond-orders for (010), (021) and (110) planes of the uranium lattice, according to TYZACK [6], are 4.565, 3.5465 and 3.367 respectively. On proportionate distribution of the sublimation energy of A uranium atom, $E_s = 4.333$ eV and the surface energy values for (010), (021) and (110) planes are found to be 6707, 5208 and 4948 erg/cm^2 respectively. The value $E_f = 1.439$ eV is obtained by substituting $\gamma = 5208$ erg/cm^2 in the above equation. The surface energy of the (021) plane is chosen as, at higher temperatures, it becomes the closest packed plane and its bond-order values remain unchanged.

The concentration of the thermal vacancies quenched-in from 913°K and corresponding to $E_f = 1.439$ eV is further estimated to be of the order of 10^{-8}.

4. 2. Resistivity decay at 77°K and evidence for impurity dispersion

In the present studies the quenched-in resistivity of alpha-uranium such as 0.139 $\mu\Omega$ cm for $T_Q = 763$°K is found to be fairly high even when compared with metals with low values of E_f. The activation energy for resistivity increase (E = 0.646 eV) is also found to be low as compared with the estimated value of $E_f = 1.439$ eV. The increase in the residual resistivity due to the quenched-in thermal vacancies can be estimated provided their concentration and the cross-section for electron scattering is known. Using Seeger's value of 1.67 $\mu\Omega$cm per 1 at.% vacancy concentration as the scattering cross-section, the contribution of the quenched-in vacancies to the residual resistivity in this case is found to be negligible in view of their low supersaturation values. It, therefore, seems that the observed quenched-in resistance of alpha-uranium is to be attributed to the dispersion of impurity atoms in the lattice.

The main impurities in the present case are aluminium and carbon and their reported [7] solubilities at 700°C are of the order of 10^{-3} wt.% and 10^{-5} wt.% respectively. Higher concentrations of these impurities exist as intermetallic compounds or carbide inclusions respectively. NORTHCOTT [8] has shown that normally the impurities segregate at the sub-boundaries but get randomly dispersed in the matrix during high-temperature quenching. Re-segregation of the impurities may occur with ageing. Thus if immediately after quenching such a specimen is transferred to a temperature at which the atomic diffusion rate is low, it would exhibit a supersaturation of the dispersed impurity atoms similar to that of the quenched-in vacancies. The increase in the supersaturation value would also increase with the quenching temperature and the activation energy would be same as that for intermetallic diffusion. It is interesting to note that the observed activation energy E = 0.646 eV compares more favourably with the estimated activation energy for the diffusion of carbon in uranium ($E \simeq 0.5$ eV) than with the estimated value of E_f for the formation of a lattice vacancy.

The large increase in the quenched-in resistance of alpha-uranium is to be attributed to the low solubility of the impurities. For a high solubility value, the initial concentration of impurities in the lattice should be high and any additional dispersion during fast quenching would not change the residual resistivity in a significant way. On the other hand, if the initial

dispersion is low because of low solubility, considerable increase in resistivity would be observed due to increased dispersion of the impurity atoms.

Additional information of interest regarding the impurity dispersion in alpha-uranium has been evaluated from the decay behaviour of its quenched-in resistance. The activation energy for the resistivity decay at 77°K is found to be of the order of 0.21 eV. The resistivity decay of the quenched specimens is usually associated with the lattice vacancy migration or due to the clustering of the originally-dispersed, substitution impurities. It can also occur due to the migration of the interstitials if any are present. Since the activation energy (0.21 eV) is low for activating both vacancy-movement or clustering, it seems that decay may be due to the migration of some impurity atoms pinned in the interstitial holes during fast quenching. The largest interstitial hole in alpha-uranium is 1.36 Å in diameter, and the energy considerations show that only carbon and other elements of low atomic weight which may be present in the metal can occupy these sites. The activation energies for putting other impurity atoms into the holes are too high. The activation energy for putting a carbon atom into an interstitial hole in uranium has been calculated on the basis of BROOKS' elastic distortion model [9], similar to the one assumed for vacancies, and the energy is found to be 0.08 eV. The probable concentration of the carbon atoms occupying interstitial positions at room temperature corresponding to this energy is further estimated to be of the order of 10^{-2}. Since the actual atomic solubility of carbon in alpha-uranium is only 60 ppm, most of these carbon atoms dispersed interstitially during quenching would exist in an unstable state and would anneal-out with ageing. This migration of carbon atoms to the sinks would be accompanied by low-energy resistivity-decay as observed here. From the resistivity-decay curves (Fig. 2a) the concentration of such atoms is roughly estimated to be about 10^{-4}. It may be further pointed out that the atomic binding forces in uranium alter considerably with changing temperature. The activation energy for interstitial diffusion would also, therefore, exhibit some variation with temperature.

4.3. Residual-resistivity decay at 303°K

A second stage of the quenched-in resistivity decay in this case is found to occur at room temperature (303°K) with an activation energy of about 1.0 eV. Both on temperature and energy considerations the decay seems to be associated with the annihilation of the quenched-in lattice vacancies. Such an annihilation normally occurs by the absorption of the vacancies at the grain boundaries, dislocation jogs or by interstitial recombination during their random movement within the metal. SIEGLE and OPINSKY [10] have shown that the recombination probability for alpha-uranium is equal to $C_v \times 5\, C_i/2$ where C_i and C_v are the interstitial and vacancy concentrations respectively. Putting ν_i and ν_v as the jump frequencies for interstitials and vacancies respectively, the corresponding recombination rate per unit volume can be further estimated as $5(C_i \times C_v)(\nu_i + \nu_v)N$. In the present case the probability of annihilation of the vacancies by recombination with interstitially located carbon atoms is found to be small because of the low supersaturation of the vacancies. Though the recombination rate rises with in-

creasing temperature, it is estimated that only a small fraction of the quenched vacancies would recombine. The majority of the vacancies are expected to migrate to the sinks.

Recently, DAMASK and DIENES [4] have shown that, in the case of impure metals, the impurity atoms act as traps and usually retard their migration rate to sinks by forming impurity-vacancy complexes. The decay constant observed in such a case is, therefore, a composite rate constant for the decay of both vacancies and impurity-vacancy complexes. LOMER and COTTRELL [11] have further shown that if the impurity concentration (C) is high as compared to that of the traps and the vacancies, the jump frequency for the vacancies is given by

$$f = \frac{z \cdot \nu}{C} \exp \cdot \left(- \frac{E_M + B}{kT} \right) \qquad (6)$$

and the resistivity decay is represented by Eq. (3) rather than by Eq. (2).

The value of $(E_M + B)$ for the residual resistivity decay as given earlier has, therefore, been evaluated using Eq. (3) for $C = 3 \times 10^{-3}$ and $Z = 4$. The latter takes into account the anisotropy of the uranium lattice. Slight variations in the activation energy values are observed for specimens for which recovery was examined in only one stage. The variation seems to be due to the overlapping of the fast-decaying interstitially located carbon atoms on the slow mobilities of the vacancies and the complexes. Assuming the value of B to be about 0.3 eV, the activation energy for the migration of a lattice vacancy in uranium should be about 0.7 eV. It is significant that the sum of the activation energy $E_f + E_M = 2.139$ eV as estimated here compares favourably with the activation energy of the self-diffusion for alpha-uranium ($E_d = 2.32$ eV) [12].

It is also seen from Fig. 2a and b that a considerable fraction of the quenched-in resistance of uranium decays during the second stage. Further, this fraction is too large to be accounted for by the migration of the quenched-in vacancies alone. The observed resistivity decay, therefore, seems to be associated with a probable clustering of the impurity atoms. HARRISON [13] has shown that the scattering cross-section of an impurity atom is reduced by 30 to 40% for a cluster size of about 10 atoms. These calculations were made for only monovalent and trivalent metals. Assuming these results to be suitable approximations for the cases considered, from the present experiments clusters of a size as large as four to five atoms may be expected.

ACKNOWLEDGEMENTS

The authors wish to thank Dr. Brahm Prakash, the Head of the Metallurgy Division, for his keen interest and encouragement during the course of these investigations. The able assistance of Shri S. J. Vijaykar in carrying out the experiments is gratefully acknowledged.

REFERENCES

[1] KAUFFMAN, J.W. and KOEHLAR, J.S., Phys. Rev. 88 (1952) 149.
[2] BRADSHAW, F.S. and PEARSON, S., Phil. Mag. 2 (1957) 570.
[3] COTTRELL, A.H., Vacancies and other point defects in metals, Inst. Metals (1958) 1.
[4] DAMASK, A.J. and DIENES, G.J., Phys. Rev. 120 (1960) 99.
[5] BROOKS, H., Impurities and Imperfections, Amer. Soc. Metals (1955) 6.
[6] TYZACK, C., U.K.A.E.A. Rpt. I G 49 (RD/ C) (1959).
[7] BLUMENTHAL, J.B., J. nucl. Mat. 2 (1960) 197.
[8] NORTHCOTT, L., J. Inst. Metals 59 (1936) 225.
[9] BROOKS, H., Impurities and Imperfections, Amer. Soc. Metals (1955) 8.
[10] SIEGLE, L.L. and OPINSKY, A.J., USAEC Rpt. SEP-160 (1954).
[11] LOMER, W.M. and COTTRELL, A.H., Phil. Mag. 46 (1955) 711.
[12] HOLDEN, A.N., Physical Metallurgy of Uranium, Addison-Wesley (1958) 161.
[13] HARRISON, W.A., Acta Met. 8 (1960) 168.

ВНУТРЕННЕЕ ТРЕНИЕ В УРАНЕ

В.Е. ИВАНОВ и Б.И.ШАПОВАЛ

СССР

Abstract — Résumé — Аннотация — Resumen

INTERNAL FRICTION IN URANIUM. The paper explains a new method of determining internal friction in metals. Unlike existing procedures, the new method involves measurements of forced oscillations, when variation in the internal friction of the metal under investigation, induced by whatever cause, is indicated by change in the amplitude of the resonance oscillations. (Measurements are made when the amplitude is low; i.e. when internal friction is independent of amplitude.)

Using this method it is possible to measure the internal friction over a wide range of rates of heating and cooling of the sample. The curves showing the temperature-dependent amplitude changes can be recorded automatically, without the intervention of the experimenter, which is of course important when working with radioactive materials.

The internal friction Q^{-1} in uranium was studied in the temperature range 20 - 500° C, and a maximum value for Q^{-1} was found at 250° C.

The height of this maximum depends on the rate of temperature variation, a finding which corresponds to the observation made when carrying out measurements on zirconium regarding the existence of a "hydride" maximum. Additional experiments on the annealing of uranium in a hydrogen atmosphere confirm the hypothesis that the existence of a maximum is linked with the formation of uranium hydride, although it is not out of the question that the appearance of a maximum may also be due, in this case, to the influence of stresses within the sample. The role of stresses needs further investigation. When the material cools from 500° C to ambient temperature, internal friction does not return to its initial level.

It is found that the internal friction is subject to hysteresis which, generally speaking, is characteristic of phase transformations. It is suggested that the processes of formation and destruction of uranium hydrides during the thermal cycling of uranium rods may be one of the causes of the variations in dimensions which occur.

FRICTION INTERNE DANS L'URANIUM. Les auteurs exposent une nouvelle méthode d'évaluation de la friction interne dans les métaux; elle se distingue des procédés appliqués jusqu'ici par le fait qu'on emploie des oscillations forcées et que l'on détermine les variations de la friction interne dans le métal étudié en fonction de divers facteurs, d'après les variations de l'amplitude des oscillations de résonance. (On procède aux mesures quand l'amplitude est faible, c'est-à-dire lorsque la friction interne ne dépend pas de l'amplitude.)

Cette méthode permet de mesurer la friction interne pour une gamme étendue de vitesses de réchauffement et de refroidissement de l'échantillon. Les courbes d'amplitude en fonction de la température peuvent être enregistrées automatiquement, sans l'intervention de l'expérimentateur, ce qui est essentiel dans l'étude des matériaux radioactifs.

La friction interne Q^{-1} dans l'uranium a été étudiée pour une gamme de températures comprises entre 20 et 500°C. On a observé la friction maximum à 250°C. Comme on l'a constaté lors de mesures faites sur le zirconium, à propos de l'existence d'un maximum d'«hydruration», la hauteur du maximum observé dépend de la vitesse de variation de la température. Des essais complémentaires de recuit d'uranium dans une atmosphère d'hydrogène confirment l'hypothèse selon laquelle l'existence d'un maximum est liée à la formation d'un hydrure d'uranium, mais il n'est pas exclu que l'apparition d'un maximum puisse être également due, dans une certaine mesure, à l'influence des tensions à l'intérieur de l'échantillon. Le rôle des tensions internes doit encore faire l'objet de recherches. Lorsque le matériau passe de 500° C à la température ambiante, l'intensité de la friction interne ne reprend pas sa valeur initiale.

On constate que la friction interne est soumise au phénomène d'hystérésis qui caractérise d'une manière générale les transformations périodiques. Les auteurs supposent que les processus de formation et de destruction des hydrures d'uranium lors du traitement thermique cyclique des barres d'uranium peuvent être l'une des causes des variations de dimensions constatées.

ВНУТРЕННЕЕ ТРЕНИЕ В УРАНЕ. Разработана новая методика определения внутреннего трения в металлах. В отличие от ранее существовавших применяются измерения на вынужденных колебаниях, когда мерой изменения внутреннего трения исследуемого металла в зависимости от тех или иных причин служит изменение амплитуды резонансных колебаний. (Измерения ведутся при малых амплитудах, когда внутреннее трение от амплитуды не зависит).

Методика позволяет измерять внутреннее трение в широком интервале скоростей нагрева и охлаждения образца. Может быть применена автоматическая запись кривой изменения амплитуды в зависимости от температуры без участия экспериментатора, что существенно при работе с радиоактивными материалами.

Внутренее трение Q^{-1} урана исследовалось в интервале температур 20 - 500°С. Обнаружен максимум Q^{-1} при температуре 250°С. Аналогично тому, как это наблюдалось при измерениях на цирконии в области существования "гидродного" максимума, высота обнаруженного максимума зависит от скорости изменения температуры. Дополнительные опыты с отжигом урана в атмосфере водорода подтверждают предположение о том, что существование максимума связано с образованием гидрида урана, хотя не исключена в данном случае возможность влияния на появление максимума внутренних напряжений в образце. Роль напряжений должна быть выяснена дальнейшими исследованиями. При охлаждении от 500°С до комнатной температуры уровень внутреннего трения в исходное состояние не возвращается. Кроме этого наблюдается гистерезис внутреннего трения, что вообще характерно для фазовых превращений.

Высказывается предположение, что процессы образования и распада гидридов урана при циклической термообработке стержня урана могут являться одной из причин изменения его размеров.

EL ROZAMIENTO INTERNO EN EL URANIO. Los autores describen un nuevo método para la determinación del rozamiento interno en los metales. A diferencia de los anteriores, este método se basa en la medición de las oscilaciones forzadas, en los casos en que la variación de amplitud de las oscilaciones de resonancia puede servir para medir la variación del rozamiento interno del metal estudiado, sea cual fuere la causa que lo provoca. (Cuando el rozamiento interno no depende de la amplitud, las mediciones pueden efectuarse con amplitudes pequeñas.)

El método descrito permite medir el rozamiento interno dentro de un extenso intervalo de velocidades de calentamiento y de enfriamiento de la probeta. Es posible registrar automáticamente la curva de variación de la amplitud en función de la temperatura, sin intervención del experimentador, lo que significa una ventaja decisiva cuando se trabaja con sustancias radiactivas.

Los autores han estudiado la variación del rozamiento interno Q^{-1} en el uranio, dentro de un intervalo de temperatura de 20 a 500°C. Han observado que el valor máximo de Q^{-1} corresponde a una temperatura de 250°C, y que, lo mismo que en las determinaciones correspondientes a la zona de existencia del máximo "hidrúrico" en el caso del circonio, la magnitud del máximo hallado depende de la velocidad de variación de la temperatura. Ciertos experimentos complementarios consistentes en el recocido de uranio en atmósfera de hidrógeno confirmaron la hipótesis de que la presencia del máximo está relacionada con la formación del hidruro de uranio, aunque no se excluya en ciertos casos la posibilidad de que intervengan en este fenómeno, en cierta medida, las tensiones internas en la probeta. Será preciso efectuar nuevos estudios para dilucidar el papel que desempeñan dichas tensiones. Durante el enfriamiento desde los 500°C hasta la temperatura ambiente se comprueba que el rozamiento no vuelve a alcanzar el valor inicial.

Se ha observado que en la variación del rozamiento interno se manifiesta cierta histéresis, cosa que, por otra parte, es característica de las transformaciones de fase. Los autores proponen una hipótesis, en virtud de la cual los procesos de formación y descomposición de los hidruros de uranio en el transcurso del ciclado térmico de una barra de uranio podrían ser una de las causas de la variación de sus dimensiones.

ВВЕДЕНИЕ

В последнее время метод внутреннего трения приобретает значение в изучении структуры и свойств металлов. Весьма удобным оказывается применение его в целях исследования влияния малых количеств примесей. В данной работе изучается поведение водорода в уране.

МЕТОДИКА И ОБРАЗЦЫ

Наиболее широко распространенным методом определения внутреннего трения Q^{-1} является измерение скорости затухания свободных колебаний проволочных образцов. Однако использование этого метода затруднительно в том случае, когда необходимо определять Q^{-1} в зависимости от температуры при больших скоростях нагрева или охлаждения. В этих условиях оказалось более удобным применение вынужденных колебаний при резонансе, когда мерой изменения внутреннего трения может служить величина изменения амплитуды резонанса.

В случае резонанса можно записать:

$$\delta = \frac{A}{A_p \cdot \omega_p^2}, \qquad (1)$$

где A - константа, пропорциональная величине вынуждающей силы; A_p - резонансная амплитуда; ω_p - резонансная частота; δ - логарифметический декремент.

Отсюда видно, что если сохранять величину (A) постоянной, то при данной резонансной частоте (ω_p) изменения (δ) в зависимости от тех или иных причин будут полностью характеризоваться изменениями величины резонансной амплитуды (A_p).

Эти рассуждения справедливы, конечно, лишь в том случае, когда внутреннее трение не зависит от амплитуды колебаний, т.е. при амплитудах, соответствующих величине относительной деформации (ϵ) от 10^{-5} и ниже.

Установка для измерений Q^{-1} по этому методу устроена следующим образом (рис.1). В металлическом каркасе 1 жестко монти-

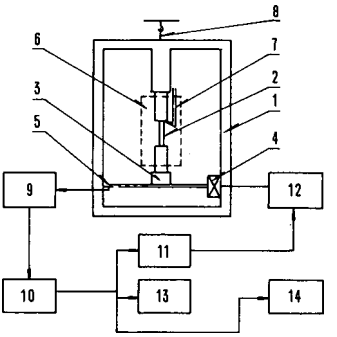


Рис.1

Схема установки:
1 - металлический каркас; 2 - исследуемый образец;
3 - траверса; 4 - соленоиды; 5 - датчик; 6 - трубчатая печь;
7 - термопара; 8 - гибкий тросик; 9 - преобразователь;
10 - усилитель; 11 - ограничитель; 12 - усилитель;
13 - вольтметр.

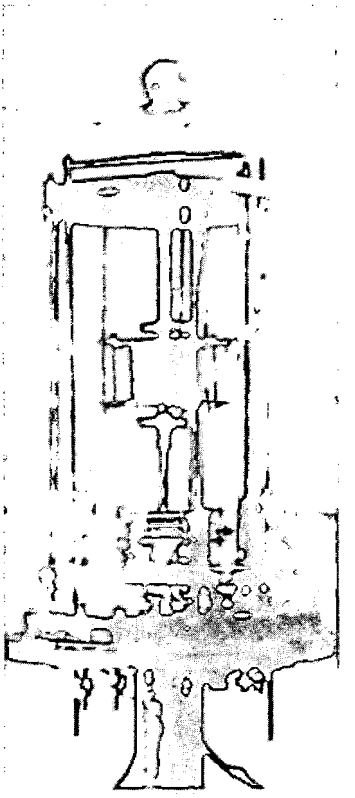


Рис.2

Внешний вид установки.

руется одним концом образец исследуемого металла 2. К нижнему, свободному, концу образца крепится траверса 3, посредством которой в образце при помощи соленоидов 4 возбуждаются крутильные колебания. (На рисунке с целью упрощения показан один соленоид). На траверсе укреплена система подвижных пластин емкостного датчика 5, который служит для измерения амплитуды колебания; система неподвижных пластин монтируется на каркасе. Рабочая часть образца помещена в трубчатой печи 6. Для измерения температуры служит термопара 7.

Для уменьшения нежелательной утечки энергии, сообщаемой образцу, каркас с приспособлениями, которые на нем смонтированы, подвешивается на опорах при помощи тонкого гибкого тросика 8 и помещается в вакуумную камеру (рис.2). Измерения ведутся при остаточном давлении 10^{-5} мм рт.ст.

Чтобы добиться большой точности измерения, необходимо обеспечить выполнение следующих условий:

1. Измерения должны проводиться точно на резонансной частоте; вследствие большой остроты резонансного пика малейшее от-

клонение от резонансной частоты приводит к большим погрешностям в измерениях.

2. Амплитуда колебаний образца, соответствующая малым относительным деформациям $\epsilon = 10^{-5} \div 10^{-7}$, должна измеряться с большой точностью.

3. Необходимо обеспечить строгое постоянство во времени возбуждающей силы.

В наших опытах эти требования удовлетворялись применением радиотехнических методов. Периодические изменения емкости, происходящие вследствие колебаний образца, с помощью датчика 5 и преобразователя 9 превращаются в электрические колебания, которые затем усиливаются четырехкаскадным усилителем низкой частоты 10, с отрицательной обратной связью до значений 100 ÷ 150 в. Как преобразователь так и усилитель в рабочем диапазоне должны иметь линейные характеристики.

Усиленные электрические колебания подаются через ограничитель амплитуды 11 на усилитель мощности 12. Последний осуществляет раскачку образца путем подачи тока в соленоиды 4. Цепь: образец - датчик - усилители - соленоиды представляет собой автоколебательную систему, находящуюся в резонансе. Необходимо отметить, что в подобного рода устройствах существует опасность ухода от резонанса вследствие сдвига фазы. Однако при соответствующим образом подобранных электрических и механических параметрах системы этого можно практически избежать. Перед каждым опытом проводится проверка системы на резонансные колебания с помощью звукового генератора. Этим выполняется первое условие. Наличие в цепи амплитудного ограничателя удовлетворяет третьему условию.

Для измерения амплитуды колебаний и ее зависимости от температуры нагрева образца служит ламповый вольтметр 13. Наблюдение за формой колебаний ведется с помощью электронного осциллографа. Осциллограф необходим также и для градуировки системы. Дело в том, что в выражении для логарифмического декремента (1) трудно вычислить величину (δ), т.к. значение (A), или возбуждающая сила, определяется недостаточно точно. Эту трудность легко обойти, предварительно проградуировав прибор по затуханию свободных колебаний при помощи осциллографа и секундомера. Зная частоту колебаний и время половинного спада амплитуды, можно для комнатной температуры с хорошей точностью определить величину Q^{-1}, т.е. получить одну градуировочную точку на кривой зависимости от температуры. Заметив соответствующее данной точке значение резонансной амплитуды на ламповом вольтметре, можно в дальнейшем следить лишь за изменением последней.

В описываемом устройстве предусмотрена автоматическая запись кривой изменения резонансной амплитуды в зависимости от температуры. В сочетании с приспособлением для автоматического линейного во времени подъема температуры записывающее устройство позволяет получить кривую внутреннего трения без участия оператора, что существенно при работе с радиоактивными материалами.

Для измерений используются цилиндрические образцы длиной 100 и диаметром 10 мм. В средней части образец проточен на длине 20 мм до диаметра 3 мм.

Измерения, проведенные на материалах с хорошо известными характеристиками внутреннего трения [1] дали значения Q^{-1}, удовлетворительно совпадающие с данными, приведенными в литературе [2].

Результаты экспериментов

Для опытов был использован металлический уран, полученный прессованием с последующей холодной протяжкой и отжигом. Чистота металла - 99,9%. Употребляемая частота колебаний составляла 99,9 гц при комнатной температуре. В интервале температур 20 ÷ 300°С у исследуемых образцов наблюдалось увеличение внутреннего трения, которое зависело от скорости нагрева образца. На рис.3 кривой I

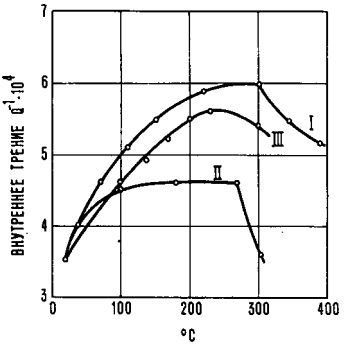


Рис.3

Внутреннее трение урана после различных обработок.

представлена температурная зависимость внутреннего трения Q^{-1}. Скорость нагрева образца составляла 10 град/мин. Как видно, в этом случае в области температур 220 ÷ 300°С Q^{-1} достигает максимального значения. Как известно из литературных данных [3], в температурном интервале 225 ÷ 250°С происходит интенсивное образование гидридов, которые распадаются выше 300°С. Возникает предположение, что в данном случае причиной появления максимума является водород, находящийся в металле. Так как присутствующий в уране водород удаляется отжигом в высоком вакууме, то были проведены измерения на образцах, отожженных при давлении 10^{-5} мм рт.ст. и температуре 640°С в течение трех часов. Измерения Q^{-1} этих образцов при той-же скорости нагрева (10 град/мин), что и в предыдущем опыте, показывают, что максимум в области 220 ÷ 300°С значительно уменьшился и что форма его изменилась (кривая II). В дальнейшем этот образец был нагрет в атмосфере водорода при давлении 100 мм

рт.ст. до температуры 200°С и выдерживался в этих условиях в течение четырех часов. Затем были произведены измерения Q^{-1} град/мин. Результаты опыта, представленные кривой III (рис.3), вновь показывают на возрастание максимума. Таким образом, эти опыты могут служить подтверждением высказанного предположения, что появление максимума Q^{-1} связано с процессами выделения гидрида урана. Эти результаты интересно сравнить с измерениями внутреннего трения в цирконии, проведенными нами аналогичным методом.(рис.4). Здесь представлены результаты измерений, про-

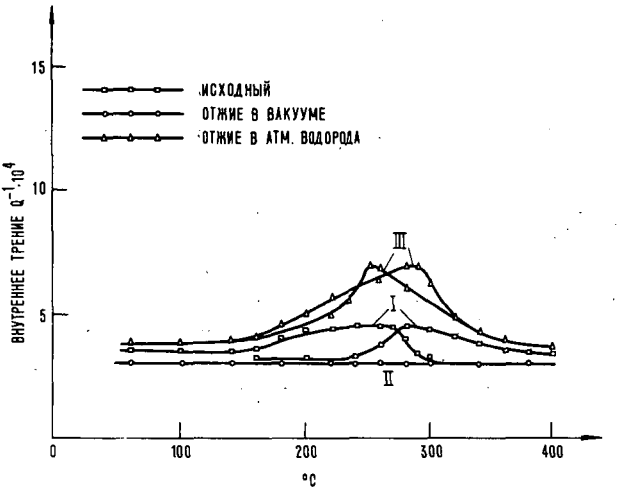


Рис.4

Внутреннее трение циркония.

веденных при одинаковых скоростях нагрева и охлаждения в случае исходного (кривые I), отожженного в вакууме (кривая II) и отожженного в водороде (кривые III) циркония. Любопытно отметить, что после отжига в атмосфере водорода появляется гистерезис внутреннего трения, в то время как на исходном цирконии его не наблюдалось. Можно было бы предположить, что появление пика внутреннего трения в уране вызывается влиянием внутренних напряжений в образце вследствие анизатропии свойств металла; несомненно, что напряжения могут оказывать значительные влияния на ход внутреннего трения, однако рассматриваемый процесс имеет обратимый характер, что можно объяснить тем, что свободный водород, образовавшийся при разложении гидрида во время нагрева до 400°С, при охлаждении образца вновь вступает в реакцию с ураном, образуя гидрид. При охлаждении образца пик, обусловленный образованием гидридов, появляется при более низкой температуре (рис.5). Вместе с тем уровень Q^{-1} не достигает исходного состояния и повышается с увеличением числа циклов нагрева и охлаждения. Возможно, что при образовании гидрида урана возни-

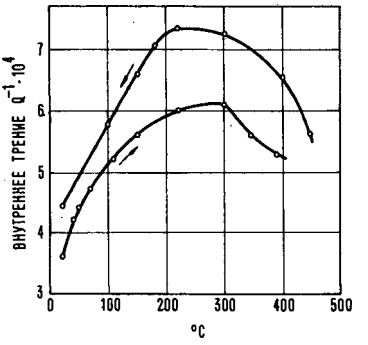


Рис.5

Внутреннее трение урана при нагреве и охлаждении.

кающие напряжения приводят к пластическому деформированию урана и появлению дефектов кристаллического строения. При дальнейшем нагревании, когда происходит распад гидрида, в решетке урана могут появляться пустоты, а при многократном повторении нагрева и охлаждения эти процессы проявляются в виде повышения фона внутреннего трения. Возможно, что такие процессы являются одной из причин изменения формы урановых стержней при циклической термообработке.

ЛИТЕРАТУРА

[1] ИВАНОВ В.Е., ШАПОВАЛ Б.И., АМОНЕНКО В.М. Ф.М.М. т.2, вып.1 (1961).
[2] ГАРБЕР Р.И., КОВАЛЕВ А.И. Ф.М.М. т.4, вып.5 (1959).
[3] КАЦ Дж., РАБИНОВИЧ Е. Химия урана. т.1, Изд.иностр.лит.,1954, стр.165

THE SELF-IRRADIATION OF PLUTONIUM AND ITS DELTA ALLOYS*

C.E. OLSEN, R.O. ELLIOTT AND T.A. SANDENAW
LOS ALAMOS SCIENTIFIC LABORATORY,
UNIVERSITY OF CALIFORNIA, LOS ALAMOS, NEW MEXICO

Abstract — Résumé — Аннотация — Resumen

THE SELF-IRRADIATION OF PLUTONIUM AND ITS DELTA ALLOYS. Electrical resistivity and heat capacity measurements have shown that self-irradiation from the alpha activity in plutonium produces damage at low temperatures. Measurements were made on specimens of nominally pure, α-phase plutonium and on specimens of plutonium-rich, δ-phase, solid-solution alloys containing aluminium. The resistivity was found to increase linearly with time at 20.1°K and 4.5°K in both phases, but the rates of increase in α-phase are significantly higher than in δ-phase. Annealing of stored damage was studied by means of electrical resistivity and heat capacity measurements, and the results from both types of measurements are in concordance. Calculations by Vineyard on self-irradiation damage in plutonium are presented, and differences in the radiation damage behaviours of α-phase and δ-phase are discussed and correlated with differences in other physical properties of these phases.

AUTO-IRRADIATION DU PLUTONIUM ET DE SES ALLIAGES DELTA. Les mesures de la résistivité électrique et de la capacité calorifique montrent que l'auto-irradiation due au rayonnement alpha du plutonium cause des dommages à basse température. Les auteurs ont fait des mesures sur des échantillons de plutonium de phase alpha, virtuellement pur, et des échantillons d'alliages riches en plutonium de phase delta, et contenant de l'aluminium en solution solide. Ils ont constaté que, dans les deux phases, la résistivité augmentait avec le temps selon une loi linéaire à 20,1°K et à 4,5°K, mais que les vitesses d'accroissement pour la phase alpha étaient considérablement plus élevées que pour la phase delta. Ils ont étudié le recuit des dommages accumulés en faisant des mesures de la résistivité électrique et de la capacité calorifique; les résultats de ces deux types de mesures concordaient entre eux. Les auteurs exposent les calculs de Vineyard sur les dommages par auto-irradiation; ils examinent les différences de comportement entre la phase alpha et la phase delta, et déterminent la corrélation qui existe entre ces différences et les différences d'autres propriétés physiques de ces phases.

САМООБЛУЧЕНИЕ ПЛУТОНИЯ И ЕГО ДЕЛЬТА-СПЛАВОВ. Измерение удельного электросопротивления и теплоемкости показали, что при низких температурах самооблучение от альфа-активности в плутонии вызывает повреждение. Измерения проводились на образцах номинально чистого плутония альфа-фазы и на образцах, богатых плутонием дельта-фазовых твердорастворных сплавов, содержащих алюминий. Было установлено, что удельное сопротивление возрастает линейно во времени при 20,1°К и 4,5°К, но величина возрастания в α-фазе значительно больше, чем в δ-фазе. Отжиг образовавшегося повреждения изучался с помощью измерений удельной электропроводимости и теплоемкости. Результаты, полученные с помощью обоих типов измерений, совпадают. Приводятся вычесленные Виньярдом повреждения от самооблучения в плутонии, обсуждаются различные степени повреждения в α- и δ-фазах и дается сравнение с различиями в других физических свойствах этих фаз.

LA AUTOIRRADIACION DEL PLUTONIO Y DE SUS ALEACIONES δ. Las determinaciones de la resistividad eléctrica y del calor específico han demostrado que, a bajas temperaturas, la autoirradiación originada por la actividad alfa del plutonio causa daños al mismo. Los autores efectuaron mediciones con muestras de plutonio en fase α, nominalmente puro, y con muestras de aleaciones de aluminio en solución sólida, en fase δ, ricas en plutonio. Comprobaron que la resistividad aumenta linealmente en función del tiempo, a 20,1° K y 4,5° K en ambas fases, pero que el índice de aumento en la fase α es apreciablemente mayor que en la fase δ. Se

* Work performed under the auspices of the United States Atomic Energy Commission.

estudió el efecto del recocido sobre el daño acumulado, midiendo la resistividad eléctrica y el calor específico, y se comprobó que los resultados obtenidos por ambos métodos concuerdan. Los autores presentan los resultados de evaluaciones del daño causado por la autoirradiación en el plutonio, según el método de Vineyard, examinan las diferencias observadas en la manifestación de los efectos de los daños causados por las radiaciones en fase α y en fase δ y las relacionan con las diferencias observadas en otras propiedades físicas del metal en dichas fases.

1. INTRODUCTION

The effects of radiation damage on a wide variety of materials have been studied and may excellent review articles are available [1]. These studies have been concerned almost exclusively with radiation damage effects produced by bombardment with high-energy particles, such as protons, deuterons, electrons and neutrons, that enter the material from external sources. The results show that the electrical resistivity of metals such as copper, silver and gold increases when these metals are irradiated at low temperatures, and that these increases are proportional to the intensity of the radiation [2]. The annealing of stored radiation damage occurs at definite temperatures as evidenced, for example, by steps in the resistivity-versus-temperature curves on heating. The damage is retained to relatively high temperatures (i.e. 24 to 200° C or sometimes higher) in a number of metals before annealing occurs and the annealing processes have been interpreted in terms of interstitial-vacancy migration [1]. Radiation damage investigations have also been made on nuclear materials, notably uranium and its alloys, under fission conditions [1]. The authors did not find any reference in the literature, however, in which the effects of self-irradiation damage in radioactive metals or alloys were mentioned, although the instability of radioactive compounds is mentioned and some self-damage investigations have been made on metamict minerals containing uranium and thorium [1].

Pu^{239} has a half-life of 24 360 ± 100 yr and decays by emission of an alpha particle with an energy of about 5.147 MeV [3]. The residual U^{235} nucleus recoils with an energy of about 87 keV. Pu^{240} decays by a similar scheme and has a half-life of 6600 yr. It emits an alpha particle with an energy of about 5.162 MeV and the residual U^{236} nucleus also recoils with an energy of about 87 keV [3]. These isotopes also undergo spontaneous fission but this disintegration process is a minor one. Calculations by DEMPSEY and KAY [4] indicate that helium accumulation will not produce any appreciable effect on the physical properties of α-plutonium at room temperature in less than one century. The present work was initiated when it was observed that the resistivity of α-plutonium was lowest when the specimens were quenched directly to 20° K (in comparison with slow cooling from 300 to 20° K over a period of 3 d). This effect was interpreted as arising from self-damage produced by the alpha activity in the specimens and further investigation showed that the resistivity increased linearly as a function of time at 20° K [5].

The room temperature α-phase allotrope of metallic plutonium is simple monoclinic with 16 atoms per unit cell [6]. The unit cell dimensions at 25°C are: $a = 6.182 \pm 0.001$ Å, $b = 4.826 \pm 0.001$ Å, $c = 10.956 \pm 0.001$ Å and $\beta = 101.74° \pm 0.01°$; the calculated density is 19.84 g/cm^3. The δ-phase allotrope of plutonium is face-centred-cubic and is stable between 319 and 451°C on heating.

At 320°C its unit cell dimension is 4.6371 ± 0.0004 A and the calculated density is 15.92 g/cm³ [6]. Delta phase can easily be retained to room temperature and below by alloying. These phases differ widely in some properties [7], as might be expected from their differences in crystal structure. Similarities between low-temperature physical properties of these phases have also been noted, however, which suggest that crystal structure is not necessarily always the dominant factor in determining the behaviour of plutonium [8, 9, 10]. We undertook the present work in order to study in detail the self-irradiation damage behaviours of the alpha and delta phases, to compare these behaviours and to attempt to correlate the results with other physical properties of these phases.

2. ELECTRICAL RESISTIVITY MEASUREMENTS

2.1. Specimen preparation

Since complete information on specimen preparation, experimental apparatus and procedure and chemical analyses of the specimens is given elsewhere [5, 10, 11], only a brief summary of these items is given here. Specimen labelling in the present paper is identical with that used previously [5, 10], and information about the electrical properties of these specimens in the "undamaged" states can be obtained by referring to our earlier work.

Specimens were induction-melted and cast into MgO crucibles to form cylindrical ingots 0.65 cm in diameter by 2.8-cm long. The alloy ingots were sealed within Pyrex capsules (either evacuated or filled with 0.5 atm of argon gas) and homogenized for at least 200 h at 450° C, air-quenched to room temperature and machined to form right cylinders 0.61-cm diameter by 2.54-cm long. Diameters and lengths of the specimens were measured with micrometer calipers to ± 0.025 mm before and after each resistivity run. Densities were also measured before and after each run by using the standard method of weighing the specimens in air and in bromobenzene. The isotopic analyses of the plutonium used were typically 94 to 95% Pu^{239}, 4 to 5% Pu^{240} and usually less than 0.5% Pu^{241}. Work on plutonium of similar isotopic composition was reported previously by SANDENAW et al. [12].

2.2. Apparatus and procedure

A copper holder allowed four specimens to be measured during each run. The specimens were insulated from the holder by thin Lucite sleeves. The current contacts at the ends of each rod were insulated and spring-loaded and were made of gold-plated steel. Potential contacts (situated along the longitudinal surfaces of the specimen rods) were also insulated and spring-loaded but were made of tungsten. The probe separation was about 1.5 cm. Measurements were made by a potentiometer method and the current through and voltage across the specimens were measured simultaneously. The specimen potential was measured by using a bucking circuit, which provided compensation for static thermal EMF's [11]. Temperatures

were measured with two 'calibrated' copper-constantan thermocouples that had been soft-soldered to the copper holder. The thermocouple calibration data were reduced to a sixth-order polynomial expression for the region below 76°K and to a third-order polynomial expression for the region above 76°K by the 'method of least-squares' fitting of the calibration points. In addition, cemented to the holder were two carbon resistor thermometers which were also used to measure very low temperatures. Their resistances were measured with an alternating-current bridge similar to that described by BLAKE et al. [13], and the resistor calibration data were reduced to the analytic form proposed by CLEMENT and QUINNEL [14].

The specimen holder was mounted in a vacuum-tight demountable brass can, and the assembly was suspended in the cryostat by means of an Inconel tube, which terminated in a vacuum-tight head. The electrical leads passed out of the head through vacuum-tight, insulated Kovar seals. The cryostat was a standard nitrogen-jacketed type, and the assembly had pumping connection that allowed the inner Dewar and the inner Dewar jacket to be evacuated or filled with helium gas at any desired pressure.

The following temperature cycles were used in the investigation. The so-called "normal" run was one in which the samples were cooled slowly from ~300 to ~77°K in approximately 9 h. The sample was held at the lower temperature overnight and then cooled to ~48°K by adding liquid nitrogen to the cryostat and pumping. Data were taken between 48 and 80°K while the samples were slowly warmed. Approximately 4 h were required to cover this interval. The samples were stored overnight at ~77°K, and then cooled the next morning with either liquid helium or hydrogen. The samples were cooled to the lowest obtainable temperatures (~2°K for He or ~10°K for H_2) by pumping. The samples were then warmed to ~77°K, which took approximately 4 to 6 h. Finally they were stored overnight at ~77°K and then warmed to 300°K, over approximately 9 h. The "quenched" runs were made by cooling the samples directly to ~20°K from room temperature. The actual sample cool-down time was approximately 1/2 h. The hydrogen was pumped to obtain the lowest possible temperature, then the samples were warmed to room temperature, the whole operation taking approximately 9 h. Resistivities were measured continuously in sequence among all four specimens during these temperature changes. The normal boiling point of liquid hydrogen is ~19.6°K at Los Alamos barometric pressure, typically 585 to 590 mm of Hg, and the measured specimen temperature corresponding to this bath temperature was 20.1 °K. Similarly, the bath temperature of boiling liquid helium is approximately 3.96°K at Los Alamos, and the corresponding specimen temperature was estimated to be ~4.5°K.

The build-up and storage of self-irradiation damage were measured by holding the specimens at the normal boiling points of liquid helium, hydrogen or nitrogen or at the triple points of hydrogen and nitrogen and recording their resistivities as a function of time. A manostat was used to regulate the pressure and consequently to maintain constant temperature at the triple points. The annealing of stored self-irradiation damage was studied in two ways: (1) by measuring resistivities continuously in sequence as the specimens were slowly warmed to room temperature; and (2) by measuring changes

in the resistivity at 20°K after the specimens were warmed slowly to various annealing temperatures* and then quenched back to 20°K. The latter technique was used to study annealing processes in α-plutonium only, and changes in the resistivity at 20°K were taken as indicative of annealing.

2.3. Electrical resistivity results and discussion

2.3.1. Behaviour of nominally pure α-phase plutonium. Measurements of the increase in resistivity as a function of time at constant temperature show large self-damage effects in α-plutonium at 20°K and below. Runs were made at ~4.5, 20.1, 64.7 and 77.1°K, and experimental data for α-plutonium specimen No.2 are shown in Fig. 1. The specific resistivity in-

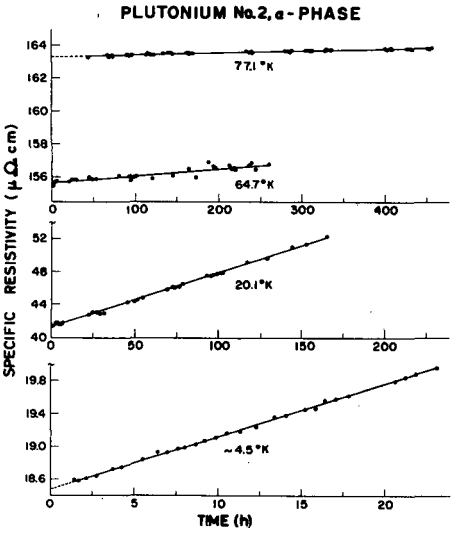


Fig. 1

Specific resistivity as a function of time for nominally pure α-plutonium at ~ 4.5, 20.1, 64.7 and 77.1°K.

creased linearly with respect to time at each temperature and the data were least-squares-fitted to the expression

$$\rho = \rho_0 + \dot{\rho}(t), \tag{1}$$

where ρ_0 is in $\mu\Omega$cm, ρ_0 is the value of ρ_0 in $\mu\Omega$cm at zero time, $\dot{\rho}_0$ is $d\rho/dt$ in $\mu\Omega$cm/h, and t is time in hours. (Similar observations were made on δ-phase solid-solution alloys containing aluminium and cerium. These ex-

* The term "annealing temperature" has the following two different meanings in this paper: (1) the temperature to which specimens were warmed: and (2) the temperature at which annealing of damage actually occurred. The meaning intended will be evident from the context.

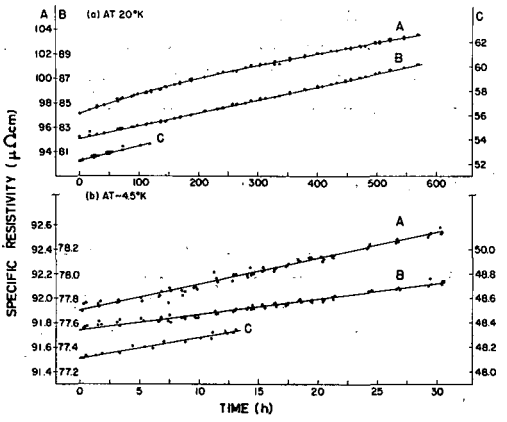


Fig. 2

Specific resistivity as a function of time for plutonium-rich δ-phase and δ + α-phase mixtures in solid solution alloys containing aluminium and cerium at 20°K and ~ 4.5°K
Curve A is for 0.5% Al-50% α-50% β phase mixture
Curve B is for 3.4% Al-100% δ-phase
Curve C is for 8% Ce-100% δ-phase

perimental data are shown in Fig. 2 and are discussed below.) A summary of the results is given in Table I for three different α-plutonium specimens. The data show that within experimental error the resistivity increases linearly with time and there is no evidence for curvature or saturation within the time periods specified in Table I. The rates of increase for each specimen at a given temperature are about the same, showing that a comparable amount of damage is produced in each specimen. The rates of increase are slightly lower in each specimen at ~ 4.5°K than at 20.1°K. Fig. 3 includes resistivity-versus-temperature curves for α-plutonium specimen #2 and for a δ-phase alloy specimen containing 3.4 at.% aluminium. These curves illustrate the electrical behaviours of alpha and delta phases in the "damaged" and "undamaged" states and show qualitatively that most of the self-irradiation damage anneals out at the temperature of the resistivity maximum, i.e. ~ 105°K for α-plutonium. Note that there is no evidence for discontinuous steps in the α-plutonium "damaged" curve, such as are typically observed on annealing of stored damage in normal metals.

There is strong evidence [5, 15] that α-plutonium undergoes a low-temperature transformation similar to that reported for α-uranium [16]. Elastic constant, resistivity, thermal expansion, Hall-coefficient, specific heat and thermo-electric power measurements show evidence for a phase change near 42°K in α-uranium, and X-ray diffraction data have shown that this phase change involves a change in lattice expansion characteristics rather than a change in crystal symmetry [16]. Evidence for similar behaviour in α-plutonium is shown in Figs. 4a and 4b. The ρ/T-versus-T plots give information on the electrical behaviour of α-plutonium that is not obvious from the ρ-versus-T plots shown in Fig. 3. Results in Fig. 4b

TABLE I

BUILD-UP OF SELF-IRRADIATION DAMAGE IN PLUTONIUM AND ITS SOLID SOLUTION ALLOYS

(Based on electrical resistivity measurements)

	Temperature (°K)	Initial ρ_0 ($\mu\Omega$ cm)	Average linear Rate of increase ρ_T ($\mu\Omega$cm/h)	Time (h)	Standard error ($\mu\Omega$cm)
α-phase [5]	(a) Plutonium No.1; density (297°K) = 19.535 g/cm^3				
	~ 4.5	22.531	0.0616	23.1	± 0.0137
	20.1 ± 0.1	44.982	0.0635	165	± 0.148
	64.7 ± 0.2	151.14	0.00367	260	± 0.145
	77.1 ± 0.1	158.22	0.00123	475	± 0.0426
	(b) Plutonium No.2; density (297°K) = 19.475 g/cm^3				
	~ 4.5	18.493	0.0637	23.1	± 0.0161
	20.1 ± 0.1	41.295	0.0656	165	± 0.167
	64.7 ± 0.2	155.66	0.00425	260	± 0.173
	77.1 ± 0.1	163.27	0.00136	475	± 0.0304
	(c) Plutonium No.3; density (297°K) = 19.50 g/cm^3				
	~ 4.5	25.475	0.0671	23.1	± 0.0195
	20.1 ± 0.1	47.067	0.0682	165	± 0.149
	64.7 ± 0.2	157.29	0.00361	260	± 0.153
	77.1 ± 0.1	164.30	0.00169	475	± 0.0528
δ-phase	(a) 96.6 at.% Pu-3.4 at.% Al; density (297°K) = 15.57 g/cm^3				
	~ 4.5	77.544	0.0124	30.6	± 0.0174
	20.1 ± 0.2	82.056	0.0107	569	± 0.0572
	65.0 ± 0.2	102.14	0.0018	279	± 0.0817
	76.7 ± 0.3	105.50	0.0014	428	± 0.0285

TABLE I (cont.)

	Temperature (°K)	Initial ρ_0 (μΩcm)	Average linear Rate of increase $\dot{\rho}_T$ (μΩcm/h)	Time (h)	Standard error (μΩcm)
δ-phase	(b) 92.0 at.% Pu-8.0 at.% Ce; density (297°K) = 15.18 g/cm^3				
	~ 4.5	48.111	0.0166	13.1	± 0.0154
	13.5 ± 0.6	51.740	0.0143	72.6	± 0.1731
	19.8 ± 0.2	52.237	0.0123	118	± 0.0640
	76.8 ± 0.1	86.118	0.0023	646	± 0.0888
50% α-phase 50% δ-phase (mixture)	(a) 98.8 at.% Pu-1.2 at.% Al; density (297°K) = 17.63 g/cm^3 (estimated)				
	~ 4.5	91.897	0.0213	30.5	± 0.0264
	20.1 ± 0.2	97.235	*	569	± 0.0635
	64.9 ± 0.2	131.32	**	279	± 0.0905
	76.6 ± 0.1	136.16	0.0011	428	± 0.0533

* Average rate of increase followed parabolic law:
$\rho = 97.235 + 0.0149\ t - 6.96 \times 10^{-6} t^2$, where ρ is in μΩcm and t is in hours.

** $\rho = 131.32 + 0.0035\ t - 9.20 \times 10^{-6} t^2$.

(plutonium No. 1) show that with increasing temperature the ρ / T ratio decreases rapidly between ~4.5 and 18°K, reaches a minimum near 18°K, increases to a peak near 50°K and then decreases gradually to 300°K. Figs. 4a and 4b show that this low-temperature anomaly in α-plutonium is related both to self-irradiation damage and to impurity content in the same way. Thermal expansion and heat capacity measurements [12, 15] provide supporting evidence for a low-temperature transformation. The thermal expansion and heat-capacity behaviour of α-plutonium are strongly dependent on the holding time and temperature at low temperatures, which suggests the existence of a radiation-induced or radiation-accelerated change.

The data for α-plutonium specimen No.2 show that the ratio of rates of increase at 20.1 and 64.7°K is 15.4 to 1 (see Table I), while the ratio of the differences in resistivity between the "damaged" and "undamaged" curves at 20.1 and 64.7°K is only 4.4 to 1 (see Fig. 3). This apparent discrepancy in the results led us to analyse carefully the differences between the "damaged" and "undamaged" curves at constant temperature. A common temperature was selected and the two nearest data points above and the two nearest data points below this common temperature were least-squares-fitted to the third-order polynomial equation

$$\rho = B_1 + B_2 T + B_3 T^2 + B_4 T^3, \qquad (2)$$

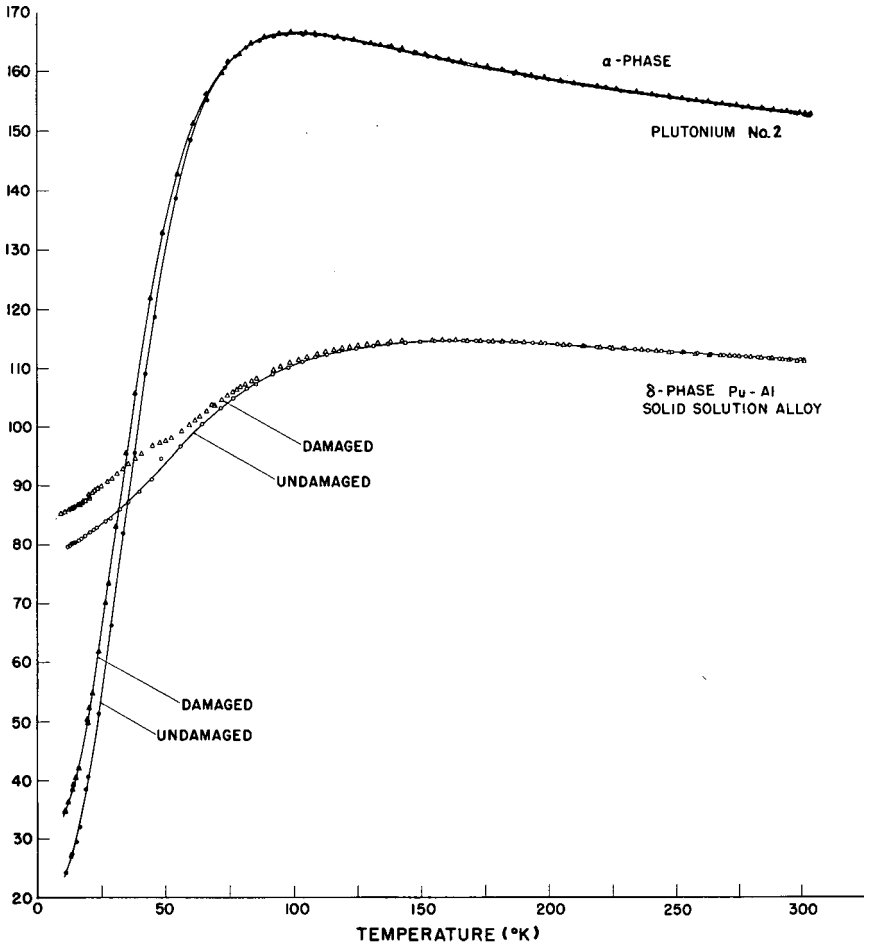


Fig. 3

Specific resistivity as a function of temperature for nominally pure α-plutonium and for a plutonium-rich δ-alloy containing 3.4 at.% aluminium - 96.6 at.% plutonium

o● Data taken immediately after quenching from 300 to 20°K to give the "undamaged" curves.

▲ Data taken after quenching from 300 to 20°K and holding at 20°K for 1 week for the "damaged" α-phase curves

Δ Data taken after quenching from 300 to 20°K and holding at 20°K for 3.4 weeks for the "damaged" δ-phase curve

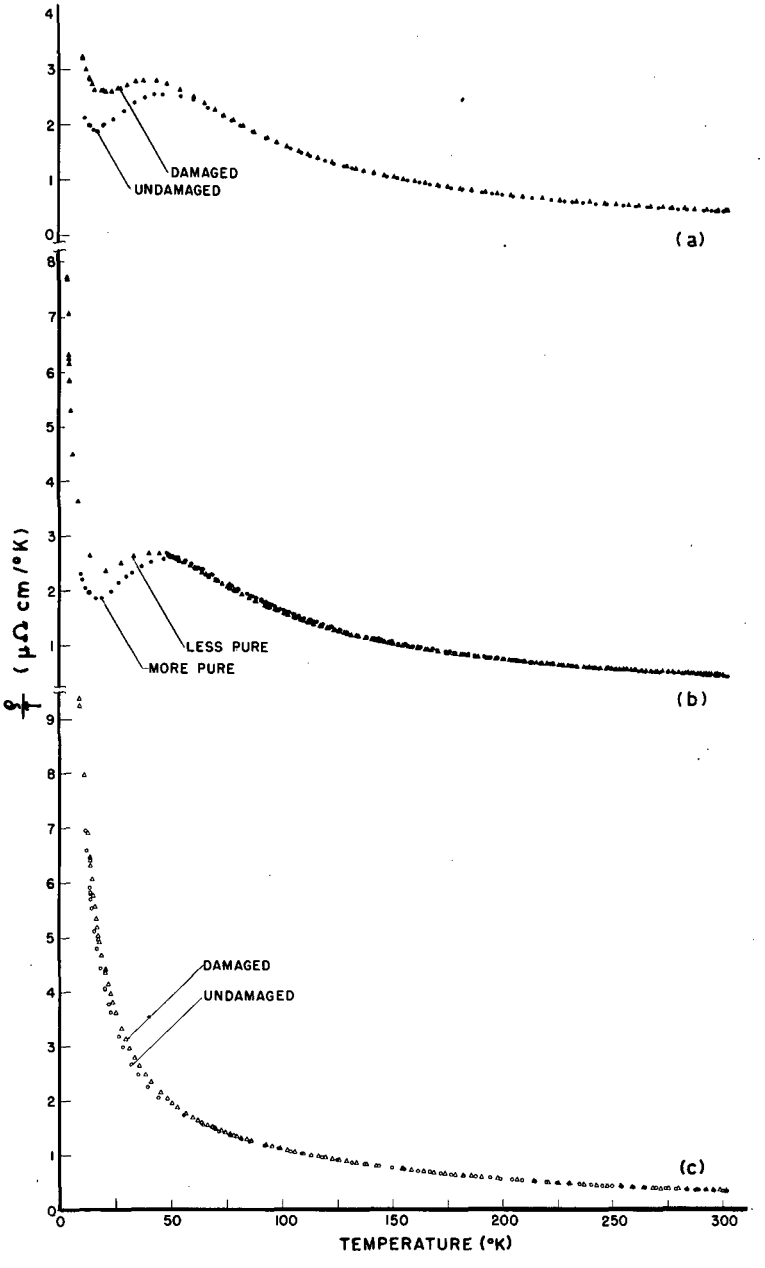


Fig. 4

(for caption see opposite)

Fig. 4

Ratio of electrical resistivity to absolute temperature as a function of absolute temperature
(a) Nominally pure α-phase plutonium No. 2 for which data were taken on heating only
- ● Data taken immediately after quenching from 300 to 20°K.
- ▲ Data taken after quenching from 300 to 20° and holding at 20°K for 1 week.

(b) α-phase plutonium specimens for which data were taken on heating and cooling
- ● Plutonium No. 1 ▲ Plutonium No. 2

(c) 96.6 at.% plutonium - 3.4 at.% aluminium δ-phase solid solution alloy for which data were taken on heating only
- o Data taken immediately after quenching from 300° to 20°K.
- Δ Data taken after quenching from 300° to 20°K and holding at 20°K for 3.4 weeks.

where ρ is $\mu\Omega$cm, T is the temperature in °K and B_1, B_2, B_3 and B_4 are constants. The "damaged" and "undamaged" resistivities (see Fig. 3) were then computed at the common temperature, and the differences, $\Delta\rho_T$ in $\mu\Omega$cm, are shown plotted as a function of temperature in Fig. 5. The complete curve for α-plutonium specimen No. 2 is shown in Fig. 5a with inserts for portions

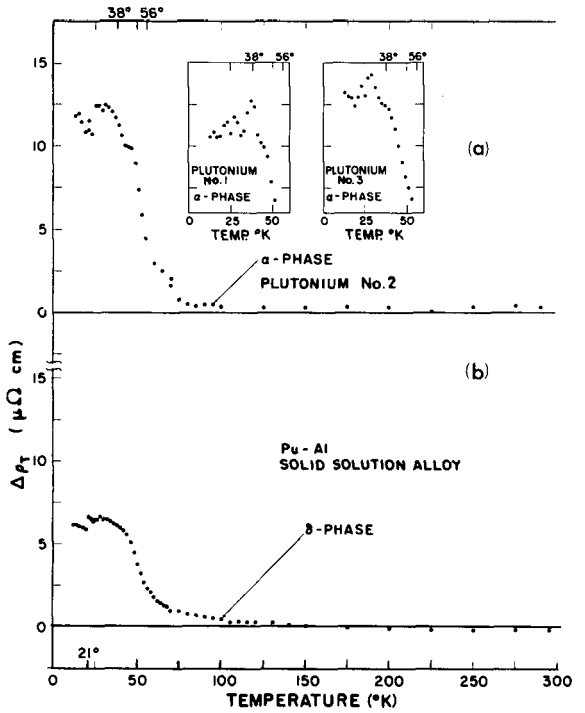


Fig. 5

Annealing of self-irradiation damage in plutonium
Difference in specific resistivity between "damaged" and "undamaged" curves shown in Fig. 3 (at constant temperature) are plotted as a function of absolute temperature for:
(a) nominally pure α-plutonium; and
(b) 96.6 at.% plutonium - 3.4 at.% aluminium, δ-phase solid solution alloy
96.6 at.% plutonium - 3.4 at.% aluminium

of the curves for two other α-plutonium specimens. (A similar delta-rho curve, $\Delta\rho_T$ versus T, for a δ-alloy containing 3.4 at.% aluminium is shown in Fig. 5b.) The delta-rho curves for the α-phase are semi-quantitatively in agreement and show a wealth of detail not evident in the ρ-versus-T curves in Fig. 3. The α-phase specimens show increasing $\Delta\rho_T$ values with increasing temperature to 30 or 38°K, which is consistent with the observation of slightly higher rates of increase at 20.1°K than at ~4.5°K, as given in Table I. Assuming that no appreciable annealing of damage occurs in this range from 4.5 to 20°K, it then appears that the relative increase in resistivity due to self-damage is greater at 20 than at 4.5°K, either because of the curvature of the resistivity versus temperature curve or, as is more likely, because of the differences in the radiation damage effects due to differences in the properties of plutonium at these two temperatures. The dip that occurs above 20°K in all three α-phase specimens appears to be significant and resembles the dips observed in the thermal recovery of deuteron-bombared gold [17]. The curves for all three α-plutonium specimens also show a definite step at or near 40°K. Another step appears in the delta rho curve of specimen 2 at 65°K but it is not strongly evident in either specimen 1 or specimen 3. Minor variations may arise from differences in impurity content, isotopic content and/or differences in the physical states of the specimens. The delta-rho curves also show that thermal recovery is essentially completed at 105°K, the temperature of the resistivity maximum, in agreement with data shown in Fig. 3. Small resistivity increases persist to room temperature, however, and it has not been established whether this effect is due to retained damage, a sluggish recovery or stress relief. Stress relief could account for the small resistivity increases that persist to room temperature, since the resistivity of α-plutonium increases with increased purity above 100°K [5]. The ratio of the rate of increase $\dot{\rho}_T / \dot{\rho}_{20.1°K}$ are 0.058, 0.065 and 0.053 at 64.7°K and 0.019, 0.021 and 0.025 at 77.1°K for specimens 1, 2 and 3 respectively, while the ratios of delta-rho $\Delta\rho_T / \Delta\rho_{20.1°K}$ are 0.130, 0.226 and 0.137 at 64.7°K and 0.020, 0.047 and 0.025 at 77.1°K for specimens 1, 2 and 3 respectively. The values at 77.1°K are in good agreement, but at 64.7°K the delta-rho ratios are higher than the rate of increase ratios, which indicates that there is some sluggishness in thermal recovery at this temperature.

The annealing of stored radiation damage in α-plutonium was also determined by measuring changes in the resistivity at 20°K after the specimens had been warmed slowly at about 0.1 to 0.2°K/min to various annealing temperatures and then quenched back to 20°K. The specimens had first been held at 20°K in order to build up and store large amounts of damage before annealing. The annealing temperatures were about 38, 56, 80, 77, 110, 224 and 300°K. A summary of these annealing data is given in Table II. The specimens were held at each annealing temperature for at least 10 to 30 min, and during this period the resistivities were measured as a function of time in order to obtain information on the kinetics of the annealing process. No drifting of resistivity was observed, which indicated that thermal recovery at these temperatures was either very rapid or very slow. The experimental evidence suggests that equilibrium is established rapidly at low temperatures, but that there may be some sluggishness in recovery above 77°K. This behaviour is consistent with a recovery process involving long-

TABLE II

ANNEALING OF SELF-IRRADIATION DAMAGE STORED IN α-PLUTONIUM HELD AT 20°K
(Based on electrical resistivity measurements)

Annealing temperature* (°K)	Damage stored before anneal $\Delta\rho_{20°K}$ ($\mu\Omega$cm)	Damage remaining after anneal $\Delta\rho'_{20°K}$ ($\mu\Omega$cm)	Damage annealed out $\Delta\rho''_{20°K}$ ($\mu\Omega$cm)	Damage annealed out $\frac{\Delta\rho''_{20°K}}{\Delta\rho_{20°K}} \times 100$ (%)
(a) Plutonium No. 1				
38.3	11.13	11.31	-0.18	-1.6
56.0	12.82	12.34	0.48	3.7
79.6	13.19	9.61	3.58	27.1
77.1**	14.64	11.03	3.61	24.7
110.0	13.88	9.91	3.97	28.6
223.8	11.50	5.43	6.07	52.8
300.7	5.43	3.41	2.02	37.2
Totals: -	22.96 +		19.55	
(b) Plutonium No. 2				
38.3	12.68	13.04	-0.36	-2.8
55.9	14.20	13.60	0.60	4.2
80.4	14.50	10.84	3.66	25.2
77.1**	16.50	12.38	4.12	25.0
110.1	15.74	11.39	4.35	27.6
226.3	12.57	7.00	5.57	44.3
300.7	7.00	4.35	2.65	37.9
Totals: -	24.94 +		20.59	
(c) Plutonium No. 3				
38.2	14.15	14.43	-0.28	-2.0
55.9	15.69	15.32	0.37	2.4
80.0	16.21	12.97	3.24	20.0
77.1**	18.28	13.76	4.52	24.7
110.1	17.77	13.01	4.76	26.8
225.0	14.15	8.69	5.46	38.6
300.1	8.69	7.28	1.41	16.2
Totals: -	26.76 +		19.48	

* Heating rate from 20°K to the annealing temperature was approximately 0.1 to 0.2 deg/min.

** No substantial change in resistivity was observed during the holding at this temperature for 7 h.

\+ The total damage stored during the entire experiment is equal to the total damage that annealed out plus the damage remaining after the last annealing run to 300°K.

range, interstitial-vacancy migration. The annealing runs to 38 and 56°K are especially interesting. The delta-rho curve of α-plutonium specimen 2, shown in Fig. 5a, indicates that 80% of the stored damage annealed out at 56°K, while the data in Table II show that only 4.2% annealed out at this temperature. This result can be interpreted in either of the following ways: (1) that the damage anneals out on warming and then reconstitutes itself rapidly on cooling back to 20°K; or (2) that there is a change in the physical properties of plutonium in the temperature region between 20 and 56°K. The second explanation is the more plausible and is in agreement with the heat-capacity data discussed below. The delta-rho curves of α-plutonium show the combined effects of self-irradiation damage and a low-temperature transformation. The small increases in resistivities at 20°K after the annealing run to 38°K (see Table II) are believed to be due to additional damage stored during heating, holding and cooling below the recovery temperature, and apparently no appreciable annealing occurred below 38°K. Consequently, this low-temperature transformation in plutonium must occur in the region between 38 and 56°K.

2.3.2. Behaviour of δ-alloys containing aluminium and cerium. Delta-phase solid-solution alloys may be either stable or metastable at room temperature. Metastable δ-alloys may transform to an equilibrium phase mixture, such as $\delta + \alpha$, when cooled to low temperatures. Electrical resistivity measurements [10] on plutonium-rich, metastable δ-alloys containing either aluminium or cerium show evidence of irreversible, partly reversible and completely reversible $\delta \leftrightarrows \alpha$ transformations at low temperatures, the extent of reversibility increasing with increased amounts of alloying additions. The δ-alloy compositions used in the present work were selected so that self-damage behaviour could be determined in stable δ-phase alloys and in a metastable δ-alloy that would transform to a 50/50 mixture of δ and α when cooled to low temperature. The results are compared with those of α-phase plutonium, and the self-damage behaviour of the metastable δ-alloy is examined from the viewpoint of possible phase-transformation effects.

Resistivity increases were measured as a function of time in plutonium-rich alloys at ~4.5, 13.5, ~20 and ~77°K. The experimental data at 4.5 and 20°K are shown in Fig. 2 and a summary of all the results is given in Table I. The specific resistivity increased linearly with respect to time at each temperature except at 20.1 and 64.9°K for the alloy containing 1.2 at.% aluminium. The build-up of self-damage in this alloy obeys the parabolic law that is given at the bottom of Table I. (The holding time at ~4.5°K was insufficient for determining whether or not the build-up at this temperature also obeys a similar parabolic law.) Resistivity-versus-temperature curves for a stable δ-alloy containing 3.4 at.% aluminium in the "undamaged" and "damaged" states are shown in Fig. 3 and the same data are shown replotted as ρ/T versus T in Fig. 4c and as $\Delta\rho_T$ versus T in Fig. 5b.

Self-damage effects are qualitatively similar in delta and alpha phases although the rates of increase are appreciably less in delta phase than in

TABLE III

SUMMARY OF DATA USED IN CALCULATING THE CONSTANT, A, IN THE EXPRESSION: $\dot{\rho} = A(\rho_{Max} - \rho_{0°K})\, x_{Pu}\, d$

Specimen description		Density at 24°C d (g/cm^3)	$(\rho_{Max} - \rho_{0°K})$* ($\mu\Omega cm$)	$\dot{\rho}_{4.5°K}$ ($\mu\Omega cm/h$)	x_{Pu}	A $cm^3/g\,h$ (10^5)
α-phase Pu	Specimen No.1	19.535	134.1	0.0616	1.000	2.35
	Specimen No.2	19.475	150.1	0.0637	1.000	2.18
	Specimen No.3	19.50	139.3	0.0671	1.000	2.47
Pu-rich δ-phase	3.4 at.% Al	15.57	36.4	0.0124	0.966	2.26
	8.0 at.% Ce	15.19	56.5	0.0166	0.920	2.13

* Data for α-phase were taken from [5], and data for δ-phase were taken from [10].

alpha phase at 4.5 and 20°K. It was found empirically that the data for both delta and alpha phases can be fitted to the following expression:

$$\dot{\rho} = A(\rho_{Max} - \rho_{0°K})\, x_{Pu}\, d, \qquad (3)$$

where $\dot{\rho}$ is $d\rho/dt$ in $\mu\Omega$ cm/h at constant temperature, A is a constant that depends on the isotopic content of plutonium, $(\rho_{Max} - \rho_{0°K})$ is the resistivity maximum corrected for the residual term and is in $\mu\Omega$ cm, x_{Pu} is atomic fraction of plutonium and d is the density in g/cm^3. The results of this calculation, given in Table III, indicate that (to within ± 10%) the electrical behaviour of plutonium due to self-irradiation damage depends on the plutonium content, the specimen density and the difference between the resistivity maximum and the residual resistivity. Small differences in the values of A given in Table III may be due partly to variations in the isotopic compositions of plutonium in the specimens. Eq. (3) best fits the data at ~4.5°K.

The complete curve of $\Delta\rho$ as a function of temperature is shown in Fig. 5b for the stable δ-alloy containing 3.4 at.% aluminium. $\Delta\rho$ decreases slightly with increasing temperature between 10 and 21°K, in agreement with the data on rates of build-up of damage in this alloy at ~4.5 and 20.1°K (see Table I). At 21°K, however, there is an abrupt increase in $\Delta\rho$, and with increasing temperature the $\Delta\rho$ curve shows a slight dip at 24°K and a rapid decrease near 50°K. The abrupt increase or step at 21°K is also evident in the ρ-versus-T "damaged" curve for this alloy, shown in Fig. 3. This δ-alloy composition is near the $\alpha + \delta/\delta$ solvus phase boundary at low temperature [10], and the data appear to be consistent with the possibility of a radiation-induced phase transformation from δ-phase to a $\delta + \alpha$-phase

mixture during holding at temperatures below 21°K. According to this interpretation the step at 21°K on warming, after holding at 20.1°K for 3.4 weeks, would be due to the $\delta + \alpha$-phase mixture retransforming to δ-phase. Heat-capacity measurements on a δ-alloy of the same composition offer confirmatory evidence for this interpretation and these results are discussed later in this paper. The rapid decrease in $\Delta\rho$ near 50°K is similar to that observed in α-plutonium. No annealing measurements of the type where the specimen is warmed to various annealing temperatures and then quenched to 20°K have been made on δ-alloys, but this rapid decrease in $\Delta\rho$ at 50°K is being investigated at present. It is possible that this behaviour may also involve a low-temperature transformation similar to that proposed for α-phase plutonium. The ρ/T-versus-T curves for δ-phase (see Fig. 4c), however, fail to reveal evidence of an anomaly near 50°K, such as occurs in α-plutonium (see Figs. 4a and 4b) and this behaviour is most likely to be due to annealing.

The rates of increase of resistivity with time at 20.1 and at 64.9°K due to self-damage in the metastable δ-alloy specimen containing 1.2 at.% aluminium are noteworthy because these rates of increase follow a parabolic instead of a linear law. This specimen was initially 100% δ-phase, and it transformed irreversibly, starting at 256°K on cooling, to a phase mixture consisting of about 50% α and 50% δ [10]. The initial rate of increase in this specimen at 20.1°K was appreciably higher than it was after the specimen had been held at 20.1°K for 3.4 weeks. The latter rate is nearly the same as was the linear rate of increase in the stable δ-alloy containing 3.4 at.% aluminium (see Fig. 2a). This change in the rate of increase in the 1.2 at.% aluminium alloy with time at 20.1°K suggests a change in phase compositions toward a higher content of δ-phase, i.e. a radiation-induced phase change from stable alpha to metastable delta, which is retained because of the low temperature. This explanation is contradictory to experimental fact, however, since the ρ-versus-T curve of this 1.2 at.% aluminium-alloy specimen (after storage of self-damage by holding at 20.1°K) closely resembles the "damaged" curve of the δ-alloy shown in Fig. 3, except in the region between 40 and 60°K where the curve is smoother and shows no evidence of any flattening in the resistivity. The parabolic build-up of self-damage in plutonium-rich alloys needs further investigation; it is obviously more complicated than described here.

3. HEAT CAPACITY MEASUREMENTS

3.1. Specimen preparation

The α-phase plutonium specimen was prepared from exceptionally high-purity, electro-refined plutonium and complete descriptions of the chemical analysis, experimental apparatus and procedure, thermodynamic properties and self damage effects are given elsewhere [18]. Only a brief summary of these results is included in the present paper; details can be obtained by referring to the earlier paper.

The plutonium-rich δ-alloy containing 3.4 at % aluminium was arc-melted and then cast in vacuo into an MgO crucible in an induction furnace to form

a cylindrical ingot. The ingot was wrapped in tantalum foil and sealed within a Pyrex capsule containing 0.5 atm of argon gas, homogenized for more than 200 h at 450 ± 10°C and air-cooled to room temperature. The specimen density after heat treatment was 15.59 g/cm^3. The specimen was then machined to the final dimensions of 0.85 ± 0.04-cm diam. and 4.69 ± 0.04-cm long. The rate of heat generation due to the radioactivity in this specimen was 2.161 ± 0.004 mW/g. This δ-alloy specimen was prepared from the same metallic plutonium stock that was used to prepare α-plutonium specimen #2.

3.2. Apparatus and procedure

The heat capacity measurements were obtained by utilizing the self-heating property of plutonium. The apparatus and procedure are described elsewhere [12], and that publication should be consulted for details.

The α-phase plutonium and δ-alloy specimens were canned in the same manner. Each specimen was sealed within a fully-annealed copper capsule containing 1 atm of helium gas. The capsule sealing was accomplished by first crimping the open end in an arbor press and then Heliarc-welding the crimped end. The copper walls of each capsule were gently squeezed against the specimens to improve the thermal contact. Lack of reproducibility below 25°K in the first set of measurements on the δ-alloy specimen indicated that this specimen contracted away from the capsule. Reasons for this behaviour are discussed below. This specimen was re-canned and no further difficulties were experienced. The weights of the copper capsule and the δ-alloy specimen after being re-canned were 30.705, and 60.107 g, respectively. The atomic weight of plutonium was taken to be 239.11 (chemical scale) and the gram-calorie was taken to be equivalent to 4.184 J (abs.).

The specimens were held at the temperatures of boiling liquid nitrogen, hydrogen or helium for varying lengths of time in order to store energy due to self-damage. The δ-alloy specimen was not held at the boiling point of liquid nitrogen, however, since it was known that the rate of energy storage at this temperature would be low. It was held at ~3.96°K for 2 and 8 h in order to examine short-term effects under conditions of maximum damage retention. Measurements in the "undamaged" state were made after cooling the δ-alloy specimen slowly from 300 to 209°K overnight and from 209 to ~3.96°K in 110 min. The specimen was held at ~3.96°K for 45 min before starting the "undamaged" run. Measurements in the "self-damaged" states were obtained by holding the specimens at ~19.6°K for 24 h and for either 163 or 184 h.

3.3. Heat capacity results and discussion

The low-temperature heat-capacity behaviour of the δ-alloy specimen in the "undamaged" and various "self-damaged" states is shown in Fig. 7, and a comparison of the "self-damaged" heat-capacity behaviours of the α-phase and δ-phase specimens is shown in Fig. 8. The low-temperature heat-capacity, electrical-resistivity and thermal-expansion behaviours of an undamaged, stable δ-alloy containing 8 at.% aluminium were given in an earlier paper by SANDENAW [8].

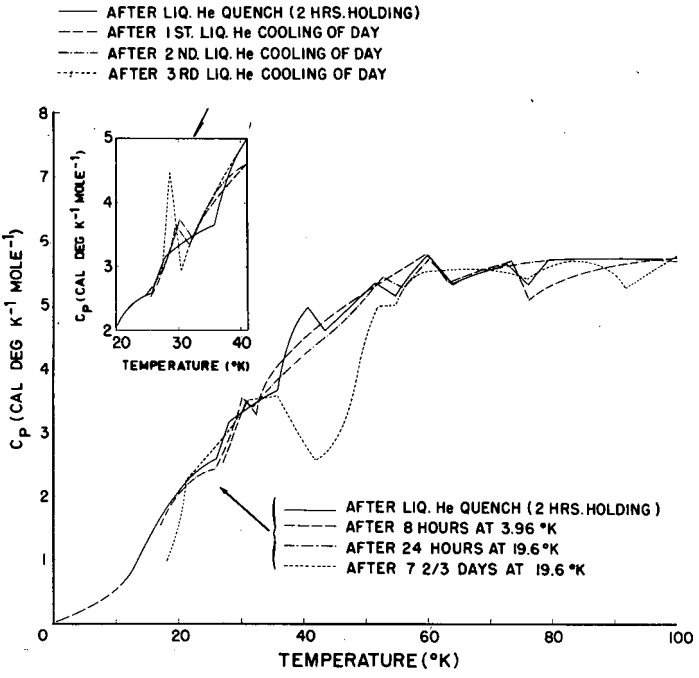


Fig. 6

Heat capacity as a function of absolute temperature for a 96.6 at.% plutonium - 3.4 at.% aluminium, δ-phase alloy between ~ 3.96 and 100°K after holding for various times at either ~ 3.96 or ~ 19.6°K (The insert shows data between 20 and 40°K after quenching from 300 to ~ 3.96°K, and then after repeated coolings (on the same day) to ~ 3.96°K with liquid helium)

A large number of anomalies were observed during the early stages of heat-capacity work on plutonium, and their origins were not readily explained. Observations on standard substances indicated that the anomalies in question were not due to the apparatus. The situation was further complicated by the lack of reproducibility of data from the plutonium specimens. These difficulties are still present in the heat-capacity work but they are becoming easier to understand and explain as data on self-irradiation and phase transitions in plutonium and its δ-alloys at low temperature become available. In the present work, for example, out of six heat-capacity runs made on the δ-alloy specimen, the peak between 29 and 31°K was observed five times, the peak between 40 and 43°K was observed three times, the peak between 51.5 and 53°K was observed four times, the peak at 60°K was observed six times and the peak between 67 and 74°K was observed four times. Also, the first low-temperature heat-capacity runs after the specimens had been at room temperature usually either failed to show any peaks or the peaks were small. These peaks became more pronounced, however, when the specimens were held at low temperatures or when repeated low-temperature runs were made during which the specimen temperatures did not exceed ~100°K. The rates of energy storage due to self-damage in

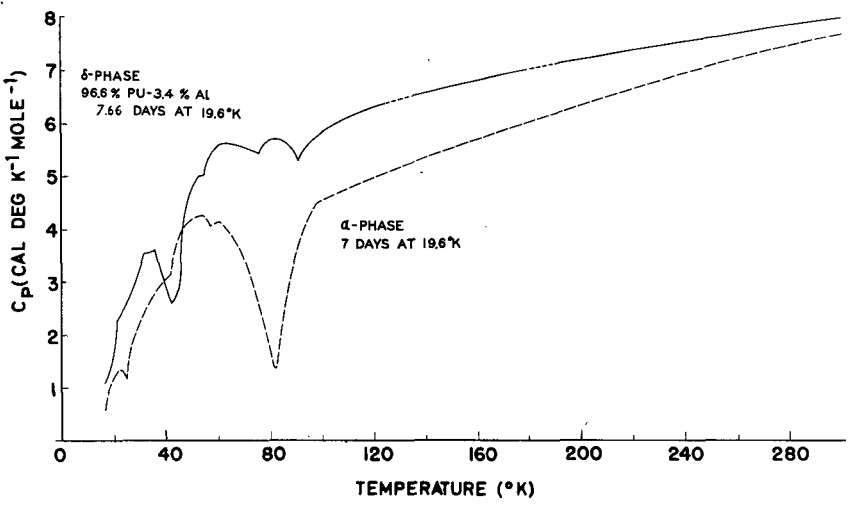


Fig. 7

Heat capacity as a function of absolute temperature for high-purity electro-refined α-plutonium and for a 96.6 at.% plutonium - 3.4 at.% aluminium δ-phase alloy (Data were taken after holding for about 1 week at ~ 19.6°K)

plutonium indicate that detectable heat-capacity effects should be evident after specimens are held for only a few hours at low temperature.

Comparison between the low-temperature heat-capacity behaviour of α-phase plutonium and δ-phase alloys containing 3.4 and 8 at.% aluminium [8] shows that above 30°K there is in general a parallel in their behaviours if one ignores the presence of peaks. The number of peaks, and the temperatures at which they occur, vary depending on differences in crystal structure and alloy composition, as might be expected. Below 30°K, the δ-alloy specimen containing 3.4 at.% aluminium shows a sigmoidal variation of heat capacity with temperature, a behaviour that is characteristic of a phase change (see Fig. 6).

Heat capacity curves of the δ-alloy specimen containing 3.4 at % aluminium are shown in Fig. 6 for various holding times at ~3.96° and ~19.6°K. A summary of these results is given in Table IV, and a summary showing a comparison between the "self-damaged" α-phase and δ-alloy specimens is given in Table V. The values for stored energy due to self-damage were obtained by taking the summed enthalpy difference between the "damaged" and "undamaged" conditions to 100°K. The results reveal a storage of 62 cal/mole after 163 h at ~19.6°K for α-plutonium [18] and 40 cal/mole after 184 h at ~19.6°K for the δ-alloy containing 3.4 at.% aluminium, or 0.38_0cal/mole- and 0.21_7 cal/mole-h for α- and δ-phases, respectively. The heat-capacity curve for α-plutonium, see Fig. 7, shows that thermal recovery occurs mostly between 46 and 100°K, which is in good agreement with the electrical resistivity results. Thermal recovery in the δ-alloy containing 3.4 at.% aluminium starts near 32°K and most of the stored energy

TABLE IV

HEAT CAPACITY, C_p, AND ENTHALPY, $H_T - H_0$, OF A PLUTONIUM-RICH δ-ALLOY SPECIMEN CONTAINING 3.4 at.% ALUMINIUM, FOR THE "UNDAMAGED" AND "SELF-DAMAGED" STATES

Temperature (°K)	C_p (cal mole^{-1} deg^{-1})			$H_T - H_0$ (cal/mole)		
	Undamaged	Self-Damaged*		Undamaged	Self-Damaged*	
		(24 h)	(184 h)		(24 h)	(184 h)
25	2.54	2.42	2.68	28	30	23
50	5.22	5.12	4.52	124	124	100
75	5.42	5.80	5.46	267	262	236
100	5.70	5.82	5.78	419	410	379
150	6.60	6.76	6.70	736	732	693
200	6.90	7.25	7.20	1066	1070	1030
273.15	7.70	-	7.75	1660	-	1570
298.15	7.90	-	7.97	1795	-	1768

* After storage of self-irradiation damage by holding at ~19.6°K for the specified times.

is released by the time 50°K is reached, although the slight dips in the heat-capacity curve between 63 and 100°K may indicate further annealing (see Fig. 7).

4. CORRELATION OF ELECTRICAL RESISTIVITY AND HEAT CAPACITY RESULTS

Self-irradiation damage work on plutonium provides confirmation of the heat-capacity anomalies observed in both α-phase and δ-phase plutonium. In α-phase, for example, the small dip in Δρ above 20°K corresponds with a heat-capacity peak in the same temperature region. Similarly, steps in the Δρ curves near 40, 50 and 65°K also correspond with heat-capacity peaks near these temperatures. Correlation between resistivity and heat-capacity results for the δ-alloy containing 3.4 at.% aluminium is similar, and it is very likely that the heat-capacity anomalies observed in the δ-alloy containing 8 at.% aluminium [8] also have their origins in self-damage at low temperatures. Heat-capacity measurements are either more sensitive than the resistivity measurements or sensitive in a different way to the effects of radiation damage in plutonium. The rates of energy storage due to self-damage below the annealing temperatures are ~0.38 cal/mole-h and ~0.22 cal/mole-h for α- and δ-phases, respectively. These rates indicate that

TABLE V

COMPARISON OF HEAT CAPACITY, C_p, AND ENTHALPY, $H_T - H_0$, OF α-PHASE PLUTONIUM AND A δ-ALLOY CONTAINING 3.4 at. % ALUMINIUM "SELF-DAMAGED" STATES

Temperature (°K)	C_p (cal mole^{-1} deg K^{-1})		$H_T - H_0$ (cal/mole)*	
	α-phase (163 h)	δ-phase (184 h)	α-phase (163 h)	δ-phase (184 h)
25	1.20	2.68	12.7	23.0
50	4.24	4.52	87	100
75	2.68	5.46	183	236
100	4.52	5.78	258	379
150	5.54	6.70	513	693
200	6.35	7.20	816	1030
273.15	7.40	7.75	1327	1570
298.15	7.70	7.97	1519	1768

* After storage of self-irradiation damage by holding at ~19.6°K for the specified times.

heat-capacity effects should be observable after relatively short holding times below 100°K, and especially after short holding times below 46 or 32°K for α- or δ-phase, respectively.

The rate of increase in resistivity with time due to self-damage effects was found empirically to obey Eq. (3) for both α-phase and δ-phase plutonium. This relationship appears also to apply qualitatively (but not quantitatively) to the storage of energy as determined from the heat capacity measurements. Eq. (3) suggests that the storage of energy due to self-damage should be directly proportional to the specimen density and atomic fraction of plutonium, and this relationship predicts a rate of energy storage of 0.295 cal/mole/h for the δ-alloy containing 3.4 at.% aluminium. The experimentally observed rate is appreciably less than this calculated rate. ELLIOTT and GSCHNEIDNER [19] have shown that this δ-alloy transforms irreversibly under hydrostatic compression at room temperature. The transformation occurs at 7020 atm and is due to a change from δ-phase to a $\delta + \alpha$-phase mixture. The low-temperature electrical resistivity and heat capacity of this δ-alloy also suggest such a phase change, and a radiation-induced or radiation-accelerated phase transformation was postulated above in section 2.3. Absence of evidence for a thermal arrest at 21°K in the heat-capacity data and differences in the measured and calculated rates of

energy storage in this alloy could be the result of homogeneously stored radiation damage providing the energy for the phase transformation. This interpretation implies that consideration must be given to the effects that stored energy and self-irradiation might have on any processes involving energy changes in plutonium and its alloys. It is quite possible that the actual energy from self-irradiation in plutonium is greater than the measured value obtained from heat-capacity data.

5. RADIATION DAMAGE CALCULATIONS

(The calculations presented in this section are by G. H. Vineyard, who made them at Los Alamos during the summer of 1961, and they are included in this paper with his permission.)

5.1. Particle ranges

Pu^{239} and Pu^{240} decay by the schemes given in the introduction. The α-particle travels a few microns in the material and then comes to rest, presumably as an interstitial helium atom. The range of the α-particle has not been determined in metallic plutonium or its δ-alloys, but estimates can be readily made by using either WILSON's chart [20] or the BRAGG-KLEEMAN rule [21]. Wilson's chart shows the range of a 5-MeV α-particle in material of $Z = 94$ to be 10^{-2} g/cm^2. This range corresponds to 5×10^{-4} cm in α-phase plutonium and to 6.3×10^{-4} cm in δ-phase plutonium. The Bragg-Kleeman rule gives 6.2×10^{-4} cm for α-phase and 7.7×10^{-4} cm for δ-phase plutonium. There is approximate agreement between the two methods, although the chart values are probably better than the Bragg-Kleeman values; consequently the chart values are used here. The range of the recoiling uranium nucleus can also be estimated from the data of Van LINT et al. [22] and from the observations of HOLMES and LEIBFRIED [23] and is estimated to be approximately 60 Å in plutonium.

5.2. Number of displacements

The threshold energy for permanent displacement E_d has not been measured for α-plutonium. This threshold occurs at 25 eV in many metals, however, and this value was used in the calculations. The recoiling uranium nucleus is created at an energy well below the ionization threshold energy and the number of Frenkel pairs produced by the recoil will be $\nu \simeq E/2E_d$, assuming simple cascade theory [24]. The number of Frenkel pairs per uranium recoil is thus estimated to be 1740. This rule has been found to give results that are too high by factors of 2 to 10 for common metals. Allowing for uncertainties in E_d, the number of displacements produced by the recoiling uranium nucleus could range from as low as 80 to as high as 3500. A best guess at present would be about 1000. The computation of the number of displacements produced by the primary α-particle is complicated, but following the methods outlined by DIENES and VINEYARD [25], it leads to a prediction of approximately 800 displacements by each α-particle. Thus the total number of displacements per disintegration is predicted to be about 1800.

WALKER [26] has proposed a rough rule of thumb that says that a 1% concentration of Frenkel pairs in a substance should cause an increase of residual resistivity that is about equal to the difference between the substance's room-temperature resistivity and its residual resistivity at absolute zero. This resistivity difference is about 120 $\mu\Omega$ cm for α-phase plutonium, and its average linear rate of increase due to self-damage at 20.1°K is 0.065 $\mu\Omega$ cm/h. By using these data and Walker's rule of thumb, one calculates 1670 Frenkel pairs per disintegration, which is in good agreement with the previous estimates. Assuming energy storage at 5 eV per Frenkel pair, one calculates a storage of approximately 107 cal/mole per week in α-phase plutonium at 20°K. The experimental value of 62 cal/mole per week is in good agreement with this estimate, if allowances are made for uncertainties.

ACKNOWLEDGEMENTS

The authors wish to thank V. O. Struebing for preparing the specimens; R. R. Gilmore for machining and canning the specimens; Bertha G. Fagan and Josephine E. Powers for making the IBM 704 resistivity and least-squares calculations, respectively; and W. N. Miner for editing the final manuscript. We also wish to express our gratitude to Dr. R. B. Gibney for his valuable criticism of the final manuscript and to Dr. George H. Vineyard, of Brookhaven National Laboratory and Los Alamos Scientific Laboratory Consultant, for making the radiation damage calculations.

REFERENCES

[1] General references for reviews on radiation damage work are given below. This list is obviously not complete and does not include references to reviews on specialized topics.
(a) SEITZ, F. and KOEHLER, J.S., Solid State Physics,(SEITZ, F. and TURNBULL, D.,Eds.) Academic Press Inc., New York 2 (1956) 305-448.
(b) DIENES, G.J. and VINEYARD, G.H., Radiation Effects in Solids, Interscience Publ. Inc., New York (1957).
(c) The Effects of Radiation in Materials, (HARWOOD, J.J., HAUSNER, H.H., MORSE, J.G. and RAUCH, W.G., Eds.) Reinhold Publ. Corp., New York (1958).
(d) Progress in Nuclear Energy (FINNISTON, H.M. and HOWE, J.P., Eds.) Pergamon Press, London, Series V, 1 (1956) 553-720.
(e) Ibid., Series V 2 (1959) 475-569.
(f) Ibid., Series V 3 (1961) 161-398.
(g) BILLINGTON, D.S. and CRAWFORD, J.H., Jr., Radiation Damage in Solids, Princeton Univ. Press (1961).
[2] COOPER, H.G., KOEHLER, J.S. and MARX, J.W., Phys. Rev. 94 (1954) 496.
[3] SEABORG, G.T. and KATZ, J.J., The Actinide Elements, McGraw-Hill, New York (1954) 194-200.
[4] DEMPSEY, E. and KAY, A.E., J. Inst. Metals 86 (1958) 379.
[5] OLSEN, C.E. and ELLIOTT, R.O., J. Phys. Chem. Solids, in press.
[6] ZACHARIASEN, W.H., The Metal Plutonium, Univ. Chicago Press, Chicago (1961) 99-107.
[7] MINER, W.N. et al., Rare Metals Handbook, (HAMPEL, C.A., Ed.) Reinhold Publ. Corp., New York 2nd ed (1961) 336-392.
[8] SANDENAW, T.A., J. Phys. Chem. Solids 16 (1960) 329.
[9] LEE, J.A., MEADEN, G.T. and MENDELSSOHN, K., Cryogenics 1 (1960) 52.
[10] ELLIOTT, R.O., OLSEN, C.E. and LOUIE, J., J. Phys. Chem. Solids, in press.
[11] OLSEN, C.E., USAEC Rpt. LA-2406 (1960).

[12] SANDENAW, T.A., OLSEN, C.E. and GIBNEY, R.B., Plutonium 1960, (GRISON, E., LORD, W.B.H. and FOWLER, R.D., Eds.) Cleaver-Hume Press Ltd., London (1961) 66-79.
[13] BLAKE, C., CHASE, C.E. and MAXWELL, E., Rev. Sci. Instr. 29 (1958) 715.
[14] CLEMENT, J.R. and QUINNEL, E.H., Rev. Sci. Instr. 23 (1952) 213.
[15] SANDENAW, T.A., Plutonium 1960, (GRISON, E., LORD, W.B.H. and FOWLER, R.D., Eds.) Cleaver-Hume Press Ltd., London (1961) 79-90.
[16] FISHER, E.S. and McSKIMIN, H.J., Phys. Rev. 124 (1961) 67.
[17] COOPER, H.G., KOEHLER, J.S. and MARX, J.W., Phys. Rev. 97 (1955) 599.
[18] SANDENAW, T.A., J. Phys. Chem. Solids, in press.
[19] ELLIOTT, R.O. and GSCHNEIDNER, K.A., Jr., Extractive and Physical Metallurgy of Plutonium and Its Alloys, (WILKINSON, W.D., Ed.) Interscience Publ. Inc., New York (1960) 243-262.
[20] BETHE, H.A. and ASHKIN, J., Experimental Nuclear Physics, (SEGRÉ, E., Ed.) John Wiley and Sons, Inc., New York 1 (1953) 222.
[21] EVANS, R.D., The Atomic Nucleus, McGraw-Hill Book Co., New York (1955) 652.
[22] Van LINT, V.A.J., SCHMITT, R.A. and SUFFREDINI, C.S., Phys. Rev. 121 (1961) 1457.
[23] HOLMES, D.K. and LEIBFRIED, G., J. Appl. Phys. 31 (1960) 1046.
[24] DIENES, G.J. and VINEYARD, G.H., Radiation Effects in Solids, Interscience Publ. Inc., New York (1957) Chap. II.
[25] Ibid., Chap. I.
[26] WALKER, R.M., private communication to G.H. Vineyard.

THE CRACKING OF IRRADIATED URANIUM

R.G. BELLAMY
ATOMIC ENERGY RESEARCH ESTABLISHMENT, HARWELL,
BERKS., ENGLAND

Abstract — Résumé — Аннотация — Resumen

THE CRACKING OF IRRADIATED URANIUM. Structural features other than fission-product gas bubbles seen in unrestrained, unalloyed uranium irradiated in the alpha range to burn-ups of up to 0.7% of all atoms are described. The main features are:

(1) Brittle grain-boundary cracks in which the grains appear to have parted without plastic deformation. These cracks are associated with thermal cycling and high maximum temperatures (~600° C).

(2) Transgranular cracks, which are comparatively rare. It is suggested that they may be related to the pseudo-cleavage or "twin parting" observed in unirradiated uranium by Cahn.

(3) Grain boundary "creep voids" believed to arise from the coalescence of vacancies under tensile stress. The voids may form a path for crack propagation or may themselves coalesce to form cracks.

Apart from the direct effects of these features in increasing the volume and changing the thermal conductivity and mechanical properties of the uranium, a mechanism is discussed by which cracks may accumulate fission-product gas and cause further volume increases. The possible effects of structural variations in the uranium and of restraint during irradiation on the incidence of cracking and void formation are considered.

FISSURATION DE L'URANIUM IRRADIÉ. L'auteur décrit les modifications structurelles (autres que celles qui sont dues aux bulles gazeuses résultant de la fission) qui apparaissent dans de l'uranium non allié, non soumis à des contraintes, irradié dans la gamme des températures de la phase alpha de l'uranium, les taux de combustion atteignant 0,7% pour tous les atomes. On observe les principales modifications suivantes :

1. Des fissures aux joints de grain fragiles, dans lesquels les grains semblent s'être disjoints sans déformation plastique. Ces fissures se forment généralement dans de l'uranium soumis au cyclage thermique, ou porté à des températures élevées (environ 600° C).

2. Des fissures transgranulaires qui sont relativement rares et se rattachent peut-être au pseudo-clivage avec «désagrégation des macles» observé par Cahn dans l'uranium non irradié.

3. Des «vides de fluage» aux joints de grain que l'on pense provenir de l'agrégation des lacunes sous l'effet des contraintes de traction. Ces vides peuvent former une voie de propagation pour les fissures ou bien fusionner pour former des fissures.

A part les effets directs de ces modificztions (augmentation du volume et modification de la conductibilité thermique et des propriétés mécaniques de l'uranium) l'auteur étudie un mécanisme par lequel de gaz produit par la fission peut s'accumuler dans les fissures et provoquer une nouvelle augmentation de volume. Il étudie aussi les effets possibles des modifications structurelles de l'uranium et les ettets de contraintes pendant l'irradiation, sur la formation des fissures et des vides.

ОБРАЗОВАНИЕ ТРЕЩИН В ОБЛУЧЕННОМ УРАНЕ. Описаны структурные изменения, кроме связанных с образованием газовых пузырьков, наблюдаемые в неограниченном нелегированном уране, облученном в альфа-фазе при выгорании до 0,7% всех атомов. Главными чертами является следующее:

1. Трещины на границе хрупких зерен появляются, по-видимому, без пластической деформации. Появление этих трещин связано, как полагают, с тепловым циклом и высокими максимальными температурами (~600°C).

2. Трансгранулярные трещины, наблюдаемые сравнительно редко. Предполагается, что они могут быть связаны с псевдотрещинами или "близнецовым разделением", наблюдавшимся в необлученном уране Каном.

3. "Пустоты смещения" на границах зерен, которые, как полагают, возникают в связи со сращиванием вакансий, происходящих под воздействием сил разрыва. Пустоты образуют, возможно, путь для распространения трещин или же сами сращиваются, образуя трещины.

Кроме непосредственного влияния этих причин на увеличение объема и изменение теплопроводимости и механических свойств урана, рассматривается еще механизм возможного скопления в трещинах

газовых продуктов деления, что приведет к дальнейшему увеличению объема. Рассматривается возможное влияние структурных изменений в уране и его сжатия в течение облучения на частоту образования трещин и пустот.

AGRIETAMIENTO DEL URANIO IRRADIADO. El autor describe las características estructurales distintas de las burbujas de productos de fisión gaseosos, que se observan en probetas de uranio puro, no sujetas a restricciones, irradiadas en el intervalo alfa hasta alcanzar un grado de combustión de 0,7 por ciento del total de los átomos. Las principales características son las siguientes:

1) Grietas por fragilidad en los bordes de granos, en las cuales éstos parecen separarse sin sufrir una deformación plástica previa. Estas grietas se relacionan con el ciclado térmico y con temperaturas máximas elevadas (aproximadamente 600° C).

2) Grietas transgranulares, relativamente poco frecuentes. El autor sugiere que pueden provenir del pseudoclivaje, o "separación de maclas", observado por Cahn en el uranio sin irradiar.

3) "Huecos de fluencia" en los bordes de granos, que se suponen originados por la coalescencia de vacantes por efecto de un esfuerzo de tracción. Dichas vacantes pueden abrir un camino por el que se propaga la grieta o bien pueden unirse para formar grietas ellos mismos.

Aparte de la influencia directa que pueden ejercer estos fenómenos en el aumento de volumen y en la modificación de la conductividad térmica y de las propiedades mecánicas del uranio, el autor estudia un mecanismo que podría dar lugar a la acumulación de productos de fisión gaseosos en las grietas, provocando así nuevos aumentos de volumen. Examina luego los posibles efectos de las variaciones estructurales del uranio y de la imposición de restricciones durante la irradiación sobre la frecuencia de la aparición de grietas y de la formación de huecos.

1. INTRODUCTION

Metallurgical phenomena which have so far proved to be of the greatest technological importance in the irradiation of uranium metal in the alpha range, and have consequently received most attention, are the growth and swelling phenomena. Experiments have indicated that growth ceases above about 500° C whereas it was originally postulated that the severity of swelling would increase with temperature in the high alpha range. Experimental evidence suggests, however, that the swelling of adjusted alpha-uranium is not very temperature-dependent, although there is some evidence for a sharp maximum in the region of 450° C [1]. Incidental to the metallographic examination of the fission-gas bubbles additional features have been observed which contribute to swelling, in particular cracking and grain-boundary void-formation, and which are the subject of the present paper.

PUGH has reported that about one in three of early AERE uranium specimens irradiated to 0.4% burn-up in the range 450-600° C showed patches of alpha grain-boundary cracking, and he ascribed this cracking to a combination of irradiation embrittlement and internal stressing caused by thermal cycling [1]. A smaller number of these specimens, mainly those without cracks, showed grain-boundary voids, although it was believed possible that these could be an etching effect. The sporadic appearance of these phenomena suggested that minor variations in composition were important.

If swelling due to fission-gas bubbles can be successfully controlled, swelling due to cracking and grain-boundary void-formation will increase in relative importance. At AERE evidence has accumulated that at 550-625° C swelling due to fission-gas bubbles is restricted in beta-quenched uranium containing additions of iron and aluminium, and that cracking and grain-boundary voids then play a substantial part in the total volume increase [2].

2. EXPERIMENTAL WORK

2.1. Techniques

The majority of the samples were enriched, magnesium-reduced uranium, "adjusted" with a grain-refining addition of 200-500 ppm iron and 500-1200 ppm aluminium [3], vacuum-cast and beta-quenched from 730° C. Cylinders 0.2-0.4-in diam. and 0.3-1.6-in long were machined and irradiated without restraint in liquid sodium [4] to burn-ups of up to 0.8% of all atoms. A detailed description of the methods of remote preparation and examination has been given elsewhere [5]; briefly, three types of metallographic examination were used:

(1) mechanical polishing with fine paste, and optical examination of cracks, voids and inclusions;
(2) attack polishing with a chromic acid/nitric acid mixture and examination under polarized light; and
(3) cathodic vacuum-etching, usually followed by replication and electron-microscope examination of the carbon replica.

The chemical reactivity of uranium appears to increase on irradiation and it is rapidly attacked by the usual chemical etching reagents. There is a suspicion that artefacts may be produced in this way, and at AERE cathodic vacuum-etching is regarded as advisable for examination at magnifications above 500 times, and essential for electron-microscope examination by the carbon-replica technique. HYAM [6] has suggested that even cathodic vacuum-etching may cause significant enlargement and rounding of very small voids (<1000 Å) in uranium. While fractography is less likely to give artefacts it does not produce a random section. A compromise solution is to study large voids and cracks and the numerical distribution of small voids and other microstructural features by sectioning and cathodic vacuum-etching, while the dimensions and shape of individual small features are examined by fractography.

2.2. Observations

The structural features seen in irradiated uranium in addition to fission-gas bubbles were mainly grain-boundary creep voids of various sizes in uranium irradiated below 450° C, and cracks observed only in specimens irradiated at or above 450° C. The cracks could be classified into three types, as follows:

Type I. Brittle grain-boundary cracks, with sharp edges and tips, in which the individual alpha grains appear to have parted without much plastic deformation of the grains (Fig. 1). This type of cracking was most marked in specimens in which the maximum irradiation temperature was above 550° C.

Type II. Strings of grain-boundary voids which in some cases had coalesced to form cracks (Fig. 2). These cracks are relatively smooth and blunt-ended, and the edges do not "match" as well as those of Type I brittle cracks. The sub-grain boundaries also frequently showed complete networks of smaller voids, but cracking along these networks was very rare.

Type III. Brittle transgranular cracks (Fig. 3). These cracks are very much rarer than Types I and II; they are usually straight, thin (0.5-5 μm),

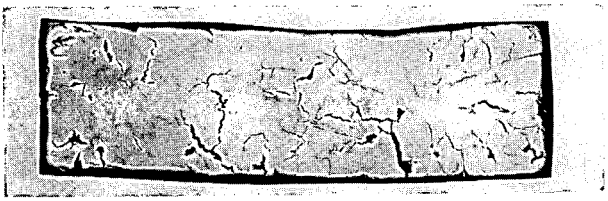


Fig. 1

Uranium irradiated to 0.7% burn-up at 550°C, showing extensive brittle grain-boundary cracks (Type I)

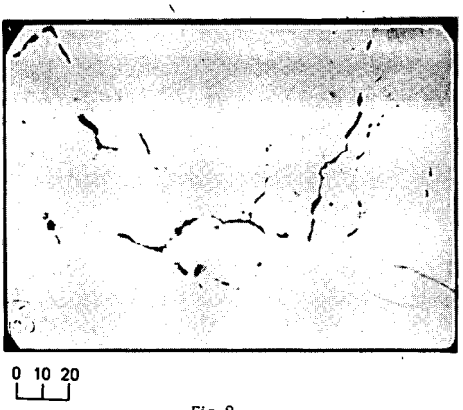


Fig. 2

Uranium irradiated to 0.5% burn-up at 575°C showing grain-boundary voids coalescing to form cracks (Type II)
Sub-grain boundary voids are also visible



Fig. 3

Brittle transgranular crack (Type III) in irradiated uranium

sharp at the tip, and frequently lie in a staggered, parallel series with a step or a short curved tip between successive cracks. The great majority begin or end at a grain boundary. Type III cracks are often parallel to twins, and in some instances appear to have occurred by parting along twin boundary (Fig. 4).



Fig. 4

Irradiated uranium tensile test piece showing transgranular crack (Type III) at twin boundary

In any cracked specimen a representative of each type of crack could usually be found (Fig. 5), and the two types of intergranular crack were not

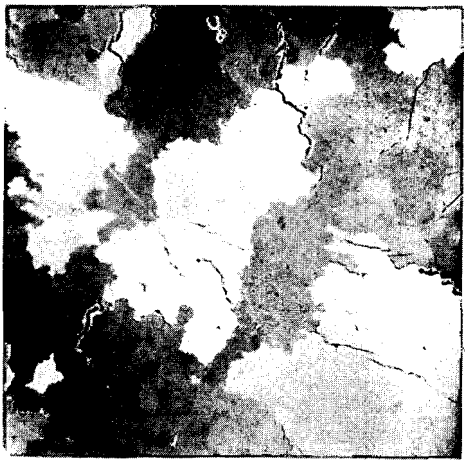


Fig. 5

Uranium irradiated to 0.5% burn-up at 575°C showing all types of crack

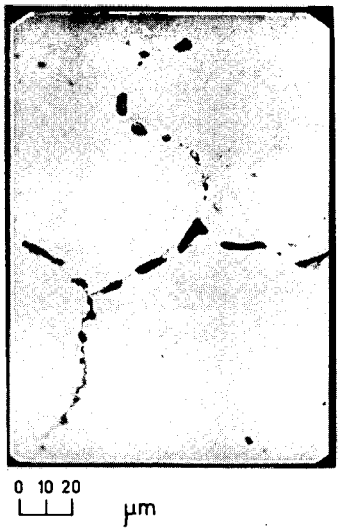


Fig. 6

Grain boundary voids (Type II) which have been traversed by a brittle crack (Type I)

always separate and distinct. Fig. 6, for example shows a row of Type-II grain-boundary voids which have been traversed by a Type-I brittle crack before coalescence has occurred. The distinction could be even less sharp, with a brittle Type-I crack becoming ragged and eventually breaking up into a string of voids. Type-I brittle grain-boundary cracks sometimes predominated, e. g. Fig. 1, a specimen taken to 0.7% burn-up at 550-580° C; their extent was not always a function of burn-up, however, and extensive brittle grain-boundary cracking was found in a specimen taken to only 0.05% burn-up which had undergone severe thermal cycling; no Type-II void cracking was observed in this specimen. Predominant Type-II cracking was not found, but was sometimes as extensive as Type-I cracking in the same specimen. Type-I brittle grain-boundary cracks occasionally tended to increase at the surface of a specimen, but cracking was otherwise relatively uniform. It was observed to some extent in each of ten specimens of adjusted, beta-quenched uranium irradiated at 575° C to burn-ups ranging from 0.21 to 0.7%.

3. DISCUSSION

3. 1. The origins of irradiation cracking

3. 1. 1. Brittle alpha grain-boundary cracking was ascribed by PUGH to a combination of irradiation embrittlement and thermal-cycling stresses due to anisotropic thermal expansion [1]. In support are the facts that cracking is observed only in specimens irradiated above 450° C, or after post-irradiation thermal cycling of specimens irradiated at lower temperatures, and that it is not observed either after thermally cycling unirradiated uranium or after irradiating uranium at a constant temperature in the high alpha

range. All but the smallest thermal cycles are due to occasional cooling from the nominal irradiation temperature, usually due to operational requirements of the reactor. Typical thermal histories are shown in Table I.

TABLE I

TYPICAL THERMAL HISTORIES

Specimen (Number)	Burn-up (%)	Number of cycles		
		<15°C	15-100°C	>100°C
845 (see Fig. 1)	0.7	3184	18	64
118	0.16	N.D.	110	23

The largest cycles occur during reactor shut-downs when the specimen cools to room temperature. The differential strain per deg C temperature change between adjacent grains having maximum mismatch (i. e. [100], the direction of maximum thermal expansion of one grain, lies parallel to [010], the direction of minimum thermal expansion of the other) increases exponentially with mean temperature. In unirradiated uranium the strain can be accommodated plastically, but loss of ductility is an early effect of irradiation. Thus the maximum internal strain on cooling from 600° C to room temperature is 2%, and the ductility of uranium irradiated to 0.02% is about 1% at 600° C. The grain boundary is the region of greatest strain-gradient, and for medium strain rates grain-boundary relaxation occurs at about 450° C in uranium. Failure will therefore occur preferentially at the grain-boundaries as a Type-I brittle crack above 450° C, conforming with the general observation that grain-boundary cracking of this type becomes more likely the higher the temperature. Hence in irradiated uranium Type-I grain-boundary cracking is observed only in specimens in which the irradiation temperature exceeded 450° C, both because the total strain on cooling and heating was greater and because the tendency for grain-boundary cracking was greater.

The sporadic occurrence of cracks reported in earlier work [1] suggests structure sensitivity. Non-uniform grain-boundary phenomena, e. g. second phase particles, might be potential crack initiators. It is interesting that the cracks occurred more uniformly and frequently in adjusted, beta-quenched uranium where grain-boundary particles (UAl_2, U_6Fe) are likely to exist.

3.1.2. Type-II grain-boundary void cracks are believed to be initiated from strings of creep voids, of the type observed by GREENWOOD et al. and HULL and RIMMER [7, 8] in grain boundaries under tensile stress, but their formation is complicated by the vacancies and inert gases produced by fission. A tensile stress (σ) across a grain boundary generates vacancies which tend to condense by random nucleation, or on pre-existing porosity, second-phase particles, etc. Voids are formed in this way on carbide particles in uranium tensile-test specimens pulled at high temperatures [9]. The driving force

for growth is the resultant stress at the void surface, which in a true void is given by $\sigma - (2\gamma/r)$, where γ is the surface energy and r the void radius. When $r < (2\gamma/\sigma)$ the voids tend to close by sintering. During irradiation, however, fission events will increase the vacancy concentration, fission-gas bubbles in the grain boundary will act as nuclei, and fission-gas atoms may enter and stabilize pre-existing void nuclei. The condition for void growth will then be $r \geq 2\gamma/(\sigma + p)$, where p is the pressure of fission gas in the void; if $p > (2\gamma/r)$ the void will continue to grow even at zero grain-boundary stress. There will in fact be a continuous transition, depending on local conditions, between creep voids and fission-gas bubbles in the grain boundaries. Since gas pressure increases the force tending to maximum volume and hence minimum surface area, a true-fission gas bubble should approach a spherical shape more closely than a true creep void, which may assume a polyhedral shape to reduce surface energy.

The tensile stresses produced at the grain boundaries of polycrystalline uranium by anisotropic thermal expansion depend very much on the local grain configuration; it is known that at high temperatures local plastic deformation occurs, however, so that the yield stress ($\sim 10^9$ dyn/cm^2 in unirradiated uranium at 500°C) can be taken as a maximum permissible stress. Taking $\gamma \simeq 1000$ dyn/cm, the smallest critical nucleus radius is 2×10^{-6} cm (0.02 μm). The mean pressure of gas in a specimen showing 5% volume increase after irradiation at 500° C to 0.5% burn-up should be 1.4×10^8 dyn/cm^2. This is smaller than σ_{max}, and although the pressure tends to be higher in the smaller bubbles, it can be concluded that during irradiation thermal-cycling stresses are still capable of playing a significant part in the growth of grain-boundary voids.

The occasional lack of distinction between Type-I brittle cracks and Type II-void cracks is to be expected, since, for example, a boundary weakened by creep voids may suddenly undergo brittle failure. However, early in the irradiation period, void cracking is less likely than brittle failure. The small degree of mis-orientation at sub-grain boundaries and the consequent low grain-boundary stresses are an adequate explanation of the absence of cracking there, but the networks of small voids are correspondingly difficult to explain. Unirradiated uranium with iron and aluminium additions has shown similar networks of second-phase particles at the sub-grain boundaries. The voids may be nucleated by these particles during irradiation; alternatively they may be a preparative effect due to the removal of particles during polishing or etching. No such effect is found in unirradiated uranium, however, and the voids have been observed in irradiated uranium using all the preparative techniques described above. It seems probable that second-phase particles in the grain or sub-grain boundaries will play a significant part in irradiation cracking.

3.1.3. Type III-transgranular cracks are assumed, like the intergranular Types I and II, to be produced by the thermal-cycling stresses. These cracks often straddle the narrowest part of an hour-glass shaped grain in which the keying effect of adjacent grains restricts the relief of tensile stress by grain-boundary sliding or cracking. However, they are believed to occur primarily at the lower end of the thermal cycle, where failure is, in any case, less likely to occur at the grain boundary. The strain will be greatest,

and the crack will be most likely to be initiated, at the grain boundary, as is in fact observed. The cracks appear to be brittle failure along one or more parallel planes. The tear lines may be cleavage steps accommodating the plane of failure to a tensile stress to which it is not quite normal; screw dislocations may play an important part in forming these cleavage steps [10].

CAHN [11] observed what appeared to be cleavage facets in unirradiated uranium. The only 'cleavage plane' which could be identified coincided with (172); Cahn also found many twins of the second kind with an irrational twinning plane close to (172) and concluded that this was not true cleavage but 'parting' along a twin boundary, more usually met with in minerals. Twins due to thermal-cycling stresses are very thin; some or all of the Type-III transgranular cracks may be 'twin partings' in which the crack has obscured the twin. The uranium sample of Fig. 5 was plastically deformed after irradiation, producing thick twins.

3. 2. Secondary effects of irradiation cracking

3. 2. 1. Breakaway swelling. Cracks may modify the subsequent irradiation behaviour of the uranium and cracks occurring early in the irradiation may themselves be modified. In Fig. 7 is shown a severely swollen specimen of irradiated (unadjusted) uranium containing wide, ragged fissures believed to be grain-boundary cracks opened by the pressure of accumulated fission gas. The volume of uranium from which a large void collects gas atoms by random-walk diffusion is a product of its surface area and the mean linear distance a gas atom travels before being captured by a fission-gas bubble or other nucleating body. The large surface-area-to-volume ratio of the lenticular cracks favours gas capture.

The expansion of gas-filled cracks into a more nearly spherical shape by creep relaxation was simulated by prolonged hot-hardness tests on unirradiated uranium. The load-time curve, extrapolated to 100 d, showed

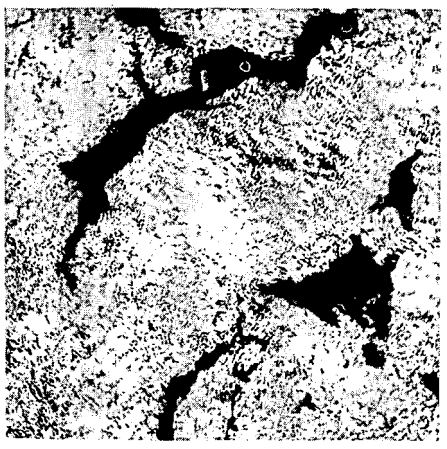


Fig. 7

Ragged fissures, believed to be opened grain-boundary cracks, in unadjusted uranium showing 34% volume increase at 0.46% burn-up

a minimum equilibrium load at 550° C of 0.15 kg/mm^2. The mean fission-gas pressure in the voids of unadjusted uranium irradiated at 550° C to 0.7% burn-up in 100 d, volume increase 31%, was calculated to be 0.34 kg/mm^2, which is in reasonable agreement with the hot-hardness result.

In beta-quenched uranium adjusted with iron and aluminium the irradiation cracks remained relatively narrow; overall volume increases were smaller than in unadjusted uranium, and breakaway swelling was not observed at burn-ups up to 0.7% [2]. Because a very large number per unit volume of fission-gas bubbles are nucleated, in adjusted uranium, their subsequent growth by coalescence is prevented. Owing to surface-energy effects the equilibrium pressure in small bubbles is high, and a given quantity of gas can be accommodated with less volume increase than in a smaller number of large bubbles. This would seem a sufficient explanation of the crack stability, since the increased bubble density will reduce the diffusion distance and hence reduce the volume of uranium from which a given crack can accumulate fission-gas atoms. Thus in adjusted uranium the second form of breakaway swelling is also retarded.

3.2.2. Thermal conductivity. Cracking will reduce the thermal conductivity of a uranium fuel element, with a consequent increase in its centre temperature. Circumferential cracking will have the most serious effect whereas the hoop stresses produced in the fuel element by the expansion of its core would be most readily relieved by radial cracking. Gross cracking, associated with rapid and large thermal cycles, generally takes a radial form.

3.2.3. Other effects. In most reactor concepts the uranium fuel element is to some extent a structural member, which is a further limitation on the amount of cracking which can be tolerated. Also the extent of fission-gas may be increased by cracks opening to the surface of the fuel rod.

3.3. The further study of irradiation cracking

Post-irradiation heat-treatment and the irradiation of uranium under restraint have been proposed as techniques for the further study of irradiation cracking. If the interpretation of crack origins given above is correct, post-irradiation thermal cycling of uranium irradiated below 450°C should be a suitable means of studying Type-I brittle intergranular cracks and Type-III brittle transgranular cracks. This technique is usually more flexible than an in-pile experiment. Data on the minimum combinations of thermal cycling and burn-up required to produce cracking and the effects of composition of structure (e.g. the presence of grain-boundary particles) could be obtained in this way. The formation of Type-II voids and cracks is probably more directly and continuously affected by fission events, and less easily simulated in out-of-pile experiments.

If uranium undergoing irradiation is under an external pressure P, the condition for growth of a void by vacancy condensation becomes

$$r > \frac{2\gamma}{\sigma + p - P} .$$

If $P \simeq \sigma + p$, therefore, growth will be inhibited until the accumulation of fission-gas atoms raises p significantly. Taking the values of σ and p considered earlier, this inhibition will require an external pressure of the order of $10^9 dyn/cm^2$, or approximately 15 000 lb/in^2. This is very much larger than pressures normally applied; the Calder Hall coolant pressure, for example, is only 150 lb/in^2, while at the highest operating temperatures the restraint due to the Magnox can is probably negligible. However, since this pressure is calculated for complete inhibition at high levels of thermal stress (≡ 30°C temperature change) a significant reduction of creep void growth can also be expected at lower restraining pressures.

4. SUMMARY AND CONCLUSIONS

4.1. Alpha uranium cracks during irradiation only when thermal cycling with a maximum temperature above 450°C occurs.

4.2. The stresses producing cracking are due to anisotropic expansion of the uranium during thermal cycling; brittle cracking occurs when irradiation embrittlement prevents these stresses being accommodated by plastic flow.

4.3. Three types of crack have been classified and are summarized below.

Type I. Intergranular brittle cracking, which can occur at low irradiation levels, and is due to large stresses produced by cycling at high temperatures (~ 600°C) where the grain boundaries are weak.

Type II. Intergranular void cracking is due to the coalescence of vacancies and fission-gas atoms at grain boundaries under tensile stress, and has not been observed at low burn-ups (~ 0.05%).

Type III. Transgranular brittle cracking is believed to be associated with large stresses at relatively low temperatures, e.g. the bottom of a large thermal cycle, where grain-boundary failure is less likely.

4.4. In Type-II intergranular void cracking a continuous transition can occur between true creep voids due to vacancy coalescence, and gas bubbles due to fission-gas atom diffusion. Analysis of the forces producing void growth suggests that thermal-cycling stresses can play a larger part than fission-gas pressure, and that effective restraint requires pressures of $10^3 - 10^4$ lb/in^2.

4.5. Intergranular cracks in badly swollen uranium appear to have opened under the internal pressure of fission gases. This did not occur in beta-quenched uranium samples containing iron and aluminium additions which were irradiated at 550-600°C [4]. An adequate explanation is based on the assumption that these specimens, which swelled very little, did so because the fission gases were precipitated in a very large number of small bubbles. This would reduce not only the total volume increase, but the amount of gas available to enter the cracks.

ACKNOWLEDGEMENTS

Many members of Metallurgy Division, AERE, helped in the preparation, irradiation and examination of the specimens described in this paper. The metallography, in particular, was largely carried out by J.E. Bainbridge and D.V.C. Jones.

REFERENCES

[1] PUGH, S.F., J. nucl. Materials 4 177 (1961).
[2] BELLAMY, R.G., Symp. Uranium and Graphite, Inst. Metals (20-21 March 1962).
[3] JEPSON, M.D. and SLATTERY, G., Brit. Pat. 863492 (1961).
[4] PLAIL, O.S., Proc. 2nd UN Int. Conf. PUAE 5 (1958) 543.
[5] EVANS, J.H. and VENABLES, J.H., Ninth Hot Labs. and Equipment Conf. of the Amer. Nucl. Soc. (1961).
[6] HYAM, E.D., U.K.A.E.A., private communication.
[7] GREENWOOD, J.N. et al., Acta. Met. 2 (1954) 250.
[8] HULL, D. and RIMMER, E., AERE Rpt. M/R 2804.
[9] DAVIES, D.M. and MARTIN, J.W., J. nucl. Mat. 3 (1961) 156.
[10] GILMAN, J.J., Plasticity, Pergamon Press, London (1961).
[11] CAHN, R.W., AERE Rpt. M/R 740 (1951).

ÉTUDE DE LA DIFFUSION ET DE LA PRÉCIPITATION DES GAZ RARES DANS LES MÉTAUX

M. GILBERT BREBEC, VIVIANE LÉVY, JEAN LETEURTRE ET YVES ADDA
CENTRE D'ÉTUDES NUCLÉAIRES DE SACLAY,
GIF-SUR-YVETTE (S. et O.), FRANCE

Abstract — Résumé – Аннотация — Resumen

A STUDY OF THE DIFFUSION AND PRECIPITATION OF RARE GASES IN METALS. In an attempt to explain the mechanism of swelling of irradiated uranium, we studied the behaviour of various rare gases (helium, argon, krypton, xenon) in several metals (silver, zirconium, uranium).

Rare-gas/metal alloys of different concentrations were produced by electric discharge. It was shown that the introduction mechanism is probably based on the penetration of rare gas ions into the metallic lattice combined with redeposition. Using these alloys we studied:

(a) Changes in the crystal lattice, including variations in crystal parameter due to introduction of rare gases into the lattice, and formation of defects through bombardment by the rare gas ions.
(b) Diffusion of the Xe and Kr fission gases in various metals (silver, uranium).
(c) Precipitation of rare gases (helium, argon, xenon, krypton) in the form of bubbles in various metals (silver, uranium, zirconium). These studies were carried out partly by optical microscopy and partly by transmission electron microscopy.

ÉTUDE DE LA DIFFUSION ET DE LA PRÉCIPITATION DES GAZ RARES DANS LES MÉTAUX. En vue d'essayer de préciser les mécanismes du gonflement de l'uranium irradié nous avons étudié le comportement de différents gaz rares (hélium, argon, krypton, xénon) dans différents métaux (argent, zirconium, uranium).

Des alliages gaz rare-métal de différentes concentrations ont été réalisés par décharge électrique. On a montré que le mécanisme d'introduction est probablement basé sur une pénétration des ions gaz rare dans le réseau métallique combinée à une redéposition. Sur de tels alliages nous avons étudié:

a) Les modifications du réseau cristallin.
   - Variations de paramètre cristallin dû à l'introduction des gaz rares dans le réseau.
   - Création de défauts dus au bombardement par les ions gaz rares.
b) La diffusion des gaz de fission Xe et Kr dans différents métaux (argent, uranium).
c) La précipitation des gaz rares (hélium, argon, xénon, krypton) sous forme de bulles dans différents métaux (argent, uranium, zirconium). Ces études ont été effectuées soit par microscopie optique, soit par microscopie électronique par transmission.

ИЗУЧЕНИЕ РАСПРОСТРАНЕНИЯ И ОСАЖДЕНИЯ ИНЕРТНЫХ ГАЗОВ В МЕТАЛЛАХ. В целях уточнения механизмов вспучивания облученного урана авторы изучили поведение различных инертных газов (гелий, аргон, криптон, ксенон) в различных металлах (серебро, цирконий, уран).

С помощью электрического разряда были получены сплавы метал - инертный газ различной концентрации. Было показано, что механизм введения возможно основывается на проникновении ионов инертного газа в кристаллическую решетку металла, которое сопровождается переотложением. На подобных сплавах авторы изучили:

а) изменения кристаллической решетки; изменение кристаллического параметра, которое происходит из-за введения инертных газов в решетку; возникновение дефектов, происходящих в результате бомбардировки ионами инертных газов;

б) распространение газообразных продуктов деления ксенона и криптона в различных металлах (серебро, уран);

в) осаждение инертных газов (гелий, аргон, ксенон, криптон) в виде пузырьков в различных металлах (серебро, уран, цирконий). Эти исследования были проведены при помощи оптического микроскопа или при помощи электронного микроскопа с передачей на экран.

ESTUDIO DE LA DIFUSIÓN Y DE LA PRECIPITACIÓN DE LOS GASES NOBLES EN LOS METALES. Con el propósito de conocer mejor los mecanismos que intervienen en el crecimiento del uranio, los autores han estudiado el comportamiento de una serie de gases nobles (helio, argón, criptón, xenón), en diversos metales (plata, zirconio, uranio).

Han preparado, por descarga eléctrica, aleaciones gas noble-metal de diferentes concentractiones y han demostrado que el mecanismo de introducción se basa probablemente en una penetración de los iones del gas noble en la red metálica, combinada con una resedimentación. En tales aleaciones, los autores han estudiado:

a) Las modificaciones de la red cristalina.
Variaciones de parámetro cristalino debido a la introducción de gases nobles en la red.
Creación de defectos debidos al bombardeo del metal por iones de los gases nobles.

b) La difusión de los gases de fisión Xe y Kr en diferentes metales (plata, uranio).

c) La precipitación de los gases nobles (helio, argón, xenón, criptón) bajo forma de burbujas en diferentes metales (plata, uranio, zirconio). Estos estudios se han efectuado por microscopía óptica y por microscopía electrónica de transmisión.

INTRODUCTION

La formation de gaz rares au cours de l'irradiation de certains matériaux nucléaires (U, Pu et leurs alliages, Be, etc.) pose de nombreux problèmes à la technologie des réacteurs car leur présence modifie beaucoup les propriétés mécaniques de ces matériaux. Plusieurs phénomènes accompagnent la formation de gaz rares au sein des matériaux irradiés; l'un des plus importants est le gonflement, essentiellement dû à la précipitation des atomes de gaz rares sous forme de bulles. En effet les gaz rares sont très peu solubles dans les métaux, si bien que l'irradiation crée de très fortes sursaturations à des températures trop basses pour que toute diffusion soit possible; lorsqu'on élève la température les atomes deviennent mobiles et précipitent en bulles de plus ou moins grandes dimensions.

L'étude théorique du gonflement est très complexe et nécessite la connaissance de nombreux paramètres tels que la mobilité des atomes de gaz et des lacunes dans le réseau, et celle du mécanisme de germination des bulles.

Il était donc très intéressant d'essayer de déterminer ces différents facteurs. L'utilisation de matériaux irradiés pour ces études, outre la complexité théorique qui résulte de la pluralité des produits de fission, pose des problèmes technologiques délicats (manipulation de produits très actifs). Nous avons donc effectué nos études sur des systèmes métal-gaz rare plus simples où le gaz rare est introduit dans le métal par décharge électrique.

Sur de tels échantillons nous avons étudié:

1° Les modifications du réseau cristallin.

2° La précipitation des gaz rares sous forme de bulles.

3° La diffusion des gaz rares dans le métal.

I. MÉTHODE D'INTRODUCTION DES GAZ RARES DANS LE MÉTAL

Les alliages métal-gaz rare ont été préparés par décharge électrique [1]. Cette méthode très générale permet de réaliser des alliages métal-gaz rare différant par la nature du gaz rare ou par celle du métal. Elle permet en outre de faire varier la concentration du gaz rare dans le métal dans de grandes limites.

Le principe de la méthode est le suivant :

On applique une différence de potentiel de quelques centaines de volts entre une anode de nickel et deux cathodes planes (du métal à charger) disposées face à face (fig. 1). L'une des cathodes C_2 est reliée directement

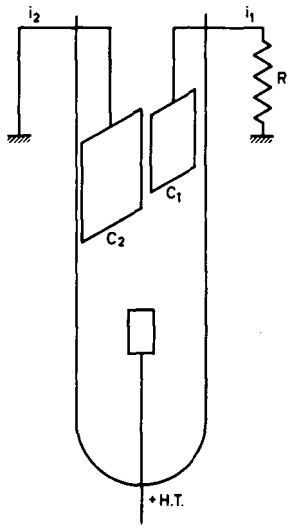


Figure 1

Tube de décharge avec deux cathodes plates.

à la terre; elle est donc au potentiel zéro. La seconde C_1 est polarisée, par une résistance R judicieusement choisie, à un potentiel compris entre 0 et celui de l'anode. Ces différentes électrodes sont placées dans une atmosphère du gaz rare à étudier, à une pression comprise entre 0, 1 et 1 mm de Hg.

On constate après décharge que :

a) La cathode reliée à la terre s'amincit au profit de la cathode polarisée par la résistance. On note sur celle-ci la formation d'un dépôt métallique d'épaisseur uniforme qui peut être aisément mis en évidence par microscopie optique (fig. 2).

b) La concentration en gaz est la même en tout point de la surface de la cathode.

c) La quantité de gaz fixée sur la cathode polarisée par la résistance dépend de la différence de potentiel (V-v) entre les deux cathodes. Elle augmente lorsque V-v diminue (fig. 3). Ces observations sont en accord avec le mécanisme proposé par les auteurs dans une publication antérieure [1].

Nous avons donc obtenu par cette méthode des alliages métal-gaz rare dans lesquels la concentration en gaz varie de 10^{-6} à $4 \cdot 10^{-2}$ at. Ces valeurs ont été déterminées soit au microanalyseur à sonde électronique de Castaing (pour les concentrations élevées) soit par analyse au moyen d'isotopes radioactifs. Les sytèmes étudiés ont été Ag-Kr, U-Kr.

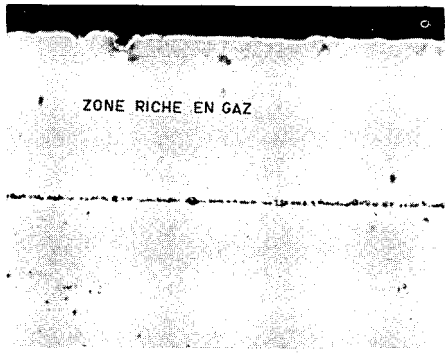


Figure 2

Décharge de krypton dans l'argent.

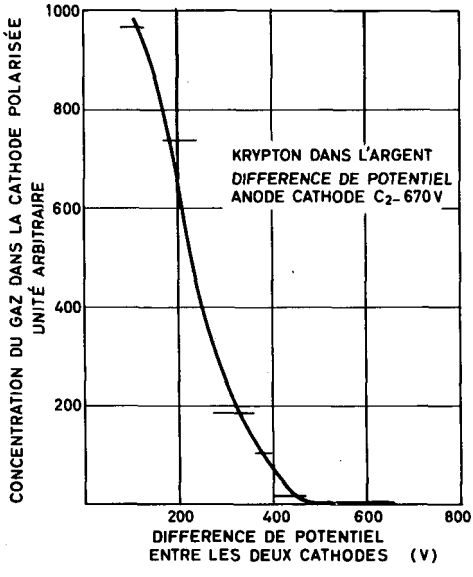


Figure 3

Variation de la concentration moyenne en gaz rare de la cathode polarisée C_1 en fonction de la différence de potentiel entre les deux cathodes.

II. MODIFICATIONS DU RÉSEAU CRISTALLIN

Le processus d'introduction des gaz étant une pénétration du gaz rare dans le métal par choc combinée à une redéposition d'atomes métalliques par attaque cathodique, nous avons vérifié que les couches métalliques riches en gaz obtenues sont constituées de métal massif. En effet les micrographies et les clichés de diffraction électronique effectués sur de tels échantillons après amincissement électrolytique sont analogues à ceux obtenus sur n'im-

porte quel métal massif. Cependant, comme dans l'irradiation, le bombardement ionique crée de nombreux défauts dans le réseau cristallin; d'autre part, la présence de gaz rares dans le métal peut perturber le réseau cristallin.

A. Défauts du réseau introduits par le bombardement ionique

Comme on l'avait déjà constaté pour les décharges en cathode creuse [2], il existe de nombreux défauts du réseau dans les dépôts métalliques contenant des gaz rares.

Ces couches métalliques sont amincies par une technique électrolytique et les fragments sont examinés par transmission au microscope électronique en double condenseur sous une tension de 100 kV.

Nos observations ont porté sur les systèmes argent-krypton et uranium-krypton.

Système argent-krypton : Nous avons pu mettre en évidence des tétraèdres de fautes d'empilement (fig. 4 et 5) analogues à ceux qui ont été observés par Silcox et Hirsch par recuit de lacunes trempées. On note aussi de nombreux petits défauts triangulaires (fig. 4); ils correspondent à des triangles équilatéraux dans les plans [111], les directions des côtés étant (110).

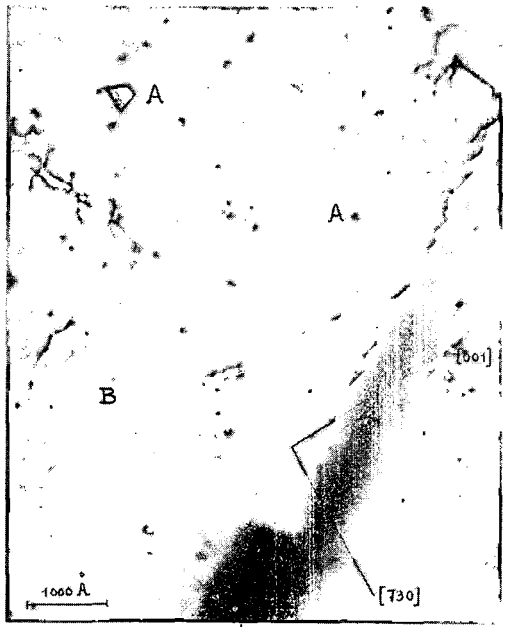


Figure 4

A: Tétraèdres de faute d'empilement.
B: Défauts triangulaires situés dans les plans [111] les côtés étant parallèles à (110).



Figure 5

A: Tétraèdres de faute d'empilement.
B: Boucle de dislocation.

On trouve aussi de petites boucles de dislocations (fig. 5) ainsi que de nombreuses dislocations (fig. 6) dont certaines sont spiralées. De plus on voit souvent des fautes d'empilement entre les deux partielles d'une dislocation dissociée (fig. 7).

Système uranium-krypton: L'amincissement a été effectué par la technique décrite par HUDSON, WESTMACOTT et MAKIN [3]. Les observations au microscope électronique ont montré que la zone riche en gaz est constituée de très petits grains (souvent inférieurs au micron). Comme dans le cas de l'argent on observe de nombreux défauts et en particulier la présence de nombreuses boucles de dislocation de 50 à 300 Å de diamètre (fig. 8).

B. Modifications du réseau cristallin en fonction de la teneur en gaz rare

Pour préciser la structure des alliages métal-gaz rare préparés par décharge électrique nous avons étudié les variations du paramètre cristallin de l'argent en fonction de la teneur en krypton.

Nous avons pu mettre en évidence les faits suivants:

1° Pour les faibles concentrations (inférieures à $2 \cdot 10^{-3}$at environ), le paramètre de l'argent croît en fonction de la teneur en gaz rare (tableau I). Ces variations sont de l'ordre de grandeur de celles prévues par la loi de Vegard.

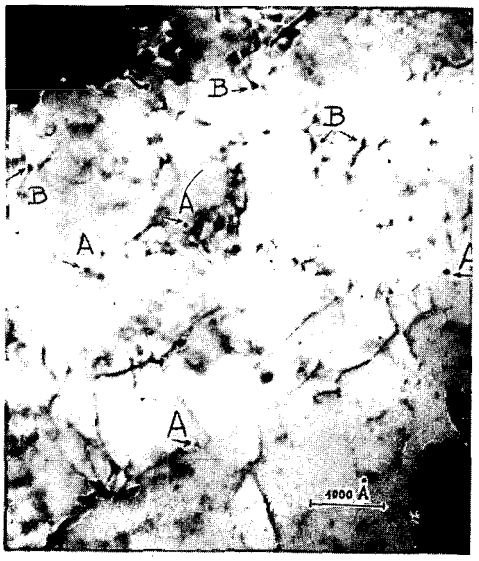


Figure 6

Défauts triangulaires en A.
Noeuds de dislocation étalés en B. Le rayon de courbure de la partielle indiquée par la flèche est 150 Å. On peut en déduire l'énergie de faute d'empilement par la formule:

D'où :

$$\gamma = \frac{\mu b^2}{2R}$$

μ = module de cisaillement
$= 2,6 \cdot 10^{11}$ dyne/cm^2
b = vecteur de Burgers 2 A

γ 32 ergs/cm^2.



Figure 7

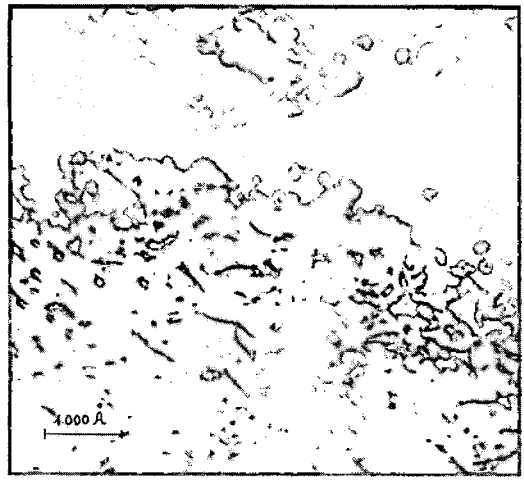


Figure 8

TABLEAU I

VARIATIONS DU PARAMÈTRE EN FONCTION DE LA TENEUR EN GAZ RARE

Concentration en gaz (atomes)	Paramètre
0	4,0756
10^{-6}	4,0756
$2,1 \cdot 10^{-4}$	4,0763
$4,1 \cdot 10^{-4}$	4,0770
$1,2 \cdot 10^{-3}$	4,0775
$1,8 \cdot 10^{-3}$	4,0781
$7,4 \cdot 10^{-3}$	4,0756
$9,6 \cdot 10^{-3}$	4,0756

2° Pour les fortes concentrations (supérieures à $5 \cdot 10^{-3}$ at environ), on n'observe aucune variation de paramètre.

Les résultats sont indiqués sur la figure 9.

Des échantillons correspondant à chacune de ces deux catégories ont été examinés au microscope électronique en transmission. Les résultats obtenus semblent indiquer qu'il n'est pas possible de mettre en évidence des bulles de gaz rare dans les échantillons présentant une variation de paramètre (fig. 5 et 7). Par contre sur les échantillons contenant de fortes

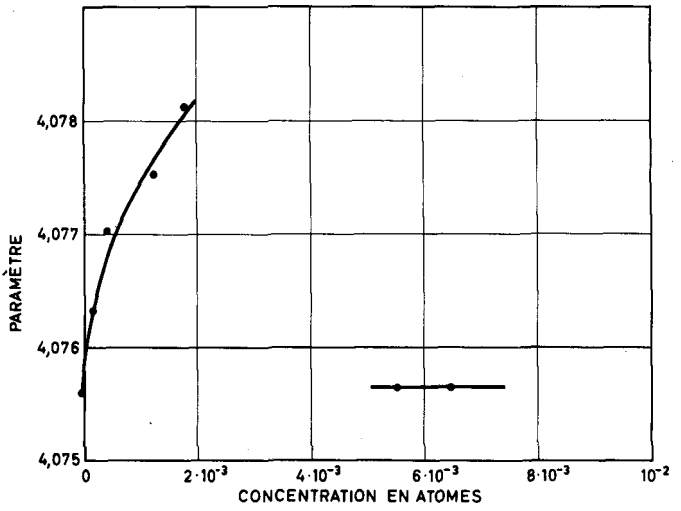


Figure 9

Variation du paramètre de l'argent en fonction de la concentration en krypton.



Figure 10

Micrographie électronique d'un échantillon d'argent contenant du krypton à une teneur supérieure à $5 \cdot 10^{-3}$ atomes.

concentrations en gaz rare et dont le paramètre cristallin est inchangé on observe toujours une précipitation du gaz en bulles (fig. 10).

On pourrait donc penser que pour les faibles teneurs les atomes de gaz rares sont en position de substitution dans le réseau; cette solution

solide est sans doute thermodynamiquement instable si l'on en croit les évaluations théoriques de la solubilité des gaz rares dans les métaux.

Lorsque la teneur en gaz rare dans le métal croît, la sursaturation peut être suffisamment grande pour qu'il y ait précipitation dans les conditions de la décharge électrique (température de l'ordre de 300°C).

III. ÉTUDE DE LA PRÉCIPITATION DES GAZ RARES

Les études ont été faites par microscopie optique et électronique.

A. Système gaz rare-argent

L'étude de la précipitation des gaz rares dans l'argent a permis de mettre en évidence l'influence très forte de la concentration en gaz sur la température de début de précipitation.

En effet l'observation au microscope électronique d'échantillons bruts de décharge conduit aux constatations suivantes :

a) si la teneur en gaz est élevée (supérieure à $5 \cdot 10^{-3}$at) il y a précipitation de bulles dans tous les cas (fig. 10),

b) si la teneur en gaz est inférieure à $2 \cdot 10^{-3}$ at on ne voit pas de bulles (fig. 5 et 7).

Comme la température en cours de décharge est sensiblement la même dans les deux cas (300°C) on pourrait penser, par analogie avec la précipitation dans une solution solide sursaturée, que la nucléation des bulles est d'autant plus facile que la concentration est plus élevée.

Dans le but d'essayer de préciser les mécanismes de germination et de croissance des bulles nous avons effectué des traitements thermiques sur des échantillons de différentes concentrations.

Cas des concentrations élevées

Les micrographies optiques de tels échantillons non traités thermiquement ne permettent pas la mise en évidence de bulles de gaz rare (fig. 2) bien que l'observation au microscope électronique révèle l'existence de bulles de 50 à 300 Å de diamètre (fig. 10).

Si on traite ces échantillons 244 h à 300° on voit apparaître des bulles dont la dimension varie de 0, 2 à 2 μ. Après un traitement de 2 h à 850°, les bulles atteignent plusieurs microns de diamètre (fig. 11).

La microscopie optique ne permettant pas de voir les bulles de très faibles dimensions ni d'effectuer des observations précises sur la dimension ou la forme des bulles nous avons effectué des examens au microscope électronique en transmission.

Après le recuit à 850° on observe des bulles de taille variable (fig. 12). Ces bulles ont des formes polyédriques. Ce fait avait déjà été observé pour les bulles d'hélium dans l'argent (fig. 13). Les faces du polyèdre sont des plans denses [111] ou [100].

Efin les bulles sont presque toujours situées sur les dislocations (fig. 13 et 14).



Figure 11

Bulles de krypton dans l'argent.
Echantillon recuit pendant 2 h à 850°.

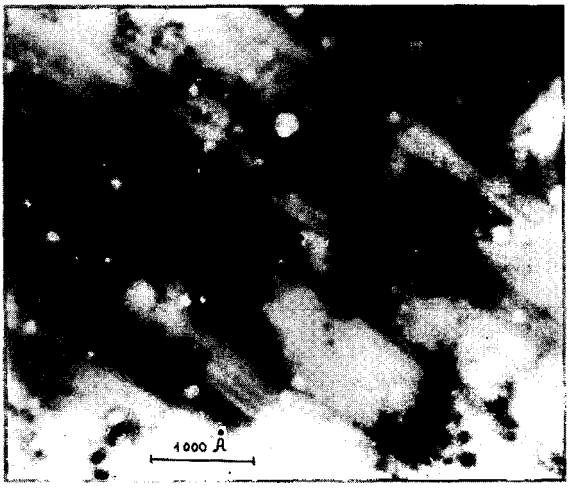


Figure 12

Bulles de krypton dans l'argent.
Echantillon recuit pendant 2 h à 850°.

Cas des faibles teneurs

Après un traitement thermique de 25 h à 400° nous n'avons pu mettre en évidence la présence de bulles de gaz (fig. 15). Cependant à 700° la précipitation est très rapide. Deux heures de traitement sont suffisantes pour faire apparaître de nombreuses bulles d'une centaine d'Angströms.

Ces bulles, comme précédemment, sont polyèdriques et situées le long des dislocations.

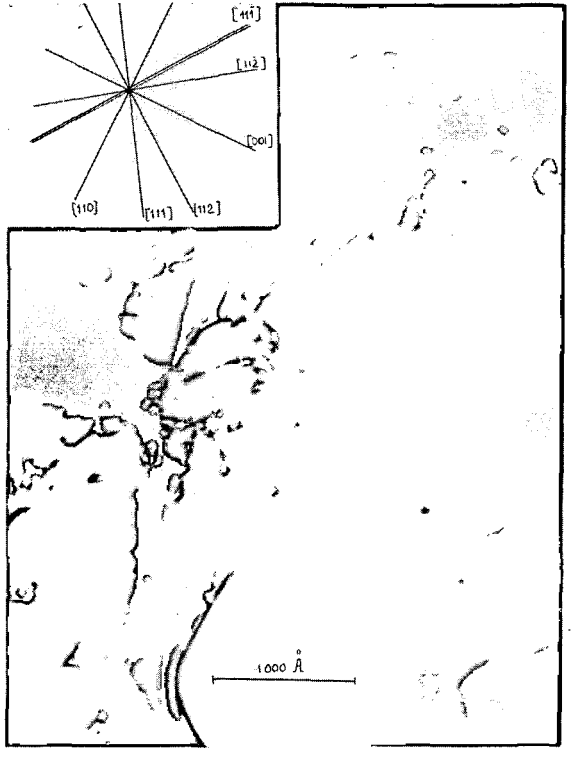


Figure 13

Bulles d'hélium dans l'argent. Les axes cristallographiques sont portés sur la photo. Les bulles sont polyédriques et les plans des polyèdres sont [111] et [100].

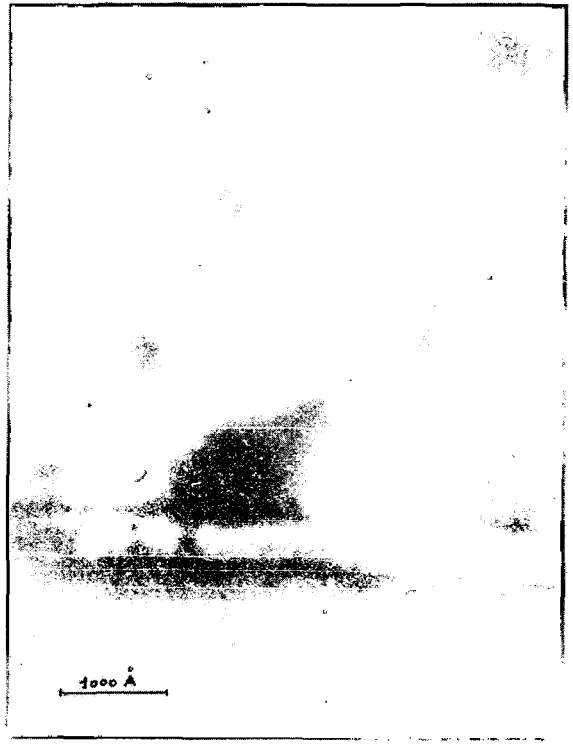


Figure 14

Bulles de krypton dans l'argent.
Echantillon recuit pendant 2 h à 850°.



Figure 15

Krypton dans l'argent.
Echantillon recuit pendant 25 heures à 400°
(on note l'absence de bulles).

B. Système gaz rare-uranium

Les études n'ont été faites que dans le cas du krypton.

Sur des échantillons bruts de décharge nous n'avons pu mettre en évidence de bulles de krypton par microscopie optique ou par microscopie électronique en transmission (fig. 8). Ces échantillons ont été soumis à différents traitements thermiques.

En phase γ

Pour des traitements de 1 à 63 h à 950° on observe au microscope optique la formation de bulles de grandes dimensions dans les régions les plus riches en gaz. Le diamètre moyen de ces bulles croît en fonction de la durée du traitement (fig. 16).

En phase α

Les traitements ont été effectués à 620°.

Par microscopie optique il est difficile de mettre en évidence la présence de bulles. Néanmoins pour un traitement de 500 h il semble qu'il y ait une précipitation de bulles le long des joints de grains. Des observations au microscope électronique sur répliques ont confirmé ce fait. Les bulles observées ont environ 2000 Å de diamètre (fig. 17).

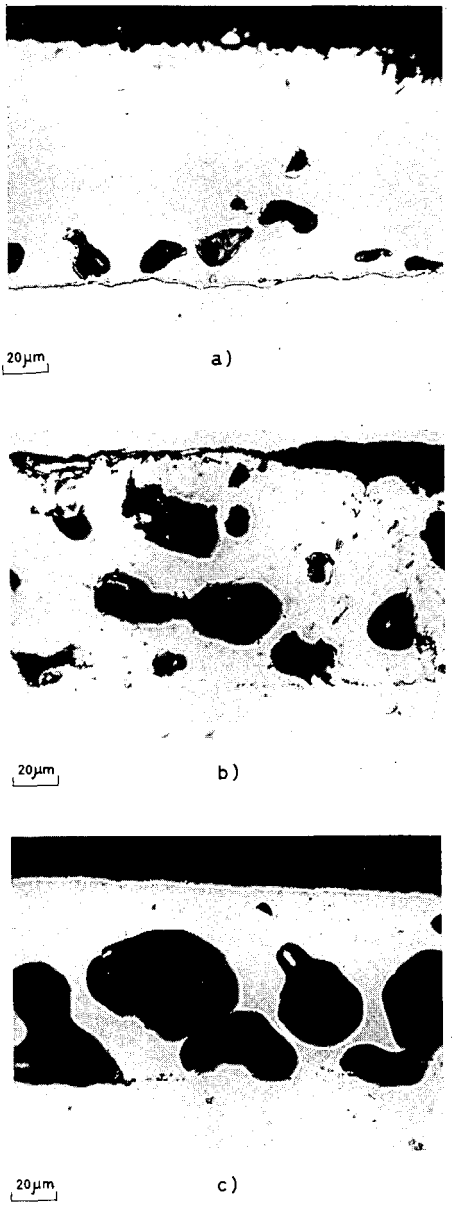


Figure 16

Bulles de krypton dans l'uranium.

a) 1 h à 900°
b) 24 h à 900°
c) 63 h à 900°

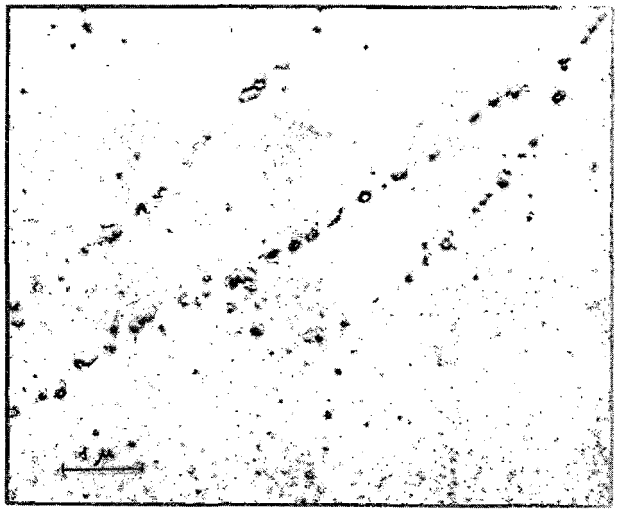


Figure 17

620°, 500 h; réplique.

Nous avons pu en effectuant des micrographies électroniques par transmission montrer la présence de bulles après 1 heure de traitement à 620°. Les bulles ont 50 - 200 Å de diamètre et sont réparties sensiblement avec uniformité sur toute la lame mince (fig. 18).

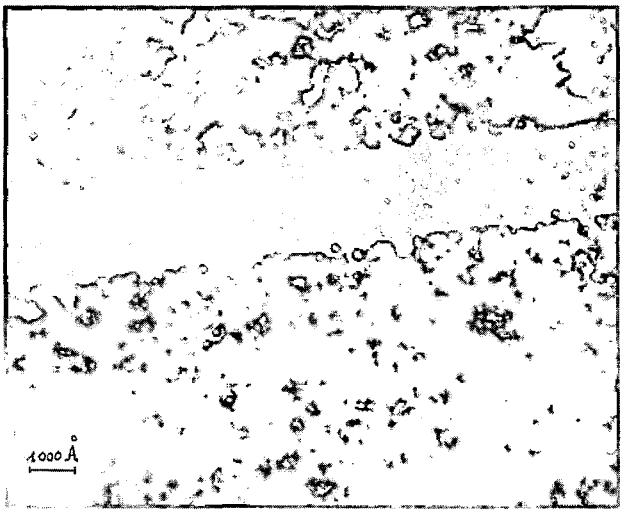


Figure 18

620°, 1 h; examen en transmission.

IV. ÉTUDE DE LA DIFFUSION DES GAZ RARES

A. Principe de la méthode

La méthode utilisée consiste à traiter sous vide des échantillons contenant des gaz rares introduits par décharge électrique et à mesurer la quantité de gaz dégagés en fonction de la température et du temps.

Suivant les conditions géométriques la solution de la 2e loi de Fick conduit à des équations différentes. Nos études ont été effectuées sur 2 types d'échantillons : échantillons bruts de décharge et « soudures» obtenues en soudant deux échantillons bruts de décharge, les zones riches en gaz étant disposées face à face (fig. 20).

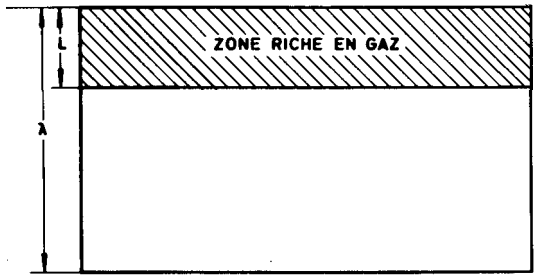


Figure 19

Cas des échantillons bruts de décharge.

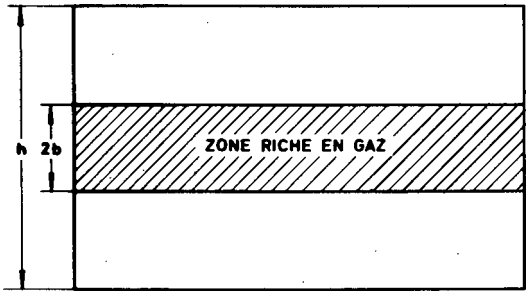


Figure 20

Cas des soudures.

Cas des échantillons bruts de décharge (fig. 19).

Si l'on suppose que l'épaisseur L de la zone chargée en gaz est uniforme et que la concentration C_0 du gaz dans cette couche est constante, la solution de la deuxième loi de Fick [4] montre que la quantité de gaz Q_t qui s'échappe après un chauffage sous vide, à une température T pendant le temps t, est reliée aux constantes de diffusion par la relation :

$$\frac{Q_t}{Q_0} = 1 - \frac{8}{\pi^2 k} \sum_{n=0}^{\infty} \frac{1}{(2n+1)^2} \sin^2 \frac{(2n+1)\pi k}{2} \exp - \left[(2n+1)^2 \pi^2 \frac{Dt}{\lambda^2} \right] \quad (1)$$

où

λ est l'épaisseur totale de la feuille,

$k = L/\lambda$,

D est le coefficient de diffusion, et

Q_0 la quantité de gaz initialement contenue dans l'échantillon.

Connaissant le rapport Q_t/Q_0, k, λ et t on peut donc déterminer D si l'on connaît le réseau de courbes donnant la variation de Q_t/Q_0 en fonction de $\varphi = D_t/\lambda^2$ pour les différentes valeurs de k. La série de l'expression (1) ne converge pas très rapidement surtout pour les faibles valeurs de φ ; ces courbes ont été déterminées à l'aide d'un calculateur électronique (fig. 21).

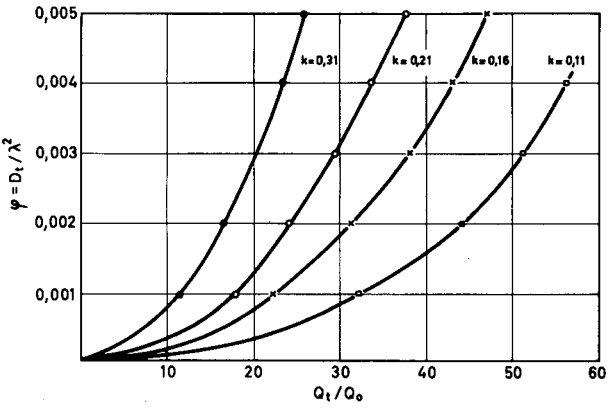


Figure 21

Variation de

$$\frac{Qt}{Q_0} = 1 - \frac{8}{\pi^2 k} \sum_{n=0}^{\infty} \frac{1}{(2n+1)^2} \sin^2 \frac{(2n+1)\pi k}{2} \exp \left[-(2n+1)^2 \pi^2 \varphi \right]$$

en fonction de

$$\varphi = \frac{Dt}{\lambda^2} \text{ et } k = \frac{L}{\lambda}.$$

Cas des soudures (fig. 20)

Dans ce cas la solution de l'équation de Fick est

$$\frac{Q_t}{Q_0} = 1 - \frac{4}{\pi^2 \alpha} \sum_{n=1}^{\infty} \frac{(-1)^{n+1}}{(2n-1)^2} \exp - \left[(2n-1)^2 \pi^2 \gamma \right] \sin (2n-1)\pi\alpha$$

où

$\alpha = b/h$,

$\gamma = Dt/h^2$,

Q_t et Q_0 ont les mêmes significations que précédemment,

2b est l'épaisseur de la zone riche en gaz, et h l'épaisseur totale.

Comme précédemment on peut déterminer D si l'on connaît Q_t/Q_0, b, h ainsi que la courbe donnant la variation de Q_t/Q_0 en fonction de $\gamma = Dt/h^2$ (fig. 22).

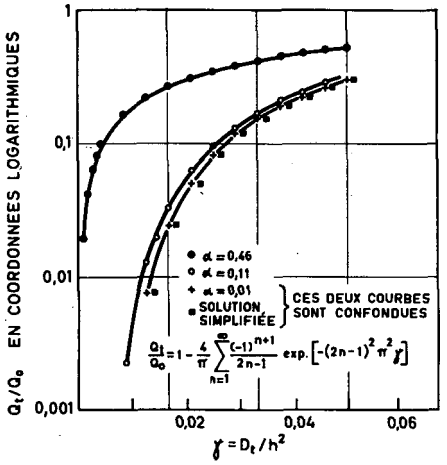


Figure 22

Variation de:

$$\frac{Q_t}{Q_0} = 1 - \frac{4}{\pi^2 \alpha} \sum_{n=1}^{\infty} \frac{(-1)^{n+1}}{(2n-1)^2} \exp\left[-(2n-1)^2 \pi^2 \gamma\right] \sin(2n-1)\pi\alpha$$

en fonction de

$$\alpha = \frac{b}{h} \qquad \gamma = \frac{Dt}{h^2}$$

L'épaisseur de la zone riche en gaz est déterminée par abrasion et mesures d'activité à différents niveaux, l'épaisseur totale est mesurée au moyen d'un comparateur et Q_t/Q_0 est obtenu en mesurant l'activité des gaz extraits au cours du traitement thermique, puis celle des gaz recueillis en fondant l'échantillon. Ces deux activités mesurées dans les mêmes conditions étant proportionnelles à Q_t et Q_0, leur rapport donne Q_t/Q_0.

B. Résultats

Nos études sont relatives aux systèmes argent-krypton, argent-xénon et krypton-uranium.

Cas de l'argent

Nous avons déterminé les coefficients de diffusion du krypton et du xénon dans l'argent dans les cas suivants:

a) échantillons bruts de décharge - la couche riche en gaz ayant une épaisseur soit faible (10 μ) soit forte (100 μ) par rapport à l'épaisseur totale (300 μ),

b) soudures obtenues en soudant face à face deux échantillons bruts de décharge.

Les coefficients de diffusion obtenus suivant dans chaque cas la loi d'Arrhenius, nous avons donc pu tracer les droites donnant la variation de log D en fonction de l'inverse de la température absolue.

Ces résultats sont indiqués sur la figure 23 où nous avons également porté les courbes déterminées à partir de soudures par LECLAIRE [5] pour

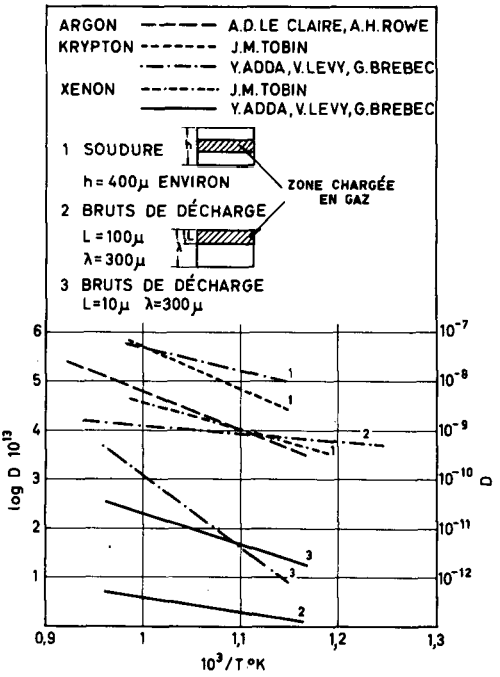


Figure 23

Diffusion des gaz rares dans l'argent.

la diffusion de l'argon dans l'argent et celles de TOBIN [6, 7] concernant la diffusion du krypton et du xénon.

Plusieurs remarques s'imposent :

1° Pour chaque géométrie les résultats sont à peu près reproductibles mais les coefficients de diffusion diffèrent notablement lorsque les conditions géométriques changent. En particulier ceux déterminés sur des soudures sont beaucoup plus élevés que ceux déterminés sur des échantillons bruts de décharge.

2° Dans le cas des soudures les résultats que nous avons déterminés sont du même ordre de grandeur que ceux obtenus par TOBIN [6, 7].

3° Enfin il est bon de noter que dans nos expériences les cinétiques de diffusion sont conformes à la théorie pour les échantillons bruts de dé-

charge ce qui n'est pas le cas des soudures. Dans ce cas la plus grande partie du gaz rare est éliminée durant les premières minutes du chauffage.

Cas de l'uranium

Les expériences de diffusion concernent le système uranium-krypton exclusivement. Les essais ont été effectués principalement sur des échantillons bruts de décharge. Néanmoins en phase γ nous avons effectué quelques essais sur des soudures.

Les résultats obtenus sont reproductibles pour chaque géométrie, ils permettent la détermination du coefficient de diffusion aux différentes températures.

La figure 24 donne la variation du coefficient de diffusion en fonction de la température. On peut noter que :

1° Les coefficients de diffusion du krypton dans l'uranium déterminés à partir d'échantillons chargés en gaz par décharge électrique sont supérieurs à ceux mesurés sur l'uranium irradié [8, 9, 10].

2° La variation du coefficient de diffusion en fonction de la température présente une augmentation brusque du coefficient de diffusion lorsqu'on passe de la phase β à la phase γ. Ce phénomène déjà noté pour l'autodiffusion de la phase β à la phase γ. Ce phénomène déjà noté pour l'autodiffusion de l'uranium [11, 12] et la diffusion de certains solutés dans l'uranium (silicium, fer) [13] n'a jamais été signalé dans la littérature pour la diffusion du krypton dans l'uranium irradié.

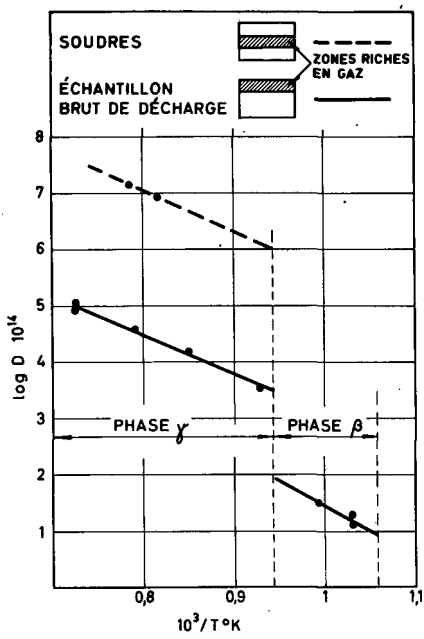


Figure 24

Diffusion du krypton dans l'uranium.

3° Comme dans le cas de l'argent les coefficients de diffusion obtenus diffèrent suivant la géométrie de l'échantillon utilisé. Ils sont environ cent fois plus élevés dans le cas des soudures.

C. Discussion

Le fait que des échantillons de géométrie différente conduisent dans les mêmes conditions à des coefficients de diffusion différents indique sûrement que l'élimination des gaz rares au cours des traitements thermiques sous vide ne s'effectue pas dans tous les cas par un simple processus de diffusion.

On peut tout d'abord noter, d'après les études publiées sur la diffusion des gaz rares dans les métaux, que les résultats obtenus sont très dispersés et que de nombreuses anomalies ont été déjà observées.

Les tentatives d'interprétation, quand elles existent font généralement appel à la diffusion du gaz le long des joints de grains et des dislocations, ou à la précipitation du gaz sous forme de bulles.

Les résultats obtenus dans notre étude ne peuvent sûrement pas être interprétés par une diffusion préférentielle aux joints de grains. En effet la zone riche en gaz étant constituée de très petits cristaux les coefficients de diffusion mesurés dans le cas de soudures devraient être inférieurs à ceux déterminés à partir d'échantillons bruts de décharge. C'est le contraire qui est observé expérimentalement.

Dans les sytèmes que nous avons étudiés la précipitation du gaz intervient certainement. En effet nous avons pu montrer par des micrographies optiques et électroniques que lors de traitements thermiques analogues à ceux effectués dans nos expériences de diffusion on observe la formation de bulles. La présence de ces bulles peut en effet influencer considérablement les valeurs des coefficients de diffusion.

Si le gaz contenu dans les bulles ne peut retourner en solution dans le réseau, la partie de gaz précipité n'interviendra pas dans la diffusion; la valeur Q_t/Q_0 sera donc erronée par défaut et les coefficients de diffusion mesurés seront trop faibles. D'autre part il est possible que lors des traitements de diffusion, il y ait intercommunication des bulles et élimination du gaz rare par les microfissures ainsi formées. Dans ce cas les coefficients de diffusion mesurés expérimentalement seront erronés par excès.

Afin d'essayer de préciser le rôle de la précipitation des gaz rares et celui de l'élimination des gaz par intercommunication des bulles (et formation de microfissures), nous avons étudié la diffusion du krypton dans l'argent dans les conditions suivantes :

Les échantillons étaient réalisés en soudant une zone métallique riche en gaz entre deux plaquettes d'argent recuit (fig. 25). Dans ces conditions, si la soudure est parfaite l'élimination des gaz rares ne pourra se faire que par diffusion à travers le métal massif.

Les essais de diffusion ont montré des différences notables entre le comportement de tels échantillons et celui des soudures précédemment étudiées. Les résultats des cinétiques de diffusion sont groupés sur la figure 26. On peut noter en particulier que dans le cas des soudures du type II (fig. 25) il y a au début du chauffage, à toutes les températures, une période

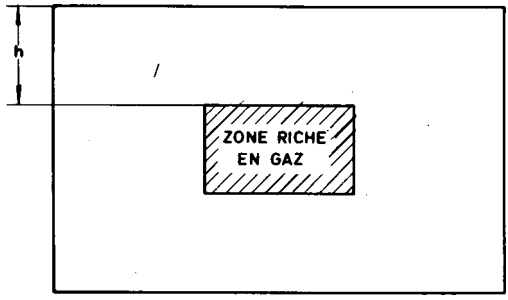


Figure 25

Cas des soudures du type II.

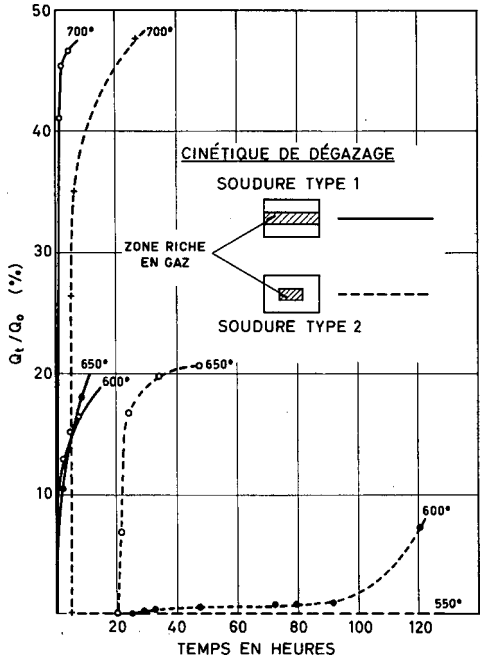


Figure 26

Diffusion du krypton dans l'argent.

d'induction pendant laquelle le gaz n'est pas éliminé. La durée de cette période d'induction décroît lorsque la température augmente.

Il semblerait donc que l'élimination des gaz dans les premières minutes du chauffage, lors des essais effectués sur les soudures du type I, soit due à un départ du gaz par les côtés de la soudure, probablement par des micro-fissures.

De plus, il faut remarquer sur les courbes de la figure 26 une différence notable entre les cinétiques de diffusion au-dessus de 650° et en dessous de

cette température. A 600° on a une élimination lente et progressive du gaz pendant de nombreuses heures alors qu'au-dessus de 650° l'allure de la cinétique ressemble à celle des soudures classiques (type I) mais décalée de la période d'induction.

On peut donc penser que, aux basses températures seulement, l'élimination des gaz est due à un processus de diffusion. Aux températures supérieures à 650° la pression existant dans les bulles pourrait conduire à la formation de fissures le long de l'interface de soudure et à l'élimination du gaz par ces fissures.

Enfin, il faut remarquer que dans le cas des essais effectués à 600° l'application de la méthode décrite ci-dessus pour la détermination des coefficients de diffusion conduit à des valeurs trop faibles, car le gaz contenu dans les bulles n'intervient pas dans la diffusion.

Cependant de telles expériences peuvent permettre de déterminer les coefficients de diffusion à partir des périodes d'induction si l'on suppose que l'on a un état stationnaire [14]. Dans ce cas la solution des équations de Fick conduit à

$$D = \frac{h^2}{6\theta}$$

où θ est la période d'induction en secondes et h l'épaisseur moitié de la soudure en cm.

La valeur déterminée à 600° est $2 \cdot 10^{-9}$ cm^2/s.

V. CONCLUSION

Dans notre travail nous avons préparé par décharge électrique des échantillons métalliques contenant des gaz rares à des teneurs variables. En particulier nous avons pu réaliser des solutions solides métal-gaz rare, dans lesquelles les atomes de gaz rares sont probablement en position de substitution dans le réseau.

Sur les échantillons contenant des gaz rares introduits par décharge électrique nous avons étudié la précipitation des gaz rares en bulles par microscopie optique et électronique.

Enfin, sur de tels alliages nous avons étudié la diffusion du gaz rare dans le métal : nous avons pu montrer que la précipitation des gaz rares en bulles lors de traitements de diffusion perturbe la mesure des coefficients de diffusion. Néanmoins il semble possible en utilisant des conditions géométriques convenables de déterminer les coefficients de diffusion avec précision.

RÉFÉRENCES

[1] BREBEC, G., LEVY, V., BENDAZZOLI, M. et ADDA, Y., Comptes rendus de l'Académie des Sciences (à paraître).

[2] LETEURTRE, J., LEVY, V., QUERE, Y. et ADDA, Y., 5e Colloque de métallurgie de Saclay, Juin 1961 (à paraître).

[3] HUDSON, B., WESTMACOTT, K.H. and MAKIN, M.J., AERE-R-3752.

[4] BREBEC, G., LEVY, V. et ADDA, Y., Rev. Métall. LVIII, 10 (1961) 743.

[5] LECLAIRE, A.D. et ROWE, A.H., Rev. Métall. 52, 2 (1955) 94.
[6] TOBIN, J.M., TID-7526.
[7] TOBIN, J.M., HW-53639.
[8] REYNOLDS, M.B., KAPL-1315.
[9] BARNES, R.S. et al., Actes 2e Conf. int. ONU util. EAFP 3 (1958) 846.
[10] WALKER, J.F., IGR-TN-W-1046.
[11] ADDA, Y. and KIRIANENKO, A., J. nucl. Mater. 2 (1959) 120.
[12] ADDA, Y., KIRIANENKO, A. and MAIRY, C., J. nucl. Mater. 3 (1959) 300.
[13] MOSSE, M., LEVY, V. et ADDA, Y., Comptes rendus de l'Académie des Sciences 250 (1960) 3171-3.
[14] BREBEC, G., LEVY, V. et ADDA, Y., Comptes rendus de l'Académie des Sciences (à paraître).

SWELLING OF URANIUM

B. A. LOOMIS
ARGONNE NATIONAL LABORATORY, ARGONNE, ILLINOIS

Abstract — Résumé — Аннотация — Resumen

SWELLING OF URANIUM. An understanding of the mechanism of swelling in irradiated uranium has been handicapped by lack of data from experiments in which the parameters are accurately known. The present concepts of swelling are based largely on data of this nature. In this study, uranium specimens with less than 0.01% impurity were irradiated below 300° C, and the swelling was induced by subsequent heat treatment outside the reactor where careful control of the temperature was possible. The results obtained by this technique were self-consistent but in considerable disagreement with the results of the in-pile investigations.

The density and porosity of irradiated uranium specimens were determined following pulse annealing in the alpha, beta and gamma phases. Both the light microscope and the electron microscope were used to study porosity. The results may be summarized as follows:

(1) Uranium specimens irradiated to 0.30% burn-up and heat-treated 75 h at temperatures less than 550° C in the α-phase swelled less than 1%.

(2) Uranium specimens (0.30% burn-up) heat-treated 75 h at temperatures between 550° C and 650° C in the α-phase swelled up to 18%. This swelling was due to bubbles with diameters up to 15μm. These results were diametrically opposed to recent data.

(3) Uranium specimens (0.30% burn-up) heat-treated 75 h at temperatures in the β-phase decreased their density by 4 - 5%. This decrease in density is apparently the result of grain-boundary cracking rather than bubble formation, as there is evidence to suggest that fission gas is retained in the matrix of the β-phase. These results suggest that a modification of the role of pressure and surface tension is required in the current theories of swelling.

(4) A uranium specimen (0.30% burn-up) heat-treated for 15 h in the γ-phase at 820° C swelled 20%. In this case the swelling was primarily due to the formation of bubbles in the vicinity of and on grain boundaries.

The explanation of these experimental results requires extensive modifications in previously suggested mechanisms of swelling; an alternative mechanism is therefore, presented.

GONFLEMENT DE L'URANIUM. Le mécanisme du gonflement de l'uranium irradié n'a pu être expliqué entièrement faute de données obtenues par des expériences dans lesquelles les paramètres étaient exactement connus. La notion actuelle de gonflement se fonde dans une large mesure sur des données de cette nature. Dans l'étude faite par l'auteur, des échantillons d'uranium à moins de 0,01% d'impuretés ont été irradiés à une température inférieure à 300° C; le gonflement a été provoqué par un traitement thermique ultérieur en dehors du réacteur, dans des conditions telles que la température pouvait être soigneusement contrôlée. Les résultats obtenus par cette méthode étaient tous concordants, mais ils différaient sensiblement des résultats des études sur le gonflement en pile.

La densité et la porosité des échantillons d'uranium irradié ont été déterminées après un recuit par impulsions dans les phases alpha, bêta et gamma. Pour l'étude de la porosité, l'auteur s'est servi à la fois du microscope orginaire et du microscope électronique. Les résultats obtenus peuvent se résumer comme suit :

1. Les échantillons d'uranium irradiés jusqu'à 0,30% et soumis à un traitement thermique pendant 75 heures, à des températures inférieures à 550° C en phase alpha, ont gonflé de moins de 1%.

2. Les échantillons d'uranium (taux de combustion de 0,30%) soumis à un traitement thermique pendant 75 heures à des températures comprises entre 550 et 650° C en phase alpha ont gonflé de 18%. Ce gonflement était dû à des bulles dont le diamètre atteignait 15 microns. Ces résultats sont diamétralement opposés aux données recueillies récemment.

3. Les échantillons d'uranium (taux de combustion de 0,30%) soumis à un traitement thermique pendant 75 heures à des températures de 700 et 740° C en phase bêta ont diminué de densité dans la proportion de 4 à 5%. Cette diminution de densité semble résulter d'une fissuration aux joints de grains et non de la formation de bulles; en effet, certains indices donnent à penser que le gaz de fission est retenu dans la matrice de la phase bêta. Ces résultats semblent indiquer que, dans les théories actuelles du gonflement, le rôle de la pression et de la tensfon superficielle est mal expliqué.

4. Un échantillon d'uranium (taux de combution de 0,30%) soumis à un traitement thermique pendant 15 heures en phase gamma à 820°C a gonflé de 20%. Dans ce cas, le gonflement était dû avant tout à la formation de bulles aux joints de grains et à proximité de ces joints.

Pour expliquer ces résultats, il faut modifier sensiblement les mécanismes de gonflement proposés. L'auteur présente donc un nouveau mécanisme.

РАЗБУХАНИЕ УРАНА. Понимание механизма разбухания облученного урана было затруднено из-за недостатка экспериментальных данных в отношении точно известных параметров. Существующие концепции разбухания основаны в значительной мере на данных этого характера. В этой работе образцы урана, содержащие менее 0,01 примесей, подверглись облучению при температуре ниже 300°С, а разбухание было достигнуто при последующей тепловой обработке вне реактора, чтобы можно было осуществить строгий контроль за температурой. Результаты, полученные с помощью этого метода, согласовывались между собой, но значительно расходились с результатами, полученными в реакторе.

Плотность и пористость облученных образцов урана была определена с помощью наблюдения за импульсом отжига в альфа-, бета-и гамма-фазах.

Для изучения пористости были использованы как обычные, так и электронные микроскопы. Результаты могут быть суммированы следующим образом:

1) Образцы урана, облученные при 0,30% выгорания и подвергнутые тепловой обработке в течение 75 часов при температурах меньших 550° в альфа-фазе, разбухали менее чем на 1%.

2) В образцах урана (0,30% выгорания), после тепловой обработки в течение 75 часов при температурах в диапазоне между 550°С и 650°С в альфа-фазе, разбухание происходило до 18%. Это разбухание вызывалось пузырьками, диаметрами до 15 мк. Эти результаты диаметрально противоположны данным, полученным за последнее время.

3) Образцы урана (0,30% выгорания), после тепловой обработки в течение 75 часов при температурах, соответствующих β-фазе, обнаружили уменьшение плотности на 4 - 5%. Это уменьшение плотности является, очевидно, результатом образования трещин на границах зерен, а не появления пузырьков, так как имеются данные, позволяющие предполагать, что газ деления удерживается в матрице β-фазы. Эти результаты указывают на то, что в существующих теориях разбухания требуется пересмотреть роль, которую придают давлению и поверхностному натяжению.

4) Образец урана (0,30% выгорания), подвергнутый тепловой обработке в γ-фазе в течение 15 часов при температуре 820°С, разбух на 20%. В этом случае разбухание вызывалось в первую очередь образованием пузырьков вблизи зерен и на их границах.

Объяснение этих экспериментальных результатов требует обширных модификаций ранее предложенных механизмов разбухания. Поэтому будет представлен альтернативный механизм.

CRECIMIENTO DEL URANIO. La falta de datos experimentales procedentes de ensayos cuyos parámetros se conozcan con toda precisión ha impedido que se adquiera una noción cabal del mecanismo causante del crecimiento que se observa en el uranio irradiado. Los conceptos actuales acerca de ese crecimiento se basan en gran parte en datos de la índole mencionada. Para efectuar el presente estudio, se irradiaron muestras de uranio con menos de 0,01 por ciento de impurezas, a temperaturas inferiores de 300° C, provocándose el crecimiento térmico subsiguiente realizado fuera del reactor, en condiciones que permitían regular cuidadosamente la temperatura. Si bien los resultados obtenidos aplicando esta técnica son coherentes, distan mucho de coincidir con los resultados de las investigaciones realizadas en el interior del reactor.

Se determinó la densidad y la porosidad de las muestras de uranio irradiadas, después de un recocido cíclico, en las fases alfa, beta y gamma. Para estudiar la porosidad, se recurrió al microscopio óptico y al microscopio electrónico. A continuación se resumen los resultados obtenidos:

1) Las muestras de uranio irradiadas hasta alcanzar un grado de combustión de 0,30 por ciento y tratadas térmicamente durante 75 horas a temperaturas inferiores a los 550° C, en fase alfa, sufrieron un crecimiento inferior al 1 por ciento.

2) En las muestras de uranio (grado de combustión: 0,30 por ciento) tratadas térmicamente durante 75 horas a temperaturas comprendidas entre 550° C y 650° C, en fase alfa, el crecimiento alcanzó a 18 por ciento. El fenómeno fue causado por burbujas de diámetros hasta 15μ. Estos resultados están en franca contradicción con algunos datos recientemente publicados.

3) En muestras de uranio (grado de combustión: 0,30 por ciento) tratadas térmicamente durante 75 horas a temperaturas correspondientes a la fase beta, se observó una disminución de densidad de 4 a 5 por ciento.

Esta disminución se debe, al parecer, al agrietamiento en los bordes del grano, más que a la formación de burbujas, ya que hay pruebas de que los gases de fisión quedan retenidos en la matriz de la fase beta. Estos resultados sugieren que es preciso modificar los papeles atribuidos a la presión y a la tensión superficial en las teorías en boga acerca del crecimiento.

4) En una muestra de uranio (grado de combustión: 0,30 por ciento) tratada térmicamente durante 15 horas en fase gamma, a 820°C, se observó un crecimiento de 20 por ciento. En este caso, el crecimiento se debe primordialmente a la formación de burbujas en la proximidad de los bordes del grano y en los bordes mismos.

Para explicar estos resultados experimentales, es preciso introducir importantes modificaciones en las teorías anteriormente expuestas acerca del mecanismo del crecimiento y, por lo tanto, el autor propondrá una nueva hipótesis basada en un mecanismo diferente.

1. INTRODUCTION

The density of uranium decreases during neutron irradiation or during annealing after irradiation. This phenomenon is called swelling. The decrease in density is due to the presence of bubbles, to the presence of cracks, and to the presence of fission products within the uranium. The bubbles are believed to result from the agglomeration of the fission product atoms, krypton and xenon.

The mechanism of bubble formation and growth, and the influence of certain factors on the magnitude of the swelling in irradiated uranium are still a subject of speculative comment. Homogeneous nucleation of bubbles [1], nucleation on dislocations [1], and nucleation on undersize and oversize atoms [2] have been considered by various investigators. It has been suggested that the bubbles grow by vacancy diffusion [1], by creep of the surrounding matrix [3], and by plastic yielding in addition to the creep processes [4]. Some of the factors suggested as influencing the magnitude of swelling are temperature, extent of burn-up, time of burn-up, and the presence of second phases [5].

Much of the previous experimental evidence for swelling in uranium has been obtained with material containing appreciable quantities of impurity and under experimental conditions which were not precisely defined. So that more precise control could be obtained over the experimental conditions under which swelling occurred, specimens of uranium, previously irradiated at a temperature too low for swelling, were heat-treated at various temperatures to produce changes in their density and microstructure. The data from the annealing experiments and from the microstructure examinations were used to evaluate qualitatively some of the factors which influenced the magnitude of swelling and to discuss the mechanisms of swelling.

2. EXPERIMENTAL MATERIALS AND PROCEDURE

A casting of uranium was prepared by melting the uranium in an evacuated induction-furnace and pouring it into a water-cooled copper mould. The casting was extruded to an 83% reduction in the cross-section area. The extruded uranium was then heat-treated at 725°C for 10 min and water quenched. This material was further annealed at 620°C for 1 h and then cooled to the ambient temperature. The uranium contained less than 0.01 at.% total impurity.

Specimens, 0.635 cm in diameter and 1.270 cm in length, were cut from the heat-treated uranium for insertion in stainless-steel irradiation capsules. Eight specimens were loaded with minimum clearances in a capsule and sealed in a helium atmosphere.

The capsules with specimens were irradiated in the Materials Test Reactor* at an estimated central metal-temperature of 275°C. After irradiation the specimens were removed from the capsule by parting the capsule wall along its length.

The irradiated specimens were annealed in a tantalum cup which was suspended in an Inconel tube. The Inconel tube was evacuated to 0.01 μm pressure and was heated by a resistance furnace. The temperature of the specimens was determined with a Chromel-Alumel thermocouple in the tantalum cup. The thermocouple was about 1 cm from the specimens. The calibration of the thermocouple was determined before and after the annealing experiments. The specimens were heated to and cooled from the annealing temperature at a rate of 4°C/min. The temperature was controlled to ±0.5°C during annealing.

The density of the irradiated specimens was determined after each annealing treatment. The amount of swelling was then expressed as the ratio of the change in density on annealing to the density of the specimen after irradiation. The density was obtained by weighing the specimens in air and in carbon tetrachloride. The weight of the specimens was determined using an analytical balance which was capable of weighing with a precision of 0.05 mg. The temperature of the carbon tetrachloride was remotely measured with a calibrated thermistor. The thermistor was placed 0.6 cm from the specimen and could detect temperature changes of 0.01°C. Prior to taking a weight measurement in the carbon tetrachloride, the specimen was immersed for a period of between 30 min and 2 h. The elapsed time depended on the amount of beta and gamma heating of the liquid by the specimen and on the amount the specimen had swelled. The maximum deviation of the density values from an average value for a specimen was ±0.02 g/cm^3.

The evolution of any radioactive fission gases on annealing could be determined by adsorbing the gases on activated charcoal cooled with liquid nitrogen. The activity of the adsorbed gases was continuously monitored by an end-window Geiger counter.

On completion of the annealing treatments, the specimens were cut into two pieces. One piece was submitted for a determination of the number of fissions which had occurred in the sample. The other piece of a specimen was ground on silicon carbide and polished with 3 and 1 μm-diamond paste. Worked metal which was formed on the specimens during the diamond-paste polishing was removed by electrolytic polishing in a solution containing five parts of orthophosphoric acid, five parts of ethylene glycol, and eight parts of ethyl alcohol and at a current density of 30 mA/cm^2 for 2 min. Cathodic etching was used as the final preparation of the polished specimens for an examination of their microstructure. The cathodic etching was done in an argon atmosphere and at a current density of about 0.3 mA/cm^2(at 4 kV) for 20 min. The argon pressure in the aparatus was 20 μm, and the specimen

* National Reactor Testing Station, Idaho Falls, USA.

was cooled during etching by conducting the heat away through an aluminium tube containing iced water.

The microstructure of the etched specimens (magnifying up to 500 diam.) was examined in an optical microscope shielded from beta and gamma radiation. For the examination of the microstructures at higher magnifications, the specimens were copied with cellulose acetate, shadowed with 80 wt.% Pt - 20 wt.% Pd alloy, and backed with carbon. The carbon-negative replicas were examined in an electron microscope.

The exposure of the specimens to the neutron flux in the reactor was reported in terms of the fraction of all atoms which had undergone fission or, expressed more briefly, at.% burn-up. The burn-up was determined from an analysis of the irradiated specimens for the fission product Cs^{137} and uranium-isotope composition.

3. EXPERIMENTAL RESULTS

The percentage decrease in density of irradiated uranium specimens after annealing at various temperatures is shown in Figs. 1 and 2. In Fig. 1, the percentage decrease in density is plotted against the annealing time for specimens annealed at the temperature indicated in the key. Each curve represents the accumulated percentage decrease in density of an individual specimen, and each point on a curve represents the total accumulated time that the specimen was held at the temperature. The annealing time does not include the time required for the specimen to heat to or cool from the annealing temperature for a density determination. In Fig. 2 the percentage decrease in density is plotted against the annealing temperature for various periods of annealing time. These curves were constructed from those in Fig. 1 by selecting the indicated annealing times.

Porosity with a diameter greater than 0.06 μm was almost non-existent in the uranium before irradiation or after irradiation to about 0.30 at.% burn-up. However, pores with a diameter between 0.02 and 0.06 μm and a concentration of approximately $10^{10}/cm^2$ were visible in both the unirradiated and the irradiated uranium. Also, no cracks were visible in the microstructure of the irradiated uranium even though the grains appeared severely distorted (Fig. 3). It was not possible to arrive at an average grain diameter in irradiated specimens because of the distortion of the grains, but the average grain diameter in the unirradiated uranium was about 60 μm. After annealing irradiated uranium at temperatures between 450 and 650°C in the alpha phase, it was observed that bubbles with a diameter greater than 0.06 μm formed on grain boundaries primarily, and also at preferential sites within the grains. For specimens which were annealed at temperatures below 550°C, it appeared that the bubbles were formed on grain boundaries or sub-grain boundaries which were present in the as-irradiated uranium. The density of these specimens decreased by less than 1% on annealing for up to 75 h. However, in specimens which were annealed at 593 and 618°C, it appeared that the bubbles were formed on grain boundaries of recrystallized material and the density of these specimens decreased to 9.75% and about 18%, respectively, on annealing for up to 75 h.

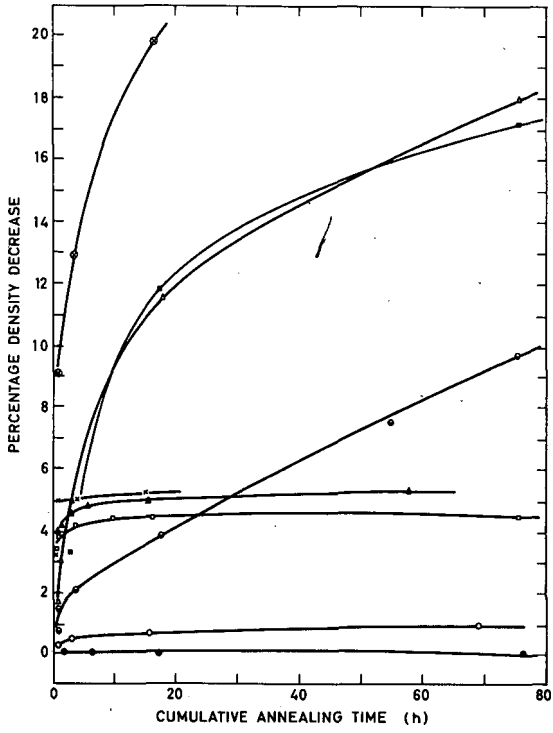


Fig.1

The effect of annealing on the swelling of irradiated uranium
(a single specimen annealed at each temperature)

●	463°C (0.29 at.% burn-up)	x	651°C (0.30 at.% burn-up)
○	548°C (0.30 at.% burn-up)	▲	700°C (0.27 at.% burn-up)
◒	593°C (0.28 at.% burn-up)	□	740°C (0.25 at.% burn-up)
■	618°C (0.24 at.% burn-up)	◉	822°C (0.24 at.% burn-up)
△	618°C (0.27 at.% burn-up)		

The microstructure of a uranium specimen annealed at 548°C for 69 h is shown in Fig. 4. The largest pores in this specimen had a diameter about 0.1 μm. The microstructure of a uranium specimen annealed at 618°C for 75 h is shown in Fig. 5. The specimen appeared to be about 75% recrystallized and the diameter of the grains was about 6 μm. Pores with diameters up to 2.5 μm and a concentration of approximately $3 \times 10^7/cm^2$ were visible in the recrystallized areas. A few pores, with diameters greater than 2.5 μm and up to 15 μm, were also visible. In those areas which were not recrystallized, numerous pores with diameters of between 0.02 and 0.06 μm appeared to be present (see Fig. 6), and relatively few larger-diameter pores were visible. Cracks were almost non-existent in specimens annealed at temperatures up to 650°C.

Extensive cracking along grain boundaries occurred in irradiated-uranium specimens annealed at 700 and 740°C in the beta phase and the porosity was

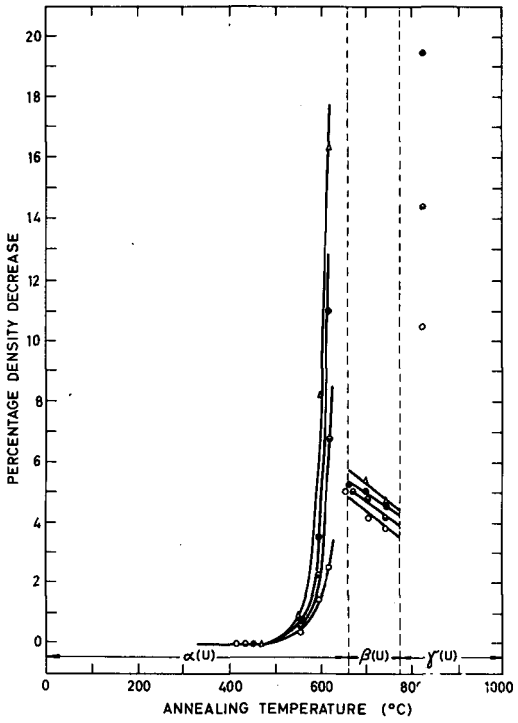


Fig. 2

The effect of annealing temperature on the swelling of irradiated uranium

○ annealed 1 h ● annealed 15 h
◒ annealed 5 h △ annealed 60 h



Fig. 3

Deformed structure in uranium after irradiation to 0.30 at.% burn-up at about 275°C

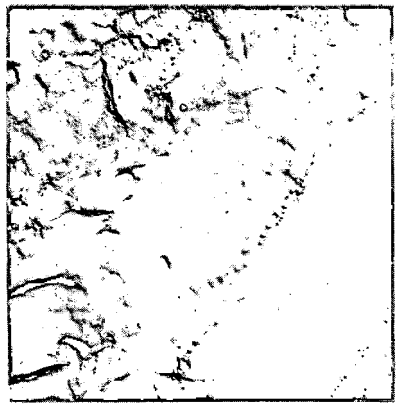


Fig. 4

Porosity in uranium irradiated to 0.30 at.% burn-up and annealed for 69 h at 548°C



Fig. 5

Recrystallized structure and porosity in uranium irradiated to 0.24 at.% burn-up and annealed for 75 h at 618°C

uniformly distributed, in contrast to specimens annealed in the alpha phase. The decrease in density of these specimens was about 5% on annealing up to 75 h. The maximum diameter of the pores observed in specimens annealed in the beta phase was 1.3 μm. The diameter of the pores, adjacent to the cracks or along grain boundaries which were not cracked, did not appear substantially greater than the diameter of pores within the grains. The diameter and distribution of porosity as well as the amount of cracking was essentially the same for specimens annealed for 30 min or up to 75 h at

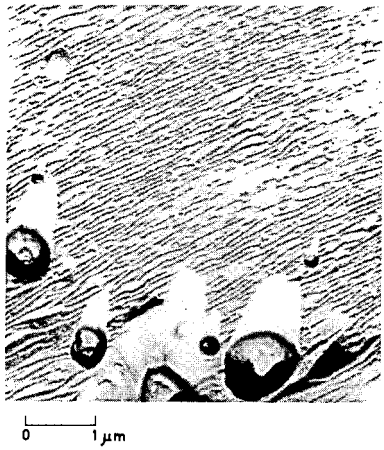


Fig. 6

Areas of large- and small-diameter porosity in uranium irradiated to 0.27 at.% burn-up and annealed for 75 h at 618°C

temperatures in the beta phase. The microstructure of a uranium specimen annealed for 30 min at 670°C in the beta phase is shown in Fig. 7. The diameter of the grains after heat treatment in the beta phase was greater than 30 μm, estimated from the location of the cracks. Even though the specimen annealed at 651°C was heated at a temperature which should have been in the alpha phase, it had a microstructure after annealing similar to specimens annealed in the beta phase, and the specimen decreased in density in a manner similar to specimens annealed at 700 and 740°C (see Fig. 1).

Pores with a diameter of up to 20 μm were present in the irradiated uranium specimen which was annealed at 822°C for 16 h in the gamma phase. The microstructure of the specimen after this heat treatment is shown in Fig. 8. The majority of the elongated pores visible in this photomicrograph were due to bubbles joining up rather than to cracks forming. The diameter of the porosity decreased with increased distance from the grain boundaries. There were numerous cracks visible in the microstructure of this specimen but cracking was not so extensive as for specimens annealed in the beta phase. The decrease in density of this specimen was 19.86%.

No detectable amount of radioactive fission-product gas was released from the irradiated specimens during the annealing experiments. This result is dependent on the sensitivity of the apparatus. However, evolution of radioactive fission gas was readily detected in the annealing of other irradiated materials with this same apparatus. Hence, the amount of gas released from the uranium specimens on annealing must have been extremely small.

4. DISCUSSION OF RESULTS

Uranium which had been irradiated at about 275°C to approximately 0.3 at.% burn-up decreased in density 1% or less on annealing for up to 75 h

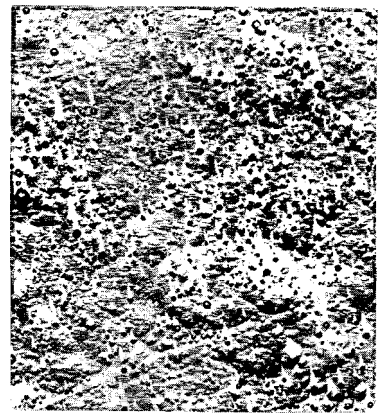


Fig. 7

Porosity in uranium irradiated to 0.28 at.% burn-up and annealed for 30 min at 670°C



Fig. 8

Porosity in uranium irradiated to 0.24 at.% burn-up and annealed for 16 h at 822°C

at temperatures less than 550°C. Above this temperature and up to the alpha-beta transformation temperature, the magnitude of swelling increased sharply with increasing temperature, as did the rate of swelling at a given temperature. These results were opposite to the data obtained by other investigators [5]. These investigators have reported that when uranium is irradiated to about 0.3 at.% burn-up at temperatures below about 300°C and subsequently annealed at temperatures in the alpha phase, the increase in volume is only of the order of 1%. In the present investigation, uranium

specimens which were irradiated under similar conditions increased in volume up to about 18% when annealed at high temperatures in the alpha phase.

This pronounced increase in the amount of swelling at about 600°C was believed to be the result of the formation of numerous bubbles with diameters up to 2.5 μm in areas which had recrystallized producing grains about 6-μm diam. The bubbles were nucleated primarily at sites along the grain boundaries and at sites of an unknown nature within the grains. The bubbles were nucleated probably as a result of diffusion of the krypton and xenon fission-product atoms to these sites. It was not fully understood why bubbles with diameters up to 2.5 μm were not able to form in the un-recrystallized areas. The pores, with diameters between 0.02 and 0.06 μm visible in the un-recrystallized areas and in the as-irradiated material as well, may have represented dislocation lines which were decorated by the krypton and xenon atoms. The swelling rate decreased, after its high initial rate, in specimens annealed at temperatures of 593 and 618°C (see Fig. 1). This was believed to be the result of the specimens approaching complete recrystallization and to the recrystallized areas becoming satiated with bubbles.

Some investigators of the swelling phenomenon have suggested that the gas pressure in bubbles was largely balanced by surface-tension forces [1, 5] and this balance was maintained by the diffusion of vacancies to the bubbles. It was consequently suggested that this balance between gas pressure and the restraining forces of the surface-tension could explain why the volume increase for a given burn-up did not rise rapidly with increase in temperature in the range 450-650°C. The surface-tension forces would not be expected to change appreciably in this temperature range. Alternatively, some investigators have suggested that creep in the matrix [3] or plastic yielding in addition to the creep process [4] governed the rate of growth of gas-filled bubbles. In this model it was assumed that the fission-product gas was distributed in bubbles and the gas pressure was balanced by the stress in the uranium matrix. In this investigation density decreases of up to 18% occurred in specimens annealed at temperatures below 650°C. Hence, the results of this investigation did not show whether the surface-tension forces and/or the strength of the uranium prevented excessive growth of the gas-filled bubbles.

A relatively low carbon content of about 0.0017 at. % in the specimens annealed in the alpha phase may have been indirectly important in determining the magnitude of swelling. The recrystallization temperature would be expected to be influenced by the amount of carbon in the uranium. It has been determined in conjunction with this investigation that uranium containing 0.11 at. % carbon and irradiated to 0.34 at. % burn-up decreased in density by only 6.51% when annealed at 620°C for 75 h. It may be that for uranium containing 0.11 at. % carbon a temperature higher than 620°C is required for recrystallization, whereby numerous small bubbles could form on the boundaries of small grains.

Cracks along grain boundaries in specimens annealed at temperatures of 700 and 740°C in the beta phase caused some of the swelling. The cracks were probably formed as a result of the allotropic transformation stresses. The largest pores observed in the microstructure of these specimens had a diameter of 1.3 μm. The number of cracks along grain boundaries and the

diameter of the bubbles within the grains were not appreciably changed after the first 30 min of annealing. Thus the pores in the specimens may have been formed on heating up to the annealing temperature in the beta phase. These observations were in agreement with the measured percentage density changes of the specimens (see Fig. 1). The absence of pores with a diameter larger than the pores observed in the microstructure of specimens annealed for 75 h at 618°C was possibly due to the higher yield strength and the large grain size of beta uranium. The unexpectedly low swelling of the specimen annealed at 651°C was probably due to a lowering of the alpha-beta transformation temperature. The lowering of the transformation temperature could have been due to the presence of fission products.

Pores with diameters up to 20 μm were visible in and along the grain boundaries of the specimen annealed for 16 h at 822°C. The diameter of the bubbles decreased with an increasing distance from the grain boundaries. The low yield strength of gamma uranium and the diffusion of vacancies from the grain boundaries to bubbles were possibly responsible for the distribution of bubble sizes. Upon first heating the specimen into the gamma phase, the appearance of the microstructure was presumably similar to that shown in Fig. 7, since the specimen was in the beta phase for about 30 min. If it is assumed that all of the krypton and xenon gas were in bubbles on heating the specimen into the gamma phase, then it is unlikely that the gas atoms would redissolve and diffuse to the vicinity of the grain boundaries to form enlarged bubbles. Hence, the enlarged bubbles on and adjacent to the grain boundaries may have been due to the diffusion of vacancies from the grain boundary source. The elongated bubbles resulted from the join up of bubbles and in some instances probably from the filling of cracks with fission gas.

5. CONCLUSIONS

(1) Uranium irradiated to about 0.30 at. % burn-up swelled (or decreased in density) on post-irradiation annealing. The amount of swelling did not increase proportionately with increasing annealing temperature. A pronounced increase in the amount of swelling began at about 600°C. This was followed by disproportionately low swelling of specimens annealed at temperatures between 650 and 740°C in the beta phase. Finally, a specimen which was annealed at 822°C in the gamma phase swelled more than specimens annealed at lower temperatures.

(2) The pronounced increase in the amount of swelling at about 600°C may have been the indirect result of recrystallization of the as-irradiated material. Numerous bubbles with diameters up to 2.5 μm were formed primarily on the grain boundaries, and also within the grains. The swelling of uranium specimens which were annealed between 650 and 740°C in the beta phase was due to cracking along grain boundaries and to bubbles with diameters up to 1.3 μm. The swelling of a uranium specimen annealed at 822°C in the gamma phase was due to the formation of bubbles with diameters up to 20 μm, primarily on or adjacent to grain boundaries, and to cracking along grain boundaries.

(3) The rate of swelling was highest during the first few hours of annealing of all specimens; it then decreased. For example, the swelling

rate was reduced to such an extent in the case of uranium specimens annealed between 650 and 740°C, that after the first 5 h of annealing the density decreased less than 1% on further annealing for periods up to 75 h.

ACKNOWLEDGEMENTS

The author is indebted to Mr. D.W. Pracht for assistance in the performance of the experiments. The author also wishes to thank Drs. H.H. Chiswik, T.H. Blewitt, and R.K. Hart for many helpful discussions. This paper is based on work performed under the auspices of the US Atomic Energy Commission.

REFERENCES

[1] GREENWOOD, G.W., FOREMAN, A.J.E. and RIMMER, D.E., J. nucl. Mat. 1 (1959) 305.
[2] BRINKMAN, J.A., Nucl. Metallurgy VI (1959) 1.
[3] FOREMAN, A.J.E., AERE Rpt. T/M 134 (1956).
[4] ENDERBY, J.A., U.K.A.E.A. Rpt. IGR-R/R 198 (1956).
[5] PUGH, S.F., J. nucl. Mat. 4 (1961) 177.

DIMENSIONAL STABILITY OF URANIUM UNDER IRRADIATION

J.H. GITTUS, V.W. ELDRED, A. STUTTARD, G. SLATTERY AND F. CHATTERLEY
U.K.A.E.A. REACTOR GROUP LABORATORIES,
SPRINGFIELDS, LANCS. AND WINDSCALE, CUMBERLAND, ENGLAND

Abstract — Résumé — Аннотация — Resumen

DIMENSIONAL STABILITY OF URANIUM UNDER IRRADIATION. The practical importance of irradiation-induced dimensional changes is outlined, and the several mechanisms leading to dimensional instability are summarized.

Changes in volume occur, attributable to the accumulation of solid and gaseous fission products and to phase changes.

Changes in shape, such as the accentuation of bow in vertically stacked uranium fuel rods, are ascribed mainly to irradiation-induced creep. Theories seeking to explain the phenomenon are reviewed, as are the laws which appear to govern irradiation creep, isothermal creep and thermal-cycling creep.

Changes in length, partly due to the presence of preferred orientation in the fuel rod have been observed and compared with physical measurements of the type of orientation present. These measurements are catalogued for a variety of uranium fuels. Methods of producing fuel of controlled texture are postulated and tested.

ÉTUDE SUR LA STABILITÉ DES DIMENSIONS DES CARTOUCHES D'URANIUM SOUS L'EFFET DES RAYONNEMENTS. Les auteurs montrent brièvement l'importance pratique des changements de dimensions que l'uranium subit sous irradiation et décrivent les grandes lignes des divers mécanismes qui peuvent provoquer cette instabilité.

Les modifications du volume sont dues à l'accumulation des produits de fission gazeux et solides ainsi qu'aux changements de phase.

Les changements de forme tels que l'accentuation de la flèche des cartouches d'uranium disposées verticalement sont attribués essentiellement au fluage radioinduit. Les auteurs examinent les théories pouvant expliquer le phénomène, ainsi que les lois qui semblent régir le fluage radioinduit, le fluage isothermique et le fluage cyclothermique.

Les changements de longueur, dus en partie à la présence d'une orientation privilégiée dans la cartouche de combustible, ont été observés et comparés aux mesures du type d'orientation. Les auteurs ont établi un répertoire de ces mesures pour un certain nombre de combustibles d'uranium. Ils ont conçu et essayé des procédés de production permettant d'obtenir des combustibles de texture prédéterminée.

ПРОСТРАНСТВЕННАЯ УСТОЙЧИВОСТЬ УРАНА ПОД ДЕЙСТВИЕМ ОБЛУЧЕНИЯ. Описывается практическое знание наведенных облучением пространственных изменений и дается сводка различных процессов, ведущих к пространственной неустойчивости.

Происходящие изменения объема объясняются накоплением твердых и газообразных продуктов деления и фазовыми изменениями.

Изменения формы, как, например, усиление прогиба вертикально установленных урановых топливных стержней, приписываются главным образом наведенной облучением ползучести. Описываются теории, пытающиеся объяснить это явление, а также законы, определяющие, по-видимому, как наведенную облучением ползучесть, так и ползучесть изотермическую и термически-циклическую.

Были произведены наблюдения над изменением длины, частично вызываемом наличием предпочтительной ориентировки в тепловыделяющих стержнях, и результаты были сопоставлены с физическими измерениями в зависимости от типа имеющейся ориентировки. Составлены таблицы результатов этих измерений для целого ряда урановых топливных материалов. Предлагаются и испытываются методы производства топливных элементов с определенным заданным строением.

ESTABILIDAD DIMENSIONAL DEL URANIO IRRADIADO. La memoria describe someramente la importancia práctica de las alteraciones dimensionales radioinducidas en el uranio y los diversos mecanismos que producen inestabilidad dimensional.

Las alteraciones de volumen observadas pueden atribuirse a la acumulación de productos de fisión sólidos y gaseosos y a cambios de fase.

Las modificaciones de forma tales como la acentuación de la curvatura de las barras combustibles de uranio dispuestas verticalmente se adscriben principalmente a la fluencia radioinducida. La memoria revisa teorías que tratan de explicar ese fenómeno, así como las leyes relativas a la fluencia bajo irradiación, fluencia isotérmica y fluencia debida al ciclado térmico.

Se han observado alteraciones de longitud, debidas en parte a la presencia de orientaciones preferentes en las barras de combustible; los resultados se comparan con las mediciones físicas del grado de orientación. Estas mediciones se han catalogado para toda una serie de combustibles de uranio. La memoria propone y analiza diversos métodos para obtener combustibles de la contextura deseada.

1. INTRODUCTION

Changes in the dimensions of fuel rods during irradiation are undesirable since they can result in rupture of the cladding, deformation of the heat transfer surface and interference between the element and the channel. A comprehensive programme of work designed to identify dimensionally stable fuel-rods for use in the Calder Hall, Chapelcross and CEGB reactors has been successfully implemented and some of the data so derived are presented in the present paper.

Two causes of these irradiation-induced dimensional changes can be identified: fission-product formation and anisotropic growth of individual grains. The distortion produced by fission products is isotopic and takes the form of an increase in volume. Both solid and gaseous fission products contribute, the latter tending to accumulate in pockets and bubbles. The growth phenomenon arises from a tendency for expansion in the [010] direction and contraction in the [100] direction when a single alpha-uranium crystal is irradiated. As a result, textured polycrystalline fuel rods will change shape under irradiation. In addition, the restraint imposed upon the anisotropic deformation of each grain by its neighbours generates internal stresses which increase the creep rate produced by external forces.

2. VOLUME CHANGES

If the fission products that accumulate in uranium during irradiation remain in solution in the metal lattice, an increase in volume of only 0.3% per 1000 MWd/t is expected. The inert fission-product gases, xenon and krypton, tend, however, to precipitate and the bubbles so formed are primarily responsible for the swelling observed at constant temperatures in the alpha phase.

The observed percentage increase in volume (Δv) of Calder Hall fuel rods on irradiation to B MWd/t is given approximately (Fig. 1) by

$$\Delta v = 10^{-3} B.$$

The scatter in the results is almost entirely attributable to experimental errors involved in determining the densities of complete rods before and after irradiation. For a given irradiation level, the volume changes do not

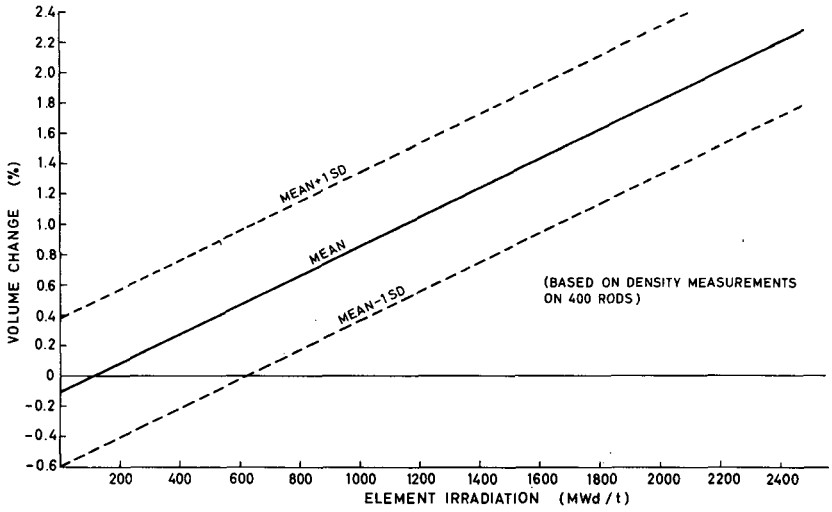


Fig. 1

Volume change in normal production Springfield's uranium rods irradiated at Calder Hall

differ significantly from one channel position to another (i.e. there is no detectable dependence of swelling on temperature or rating in the range concerned). Metallographic examination of these elements with an optical microscope has not revealed any cracking or porosity which has developed during irradiation, but numerous bubbles, small enough to be controlled by surface tension alone, have been detected with an electron microscope.

For swelling due primarily to the growth of gas bubbles controlled by surface tension forces a relationship of the form

$$\Delta v = KB^{\frac{3}{2}} + 2.4 \times 10^{-4}\ B$$

is expected, where K is a constant depending on the size and number of the bubbles, the temperature and the surface tension of uranium metal, and the second term is to allow for the effects of fission products (other than xenon and krypton) in solution. Because of the scatter involved in the data, it is not possible to distinguish between this and a linear relationship between swelling and burn-up. A value for K of 1.7×10^{-5} is, however, consistent with the measured change in volume and with the apparent size and distribution of bubbles. Little temperature dependence is to be expected for bubbles of the size observed; none has in fact been detected.

3. CREEP

The isothermal creep rate of uranium and of alpha-phase uranium alloys is increased by thermal cycling and by neutron irradiation. Vertically-stacked uranium fuel rods in a reactor are subject to both effects; the resultant creep process causes them to bow and shorten under the weight of the super-

posed elements. Bowing is the more undesirable effect since it can lead to contact with the channel wall and consequent localized over-heating. Excessive bowing may render discharge difficult. Thermal, thermal-cycling and irradiation-induced creeps have all been subject of separate experimental studies, the results of which have proved amenable to mathematical summarization.

Isothermal creep

The secondary creep rate $\dot{\epsilon}$ has been found [1] to conform to the relationship

$$\dot{\epsilon} = \sigma^n \exp [A + (B/T)],$$

where σ is the stress and T is the absolute temperature. n, A and B are constants having the best values 2.61, -0.824 and -23 400 for Calder Hall uranium. The accuracy of this relationship is illustrated in Fig. 2.

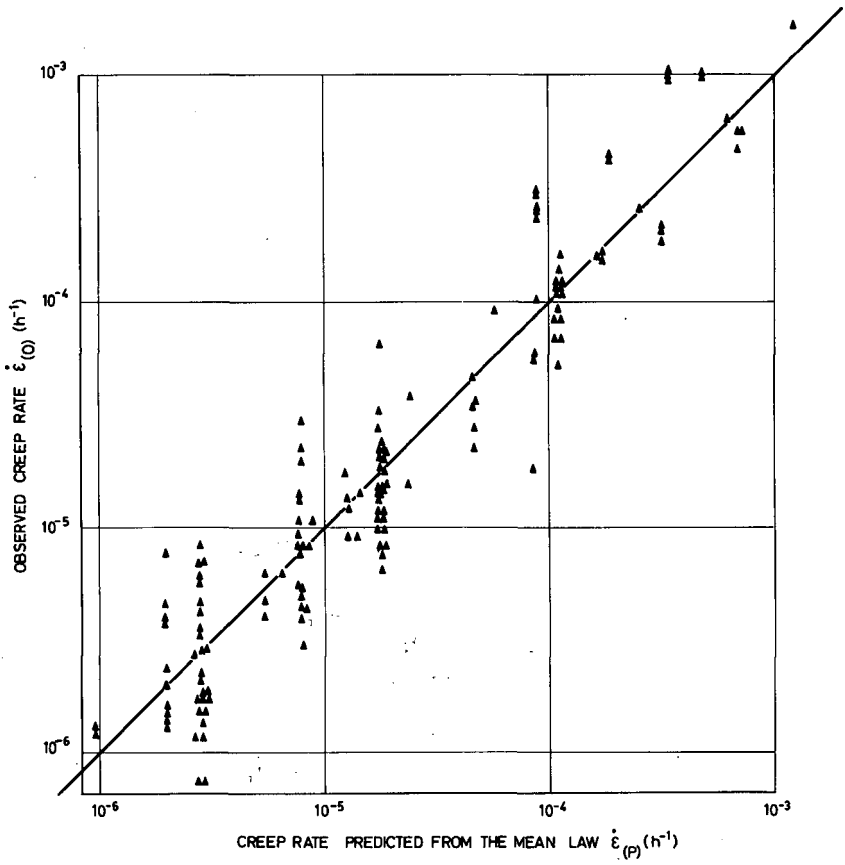


Fig. 2

Isothermal creep of alpha uranium

Thermal-cycling creep

Internal strains are produced by the conflicting, anisotropic expansion and contraction of neighbouring alpha grains when uranium is subjected to thermal cycling. Under external stress, a resolved macroscopic component of the strain produced by thermal cycling appears, supplementing the strain due to conventional thermal creep. Continuous rapid cycling of amplitude

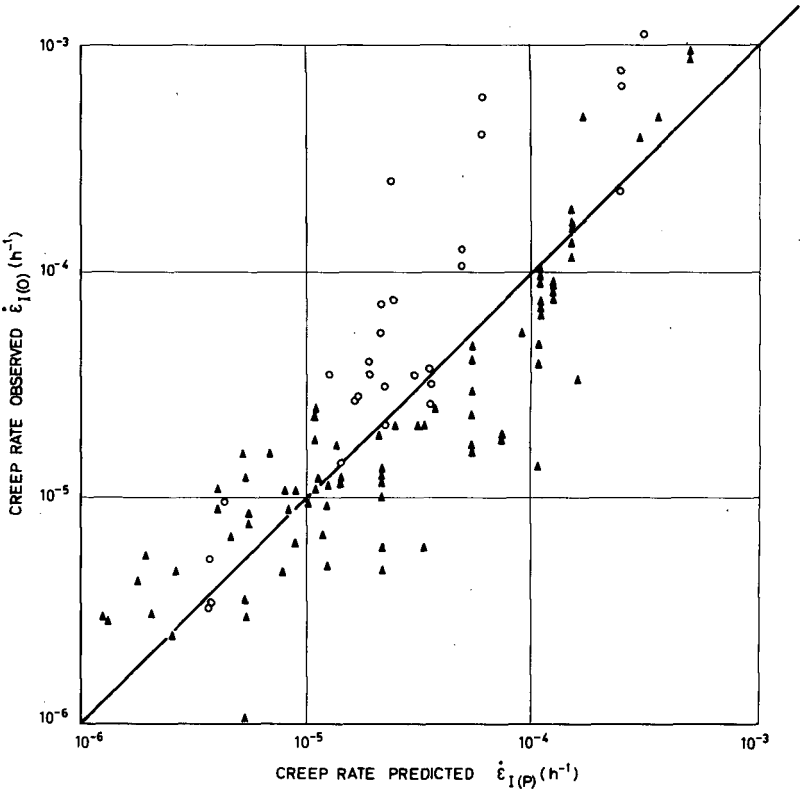


Fig. 3

Continuous thermal-cycling creep of alpha-uranium
(▲ creep results for which simple creep law is valid)

T deg C produces a secondary creep rate, which is well represented (Fig. 3 [1]) by the expression

$$\dot{\epsilon}_i = f(n)\ (\Delta T\, I_i)^{n-1} \sigma\ \exp\,[A + (B/T)],$$

where I_i is the internal stress produced by a ± 1 deg C cycle, n, A and B have the same values as before and f(n) is a constant nearly equal to unity. It may be noted that discrete cycles of large amplitude can individually produce increments of plastic strain.

Irradiation creep

Irradiation produces anisotropic internal strains comparable to those produced by thermal cycling and creep is again accelerated. The expression

$$\dot{\epsilon} = \dot{\epsilon}_g K\sigma / Y$$

has been deduced to apply where Y is the yield stress [2], $\dot{\epsilon}_g$ is the rate of single crystal [010] irradiation growth, K is a constant near to unity and σ is the applied macroscopic stress, all at the prevailing temperature.

Bowing

Considerations of the type listed above allow the problem of bowing to be examined analytically. It can be shown that the central deflection Z should be related to the initial deflection Z_0 by the expression

$$\log \frac{Z}{Z_0} = \frac{4PL^2}{\pi^3 a^4} \int_0^t \frac{dt}{\bar{E}},$$

where P is the end load, L is the free length, $\bar{E}$ is the creep modulus or stress needed to produce unit strain rate, t is the elapsed time and a is the radius.

If braces are attached to the centre of the element to minimize bow, then bowing of the unbraced regions should conform to the modified expression:

$$\log Z = \frac{4PL^2}{\pi^3 a^4} \int_0^t \frac{dt}{\bar{E}} + \text{constant}.$$

TABLE I

CREEP OF SPRINGFIELDS URANIUM

Cartridge position	Uranium temperature (°C)	Rating (MW/t)	Observed in-pile creep modulus ($\bar{E}$) (kg/m² per MW d/t	Calculated creep modulus for ± 5 deg C thermal cycles (kg/m²)
6	375	1.4	2.5×10^{10}	27000×10^{10}
5	416	2.4	large $\times 10^{10}$	55×10^{10}
4	423	2.9	140×10^{10}	43×10^{10}
3	401	3.0	4.4×10^{10}	150×10^{10}
2	344	2.6	2.4×10^{10}	39000×10^{10}
1	259	1.7	2.5×10^{10}	$(1.8 \times 10^6) \times 10^{10}$

Average creep moduli ($\bar{E}$), calculated by substituting measured values of Z into the expression, are given in Table I, indicating the increase produced by increasing temperature.

Evidently thermal and thermal-cycling creep have little effect on bowing in such a reactor, a conclusion which is supported by the behaviour of the hotter elements (Table I) and by the out-of-pile creep data. The Calder Hall reactors are base load stations and little thermal cycling occurs. Reactors designed for load following or shift operation will impose thermal cycles on the fuel rods and the contribution to bowing can be deduced from out-of-pile thermal-cycling creep data. Thus the final column of Table I shows what would be expected to happen to $\bar{E}$ if the elements in question had been subjected to a ± 5 deg C thermal cycle.

4. IRRADIATION-INDUCED ANISOTROPIC GROWTH

The [010] extension (and the equal [100] contraction) produced by the irradiation of a single alpha-uranium crystal is defined by $L = L_0 \exp(G f)$ (where L is the length measured along [010] after a fraction f of all the atoms has been fissioned, and L_0 is the original length). BUCKLEY [3] shows that at -196°C, G = 11 500 falling to 1200 at +75°C and, probably, to zero at about 500°C. He deduced a mechanism depending on the production of widely spaced groups of point defects in the displacement spikes. Thermal spike stresses are presumed to cause the vacancies to condense on one set of lattice planes and the interstitials on another. Thermally-activated mutual annihilation of the point defects is invoked as the source of temperature-dependent growth. A consequence of this phenomenon is the anisotropic growth, under irradiation, of textured fuel rods. Unlike irradiation creep (although both phenomena are attributed to the same cause), irradiation growth occurs in the absence of external load. If excessive, it can rupture the cladding surrounding the fuel rod and efforts have therefore been made to minimize it by eliminating texture.

The measurement of texture

X-ray diffraction, neutron diffraction, thermal expansivity, electrical resistivity and elasticity measurements are amongst the methods which have been adopted for the estimation of texture in uranium fuel rods. The techniques are described in this section and some results are given in the next section. The object is to derive growth indices which predict the expected irradiation-growth as a fraction of the [010] single crystal growth.

X-ray diffraction. Inverse pole figures and pole figures have been found too insensitive for the representation of diffraction data for specimens having relatively little texture and they have been superseded by a growth index (G_x) developed from the work of MORRIS [4] and STURCKEN [5].

A computer programme has been written to derive from the expression:

$$G_x = \int_0^1 \int_0^{\pi/2} P(u, \phi)(1-u^2)\cos^2\phi \, d\phi \, du,$$

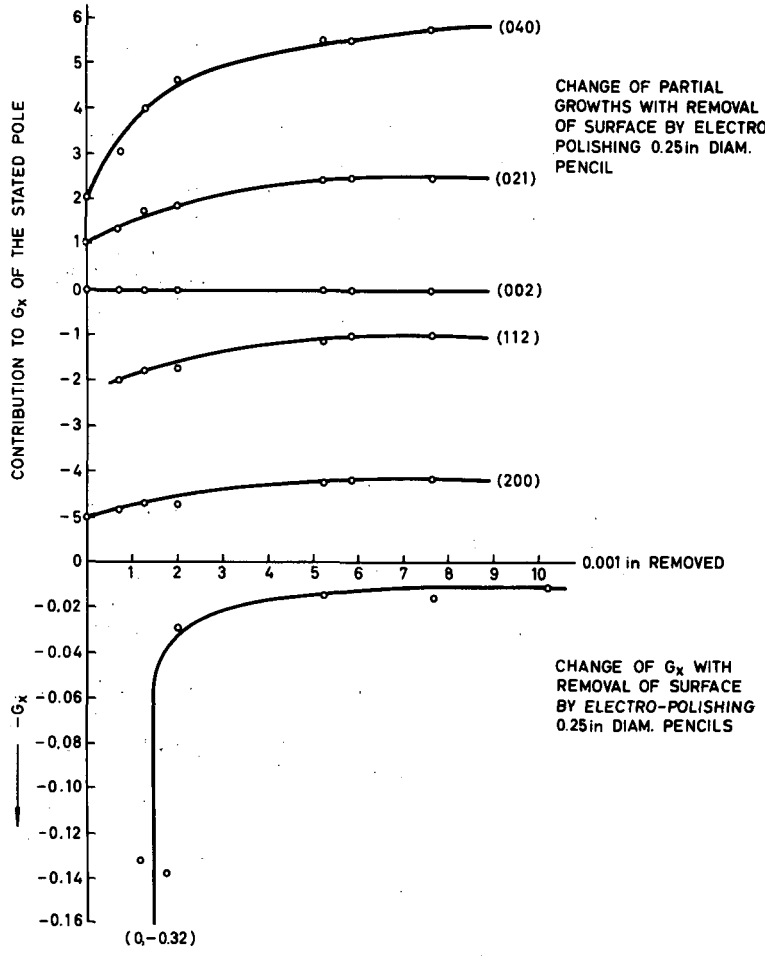


Fig. 4

The X-ray growth index (G_x)

where ϕ is the angle between the projection of the pole on the ab plane and the b axis; u is the cosine of the angle between the pole and the c axis.

$P(u, \phi)$ is a continuous function of u and ϕ such that

$$\int_0^1 \int_0^{\pi/2} P(u, \phi)\, d\phi\, du = 1.$$

G_x is designed to represent the fraction of [010] single-crystal growth which the specimen would exhibit if irradiated.

It is essential to electro-polish the specimen surface since mechanical machining produces an intense surface texture. Thus Fig. 4 shows how the

resolved contributions to irradiation growth of various poles change as the surface texture is removed and the resultant changes in G_x.

Neutron diffraction. As applied by BACON at AERE, neutron diffraction has, as an advantage over X-ray diffraction, the fact that much deeper penetration of the material occurs. Practical difficulties, however, have precluded all but the simplest experiments. Typically a comparison is made between the [010] pole intensity in and around two mutually perpendicular directions.

Thermal expansivity and electrical resistivity. Data for the single-crystal values of these properties listed in Table II [6, 7] suggest that thermal ex-

TABLE II

PHYSICAL CONSTANTS OF URANIUM SINGLE CRYSTALS

Direction	Thermal expansion (6) coefficient 20 to 100°C ($°C^{-1}$)	Electrical resistivity (7) 25°C ($\mu\Omega$cm)
[100]	(21.6 to 25.3) 10^{-6}	42.2
[010]	(-0.2 to +0.1) 10^{-6}	27.3
[001]	(17.9 to 22.0) 10^{-6}	28.0

pansion in the [010] direction is very much different from those of the other two principal crystallographic directions. Similarly, resistivity should detect [100] for textured polycrystalline specimens. Growth indices based on these considerations may be calculated from the expressions:

$$G_e = 1.06 - 0.05e,$$

where e is the expansivity, that of a random sample being presumed to be $14.5 \times 10^6 °C^{-1}$;

$$G_r = 0.07\,r - 1.95,$$

where r is the resistivity, that of a random sample being presumed to be $32.0 \mu\Omega$cm; and

$$G_{er} = G_e - G_r *,$$

where G_{er} is an index based on the combined results of expansivity and resistivity measurements.

* The possibility of deriving G_{er} in this way was first pointed out by Dr. J. Stobo, of C.A. Parsons Ltd., Nuclear Research Centre, Newcastle, England.

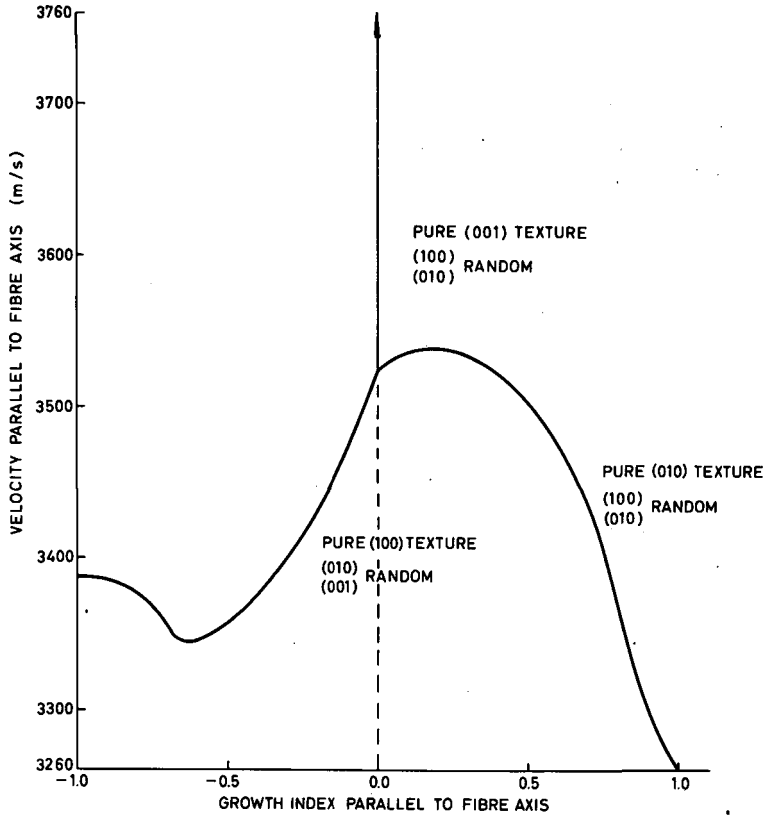


Fig. 5

The relation between compressional wave velocity and irradiation growth for three simple textures

Elasticity. Nine constants are needed to describe the elastic properties of an orthorhombic metal, such as uranium, and it has proved impracticable to calculate a growth index from simple elasticity measurements on a polycrystalline specimen. Nevertheless, measurement of the velocity of ultrasonic pulses has proved a rapid procedure and its application has been studied. The difficulty of interpreting the data so obtained is exemplified by Fig. 5, which demonstrates the theoretical relationship between irradiation growth and texture for each of the three main crystallographic directions when the other two are randomly distributed.

5. DEVELOPMENT OF URANIUM ALLOYS DEVOID OF TEXTURE

The methods of measuring texture described above have been used to assist in the development of uranium fuel rods designed to be free from irradiation growth. A further requirement was that the alpha grain size should be small (< 0.3 mm) to prevent the growth of individual surface grains puncturing the can. Most of the effort has been expended on water-quenched alloys, since these require the minimum content of alloying elements. Isothermally

transformed and as-cast fuel rods have also received attention. The work on these various systems is summarized below, together with the evolutionary development of hypotheses designed to assist alloy selection.

Water-quenched alloys

Conventional Calder Hall fuel elements are water-quenched by passing them initially through an induction coil which heats a short length into the beta phase and then through a water spray. Grain refinement may be promoted during the water-quenching of uranium by alloying it with iron and aluminium [8]. Relatively small amounts of iron and aluminium are needed to produce a satisfactorily fine grain size, and a detailed study has been made of such alloys.

Relevant continuous-cooling transformation characteristics have been established by the Jominy end-quench test. An example of the information so obtained is provided by Fig. 6. Apparently the alloying elements produce a marked dependence of the transformation temperature upon cooling rate. Fig. 7 shows the variation in grain size along the Jominy bar.

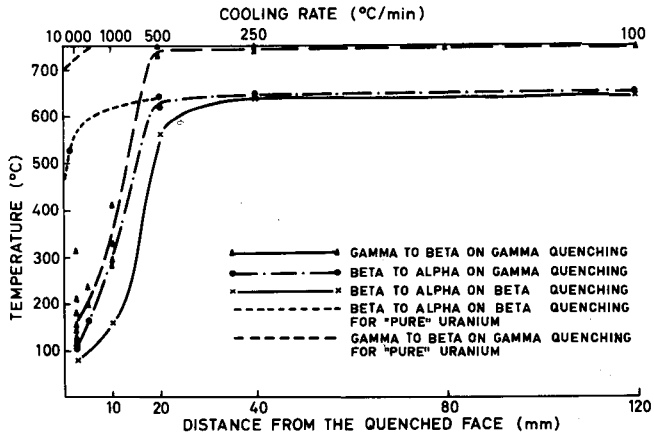


Fig. 6

The transformation temperature plotted against distance from the quenched face for dilute uranium +(Fe, Al) alloy

The texture of traverse-quenched fuel rods of this material has been established by all the previously described methods and a summary appears in Table III. Apparently the core region should exhibit a small contraction and the rim a small expansion under irradiation. The change in texture across the bar diameter is thought to derive from the stress system, the curved isotherms produced during traverse-quenching and the dependence of transformation temperature upon cooling rate. A corollary is the implication that changes in traversing speed, alloying element content etc. may

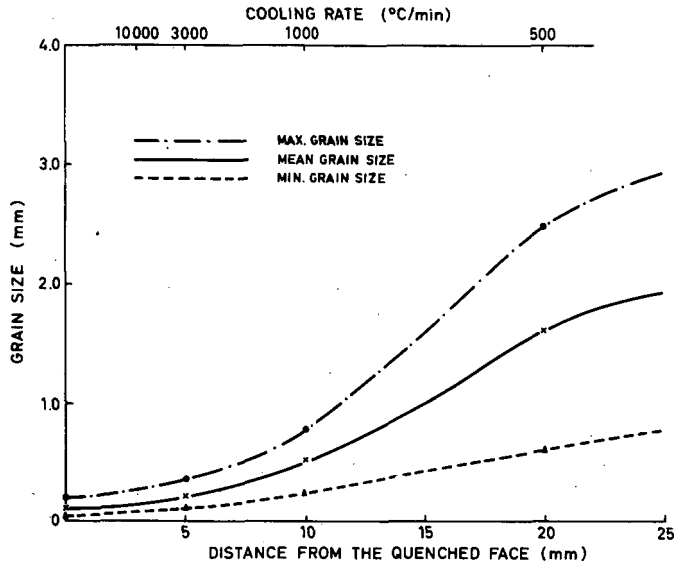


Fig. 7

Variation of grain size in dilute U-Fe-Al alloy with cooling rate

alter the relative growth indices of core and rim. Irradiation trials reported later in this paper provide a measure of support for this view.

Other alloys which have received attention include particularly those which exhibit the required fine grain size in regions of the Jominy bar remote from the water-quenched face. The slow cooling rates in those regions and the associated smaller temperature gradients should result in a lower level of texture. Structures produced in the U-Mo-Cr system are exemplified in Fig. 8. Even higher contents of niobium, chromium and molybdenum etc. can produce grain refinement at even lower cooling rates, such as those which obtain in the fuel rod when it is cooling in the mould. Such alloys are dealt with in the next section.

As-cast alloys

A prime necessity is to minimize the reactivity losses produced by the relatively large amounts of alloying element which are needed to promote grain refinement in as-cast bars.

Studies of the co-operative interactions of alloying elements have therefore been made. Fig. 9 illustrates such an effect in the U-Mo-Al system and Table IV the complementary effects of niobium and molybdenum in the U-Nb-Mo-Al system. Such as-cast alloys are sensibly devoid of texture; for example Table V shows that the thermal expansion coefficients of rim and core regions are identical for as-cast 3 at.% Mo-U fuel rods.

A further reduction in the temperature gradients which exist during transformation can be effected by the use of isothermal heat treatments.

TABLE III

TEXTURE MEASUREMENTS ON TRAVERSE-QUENCHED BETA-URANIUM

	X-ray diffraction	Neutron diffraction	Thermal expansion and electrical resistivity method			Ultrasonic velocity (m/sec)
			Thermal expansion	Electrical resistivity ($\mu\Omega$cm)	Total growth	
	G_x	Relative numbers of [010] poles	G_e	$-G_r$	G_{er}	
	(2 bars)	(2 bars)*	(20 bars)+	(20 bars)+	(20 bars)+	(20 bars)+
Rim axial direction	1 +0.033 2 +0.022	3 118 4 113	+0.004 ±0.012	+0.013 ±0.03	+0.017 ±0.04	3426 ± 14
Rim radial direction		104 97				
Core axial direction	-0.030 -0.035	98 105	-0.012 ±0.012	-0.045 ±0.03	-0.057 ±0.04	3411 ± 9
Core radial direction		124 125				

* Estimated error on each measurement ± 3 poles

\+ The spread is the standard deviation of bar-to-bar variation

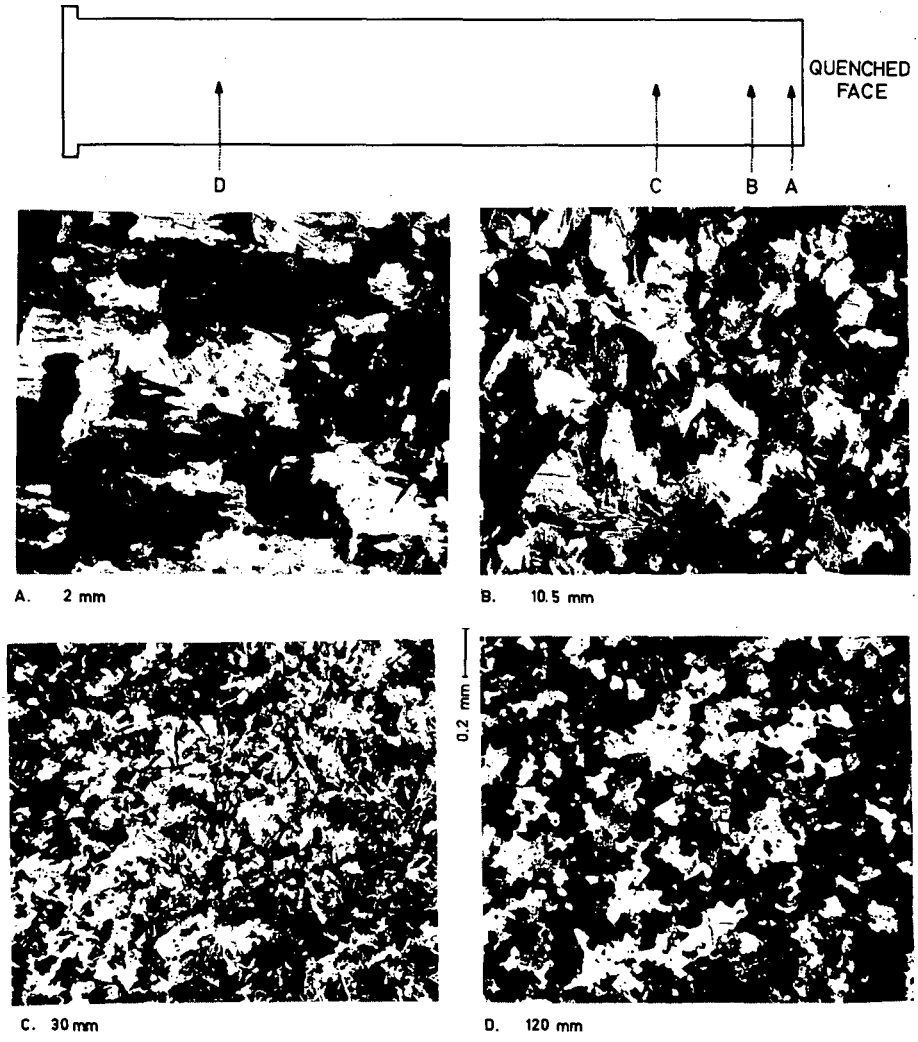


Fig. 8

Uranium + (0.3 at. % Cr + 0.1 at. % Nb) quenched from beta-phase uranium temperatures

Such alloys should have even less texture than as-cast fuel rods and their development is outlined in the next section.

Isothermally transformed alloys

The amounts of alloying elements required to permit isothermal transformation are generally smaller than the amounts which produce grain refinement in as-cast bars. Nevertheless the co-operative effects of certain

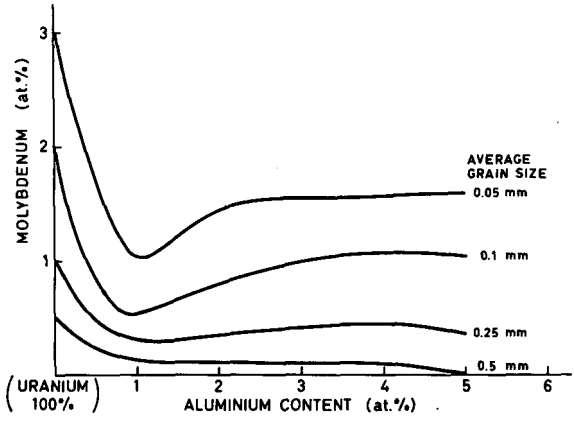


Fig. 9

Grain size variations in dilute ternary U-Mo-Al alloys as-cast

TABLE IV

GRAIN SIZES OF DILUTE U/Mo/Al AND U/Mo/Nb/Al ALLOYS

	Mo (at.%)	Nb (at.%)	Al (at.%)	Average grain size (mm)
Alloy 1	0.25	0.25	1	0.10
Alloy 2	0.5	-	1	0.10
Alloy 3	0.5	0.5	1	0.05
Alloy 4	1.0	-	1	0.06

elements have again been invoked to reduce the reactivity loss. Typical isothermal transformation diagrams are shown in Figs. 10, 11 and 12 for 0.625 at.% Mo +0.125 at.% Fe +0.625 at.% Al)-U, 0.500 at.% Cr-U and 0.500 at.% Mo +0.250 at.% Cr)-U respectively.

Table V shows that texture, determined by some of the methods outlined above, is sensibly absent from such alloys.

Mechanically worked fuel rods

Although casting is the most elementary method of making fuel rods, rolling and extrusion are potentially cheaper. A detailed survey of the texture produced by mechanical working has been made. Fig. 13 shows that the X-ray growth index (G_x) measured in the rolling direction varies with rolling temperature (at a specific reduction) and approaches zero for material rolled at 650°C. Points on this diagram are each the mean of 3 to 5 determinations. Fig. 14 illustrates the increase in G_x produced by increasing amounts of rolling reduction at room temperature.

TABLE V

TEXTURE OF ALLOYED URANIUM BARS

Material	Thermal expansion ($\times 10^{-6}$/deg C)		Neutron diffraction Number of [010] poles	
	Core	Rim	Core	Rim
Uranium + (3 at.% molybdenum)	axial 14.15 ± 0.18 8 specimens	axial 14.25 ± 0.17 8 specimens		
Uranium + {0.625 at.% molybdenum + (Fe, Al)}	14.62 ± 0.29 4 specimens	14.64 ± 0.24 4 specimens		
	14.78 ± 0.09 8 specimens	14.75 ± 0.09 8 specimens	axial 121 ± 3 125 ± 3	axial 123 ± 3 128 ± 3
Uranium + (0.500 at.% chromium)	transverse 14.72 ± 0.2 6 specimens	transverse 14.72 ± 0.2 6 specimens	transverse 136 ± 3 121 ± 3 121 ± 3 122 ± 3	transverse 131 ± 3 123 ± 3 124 ± 3

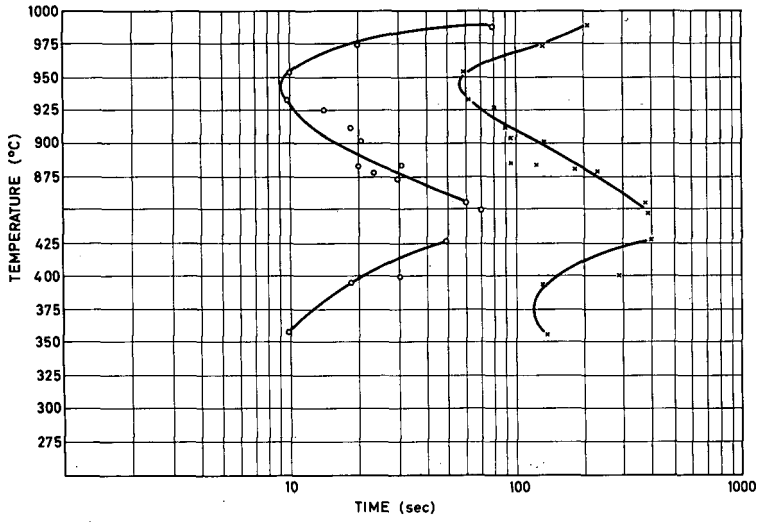


Fig. 10

Uranium + (0.625 at.% molybdenum + 0.125 at.% iron + 0.625 at.% aluminium)

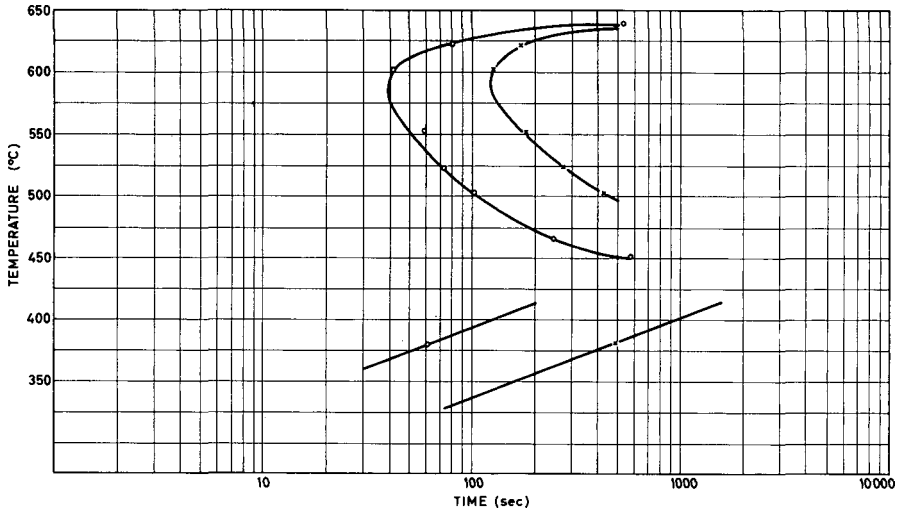


Fig. 11

T. T. T. curve of uranium + (0.500 at.% chromium)

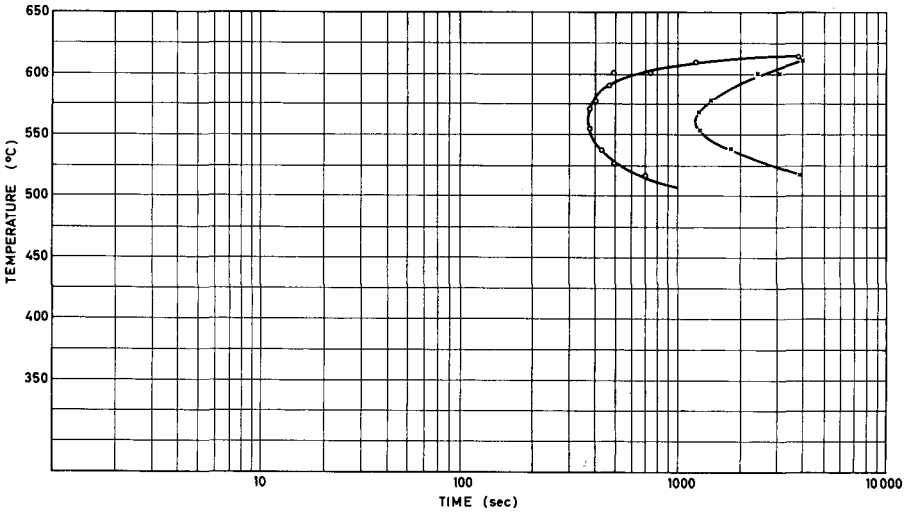


Fig. 12

T. T. T. curve of uranium + (0.500 at.% molybdenum + 0.250 at.% chromium)

6. RESULTS OF IRRADIATION EXPERIMENTS

Full-sized fuel rods made by each of the procedures exemplified in the preceding section have been irradiated in the Calder Hall and Chapelcross

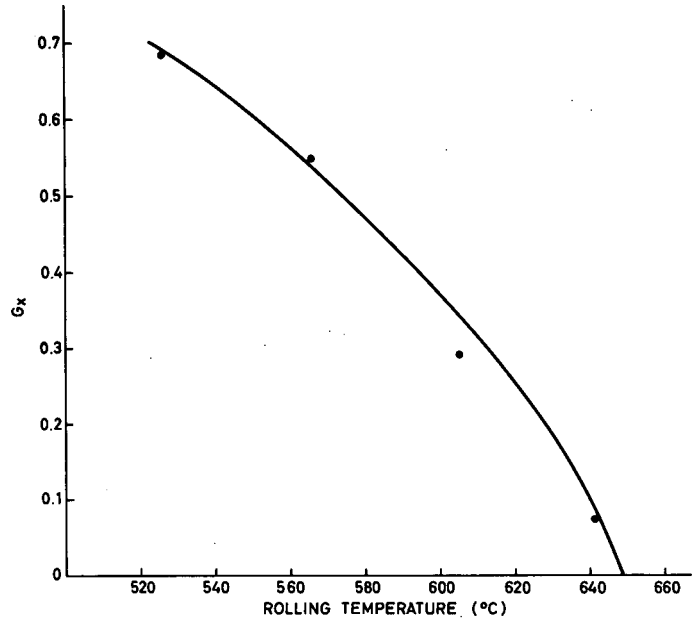


Fig. 13

Effect of rolling temperature on X-ray growth index G_x

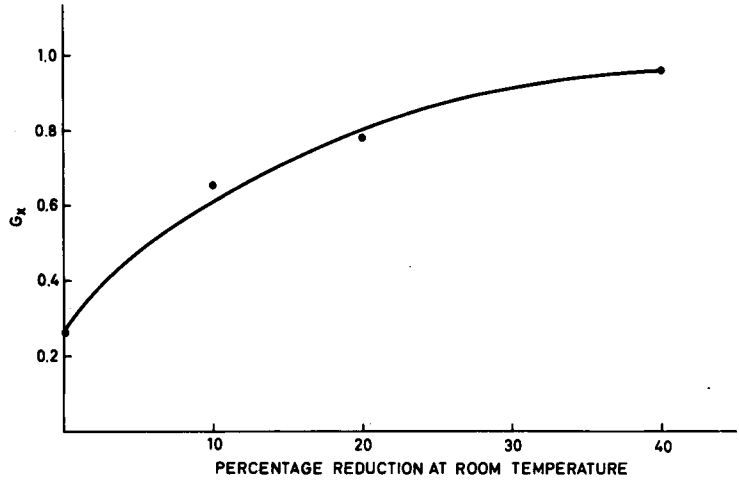


Fig. 14

Effect of rolling reduction on X-ray growth index G_x

Reactors. The results generally support the contention that measures which reduce the texture also reduce the anisotropic growth.

Water-quenched alloys

The texture in traverse-quenched uranium (see Table III) should produce axial growth in the rim and axial contraction in the core under irradiation at low temperatures. Data illustrating the irradiation-induced dimensional changes of such fuel rods are summarized in Fig. 15.

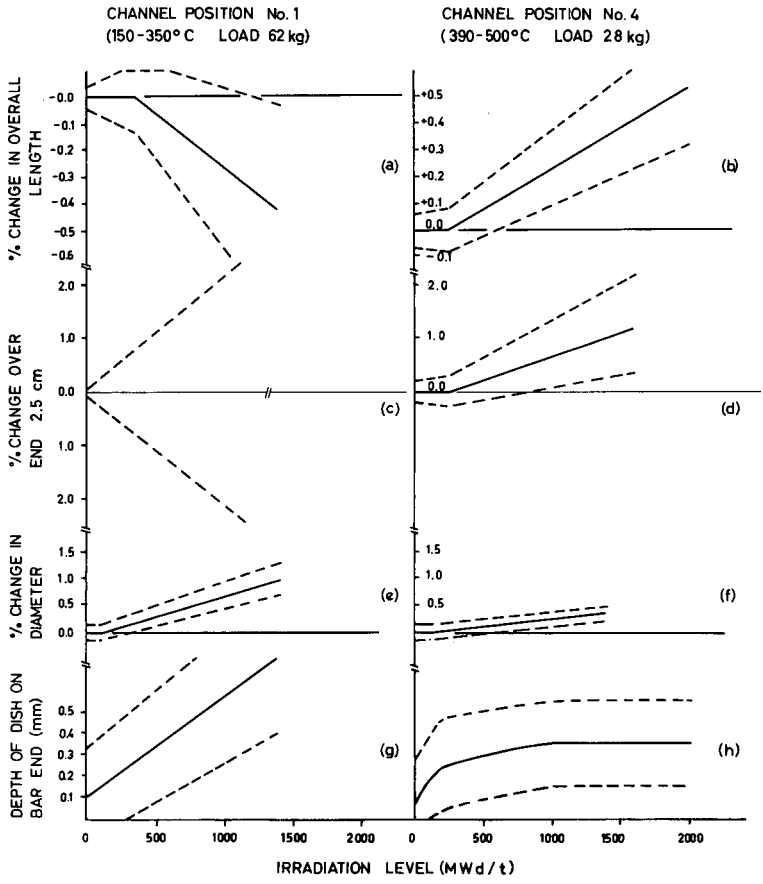


Fig. 15

Dimensional changes plotted against irradiation level (Normal production Springfields rods)

In channel position 4 (temperature 390-500°C, load 28 kg) the overall length of the average rod increases (Fig. 15(b)) by about 0.2% during irradiation to 1000 MWd/t, whereas in position 1 (temperature 150-350°C, load 62 kg) the overall length decreases by about 0.3%. The diameters at the middle of the rods increase by 0.2 and 0.7%, respectively, (Fig. 15 (f) and (c)).

Since the ends of irradiated bars are generally slightly concave and the measurement of overall length is made between flats, the change in overall length recorded is that of the cylindrical surface of the rod. The depth of the concavity at each end of the bar is measured separately and is typically 0.6 mm in position 1 (Fig. 15 (g)) and 0.4 mm in position 4 (Fig. 15 (h)) at 1000 MWd/t.

All rods have shallow cylindrical anti-ratcheting grooves machined at approximately 2.5 cm from each end and, whenever practicable, the change in this dimension has been determined. In some rods this localized change is more than an order of magnitude larger than the change in overall length (Figs. 15(c) and 15(d). In position 1 the changes may be of either sign and the mean change is zero (Fig. 15(c)) at all irradiation levels, but in position 4, where the spread is much less, the mean change does increase slightly with increasing irradiation. Failures in elements of this type are almost entirely due to the development of grain-boundary leak paths across the can wall near the ends of some of the cooler elements, where the dimensional changes are greatest and the creep ductility of the can is least.

The scatter in the estimated dimensional changes (indicated by the broken lines representing ± 1 standard deviation about the mean in Fig. 15) is well outside the error of measurement and therefore reflects real differences between rods. A reasonable explanation of the features illustrated in Fig. 15 has been arrived at as follows.

The changes in overall dimensions expected from homogeneous swelling and irradiation creep are plotted against irradiation level in Fig. 16(a) to (e). The [100] longitudinal shrinkage texture in the core of these rods is apparently more than sufficient to overcome the [010] longitudinal growth texture of the rim at the temperatures concerned. Variations in texture from rod to rod are found to be sufficient to explain the scatter in results obtained. Near the ends of the rods the core and rim exert less constraint on one another with the result that marked elongation of the rim and shrinkage of the core occur in some cases and a concavity develops on the bar ends. These effects may be assisted by different degrees of swelling in the rim and core due to flux variations.

Further support for the hypothesis that the irradiation induced dimensional changes of traverse-quenched bars depend upon the relative magnitude of the rim texture and the core texture is thought to derive from the data of Table VI. This gives the results of irradiating traverse-quenched fuel rods of varying iron and aluminium contents. The higher iron content produces the smallest depth of dish and the biggest overall length contraction, apparently because it reduces the expansion texture in the rim of the fuel rod. A body of experience has been accumulated which shows that, as might be expected from Table VI, high-iron fuel rods are less likely to rupture the ends of the cans when under irradiation than are rods of lower iron content.

As-cast and isothermally transformed alloys

The thermal expansion data of Table V suggest that texture is absent from as-cast 3 at. % Mo-U and from isothermally transformed 0.500 at. % Cr-U. Irradiation experiments have been carried out to test the hypothesis that material will not exhibit anisotropic irradiation-induced dimensional changes

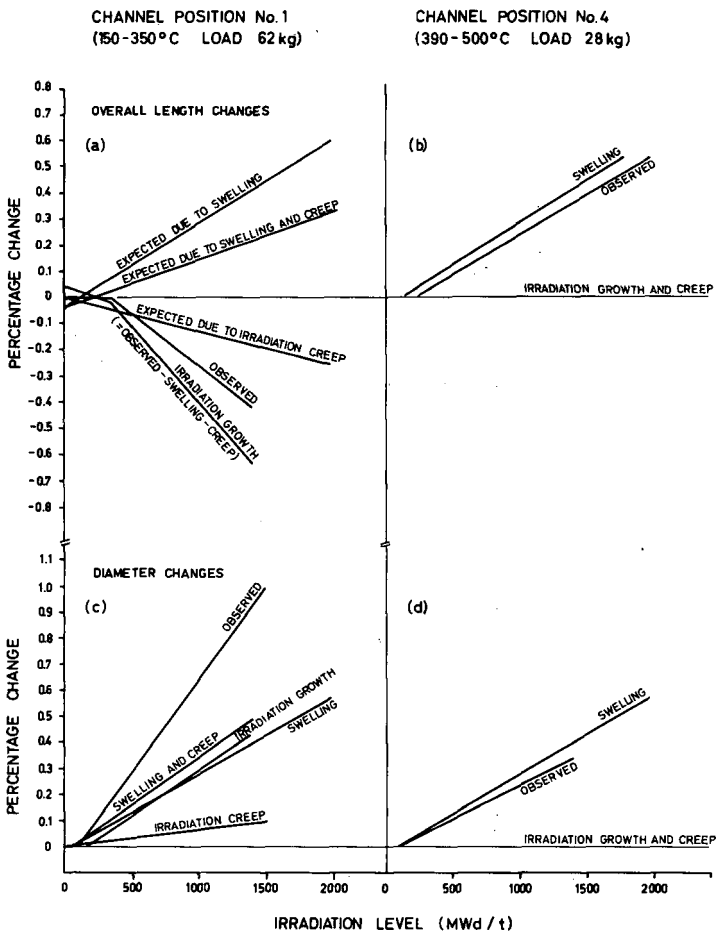


Fig. 16

Dimensional changes corrected for swelling and irradiation creep

in the cooler channel positions. Table VII typifies the results obtained, including an item from Table VI for comparison. Included also are data for rolled bar which was traverse-quenched before irradiation. The mean end-inch expansion for 0.500 at.% Cr-U is very small and the amount of the end dishing in this alloy did not differ significantly from zero. In the case of the 3 at.% Mo-U, the overall length change was, on average, expansion and was small. The rolled bar had a more or less uniform growth texture (cf. Fig. 13) in both rim and core. It is not surprising, therefore to find that dishing was small whilst the end-inch and overall length changes were both expansions.

7. DISCUSSION

During its life in a power reactor, every atom in a uranium fuel rod is violently displaced from its lattice site on many occasions. The colder mat-

TABLE VI

MEAN DIMENSIONAL CHANGES AFTER 1000 MWD/t IN LOWER CHANNEL POSITION

	low					high				
	End-inch expansion (E) (%)	Overall concentration (C) (%)	Depth of dish (mm)	Max. bow (in)	Volume increase (%)	End-inch expansion (E) (%)	Overall concentration (C) (%)	Depth of dish (mm)	Max. bow (%)	Volume increase (%)
low	2.3	0.4	0.54	0.2	1.1	1.5	1.2	0.41	0.2	0.9
high	2.5	0.1	0.87	0.2	1.0	1.7	0.9	0.23	0.2	1.0

TABLE VII

MEAN DIMENSIONAL CHANGES FOR
3 at.% Mo-U, 0.500 at.% Cr-U AND ROLLED URANIUM
(Corrected to 1000 MWd/t)

Material	End-inch expansion (%)	Overall contraction (%)	Depth of dish (mm)	Volume increase (%)
Quenched* U+Fe+Al	2.5	0.1	0.87	1.0
3 at.% Mo-U	0.40	-0.02+	-	-0.02
0.500 at.% Cr-U	0.006	0.54	0.1	1.2
Gothic-rolled 640-480°C plus a beta quench	2.5	-1.5+	0.3	-

* From Table VI for comparison

\+ I.e. these fuel rods exhibited overall expansion

erial is stressed to the yield point by irradiation growth, solid fission product atoms are produced in relative profusion and a large volume of almost insoluble gas is generated in the lattice. In view of these facts, it is hardly surprising that dimensional changes occur.

As yet it has not been possible to detect, by physical tests, the change in texture produced by altering the iron content of beta-quenched bars. However, the effect upon irradiation growth and upon the consequent failure-rate has been clearly established. Calculations suggest that the change in texture needed to produce the observed changes in dimensional stability is too small to be registered by the methods available for texture measurement.

The excellent swelling resistance of uranium alloyed with iron and aluminium and beta-quenched is to be expected from the small size of the fission-product gas bubbles, whose surface tension will result in the gas being compressed under a load approaching 1 kg mm^{-2}. Neither the iron and aluminium nor the beta-quenching operation are separately capable of imparting this property; it is only when suitably alloyed material is beta-quenched that the requisite high nucleation rate for fission-gas bubbles is achieved. Calculations have shown that when this material is irradiated the amount of swelling produced should be relatively insensitive to irradiation temperature, a conclusion which is substantiated by experience.

It is impracticable to reduce the extent of irradation-induced creep by alloying, unless large amounts of alloying elements are permissible (they are not on both reactivity and chemical grounds). However, bowing can be controlled by the use of braces etc. to support the element and does not therefore present an insurmountable problem from an engineering standpoint.

8. CONCLUSIONS

Irradiation-induced swelling of the fuel rods from Calder Hall reactors is comparatively small and exhibits no detectable temperature dependence.

In Calder Hall reactors, the bow which develops in the stacked fuel elements is greatest in the second element from the botom of the channel. It is attributed to irradiation creep.

Thermal and thermal-cycling creep do not occur significantly in the fuel rods in the Calder Hall reactors but thermal cycling in later, load-following stations should supplement the creep produced by irradiation, particularly in the hotter elements.

Traverse beta-quenched, cast, uranium bars exhibit preferred orientation of a type which qualitatively accounts for part of their anisotropic deformation in the reactor.

By alloying, fuel rods can be produced having the requisite fine grain size, as-cast or after isothermal beta-to-alpha transformation, and do not appear to exhibit preferred orientation or marked anisotropic irradiation-induced growth.

ACKNOWLEDGEMENT

The authors thank Mr. R.V. Moore, the Managing Director, and Dr. H. Kronberger, the Deputy Managing Director (Development) of the Reactor Group, U.K.A.E.A., for permission to publish this paper.

REFERENCES

[1] GARDNER, L.R.T. and MILLER, W.N., The Creep of Alpha-Uranium under isothermal and both continuous and descrete thermal cycling conditions, Symp. Uranium and Graphite, Inst. Metals (20-21 March 1962).

[2] ANDERSON, R.G. and BISHOP, J.F.W., The effect of neutron irradiation and thermal cycling on permanent deformation in uranium under load, Symp. Uranium and Graphite Inst. Metals (20-21 March 1962).

[3] BUCKLEY, S.N., Irradiation growth., AERE Rpt R-3674 (1961).

[4] MORRIS, P.R., NLCO-760 (1958).

[5] STURCKEN, E.F., NLCO-804 (1960).

[6] LLOYD, L.T., Thermal expansion of alpha-uranium single crystals, USAEC Rpt. ANL-X 5972 (June 1959).

[7] BERLINCOURT, T.G., Hall effect resistivity and magnetoresistivity of Th, U, Zr, Ti and Nb, Phys. Rev. 114 (May 1959) 969.

[8] JEPSON, M.D. and SLATTERY, G., Brit. Pat. No. 863, 492.

THE EFFECT OF IRRADIATION TEMPERATURE AND FISSION RATE ON THE RADIATION STABILITY OF THE URANIUM-10 wt.% MOLYBDENUM ALLOY

A.A. SHOUDY, W.E. McHUGH AND M.A. SILLIMAN
ATOMIC POWER DEVELOPMENT ASSOCIATES, INC.,
DETROIT, MICHIGAN

Abstract — Résumé — Аннотация — Resumen

THE EFFECT OF IRRADIATION TEMPERATURE AND FISSION RATE ON THE RADIATION STABILITY OF THE URANIUM-10 wt.% MOLYBDENUM ALLOY. The radiation stability of uranium-10 wt.% molybdenum alloy has been studied since 1955 by Atomic Power Development Associates, Inc. This radiation programme, carried out as a part of the research and design effort for the Enrico Fermi Atomic Power Plant, covered the evaluation of various radiation parameters such as fission rate, fuel temperature and burn-up.

Of these parameters studied, fission rate was found to have the most pronounced effect on the dimensional stability of the fuel alloy, particularly in the temperature range of 480 to 570° C. For material irradiated at a fission rate greater than 8×10^{13} fissions/cm^{3}s, diametral increases of about 3% were observed for burn-ups up to 7.5×10^{20} fissions/cm^3 at temperatures less than 630° C. At fission rates less than 6×10^{13} fissions/cm^{3}s and radiation temperatures of 480 - 570° C, the diameter changes become increasingly larger for decreasing fission rates. Post-irradiation examination has shown that the loss of dimensional stability can be directly related to the transformation kinetics of the fuel alloy while under irradiation. At high fission rates, the metastable gamma phase continues to exist and the diameter changes are small and relatively insensitive to burn-up. At progressively lower fission rates, the alloy transforms partially or completely to the equilibrium alpha plus delta (or gamma) phases, the degree of transformation depending on the absolute fission rate and the radiation temperature. Under these conditions, diameter increases for burn-ups of about 5×10^{20} fissions/cm^3 range from 3 to 14% for fission rates of 5×10^{13} to 2×10^{13} fissions/cm^{3}s respectively, and are highly dependent on burn-up.

This paper presents data relating dimensional stability to burn-up, radiation temperature and fission rate for zirconium-clad uranium-10 wt.% molybdenum fuel pins. These specimens were fabricated according to the fuel specifications for the Enrico Fermi Reactor.

INFLUENCE DE LA TEMPÉRATURE D'IRRADIATION ET DU TAUX DE FISSION SUR LA RADIOSTABILITÉ DE L'ALLIAGE URANIUM-MOLYBDÈNE (10% EN POIDS DE Mo). Depuis 1955, la société Atomic Power Development Associates, Inc. poursuit des études sur la radiostabilité de l'alliage uranium-molybdène à 10% en poids de Mo. Ce programme, qui a été entrepris dans le cadre des recherches et des études ayant trait à la construction de la Centrale nucléaire Enrico Fermi, comporte une évaluation de divers paramètres, tels que le taux de fission, la température du combustible et le taux de combustion.

Les auteurs ont constaté que, parmi les divers paramètres étudiés, c'est le taux de fission qui avait l'effet le plus prononcé sur la stabilité dimensionelle de l'alliage, notamment dans la gamme de températures comprise entre 480 et 570° C. Pour les matériaux irradiés à un taux de fission supérieur à $8 \cdot 10^{13}$ fissions par cm$^3 \cdot$ s, on a observé des augmentations diamétrales d'environ 3% pour des taux de combustion allant jusqu'à $7,5 \cdot 10^{20}$ fissions/cm^3, à des températures inférieures à 630° C. Pour des taux de fission inférieurs à $6 \cdot 10^{13}$ fissions/cm$^3 \cdot$ s et des températures d'irradiation comprises entre 480 et 570° C, les variations de diamètre augmentent progressivement lorsque les taux de fission diminuent. Un examen après irradiation montre que l'on peut établir une relation directe entre la perte de stabilité dimensionnelle et la cinétique de transformation de l'alliage sous irradiation. A des taux de fission élevés, la phase gamma métastable subsiste; les variations de diamètre sont faibles et dépendent relativement peu du taux de combustion. A mesure que les taux de fission diminuent, l'alliage se transforme, en tout ou en partie, en des phases d'équilibre alpha plus delta (ou gamma), le degré de transformation étant fonction du taux de fission absolu et de la température d'irradiation. Dans ces conditions, les augmentations de diamètre à des taux de combustion d'environ $5 \cdot 10^{20}$ fissions/cm^3 varient de 3 à 14% pour des taux de fission allant de $5 \cdot 10^{13}$ à $2 \cdot 10^{13}$ fissions/cm$^3 \cdot$ s respectivement, et dépendent dans une grande mesure du taux de combustion.

Les auteurs présentent des données permettant d'établir une relation entre la stabilité dimensionnelle, d'une part, et le taux de combustion, la température d'irradiation et le taux de fission, d'autre part, pour des aiguilles en alliage d'uranium-molybdène à 10% en poids de Mo, gainées de zirconium. Pour la fabrication des échantillons, on s'était conformé aux spécifications fixées pour le combustible destiné au réacteur Enrico Fermi.

ВОЗДЕЙСТВИЕ ТЕМПЕРАТУРЫ ПРИ ОБЛУЧЕНИИ И СКОРОСТИ ДЕЛЕНИЯ НА РАДИАЦИОННУЮ УСТОЙЧИВОСТЬ СПЛАВА УРАНА С МОЛИБДЕНОМ (10 вес %). Радиационная устойчивость сплава урана с молиденом (10 вес %) изучалась компанией "Атомик пауэр девелопмент ассошиейтс, инк." с 1955 года. Это была часть исследовательской и конструкторской работы для атомной энергетической установки Энрико Ферми. Она охватывала определение различных параметров радиации, таких, как скорость деления, температура топлива и выгорание.

Было установлено, что изо всех этих излученных параметров скорость деления оказывает наиболее ярко выраженное влияние на размерную устойчивость топливного сплава, в особенности в диапазоне температур от 480° до 570°С. Было установлено, что для материала, облученного при скорости деления большей чем $8 \cdot 10^{13}$ делений на $см^3$/сек, происходит увеличение в диаметре приблизительно на 3% при выгораниях до $7{,}5 \cdot 10^{20}$ делений на 1 $см^3$ при температурах меньших 630°С. При скоростях деления меньших $6 \cdot 10^{13}$ делений на $см^3$/сек и температурах радиации от 480° до 570°С изменения в диаметре становятся в возрастающей степени больше для падающих скоростей деления. Изучение после облучения показало, что потеря размерной устойчивости может быть непосредственно связана с кинетикой трансформации топливного сплава во время его облучения. При высоких скоростях деления метастабильная гамма-фаза не исчезает, а величина изменений диаметра мала и относительно нечувствительна к выгоранию. При уменьшающихся скоростях деления происходит частичный или полный переход сплава в фазы равновесия альфа плюс дельта (или гамма), причем степень перехода зависит от абсолютной скорости деления и температуры радиации. При этих условиях увеличение диаметра при выгораниях около $5 \cdot 10^{20}$ делений на $1см^3$ происходит в диапазоне от 3 до 14% для скоростей деления соответственно от $5 \cdot 10^{13}$ до $2 \cdot 10^{13}$ делений на $см^3$/сек и сильно зависит от выгорания.

В этом документе приводятся данные зависимости размерной устойчивости от выгорания, температуры радиации и скорости деления для тонких тепловыделяющих элементов, имеющих форму стержней, изготовленных из сплава урана с 10 весовыми частями молибдена, с покрытием из циркония. Эти образцы были изготовлены в соответствии с топливными спецификациями реактора Энрико Ферми.

EFECTO DE LA TEMPERATURA DE IRRADIACIÓN Y DE LA VELOCIDAD ESPECÍFICA DE FISIÓN SOBRE LA RADIOESTABILIDAD DE LA ALEACIÓN DE URANIO CON 10 POR CIENTO EN PESO DE MOLIBDENO. Desde el año 1955 la Atomic Power Development Associates, Inc., ha venido estudiando la radioestabilidad de la aleación de uranio con 10 por ciento en peso de molibdeno. Este programa de estudio, que forma parte de las actividades de estudios y proyectos de la Enrico Fermi Atomic Power Plant, comprendía la evaluación de parámetros tales como la velocidad específica de fisión, la temperatura del combustible y el grado de combustión del mismo.

Se comprobó que, de todos los parámetros estudiados, la velocidad específica de fisión es el que ejerce el efecto más pronunciado sobre la estabilidad dimensional de la mencionada aleación combustible, particularmente entre 480 y 570°C. En el material irradiado a velocidades específicas de fisión superiores a $8 \cdot 10^{13}$ fisiones/$cm^3 \cdot s$, se observaron incrementos diametrales de alrededor del 3 por ciento, en correspondencia con grados de combustión hasta de $7{,}5 \cdot 10^{20}$ fisiones/cm^3, a temperaturas inferiores a 630°C. Tratándose de velocidades específicas de fisión menores que $6 \cdot 10^{13}$ fisiones/$cm \cdot s$ y temperaturas de irradiatión comprendidas entre 480 y 570°C, los cambios de diámetro se hacen cada vez mayores a medida que disminuyen las velocidades específicas de fisión. El examen ulterior a la irradiación ha demostrado que la pérdida de estabilidad dimensional puede vincularse directamente con la cinética de la transformación de la aleación combustible en el curso de su irradiación. A velocidades específicas de fisión elevadas, subsiste la fase gamma metaestable, y los cambios de diámetro son pequeños y relativamente independientes del grado de combustión. Al disminuir gradualmente las velocidades específicas de fisión, la estructura de la aleación se transforma parcial o totalmente, pasando a las fases de equilibrio alfa más delta (o gamma); el grado de la transformación depende de la velocidad específica de fisión absoluta y de la temperatura de irradiación. En estas condiciones, los aumentos de diámetro, en correspondencia con grados de combustión de alrededor de $5 \cdot 10^{20}$ fisiones/cm^3, oscilan entre 3 y 14 por ciento para velocidades específicas de fisión de $5 \cdot 10^{13}$ y $2 \cdot 10^{13}$ fisiones/$cm^3 \cdot s$ respectivamente, y dependen en gran medida del grado de combustión.

En esta memoria se presentan datos que permiten establecer una relación entre la estabilidad dimensional y el grado de combustión, la temperatura de irradiación y la velocidad específica de fisión, en el caso de agujas combustibles de uranio con 10 por ciento en peso de molibdeno, revestidas de zirconio. Estas muestras se elaboraron siguiendo las especificaciones referentes al combustible destinado al reactor Enrico Fermi.

1. INTRODUCTION

Uranium 10 wt.% molybdenum alloy was selected as the fuel for the first core loading of the Enrico Fermi Atomic Power Reactor on the basis of an irradiation screening programme [1] carried out by Battelle Memorial Institute under the sponsorship of Atomic Power Development Associates, Inc. Since that time, a comprehensive radiation programme has been in progress to determine the effects of several variables that would be encountered during reactor operation on radiation stability and to determine the burn-up that could be achieved without excessive fuel swelling. The variables studied included such items as burn-up, fission rate, radiation temperature, post-fabrication heat-treatment and alloy composition. Results of this radiation programme have previously been reported [2, 3]. SILLIMAN et al.[3] pointed out that significant differences in radiation stability resulted from high and low fission rates in the temperature range of about 925 to 1100°F. At that time, the data covered only the maximum and minimum fission rates to be encountered in the Fermi reactor in this temperature range, 8×10^{13} and 2.5×10^{13} fissions cm^{-3} s^{-1}, respectively. These data effectively confirmed that a critical fission rate did exist below which the U-10 wt.% Mo alloy would transform to the thermally stable $\alpha + \delta$-phases, as had been proposed by THOMAS and others at Bettis Atomic Power Laboratory [4]. It was indicated from these experiments that the critical fission rate for maintaining the γ-phase in the Fermi-type, wrought U-10 wt.% Mo fuel-pins appeared to be between 4×10^{13} and 8×10^{13} fissions cm^{-3} s^{-1} for the temperature range 925 to 1045°F.

At that time, a more detailed irradiation programme was initiated to investigate the effect of fission rate on the transformation kinetics and radiation stability of the Fermi reactor production fuel-pins. Fission rates investigated ranged from about 1.0 to 6.0×10^{13} fissions cm^{-3} s^{-1} over a wide temperature range. This paper deals with results of this later irradiation programme and includes only that portion of the previously reported data that is pertinent to the subject of fission rate effects on transformation and/or swelling.

2. EXPERIMENTAL TECHNIQUE

2.1. Specimen preparation

The specimens used for this programme were made by approximately the same procedure used in the production fabrication of the first core loading for the Fermi reactor. In fact, some of the tests reported in this paper were run on pins taken from the actual production line. The fabrication procedure was essentially as follows :

(1) Induction-melt the alloy in vacuum.
(2) Cast in 4-in ingot.
(3) Machine ingot and extrude at 1600°F to 1.5 in.
(4) Machine extruded bar, can in zirconium sleeve, and co-extrude at 1600°F to 0.310 in.
(5) Cold-swage to reference diameter of 0.158 in. For several of the CP-5 tests, the pins were further cold-swaged to 0.126 in to achieve proper heat generation rates.
(6) Stress-relieve by vacuum heat-treatment of 1 h at 1470°F and furnace-cool.
(7) In some of the irradiation tests, fuel specimens were given a post-fabrication heat-treatment to transform the specimens to the $\alpha + \delta$-condition.

Depending on the test being run, the specimens were made from uranium enriched to 10.54, 19.0 and 25.6% U^{235}. In the fabricated condition, the test specimens were clad with 0.005 ± 0.0005 in of pure zirconium.

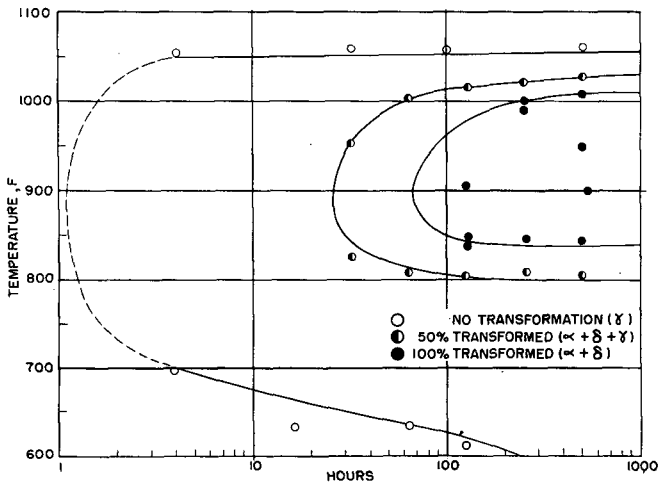
Nominal chemical composition and impurity levels for the test specimens was as follows:

Element	Composition Range
Molybdenum	10.0 ± 0.5%
Carbon	100 to 350 ppm
Iron	75 to 200 ppm
Nickel	25 to 100 ppm
Oxygen	50 to 250 ppm
Zirconium	10 to 1200 ppm

2.2. Transformation kinetics of test specimens

Transformation kinetics of the as-fabricated fuel-pins have been determined [5]. The metallographically determined time-temperature-transformation (TTT) curve resulting from this work is shown in Fig.1. For this alloy, the high-temperature γ-phase is stable above 1060°F, as shown in the equilibrium diagram (Fig.2) [6]. The γ-phase can be retained by either quenching or slow-cooling from above 1060°F to room temperature. On reheating of Fermi production fuel-pins to temperatures less than 1045°F, the γ-phase decomposes to the thermally stable $\alpha + \delta$-phases, as indicated in Fig.1. The nose of the TTT curve appears to be about 900°F.

2.2.1. Irradiation procedure. Irradiation tests reported here were carried out in both the CP-5 and MTR reactors. In the case of the MTR tests, specimens $1\frac{1}{2}$-in long and 0.158-in diam. were irradiated in capsules. Six specimens were tested in each of six capsules. Three of the specimens in each capsule were in the as-fabricated γ-condition while the remaining three were given a post-fabrication heat-treatment to transform the alloy to the $\alpha + \delta$-condition. (The details of the transformation heat-treatment are given later in this report.) The specimens were NaK-bonded in stainless-steel



T-T-T CURVE FOR U-10 W/O Mo

Fig. 1

TTT curve for U-10 wt.% Mo fabricated into fuel pins (phases present determined metallographically)

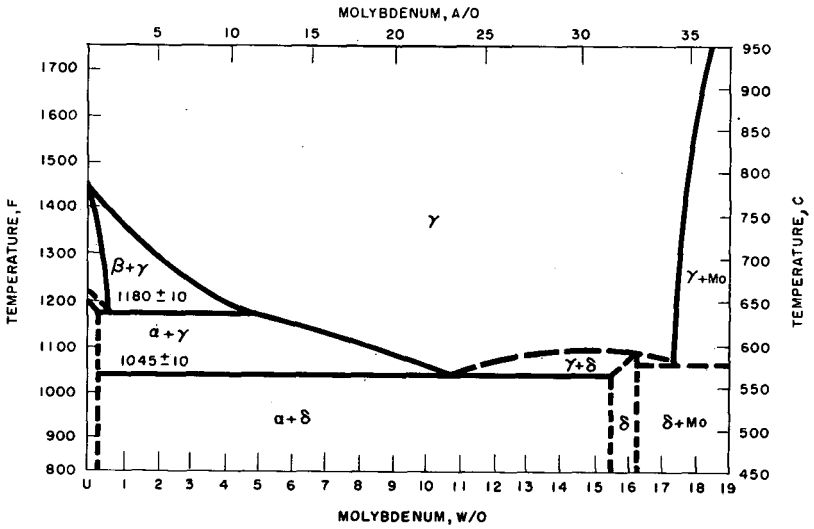


Fig. 2

U-Mo equilibrium diagram to 19 wt.% Mo [6]

capsules of double-walled construction. A helium-filled annulus between the inner and outer walls was sized to give sufficient heat resistance so that the fuel specimens would operate in the temperature range 850 - 1050°F under

the desired fission rate. The capsules were not temperature-controlled but were equipped with thermocouples adjacent to each fuel specimen. Determination of burn-up and fission rates of this series of specimens was based on the total heat generation of the specimens as determined by the heat-meter method.

In the CP-5 programme, tests were carried out in air-cooled and water-cooled capsules. The air-cooled radiation facility has previously been described [7]. Briefly, the facility consists of: (1) a longitudinally finned, stainless-steel capsule within which a 25- or 30-in long, 0.158-in diam., fuel-pin is NaK-bonded; (2) an inner stainless-steel thimble, in which the finned capsule is inserted; and (3) an outer stainless-steel thimble. The air coolant inlet is between the finned capsule and the inner thimble, and the outlet is between the inner and outer thimbles. The capsule outer-surface temperature was monitored by 10 thermocouples located at the fin roots and positioned in a spiral pattern at 3-in intervals along the capsule. Two additional thermocouples were used to monitor the inlet and outlet air temperatures. The capsule-surface temperature, and thus the fuel-pin temperature, was controlled by the air-coolant flow rate. The one major modification to this radiation facility over that previously described was the design of a bottom-loading device that allowed an irradiated fuel pin to be re-inserted into the reactor by remote handling. This modification permitted a single fuel pin to be irradiated, examined non-destructively, and then reinserted in the reactor for an additional burn-up increment.

The water-cooled facility has also been described in detail [8]. Briefly, it consists of a 15-in-long fuel specimen of either 0.126-in or 0.158-in diam., NaK-bonded in a finned tube. The capsule is completed by shrink-fitting a sleeve over the fins. In the reactor, the capsule is fixed within a D_2O-filled pressure vessel. Thus, the heat generated within the fuel specimen was conducted through the fins, into the sleeve and into the D_2O, causing nucleate boiling. The ultimate heat sink was the reactor coolant (D_2O) continuously flowing outside the pressure-vessel wall. The temperature of the boiling-D_2O annulus was controlled by regulation of the over-pressure. The temperature drop between the specimen and the D_2O was predominately determined by the fin thickness, which was individually selected in each experiment. As in the case of the air-cooled capsules, the temperature of the finned capsule was monitored by thermocouples attached to the fin-roots along the axis of the capsule. This capsule design was also modified to permit reinsertion of irradiated fuel pins.

3. EXPERIMENTAL RESULTS

3.1. MTR irradiation programme

As previously indicated, three of the specimens in each MTR capsule were irradiated in the as-fabricated condition while three were irradiated as fully or partially transformed to the $\alpha + \delta$-condition. A typical area of the γ-structure of the as-fabricated specimens is shown in Fig. 3. The transformation heat-treatment given the specimens in capsules 35-1 and

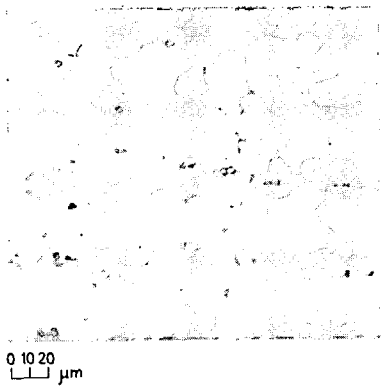


Fig. 3

Typical microstructure of as-fabricated specimens

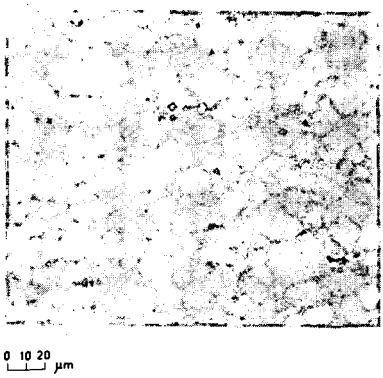


Fig. 4

Typical microstructure of specimens transformed after 100 h at 930°F

35-2 was 100 h at 930°F. This treatment results in a fully transformed structure, a typical area of which is shown in Fig. 4. The specimens used in the remaining capsules were mistakenly given a heat-treatment of 100 h at 1120°F. This was corrected by heating at 930°F for 63 h. By comparison with microstructures of previous heat-treatment studies, it was concluded that the 1120°F treatment had little or no effect on the structure and that transformation at 930°F would proceed as indicated by the TTT diagram. This heat treatment resulted in greater than 80% transformation to the $\alpha + \delta$-phases, as determined by electrical resistivity measurements and metallographic examination. A typical area of the microstructure of these specimens is shown in Fig. 5.

The operating conditions and test results of the six MTR capsules are given in Table I. The indicated burn-ups were calculated by the heat-meter method. Burn-ups for the specimens in capsules 35-1 and 35-3 were also determined, but not reported here, by analyses of dosimeter wires and were

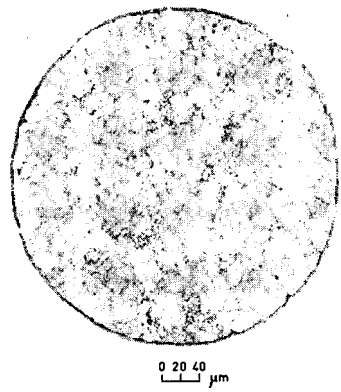


Fig. 5

Typical microstructure of samples heat treated at 1100°F for 100 h and a further 63 h at 930°F

within 15% of those determined by the heat-meter method. For this reason, additional dosimetry work was not done.

Dimensional changes were small (less than 2% diameter increase) for the specimens irradiated to burn-ups up to 1.0 at.% at temperatures ranging to about 900°F (capsules 35-1, 2 and 5). Specimens in these capsules were determined, by post-irradiation electrical-resistivity measurements and/or metallographic examination, to be in the γ-phase. Pre-irradiation and post-irradiation electrical resistivity data for four specimens in 35-1 are given in Table II. Also shown are values corrected for volume increases of the specimens. This correction was based on a method for correcting thermal conductivity measurements as presented by ODELEVSKI [9]. The correction is made on the assumption that the fission gas is dispersed in sub-microscopic voids in a uniform fashion throughout the fuel and that the gas has zero electrical conductivity. Metallographic examination of specimens 14 and 15 of capsule 35-2, and 8 and 9 of capsule 35-5 also indicated that these specimens were entirely in the γ-phase, typical microstructures of which are shown in Fig. 6. In all the metallographic work, an electrolytic-chromic acid etch was used, except where otherwise indicated. It is apparent, therefore, that under the irradiation conditions indicated the fission rates were sufficient to cause the transformed specimens to revert to the metastable γ-phase and to retain the γ-structure of those specimens that were originally in the γ-phase.

The specimens in the other three capsules (35-3, 4 and 7) were irradiated at only slightly higher temperatures and fission rates but received burn-ups comparable to those previously discussed. However, these specimens swelled considerably more than did the others, as is shown in Fig. 7. It is further pointed out that the specimens in capsule 35-4 were originally irradiated at fission rates and temperatures comparable to those of capsule 35-5. After 0.8 at.% burn-up, capsule 35-4 was shifted to a higher flux facility, where it received an additional 0.25 at.% burn-up. If one assumes

TABLE I

CONDITIONS AND RESULTS OF MTR RADIATION PROGRAMME

Capsule (No.)	Specimen (No.)	Initial phases and heat treatment[a]	Reactor full power time (h)	Mean temperature range (°F)	Approximate fission rate (10^{13} fissions $cm^{-3} s^{-1}$)	Burn-up (Total at.%)	Changes			Post-irradiation phases present	
							Length (%)	Diam. (%)	Density (%)	Determined by metallography	Determined by electrical resistivity
35-1	2	γ -(0)	2420	780-890	3.5	0.62	+1.3	+1.8	-4.0	-	-
	3	α+δ -(1)	"	770-900	3.5	0.62	+1.5	+1.2	-4.2	-	-
	8	γ -(0)	"	810-900	3.6	0.64	+1.0	+0.6	-2.8	-	γ
	9	α+δ -(1)	"	810-900	3.6	0.63	+0.3	+1.9	-5.4	-	γ
	11	γ -(0)	"	815-915[c]	3.6[c]	0.63[c]	+0.6	+1.3	-4.2	-	γ
	12	α+δ -(1)	"	820-930	3.6	0.63	+1.4	+1.2	-3.8	-	γ
35-2	6	α+δ -(1)	4490	640-800	3.00	0.91	+0.8	+1.0	-2.5	-	-
	5	γ -(0)	"	640-800	3.05	0.93	+0.8	+0.6	-2.2	-	-
	15	α+δ -(1)	"	650-845	3.20	0.96	+1.0	+0.8	-2.9	γ	-
	14	γ -(0)	"	675-880	3.30	0.99	+0.8	+0.6	-2.3	γ	-
	18	α+δ -(1)	"	695-885	3.30	0.99	+1.0	+0.9	-2.8	-	-
	17	γ -(0)	"	695-870	3.25	0.97	+0.7	+0.7	-2.4	-	-
35-3	2	γ -(2)	1750	985-1020	4.2	0.54	+2.8	+2.9	-8.4	-	γ+α+δ
	3	α+δ+γ -(2)	"	940-1010	4.2	0.54	+3.6	+3.4	-9.7	-	γ+α+δ
	5	γ -(0)	"	970-1000	4.1	0.53	+3.6	+3.5	-9.7	α+δ+γ	γ+α+δ

TABLE I (cont'd)

Capsule (No.)	Specimen (No.)	Initial phases and heat treatment [a]	Reactor full power time (h)	Mean temperature range (°F)	Approximate fission rate (10^{13} fissions $cm^{-3} s^{-1}$)	Burn-up (Total at.%)	Changes			Post-irradiation phases present	
							Length (%)	Diam. (%)	Density (%)	Determined by metallography	Determined by electrical resistivity
	5	γ -(0)	3460	750-830	3.25	0.77	+0.5	+0.4	-1.8	-	-
	6	α+χ+γ -(2)	"	755-870	3.25	0.77	+1.0	+1.0	-3.0	-	-
	8	γ -(0)	"	750-870	3.30	0.78	+0.6	+0.4	-2.0	γ	-
	9	α+δ+γ -(2)	"	740-835	3.20	0.76	+1.9	+0.6	-4.8	γ	-
35.7	58	γ -(0)	2930	950-1040	4.3	0.90	+4.1	Not measured		-	-
	59	α+δ+γ -(2)	"	970-1065	4.4	0.93	+5.1	Not measured		-	-
	61	γ -(0)	"	1005-1080	4.5	0.96	+5.4	+7.3	-16.6	γ(α+δ at edge)	-
	62	α+δ+γ -(2)	"	1005-1115	4.8	1.00	+6.3	+9.0	-19.8	γ(α+δ at edge)	-
	64	γ -(0)	"	1005-1115	4.8	1.00	+4.7	+6.2	-15.2	-	-
	65	α+δ+γ -(2)	"	1005-1115	4.7	0.99	+5.2	+9.0	-18.2	-	-

[a] Heat treatments of test specimens: (0) As-received γ
(1) 100 h at 930°F
(2) 100 h at 1110°F + 63 h at 930°F

[b] This capsule was removed from the reactor and re-inserted in a higher-flux facility.

[c] Thermocouple adjacent to specimen failed; temperature, fission rate and burn-up estimated on basis of adjacent thermocouple data.

TABLE I (cont'd)

Capsule (No.)	Specimen (No.)	Initial phases and heat treatment[a]	Reactor full power time (h)	Mean temperature range (°F)	Approximate fission rate (10^{13} fissions $cm^{-3} s^{-1}$)	Burn-up (Total at.%)	Changes			Post-irradiation phases present	
							Length (%)	Diam. (%)	Density (%)	Determined by metallography	Determined by electrical resistivity
35-3	6	α+δ+γ -(2)	1750	965-995	4.1	0.52	+3.6	+3.4	-9.8	α+δ+γ	γ+α+δ
	8	γ -(0)	"	965-995	4.1	0.52	-	+3.4	-7.3	-	γ+α+δ
	9	α+δ+γ -(2)	"	910-960	4.0	0.49	+2.0	+2.1	-5.9	-	γ+α+δ
35-4[b]	12	α+δ+γ -(2)	3892+	700-815	3.0	0.75					
			768	1000-1010	4.3	0.24 1.09	+5.0	Not measured		-	-
	11	γ -(0)	"	720-825	3.1	0.76					
				1005-1020	4.5	0.25 1.11	+5.5	Not measured		-	-
	15	α+δ+γ -(2)	"	730-830[c]	3.1[c]	-					
				1020-1040	4.6	- 1.13[c]	+6.4	+8.8	-19.3	α+δ+γ	-
	14	γ -(0)	"	740-835	3.2	0.80					
				1040-1050	4.7	0.26 1.16	+5.3	+6.4	-15.6	α+δ+γ	-
	18	α+δ+γ -(2)	"	725-820	3.1	0.79					
				1000-1020	4.5	0.25 1.14	+6.5	+7.8	-17.8	-	-
	17	γ -(0)	"	695-760	2.9	0.81					
				835-955	4.2	0.23 1.04	+4.8	+4.7	-11.7	-	-
35-5	2	γ -(0)	3460	-	3.20	0.76	+0.6	+1.1	-2.1	-	-
	3	α+δ+γ -(2)	"	750-840	3.20	0.76	+0.9	+0.8	-3.1	-	-

TABLE II

ELECTRICAL RESISTIVITY DATA FOR SPECIMENS FROM CAPSULES 35-1 AND 35-3

Capsule (No.)	Specimen (No.)	Initial phases	Electrical resistivity ($\mu\Omega$cm)		
			Pre-irradiation	Post-irradiation	Corrected [a]
35-1	8	γ	55.76	56.60	55.50
	9	$\alpha+\delta$	34.69	59.30	56.00
	11	γ	55.40	57.60	55.20
	12	$\alpha+\delta$	34.41	58.23	56.40
35-3	2	γ	56.48	54.76	49.20
	3	$\alpha+\delta+\gamma$	38.67	54.80	48.30
	5	γ	55.78	56.40	49.60
	6	$\alpha+\delta+\gamma$	36.61	55.55	49.00
	8	γ	55.93	57.30	52.30
	9	$\alpha+\delta+\gamma$	35.36	58.15	54.20

[a] Corrected values are to allow for volume increase of specimens. This correction was made by allowing a 2.3% volume increase per 1 at.% burn-up due to solid fission products. It was assumed that:

(1) Volume increase due to solid fission products would have no effect on the resistivity;

(2) Volume increase due to fission gases would have a significant effect on resistivity. The correction is based on zero conductivity of these fission gases.

that at the time of the shift the specimens were comparable to those in capsule 35-5, then the large diameter increases all occurred during the final 0.25 at.% burn-up.

As in the case of the other capsules, post-irradiation examination of these specimens was carried out to determine the metallurgical-structure. Electrical resistivity measurements were made on the specimens in capsule 35-3 and are reported in Table II. The data, after correction for swelling, indicate that the specimens had transformed to some extent. However, the analysis of the resistivity measurements is complicated by the fact that the thermally stable δ-phase may disorder under irradiation and indicate the presences of the γ-phase, as suggested by BLEIBERG [10]. Bleiberg proposed that a small decrease in the electrical resistivity of the γ-phase after irradiation could be caused by partial ordering of this structure. With the high burn-ups of the specimens in capsule 35-3, it is believed that the solid fission-product impurities (resistivity uncorrected volume increase) would increase the resistivity of the γ-structure and could compensate in this way for this ordering effect; and that the resistivity is, indeed, indicating a partial transformation to the $\alpha+\delta$-phases. Admittedly this interpretation

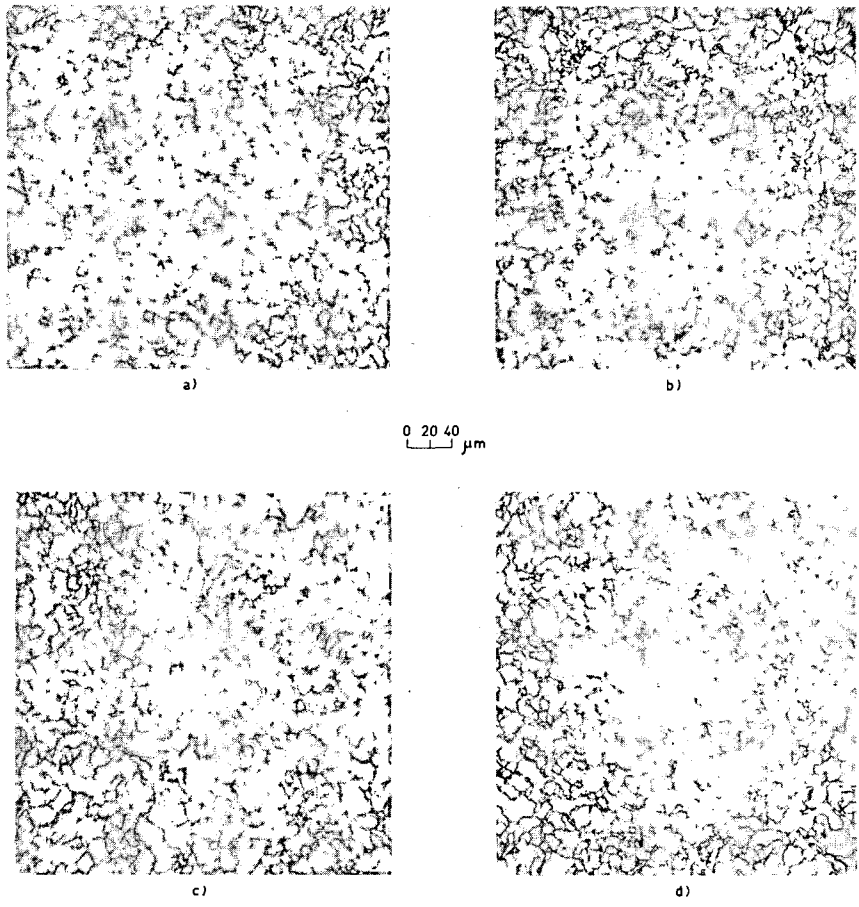


Fig. 6

Microstructure of specimens irradiated at temperatures of less than 900°F and fission rates of less than 3.6×10^{13} fissions cm^{-3} s^{-1}

(a) Specimen 14, from 35-2: pre-irradiation = γ-phase, post-irradiation = γ-phase
(b) Specimen 15, from 35-2: pre-irradiation = α+δ+γ phases, post-irradiation = γ-phase
(c) Specimen 8, from 35-5: pre-irradiation = γ-phase, post-irradiation = γ-phase
(d) Specimen 9, from 35-5: pre-irradiation = α+δ+γ-phase, post-irradiation = γ-phase

is open to argument. There is no question that the specimens with the initial α+δ-structure have partially reverted to the γ-phase. Metallographic examination of specimens 5 and 6 of capsule 35-3 indicated that some transformation of the γ-structure to the thermally stable phases had indeed occurred and that the specimen which was originally α+δ+γ contained a greater percentage of the γ-phase than it did before irradiation. Microstructures of these two specimens are shown in Fig. 8. Metallography of these specimens was exceedingly difficult; but following a series of etching procedures, it was concluded that some α-phase was present in both cases,

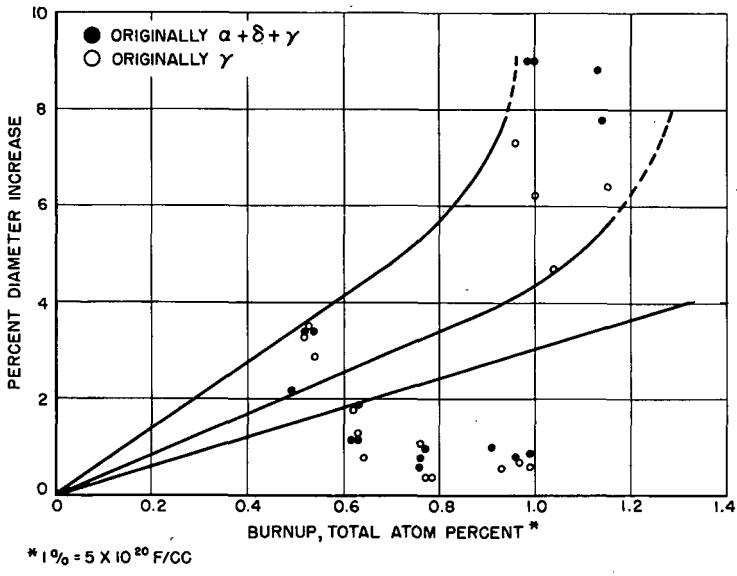


Fig.7

Diameter changes against burn-up for two fission-rate and temperature ranges of MTR specimens

A: Partial transformation after irradiation; fission rate $(4.0 - 4.8) \times 10^{13}$ fissions cm^{-3} s^{-1}
centre temperature 950 - 1115° F

B: γ-phase after irradiation; fission rate $(3.0 - 3.6) \times 10^{13}$ fissions cm^{-3} s^{-1}
centre temperature 640 - 900° F

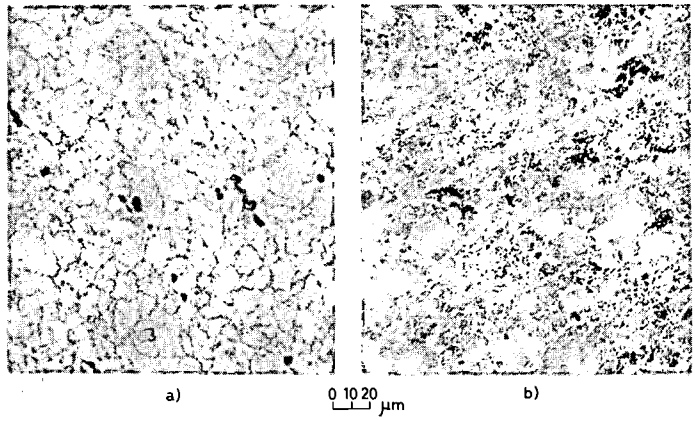


Fig.8

Microstructure of specimens irradiated at 965 - 1000° F at a fission rate of 4.1×10^{13} fissions cm^{-3} s^{-1}

(a) Specimen 5, from 35-3: pre-irradiation = γ-phase; post-irradiation = γ+α+δ-phase
(b) Specimen 6, from 35-3: pre-irradiation = α+γ+δ-phase, post-irradiation = γ+α+δ-phase

and that there was more α-phase present in specimen 6, which was originally transformed. The transformation products appeared more spheroidal than is usually found in the thermally transformed alloy.

Metallographic examinations of specimens from capsules 35-4 and 35-7 were also carried out. Specimens 14 and 15 of capsule 35-4 showed a predominately $\alpha + \delta$-structure (Fig. 9), with the γ-phase being evident near the

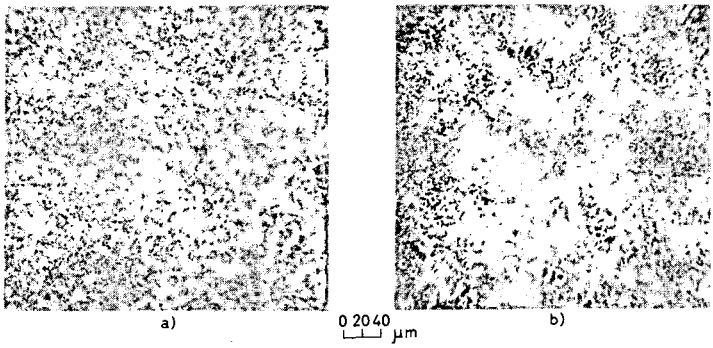


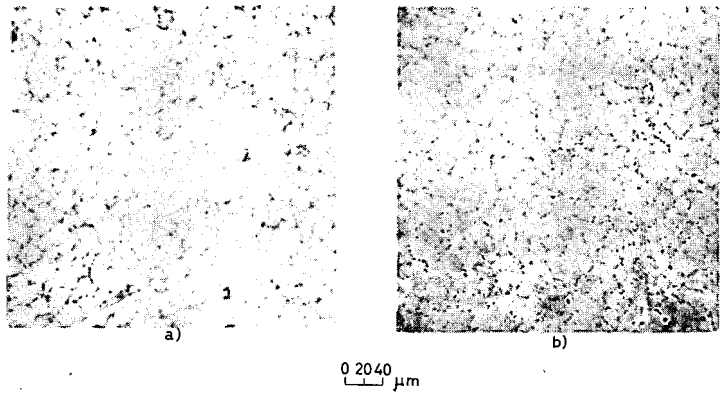
Fig. 9

Microstructure of specimens irradiated at 730 - 835°F at a fission rate of 3.1×10^{13} fissions $cm^{-3} s^{-1}$ and then shifted to 1020 - 1050°F at 4.6×10^{13} fissions $cm^{-3} s^{-1}$

(a) Specimen 14, from 35-4: pre-irradiation = γ-phase, post-irradiation = $\alpha+\delta+\gamma$-phase
(b) Specimen 15, from 35-4: pre-irradiation = $\alpha+\delta+\gamma$-phase, post-irradiation = $\alpha+\delta+\gamma$-phase

centre. As in the case of capsule 35-3, some difficulty was encountered in metallographic identification of the structure. In this case, however, it was further complicated by what appeared to be fission-gas bubbles in the matrix. However, it is clear that some α-phase is present. In some instances, the normal lamellar transformation product was seen, but again the transformation products appear more spheroidal than is usually observed. As in the case of specimen 6 from capsule 35-3, more α-phase appeared to be present in specimen 15, which was originally transformed. Shown in Figs. 10a and b are typical sections near the centre of sample 61 of capsule 35-7; Fig. 10c shows a section near the edge. It appears that the material at the centre is in the γ-phase (its pre-irradiation condition), with voids or precipitated particles outlining the grains, while at the edge there is a small amount of transformation product. The same general observations may be made for specimen 62, which was originally transformed (Fig. 11). The occurrence of this transformation gradient from the centre to the edge may be explained by the high operating temperature of the fuel, as indicated in Table I, and the temperature drop across the fuel pin which amounts to $\sim$100°F. Because these samples were close to the eutectoid temperature, the centre region of the specimens may have been shifting from the normally γ-temperature range to the $\alpha + \delta$-temperature range during various reactor cycles.

Referring back to Fig. 7, it appears that those specimens which did not swell appreciably were all in the γ-phase, while those that did swell had



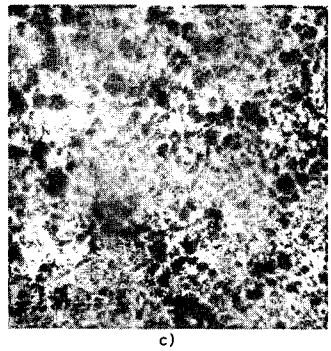


Fig. 10

Microstructures of specimen 61 from 35-7

Pre-irradiation = γ-phase, post-irradiation = predominantly γ-phase except for α+δ-phase near edge. Temperatures 1005 - 1080°F at a fission rate of 4.5×10^{13} fissions $cm^{-3} s^{-1}$

(a) Centre of specimen (b) As (a), but heat-etched

(c) Edge of specimen, note presence of lamellae (heat-etched)

transformed or remained in the α+δ-condition, at least to some extent. It was on this basis that the curves for the two metallurgical conditions were drawn.

A summary of the results and observations of the MTR radiation specimens is as follows:

(1) All the samples irradiated in capsules 35-1, 2 and 5 were either retained in or transformed to the γ-phase by irradiation at fission rates of 3.0 to 3.6×10^{13} fissions cm^{-3} s^{-1} and centre-line temperatures between about 640 and 900°F.

(2) Specimens irradiated in capsule 35-4, first at 695 to 835°F, and then at 935 to 1050°F, swelled during irradiation at the higher temperature. This is based upon the observation that other specimens irradiated at the

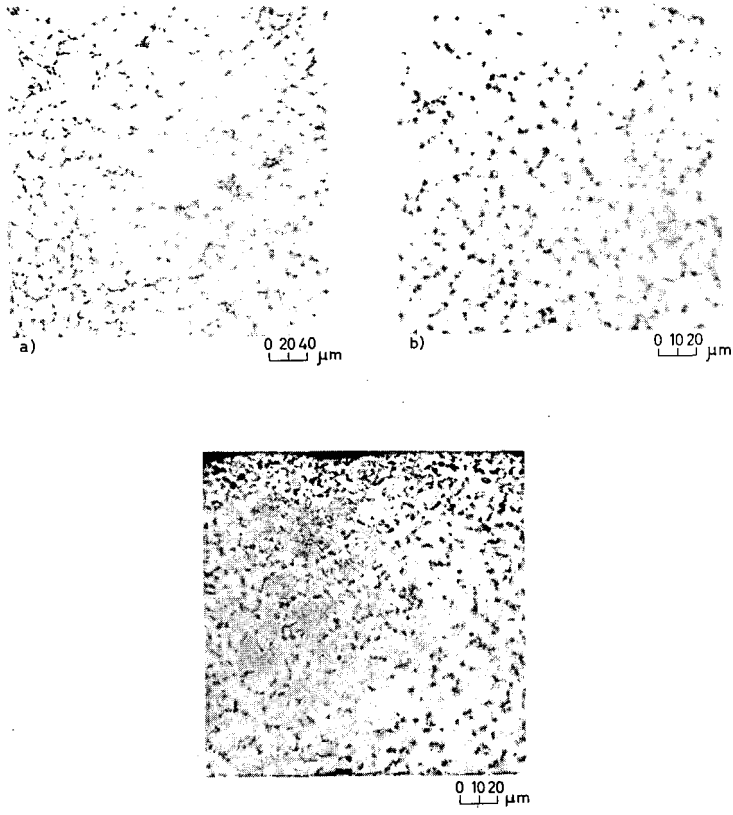


Fig. 11

Microstructures of specimen 62 from 35-7

Pre-irradiation = α+δ+γ-phase, post-irradiation = predominantly γ-phase except for α+δ-phase near edge. Temperatures 1005 - 1115°F at a fission rate of 4.8×10^{13} fissions $cm^{-3}\ s^{-1}$

(a) Centre of specimen (b) As (a), but heat-etched

(c) Edge of specimen: note presence of lamellae (heat-etched)

lower temperature range, at similar fission rates and to about the same burn-up, did not swell excessively.

(3) Specimens from 35-3 and 35-4 showed significant amounts of transformation product although not the equilibrium amount. The identification of the transformed phases by metallographic techniques was extremely difficult but reasonably conclusive.

The appearance of the transformed products resulting during irradiation is more spheroidal than lamellar, which is normally found in thermally transforming this alloy in the absence of irradiation. At the temperature ranges for samples in capsules 35-3 and 35-4, it would appear that a fission rate of ~ 4.0 to 4.5×10^{13} fissions $cm^{-3}\ s^{-1}$ is not sufficient to maintain the γ-phase completely or to put back into solution the thermally stable phases.

(4) The amount of swelling for a given burn-up appears to be only slightly affected by the phases present before irradiation, particularly when the material is irradiated under conditions where the γ-phase is stable, see Fig. 7. Under irradiation conditions where the $\alpha + \delta$-phases are stable, the specimens that were originally transformed show slightly more swelling than those that were γ.

(5) It is not clear whether swelling of the 35-7 specimens is caused by transformation or by the high-temperature irradiation of the γ-phase.

3.2. CP-5 irradiation programme

Shown in Table III are the irradiation conditions and over-all specimen changes that occurred due to irradiation. Also included are the initial phases of each U-10 wt.% Mo pin and the heat-treatments which were given to the as-fabricated pins. In all cases where it was desired to transform the pins to the $\alpha + \delta$-phases before irradiation, a minimum time of 72 h at a temperature of 930°F was used. Specimens CP-5-6e, 7e and 7ec were swaged from 0.158-in to 0.126-in diam. and then given a stress-relief heat-treatment at 1470°F for one hour. These samples were zirconium-clad, but because of the additional cold-swaging, the thickness was decreased from the nominal 0.005 in to ~0.004 in.

As shown in Table II, the over-all density of all specimens decreased and, in all but one case (CP-5-7a), the length increased, as would be expected. The CP-5-7a pin was the only instance of a decrease in length noted in this series of tests and is quite uncommon for this alloy. A sample mix-up was suspected, but upon further examination it seemed that the effect was real and has not been explained. The re-encapsulation and re-insertion procedure, as previously discussed, was successfully followed for the CP-5-5b and 6e specimens and there is, therefore, a second burn-up increment for these pins.

3.2.1. General appearance. The general appearance of the CP-5-5a, 6a and 7a samples was extremely good. There was no evidence of zirconium-cladding cracks or warping. After the first burn-up increment of CP-5-5b, a dark coating, assumed to be oxide, covered the specimen cladding. There was no evidence of cracking of the cladding and the element was, therefore, re-encapsulated for additional burn-up accumulation. After an average total burn-up of 0.83 at.%, the general appearance remained unchanged except for a large crack which extended from the bottom of the sample to about 6 in from the bottom. The reason for this cracking is not known at present. Because of this crack, any diameter measurements in this area would be meaningless.

The appearance of the CP-5-6e specimen after the first burn-up increment was good with no evidence of cracking or significant cladding discoloration. After the second burn-up increment, the clad surface was blackened and small axial "hairline" cracks extended over most of the length but no large fissures were observed. The cracks are believed to be associated with the embrittling effect of oxygen diffusion into the zirconium cladding, the oxygen being present as an impurity in the NaK. At 3 in from the

TABLE III

DATA SUMMARY ON CP-5 IRRADIATION CONDITIONS AND OVER-ALL CHANGES

	CP5-5a	CP5-6a	CP5-7a	CP5-5b 1st Inc.	CP5-5b 2nd Inc.	CP5-6e 1st Inc.	CP5-6e 2nd Inc.	CP5-7e	CP5-7ec
Initial phases and heat treatment[a]	α+δ-(1)	α+δ-(2)	γ - (3)	α+δ-(1)		α+δ-(4.2)		γ - (4)	γ - (4)
Capsule type	Air-cooled	Water boiler	Water boiler	Air-cooled		Water boiler		Water boiler	Water boiler
Time in-pile (h)	4510	4424	4405	3290	2598	670	2690	650	2210
Average burn-up (total at.%)	0.31	0.33	0.31	0.52	0.83 (total)	0.21	1.0 (total)	0.21	0.67
Length change (%)	+1.12	+0.39	-2.45	+3.2	+5.6 (total)	+0.31	- c	- c	- c
Density decrease (%)	-1.97	-3.8	-1.6	-5.5	-15.7 (total)	-3.26	-10.98 (total)	-2.92	-7.1
Average Fission Rate (10^{13} fissions $cm^{-3} s^{-1}$	1.1	1.44	1.44	1.3/2.6	2.4	5.4	5.4	4.7	5.7
Original diameter (in)	0.158	0.158	0.158	0.158		0.126		0.126	0.126
Original length (in)	25.13	15.38	15.92	30.0		14.95		15.0	15.0

[a] Heat-treatment

(1) 96 h at 930°F
(2) 72 h at 930°F
(3) γ as fabricated
(4) γ as fabricated + swaging + 1 h at 1470°F.

[b] See figures for local burn-up.

[c] Top end appeared to have melted due to poor thermal bond.

top of this specimen, several small sections of the cladding were flaked-off and the upper 2 in showed considerable damage to cladding and swelling of the specimen. It is believed that excessive temperatures were encountered locally near the top of the pin because of a poor NaK bond. A poor NaK bond was also thought to have affected the CP-5-7e pin at the low temperature end (top) and, again, this region showed considerable damage while the remainder of the pin was in good condition. The CP-5-7ec pin had about the same general appearance as the 6e pin after the second burn-up increment and included a dark surface coating of what was assumed to be oxide. The top of this pin was severely damaged by what was assumed to be excessive temperatures resulting from a poor thermal bond. Axial "hairline" cracks also extended along the length of this sample. These "hairline" cracks, and those mentioned previously, would not have a significant influence on dimensional measurements.

3.2.2. Diameter changes. Shown in Figs. 12 to 19 are the changes in diameter that occurred at various intervals along the length of the CP-5 irradiated pins. Also shown are the central metal temperature, burn-up and fission rates that were associated with these changes. The changes shown are calculated from the average of at least two micrometer measurements taken 90° apart, both before and after irradiation.

The diameter changes incurred by pins CP-5-5a, 6a and 7a, as shown in Figs. 12, 13 and 14, respectively, are all less than 2%. Since these changes are so small and were obtained at low burn-ups, they are not considered significant and are presented only for completeness in reporting the data. It may be seen in Fig. 12 that the diameter appeared to decrease slightly at temperatures up to 1000°F, and then increased slightly at higher

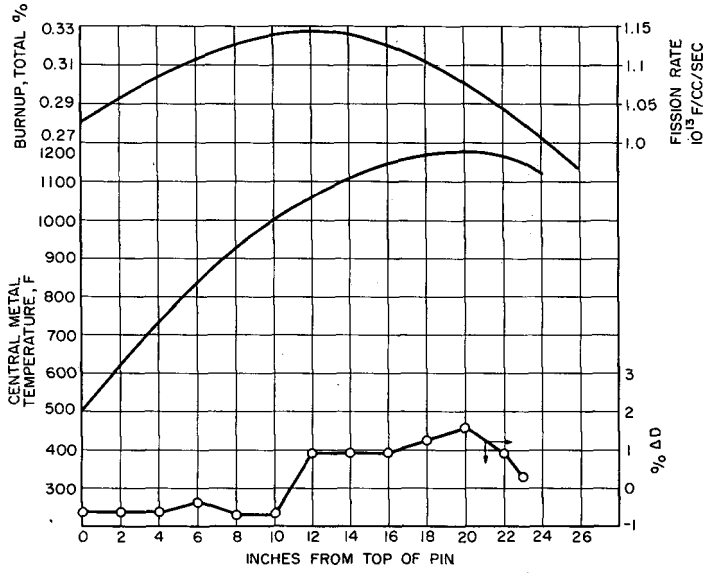


Fig. 12

Results of CP-5-5a irradiation

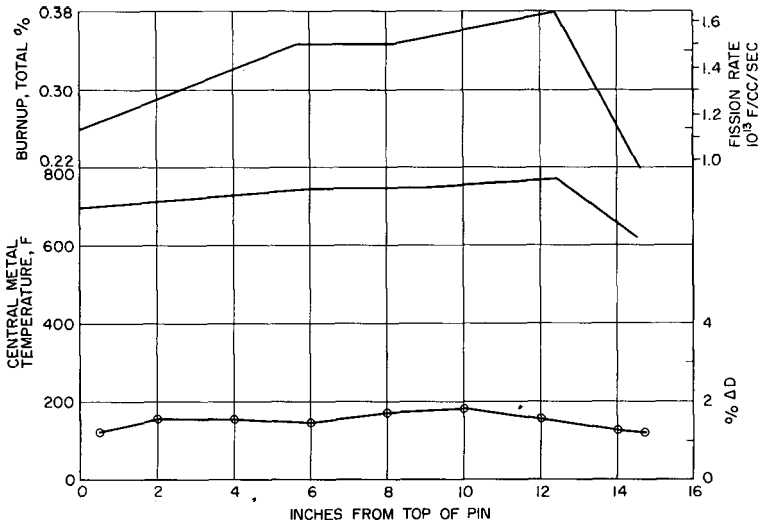


Fig. 13

Results of CP-5-6A irradiation

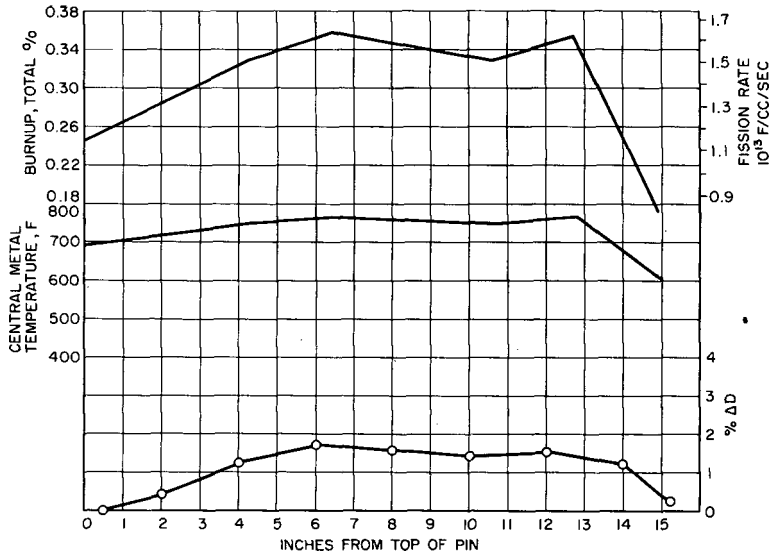


Fig. 14

Results of CP-5-7a irradiation

temperatures. As shown in Fig. 13, there was an almost uniform diameter increase of ~1.5% over the entire length of the 6a pin. The diameter increase of the 7a pin was also nearly uniform along its length and was about 1.5% as shown in Fig. 14.

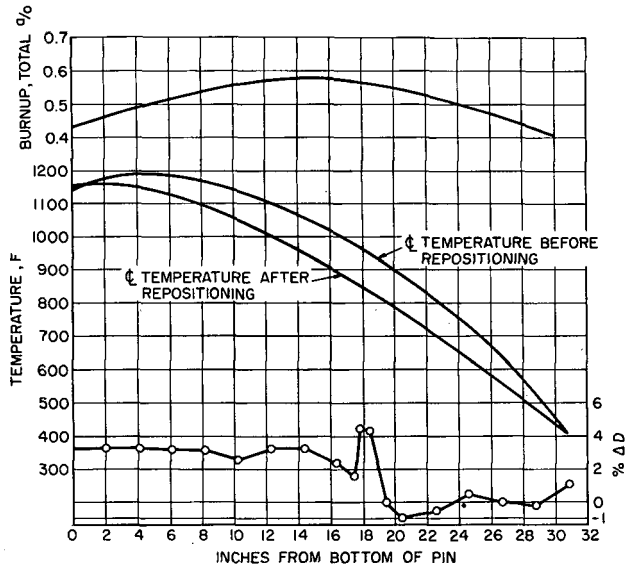


Fig. 15

Results of CP-5-5b irradiation

(first burn-up increment)

Diameter changes for the first burn-up increment (average 0.52 at.% burn-up) of the 5b pin are shown in Fig. 15. During this irradiation increment the CP-5 reactor power level was increased from 2.2 to 4.6 MW. To obtain the same approximate temperatures along the length of the pin, the capsule was repositioned in the reactor before the reactor power was increased. The result of this repositioning on the temperature is indicated, but only the average burn-up values for this increment are shown. The average burn-up was 0.3 at.% before repositioning, which corresponded to an average fission rate of 1.3×10^{13} fissions $cm^{-3}\ s^{-1}$. There was little diameter change for this increment at central metal temperatures of $< 800°F$. The maximum swelling occurred where the temperature was 970°F before repositioning (burn-up = 0.33 at.%) and 850°F after repositioning (additional burn-up = 0.24 at.%). This peak was checked several times and is considered real. It is, of course, not clear whether the diameter increase occurred before or after repositioning. The higher-temperature portion of this pin had a rather uniform swelling of between 2.5 to 3.3% diameter increase as shown. The results of the second burn-up increment of CP-5-5b are shown in Fig. 16. The calculated temperatures along the length of the pin were about the same as the repositioned first burn-up increment portion, since it was reinserted into the same reactor position. Included in this curve is the fission rate, temperature, total burn-up and diameter change. A large fissure was detected and extended over the lower 6 in of the pin, as indicated. Diameter measurements taken at 6 in from the bottom and below are, therefore, not meaningful. A maximum of 13.5% diameter increase

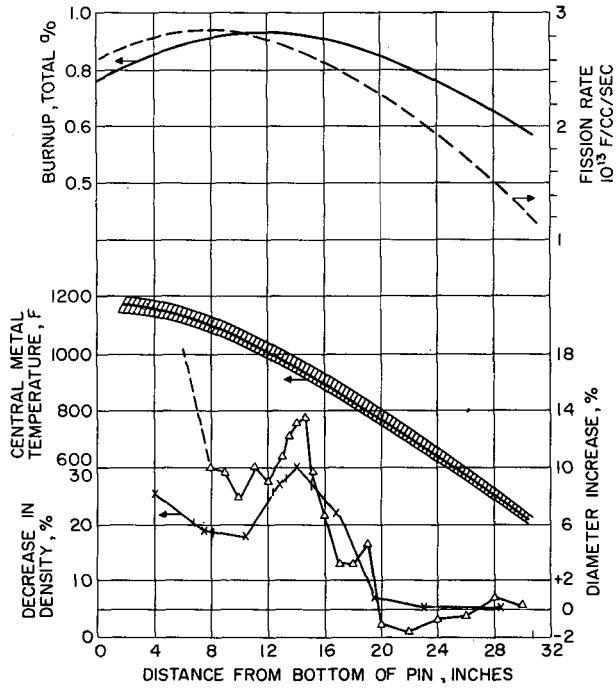


Fig. 16

Results of CP-5-5b irradiation

was observed at the 14-in point and corresponds to a temperature of 960°F and burn-up of 0.92 at.%. The cladding was intact and without cracks at this point. At higher temperatures (up to the fissure) the diameter was significantly less, although the total burn-up was essentially the same. Between the 8-in and 12-in points, where the temperature was between 1000 and 1100°F, the diameter increase was from 8 to 10%. This diameter increase peak was very much like the results of the CP-5-1 pin reported by SILLIMAN et al. [3] where the maximum diameter increase occurred at 975°F and the burn-up increased slightly with increasing temperature above 975°F, while the diameter decreased. Below 960°F the percentage of diameter change decreased rapidly to the point where the maximum swelling of the first burn-up increment was found (~ 19 in). There is a small linear transposition of this point, as may be seen by comparing Figs. 15 and 16, caused by the longitudinal growth of the specimen due to irradiation. It is interesting to point out that at this position the diameter did not increase over that found for the first burn-up increment. In order to confirm the diameter increase curves, density values were taken after the pin was sectioned into various lengths. In Fig. 16 the average density changes are shown for various lengths of the pin. The vertical lines shown indicate the sample length on each side of the point. It is, therefore, obvious that the largest density change did occur at the 14-in point (30%), confirming the diameter data in this respect.

The results of the first and second burn-up increments of the CP-5-6e pin are shown in Fig. 17. The fission rates and temperatures were identical in each of these increments, since they were re-inserted into the identical

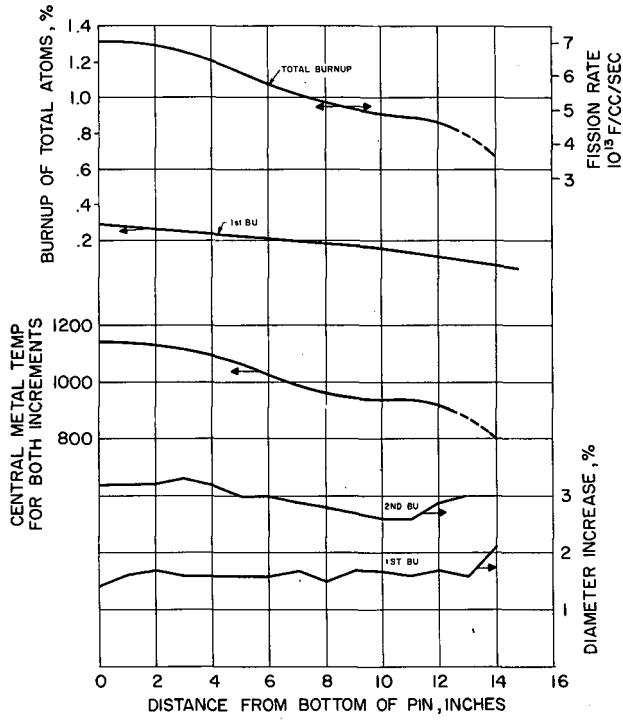


Fig. 17

Results of CP-5-6e irradiation

position in the reactor. The diameter increase after the first burn-up increment was an almost uniform 1.6% as shown, and, after the second burn-up increment, was 3 ± 0.4% over the entire length, except near the top where the specimen was damaged and may have melted, as previously mentioned. In the temperature range of 930 to 1060°F the sample only increased from 2.6 to 3% when irradiated at fission rates of from (5 to 6) × 10^{13} fissions cm^{-3} s^{-1} for burn-ups between 0.9 and 1.1 at.%.

Figs. 18 and 19 show the diameter changes incurred by the CP-5-7e and 7ec pins. The 7e pin exhibited an almost uniform diameter increase varying between 1.2 and 2.1% at temperatures between 780 and 1180°F and corresponding fission rates and burn-ups from (3.3 to 7.0) × 10^{13} fissions cm^{-3} s^{-1} and 0.14 to 0.31 at.% burn-up. The 7ec sample also exhibited an almost uniform increase along its length of 3 ± 0.4%, except where melting had apparently occurred. Fission rates ranged from (4.5 to 6.7) × 10^{13} fissions cm^{-3} s^{-1} with corresponding burn-up values of 0.53 to 0.8 at.%.

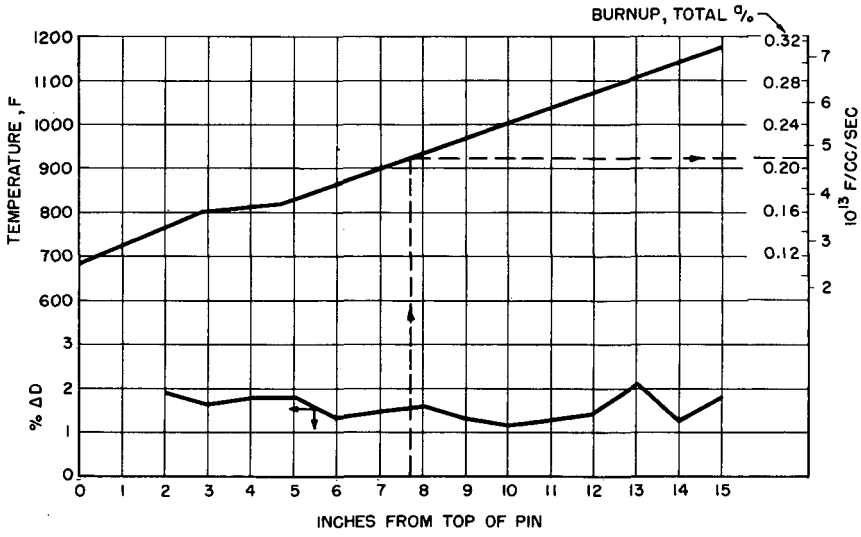


Fig. 18

Results of CP-5-7e irradiation

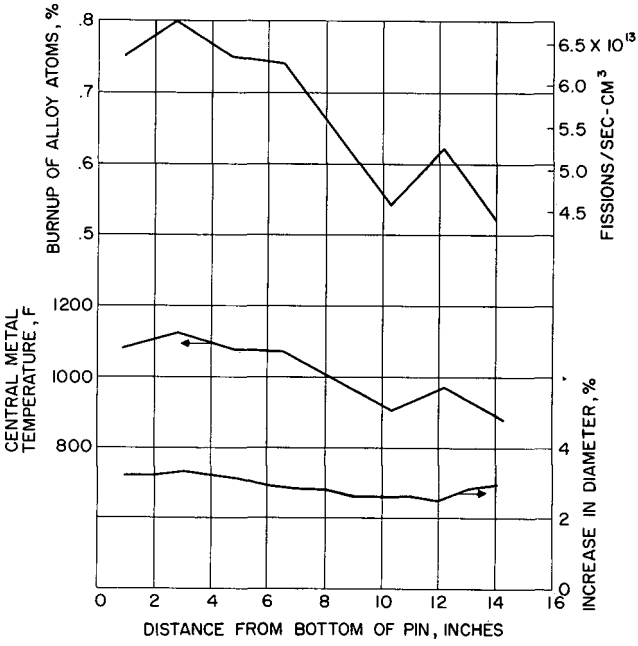


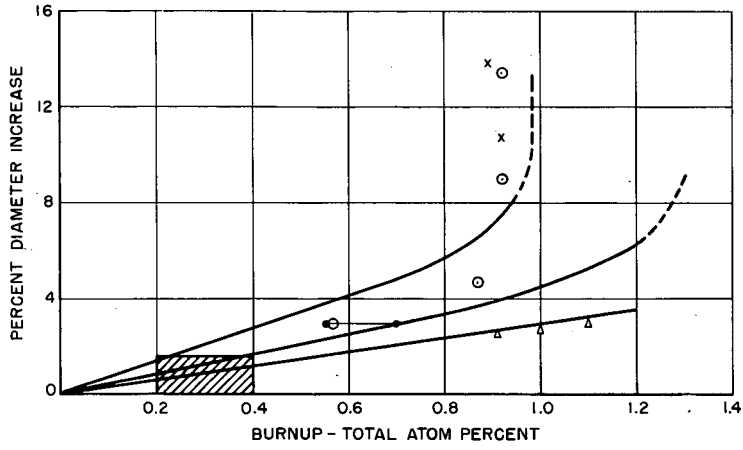
Fig. 19

Results of CP-5 7ec irradiation

4. DISCUSSION

As discussed in previously reported data [2], it was determined that at fission rates greater than 8×10^{13} fissions cm^{-3} s^{-1}, and over the temperature range of 900 to 1100°F, the U-10 wt.% Mo alloy swelled very little as a result of burn-ups up to about 1.2 at.%. The data herein reported and those previously reported by SILLIMAN et al. [3] show that large fuel swelling does occur at temperatures in the range of 960-1050°F, provided the fission rate is of the order of 4×10^{13} fissions cm^{-3} s^{-1} or less. It is also shown by the CP-5-1 [3] and the CP-5-5b pins that this is not simply a temperature or material strength effect, since swelling has been observed to decrease with increasing temperature above about 975°F and at comparable or higher burn-ups.

The curves representing the effect of the irradiation conditions illustrated in Fig. 7 for the MTR tests have been replotted in Fig. 20, together with pertinent data points (Table IV) from the CP-5 tests. A band has been shown for the low burn-up points of the CP-5 tests. Again, it is seen that for burn-ups greater than 0.5 at.% the swelling appears to fall in two groups. The data from the CP-5-6e pin put it in the low swelling range, while the other specimens, with the exception of the 7ec sample which spans the range,



DIAMETER CHANGES VS BURNUP

Fig. 20

Diameter changes plotted against burn-up for selected CP5 points plotted using the MTR curves (see Fig. 7).

TABLE IV

SELECTED CP-5 SWELLING POINTS

Sample designation	Temperature range (°F)	Burn-up range (at.%)	Fission rate (10^{13} fissions $cm^{-3}s^{-1}$)	Diameter increase (%)
CP5-1	975	0.89	2.5	13.9
	1025	0.92	2.5	10.7
CP5-5b(1st)	960	0.57	~2.7	3.0
CP5-5b(2nd)	900	0.87	2.5	4 7
	960	0.92	2.7	13.5
	1060	0.92	2 8	9.0
CP5-6e(2nd)	930-1050	0.91-1.1	5-6	2.6-3.0
CP5-7ec	930-1060	0.56-0.7	4.7 to 6.3	3 max.

appear to be in the high swelling range. Where post-irradiation metallographic examinations and electrical resistivity measurements have been made, it was indicated that the excessive swelling is associated with either complete or partial transformation of the γ-phase to the $\alpha + \delta$ phases.

Unfortunately, the metallographic examination of the CP-5 test specimens was not completed in time for inclusion in this paper. However, without benefit of this information, if we now select the data points of both the MTR and CP-5 samples, where burn-ups of 1.0 ± 0.15 at.% were achieved, at temperatures of ~975°F, and plot their diameter increase as a function of fission rate, we see essentially a linear dependence of swelling on fission rate as shown in Fig. 21. The origin of the data points used for this plot are indicated on the curve. The specimens of 35-4 were plotted here although they operated at temperatures somewhat higher than 975°F. Since it was shown that the higher temperature would not result in greater swelling, we felt we coult justifiably plot these results on this curve. Of these data, the CP-5-1 point has indirectly been identified as having an $\alpha + \delta$-structure [3], the 35-4 specimen is identified as partially transformed, while the MTR data at high fission rates were believed to refer to γ-phase [2]. Identification of the microstructure of the CP-5-5b and 6e specimens is currently in progress, but on the basis of this curve it would appear that they should be essentially $\alpha + \delta$ and γ-phase respectively. It is not clear that the swelling is due solely to the transformation and the poor stability of the alpha structure, since the possibility remains that the swelling could be the result of the increased time allowing swelling to take place by a creep mechanism. An experiment would have to be especially designed with this specific objective, to separate these two possibilities.

At irradiation temperatures of 800 to 900°F, it has been shown by the MTR results that the γ-phase is thermally stable at fission rates of 3.6×10^{13} fissions $cm^{-3}s^{-1}$, and the alloy resists swelling during irradiation. BLEIBERG et al. [10] demonstrated that the $\alpha + \delta$-phases, when irradiated at low temperature, revert to the γ-phase and, while this reversion was

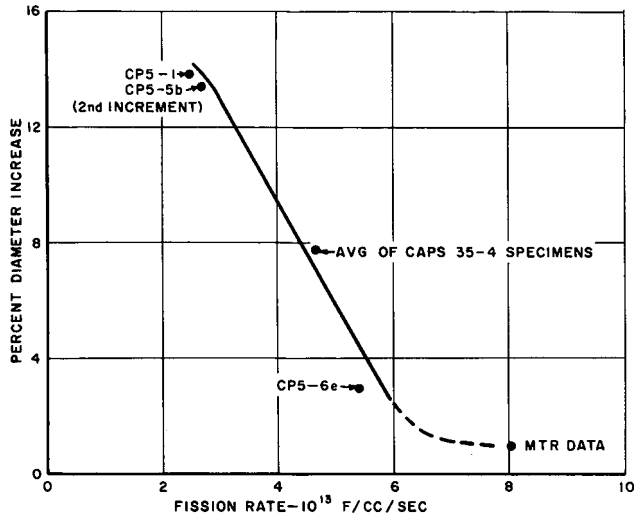


Fig. 21

Diameter changes plotted against fission rate for U-10 wt.% Mo specimens irradiated at ~975°F to burn-ups of 9.0 ± 0 15 total at.%

detected by X-ray diffraction and electrical resistivity, the $\alpha+\delta$-structure persisted metallographically. In our work, in which the $\alpha+\delta$-phases reverted to the γ-phases at temperatures of 800 to 900°F, the γ-structure was plainly detected and was confirmed by electrical resistivity measurements.

Metallographic identification of the metallurgical structure of the specimens irradiated at temperatures greater than 960°F was extremely difficult. This was believed to be due in part to the swelling that had occurred in these specimens and, to some extent, to differences of the structure after high-temperature irradiation. The transformation products, in general, appear to be more spheroidal and finer than for material thermally transformed at those temperatures.

Although phase identification by metallographic and electrical resistivity techniques seems reasonably certain, more positive identification by X-ray diffraction would be desirable.

5. CONCLUSIONS

On the basis of this work, the following conclusions have been drawn for U-10 wt.% Mo alloy fabricated in such a manner as to give transformation kinetics comparable to those shown in Fig. 1:

(1) A fission rate of 3.6×10^{13} fissions cm^{-3} s^{-1} is sufficient to maintain the γ-phase or cause the $\alpha+\delta$-phases to revert to γ-phase during irradiation at temperatures up to about 860°F. Under these conditions, the dimensional stability of the fuel is good for burn-ups to at least 1.0 at.%.

(2) At temperatures greater than about 930°F, a fission rate of 7×10^{13} fissions $cm^{-3}\ s^{-1}$ or greater is necessary to maintain the γ-phase or cause the $\alpha + \delta$-phases to revert to γ-phase during exposures of up to ~1.0 at.% burn-up.

(3) At an irradiation temperature of about 975°F, diameter increase at 1.0 ± 0.15 at.% burn-up appears to be a linear function of and inversely proportional to the fission rate between 2.5 and 7.0×10^{13} fissions $cm^{-3}\ s^{-1}$.

(4) For radiation in the temperature range of 950-1050°F and for fission rates of ~2.5×10^{13} fissions $cm^{-3} s^{-1}$, the swelling of the U-10 wt.% Mo alloy will increase rapidly with burn-ups > 0.5 at.% and will approach a diameter increase of ~14% at 0.9 at.% burn-up. The mechanism for the swelling is not clearly understood, but it is suggested that it is associated with the α-phase.

(5) The swelling characteristics during irradiation are only slightly influenced by the phases present in the alloy before irradiation.

ACKNOWLEDGEMENTS

The authors are indebted to numerous engineers and technicians at the Argonne National Laboratory, where the CP-5 tests were conducted, and at Battelle Memorial Institute, where the MTR capsules were designed and fabricated and the samples examined before and after irradiation. The successful completion of this programme would not have been possible without their willing co-operation.

We are particularly appreciative of the efforts of W.E. Murr and A.A. Bauer for their assistance in the MTR phase of this work. All of the metallographic studies connected with this programme were carried out at the Battelle Memorial Institute hot-cell facility.

Finally, we would like to acknowledge the assistance of P.R. Huebotter of Atomic Power Development Associates and A D. Smart of the Detroit Edison Company for the many contributions they have made.

REFERENCES

[1] CAULKINS, G.D., GATES, J.E., BAUER, A.A. and ROUGH, F.A., Radiation Stability Studies on Binary Uranium Alloy, 2nd Nucl.Engng. and Science Conf., Battelle Memorial Institute, Paper NESC-109 (March 1957).

[2] LEESER, D.O., ROUGH, F.A., and BAUER, A.A., Radiation Stability of Fuel Elements for the Enrico Fermi Power Reactor, Proc. 2nd UN Int.Conf. PUAE 5 (1958) 587.

[3] SILLIMAN, M.A., SHOUDY, A.A., HUEBOTTER, P.R. and BLESSING, W.G., Irradiation Testing of Enrico Fermi Protytype Fuel Pins in the CP-5 Reactor, ASTM Special Tech. Publ. No. 286.

[4] THOMAS, D.C. and FILLNOW, R., Bettis Atomic Power Laboratory, private communication.

[5] Work to be published.

[6] DWIGHT, A.E., The uranium-molybdenum equilibrium diagram below 900°C, J.nucl.Mat. 2 (1960) 81.

[7] USAEC Rpt. ANL-5371, (Oct. - Dec. 1954).

[8] SCHILTZ, R.J., MONAWICK, J.H. and SOWA, E.S., Fuel Irradiation Facilities, USAEC Rpt. ANL-5940 (Nov.1958).

[9] ODELEVSKI, V.I., Calculations of Generalized Conductivity of Heterogeneous Systems, Zhur Telsh, Fig. 21 (1951) 667.

[10] BLEIBERG, M.L., JONES, L.S. and LUSTMAN, B., Phase Changes in Pile-Irradiated Uranium-Base Alloys, J. appl. Phys. 27 1 (Nov. 1956).

QUELQUES RESULTATS D'IRRADIATION SUR LES COMBUSTIBLES ENVISAGES POUR «RAPSODIE»

J.-P. MUSTELIER
CENTRE D'ÉTUDES NUCLÉAIRES DE SACLAY,
GIF-SUR-YVETTE (S. et O.) FRANCE

Abstract — Résumé — Аннотация — Resumen

SOME EFFECTS OF IRRADIATION ON THE FUEL TYPES UNDER CONSIDERATION FOR THE "RAPSODIE" REACTOR. Two types of fuel are being considered for use in the core of the "Rapsodie" reactor: the UPuMo alloy, containing 20% plutonium and 10% molybdenum, and the mixed oxide UO_2PuO_2, containing 25% PuO_2. The results of the irradiation tests which the authors carried out on fuel elements of these types are as follows:

(1) UPuMo alloys: Twenty-four samples of as-cast UPuMo alloy were irradiated in the EL3 reactor at burn-ups between 4400 MWd/t and 8300 MWd/t. The unclad samples were immersed in liquid sodium at various temperatures from 400 to 525°C. Examination of the samples following irradiation showed that they had increased in volume by between 30% and 104%. The bubbles causing this swelling can be seen in the micrographs:

(2) Oxides: Six fuel elements in the form of needles, four consisting of enriched uranium oxide and two of the mixed oxide UO_2PuO_2, were irradiated in the EL3 reactor. The temperature of the cladding was 450°C and the specific power was between 1000 and 1750 W/cm³. Examination of the needles provided some data on their behaviour under irradiation.

QUELQUES RÉSULTATS D'IRRADIATION SUR LES COMBUSTIBLES ENVISAGÉS POUR «RAPSODIE». Deux combustibles sont à l'étude pour le cœur de RAPSODIE: l'alliage UPuMo à 20% de plutonium et 10% de molybdène et l'oxyde mixte UO_2PuO_2 à 25% de PuO_2. Les résultats des essais d'irradiation que nous avons effectués sur ces combustibles sont les suivants:

1. Alliages UPuMo: 24 échantillons d'alliage UPuMo brut de coulée ont été irradiés dans la pile EL3 à des taux de combustion étagés entre 4400 MWj/t et 8300 MWj/t. Les échantillons non gainés étaient immergés dans du sodium liquide à différentes températures allant de 400 à 525°C. Les examens après irradiations ont permis de constater des augmentations de volume des échantillons comprises entre 30 et 104%. Les micrographies mettent en évidence les bulles responsables de ce gonflement.

2. Oxydes: Six aiguilles combustibles dont quatre en oxyde d'uranium enrichi et deux en oxyde mixte UO_2PuO_2 ont été irradiées dans EL3. La température de gaine était de 450° et les puissances spécifiques de 1000 à 1750 W/cm³. L'examen des aiguilles apporte un certain nombre de renseignements sur leur comportement à l'irradiation.

НЕКОТОРЫЕ РЕЗУЛЬТАТЫ ПО ОБЛУЧЕНИЮ ЯДЕРНОГО ТОПЛИВА, ПРЕДУСМОТРЕННОГО ДЛЯ РЕАКТОРА "RAPSODIE". Для активной зоны реактора "RAPSODIE" изучаются два вида топлива: сплав U - Pu - Mo, содержащий 20% плутония и 10% молибдена, и смешанная окись UO_2PuO_2, содержащая 25% PuO_2. Были получены следующие результаты после облучения этих видов топлива:

1) Сплав U - Pu - Mo: 24 образца неочищенного сплава U - Pu - Mo в виде расплавленной массы были облучены в реакторе типа EL-3 в виде расплавленной массы были облучены в реакторе типа EL-3 при степенях выгорания в пределах от 4,400 мгвт-день/т до 8,300 мгвт-день/т. Голые ооразцы погружались в жидкий натрий при различных температурах от 400 до 525°C. Обследование, проведенное после облучения, позволило установить увеличение объема этих образцов в пределах 30 - 104%. Микрографические исследования выявили наличие пузырьков, образовавших это вздутие.

2) Окиси: шесть тепловыделяющих элементов пруткового типа, четыре из которых состояли из окиси обогащенного урана и два из смеси окисей UO_2PuO_2, были облучены в реакторе типа EL-3 . Температура защитной оболочки равнялась 450°, а удельная мощность от 1000 до 1750 вт/см³. Исследование тепловыделяющих элементов пруткового типа дает некоторые сведения относительно их поведения при облучении.

ALGUNOS RESULTADOS DE LA IRRADIACION DE LOS COMBUSTIBLES DESTINADOS AL REACTOR RAPSODIE. Se están estudiando dos posibles combustibles para el cuerpo del reactor Rapsodie: la aleación U-Pu-Mo, con el 20 por ciento de plutonio y el 10 por ciento de molibdeno, y el óxido mixto UO_2PuO_2, con el 25 por ciento de PuO_2. Los resultados en los ensayos de irradiación realizados con estos combustibles son los siguientes:

1) Aleaciones U-Pu-Mo: En el reactor EL3 se irradiaron 24 muestras de aleación U-Pu-Mo bruta de colada a grados de combustión que oscilaban entre 4400 MWd/t y 8300 MWd/t. Se trataba de muestras sin envainar sumergidas en sodio líquido a temperautras comprendidas entre 400 y 525° C. Los exámenes efectuados después de la irradiación permitieron comprobar aumentos de volumen de las muestras que varían entre el 30 y 104 por ciento. En las microfotografías se pudieron observar las burbujas responsables de ese crecimiento.

2) Oxidos: En el reactor EL3 se irradian seis agujas combustibles, a saber, cuatro de óxido de uranio enriquecido y dos del óxido mixto UO_2PuO_2. La temperatura en la vaina era de 450° C y las potencias específicas, de 1000 a 1750 W/cm^3. El examen de las agujas proporciona una serie de datos sobre la manera en que el material se comporta frente a las radiaciones.

Les problèmes posés par la mise au point d'un élément combustible de réacteur rapide sont nombreux et bien connus; dans le cas du réacteur RAPSODIE l'un d'entre eux, et non le moindre, peut se résumer en ces quelques mots: atteindre un taux de combustion très élevé dans un combustible riche en uranium, et contenant une proportion importante de plutonium.

C'est dans ce sens qu'un programme d'irradiation a été entrepris. Deux voies différentes ont été choisies: dans l'une d'elles le combustible est un alliage uranium-plutonium-molybdène; les irradiations ont été faites sur de petits échantillons non gainés. Dans l'autre version, le combustible est un oxyde mixte d'uranium et de plutonium; les irradiations ont été réalisées sur des aiguilles en vraie grandeur.

L'exposé qui suit donnera en deux chapitres distincts les résultats de ces premières irradiations.

II. RÉSUMÉ ET CONCLUSIONS

Deux combustibles sont à l'étude pour le cœur du réacteur rapide RAPSODIE: l'alliage UPuMo et l'oxyde mixte UO_2PuO_2. Les résultats des essais d'irradiation que nous avons effectués sur ces combustibles sont les suivants:

1. Alliages UPuMo

Vingt-quatre échantillons à 20% de plutonium et 8, 10, 12% de molybdène bruts de coulée ont été irradiés dans la pile EL 3 à des taux de combustion étagés entre 4400 et 8300 MWj/t. Les échantillons, non gainés, étaient immergés dans du sodium liquide à différentes températures allant de 400 à 525°C. Les examens des échantillons irradiés ont permis de constater des augmentations de volume comprises entre 30 et 104%. Les micrographies mettent en évidence les bulles responsables de ce gonflement.

2. Oxydes

Cinq aiguilles combustibles dont quatre en oxyde d'uranium enrichi et une en oxyde mixte UO_2PuO_2 ont été irradiées dans la pile EL 3. La température de gaine était voisine de 450°C et les puissances spécifiques com-

prises entre 1000 et 1750 W/cm^3. L'examen des aiguilles a montré leur bonne stabilité dimensionnelle. Un grossissement considérable du grain de l'oxyde associé à une cavité centrale a été constaté sur deux aiguilles.

Les résultats obtenus dans le cas de l'oxyde sont encourageants; ils demandent cependant à être confirmés par des irradiations à des taux de combustion beaucoup plus élevés; quant au comportement des alliages UPuMo, la seule solution qui semble offerte est celle d'un gainage suffisemment résistant pour limiter le gonflement.

III. IRRADIATION D'ÉCHANTILLONS D'ALLIAGES URANIUM-PLUTONIUM-MOLYBDÈNE

1. Dispositif d'irradiation

Les échantillons à irradier, décrits plus complètement au paragraphe 3, étaient ving-quatre cylindres de 4,3 mm de diamètre et de 20 mm de longueur. La teneur en plutonium était de 20% en poids. Non gainés, ils étaient placés trois par trois, maintenus par des étagères, dans des containers en zircaloy-2.

Remplis d'une quantité connue de soduim, les containers sont fermés, puis montés horizontalement dans un ensemble d'irradiation placé dans le canal horizontal H 3 de la pile EL 3. Chaque container possède un doigt de gant qui plonge dans le sodium; le doigt de gant contient un thermocouple qui permet de mesurer la température du soduim.

Le refroidissement des échantillons est assuré par un liquide organique («dowtherm») qui circule autour des containers. Pour assurer entre le sodium et le liquide de refroidissement un gradient thermique suffisant, la paroi des containers, très épaisse, est en outre évidée par de nombreux perçages longitudinaux.

Une régulation qui fait varier la température du « dowtherm» par l'intermédiaire de réchauffeurs et de refroidisseurs maintient constante la température du sodium de l'un des containers.

La boucle d'irradiation, tant dans sa partie en pile comme dans sa machinerie, a été décrite de façon complète dans la référence [1].

2. Conditions de l'irradiation

L'irradiation a duré quatre cycles de vingt jours. Le tableau I donne les températures moyennes du sodium qui entoure les échantillons, et les taux de combustion*. Ces valeurs demandent quelques éclaircissements:

a) Les puissances spécifiques et les taux de combustion sont obtenus par le calcul de l'échange de chaleur entre le sodium et le dowtherm au travers de chaque container. Des analyses radiochimiques de césium et de strontium, réalisées sur des échantillons d'uranium placés dans le même dispositif permettent de recouper les résultats précédents à moins de 15% près.

---

* Le tableau I se borne à donner les valeurs qui concernent les huit échantillons examinés après irradiation.

TABLEAU I

IRRADIATION D'ALLIAGES URANIUM-PLUTONIUM-MOLYBDÈNE

Echantillons	Composition pondérale (%)			Température moyenne du Na (°C)	Taux de combustion (MWJ/t)	Augmentation de longueur (%)	Augmentation de diamètre (%)	Densité avant irradiation (g/cm^3)	Densité après irradiation (g/cm^3)	Augmentation de volume (%)
	U	Pu	Mo							
A4	68	20	12	410	4400	-	33,5	17,01	8,9	90,5
B4	70	20	10	410	4400	10	9,5	17,17	12,64	36
C4	72	20	8	410	4400	8,5	13,5	16,91	13	30
A2	68	20	12	485	7100	11	23,5	16,96	10,1	68,5
B2	70	20	10	485	7100	11,5	26	17,29	10,3	68
A5	68	20	12	525	8300	16,5	28,5	16,84	9,53	76,5
B5	70	20	10	525	8300	10,5	23	17,24	10,5	64
C5	72	20	8	525	8300	9	47	18,19	8,9	104,5

b) La dépression du flux de neutrons thermiques au cœur des échantillons est très forte. Aussi y a-t-il un rapport 2,2 entre les taux de combustion moyens donnés dans le tableau I et les taux de combustion à la surface des échantillons.

c) La température mesurée est celle du sodium; il est permis d'admettre qu'elle est très voisine de celle de la surface des échantillons. Une vérification expérimentale a pu en être faite sur des échantillons d'alliage uranium-molybdène à 11,4% en poids de molybdène, placés dans le même dispositif d'irradiation; un examen micrographique après irradiation a mis en évidence une structure à deux phases; ceci permet d'affirmer que la surface des échantillons était à une température inférieure à celle de l'entectoïde. La température du sodium s'était effectivement maintenue à 30°C environ au-dessous de cette température.

Un calcul approximatif montre en outre que le gradient de température entre le centre et la surface des échantillons ne peut dépasser 40°C.

3. Résultats de l'irradiation

a) Echantillons non irradiés [2]

Les alliages ont été élaborés au four à arc, coulés en moule de cuivre et usinés. Les teneurs en uranium, plutonium et molybdène des échantillons obtenus, ainsi que la densité de chacun des échantillons sont données dans le tableau I.

La structure des échantillons a été étudiée par micrographie et par rayons X. Bruts de coulée, ils possèdent tous une structure cubique γ non homogène; cette hétérogénéité de la structure est due à l'écart important entre le liquidus et le solidus.

b) Echantillons irradiés

L'examen des échantillons irradiés a été réalisée dans un ensemble de cellules α, β, γ [3]. Ces cellules, étanches et sous azote, sont équipés d'un manipulateur à transmission magnétique. La figure 1 montre une vue de l'intérieur de deux de ces cellules: tronçonnage et préparation métallographique.

La figure 2 montre les photos de quelques échantillons après irradiation. Hormis l'échantillon A 4, dont l'extrémité a été cassée au cours du démontage, les échantillons sont en général bien conservés; leur surface est peu oxydée, et les rayures d'usinage sont encore nettement visibles. Le gonflement est assez homogène; les extrémités de certains échantillons (fig. 2, échantillon B 4) prennent cependant la forme de massues.

La tôle de zirconium qui fixe les échantillons s'est parfois profondément encastrée, provoquant de ce fait une rainure profonde (fig. 2, échantillon A 5).

c) Changements de dimensions et de volume

Les dimensions des échantillons irradiés ont été mesurées au palmer. Les densités ont été déterminées par la méthode de la poussée hydrostatique dans du xylène; la précision des mesures est de 1%.

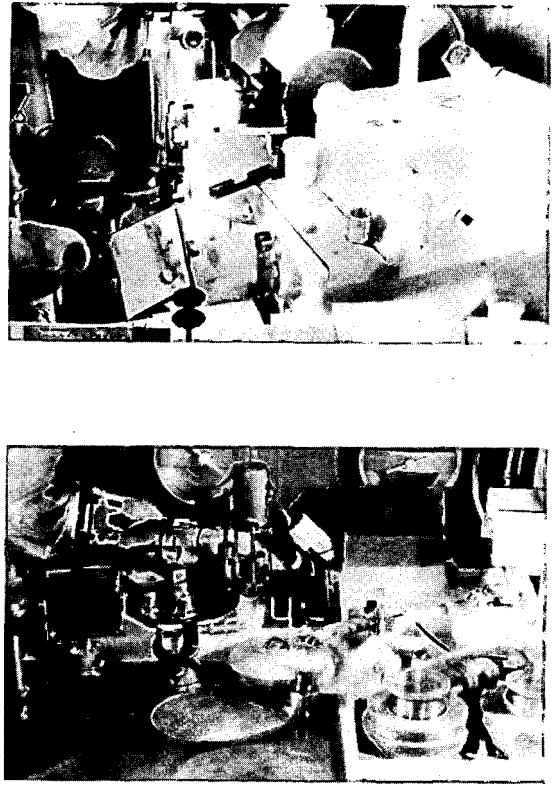


Figure 1

Ligne α,β, γ.

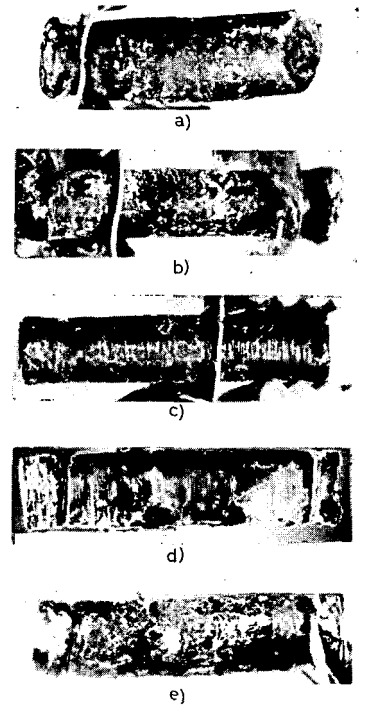


Figure 2

Echantillons UPuMo irradiés.
a) Echantillon A 4 – b) Echantillon B 4
c) Echantillon C 4 – d) Echantillon A 5
e) Echantillon B 5.

Les changements de diamètre, de longueur et de volume sont indiqués dans le tableau I.

d) Aspect micrographique

Après enrobage, polissage mécanique et nettoyage aux ultra-sons, l'extrémité de l'échantillon B 5 a été examinée; la figure 3 a montre une coupe micrographique de cet échantillon. Apparemment non fissuré, il contient par contre une porosité considérable. La répartition des bulles n'est pas homogène. Deux zones se différencient nettement, dont l'une, périphérique, contient des bulles plus grosses que l'autre (fig. 3b). La taille des bulles

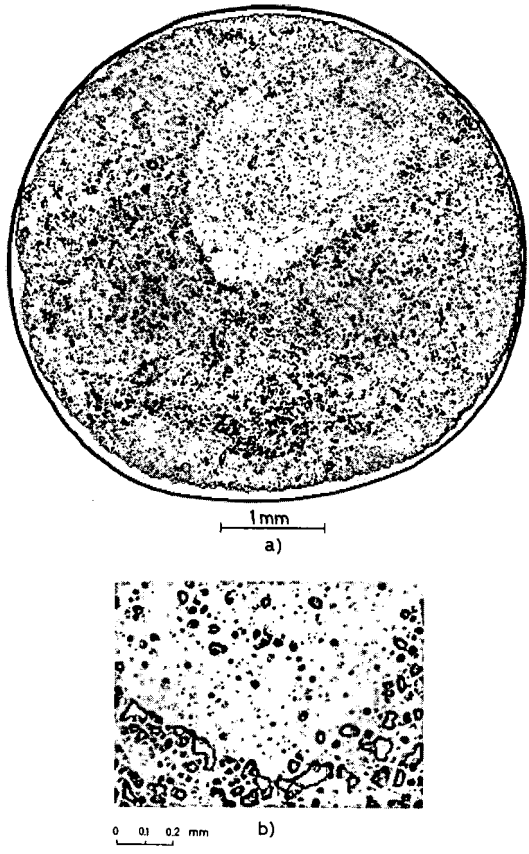


Figure 3

Echantillon B 5.
a) Coupe micrographique – b) Porosités.

est très variable; elle s'étage entre 1 et 50μ, la limite de résolution du microscope étant de 1μ environ. Un calcul du gonflement par la mesure du rapport entre la surface des bulles et celle du métal rend bien compte de l'augmentation de volume observée par densité.

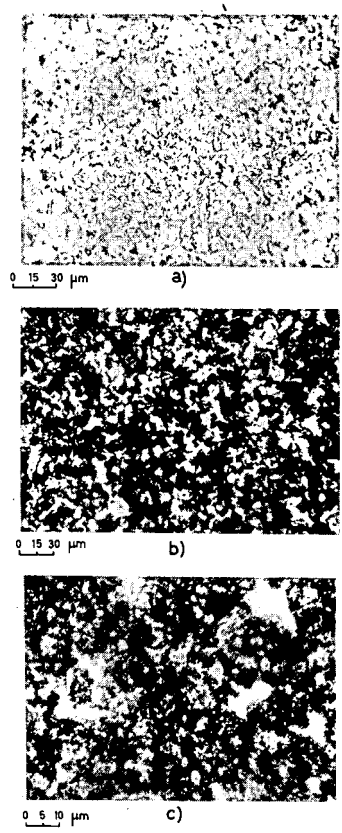


Figure 4
Structure micrographique de l'échantillon B5.
a) Avant irradiation – b) et c) Après irradiation (c) est trois fois plus agrandie que b)).

La figure 4a montre la structure micrographique de l'échantillon B5 avant irradiation. Comme nous l'avons indiqué plus haut (par. 3a), la structure cubique γ n'est pas homogène: les zones claires, riches en molybdène, et les zones sombres, plus pauvres, correspondent à la ségrégation au cours de la solidification.

Un polissage électrolytique a permis de mettre en évidence la structure de l'alliage irradié. Les conditions étaient les suivantes:

Bain:	PO_4H_3	100 cm³	2 parts
	$P_2O_7H_4$	40 g	
	CrO_3	2 g	
	H_2O	50 cm³	
	C_2H_5OH		1 part

Température:	10°C
Tension de polissage:	5 V
Durée:	20 s

Sur les micrographies de la figure 4b, faites sur l'échantillon irradié, on retrouve la ségrégation observée avant irradiation. Cependant, dans les zones pauvres en molybdène, on constate à fort grossissement une décomposition fine de la phase γ. C'est l'effet qu'on pouvait attendre d'un traitement thermique prolongé à la température d'irradiation. L'irradiation semble donc n'avoir joué aucun rôle: malgré la densité de fission assez élevé ($\sim 7 \cdot 10^{13}$ fissions/cm$^3 \cdot$ s) elle n'a pu homogénéiser la phase γ.

e) Conclusions

Les résultats précédents amènent un certain nombre de remarques:

1. Le gonflement des échantillons est considérable, et ceci malgré des températures d'irradiation relativement modérées.

2. La teneur en molybdène dans l'intervalle de composition étudié ne semble pas jouer un role significatif.

3. Le gonflement s'accroît avec le taux de combustion. Les résultats sont cependant difficilement comparables d'un échantillon à l'autre; en particulier A4 a gonflé beaucoup plus que les échantillons B4 et C4. On retrouve ici le caractère aléatoire fréquemment observé des gonflements exagérés, dont les valeurs varient souvent du simple au double dans des conditions apparemment identiques.

Nous avons calculé une valeur moyenne de la pression des gaz de fission dans les différents échantillons à la température d'irradiation. Cette valeur est obtenue en supposant que le gaz occupe, à une pression uniforme, le volume offert par le gonflement. Les résultats ont été portés dans le tableau II. On constate que, hormis l'échantillon A4, les valeurs obtenues sont assez voisines et oscillent autour de 15 à 18 kg/cm^2. Cette valeur, si dénuée de sens physique qu'elle soit, est cependant une mesure de la résistance du métal au gonflement.

TABLEAU II

RÉSISTANCE AU GONFLEMENT DE L'ALLIAGE UPuMo

Echantillons	Volume de gaz par cm^3 de métal (TPN)	Pression du gaz à la température d'irradiation (kg/cm^2)
A4	2,14	6,2
B4	2,16	15,6
C4	2,13	18,2
A2	3,46	14,5
B2	3,53	15
A5	4,01	15,5
B5	4,10	19
C5	4,33	12,3

Il est cependant probable qu'aux très bas taux de combustion, tant que le gonflement reste faible et les bulles très petites, la résistance au gonflement opposé par l'énergie de surface du métal doit conduire à des valeurs de la pression moyenne beaucoup plus fortes. Il pourrait en être de même en présence d'une gaine épaisse qui limiterait le gonflement à quelques pour cent: les bulles restant petites, la contribution du combustible lui-même à la limitation du gonflement pourrait garder une valeur très supérieure à 18 kg/cm^2.

IV. IRRADIATION D'AIGUILLES COMBUSTIBLES EN OXYDE

Les irradiations d'oxydes combustibles ont été entreprises non plus sous la forme d'échantillons, mais directement sous la forme d'éléments combustibles adaptés au réacteur rapide RAPSODIE; cette décision a amené à fixer un certain nombre de paramètres dont les principaux sont les suivants:

a) les cotes des aiguilles;
b) la température du sodium entourant l'aiguille, 450°C;
c) la puissance spécifique, pour laquelle deux valeurs ont été choisies: 875 W/cm^3 et 1750 W/cm^3; ces puissances correspondent respectivement au fonctionnement de RAPSODIE à 10 MW et 20 MW.

Cinq aiguilles ont été irradiées: parmi elles, quatre aiguilles en oxyde d'uranium enrichi qui ont permis de mettre la méthode au point et servent de référence, et une aiguille en oxyde mixte d'uranium et de plutonium à 9,3% de plutonium.

1. Fabrication du combustible

La fabrication des pastilles a été décrite dans d'autres publications [4]. Nous en rappellerons les éléments essentiels.

Les pastilles d'oxyde d'uranium enrichi destinées aux quatre premières aiguilles (UR 5, UR 10, UR 5A et UR 10A) ont été préparées à partir de poudres d'oxydes d'uranium naturel et d'uranium enrichi. Ces poudres, mélangées avec un liant (camphre et stéarine), mises en forme sous une pression de 4 t/cm^2, sont ensuite frittées pendant 4 h à 1500°C sous atmosphère d'hydrogène (frittage naturel).

Les pastilles ainsi obtenues sont pratiquement stoéchiométriques. Leurs caractéristiques sont les suivantes:

Densité: 10,1 g/cm^3, soit 92% de la densité théorique.
Diamètre: 5,7 ± 0,05 mm.
Hauteur: 9 mm.

Les pastilles d'oxyde mixte d'uranium et de plutonium à 9,3% de PuO_2, destinées aux aiguilles R 20-1 et R 20-2, ont été préparées par calcination à 400°C et par réduction à 600°C de peroxyde mixte uranium-plutonium. La poudre ainsi obtenue, de surface spécifique 7 m^2/g, a été pressée avec un liant (camphre et stéarine) pour donner des pastilles d'une densité de 7 g/cm^3. Les pastilles ont alors subi un frittage naturel de 4 h à 1500°C sous hydrogène. Les pastilles ainsi obtenues, pratiquement stoéchiométriques, ont les caractéristiques suivantes:

Densité: 10,48, soit 95,2% de la densité théorique.
Diamètres extrèmes: 5,78 à 5,85 mm.
Hauteur moyenne: 11,5 mm.

2. Fabrication des aiguilles [5]

L'aiguille, dont le plan est représenté sur la figure 5, est constituée d'un empilement de pastilles d'environ 350 mm de hauteur. Une gaine d'acier inoxydable est appliquée sur les pastilles par tréfilage et martelage. La colonne de pastilles se termine vers le bas par une rondelle isolante en alumine. Dans la partie supérieure, la colonne de pastilles se prolonge par une rondelle d'alumine percée d'un trou, une rondelle d'acier inoxydable percée elle aussi, et un espace d'expansion pour les gaz de fission. Cet espace d'expansion a un volume de 1 cm^3 environ. Un bouchon en acier inoxydable est soudé, par soudure à la molette, à chaque extrémité de l'aiguille.

3. Les dispositifs d'irradiation [6]

Pour irradier les aiguilles aux deux puissances spécifiques qui ont été choisies (875 et 1750 W/cm^3), il a fallu réaliser deux dispositifs différents. Leur principe étant analogue, nous nous bornerons à décrire sommairement le dispositif correspondant à RAPSODIE 20 MW (puissance spécifique 1750 W/cm^3). La figure 6 est un plan de ce dispositif. L'aiguille est placée dans un container étanche en acier inoxydable (106). Ce container est rempli d'une quantité convenable de sodium purifié. Il est d'abord placé dans un tube à paroi épaisse (105) (126) en zircaloy-2 qui constitue une seconde étanchéité.

Le contact thermique zircaloy-2-inox entre les deux tubes concentriques est assuré par les dilatations thermiques pendant l'irradiation. Alors qu'il existe à froid un jeu de 1 à 1,25 dixième de mm, il se produit à chaud un frettage dont la pression est de l'ordre de 10 kg/mm^2; cette valeur conduit à une contrainte de cisaillement maximum dans le zircaloy inférieure à la limite élastique du métal.

Un thermocouple chromel-alumel gainé d'acier inoxydable passe, par une étanchéité mécanique, au travers du premier container; il traverse ensuite le second container par une soudure réalisée à la machine à souder par résistance et plonge ainsi dans le sodium à mi-hauteur de l'aiguille.

Le dispositif est placé dans l'eau lourde de refroidissement de la pile EL 3, à la place d'un élément combustible quelconque; le gradient entre la température du sodium (450°C) et celle de l'eau lourde (25°C) se produit en grande partie dans l'épaisseur du tube de zircaloy. La réalisation d'un film de sodium continu a posé un problème délicat et si sa mise au point est maintenant chose faite, on verra au paragraphe 5 qu'un film de sodium imparfait a été à l'origine d'un certain nombre de ruptures de gaine.

4. Les irradiations

Afin d'obtenir une puissance spécifique convenable, l'emplacement

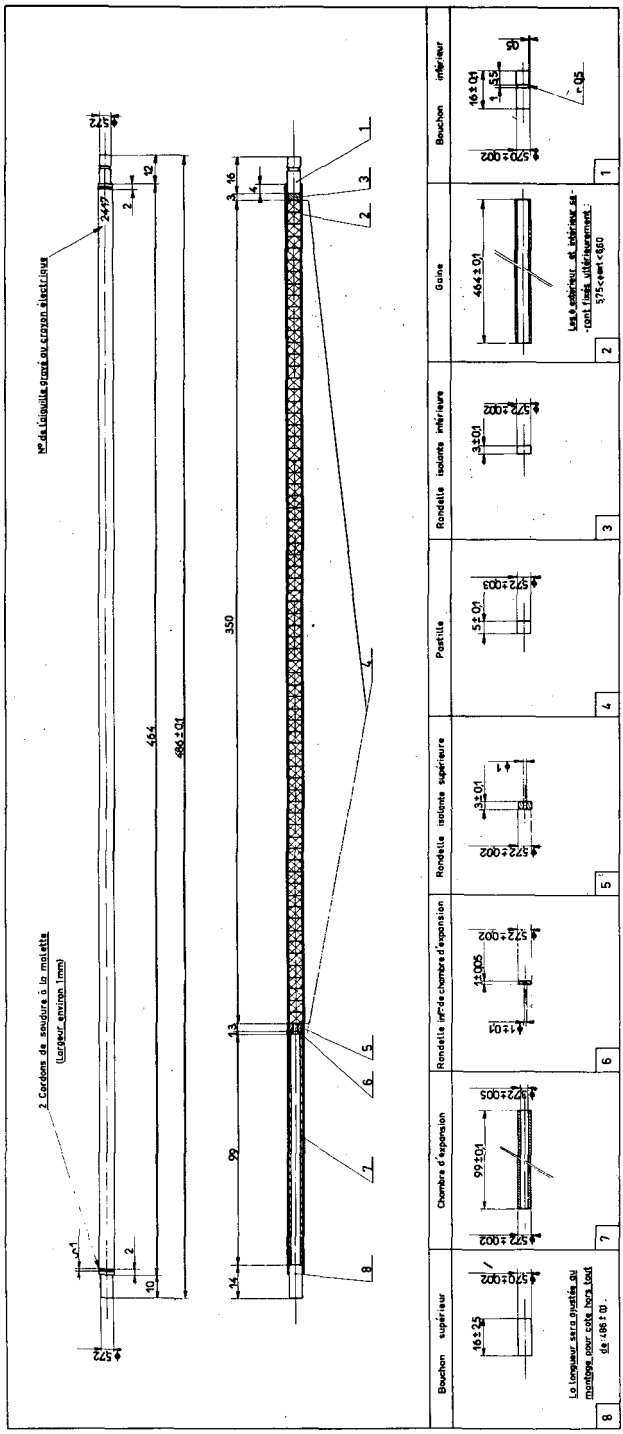


Figure 5
Plan d'aiguille.

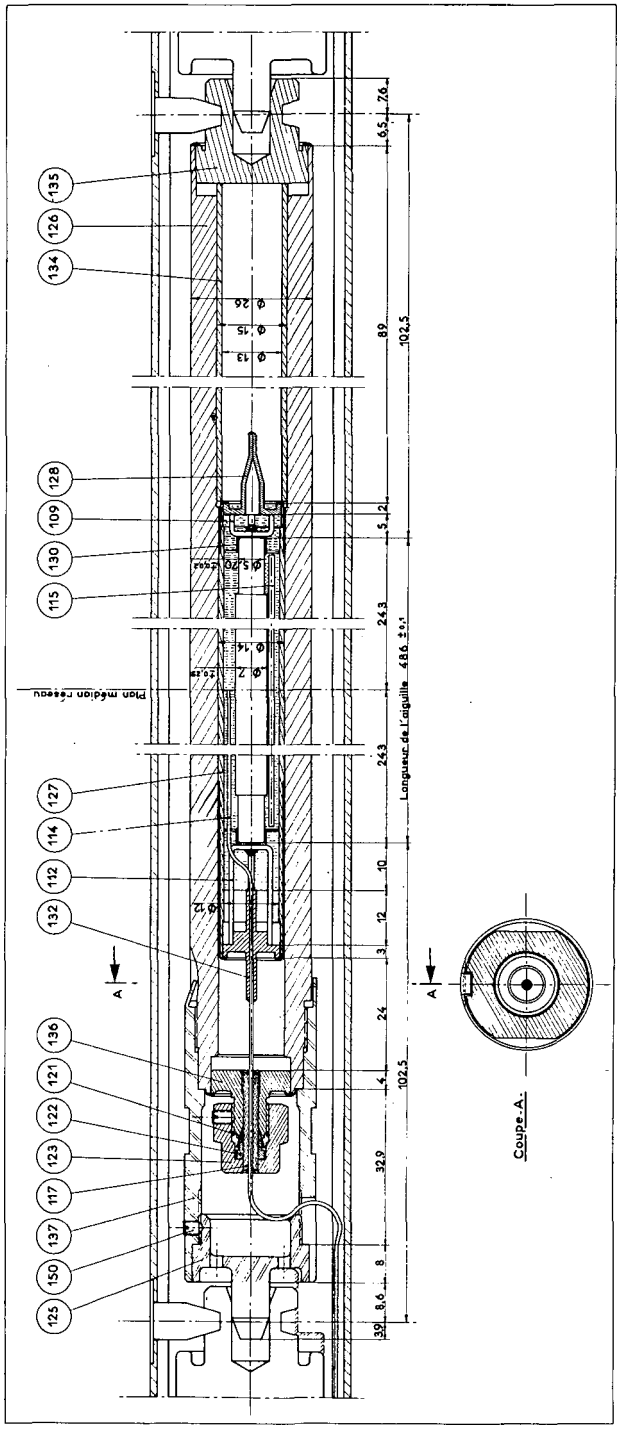


Figure 6
Dispositif d'irradiation du réacteur RAPSODIE.

TABLEAU III

Aiguilles	Nature	Durée d'irradiation	Puissance spécifique (W/cm³)		Température du Na (°C)		Intégrale de conductibilité moyenne
			max.	moy.	max.	moy.	(W/cm)
UR 5	UO enrichi 5%	60 h	950		505		18,5
UR 10	UO enrichi 10%	60 h	1725		410		32
UR 5A	UO enrichi 5%	20 j		1090	597	572	21
UR 10A	UO enrichi 10%	20 j	1725	1580	410	375	29,5
R 20-1	UO PuO à 9,3% de PUO	33 j	1720	1650	410	393	30,2

du dispositif en pile est déterminé par un calcul qui tient compte des flux de neutrons dans la pile et de la quantité de matière fissile [6].

La température atteinte par le sodium au cours de l'irradiation permet ensuite, par le calcul des échanges thermiques avec l'eau lourde de refroidissement, de déterminer les puissances réelles dégagées par les aiguilles. Des mesures des intensités de rayonnement émises par les aiguilles après irradiation permettent de comparer et de vérifier les résultats.

Le tableau III résume les paramètres des irradiations des différentes aiguilles; on remarquera que pour chaque aiguille deux valeurs de puissance spécifique sont indiquées. Il se produit en effet, à la première montée en puissance du réacteur, un maximum de puissance dans l'aiguille, suivi d'une décroissance d'environ 10%. Ce phénomène est probablement dû à l'apparition progressive dans l'aiguille des poisons xénon et samarium.

5. Examen après irradiation

Il faut tout d'abord indiquer le point suivant: l'examen des aiguilles irradiées a mis en évidence des ruptures de gaine sur les aiguilles UR 5, Ur 10 et R 20-1; l'observation micrographique a permis de préciser que dans chaque cas il y avait échauffement et fusion locale de la gaine. Ces fusions ont été attribuées à des défauts du film de sodium entourant l'aiguille.

Les aiguilles vont alors se diviser en deux classes: celles où le sodium a pénétré dans l'oxyde et celles où le sodium n'a pu pénétrer.

a) Aiguilles contenant du sodium

L'examen macrographique de coupes des aiguilles UR 5, UR 10 et UR 5A a révélé la présence de sodium entre l'oxyde et la gaine et dans toutes les fissures de l'oxyde. L'aspect général de l'oxyde de toutes ces aiguilles est semblable à celui de l'oxyde non irradié; la figure 7a est par exemple la photographie d'une coupe de l'aiguille UR 10. On y remarque quelques

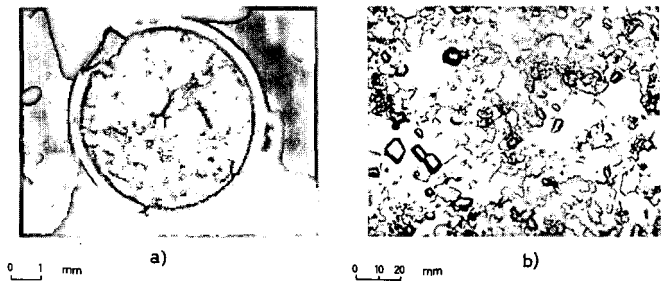


Figure 7

Aiguille UR 10.
a) Coupe transversale – b) Aspect micrographique.

fissures irrégulières dont l'origine peut très bien être attribuée au martelage que les aiguilles ont subi à la fabrication.

L'examen micrographique après polissage au diamant et attaque ionique n'a pas amené de renseignements supplémentaires. Aucun grossissement du grain n'a pu être décelé (fig. 7b) même dans le cas de l'aiguille UR 10 dont la puissance spécifique était cependant de 1720 W/cm^3.

b) Aiguilles ne contenant pas de sodium

Ce sont les aiguilles UR 10A et R 20-1.

Aiguille UR 10A:

L'aiguille est absolument intacte; ni son diamètre ni sa longueur n'ont subi de modifications. Les coupes effectuées dans l'aiguille ont l'aspect de la figure 8a; on y remarque une cavité centrale et des fissures radiales accompagnées de quelques fissures circonférentielles. Le trou central s'étend d'une extrémité à l'autre de l'aiguille. Son diamètre varie entre 0,5 et 0,8 mm et souvent d'un bout à l'autre d'une même pastille, comme on peut le voir sur la coupe longitudinale de la figure 8b. On observe d'autre part la soudure partielle des pastilles les unes aux autres.

Une coupe longitudinale de l'espace d'expansion (fig. 8c) qui prolonge l'aiguille a permis de mettre en évidence, sur les parois de cet espace, un dépôt de cristaux d'UO_2 qui forment un revêtement continu. Il s'agit là très certainement d'un phénomène de transport et de condensation en phase vapeur de l'oxyde d'uranium.

La structure de l'oxyde a été mise en évidence par attaque ionique. La coupe micrographique de la figure 9 permet de constater, autour du trou central, une couronne de cristaux basaltiques. L'étude de cette coupe à un grossissement plus élevé permet de distinguer, de la périphérie au centre, une succession d'aspects micrographiques différents:

1° Une zone périphérique à grains fins où l'on retrouve l'aspect micrographique de l'oxyde d'uranium non irradié; les porosités sont très nombreuses.

2° Une zone assez étroite où le grain a grossi tout en restant équiaxe (fig. 10b et c).

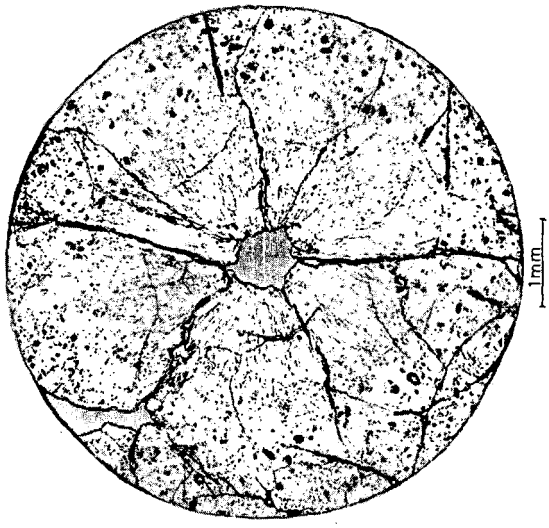


Figure 9
Coupe micrographique de l'aiguille UR 10A.

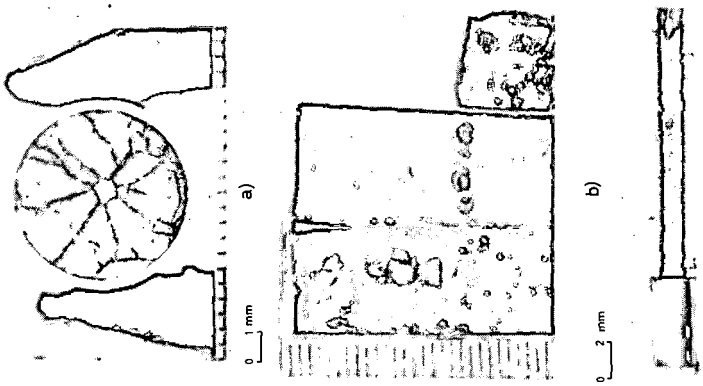


Figure 8
Aiguille UR 10 A.
a) Coupe transversale – b) Coupe longitudinale
c) Espace d'expansion.

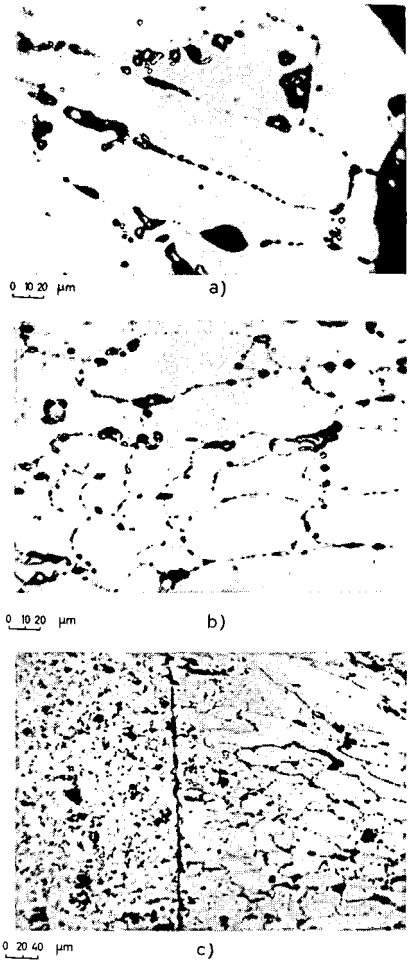


Figure 10

a) Bord du trou central – b) Vers le trou central
c) Fissure perpendiculaire du rayon.

3° Une zone de gros grains basaltiques orientés vers le trou central (fig. 10a). Ces grains contiennent très peu de porosités; les joints de grains, par contre, sont décorés de nombreux petits trous.

Afin de rendre compte de manière plus précise du grossissement du grain, nous avons tracé la courbe du nombre de grains par unité de surface de l'échantillon en fonction du rayon (fig. 11); on constate sur cette courbe que la variation de la taille des grains se produit en majeure partie dans une zone assez étroite; cette zone est celle du grossissement de grain.

Aiguille R 20-1:

L'aiguille R 20-1 a subi pendant l'irradiation une rupture de gaine.

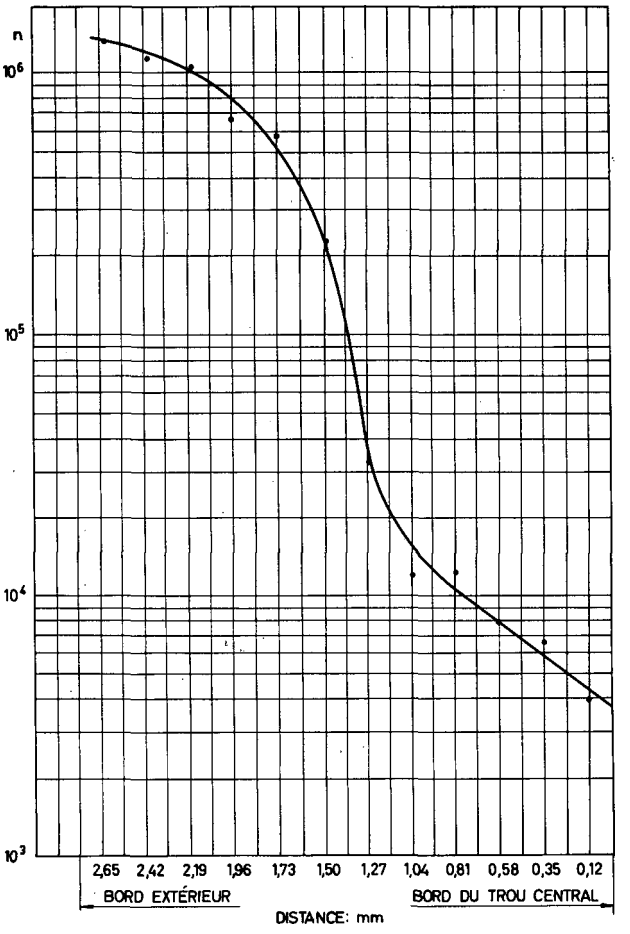


Figure 11

Aiguille UR 10A, éch. n° 2.
n = f (distance)
n: grains/cm² (éch.).

Des coupes transversales successives de l'aiguille n'ont révélé la présence de sodium qu'au voisinage de la rupture.

L'oxyde, comme dans le cas de l'aiguille UR 10A, contient une cavité centrale dont le diamètre varie entre 0,2 et 0,5 mm. On retrouve sur toutes les sections (fig. 12) un double réseau de fissures: des fissures radiales aboutissant au trou central et des fissures circonférentielles non loin de la périphérie de l'échantillon. La structure micrographique de l'UO_2PuO_2 n'a pas été étudiée. Il est cependant possible d'identifier, sur la figure 12, une zone centrale de grains de grandes dimensions, allongés dans la direction du trou central.

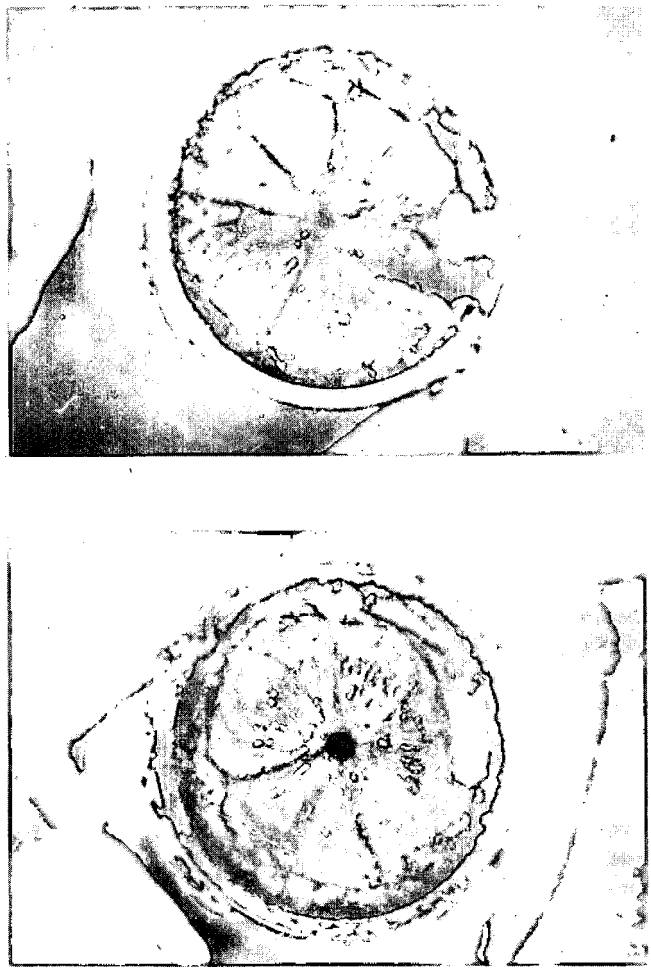


Figure 12
Coupes transversales de l'aiguille R 20-1.

6. Intégrales de conductibilité et températures

Le calcul des intégrales de conductibilité permet, si l'on connaît la conductibilité du combustible à toutes températures, de déterminer la répartition des températures dans une section droite. Dans le cas d'un combustible enrichi, où la dépression de flux est importante, l'intégrale de conductibilité a pour valeur [7]

$$\int_{T_s}^{T_r} k(\theta)d\theta = \frac{Q\pi a^2}{4\pi} \frac{I_0(Xa) - I_0(Xr)}{\frac{Xa}{2} I_1(Xa)}$$

avec les notations

$k(\theta)$: conductibilité thermique de l'oxyde à la température θ,
a: rayon de la pastille d'oxyde,
T_s: température à la surface de l'oxyde,
T_0: température au cœur de l'oxyde,
T_r: température sur un rayon r,
X: inverse de la longueur de diffusion corrigée de l'oxyde,
I_0, I_1: fonctions de Bessel modifiées de 1re espèce,
Q: puissance spécifique moyenne en W/cm^3.

Les intégrales de conductibilité entre les limites T_s et T_0 ont été calculées pour les différentes aiguilles. Elles figurent dans le tableau III.

A partir de l'intégrale de conductibilité nous avons tenté de déterminer la répartition des températures dans une section de l'aiguille UR 10A (fig.9). En ce qui concerne les conductibilités thermiques, nous avons adopté en tenant compte de la densité de l'oxyde, les valeurs préconisées par ROSS [8]. Il est en outre nécessaire de connaître la température en un point de l'oxyde; la température de surface T_s de l'oxyde étant difficile à déterminer, nous avons préféré admettre que dans la zone assez étroite où le grossissement de grain apparaît (fig. 11), et d'après les valeurs publiées [9], la température est de l'ordre de 1550°C.

Ceci nous a conduit, pour la section droite de l'aiguille UR 10A (tableau III) dont l'intégrale de conductibilité a pour valeur

$$\int_{T_s}^{T_0} k(\theta)d\theta = 29,4 \text{ W/cm}$$

à une température T_s de la surface de l'oxyde égale à 700°C, et à une température centrale T_0 de 1860°C.

Ces résultats amènent un certain nombre de remarques:

1° Le gradient entre la température de surface de l'oxyde T_s (700°C) et celle du sodium, qui est de 376°C, conduit à un coefficient de transfert de chaleur entre l'oxyde et sa gaine dont la valeur (0,75 $W/cm^2/°C$) est raisonnable.

2° Dans le cas de l'aiguille UR 10, dont l'intégrale de conductibilité atteint 32 W/cm, aucun grossissement de grain n'a été observé dans l'oxyde. Compte tenue de la durée de l'irradiation (60 h), ceci permet d'assurer que la température de l'oxyde n'a pas dépassé 1650°C. Il apparaît alors comme certain que la présence de sodium dans l'aiguille a augmenté considérablement le coefficient de transfert entre l'oxyde et la gaine, abaissant ainsi le niveau des températures dans l'oxyde. Ce phénomène ne s'est pas produit dans l'aiguille R 20-1, comme on l'a vu au paragraphe 5, la pénétration du sodium dans l'oxyde étant très limitée.

7. Conclusion

Les résultats précédents, en particulier ceux qui concernent UR 10A et R 20-1, permettent de préciser un certain nombre de points:

1° Les aiguilles combustibles supportent sans déformation des irradiations à la puissance spécifique de 1750 W/cm³ pourvu que le film de sodium extérieur à la gaine soit sans défaut.

2° La présence accidentelle de sodium dans la gaine au contact avec l'oxyde n'a entrainé aucun inconvénient particulier pour le combustible.

3° L'oxyde mixte UO_2PuO_2 s'est comporté d'une façon tout à fait comparable à l'oxyde d'uranium enrichi.

Ces résultats sont encourageants; ils doivent cependant être complétés par l'étude du comportement des gaz de fission, et confirmés par des irradiations de longue durée.

RÉFÉRENCES

[1] BESSE, R. et RATIER, J. L. «Boucles à refroidissement par liquide organique», C. R. d'essai SECPER n°201 (Mars 1961).

[2] BOUCHER, R., ROBILLARD, A. et SAINT CRICQ, J., «Préparation d'échantillons de combustibles UPuMo pour essais d'irradiation», C. R. d'essai SECPER n°9 (Juin 1960).

[3] VALENTIN, A., Nucleonics 7, (1962) 84.

[4] BEL, A., «Fabrication de pastilles d'oxydes mixtes d'uranium et de plutonium à 11% de PuO_2», C. R. d'essai DPu SCP n°221 (Août 1961).

[5] MASSELOT, Y. et STOSSKOPF, F., «Fabrication de deux aiguilles combustibles pour irradiation dans EL3 d'oxyde d'uranium enrichi», C. R. d'essai DPu SECPER n°22 (Nov. 1960).

[6] RATIER, J. L., «Irradiation d'éléments combustibles type Rapsodie en UO_2PuO_2», C. R. d'essai DPu SECPER n°7 (Mars 1960).

[7] MIKAILOFF, H. et RATIER, J. L., «Irradiation d'aiguilles type Rapsodie en UO_2 dans la pile EL3», C. R. d'essai DPu SECPER.

[8] ROSS, A. M., "The dependance of the thermal conductivity of UO_2 on density, microstructure, stoechiometry and thermal neutron irradiation", CRFD 817.

[9] MAC EWAN, J. R., "Grain growth in sintered Uranium dioxyde", AECL 1184 CRFD 999.

B. RADIATION DAMAGE IN CERAMIC NUCLEAR FUEL

1. Review of papers and panel discussion

(Part of Session 5)

RADIATION DAMAGE IN CERAMIC NUCLEAR FUEL

Chairman: E. NAGY

Moderator: W. E. ROAKE

W. E. ROAKE*: The hour is late, and my colleagues on the Panel and I see it as a challenge to hold your interest. We will stay as long as you will have us !

I do not profess to be a metallurgist, therefore I can express a relatively unbiased opinion of the proceedings of the past two days. I have reached the conclusion that a great many of the problems of experimentation and of interpretation of the results exist because of the variations in impurity content and physical state of the "pure" metals and alloys. So, what hope of making sense have we who work with chemical compounds that disproportionate during irradiation, that contain native and fission-product impurities, that have widely varying physical properties reflecting methods of fabrication? Perhaps those are only reasons why we find ceramic nuclear fuels so fascinating. Brian Frost put it well in his paper**. He wrote, in essence, that we primarily seek something that works in the reactor, then we study the irradiation damage to help understand the practical behaviour. But the situation is improving. Now, experimenters are finding more pure materials available to work with, for example, zone-refined single-crystal UC and purified single-crystal UO_2.

It is my privilege to review the papers of this session. What I find interesting may not be that which the author considers the most important point of his paper. Each will have a later opportunity to illuminate my lack of empathy.

Eight papers are included in this panel discussion on radiation damage in ceramic nuclear fuels. Frost, Bradbury and Griffiths of Harwell in the United Kingdom submitted the paper entitled "The radiation effects in fissile oxides and carbides at low and high burn-up levels"**. This paper covers work at Harwell on uranium oxide, uranium carbide and mixed uranium-plutonium oxides and carbides. In addition, more work in the United Kingdom is discussed in the paper from Dounreay by Childs, Ogilvie, Ruckman and Whitton entitled "The low-temperature irradiation behaviour of cast uranium carbide"**. "The effect of irradiation on uranium-carbon alloys with composition near that of UC" is discussed in the paper by Accary, Darras, and Caillat from the Saclay establishment in France**. A paper by Sinizer, Webb and Berger of Atomics International in the United States covers the "Irradiation behaviour of uranium carbide" under prototypic power reactor conditions**. The paper by Bleiberg, Berman and Lustman discusses the extensive work at the Bettis Laboratory of the Westinghouse Electric Corporation on urania and zirconia-urania mixtures and on dispersions of UO_2 in beryllia or aluminia. The title of the paper is "The effects of high burn-up on oxide ceramic fuels"**. Other uranium

---

* Work performed for the United States Atomic Energy Commisssion under Contract AT(45-1)-1350.

** For full text, see section B.2.

oxide and uranium-plutonium oxide work in the United States is related in Roake's paper titled "The irradiation alteration of uranium dioxide"*. The second portion of the paper by Mustelier, of Saclay, entitled "Some results of irradiation on the fuels envisaged for the Rapsodie reactor", includes their experience with uranium-plutonium oxides*. Finally, the paper by Slooten and Hermans, of the Netherlands, and Sowden, of Harwell, discusses the "Irradiation experiments with fuel suspensions", of uranium-thorium oxide, and plutonium oxide*.

In reviewing the papers for this panel, I was pleased to find that they complement one another. There is very little overlapping of experimental conditions, of methods of investigation, or of details of fabrication of specimens. For me to review these papers in a manner which they deserve would be an impossible undertaking in the short time available. Therefore, I propose to acquaint you briefly with the contents of these papers, to point out areas where there are conflicting data, or conflicting interpretations of data, and particularly to point out the relationships among the work described. Hopefully, we may find how each piece of data fits into the mosaic that eventually will provide a coherent picture of the irradiation performance of ceramic nuclear fuels.

I would like first to discuss the carbides.

Carbide fuels

The papers in this group treat uranium-carbon alloys prepared by three methods; by casting, by reaction-sintering and by reaction-sintering under pressure. Structural differences include grain size, porosity and homogeneity.

Changes in electrical resistivity have been used to indicate the progress of radiation damage in uranium-carbon alloys. In Fig. 1 I have plotted data from Frost's and from Childs' papers, and have also included Rough's published results** for comparison. It is well known among engineers that nearly anything can be demonstrated from a log-log plot, and the authors may not recognize their data plotted this way. However, it was necessary in order to get it all on one graph.

Remarkable differences in the behaviour of the two kinds of specimens are reported. For example, Frost et al., using reaction-sintered UC, report a small increase in electrical resistivity, about 2.5% at an exposure of 10^{18} n/cm^2. Saturation was reached at approximately 10^{17}n/cm^2. Childs et al., on the other hand, show a resistivity increase of approximately 120% at 10^{18} n/cm^2 using cast UC. Saturation appears at a higher exposure in this case, and correlates with the saturation exposure reported earlier by Adam and Rogers for lattice parameter expansion. Childs' data agree in extent with those reported by Rough et al. in the United States** using cast uranium carbide.

Differences in annealing of radiation damage from the two types of carbide bodies are also revealed in the papers (Fig. 2). Frost's annealing experiments show two well-defined temperatures at which partial recovery

---

* For full text, see section B.2.

** ROUGH, F. A. and CHUBB, W., BMI-1554, Battelle Memorial Institute, Columbus, Ohio (1961) 55 pp.

from radiation-induced electrical resistivity change occurs. Approximately 30% recovery is achieved in one hour at 110 - 130°C and 70% recovery at

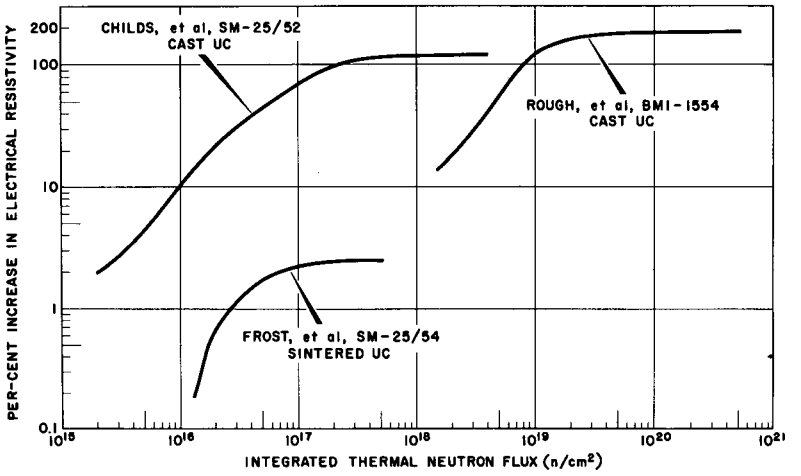


Fig. 1

Effect of neutron irradiation on electrical resistivity of uranium monocarbide
Comparison of results obtained by CHILDS et al. (these Proceedings, section B. 2) and ROUGH et al.* with cast UC, and by FROST et al. (these Proceedings, section B. 2) with sintered UC.

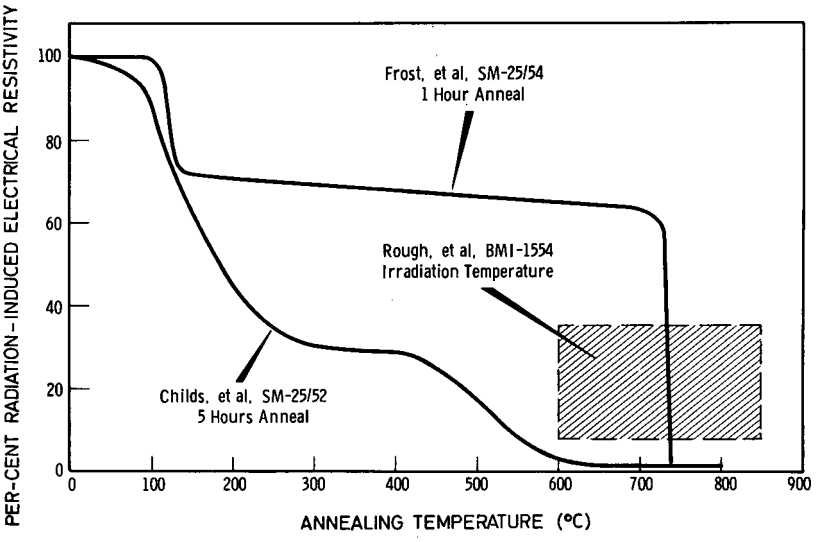


Fig. 2

Annealing of radiation-induced resistivity in uranium monocarbide
Comparison of results obtained by CHILDS et al. (these Proceedings, section B. 2), ROUGH et al.* and FROST et al. (these Proceedings, section B. 2).

* ROUGH, F. A. and CHUBB, W., BMI-1554, Battelle Memorial Institute, Columus, Ohio (1961) 55 pp.

700 - 730°C. Childs' data is quite the other way around, with approximately 70% recovery occurring at approximately 150°C during a five-hour anneal, and the remaining 30% recovery centred at approximately 510°C with no indication of change at 700°C. Resistivity data from Rough's specimens irradiated at 600 - 800°C are comparable. Perhaps Drs. Childs and Frost will illuminate the causes of the differences during the panel discussion.

All three recovery temperatures can be found in published work by Adam and Rogers of Harwell and by Bloch at Saclay in which lattice parameter change was used as an indication of recovery.

Frost shows that thermally induced vacancies in non-irradiated UC become noticeably mobile at about 670°C. From this he concluded that interstitial atoms become mobile in UC at approximately 100°C and that the second annealing stage, at 700°C, is the result of vacancy or, more probably, vacancy-cluster movement and removal from the lattice.

Frost shows nearly 50% reduction in bend strength of his specimens after 5×10^{17} n/cm^2 exposure. Concurrently a change in mode of fracture from predominantly transgranular to intergranular is noted. Childs' cast specimens also show this change, but to a lesser extent.

Irradiation tests of fuel specimens under prototypic reactor conditions are reported by Sinizer, by Frost and by Accary*.

In the Atomics International and Battelle experiments, arc-cast uranium carbide specimens were irradiated to more than 25 000 MWd/t U. Surface heat fluxes in some tests were as great as 900 000 BTU/h ft^2. Fuel surface temperature reached 838°C, in one instance, with centreline temperature reaching 1300°C. Fuel-rod diameter increases ranging between 0.4% and 3.0% were recorded. Swelling-burn-up isotherms are plotted in Sinizer's paper. They are described by an empirical equation that has practical application. Fuel compositions ranging from 4.4 to 5.3 wt.% C were tested. Fig. 3, taken from Sinizer's paper, shows the microstructure of the arc-cast UC throughout that composition range.

Frost et al. irradiated reaction-sintered UC to 15 000 MWd/t at 600°C surface temperature without unexpected incident.

Accary et al. reported irradiation of reaction-sintered UC to approximately 700 MWd/t at a maximum of 620°C.

Irradiation of hollow pellets, clad in NS-22S stainless steel (18-8 composition) was carried out in EL-3 under prototypic power reactor conditions. Fuel-element performance is reported to have been satisfactory.

Ceramographic examination of the irradiated fuel revealed grain growth, and grain boundaries that had become relatively straight and regular. This is interpreted by the author to indicate progress toward a more thermodynamically stable structure. It is interesting that the effect occurred under the influence of fission events at a relatively low temperature.

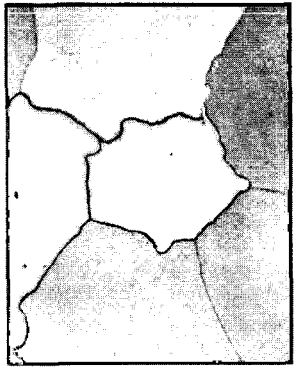
An effect that limits the in-reactor performance of some fuel-cladding combinations is the decarburizing of hyperstoichiometric UC above approximately 538°C, followed by transfer of the carbon, through the sodium or NaK heat transfer bond, to the cladding. Fig. 4 (Sinizer) shows the extent of decarburizing. Extensive technological studies, reported by Sinizer,

---

* For full text of these papers, see section B.2.



4.4 % CARBON
FREE URANIUM AT UC
GRAIN BOUNDRIES



4.79 % CARBON
EQUIAXED UC GRAINS



5.2% CARBON
WIDMANSTATTEN PATTERN OF
UC_2 PLATELETS ON (100) UC FACES

Fig. 3

Uranium-carbon alloys
(From SINIZER, D. I., WEBB, B. A. and BERGER, S., "Irradiation behaviour of uranium-carbide fuels", these Proceedings, section B. 2).



Fig. 4

UC_2 depletion during irradiation
(From SINIZER, D. L., WEBB, B. A. and BERGER, S., "Irradiation behaviour of uranium-carbide fuels", these Proceedings, section B. 2).

show that the decarburization is not sensitive to irradiation, and that subsequent transfer of the carbon causes serious embrittlement of stainless-steel cladding, as illustrated in Fig. 5. Other cladding materials capable of forming a carbide diffusion barrier layer can be used with sodium-bonded, hyperstoichiometric UC at temperatures as great as 1100°C.

Fission-gas release from both hypo- and hyperstoichiometric UC test elements was predictable from considerations of surface recoil and diffusion, as reported by Sinizer. Post-irradiation anneals of lightly irradiated reaction-sintered UC show poorer Xe^{133} retention than that of electron-beam-melted UC (Accary).

Harwell is irradiating specimens of (10 Pu, 90 U)C, and preliminary post-irradiation examinations show the behaviour to be similar to that of UC under irradiation conditions.

Oxide fuels

One of the advantages often claimed for oxide nuclear fuels in water-cooled reactors is the relative resistance to reaction with the coolant, should

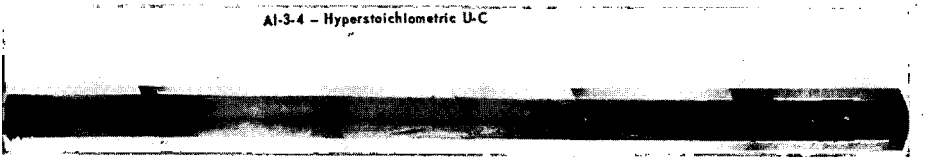


Fig. 5

Nickel cladding embrittled by carburizing during irradiation
(From SINIZER, D. L., WEBB, B. A. and BERGER, S., "Irradiation behaviour of uranium-carbide fuels", these Proceedings, section B. 2).

the cladding fail during reactor operation. Cladding costs generally comprise the largest portion of the fuel-element costs, and many experimenters would like to reduce the integrity requirements, or to do away entirely with fuel-element cladding. In experiments now begun with uranium oxide, porous-metal cladding is being investigated. The ultimate goal, of course, is to disperse the fuel as a suspension directly in the coolant. Although this concept is nearly as old as the nuclear reactor itself, most studies have been directed toward the mechanical problems of maintaining uniform suspension. Relatively few investigators have studied the effect of nuclear reactions on the fuel-coolant system.

The paper of Hermans, Sowden and Slooten reports work in progress*. Slurries of calcinated plutonia and of urania-thoria solid solution, both in dispersing and in flocculating media, were irradiated to approximately 20 MWd/t. Colloidal dispersion of as much as 50% of the plutonia could be made to occur during a very short irradiation time. The authors generalized that the extent of fuel-particle break-up per fission event depends strongly on the surface area of the particle during the early stages of fragmentation. The electron microscopy studies included in the paper show very clearly the nature of the pitting of the fuel particle surfaces, which become quite spongy in appearance, as in Fig. 6, taken from Slooten's paper. The colloidal particles were shown by X-ray diffraction and electron microscopy to have diameters of approximately 1×10^{-2} μm and to be clearly crystalline in the case of the urania-thoria slurries. The fragmentation rate was revealed to be independent of dose-rate over a range of 3 to 200×10^{7} fissions/mg s. The tentative explanation proposed by the authors for the disintegration phenomenon is a dissolution, or a peptizing of surface atoms that have been activated by the passage of fission fragments. Fragmentation was shown to be appreciable only if the solid was irradiated in a dispersing medium. For example, a variation of fragmentation of more than one order of magnitude occurred among thoria-urania particles irradiated in supernates having a pH of 10 and 11.5. This is not greatly different from the pH of the coolant of some currently operating reactors. For instance, the specified pH of the heavy-water coolant of the Plutonium Recycle Test Reactor is in the range 9.0 – 10.5. The loading of the reactor is being gradually converted to mixed plutonium-uranium oxide fuel. One wonders about the possibility of transfer of colloidal plutonium oxide and subsequent deposition in the other parts of the primary coolant system in the event of fuel-element cladding failure. I would like to hear Mel Bleiberg's comments.

The effects of irradiation on many properties of UO_2 are now relatively well defined in low to moderate temperature ranges. Particularly well studied is the release of gaseous fission products. The change in thermal conductivity of the fuel with irradiation and with operating temperature, and changes in microstructure and associated physical properties at both low and high burn-ups have been demonstrated. The papers of this panel session illustrate perhaps more than in the past the effect of fuel-element geometries and operating conditions on the extent and importance of the irradiation damage to the fuel. With each succeeding reactor that is built the conditions become increasingly severe. It is not inappropriate to consider that, in

* For full text, see section B.2.



Fig. 6

Electron micrographs showing surface of UO_2 - 80 wt. % ThO_2 before (left) and after (right) irradiation to 2×10^{16} n/cm^2 in a dispersing medium (From HERMANS, M. E. A. et al., "Irradiation experiments with fuel suspensions", these Proceedings, section B. 2).

the relatively near future, solid, liquid and gaseous UO_2 may coexist in the operating fuel element, that steep temperature gradients will extend from slightly above coolant temperature to slightly above 2800°C, and that operation of the fuel to the burn-ups already demonstrated to be possible will cause wide variations of chemical composition throughout the fuel. Similarly, these conditions will be continuously varied, as is normal in the operation of a nuclear reactor. Therefore we hope to leave you with one idea firmly in mind, that the radiation effects we are concerned with are a complex, continuously variable interrelation of radiation damage, thermal and chemical effects; and, further, that we should be able to utilize many of these effects to our advantage.

The paper by Bleiberg, Berman and Lustman* presents a remarkably complete study of the performance of several fuel materials evaluated for use in an advanced plate-geometry element in the Pressurized Water Reactor. This paper is an example of the investigative approach that is becoming common wherein basic studies are often carried out to explain the results of tests carried out under prototypic reactor conditions.

The Westinghouse experiments carried oxide ceramic fuel materials of high-density sintered UO_2, of $ZrO_2 + UO_2$, and of two phase dispersions of UO_2 in matrices of BeO or Al_2O_3 to exposures as great as 36×10^{20} fissions/cm^3, and at fuel centreline temperatures as great as 2100°C.

This paper is concerned in extensive detail with the appreciable change in performance of UO_2 that occurs after approximately 17×10^{20} fissions/cm^3, as illustrated in Fig. 7, taken from Bleiberg's paper. Below that exposure UO_2 was shown to exhibit an apparent volume change of 0.16% per 10^{20} fissions/cm^3. At higher exposures the rate increased to 0.7% per 10^{20} fissions/cm^3. The behaviour of the zirconia-based fuel is slightly different in that it swells uniformly at 0.7% per 10^{20} fissions/cm^3 to at least 35×10^{20} fissions/cm^3. However, the sintered, zirconia-based fuel plates pass through an initial volume decrease that is the result of complete densification of the fuel at exposures below 6×10^{20} fissions/cm^3. The data indicate that this difference between UO_2 and zirconia-base fuel probably reflects the difference in plasticity under fission-fragment bombardment. The zirconia-base fuel exhibited a creep rate, under irradiation, at least five times greater than that of cubic UO_2. Homogenizing of multiphase compositions into a metastable cubic structure occurred at about 9×10^{20} fissions/cm^3.

UO_2 dispersed in beryllia showed a slighly higher swelling rate of approximately 1% per 10^{20} fissions/cm^3. Porosity disappeared at very low burn-up, as in the case of the zirconia-base fuels.

The swelling behaviour of UO_2 dispersed in alumina reflects an entirely different phenomenon, operating at low irradiation temperatures, that makes the result from the alumina dispersion not comparable with those from the other fuel materials. For example, Al_2O_3 plus 21 wt.% UO_2 swelled approximately 19% before an exposure of 10^{20} fissions/cm^3 was reached. Little or no further swelling was noted during exposures to 5×10^{20} fissions/cm^3.

Fig. 8, from Bleiberg's paper, shows that the retention of fission gases by these fuel materials was similar, and is related to volume diffusion theory and to the changes occurring in the microstructure of the fuel. It

* For full text, see section B. 2.

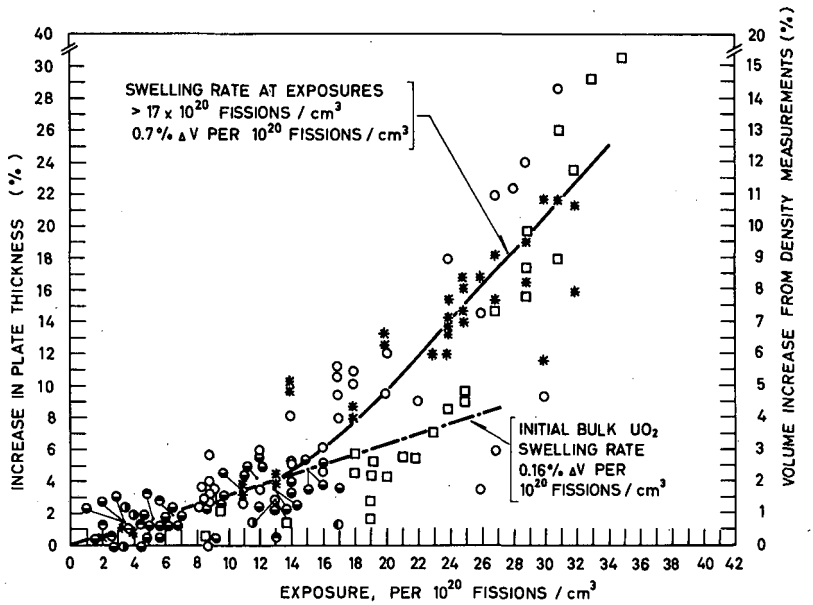


Fig. 7

Solid volume swelling of bulk UO_2
* ● % ΔV from gravimetric density measurements
% Δt from plate measurements:

	Fuel thickness (in)	Density (%)	Q/A x 10^{-5}	Temperature range (°F)
○	0.04	96	3 - 7	1340 - 2200
◑	0.08	96	3 - 4	1620 - 1700
◒	0.10	96	5 - 7	2300 - 3200
◐	0.12	96	3 - 4	2300 - 2600
◓	0.16	96	4 - 7	2420 - 3840
□	0.04	88	6 - 7	2110 - 2385

(From BLEIBERG, M. L., BERMAN, R. H. and LUSTMAN, B., "Effects of high burn-up on oxide ceramic fuels", these Proceedings, section B. 2)

is indicated that, at the low-to-moderate fuel temperatures of these irradiations, the results of the electron micrographic examinations are consistent with migration of solid and gaseous fission products to grain or to sub-grain boundaries. There, precipitation of the gas occurs until structural fragmentation permits external release of the fission gases, at approximately 20×10^{20} fissions/cm^3. Zirconia-base fuels have a higher fission gas diffusivity than does UO_2. However, this is partially compensated by the increased path-length required for external release after the fuel has become completely dense during the early stages of irradiation. This provides greater availability of gas for the bubbles and they are expected to

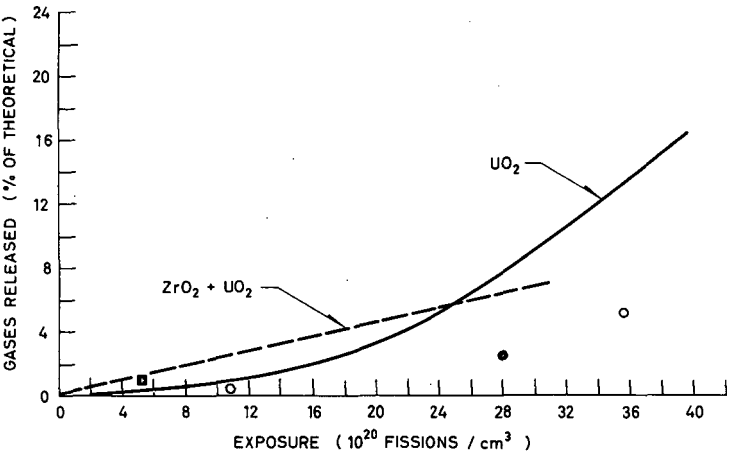


Fig. 8

Comparison of fission-gas release from oxide ceramic materials
O BeO + 65 wt. % UO_2
● BeO + 51 wt. % UO_2
□ Al_2O_3 + 21 wt. % UO_2

(From BLEIBERG, M. L., BERMAN, R. H. and LUSTMAN, B., "Effects of high burn-up on oxide ceramic fuels", these Proceedings, section B. 2)

be easier to precipitate because of the greater plasticity of the zirconia-base fuel during irradiation. This effect is illustrated in the paper by showing extensive precipitation of gases in the zirconia-base fuel irradiated under conditions where no evidence of precipitation is seen in the sintered UO_2, Fig. 9.

The paper by Frost, Bradbury and Griffiths*, however, contains an electron micrograph (shown in Fig. 10) of a columnar grain growth region in UO_2, irradiated at temperatures above approximately 1800°C, that seems to show bubble formation due to fission-gas nucleation. In a similar electron micrograph (Fig. 11) of a 1% PuO_2 - UO_2 fuel, non-random alignment of bubbles is quite evident, and it may be that the nucleation occurs principally along the dislocation lines of single crystals. In the paper by Roake*, several photomosaics of cross-sections of irradiated fuel rods (Fig. 12, for example) show extensive accumulation of porosity along boundaries of single columnar grains in fuel irradiated at greater than 2400°C. In other instances (Fig. 13) the sub-grain structure is made apparent in optical micrographs by the resolution of the low-angle boundaries by an accumulation of very small pores. Electron microscopy has not yet been attempted. Further evidence of accommodation of fission products in the fuel structure, but not in the lattice, is seen by Bleiberg in the relatively greater ease of etching of grain boundaries in irradiated UO_2, in the precipitation of uranium or uranium/fission-product alloys from high-temperature-irradiated fuels,

* For full text, see section B. 2.

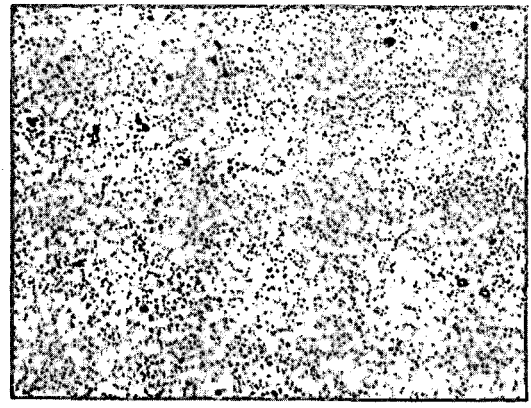


Fig. 9

Fission-gas bubbles precipitated in ZrO_2 - 36.8 wt. % UO_2
after 25.1×10^{20} fissions/cm^3
(From BLEIBERG, M. L., BERMAN, R. H. and LUSTMAN, B.,
"Effects of high burn-up on oxide ceramic fuels",
these Proceedings, section B. 2)

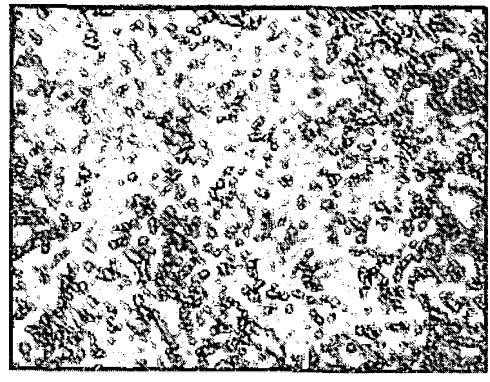


Fig. 10

Electron micrograph of columnar grain interior in irradiated UO_2,
showing what may be fission-gas bubbles
(From FROST, B. R. T., BRADBURY, B. T. and GRIFFITHS, L. B.,
"Irradiation effects in fissile oxides and carbides at low and high burn-up levels",
these Proceedings, section B. 2)

and in the X-ray diffraction patterns that show no significant effect of high burn-up on unit cell size or on the degree of internal strain.

These last results are not in conflict with those published earlier by Bloch, of Saclay, because of the saturation observed at approximately 10^{17} fissions/cm^3.

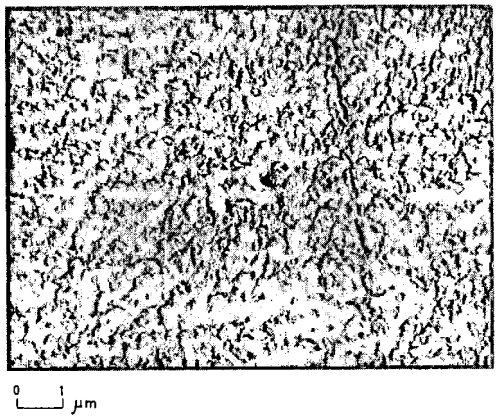


Fig. 11

Electron micrograph of a columnar grain interior in irradiated 1% PuO_2/UO_2, showing non-random distribution of gas bubbles
(From FROST, B. R. T., BRADBURY, B. T. and GRIFFITHS, L. B., "Irradiation effects in fissile oxides and carbides at low and high burn-up levels", these Proceedings, section B. 2)

Precipitation of white metallic phase in fuel plates irradiated to produce columnar-grain formation is not unique to the Bettis plate geometry. Extensive precipitation of beta uranium throughout the columnar-grain region of cylindrical Uo_2 fuel rods is reported in the paper submitted from Hanford Laboratories. The Hanford investigators believe that the precipitated uranium results from quenching a stable sub-stoichiometric UO_2 that exists at high temperatures, as also proposed by Rothwell at Harwell. The precipitate is not necessarily indicative of high exposure, but primarily of high temperature. These observations somewhat parallel those of Bleiberg et al. in which the greater concentration of precipitated particles observed in ZrO_2 - UO_2 fuel plates is held to be consistent with the greater susceptibility of sub-stoichiometry of the latter fuel system.

The results of Frost, Bradbury and Griffiths' duplex capsule experiments support Bleiberg's contention that the "breakaway" exposure for UO_2 swelling is independent of temperature, but strongly dependent on restraint. Enriched UO_2 pellets were thermally insulated with a surrounding hollow cylinder of naturally enriched UO_2. These specimens were irradiated to $3 - 8 \times 10^{20}$ fissions/cm^3 with surface and centre temperatures of the order of 1000°C and 1600 - 1800°C respectively. No swelling was observed, although the onset of gas-bubble precipitation mentioned earlier may have foreshadowed such an event at greater exposure. The addition of 1% or 10% plutonium as a co-precipitated oxide did not appear to modify the irradiation performance of UO_2, except that an unidentified second phase was observed that appears very similar to that reported earlier by Bates and Roake in a 1% Pu-U oxide element.

In the paper by Mustelier*, four test elements containing sintered, enriched UO_2 were irradiated to establish a basis for comparison with the later

* For full text, see section A. 2.

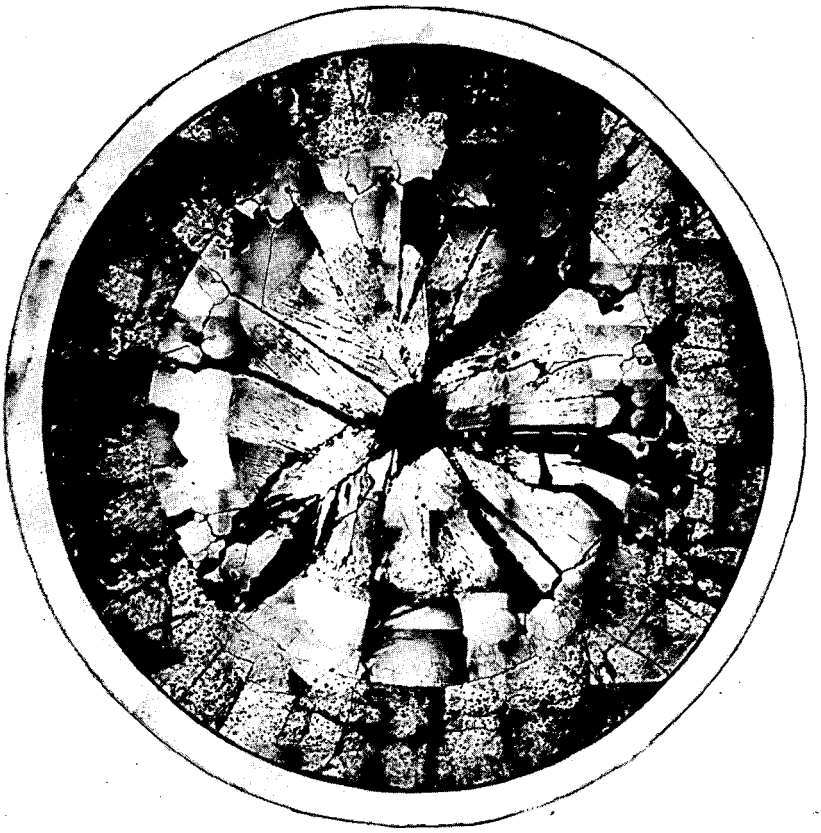


Fig. 12

Irradiated, sintered UO_2 pellet cross-section, test GEH-14-189
(From ROAKE, W. E., "Irradiation alteration of uranium dioxide", these Proceedings, section B. 2)

element containing (9.3wt. % Pu-U)O_2 pellets that were prepared from co-precipitated peroxide. These elements were irradiated under prototypic conditions for the "Rapsodie" reactor; that is, 450°C cladding temperature, and at a specific power of 1000 to 1750 W/cm^3. Well-developed regions of equiaxed grain growth and columnar-grain structure are shown in the paper for both UO_2 and (Pu, U)O_2 elements. The author refers to the columnar grain region as "basaltic" grains, which I take to mean grains solidified from the melt. I disagree with this interpretation, and perhaps we can argue the point during the panel discussions.

In some of the test elements, an external sodium heat-transfer bond failed to wet the stainless-steel cladding completely. The net result was that the cladding failed and sodium entered the fuel cavity. In those instances no structural change of the fuel occurred, even though heat ratings comparable with those mentioned earlier were maintained. This, of course, illustrates the marked improvement in overall heat-transfer rate when a metallic

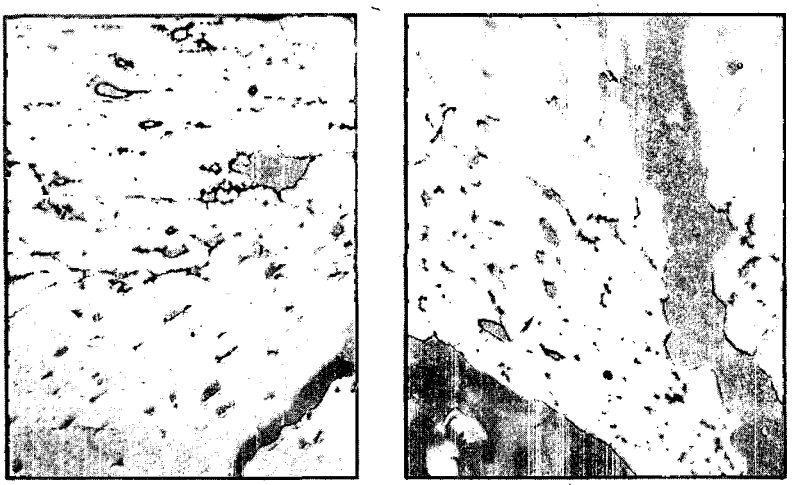


Fig. 13

Porosity accumulated at low-angle boundaries in large columnar grain region of irradiated UO_2
(From ROAKE, W. E., "Irradiation alteration of uranium dioxide",
these Proceedings, section B. 2)

bond is present, as was also shown earlier by Kittel and colleagues at Argonne National Laboratory, using a molten-lead heat-transfer bond.

Thermal conductivity; relocation of fission fragments, and plutonium; homogenizing of mixed fuels; and the mechanical performance of high-rated fuel rods are dominated by the phenomenon of columnar-grain growth, where fuel temperatures exceed approximately 1800°C. Several illustrations in Roake's paper show that the general configuration comprising concentric regions of unchanged microstructure, equiaxed grain growth, small columnar grains, large columnar grains and a central, porous, large columnar-grain region is common to high-rated irradiated fuel rods contianing sintered UO_2, particulate UO_2, or mixtures of UO_2 and ThO_2 or PuO_2. The effect of radial columnar-grain structure on enhanced heat transfer, published earlier by Bates, is supported by extensive additional data as well as by measurements showing that the thermal conductivity of non-irradiated, single crystal UO_2 is approximately twice that of polycrystalline UO_2, even at 800°C. The measurements reported here were made by Deem and colleagues in a co-operative study by Hanford Laboratories and Battelle Memorial Institute.

Measurements of the thermal conductivity of polycrystalline UO_2 specimens irradiated at less than 100°C temperature to 10^{18} fissions/cm^3 showed a decrease of at least 50% from the non-irradiated value (Fig. 14). Annealing studies demonstrated three stages of recovery of thermal conductivity at temperatures that correlate well with the data on annealing of irradiation-induced changes of lattice parameter published by Bloch. With the possible exception of the lowest-temperature annealing stage, no saturation of damage has yet been observed.

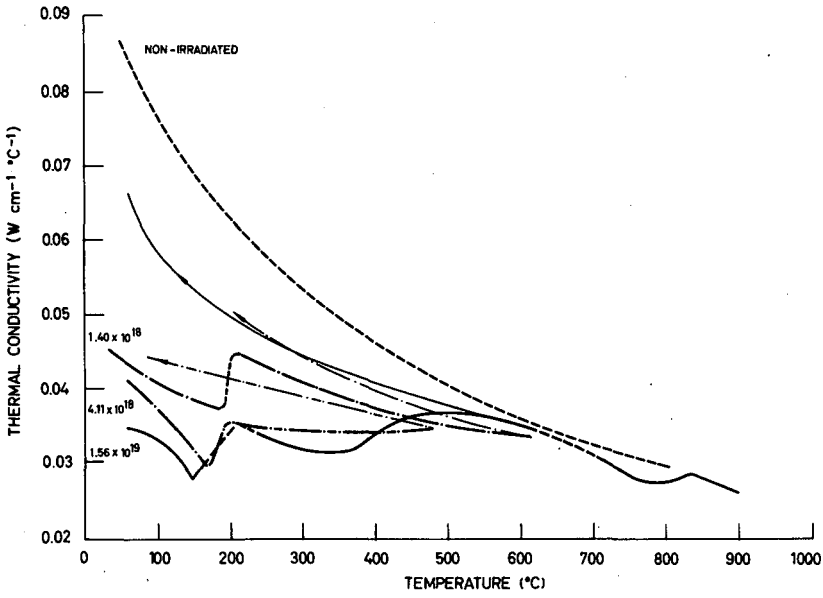


Fig. 14

Effect of irradiation on the thermal conductivity of sintered uranium dioxide
(From ROAKE, W. E., "Irradiation alteration of uranium dioxide",
these Proceedings, section B. 2)

Electrical conductivity (Fig. 15) changes in the same irradiated specimens showed no correlation with the annealing temperatures indicated by the thermal conductivity data. An initial decrease in electrical conductivity

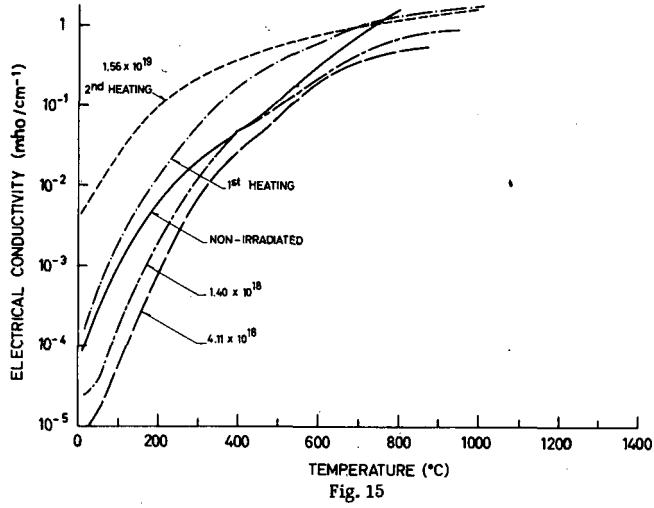


Fig. 15

Electrical conductivity of polycrystalline UO_2
(From ROAKE, W. E., "Irradiation alteration of uranium dioxide",
these Proceedings, section B. 2)

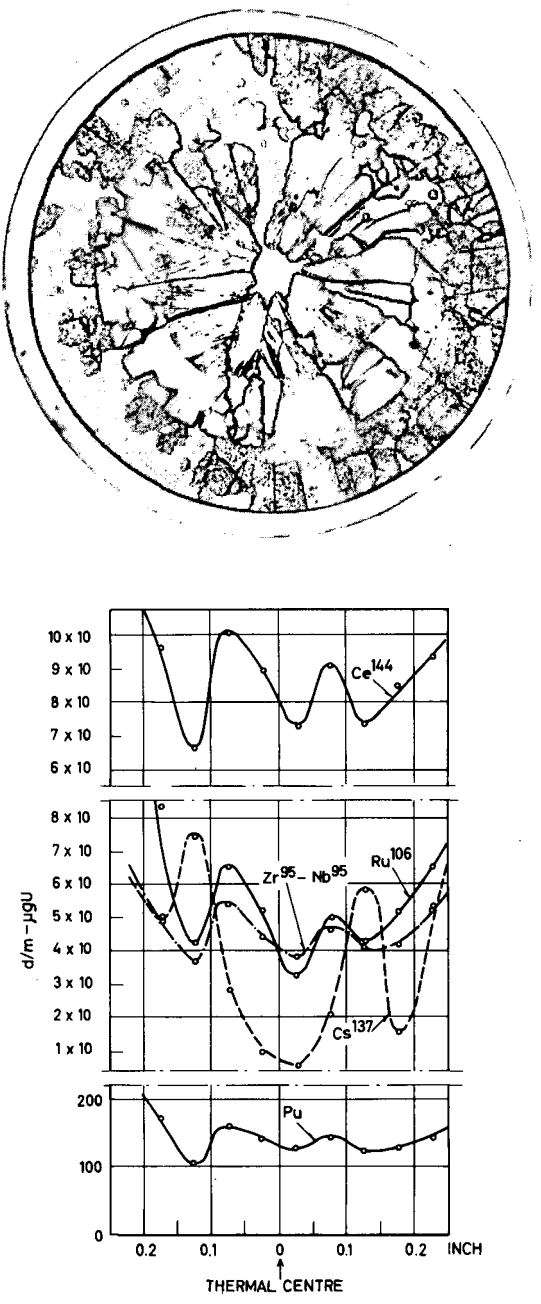


Fig. 16

Fission-fragment distribution in irradiated, sintered UO_2 pellet
(From ROAKE, W. E., "Irradiation alteration of uranium dioxide", these Proceedings, section B. 2)

is reserved beyond 4×10^{18} fissions /cm^3 and at 1.5×10^{19} fissions/cm^3 the electrical conductivity is greater than for the non-irradiated specimen. Other single-crystal specimens irradiated at low temperature are currently being examined by both replica and direct-reflection electron microscopy. In these specimens, the hardness of the crystals was shown to be appreciably increased. The appreciable increase in melting point at moderate exposures was shown to reverse, and high-burn-up specimens supplied by Westinghouse had a lower melting point than non-irradiated UO_2.

Migration of fission products and plutonium in irradiated UO_2 is associated with columnar grain growth (Fig. 16). Concentration variations of 2 - 10 are illustrated for several fission fragments and plutonium.

It was mentioned earlier in this review that improved understanding of irradiation effects permits us to make virtues out of necessities. For example, Bleiberg and his colleagues have demonstrated their understanding of swelling in UO_2 by developing a method for fabricating a porous, sintered UO_2 having only approximately 88% bulk density, but high interpore fuel density. That this material has a failure exposure in the PWR fuel plate geometry more than twice as great as that of 96% dense UO_2 is shown in Fig. 17, from Bleiberg's paper.

At Hanford Laboratories, engineers are using the columnar grain growth phenomenon to simplify fuel element fabrication techniques. Probably more effort is expended in calculating hot-spot effects in test elements than in any other part of the thermal-hydraulic calculations. As a result of this, probably more effort is expended assuring fuel homogeneity than in any other aspect of fabrication of fuels of mixed enrichment, such as UO_2 plus PuO_2. We do not now believe this effort is entirely warranted. Hot spots produce columnar grain growth and columnar grain growth effectively homogenizes mixtures of UO_2 and PuO_2 or ThO_2. In a "test to end all tests", severe initial hot spots were prefabricated by placing 3-mm-diam. lumps of 93%-enriched $U^{235}O_2$ against the inner cladding surface of a fuel element containing vibrationally compacted UO_2 having an average enrichment of only 1.6% U^{235}. Assuming no relocation, one would calculate boiling burn-out and melting of the cladding. However, the gross relocation of the highly enriched fuel by the mechanism of sublimation, diffusion and redeposition occurred so rapidly that only slight discoloration of the cladding exterior marked the original position of the enriched pellet.

Fig. 18 shows a longitudinal cross-section of the fuel rod and its autoradiograph. The autoradiograph clearly reveals how the enriched UO_2 moved from its position adjacent to the cladding into the centre of the fuel rod. The columnar grain structure shown here is sometimes mistaken for equiaxed grains, but this appearance is that of columnar grains cut at an angle of approximately 30° to their long axis. I will conclude this review with a motion picture of 22 seconds duration that illustrates that statement. The film shows the change of surface appearance of the cross-section of a similar fuel rod as it is ground away over a distance of approximately 0.5 in. In one sense it provides a three-dimensional interior view of the irradiated fuel. The growth directions of the columnar grains are clearly evident.

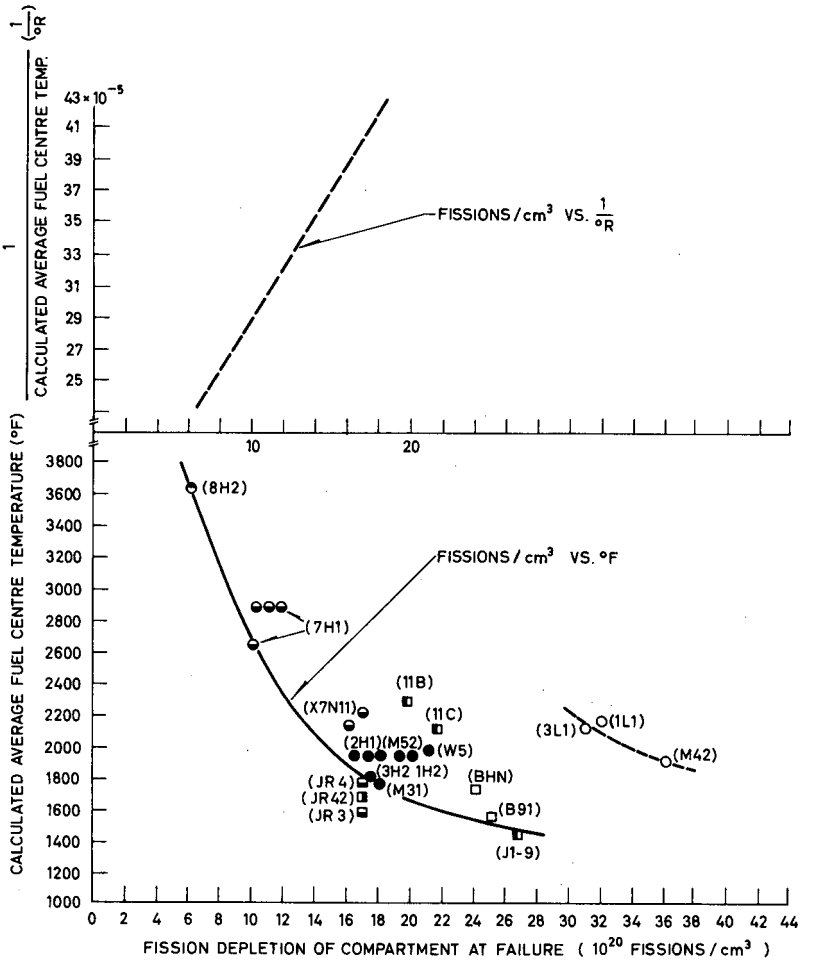


Fig. 17

Comparison of centreline fuel temperatures for failed UO_2 and $ZrO_2 + UO_2$ compartments
(Pressure-bonded elements only)

	Thickness (in)	Density (%)
◧ ZrO_2 + 25 wt. % UO_2	0.036	96
◨ ZrO_2 + 34 wt. % UO_2	0.036	96
◧ ZrO_2 + 46 wt. % UO_2	0.020	90
□ ZrO_2 + 34 wt. % UO_2	0.036	90
○ Bulk UO_2 fuel	0.040	88
● Bulk UO_2 fuel	0.040	96
◒ Bulk UO_2 fuel	0.100	96
◓ Bulk UO_2 fuel	0.160	96

(From BLEIBERG, M. L., BERMAN, R. H. and LUSTMAN, B.,
"Effects of high burn-up on oxide ceramic fuels",
these Proceedings, section B. 2)

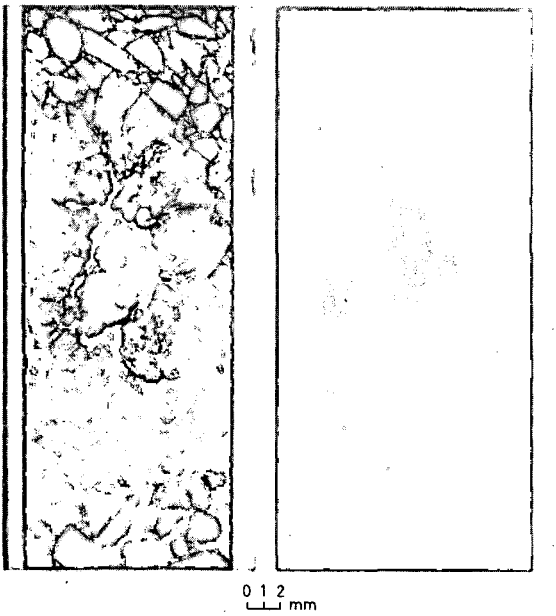


Fig. 18

Longitudinal section of an irradiated, vibrationally compacted UO_2 fuel rod near the position of an initially severe hot spot

(Film showing, with commentary)

I thank you all for your attention. We will now proceed with the panel discussion to give my colleagues an opportunity to repair whatever damage I may have done to their professional reputations !

PANEL DISCUSSION

W.E. ROAKE: May I ask Dr. Frost and Dr. Childs if they would like to comment on the remarkable difference that we revealed earlier between the two types of uranium carbide, that which is arc-cast and that which is prepared by sintering?

B.G. CHILDS: I think that what we are looking at when we measure the change in resistivity of uranium carbide is scattering of conduction electrons by uranium atoms displaced from their normal lattice sites – either displaced interstitially in the lattice or displaced into carbon lattice sites. So I would imagine that the reason for the difference is that in the case of the melted and cast material we have a high concentration of uranium interstitials and in the case of the reaction-sintered material for some reason we have not. The only reason I can think of for this is that in the reaction-sintered material there must be a very high density of sinks for uranium interstitial atoms, either dislocations or porosity, and that these things are mopping up the uranium interstitials as they are created.

B.R.T. FROST: I think that we would essentially agree with that. Our views were that the reaction-sintered material contained something like 9% porosity and, as Dr. Childs says, these were acting as sinks for the lattice defects. There is another thing I would like to add, perhaps to confuse the situation a little further, on the question of radiation damage in uranium carbide. Dr. Adam and Mr. Rogers, who published lattice parameter change curves for uranium carbide versus irradiation dose have recently reexamined their old data and have obtained some newer data. It seems from the lattice parameter changes that the build-up to saturation occurs in two steps. One type of defect is being formed and saturated, and when it saturates another type of defect can then form. This suggests, perhaps, that interstitials which are likely to affect the lattice parameter more than do vacancies saturate. Then clusters form. The other thing, which I think Mr. Childs points out in his paper, is that unlike a pure metal we are dealing with a two-element compound and we can have uranium and carbon interstitials – we can have uranium and carbon clusters, and this is going to complicate the radiation damage pattern in this material very considerably.

W.E. ROAKE: Dave Sinizer, I wonder if you would like to comment on the relative merits of arc-cast uranium carbide and sintered uranium carbide, recognizing of course that your opinion is biased, and perhaps we can get an equally biased argument out of Brian.

D.I. SINIZER: The advantages that we see for cast uranium carbide are primarily from the standpoint of fabrication. We started our programme some years ago in the direction of using slightly hyperstoichiometric carbide – that is with UC_2 platelets present in the UC grains. The reason for this choice before we started working intensively on uranium carbides was the thought that perhaps the free uranium in the grain boundaries might result in some irradiation instability. However, the results that we have obtained so far indicate that in the region close to stoichiometric on both the hypo- and the hyperstoichiometric side the radiation damage or the swelling that we have observed, and the fission-gas release, are not affected by carbon content. I am straying somewhat from the original problem, but we

have come to the conclusion, on the basis of the carbon transfer problem revealed in out-of-pile tests and in our irradiation tests, that stoichiometric or hypostoichiometric material will be satisfactory for the high-temperature sodium-cooled reactors that we are planning for the future. We feel that this material will be satisfactory with stainless-steel cladding to central temperatures of 2000°F, and we do not foresee any problem in the fabrication of either hyper-or hypostoichiometric fuel. The major reason for our interest in arc-cast uranium carbide, however, stems from the cost of fabrication, which we feel will be less for the arc-cast material. Our calculations have indicated a fuel-cycle cost of less than 2 mills/kWh based on American methods of calculation. How that translates into your own current technology I am not prepared to comment at the present time.

B.R.T. FROST: We have tended to concentrate more on sintered material because I think our applications are somewhat different – we are not thinking in terms of UC as a thermal reactor fuel but rather of mixed uranium-plutonium carbide as a fast reactor fuel. In this case fabrication has to be carried out under glove-box conditions and with rather strict criticality limitations, and we feel that the sintering process is rather more adaptable to these conditions. We have recently succeeded in producing high-density mixed plutonium-uranium carbide by a direct sintering process, as I think some of the laboratories have in the United States, and this seems to be a pretty satisfactory product. We have another application for uranium carbide in that we are interested in using it as a cathode material in a direct-conversion diode. In this case we add zirconium carbide to improve its properties. It may be of interest to some of you that one of these operated successfully in-reactor last week and did not drop to pieces, as many people had predicted. So our experience with sintered uranium carbide material is quite favourable. The material which we have irradiated to about 15 000 MWd/t seems to have behaved very much as we had hoped.

W.E. ROAKE: Thank you, Brian. Now, I would like to add a little more fuel to the fire. Brian mentioned the difficulties of working in dry-box conditions – glove-box conditions – and any of you who have worked with plutonium are certainly familiar with this. I should like to point out that the Plutonium Metallurgy group at Hanford, under Oz Wick and Ivor Thomas, are now making arc-cast plutonium carbide, and mixtures with uranium carbide, in a glove-box and as a matter of fact are machining this material, grinding it and cutting it under dry conditions.

B.R.T. FROST: We also have done this at Harwell and I think Mr. Childs will tell you that they have also done it at Dounreay, but we think that on a production basis the sintering method might be more amenable.

D.I. SINIZER: I should like to say that Mr. Frost's point is very well taken that the application of the material might well govern the kind of fabrication that is to be used. I have here a slide showing a typical as-cast slug of uranium carbide. This particular one is approximately 7/8 in in diameter by about 6 in long. You can see a typical as-cast surface on it, which might look bad for certain types of application, such as the diode that Mr. Frost mentioned, but for the type of thermal reactor fuel that we are using at Atomics International it is highly satisfactory. This fuel goes into a fuel element where the cast slugs, such as you see here, have the head cut off and the bottom squared with the axis of the cylindrical slug. The slugs are

stacked end-to-end in a fuel element and sodium-or NaK-bonded to a stainless-steel cladding. In this type of fuel element imperfections in the surface are of no consequence in the operation of the reactor, since there is a good thermal bond between the fuel and the cladding, and eventually out to the ultimate heat-removal medium, the sodium coolant of the reactor. For this type of application we feel that this kind of fuel element will be highly satisfactory. At the bottom of the slide you see a ground surface which we have tested in irradiation capsules, but only for the purpose of discovering any differences that might exist between the two forms of fuel. We have discovered none, I might add, in our very brief comparison experiments.

W.E. ROAKE: Dr. Slooten, perhaps you would like to elaborate on your dispersion fuels.

H.S.G. SLOOTEN: Yes. I think you have made a very good job of compressing the work we have done into a very short time. It wasn't too hard a job, anyway, because it was a rather small amount of work. But I think the points I would like to stress again are that, in the first place, the effect we found – the break-up of the 5-μm fuel particles – occurs within a very short time, within exposures not at all comparable with the exposures you usually think of when you think of reactor applications. In the second place I would like to stress the fact that the break-up is to a very large extent governed by the chemical conditions under which the irradiation is taking place. This, in connection with the fact that the effect is also proportional to the original surface area of our particles, led us to believe that it is essentially a surface effect, and this brought us to the hypothesis that it is most likely a dissolution or peptization of our material after the passage of a fission fragment. Now this leaves us with the problem of why. It is especially clear in the electron micrographs of the fuel irradiated in a non-dispersing medium that no evidence of damage to the surface is seen at all. But we still have to find out exactly what this situation is.

W.E. ROAKE: Thank you, Dr. Slooten. I wonder, Dr. Bleiberg, do you have anything to add to that?

M.L. BLEIBERG: No, not really. You brought up a very interesting point – significantly, one not covered in my paper, – about the irradiation of intentionally defected UO_2 fuel-plates in this case. However, what I'm going to describe briefly is available in WAPD-263; also it is discussed very briefly in a book called, I believe, "UO_2 Applications" edited by J. Belle, in the chapter written by Lustman. Under a certain set of circumstances, such as you would have by having an intentional hole in a plate-type element, we have demonstrated that significant amounts of UO_2 corrode away in recirculating, hot water test loops. Lustman suggested that the mechanism by which this occurs involves radiolytic decomposition of the water in the immediate vicinity of the UO_2, and the subsequent formation of hydrogen peroxide oxidizes the UO_2 to UO_3, which sloughs off. So this reaction is really governed by the hydrogen concentration, because that controls the back reaction. This may explain why the same effect is not noted in a fuel rod in which you can trap a hydrogen-enriched atmosphere as a result of corrosion of the Zircaloy cladding.

W.E. ROAKE: There were a great number of topics covered in Dr. Bleiberg's paper which I didn't cover in review. While you have the audience at your disposal, Mel, why don't you take the floor?

M.L. BLEIBERG: I know it's getting late and I certainly don't want to prolong the session unduly. I think there are four significant observations made in this paper. The first is that the swelling rate of the zirconia-based UO_2 fuel mixtures and BeO are identical. The true swelling rate is the same but the variability and dimensional changes observed during irradiation are related to the plasticity of these materials.

The second interesting item that we noted was that we can take the diffusion model that has been developed for rod-type fuel elements at exposures orders of magnitude lower than our fuel plates have reacted, and by making a few assumptions actually show that fission-gas release can be described by this model of diffusion from a hypothetical sphere, up to exposures of about 40×10^{20} fissions/cm^3.

Another interesting item is the irradiation-induced phase changes in zirconia-UO_2 fuel system. This is a rather complicated fuel system. However, after relatively short irradiations the multiple phases become single phases, even tetragonal. This in turn becomes cubic, and this ultimate cubic phase is predictable on the basis of Vegard's Law. This is a rather unexpected result.

The other item that I would like to mention is that we see much evidence, as does Dr. Roake and other investigators, of fission-product migration and segregation at grain boundaries and at sub-grain boundaries. And this agrees with our X-ray diffraction studies on UO_2 in which roughly 17% of the uranium atoms have fissioned, from which we obtain sharp X-ray diffraction patterns, sharp cubic patterns, of the UO_2 lattice. There is essentially no line broadening, so the fission products are not in the lattice. Rather, they segregate at the grain boundaries and then at the sub-grain boundaries. We also see evidence of precipitation at high burn-ups at high temperatures – precipitation of the volatile as well as the non-volatile fission products.

E.L.F. VANDEN BEMDEN: Je voudrais poser une ou deux questions aux auteurs qui ont parlé des combustibles UO_2 enrichis à l'oxyde de plutonium, et la première question est relative à l'instabilité de l'oxyde de plutonium. D'après l'expérience de laboratoire et des expériences que nous avons réalisées nous-mêmes, on sait que cet oxyde est instable sous vide à des températures relativement basses, de l'ordre de 1500°C, et instable également dans des gaz rares, tels que l'argon, à des températures beaucoup plus hautes, voisines de la température de fusion. Est-ce que cette instabilité ne peut pas être responsable de cette apparition ou de la présence de cette seconde phase mentionnée par le rapport de Hanford il y a un an et demi et par le rapport présent de M. Frost ?

La deuxième question est relative à la diffusion possible du PuO_2 dans le combustible UO_2-PuO_2. Je parle ici de diffusion longitudinale, par exemple, due à des gradients thermiques, et en particulier est-ce qu'une expérience telle que l'expérience appelée Princess Experiment, l'expérience du hot spot, a été faite avec du PuO_2 à Hanford ?

B.R.T. FROST: Yes, I think this could be explicable on the basis of a high-temperature phase diagram. Our statement that we thought the particle was non-fissile was mainly based on etching characteristics and the complete absence of any gas bubbles or anything of that nature in that particular phase. But this does not rule out the possibility of its being a second

uranium-plutonium-oxygen phase. We deliberately avoided being too specific about what it was.

W.E. ROAKE: As I understand the second part of your question, you are concerned with the movement of plutonium in the hot-spot experiment. That particular experiment was not carried out with plutonium but with enriched UO_2 lumps in natural UO_2. However, we have translated the results into methods of fabricating mixed plutonium-uranium oxide fuel for the plutonium-recycle test reactor. Rather than attempting to fabricate a uniformly enriched mixed oxide, the technique now used for loading the swaged or the vibrationally compacted fuel rods is to blend mechanically a relatively small volume percent of a highly enriched plutonium compound with natural UO_2. We do not yet have all the answers to the problem of the plutonium-migration – as with the fission-product migration. We think it's associated with something akin to a vapour-phase zone-refining process which occurs by the same mechanism that is responsible for the solid-state growth of columnar grains, i.e. the movement of a void towards the centre by sublimation of the UO_2 from the hot side and redeposition on the cold side. We also have some other ideas now about interaction of moving pores with grain boundaries. What effect these migrations have on reactor operation and safety I cannot discuss at this time.

M.E.A. HERMANS: I have a question for Dr. Bleiberg. The experiment you described gives an opportunity to get some more information about the phenomenon which occurs in the disintegration of the fuel. Your proposal is the same as we started to investigate and in that case we expected we might find two or three hydrates in the debris of the colloidal material. We have tried and failed to find these. At least we think that we have mixed oxides. The second point is that in our work we irradiated fuels with a high thoria content and uranium oxide. In these cases, too, the same number of atoms were lost from the particle per fission as for uranium oxide. I would like to know your view on this point – I would think that the experiment you described might give an explanation for uranium oxide or mixed oxide fuels with a high uranium oxide content. But I am wondering whether you could comment about fuels, like those we have, containing 85% thorium oxide or even higher.

M.L. BLEIBERG: That's a very good point. In our paper we show a metallographic longitudinal fuel cross-section. From the hole created by the corrosion, through a transition zone to normal UO_2, the region between the hole and the normal UO_2 seems to have the same appearance as that shown by Shaner in his metallographic study of the uranium-oxygen phase diagram. From that we concluded that this was UO_{2+x}. But your point is quite interesting, in that this phenomenon would not necessarily be active in thoria, and in 80% thoria – 20% wt.% UO_2.

B.R.T. FROST: May I raise a question with Dr. Bleiberg and Dr. Roake? They both report seeing free uranium in high-temperature regions of UO_2. As Dr. Roake says, Rothwell at Harwell observed this and I also believe this was observed at Chalk River in UO_2 heated to high temperatures in a flowing gas stream and when the UO_2 became substoichiometric, if one can use this expression. When the UO_{2-x} cooled down uranium was precipitated in order that stoichiometric UO_2 could form. Now we had always postulated that this could not happen in a fuel element because one could

not drain off the excess oxygen. But I believe, on the basis of private discussions with Dr. Bleiberg, that he has an explanation for the appearance of free uranium in his high-burn-up UO_2 specimens.

M.L. BLEIBERG: I guess it would be possible to show some electron micrographs very quickly. I think this would save me a thousand words.

When we first observed the spherical white precipitates we made a very extensive investigation to see what they could be. We investigated uranium carbide and nitride and other things, like alumina, which was mentioned earlier, tonight. We decided it could not be uranium because it was chemically inert. However, the explanation that we offer is that it is the same phenomenon that Dr. Roake described and which Lewis from Chalk River has reported. The difference in our case is due to the large concentration of cations associated with the grain boundaries. And this is what I should like to show. It is rather difficult to describe. This slide shows an electron micrograph of unirradiated, 96% dense UO_2. It is chemically etched and the pores you see are typical of the sloping grain boundaries – I am sure you have seen similar things before.

The next slide shows UO_2 irradiated at the relative low temperatures that we have been interested in, up to about 13×10^{20} fissions/cm^3. The etching action on the material at the grain boundaries is quite apparent. Now we believe this material is the fission fragments. With further exposure, you can see what happens more clearly.

In the next slide, we see that the grain boundaries subdivide, and then continue to subdivide until finally you get a grain diameter of the order of one tenth to one half a micron, as you see in this slide. So this is our "reducing atmosphere" and this is where the oxygen goes at high temperature. These fission-product cations are highly substoichiometric and will readily absorb the released oxygen. During cooling to where UO_2 again is stable, the excess uranium metal is probably precipitated, but it undoubtedly reacts with the zirconium, the niobium and the other soluble fission products. This is the reason why it seemed chemically inert.

D.I. SINIZER: Might I suggest another possibility that could explain some of the substoichiometry? The oxygen is released, it is true, by the fission of a uranium atom, but the fission products that are formed are more than enough to take care of that released oxygen. I am referring to the fission products that remain in the lattice. Some years ago we made some calculations which indicated that this was the case. As a matter of side interest, this is also true for uranium carbide. There are sufficient stable carbide-formers in the fission products to take care of the carbon that is released when a uranium atom fissions.

M.L. BLEIBERG: I would like to make one other comment. There have been many balances made of the fission products and oxygen. Naturally our conclusions are based on a body of data. Another relatively important piece of information that is described in our paper but has not been mentioned here is that we see rather conclusive evidence that the inside surface of our Zircaloy cladding is oxidized. A grey film forms on the inner surface of the cladding. The amount and thickness of this phase is solely a function of irradiation exposure. We have not definitely identified it as ZrO_2. It has approximately the hardness of ZrO_2 and tentatively I think it is safe to say that it is ZrO_2. A quick calculation showed that it

would take 18 - 25% of the total oxygen released in fission to account for the thickness of the proposed ZrO_2 film that we see on the inside. So it is not all taken up by the fuel.

D.I. SINIZER: In reprocessing work that has been done at various sites it seems to be indicated that the thermodynamically stable form is a UO_2 and that zirconium would remain behind in the uranium metal, in the oxidizing - oxidating slagging work, for example. This would indicate that the zirconium oxide is less stable than the uranium oxide. Might this film not be some of the rare-earth oxides which would appear as fission products after the fission of uranium?

M.L. BLEIBERG: It is hard to see how the rare earths, which have such a low fission yield, could possibly give 8-μm-thick films on the inside.

B. LIEBMANN: I would like to put two questions, one to Dr. Sinizer and the other to Dr. Roake. The one to Dr. Sinizer is a very simple one. In the irradiation tests with cast uranium carbide slugs described in your paper, and in all tests I know of, the difference between surface temperature and the centreline temperature is relatively small, in the neighbourhood of 500 deg C, and the centreline temperature is kept below 1350°C. Now what I want to ask is, is there no incentive for going higher with the centreline temperature? Or doesn't one dare to do it? It seems you are giving away some of the advantages which you have with uranium carbide if you do not go up higher, such as higher heat ratings and the benefit of the high thermal conductivity of UC.

The second question is concerned with the thermal conductivity of UO_2. Dr. Roake, in your paper, and in papers by Bates and by Murtha and Chernock, it has been reported that the thermal conductivity of UO_2 increases at temperatures over 1200°C. The range of temperature where this increase takes place corresponds with the range where you have columnar-grain growth. It has been suggested that the increase of conductivity is due to radiant heat transfer. I would like to know whether this has been established by out-of-pile measurements, since the fact that columnar-grain growth and increased conductivity occur together suggests that these perfect large single crystals that form may have a much better conductivity than small-grained UO_2, even if radiant heat transfer is not important.

D.I. SINIZER: I might discuss the thermal conductivity of carbide a little bit in preparation for answering the question. The out-of-pile thermal conductivity has been found to be about 0.05 or 0.056 - equivalent to about 13 - 13.5 BTU – over a wide range of temperatures, and to be relatively independent of carbon content for specimens nearly stoichiometric. Our irradiation tests have indicated that this is a fairly good value to use, even under irradiation and after relatively long irradiation. We have inferred thermal conductivity from our in-pile irradiations to be between 11 and 14.5, which represents pretty good agreement with the 13.5 we measure out of pile. For this reason we feel we are justified in using the out-of-pile thermal conductivity as a good measure of the thermal conductivity we can achieve in a fuel element. Now as far as going to higher centreline temperatures is concerned, the central temperature we get is very nearly chosen for us by the requirement that the sodium coolant used in the sodium reactor be in the neighbourhood of 1200°F (about 1650°C). This will govern the central temperature that we can achieve for the heat fluxes that we envision as being

practical for our sodium reactors, which run in the neighbourhood of a million BTU/hr ft^2 for hot channels, so that we take what we will get on the basis of the surface temperature that is consistent with the use of sodium coolant. Now in the written version of the paper that I presented* is a curve which indicates that the diametral change, which is of great significance in our type of fuel element, is going to increase by a function which is related to nearly the fifth power of the absolute temperature. Going up higher than about 2000 at the present time with unalloyed uranium carbide may be a dangerous business, in our view.

W.E. ROAKE: I'll use two slides, if I may, to save a couple of thousand words.

Our selection of radiant energy transfer as an explanation of the increased heat-transfer rates deduced from post-irradiation examination of irradiated, high-rated UO_2 fuel elements came about because of the good fit of the experimental data with theory. If you will recall Bates' paper, the solid line shown in his graph, and in Fig. 22 of my present paper**, is the sum of the curve describing the conventional reciprocal temperature relationship of the thermal conductivity of polycrystalline UO_2, and the curve describing the "conductivity" due to radiant energy transfer. The latter component was computed from values, published by Ackerman, of the infra-red transmission of thin films of UO_2, which we assume behave effectively as thin single crystals. What we are talking about is, we think, radiant heat transfer mostly through the region of the columnar grains that are, effectively, single crystals; and to some degree, through the porosity that develops at later exposure in the hotter portion of the columnar grain region. The out-of-reactor measurements by Murtha and Chernock and, of course, the Daniel and Deem conductivity curve for the single crystal at lower temperatures all support our contention. I must point out that our post-mortem analyses of irradiated test elements assume that certain phenomena, such as the onset of columnar grain growth, occur during irradiation at the same temperature at which we observe them out-of-reactor. This may be a fault in our reasoning, but we don't think a serious one. Also, we admit the treatment is somewhat naive in that we have not indicated the effects of fission products and irradiation-induced defects, but we hope to improve our understanding, a slow process, with irradiation experiments.

B. DUNNINGTON: I would like to go back to the marked difference in damage noted by Mr. Childs and Mr. Frost between powder metallurgy and arc-cast uranium carbide. The tentative explanation that was offered, essentially a mechanism for annealing-out defects, suggests that perhaps the dimensional instability or swelling at very high burn-up might also be different for these two types of material. I'd be very interested in their comments and in Mr. Sinizer's comments.

D.I. SINIZER: I might bring up the question of what part the purely mechanical damage that you might get in a cast uranium carbide through exposure to the atmosphere could play in the observed increase in resistivity. I wonder if Childs or Frost might comment on that?

---

* SINIZER, D.I., WEBB, B.A. and BERGER, S., "Irradiation behaviour of uranium carbide fuels", these Proceedings, section B.2.

** ROAKE, W.E., "Irradiation alteration of uranium dioxide", these Proceedings, section B.2.

B.G. CHILDS: I have no comment on that point. I think there is one relevant thing that one might say about this, and that is that the reaction-sintered material appears to exhibit a greater plasticity under some circumstances than does the arc-melted material. Some experiments have been done at Harwell, which Dr. Frost may like to comment on, on measuring the creep rate of the reaction-sintered material under static loading. It appears that this material creeps at a much lower temperature than does the arc-melted material, so that this might possibly give rise to swelling at lower burn-ups.

B.R.T. FROST: What you said was true, but in fact we recently discovered that higher creep rate was associated with free uranium in the uranium carbide, and if the carbide is hyperstoichiometric, then it does not creep appreciably until the same temperatures as found with cast material. The other thing is, of course, that there may be some advantage in having some free volume in the form of pore space in the sintered material to accommodate fission gases. This may help to give better dimensional stability.

B.G. CHILDS: One further point in connection with this subject is that I would imagine that in the reaction-sintered material which has never been heated to a very high temperature, but has only been up to about 1400° for only a very few minutes, you would probably have a very high dislocation density compared with the arc-melted and cast material. The dislocations may well serve as nucleation sites for bubbles of fission gases and in this case the bubbles may be nucleated on a very fine scale indeed. They may be very, very small compared with the bubbles of gas nucleated in the arc-melted material. Whether this a good thing or not I wouldn't like to say.

I would like to raise a point in connection with Dr. Roake's statement that there is no correlation between the annealing behaviour shown in the thermal conductivity of uranium dioxide and the behaviour shown by the electrical resistivity. In fact, workers at the Battelle Memorial Institute (BMI) have published electrical conductivity data which can be interpreted to show two annealing stages. If I may just draw a curve on the blackboard it will illustrate what I mean. I've tried to plot the data given by the BMI workers in the form of the logarithm of the electrical conductivity plotted upwards against the inverse temperature plotted horizontally. The upper straight line is the results for the unirradiated material. The lower curve shows the behaviour of irradiated material on being warmed up, in other words, moving to the left on that curve, and you can in fact see two distinct steps at the same annealing temperatures that the thermal conductivity anneals out at. I am wondering whether in Dr. Roake's material he is showing two effects, that perhaps at lower burn-ups he is getting a reduction in the electrical conductivity due to radiation damage and perhaps at higher burn-ups he may be getting a complicated effect due to oxidation of his UO_2 which would tend to increase the thermal conductivity again.

W.E. ROAKE: I think you may well be right about two effects. The work reported here was, as I mentioned earlier, done cooperatively by Lee Daniels at Hanford, and Deem and Matolich of Battelle Memorial Institute. I can relate Dr. Daniels' thoughts on this matter. He believes that the major effects of irradiation on conductivity are perhaps related to both changes in the physical state and in the oxidation state.

E. NAGY (Chairman): If there are no further comments I should like to ask Dr. Roake to sum up the results of this discussion.

W.E. ROAKE (Moderator): I don't think I should try to summarize this discussion further. I don't know if we solved any problems today, although we certainly aired several! I hope we have clarified some points in the minds of what I consider to be an extremely durable audience. Thank you all for staying. I think we would all like to go to dinner.

B. RADIATION DAMAGE IN CERAMIC NUCLEAR FUEL

2. Full text of papers

IRRADIATION EFFECTS IN FISSILE OXIDES AND CARBIDES AT LOW AND HIGH BURN-UP LEVELS

B.R.T. FROST, B.T. BRADBURY AND L.B. GRIFFITHS
METALLURGY DIVISION, ATOMIC ENERGY RESEARCH ESTABLISHMENT, HARWELL, BERKS., ENGLAND

Abstract — Résumé — Аннотация — Resumen

IRRADIATION EFFECTS IN FISSILE OXIDES AND CARBIDES AT LOW AND HIGH BURN-UP LEVELS. Structural changes occurring in UO_2 and in UC during irradiation to burn-ups between 100 and 10 000 MWd/t have been studied by optical and electron microscope techniques. In particular, the change in mode of fracture from transgranular to intergranular and a decrease in bond strength with increasing radiation dose have been observed.

Radiation damage in UC has been studied by measurements of the variation in electrical resistivity with dose on cold irradiated materials, this technique being used subsequently to study the temperature, the mechanism and the kinetics of annealing.

A series of pellets of UO_2, UO_2-PuO_2 solid solution, UC and PuC-UC solid solution have been irradiated in stainless-steel containers to burn-ups in the range 15 000-54 000 MWd/t, the oxide centre temperatures being in the range 900-1600°C and the carbide centre temperatures about 800°C. Post-irradiation examination includes fission-gas analysis, measurement of dimensional changes and a study of structural changes by optical and electron microscopy.

EFFETS DE L'IRRADIATION SUR LES OXYDES ET CARBURES FISSILES A DES TAUX DE COMBUSTION FAIBLES ET ÉLEVÉS. Les auteurs ont étudié au microscope optique et au microscope électronique les modifications structruelles qui se produisent dans l'UO_2 et l'UC irradiés avec des taux de combustion compris entre 100 et 10 000 MWj/t. Ils ont constaté notamment un changement de mode de fracture qui, de transgranulaire, devient intergranulaire, et une diminution de la résistance au flambage lorsqu'on augmente la dose de rayonnements.

Ils ont étudié les dommages causés par les rayonnements dans l'UC en mesurant les variations de la résistivité selon la dose dans des matières irradiées à froid; ils emploient ensuite cette méthode pour étudier les températures, le mécanisme et la cinétique du recuit.

Une série de pastilles d'UO_2, d'UO_2-PuO_2 en solution solide, d'UC et de PuC-UC en solution solide, ont été irradiées successivement dans des récipients en acier inoxydable à des taux de combustion de l'ordre de 15 000 à 54 000 MWj/t, les températures centrales étant de l'ordre de 900 à 1600°C pour l'oxyde et d'environ 800°C pour le carbure. Après l'irradiation on a analysé le gaz produit par la fission, mesuré les modifications dimensionnelles et étudié les modifications structurelles au microscope optique et au microscope électronique.

ВЛИЯНИЕ ОБЛУЧЕНИЯ НА РАСЩЕПЛЯЮЩИЕСЯ ОКСИДЫ И КАРБИДЫ ПРИ НИЗКИХ И ВЫСОКИХ УРОВНЯХ ВЫГОРАНИЯ. Структурные изменения, возникающие в UO_2 и UC в течение облучения при выгораниях между 100 и 10 000 мгвт-дней/т были изучены с применением оптических и электронных микроскопов. В частности, осуществлялось наблюдение за изменением вида трещины от трансгранулярной и уменьшением силы сгибания при увеличении дозы радиации.

Радиационное повреждение в UC изучалось по изменению электронного сопротивления в зависимости от дозы для холодного облученного материала. Эта техника используется затем для изучения температуры и механизма отжига и его кинетики.

Несколько лепешек UO_2, UO_2 - PuO_2 и UC и PuC - UC, образующих твердый раствор, были облучены в контейнерах из нержавеющей стали при выгораниях в интервале 15 000 - 54 000 мгвт-дней/т. Температура центра оксида была порядка 900 - 1600°C, а температура центра карбида около 800°C. Изучение после облучения включает анализ газа деления, измерение изменений в размерах и изучение структурных изменений с помощью оптических и электронных микроскопов.

EFECTOS DE LA IRRADIACIÓN SOBRE LOS ÓXIDOS Y CARBUROS FISIONABLES PARA GRADOS DE COMBUSTION BAJOS Y ELEVADOS. Aplicando técnicas de microscopía óptica y electrónica, los autores estu-

diaron las alteraciones estructurales que la irradiatión provoca en el UO_2 y el UC, en correspondencia con grados de combustión comprendidos entre 100 y 10 000 MWd/t(e). En particular, observaron cómo cambia el modo de fractura de transgranular a intergranular y cómo disminuye la resistencia a la flexión al aumentar la dosis de radiación.

También estudiaron los daños causados por la radiación en el UC, midiendo la variación de la resistividad eléctrica en función de la dosis, en el material frío irradiado y aplicaron ulteriormente la misma técnica para estudiar las temperaturas de recocido y el mecanismo y la cinética del recocido.

Irradiaron una serie de bolillas de UO_2, una solución sólida de UO_2-PuO_2 y una solución sólida de UC y de PuC-UC, en recipientes de acero inoxidable, hasta alcanzar grados de combustión del orden de 15 000 a 54 000 MWd/t(e), manteniendo las temperaturas centrales del óxido entre los 900 y 1600°C y las del carburo en los 800°C, aproximadamente. Los exámenes posteriores a la irradiación comprendieron el análisis de los gases de fisión, la medición de los cambios dimensionales y el estudio de las alteraciones estructurales por microscopía óptica y electrónica.

1. INTRODUCTION

In the field of nuclear fuel-element development a considerable effort is being devoted to studies of ceramic fuels. Almost all the water-moderated reactors being designed or constructed in the world today will be fuelled with an oxide fuel; most of the fast reactors under development are planned as using an oxide or carbide fuel and all the advanced types of gas-cooled graphite-moderated reactors will employ an oxide or carbide fuel. The reason for this interest in ceramic fuels lies in their ability to remain dimensionally stable at higher temperatures and to higher burn-ups than metallic fuels and in their property of retaining large quantities of gaseous fission products. These fuels are not, however, without their difficulties. Being ceramics they are brittle up to about 1000°C and, in the case of oxides, their thermal conductivity is low; the combination of these two factors results in poor resistance to thermal stresses. Moreover the fact that they are chemical compounds of two or more elements which exhibit some degree of covalent and/or ionic bonding and have the ability to exist over a range of compositions tends to complicate any detailed analysis of their properties. Nevertheless many of their more relevant physical properties have been measured on fairly pure, dense material and a qualitative picture of their behaviour under irradiation is beginning to emerge. This paper describes some attempts to complete this qualitative picture and to place the irradiation studies on a more quantitative basis.

Studies of irradiation effects in fissile materials can be subdivided into three main classes:

(i) Thermal effects which are a consequence of the fuel being a volume heat source; the most important practical example is the grain growth in UO_2 at high temperatures. This paper will only discuss such effects where they influence the movement of fission products and of point defects.

(ii) Point defects manifest themselves particularly in studies of fissile materials at low burn-ups. This is primarily because their density saturates at low burn-up levels when the fission spikes overlap. The main justification for studying them is to advance the understanding of the physical properties of the material. However, when a material is fissioning at a high rate, at a temperature where

the defects are reasonably mobile, then stable clusters might be formed.

(iii) Fission product effects which become of over-riding importance at practical burn-up levels. They are significant in two senses; firstly the volatile species may agglomerate within the fuel or within the fuel element and exert high pressures, and secondly the non-volatile species may influence the structure and properties of the fuel itself.

These effects have been studied at Harwell in UC and PuC-UC solid solutions and in UO_2 and PuO_2-UO_2 solid solutions.

2. CARBIDES

In many respects uranium monocarbide (UC) and solid solutions of UC containing plutonium are simpler materials on which to study irradiation effects than are UO_2 or PuO_2-UO_2. The monocarbides have a simple NaCl-type crystal structure, are stoichiometric compounds and have metallic transport properties, being dominated by the large uranium atoms. Moreover, the somewhat lower melting point permits the use of a wider range of fabrication techniques, particularly that of arc-melting in addition to sintering and hot pressing. On the other hand it is not very easy to produce single phase structures. Free uranium or UC_2 may be associated with UC and either Pu-U solution or a mixed sesquicarbide $(Pu,U)_2C_3$ with the (Pu,U)C solid solution: these second phases may influence the behaviour under irradiation.

2.1 The nature of radiation damage in UC

Electrical resistivity measurements have been used to follow the build-up of radiation damage in UC and to determine the temperatures at which annealing occurs. These measurements have followed some earlier experiments by ADAM and ROGERS [1] at Harwell and by BLOCH [2] at Saclay in which lattice parameter changes, determined by X-ray diffraction powder-methods, were used to study the same processes.

The resistivity test specimens consisted of square-section rods measuring 0.1 in × 0.1 in × 1.0 in, fabricated by the reaction sintering process [3] to a density of 91.8% theoretical. In this method, freshly-pickled calcium-reduced uranium powder (particle diameter about 40 μm) is intimately mixed with fine graphite powder (surface area 115 m^2/g) and compacted cold under a pressure of 6300 kg/cm^2 to give a green density of about 12.4 g/cm^3 or 91% theoretical density. The pellets are loaded rapidly into a furnace held at 1125°C. The pellet temperatures rise rapidly to the reaction temperature of 800°C and the exothermic reaction raises it still more rapidly to above the melting point of uranium. The process is therefore one of liquid phase sintering which helps to ensure a high-density product and a high proportion of closed-porosity. The product is further annealed at 1400°C for periods of up to 24 hours to homogenize the structure; Fig. 1 shows a typical microstructure in which some free uranium and graphite is still present, the uranium being between 0.5% and 1.0% of the total volume. After annealing,

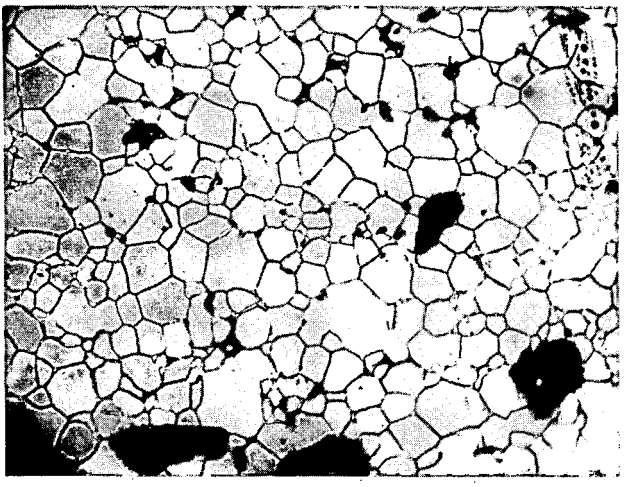


Fig. 1

Reaction-sintered UC - typical section

the rods are ground to size on silicon carbide laps and under a dehydrated lubricant. They are then sealed in helium-filled aluminium containers and irradiated in the BEPO* reactor at a thermal neutron flux of 1.2×10^{12} n/cm^2 for varying times at a temperature of 70°C to produce neutron doses of between 10^{16} and 10^{18} n/cm^2. After irradiation the specimens remain in their cans until they are required for resistivity measurements. Resistivities are measured by a conventional four-probe potentiometric technique in an atmosphere of dry argon inside a cell shielded with 2-in lead bricks. The results of the measurements of resistivity with increasing neutron dose are plotted in Fig.2, which shows that the radiation-induced resistivity change begins to saturate at about 10^{17} n/cm^2, reaching a value of 2.8% at 10^{18} n/cm^2. The general trend is similar to that observed by Adam and Rogers, whose curve for lattice parameter versus neutron dose is shown in Fig.3. From these curves estimates were made of the number of atoms affected per fission event.

Adam and Rogers demonstrated that their curve for unit cell expansion of UC plotted against neutron dose followed a relationship of the type $Y = 1 - \exp\{-\gamma n\}$, where Y is the fraction of atoms affected in the crystal by fission events, n is the neutron dose and γ is a constant for a given material.

If the fractional change in unit cell size $\Delta a/a$ is proportional to the fraction of atoms affected by the passage of fission fragments, then $\Delta a/a = A(1 - \exp\{-\gamma n\})$. The number of fission events per atom of material irradiated to a neutron dose $n = \sigma_f n$, where σ_f is the fission cross-section. Thus $\gamma n = k\sigma_f n$, where $k = \gamma/\sigma_f$, the number of atoms affected per fission event. Similar reasoning was applied to the resistivity curves and both gave a value of k approximately equal to 1.4×10^7. This number is similar to

* BEPO: British Experimental Pile Operation, AERE, Harwell, UK.

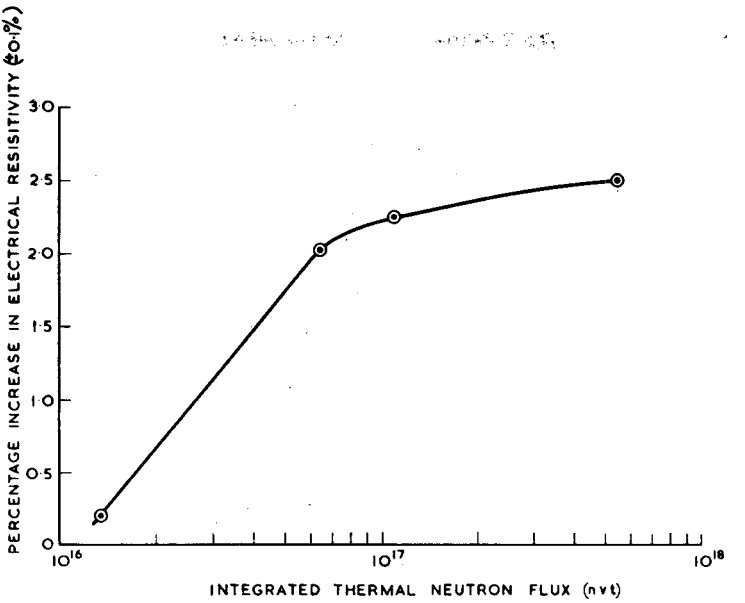


Fig. 2

Effect of neutron bombardment in BEPO reactor upon electrical resistivity of UC

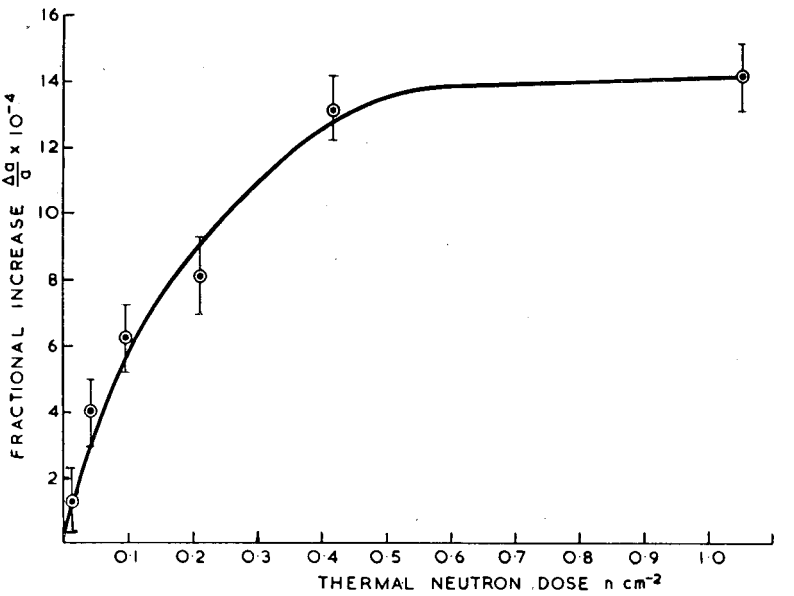


Fig. 3

Fractional increase in unit cell size in UC with irradiation in BEPO [1]

that obtained for U_3O_8 from stored energy measurements [4] but is somewhat higher than the values for uranium and its alloys.

The electrical resistivity change of only a few per cent contrasts markedly with the results obtained by workers at the Battelle Memorial Institute [5] and at Dounreay [6], both of whom used arc-cast material for their studies. It seems that the difference must be due to the different natures of the material rather than to differences in neutron energy and dose rate since the results on arc-cast material gave similar increases in two different reactors and in different positions in these reactors. The sintered material contains more pores than the arc-cast and is of smaller grain size and therefore has a higher grain-boundary area, both effects providing a larger number of sinks for defects at a smaller spacing. It is possible that the observed differences in resistivity are due to the greater degree of annealing of defects occurring during irradiation in the sintered material than in the cast.

After these measurements the specimens were subjected to a series of isothermal anneals of one hour duration at a series of temperatures from 100 to 800°C. After each anneal the resistivity was remeasured; the resultant curve of resistivity change versus temperature is shown in Fig. 4. Two well-defined decay stages are observed, one at 110 - 130°C and the other at 700 - 730°C, about 30% of the "extra-resistivity" annealing out at the lower temperature. This contrasts with the similar recovery curves obtained by Adam and Rogers at Harwell and by Bloch at Saclay using lattice parameter changes as an indication of annealing. Adam and Rogers observed

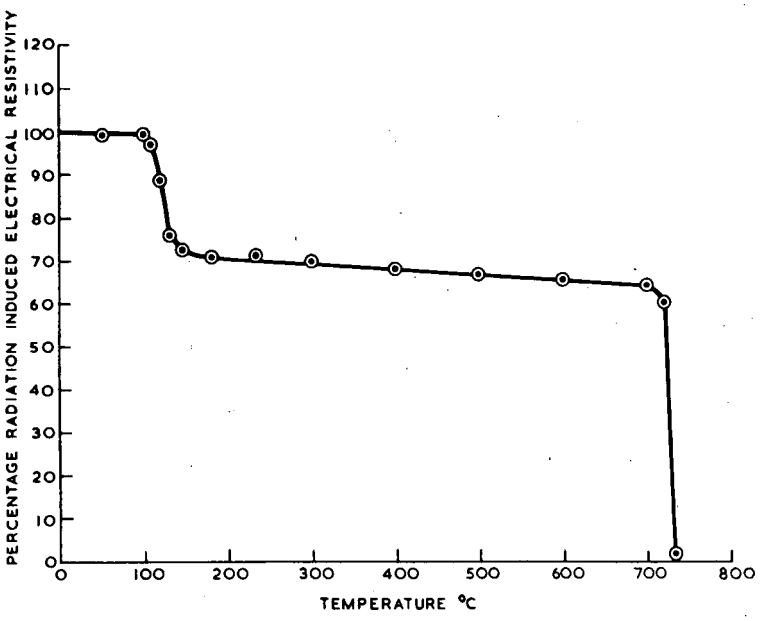


Fig. 4

Annealing of radiation-induced resistivity in UC
(Anneals carried out in 1h steps at temperatures shown)

steps at 100 and 550°C but did not anneal up to 700°C, while Bloch observed steps at 100, 550 and 700°C.

Further resistivity experiments were carried out on un-irradiated, sintered UC to assist in the interpretation of the annealing behaviour. Thin bars of UC were heated to temperatures in the range 1300 - 1500°C and quenched in a helium blast to retain the thermally-induced vacancies. The resistivity of these specimens was then measured at room temperature, after a similar series of isothermal anneals to those carried out on the irradiated material. One result is plotted in Fig. 5. Only one annealing

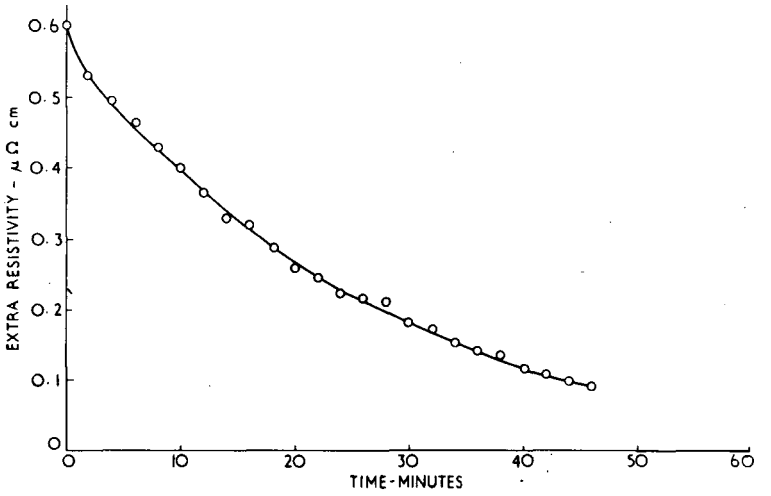


Fig. 5

Annealing of thermally induced vacancies in UC

step is observed; this is at 670°C and indicates that the highest-temperature radiation damage annealing step corresponds to vacancy movement. Values for the activation energies of vacancy formation and migration obtained from these experiments are 2.8 eV and 1.1 eV respectively.

It is apparent from the results obtained that readily detectable damage occurs in the UC lattice following quite small neutron doses. The unit cell size of solids in general tends to be insensitive to vacant sites, but varies quite considerably when interstitial atoms are produced in the lattice. From the fact that a fairly large proportion of the lattice parameter increase anneals out in the first of the decay steps observed, together with the information regarding vacancy annealing obtained from the quenching experiments, i.e. that no annealing occurs below 670°C, it is concluded that interstitials become mobile in UC at about 100°C and account for most of stage one, while the 700°C stage results mainly from vacancy movement and subsequent removal from the lattice. This very general overall picture is almost certainly a simplification of the actual situation. As yet insufficient information is available to enable a more detailed interpretation of the experimental observations. No account has been taken of the possible grouping of defects into clusters thereby modifying annealing kinetics, nor has any

explanation been attempted for the annealing stage at 550°C observed by French workers. The development of thin-film transmission electron microscope techniques for UC should determine the extent to which clustering occurs. Some preliminary attempts at this by workers at the Aeon Laboratories, Egham, Surrey, England (using a diamond-microtome technique) and at Harwell (using chemical thinning techniques) give promise of success in preparing sufficiently thin sections for electron transmission.

2.2 The consequences of radiation damage in UC

Having established that radiation-induced defects can remain in UC at temperatures up to 700°C, it is important to determine their effect on physical and mechanical properties. As a start to such studies the effect of neutron doses in the range 10^{16} to 10^{18} n/cm^2 on the mechanical strength of UC has been investigated. Bars of similar size and composition to those used for resistivity measurements were irradiated under similar conditions in the BEPO reactor. After irradiation they were subjected at room temperature to a three-point bend test on an Instron testing machine located in a concrete cell and the variation in bend strength with dose was found. A marked drop in strength occurs at doses in excess of 10^{17} n/cm^2, as shown in Table I, which lists some typical results. Electron micrographs of replicas of the fractured surfaces were taken from all the specimens. Replicas were prepared using a two-stage Bex film - carbon replica technique, and the electron micrographs were taken on a Phillips EM 100 microscope. The unirradiated specimens and those irradiated to low doses showed fracture patterns characteristic of transgranular fracture, as shown in Fig. 6, but those irradiated to higher doses, which gave approximately 50% lower bend strengths, showed patterns characteristic of intergranular failure together with holes or cracks at the grain boundaries, Fig.7. This behaviour is very similar to that observed in UO_2 by NEWKIRK, DANIEL and MASTEL [7]. It is uncertain to what extent the effects are due to point defects and to what extent to fission fragments. At these doses the concentrations of the latter are very low and it may be that the grain boundaries are weakened by the accumulation of defects and the grain interiors are strengthened by dislocation locking, these causing preferential failure in the grain boundaries.

TABLE I

THE EFFECT OF IRRADIATION
UPON THE BEND RUPTURE STRENGTH OF SINTERED UC

Bend strength (kg/mm^2)	Integrated thermal neutron flux (n/cm^2)
9.6	nil
8.8	5×10^{17}
4.9	10^{18}



Fig. 6

Electron micrograph of fracture surface of sintered UC (unirradiated)

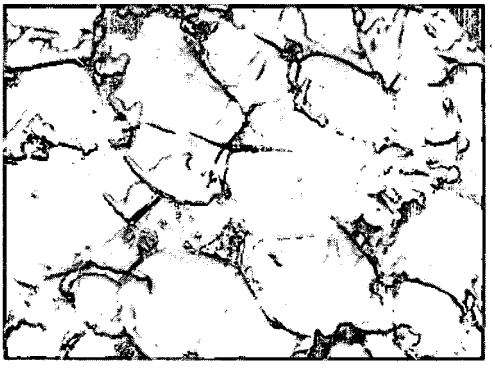


Fig. 7

Electron micrograph of fracture surface of lightly irradiated UC

2.3 Technological studies

Technological interest in monocarbide fuels in the U.K.A.E.A. is focussed primarily, but not exclusively, on their use as fast-reactor fuels. This implies a predominant interest in plutonium-uranium carbide solid solutions and in their capability of achieving high burn-ups at high ratings and high temperatures. Preliminary irradiation studies have, therefore, been aimed at irradiating PuC-UC to high burn-ups, a target of 5% burn-up of U + Pu atoms being the general aim. At the same time samples of UC have been irradiated to burn-ups of interest in thermal-reactor applications (about 15 000 MWd/t).

2.4. (Pu, U)C specimens

For use as the fuel in large, dilute fast-reactor cores interest is centred on mixed carbides with plutonium contents in the range 10 to 20 wt.% plutonium, with a peak rating of 200 W/g and a mean maximum burn-up in the range 5 to 10% of (U + Pu) atoms. To date the only published information on the behaviour of carbide fuels to appreciable burn-ups is that obtained at the Battelle Memorial Institute [8] on arc-cast UC taken to 25 000 MWd/t at surface heat ratings of up to 300 W/cm^2 or about 45 W/g and centre temperatures of up to about 850°C. The specimens exhibited good dimensional stability and the fission-gas release values corresponded closely with those expected from recoil. These results are reasonable in the light of measurements by LONG and FINDLAY [9] on the release of Xe^{133} from UC on annealing lightly irradiated material. They found that the true diffusion coefficient, D, was lower by an order of magnitude than the corresponding value for UO_2 at the same temperature, but that the apparent diffusion coefficient, D^1, was higher for UC due to a larger surface area; recent advances in fabrication techniques may well have eliminated this difference.

Work is in hand at Harwell and elsewhere to establish fabrication techniques and the physical properties of (Pu, U)C. It is important that the favourable properties should remain with the addition of up to 20% Pu and after irradiation. It has already been established that the plutonium addition lowers the thermal conductivity, but not excessively: even at 15 wt.% Pu the value for carbide is three to four times that of UO_2[10]. It should, therefore, be possible to irradiate fuel of reasonable dimensions (say 1-cm diam.) under the conditions listed above without excessively high centre temperatures.

As the first step in a series of technological studies of the irradiation behaviour of (Pu, U)C, four specimens of 10 wt.% Pu content were irradiated to rather lower ratings and burn-ups than those required for future fast reactors. Four rods were arc-cast by melting together UC and PuC buttons on the water-cooled copper hearth of a non-consumable arc furnace using a tungsten electrode. The specimens were "cast" by inducing them to run into a depression in the hearth, as opposed to the now more usual methods of "drop" or "skull" casting. After solidification the rods were ground on laps to 0.25-cm diam., their characteristics were measured (described later) and they were inserted in stainless-steel cans of 0.5-mm wall thickness to give a fuel-to-can gap of 0.025 mm. The cans were sealed at the ends by welding under pure helium at a reduced pressure. These cans were sealed in sodium-filled capsules (to assist heat transfer) which were placed in a light-water-cooled rig in a 7-in (17.75-cm) horizontal facility in the PLUTO* reactor. Cobalt flux monitors were attached to the specimens and mineral-insulated thermocouples were used to measure individual-specimen can surface-temperatures. No auxiliary heaters were supplied so that specimen heating was entirely nuclear and temperatures were controlled by adjustment of the gas gap between the outer wall of the sodium-filled capsule and the inner wall of the water-cooled heat sink. Specimen temperatures were, therefore, dependent on the reactor power level.

* PLUTO: Pluto Reactor. AERE, Harwell, UK.

After irradiation for a period of 232 d, the rig was withdrawn from the reactor and dismantled to recover the specimens, among which were oxides (see below) as well as the carbides. In general, the post-irradiation examination followed the pattern of the pre-irradiation characterization with some important additions. Tests performed before and after irradiation were:

(i) Density (real and apparent)
(ii) Optical microscopy
(iii) Electron microscopy (replicas)
(iv) Can (external dimensions)

Additional tests included:

(v) Can puncture for fission gas analysis by mass spectrometry
(vi) Radiochemical analysis to determine burn-up levels.

Data available on two of the samples irradiated are listed in Table II. Electron and optical microscopy of the unirradiated samples showed that they were not single-phase. A small proportion of a light etching phase, which could be Pu-U metal solid solution or free tungsten from the arc melting furnace electrode, is clearly visible in the grain boundaries in Fig. 8. After irradiation this structure is little altered (Fig. 9). However, careful examination of an as-polished section shows signs of intergranular cracking, the origin of which is uncertain; it could be simply intergranular corrosion by contaminants in the argon atmosphere of the hot cells or it could be a manifestation of a type of powdering which other workers have observed after irradiation at lower temperatures. Since it was not observed by BMI workers it may be due to corrosion.

The percentage release of fission gases is very low but, as with the BMI results for UC, this is consistent with present information on fission

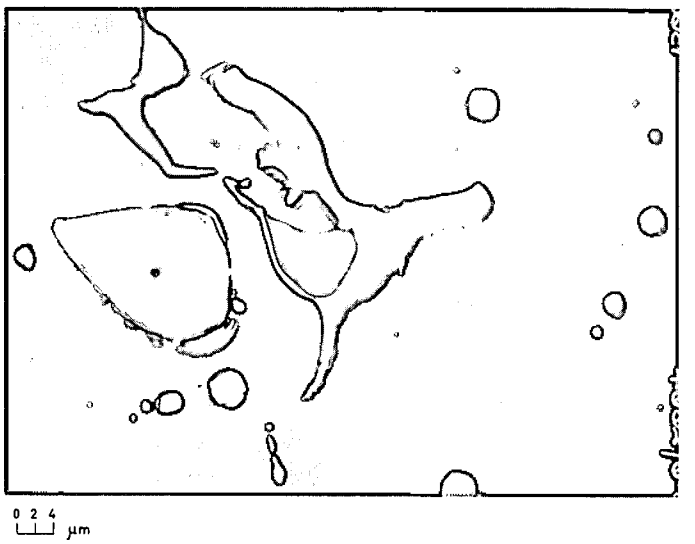


Fig. 8

10% PuC-UC arc-cast specimen, unirradiated

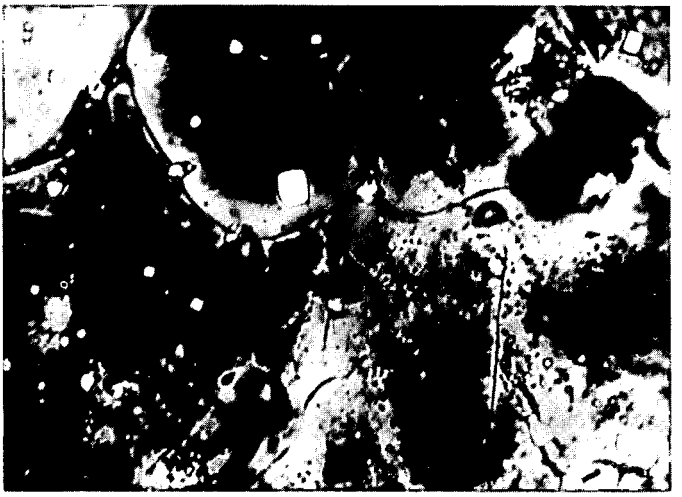


Fig. 9

10% PuC-UC arc-cast specimen, irradiated to 17 800 MWd/t

gas diffusion. At the temperatures experienced by these specimens, release would be almost entirely by a recoil or "knock-out" mechanism [9]. Since recoils are energetic they probably result in re-absorption of the fission fragments, so a more likely mechanism for gas release is knocking out by nearby fission events.

The external dimensions of the cans were virtually unaltered after irradiation; this is consistent with the micrographic and gas release observations.

These results suggest that the irradiation behaviour of (Pu,U)C to modest burn-ups at modest ratings is similar to that of UC. Specimens of high density (~ 98% theoretical) 15 wt.% PuC-UC in arc-cast and sintered form will be irradiated to burn-ups in the range 4 to 8% (Pu + U) atoms during the next 12 to 18 months to establish whether this promising behaviour is extended to the conditions required by fast reactor design.

3. OXIDES

Due to the wide practical application of UO_2 as a reactor fuel more information is available on its irradiation behaviour than is the case for UC. At low burn-ups the build-up of damage (or stored energy) and its annealing have been studied by following lattice parameter changes [11], the release of gaseous fission products on heating has been studied extensively and is understood in a qualitative manner [12], and fractographic studies have established a change in the mode of fracture at low irradiation levels similar to that described above for UC [7]. At high burn-up levels the irradiation effects of most significance appear to be thermal in origin, i.e. radial and circumferential cracking, grain growth and associated increases in fission gas release. However, a number of effects are still not adequately explained:

(i) The precise mechanism of enhanced gas release in the regions of equi-axed and columnar grain growth.
(ii) Dimensional stability at high burn-ups at high temperatures.
(iii) The effects of plutonium additions on the irradiation behaviour.

Interest in the application of UO_2 and PuO_2-UO_2 to advanced reactor systems has led to a study of these factors at Harwell.

3.1. Enhanced gas release

As an approach to understanding the mechanism of fission gas movement in UO_2, electron microscope replica-techniques have been applied to the study of UO_2 irradiated to burn-ups of 5000-10 000 MWd/t, with centre temperatures of up to 2000°C and higher.

Unlike metallic uranium, sintered UO_2 is a porous material and contains a void volume in the form of closed pores. This void volume is therefore available for containment of the gaseous fission products generated during irradiation. It is therefore important to study the irradiated oxide at high magnifications to determine whether the gas atoms nucleate into bubbles on a sub-optical scale as in the case of uranium metal [13], whether they collect in the closed pores or remain in "solution" in the UO_2 lattice.

A two-stage Bex film-carbon replica technique was used to study the microstructure of specimens of irradiated uranium oxide at high magnifications. Plastic replicas of as-polished and polished-and-etched surfaces of irradiated UO_2 were made in a lead cell, the first replica being rejected due to pick-up of active dust. The subsequent replicas could then be handled in the open laboratory and in an unshielded electron microscope, which was in this case a Phillips model EM 100.

The electron micrographs shown in Fig. 10 illustrate the transition in microstructure across the radius of a cylindrical pellet of irradiated uranium oxide. Fig. 10a is a typical electron micrograph of the unirradiated uranium oxide and shows the general grain structure (grain size ~ 10 μm) and the individual closed pores (0.1-0.25 μm diam.) situated mainly in grain interiors. Figs. 10b, c and d show the microstructure of the uranium oxide after irradiation, and represent the transition from the outer region (b), through the equi-axed grain growth region (c) into the columnar grain growth region (d). One striking feature of the irradiated-specimen microstructures is the marked absence of grain interior porosity as compared to the microstructure before irradiation. After irradiation, most of the porosity, in regions where grain growth has occurred, is situated at the grain boundaries. This is probably due to the fact that the grain boundaries have either swept the original grain interior pores with them during the process of grain growth or have become anchored at the pores; some redistribution of pores does seem to have occurred. Fig. 10d represents an area of the irradiated specimen where onset of columnar grain growth occurs. Grain boundary porosity is very evident in Fig. 10d and if, in fact, these pores do contain fission gases, then it seems reasonable to suppose that these gases will have a path of easy escape along the radially directed grain boundaries. This observation is therefore consistent with the fact that fission-gas release values are usually high for UO_2 specimens exhibiting columnar grain growth, com-

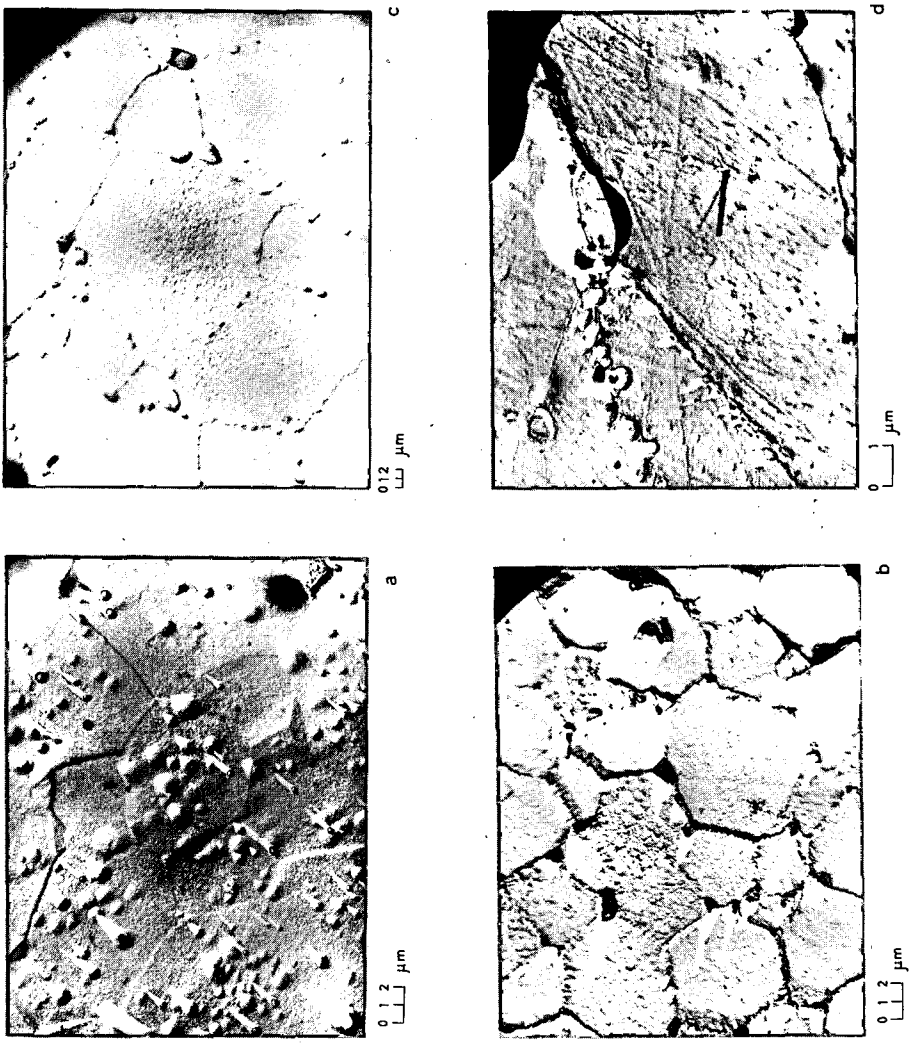


Fig. 10
A series of electron micrographs of irradiated UO_2

pared with the values for specimens in which columnar grain growth is absent [14].

In an attempt to improve the resolution of the replica technique, thinner Bex film (0.002-in instead of the 0.004-in Bex film used in obtaining Fig. 10) has been used to replicate the surface of the irradiated specimen shown in Fig. 11. Some effects not previously observed have been noted.

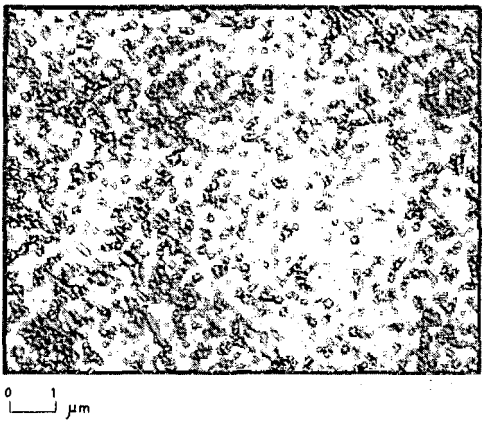


Fig. 11

Electron micrograph of grain growth region in UO_2
(this is believed to illustrate the formation of gas bubbles)

Grain-boundary cavities have again been observed in the equi-axed and columnar grain growth regions but in addition to this effect, there is a new feature in grain interiors in both these regions. Fig. 11 illustrates this feature in the columnar grain growth region of irradiated UO_2. At the present time it is thought that this may represent a fine scale of bubble formation due to fission-gas nucleation, the bubbles being about 400Å diam. and often occurring in clusters or along lines in groups of three or four. This latter effect can be seen if Fig. 11 is inspected closely. Fig. 12 illustrates a similar feature in irradiated 1% PuO_2-UO_2 where alignment of the 'bubbles' is even more pronounced. Thus, the distribution of these bubbles is non-random and it may be that nucleation is often occurring preferentially along dislocation lines, which would account for the alignment observed. If these are bubbles, they do not appear to have any influence on the dimensional stability of UO_2 until very high burn-ups are attained. They may, however, facilitate the formation of the large bubbles observed in UO_2 particles in cermets taken to high burn-ups [15, 16] and in bulk UO_2[17].

Finally, large unidentified inclusions in irradiated 1% PuO_2-UO_2 are frequently observed (see Fig. 13) and in all cases, phase boundary nucleation of bubbles is very pronounced. As can be seen, these bubbles are segregated at the boundary between the matrix and the second phase but appear on the second-phase side of the boundary. This phase may be an impurity inclusion introduced during the fabrication process, e.g. alumina or aluminous porcelain introduced during ball-milling operations. If this is the case, then the

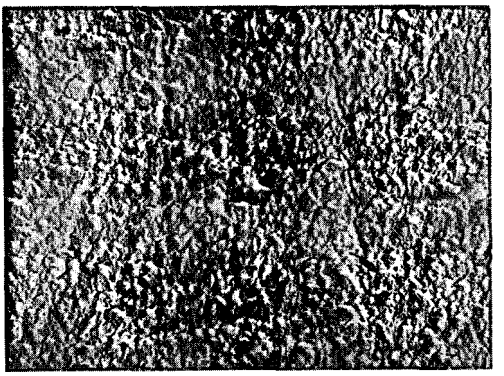


Fig. 12

Electron micrograph of columnar grain interior in 1% PuO_2-UO_2.

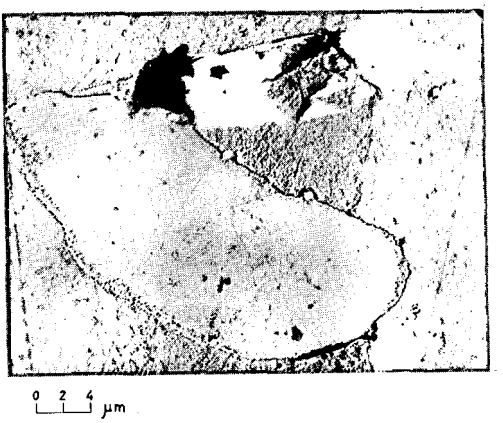


Fig. 13

Non-fissile inclusion in irradiated 1% PuO_2-UO_2

narrow area adjacent to the phase boundary in Fig. 13, in which the bubbles are seen, may represent the recoil distance of the fissile matrix atoms into the second-phase inclusion. This is an inverse of the recoil zone in steel surrounding UO_2 particles in cermet fuels. Further work is planned to interpret this observation more fully.

The general indications of the electron microscopy are, therefore, that, in addition to the containment of fission gases by closed porosity in irradiated UO_2 and solid solutions of PuO_2 in UO_2, there seems to be a non-random distribution of what appear to be gas bubbles throughout the grain interiors. It is thought that the size of these bubbles would be better represented by replicas prepared from fracture surfaces of the irradiated samples than from polished and etched surfaces. In the latter case, the size of the bubbles may be slightly distorted. Accordingly, fractography of irradiated UO_2 is at present under way.

Since thin-film work on uranium oxide is not very far advanced, direct observations of the nucleating sites for fission-product gas has not yet been possible, but it is hoped that this will be achieved in the near future.

3.2. High-burn-up experiments

The irradiation behaviour of cold-pressed and sintered UO_2 at high burn-up levels has been studied directly by BLEIBERG [15] and indirectly, in cermet fuels [16]. In all these cases, however, the fuel surface and centre temperatures were relatively low, of the order of 300 and 800°C respectively. At these temperatures, fission-gas release is controlled by recoil or knock-out and the UO_2 matrix has high strength and low ductility. An interest in the possible use of oxide fuels in advanced gas-cooled thermal reactors, and in fast reactors, led to a study of the irradiation behaviour of UO_2 and PuO_2-UO_2 solid solution fuels at burn-ups in the range 10 000-60 000 MWd/t and with surface and centre temperatures of about 600 and 1600°C respectively This study is still in progress and some of the earlier results will be given here.

The irradiation of fuel specimens to high burn-up at high fission rates in the type of capsule used in Metallurgy Division, Harwell, raises some difficulties. The capsule containing the canned UO_2 sample is filled with sodium to assist in heat removal to a water-cooled "sink". It is essential that the sodium at the specimen surface should not boil, otherwise temperature control would become impossible. The limiting surface heat rating above which sodium film boiling is liable to occur is 120 W/cm^2, although this is believed to be a conservative figure. This imposes a restriction in terms of heat output and specimen diameter. To ease these problems in the high burn-up UO_2 irradiations a somewhat novel fuel configuration was adopted: UO_2 pellets containing 30% U^{235} of 0.254-cm diam. were made by conventional cold-pressing and sintering techniques, the final sintering being carried out at 1650°C in a hydrogen atmosphere. Hollow pellets were made from natural UO_2, 0.635-cm external diameter, 0.254-cm internal diameter. The two pellet types were then ground until the enriched pellets fitted tightly into the central hole in the natural pellets. This combination allowed the central pins to run at high temperatures and at high heat ratings. These "duplex" specimens were canned in helium-filled stainless-steel cans and were irradiated under similar conditions to the (Pu, U)C specimens described above, i.e. in a water-cooled rig in the PLUTO 7H2L facility for 232 d.

To investigate behaviour over a somewhat lower burn-up range and to study the effect of plutonium additions, a series of specimens were prepared and irradiated in the same rig as the "duplex" UO_2 samples. These lower-burn-up samples were enriched to 10 wt.% U^{235} or 10 wt.% Pu^{239} and were of 0.635-cm diam. The plutonium-containing samples were prepared by a co-precipitation method (as opposed to physical mixing of the powders) to ensure a uniform solid solution. These also were canned in helium-filled stainless-steel cans.

Before canning, all pellets were carefully examined. Their external dimensions were measured on a Sigma comparator to within ± 2.5 μm; by

an adaptation of the classical Archimedes method, real and apparent densities were determined to give values for open and closed porosity; finally the end face of each pellet was prepared for microscopic examination and photographed; after canning the external dimensions of the cans were also measured to within ± 2.5 μm. The samples were, therefore, well characterized. After irradiation similar measurements were performed inside αβγ-shielded cells. In addition the cans were punctured; the contained gases removed to a highly evacuated vessel of known volume and samples were removed for mass spectrometric analysis for xenon and krypton. At the time of writing the external dimensions of all the cans have been checked, gas sampling has been performed on 5 "duplex" specimens and on two PuO_2-UO_2 specimens and a preliminary metallographic examination carried out on two of the duplex samples. The data obtained are summarized in Table II.

It will be noted that the changes in diameters of the cans were negligibly small in every case. The gas release values do not correlate well with any of the variables such as burn-up or centre temperature, although these have not been measured directly. In the case of the duplex specimens the double gas gap makes the estimation of centre temperature very difficult. The values quoted assume that the high temperature in the central pin causes it to expand and press tightly against the natural UO_2 annulus thereby eliminating that gas gap. The microstructures should provide another indication for the magnitudes of the gas release values. The central pellets show no evidence of grain growth having occurred during irradiation but the photomicrograph of specimen PH18 enriched core (Fig. 14) shows extensive porosity in the grain boundaries which was not present in the unirradiated samples. This effect seems to be an extension to a larger scale of that observed in the electron microscope replicas of UO_2 irradiated to lower

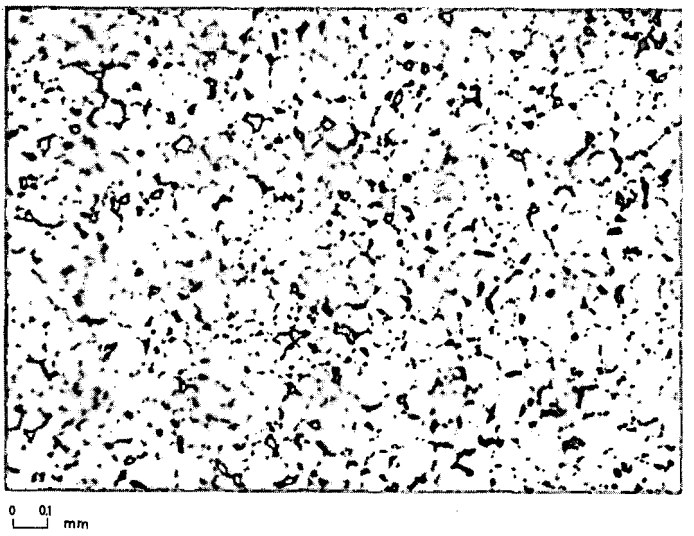


Fig. 14

Enriched UO_2 core of high-burn-up duplex specimen

TABLE II

PRE- AND POST-IRRADIATION DATA ON FUEL SPECIMENS TESTED

Specimen reference number	Fuel type	Linear heat rating	Rating	Estimated centre temperature	Estimated burn-up	Volume of Xe produced	Total vol. of gas collected	Volume of Xe collected	Gas Release	Ratio Xe/Kr	Can diameter change	
											Pre-irrad.	Post-irrad.
		(W/cm)	(W/g of fuel)	(°C)	(MWd/t)	(cm^3)	(cm^3)	(cm^3)	(%)		(in)	(in)
PH 8	Duplex	108 (centre)	176	1480	44 200	2.59	1.01	0.45	17	3.45	0.2930	0.2935
PH 9	Duplex	85 (centre)	147	1250	36 600	2.25	2.1×10^{-2}	1.26×10^{-5}	--	--	0.2935	0.2937
PH 10	Duplex	131	213	1740	53 300	3.16	0.17	0.15	4.75	13	0.2915	0.2917
PH 11	Duplex	108	176	1530	44 200	2.64	1.08×10^{-2}	4.3×10^{-3}	--	6	0.2925	0.2930
PH 18	Duplex	108	176	1530	44 200	2.64	2.07	1.77	66	7.2	0.2915	0.2915
PH 13	10 wt% (Pu, U) C	49.5	76.5	600	19 000	1.28	4.64×10^{-3}	3.4×10^{-4}	2.65×10^{-2}	--	0.1437	0.1438
PH 14	10 wt% (Pu, U) C	59.5	91.5	750	22 800	1.13	10.1×10^{-3}	1.32×10^{-5}	1.17×10^{-3}	--	0.1437	0.1437
PH 15	10 wt% PuO_2-UO_2	168	73	1170	12 700	4.72	2.7×10^{-2}	6.8×10^{-3}	0.144	22.5	Not available	
PH 16	10 wt% PuO_2-UO_2	168	73	1170	12 700	4.72	0.25	Not known		19	0.2925	0.2927

burn-ups, described in the previous section. This may, in fact, be an intermediate stage towards the formation of large bubbles as observed in UO_2 taken to still higher burn-ups. In the duplex cores the bulk of the UO_2 is at temperatures where the creep strength is beginning to fall rapidly and where plastic deformation can occur fairly easily [18]. If, in fact, the diffusion of fission gases along grain boundaries is not very rapid, the grain boundary pores or voids may collect gases and eventually exert a sufficient pressure on the matrix to cause plastic flow and bubble enlargement, as observed by BARNEY [15] and others. A detailed study of this behaviour requires the development of reliable techniques for thinning bulk UO_2 for transmission studies in the electron microscope; such techniques are still at an early stage of development.

There is insufficient evidence to say whether the presence of 10% plutonium modifies the irradiation behaviour of UO_2. Earlier work on 1% PuO_2-UO_2 taken to a lower burn-up level [19] indicated that the presence of the plutonium had no effect. At the higher plutonium content, one factor of possible importance may be found in the tendency for UO_2 to take an excess of oxygen into solution and for PuO_2 to form an oxygen-deficient structure. This would require a phase separation unlikely from energy considerations.

4. CONCLUSIONS

(1) The build-up of radiation damage in sintered UC and its annealing have been studied by the electrical resistivity technique. The indication is that interstitials become mobile at 100-130°C and vacancies become mobile at about 700°C. The X-ray diffraction measurements indicate that a distinction between uranium and carbon interstitials and vacancies should be made and that some defect-clustering may occur.

(2) A preliminary study of the behaviour of 10% PuC-UC to burn-ups of about 20 000 MWd/t suggests that at temperatures of between 500 and 800°C the rate of fission-gas release is very low, probably being solely due to recoil, or more probably to knock-out, of gas atoms near the surface of the fuel or grains by recoiling fission fragments.

(3) Electron microscope replicas of irradiated UO_2 and 1% PuO_2-UO_2 suggest that two important phenomena may be occurring: grain growth causes the closed pores to concentrate in the grain boundaries and small bubbles of about 400Å diameter may be forming in the grain interiors.

(4) Preliminary results of a study of the irradiation behaviour of UO_2 and PuO_2-UO_2 to high burn-ups suggest that no drastic structural changes such as swelling have occurred within the burn-up and temperature range covered to date but that a concentration of pores at the grain boundaries may foreshadow swelling at higher burn-ups or with less restraint.

ACKNOWLEDGEMENTS

The assistance of members of the Ceramic Fuel Irradiation and Irradiation Services Groups of Metallurgy Division, A.E.R.E., in the experimental work described in this paper is gratefully acknowledged. In particu-

lar we would like to acknowledge the efforts of Messrs. H. Venables, J. Lambert and J. Cole.

REFERENCES

[1] ADAM, J. and ROGERS, M. D., Reactor Sci. Tech. 14 (1961) 51.
[2] BLOCH, J. and MARCHEIX, C., CEA-202 (March 1961).
[3] HEDGER, H.J. and REGAN, M.C., Proc. Plansee Conf. (1961).
[4] CHILDS, B.G. and McGURN, J., AECL Rpt CR Met-868 (1959).
[5] ROUGH, F.A. and CHUBB, W., USAEC Rpt. - BMI-1554 (1961).
[6] CHILDS, B.G., these Proceedings.
[7] NEWKIRK, H.W. Jr., DANIEL, J.L. and MASTEL, B., J. Nucl. Mat. 2 (1960) 269.
[8] HARE, A.W. and ROUGH, F.A., USAEC Rpt. BMI-1491 (1961).
[9] FINDLAY, J. and LONG, G., private communication.
[10] RUSSELL, L.E., private communication.
[11] BLOCH, J., J. Nuc. Mat. 3 (1961) 237.
[12] ROBERTSON, J.A.L., BAIN, A.S., ALLISON, G.M. and STEVENS, W.H., Nuclear Metallurgy, Amer. Inst. Mech. Engnrs., VI (AECL-890) (1960).
[13] PUGH, S.F., J. Nucl. Mat. 4 (1961) 177.
[14] LAWSON, V.B. and MacEWAN, J.R., CRFD-915 (AECL-994 (1960).
[15] BARNEY, W.K., Proc. 2nd UN Conf. PUAE 6 (1958) 677.
[16] LAMBERT, J.D.B., unpublished work.
[17] BLEIBERG, M., these Proceedings.
[18] HALL, A., SCOTT, R. and WILLIAMS, J., J. Nuc. Mat. 1 (1959) 28.
[19] SAYERS, J.B. and WORTH, J.H., Power Reactor Experiments, IAEA, Vienna (196).

THE LOW-TEMPERATURE IRRADIATION BEHAVIOUR OF CAST URANIUM CARBIDE

B.G. CHILDS, A. OGILVIE, J.C. RUCKMAN AND J.L. WHITTON
DOUNREAY EXPERIMENTAL REACTOR ESTABLISHMENT,
CAITHNESS, SCOTLAND

Abstract — Résumé — Аннотация — Resumen

THE LOW-TEMPERATURE IRRADIATION BEHAVIOUR OF CAST URANIUM CARBIDE. The electrical resistivity, at 20°C, of cast uranium monocarbide has been measured as a function of neutron exposure over the range 0 - 10^{19} n/cm^2. The specimens, which were of natural isotopic content, were irradiated at temperatures estimated to be less than 80°C.

The resistivity increased with exposure in an inverse exponential fashion, increases of up to 150% of the original values being observed for previously annealed specimens containing precipitated UC_2. Pure specimens which were free from UC_2, and also UC_2-containing specimens which had been contaminated by tungsten during the melting process, increased rather less in resistivity - typically by 114% after 10^{19} n/cm^2.

On subsequently annealing the specimens in a series of increasing temperature steps, between 50% and 70% of the fractional resistivity increment was removed over the interval 20°C - 300°C. Virtually complete recovery of the original resistivity values occurred below 800°C.

Lattice parameter and microstructural changes were also observed in these specimens.

COMPORTEMENT DU CARBURE D'URANIUM MOULÉ, IRRADIÉ A BASSE TEMPÉRATURE. La résistivité électrique à 20°C du monocarbure d'uranium moulé a été mesurée en fonction de l'exposition à des flux de neutrons d'une densité allant jusqu'à 10^{19}n/cm^2. Les échantillons, qui étaient des composés d'isotopes naturels, ont été irradiés à des températures estimées inférieures à 80°C.

La résistivité est une fonction exponentielle inverse de la radioexposition; on a observé des accroissements atteignant 150% des valeurs initiales pour des échantillons préalablement recuits contenant un précipité de carbure d'uranium. Des échantillons purs dépourvus d'UC_2 et, d'autre part, des échantillons contenant de l'UC_2 contaminés par du tungstène au cours des opérations de fonderie ont accusé une augmentation de résistivité moins élevée (114% après irradiation par un flux de 10^{19} n/cm^2).

Si l'on procède ensuite au recuit des échantillons en augmentant progressivement la température, on constate que 50 à 70% de l'accroissement fractionnaire de la résistivité disparaît dans l'intervalle de 20 à 300°C. La résistivité retrouve pratiquement sa valeur initiale au-dessous de 800°C.

Les auteurs ont également observé sur ces échantillons les paramètres de réseau et les modifications microstructurelles.

СВОЙСТВА ЛИТОГО КАРБИДА УРАНА, ОБЛУЧЕННОГО ПРИ НИЗКОЙ ТЕМПЕРАТУРЕ. Электрическое сопротивление литого монокарбида урана было измерено при 20°C в зависимости от нейтронного облучения в диапазоне от 0 до 10^{19} н/см^2. Образцы с нормальным содержанием изотопов облучались при температурах, считавшихся ниже 80°C.

При облучении сопротивление увеличивалось как обратная экспоненциальная функция. Для ранее отожженных образцов, содержащих осажденный UC_2, наблюдались увеличения до 150% первоначальной величины. Чистые образцы, свободные от UC_2, а также образцы, содержащие UC_2 и загрязненные вольфрамом в процессе плавления, дали значительно меньшее увеличение сопротивления - обычно на 114% после 10^{19} н/см^2. При последующем отжиге образцов при возрастающих температурах в интервале 20°C - 300°C устраняются от 50 до 70% от начальной величины увеличения сопротивления. Полное восстановление первоначальных величин сопротивления происходило фактически при температуре ниже 800°C.

В этих образцах наблюдались также изменения параметра решетки и микроструктуры.

EFECTOS DE LA IRRADIACIÓN A BAJA TEMPERATURA SOBRE EL CARBURO DE URANIO FUNDIDO. Los autores han medido la variación de la resistividad eléctrica del monocarburo de uranio fundido, a 20°C,

en función de dosis neutrónicas comprendidas entre 0 y 10^{19} n/cm^2. Las probetas, de composición isotópica natural, se irradiaron a temperaturas inferiores a 80°C.

La resistividad aumenta con la exposición según una ley exponencial inversa, habiéndose observado incrementos que llegan hasta el 150 por ciento de los valores originales en el caso de probetas previamente recocidas que contienen UC_2 precipitado. En las probetas exentas de UC_2, y también en las que contienen UC_2 pero que fueron contaminadas por wolframio durante el proceso de fusión, los aumentos de resistividad observados son bastante menores, siendo el valor característico el 114 por ciento, que se registra en correspondencia con una dosis de 10^{19} n/cm^2.

Al recocer ulteriormente las probetas en una serie de aumentos de temperatura escalonados, se pudo anular entre 50 y 70 por ciento del incremento de resistividad fraccionario, dentro del intervalo 20°C a 300°C. Por debajo de los 800°C, se observó una recuperación prácticamente total de los valores originales de la resistividad.

También estudiaron los autores en las mismas probetas los parámetros del reticulado y los cambios microestructurales.

1. INTRODUCTION

The considerable interest which has recently developed in the use of uranium carbide as a reactor fuel has lead to a number of high burn-up fuel-element irradiations [1-4] in which technologically important properties such as swelling, cracking and the release of fission-product gases have been investigated. Rather less attention, however, has been devoted to experiments aimed at discovering the basic mechanisms of radiation damage in the material. Such experiments are, nevertheless, of value both in adding to the general body of knowledge concerning radiation-damage processes in fissile materials and also as a long term support to the technological studies. Only through a detailed understanding of the irradiation effects can complete confidence in the behaviour of the fuel under all service conditions be achieved and its optimum performance realised.

As a contribution to this understanding, a programme of basic irradiation-experiments on UC has been initiated at the U.K.A.E.A. Experimental Reactor Establishment, Dounreay. The results obtained in the work up to the present time, are reported in this paper.

2. EXPERIMENTAL DETAILS

2.1. Specimens

The uranium carbide specimens were in the form of cylindrical rods, 0.3-cm diam. by 3-cm long, and had compositions varying between 4.5 and 5.5 wt.% carbon. They were produced* by melting natural uranium metal in contact with graphite chips on the water-cooled hearth of an argon-arc furnace. The uranium-carbon alloy buttons thus formed were inverted and remelted six times, in order to make them homogeneous in composition, and were then cast into thin-walled graphite moulds. Both the tilt-pouring and the drop-casting techniques were used, the moulds being pre-heated

* Produced by C.A. Parsons & Co. Ltd., Nuclear Research Centre, Fossway, Newcastle-upon-Tyne, 6, see Ref. [5].

to at least 800°C to improve their penetration by the liquid. After casting, the specimens were extracted from the moulds and annealed in vacuo, usually for 5 h at 1700°C, which enabled them to develop an equilibrium grain structure.

The small diameter of the moulds made it difficult to produce specimens free from casting defects due to the volume contraction of UC on solidification. Mostly these took the form of isolated cavities distributed along the axis of the specimens. γ-radiographs of some of the specimens, showing these cavities, are reproduced in Fig. 1. Some specimens also contained radial cracks due to thermal shock on cooling.

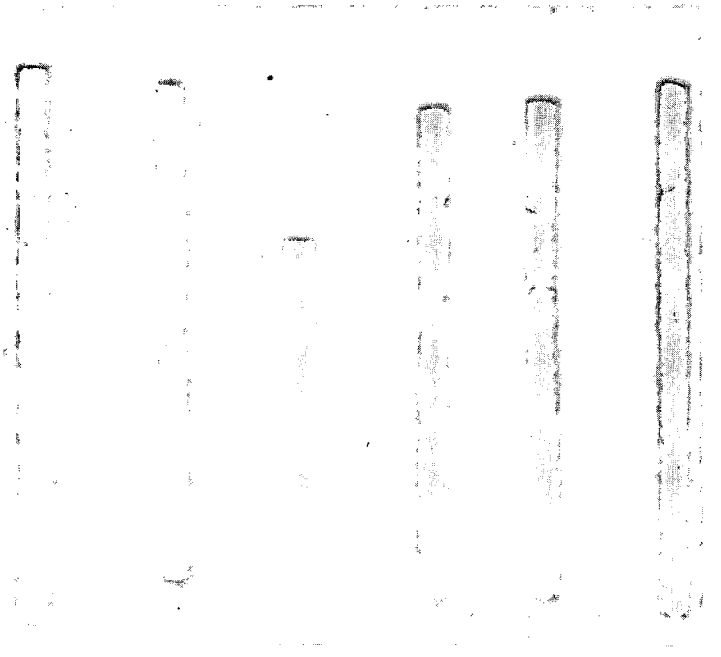


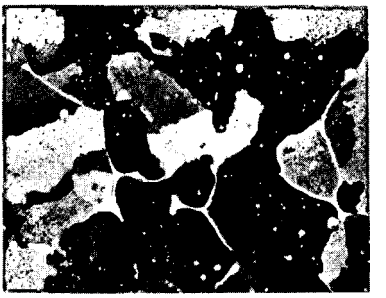
Fig.1

Radiographs of UC specimens

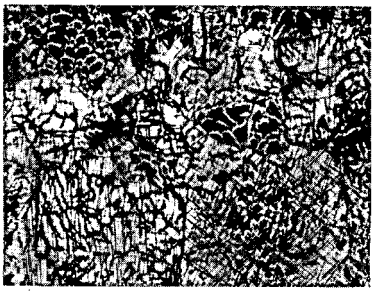
The first specimens were made using a tungsten electrode in the arc furnace and, in consequence, were contaminated by 1-2 wt.% of tungsten; to avoid such contamination later specimens were produced using a graphite electrode . The presence of tungsten affected the specimen microstructure by inhibiting grain growth during the annealing stage. The grains in the tungsten-containing specimens (see Fig. 2) were small and very irregular in shape compared to those in tungsten-free specimens. In addition, "coring-type" concentration-gradient patterns were visible in the micrographs of the contaminated specimens, even after annealing at 1800°C. These gradients were formed as a result of dendritic crystal growth during solidification from the melt. They are believed to be due to the local concentration, by a zone-refining mechanism, of the tungsten dissolved in the UC matrix. This is supported by the fact that the lattice spacing for the specimens con-



a)



b)



c)

Fig. 2

Microstructure of tungsten-containing specimens

(a) specimen 31, showing relatively well-developed grain structure with traces of tungsten concentration gradients

(b) specimen 45, showing irregularly shaped grains with free uranium at boundaries

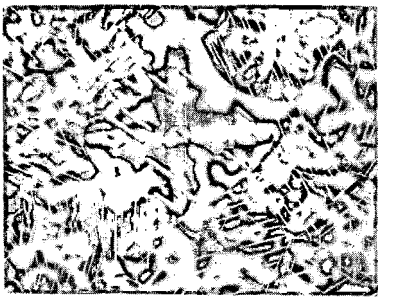
(c) specimen 42, showing tungsten concentration gradients and UC_2 precipitate

taining tungsten was abnormally low compared to that for tungsten-free material (4.9520 Å instead of 4.9600 Å). Metallic tungsten, detected by X-ray diffraction, was also visible in the specimens, being dispersed as a fine precipitate throughout the grains.

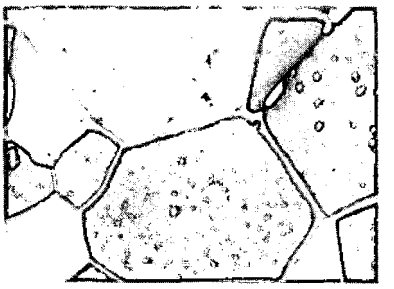
The tungsten-free specimens (Fig.3) were composed of large (200-800 μm diameter) polyhedral grains with no indication, in the annealed condition, of concentration gradients. Specimens with more than 4.8 wt.% carbon contained the tetragonal UC_2 phase, dispersed both as Widmanstätten-type precipitates of flat needles lying on $\langle 100 \rangle$ planes in the UC matrix and also as thin sheets along the boundaries of the UC grains. In specimens with less than 4.8 wt.% carbon, the excess uranium metal was mostly distributed around the UC grains with, in addition, a fine precipitate of spherical particles within the grains. Typical analyses of the specimens are shown in Table I.



a)



b)



c)

Fig. 3

Microstructure of tungsten-free specimens

(a) specimen 53, showing normal UC_2 distribution

(b) specimen 61, unannealed (as-cast), showing carbon concentration gradients and fine-scale UC_2 precipitate

(c) specimen 65, showing free uranium at grain boundaries

2.2. Irradiation technique

The specimens were irradiated in 4V and 4VG positions in the Materials Testing Reactor, Dounreay, in a thermal neutron flux which varied between 1.3×10^{12} and 1.4×10^{13} n cm^{-2} s^{-1}. The specimen capsules (see Fig. 4) were made from stainless steel and designed so that the operations of inserting the specimens, evacuating, filling with helium, and sealing could be performed by remote handling. This made it possible to irradiate individual specimens to an increasingly high series of exposures and so to compare effects in one specimen with those in another over a range of exposure values.

Each capsule was sealed by forcing a conical steel plug into a mating conical hole at its open end. A preformed aluminium gasket, placed between the two conical surfaces, was sheared by this operation and forced into close physical contact with them.

The neutron exposure of the specimens was measured by the cobalt activation method assuming the Co^{59} absorption cross-section to be 38.0 b.

TABLE I

ANALYTICAL DATA FOR URANIUM CARBIDE SPECIMENS

1. Tungsten-containing specimens

Specimen number	Carbon content (wt.%)	Impurity content-gases (wt. ppm)			Impurity content-tungsten (wt.%)
		O_2	N_2	H_2	
28	4.6	36	350	400	1.5
29	4.7	47	400	400	1.7
30	4.8*	-	-	-	0.9
39	4.4	275	160	14	2.1
41	4.8*	270	250	19	2.2
46	4.5	< 20	830	47	1.1
51	4.8*	-	-	-	3.0

TABLE I (cont.)

2. Tungsten-free specimens

Specimen number	Carbon content (wt. %)	Impurity content-gases (wt. ppm)			Impurity content-metals (wt. ppm)								
		O_2	Ni_2	H_2	W	Al	Ca	Cr	Fe	Mg	Mo	Mn	Ni
54	4.9*				n (25)	60	40	n (10)	n (10)	n (10)	n (30)	n (15)	n (30)
60	4.6												
62	5.0				n	n (30)	20	n	n	35	n	n	n
63	4.7												
66	4.4				n	n	25	n	n	80	n	n	n
73	5.5*	200	420	20									
74	5.6	155	525	15	n	50	50	n	15	30	n	2	n
77	5.5	235	620	20	n	100	40	n	15	30	n	2	n

* composition inferred from appearance of microstructure

n not detected

( ) parenthesis indicate the detection limit

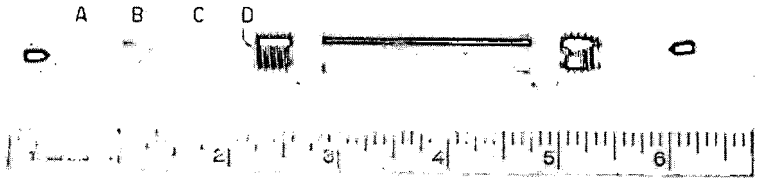


Fig. 4

Specimen capsules
(The scale is in inches)

A: cobalt-foil flux-monitor

B: conical steel plug

C: aluminium gasket

D: conical opening

The cobalt foils were placed in tapped holes at either end of the capsule; the relationship of the flux at these positions to that at the specimen position was determined by a separate calibration experiment. During irradiation, the capsules were immersed in water at 40°C. The estimated maximum specimen-temperature was 80°C.

2.3. Resistivity-measurement

The electrical resistance of the specimens was measured at 20°C using the twin potentiometer apparatus shown in Fig. 5. This was designed so that the resistance of both short (1.5 cm) and standard length (3 cm) specimens could be measured. Thus, even if a specimen broke during a series of irradiations and measurements, it was usually possible to continue the measurements using one of the pieces, although the accuracy was reduced.

Each section of the apparatus contained a pair of inverted V-shaped steel probes which made a two point contact at each end of the specimen. A known current was passed into and out of the specimen through these contacts. A second set of probes, consisting of two sharpened tungsten knife edges, fixed to an insulating block, contacted the specimen in-between the current probes and served to measure the potential drop along it.

Both the specimen support and the potential-probe block were arranged to rotate independently about the same axis. In this way the contact pressure at each of the four current-probe contact points was equalized. This was also the case for the two potential probes.

The potential measurements were made with the current flowing in each direction to compensate for thermoelectric voltages in the circuit. During measurement the specimens were immersed in CCl_4 at a temperature of 20.0 ± 0.1°C. This was maintained by circulating thermostatically-controlled water between the double walls of the brass tank which contained the apparatus.

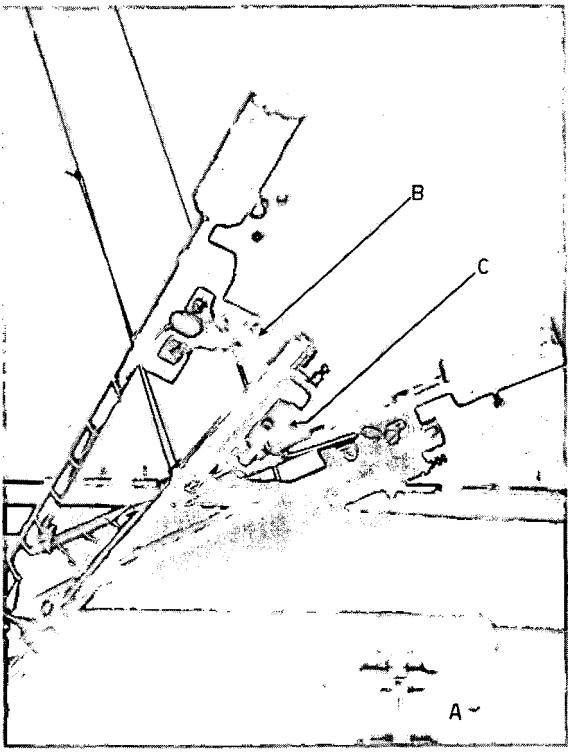


Fig.5

Resistivity measurement apparatus

A: specimen

B: current probes

C: potential probes

Apparent resistivity values for the specimens were calculated from the measured resistances using an average value for the cross-sectional area. This figure was obtained from measurements of the specimen diameter at a number of positions along its length. In this calculation the influence of the cracks and cavities on the effective area and length of the specimens was ignored.

2.4. Lattice parameter measurement

The uranium carbide lattice-parameter was measured, at various exposure levels, for three UC specimens similar to those used for resistivity measurements. After annealing, each specimen was broken into a number of 3-mm long fragments and alternate fragments from along the length of the specimen were irradiated to an exposure in the range 5×10^{15} to 10^{19} n/cm^2.

After irradiation, the average lattice parameter of each of these fragments was measured by the technique described below. The remaining fragments of the specimen were used to give accurate parameter values for the unirradiated condition and to check that no significant variation in parameter had occurred along the length of the specimen.

Before measurement, each fragment was ground to powder under CCl_4 in a pestle and mortar and the powder was then mixed with canada balsam to form a thick paste. This was smeared into a recess (1.2-cm diam. by 0.005-cm deep) in the flat surface of a Perspex mount and allowed to set. The Perspex mount made it possible to locate the specimen surface accurately in coincidence with the central axis of the X-ray diffractometer (see Fig.6) used for the parameter measurement. This instrument, which has been described in detail elsewhere [6], was of a conventional type apart from the arrangements made to prevent the β- and γ-radiation from the radioactive specimen swamping the X-ray signal at the detector.

The collimated, monochromatic (Cu K α) X-ray beam, after diffraction at the specimen, was deflected by a quartz crystal monochrometer into a proportional gas-counter. Suitably arranged lead shielding intercepted the undeflected radiation from the specimen and thus reduced the background

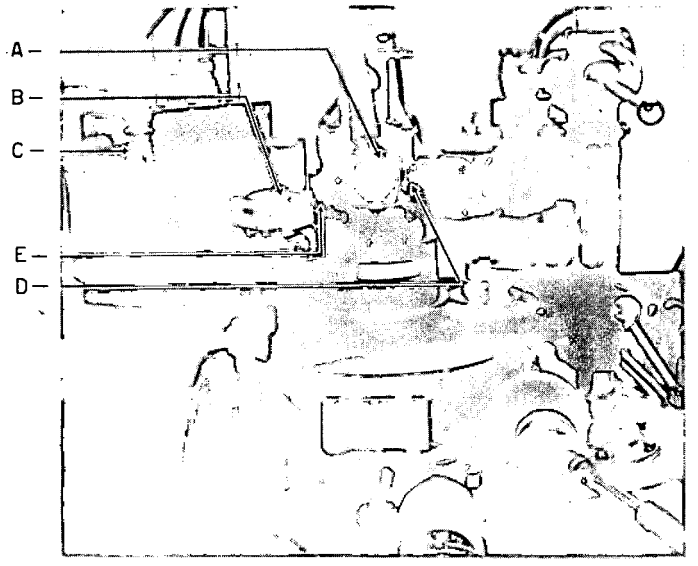


Fig.6

X-ray diffractometer

A: specimen housing

B: quartz crystal

C: counter

D: collimator

E: slit

radiation level at the counter. This level was further reduced by passing the counter output into an analyser which rejected all signals falling outside the energy range of the Cu Kα radiation.

The (440), (531) and (600) X-ray peaks, at Bragg angles of about 61°30', 66°50' and 68°50', respectively, were scanned for each specimen, the counter and quartz crystal rotating as a unit about the diffractometer axis. Initially, both point counting and continuous recording, at a counter speed of 0.006° (θ) per min were used. However, when the results obtained by the two methods were found to agree to within the limits of accuracy of the instrument, it was decided to use only continuous recording for the remaining specimens. During the scans the specimen was rotated so as to bring more planes into a reflecting position.

In the diffractometer oxidation of the specimen was avoided by enclosing it in an argon-filled housing. This was fitted with a thin plastic window transparent to the X-ray beam.

To calculate the parameter value from the recorded diffraction peak positions, each peak (Cu Kα doublet) was truncated using the method described by LADELL, PARRISH and TAYLOR [7] and the centre of gravity of the portion above the truncating line was determined. The value of 1.541853 Å given by LADELL, PARRISH and TAYLOR [8] for the wavelength centroid of the Cu Kα spectral distribution was substituted in the Bragg formula, together with the angular position of the peak centroid, and a value obtained for the apparent lattice parameter corresponding to the particular diffraction angle, θ. The values for the three peaks were corrected for possible error, due to slight displacement of the specimen surface from the diffractometer axis, by plotting them against $\cos^2\theta$ and extrapolating to $\cos^2\theta = 0$. Finally, this extrapolated value was corrected for specimen refraction effects.

In the calculation, no account was taken of Lorentz, polarization or dispersion errors since these were expected to introduce an error of less than 0.01° (θ) at the high angles where the measurements were made. Also, because of the high absorption-coefficient of uranium carbide, the specimen transparency error was negligible. The specimen flatness-error was also very small.

3. RESULTS

3.1. Resistivity change on irradiation

The resistivities of the specimens before irradiation (see Table II) varied between 36×10^{-6} and 53×10^{-6} Ωcm, the values for the tungsten-containig specimens (average = 46.1×10^{-6} Ωcm) being significantly higher than those for the tungsten-free specimens (average = 38.5×10^{-6} Ωcm). The latter figures, also are somewhat higher than the accepted value of 35.0×10^{-6} Ωcm at 20°C for pure dense UC obtained by workers [9] at the Battelle Memorial Institute.

Much of the difference for the tungsten-free specimens can be attributed to the casting defects mentioned previously. Thus, for example, it may be shown that a single spherical cavity having a diameter equal to half the

TABLE II

COMPOSITION, MICROSTRUCTURE AND RESISTIVITY OF SPECIMENS BEFORE IRRADIATION

1. Tungsten-containing specimens

Specimen number	Carbon content (wt.%)	Microstructure (see key below)	Apparent resistivity at 20°C (10^6 Ωcm)
25	4.8 ≠	vi (80), c, W	49.4
30	4.8 *	r (200), lc	47.9
31	4.7 *	r (250), lc, U (see Fig. 2)	45.5
33	4.8 ≠		47.6
34	4.9 *	r (100), lc, UC_2	53.3
35	4.8 ≠		46.6
36	4.5		40.2
37	4.5 ≠		40.7
38	4.5 ≠	vi (80), U	40.7
42	5.0	i (100), c, UC_2 (see Fig. 2)	51.4
43	4.5 ≠		-
45	4.5	vi (100), U (see Fig. 2)	43.3
51	4.8 *	vi (50), hc, W	44.9

2. Tungsten-free specimens

Specimen number	Carbon content (wt.%)	Microstructure (see key below)	Apparent resistivity at 20°C (10^{-6}Ωcm)
53	5.0 *	r (150), UC_2, (see Fig. 3)	40.4
54	4.9 *	r (150), UC_2	37.8
57	4.9 *	r (150), u, UC_2	39.4
58	4.9	r (50), u, UC_2	36.3
61	4.8	r (75), u, UC_2 (see Fig. 3)	37.0
62	5.0	vr (400), UC_2	36.2
63	4.7	vr (750)	37.6
64	4.9	vr (150), UC_2	35.8

TABLE II (cont.)

2. Tungsten-free specimens (cont.)

Specimen number	Carbon content (wt.%)	Microstructure (see key below)	Apparent resistivity at 20°C (10^6 Ωcm)
65	4.5	vr (400), U	-
66	4.4	r (300), U (see Fig. 3)	43.1
67	4.5	vr (600)	40.6
71	5.4	U_2C_3	-
72	5.5 *	(80), UC_2, U_2C_3	67.7
76	5.5	(80), UC_2, (U_2C_3 ?)	38.9

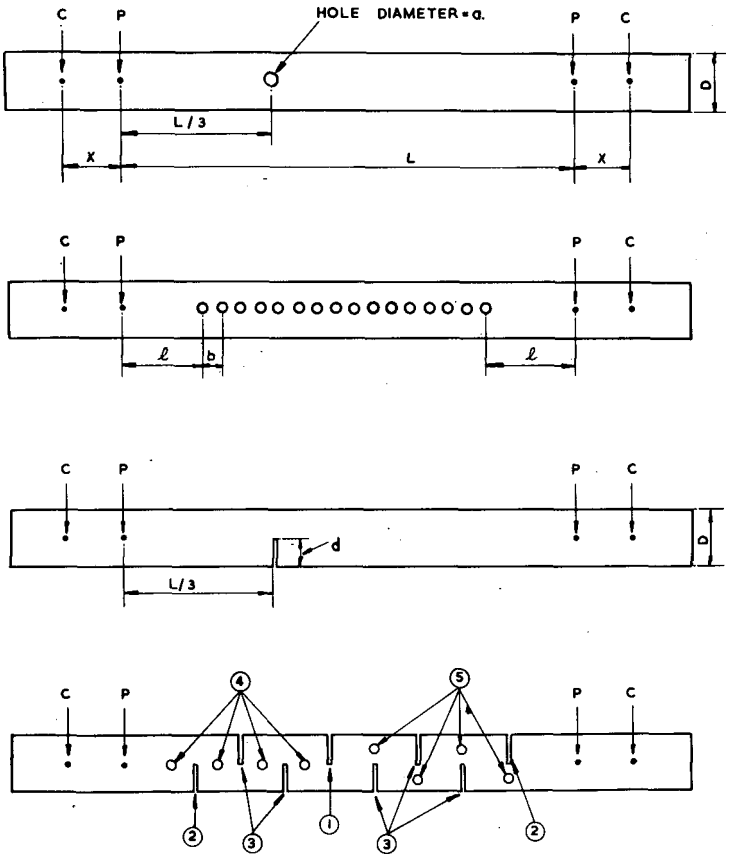
Key

≠	nominal composition
*	composition inferred from appearance of microstructure
vi	very irregularly shaped grains
i	irregularly shaped grains
r	regular, quite-well-developed polyhedral grains
vr	very regularly shaped polyhedral grains
(80)	average grain size in μm
lc	light } coring-type concentration gradient patterns believed due to W in solution
c	medium }
hc	heavy }
W	precipitated metallic W
u	unannealed (as-cast) specimens showing carbon concentration gradients
U	metallic U around UC grain boundaries
UC_2	Widmanstätten-type precipitate of UC_2
U_2C_3	U_2C_3 around UC grain boundaries

The estimated error in resistivity is ±1% or $\pm 0.5 \times 10^{-6}$ Ωcm, whichever is the smaller.

specimen diameter, or a single transverse crack having an area equal to half the specimen cross-sectional area, should increase the apparent resistivity of a 2-cm long specimen by about 5%. These predicted figures were confirmed in tests (summarized in Fig. 7) using metal strips in which holes and slots were cut to simulate the casting defects in the actual specimens. From these tests and from the observed incidence of casting defects, apparent resistivity values up to about 40×10^{-6} Ωcm are to be expected for the tungsten-free specimens.

The additional resistivity increment of about 8×10^{-6} Ωcm for the tungsten-containing specimens was probably due to tungsten dissolved in the UC lattice. This increment was observed for specimens showing tungsten concentration-gradient patterns irrespective of the additional presence of dispersed metallic tungsten.



1. SINGLE CAVITY
2. MULTIPLE CAVITIES
3. SINGLE CRACK
4. MIXTURES OF CRACKS AND CAVITIES

Fig. 7

Experiments simulating the effects of cavities and cracks in UC specimens

1. Single cavity

Steel strip: thickness 0.025 cm, L = 9.5 cm, D = 1.5 cm, X = 2.0 cm (potential drop independent of X for X > 1.0 cm).
Up to a/d = 0.45, percent resistance increase for single hole at L/3 varies as $(a/d)^2$
For spherical cavity in UC rod with diameter = 0.5 rod diameter, equivalent (a/d) in strip experiment = 0.25.
Corresponding resistance increase = 2.1%.

2. Multiple cavities

Steel strip: thickness 0.025 cm, h = 30 cm, D = 1.3 cm, X = 2.0 cm, a = 0.4 cm.
For 1, 2, 3, and 5 holes drilled with separation distances decreasing down to 2 cm, percent resistance in-

crease per hole is 1.41%. For 9 holes, 1 cm apart, resistance increase per hole is 1.38%: for 16 holes, 0.5 cm apart, it is 1.36%.

3. Single crack

Steel strip: thickness 0.025 cm, L = 11 cm, D = 1.5 cm, X = 2.0 cm.
For slit lengths, d, up to 0.5 D, percentage resistance increase varies as $(d/D)^2$
For transverse crack in UC rod with area = 0.5 rod cross-sectional area, equivalent resistance increase in strip experiment = 4.0%.

4. Mixtures of cracks and cavities

Strips of steel, copper and tantalum: steel thickness 0.025 cm; L = 16 cm, D = 1.3 cm, X = 2.0 cm. Hole diameters = 0.4 cm, slit lengths = 0.65 cm. Values of R_S/R_C and R_T/R_C (where R_C, R_S, R_T are resistances of copper, steel and tantalum strips) for various configurations of cracks and cavities are as follows:-

Configuration	Percent increase in R_C	R_S/R_C	R_T/R_C
Initial	0	5.43	10.51
Slit (1)	4.7	5.07	10.42
Slits (1) and (2)	13.0	5.00	10.29
Slits (1), (2) and (3)	37.0	4.97	10.14
Slits (1), (2), (3) and holes (4)	43.5	4.98	10.13
Slits (1), (2), (3) holes (4) and (5)	59.0	5.18	10.03

Thus the ratios of the resistances of strips of different resistivities are almost unaffected by increasingly complex configurations of holes and slits.

The changes, ΔR, in the apparent resistivities of the specimens on irradiation, are shown as a function of exposure in Fig. 8. Considering an individual specimen, for example specimen 38, ΔR increased from a very low value at a dose of 10^{15} n/cm^2 to a limiting value of 46×10^{-6} Ωcm at about 10^{18} n/cm^2; this value was not exceeded for higher exposures reaching 1.6×10^{19} n/cm^2. The limiting resistivity increases for all the specimens covered a range of values between 46×10^{-6} and 62×10^{-6} Ωcm.

The tungsten-containing specimens' resistivity increased significantly less than did the tungsten-free specimens, the average limiting ΔR values for the two groups being 49.8×10^{-6} and 56.3×10^{-6} Ωcm, respectively. Some of the scatter within the individual groups is connected with the scatter in the original resistivity values since the isolated casting defects (see Fig. 7) increase the apparent resistivity of a specimen, relative to its true resistivity, by a geometrical factor which is independent of exposure. In this case, the change in resistivity on irradiation, expressed as a percentage of the original value, should be the same for all otherwise similar specimens at a given exposure.

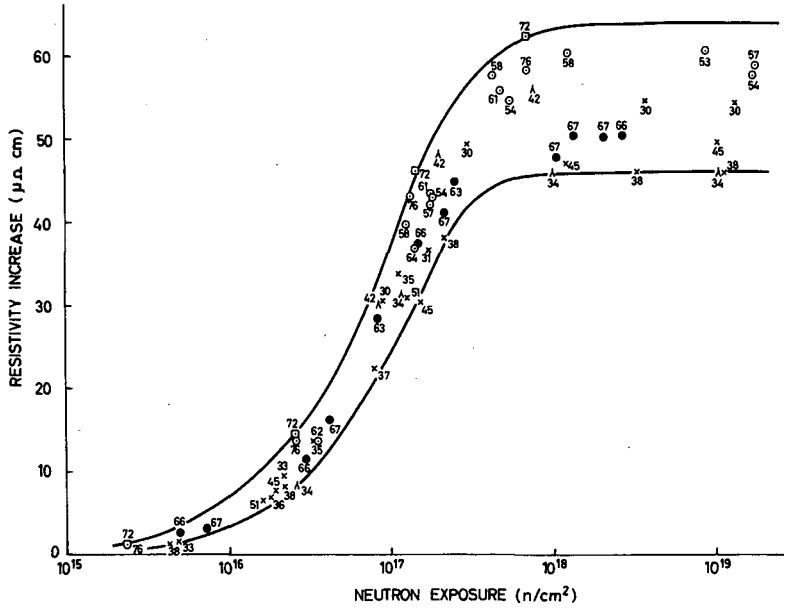


Fig. 8

Absolute resistivity increase with exposure for irradiated uranium carbide

Tungsten-free	⊙	carbon-rich (UC_2): 53, 54, 57, 58, 61, 62, 64
	⊡	carbon-rich (U_2C_3): 72
	●	uranium-rich or stoichiometric: 63, 66, 67
Containing tungsten	λ	carbon-rich (UC_2) : 34, 42
	X	uranium-rich or stoichiometric: 30, 31, 32, 35, 36, 37, 38, 45, 51

The percentage resistivity changes, P, of the specimens are shown plotted as a function of exposure in Fig. 9. With few exceptions the points are grouped along two main curves. All the tungsten-containing specimens, except for specimen 34, fall on the lower curve with a limiting P-value of 115%. These specimens had carbon contents from 4.5 - 5.0 wt.% C and possessed widely differing microstructures containing either free uranium or UC_2 (see Fig. 2 and Table II).

Most of the tungsten-free specimens gave points on the upper curve of Fig. 9 with a limiting P-value of 156%. All of these specimens were slightly rich in carbon and in every case UC_2 was found in their microstructure (see Fig. 3). The resistivity of specimens 66 and 67 which, in contrast, were uranium-rich and showed no trace of UC_2 increased much less – only slightly more in fact than the tungsten-containing specimens. The points for specimen 63, which was apparently stoichiometric in composition, also lay significantly below the curve for the carbon-rich specimens.

Specimen 72 contained the U_2C_3 phase dispersed around the UC grains and, in consequence [9] had a high initial resistivity. This was responsible

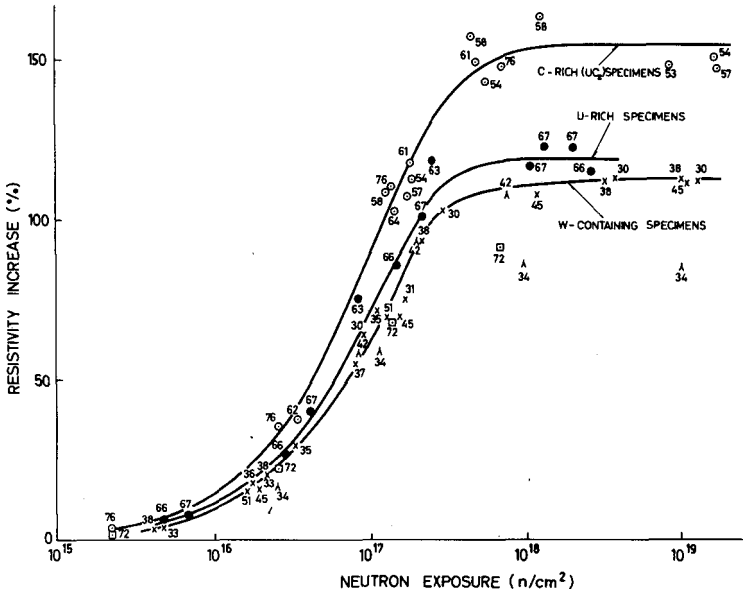


Fig. 9

Percentage resistivity increase with exposure for irradiated uranium carbide

Tungsten-free
- ⊙ carbon-rich (UC_2): 53, 54, 57, 58, 61, 62, 64
- ⊡ carbon-rich (U_2C_3): 72
- ● uranium-rich or stoichiometric: 63, 66, 67

Containing tungsten
- λ carbon-rich (UC_2) : 34, 42
- X uranium-rich or stoichiometric: 30, 31, 32, 35, 36, 37, 38, 45, 51

for the lower P-values shown by the specimen since its absolute resistivity increase was relatively high.

Three carbon-rich specimens, 57, 58 and 61, which were not annealed before irradiation, behaved similarly to annealed specimens of similar composition despite the presence in them (see Fig.3) of carbon concentration-gradients and a poorly developed UC_2 precipitate structure. No major effect of neutron flux, as opposed to total exposure, on the resitivity increases was found for fluxes in the range 1.2×10^{12} to 1.3×10^{13} n cm^{-2} s^{-1}. Such an effect was thought possible for two reasons:—

(1) Because of consequent variations in the specimen temperature during irradiation, leading to partial annealing-out (see section 3.2) of the resistivity change; and

(2) Because of possible interactions between lattice defects which might depend on the rate of defect production and hence on the flux. The absence of any major effect can be seen from the behaviour of specimens 58 and 61 which were irradiated first, in an average flux of 1.0×10^{13} n cm^{-2} s^{-1} up to exposures of about 1.5×10^{17} n/cm^2 and then, in a flux of 1.2×10^{12} n cm^{-2} s^{-1}, to above 5×10^{17} n/cm^2. Considering the upper curve in Fig. 9, the percen-

tage resistivity increases after the second, low flux irradiation were only slightly higher than those resulting from initial, high flux irradiation. The eightfold decrease in flux increased P at given exposure by a factor of only 1.03. This finding was confirmed by re-irradiating specimen 66 in a low flux once the resistivity changes resulting from the earlier, high flux irradiations had been annealed out. The effect of reducing the flux from 8.2×10^{12} to 1.4×10^{12} n cm^{-2}s^{-1} was to increase P at given exposure by a factor of 1.07.

The possibility that a variation in P could be associated with the slight variations in diameter of specimens cast into different moulds was also considered. These caused the radial gap between the specimens and the capsule wall to vary between 6×10^{-3} and 18×10^{-3} cm and at maximum flux produced an estimated variation in specimen temperature of 26°C (55-81°C). No such effect, however, was found. Thus, specimens 58 and 61 which were respectively larger and smaller in diameter than specimen 66 both gave the same percentage increase in resistivity at 1.5×10^{17} n/cm^2 exposure, while specimen 66 itself, though irradiated in the same flux, showed a smaller increase. Specimen 67, moreover, increased similarly to specimen 66 although its diameter was 0.008 cm less.

3.2. Annealing behaviour

Ten of the specimens, representative in microstructure and composition of the remainder were irradiated to various exposures and were then annealed in vacuo for 5-h periods at successively increasing temperatures up to 1000°C. Their resistivities were measured at 20°C before and after each anneal and values of the recovery parameter F calculated for each exposure.

F is given by the expression

$$F = \frac{R - R_0}{R_I - R_0},$$

where R_0, R_I and R are the resistivities measured before irradiation, after irradiation and after annealing respectively.

Typical annealing curves showing F as a function of annealing temperature are reproduced in Fig. 10. These all show the same general features, namely a major recovery stage centred at 150°C in which most of the resistivity change annealed out, followed by a secondary stage at 510°C in which all or part of the residual change was removed.

Referring to Table III, the fractional change $(1 - F)_{400}$ annealed out in the first stage up to 400°C, varied from 0.55 for specimen 53 up to 0.72 for specimens 38 and 64. The total change annealed out up to 1000°C, $(1 - F)_{1000}$, varied from 0.785 for specimen 53 to 1.035 for specimen 38.

At both temperatures the values of (1 - F) for specimen 53 were anomalously low, this behaviour being accompanied (see section 3.4) by the disappearance of the UC_2 phase from the specimen. Similar, though much less pronounced, annealing characteristics were shown by the other tungsten-free specimens containing the UC_2 phase. In particular, for specimens

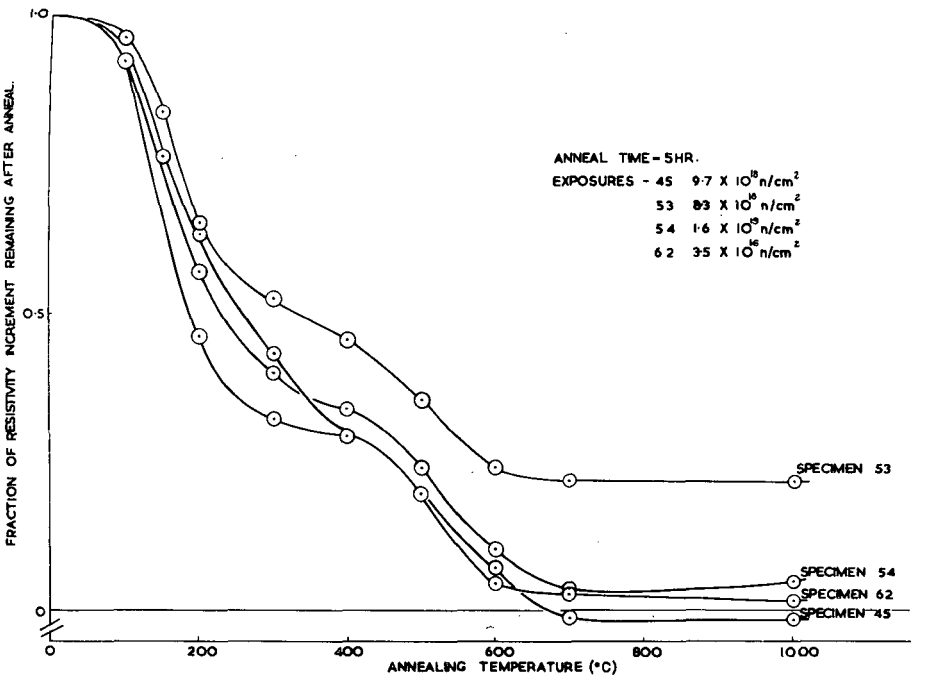


Fig. 10

Decrease in resistivity with annealing for irradiated uranium carbide

54 and 57, the residual F values after the 1000°C anneal were significantly positive at about 0.05.

The tungsten-containing specimens 38, 45 and 51 all gave resistivity values after the final anneal which were significantly lower than their original resistivities, even though the specimens had been annealed before irradiation at temperatures well above 1000°C.

It seems likely, both for the specimens showing incomplete annealing and for those showing over-annealing, that the same fraction of the total change annealed out was removed in the first annealing stage. Thus, values of the ratio $(1 - F)_{400}/(1 - F)_{1000}$ are nearly constant at 0.70 for specimens irradiated to above 7.5×10^{17} n/cm^2. The corresponding values for the two specimens, 62 and 64, irradiated up to 1.2×10^{17} n/cm^2 are slightly higher (0.72 and 0.73) but this difference is barely significant.

One other noteworthy feature, apparent from Fig. 10, concerns the relative width or degree of resolution of the two stages in the different specimens. The stages were much more clearly resolvable for the low exposure tungsten-free specimens than for the high exposure tungsten-containing specimens. Thus, for specimen 45 (tungsten-containing, 9.7×10^{18} n/cm^2) the stages were broadened and overlapped while for specimen 62 (tungsten-free, 3.5×10^{16} n/cm^2) they were well separated.

TABLE III

ANNEALING BEHAVIOUR OF SPECIMENS

Specimen number	Neutron exposure (n/cm^2)	Fraction of resistivity increment annealed out $(1-F)_T$		$\frac{(1-F)_{400}}{(1-F)_{1000}}$
		T = 400°C	T = 1000°C	
31	1.7(17)	0.71	-	-
38	7.5(17)	0.72	1.035	0.70
45	9.7(18)	0.70	1.015	0.70
51	7.5(17)	0.71	1.020	0.71
53	8.2(18)	0.55	0.785	0.70
54	1.6(19)	0.66	0.955	0.69
57	1.6(19)	0.65	0.945	0.69
62	3.5(16)	0.71	0.985	0.72
64	1.2(17)	0.72	0.985	0.73
66	2.25(18)	0.68	1.000	0.68

Note: The neutron exposure is given in floating point notation,

i.e. $1.7(17) \equiv 1.7 \times 10^{17}$

3.3. Lattice parameter changes

The three specimens 43, 65 and 71 used for lattice parameter measurement were respectively, tungsten-containing; tungsten-free uranium-rich; and tungsten-free carbon-rich. Specimen 65 (4.5 wt.% C) contained free uranium and specimen 71 (5.4 wt.% C) U_2C_3 distributed around the UC grains. Specimen 43 had an exceptionally irregular grain structure despite its annealing treatment (5 h at 1800°C) and no second phase could be detected in it. The UC lattice parameter values before irradiation were: 43 - a = 4.9525 ± 0.0005 Å; 65 - a = 4.9539 ± 0.0005 Å and 71 - a = 4.95725 ± 0.0005 Å.

The fractional increases in lattice parameter $\Delta a/a$ on irradiation of the specimens are shown plotted against the logarithm of exposure (Fig. 11). Also shown are some values obtained by ADAM [10] and by FREAS et al.[11]. The $\Delta a/a$ values for specimen 71 rose to 1.5×10^{-3} at 4.9×10^{17} n/cm^2, in good agreement with the values of the other workers *. Significantly smaller increases, however, were found for specimens 43 and 65. Moreover, the parameter of 43, in contrast to the findings of Freas et al., decreased significantly between the exposures 6.4×10^{17} and 4.6×10^{18} n/cm^2.

* Recent experiments on another carbon-rich specimen (number 83, 4.84 wt.% C, UC_2 containing) have confirmed this relatively large increase. $\Delta a/a$ for 83 was 1.45×10^{-3} at 1.73×10^{17} n/cm^2.

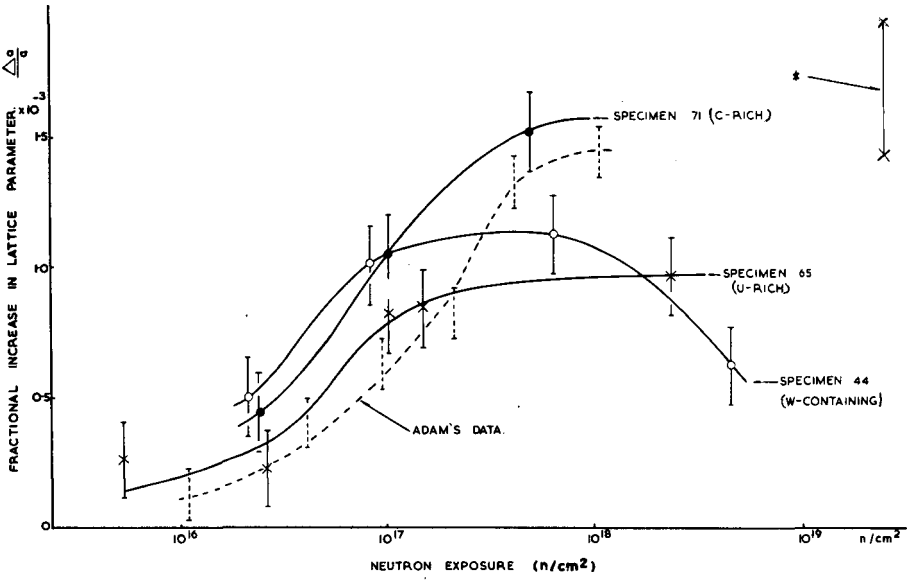


Fig. 11

Increase in lattice parameter with exposure for irradiated uranium carbide
*Range of values from FREAS et al. [11], exposures (0.24 - 4.7) 10^{20} n/cm²

The U_2C_3 lattice parameter in specimen 71 (originally 8.0885 ± 0.0005 Å) also increased on irradiation although to a lesser extent than the UC parameter. After 4.9×10^{17} n/cm², $\Delta a/a$ was 8.7×10^{-4}, This contrasts with a lattice contraction of 1.4×10^{-3} at 0.2 at.% burn-up reported by FREAS et al. [11].

3.4. Electron-microscopic examination

In order to check whether the resistivity and lattice parameter changes were accompanied by visible changes in microstructure, surface replicas of several specimens were examined at high magnification under an electron microscope *. The replicas were prepared, in the usual way, by first pressing a softened cellulose acetate film (0.008-cm thick) against the specimen surface and then, when the film had hardened, removing it from the specimen and evaporating onto it, in succession, a Au-Pd alloy deposit at an oblique angle followed by carbon at normal incidence. The cellulose acetate was then dissolved off the carbon film and the latter transferred to a microscope grid for examination.

Most of the examinations were made on pieces of one typical tungsten-free carbon-rich specimen (number 59) which were irradiated individually to an exposure between 0 and 6.5×10^{17} n/cm². After irradiation, replicas were taken of (1) the original (pre-irradiation) polished and etched surface,

* Siemens Elmiskop I.

(2) a freshly fractured surface, and (3) a freshly polished and etched surface. The irradiated piece was then annealed in a vacuum of 10^{-4} torr, at 700-1500°C and further replicas taken of (4) the original (number 1) polished surface, and (5) a second, newly prepared, polished and etched surface.

By far the most significant changes took place at the exposed surface during irradiation (1) and annealing (4) (see Figs. 12a-12c). A pattern of cracks or deep grooves was formed in the surface, parallel to the edges of the UC_2 needles, with additional shorter (up to 5-μm long) grooves in the areas of UC between the needles. These latter grooves were curved and appeared to initiate as a series of disconnected "pits" (Fig. 12d) each about 300 Å in diameter. In addition, the grain boundaries became deeply indented. Another characteristic feature of the annealed specimen surfaces was the presence of shallow depressions around some of UC_2 needles. These appeared to form by spalling (Fig. 12e) perhaps as a result of the propagation of the curved cracks.

The surfaces examined after irradiation showed a general roughening (Fig. 12f) which became more pronounced, though not very systematically so, with increased exposure. It is not known at present to what extent these and the other changes were due to irradiation as distinct to corrosion effects.

After the exposed surfaces had been ground away and the specimens re-polished, no unusual features, which might have resulted from the irradiation, could be detected. In particular the UC_2 needles appeared unaltered in density, size and shape (Figs. 13a, b) even at region close to their pointed tips (Figs. 13c, d) which might be expected to be particularly sensitive to radiation damage. Also, no bubbles or voids greater in diameter than 100 Å (the limit of resolution of the replicas), or any microcracks longer than 100 Å were visible.

Some changes were apparent in the mode of fracture of the irradiated specimens. Before irradiation, fracture occurred exclusively by transgranular crack propagation, fracture patterns such as those of Fig. 14a being obtained. After irradiation, however, a proportion – estimated at about 10% – of the surface area showed signs of intergranular fracture (Fig. 14b). This proportion did not vary significantly with the actual exposure of the sample.

As well as specimen 59, several resistivity specimens (34, 42, 53, 54) were examined after irradiation up to 1.6×10^{19} n/cm^2 and annealing. In particular, specimen 53 was chosen for examination because of its abnormal annealing behaviour and 54 because it was similar in composition and treatment to 53 but behaved normally on annealing. The microstructure of 53 was found to be quite different both from its original structure before irradiation and from that of 54. The normal distribution of UC_2 needles, visible in the specimen before irradiation, had disappeared completely and was replaced, within the original grain structure, by a pattern of irregularly shaped regions partly bounded by cracks. These regions (see Fig. 15) appeared to be harder than the UC matrix since they were relatively unmarked by the scratches left in the surface after polishing. In contrast, specimen 54 appeared to have a normal unchanged UC_2 distribution. Specimens 59 (1000°C anneal but lower exposure), 34 (similar exposure but tungsten-containing and 300°C anneal) and 42 (lower exposure, tungsten-containing

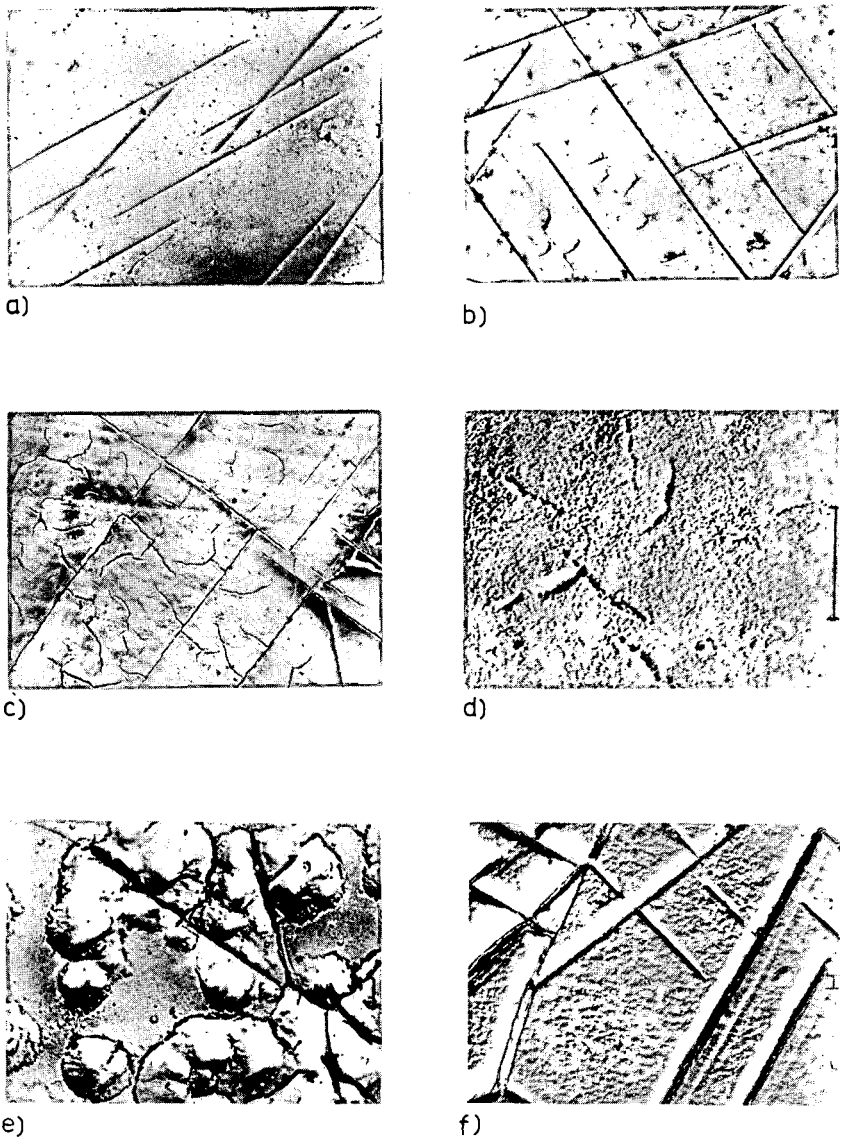


Fig. 12

Surface changes due to irradiation
Replicas taken of the originally polished and etched surface of specimen 59 after the various treatments listed

(a) before irradiation
(b) irradiated to 5.1×10^{15} n/cm^2
(c) irradiated to 2.6×10^{16} n/cm^2
(d) as (c) but showing the discontinuous nature of the grooves at high magnification
(e) irradiated to 5.1×10^{15} n/cm^2 and annealed for 5 h at 700°C
(f) irradiated to 7.9×10^{17} n/cm^2

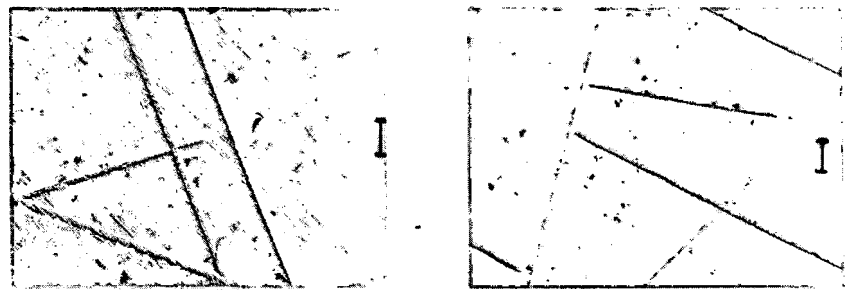


Fig. 13

Internal microstructure of specimen 59 after irradiation

(a) original structure
(b) after irradiation to 1.4×10^{17} n/cm^2

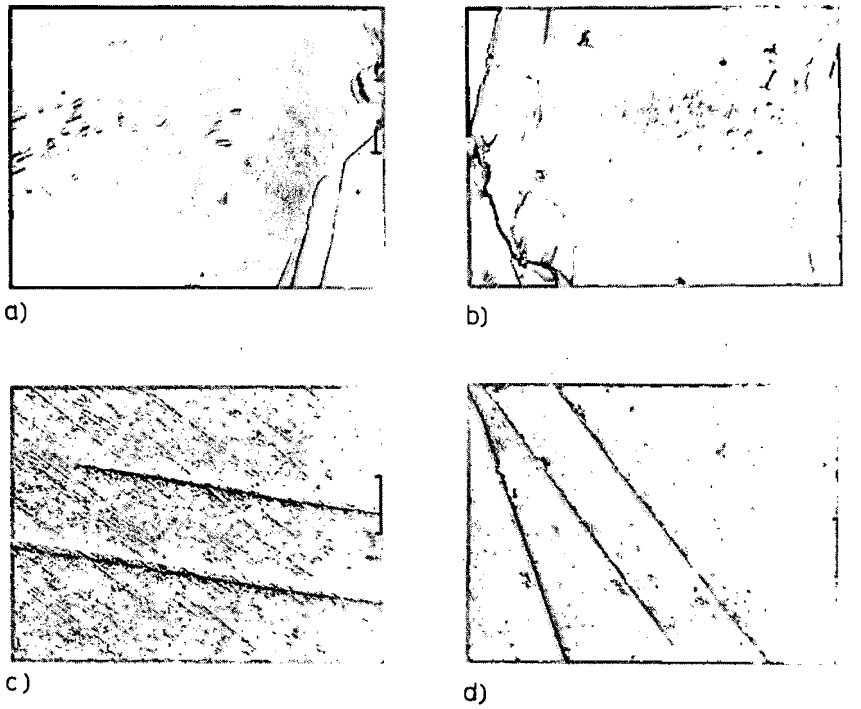


Fig. 14

Fracture surface replicas before and after irradiation

(a) normal transgranular fracture pattern before irradiation
(b) showing partially intergranular fracture after irradiation to 7.9×10^{17} n/cm^2
(c) showing tips of UC_2 needles before irradiation
(d) as (c) after irradiation to 1.4×10^{17} n/cm^2

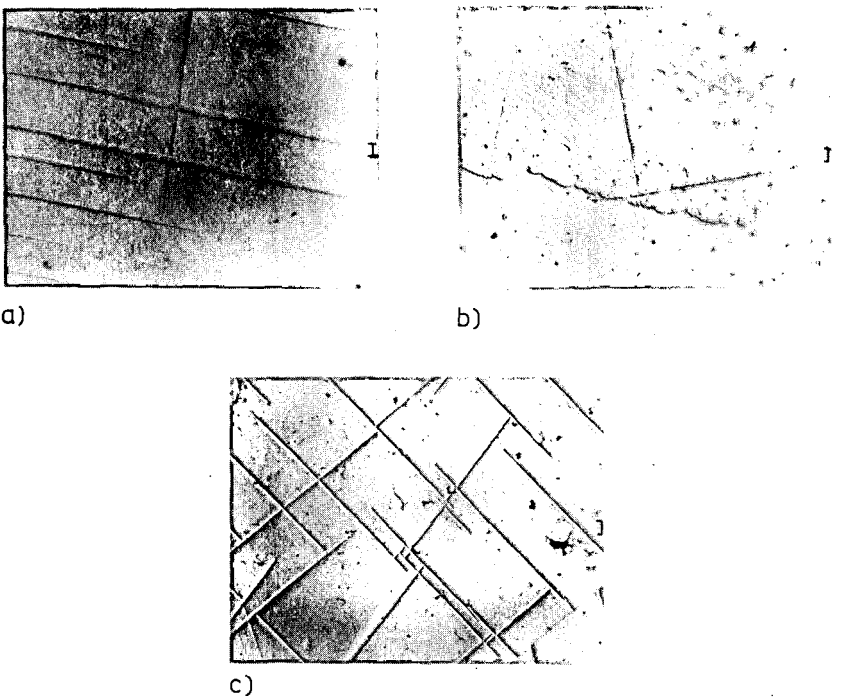


Fig. 15

Internal microstructure of specimens after irradiation and annealing

(a) specimen 53 before irradiation
(b) specimen 53 after irradiation to 8.2×10^{18} n/cm^2 and annealing up to 1000°C
(c) specimen 59 after irradiation to 7.8×10^{17} n/cm^2 and annealing for 5 h at 1000°C

and unannealed) were also apparently unchanged in structure. No explanation of the changes in 53 is possible at the present time.

4. DISCUSSION

Uranium carbide behaves, in its electronic properties, in a typically metallic fashion. Thus, its electrical resistivity is relatively low (roughly equal to that of Zr, U and Hf) and increases with temperature while its thermal conductivity obeys the Wiedemann-Franz relation and is correspondingly high. Its electronic specific heat and paramagnetic susceptibility are also high, suggesting a high density of electron states at the Fermi surface.

In these circumstances it is, perhaps, surprising that the limiting resistivity-increases on irradiation (as shown by our specimens) should be so great when compared to those normally found (see Table IV) for metals irradiated at about 80°C. The differences are marked even in comparison with uranium and its alloys in which the lattice damage responsible for the resistivity increase is produced, as in UC, by fission-fragment bombardment.

TABLE IV

INCREASE IN RESISTIVITY OF METALS AND ALLOYS ON IRRADIATION

Metal	Reference	Maximum exposure		T_i (°C)	T_m (°C)	Resistivity increase (%)	Comments
		(n/cm^2)	(at. % U burn-up)				
Cu	[18]	6×10^{20}		90	20	9.5	For all metals the resistivity change is relatively insensitive to exposure over the range $(2-6) \times 10^{20}$ n/cm^2
Ni	[18]	6×10^{20}		90	20	4.5	
αTi	[18]	6×10^{20}		90	20	7.5	
αZr	[18]	6×10^{20}		90	20	6.4	
αFe	[18]	6×10^{20}		90	20	9.1	
Mo	[18]	6×10^{20}		90	20	22.7	
Mo	[19]	1.8×10^{19}	("fast" flux)	30	0	15	
W	[19]	1.8×10^{19}	("fast" flux)	30	0	24	
Pt	[21]	2×10^{20}	(E > 1.2 keV)	50	-196	36	
αU	[15]	1.6×10^{18}	7×10^{-4}	?	-196	6	Resistivity change saturates below 9×10^{-5} at. % burn-up.
γ(U-20 at. % Mo)	[20]	2.9×10^{19}	4×10^{-1}	45	45	-2.4	Resistivity change saturates below 5×10^{-3} at. % burn-up.
γ(U-22 at. % Nb)	[22]	2.7×10^{20}	1.2×10^{-1}	132 - 167	20	4.0 max	Resistivity rises to a maximum at 9×10^{-2} at. % burn-up and then decreases to less than its original value.
					-196	2.0 max	

TABLE IV (cont.)

Metal	Reference	Maximum exposure (n/cm^2)	Maximum exposure (at. % U burn-up)	T_i (°C)	T_m (°C)	Resistivity increase (%)	Comments
ϵ U_3Si	[22]	3.6×10^{20}	1.4×10^{-2}	94 - 242	20 -196	40 240	Temperature coefficient of resistivity is changed by irradiation. Change saturates below 3.8×10^{-2} at. % burn-up.

Note: The neutron exposure figures relate to thermal flux unless otherwise stated, T_i and T_m are, respectively, the temperatures of irradiation and measurement.

There appear to be three main reasons for this. First, because of the relatively high melting point of UC (2400°C) there will be a tendency for lattice defects to be relatively less mobile at a particular temperature in UC than in most metals. For a given damage rate this will produce a higher equilibrium defect concentration and, correspondingly, a higher resistivity increment. Thus, the two high-melting-point metals, Mo and W, in Table IV both show relatively large resistivity increases on fast-neutron irradiation.

Secondly, because it contains two types of atom on separate sub-lattices, the UC structure can be disordered in several ways additional to those possible in a simple monatomic metal. Not only may single vacancies and interstitial atoms, or simple groupings of these, be formed but it is also possible for the ordered distribution of C and U atoms on the lattice sites to be disarranged so that some U atoms occupy C lattice sites and vice-versa. An additional resistivity increment will be associated with this disorder.

This effect has been demonstrated for ordered alloys such as Cu_3Au in which it is possible to retain a disordered structure by quenching from a high temperature. Resistivity increases of up to 120% were found by SIEGEL [12] for ordered Cu_3Au after exposure at 50°C to 3.3×10^{19} fast-neutrons/cm^2. In contrast, initially disordered Cu_3Au showed increases of less than 1% after the same exposure.

The behaviour of beta brass (40 at.% Zn, 60 at.% Cu) is even more interesting since the tendency to order in this alloy is so great that it has not been found possible to retain, even at room temperature, the disordered structure obtained by quenching. EGGLESTON and BOWMAN [13] obtained a 90% resistivity increase after irradiation at -100°C with 33 MeV alpha particles, which was attributed to the creation of disorder. The increase annealed out at -40°C.

A third possible reason for the behaviour of UC may arise from the nature of its bonding which, though partly metallic, still shows certain characteristically covalent features. Any tendency to bond-directionality (particularly by the carbon atoms) may well result in changes in the degree of overlap of the electron clouds from adjacent atoms when the local atomic arrangement is disturbed. This, in turn, would change the conduction-electron density and, more generally, the shape of the electron energy band. In this way the intrinsic resistivity of the material would be affected irrespective of additional changes due to electron scattering by defects. Further experiments are needed before the relative magnitudes of these three effects can be assessed.

Even larger resistivity increases than those in our experiments have been found in arc-melted carbon-rich UC by workers [11] at the Battelle Memorial Institute. Their values ranged from 170% at 0.01 at.% U burn-up (equivalent to 2.4×10^{19} n/cm^2 for natural UC) to 195% at 0.18 at.% U burn-up. In marked contrast, however, very much smaller increases – less than 3% at 10^{18} n/cm^2 – have been found by GRIFFITHS [14] for reaction-sintered UC specimens irradiated below 70°C. These specimens, produced by heating cold-pressed mixtures of the elemental powders, were porous (about 91% theoretical density) and contained regions of incomplete reaction, both free

uranium and graphite being present. The average grain size was 20 μm compared with 50-400 μm for our tungsten-free specimens.

The small resistivity increase is probably connected with these structural features and with the high dislocation concentration expected to accompany them since, by acting as sinks for the continuous annihilation of the radiation-induced defects, they should prevent the defect concentration building up to levels as large as those in our specimens.

Considering our results in detail, one feature requiring explanation is the relatively small resistivity increase shown by the uranium-rich specimens compared with that for the carbon-rich specimens. It might be argued that this reflects the smaller resistivity change in uranium itself since P would be expected to vary in some fashion from 6% for pure U [15] to 156% for slightly carbon-rich UC. Some doubt is thrown on this simple explanation, however, by the suppression or even reversal of the effect in the tungsten-containing specimens.

An alternative possibility follows from the work of WILLIAMS et al. [16] on the variation with composition of the UC lattice parameter in arc-melted uranium-carbon alloys. The parameter, for specimens in the "as melted" condition, remained constant at 4.9600 Å as the alloy's carbon content was reduced from 7.0 to 4.85 wt.% (cf. UC composition of 4.80 wt.% C). Below this composition, the parameter fell to a minimum of 4.9520 Å at 3.8 wt.% C before rising again to 4.9562 Å at 2.4 wt.% C.

Annealing the specimens at 1300°C increased the parameter for compositions below 4.85 wt.% C, that for the higher carbon contents remaining unchanged. However, even after annealing for 88 h, the parameter at 3.8 wt.%C (4.9578 Å) was still low.

These results were taken by Williams et al. as evidence for the high temperature solubility of uranium in UC, the uranium being, at least partially, retained in solution on quenching to room temperature. Nothing is known at present about the lattice defect structure of these solutions but, whatever this should be, it is likely to affect their irradiation behaviour. For example, an excess concentration of carbon vacancies would reduce the resistivity increment by providing sinks at which the carbon interstitials, created by irradiation, could be annihilated.

The above observations suggest that the low parameter values for specimens 43 and 66 in our experiment also resulted from solution of some of the excess tungsten or uranium in the UC phase, the cooling rate, following the 1700°C anneal, being too rapid for the solutions to achieve their equilibrium room-temperature concentrations. If this is so, the relatively small parameter increases of these specimens on irradiation and also the correspondingly small resistivity increases for the uranium-rich and the tungsten-containing specimens, were most probably due to the associated initial defect structure of their UC matrices.

This hypothesis also explains why the percentage resistivity changes were not directly related to carbon content over the whole range from 4.5 to 5.4 wt.% C, the increases in the UC_2 containing specimens being apparently independent of the composition. The freedom of UC from quenching defects for solutions above 4.85 wt.% C would result in the carbon-rich specimens behaving similarly on irradiation – at least up to concentrations at which their UC_2 content began to have some effect.

Another interesting feature of our results concerns the equation governing the increase in P with exposure. Many properties of fissile materials change on irradiation according to a relation of the type

$$P = P_\infty \, (1 - \exp[-a\Phi]), \tag{1}$$

where Φ is the exposure and a is a constant with the dimensions of area. It is usually assumed that this behaviour results from each fission fragment damaging a certain sharply defined volume of the material to saturation. In this case, further accumulation of damage in the specimen as a whole ceases once every part of it has been crossed once by the damage volume of a fission fragment. To test this assumption for our data, values of the left hand side of the equivalent relation

$$\log\left(\frac{P_\infty}{P_\infty - P}\right) = a\Phi$$

were plotted against Φ (see Fig. 16), the P_∞ value for each specimen being taken as equal to the limiting P value above 5×10^{18} n/cm^2. The curve drawn through the points on Fig. 16 is taken from Fig. 17 where the resistivity results are plotted in the reduced form of P/P_∞ as a function of log Φ.

It is apparent from Fig. 16 that Eq. (1) is obeyed very well up to about 2×10^{17} n/cm^2 but that it fails above this, the measured P values not tending

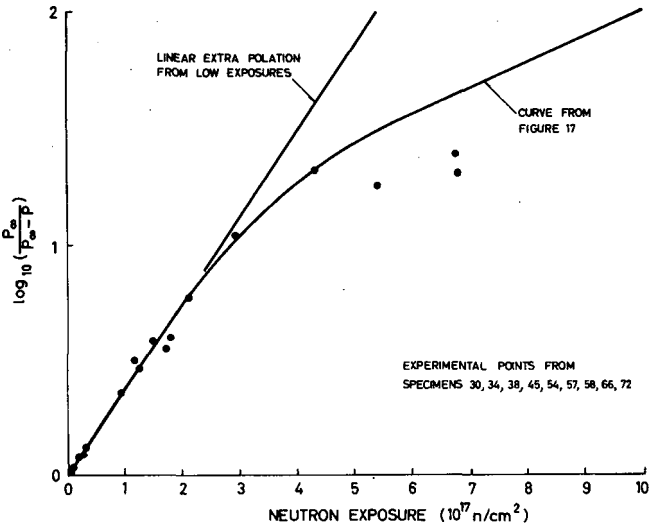


Fig. 16

Variation of $\log_{10}\{P_\infty/(P_\infty - P)\}$ with exposure

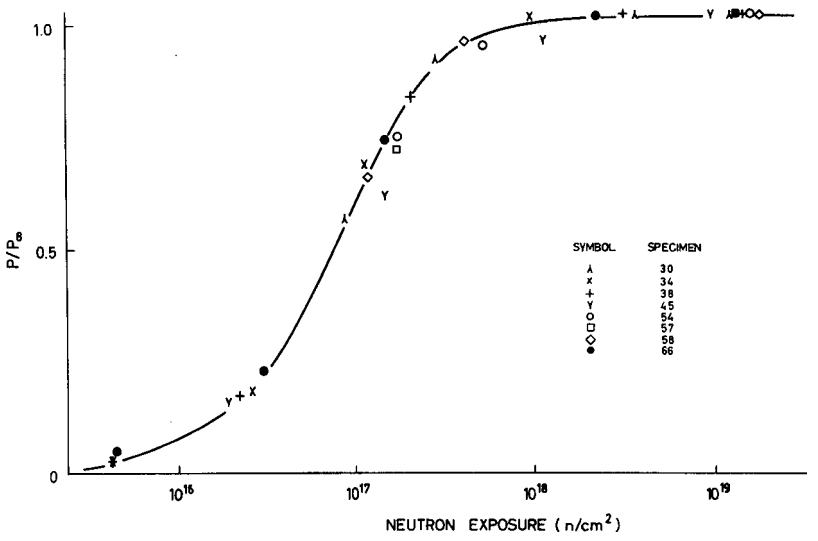


Fig. 17

Variation of normalized resistivity (P/P_∞) with exposure

sufficiently rapidly to P_∞. One possible explanation for this is that the resistivity increase is actually a two stage effect with

$$P = A_\infty (1 - \exp[-a\Phi]) + B(\Phi), \qquad (2)$$

in which the individual terms increase to limiting values A_∞ and B_∞ at about 5×10^{17} and 5×10^{18} n/cm^2 respectively. Below 10^{-17} n/cm^2, B would be negligible and would be P small enough for A_∞ to be replaced by P_∞ without serious error. Eq. (2) would then reduce to Eq. (1) as required.

If this explanation were correct it would be logical to expect the defect configurations associated with stages A and B to be different and thus to anneal out at different temperatures in some way dependent on exposure. The behaviour of the two annealing stages, however, is independent of exposure, implying rather that the corresponding defects are created simultaneously in constant ratio to each other.

It is likely, therefore, that the above explanation is not the correct one and that each fission fragment does not in fact damage a sharply defined region in UC to saturation. Each part of the specimen may have to be crossed several times by fragments before local defect saturation is achieved.

The annealing behaviour of our specimens differs from that found by GRIFFITHS [14] for reaction-sintered UC. In his specimens the resistivity increments annealed out (1 h anneals) in two very sharply defined stages at 120 and 720°C, instead of in relatively wide stages at 150 and 510°C as

found by us. Moreover, only 30% of the increment annealed out in the low temperature stage compared with 70% in our specimens. These differences are probably connected with the differences in irradiation behaviour already referred to.

ADAM [17] has found that the lattice parameter increment in UC anneals out in two or possibly three stages. Approximately 60% is removed in the range 80-150°C and 30% in the range 500-600°C, the remaining 10% of the increment being left unannealed at 600°C. These annealing temperatures and fractions correspond quite well to those found for our specimens. Moreover in Adam's specimens, like ours, the stages are relatively broad.

As mentioned in section 3.2, we have observed some differences, mainly slight, in the annealing behaviour of individual specimens. The incomplete annealing of specimen 53 was apparently due to the breaking up of the UC_2 structure and the associated formation of micro-cracks. However since 53 behaved normally on irradiation (cf. with 54 and 57) these changes probably occurred progressively during the annealing. Further work is required to discover the reasons for them.

The over-annealing of the tungsten-containing specimens was probably due to a change on irradiation in the state of distribution of the tungsten atoms in the UC lattice. The specimens were annealed before irradiation at much higher temperatures than those reached afterwards, so that an explanation based on thermal annealing alone is not valid. It is possible that some of the dissolved tungsten atoms may have aggregated as a result of the migration of lattice defects on annealing, the effect per atom on the resistivity being, no doubt, smaller for atoms in clusters than for those dispersed in solution.

5. CONCLUSIONS

The main conclusions of the work so far may be summarized as follows:

(1) Increases of up to 160% in electrical resistivity occur for UC specimens irradiated at low temperatures to exposures up to 1.6×10^{19} n/cm^2 (0.006 at.%U burn-up). These increases are somewhat greater for specimens containing UC_2 than for those containing free uranium.

(2) The form of the increases is not consistent with the simple model, apparently valid for other fissile materials, in which each fission fragment is assumed to damage to saturation a well-defined volume of the specimen.

(3) The lattice parameters of the specimens also increased, $\Delta a/a$ rising to 1.5×10^{-3} at 4.9×10^{17} n/cm^2. Again, the change for a UC_2-containing specimen was greater than that for one containing free uranium.

(4) The effect of tungsten impurity is to suppress the additional changes in the UC_2-containing specimens. It is believed that both this effect and the smaller changes for the uranium-rich specimens are associated with the UC defect structures due to uranium or tungsten in solution in the lattice.

(5) On annealing, the original resistivity value is recovered, almost completely, in two stages (for 5 h anneals) centred at 150 and 510°C. The fractional recovery in the two stages seems to be independent of exposure at least between 3.5×10^{16} and 1.6×10^{19} n/cm^2.

(6) With one exception, no major changes in microstructure have been observed in the specimens. The reasons for the disappearance of the UC_2 phase in the exceptional specimen have not yet been established.
(7) Considerable changes occurred at the specimen surfaces both on irradiation and on annealing. These led to the formation of grooves and cracks and to a general roughening of the surface. The extent to which this is an irradiation as opposed to a thermal or corrosion effect is not known at present. On irradiation a tendency towards intercrystalline, as opposed to transgranular, fracture was also observed.
(8) It is not considered profitable at the present time to speculate about the nature of the defects responsible for the property changes.

ACKNOWLEDGEMENTS

We are indebted to Mr. A. Fraser, Metallurgy Division DERE, for metallographic examination of the specimens before irradiation, to members of the Analytical Group DERE under Mr. A. Ross for the chemical analyses and to Mr. J. Rose, DMTR, for preparing specimen replicas for the electron microscope. The irradiations were performed by members of the Operations Group, DMTR under Mr. G. Leet.

We are also most grateful to Dr. R. Hurst, DERE, Mr. J.L. Phillips, Head, Reactor Division DERE and Mr. J.R. Atkinson, Project Manager, DMTR for interest and support in the work.

REFERENCES

[1] HARE, A.W., ALFANT, S., ROUGH, F.A. and SINIZER, D.I., Further Results of Irradiation of Uranium Carbide, Nucl. Sci. Engng 10 (1961) 24.
[2] HARE, A.W. and ROUGH, F.A., The Effect of High-Burnup Irradiation of Massive Uranium Carbide, USAEC Rpt. BMI-1491 (1961).
[3] Proceedings of the uranium carbide meeting held at Oak Ridge National Laboratory, December, 1960 USAEC Rpt. TID-7603 (1960).
[4] FROST, B.R.T., GRIFFITHS, L. and BRADBURY, B.T., Irradiation effect in fissile oxides and carbides at high and low burnup levels, these Proceedings.
[5] MICHIE, G.M. and BROWN, D.J., Experience in arc melting and casting uranium monocarbide, Brit. Ceramic Soc. Conf. on Ceramics in Nuclear Science, AERE Harwell (Nov.1961). To be published in the J. Brit. Ceramic Soc.
[6] RUCKMAN, J.C., SANDERSON, H.M. and PRESTON, R.R., Design and construction of an X-ray diffractometer for the study of α, β, γ – active materials, U.K.A.E.A. Reactor Group (TRC) Rpt. 187 (D) (1962).
[7] LADELL, J., PARRISH, W. and TAYLOR, J., Centre-of-gravity method of precision lattice parameter determination, Acta Crystallographica 12 (1959) 253.
[8] LADELL, J., PARRISH, W. and TAYLOR, J., Interpretation of diffractometer line profiles, Acta Crystallographica 12 (1959) 561.
[9] ROUGH, F.A. and CHUBB, W., Progress in the development of uranium carbide-type fuels, USAEC Rpt. BMI 1488 (1960).
[10] ADAM, J. and ROGERS, M.D., X-ray diffraction studies of fission fragment damage in uranium carbide and nitride, Reactor Sci. Technol. 14 (1961) 51.
[11] FREAS, D.G., AUSTIN, A.E. and ROUGH, F.A., Mechanism of irradiation damage in uranium monocarbide, Paper 105(i) presented at A.S.T.M. Symp. Atlantic City, (June 1961). To be published in the Proc. Amer. Soc. Testing Materials.

[12] SIEGEL, S., Effect of neutron bombardment on order in the alloy Cu_3Au, Phys. Rev. 75 (1949) 1823.
[13] EGGLESTON, R.R. and BOWMAN, F.E., Radiation damage of beta-brass, J. appl. Phys. 24 (1953) 229.
[14] GRIFFITHS, L.B., The effect of irradiation and post-irradiation annealing on the electrical resistivity of uranium, J. nucl. Mat. 4 (1961) 336.
[15] QUÉRÉ, V. and NAKACHE, F., Determination of the volume of a fission spike in uranium, J. Nucl. Mat. 2 (1959) 203.
[16] WILLIAMS, J., SAMBELL, R.A.J. and WILKINSON, D., The variation of unit cell-edge of uranium monocarbide in arc-melted uranium-carbon alloys, J. Less - Common Metals 2 (1960) 352.
[17] ADAM, J., AERE Harwell, private communication.
[18] BRUCH, C.A., McHUGH, W.E. and HOCKENBURY, R.W., Variations in radiation damage to metals, J. Metals 8 (1956) 1362.
[19] KINCHIN, G.H. and THOMPSON, M.W., Irradiation damage and recovery in molybdenum and tungsten, J. nucl. Energy 6 (1958) 275.
[20] BLEIBERG, M.L., Effect of fission rate and lamella specing upon the irradiation - induced phase transformation of U - 9 wt.% Mo alloy, J. nucl. Mat. 2 (1959) 182.
[21] PIERCY, G.R., Point defects in platinum, Atomic Energy of Canada Ltd., Rpt. CRMet - 782 (1958).
[22] BLEIBERG, M.L. and EICHENBERG, J.D., Development and properties of uranium-base alloys corrosion resistant in high temperature water. Part 4. Radiation stability, USAEC Rpt. WAPD - 127, Pt.4(1957).

EFFET DE L'IRRADIATION DANS EL. 3 SUR LES ALLIAGES URANIUM-CARBONE DE COMPOSITION VOISINE DE UC PRÉPARÉS PAR FRITTAGE-RÉACTION SOUS CHARGE

A. ACCARY, R. DARRAS ET R. CAILLAT
CENTRE D'ÉTUDES NUCLÉAIRES DE SACLAY, FRANCE

Abstract — Résumé — Аннотация — Resumen

EFECTO DE LA IRRADIACIÓN EN EL REACTOR EL. 3 SOBRE LAS ALEACIONES URANIO-CARBONO DE COMPOSICIÓN PRÓXIMA A LA DEL UC, PREPARADAS POR SINTERIZACIÓN-REACCIÓN A PRESIÓN. Una barra experimental anular de 280 mm de longitud, por 30 mm de diámetro exterior y 20 mm de diámetro interior, de una aleación de uranio-carbono con un contenido de 4,6 por ciento en peso de carbono, obtenida por sinterización-reacción a presión a 1000°C y sometida a un tratamiento térmico de estabilización a 1200°C, fue irradiada hasta alcanzar un grado de combustión de unos 700 MWd/t en el reticulado del reactor EL. 3.

La temperatura máxima de las probetas se mantuvo próxima a 620°C. A pesar de bruscas variaciones de la temperatura, debidas al cambio de régimen del reactor, se ha podido comprobar, observando la evolución de la temperatura del combustible, que éste soportaba satisfactoriamente el tratamiento.

Los exámenes macro y micrográficos efectuados después de la irradiación han permitido precisar las observaciones realizadas en el curso de la irradiación.

Asimismo, se han calentado hasta 1400°C, en el vacío, pequeñas probetas débilmente irradiadas a una temperatura próxima a la ambiente y se ha medido la velocidad de desprendimiento de xenón-133, determinando así un coeficiente aparente de difusión D'.

Se han comparado muestras preparadas por sinterización-reacción a presión con muestras fundidas por bombardeo electrónico. En estas últimas, la retención de los gases de fisión parece ser más eficaz que en las primeras.

EFFET DE L'IRRADIATION DANS EL. 3 SUR LES ALLIAGES URANIUM-CARBONE DE COMPOSITION VOISINE DE UC PREPARÉS PAR FRITTAGE-RÉACTION SOUS CHARGE. Une barre expérimentale annulaire, de 280 mm de long sur 30 mm de diamètre extérieur et 20 mm de diamètre intérieur, d'un alliage uranium-carbone à 4,6% en poids de carbone, préparé par frittage-réaction sous charge à 1000°C et soumis à un traitement thermique de stabilisation à 1200°C, a été irradiée jusqu'à un taux de combustion d'environ 700 MWj/t dans le réseau du réacteur EL. 3.

La température maximum des éprouvettes a été maintenue voisine de 620°C. Malgré les variations brutales de température dues au changement de régime du réacteur, on a pu se rendre compte, en suivant l'évolution de la température du combustible, que celui-ci a subi ce traitement d'une manière satisfaisante.

Les examens macrographiques ainsi qui micrographiques, après irradiation, ont précisé les observations faites au cours de l'irradiation.

Par ailleurs, on a chauffé à 1400°C, sous vide, de petites éprouvettes faiblement irradiées à une température voisine de la température ambiante, et on a mesuré la vitesse de dégagement du ^{133}Xe, déterminant ainsi un coefficient apparent de diffusion D'.

On a comparé des échantillons préparés par frittage-réaction sous charge et des échantillons préparés par fusion sous bombardement électronique. Ces derniers paraissent mieux retenir les gaz de fission que les premiers.

ДЕЙСТВИЕ ОБЛУЧЕНИЯ В РЕАКТОРЕ EL.3 НА СПЛАВЫ УРАНА-УГЛЕРОДА, ПРИБЛИЖАЮЩИЕСЯ ПО СОСТАВУ К UC, ИЗГОТОВЛЕННЫЕ ПРИ РЕАКЦИИ СПЕКАНИЯ ПОД НАГРУЗКОЙ. Пустотелый экспериментальный топливный стержень длиной 280 мм с внешним диаметром 30 мм и внутренним диаметром 20 мм из углеродно-уранового сплава, содержащего 4,6 вес % углерода, изготовленный при реакции спекания под нагрузкой при температуре в 1000°C, был облучен до степени выгорания приблизительно в 700 мгвт-дней/т в решетке реактора EL.3.

* Mémoire rédigé d'après un travail effectué dans le cadre du contrat USA/EURATOM - 0.12.60.5.RDF [1]

Максимальная температура образцов поддерживалась на уровне 620°. Несмотря на резкие колебания температуры, вызываемые изменением режима реактора, на основании изменения температуры оплива можно убедится, что оно выдержало эту обработку удовлетворительно.

Макро- и микрографический анализы после облучения позволили уточнить наблюдения, сделанные во время облучения.

Помимо этого, были нагреты до 1400°C в вакууме небольшие слабооблученные при комнатной температуре образцы, и была измерена скорость выделения ксенона-133, что позволило определить видимый коэффициент диффузии D' .

Были сравнены образцы, изготовленные при реакции спекания под нагрузкой, с образцами, изготовленными плавлением под действием электронной бомбардировки. Эти последние образцы, по-видимому, лучше удерживают газообразные продукты деления, чем предыдущие.

EFFECT OF IRRADIATION IN EL.3 ON URANIUM-CARBON ALLOYS OF COMPOSITION CLOSE TO THAT OF UC AND PREPARED BY SINTERING REACTION UNDER LOAD. An experimental annular rod (280 mm long, 30 mm external and 20 mm internal diameter), composed of a uranium-carbon alloy (4.6% carbon by weight), prepared by sintering at 1000°C under load and subjected to stabilization heat-treatment at 1200°C, was irradiated to a burn-up of 700 MWd/t in the lattice of the EL.3 reactor.

The maximum temperature of the test pieces was kept in the neighbourhood of 620°. In spite of abrupt variations in temperature, due to the changing operating conditions of the reactor, it was possible by following the changes in the fuel temperature to ascertain that the latter had undergone the treatment satisfactorily.

Macrographic and micrographic examinations after irradiation confirmed and extended the observations made during irradiation.

In addition, small test pieces, which had been weakly irradiated at approximately ambient temperature, were heated to 1400°C in a vacuum and the rate of liberation of xenon-133 was measured, giving a value for an apparent coefficient of diffusion, D'.

Samples prepared by sintering reaction under load and by fusion under electronic bombardment were compared. The latter appeared to retain the fission gases better than the former.

1. INTRODUCTION

Le présent mémoire décrit la méthode expérimentale que nous avons utilisée pour irradier dans le réacteur EL3 à Saclay un barreau préparé par frittage-réaction sous charge, d'alliage uranium-carbone de composition voisine du monocarbure.

Cette irradiation a été faite dans des conditions similaires à celles de l'utilisation éventuelle de ce matériau dans un réacteur de puissance, c'est-à-dire à des températures d'environ 600°C.

Dans une deuxième partie, afin de classer les différents produits aujourd'hui disponibles, des essais préliminaires de libération des gaz de fission à chaud ont été réalisés, après irradiations de petits échantillons d'alliages uranium-carbone, de composition voisine de celle du monocarbure. Ces irradiations ont révélé que, selon toute probabilité, la rétention des gaz de fission par le produit préparé par bombardement électronique est meilleure que celle des produits préparés par frittage-réaction sous charge.

2. IRRADIATIONS DANS EL3

2.1. Techniques d'irradiation

Pour éviter des réactions chimiques entre les alliages uranium-carbone plus riches que UC en carbone et les aciers inoxydables du type 18/8 [2], et compte tenu de la nécessité où nous nous trouvions, cependant, d'opérer

dans une gaine en acier inoxydable, nous avons choisi un alliage uranium-carbone à 4,6% de carbone, c'est-à-dire légèrement moins riche en carbone que la composition stoéchiométrique.

D'autre part, afin de rendre ces irradiations aussi sûres que possible du point de vue du fonctionnement de la pile, nous les avons menées en utilisant une gaine épaisse (1 mm) d'acier inoxydable du type Ugine NS22S; ceci nous a conduits à construire une cartouche en inox réalisée par le Service de technologie du CEN de Saclay, présentant approximativement les cotes normales des cartouches de EL3 et dont le plan est indiqué figure 1.

Comme on le voit sur ce document, le combustible composé d'anneaux empilés constitue un manchon cylindrique, forme que nous avons été amenés à lui donner pour pouvoir atteindre les températures visées et les taux de fission souhaités.

Ces anneaux sont enfilés sur un tube d'alumine qui les maintient en position au cas où l'irradiation entraîne la rupture des pièces de carbure.

On remarque également sur ce plan deux thermocouples, dont l'un indique la température maximum dans l'axe du tube d'alumine, et l'autre la température à l'interface alumine-carbure d'uranium.

Les extrémités du manchon de carbure d'uranium sont isolées des bouchons de la cartouche par des intermédiaires en alumine destinés à éviter une élévation dangereuse de la température de ces derniers.

Comme on peut le remarquer, nous nous sommes efforcés dans la construction de cette cartouche de placer le carbure dans des conditions aussi voisins que possible de celles d'une éventuelle utilisation dans une pile de puissance.

Nous avons donné la forme d'un manchon au combustible, de manière à pouvoir obtenir une température prévue de l'ordre de 600°C au point chaud, dans les limites de possibilités de refroidissement offertes par les canaux de EL3. On sait que dans EL3, le refroidissement d'un élément combustible est fait par circulation d'eau lourde dans l'espace annulaire compris entre celui-ci et la paroi de la cellule constituée par un tube coaxial à l'élément combustible.

2.2. Contrôle du comportement de l'élément combustible en cours d'irradiation

Au cours de cette expérience, nous avons contrôlé à la fois le comportement de la gaine en acier inoxydable et celui du matériau combustible lui-même.

Pour ceci nous avons utilisé une méthode d'analyse thermique. Cette méthode consiste à enregistrer d'une manière continue la température indiquée par les deux thermocouples mentionnés ci-dessus.

En effet, une modification de la nature du contact entre la gaine et le combustible, ou une modification de la géométrie de ce combustible, aurait entraîné des variations des températures indiquées. Donc, dans la mesure où, pour une puissance déterminée de la pile, les températures atteintes sont reproductibles et constantes, on peut conclure que l'élément combustible reste identique à lui-même, au point de vue géométrique et, vraisemblablement, physico-chimique.

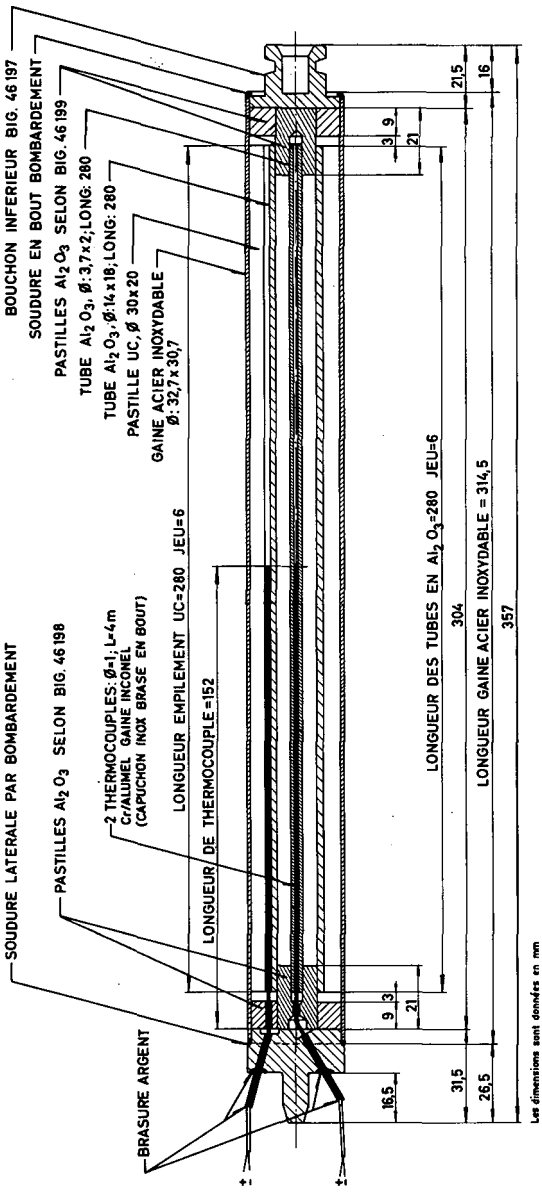


Figure 1

Barreau au carbure d'uranium type EL3

2.3. Contrôle hors pile du comportement de l'élément combustible

L'irradiation, d'une durée totale de 89 jours, a été séparée en deux cycles, l'un de 33 jours et l'autre de 56 jours, entre lesquels nous avons retiré l'élément combustible de la pile et nous l'avons observé par radiographie, ceci dans le but de mettre en évidence les défauts possibles du combustible ou de la gaine.

A la suite de l'irradiation, et après avoir ouvert la cartouche, nous avons observé par micrographie le carbure d'uranium ainsi que l'acier inoxydable de la gaine, et nous avons comparé l'aspect de ceux-ci à celui de ces matériaux avant irradiation.

2.4. Résultats d'irradiation

L'irradiation a été effectuée sous un flux maximum de $4,14 \cdot 10^{13} n/cm^2 \cdot s$ à une température maximum de régime de 620°C, sans jamais dépasser 680°C.

Par suite d'un incident survenu à la pile pendant le deuxième cycle, le flux neutronique a été ramené à $2,96 \cdot 10^{13} n/cm^2 \cdot s$, ce qui a porté la température à 500°C.

Ainsi le taux de combustion total à la fin du deuxième cycle d'irradiation était d'environ 700 MW j/t (évalué d'après la puissance du réacteur).

Nous avons comparé les radiographies effectuées à la fin du premier cycle ainsi qu'à la fin du deuxième cycle à celle effectuée avant irradiation et nous n'avons constaté aucune évolution sensible de l'image obtenue.

En ce qui concerne la température, les graphiques (fig. 2, 3 et 4) montrent que:

A la suite des différents arrêts du réacteur et pour une puissance déterminée de ce dernier, correspond une température du combustible reproductible avec une marge de ± 20°C (température en régime permanent). Il faut remarquer que ces variations de température sont de l'ordre de grandeur de l'incertitude sur la puissance du réacteur, et qu'en conséquence on peut en conclure qu'au cours des deux cycles d'irradiation, aucune modification notable, ni de la gaine, ni du combustible, ne s'est manifestée.

On remarquera que la température indiquée sur le thermocouple axial est supérieure d'environ 100°C à celle qui est indiquée par le thermocouple en contact avec le combustible. Cette différence doit être attribuée à l'échauffement dû aux rayons γ du thermocouple central.

Notons que pendant 7 jours de fonctionnement (fig. 3) à une puissance de 12,5 MW du réacteur, nous avons constaté des oscillations cycliques de température enregistrée par le thermocouple situé à l'interface alumine-carbure d'uranium (alors que le thermocouple central indiquait une température constante).

Nous pensons que ces variations de température étaient dues à des dilatations et contractions successives du carbure et de la gaine en acier inoxydable amenant alternativement un bon puis un mauvais contact entre ces deux matériaux, processus faisant varier les pertes calorifiques et, partant, la température du combustible.

Nous avons constaté à nouveau ce phénomène pendant deux jours pour la même puissance du réacteur, ce qui confirme notre hypothèse explicative

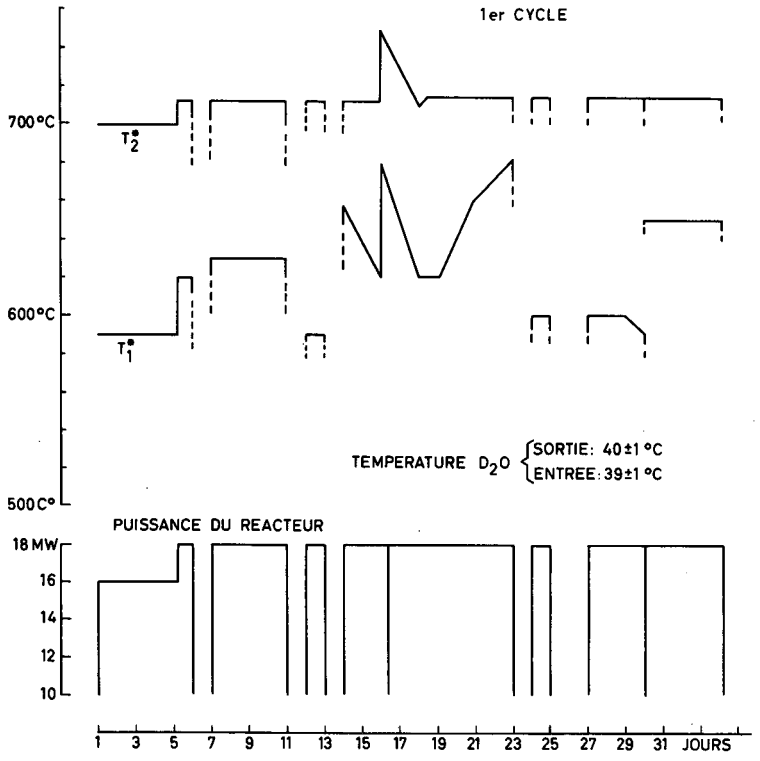


Figure 2

Irradiation du monocarbure d'uranium sous un flux moyen ($\alpha = 0,5$) dans EL3
*T_1 = température sur la paroi intérieure du barreau annulaire de UC.
*T_2 = température au cœur de la cartouche.

puisque, au-dessus de cette puissance, le contact est assuré d'une manière permanente, avec suffisamment d'efficacité, pour proscrire des variations cycliques de température.

Les micrographies (fig. 5 et 5bis) montrent que, comparativement au carbure d'uranium avant irradiation, ce matériau après irradiation a subi un léger grossissement de grain et une régularisation de la forme des joints séparant ceux-ci, indiquant une évolution vers un état d'équilibre physico-chimique plus stable.

Par ailleurs, l'examen de l'acier inoxydable de la gaine n'a pas révélé de modifications profondes de sa structure.

En résumé, la radiographie ainsi que l'analyse thermique et la micrographie s'accordent pour permettre de conclure à un comportement satisfaisant de l'élément combustible pendant l'irradiation que nous avons pratiquée. De plus, les modifications d'aspect micrographique de l'alliage uranium-carbone utilisé indiquent une évolution de celui-ci vers un état thermodynamiquement plus stable. Il faut donc admettre que la température de 500 - 600°C est déjà suffisante pour provoquer une restauration permanente

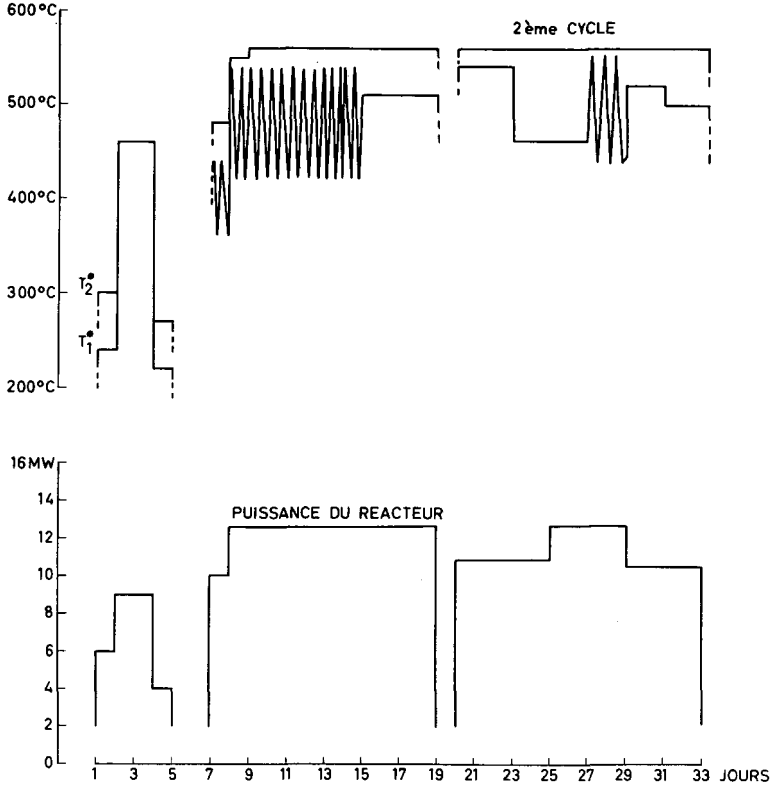


Figure 3

Irradiation du monocarbure d'uranium sous un flux moyen ($\alpha = 0,5$) dans EL3
*T_1 = température sur la paroi intérieure du barreau annulaire de UC.
*T_2 = température au cœur de la cartouche.

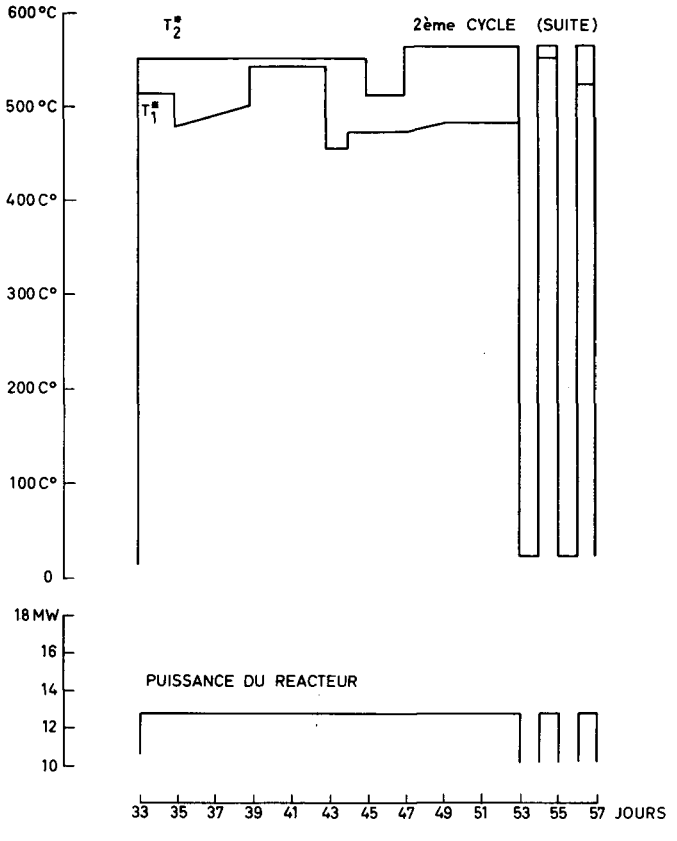


Figure 4

Irradiation du monocarbure d'uranium sous un flux moyen ($\alpha = 0,5$) en EL3
*T_1 = température sur la paroi intérieure du barreau annulaire de UC.
*T_2 = température au cœur de la cartouche.

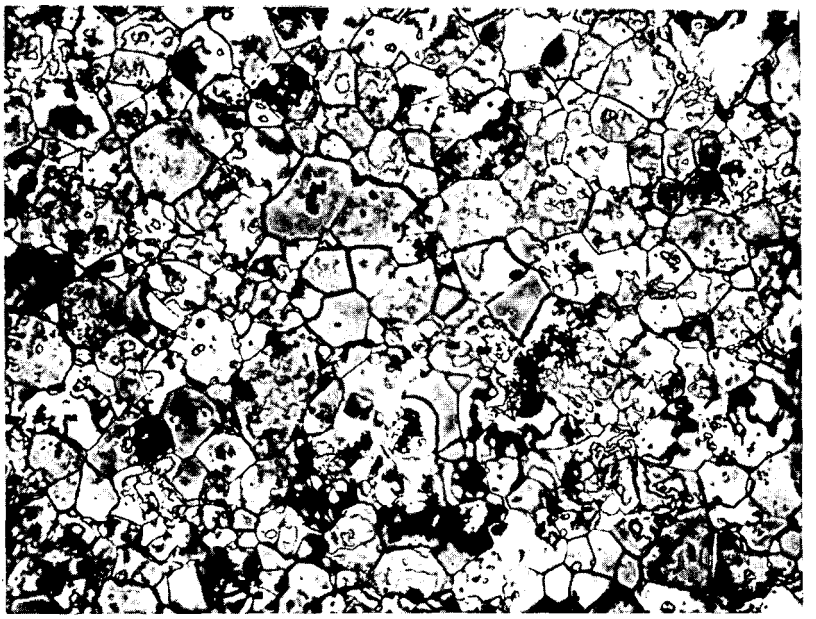


Figure 5

UC(4, 6% de carbone)
avant irradiation.

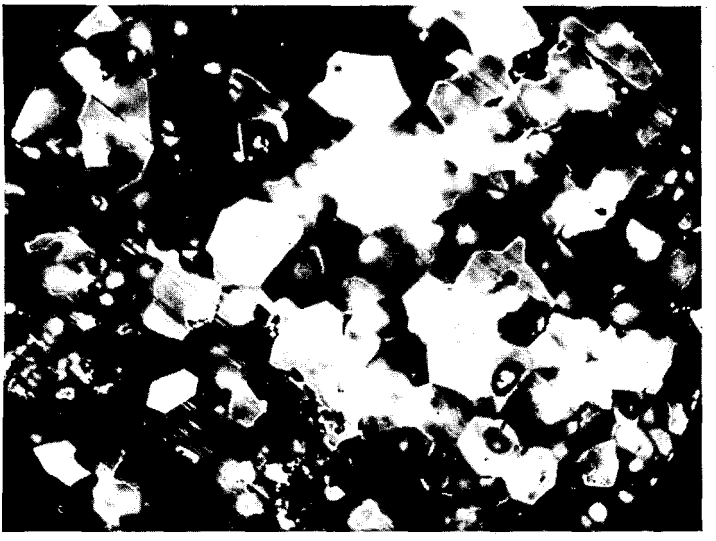


Figure 5bis

UC(4, 6% de carbone)
après irradiation (700 MWj/t).

de la structure du monocarbure d'uranium, lorsque celle-ci est perturbée par les fissions.

3. EXTRACTION DES GAZ DE FISSION APRÈS IRRADIATION

3.1. Principe

Les échantillons d'environ 50 mg sont irradiés dans EL2 à une température voisine de la température ambiante pendant environ une semaine, après quoi ils sont chauffés dans un four à 1400°C et les gaz dégagés entraînés par un courant d'He sont recueillis en permanence (fig. 6).

La quantité de ^{133}Ke est mesurée par comptage à l'aide d'un scintillateur. Elle est rapportée à la quantité totale présente dans l'échantillon. Ceci permet de calculer un coefficient de diffusion apparent D', D' étant relié au coefficient D de diffusion chimique par la relation:

$$D' = \frac{D}{a^2} ,$$

a étant une constante géométrique tenant compte de la structure de l'échantillon [3, 4].

3.2. Résultats de l'extraction des gaz de fission

La méthode expérimentale précédente a été appliquée à des échantillons préparés soit par frittage-réaction sous charge, soit par fusion par bombardement électronique.

TABLEAU I

RÉSULTATS DE L'EXTRACTION DES GAZ DE FISSION

Nature des échantillons	Procédé de fabrication	Repère	D'1400°C
UC:d = 13,4 (lot 27)	Frittage-réaction sous charge	B_2	$1,7 \cdot 10^{-12}$/s
	"	B_3	$5,6 \cdot 10^{-13}$/s
	"	B_4	$1,1 \cdot 10^{-12}$/s
UC:d = 13,5 (lot 30)	Frittage-réaction sous charge	B_5	$2,6 \cdot 10^{-11}$/s
	"	B_7	$2,8 \cdot 10^{-11}$/s
UC:d = 13,6	Fusion par bombardement électronique	B_8	$4,2 \cdot 10^{-14}$/s
"	"	B_9	$1,6 \cdot 10^{-13}$/s

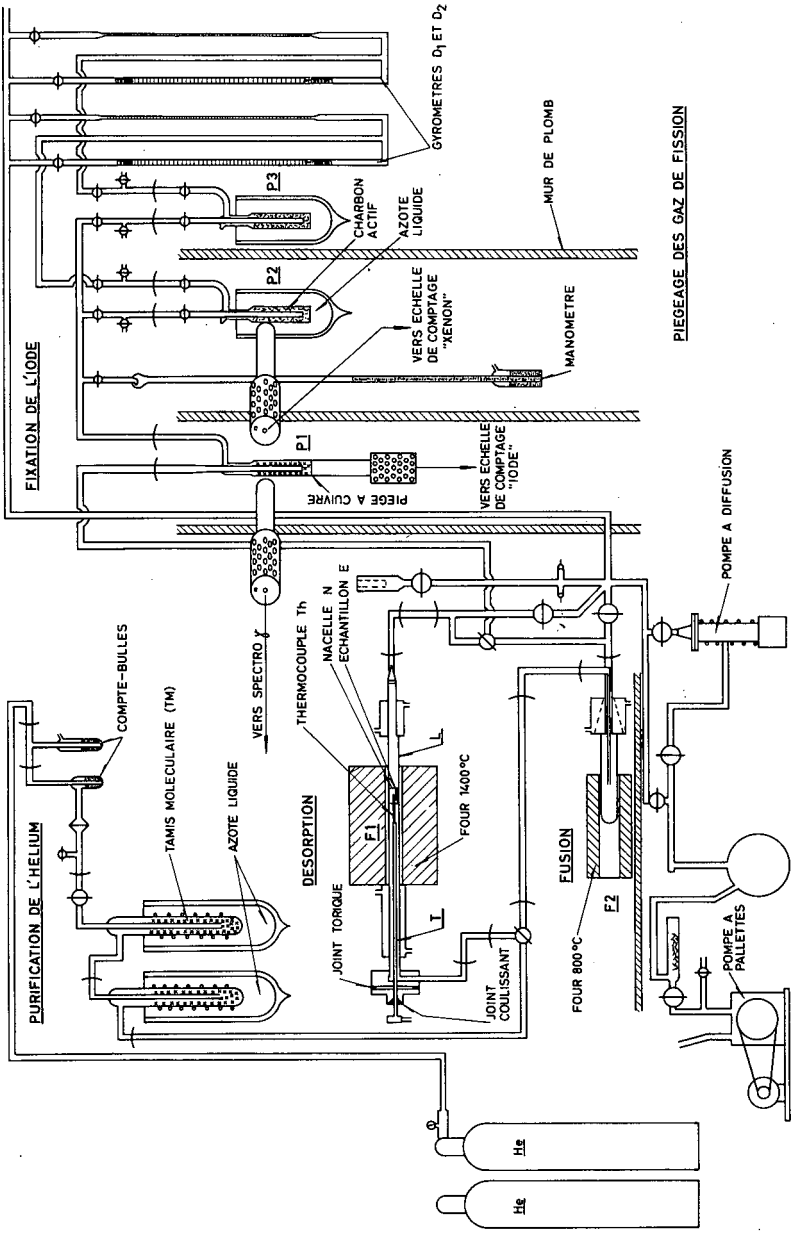


Figure 6

Appareil d'extraction et de recueil des gaz de fission.

Les résultats obtenus pour les deux types d'échantillons sont rassemblés dans le tableau I. Les valeurs D' rassemblées dans celui-ci présentent une dispersion notable. On note qu'elles encadrent celles qui sont déterminées dans les même conditions expérimentales sur le bioxyde d'uranium stoéchiométrique (D' de l'ordre de $6 \cdot 10^{-13}$/s pour une densité de 10,6 g/cm^3) [5]. De plus, on voit que le comportement du monocarbure d'uranium fondu par bombardement électronique paraît sensiblement meilleur que celui du produit obtenu par frittage-réaction sous charge.

Il faudrait peut-être relier la différence de comportement entre le carbure d'uranium préparé par frittage-réaction sous charge et celui préparé par fusion par bombardement électronique, à la différence très importante de la grosseur de grains entre les deux produits. En effet, la taille du grain du produit préparé par fusion par bombardement électronique est telle que chacun des échantillons est pratiquement constitué par un monocristal, tandis que celle du grain du produit préparé par frittage-réaction sous charge est très petite et chaque éprouvette est constituée d'un grand nombre de cristallites séparées par des joints de grain qui peuvent constituer des chemins préférentiels de diffusion du ^{133}Xe.

4. CONCLUSION

Les irradiations dans EL3 à une température comprise entre 500 et 600°C de monocarbure d'uranium à 4,6% de C préparé par frittage-réaction sous charge ont permis de montrer la bonne tenue de ce matériau ainsi que sa compatibilité avec l'acier inoxydable utilisé comme gaine.

Par ailleurs elles ont montré que dans nos conditions expérimentales l'alliage uranium-carbone utilisé évoluait au cours de l'irradiation vers un état structural plus parfait que celui du produit de départ.

Enfin, nos premiers essais sur l'étude du dégagement hors pile à chaud des gaz de fission montrent que le monocarbure d'uranium préparé par frittage-réaction sous charge paraît retenir les gaz de fission sensiblement aussi bien que le dioxyde d'uranium et que le monocarbure d'uranium préparé par fusion par bombardement électronique semble se comporter sous ce rapport d'une manière encore plus satisfaisante.

REMERCIEMENTS

Nous remercions Messieurs Genthon et Goinguenet et Mademoiselle Collet (Service de physique et expérimentation) qui ont fait les calculs neutroniques et thermiques, Madame Vignesoult et Mademoiselle Bazire (LECI) qui ont effectué la micrographie du carbure d'uranium ainsi que Monsieur Berry (Section d'étude de la corrosion par les gaz et par les métaux liquides) qui a dirigé les opérations d'extraction des gaz.

RÉFÉRENCES

[1] ROUSSET, P., Contrat USA/EURATOM - 012.60.5.RDF Rap. trim. n° 1 (1960).
ROUSSET, P. et MANSARD, B., Contrat USA/ EURATOM-012.60.5.RDF Rap. trim. n°2 et 3 (1961), n°4 et 5 (1962)
[2] SINIZER, D.I., TID 7589 (1960)5.

[3] BOOTH, A. and RYMER, G. T., CRDC 720 (1958), Chalk River, Ontario, . CRDC 720- August 1958.
[4] DARRAS, R. et BERRY, J.L., Industries atomiques, 3(1961)83.
[5] BERRY, J., DARRAS, R. et CHEVILLIARD, H., Communication personelle.

IRRADIATION BEHAVIOUR OF URANIUM CARBIDE FUELS

D. I. SINIZER, B. A. WEBB AND S. BERGER
ATOMICS INTERNATIONAL, CANOGA PARK, CALIFORNIA

Abstract — Résumé — Аннотация — Resumen

IRRADIATION BEHAVIOUR OF URANIUM CARBIDE FUELS. Arc-cast uranium-carbon fuels near stoichiometric UC in composition have been irradiated in sodium or NaK-bonded stainless-steel capsules at centre temperatures to 1950°F (1065°C) [average temperature to 1750°F (950°C)] to burn-ups of 25 000 MWd/MTU. Stoichiometric and slightly hyperstoichiometric fuels show approximately linear increase in diameter with burn-up to 25 000 MWd/MTU. At 1500°F (815°C) average centre temperature, diameter increase is less than 3% after 25 000 MWd/MTU and correspondingly lower at low fuel temperature. At 1000°F (540°C) average temperature, observed volume change is about equal to the change expected from fission product accumulation. Fission-gas release is estimated at less than 1% after 25 000 MWd/MTU at 1700°F (926°C) centre temperature. This is extrapolated from experimental data up to 15 000 MWd/MTU at 1700°F (926°C). Transfer of carbon from hyperstoichiometric U-C fuel to stainless-steel cladding across the sodium bond has been observed in both in-pile and out-of-pile experiments. There is no evidence in our view to support the possibility of irradiation-induced acceleration of the carbon transfer process.

Two mechanisms appear to be operative simultaneously. At temperatures above 1000°F (540°C) the UC_2 phase is selectively attacked by sodium or NaK, removing a carbon atom which goes into solution in the Na, and then transforming the body-centred tetragonal UC_2 to face-centred cubic UC. Voids are left at sites formerly occupied by the lower-density UC_2 phase. This process is clearly evident in out-of-pile isothermal compatibility tests and is the rate-controlling step in carbon transfer to the cladding. Under irradiation there is evidence of diffusion occurring in the UC phase which results in healing of the voids at former UC_2 sites. This healing is thought to be accelerated by the compressive stress in the fuel induced by the extreme temperature gradient during irradiation. The result is a void-free, single-phase microstructure in the decarburized region of the originally hyperstoichiometric fuel. No carbon transfer is observed with hypostoichiometric U-C.

Carbon removed from hyperstoichiometric U-C fuel is readily transferred across the Na bond to carburize stainless-steel cladding in both in-pile and out-of-pile experiments. This transfer represents a possible limitation of choice of fuel composition for Na-bonded stainless-steel-clad elements. Nevertheless, available data lead to the present conclusions that stoichiometric or hyperstoichiometric U-C Na-bonded to stainless steel can be effectively used in Na-cooled power reactors. Fission-gas release or fuel swelling do not represent limitations under presently conceived Na-cooled reactor conditions. Alternative cladding materials such as Cb alloys or gas-bonded fuel elements may be required for ultra-high-temperature applications.

COMPORTEMENT DES CARBURES D'URANIUM SOUS L'EFFET DE L'IRRADIATION. Des combustibles UC ayant une composition quasi stoechiométrique, obtenus par fusion à l'arc électrique et enfermés dans des gaines en acier inoxydable avec lien de sodium ou de NaK, ont été irradiés à des températures au centre allant jusqu'à 1950°F (1065°C) [température moyenne: 1750°F (950°C)] et des taux de combustion allant jusqu'à 25 000 MWj/t d'U. Les combustibles stoechiométriques et légèrement hyperstoechiométriques accusent une augmentation à peu près linéaire du diamètre pour des taux de combustion allant jusqu'à 25 000 MWj/t d'U. Pour une température au centre moyenne de 1500°F (815°C), l'augmentation de diamètre est inférieure à 3% au-dessus de 25 000 MWj/t d'U; elle est proportionnellement moindre losque la température du combustible s'abaisse. A la température moyenne de 1000°F (540°C), on observe une dilatation qui est à peu près égal à celle que l'on peut prévoir du fait de l'accumulation des produits de fission. La libération des gaz de fission est estimée à moins de 1% au-dessus de 25 000 MWj/t d'U, pour une température au centre de 1700°F (926°C). Ce chiffre est obtenu par extrapolation des données expérimentales pour des taux de combustion allant jusqu'à 15 000 MWj/t d'U, à la même température. Dans des expériences en pile et hors pile, on a constaté qu'une certaine quantité de carbone du combustible hyperstoechiométrique UC passe, à travers le lien de sodium, dans la gaine en acier inoxydable. De l'avis des auteurs, rien ne prouve que le processus de transfert du carbone soit accéléré par l'irradiation.

Deux mécanismes semblent entrer en jeu simultanément. A des températures supérieures à 1000°F(540°C), la phase UC_2 est attaquée en préférence par le sodium ou le NaK; de ce fait, il y a perte d'un atome de carbone, qui se dissout dans le Na, et transformation de UC_2 tétragonal à mailles centrées en UC cubique à faces centrées. Il reste des lacunes dans les sites précédemment occupés par la phase UC_2 à faible densité. Ce processus est très net dans les essais hors pile de compatibilité isothermique: il permet de déterminer le transfert de carbone dans la gaine. Sous l'effet de l'irradiation, on peut observer dans la phase UC une diffusion qui a pour résultat la«guérison»des lacunes dans les anciens sites de UC_2. On pense que cette guérison est accélérée par l'effort de compression du combustible, résultant du gradient de température maximum pendant l'irradiation. Il en résulte une microstructure en phase simple, sans lacunes, dans la région décarburée du combustible initialement hyperstoechiométrique. Aucun transfert de carbone n'intervient pour le UC hypostoechiométrique.

Dans les expériences en pile comme dans celles hors pile, le carbone détaché du combustible UC hyperstoechiométrique traverse aisément le lien de Na, pour carburer la gaine en acier inoxydable. Ce transfert impose peut-être une limitation dans la composition du combustible devant être contenu dans des gaines en acier inoxydable avec lien de Na. Néanmoins, les données dont on dispose actuellement permettent de conclure que le combustible UC stoechiométrique ou hypostoechiométrique, dans une gaine en acier inoxydable avec lien de Na peut être efficacement utilisé dans les réacteurs de puissance refroidis au sodium. La libération des gaz de fission et la dilatation du combustible ne constituent pas des limitations pour les réacteurs refroidis au sodium tels qu'ils sont conçus actuellement. D'autres matériaux de gainage, tels que des alliages de Cb, ou des cartouches de combustible avec lien gazeux pourront être nécessaires pour les températures très élevées.

ПОВЕДЕНИЕ УРАНО-КАРБИДНОГО ТОПЛИВА ПРИ ОБЛУЧЕНИИ. Топливный стержень в виде литой дуги из урана-углерода, близкий по своему строению к стехиометрическому UC, подвергался облучению в натриевой или NaK-смеси, заключенной в капсулу из нержавеющей стали при температурах в центре 1065° (средняя температура 950°C) при выгорании 25 000 мгвт-дней/т. Стехиометрическое и слегка гиперстехиометрическое топливо показывает приблизительное линейное увеличение в диаметре с выгоранием до 25 000 мгвт-дней/т. При средней температуре в центре (815°) увеличение диаметра происходит менее чем на 3% после 25 000 мгвт-дней/т и соответственно еще меньше при низких температурах топлива. При средней температуре в 1000°F (540°C) наблюдаемое изменение в объеме почти равно изменению, происходящему при аккумуляции продуктов деления. Высвобождение газообразных продуктов деления едва достигает 1% после 25 000 мгвт-дней/т при температуре в центре 926°C. Такой расчет экстраполирован из экспериментальных данных при 15 000 мгвт-дней/т и при температуре 926°C. Перенос углерода из гиперстехиометрического топлива U-C в оболочку из нержавеющей стали через диффузионный слой натрия наблюдался в опытах как внутри реактора, так и вне реактора. По нашему мнению, нет данных, подтверждающих возможность ускорения процесса переноса углерода путем облучения.

Представляется, что два механизма должны действовать одновременно. При температурах выше 540°C Na или NaK селективно реагируют с UC_2, удаляя атом углерода, который растворяется в Na, и преобразуя объемно-центрированный тетрагональный UC_2 в гренецентрированный кубический UC. Образуются пустоты в местах, прежде заполненных фазой UC_2 низкой плотности. Этот процесс совершенно очевиден в опытах по изотермической совместимости вне реактора, и он дает возможность регулировать скорость переноса углерода в оболочку. Доказано, что при облучении происходит диффузия, происходящая в фазе UC, в результате которой идет заполнение пустот в прежних местах UC_2. Думается, что это заполнение должно ускоряться при сжатии топлива, вызываемом высоким температурным градиентом во время облучения. В результате получается свободная от пустоты однофазная микроструктура в обезуглероженном районе первоначально гиперстехиометрического топлива. В гиперстехиометрическом UC не наблюдается переноса углерода.

Углерод, удаленный из гиперстехиометрического топлива UC, легко переносится через диффузионный слой Na в науглероженную оболочку из нержавеющей стали, что подтверждается опытами внутри и вне реактора. Этот перенос представляет некоторое ограничение в выборе состава топлива для элементов, покрытых нержавеющей сталью и имеющих диффузионный слой Na. Тем не менее, на основе имеющихся данных можно сделать вывод, что стехиометрическое или гиперстехиометрическое топливо UC с диффузионным слоем Na в нержавеющей стали может эффективно использоваться в энергореакторах с натриевым охладителем. Высвобождение газообразных продуктов деления или набухание топлива не ограничивает понимание существующих условий в реакторе с натриевым охлаждением. Другие материалы,

пригодные для оболочки, такие как сплавы Cb или топливные элементы с газовым диффузионным слоем, могут потребоваться при использовании ультравысокой температуры.

COMPORTAMIENTO DE LOS COMBUSTIBLES DE CARBURO DE URANIO FRENTE A LA IRRADIACIÓN. Los autores irradiaron combustibles de carburo de uranio fundidos al arco, de composición próxima a la del UC estequiométrico, en cápsulas de acero inoxidable con unión térmica de sodio o de aleación sodio-potasio (temperaturas centrales hasta 1065°C, temperaturas medias hasta 950°C), hasta alcanzar grados de combustión de 25 000 MWd/t de uranio. En los combustibles de composición estequiométrica o levemente hiperestequiométrica, se observa que el aumento del diámetro es aproximadamente proporcional al coeficiente de consumo hasta los 25 000 MWd/t de uranio. Cuando la temperatura media en el centro alcanza a 815°C, el diámetro aumenta en menos de 3 por ciento, al exceder el grado de combustión de los 25 000 MWd/t de uranio, y disminuye en proporción al decrecer la temperatura del combustible. A una temperatura media de 540°C, la variación de volumen observada es aproximadamente igual a la que la acumulación de productos de fisión debería producir teóricamente. El desprendimiento de gases de fisión se evalúa en menos del 1 por ciento, cuando se superan los 25 000 MWd/t de uranio, a una temperatura central de 926°C. El mencionado valor se obtiene por extrapolación, partiendo de los datos experimentales obtenidos hasta los 15 000 MWd/t de uranio, a 926°C. Tanto en los experimentos realizados en el reactor como fuera del mismo, se ha observado transporte de carbono del combustible de UC hiperestequiométrico hacia el revestimiento de acero inoxidable, a través de la unión térmica de sodio. A juicio de los autores, no hay ningún indicio que confirme la suposición de que el proceso de transporte de carbono pueda ser acelerado por la irradiación.

Al parecer, dos mecanismos intervienen simultáneamente. A temperaturas superiores a los 540°C, el sodio, o la aleación sodio-potasio, atacan selectivamente la fase UC_2 , expulsando un átomo de carbono que pasa a disolverse en el sodio y dando lugar a la transformación del UC_2 tetragonal centrado en el cuerpo en UC cúbico centrado en las caras. En los lugares ocupados previamente por la fase UC_2, de menor densidad, quedan los huecos respectivos. Este proceso se manifiesta claramente en los ensayos de compatibilidad isotérmica efectuados fuera del reactor y constituye el factor que regula la velocidad del transporte del carbono al revestimiento. En el curso de la irradiación, hay indicios de que tiene lugar una difusión en la fase UC, cuya consecuencia es el relleno de los huecos en los lugares ocupados previamente por el UC_2. Se supone que esta recuperación se acelera gracias al esfuerzo de compresión que ejerce sobre el combustible el acentuado gradiente de temperatura durante la irradiación. Como resultado, se tiene una microestructura de fase única, exenta de huecos, en la región decarburada del combustible originalmente hiperestequiométrico. No se registra ningún transporte de carbono cuando la composición del UC es hipoestequiométrica.

El carbono procedente del combustible de UC hiperestequiométrico es transportado fácilmente a través de la unión térmica de sodio, carburando el revestimiento de acero inoxidable, tanto en los experimentos dentro del reactor como en los experimentos fuera del mismo. Este transporte podría imponer una restricción en la elección de la composición del combustible en el caso de elementos revestidos de acero inoxidable con unión térmica de sodio. Con todo, los datos disponsibles permiten llegar a la conclusión de que el UC estequiométrico o hipoestequiométrico, unido al acero inoxidable mediante sodio, puede usarse con buenos resultados en los reactores refrigerados por sodio. El desprendimiento de gases de fisión o el crecimiento del combustible no significan limitaciones, en las condiciones de funcionamiento de los reactores refrigerados por sodio, tal como se los concibe actualmente. Para aplicaciones a temperaturas ultraelevadas, es posible que se necesiten otros materiales de revestimiento, tales como aleaciones de Cb o elementos combustibles con uniones térmicas gaseosas.

1. INTRODUCTION

Results of recent irradiation experiments and out-of-pile studies on arc-cast uranium-carbon alloys near stoichiometric uranium monocarbide in composition have continued to demonstrate the importance of these fuels for high-temperature, high-burn-up reactors. The known physical properties of UC, especially its high thermal conductivity and high uranium density compared to competitive refractory fuels, make it important for high-temperature reactors, particularly the large sodium-cooled reactors capable of delivering steam at temperatures up to 1050°F (567°C). The high

thermal conductivity of uranium carbide permits the fuel in the form of relatively large diameter rods to match the heat-transfer capability of the sodium coolant without reaching excessive central temperatures.

Irradiation stability and fission-gas retention are significant fuel parameters in the design of power reactors. A basic understanding of these parameters at temperatures and burn-ups of interest to power reactor design is the objective of the U-C development programme at Atomics International. In this integrated programme, out-of-pile physical and mechanical properties of uranium-carbon alloys and their compatibility with cladding, fuel-element bonding media and reactor coolants are being determined. Understanding of irradiation stability and the behaviour of fuel materials are being established for a wide range of temperature and burn-up conditions. Knowledge of irradiation behaviour determined from small-scale capsule experiments permits scale-up to irradiation behaviour of prototype fuel elements. As a later step in the fuel development programme, full-scale fuel elements are being designed and fabricated for operation in full-scale reactors such as the SRE*, or the HNPF+. The ultimate goal of the programme is the operation of power reactors with a full core loading of uranium carbide producing electrical power at an economically attractive fuel-cycle cost.

2. U-C IRRADIATION

2.1. Irradiation programme

The first irradiation of arc-cas uranium carbide was made on a series of six capsules irradiated by Battelle Memorial Institute for Atomics International [1]. In these experiments four capsules containing U-C hyperstoichiometric with respect to carbon, one capsule with stoichiometric UC and one capsule with hypostoichiometric U-C were irradiated. The differences between these three types of uranium-carbon alloys are shown in Fig. 1. Hypostoichiometric U-C with less than 4.8 wt.% carbon contains face-centred UC grains with a grain-boundary network of metallic uranium. The amount of free uranium increases as the carbon content decreases below 4.8 wt.%. Stoichiometric UC with 4.8 wt.% carbon contains only equiaxed uranium monocarbide grains. Hyperstoichiometric U-C with more than 4.8 wt.% caroon contains body-centred tetragonal UC_2 platelets located on the (100) faces of the UC grains. In this paper the symbol UC will represent stoichiometric uranium monocarbide, while the symbol U-C (with a hyphen between U and C) will represent uranium-carbon alloys of composition other than stoichiometric.

Pertinent data from these first six capsules labelled BMI 23-1 to BMI 23-6 are listed in Table I [1]. In these experiments, a 5-in (12.7 cm) column of 3/8-in (0.95 cm) diameter fuel, NaK-bonded to Type 304 stainless-steel (18Cr-8Ni) capsules, were irradiated to burn-ups up to 25 000 MWd/t at centre temperatures reaching 1375°F (746°C). Heat flux was at levels

* SRE: Sodium Reactor Experiment; Santa Susana, California

\+ HNPF: Hallam Nuclear Power Facility; Hallam, Nebraska



(a) (b) (c)

Fig.1

Uranium-carbon alloys

(a) 4.40% carbon, free uranium at UC grain boundaries
(b) 4.79% carbon, equiaxed UC grains
(c) 5.20% carbon, Widmanstatten pattern of UC_2 platelets on [100] UC faces

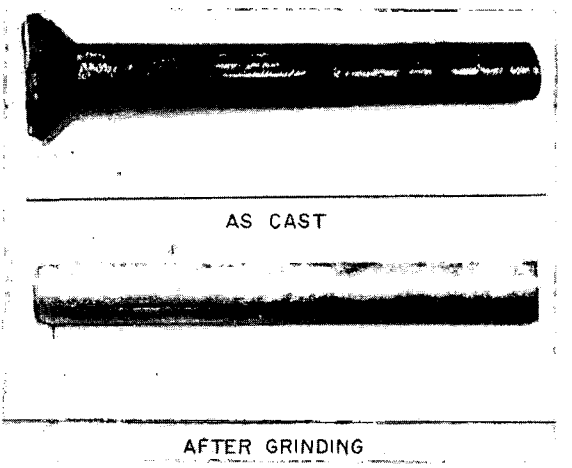


Fig.2

Arc cast UC fuel slug

expected in power reactor fuel elements. Dimensional stability was good and fission gas release was very nearly equal to that released by recoil from the nominal fuel surface. The results of these irradiations are plotted in the graphs of irradiation swelling and fission-gas release in this paper.

More recently, six additional capsule irradiation tests have been completed by Atomics International. Other tests are still in progress. Results of the six completed irradiations are listed in Table II. These capsules contained both hyperstoichiometric and hypostoichiometric U-C with carbon ranging from 4.4 to 5.0 wt.%.

TABLE I

U-C IRRADIATIONS*

Capsule	BMI 23-1	BMI 23-2	BMI 23-3	BMI 23-4	BMI 23-5	BMI 23-6
Test site	MTR	MTR	MTR	MTR	MTR	MTR
Fuel carbon content (wt.%)	5.2	5.3	5.0	5.2	4.6	4.8
Bonding medium	NaK	NaK	NaK	NaK	NaK	NaK
Fuel diameter (in)	3/8	3/8	3/8	3/8	3/8	3/8
(cm)	0.95	0.95	0.95	0.95	0.95	0.95
Fuel length (in)	5	5	5	5	5	5
(cm)	12.7	12.7	12.7	12.7	12.7	12.7
Peak burn-up (MWd/t)	1780	7800	15 700	25 200	8600	6500
Average temp. - Surface (°F)	770	915	765	660	880	950
- Surface (°C)	410	488	407	347	469	510
- Centre (°F)	1300	1375	1 180	1 080	1330	1375
- Centre (°C)	704	746	630	580	721	745
Peak temp. - Surface (°F)	900	1070	800	-	990	1030
(measured) - Surface (°C)	480	575	426	-	532	553
- Centre (°F)	1600	1830	1 550	-	1 420	-
- Centre (°C)	871	999	861	-	771	-
Average surface heat generation ($BTU\ h^{-1}\ ft^{-2}$)	680 000	880 000	750 000	610 000	900 000	600 000
Average surface heat generation (W/cm^2)	215	277	236	192	284	189
Density decrease (%)	0.8	0.6 - 2.0	1.8	3.4	2.4	1.2
Diameter increase (%)	0.4	0.9	0.8	1.4	0.8	0.5
Fission-gas release (% Kr^{86})	0.04	0.04	-	-	0.04	0.04

* Series completed in 1960.

TABLE II

RECENT U-C IRRADIATIONS

Capsule	AI 3 - 1	AI 3 - 4	AI 5 - 1	NAA 48-1	NAA 48-2	NAA 48 - 6
Test site	WTR	GETR	WTR	MTR	MTR	MTR
Fuel carbon content (wt.%)	4.4 - 4.7	4.8 - 5.0	4.8 - 5.0	4.8 - 5.0	4.8 - 5.0	4.8 - 5.0
Cladding	304 SS	NI	304 SS	304 SS	304 SS	304 SS
Bonding medium	Na	Na	NaK	NaK	NaK	NaK
Annulus width* (in)	0.015	0.050	0.005	0.005	0.005	0.015
(cm)	0.038	0.127	0.013	0.013	0.013	0.038
Fuel diameter (in)	0.5	0.5	0.5	0.5	0.5	0.5
(cm)	1.27	1.27	1.27	1.27	1.27	1.27
Fuel length (in)	12	12	18	18	18	18
(cm)	30.48	30.48	45.72	45.72	45.72	45.72
Peak burn-up (MWd/t)	7500	16600	7500	8000	20 000	7000
Peak temp. - Surface (°F)	1540	1190	1000	1000	950	1390
- Surface (°C)	838	633	538	538	510	755
- Centre (°F)	2430	1850	1850	1950	1750	2350
- Centre (°C)	1332	1010	1010	1065	927	1288
Diameter increase (%)	2.5	1.8	0.7	1.7	2.2	3.0
Fission gas release (% Kr^{85})	1.58	0.18	0.06	--	1.3	0.74

* Between fuel and cladding

2.2. Irradiation test procedure

2.2.1. Materials. The U-C listed in Tables I and II was prepared by arc-melting and casting [2]. In this technique, elemental uranium and carbon are melted under vacuum in a direct current arc on a water-cooled graphite hearth. The carbon content of the alloyed buttons is adjusted to allow for some carbon pick-up in the subsequent casting operation. The buttons are arc-remelted in a similar water-cooled hearth with a mould cavity of the proper size below the hearth. The cavity is sealed with a thin carbon diaphragm to prevent the melt from entering the cavity prematurely. When a sufficiently large pool of molten U-C is formed, the diaphragm burns through, dropping the melt into the cavity where it solidifies into a cylindrical slug.

In the irradiation programme summarized in Table II all slugs were 10% enriched and were a nominal 1/2-in (1.27-cm) in diameter. All slugs were irradiated with as-cast surfaces. Casting imperfections on the slug surfaces are acceptable because the Na or NaK, which bonds the fuel to the cladding, fills the surface irregularities and prevents hot spots during irradiation. A typical arc-cast U-C slug is shown in Figure 2.

2.2.2. Capsules. All the irradiation capsules were made of Type 304 stainless steel (18Cr-8Ni) with the exception of AI 3-4, whose cladding was nickel. In the AI 3 capsule series, the U-C fuel was bonded to the cladding with purified Na, while in the NAA 48 and AI 5 experiments, the bonding medium was purified, eutectic NaK (78%K-22%Na). No differences in the irradiation behaviour of the capsules can be correlated with the bonding medium. After loading with fuel and Na or NaK, the capsules were sealed by heliarc welding. A helium-filled space was left above the fuel for collection of fission gas.

The fuel column was about 12-in (30.5-cm) long in the AI 3 series and about 18-in (46-cm) long in the NAA 48 and AI 5 series. Bond annulus width was 0.005 in (0.013 cm) in the AI 5-1, NAA 48-1 and NAA 48-2 capsules, and exceeded 0.015 in. (0.038 cm) in all other capsules. The sealed fuel capsules were NaK-bonded to a second stainless-steel capsule. The outer NaK annulus provided sufficient thermal resistance in the heat flow path to control the fuel surface and centre temperatures. Thermocouples were placed in the fuel centre and at appropriate positions in the outer NaK annulus. The sealed, inner, fuel capsules simulated the type of fuel element commonly used in sodium-cooled reactors designed by Atomics International [3].

2.2.3. Irradiation tests. Irradiations were carried out in several reactors as indicated in Tables I and II. In all cases experiments were subject to temperature and flux variations typical of the test reactors used for such experiments. A typical fuel surface and centre temperature history is shown in Fig. 3, taken from continuous temperature recordings made during the irradiation of AI 3-1, at a point $4\frac{1}{2}$ in (11.4 cm) from the bottom of the 12-in (30.5 cm) capsule. Surface and centre temperatures were calculated from observed thermocouple readings in the NaK annulus outside the sealed fuel capsule. The out-of-pile thermal conductivity of U-C (13.3 BTU h^{-1} $°F^{-1}$ ft^{-1}

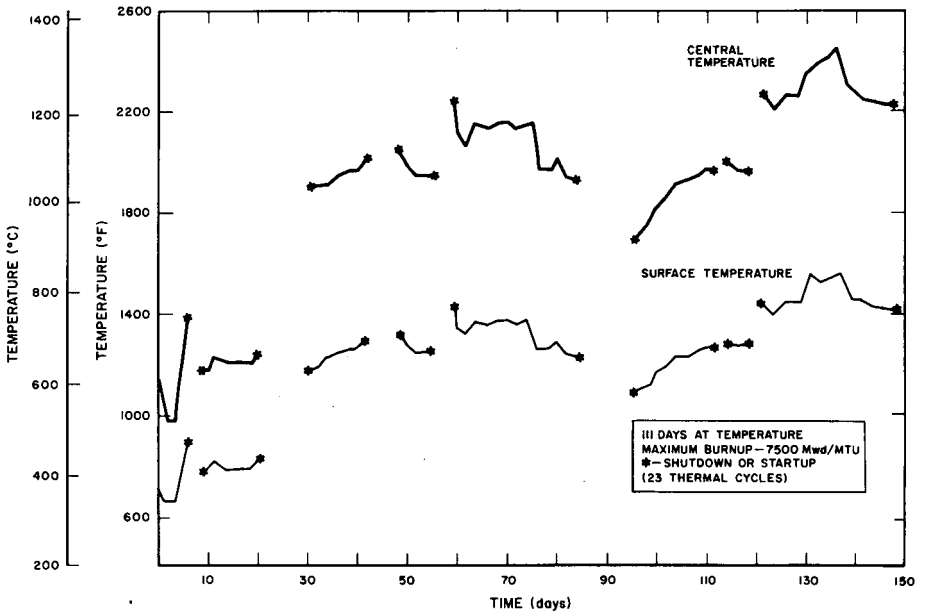


Fig. 3

Irradiation history of AI-3-1

or 0.055 cal $s^{-1}cm^{-1}$ $°C^{-1}$ was used in calculating the centre and surface temperatures of Fig. 3. Sufficient evidence has accumulated from irradiation experiments to justify use of out-of-pile thermal conductivity in calculating slug temperatures during in-pile experiments [4].

In the 10%-enriched fuel used in these experiments, U-C fuel accumulates burn-up at the rate of about 60 to 70 MWd/t each day. In the typical irradiation cycle shown in Fig. 3 the fuel was subject to 23 thermal cycles resulting from reactor scrams or shut-downs. Heat generation rates varied in all irradiations from about 600 000 to 900 000 BTU h^{-1} ft^{-2} (190-285 W/cm^2).

2.2.4. Hot cell examination. In the first step of the post-irradiation examination, the outer NaK annulus was probed for fission gas released during irradiation. If no gas was collected, it was evident that the inner capsule was intact. The outer capsule cladding was slit and removed, and the inner capsule was removed and photographed. Fig. 4 shows the typical appearance of an irradiated capsule with hypostoichiometric fuel (AI 3-1) and one with hyperstoichiometric fuel (AI 3-4). The AI 3-4 cladding, shown in Fig. 4, was nickel but the cracks were similar in appearance to those in the stainless steel cladding of other capsules listed in Table III.

The inner capsule was scanned along its entire length for gamma activity to establish a burn-up profile. A typical burn-up profile determined by gamma scanning of AI 3-1 is shown in Fig. 5. The temperature history shown in Fig. 3 was taken at the point marked 'T' in Fig. 5. At this point maximum burn-up was estimated to be 7500 MWd/t by comparison of the

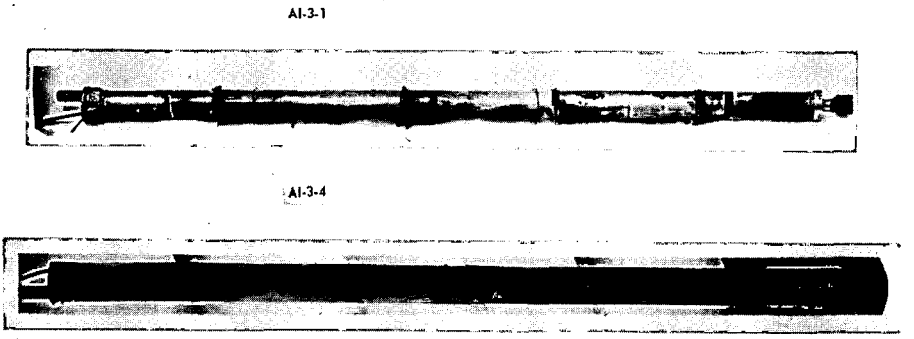


Fig.4

Irradiated cladding from AI-3-4 and AI-3-1

(a) AI-3-1, hypostoichiometric UC
(b) AI-3-4, hypostoichiometric UC

capsule activity with Cs^{137} and Co^{60} standards. (This burn-up determination is subject to confirmation by radiochemical analysis of the irradiated fuel for Cs^{137} and U^{236}). The inner capsule was punctured to collect fission gas which was captured in two activated-charcoal traps in series. In general, the first trap collected about 95 to 99% of the total fission gas and the remainder was collected in the second trap. The gas was analysed for Kr^{85} on a 256-channel gamma pulse-height analyser to determine fission-gas release.

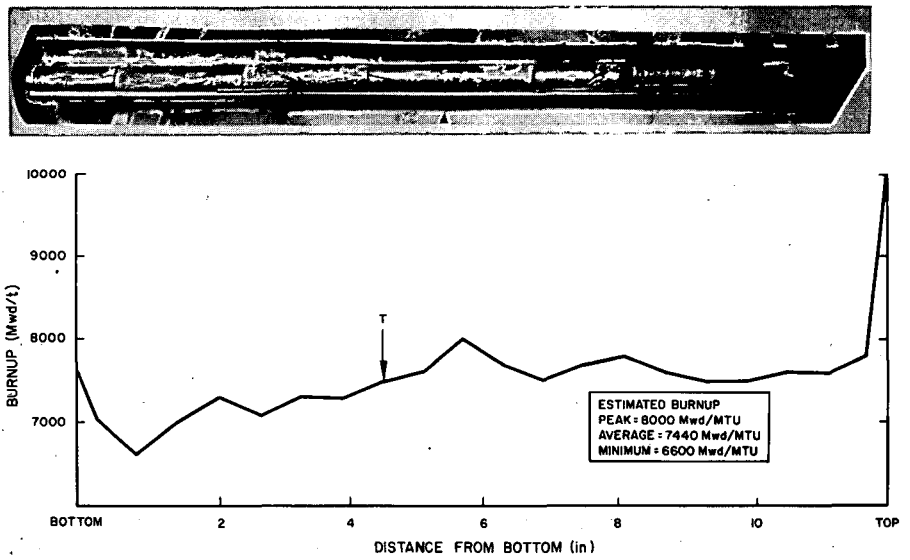


Fig.5

Irradiated fuel and burn-up profile of AI-3-1

TABLE III

EFFECT OF IRRADIATION ON TYPE-304 STAINLESS-STEEL CLADDING

Capsule	AI 3-1	AI 5-1	NAA 48-1	NAA 48-2	NAA 48-6
Fuel carbon content (wt. %)	4.4 - 4.7	4.8 - 5.0	4.8 - 5.0	4.8 - 5.0	4.8 - 5.0
Burn-up (MWd/t)	7500	77 500	8000	20 000	7500
Diameter increase (%)	2.5	0.7	1.7	2.2	3.0
Bond annulus/slug diameter (%)	6	2	2	2	6
C content (wt.%)					
Pre-irradiation	<0.08	<0.08	<0.08	<0.08	<0.08
Post-irradiation (max.)	<0.08	<0.68	1.26	0.95	1.39
Cladding condition	Intact	Cracked	Cracked	Cracked	Intact

After this procedure the cladding was slit longitudinally to expose the fuel. Typical appearance of the fuel is shown in Fig. 5. Dimensional measurements of the fuel were made after removal of the Na or NaK by vacuum distillation. Samples of fuel and cladding were prepared for metallographic examination and, in some cases, replicas were prepared for electron-microscopic examination.

3. EXPERIMENTAL OBSERVATIONS

3.1. Fuel behaviour

3.1.1. Fuel cracking. The form and type of cracking seen in the most recent capsule experiments are the same as reported earlier for the BMI 23-1 to 23-6 irradiations [1]. The slugs appear to fracture either on radial planes or on planes perpendicular to the slug axis, forming relatively large wedge-shaped pieces. The observed pattern is typical of thermal-stress-induced cracking in brittle materials.

Typical appearance of fuel slugs from a hypostoichiometric capsule, AI 3-1, is shown in Fig. 5, but the cracking is typical of both hyper- and hypostoichiometric U-C. The observed cracking is predictable in view of the steep temperature gradient of about 3200°F/in (750°C/cm). In spite of the cracking, however, there was no redistribution of the fuel within the cladding because of the nature of the crack pattern. Fuel cracking to the degree observed in these experiments is not believed to be detrimental in any way to the performance of U-C as a high-temperature sodium-reactor fuel.

3.1.2. Dimensional changes during irradiation. In Fig. 6 data points for U-C irradiations in Tables I and II are plotted as percentage change in diameter against burn-up. The average centre-line temperature (°F) associated with each point is placed next to that point. Linear isotherms of swelling against burn-up have been drawn on Fig. 6 for various average centre-line temperatures between 1000 and 1900°F (538-1038°C). The isotherm for 1900°F (1038°C) is based on only one observation and is therefore dotted. All of these isotherms must be regarded as tentative since insufficient data exist to verify the linearity assumed. Further testing is in progress to confirm the tentative functional relationship.

Some notes on the method of plotting data for Fig. 6 are essential to avoid misinterpretation of the information. Wherever data were available from centre thermocouple readings during irradiation experiments these data were plotted. However, most of the temperature data were based on calculation of centre temperatures from thermocouples in the NaK annulus outside the inner fuel container. Time-averaged fuel centre-line temperatures for each capsule, determined from automatically recorded time-temperature charts, are plotted for each capsule.

The diameter changes used as the ordinate in Fig. 6 were based on post-irradiation hot-cell measurements. Most of the observed changes are less than 2%, which is equivalent to a change of about 0.010 in (0.25 cm) for a slug diameter of 0.500 in (1.27 cm). The accuracy of in-cell diameter measurements is probably no better than ± 0.003 in. (± 0.1 cm) so that

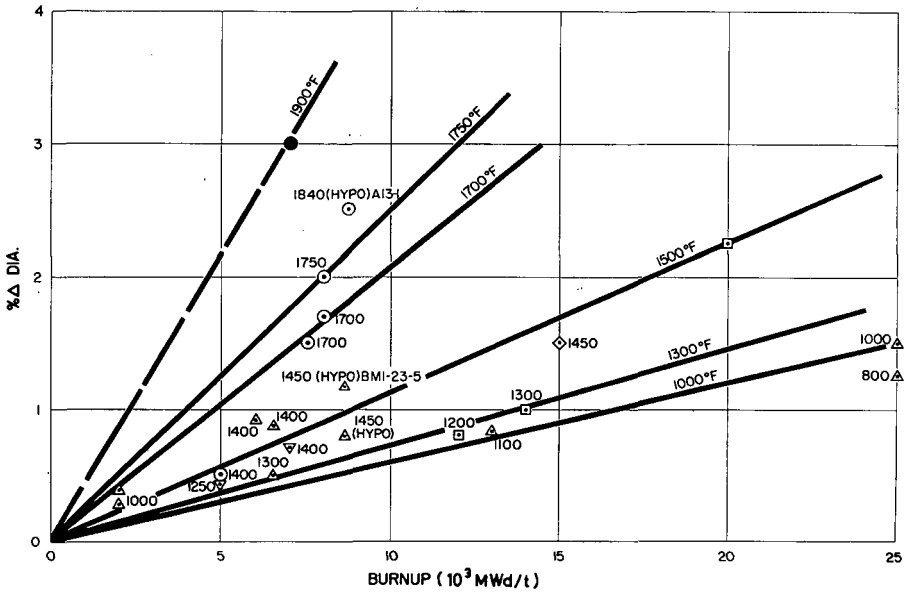


Fig. 6

Irradiation-induced swelling of cast uranium carbide

△ BMI capsules ⊡ NAA-48-2
○ NAA-48-1 ◇ AI-3-4
▽ AI-5-1 ● NAA-48-6
⊙ AI-3-1

large errors can be introduced in the reported percentage change in diameter after irradiation. Error can be introduced into the post-irradiation diameter measurements from slug cracking. It is, therefore, felt that the reported values for diameter change are probably conservatively high.

Since the swelling-burn-up isotherms in Fig. 6 are assumed to be linear as a first approximation, the swelling per atom percent burn-up is linear for each isotherm. In Fig. 7 the diametral swelling per at. % burn-up has been plotted against time-averaged fuel centre-line temperature against the fifth power of the empirical parameter τ given by

$$\tau = 10^{-3}\ T_R\ -\ 1,$$

where T is the time-averaged centre-line temperature in °R (absolute Fahrenheit units). All the data of Fig. 6 have been reduced to the single linear relationship of Fig. 7 represented by the empirical equation

$$R_D = 0.6 + 0.77\ \tau^5, \qquad (1)$$

where R_D is the percentage diametral increase per at. % burn-up. This empirical correlation is based on data from Fig. 6 in the range of 1400 to 1750°F (760-955°C) and is extrapolated to time-averaged centre-line tempera-

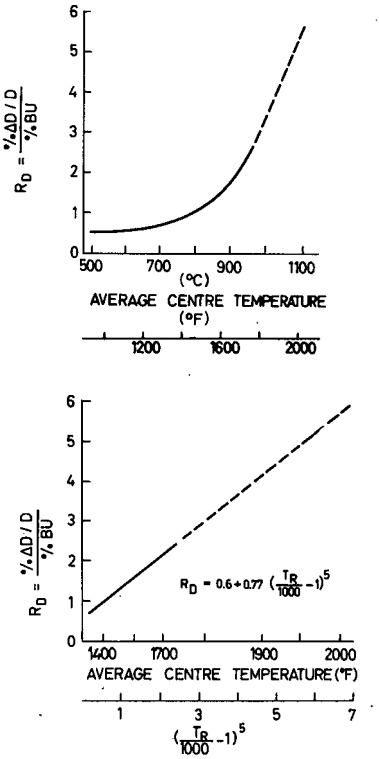


Fig. 7

Empirical curves for correlation of diameter changes in irradiated cast uranium carbide

tures to 2000°F (1083°C). This is the temperature range of interest in sodium-cooled reactors. A comparison of measured swelling and the swelling predicted from Eq. (1) for randomly chosen slugs from several capsules is given in Table IV. In all cases agreement is good.

3.1.3. Fission-gas release. Fission-gas release from U-C irradiation capsules was measured during post-irradiation examination. The total gas produced was calculated from the capsule burn-up. The percentage release is plotted in Fig. 8. Observed fission-gas release from hyperstoichiometric and hypostoichiometric irradiation capsules has been low, with the exception of capsules in which significant diffusion reaction occurred between the fuel and the stainless-steel thermocouple sheath. In all other cases the measured release has been in good agreement with the calculated values based on release by surface recoil and diffusion. It is felt that the fission-gas release observed in these experiments can be accommodated in adequately designed sodium-reactor fuel elements. Methods for predicting gas release based on recoil from the slug surface and diffusion of fission gas at irradiation temperature are discussed in the Appendix.

TABLE IV

COMPARISON OF OBSERVED AND CALCULATED SWELLING

Capsule	Burn-up (MWd/t)	C (wt.%)	Average Centre Temp. (°F)	R_D	Swelling, calculated (%)	ΔD/D Observed (%)
NAA 48-1 (Top)	5000	5.0	1450	0.8	0.7	0.6
NAA 48-1 (Aver.)	8000	4.9	1675	1.9	1.5	1.7
NAA 48-1 (Bottom)	8000	5.0	1900	4.1	3.2	2.8
BMI 23-3 (Aver.)	15700	5.0	1190	0.6	0.9	0.8
AI 3-1 (Top)	7700	4.3	1875	3.8	2.8	2.5
AI 3-1 (T)*	7500	4.3	1960	5.0	3.8	4.4
AI 3-1 (Bottom)	6600	4.4	1780	2.7	1.8	3.0
AI 3-1 (Aver.)	7500	4.5	1860	3.7	2.8	3.4

* Point T of Fig. 5

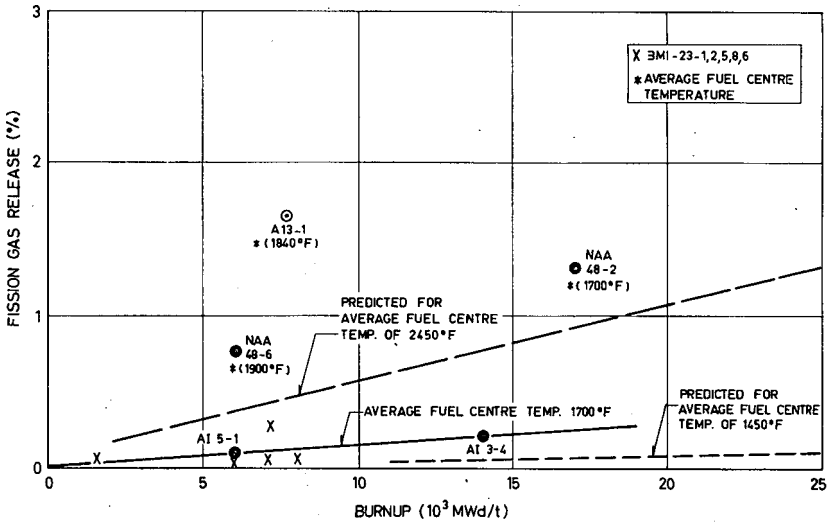


Fig. 8

Fission gas release from uranium carbide

3.1.4. Metallographic examination. From the uranium-carbon phase diagram [3] no metallographic change is expected in a neutron-free environment at temperatures reported in this study. Metallographic examination of sections taken from irradiated fuel slugs confirmed this expected behaviour and failed to disclose any irradiation-induced changes. It was observed, however, that hyperstoichiometric fuel slugs which operated for long periods at temperatures above 1000°F (538°C) had been reduced to stoichiometric. The UC_2 platelets originally present in the microstructure had disappeared from the centre outward and, depending on the temperature, the fuel either had a thin band around the periphery which contained the UC_2 precipitate or was completely devoid of UC_2.

Fig. 9 shows a micrograph taken near the surface of the U-C in BMI 23-2 after irradiation. Before irradiation, the U-C was uniformly hyperstoichiometric. The post-irradiation micrograph shows that a two-phase UC plus UC_2 structure exists to a depth of about 0.060 in (0.15 cm). Below this depth only the single-phase UC is found. It is hypothesized that contact with the high-temperature sodium in the thermocouple hole has removed carbon from the interior of the sample leaving behind only the single-phase UC structure.

Similar depletion of carbon from hyperstoichiometric U-C fuel has been observed in the more recent U-C irradiations typified in Fig. 10 (taken from the composite edge-to-centre micrograph of NAA 48-2). The fuel from NAA 48-2 was originally hyperstoichiometric, but no UC_2 remains in the structure after irradiation in a NaK-filled capsule. Adjacent fields not photographed showed slight amounts of UC_2 still present near the fuel rod periphery.

Out-of-pile tests [5] have shown that the observed carbon depletion



Fig. 9

UC_2 depletion during irradiation





Fig. 10

Diffusion reaction between UC and stainless steel at temperatures above 2000°F

(a) Post-irradiation composite of NAA-48-2 from edge of thermocouple hole
(b) Out-of-pile reaction of UC (5.2 wt.% C) with type-304 stainless steel after 382 hours at 2000°F (1083°C)

cannot result from carbon diffusion down a thermal gradient in the fuel under irradiation. Also, it has been calculated [4] that there are at least enough stable carbide-forming fission product elements to combine with the carbon

atom released by the fission of the uranium atom from U-C. If this carbon deficiency after fission had contributed to the observed carbon depletion it is more probable that carbon would be depleted near the fuel surface where fission density is greatest. Since carbon depletion is observed in the centre rather than at the surface, the suggested mechanism cannot operate. The observed depletion can be explained, however, by considering the interaction between sodium and hyperstoichiometric U-C.

3.2. Cladding behaviour

3.2.1. U-C as a carbon source. Five of the six capsules of Table II contained only hyperstoichiometric U-C (> 4.8 wt.% C) clad in Type 304 stainless steel. In each case the cladding was carburized during irradiation from the original 0.06 - 0.08% to as high as 1.34%. This behaviour has been duplicated in out-of-pile experiments where carbon can be transferred from hyperstoichiometric U-C to stainless-steel cladding across a Na or NaK bonding layer [3, 6]. The transfer occurs readily at temperatures above 1000°F (538°C). In AI 3-1 which contained hypostoichiometric U-C (< 4.8% C) the Type 304 stainless-steel cladding was uncarburized after over 2600 h at irradiation temperature and flux. This again confirms out-of-pile behaviour where no carbon transfer is observed with hypostoichiometric U-C even up to 12 000 h at 1600°F (870°C) [6].

In order to account for the observed carburization of cladding in both in-pile and out-of-pile tests, it is obvious that a carbon source must be present. The excess carbon over stoichiometric in hyperstoichiometric fuel represents such a source.

In BMI 23-2 (Table I) [7] U-C containing 5.3% carbon was irradiated to 6000 MWd/t in six cycles at MTR with a maximum centre-line temperature of 1830°F (1000°C) and an average centre-line temperature of 1380°F (749°C). Maximum surface temperature was 1070°F (577°C) with an average of 916°F (491°C). The U-C was held at irradiation temperature for a total of about 3000 h. In this test the U-C, about 3/8 in (0.93 cm) in diameter, contained an axially drilled thermocouple hole about 3/32 in (0.23 cm) in diameter. The resulting carbon depletion is shown in Fig. 9.

The microstructural changes observed in irradiated hyperstoichiometric UC were compared with similar changes occurring in out-of-pile U-C/Na/304 SS compatibility tests. It has been shown [6] that the observed disappearance of the UC_2 platelets originally present in the U-C microstructure was a direct result of reaction of the UC_2 phase with the sodium bond at the contact interface with subsequent transfer of carbon through the sodium bond to the cladding. There seems to be no acceleration of this effect due to irradiation.

At relatively low temperatures (~1000°F or 538°C) the UC_2 in hyperstoichiometric U-C is attacked by sodium. This attack reduces UC_2 (body-centred tetragonal with two carbon atoms located at points corresponding to the single carbon atom sites in the UC structure) to the face-centred-cubic UC structure with a corresponding lattice contraction. Only the UC_2 phase is reduced by sodium. The UC phase is stable in sodium for times at least to 12 000 h at temperatures to 1600°F (871°C). If no carbon sink exists, the reaction will proceed only until the carbon activity in sodium

and in UC_2 are equal. This is not the case in Type 304 stainless-steel capsules since the capsule wall acts as a nearly infinite carbon sink.

When UC_2 is reduced to UC by sodium, a void is left at the former UC_2 site. Since the UC_2 platelets in the structure are interconnected [3], the voids formed when the UC_2 is reduced to UC are also interconnected, permitting penetration of the unsaturated sodium into the structure. As long as this sodium penetration is possible, the decarburization rate of hyperstoichiometric U-C remains relatively constant at constant temperature as seen in Fig. 11. Hypostoichiometric specimens are not decarburized under the same conditions.

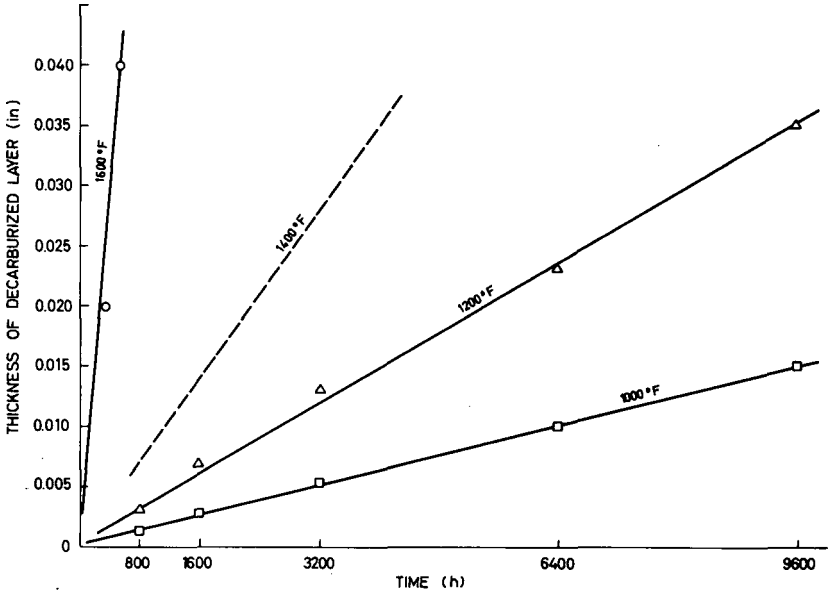


Fig.11

Increase of decarburization of hyperstoichiometric uranium-carbon alloy with time

(Decarburization depth is independent of slug diameter and carbon content when large volumes of stainless steel are present acting as an infinite sink)

During irradiation, penetration of sodium into cracks in the fuel slug can move the UC_2/Na interface to higher-temperature regions in the interior of the slug where the decarburization rate is greater. This causes decarburization primarily in the central regions of the slug and results in the microstructure observed in irradiated hyperstoichiometric U-C specimens shown in Figs. 9 and 10.

3.2.2. Cladding carburization. In the hyperstoichiometric U-C/Na/304 stainless-steel system, the decarburization of U-C is accompanied by carburization of the stainless-steel capsule wall [6]. As seen from Fig. 11, the decarburization is linear with time. It is therefore unlikely that diffusion of carbon through sodium or through the cladding is rate-controlling since a diffusion rate-controlled process should lead to a decarburization linear

with the square root of time. The data of Fig. 12 show that the rate of carburization of the Type 304 stainless steel is strongly dependent on the carbon content of the U-C. Otherwise, carburization of the cladding would occur in a manner similar to the carburization of Type 304 stainless steel in carbon-saturated sodium [8]. Fig. 13 shows the carbon concentration gradient found in Type 304 stainless steel carburized in carbon-saturated sodium (corresponding to an infinite carbon source), for 100 h at 1200°F (649°C). The surface concentration (3.1%) is in equilibrium with the carbon in carbon-saturated sodium at this temperature [8]. However, hyper-

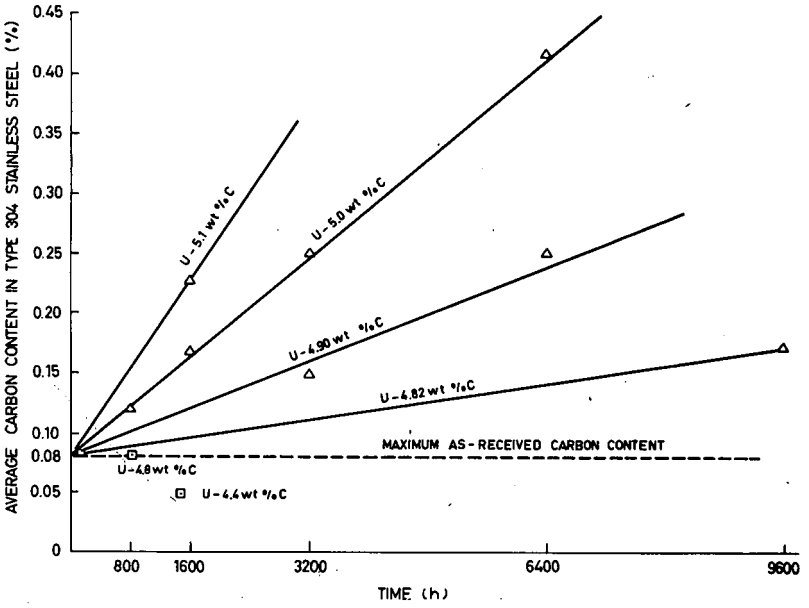


Fig. 12

Carburization of Type-304 stainless steel by uranium-carbon alloys at 1200°F

stoichiometric U-C does not represent an infinite source. The surface carbon content of the cladding in the U-C/Na/304 system is only 1.0% even after 6400 h at 1200°F (649°C). Apparently carbon has been supplied to the steel surface at a rate much slower than the maximum possible carburization rate of the steel at 1200°F (649°C). Therefore, it is concluded that the rate of removal of carbon from the hyperstoichiometric U-C is the rate-controlling step in the cladding carburization.

3.2.3. Cladding embrittlement. In four of the five capsules where the cladding was carburized by transfer of carbon from hyperstoichiometric fuel, the cladding showed longitudinal cracks after carburization during irradiation, as shown in Fig. 4. These longitudinal cracks, typical of brittle failure, occurred only in capsules which contained hyperstoichiometric U-C fuel. Carbon analyses of samples adjacent to cracks indicated that carbon

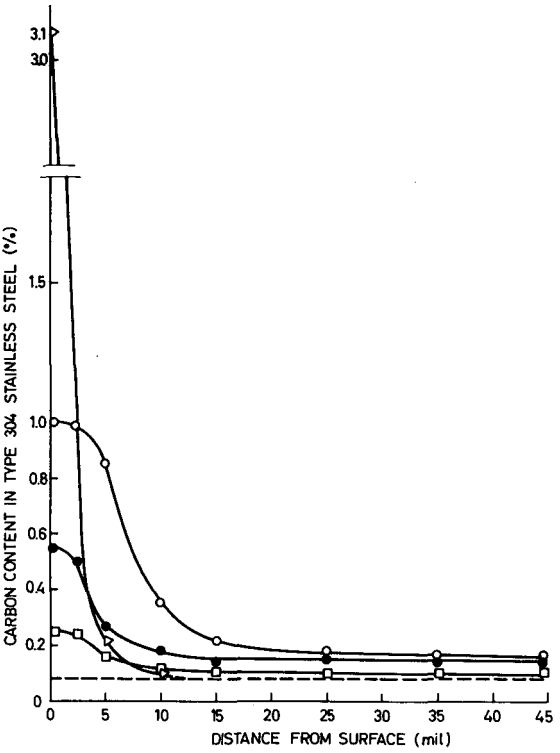


Fig. 13

Carbon gradient in Type-304 stainless steel carburized at 1200°F

▷ 100 hr - carbon-saturated sodium

○ 6400 hr
● 3200 hr
□ 800 hr
} U-50 wt.% C specimens as carbon source

content in the cladding had increased to as much as 1.4 wt. %. However, cladding from irradiated capsules containing hypostoichiometric U-C was uncarburized. It remained intact during irradiation as shown in Fig. 4 and was ductile in bend tests after irradiation. Although failure occurred only in fuel tubes containing hyperstoichiometric U-C fuel, the cause of the cracking can only be hypothesized at this time. It is thought that the combination of loss of ductility due to carburization, coupled with pressure exerted by the fuel swelling after filling the thin annulus, precipitated the failure. Strain rate may be a significant contributing factor in causing brittle failure. Had the stainless-steel cladding not been carburized, it is felt that the fuel swelling could have been accommodated by elongation of ductile cladding.

In one capsule, NAA 48-6, the cladding was carburized as expected but it remained intact during irradiation. It is felt that the increased expansion space provided by the 0.015-in (0.038 cm) annulus of this capsule

prevented cracking of the cladding. Cladding of NAA 48-1, a similar capsule with a 0.005-in (0.013 cm) instead of a 0.015-in (0.038 cm) annulus, cracked after irradiation under similar temperature and burn-up conditions. If this hypothesis is correct, NAA 48-6 cladding might also have cracked if the irradiation had continued. If the fuel swelled enough to be in contact with the cladding and subsequently exerted pressure at a slow strain rate on the carburized cladding by further swelling, cracking could result.

Cracking of the nickel cladding of AI 3-4 is as yet unexplained. The nickel cladding was specified for this capsule to provide a lower thermal resistance because of its high thermal conductivity and thereby decrease thermal stress in the cladding. Out-of-pile compatibility capsules with U-C in nickel cladding have revealed no carburization of the nickel cladding [4] in spite of the very high diffusion rate reported for carbon in nickel [9]. It has also been reported [10] that nickel is not carburized in contact-pairs with graphite but that graphitization can occur when diffusion occurs at 1700°F (927°C) followed by aging at lower temperatures. It is possible that graphitization may have occurred in AI 3-4 where the NaK in the outer capsule annulus may have acted as a carbon sink and permitted rapid diffusion of carbon from hyperstoichiometric U-C through the nickel cladding. Further study is necessary to explain the observed phenomenon.

3.2.4. Diffusion reactions between U-C and stainless steel. An additional effect was noted in capsules which had central thermocouples sheathed in stainless steel and which underwent temperature excursions exceeding capsule design conditions. Visual examination indicated a diffusion reaction had occurred between the Type 304 stainless-steel thermocouple sheath and the U-C fuel. A liquid phase formed which fused the fuel slugs together. Metallographic examination of a cross-section of a slug from NAA 48-2 is illustrated in Fig. 10a, Fig. 10b shows a similar diffusion reaction between hyperstoichiometric U-C (5.2 wt.%) and Type 304 stainless steel in out-of-pile tests for 382 h at 2000°F (1076°C). A diffusion reaction has occurred between stainless steel and U-C resulting in carbon depletion in the diffusion zone and formation of a solid elemental uranium phase, probably containing minute amounts of iron and carbon in solid solution.

This reaction is of little interest in the practical design of a fuel element since contact between U-C and stainless steel in a fuel element can only occur at the low interface temperature in the vicinity of 1200°F (649°C) where the diffusion rates are extremely low. The observed diffusion reaction can be significant only in an instrumented irradiation experiment where a stainless-steel-sheathed thermocouple is in contact with fuel at high temperatures.

3.2.5. Compatibility of U-C with Zr-alloys. Because of the demonstrated carburization and embrittlement of stainless-steel cladding by hyperstoichiometric U-C, it is necessary to use hypostoichiometric U-C with such cladding. However, it is possible to use hyperstoichiometric U-C with a sodium bond in cladding materials such as zirconium or niobium alloys. In carburization of these materials by hyperstoichiometric U-C a thin carbide diffusion barrier forms on the cladding surface [11]. Diffusion of carbon through the carbide layer is the rate-controlling process. Unlike the carburization of stainless

steel by hyperstoichiometric U-C, carburization of Zr- and Nb-alloys is independent of fuel temperature and fuel carbon content, and depends only on the cladding temperature. Diffusion rates are extremely slow at cladding temperatures below 1200°F (649°C).

A high-strength Zr-alloy, known as 3Z1, has been developed by Atomics International [12] for use in sodium systems. The compatibility of this alloy with U-C is now being studied. When U-C is in direct contact with Zr or 3Z1 at high temperatures for prolonged periods of time, a diffusion layer forms. The nature of the diffusion layer depends on the temperature at which diffusion takes place and the composition of the U-C. Above 2040°F (1116°C) a liquid phase forms at the U-C/Zr interface [3]. Below 2040°F (1116°C) the reaction is substantially the same, except the uranium containing zirconium and carbon in solid solution is in the solid state. Based on diffusion tests performed at Atomics International combined with diffusion coefficients determined at Saclay [11], the growth of the reaction zone appears to follow a typical diffusion-controlled, parabolic, rate law. The temperature dependence of the reaction obeys the Arrhenius equation. The results, based on extrapolation of test results up to 1000 h at 1670°F (910°C), are shown in Fig. 14. The reaction rate with 3Z1 appears to be significantly slower than with unalloyed zirconium at the same temperature. The diffusion layer between U-C and 3Z1 will be only 0.002-in (0.005 mm) thick after three years at 1670°F (910°C). Thickness will be significantly less at the reference cladding temperature of 1200°F (649°C).

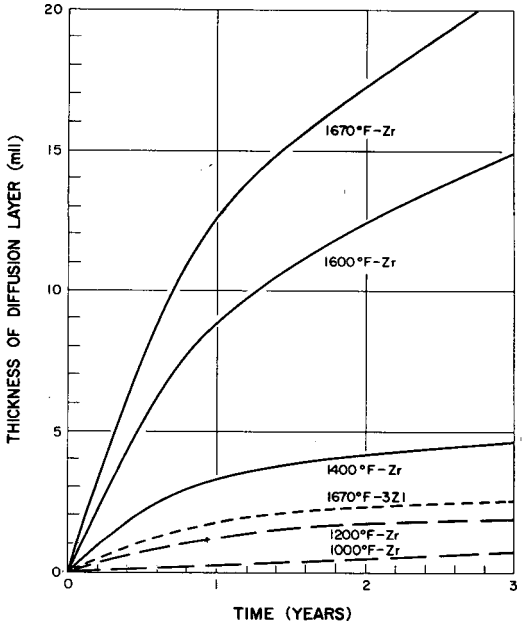


Fig. 14

Interdiffusion of uranium-carbon and -zirconium alloys

4. CONCLUSIONS

Stoichiometric or hypostoichiometric U-C Na-bonded to stainless steel can be effectively used in Na-cooled power reactors to centre temperatures of 2000°F (1093°C) and burn-up of 25 000 MWd/t with cladding temperature of 1200°F (649°C). Alternatively, 3Z1 clad, Na-bonded elements with hyperstoichiometric U-C can be used to the same central temperature and burn-up. In these elements cladding temperature would be limited by the cladding strength to about 1150°F (621°C).

Observations of diametral swelling on arc-cast U-C bonded with Na or NaK can be correlated by the empirical equation

$$R_D = 0.6 + 0.77\ (10^{-3}\ T_R\ -1)^5,$$

where R_D is the percentage diametral swelling per percentage burn-up and T_R is the centre temperature in degrees Rankine (°R).

Fission-gas release from both hypostoichiometric and hyperstoichiometric U-C is low and predictable with good accuracy from the calculated curves. Fission-gas release increases in cases where there is a diffusion reaction between fuel and cladding or thermocouple sheaths to form a liquid or solid metallic phase. In general, this can be of significance in instrumented capsule tests where a central thermocouple sheath can operate at a relatively high temperature. It is of less significance in a fuel element where fuel-cladding contact occurs only at relatively low surface temperatures and hence the reaction rate is probably insignificant.

Fission-gas release or fuel swelling do not represent limitations on the use of U-C fuel elements under presently conceived sodium-cooled reactor conditions. Observed swelling and fission-gas release rates can be accommodated in properly designed elements.

Transfer of carbon from hyperstoichiometric U-C fuel to stainless-steel cladding across the sodium bond has been observed in both in-pile and out-of-pile experiments. There is no evidence to support the possibility of irradiation-induced acceleration of the carbon transfer process. At relatively low temperatures UC_2 is readily attacked, with Na or NaK removing a carbon atom which then goes into solution in the liquid metal. The body-centred-tetragonal UC_2 is converted fo face-centred-cubic UC. Voids are left at sites formerly occupied by the UC_2 phase. This process is the rate-controlling step in carbon transfer at low temperatures; at higher temperatures there is evidence of carbon transfer by diffusion of carbon through UC. A single-phase microstructure results after the high-temperature carbon-transfer process. This structure has been observed at the centre of U-C fuel slugs after irradiation. No carbon transfer is observed with hypostoichiometric U-C under irradiation.

Carbon removed from hyperstoichiometric U-C fuel is readily transferred across the Na bond to carburize and embrittle stainless-steel cladding in both in-pile and out-of-pile experiments. This transfer represents a possible limitation of choice of fuel composition for Na-bonded, stainless-steel clad elements.

Fuel cracking is observed in irradiation experiments occurring on either transverse or radial planes, probably because of thermal stresses. The

observed crack pattern is not believed to be detrimental to performance of U-C fuels. The crack pattern is similar for both hypostoichiometric and hyperstoichiometric fuel.

ACKNOWLEDGEMENTS

The work described in this paper was performed for the United States Atomic Energy Commission by Atomics International under Contract AT (11-1) GEN-8. Permission to publish the results is gratefully acknowledged. The authors appreciate the invaluable assistance of members of the Staff at Atomics International who participated in the work and in compiling and editing this paper. The particular contributions of Dr. H. Pearlman and Messrs. P.E. Elkins, R.D. Hahn, W. McCarty and J. Leirich are acknowledged. Mr. C. Coffindaffer helped in preparing the manuscript.

APPENDIX

RELEASE OF FISSION GAS FROM UC

A-1. INTRODUCTION

The fissioning of uranium results in the formation of about 25 fission-product elements ranging in mass numbers from 72 to 161. For a uranium-carbide fuel element, it has been calculated that about half of the fission product elements react with the carbon atoms released by fission of uranium atoms to form stable carbide compounds. Of the remaining atoms, approximately 29% are Xe atoms and 4% are Kr atoms. Calculated fission-gas release is nearly independent of atomic mass, so the calculated results are valid for either Xe or Kr.

Fission products can be released from a fuel element either by recoil of fission products from the fuel material, by solid-state diffusion of the fission products in the fuel lattice, or by corrosion and/or erosion. The third possibility will not be considered in this report.

A-2. THEORY

A-2.1. Release by recoil

The energy of the fission fragments is sufficient to cause recoil with a range of 5 to 9 mg/cm^2, depending upon the atomic mass. These values have been measured for UO_2 [13]. Calculations from data on the release by recoil of Kr^{85} from UC indicate a range within 25% of the UO_2 values. An average fission-fragment atomic mass of 110 is assumed, corresponding to a range of 7.5 mg/cm^2. For a UC density of 13.6 g/cm^3 this corresponds to a linear range of 5.5×10^{-4}cm, assumed to be independent of temperature. The assumption is valid since the range will change by less than 4% for a 2200°F (1222°C) temperature change.

The fraction of the fission products released by recoil is independent of fission product half-life and may be expressed as follows

$$F_r = \frac{RS}{4} \frac{\phi_m}{\phi_a}, \quad (1)$$

where F_r is the fraction released by recoil, R is the recoil range (cm), S is the surface-area-to-volume ratio of the fuel element (cm^2/cm^3) and ϕ_m/ϕ_a is the peak-to-average thermal-neutron flux ratio in the fuel.

In the case of a cylindrical fuel element where the height is greater than twice the diameter ($\mathfrak{D}$) Eq. (1) may be rewritten (with a less than 25% error) as $F_r = R/\mathfrak{D}\, \phi_m/\phi_a$. (2)

A-2.2. Release by diffusion

The geometrical model used to describe release by diffusion is assumed to be spherical [14]. The actual structure of the fuel element is easily replaced with this idealized structure by use of the equation [13]

$$a = 3d/S \quad (3)$$

where a is the radius of the equivalent sphere, d is the fraction of theoretical density and S is the total surface area to volume ratio of the actual fuel element.

The diffusion equation for the concentration of any stable isotope in the sphere is as follows

$$\frac{\partial C}{\partial t} = \frac{D}{r} \frac{\partial^2 (rC) + B}{\partial r^2}, \quad (4)$$

where C is the concentration in the sphere (atoms/cm^3), t is the time (s), D is the diffusion coefficient (cm^2/s), r is the radial co-ordinate in the sphere (cm) and B is the production rate (atoms $cm^{-3}\, s^{-1}$).

The initial and boundary conditions for the above equation are C = 0 at r = a = radius of sphere, and C = 0 at t = 0.

Eq. (4) has been solved [15, 16] to give the fractional release. This solution is:

$$F_d = 1 - \frac{1}{15 D't} + \frac{6}{\pi^4 D't} \sum_{n=1}^{\infty} \frac{\exp[-n^2\pi^2 D't]}{n^4} \quad (5)$$

where F_d is the fraction of the stable fission product released and $D' = D/a^2$. Eq. (5) has been put into graphic form [15, 16].

The diffusion coefficient (D) is strongly dependent on temperature as is shown in the following equation

$$D = D_0 \exp[-Q/R_T], \quad (6)$$

where D_0 is a constant dependent upon both the material and the isotope

diffusing through it, Q is the activation energy, again dependent upon the diffusing isotope and the material, R is the universal gas constant and T is the absolute temperature.

A-3. PROCEDURE

The fraction released by recoil may be calculated from Eq. (2). For a $\frac{1}{2}$-in diam. uranium carbide fuel rod of density 13.6 g/cm^3, the fraction released is 4.3×10^{-2}% based on an average recoil range of 7.5 mg/cm^2 and a uniform neutron flux through the element.

The procedure for determining the fraction released by diffusion is as follows:

(1) Experimental results from Chalk River [14] using 4.8% massive UC gave an average value of D' as 2.7×10^{-10} s^{-1} at a temperature of 1400°C.

(2) The value of D' for a $\frac{1}{2}$-in (1.27-cm) diam. UC fuel element is determined from Eq. (3) and the relationship $D' = D/a^2$. For a smooth surfaced rod whose height is greater than 1 in (2.54 cm), the value of $D' = 1.87 \times 10^{-12}$ s^{-1} at a temperature of 1400°C.

(3) The value of D' at temperatures other than 1400°C is calculated from Eq. (6) and an activation energy of 45 kcal/mole [17].

(4) The fraction released due to diffusion, F_d, is determined for various values of D't from Eq. (5).

(5) For $\frac{1}{2}$-in (1.27-cm) diam. UC rods, the calculated centre-to-surface temperature difference is 400°F (222°C) for a centre temperature of 650°F (343°C), and 850°F (472°C) for a centre temperature of 2350°F (1288°C). A simple integration can be obtained using a three-point Simpson's Rule approximation:

$$F_d = \frac{1}{6} [F_{d_{(T_a)}} + 4 F_{d_{(T_m)}} + F_{d_{(T_s)}}], \quad (7)$$

where T_s is the surface temperature, T_a is the axial or centre temperature and T_m is the mean temperature given by (Ta + Ts)/2.

Since the last term in Eq. (7) is always negligible we can rewrite the equation as:

$$F_d = \frac{1}{6} [F_{d_{(T_a)}} + 4 F_{d_{(T_m)}}]. \quad (8)$$

A-4. RESULTS

Figs. 15 and 16 show the percentage of fission gas released from recoil and diffusion as a function of mean temperature. The calculations are based on $\frac{1}{2}$-in (1.27-cm) diam. UC rods.

Fig. 17 shows the total percentage of fission gas released from $\frac{1}{2}$-in (1.27 cm) rods as a function of in-pile time. Two different fuel-element mean temperatures are included to show the strong effect of temperature on release fraction.

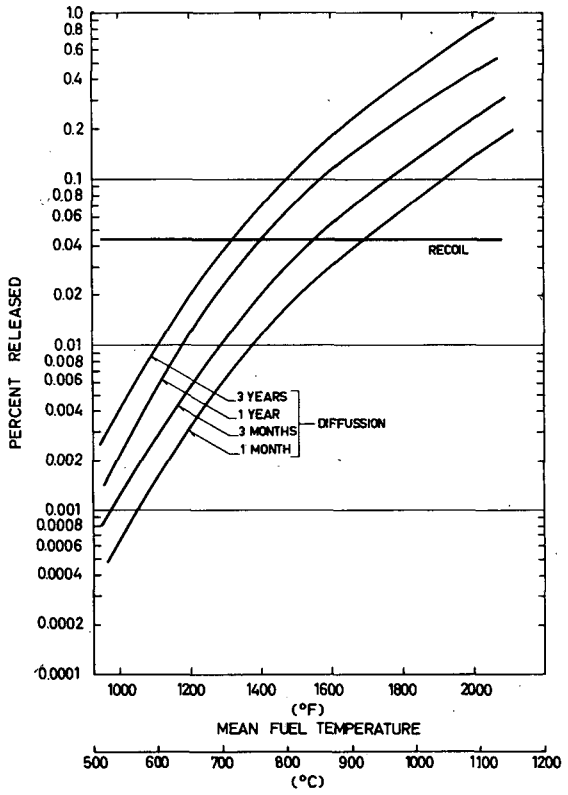


Fig.15

Fission gas release calculated from recoil and diffusion from ½-in diam. (1.27-cm diam.) UC rods.

$$* \quad T_{MEAN} = \frac{T_{AXIAL} + T_{SURFACE}}{2}$$

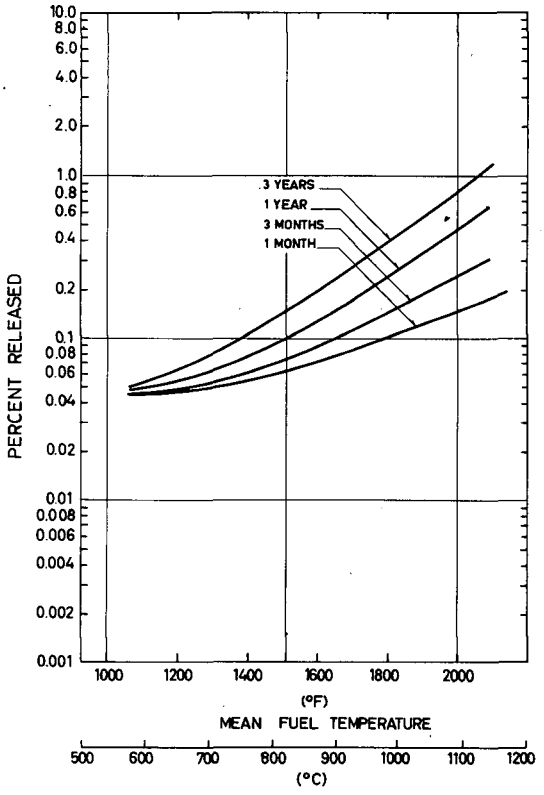


Fig. 16

Variation of total calculated fission gas release from ½-in diam. (1.27 cm diam.) UC rods with temperature

$$* \quad T_{MEAN} = \frac{T_{AXIAL} + T_{SURFACE}}{2}$$

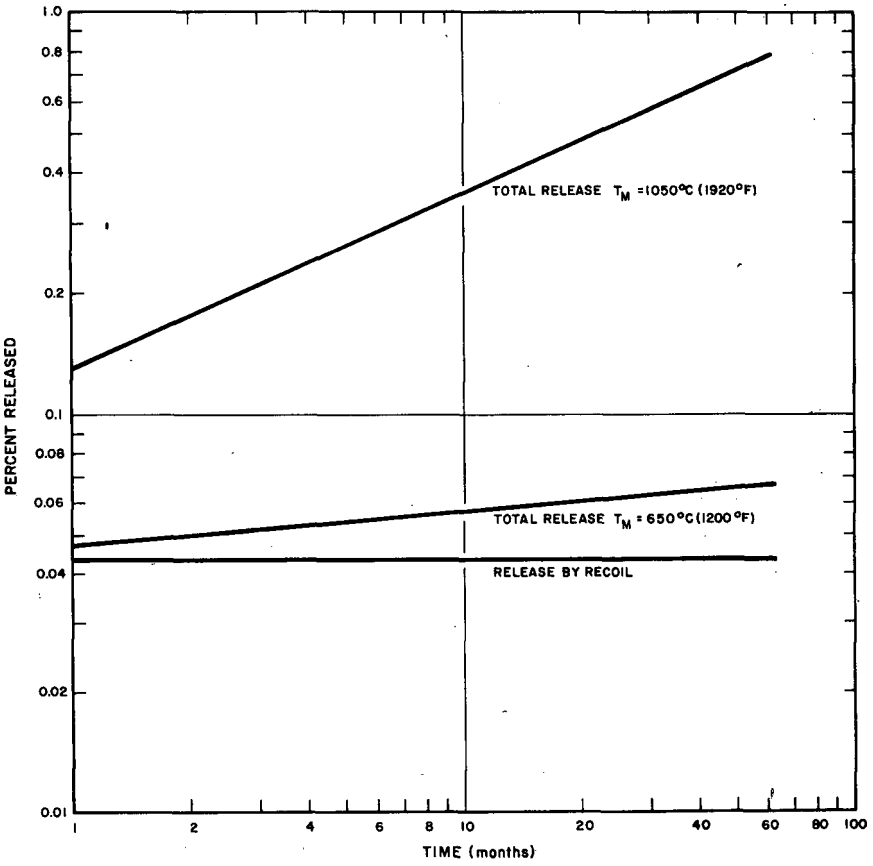


Fig. 17

Variation of total calculated fission gas release from $\frac{1}{2}$-in diam. (1.27 cm diam.) UC rods with temperature

$$T_M^* = \frac{T_{AXIAL} + T_{SURFACE}}{2}$$

Fig. 18 indicates the variation in the calculated fission gas release as a function of fuel rod diameter. The variation is referenced to a $\frac{1}{2}$-in (1.27 cm) diameter.

Fuel element damage by cracking during irradiation may be sufficient to account for measured fission-gas release appreciably greater than the calculated amount. The factor by which surface area must increase to account for fission-gas release greater than calculated is given by the ratio of observed to calculated fission-gas release. For example, in a hypothetical case where observed fission-gas release is 1% and calculated release is 0.2%, a surface increase by a factor of five due to cracking could account for the difference.

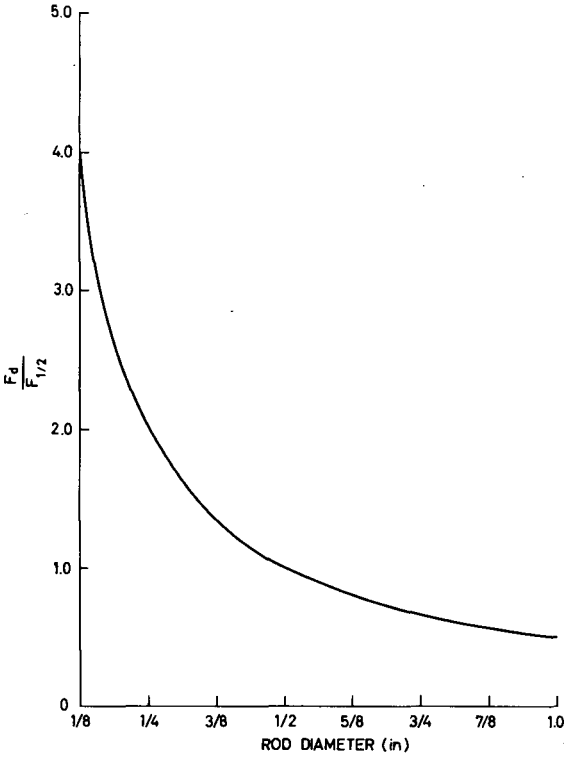


Fig.18

Fission gas release calculated for various rod diameters

REFERENCES

[1] ROUGH, F.A., Status of Irradiation of Bulk UC, Proc. Symp. on UC as Reactor Fuel Material, (4 April 1961) USAEC Rpt. TID 7614.

[2] BINSTOCK, M.H., Arc Melting and Casting of UC, ibid.

[3] SINIZER, D.I., Application of Uranium Carbide to Power Reactors, ibid.

[4] Unpublished information - Atomics International.

[5] Bimonthly Technical Progress Report, USAEC Rpt. NAA-SR-5242 (Mar. - Apr. 1960) 1D10.

[6] WEBB, B.A., Carburization of Austenitic Stainless Steel by Uranium Carbides in Sodium System, USAEC Rpt. NAA-SR-6246 (Feb. 1962).

[7] HARE, A.W. and ROUGH, F.A., Irradiation Effects on Massive UC, USAEC Rpt. BMI 1452 (July 1960).

[8] ANDERSON, W.J. and SNEESBY, G.V., Carburization of Austenitic Stainless Steel in Liquid Sodium, USAEC Rpt. NAA-SR-5282 (Sep. 1960).

[9] LANDER, J.J., KERN, H.E. and BEACH, A.L., Solubility and Diffusion Coefficient of Carbon in Nickel, J. appl. Phys. 23 (1952) 1305.

[10] BOKROS, J.C., Graphite-Metal Compatibility at Elevated Temperatures, J. Nuc. Mat. 3, 1 (Jan. 1961) 89.

[11] ACCARY, A. and TROUVE, J., Application des Methodes Microscopique a l'Etude de la Reaction Entre de Carbure d'Uranium et le Zirconium Metallique, Mem. Soc. Chim. (1960).

[12] WAGNER, R.K., KLINE, H.E. and SINIZER, D.I., Zirconium Alloys for Cladding High Temperature Fuel Elements, Nuclear Metallurgy, A Symposium on Metallic Moderator and Cladding Materials, Amer. Inst. Mech. Engnrs., IMD, VII, Special Report Series 10, (Oct.1960).

[13] EICHENBERG, J.D., et al., Effects of Irradiation on Bulk UO_2, USAEC Rpt. WAPD-183 (Oct. 1957).

[14] AECL Chalk River Progress Rpt. FD-34-5.

[15] BOETH, A.H., A Method of Calculating Fission Gas Diffusion from UO_2 Fuel, AECL Rpt. CRDC-721, (Sep. 1957).

[16] BECK, S.D., The Diffusion of Radioactive Fission Products from Porous Fuel Elements, USAEC Rpt. BMI-1433 (18 April 1960).

[17] LINDNER, R. and MATYKE, H., Diffusion Radioaktiver Edelgase in Uranoxyden und Uranmonokarbide, Z. Naturf. 14a (Nov. 1959) 1074-1077.

EFFECTS OF HIGH BURN-UP ON OXIDE CERAMIC FUELS

M. L. BLEIBERG, R. M. BERMAN AND B. LUSTMAN
BETTIS ATOMIC POWER LABORATORY,
PITTSBURGH, PENNSYLVANIA

Abstract — Résumé — Аннотация — Resumen

EFFECTS OF HIGH BURN-UP ON OXIDE CERAMIC FUELS. The irradiation stability of oxide ceramic fuels to high burn-ups has been the subject of a continuing research effort at the Bettis Atomic Power Laboratory in conjunction with the development of a second (Shippingport) core. The core blanket region will contain bulk UO_2 capable of high burn-ups. The in-pile properties of this material were investigated to burn-ups up to about 40×10^{20} fission/cm^3 (127 000 MWd/t, 17 at.% U atoms fissioned). Also, extensive development was carried out on an oxide ceramic fuel material for the core seed region. These investigations included 93% enriched UO_2 in solid solution with ZrO_2, and enriched UO_2 dispersed in matrices of BeO and Al_2O_3. These materials were tested in a similar manner as the bulk UO_2.

The irradiation-induced volume changes in these oxide fuel materials to high burn-ups are compared, and the factors influencing the fuel swelling are described. The fraction of the theoretically produced fission gases released in-pile from the fuel is shown to be related to fuel burn-up and operating temperature. These results are compared with those predicted by volume diffusion theory utilizing post-irradiation diffusion data. Profound changes in microstructure and crystal structure occur in these fuels, and these are described and related to the swelling behaviour.

EFFETS DE TAUX DE COMBUSTION ÉLEVÉS SUR LES OXYDES CÉRAMIQUES COMBUSTIBLES. La stabilité des oxydes céramiques combustibles, lors d'une irradiation à des taux de combustion élevés, a fait l'objet de recherches systématiques au Laboratoire d'énergie atomique Bettis, en vue de la mise au point d'un deuxième cœur pour le réacteur de Shippingport. La zone fertile contiendra une masse d'UO_2 susceptible de taux de combustion élevés. Le comportement de cette matière dans le réacteur a été étudié pour des taux de combustion allant jusqu'à environ $40 \cdot 10^{20}$ fissions/cm^3 (127 000 MWj/t, 17% d'atomes d'U désintégrés). En outre, de nombreux travaux ont été exécutés sur un oxyde céramique combustible destiné à la zone active du cœur. Les recherches ont notamment porté sur le l'UO_2 enrichi à 93% en solution solide avec du ZrO_2, et sur de l'UO_2 enrichi, dispersé dans les matrices de BeO et Al_2O_3. Ces matières ont fait l'objet d'essais analogues à ceux auxquels a été soumise la masse d'UO_2.

Les auteurs comparent les modifications du volume de ces oxydes combustibles, provoquées par l'irradiation à des taux de combustion élevés, et ils indiquent les facteurs qui agissent sur le gonflement du combustible. Ils montrent que la fraction des gaz de fission théoriquement produits, qui est dégagée par le combustible à l'intérieur du réacteur, est fonction du taux de combustion et de la température de fonctionnement. Ils comparent ces résultats à ceux que prévoit la théorie de la diffusion volumique, en se fondant sur des données relatives à la diffusion après irradiation. La microstructure et la structure cristalline des combustibles considérés subissent de profondes modifications que les auteurs décrivent en les rapprochant des phénomènes de gonflement.

ВЛИЯНИЕ ГЛУБОКОГО ВЫГОРАНИЯ НА КЕРАМИЧЕСКОЕ ОКСИДНОЕ ТОПЛИВО. Стойкость к облучению керамического оксидного топлива при глубоком выгорании явилась предметом продолжительных исследовательских усилий в атомно-энергетической лаборатории Беттис в связи с разработкой второй (Shippingport) активной зоны. Оболочка зоны воспроизводства будет содержать массу UO_2, способного к глубокому выгоранию. Были исследованы свойства этого материала внутри реактора при выгораниях, достигающих приблизительно $40 \cdot 10^{20}$ делений/см^3 (127 000 мгвт-дней/т, 17 ат% разделившихся атомов урана). Широкие исследования также выполнялись с керамическим оксидным топливным материалом для района запальной сборки активной зоны. Эти исследования включали UO_2, обогащенный до 93% в твердом растворе с ZrO_2, и обогащенный UO_2, рассеянный в матрицах BeO и Al_2O_3. Эти материалы были испытаны аналогично массе UO_2.

Сравнивается изменение объема, вызванное радиацией в этих керамических оксидных топливных материалах при глубоком выгорании и описываются факторы, влияющие на разбухание топлива. Часть теоретически получаемых газообразных продуктов деления, освобожденных внутри реактора из топлива, как показано, связана с выгоранием топлива и с рабочей температурой. Эти результаты сравниваются с результатами, предсказанными теорией объемной диффузии, которая использует данные диффузии после облучения. В микроструктуре и кристаллической структуре этого топлива происходят глубокие изменения, которые описываются и связываются с поведением топлива при разбухании.

EFECTOS DE UN ELEVADO GRADO DE COMBUSTIÓN SOBRE LOS COMBUSTIBLES A BASE DE ÓXIDOS CERÁMICOS. Con miras al desarrollo de un segundo cuerpo para el reactor de Shippingport, se ha venido estudiando minuciosamente en el Bettis Atomic Power Laboratory la estabilidad a la irradiación hasta elevados grados de combustión de los combustibles a base de óxidos cerámicos. La zona de la envoltura fértil contendrá UO_2 en masa capaz de alcanzar elevados grados de combustión. Se investigaron las propiedades de este material en el interior del reactor a grados de combustión de hasta unos 40×10^{20} fisiones/cm^3 (127 000 MWd/t, que corresponden a la fisión del 17% de los átomos de U). Tambien se estudió muy extensamente un material combustible a base de óxidos cerámicos para la zona de siembra del cuerpo de reactor. Estas investigaciones se efectuaron con UO_2 enriquecido al 93 por ciento en solución sólida en ZrO_2, y UO_2 enriquecido dispersado en matrices de BeO y Al_2O_3, que fueron ensayados de manera similar al UO_2 en masa.

La memoria compara los cambios de volumen inducidos por las radiaciones a grados elevados de combustión en estos materiales a base de óxidos y describe los factores que ejercen influencia sobre el crecimiento cristalino del combustible. Demuestra que el cociente gases de fisión liberados en el reactor/gases de fisión producidos teóricamente depende del grado de combustión y de la temperatura de trabajo. Compara estos resultados con los que predice la teoría de difusión en volumen basándose en datos sobre la difusión obtenidos después de la irradiación. La microestructura y la estructura cristalina de estos combustibles sufren cambios muy marcados, que la memoria describe y relaciona con el fenómeno de crecimiento.

1. INTRODUCTION

The excellent stability of UO_2 under irradiation has been reported by many investigators and has been recently reviewed by LUSTMAN [1]. These results have led to increased interest in the stability of oxide ceramic fuel materials among which, in addition to UO_2, are fuels containing UO_2 dispersed in matrices of BeO and Al_2O_3 as well as UO_2 in solid solution with ZrO_2 and $ZrO_2 + CaO_2$ [2, 5]. In general, the previously published information has been obtained on samples of fuel pellets sheathed in metallic tubes and therefore, as a result of temperature limitations on allowable fissioning rates, the material was exposed to relatively low levels of fission-fragment damage.

Of particular interest to the developmental programme for the second core of the Shippingport (PWR) reactor* is the irradiation stability of oxide ceramic fuels to high burn-ups. This is a consequence of the design criteria for this core of increased power and lifetime over that of PWR core I. The core will consist of a natural UO_2 blanket surrounding a U^{235}-enriched seed, which drives the blanket and which shares equally the total power generated. In order to maximize the heat-transfer surface and to reduce the fuel temperatures, the fuel will be incorporated in plate form; these design parameters are described in more detail by SHERMAN [6]. Consequently, the irradiation test programmes described herein were designed to determine the in-pile behaviour of oxide ceramic fuel materials up to exposures

* Pressurized Water Reactor: Shippingport, Pa, USA

of about 40×10^{20} fission/cm^3 (127 000 MWd/t, 17 at.% uranium fission in UO_2) in fuel geometries similar to those of the core II fuel elements and in-pile thermal conditions which were equal to or more severe than those anticipated in the PWR-2 core. Therefore the various materials investigated were run under essentially identical conditions, thus permitting direct comparison of the behaviour.

This report summarizes the effects of fission-fragment bombardment on the structure, dimensions, and properties of unalloyed, bulk UO_2, and UO_2 in single or multi-phase solid solution with ZrO_2. Also discussed in this report is the change observed in the ceramic materials BeO and Al_2O_3 in which UO_2 has been homogeneously dispersed as small particles (nominal sizes 5 - 10 μm diam.) so that the relative stability of these non-fissionable materials as matrices could be compared to that of UO_2 and $ZrO_2 + UO_2$. The various oxide ceramic materials are compared on the basis of fuel volume changes, ability to retain the generated, noble fission-gases and structural changes.

2. EXPERIMENTAL TECHNIQUES

2.1. Sample preparation

All of the samples used in this investigation were plate-type fuel elements which consisted of ceramic fuel cores, bonded with Zircaloy-2 cladding. A sketch of a multi-compartment fuel element in exploded view is shown in Fig. 1.

The bulk UO_2 wafers were prepared both by mechanical and chemical mixing of enriched and natural UO_2 powders to obtain the desired enrichments. The powders were agglomerated with a volatile binder, pressed into a briquette and sintered to high density at 1700-1750°C in a hydrogen atmosphere. Final dimensions were obtained by grinding with 240 silicon-carbide grit. A similar technique was utilized for the ZrO_2-UO_2 wafers except that the blended, finely-subdivided (< 1 μm) reactor-grade ZrO_2 and enriched UO_2 powders were pre-calcined at 1700°C and then recomminuted to < 1 μm size before the final pressing and sintering in order to assure micro-homogeneity. Before insertion into the fuel element, all fuel cores were coated with 2-3 μm of carbon (usually by pyrolytic decomposition of CH_4) to prevent reaction between UO_2 and the zirconium-alloy cladding during the bonding process. Where wafers of a density less than 95-98% were to be irradiated, additional amounts of binder (polyvinyl alcohol) were incorporated in the briquettes; this volatilized and left microscopic voids after sintering.

The ceramic dispersion fuel cores, which contained 21 wt.% UO_2 dispersed in Al_2O_3 or either 51 or 65 wt.% UO_2 dispersed in BeO, were made in an analogous manner to the bulk UO_2. The high-density enriched UO_2 particles were prepared by crushing and sieve sizing; these particles were then mechanically mixed with the fine BeO or Al_2O_3 matrix powder, pressed into briquettes, sintered to high density and then ground to the final size. Only dispersions containing "fine" UO_2 particles in which the matrix phase is uniformly bombarded with fission fragments are considered in this report.

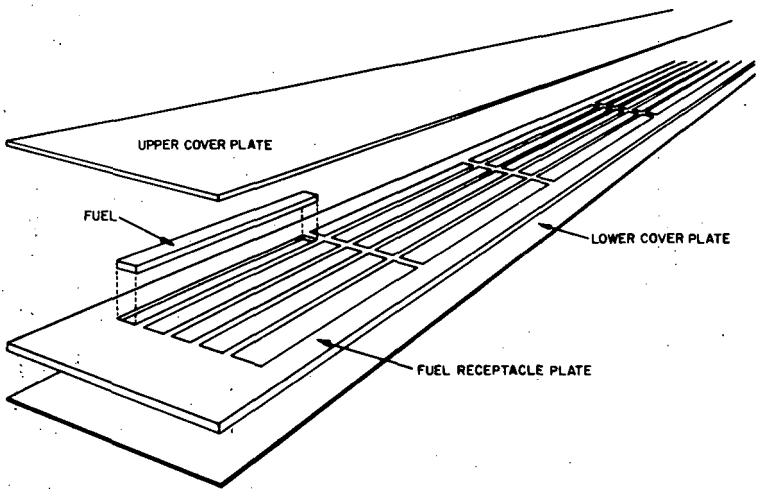


Fig. 1

Schematic representation of cladding and fuel components for a compartmented, oxide, plate-type fuel element

In the Al_2O_3 matrix materials, the UO_2 particle diameters varied from about 1 to 10 μm, and may be considered as having a nominal diameter of about 5 μm. In the BeO matrix, the UO_2 showed a somewhat similar variation with an occasional particle ranging up to 50 μm; in this case the nominal particle size is considered as 10 μm. These were true dispersions in the sense that the dispersed phase and the matrix phase were pure components with no detectable mutual solid solubility.

The fuel-element samples considered in this investigation were clad with Zircaloy-2 or 4. The fabrication of samples containing these fuel cores was accomplished by both copper-eutectic diffusion bonding and by pressure bonding. In the former process, the fuel receptacle was coated with 0.15 - 0.20 mil* of copper. The receptacle, fuel cores and cover plates were assembled and the cover plates edge-welded to the receptacle in a vacuum chamber. The assembly was then bonded for 1 h at 1000°C and 60 lb/in^2 overpressure of helium. Further details on this bonding procedure have been reported by WOLFE et al. [7]. In the pressure-bonding procedure, the zirconium-alloy components were abraded and cleaned, and assembled with the fuel cores into a fuel element. The assembled elements were then bonded at 1525°F for 4 h at 10 000 lb/in^2. The details of the pressure-bonding technique have been reported by PAPROCKI et al. [8]. The only significant difference between these bonding methods with respect to fuel behaviour is that in the former case about 10% void volume can be (and usually was) incorporated in the fuel compartment external to the oxide wafer, whereas in the latter, no void volume external to the water could be included.

* mil = 0.001 in.

The samples included in this investigation are listed in Table I by sample numbers, along with type of fuel core, bonding technique, number of fuel compartments per sample and compartment geometry. The in-pile operating parameters of all samples are listed in Table II.

2.2. Irradiation

Irradiation testing of all but two of these samples was conducted in pressurized hot-water loops designed to simulate the conditions of operation in the Shippingport (PWR) reactor. A complete description of the loop-testing technique has been given by COHEN and WROUGHTON [9]. The samples were tested in the VH-3 loop and the WAPD-30 loop in MTR, the J-10 loop in ETR, the X-3, X-6, and CR-V loops in the NRX reactor and the J-16 loop in NRU at Chalk River, Canada. The loop water pressure varied from 1140 to 2200 lb/in^2 and the bulk water temperature from 480 to 540°F. The loop water was monitored to detect the presence of fission products and it was by this means that sample failure, if it occurred, was detected. In these cases, the sample was removed either immediately or at the most convenient scheduled reactor shut-down. In addition, the samples were periodically removed from the loops and subjected to an interim dimensional and visual examination and then re-inserted into the loop for additional exposure. Upon completion of the test, the samples were subjected to a complete examination in the Bettis Hot Laboratory. Two samples of interest, containing BeO + 65 wt. % UO_2 or BeO + 51 wt. % UO_2 respectively, were irradiated in pressurized NaK-filled capsules (59-2, B3-35; and 59-3, PB# 3) and these are also shown in Tables I and II.

2.3. Post-irradiation evaluation

Post-irradiation evaluation of these fuel elements consisted of dimensional measurements, density measurements of the fuel, determination of fission-gas release, metallographic examination of the fuel and cladding and X-ray diffraction analyses. Dimensional measurements were made on the thicknesses of the fuel elements over fuel cores using a micrometer operated remotely by Selsyn motors. Density measurements were made by conventional immersion-weighing techniques modified for remote operation and residual specimen activity; the specific technique is described by DANIEL et al. [11]. Fission-gas release determinations were performed on each undefected fuel element by puncturing the cladding while the element was contained in an evacuated chamber. Gases entrapped in the fuel-compartment void volume expanded into the chamber and the pressure changes were monitored to furnish a measure of the total gas release; from the chamber the gases were pumped into sampling flasks. The collected gases were counted for Kr^{85} and also analysed by mass-spectrometric techniques for the total quantity of gases present. These results were compared with the total theoretical amount of stable fission gases produced and the percentage of gas release calculated. Metallography was performed by remote hot-laboratory techniques on samples cut from the fuel elements by a water-submerged, abrasive cut-off wheel. The X-ray diffraction analyses were performed on pieces of fuel cores using a double-crystal

TABLE I

DESCRIPTION OF TEST ELEMENTS

		COMPOSITION	FUEL VARIABLES		FUEL ELEMENT VARIABLES				
Test	Element		Av. fuel density	Nominal fuel dimensions	Bonding method	Bonding temperature	Array	Cladding material	Cladding thickness
(No.)	(No.)	(wt. %)	(% TD)	(in)		(°F)			(mil)
A.				BULK UO_2 FUEL					
CRV-m	I21	37.0	96	0.040×0.50 ×3.0	CuD.B.	1850 (½ hr)	4 × 3	Zr-2	21
	J23	37.0	96	0.040×0.50 ×3.0	CuD.B.	1850 (½ hr)	8 × 3	Zr-2	24
	D107	16.2	96	0.12 ×0.375×3.0	CuD.B.	1850 (½ hr)	5 × 3	Zr-2	21
	E9	20.5	96	0.08 ×0.50 ×3.0	CuD.B.	1850 (½ hr)	4 × 3	Zr-2	25
	C112	20.5	96	0.08 ×0.375×3.0	CuD.B.	1850 (½ hr)	5 × 3	Zr-2	24
	A104	20.5	96	0.08 ×0.250×3.0	CuD.B.	1850 (½ hr)	7 × 3	Zr-2	21
	B26	16.2	96	0.12 ×0.250×3.0	CuD.B.	1850 (½ hr)	6 × 3	Zr-2	24
	C6	20.5	96	0.08 ×0.375×3.0	CuD.B.	1850 (½ hr)	5 × 3	Zr-2	24
	G102	12.4	96	0.16 ×0.375×3.0	CuD.B.	1850 (½ hr)	4 × 3	Zr-2	21
	F13	12.4	96	0.16 ×0.25 ×3.0	CuD.B.	1850 (½ hr)	6 × 3	Zr-2	24
X3L	X1B32	20.3	98	2 comp: 0.10×0.25×6.0 4 comp: 0.10×0.25×1.5	CuD.B.	1900 (1 hr)	2 × 3	Ni-free Zr-2	20

enrichment

	X2N10	14.8	97	2 comp: 0.10×0.25×6.0 4 comp: 0.10×0.25×1.5	CuD.B.	1900 (1 hr)	2 × 3	Zr-4	20
	X3N10	52.1	97	2 comp: 0.04×0.25×6.0 4 comp: 0.04×0.25×1.5	CuD.B.	1900 (1 hr)	2 × 3	Zr-4	17
	X4B42	52.1	97	2 comp: 0.04×0.25×6.0 4 comp: 0.04×0.25×1.5	CuD.B.	1850 (1 hr)	2 × 3	Ni-free Zr-2	17
	X5N11	60.4	98	0.04 ×0.50 ×3.0	CuD.B.	1900 (1 hr)	Single	Zr-4	17
	X6N12	16.6	98	0.10 ×0.50 ×3.0	CuD.B.	1900 (1 hr)	Single	Zr-4	20
	X7N11	20.3	98	2 comp: 0.1 ×0.25×6.0 4 comp: 0.1 ×0.25×1.5	IPB	1550 (4 hr)	2 × 3	Zr-4	20
X3M	M11, Tier 1	20.3	98	0.10 ×0.25 ×1.5	IPB	1550 (4 hr)	2 × 6	Ni-free Zr-2	20
	M11, Tier 2	20.3	90	0.10 ×0.25 ×1.5	IPB	1550 (4 hr)	2 × 6	Ni-free Zr-2	20
	M22, Tier 1	14.8	97	0.10 ×0.25 ×1.5	IPB	1550 (4 hr)	2 × 6	Ni-free Zr-2	20
	M31	52.1	97	0.04 ×0.25 ×1.5	IPB	1550 (4 hr)	2 × 6	Ni-free Zr-2	20
	M42	52.1	88	0.04 ×0.25 ×1.5	IPB	1550 (4 hr)	2 × 6	Ni-free Zr-2	20
	M52, Tier 1	60.4	96	0.04 ×0.25 ×1.5	IPB	1550 (4 hr)	2 × 2	Ni-free Zr-2	20
	M72	20.3	98	0.04 ×0.25 ×1.5	IPB	1550 (4 hr)	2 × 6	Ni-free Zr-2	20
X1P	1H2	52.0	97	0.04 ×0.25 ×1.5	IPB	1550 (4 hr)	2 × 3	Ni-free Zr-2	20
	2H1	55.4	96	0.04 ×0.25 ×1.5	IPB	1550 (4 hr)	2 × 3	Ni-free Zr-2	20
	2H2	55.4	96	0.04 ×0.25 ×1.5	IPB	1550 (4 hr)	2 × 3	Ni-free Zr-2	20
	3H2	55.4	96	0.04 ×0.25 ×1.5	IPB	1550 (4 hr)	2 × 3	Ni-free Zr-2	20
	4H2	52.0	97	0.04 ×0.25 ×1.5	IPB	1550 (4 hr)	2 × 3	Ni-free Zr-2	20
	5H1	63.7	96	0.04 ×0.50 ×1.5	IPB	1550 (4 hr)	4 × 3	Ni-free Zr-2	20

enrichment

TABLE I cont.

		COMPOSITION	FUEL VARIABLES		FUEL ELEMENT VARIABLES				
Test	Element		Av. fuel density	Nominal fuel dimensions	Bonding method	Bonding temperature	Array	Cladding material	Cladding thickness
(No.)	(No.)	(wt. %)	(% TD)	(in)		(°F)			(mil)
A. cont.				BULK OF UO_2 FUEL					
X1P (cont.)	6H2	63.7	97	0.04 ×0.125×1.5	IPB	1550 (4 hr)	4 × 3	Ni-free Zr-2	20
	7H1	35.0	96	0.10 ×0.25 ×1.5	IPB	1550 (4 hr)	4 × 3	Ni-free Zr-2	20
	8H2	21.4	97	0.160×0.25 ×1.5	IPB	1550 (4 hr)	4 × 3	Ni-free Zr-2	20
	9H1	63.7	96	0.04 ×0.25 ×1.5	IPB	1550 (4 hr)	4 × 3	Ni-free Zr-2	20
	1L1	63.7	89	0.04 ×0.25 ×1.5	IPB	1550 (4 hr)	4 × 3	Ni-free Zr-2	20
	1L2	63.7	89	0.04 ×0.25 ×1.5	IPB	1550 (4 hr)	4 × 3	Ni-free Zr-2	20
	2L1	55.4	87	0.04 ×0.25 ×1.5	IPB	1550 (4 hr)	4 × 3	Ni-free Zr-2	18
	2L2	55.4	87	0.04 ×0.25 ×1.5	IPB	1550 (4 hr)	4 × 3	Ni-free Zr-2	20
	3L1	55.4	89	0.04 ×0.25 ×1.5	IPB	1550 (4 hr)	4 × 3	Ni-free Zr-2	20
	4L1	63.7	88	0.04 ×0.25 ×1.5	IPB	1550 (4 hr)	4 × 3	Ni-free Zr-2	20
VH3-23	W5	60.4	98	0.030×0.25 ×1.5	IPB	1550 (4 hr)	1 × 4	Ni-free Zr-2	15
VH3-28	H11	60.4	97	1 comp: 0.036×0.25×1.5 1 comp: 0.036×0.25×4.5	PackP.B.	1560 (4 hr)	1 × 2	Ni-free Zr-2	20
29-13	7	6.0	97	0.08 ×0.25 ×3.0	CuD.B.	1832 (½ hr)	1 × 2	Zr-2	25

enrichment

	8	3.8	97	0.08 ×0.25 ×3.0	CuD.B.	1832 (½ hr)	1 × 2	Zr-2	25
	9	3.8	97	0.08 ×0.25 ×3.0	CuD.B.	1832 (½ hr)	1 × 2	Zr-2	25
30-5	52	7.1	97	0.10 ×0.50 ×3.0	CuD.B.	1832 (½ hr)	3 × 3	Zr-2	21
	55	7.1	97	0.10 ×0.50 ×3.0	FeD.B.	1832 (½ hr)	3 × 3	Zr-2	21
X-1-m	X1	14.0	94	0.120×0.50 ×2.0	CuD.B.	1832 (½ hr)	1 × 3	Zr-2	25
29-10	b	6.1	96	0.038×0.42 ×1.0	NiD.B.	1876 (2 hr)	1 × 4	Zr-2	17
	c	6.1	96	0.038×0.42 ×1.0	NiD.B.	1876 (2 hr)	1 × 4	Zr-2	17
X-1-c	X-102	11.2	97	0.100×0.25 ×6.0	CuD.B.	1832 (½ hr)	2 × 2	Zr-2	21
	X1B	11.2	97	0.100×0.25 ×6.0	P.B.	1550 (4 hr)	2 × 2	Zr-2	21
	X3B	12.3	97	0.100×0.25 ×6.0	P.B.	1550 (4 hr)	2 × 2	Zr-2	21
	X103	11.2	97	0.100×0.25 ×6.0	CuD.B.	1832 (½ hr)	2 × 2	Zr-2	21
	X205	12.3	97	0.100×0.25 ×6.0	CuD.B.	1832 (½ hr)	2 × 2	Zr-2	21
B.				UO_2 DISPERSED IN Al_2O_3 AND BeO					
29-10	1	Al_2O_3 - 21.0 UO_2 (nominal 5 μm particle size)	96	0.036×0.51 ×1.0	NiD.B.	1870 (2 hr)	1 × 4	Zr-2	17
30-3	T04	Al_2O_3 - 21.0 UO_2 (nominal 5 μm particle size)	96	0.080×0.61 ×0.61	NiD.B.	1870 (2 hr)	3 × 14	Zr-2	25
	T17	Al_2O_3 - 21.0 UO_2 (nominal 5 μm particle size)	96	0.080×0.61 ×0.61	NiD.B.	1870 (2 hr)	3 × 14	Zr-2	25

enrichment

TABLE I cont.

		COMPOSITION	FUEL VARIABLES		FUEL ELEMENT VARIABLES				
Test	Element		Av. fuel density	Nominal fuel dimensions	Bonding method	Bonding temperature	Array	Cladding material	Cladding thickness
(No.)	(No.)	(wt. %)	(% TD)	(in)		(°F)			(mil)
B. cont.			UO_2 DISPERSED IN Al_2O_3 AND BeO						
29-22	9	BeO - 65.0 UO_2 (nominal 10 μm particle size	97	0.030×0.25 ×1.5	CuD.B.	1832 ($\frac{1}{2}$ hr)	1 × 4	Zr-2	15
59-2	B3-35	BeO - 65.0 UO_2 (nominal 10 μm particle size)	97	0.020×0.25 ×1.5	CuD.B.	1832 ($\frac{1}{2}$ hr)	2 × 2	Zr-2	20
59-3	PB # 3	BeO - 51.0 UO_2 (nominal 10 μm particle size)	97	0.030×0.25 ×1.5	P.B.	1550 (4 hr)	2 × 2	Zr-2	18
C.			ZrO_2 - BASED FUELS						
J-16	13A	ZrO_2 - 25.6 UO_2	91.2	0.25 ×1.5 ×0.036	IPB	1550 (4 hr)	2 × 3	Ni-free Zr-2	20
	14A	ZrO_2 - 25.3 UO_2	95.2	0.25 ×1.5 ×0.036	IPB	1550 (4 hr)	2 × 3	Ni-free Zr-2	20
	14C	ZrO_2 - 25.1 UO_2	89.9	0.25 ×1.5 ×0.036	IPB	1550 (4 hr)	2 × 3	Ni-free Zr-2	20

	16D	ZrO_2 - 26.1 UO_2	95.6	0.25 ×1.5 ×0.036	IPB	1550 (4 hr)	2 × 3	Ni-free Zr-2	20
	BFD	ZrO_2 - 25.8 UO_2	93.9	0.25 ×1.5 ×0.036	IPB	1550 (4 hr)	2 × 3	Ni-free Zr-2	20
	BFL	ZrO_2 - 25.8 UO_2	94.9	0.25 ×1.5 ×0.046	IPB	1550 (4 hr)	2 × 3	Ni-free Zr-2	15
	BFM	ZrO_2 - 26.1 UO_2	88.5	0.25 ×1.5 ×0.046	IPB	1550 (4 hr)	2 × 3	Ni-free Zr-2	15
	BFN	ZrO_2 - 26.1 UO_2	88.3	0.25 ×1.5 ×0.036	IPB	1550 (4 hr)	2 × 3	Ni-free Zr-2	20
	BJD	ZrO_2 - 25.8 UO_2	96.8	0.25 ×1.5 ×0.036	IPB	1550 (4 hr)	2 × 3	Ni-free Zr-2	20
J-10	JR-42	ZrO_2 - 26.1 UO_2	95.2	0.25 ×1.5 ×0.036	IPB	1550 (4 hr)	3 × 4	Ni-free Zr-2	20
J-16	BFV	ZrO_2 - 30.0 UO_2	96.3	0.25 ×1.5 ×0.036	IPB	1550 (4 hr)	2 × 3	Ni-free Zr-2	20
	BFW	ZrO_2 - 29.8 UO_2	94.6	0.25 ×1.5 ×0.036	IPB	1550 (4 hr)	2 × 3	Ni-free Zr-2	20
	B91	ZrO_2 - 36.8 UO_2	96.1	0.25 ×1.5 ×0.036	IPB	1550 (4 hr)	2 × 3	Ni-free Zr-2	20
	B92	ZrO_2 - 36.8 UO_2	96.1	0.25 ×1.5 ×0.036	IPB	1550 (4 hr)	2 × 3	Ni-free Zr-2	20
	CLA	ZrO_2 - 36.5 UO_2 - 1.0 Fe	96.0	0.25 ×1.5 ×0.036	*PPB + BQ	1550 (4 hr)	2 × 3	Ni-free Zr-2	20
	CLD	ZrO_2 - 36.5 UO_2 - 0.5 Fe	96.0	0.25 ×1.5 ×0.036	*PPB + BQ	1550 (4 hr)	2 × 3	N -free Zr-2	20
	CLE	ZrO_2 - 36.5 UO_2 - 1.0 Fe	96.0	0.25 ×1.5 ×0.036	*PPB + BQ	1550 (4 hr)	2 × 3	Ni-free Zr-2	20
	CLG	ZrO_2 - 36.5 UO_2 - 0.5 Fe	96.0	0.25 ×1.5 ×0.036	*PPB + BQ	1550 (4 hr)	2 × 3	Ni-free Zr-2	20
J-10	J28	ZrO_2 - 35.5 UO_2	97.5	0.25 ×1.5 ×0.030	IPB	1550 (4 hr)	3 × 2	Ni-free Zr-2	15
	J30	ZrO_2 - 35.3 UO_2	97.4	0.25 ×1.5 ×0.030	CDB	1850 (1 hr)	3 × 2	Ni-free Zr-2	15
	J35	ZrO_2 - 35.3 UO_2	97.7	0.25 ×1.5 ×0.030	CDB	1850 (1 hr)	3 × 2	Ni-free Zr-2	15
	J37	ZrO_2 - 35.3 UO_2	97.4	0.25 ×1.5 ×0.030	CDB	1850 (1 hr)	3 × 2	Ni-free Zr-2	15
	JR3	ZrO_2 - 35.8 UO_2	98.4	0.25 ×1.5 ×0.036	IPB	1550 (4 hr)	3 × 4	Ni-free Zr-2	20
	JR4	ZrO_2 - 35.8 UO_2	98.8	0.25 ×1.5 ×0.036	IPB	1550 (4 hr)	3 × 4	Ni-free Zr-2	20
	PB1	ZrO_2 - 35.5 UO_2	97.4	0.25 ×1.5 ×0.030	IPB	1550 (4 hr)	3 × 4	Ni-free Zr-2	15
VH-3	2	ZrO_2 - 34.6 UO_2	96.9	0.25 ×1.5 ×0.030	CDB	1850 (1 hr)	1 × 1	Ni-free Zr-2	16

* BQ - 10 minutes at 1900°F in gas-filled bulb and quenched in water without breaking bulb.

TABLE I cont.

		COMPOSITION	FUEL VARIABLES		FUEL ELEMENT VARIABLES				
Test	Element		Av. fuel density	Nominal fuel dimensions	Bonding method	Bonding temperature	Array	Cladding material	Cladding thickness
(No.)	(No.)	(wt. %)	(% TD)	(in)		(°F)			(mil)
C. cont.				ZrO_2 - BASED FUELS					
M-13	7GA	ZrO_2 - 34.4 UO_2	97.2	0.25 ×1.5 ×0.030	CDB	1850 (1 hr)	2 × 1	Ni-free Zr-2	15
M13/J16	7GB	ZrO_2 - 34.4 UO_2	97.2	0.25 ×1.5 ×0.030	CDB	1850 (1 hr)	2 × 1	Ni-free Zr-2	15
J-16	12A	ZrO_2 - 35.8 UO_2	97.1	0.25 ×1.5 ×0.036	IPB	1550 (4 hr)	2 × 3	Ni-free Zr-2	20
	12D	ZrO_2 - 37.0 UO_2	87.8	0.25 ×1.5 ×0.036	IPB	1550 (4 hr)	2 × 3	Ni-free Zr-2	20
	15B	ZrO_2 - 37.1 UO_2	88.4	0.25 ×1.5 ×0.036	IPB	1550 (4 hr)	2 × 3	Ni-free Zr-2	20
	16A	ZrO_2 - 35.8 UO_2	98.1	0.25 ×1.5 ×0.036	IPB	1550 (4 hr)	2 × 3	Ni-free Zr-2	20
	BFP	ZrO_2 - 34.6 UO_2	95.7	0.25 ×1.5 ×0.040	*IPB + BQ	1550 (4 hr)	2 × 3	Ni-free Zr-2	18
	BFR	ZrO_2 - 34.6 UO_2	95.7	0.25 ×1.5 ×0.040	*IPB + BQ	1550 (4 hr)	2 × 3	Ni-free Zr-2	18
	BFT	ZrO_2 - 35.7 UO_2	96.8	0.25 ×1.5 ×0.036	IPB	1550 (4 hr)	2 × 3	Ni-free Zr-2	20
	BFY	ZrO_2 - 34.6 UO_2	96.1	0.25 ×1.5 ×0.040	IPB	1550 (4 hr)	2 × 3	Ni-free Zr-2	18
	BFZ	ZrO_2 - 34.6 UO_2	96.1	0.25 ×1.5 ×0.040	IPB	1550 (4 hr)	2 × 3	Ni-free Zr-2	18
	BHA	ZrO_2 - 34.6 UO_2	96.0	0.25 ×1.5 ×0.040	IPB	1550 (4 hr)	2 × 3	Ni-free Zr-2	18
	BHB	ZrO_2 - 34.6 UO_2	95.5	0.25 ×1.5 ×0.040	IPB	1550 (4 hr)	2 × 3	Ni-free Zr-2	18
	BHC	ZrO_2 - 34.6 UO_2	95.4	0.25 ×1.5 ×0.040	IPB	1550 (4 hr)	2 × 3	Ni-free Zr-2	18

	BHD	ZrO_2 - 34.6 UO_2	95.4	0.25 ×1.5 ×0.040	IPB	1550 (4 hr)	2 × 3	Ni-free Zr-2	18
	BHE	ZrO_2 - 34.6 UO_2	95.7	0.25 ×1.5 ×0.040	IPB	1550 (4 hr)	2 × 3	Ni-free Zr-2	18
	BHF	ZrO_2 - 34.6 UO_2	95.4	0.25 ×1.5 ×0.040	IPB	1550 (4 hr)	2 × 3	Ni-free Zr-2	18
	BHH	ZrO_2 - 34.6 UO_2	95.5	0.25 ×1.5 ×0.040	IPB	1550 (4 hr)	2 × 3	Ni-free Zr-2	18
	BHJ	ZrO_2 - 34.9 UO_2	89.2	0.25 ×1.5 ×0.040	IPB	1550 (4 hr)	2 × 3	Ni-free Zr-2	18
	BHK	ZrO_2 - 34.9 UO_2	89.4	0.25 ×1.5 ×0.040	IPB	1550 (4 hr)	2 × 3	Ni-free Zr-2	18
	BHL	ZrO_2 - 34.9 UO_2	89.7	0.25 ×1.5 ×0.040	IPB	1550 (4 hr)	2 × 3	Ni-free Zr-2	18
	BHM	ZrO_2 - 34.9 UO_2	90.7	0.25 ×1.5 ×0.040	IPB	1550 (4 hr)	2 × 3	Ni-free Zr-2	18
	BHN	ZrO_2 - 34.9 UO_2	90.8	0.25 ×1.5 ×0.040	IPB	1550 (4 hr)	2 × 3	Ni-free Zr-2	18
	BHO	ZrO_2 - 34.9 UO_2	89.2	0.25 ×1.5 ×0.040	IPB	1550 (4 hr)	2 × 3	Ni-free Zr-2	18
	BHP	ZrO_2 - 34.9 UO_2	89.2	0.25 ×1.5 ×0.040	IPB	1550 (4 hr)	2 × 3	Ni-free Zr-2	18
	BHR	ZrO_2 - 34.9 UO_2	90.3	0.25 ×1.5 ×0.040	IPB	1550 (4 hr)	2 × 3	Ni-free Zr-2	18
	BHS	ZrO_2 - 34.9 UO_2	89.3	0.25 ×1.5 ×0.040	IPB	1550 (4 hr)	2 × 3	Ni-free Zr-2	18
	11B	ZrO_2 - 47.1 UO_2	97.5	0.25 ×1.5 ×0.036	IPB	1550 (4 hr)	2 × 3	Ni-free Zr-2	20
	11C	ZrO_2 - 47.1 UO_2	97.7	0.25 ×1.5 ×0.036	IPB	1550 (4 hr)	2 × 3	Ni-free Zr-2	20
	13C	ZrO_2 - 47.1 UO_2	96.2	0.25 ×1.5 ×0.036	IPB	1550 (4 hr)	2 × 3	Ni-free Zr-2	20
	BFU	ZrO_2 - 46.5 UO_2	89.6	0.25 ×1.5 ×0.025	IPB	1550 (4 hr)	2 × 3	Ni-free Zr-2	25
	BJO	ZrO_2 - 46.5 UO_2	89.6	0.25 ×1.5 ×0.025	IPB	1550 (4 hr)	2 × 3	Ni-free Zr-2	25
M13/J16	B71	ZrO_2 - 47.0 UO_2	95.5	0.25 ×1.5 ×0.025	IPB	1550 (4 hr)	2 × 3	Ni-free Zr-2	25
J-10	J1-9	ZrO_2 - 46.5 UO_2	97.2	0.25 ×1.5 ×0.030	IPB	1550 (4 hr)	3 × 4	Ni-free Zr-2	20
	J1-10	ZrO_2 - 46.5 UO_2	97.2	0.25 ×1.5 ×0.030	IPB	1550 (4 hr)	3 × 4	Ni-free Zr-2	20
	J64	ZrO_2 - 46.5 UO_2	97.2	0.25 ×1.5 ×0.020	IPB	1550 (4 hr)	3 × 4	Ni-free Zr-2	20
	JR34	ZrO_2 - 46.0 UO_2	96.0	0.25 ×1.5 ×0.036	IPB	1550 (4 hr)	3 × 4	Ni-free Zr-2	20

* BQ - 10 minutes at 1900°F in gas-filled bulb and quenched in water without breaking bulb.

TABLE I cont.

Test	Element	COMPOSITION	FUEL VARIABLES		FUEL ELEMENT VARIABLES				
			Av. fuel density	Nominal fuel dimensions	Bonding method	Bonding temperature	Array	Cladding material	Cladding thickness
(No.)	(No.)	(wt. %)	(% TD)	(in)		(°F)			(mil)
C. cont.				ZrO_2 - BASED FUELS					
VH-3	W-3	ZrO_2 - 47.0 UO_2	95.5	0.25 × 1.5 × 0.030	IPB	1550 (4 hr)	1 × 4	Ni-free Zr-2	165
J-10	J1-2	ZrO_2 - 18.0 UO_2	96	0.25 × 1.5 × 0.040	IPB	1550 (4 hr)	3 × 4	Ni-free Zr-2	15
	J1-3	ZrO_2 - 18.0 UO_2	96	0.25 × 1.5 × 0.040	IPB	1550 (4 hr)	3 × 4	Ni-free Zr-2	15
	J50	ZrO_2 - 18.0 UO_2	96	0.25 × 1.5 × 0.040	CDB	1850 (1 hr)	3 × 2	Ni-free Zr-2	15
	J51	ZrO_2 - 18.0 UO_2	96	0.25 × 1.5 × 0.040	CDB	1850 (1 hr)	3 × 2	Ni-free Zr-2	15
J-16	BJB	ZrO_2 - 18.7 UO_2	95.2	0.25 × 1.5 × 0.036	IPB	1550 (4 hr)	2 × 3	Ni-free Zr-2	20
	BJC	ZrO_2 - 18.7 UO_2	87.6	0.25 × 1.5 × 0.036	IPB	1550 (4 hr)	2 × 3	Ni-free Zr-2	20
	BHY	ZrO_2 - 60.8 UO_2	96.4	0.25 × 1.5 × 0.036	IPB	1550 (4 hr)	2 × 3	Ni-free Zr-2	20
	BHZ	ZrO_2 - 60.8 UO_2	98.1	0.25 × 1.5 × 0.036	IPB	1550 (4 hr)	2 × 3	Ni-free Zr-2	20
	BHX	ZrO_2 - 80.6 UO_2	98.8	0.25 × 1.5 × 0.036	IPB	1550 (4 hr)	2 × 3	Ni-free Zr-2	20
	BHV	ZrO_2 - 87.2 UO_2	97.7	0.25 × 1.5 × 0.036	IPB	1550 (4 hr)	2 × 3	Ni-free Zr-2	20
	BHW	ZrO_2 - 87.2 UO_2	97.4	0.25 × 1.5 × 0.036	IPB	1550 (4 hr)	2 × 3	Ni-free Zr-2	20
	BHT	ZrO_2 - 93.5 UO_2	96.4	0.25 × 1.5 × 0.036	IPB	1550 (4 hr)	2 × 3	Ni-free Zr-2	20
	BHU	ZrO_2 - 93.5 UO_2	92.0	0.25 × 1.5 × 0.036	IPB	1550 (4 hr)	2 × 3	Ni-free Zr-2	20
	M52T2	ZrO_2 - 94.0 UO_2	96	0.25 × 1.5 × 0.040	IPB	1550 (4 hr)	1 × 2	Ni-free Zr-2	20

spectrometer. The X-ray apparatus was described previously by BERMAN et al. [10].

3. FUEL VOLUME CHANGES

3.1. General considerations of fuel-plate geometry and factors limiting attainable burn-ups of plate bulk oxide fuel elements

During the irradiation tests, scheduled periodic examinations of dimension-changes in the fuel element geometry used in these experiments permitted a sensitive measurement of the fuel volume changes to be followed. The behaviour of oxide seed-fuel materials in plate-type geometries has been discussed in great detail by DANIEL et al. and RUBIN et al. [11, 12] and is reviewed here. In these test samples, the fuel and the cladding remained in intimate contact throughout the irradiation test for elements which operated at low temperatures and is illustrated in Fig. 2 for sample J23

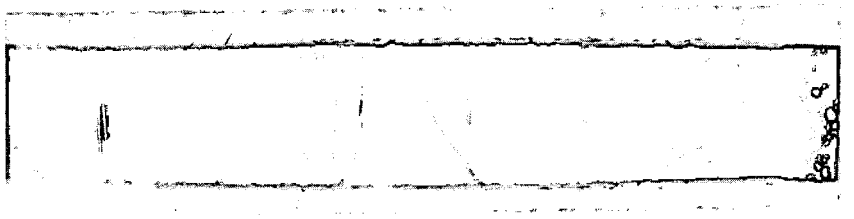


Fig. 2

Montage of element (as-polished) J23, compartment 16, after 30×10^{20} fissions/cm^3
(Note the contact between fuel and cladding and the pillow-shaped fuel swelling.
This element operated at 300 000 BTU h^{-1} ft^{-2} and contained 0.040-in thick UO_2 fuel)

[Original × 75]

containing 0.040-in thick UO_2 fuel, which operated at 300 000 BTU h^{-1} ft^{-2} up to 30×10^{20} fissions/cm^3. This figure shows the intimate contact between fuel and cladding which persisted up to these high exposures and also shows the relative plasticity of the irradiated UO_2 where it swelled into a pillow-shape, with the maximum swelling occurring at the compartment centre where the least restraint existed. This behaviour is typical of the oxide ceramic fuel materials considered here. Fuel elements which operated at high fuel temperatures showed the same behaviour until just before element failure (defined as rupture of the cladding) where they developed a gas-filled thermally insulating gap. Such a condition is illustrated in Fig. 3, where element M31, which did not fail in-pile, shows a fuel-cladding gap of about 1 mil and is typical of that observed in elements operating at high fuel-depletion rates. It is interesting to note that in the investigation of COHEN et al., the contact conductance between fuel and sheath of rod-type elements was insensitive to large gaps and this was attributed to the radial cracking of the UO_2 fuel pellet within the sheath [13] and the rearrangement of the fuel to effect a constant effective gap width. However, in the case of the plate geometry considered here, the edges of the fuel are supported by the cladding and the fuel platelet remains suspended between the cladding in

TABLE II

IN-PILE OPERATING CONDITIONS

Test	Element	Composition	Average start-up heat flux	Average start-up fuel ℄ temperature	Bulk water temperature	Loop pressure	Total EFPD	Total fissions
(No.)	(No.)	(wt. %)	(10^5 BTU h^{-1} ft^{-2})	(°F)	(°F)	(lb/in^2)		(10^{20} fissions/cm^3)
A.				BULK UO_2 FUEL				
CRV-m	I21	37.0	3.6	1340	(Loop inlet	Initially 2200 for all	401	29.0
	J23	37.0	3.6	1340	525°F	CRV-m elements;	406	30.0
	D107	16.2	3.3	2320	while at	reduced to 1140 after	632	17.0
	E9	20.5	3.5	1620	2200 lb/in^2	107-EFPD.	107	3.5
	C112	20.5	3.6	1650	and 490°F		333	13.0
	A104	20.5	3.9	1745	while at		333	13.0
	B26	16.2	3.8	2590	1140 lb/in^2)		632	17.0
	C6	20.5	3.6	1650			107	3.6
	G102	12.4	4.0	2420			107	1.9
	F13	12.4	4.0	2420			632	13.0
X3L	X1B32	20.3	5.6	2580	490	2000	476	17.0
	X2N10	14.8	5.6	2620	496	2000	191	6.8
	X3N10	52.1	7.0	2360	502	2000	191	22.0
	X4B42	52.1	7.0	2360	511	2000	121	14.0

enrichment

	X5N11	60.4	6.9	2340	518	2000	191	22.0
	X6N12	16.6	5.1	2300	521	2000	501	15.0
	X7N11	20.3	5.1	2300	523	2000	440	15.0
X3M	M31	52.1	7.0	2120	502	2000	164	20.0
	M42	52.1	6.4	2110	511	2000	338	35.0
	M52, Tier 1	60.4	6.9	2100	518	2000	164	20.0
	M72	20.3	7.0	3200	502	2000	103	5.9
X1P	1H2	52.0	7.0	2125	476	2000	145	18.0
	2H1	55.4	6.9	2100	468	2000	141	17.0
	2H2	55.4	6.5	2200	464	2000 (lowered to 1700 after ? EFPD)	197	21.0
	3H2	55.4	6.9	2100	468	2000	150	18.0
	4H2	52.0	7.0	2125	476	2000	139	17.0
	5H1	63.7	6.9	2200	484	2000	150	19.0
	6H2	63.7	6.9	2315	464	2000 (lowered to 1700 after ? EFPD)	262	31.0
	7H1	35.0	6.9	3160	488	2000 (lowered to 1700 after ? EFPD)	231	11.0
	8H2	21.4	7.0	3840	460	2000 (lowered to 1700 after 139 EFPD)	198	6.2
	1L1	63.7	6.7	2385	480	2000 (lowered to 1700 after 139 EFPD)	262	18.0
	2L1	55.4						

enrichment

TABLE II cont.

Test	Element	Composition	Average start-up heat flux	Average start-up fuel ℄ temperature	Bulk water temperature	Loop pressure	Total EFPD	Total fissions
(No.)	(No.)	(wt. %)	(10^5 BTU h^{-1} ft^{-2})	(°F)	(°F)	(lb/in^2)		(10^{20} fissions/cm^3)
A. cont.				BULK UO_2 FUEL				
X1P (cont.)	2L2	55.4	6.5	2335	472	2000	141	18.0
	3L1	55.4	6.5	2335	472	2000 (lowered to 1700 after 159 EFPD)	260	31.0
	4L1	63.7	6.7	2395	480	2000	138	18.0
VH3-23	W5	60.4	6.7	1800	464	2200	107	14 to 21
VH3-28	H11	60.4	7.2	1900	464	1700	163	17 to 25
29-13	7	6.0	3.9	1700	450	2200	63	2.4
	8	3.8	5.5	2210	450	2200	63	3.4
	9	3.8	4.0	1730	450	2200	63	2.3
30-5	52	7.1	1.7	1190	535	2200	231	3.0
	55	7.1	1.7	1190	535	2200	231	3.0
X-1-m	X1	14.0	4.9	3190	490	2000	32	1.2
29-10	b	6.1	5.5	1715	450	2200	65	5.6
	c	6.1	2.9	1120	450	2200	65	3.0
X-1-c	X-102	11.2	5.8	2730	475	2000	65	1.9

enrichment

	X-1-B	11.2 ↑ enrichment	5.7	2700	475	2000	152	5.8
	X-3-B	12.3	5.0	2525	475	2000	152	5.8
	X-103	11.2	5.8	2735	475	2000	87	2.6
	X-205	12.3 ↓	5.5	2620	475	2000	152	5.8
B.				UO_2 DISPERSED IN Al_2O_3 AND BeO				
29-10	1	Al_2O_3 - 21.0 UO_2 (nominal 5 μm particle size)	5.25	1360	450	2200	65	4.0
30-3	T04	Al_2O_3 - 21.0 UO_2 (nominal 5 μm particle size)	4.0	1440	540	2200	36	0.9
	T17	Al_2O_3 - 21.0 UO_2 (nominal 5 μm particle size)	4.0	1440	540	2200	36	0.9
29-22	9	BeO - 65.0 UO_2 (nominal 10 μm particle size)	6.2	1270	450	2200	229	14.2
59-2	B3-35	BeO - 65.0 UO_2 (nominal 10 μm particle size)	7.2	1580	NaK-filled Capsule Test	500	165	35.7
59-3	PR # 3	BeO - 51.0 UO_2 (nominal 10 μm particle size)	9.5	2060		100	185	28.0

TABLE II cont.

Test	Element	Composition	Average start-up heat flux	Average start-up fuel ℄ temperature	Bulk water temperature	Loop pressure	Total EFPD	Total fissions
(No.)	(No.)	(wt. %)	(10^5 BTU h^{-1} ft^{-2})	(°F)	(°F)	(lb/in^2)		(10^{20} fissions/cm^3)
C.				ZrO_2-BASED FUELS				
J-16	13A	ZrO_2-25.6 UO_2	5.83	1843	490	2000	327	21.8
	14A	ZrO_2-25.3 UO_2	6.33	1908	490	2000	327	22.6
	14C	ZrO_2-25.1 UO_2	5.79	1615	490	2000	125	11.1
	16D	ZrO_2-26.1 UO_2	6.35	1912	490	2000	327	23.2
	BFD	ZrO_2-25.8 UO_2	6.04	1874	490	2000	239	21.8
	BFL	ZrO_2-25.8 UO_2	6.85	2134	490	2000	239	22.0
	BFM	ZrO_2-26.1 UO_2	6.25	2053	490	2000	239	20.5
	BFN	ZrO_2-26.1 UO_2	5.97	1875	490	2000	239	20.6
	BJD	ZrO_2-25.8 UO_2	5.86	1803	490	2000	239	21.4
J-10	JR42	ZrO_2-26.1 UO_2	3.32	1173	490	2200/2000	175	16.4
J-16	BFV	ZrO_2-29.6 UO_2	5.65	1755	490	2000	239	22.5
	BFW	ZrO_2-29.6 UO_2	3.37	1180	490	2000	239	13.6
VH-3	2	ZrO_2-34.6 UO_2	5.5	2070	450	2200/2000	379	36.2
M-13	7GA	ZrO_2-34.4 UO_2	4.59	2120	450	1700	102	10.9
M13/J16	7GB	ZrO_2-34.4 UO_2	6.90	2120	490	1700/2000	262	29.5

J-16	12A	ZrO_2 - 35.8 UO_2	7.65	2204	490	2000	235	28.0
	12D	ZrO_2 - 37.0 UO_2	6.48	1993	490	2000	285	29.7
	15B	ZrO_2 - 37.1 UO_2	7.47	2223	490	2000	327	32.5
	16A	ZrO_2 - 35.8 UO_2	7.44	2157	490	2000	235	28.1
	BFP	ZrO_2 - 34.6 UO_2	7.26	2160	490	2000	197	23.6
	BFR	ZrO_2 - 34.6 UO_2	7.26	2160	490	2000	197	23.6
	BFT	ZrO_2 - 35.7 UO_2	8.08	2300	490	2000	197	26.2
	BFY	ZrO_2 - 34.6 UO_2	8.20	2376	490	2000	147	20.9
	BFZ	ZrO_2 - 34.6 UO_2	8.20	2376	490	2000	147	19.3
	BHA	ZrO_2 - 34.6 UO_2	8.10	2353	490	2000	147	18.9
	BHB	ZrO_2 - 34.6 UO_2	8.35	2411	490	2000	37	5.8
	BHC	ZrO_2 - 34.6 UO_2	6.91	2080	490	2000	80	9.6
	BHD	ZrO_2 - 34.6 UO_2	6.85	2065	490	2000	197	21.5
	BHE	ZrO_2 - 34.6 UO_2	6.55	1997	490	2000	197	23.1
	BHF	ZrO_2 - 34.6 UO_2	6.20	2125	490	2000	147	17.6
	BHH	ZrO_2 - 34.6 UO_2	8.70	2491	490	2000	160	20.1
	BHJ	ZrO_2 - 34.9 UO_2	7.72	2343	490	2000	197	22.9
	BHK	ZrO_2 - 34.9 UO_2	7.70	2338	490	2000	147	17.5
	BHL	ZrO_2 - 34.9 UO_2	8.15	2440	490	2000	37	5.3
	BHM	ZrO_2 - 34.9 UO_2	8.05	2422	490	2000	80	10.0
	BHN	ZrO_2 - 34.9 UO_2	6.74	2108	490	2000	239	24.1
	BHO	ZrO_2 - 34.9 UO_2	5.95	1918	490	2000	239	23.5
	BHP	ZrO_2 - 34.9 UO_2	7.85	2374	490	2000	202	23.5
	BHR	ZrO_2 - 34.9 UO_2	7.42	2271	490	2000	159	18.9

TABLE II cont.

Test	Element	Composition	Average start-up heat flux	Average start-up fuel ℄ temperature	Bulk water temperature	Loop pressure	Total EFPD	Total fissions
(No.)	(No.)	(wt. %)	(10^5 BTU h^{-1} ft^{-2})	(°F)	(°F)	(lb/in^2)		(10^{20} fissions/cm^3)
C. cont.				ZrO_2-BASED FUEL				
J-16 (cont.)	BHS	ZrO_2-34.9 UO_2	7.37	2259	490	2000	159	19.0
	B91	ZrO_2-34.9 UO_2	3.65/6.03	1230	490	2000	217	25.1
	B92	ZrO_2-34.9 UO_2	3.41/5.30	1165	490	2000	217	24.4
	CLA	ZrO_2-36.5 UO_2	8.05	2100	490	2000	92	12.6
	CLD	ZrO_2-36.5 UO_2	8.15	2120	490	2000	92	14.0
	CLE	ZrO_2-36.5 UO_2	8.05	2100	490	2000	92	12.6
	CLG	ZrO_2-36.5 UO_2	7.73	2036	490	2000	92	14.4
J-10	J28	ZrO_2-35.5 UO_2	6.21	1643	490	2200/1500	200	22.0
	JR3	ZrO_2-35.8 UO_2	3.36/8.50	1180	490	2200/1500	160	16.7
	JR4	ZrO_2-35.8 UO_2	7.43	2000	490	2200/1500	153	16.3
	PB1	ZrO_2-35.5 UO_2	6.26	1650	490	2200/1500	179	23.2
J-16	11B	ZrO_2-47.1 UO_2	8.70	2440	490	2000	125	19.9
	11C	ZrO_2-47.1 UO_2	8.25	2340	490	2000	125	21.2
	13C	ZrO_2-47.1 UO_2	8.10	2305	490	2000	125	20.0
	BFU	ZrO_2-46.5 UO_2	7.02	1971	490	2000	189	33.7
	BJO	ZrO_2-46.5 UO_2	5.90	1735	490	2000	92	18.8

M13/J16	B71	ZrO_2 - 46.5 UO_2	6.72	1868	490	1700/2000	167	27.1
J-10	J1-9	ZrO_2 - 46.5 UO_2	6.50	1610	490	2000	157	26.5
	J1-10	ZrO_2 - 46.5 UO_2	6.43	1600	490	2000	157	28.3
	J-64	ZrO_2 - 46.5 UO_2	6.06	1540	490	2200	144	23.7
VH-3	W-3	ZrO_2 - 46.5 UO_2	8.83	2178	450	2000	266	33.1
J-10	J1-2	ZrO_2 - 18.0 UO_2	4.93	1526	490	2200	55	4.0
J1-3	J1-3	ZrO_2 - 18.0 UO_2	4.96	1522	490	2200	55	4.0
	J50	ZrO_2 - 18.0 UO_2	5.28	1591	490	2200	55	4.2
	J51	ZrO_2 - 18.0 UO_2	5.34	1604	490	2200	55	4.3
J-16	BJB	ZrO_2 - 18.7 UO_2	5.05	1620	490	2000	239	15.7
	BJC	ZrO_2 - 18.7 UO_2	4.63	1570	490	2000	239	14.4
	BHY	ZrO_2 - 60.8 UO_2	6.91	2040	490	2000	239	25.8
	BHZ	ZrO_2 - 60.8 UO_2	5.67	1763	490	2000	239	22.4
	BHX	ZrO_2 -80.6 UO_2	6.87	2030	490	2000	147	17.5
	BHV	ZrO_2 -87.2 UO_2	6.18	1880	490	2000	239	24.0
	BHW	ZrO_2 - 87.2 UO_2	4.24	1440	490	2000	147	18.8
	BHT	ZrO_2 - 93.5 UO_2	6.18	1875	490	2000	197	21.4
	BHU	ZrO_2 - 93.5 UO_2	6.76	2050	490	2000	239	23.5

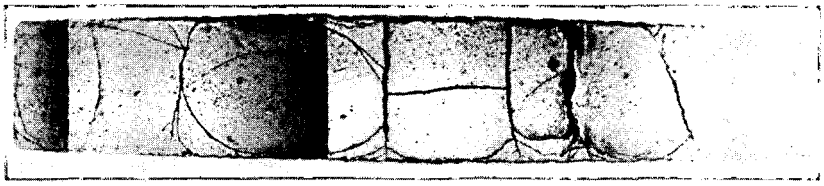


Fig. 3

Montage of element (as-polished) M31, compartment 1A, which did not rupture in-pile after 20×10^{20} fissions/cm^3
(Note the gap between fuel and cladding. This element operated at 630 000 BTU h^{-1} ft^{-2} and contained 0.040-in thick bulk UO_2 fuel)

[Original × 75]



Fig. 4

Montage of element (as-polished) M52, compartment 1A, which swelled 0.037 in after 20×10^{20} fissions/cm^3 and did not rupture in-pile
(Note the large gap between fuel and cladding and the severe overheating of the bulk UO_2 fuel. This element operated at 600 000 BTU h^{-1} ft^{-2} and contained 0.040-in thick UO_2 fuel)

[Original × 75]

spite of fuel cracking. Thus, severe overheating of the fuel is possible in this geometry and this is shown in Fig. 4 for element M52, containing 0.040 in thick UO_2.

The gaps illustrated in Figs. 3 and 4 were observed after irradiation; it is shown below that they also existed in the essential 'high-pressure water, in-pile loop' environment during irradiation. In the case of a total gap of 1 mil (i.e. $\frac{1}{2}$ mil on each fuel interface) it can be shown for element M31 (Fig. 3) that the measured fission-gas release (described in section 4) was equivalent to 6.9×10^{18} gas atoms per fuel compartment. At room temperature the pressure necessary to cause this deflection has been shown by LOSCO et al. to be 450 lb/in^2 [14]. Therefore the total gas volume at this pressure is calculated to be 9.2×10^{-3} cm^3 at room temperature. The volume corresponding to the clad deflection is 3.1×10^{-3} cm^3, and therefore the remainder of the gas volume, 6.1×10^{-3} cm^3, consists of the volume between fuel cracks shown in Fig. 3. At operating conditions in-pile, the gas pressure was 2450 lb/in^2 (2000 lb/in^2 system pressure + 450 lb/in^2 cladding pressure) and the average gas temperature was 1000°K, corresponding

to the estimated average fuel temperature. Furthermore, it was assumed that, due to the differential thermal expansion of fuel and cladding, the cracks shown in Fig. 3 were closed. With these assumptions, the gas pressure would create a total fuel-cladding gap of 1.6 mil. Thus it may be reasonably assumed that the gaps observed in destructive examination did exist in-pile and are of essentially the same magnitude as those observed during post-irradiation examination.

Throughout the entire life of fuel elements operating at the lower temperatures and, for elements operating at high temperatures, up to the time of element failure (since the cladding and the fuel remained in intimate contact to this time) the fuel centre-line temperatures of the plate elements can be calculated with a reasonable amount of assurance using one-dimensional heat flow theory. These calculations were performed as follows.

$$T_{CL}\,(\text{fuel}) = \Delta T(\text{fuel}) + \Delta T(\text{gap}) + \Delta T\,(\text{clad}) + \Delta T(\text{film}) + T_A$$

where

$$\Delta T_{CL}\,(\text{fuel}) = \frac{[Q/A]\ t(\text{fuel})}{48\quad K(\text{fuel})}$$

$\left\{\begin{array}{l} Q/A = \text{heat flux (BTU h}^{-1}\text{ft}^{-2}) \\ t(\text{fuel}) = \text{fuel thickness (in)} \\ K(\text{fuel}) = \text{thermal conductivity of fuel} \\ \qquad (\text{BTU h}^{-1}\,^{\circ}\text{F}^{-1}\text{ft}^{-1}) \end{array}\right\}$,

$$\Delta T(\text{gap}) = \frac{Q/A}{C}$$

C = gap conductance (BTU $h^{-1}\,^{\circ}F^{-1}ft^{-2}$),

$$\Delta T\,(\text{clad}) = \frac{[Q/A]\ t(\text{clad})}{12\quad K(\text{clad})}$$

$\left\{\begin{array}{l} t(\text{clad}) = \text{cladding thickness (in)} \\ K(\text{clad}) = \text{thermal conductivity of clad} \\ \qquad (7.52\ \text{BTU h}^{-1}\,^{\circ}\text{F}^{-1}\text{ft}^{-1}) \end{array}\right\}$,

$$\Delta T(\text{film}) = \frac{Q/A}{h}$$

$\left\{\begin{array}{l} h = \text{film coefficient} = 8000 \\ \quad (\text{BTU h}^{-1}\,^{\circ}\text{F}^{-1}\text{ft}^{-2}) \end{array}\right\}$,

and T_A = ambient temperature or average bulk water temperature

A value of thermal conductivity of 1 BTU $h^{-1}\,^{\circ}F^{-1}ft^{-1}$ was used for UO_2 and $ZrO_2 + UO_2$ fuels based on the data of DANIEL et al. [15] in Fig. 5. These results show that, at the burn-ups under consideration here [(6 to 36) $\times 10^{20}$ fissions/cm^3], a decrease in thermal conductivity of UO_2 of about 40% at 525°C (976°F) is a reasonable estimate for an average value of thermal conductivity of bulk UO_2. Assuming that a similar decrease occurs over the temperature range of interest here, i.e. up to about 3600°F, and using the unirradiated conductivity-data of Kingery as described by COHEN et al. [13], then the value of 1 BTU $h^{-1}\,^{\circ}F^{-1}ft^{-1}$ for UO_2 is felt to be reasonably conservative. These results also show that essentially no change in the effective thermal conductivity of $ZrO_2 + 46$ wt.% UO_2 and $ZrO_2 + 34$ wt.% UO_2 fuel materials occur up to about 10×10^{20} fissions/cm^3 and therefore the value of 1 BTU $h^{-1}\,^{\circ}F^{-1}ft^{-1}$ was utilized in these calculations. In the case of the UO_2 dispersed in Al_2O_3 and BeO matrices, it was assumed that the fuel body exhibited the thermal conductivity of the continuous matrix phase and

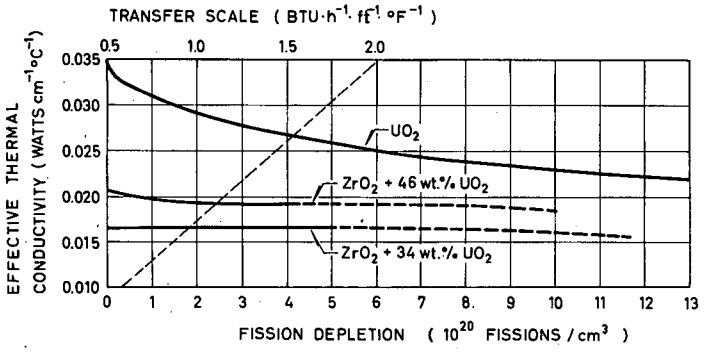


Fig. 5

Effective thermal conductivity of oxide ceramic fuels during irradiation at an average fuel temperature of 525°C

the values utilized here were 2 and 35 BTU $h^{-1}°F^{-1}ft^{-1}$ for the $Al_2O_3+UO_2$ and $BeO+UO_2$ fuel materials, respectively. In addition to these data, a small correction was made for the closed porosity of the samples in which the thermal conductivity was assumed to be reduced by the fractional density from the theoretical (i.e. 0.89 BTU $h^{-1}°F^{-1}ft^{-1}$ was used for 89% theoretical density fuel, UO_2-fuel platelet).

The data of COHEN et al. [13] were utilized to determine the contact conductance value of the plates in-pile. These irradiation tests allowed measurements of contact conductances between cold-pressed and sintered UO_2 and sheath materials in fuel-element samples to be made and these measurements were shown to agree qualitatively with the predictions of the Cetinkale-Fishenden theory. Thus, these data are applicable for the conditions of the tests described here and using the data of Cohen et al. the contact conductance values shown in Table III b were utilized for the loop water pressures of the samples. On the basis of these results, the in-pile limitations of the plate-type elements were established and were found to be sensitive to fuel temperatures as shown in Fig. 6 and Table III (a).

An explanation for the temperature variation of critical burn-up for compartment failure for bulk UO_2 and ZrO_2+UO_2 fuel materials is given by DANIEL et al. [11] and RUBIN et al. [12]. It is postulated by them that, at low temperatures, a combination of fuel swelling and internal precipitation of fission gases limits attainable fission depletions in UO_2 and ZrO_2+UO_2 fuels to a deflection of about 8 mil of the cladding (for $\frac{1}{4}$-in wide compartments with about 0.020 in of cladding, based on minimum values of Zircaloy-cladding ductility). As the fuel operating temperature is raised, the volume occupied by internally precipitated gases increases (see section 4). Furthermore, the amount of externally released gas relative to that precipitated internally increases, the former tending to deflect the cladding away from the fuel. Unlike the case of rod-type fuel elements, in which pellet fracture tends to maintain gap thicknesses at a constant maximum value, a plate fuel tends to remain centred within the element or to adhere to one cladding face only (shown in Figs. 3 and 4). These cladding deflections introduce large

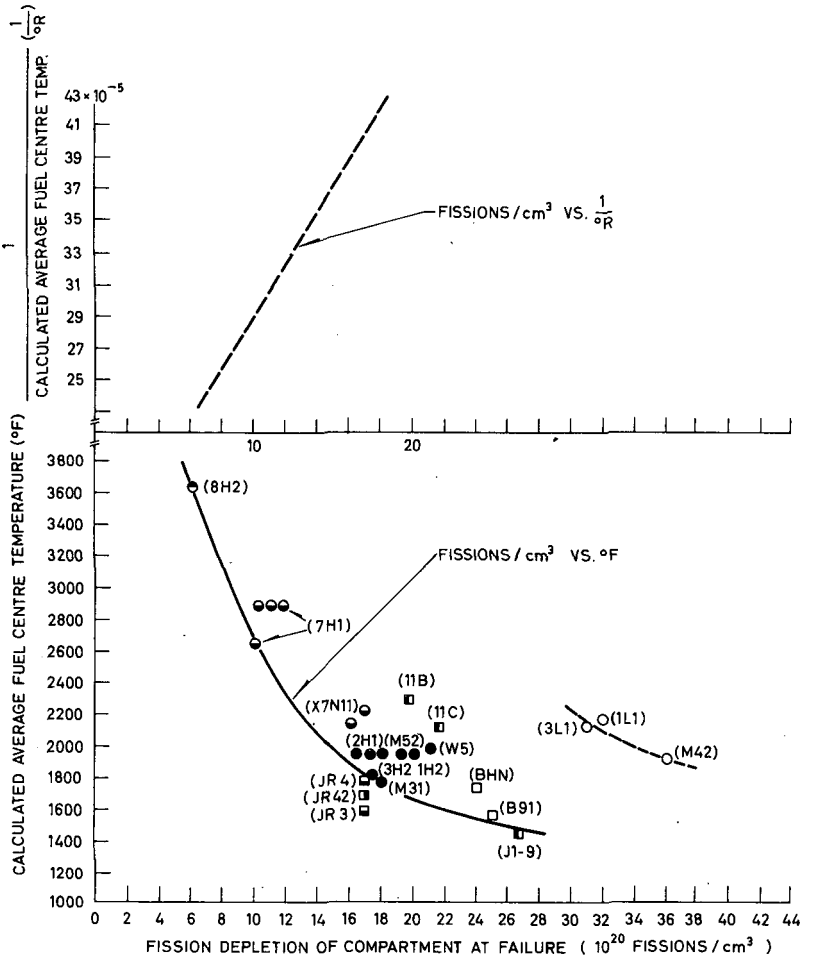


Fig. 6

Comparison of centre-line fuel temperatures for failed UO_2 and ZrO_2 - UO_2 compartments (Pressure-bonded elements only)

ZrO_2 - UO_2 fuel

- ZrO_2 - 25 wt. % UO_2, 0.036-in thick, 96% theoretical density
- ZrO_2 - 34 wt. % UO_2, 0.036-in thick, 96% theoretical density
- ZrO_2 - 34 wt. % UO_2, 0.036-in thick, 90% theoretical density
- ZrO_2 - 46 wt. % UO_2, 0.020- to 0.036-in thick, 90% theoretical density

Bulk UO_2 fuel

- 0.040-in thick, 88% theoretical density
- 0.040-in thick, 96% theoretical density
- 0.100-in thick, 96% theoretical density
- 0.160-in thick, 96% theoretical density

TABLE III

FUEL TEMPERATURE AND EXPOSURE OF FAILED PRESSURE-BONDED ELEMENTS CONTAINING UO_2 AND ZrO_2 - UO_2 FUELS

Element	Composition	Average heat flux	Calculated Av. centre-temperature	Burn-up at failure
(No.)	(values are wt. %)	(10^5 BTU h^{-1} ft^{-2})	(°F)	(10^{20} fissions/cm^3)
X7N11	UO_2	4.6	2140	16
X7N11	UO_2	4.6	2140	16
X7N11	UO_2	4.8	2210	17
M31	UO_2	5.7	1820	17 - 18
M42	UO_2	5.6	1910	36
M52	UO_2	6.3	1960	19 - 20
M52	UO_2	6.3	1960	19 - 20
1H2	UO_2	6.3	1960	18
2H1	UO_2	6.3	1960	17
3H2	UO_2	6.3	1960	18
5H1	UO_2	6.4	1980	19
6H2	UO_2	5.9	2050	31
7H1	UO_2	6.2	2900	11
7H1	UO_2	6.2	2900	11

7H1	UO_2	5.6	2660	10
7H1	UO_2	6.2	2900	11
8H2	UO_2	6.6	3650	6.2
1L1	UO_2	5.9	2160	32
3L1	UO_2	5.7	2110	31
W5	UO_2	6.5	1760	18
W5	UO_2	7.6	1980	21
11B	ZrO_2 - 47.1 UO_2	7.9	2285	19.9
11C	ZrO_2 - 47.1 UO_2	8.5	2150	21.2
JR4	ZrO_2 - 35.8 UO_2	5.4	1750	17.5
JR42	ZrO_2 - 26.1 UO_2	4.7	1700	16.4
JR3	ZrO_2 - 35.8 UO_2	5.2	2215	16.7
BHN	ZrO_2 - 34.9 UO_2	5.1	1725	24.1
B91	ZrO_2 - 36.8 UO_2	5.8	1525	25.1
J1-9	ZrO_2 - 46.5 UO_2	8.4	1390	26.5
JR-4	ZrO_2 - 35.5 UO_2	5.5	1750	17.5

values of gap (ΔT) which still further elevate fuel operating temperatures and favour an even greater external release of gas, still more cladding deflection, etc. Thus, as operating temperatures are continuously elevated and because increasing pressures are applied by the fission gases, the limit of cladding ductility is reached at even lower fission depletions. Due to the pronounced influence of operating temperature, the data of Fig. 6 (shown by the plot against 1/T) indicate that the critical burn-up for compartment failure (BU_{crit}) varies inversely to average fuel centre-temperature in °R*, i.e.

$$BU_{crit} \simeq 1/T(°R).$$

The factor, other than temperature, which has most influence on the compartment life of UO_2 fuel-element plates is fuel density, as is also shown by Fig. 6. The increased lifetime of samples containing low-density UO_2 is in sharp contrast to the behaviour of samples containing low-density ZrO_2 + 34 wt. % UO_2 which show no increased lifetime over high-density fuel. This is discussed in greater detail in sections 3.2 and 3.4 to follow.

3.2. Bulk UO_2

The dimensional changes measured as the maximum thickness-increase at the compartment centre-line on the fuel elements containing bulk UO_2 at the interim examinations are shown in Fig. 7, where the average value of the compartment centre-line thickness-change (expressed as a percentage of the original fuel thickness for each plate) is shown as a function of fission depletions, operating heat flux and fuel thickness. As the discussion in section 3.1 above and Fig. 2 indicated, these dimensional changes are directly related to the fuel volume changes by a ratio of about two to one, due to the approximately paraboloid shape of the swelled fuel. The change in fuel volume was determined for a number of samples by a wet-density measurement after completion of the irradiation tests and is shown in Table IV. These values are in good agreement with the dimensional data shown in Fig. 7 where the volume swelling of UO_2 with exposure is shown. It may be seen that this material has an initial swelling rate of 0.16% ΔV per 10^{20} fissions/cm^3 and this value appears to be independent of fuel temperature in the range of about 1340 to 3840°F and up to exposures of (16 to 20) $\times 10^{20}$ fissions/cm^3. These results demonstrate one of the features differentiating bulk UO_2 from metallic uranium-bearing fuels. In metallic fuels, the inability of the insoluble fission gases to diffuse over appreciable distances and their internal precipitation even at low exposures result in a marked variation of the amount of swelling with fuel temperature [16, 17]. In bulk UO_2, however, these gases are better accommodated within the oxide structure (although probably not, as will be described later, within the crystal lattice) and, as will be shown in section 4, can diffuse through the UO_2 lattice; hence no significant difference in swelling rate is observed with temperature.

---

* °R: Temperature on the Rankine scale, an absolute scale based on °F.

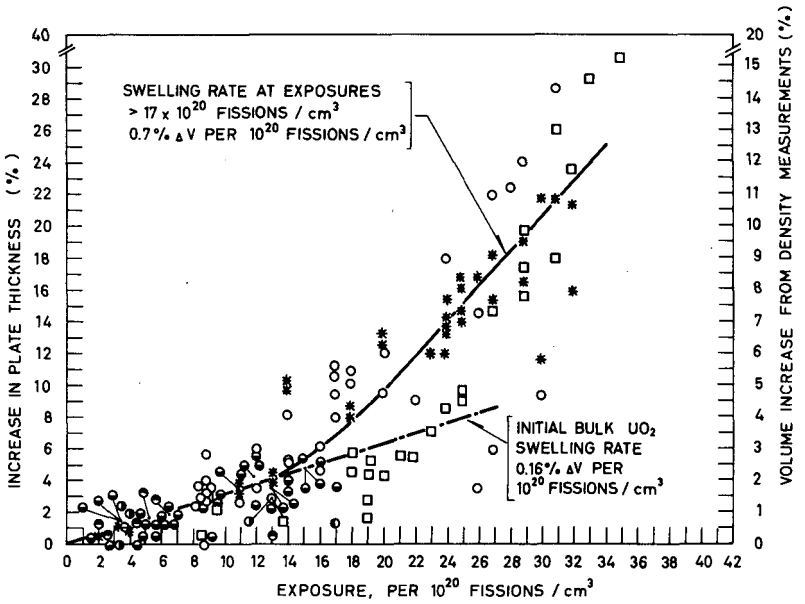


Fig. 7

Solid volume swelling of bulk UO_2

Symbol	Fuel thickness (mil)	Theoretical density	Heat flux Q/A (BTU h^{-1} ft^{-2})	Temperature range (°F)
○	40	96%	(3 to 7) × 10^5	1340 to 2200
◑	80	96%	(3 to 4) × 10^5	1620 to 1700
◒	100	96%	(5 to 7) × 10^5	2300 to 3200
◐	120	96%	(3 to 4) × 10^5	2300 to 2600
◓	160	96%	(4 to 7) × 10^5	2420 to 3840
□	40	96%	(6 to 7) × 10^5	2110 to 2385

* % ΔV from gravimetric density measurements

% Δt from plate measurements (micrometer measurements)

TABLE IV

POST-IRRADIATION GRAVIMETRIC DENSITY MEASUREMENTS ON BULK UO_2

Element	Comp.	Composition	Burn-up	Density before (A) and after (B) irradiation		ΔV
				A	B	
(No.)		(values are wt. %)	(10^{20} fissions/cm^3)	(g/cm^3)	(g/cm^3)	(%)
I-21	2	UO_2	25	10.56	9.83	7.3
I-21	6	UO_2	24	10.56	9.85	7.1
I-21	6	UO_2	24	10.56	9.90	6.7
I-21	9	UO_2	30	10.56	9.53	10.8
I-21	10	UO_2	25	10.56	9.79	8.0
J-23	12	UO_2	23	10.56	9 97	6.0
J-23	21	UO_2	24	10.56	9.81	7.7
J-23	9	UO_2	31	10.56	9.53	10.8
J-23	23	UO_2	25	10.56	9.73	8.4
J-23	23	UO_2	27	10.56	9.67	9.1
J-23	10	UO_2	26	10.56	9.74	8.4
J-23	11	UO_2	24	10.56	9.97	6.0
J-23	5	UO_2	24	10.56	9.87	7.0
J-23	6	UO_2	25	10.56	9.85	7.1
J-23	7	UO_2	27	10.56	9.81	7 7

J-23	8	UO_2	32	10.56	9.55	10.7
C112	11	UO_2	13	10.59	10.36	2.0
C6	15	UO_2	3.8	10.59	10.50	0.8
G102	9	UO_2	2.0	10.63	10.61	0.2
F13	13	UO_2	13	10.55	10.31	2.2
E9	9	UO_2	3.8	10.60	10.55	0.5
X4B42	2E	UO_2	14	10.66	10.12	5.1
M31	1A	UO_2	20	10.57	9.91	6.6
M31	2A	UO_2	20	10.61	9.98	6.3
M31	1E	UO_2	18	10.65	10.24	4.0
M31	2E	UO_2	18	10.66	10.21	4.4
X4B42	1E	UO_2	14	10.66	10.17	4.9
7H1	1C	UO_2	11	10.52	10.38	1.6
7H1	2C	UO_2	11	10.52	10.34	1.9
J-23	24	UO_2	32	10.56	9.76	7.9
I-21	1	UO_2	30	10.56	9.97	5.8
I-21	5	UO_2	29	10.56	9.64	9.5
I-21	5	UO_2	29	10.56	9.75, 9.79	8.2
BHL	A	ZrO_2 - 34.9 UO_2	5.7	6.39	7.08	-6.7
	B				6.69	-6.7
	D				6.77	-6.7
	E				6.76	-6.7
	M-1				6.80	-6.7
	M-2				6.82	-6.7

TABLE IV cont.

Element	Comp.	Composition	Burn-up	Density before (A) and after (B) irradiation A	B	ΔV
(No.)		(values are wt.%)	(10^{20} fissions/cm^3)	(g/cm^3)	(g/cm^3)	(%)
BHB	A	ZrO_2 - 34.6 UO_2	5 8	6.86	6.81	-1.0
	B				6.89	-1.0
	D				7.03	-1.0
	E				7.04	-1.0
	M-1				6.89	-1.0
	M-2				6.94	-1.0
BHC	A	ZrO_2 - 34.6 UO_2	9.6	6.85	6.78	3.6
	B				6.49	3.6
	D				5.96	3.6
	E				6.39	3.6
	M-1				6.67	3.6
	M-2				6 69	3.6
BHM	A	ZrO_2 - 34.9 UO_2	10.0	6.53	6.87	-3.2
	B				6.63	-3.2
	D				6.73	-3.2
	E				7.29	-3.2
	M-1				6.70	-3.2
	M-2				6.77	-3.2

7GA	A	ZrO_2 - 34.4 UO_2	10.9	7.03	6.62	4.8
	D				6.79	4.8
14C	B	ZrO_2 - 25.1 UO_2	11.1	6.18	6.20	-2.5
	E				6.56	-2.5
B3-11		ZrO_2 - 18.7 UO_2	11.6	6.32	6.15	2.7
JR-4	M-1	ZrO_2 - 35.8 UO_2	16.3	7.13	6.85	6.0
	M-2				6.61	6.0
BHK	A	ZrO_2 - 34.9 UO_2	17.5	6.43	6.23	3.3
	D				6.68	3.3
	M-1				5.96	3.3
	M-2				6.01	3.3
BHW	B	ZrO_2 - 87.2 UO_2	18.5	9.59	8.89	6.7
	C				9.18	6.7
	E				8.96	6.7
	F				8.76	6.7
BFZ	A	ZrO_2 - 34.6 UO_2	19.7	6.91	6.18	9.8
	B				6.27	9.8
	D				6.21	9.8
	E				6.36	9.8
	M-1				6.16	9.8
	M-2				6.18	9.8
11B	A	ZrO_2 - 47.1 UO_2	19.9	7.45	6.53	13.4
	D				6.50	13.4

TABLE IV cont.

Element	Comp.	Composition	Burn-up	Density before (A) and after (B) irradiation		ΔV
				A	B	
(No.)		(values are wt. %)	(10^{20} fissions/cm^3)	(g/cm^3)	(g/cm^3)	(%)
13C	B	ZrO_2 - 47.1 UO_2	20.0	7.38	6.73	12.3
	E				6.44	12.3
BHH	A	ZrO_2 - 34.6 UO_2	20.1	6.87	6.30	9.0
	D				6.21	9.0
B3-36		ZrO_2 - 26.4 UO_2	20.1	6.75	6.03	9.8
					6.15	9.8
BHD	A	ZrO_2 - 34.6 UO_2	21.5	6.91	6.22	9.6
	D				6.27	9.6
B92	A	ZrO_2 - 36.8 UO_2	24.4	6.91	6.27	12.0
	D				6.07	12.0
B91	A	ZrO_2 - 36.8 UO_2	25.1	6.91	6.17	12.0
	D				6.18	12.0
B3-6		ZrO_2 - 35.5 UO_2	26.1	7.03	6.12	12.9
PB-2		ZrO_2 - 35.1 UO_2	26.3	7.05	6.13	12.9
					6.15	12.9
J1-10	C	ZrO_2 - 46.5 UO_2	28.2	7.44	6.02	23.5

W3	B	ZrO_2-47.0 UO_2	34.0	7.30	6.03	20.5
	C				6.09	20.5
B3-29		ZrO_2-46.5 UO_2	40.2	7.46	6.06	18.0
					6.18	18.0
29-22 # 9	-	BeO + 65.0 UO_2 (nominal 10 μm particle size)	10.8	5.48	5.20	5.5
59-2, B3-35	-	BeO + 65.0 UO_2 (nominal 10 μm particle size)	35.7	5.47	4.16/4.35	29.0 (Av.)
59-3, PB # 3	2	BeO + 51.0 UO_2 (nominal 10 μm particle size)	28.0	-	-	24.0 *
14-27, A-3	-	Al_2O_3 + 21.0 UO_2 (nominal 5 μm particle size)	2.74	4.46	3.68	18.5
14-27, A-4	-	Al_2O_3 + 21.0 UO_2 (nominal 5 μm particle size)	2.33	4.46	3.57	19.9
14-27, B-1	-	Al_2O_3 + 21.0 UO_2 (nominal 5 μm particle size)	1.25	4.46	3.66	17.9

* Determined from Δ thickness measurement on fuel plate sample.

TABLE IV cont.

Element	Comp.	Composition	Burn-up	Density before (A) and after (B) irradiation		ΔV
				A	B	
(No.)		(values are wt. %)	(10^{20} fissions/cm^3)	(g/cm^3)	(g/cm^3)	(%)
14-28, A-10	-	Al_2O_3+21.0 UO_2 (nominal 5 μm particle size)	10.8	4.46	3.59	19.7
14-28, A-6	-	Al_2O_3+21.0 UO_2 (nominal 5 μm particle size)	6.9	4.46	3.62	18.8
29-10, 1	-	Al_2O_3+21.0 UO_2 (nominal 5 μm particle size)	5.25	4.50	3.71	17.4
30-3, T04	-	Al_2O_3+21.0 UO_2 (nominal 5 μm particle size)	0.92	4.40	3.73	19.5
30-3, T17	-	Al_2O_3+21.0 UO_2 (nominal 5 μm particle size)	0.92	4.40	3.73	19.5

At higher exposures, ranging from 17 to 36×10^{20} fissions/cm^3, bulk UO_2 shows a significant increase in swelling rate to a value of about 0.7%ΔV per 10^{20} fissions/cm^3. These data were obtained both on element specimens I21 and J23 containing 0.040-mil thick fuel in copper-diffusion-bonded samples containing about 6 to 10% void-compartment volume and which operated at a temperature of about 1600°F and the elements containing 88% theoretical density, 0.040-mil thick fuel (3L1, 1L1, and M42) operating at temperatures ranging from about 1950 to 2150°F. Since this is a rather narrow range of temperatures and there is appreciable scatter in these data (see Fig. 7) it is not possible to establish whether this accelerated swelling rate is also independent of temperature. However, the swelling of bulk UO_2 at these high burn-up values and over the temperature range of 1950 to 2150°F is obviously not subject to the same extreme temperature sensitivity as metallic uranium, which at 500°C swells at six times the rate observed at 400°C [16]. Therefore it may be concluded, on a relative basis, that the swelling of UO_2 is independent of temperature in the range of 1400 to 3600°F and up to exposures of 36×10^{20} fissions/cm^3 and that a discontinuity in the increase of swelling rate occurs at about 17×10^{20} fissions/cm^3; below this exposure value the swelling rate is 0.16%ΔV per 10^{20} fissions/cm^3 and above this exposure value the swelling rate is 0.7%ΔV per 10^{20}fissions/cm^3. It is of interest to compare these swelling rates in bulk UO_2, partially constrained within the platelet structure of Fig. 1, with those observed in highly-restrained UO_2 particles contained in dispersion fuel-element samples at fission depletions in the particles of the order of 100×10^{20} fissions/cm^3. WEBER [18] has correlated observations of swelling in UO_2 stainless-steel dispersions and concluded that the swelling rate of the fissile phase corresponds to a volume change of 0.14 to 0.41%ΔV per 10^{20} fissions/cm^3. Thus the swelling rate of UO_2, at depletions beyond (12 to 16) $\times 10^{20}$ fissions/cm^3, at which initially low swelling rates of 0.16%ΔV per 10^{20} fissions/cm^3, are noted, increases to a rate which is to some limited extent sensitive to temperature of operation and to the external restraint applied.

The data of Fig. 7 may be differently interpreted to indicate no change in swelling rate with UO_2 fuel depletion. As will be later discussed in more detail, UO_2 shows an irradiation-induced plasticity; thus part of the volume growth of the UO_2 would initially result in decrease of the initial porosity of the fuel platelets by flow of the UO_2 into internal voids and only when much of this initial porosity was sealed up would the true swelling rate be manifested. This hypothesis is to an extent confirmed by extrapolation of the final swelling-rate curve to zero burn-up; intersection with the ordinate axis is noted at about -8%ΔV to -10%ΔV, corresponding approximately to the initial fuel porosity in the case of the low-density fuel and to the combination of porosity and initial void-compartment volume in the higher-density fuel material. Still stronger confirmation of this is discussed below in connection with ZrO_2-UO_2 fuels, in which the much higher degree of irradiation-induced plasticity leads to an unequivocal densification of the original porosity quite early in the exposure lifetime.

Comparison of the appearance of irradiated low-density UO_2 compartments with the high-density UO_2 compartments of similar exposure described above reveals that at least two factors contributed to the greater dimensional stability of the low-density elements (see Fig. 6). A typical compart-

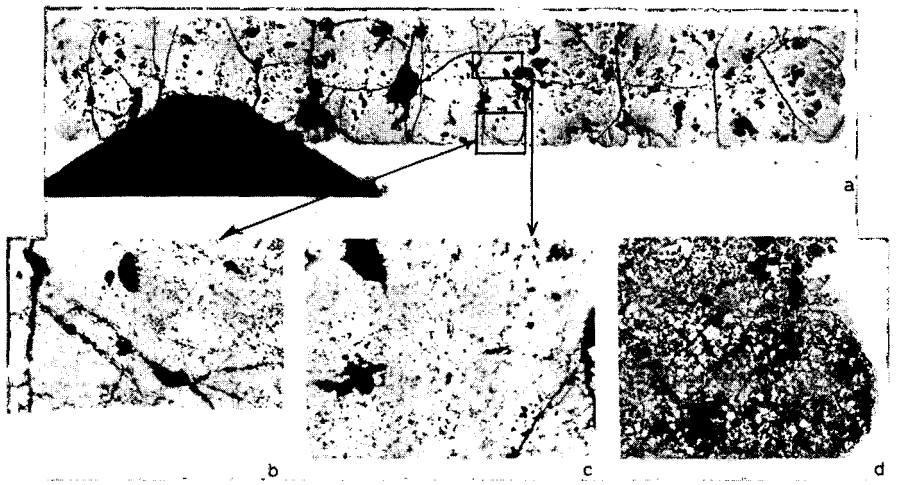


Fig. 8.1

Typical fuel structure of low-density UO_2 (88% original density) from sample 4L1 after 18×10^{20} fissions/cm^3
(The hole was drilled through cladding to remove released-fission-gases)

[Originals: (a) × 50, (b, c, d) × 400]

ment of unfailed element 4L1 (88% original density) after 18×10^{20} fissions/cm^3 is shown in Fig. 8(a); it is seen that the low-density elements had better contact between fuel and cladding both because void volume was available to contain the released fission gases internally and because the fuel and cladding were interlocked by Zircaloy "keys" extruded into numerous and relatively large surface pores of the low-density UO_2 during pressure bonding. It is significant that all the original fuel porosity has not closed up after this exposure. Were the fuel to swell during this depletion at the initial rate of $0.16\%\Delta V$ per 10^{20} fissions/cm^3 shown in Fig. 1, only about 3% porosity would have been eliminated. Indeed lineal analysis of Fig. 8(a) reveals that a porosity of about 85% remains in the fuel and the result agrees with this swelling rate. After 32×10^{20} fissions/cm^3 the original porosity was no longer present for Compartment 2A of element 1L1 (89% original density Fig. 8(b)). At this depletion, from Fig. 7, about 11% volume change should occur and, as noted in Fig. 8(b), the original porosity is to a large extent eliminated.

The elimination of voids by fuel growth (Fig. 8(a) and (b)) and the flow pattern evidenced by the high-density wafers in Figs. 2 and 3 argue for a considerable plasticity of the UO_2 under irradiation; specifically, these figures indicate that UO_2 at average fuel centre temperatures of 1340 (J23) to 1820°F (M31) can flow plastically under irradiation under the influence of stresses which at a maximum are about 2500 lb/in^2 and consist of a combination of the external loop pressure and the cladding deflection resistance. These results may be compared with the out-of-pile measurements of the plastic deformation of UO_2 by SCOTT, HALL and WILLIAMS [19]. They found for UO_2 at 1832°F, σ (lb/in^2) $= 1.45 \times 10^{20} \dot{\varepsilon}$ (sec^{-1}). For the case of

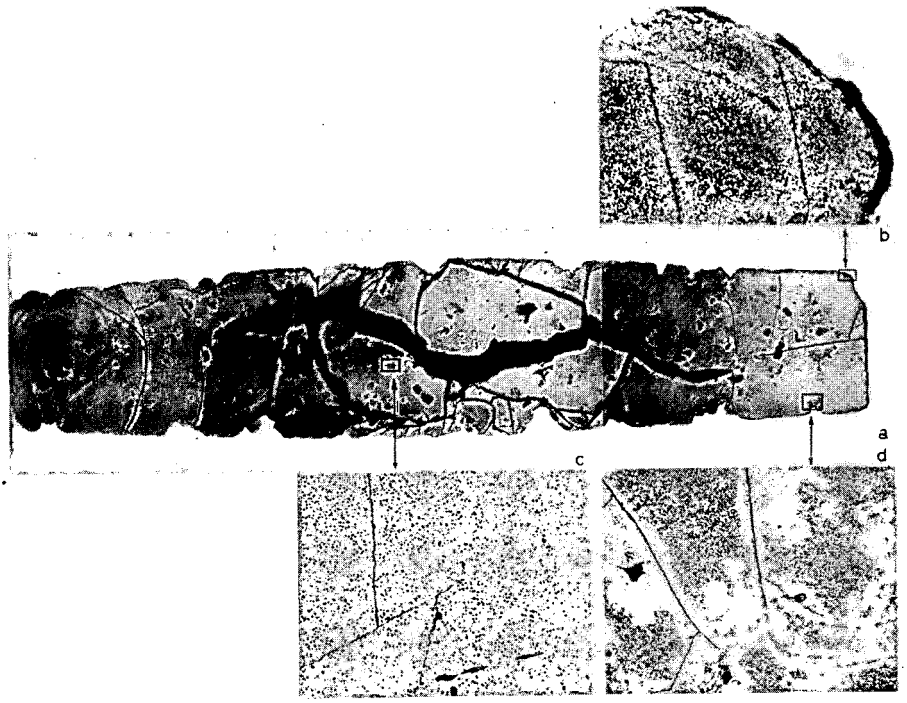


Fig. 8.2

Unfailed compartment 2A of low density element 1L1 (88% original density) after 32×10^{20} fissions/cm^3

[Originals: (a) × 50, (b,c) × 400, (d) × 150]

M31 (Fig. 3), which operated at an average central temperature of 1830°F (see Table III) for 164 EFPD and showed in-pile a maximum thickness strain of about 13%, the out-of-pile measurements predict, at a stress of 2500 lb/in^2, a strain of only about 0.3%. Thus the plastic deformation of UO_2 is accelerated by fission-product bombardment by at least a factor of 40, and a much greater effect would be predicted were a lower-temperature sample such as J23 (Fig. 2) chosen for comparison.

3.3. $ZrO_2 + UO_2$ fuel materials

In contrast to the swelling behaviour of bulk UO_2, the ZrO_2-based fuel materials decrease in volume at low exposures. The increase in density of the fuel bodies corresponds quantitatively to the residual volume of porosity left in the material after sintering. The changes in fuel volume, determined by gravimetric density measurements on the ZrO_2-based fuel materials, are shown in Table IV and Fig. 9. The rate of volume change with exposure amounts to about 0.7% ΔV per 10^{20} fissions/cm^3 for ZrO_2-base, UO_2 fuel. As noted in Fig. 9, the volume changes extrapolate at zero burn-up to the percentage of original porosity in the fuel samples. This contraction

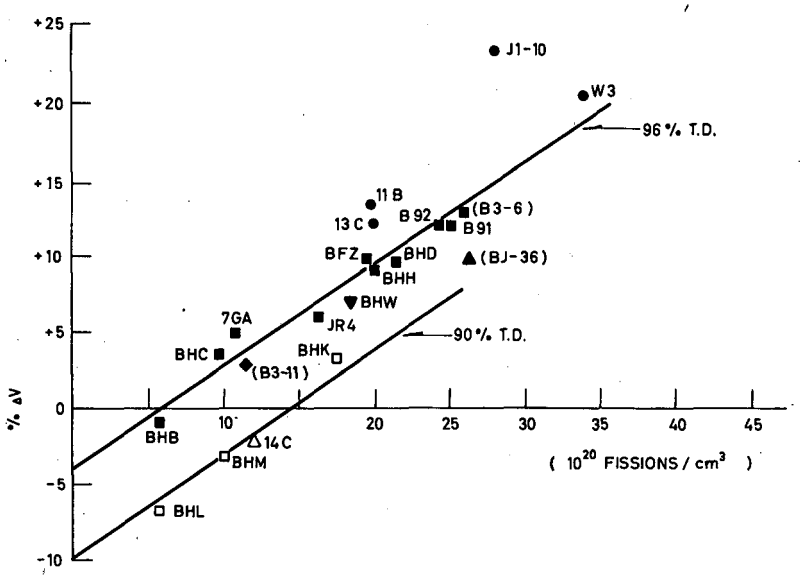


Fig. 9

Volume change of ZrO_2 - UO_2 fuels with burn-up

( ): Samples irradiated in NaK capsules
All others loop irradiated

Theoretical density		UO_2
90%	96%	(wt.%)
◇	◆	18
△	▲	25
□	■	34
○	●	46
▽	▼	87

in fuel volume is readily seen in the photomicrographs in Fig. 10 where 90% theoretical density, ZrO_2+34% UO_2 is shown at various exposures. It may be seen that sample BHL shows a reduction in compartment centre-line fuel thickness of 12% after 5.8×10^{20} fissions/cm^3; this, compared to a reduction in volume of about 6%, is in good agreement with the data shown in Fig. 9. This volume decrease is obviously caused by the filling up of the internal void volume of the fuel (see Fig. 10). As irradiation continues, the fuel swells at a rate which appears to be independent of the initial fuel porosity.

These results show that the ZrO_2-base fuel materials undergo decreases in volume equal to the total porosity of the fuel body and, unlike with bulk UO_2, these are reflected by decreases in the plate thickness at exposures

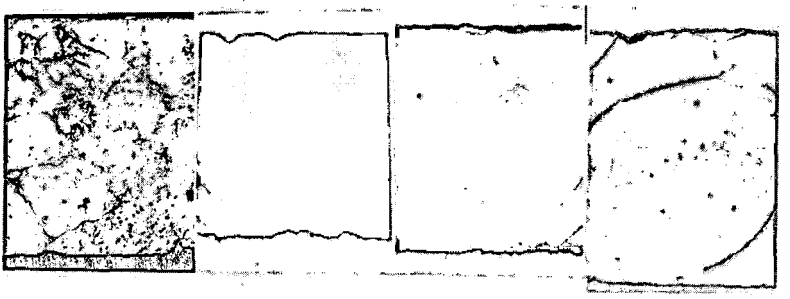


Fig. 10

Photomicrographs of ZrO_2 - 34 wt.% UO_2, initially containing 10% porosity, after various burn-ups

	Sample BHL	Sample BHL	Sample BHK
Unirradiated fuel	5.8×10^{20} fissions/cm^3	10×10^{20} fissions/cm^3	17.5×10^{20} fissions/cm^3
0.040-in thick	0.035-in thick (-12% Δt)	0.037-in thick (-8% Δt)	0.043-in thick (+8% Δt)

[Originals × 75]

less than about 6×10^{20} fissions/cm^3. Since the initial fuel porosity varied, a large amount of scatter was observed in the fuel-element thickness-changes during interim examinations. Although the specific irradiation level required to cause a density increase in ZrO_2-base fuel cannot be determined from these tests, the extrapolation of the data in Fig. 9 indicates that the fuel densification occurs at a very low burn-up (less than 5.8×10^{20} fissions/cm^3). Profound differences are thus revealed in the plasticity under fission-fragment bombardment of the UO_2 and ZrO_2-base fuel materials. Under external loads of the order of 2500 lb/in^2 the cubic-structure fuel has demonstrated an increase in creep rate of at least two orders of magnitude at a fission bombardment rate of about 10^{14} fissions/cm^3 sec. In the monoclinic-tetragonal $ZrO_2 + UO_2$ fuel (see section 5.3) complete densification had been attained at an exposure level of about 6×10^{20} fissions/cm^3 and may have been complete at much lower exposure levels. Thus this non-cubic fuel material exhibited under irradiation a creep rate which was at least five times greater than that for cubic UO_2.

The results plotted in Fig. 9 indicate that the fuel swells at a rate of about 0.7% ΔV per 10^{20} fissions/cm^3. However, examination of Table IV shows that the samples examined at low burn-up operated at high temperatures (2000 to 2400°F) while those at high exposure operated at low temperatures (1300 to 2000°F). Thus the influence, if any, of fuel in-pile temperature on swelling rate cannot be determined from the data of Fig. 10 but must be obtained from the interim dimension-examination data. However, the periodic dimension measurements conducted on these fuel-plate samples failed to give the desired information on swelling behaviour of the fuels because of two phenomena which confounded the plate-thickness measurements. The first and largest effect (described above) was the complete densification of the fuel body (see Fig. 9) where the post-irradiation gravimetric density-data extrapolate at zero burn-up to negative volume changes of the same magnitude as the fuel porosity. The second phenomenon, to be discussed in section 5.3, is a small contraction due to phase changes in these materials.

The available data do not allow for estimation of the kinetics of the fuel-densification, but the results of the X-ray examination data (section 5.3) show that the exposure required for the structural changes must be quite low.

In order to determine whether the swelling behaviour of these fuel materials varied with temperature, the thickness measurements made during each interim examination period were corrected for these two volume changes. It was assumed that the volume changes were directly reflected by the thickness measurements, as no significant changes in dimension occurred in width or length. These thickness changes were corrected by assuming that the unirradiated corrected-thickness of the fuel was the measured value corrected as follows: the corrected fuel thickness is equal to the unirradi-

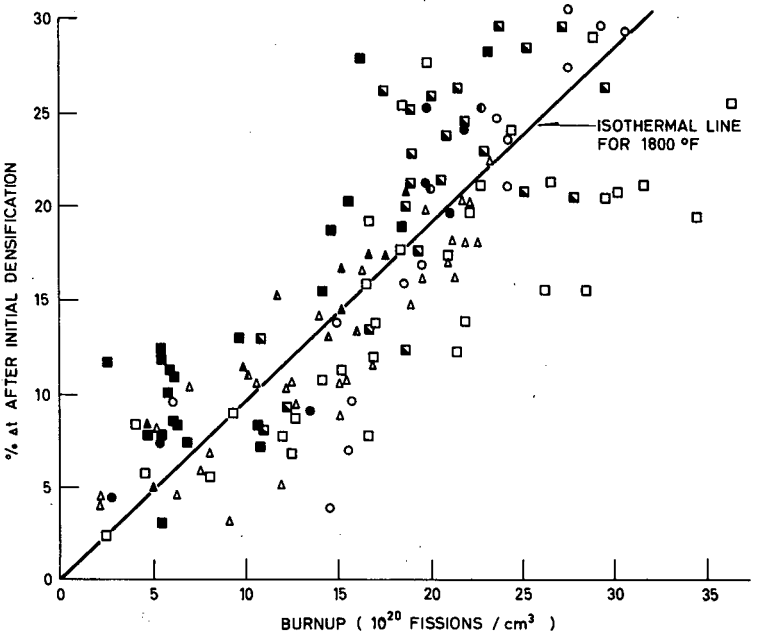


Fig. 11

Thickness change with burn-up after correction for initial densification

(wt. % UO_2) 25	34	46	Remarks
△	□	○	Centre-line temperatures below 1800°F at this and all previous examinations
▲	◪	◐	Below 1800°F at this, but above at a previous examination
▲	■	●	Above 1800°F at this examination

ated thickness multiplied by unirradiated fuel density and divided by the irradiated X-ray density. This correction was used to normalize all data for the initial fuel porosity and for the volume change due to phase changes. Using this normalization, the measured thickness changes were recalculated and are shown for ZrO_2+25%, 34% and 46% UO_2 in Fig. 11.

It is significant that the data shown in Fig. 11 extrapolate through zero at zero burn-up; this result confirms the suitability of the calculation method employed. Also, it should be emphasized that there is no evidence of "breakaway" swelling to exposures of 36×10^{20} fissions/cm^3. In order to determine the effect, if any, of temperature on the swelling rate of these fuels, the interim examination dimensional data in Fig. 12 have been compared to an arbitrary fuel centre-line temperature of 1800°F. It is quite apparent that there is good agreement between these data, and the isothermal swelling behaviour of these fuels at 1800°F can be described and corresponds to about 1% Δt per 10^{20} fissions/cm^3 or about 0.5 to 0.6% ΔV per 10^{20} fissions/cm^3, depending upon the correction for the paraboloid-shaped swelling of the plates. This is in agreement with the data from Fig. 9 of 0.7% ΔV per 10^{20} fissions/cm^3 and indicates that, in the density data, the scatter due to temperature is not unduly excessive.

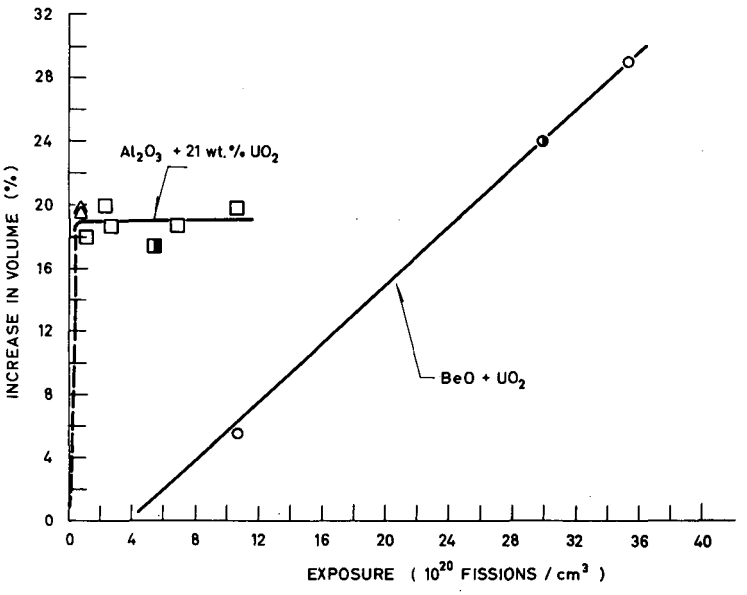


Fig. 12

Solid volume swelling of UO_2 dispersed in Al_2O_3 and BeO

○ BeO - 65 wt.% UO_2, ◐ BeO - 51 wt.% UO_2

□ WAPD 14 - 27 and 28

◨ WAPD 29-10 } Al_2O_3 - 21 wt.% UO_2

△ WAPD 30 - 3

UO_2 dispersed in Al_2O_3 and BeO

The swelling behaviour of fuels containing fine UO_2 particles (nominal 5 to 10 μm in diameter) in the oxide ceramic matrices of Al_2O_3 and BeO provides a means of comparing the stability of these non-fissionable materials under fission-fragment bombardment to the stabilities of UO_2 and $ZrO_2 + UO_2$. The irradiation performance of these dispersion fuels, containing various particle sizes of UO_2, has been reported elsewhere [3, 4].

The swelling of $BeO + UO_2$ fuels is shown in Table IV and Fig. 12. These materials also demonstrate a volume increasing with exposure and the similarity of Fig. 12, showing the swelling of $BeO + UO_2$, to Fig. 9, showing that of $ZrO_2 + UO_2$, is quite apparent. Extrapolation of the swelling curve to zero burn-up shows a volume change of -3 to -4%, which is consistent with the porosity percentage of the samples. In order to evaluate the swelling rate of the BeO materials, the matrix was considered to be uniformly exposed to fission fragments and that the swelling rate of the fuel was equal to that of the UO_2 and the BeO in the relative ratios of the volume percentages of each material. These calculations are shown in Table V. The swelling rate of the BeO was calculated for two conditions, namely, that none of the porosity of the BeO was closed and that the calculated 2.5% porosity did close. Based on these calculated swelling rates it can be concluded that the pores in the BeO do close up and that the BeO swells at a rate of about 1% ΔV per 10^{20} fissions/cm^3. This conclusion seems logical since the swelling rate of the BeO, when calculated on the basis of no pores closing, would have to increase with increasing burn-up. This does not appear to be characteristic of these materials, as is evidenced by the swelling behaviour of UO_2 and $ZrO_2 + UO_2$ discussed above. , The few data available for $BeO + UO_2$ do not permit detailed comparison of the swelling characteristics with those of UO_2 (Fig. 7) or $ZrO_2 + UO_2$ (Fig. 9). From the observation that the swelling at 10.8×10^{20} fissions/cm^3 is consistent with that at higher burn-ups, it appears reasonable to assume that original porosity has healed at this exposure by plastic flow of the BeO and that in-pile plasticity of the hexagonal structure of BeO is at least twice as great as that of UO_2 and probably approaches that of $ZrO_2 + UO_2$. Also, it is interesting to note that the swelling rate of BeO, about 1% ΔV per 10^{20} fissions/cm^3, is of the same general magnitude as that of 0.7% ΔV per 10^{20} for UO_2 and $ZrO_2 + UO_2$.

The swelling behaviour of UO_2 dispersed in Al_2O_3 is shown in Table IV and Fig. 12 and may be compared to that of bulk UO_2 shown in Fig. 7. The Al_2O_3 + 21 wt.% UO_2 fuel materials swelled by about 19% at a very low exposure of 0.9×10^{20} fissions/cm^3 and no further increase in fuel volume changes were noted up to exposures of 5.3×10^{20} fissions/cm^3. This volume change cannot be ascribed to the swelling of the UO_2 constituent of the fuel mixture. For example, in specimen 30-3 (TO4), the UO_2 particles were exposed to 4.3% of the uranium atoms fissioned and, as shown in Fig. 7, the UO_2 volume change after this exposure (10×10^{20} fissions/cm^3) is about 1.6%. Since the UO_2 constitutes only 9.2 vol.% of the fuel material, the maximum volume change which can be attributed to the UO_2 is less than 0.2%. These changes in $Al_2O_3 + UO_2$ fuel materials have been shown to take place at very low exposures (as low as 10^{16} fissions/cm^3) [1, 5]. However, this material behaves in an non-typical manner when compared with the

TABLE V

CALCULATIONS OF SWELLING RATE OF BeO

Element	UO_2 loading		Burn-up		Experimentally determined vol. change of fuel body	Experimentally determined swelling rate of fuel body	UO_2 vol. change (from experimental curve Fig. 7)	Average swelling rate of UO_2	Swelling rate of BeO	
			Depletion	U fission					No pore closing	Closure of 2.5% of open pores
(No.)	(wt. %)	(vol. %)	(10^{20} fissions/cm^3)	(at. %)	(%ΔV)	(*)	(%ΔV)	(*)	(*)	(*)
29-22 # 9	65.0	32.4	10.8	14	5.5	0.51	1.73	0.16	0.68	0.92
59-2, B3-35	65.0	32.4	35.7	53	29.0	0.812	13.3	0.37	1.02	1.10
59-3, PB3#2	51.0	21.9	28.0	67	24.0 †	0.858	9.2	0.328	1.01	1.09

* Swelling rate units: %ΔV per 10^{20} fissions/cm^3.

† From %Δt measurements.

other ceramic oxides at the relatively low temperatures of irradiation considered here and this fact has been discussed by the authors [1, 10]. Preliminary results of work by the authors has shown that post-irradiation annealing of the irradiated Al_2O_3 at about 800°C results in an increase in density toward its unirradiated value. This indicates that an intervening phenomenon, operative at the low irradiation temperatures considered here, has caused the large increases in volume which mark its characteristic swelling behaviour. Therefore these results on Al_2O_3 are not considered as directly comparable with those for the other ceramic oxide materials.

3.5. Summary of volume changes

These data show the extreme variability of the in-pile swelling behaviour of oxide ceramic materials irradiated with fission fragments. Bulk UO_2 demonstrates excellent stability and low swelling rates (0.16% ΔV per 10^{20} fissions/cm^3) up to about 17×10^{20} fissions/cm^3 and then an increased swelling rate of 0.7% ΔV per 10^{20} fissions/cm^3 at higher exposures. ZrO_2-based fuel materials showed that increase of fuel density occurred at low exposures and resulted in volume reductions which were consistent with the porosity of the fuel; then increasing exposure gave rise to a swelling rate of about 0.7% ΔV per 10^{20} fissions/cm^3. Similarly, UO_2 dispersed in BeO showed a swelling rate of about 1% ΔV per 10^{20} fissions/cm^3 for the BeO matrix, and there were indications that the original porosity of the samples healed early during irradiation. However, Al_2O_3 matrix dispersions showed very large swellings of about 19% ΔV at exposures of less than 10^{20} fissions/cm^3 and this behaviour is not typical of that observed in the other oxide ceramic materials.

This variability in fuel dimension changes has been related to the variable in-pile plasticity of these materials. The volume changes in UO_2 and $ZrO_2 + UO_2$ fuels are best expressed as consisting of a constant volume dilation of about 0.7% ΔV per 10^{20} fissions/cm^3. Detail differences in the course of swelling of the two fuels are attributed to differences in their plasticity under irradiation, ZrO_2-base materials showing higher plasticity than UO_2 materials. In the case of BeO, the rate of volume change has approximately the same value (1% ΔV per 10^{20} fissions/cm^3) and the in-pile plasticity is inferred to correspond more closely to that of the ZrO_2-based fuels. In Al_2O_3-base dispersions, the volume changes of 18% ΔV for less than 10^{20} fissions/cm^3 indicate a high degree of plasticity in-pile, but this finding is not believed to be comparable to the other oxide ceramic fuels, but rather a demonstration of a phenomenon unique to Al_2O_3 at low temperatures.

4. FISSION-GAS RELEASE

4.1. Bulk UO_2

Fission-gas release from bulk UO_2 fuel is shown in Table VI and Fig. 13 as a function of fission depletion. The relationship between these results and the fuel swelling behaviour is apparent if the gas release data of Fig. 13 are compared with the swelling data shown in Fig. 7. Qualitatively, the

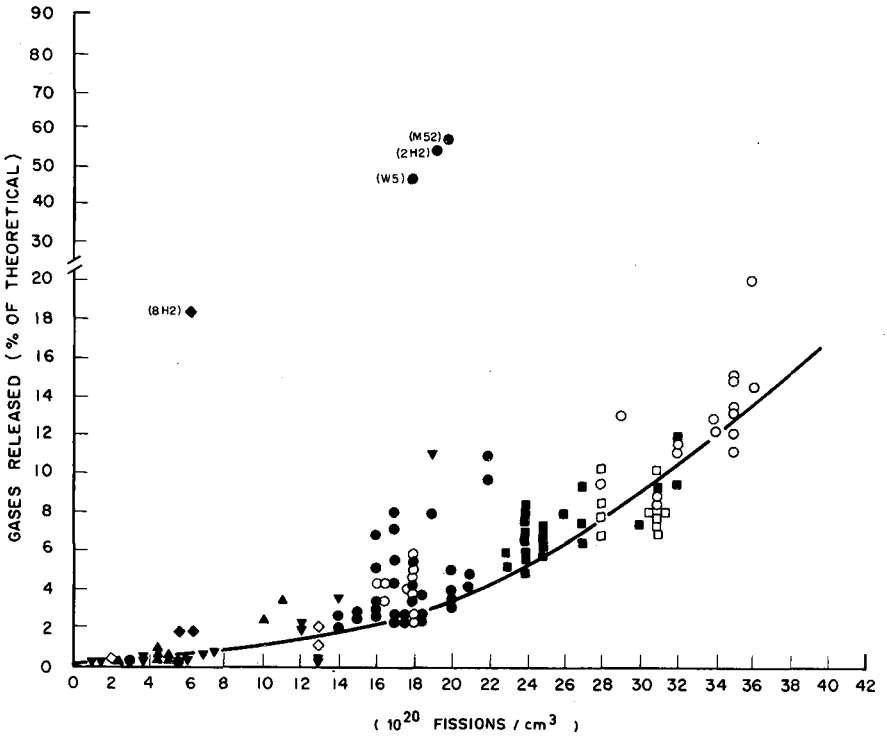


Fig. 13

Fission gas release from UO_2 plates

Symbol	Fuel thickness (in)	Width (in)	Heat flux Q/A (BTU h^{-1} ft^{-2})	Theoretical density (%)
■	0.03 - 0.04	0.25 - 0.5	$(3-4)\times10^5$	~97
□	0.04	0.125	$(6-7)\times10^5$	~97
○	0.04	0.25	$(6-7)\times10^5$	~97
●	0.03 - 0.04	0.25 - 0.5	$(5-7)\times10^5$	~97
▼	0.08 - 0.10	0.25 - 0.5	$(3-6)\times10^5$	~97
▲	0.10	0.25 - 0.5	$(6-7)\times10^5$	~97
◆	0.16	0.25	$(6-7)\times10^5$	~97
◇	0.16	0.25 - 0.5	4×10^5	~97

TABLE VI

SUMMARY OF FISSION GAS RELEASE DATA

Element (No.)	Comp.	Composition (values are wt. %)	Density (% TD)	EFPD	Burn-up (10^{20} fissions/cm^3)	Gas release (%)
I21	1(1A)	UO_2	96	401	30.0	leak
	2(2A)				25.0	7.3
	3(3A)				25.0	6.8
	4(4A)				30.0	leak
	5(1B)				29.0	leak
	6(2B)				24.0	4.9
	7(3B)				24.0	5.5
	8(4B)				29.0	leak
	9(1C)				30.0	4.5
	10(2C)				25.0	6.9
	11(3C)				25.0	6.7
	12(4C)				30.0	7.5
J23	1(1A)	UO_2	96	406	32.0	9.5
	2(2A)				27.0	6.5
	3(3A)				25.0	6.4
	4(4A)				24.0	6.6
	5(5A)				24.0	7.9

	6(6A)					25.0		5.8
	7(7A)					27.0		7.5
	8(8A)					32.0		(not drilled)
	9(1B)					31.0		(not drilled)
	10(2B)					26.0		8.0
	11(3B)					24.0		6.0
	12(4B)					23.0		6.0
	13(5B)					23.0		5.2
	14(6B)					24.0		5.9
	15(7B)					26.0		(not drilled)
	16(8B)					31.0		9.4
	17(1C)					32.0		11.9
	18(2C)					27.0		(not drilled)
	19(3C)					25.0		7.4
	20(4C)					24.0		8.4
	21(5C)					24.0		7.1
	22(6C)					25.0		(not drilled)
	23(7C)					27.0		9.4
	24(8C)					32.0		leak
C6	2	UO_2	~96	107		3.5		0.4
	7					3.5		0.2
	12					3.5		0.5
E9	2	UO_2	~96	107		3.5		0.4

TABLE VI cont.

Element (No.)	Comp.	Composition (values are wt. %)	Density (% TD)	EFPD	Burn-up (10^{20} fissions/cm^3)	Gas release (%)
E9 (cont.)	6	UO_2	~96	107	3.5	0.4
	10				3.5	0.5
C112	2	UO_2	~96	333	13.0	0.5
	7				13.0	0.4
	12				13.0	0.5
A104	2	UO_2	~96	333	13.0	0.3
	9				13.0	0.2
	16				13.0	0.3
G102	2	UO_2	~96	107	1.9	0.3
	6				1.9	0.3
	10				1.9	0.2
F13	2	UO_2	~96	632	13.0	1.0
	8				13.0	1.2
	14				13.0	2.0
X1B32	1A	UO_2	97.7	476	14.0	3.6
	1B-1E		97.6		14 - 18	leak
1F-2F	(intercomp)	UO_2	97.5	476	19.0	11.0
	2A		98.6		14.0	3.7

	2B-2E		97.4		14 - 18	leak
X2N10	F(1A)	UO_2	~97	191	6.9	0.57
B-E	1B-1E	UO_2	~97	191	6.2 - 6.7	(intercomp)
	A(1F)				7.4	0.62
	L(2A)				6.9	0.55
H-K	2B-2E	UO_2	~97	191	6.2 - 6.7	(int. def.)
	G(2F)				7.4	0.58
X3N10	A(1A)	UO_2	~97	191	22.0	leak
B-E	1B-1E	UO_2	~97	191	20.0	leak
	F(1F)				22.0	9.7
	G(2A)				22.0	11.0
H-K	2B-2E	UO_2	~97	191	20.0	leak
	L(2F)				22.0	9.7
X4B42	F(1A)	UO_2	97	121	16.0	2.6
B-E	1B-1E	UO_2	97	121	14.0	(int. def.)
	A(1F)				15.0	2.5
	L(2A)				16.0	3.0
H-K	2B-2E	UO_2	97	121	14.0	2.7
	G(2F)				15.0	2.8
X5N11	Single	UO_2	~98	191	20 - 22	leak
X6N12	Single	UO_2	~98	501	15.0	leak

TABLE VI cont.

Element	Comp.	Composition	Density	EFPD	Burn-up	Gas release
(No.)		(values are wt. %)	(% TD)		(10^{20} fissions/cm^3)	(%)
X7N11	1A	UO_2	~98	440	12.0	1.9
	1B-1E				13 - 16	leak
1F-2F	(intercomp)	UO_2	~98	440	17.0	leak
	2A				12.0	2.0
	2B-2E				13 - 16	leak
M42	1A	UO_2	85.8	327	37.0	12.0
	1B		85.8		34.0	(not drilled)
	1C		89.8		34.0	14.1
	1D		89.1		34.0	13.7
	1E		89.7		34.0	11.7
	1F		89.3		37.0	19.3
	2A		89.0		37.0	11.3
	2B		86.2		34.0	(not drilled)
	2C		88.2		34.0	15.8
	2D		86.1		34.0	15.3
	2E		90.3		34.0	12.6
	2F		86.0		37.0	14.3

M31	1A	UO_2	96.4	164	20.0	5.0
	1B		97.4		18.0	4.3
	1C		96.7		18.0	3.7
	1D		96.3		18.0	leak
	1E		97.1		18.0	3.8
	1F		96.7		20.0	3.1
	2A		96.8		20.0	3.3
	2B		97.5		18.0	2.2
	2C		97.3		18.0	2.8
	2D		97.5		18.0	2.8
	2E		97.3		18.0	2.4
	2F		96.9		20.0	4.0
M52T1	1A	UO_2	97.0	164	18 - 20	57 - 63
	1B		96.0		18 - 20	leak
M72	1A	UO_2	98.0	103	5.0	0.7
	1B		98.4		4.5	0.5
	1C		98.0		4.5	(burnout hole)
	1D		97.9		4.5	0.3
	1E		97.7		4.5	0.3
	1F		97.9		5.0	0.4
	2A		98.1		5.0	0.8
	2B		98.1		4.5	0.7
	2C		98.0		4.5	(burnout hole)

TABLE VI cont.

Element	Comp.	Composition	Density	EFPD	Burn-up	Gas release
(No.)		(values are wt. %)	(% TD)		(10^{20} fissions/cm^3)	(%)
M72 (cont.)	2D	UO_2	98.2	103	4.5	0.3
	2E		98.0		4.5	0.6
	2F		98.0		5.0	0.3
7H1	1A	UO_2	96.4	231	11.0	leak
	1B		96.2		10.0	2.3
	1C		96.0		11.0	leak
	2A		96.4		11.0	3.5
	2B		96.6		10.0	leak
	2C		96.0		11.0	leak
8H2	1A	UO_2	97.4	198	6.2	1.8
	1B		97.7		5.6	1.7
1C-2C	(intercomp)	UO_2	97.2 - 97.7		6.2	18.4
	2A		97.2		6.2	1.8
	2B		97.3		5.6	1.6
6H2	1A	UO_2	97.2	262	31.0	7.8
	1B		97.5		28.0	6.9
	1C		97.4		31.0	leak

	2A			97.4		31.0		7.1
	2B			97.4		28.0		7.8
	2C			97.4		31.0		7.9
	3A			97.3		31.0		8.0
	3B			96.9		28.0		8.5
	3C			97.0		31.0		7.2
	4A			96.7		31.0		8.1
	4B			97.2		28.0		10.4
	4C			96.9		31.0		10.3
2H1	1A	UO_2		95.9	141	17.0		8.1
	1B			97.0		15.5		3.3
	1C			96.4		17.0		7.2
	2A			96.0		17.0		5.6
	2B			96.2		15.5		5.2
	2C			96.4		17.0		leak
2H2	1A	UO_2		96.3	197	21.0		4.2
	1B			96.0		19.0		55.0
	1C			96.2		21.0		leak
	2A			96.5		21.0		4.8
	2B			96.7		19.0		leak
	2C			96.2		21.0		leak
1L1	1A	UO_2		88.0	262	32.0		11.2
	1B			88.4		29.0		13.1

TABLE VI cont.

Element (No.)	Comp.	Composition (values are wt. %)	Density (% TD)	EFPD	Burn-up (10^{20} fissions/cm^3)	Gas release (%)
1L1 (cont.)	1C	UO_2	87.4	262	32.0	11.2
	2A		89.2		32.0	leak
	2B		88.5		29.0	(not drilled)
	2C		88.6		32.0	(not drilled)
2L2	1A	UO_2	86.2	141	18.0	4.1
	1B		86.2		16.0	3.5
	1C		85.7		18.0	5.8
	2A		85.7		18.0	4.7
	2B		86.9		16.0	(not drilled)
	2C		87.2		18.0	5.2
3L1	1A	UO_2	86.3	260	31.0	9.2
	1B		88.4		28.0	9.6
	1C		89.0		31.0	8.7
	2A		89.5		31.0	(not drilled)
	2B		88.2		28.0	(not drilled)
	2C		89.2		31.0	leak
4L1	1A	UO_2	88.2	138	18.0	4.6

	1B		87.0		16.0	4.4
	1C		87.4		18.0	2.3
	2A		89.3		18.0	4.0
	2B		87.8		16.0	4.4
	2C		88.1		18.0	2.9
1H2	1A	UO_2	97.9	145	18.0	(not drilled)
	1B		97.9		16.0	(not drilled)
	1C		97.0		18.0	(not drilled)
	2A		97.0		18.0	leak
	2B		97.8		16.0	6.9
	2C		97.1		18.0	5.5
4H2	1A	UO_2	96.8	139	17.0	2.8
	1B		96.8		16.0	(not drilled)
	1C		97.4		17.0	2.7
	2A		96.6		17.0	(not drilled)
	2B		97.7		16.0	(not drilled)
	2C		96.5		17.0	(not drilled)
5H1	1A	UO_2	95.9 - 96.2	150	19.0	8.0
	1B		95.9 - 96.7		17.0	4.3
	1C		96.2 - 96.3		19.0	leak
W5	1A	UO_2	97.6	107	14.0	2.2
	1B		97.6		16.0	3.0

TABLE VI cont.

Element (No.)	Comp.	Composition (values are wt. %)	Density (% TD)	EFPD	Burn-up (10^{20} fissions/cm^3)	Gas release (%)
W5 (cont.)	1C	UO_2	97.6	107	18.0	47.0
	1D		97.3		21.0	*leak*
H11	1A-1C	UO_2	97.2	163	25.0	leak
	1D		97.2		17.0	(int. def.)
7	-	UO_2	~94	63	1.6	0.25
8	-	UO_2	~94	63	2.1	0.22
9	-	UO_2	~94	63	2.1	0.13
X1	-	UO_2	~96	32	1.2	0.30
b	-	UO_2	~94	65	5.6	0.17 - 0.3
c	-	UO_2	~94	65	3.0	0.13
S2	-	UO_2	~97	231	3.0	0.3 - 0.8
S5	-	UO_2	~97	231	3.0	0.3 - 0.6
X-102	-	UO_2	~96	65	1.9	0.09
X-1B	-	UO_2	~97	152	5.8	0.24
X-3B	-	UO_2	~97	152	5.8	0.18
X-103	-	UO_2	~97	-	2.6	0.17
X-205	2	UO_2	~97	152	5.8	0.17

29-22 #9	-	BeO - 65.0 UO_2 (nominal 10 μm particle size)	97	-	10.8	0.13
59-2, B3-35	-	BeO - 65.0 UO_2 (nominal 10 μm particle size)	97	165	35.7	5.10
59-3, PB # 3	-	BeO - 51.0 UO_2 (nominal 10 μm particle size)	97	185	28.0	2.60
29-10	-	Al_2O - 21.0 UO_2 (nominal 5 μm particle size)	96	110	5.25	1.0
BJB	D	ZrO_2 - 18.7 UO_2	95.2	239	24.1	0.9
	E					0.9
14C	B	ZrO_2 - 25.1 UO_2	89.9	125	11.1	0.8
	C					2.1
	E					2.5
	F					1.6
JR-42	A	ZrO_2 - 26.1 UO_2	95.2	175	16.4	67.0
	B					4.3
	C					7.1
	D					5.0
	E					4.8

TABLE VI cont.

Element	Comp.	Composition	Density	EFPD	Burn-up	Gas release
(No.)		(values are wt. %)	(% TD)		(10^{20} fissions/cm^3)	(%)
JR-42 (cont.)	F	ZrO_2 - 26.1 UO_2	95.2	175	16.4	3.8
	G					3.3
	H					4.5
	I					4.8
	J					4.5
	K					4.3
	L					4.4
BHL	B	ZrO_2 - 34.9 UO_2	89.7	37	5.7	1.2
	C					2.0
	E					0.95
	F					1.3
BHB	B	ZrO_2 - 34.6 UO_2	95.5	37	5.8	1.1
	C					1.6
	E					1.3
	F					3.8
BHC	B	ZrO_2 - 34.6 UO_2	95.4	80	9.6	2.7
	C					2.7

	E						2.0
	F						2.5
BHM	B	ZrO_2-34.9 UO_2	90.7	80	10.0		2.2
	C						2.5
	E						2.6
	F						2.9
7GA	A	ZrO_2-34.4 UO_2	97.2	57	10.7		1.0
	D						1.3
JR-3	A	ZrO_2-35.8 UO_2	98.4	160	16.7		4.5
	B						4.6
	C						3.2
JR-4	A	ZrO_2-35.8 UO_2	98.8	160	17.5		13.7
	B						6.3
	C						4.4
	D						3.0
	E						4.1
	F						3.1
	G						4.1
	H						2.9
BHK	A	ZrO_2-34.9 UO_2	89.4	147	17.5		5.4
	B						4.3
	C						4.6
	D						4.4

TABLE VI cont.

Element	Comp.	Composition	Density	EFPD	Burn-up	Gas release
(No.)		(values are wt. %)	(% TD)		(10^{20} fissions/cm^3)	(%)
BHK (cont.)	E	ZrO_2 - 34.9 UO_2	89.4	147	17.5	5.0
	F					5.4
BHA	C	ZrO_2 - 34.6 UO_2	96	147	18.9	5.3
	F					5.6
BFZ	A	ZrO_2 - 34.6 UO_2	96.1	147	19.7	4.9
	B					4.5
	C					27.0
	D					40.0
	E					4.6
BHH	A	ZrO_2 - 34.6 UO_2	95.5	160	20.1	4.9
	B					3.7
	D					5.4
	E					3.8
BFY	D	ZrO_2 - 34.6 UO_2	96.1	147	20.9	3.4
BHD	A	ZrO_2 - 34.6 UO_2	95.4	197	21.3	6.7
	B					4.1
						4.5

	E					3.1
BHJ	A	ZrO_2 - 34.9 UO_2	89.2	197	22.9	6.8
	B					5.3
	D					7.9
	E					6.8
BFR	A	ZrO_2 - 34.6 UO_2	95.7	197	23.6	8.4
	B					6.6
	D					6.3
	E					5.6
BHN	A	ZrO_2 - 34.9 UO_2	90.8	239	24.1	55.2
	D					7.8
B92	A	ZrO_2 - 36.8 UO_2	96.2	217	24.4	5.6
	B					5.3
	D					5.2
	E					5.7
B91	A	ZrO_2 - 36.8 UO_2	96.1	217	25.1	4.8
	C					5.1
	D					5.0
BFT	A	ZrO_2 - 35.7 UO_2	96.8	197	26.2	1.7
	B					6.1
	D					4.4
	E					3.1

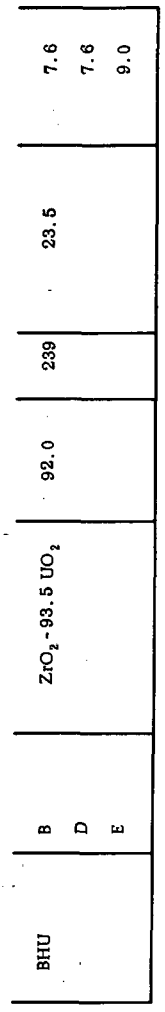
TABLE VI cont.

Element	Comp.	Composition	Density	EFPD	Burn-up	Gas release
(No.)		(values are wt. %)	(% TD)		(10^{20} fissions/cm^3)	(%)
7GB	A	ZrO_2 - 34.4 UO_2	97.2	262	29.5	6.7
	D					6.8
12D	A	ZrO_2 - 37.0 UO_2	87.8	285	29.7	4.8
	B					3.6
	D					5.6
	E					4.0
11B	B	ZrO_2 - 47.1 UO_2	97.5	125	19.9	4.0
	C					4.8
	D					5.0
	E					4.6
13C	A	ZrO_2 - 47.1 UO_2	96.2	125	20.0	3.5
	B					20.2
	C					4.7
	D					3.5
	E					4.7
	F					4.7
11C	A	ZrO_2 - 47.1 UO_2	97.7	125	21.2	3.6

	B					5.0
	D					3.9
	E					4.6
J64	A	ZrO_2-46.5 UO_2	97.2	144	23.7	3.0
	B					2.5
	C					1.8
	D					5.1
	E					3.8
	F					2.1
J1-9	A	ZrO_2-46.5 UO_2	97.2	157	26.5	6.0
	B					7.2
	D					6.2
	E					5.3
	F					4.1
	G					8.3
	H					9.1
J1-10	A	ZrO_2-46.5 UO_2	97.2	157	28.3	8.1
	B					8.8
	C					8.7
	D					7.5
	E					10.3
	F					6.7
	G					10.0

TABLE VI cont.

Element	Comp.	Composition	Density	EFPD	Burn-up	Gas release
(No.)		(values are wt. %)	(% TD)		(10^{20} fissions/cm^3)	(%)
J1-10 (cont.)	H	ZrO_2-46.5 UO_2	97.2	157	28.3	8.7
	I					12.0
	J					10.9
	K					12.5
	L					12.5
W-3	A	ZrO_2-47.0 UO_2	95.5	-	33.1	19.0
	B					13.3
	C					14.2
BFU	D	ZrO_2-46.5 UO_2	89.6	189	33.7	9.0
	E					10.7
BHX	A	ZrO_2-80.6 UO_2	98.8	147	17.5	6.1
	B					7.9
	F					27.0
BHW	B	ZrO_2-87.2 UO_2	97.4	147	18.5	5.3
	C					5.5
	E					5.5
	F					6.6


BHU
B
D
E
ZrO_2 - 93.5 UO_2
92.0
239
23.5
7.6
7.6
9.0

gas-release values exhibit a dependence on fission depletions similar to that of the volume changes. The fuel which exhibited normal swelling of 0.16% ΔV per 10^{20} fissions/cm^3 showed small gas-release rates (about 0.1% release per 10^{20} fissions/cm^3) up to about (18 to 20) $\times 10^{20}$ fissions/cm^3. However above this exposure, where accelerated swelling occurred, an increase in gas-release rate was also observed. Similarly, those compartments which showed excessive swelling and which did not rupture in-pile, due to the insulating-gas gaps described in section 3.1., showed high gas-release values. Four badly swelled but non-defective compartments were observed, W5 (1C), M52 (1A), 2H2 (1B) and 8H2 (1C-2C), and these showed gas-release values ranging from 18 to 57% of the theoretical gas-production values. Comparison of the large gas releases of these compartments with the much lower releases (1 to 11%) from unbulged compartments at the same fission depletions shows that the rate of gas-release increases rapidly near the time of failure. Such an increase in the gas-release rate would be expected to accompany an increase in fuel temperature resulting from formation of a gas gap between fuel and cladding. The increased release would, in turn, cause a larger gap until the compartment eventually ruptures.

These results show that high gas releases have been observed for at least two different reasons: (1) excessive operating temperatures caused by fuel-cladding gaps in pressure-bonded elements containing high-density UO_2 in $\frac{1}{4}$-in and $\frac{1}{2}$-in wide compartments and (2), accelerated release rates resulting from high fission depletion.

The release of fission gases from bulk UO_2 has been shown to be adequately described, at least at burn-ups below 10×10^{20} fissions/cm^3, as a solid-state diffusion process and this has recently been reviewed by LUSTMAN [1]. Following the treatment of BOOTH [20], it is assumed that volume diffusion occurs from an equivalent sphere of radius 'a', and that the fractional release for the case of irradiation occurring simultaneously with diffusion can be approximated to with fair accuracy when $\sqrt{Dt/a^2} < 1$ for gas release up to 20% by the expression

$$F_i = \frac{4}{a}\sqrt{\frac{D_i\, t}{\pi}}, \qquad (1)$$

where:
F_i is the fraction of isotope-i escaping from the solid, a is the radius (cm) of the sphere, D_i is the diffusion coefficient of isotope-i and t is the time in seconds. Also a is given by 3 (fractional theoretical density) $\div$ S, where S is the surface area (cm^2) per unit volume (cm^3).

The values of 'a' were calculated from the measured fuel-density values and the data of Ref. [1] relating this parameter to fuel surface area. Using this model, the gas-release data obtained in this investigation were examined on the basis of volume diffusion in-pile in the following manner. It was assumed that the diffusion coefficient at 1000°C varied with UO_2 depletion as reported by BELLE [1] on post-irradiation annealing of irradiated UO_2 and these results are shown in Fig. 14. It was further assumed that the activation energy for diffusion of the fission gases of -71 700 cal/mole remained un-

changed and that the correct specimen temperatures were calculated by the one-dimensional heat-transfer model described in section 3.1. Since these temperatures are time-averaged throughout sample life, the value of D at 1000°C was also averaged to that for the average fissions/cm^3 of the sample, i.e. one-half the total sample depletion. Following the same treatment utilized by Booth in analysing fuel rods, a Simpson three-point approximation rule was applied giving

$$\sqrt{D_{Total}} = \frac{1}{6}\left\{\sqrt{D(T_{CL})} + 4\sqrt{D(T_M)} + \sqrt{D(T_S)}\right\}, \qquad (2)$$

where

D_{Total} = average diffusion coefficient for the fuel
$D(T_{CL})$ = diffusion coefficient at centre-line fuel-temperature
$D(T_M)$ = diffusion coefficient at mean fuel-temperature
$D(T_S)$ = diffusion coefficient at surface fuel-temperature

Eight typical fuel plates ranging in exposure from about 4×10^{20} to 35×10^{20} fissions/cm^3 were analysed on the basis of this model and these results are shown in Fig. 14. It may be seen that the agreement between calculated and observed gas-release values is satisfactory considering the inherent inaccuracies of such a calculation. These results indicate that the observed increases in gas release at these high burn-ups can be described on the basis of volume diffusion if one assumes that the logarithm of the diffusion rate of the noble fission gases increases linearly with fuel burn-up as shown in Fig. 14. Thus, these data allow reasonable predictions of gas release from UO_2 to burn-ups of up to about 35×10^{20} fissions/cm^3. It should be pointed out that, while these results were explained on the premise that the diffusion path length 'a' remains unchanged and the volume diffusion constant varies with burn-up, they may equally well be interpreted as indicative of structural changes in the UO_2 in which the diffusion path length is decreased with increasing amounts of irradiation and the volume diffusion rate remains constant. Although this cannot be resolved by the tests described in this investigation, the observed structural effects noted in irradiated UO_2 and described in section 5 below are not inconsistent with this latter postulate. Thus the amount of released fission gases in bulk UO_2 can also be adequately described by diffusion theory and the use of a normalized diffusion coefficient (D^1) which is equal to D/a^2. The procedure has been adopted by ROBERTSON et al. [2] to predict the gas release in UO_2 fuel-rod elements. Note that the variation with burn-up of D of six orders of magnitude over a burn-up range of $(0 \text{ to } 26)\times10^{20}$ fissions/cm^3 shown in Fig. 14 requires a reduction in 'a' of three orders of magnitude if the changes observed are to be related to structure change in the UO_2.

4.2. $ZrO_2 + UO_2$ fuels

The fraction of the total fission gases released from $ZrO_2 + UO_2$ fuel materials are shown in Fig. 15 and Table VI. In a similar manner as described above for bulk UO_2, those fuel compartments subjected to overheating due to the formation of cladding-fuel gaps showed very large gas

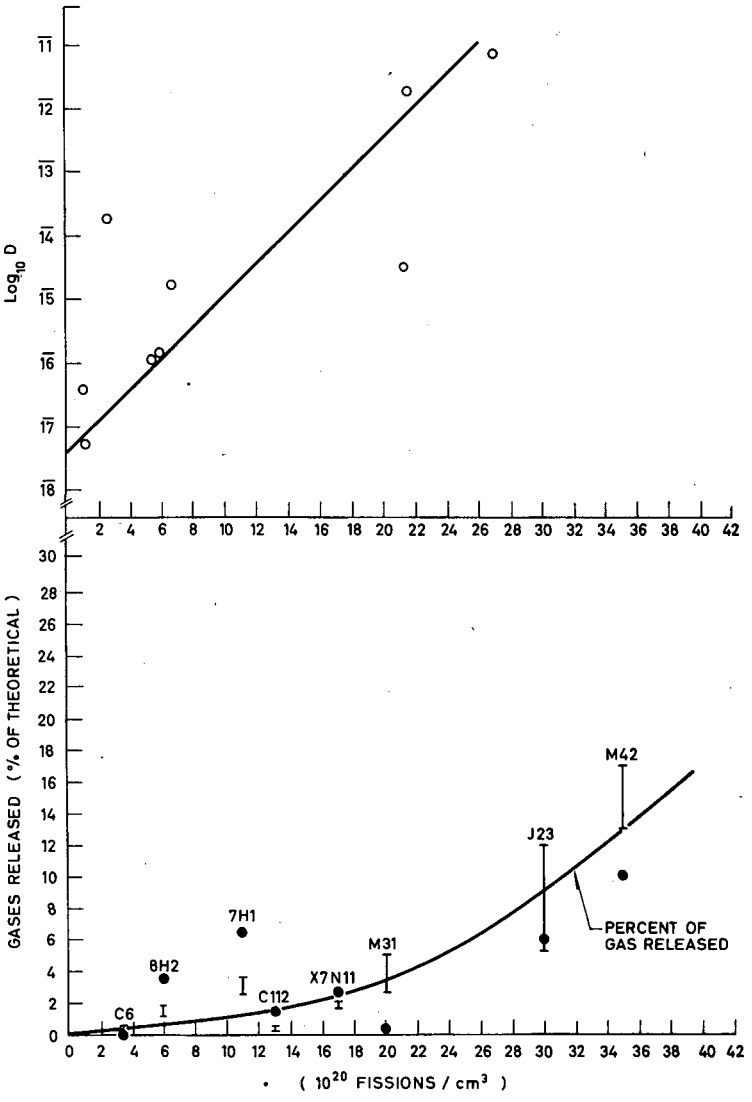


Fig. 4

Comparison of calculated and measured gas release from UO_2

○ Post-irradiation diffusion coefficient of Kr^{85} at 1000°C

M42 Sample identification

● Calculated gas release

I Measured gas release

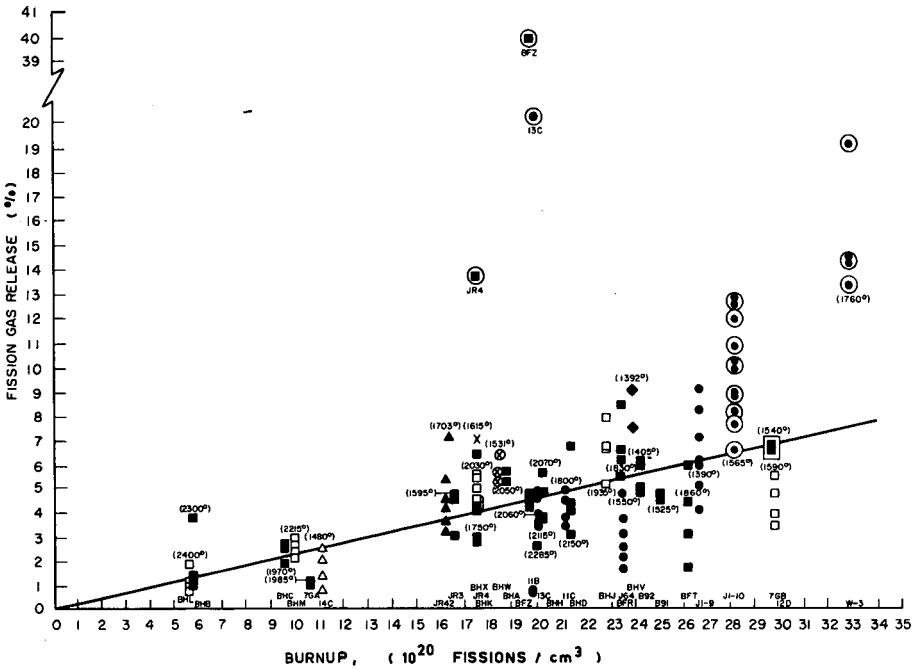


Fig. 15

Fission-gas release from ZrO_2 - UO_2 fuels

△ ZrO_2 - 25 wt. % UO_2, 90% theoretical density

▲ ZrO_2 - 25 wt. % UO_2, 96% theoretical density

□ ZrO_2 - 34 wt. % UO_2, 90% theoretical density

■ ZrO_2 - 34 wt. % UO_2, 96% theoretical density

● ZrO_2 - 46 wt. % UO_2, 96% theoretical density

× ZrO_2 - 80 wt. % UO_2, 96% theoretical density

⊗ ZrO_2 - 87 wt. % UO_2, 96% theoretical density

◆ ZrO_2 - 94 wt. % UO_2, 90% theoretical density

Copper diffusion bonded sample

These elements showed greater than 35% thickness increase; all other samples swelled less

(____°) Average operating temperature, °F

releases. The fuel which remained in contact with the cladding showed gas-release values which increased with exposure at a rate of about 0.25% release per 10^{20} fissions/cm^3 which is about twice that noted for UO_2 at exposures up to 20×10^{20} fissions/cm^3.

Comparison of these results with those obtained in UO_2 shows that, at low burn-ups, the gas release from ZrO_2-base fuels is higher than that from UO_2. However at exposures greater than about 24×10^{20} fissions/cm^3 the

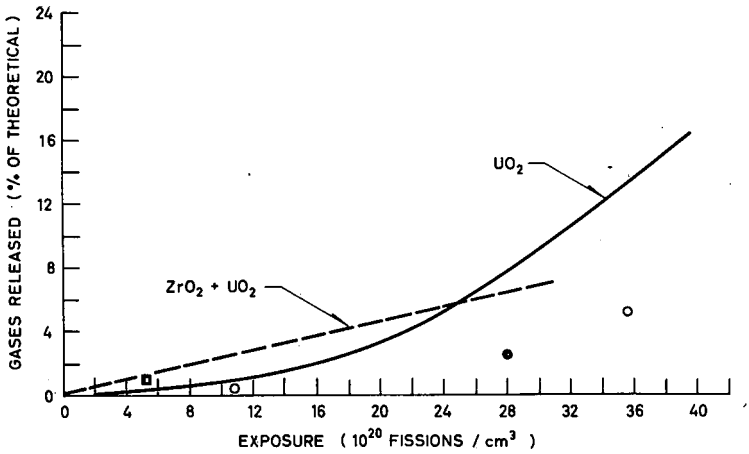


Fig. 16

Comparison of fission-gas release from oxide ceramic materials

○ BeO - 65 wt. % UO_2

● BeO - 51 wt. % UO_2

▫ Al_2O_3 - 21 wt. % UO_2

opposite situation exists. This comparison is shown in Fig. 16. CLAYTON [21] has shown that the diffusivity of the fission gases in ZrO_2-based fuels is about two orders of magnitude greater than that in UO_2. Hence, it is not surprising that this material has greater gas release than UO_2 at low exposures. It may be further presumed that, due to the increase in density of the ZrO_2-based fuel materials at low exposures (this due to the high degree of in-pile plasticity of the fuel discussed in section 3. 3), the mean free-path length 'a' is significantly increased and that the relative difference between UO_2 and ZrO_2-based fuel is much less than would be anticipated on the basis of the diffusion coefficients alone.

Another factor affecting the different fractional gas-release values of ZrO_2-based fuel materials and UO_2, described in section 5, is the precipitation of fission-gas bubbles at very low exposures in ZrO_2-based fuels; this does not occur in UO_2. Thus, in the case of the former fuel material, the precipitation of the gases in bubbles removes them from solution and hence decreases the concentration gradient for release external to the fuel wafer.

4.3. UO_2 dispersed in BeO and Al_2O_3

The total fission-gas release from the BeO + UO_2 and Al_2O_3 + UO_2 fuel materials are shown in Table VI and Fig. 16. These results show the excellent gas-retention ability of these oxide ceramic materials. Although Fig. 16 indicates that the BeO matrix is more effective in retaining the fission gases than either UO_2 or ZrO_2 + UO_2, it should be pointed out that these data on BeO at high burn-up were obtained on samples which had very low end-of-life temperatures. For example, sample B3-35 which was exposed to

35.7×10^{20} fissions/cm^3 operated at an end-of-life temperature of 740°F. This may be compared to typical ZrO_2+UO_2 or UO_2 samples which were exposed to end-of-life temperatures greater than 1100°F. Thus, assuming that the fractional gas release is diffusion-controlled, lower gas-release values would be expected from the BeO. To summarize, these results show that BeO and Al_2O_3 matrices have excellent gas-retentive abilities at least comparable with those of UO_2 and ZrO_2 + UO_2 fuel materials.

5. CHANGES IN STRUCTURE

5.1. Bulk UO_2

As a result of the behaviour of the plate elements described above in section 3.1., it was possible to characterize the changes in structure of UO_2 as a function of both burn-up and temperature in-pile. It will be shown in the following discussion that although the crystal lattice of UO_2 remains virtually unaffected by exposures up to 36×10^{20} fissions/cm^3 (15.7% of the uranium atoms fissioned), profound changes occur in fuel microstructure. These changes are characterized by a distinct change occurring at about 20×10^{20} fissions/cm^3 at low temperatures; at elevated fuel temperatures structural changes occur at lower exposures.

At exposures of less than 20×10^{20} fissions/cm^3, the only changes observed in the UO_2 microstructure were those observed at the grain boundaries. The one exception to this is that spherical white precipitates were noted at high temperatures and this is characteristic of elevated temperatures at all exposures. This is discussed in detail below. These effects are summarized in Fig. 17 which is typical of UO_2 microstructure observed at relatively low temperatures (estimated as about 1600°F). It can be seen that no gross changes in porosity or grain size occurred during irradiation. However, the grain boundaries in the irradiated material etched more rapidly and more uniformly than those in the unirradiated UO_2 and appear to be thicker. This behaviour was typical of all UO_2 examined which had been exposed to fission depletions of less than 20×10^{20} fissions/cm^3. The fuel in Fig. 17(a) can be compared to fuel from the centre of the same compartment (8H2-1C) shown in Fig. 17(b) but having an estimated maximum temperature of about 3000°F. It may be seen in Fig. 17(b) that the higher temperature resulted in pore formation at the grain boundaries and in the precipitation of the spherical white precipitates. Increased porosity at the grain boundaries, similar to that observed at the higher temperature, can also be produced by higher fission depletion at intermediate temperatures. This is illustrated by Fig. 17(c), which shows typical UO_2 after exposures of 20×10^{20} fissions/cm^3 at relatively low temperatures. It is estimated that the fuel temperature in this case was less than 2000°F, and it is significant that the fuel exhibited none of the spherical white precipitates characteristic of fuel operating at higher temperatures. The increased porosity at the grain boundaries resulting from higher temperatures or exposures correlates with the increased fission-gas releases under these conditions (see Fig. 13). It should be emphasized that although no gross changes in microstructure occurred at fission depletions of up to 20×10^{20} fissions/cm^3,

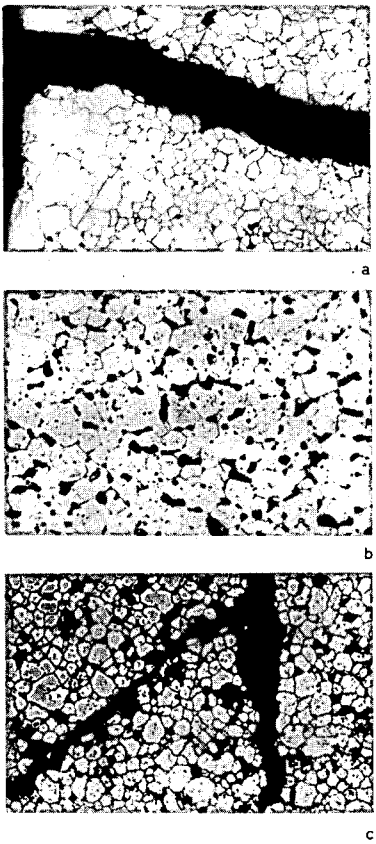


Fig. 17

Typical microstructures of UO_2 showing changes due to increased exposure up to 20×10^{20} fissions/cm^3 and due to elevated temperatures

(a)
8H2 comp. 1C, 6.2×10^{20} fissions/cm^3
Temperatures of about 1600°F

[Original × 500]

(b)
8H2 comp. 1C, 6.2×10^{20} fissions/cm^3
Temperatures of about 3000°F

[Original × 500]

(c)
M31 comp. 1A, 20×10^{20} fissions/cm^3
Temperatures of less than 2000°F

[Original × 400]

the pore formation at the grain boundaries shown in Figs. 17(b) and 17(c) are presumably related to increased mobility of the fission gases as indicated by the increased fractional gas-release values.

UO_2 exposed to fission depletions of greater than 20×10^{20} fissions/cm^3 at low temperatures (estimated as less than 2000°F) generally exhibited no grain structure when etched. Instead, the UO_2 in a given area of the sample was attacked uniformly by the etchant, resulting in a general

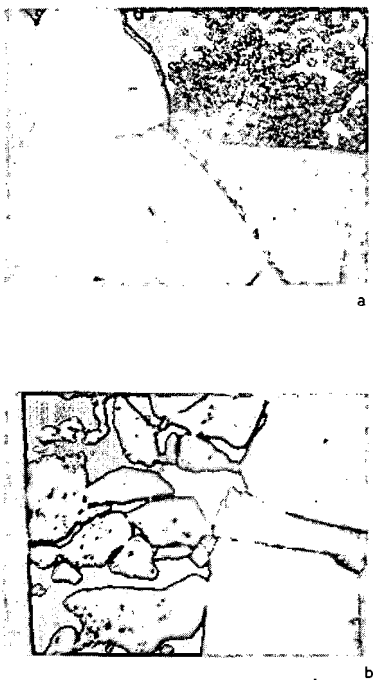


Fig. 18

Typical microstructures of fuel irradiated to greater than 20×10^{20} fissions/cm^3 at temperatures below 2000°F

(a) Fuel etched
121 comp. 5, 29×10^{20} fissions/cm^3
[Original × 250]

(b) As-polished
121 comp. 12, 30×10^{20} fissions/cm^3
(Note large fission-gas bubbles in region adjacent to fuel-clad gap)
[Original × 50]

darkening of the surface, as shown in Fig. 18(a) for compartment 5 of element I21. The fuel in this compartment operated at an average surface heat flux of 300 000 BTU $h^{-1} ft^{-2}$ to a fission depletion of 29×10^{20} fissions/cm^3. Fig. 18(a) shows that pieces of fuel in contact with the cladding etched less rapidly than pieces having poor contact, but that neither exhibited observable grain structure. The other characteristic feature of fuel at these high depletions and relatively low temperatures (Fig. 18(a)) is lack of porosity observable in the fuel. However, at higher temperatures, porosity does occur in the fuel at these burn-ups; this is shown in Fig. 18(b) where small fragments of fuel, believed to be thermally insulated since they were lodged in the void volume incorporated at the edges of the fuels, exhibited large, easily resolvable pores. It is important to note that in spite of the high fuel burn-up, no white spherical particles are present in these fuel materials irradiated at relatively low temperatures.

These observations based on light microscopy have been further clarified by preliminary results obtained by T. R. Padden of Bettis Atomic Power



Fig. 19

Electron micrograph of negative replica from unirradiated UO_2, control plate C109 (Etched with 1% H_2SO_4 in H_2O_2)

Laboratory in an electron microscopic study of UO_2 fuel material after irradiation. Typical electron micrographs obtained in this study are shown in Figs. 19, 20 and 21, and were obtained by direct observation of negative replicas stripped from the irradiated specimens. Fig. 19 shows a micrograph of unirradiated UO_2 with a typical grain size of about 15-μm diameter. The sloping planes at the grain interfaces, the pitting due to chemical etching and the pores remaining from fabrication are all characteristic of unirradiated UO_2.

The structure observed in UO_2 from plate C112 after 12.9×10^{20} fissions/cm^3 is shown in Fig. 20. No change in grain size is apparent but the grain boundaries show either precipitation of a second phase or enhanced chemical attack, agreeing with the microstructural observations noted above. The increased grain-boundary attack is presumed to result from segregation of grain boundaries of fission products as discussed below.

The microstructure of UO_2 from sample J23 after 31.3×10^{20} fissions/cm^3 is shown in Fig. 21 and it may be seen that the grains have subdivided into unit sizes of less than one micron. This behaviour was noted for fuel irradi-



Fig. 20

Electron micrograph of negative replica from UO_2, plate C112, compartment 10, irradiated to 12.9×10^{20} fissions/cm^3
(Etched with 1% H_2SO_4 in H_2O_2)

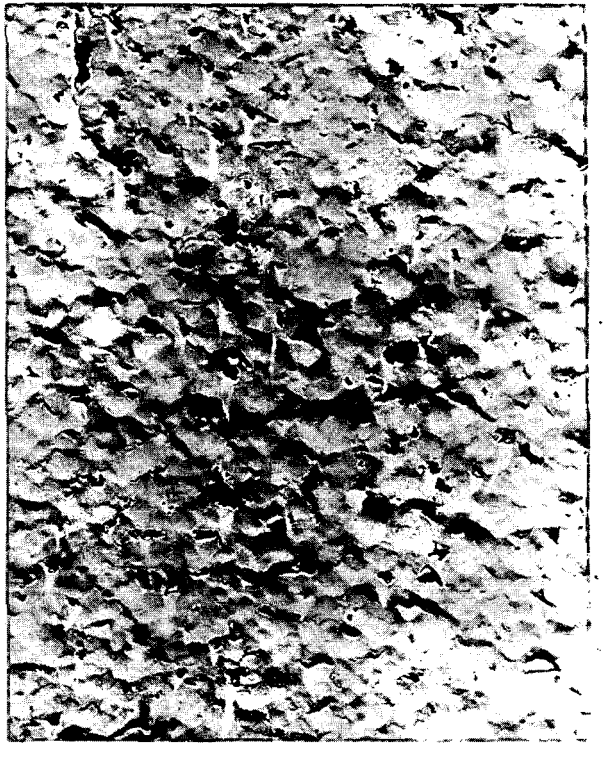


Fig. 21

Electron micrograph of negative replica from UO_2, plate J23, compartment 16, irradiated to 31.3×10^{20} fissions/cm^3
(Etched with a glow discharge)

[Original × 9400]

ated in the burn-up range of 24 to 31×10^{20} fissions/cm^3 and Fig. 21 is typical of the microstructure in this exposure range. Based on these results which indicate the formation of an extremely fine grain structure, it would not be expected that individual grains could be resolved by light microscopy.

X-ray diffraction patterns on irradiated UO_2 are consistent with the above metallographic observations. The cell sizes of the fluorite-type cubic crystal structure of UO_2 after exposures ranging from $(0.6 \text{ to } 36) \times 10^{20}$ fissions/cm^3 are shown in Table VII.

TABLE VII

CELL SIZES OF IRRADIATED UO_2

Test	Plate	Burn-up	a_0 *	Remarks
(No.)		(10^{20} fissions/cm^3)	(Å)	
unirradiated		0	5.469	
14:43-52	14:47	0.6	5.470	
30-5		2.9	5.476	Annealed 30 h, 1000°C
14-28	U-10	5.1	5.473	Annealed 30 h, 1000°C
14-28	U-11	8.3	5.466	
X3L	4	12	5.470	Annealed 30 h, 1000°C
X3L	3	21	5.470	Defected
X3L	3	21	5.465	Defected, annealed
CR-V-m	I-21	23	5.472	
X3L	4	24	5.461	Annealed 30 h, 1000°C
X3L	4	24	5.461	
CR-V-m	I-21	25	5.470	
CR-V-m	I-21	27	5.470	
CR-V-m	I-21	30	5.462	
X1P	1L1	34.5	5.466	
X3M	M42	36	5.466	

* Accuracy ±0.005 Å

The variation of the cell size from that of unirradiated UO_2 is very small. The scatter falls largely within the limits of error given as ±0.005 Å. Observations summarized by LUSTMAN [1] indicated a slight increase in the cell size of UO_2 with irradiation. This increase of 0.1% was saturated by the time an exposure of 5×10^{20} fissions/cm^3 was reached and it was attributed to the accumulation of defects in the early stages of irradiation. The unit cell size measurements in this investigation show somewhat more

scatter than for very low burn-up data, due to the increased experimental difficulties caused by sample radioactivity and therefore any further change in unit cell size is limited by the measurement error (on the other hand, see section 4.2 below). Furthermore, there is no significant change in peak broadening. The profile of the (311) peak of UO_2 from element I21, after 30×10^{20} fissions/cm^3, was determined to be 0.43° 2θ and has undergone no more broadening than the peak shown by LUSTMAN [1] of material irradiated to 3.42×10^{18} fissions/cm^3.

In plate M42 of the X-3-m test which was exposed to 36×10^{20} fissions/cm^3, about 16% of the original uranium atoms have fissioned. Among the remaining cations (including the uranium), 0.94% are ytterbium, 6.01% are zirconium, 2.37% are cerium and 4.35% are neodymium. These materials can, to the concentrations given, easily be introduced into solid solution in UO_2 as oxides, using ordinary furnace techniques. From observed values of their effect on cell size, compiled by BELLE [1], it can be calculated, using Vegard's Law, that these four fission products alone would decrease the cell size of UO_2 from 5.470 to 5.421 Å, if they were in solid solution. Other fission fragments, which cannot be accommodated so easily in the UO_2 structure, would have an even greater effect if they could be placed in solid solution by means of fission. BRINKMAN [25] estimates, on the basis of the volume of the materials in their pure solid form, that fission fragments in metallic uranium occupy about twice the volume of the uranium they replace. Even though the fission fragments may not be in elemental form in UO_2 and may not have their elemental atomic radii, it would be unusual if the fission fragments in solid solution caused a zero net volume change under a wide variety of exposures and states of decay.

The fission fragments seem to have no significant effect on the unit cell size, or on the degree of internal strain shown by the diffraction peak profile. These results suggest that the fission fragments migrate out of the UO_2 lattice and collect at grain boundaries or internal imperfections and are not uniformly or randomly distributed throughout the structure. This observation is consistent with the microstructural changes described above.

Based on the X-ray diffraction data, it seems reasonable to assume that the phase at the grain boundaries in Fig. 20 and at the sub-grain boundaries in Fig. 21 consists of segregated fission products. On this basis, the relative distribution of the fission products can be estimated. The mean grain surface area of each grain of the fuel in Fig. 20 is about 4×10^{-6} cm^2 and the volume of a grain about 10^{-9} cm^3. If it is assumed that one fission fragment can reside in each unit cell of UO_2 at the grain boundary, the thickness of the segregated zone at each grain boundary in Fig. 20 is then

$$\frac{2\times12.9\times10^{20}\times10^{-9}\times(5.47\times10^{-8})^3}{4\times10^{-6}}\simeq10^{-4}\text{ cm},$$

a value not inconsistent with the observed thicknesses. A similar correlation of the structural refinement in Fig. 21 with an assumed segregation of fission products at substructure boundaries yields a value of thickness of the latter of about 0.25×10^{-4} cm.

Compartment 1A of element M52 swelled 37 mil after 20×10^{20} fissions/cm^3 without cladding rupture, and released 57% of the theoretically-produced

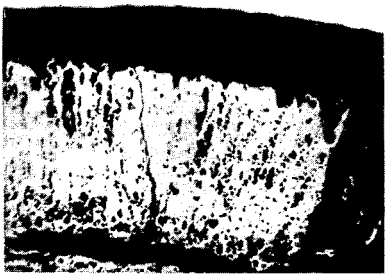
fission gases. This fuel structure (Fig. 4) shows evidence of columnar grain structure. Based on the temperature gradient evaluations made on UO_2 pellets *, irradiated to exposures lower by orders of magnitude, the maximum temperature reached by the fuel shown in Fig. 4 was greater than 1500°C (2700°F). The structure observed in this fuel platelet may thus be compared to that observed in rods irradiated at similar temperatures to such lower exposures [1, 2]. Fig. 22(a) shows the outer edge of the fuel at the compartment centre and it may be seen that large columnar grains are outlined by gas bubbles; this is typical of structures observed in rods. Also, both the uneven, jagged appearance of the fuel edge and the elongated shape of the pores indicate that vaporization and re-deposition of UO_2 together with pore migration up the thermal gradient has occurred in a manner similar to that proposed for rod elements. The most striking difference between this structure and that observed in rods is the heavy concentration of white spherical precipitates observed in this structure. These particles are shown at higher magnification in Fig. 22(b) at the centre of the fuel platelet, where it can be seen that the size and concentration is much greater than observed in other samples, i. e. Fig. 17(b). This is consistent with the interpretation that the presence of the particles is indicative of high exposure and high temperature. An investigation was conducted and reported by BELLE et al. [22] in an attempt to identify these particles on the basis that they would be either iron, uranium, uranium carbide or uranium nitride. This investigation showed conclusively that these particles were not impurities originally in the unirradiated fuel. Furthermore, the impurity concentrations in control UO_2 samples were only 220 ppm ** carbon, 98 ppm iron and 60 ppm nitrogen, which could not account for the amount of precipitate shown in Fig. 22. Metallographically similar precipitates of a white spherical phase have been noted in UO_2 heated to temperatures close to its melting point and have been identified as precipitates of uranium arising from reduction of UO_2 to a sub-stoichiometric composition at high temperatures and rejection of uranium upon cooling as the UO_2 reverts to its normal composition [23, 24]. However, the examinations reported by BELLE et al. [22] ruled out identification of these precipitates as unalloyed uranium because of their resistance to chemical etchants. It is quite likely that the precipitates consist of uranium alloyed with fission-product species such as zirconium and niobium which would greatly decrease the chemical activity of uranium. Therefore, it is believed to be a plausible assumption that these white, spherical particles are precipitated, non-volatile fission-products the concentrations of which are of the order of 10 wt. % in these high-burn-up fuels. Further verification of this premise is shown in section 5. 2 below in connection with $ZrO_2 + UO_2$ fuel materials.

5. 2. $ZrO_2 + UO_2$ fuel

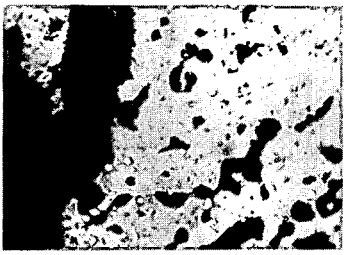
Before irradiation, the structures observed on the $ZrO_2 + UO_2$ fuel materials were in good agreement with the $ZrO_2 + UO_2$ phase diagram of

* Investigations made at Bettis Atomic Power Laboratories, Hanford Atomic Power Laboratories and Atomic Energy of Canada Ltd.

** parts per million by weight



a



b

Fig. 22

Solid precipitates and gas bubbles in bulk UO_2 (element M52, compartment 1A)

(a)
Bubble distribution along UO_2 fuel outer edge

[Original × 75]

(b)
Solid precipitates and gas bubbles at centre of fuel platelet

[Original × 400]

COHEN and SCHANER [26]. Fuel with a composition of ZrO_2 + 25 wt.% UO_2 consists of a single tetragonal phase; a typical microstructure of this material is shown in Fig. 23. Materials containing a nominal 34 or 46 wt.% UO_2 consist of appropriate amounts of two tetragonal phases, shown in Figs. 24 and 25. One of these phases is tetragonal at the temperature of formation and has the composition ZrO_2 + 29 wt.% UO_2. The other, cubic at the sintering temperature, transforms on cooling to another tetragonal phase which has a composition of ZrO_2 + (65 to 69 wt.%) UO_2, depending on the final temperature of the heat treatment.

The characteristic grain boundaries observed in the pre-irradiation microstructures of these ZrO_2-based fuels cannot be resolved by standard light microscopy after irradiation; this is illustrated in Fig. 26 for ZrO_2 + 34 wt.% UO_2 irradiated to 5.7×10^{20} fissions/cm^3. However, as discussed below, the material is still crystalline as is evidenced by the sharp X-ray diffraction patterns. This difficulty in developing grain structure by etching is similar to that observed in UO_2 at exposures greater than 20×10^{20} fissions/cm^3 (Fig. 18). However, a distinctly different feature of this material is the observed intra-microstructure bubbles, presumably filled with fission gases, which are evident at exposures as low as 5.7×10^{20} fissions/cm^3, seen in Fig. 26 for ZrO_2 + 34 wt.% UO_2 fuel. The precipitation of gas bubbles in

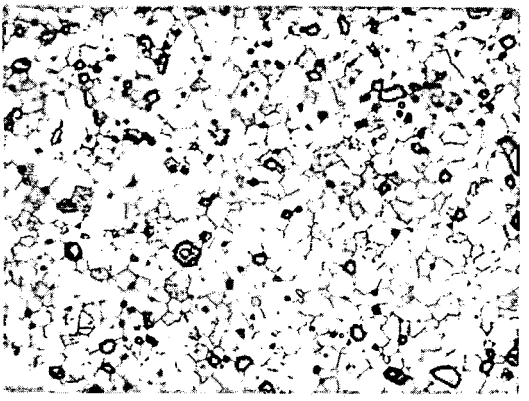


Fig. 23

Typical microstructure of unirradiated ZrO_2 - 25 wt. % UO_2

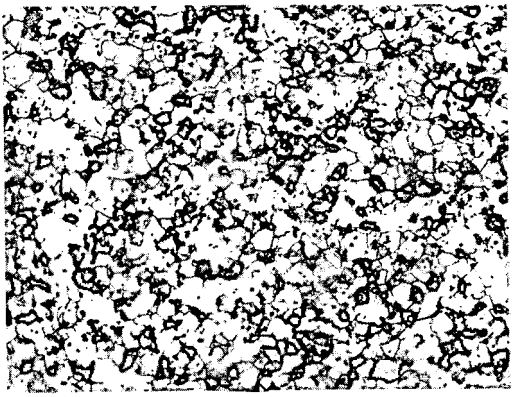


Fig. 24

Typical microstructure of unirradiated ZrO_2 - 34 wt. % UO_2

the ZrO_2-based fuel (but not in UO_2) may be attributed to the greater plasticity of the ZrO_2-base fuel materials as described in section 3 above. It may be presumed that the nucleation and growth of gas bubbles is easier in this than in UO_2 as the ZrO_2-based material is much weaker in-pile. Another factor which may contribute to this effect is the higher gas diffusivity of the ZrO_2-based fuels (described in section 4) and the increased diffusion path length for external release of gas due to the increase fuel density. Thus, it is not only easier to precipitate bubbles but also more gas is available.

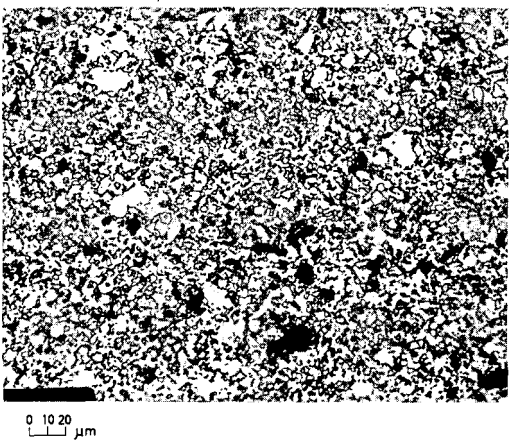


Fig. 25

Typical microstructure of unirradiated ZrO_2 - 46 wt. % UO_2

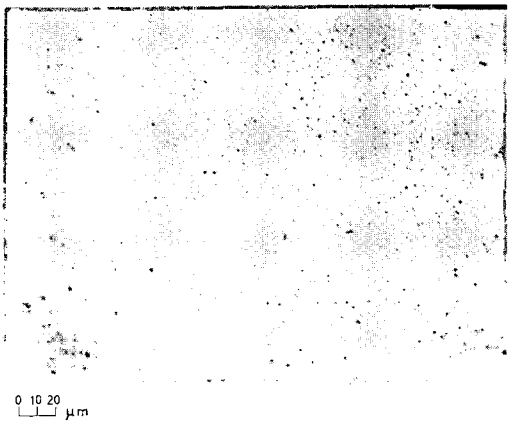


Fig. 26

Fission-gas bubbles after 5.7×10^{20} fissions/cm^3
(Element BHL containing ZrO_2 - 34.9 wt. % UO_2)

The distribution and relative abundance of fission-gas bubbles at relatively low temperatures and for various burn-ups are shown in Figs. 26, 27 and 28. These consist of ZrO_2 + 34 wt. % UO_2 fuel, originally of 96% theoretical density, irradiated to (5.7, 17.5 and 25.1)$\times 10^{20}$ fissions/cm^3, respectively. The volume occupied by pore space, as estimated by lineal analysis, varies from about 5% in the low-burn-up material (5.7×10^{20} fissions/cm^3) to 20% in the high-burn-up material (25.1×10^{20} fissions/cm^3). The fuels at the low burn-ups have considerably smaller pores, on the average, than those at higher burn-ups. The gas bubbles in Fig. 26 (5.7×10^{20} fissions/cm^3)

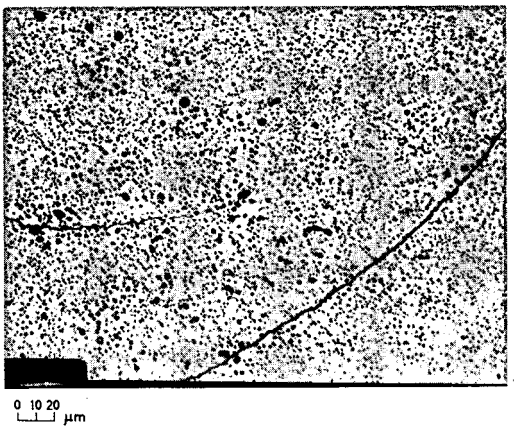


Fig. 27

Fission-gas bubbles at 17.5×10^{20} fissions/cm^3
(Element BHK containing ZrO_2 - 34 wt. % UO_2)

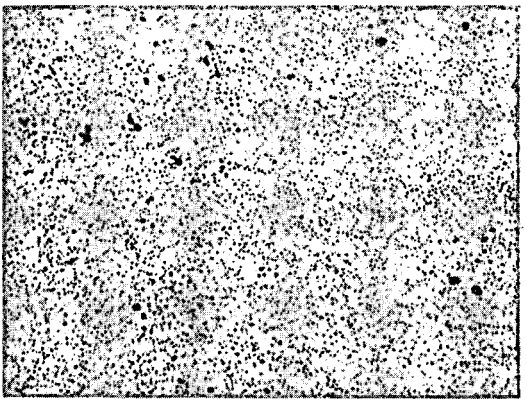


Fig. 28

Fission-gas bubbles after 25.1×10^{20} fissions/cm^3
(Element B91 containing ZrO_2 - 36.8 wt. % UO_2)

are 0.5 μm and below, with a few ranging up to 1 μm. Diffraction effects of the smaller pores make their outlines difficult to resolve. In both Figs. 27 and 28 most of the pores are 1 to 1.5 μm in diameter. Although the material of Fig. 27 received somewhat less irradiation, a larger proportion of the pores have been enlarged to 3 to 4 μm. The sample in Fig. 28 appears to contain the greater number of pores, however. These results show that the fission-gas bubble sizes and distribution in a given sample can be described in terms of the following variables: (a) the total porosity of the sample, which varies from 5 to 20% over the range from $(5.7 \text{ to } 25) \times 10^{20}$ fissions/cm^3; (b) the median

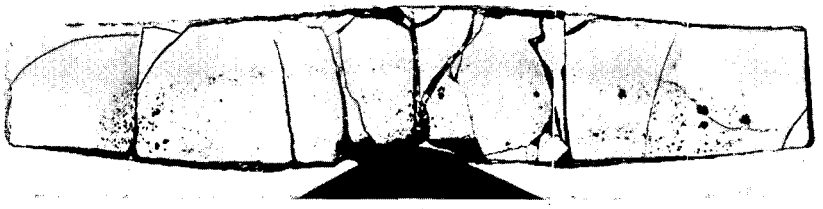


Fig. 29

Element 13C, containing ZrO_2 - 47.1 wt.% UO_2 irradiated to 20×10^{20} fissions/cm^3

diameter of the pores, which varies from 0.5 to 1.5 μm over the same exposure range; (c) the frequency of the pores that exceed the median diameter by factors of two to three. The first two values seem to depend directly on total burn-up. The third seems to be a factor depending on the operating temperature. Composition of the material and original porosity have no discernable effect due to the complete densification of the fuel, described in section 3.

The effect of temperature on the size of the bubbles is shown in Fig. 29, where samples containing ZrO_2 + 46 wt.% UO_2 fuel were overheated due to fuel-clad separation after exposures of about 20×10^{20} fissions/cm^3. This compartment had apparently formed an insulating gap on one side while the other side of the fuel remained in contact with the cladding. Thus, the presence of large bubbles (up to 75 μm in diameter) is noted, not at the centre of the platelet, but at the location of maximum fuel-temperature. The asymmetric demarcation line between "large" and "small" bubbles can be seen skewed toward the lower side of the platelet. These results show that at very high temperatures the fine gas pores agglomerate into relatively few, very large pores and this is accompanied by gross fuel-swelling.

Associated with these high-temperature fuel regions described above, white spherical particles similar to that observed in UO_2 have been observed.

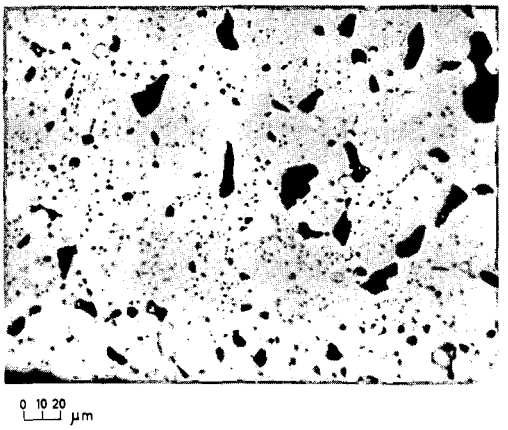


Fig. 30

Massive white particles and voids in compartment D of element BFZ, containing ZrO_2 - 34.6 wt.% UO_2 irradiated to 19.7×10^{20} fissions/cm^3

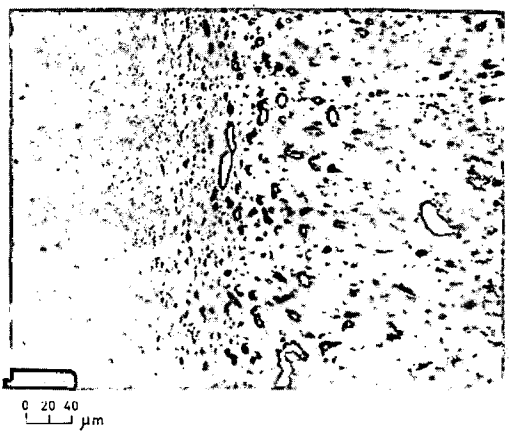


Fig. 31

White particle and thermal gradient in element 13C, containing ZrO_2 - 47.1 wt. % UO_2 irradiated to 20×10^{20} fissions/cm^3

These particles are shown in Fig. 30 in ZrO_2 + 34 wt. % UO_2 and were observed for fuel compositions ranging from ZrO_2 + 34 wt. % UO_2 to ZrO_2 + 94 wt. % UO_2. They are identical in appearance to those described in bulk UO_2 in section 5.1. The temperature dependency for the precipitation of these particles is shown in Fig. 31, where the bubble size may be used as indicative of fuel temperature. It may be seen that in the cooler region of the fuel where there are only fine bubbles, no white particles are evident. However, in the hotter fuel regions containing large, non-spherical bubbles, the white precipitates are visible even at the low magnification of Fig. 31. It is felt that these results confirm the hypothesis for UO_2 described above, i. e. these precipitates are stabilized uranium metal since $ZrO_2 + UO_2$ is known to be even more susceptible to sub-stoichiometry than UO_2 [27]. This is consistent with the much greater concentration of white particles observed in $ZrO_2 + UO_2$ fuel than in UO_2. One notable feature, observable in both Fig. 22 and Fig. 30, is that the white particle precipitates are almost invariably associated with a pore.

The ZrO_2 + 25 wt. % UO_2, heated into the 1000 - 2000°C range should consist of a single tetragonal phase. When cooled to room temperature, the cell dimensions of this phase are $a_0 = 5.154$ Å, $c_0 = 5.241$ Å. Compositions at 34 and 46 wt. % UO_2 fall, at sintering temperature, into the two-phase field in the centre of the binary diagram. In the as-sintered condition at 1650°C a zirconium-rich phase, containing about 29 wt. % UO_2, is in equilibrium with a uranium-rich phase with 69 wt. % UO_2. At 1750°C, the 29 wt. % UO_2 phase is in equilibrium with a phase containing 65 wt. % UO_2. These high-temperature phases are tetragonal at room temperature, although the resolution of the (113) and (311) peaks is barely discernible in the 69 wt. % material. Table VIII shows the cell sizes, measured at room temperature, for single phases of unirradiated material of the various compositions of interest.

Fig. 32 shows a portion of the diffraction patterns (56-63° 2 θ) of unirradiated 25, 34 and 46 wt. % UO_2 after sintering at 1650°C. The pattern

TABLE VIII

CELL SIZES OF IRRADIATED AND UNIRRADIATED UO_2 - ZrO_2

Nominal composition	Element	Burn-up	Phase designation	a_0 *	c_0 *
(wt.% UO_2)	(No.)	(10^{20} fissions/cm^3)		(Å)	(Å)
20		Unirradiated	tetragonal	5.110	5.211
			monoclinic	†	†
	10A	0.0006	tetragonal	5.099	5.201
	10B	0.002	tetragonal	5.105	5.201
	10C	0.005	tetragonal	5.123	5.201
25		Unirradiated	tetragonal	5.164	5.241
	14C	11.1	cubic	5.160	
34		Unirradiated (as sintered)	tetragonal I	5.172	5.263
			tetragonal II	5.325	5.345
		Unirradiated (coarsened)	tetragonal I	5.172	5.263
			tetragonal II	5.275	5.317
	BHL	5.7	tetragonal	5.160	5.220
	BHB	5.8	tetragonal	5.160	5.220
	BHC	9.6	cubic	5.180	
	BHM	10.0	cubic	5.180	
	7GA	10.9	cubic	5.180	
	BHH	20.1	cubic	5.182	
	BHD	21.5	cubic	5.178	
	BHJ	22.9	cubic	5.178	
	B9-2	24.4	cubic	5.180	
	B9-1	25.1	cubic	5.180	
	BFT	26.2	cubic	5.184	
	7GB	29.5	cubic	5.180	
	12D	29.7	cubic	5.180	
46		Unirradiated (The same as 34 wt.% UO_2 except for relative intensities)			
	11C	21.2	cubic	5.215	
	W3	33.1	cubic	5.217	

* Accuracy ±0.005 Å

† $a_0 = 5.14$, $b_0 = 5.204$, $c_0 = 5.311$, $\beta = 99.25°$

TABLE VIII cont.

Nominal composition	Element	Burn-up	Phase designation	a_0 *	a_0 *
(wt. % UO_2)	(No.)	(10^{20} fissions/cm^3)		(Å)	(Å)
80	BHX	20.4	cubic	5.347	
87	BHW	18.5	cubic	5.400	
94	BHT	21.4	cubic	5.423	

* Accuracy ±0.005 Å

of the ZrO_2+ 25 wt. % UO_2 shows only the (113), (311) and (222) peaks of the single tetragonal phase. The (113) and (311) peaks are clearly resolved; their separation is about 0.75° 2 θ. The other two compositions consist largely of a tetragonal phase of similar composition, plus appropriate amounts of the uranium-rich phase. This appears as an additional (222) peak at 60.8° 2 θ, and as a barely resolved doublet, (113) and (311), at 58° 2 θ, where it is partly obscured by the (113) peak of the first phase. The patterns are in good agreement with the equilibrium phases calculated from the data of Cohen and Schaner. In addition, there is often observable in all the fuels a slight amount of the monoclinic phase, in agreement with the observations of Voronov and also reported by Cohen and Schaner.

The cell sizes obtained on the double-crystal diffractometer from irradiated specimens are also listed in Table VIII. Representative portions of the diffractograms of ZrO_2 + 34 wt. % UO_2 are shown in Fig. 33. These results show that all irradiated samples of ZrO_2 + UO_2 fuel materials consist only of a single crystalline phase. Furthermore, all samples that have undergone more than 9.6×10^{20} fissions/cm^3 are cubic. BERMAN has reported [5] that ZrO_2 + 20 wt. % UO_2, which is composed initially of a mixture of the tetragonal and monoclinic phases, consists of a single tetragonal phase after exposures from 6×10^{16} to 5×10^{17} fissions/cm^3. WITTELS and SHERRILL [28] and ADAM and COX [29] irradiated monoclinic material, with the approximate composition ZrO_2 + 0.5 wt. % UO_2, to exposures of the order of 10^{16} fissions/cm^3. Both report the disappearance of the monoclinic phase. Wittels and Sherrill state that their material consists of a single cubic phase, while Adam and Cox report that the irradiated material is tetragonal. On the basis of these results on samples receiving very small amounts of irradiation, it seems reasonable to assume that the multi-phase fuels irradiated in this experiment became single-phase. The disappearance of the peaks of the additional phases cannot be ascribed to the destruction of their crystal structure, leaving only a single crystalline phase along with one or more amorphous phases that do not show on the diffractogram. It will be

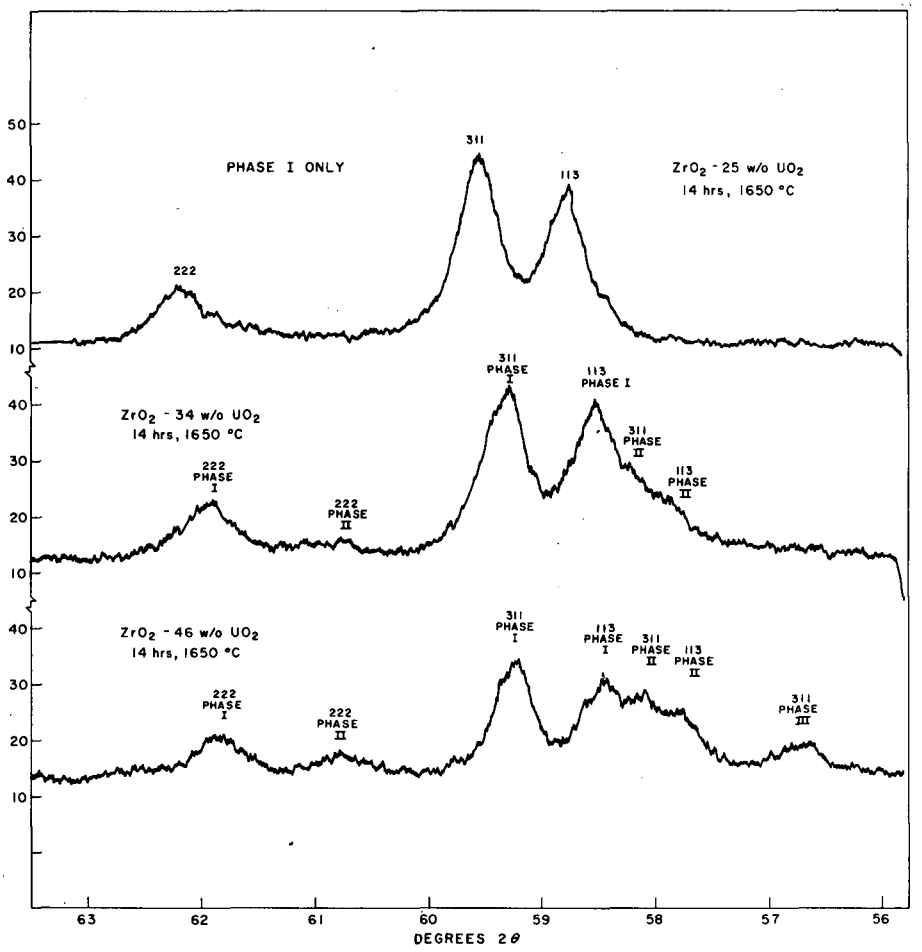


Fig. 32

Diffractograms of unirradiated ZrO_2 - UO_2 solid solutions

shown that the lattice parameters of the single phase observed correspond to the bulk composition of the entire sample, provided values appropriate to irradiated material are used in the calculations. Consider two samples, one of 34 and one of 46 wt.% UO_2, similarly heat-treated but unirradiated. These fall in the two-phase region and, by the phase rule, consist of two identical phases, differing only in the quantity of each of the phases present. Two such samples, irradiated to approximately the same exposure (see Table VIII) are BHJ (22.9×10^{20} fissions/cm^3, 34 wt.% UO_2) and 11C (21.2×10^{20} fissions/cm^3, 46 wt.% UO_2). Both consist of a single cubic phase. If one of the phases became amorphous, so that only the previously identical second phase were observed, then the diffraction patterns of this second phase should be identical; however it can be seen in Table VIII that they

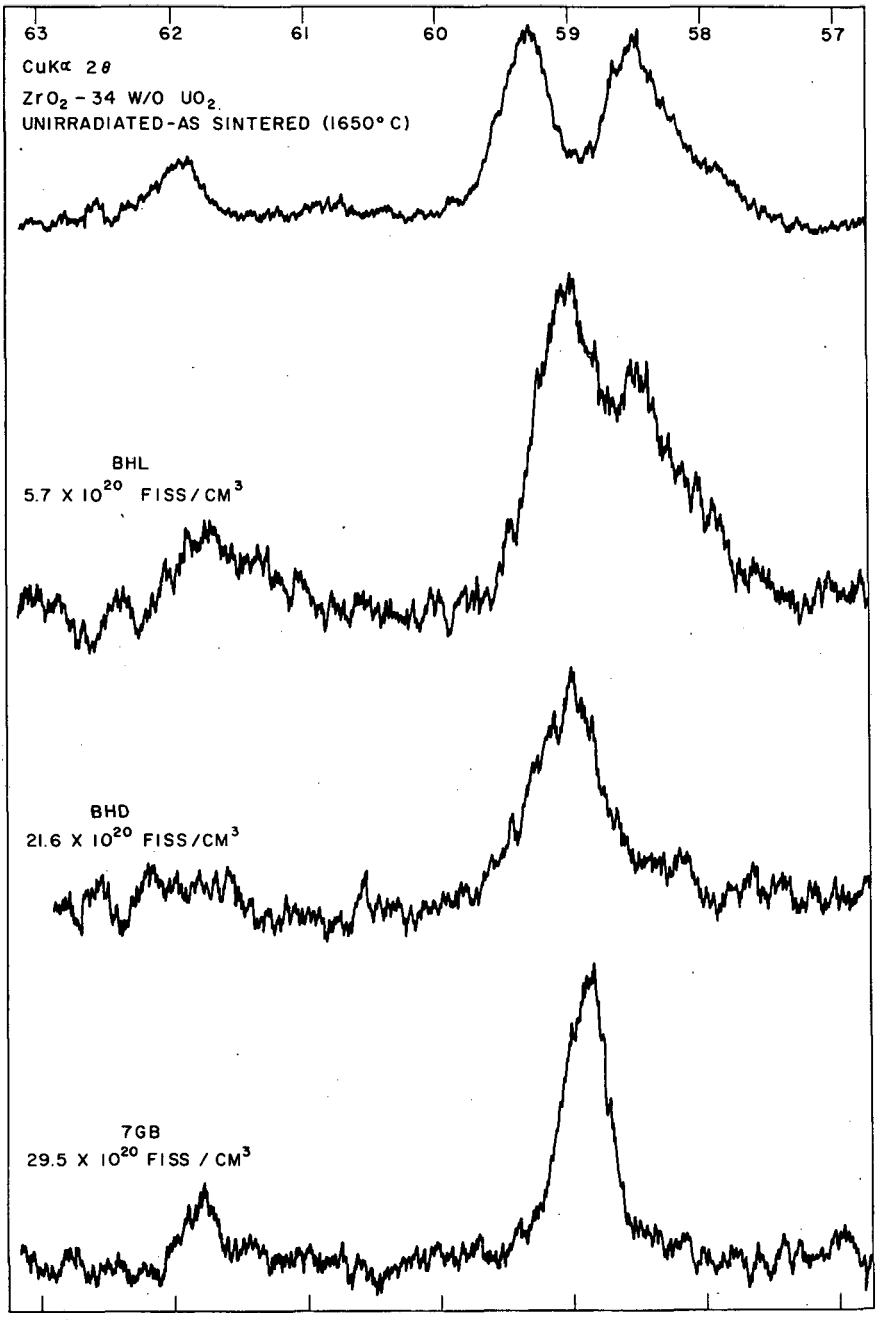


Fig. 33

Effects of fission-fragment bombardment on ZrO_2 - 34 wt. % UO_2

actually differ considerably. The cell size measured for the single cubic phase of BHJ is 5.178±0.005 Å, and for 11C, the value is 5.215 ± 0.005 Å.

Samples BHB and BHL, of slightly irradiated ZrO_2 + 34 wt.% UO_2, as well as the 20 wt.% UO_2 samples studied by Berman, are tetragonal (see Table VIII). Material of these compositions quenched from the single-phase region above 2000°C is also tetragonal at room temperature. In unirradiated material, the separation between the (113) and (311) reflections is approximately 0.76° 2 θ. In samples BHB and BHL, however, the separation is considerably less – approximately 0.55° – indicating that the c/a axial ratio has decreased to 1.012 from the value of 1.017 in unirradiated material. The cell dimensions have also decreased, such that the values for the single combined phase are not intermediate between those of the two phases of the unirradiated material. It will be shown that this decrease can be ascribed to oxidation.

These values are almost exactly those that would be predicted on the basis of a single homogenized phase obeying Vegard's Law. Calculated values, based on Vegard's Law and assuming $a_0 = 5.469$ Å for UO_2 and 5.113 Å for cubic ZrO_2, are given in Table IX for each of the compositions under

TABLE IX

CALCULATED CELL SIZES FOR ZrO_2- UO_2, BASED ON VEGARD'S LAW

Nominal composition	Calculated cell size, a_0	Av. of measured cubic cells from Table VIII, a_0
(wt.% UO_2)	(Å)	(Å)
25	5.160	5.160
34	5.180	5.180
46	5.211	5.216
80	5.344	5.347
87	5.380	5.400
94	5.427	5.423

study. These results agree closely with the observed values and it should be noted that they are unaffected by exposure up to about 33×10^{20} fissions/cm^3. A small but definite contraction of the cell volume takes place on transformation from monoclinic or tetragonal to cubic and these can be calculated from the cell size shown in Table IX. These results are presented in Table X and show that changes in density of 1.7 to 2.3% for ZrO_2 containing 25 to 46 wt.% UO_2 respectively are observed.

The merging of the (311) and (113) peaks shown in Fig. 33 for ZrO_2 + 34 wt.% UO_2 cannot be attributed to the lack of resolution of the double crystal spectrometer or the broadening of the diffraction peaks due to strain.

TABLE X

THEORETICAL DENSITIES OF ZrO_2- UO_2

Nominal composition	Pre-irradiation density	Post-irradiation density	Density increase
(wt. % UO_2)	(g/cm^3)	(g/cm^3)	(%)
25	6.767	6.883	1.71
34	7.042	7.209	2.37
46	7.502	7.672	2.27

In Fig. 33, if the diffractogram of sample 7GB is compared to that of the unirradiated material, it will be seen that the diffraction peaks are no broader and that the Bragg Angles appropriate for the the peaks of the tetragonal phase are unoccupied. It is therefore felt that the two tetragonal phases have homogenized into the single cubic, metastable, high-temperature phase.

These results indicate that the following processes are operative in this oxide binary system. First, the results of Wittels and Sherrill and of Adam and Cox show that a diffusionless transformation from the monoclinic to a system of higher symmetry takes place at exposures of the order of 10^{16} fissions/cm^3. This is consistent with other processes involving diffusionless transformations and these have been reviewed by LUSTMAN [1].

However, it is unreasonable to assume that the two-phase tetragonal structures, which are homogenized into a single tetragonal phase of composition corresponding to the bulk composition of the entire sample, would transform at this low exposure level, since such homogenization would require interdiffusion of microscopically segregated regions. Such homogenization processes have been observed in U + 9 wt. % Mo and U + 10 wt. % Nb alloys and were attributed to the action of displacement spikes occurring at the interface of the two phases and smoothing out the concentration gradients [30]. In these uranium alloys, which consist of a lamellar structure having an interlamellar spacing of about 0.5 μm, the kinetics of the homogenization reaction were such that exposures of about 5×10^{19} fissions/cm^3 were required to secure homogenization. In the ZrO_2 + UO_2 system the two tetragonal phases are present as equiaxed grains. In the case of ZrO_2 + 46 wt.% UO_2, the volume fraction of each phase is approximately equal and the grain size of each phase is about 10 μm in diameter. Hence, it would be anticipated that homogenization would take place more slowly than in U + 9 wt. % Mo alloy. Since the homogenization by fission fragments is a function of the number of fission fragments traversing the boundary of the high and low uranium content phases, the rate of homogenization would, to a first-order approximation, be proportional to the relative surface area to volume ratios. The ratio of volume to surface area in the case of the oxide relative to that of the U + Mo alloys was about 6×10^{-2} cm. Thus, homogenization in the former case would be expected to be complete by a burn-up of $(5 \times 10^{-19})/(6 \times 10^{-2})$,

or about 8×10^{20} fissions/cm^3. Since Table VIII shows that this homogenization is completed by 5.7×10^{20} fissions/cm^3, there is reasonably good experimental agreement with the above approximation.

The third process consists of the transformation of the single-phase tetragonal into a cubic structure. At the composition of ZrO_2 + 34 wt.% UO_2, this occurs gradually and is completed between (6 and 9.6) $\times 10^{20}$ fissions/cm^3. This change therefore cannot be an effect simply of the energy generated by fission. The chemical effect of the accumulating fission fragments may play a decisive role in the stabilization of the cubic phase. However, the formation of gas bubbles and white particles, the microstructural changes in the fuel and the non-dependence of cell size on fission-product concentration indicate that the proportion of fission products remaining in the crystal lattice must be quite small. It is unlikely that the fission fragments are present in sufficient concentration to shift the borders of the true stability fields in the UO_2 + ZrO_2 binary diagram to any significant extent. It may be that their effect is to suppress or retard the diffusionless transformation from cubic to tetragonal that Cohen and Schaner observed in single-phase samples of these compositions.

Another factor which may cause reversion of the ZrO_2 structure to the cubic form is the liberation of oxygen from the fuel as a result of its

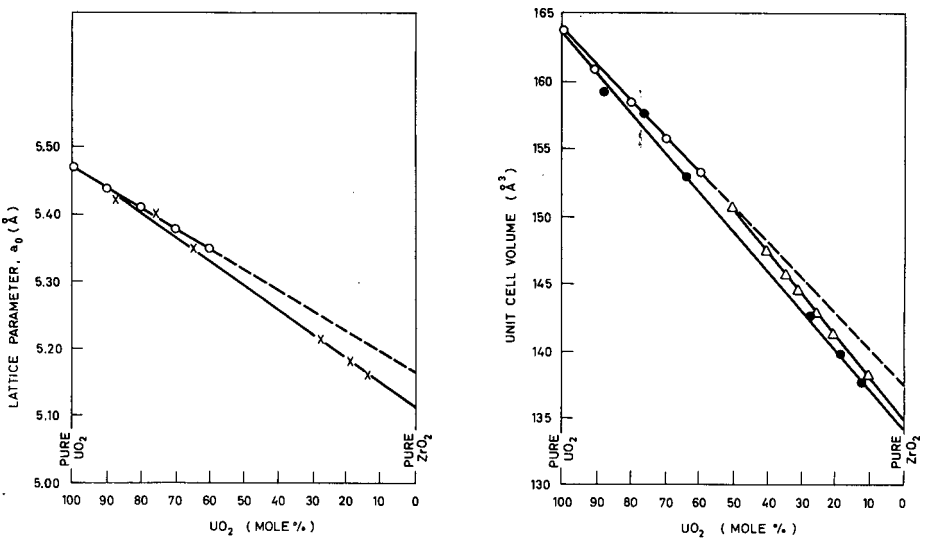


Fig. 34

Comparison of irradiated and unirradiated cubic phase in UO_2 - ZrO_2 system
(Broken line indicates extrapolated-curve for unirradiated cubic phase)

○ Unirradiated cubic

△ Unirradiated tetragonal

● Irradiated cubic (volume)

× Irradiated cubic (lattice parameter)

fissioning. As will be shown in the next section, a significant fraction of the oxygen is liberated from UO_2 and $ZrO_2 + UO_2$ during irradiation. Although no a priori reason exists for this postulate, it might be inferred that the cubic form of ZrO_2-base fuels is more stable in the presence of excess oxygen than the tetragonal form. In this connection, it is significant that GEBHARDT, SEGHEZZI and DURRSCHNABEL [35] showed different zirconium solubilities in the cubic and tetragonal forms of ZrO_2.

As discussed above, various compositions of ZrO_2-base UO_2 fuels transform to cubic crystal structure on irradiation to exposures in excess of 5×10^{20} fissions/cm^3 and the values of the unit cell parameters were shown in Table IX to agree closely with Vegard's Law interpolation between the lattice parameters of cubic UO_2 and estimated values for cubic ZrO_2. However, as shown in Fig. 34, these lattice parameters differ slightly but significantly from the parameters of the unirradiated cubic phase, measured by COHEN and SCHANER [26], and also from the values extrapolated from the measured quantities. This same effect was also noted in the homogenized single-phase, tetragonal structure of $ZrO_2 + 34$. wt. % UO_2 after 5.8×10^{20} fissions/cm^3. The significance of these differences is even more apparent when the unit cell volumes are compared as in Fig. 34. Transformation from the tetragonal to the cubic modification in the unirradiated compositions is seen to result in an increase in volume whereas transformation from the tetragonal to the irradiated cubic lattice as shown in Fig. 34 and Table X leads to an increase in fuel density. These differences between the irradiated and unirradiated cubic cell parameters and volumes are apparent even over the composition ranges in which direct measurement of both parameters is possible. It is apparent therefore that the cubic lattice formed by irradiation of $ZrO_2 + UO_2$ fuels differs significantly from the cubic lattice in the unirradiated fuels. A similar conclusion can be made in the case of the single phase tetragonal structure.

A number of speculations on the reasons for these differences may be made. For example, it might be postulated that the difference in parameters results from lattice defects introduced by fission-fragment bombardment. As discussed in the case of the UO_2 fuel parameter, changes resulting from such bombardment would be expected and have been observed to yield larger cell sizes than those found under unirradiated conditions; however, reductions in cell size are noted in Fig. 34. The solution of fission products in the lattice would be expected to cause an enlargement of the unit cell and to be a function of fission depletion. These as well as the other structural factors discussed above argue against solution of fission products in the lattice as causing the difference between the irradiated and unirradiated cell sizes. It might be further hypothesized that only the anionic fission products such as iodine and bromine dissolve in the lattice and that their chemical accommodation by oxidation of uranium ions might lead to a decrease in lattice parameter. Again, the independence of cell size on fission-fragment bombardment level argues against this postulate.

Evidence discussed in section 5. 3 below indicates that an appreciable fraction of the oxygen is liberated from the UO_2 or $ZrO_2 + UO_2$ lattice by fissioning. It may be hypothesized that the fraction of the oxygen freed by fissioning, and which does not react with the Zircaloy cladding in the interior of the fuel compartments, distributed itself throughout the fuel. It has been

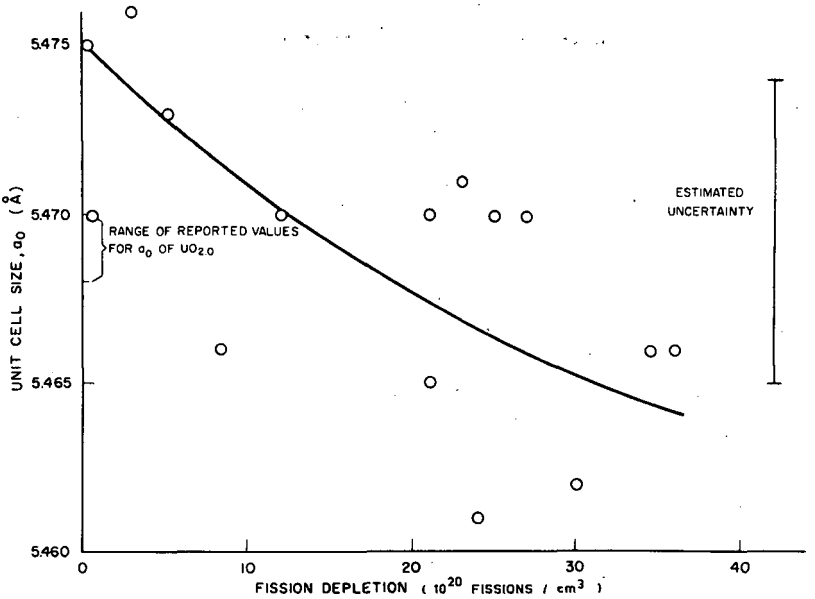


Fig. 35

Lattice parameter changes in UO_2 as a function of fission depletion

shown by Schaner that a decrease in the lattice constant of UO_2 results from solution of oxygen in UO_2 at a rate of about 0.08 Å decrease in lattice parameter per one-mole fraction of excess oxygen [36]. The change in the tetragonal lattice constant of ZrO_2 + UO_2 solid solutions with oxygen-ion content has not been measured. As shown in Fig. 35, some rather inconclusive evidence for diminution in cell sizes in UO_2 has been noted, utilizing in this plot the data tabulated in Table VII and the information reported in Ref. [1]. In the latter reference, it was indicated that very slight irradiation of UO_2 ($\simeq 10^{16}$ fissions/cm^3) resulted in an expansion of the unit cell by about 0.004 to 0.005 Å. As shown in Table VII and Fig. 35 (masked, however, by the uncertainty in measurements of lattice parameters of irradiated specimens) there is some indication that a decrease in parameter of approximately 0.01 Å. is noted with fission depletions up to about 30×10^{20} fissions/cm^3. Oxygen liberated by this amount of fission depletion would, if it all entered the UO_2 lattice, change the latter to a composition of $UO_{2.2}$ which should yield, from the data of Schaner, a decrease in lattice parameter of approximately 0.02 Å (neglecting any release of oxygen external to the fuel wafer). These results, are therefore not inconsistent with the last postulate.

It would appear to be a reasonable extension of this postulate that a cubic modification of the ZrO_2-base fuels would be stabilized only at fission depletions in excess of 5×10^{20} fissions/cm^3 corresponding to an oxygen excess of about 0.04 mole fraction. In this connection it is significant that GEBHARDT et al. [35] showed different zirconium solubilities in the cubic and tetragonal forms of unirradiated ZrO_2, with a zirconium excess tending to stabilize the cubic form to lower temperatures. It is thus postulated that

a minimum level of oxygen non-stoichiometry, which is attained at fission depletions in excess of 5×10^{20} fissions/cm^3, is required in order to stabilize in-pile the cubic modification of ZrO_2+ UO_2.

In summary, it is postulated that fission products segregate at grain boundaries or other lattice discontinuities in UO_2 and ZrO_2+ UO_2 fuels. Such concentrations lead to cation super-stoichiometry at the grain boundaries which, at elevated temperatures, can cause precipitation of high metal-content phases. Oxygen liberated as a result of the fissioning of uranium is postulated to dissolve uniformly in the oxide lattice. Further evidence for such oxygen liberation is presented in section 5.4.

5.3. UO_2 dispersed in BeO and Al_2O_3

The microstructural changes observed in BeO + 51 wt. % UO_2 after exposures of 28×10^{20} fissions/cm^3 are shown in Fig. 36. The BeO matrix can be seen to have closed the original porosity in the matrix material, consistent with the observed plasticity discussed in section 3 and inferred from Fig. 12. It is interesting to note in Fig. 36(b) that the UO_2 fuel particles are no longer angular as in the unirradiated condition (Fig. 36(a)) but have become rounded. This may be attributed to the recoil of the fission products

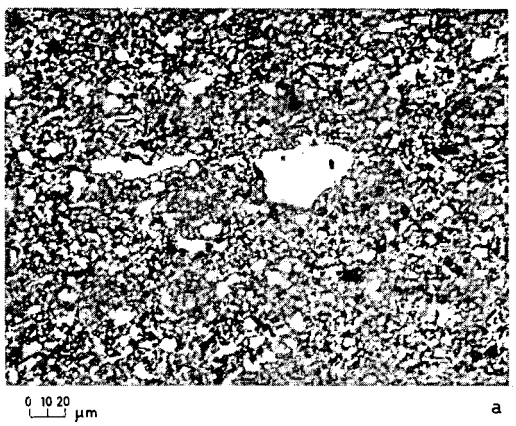


Fig. 36(a)

Unirradiated BeO - 51 wt. % UO_2

out of the fuel particles and to the swelling of the BeO matrix around them.

The pronounced effect of irradiation on the Al_2O_3 + 21 wt. % UO_2 fuel is illustrated in Fig. 37. After an irradiation of 4.0×10^{20} fissions/cm^3, no evidence of grain boundaries was observed in the Al_2O_3; much of the original porosity of the material had disappeared. The elongated swirls are attributed to the swelling of the Al_2O_3 which collapsed the original voids in the material. X-ray diffraction patterns of this material showed no diffraction profiles of either the Al_2O_3 or UO_2. However, X-ray studies on other samples of this material which had undergone only 10^{16} fissions/cm^3

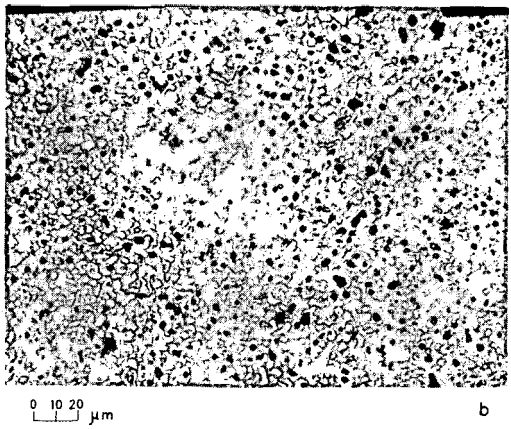


Fig. 36(b)

BeO - 51 wt. % UO_2 irradiated to 28×10^{20} fissions/cm^3

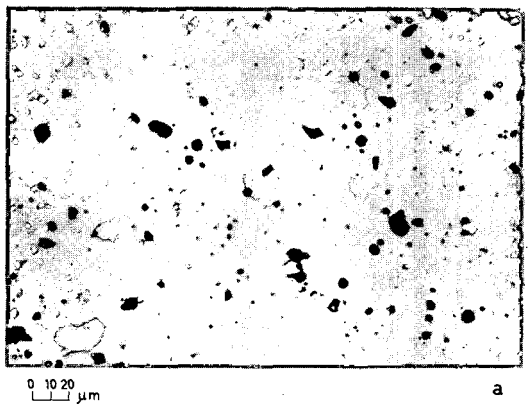


Fig. 37(a)

Unirradiated Al_2O_3 - 21 wt. % UO_2

showed X-ray diffraction patterns of UO_2, but none of Al_2O_3 [10]. Post-irradiation annealing of this material at 800°C for one hour results in restoration of the X-ray diffraction pattern. These results further confirm the postulate discussed in section 3 that a low-temperature irradiation-induced phenomenon has influenced the swelling behaviour of Al_2O_3 atypically with respect to the other oxide ceramic materials considered here.

5.4. Internal oxidation of Zircaloy cladding

An as yet unidentified grey phase was observed at the interface between the UO_2 and ZrO_2+ UO_2 fuel material and the Zircaloy cladding in compart-

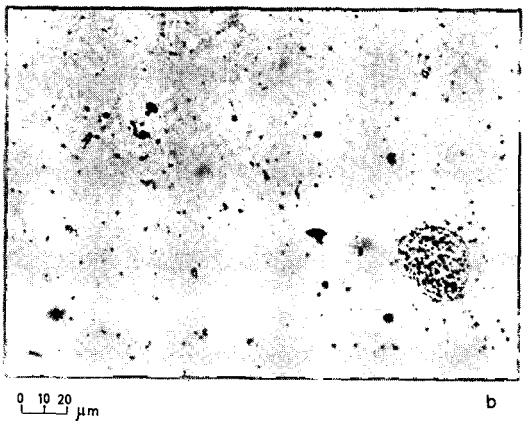


Fig. 37(b)

Al_2O_3 - 21 wt. % UO_2 irradiated to 4×10^{20} fissions/cm^3

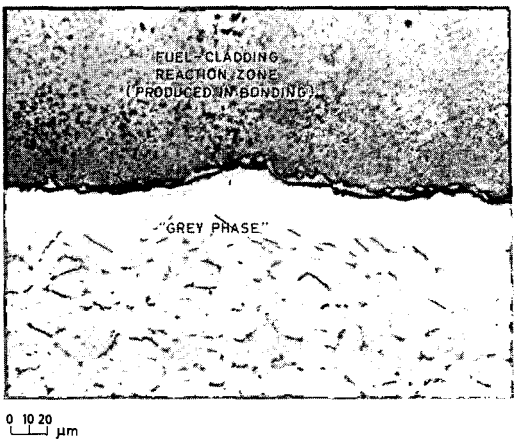


Fig. 38

Fuel-cladding interface between ZrO_2 - 25 wt. % UO_2 and Zircaloy cladding in sample 14C after 11.1×10^{20} fissions/cm^3

ments which did not rupture and become exposed to loop water. Samples at low burn-up show the grey material as a discontinuous layer, as shown in Fig. 38 for ZrO_2 + 25 wt. % UO_2 irradiated to 11×10^{20} fissions/cm^3. It can be seen in this figure that the "grey phase" is distinctly different from the interaction zone produced in Zircaloy by reaction with the fuel during fabrication operations in which the oxygen-rich Zircaloy phase also appears to be light in colour. The grey layer becomes continuous and broadens as burn-up progresses, as shown by the measurements in Table XI for samples containing ZrO_2 -base fuel and as exemplified by Fig. 39 of sample 12D containing ZrO_2 + 37% UO_2 at 29.7×10^{20} fissions/cm^3. These results indicate

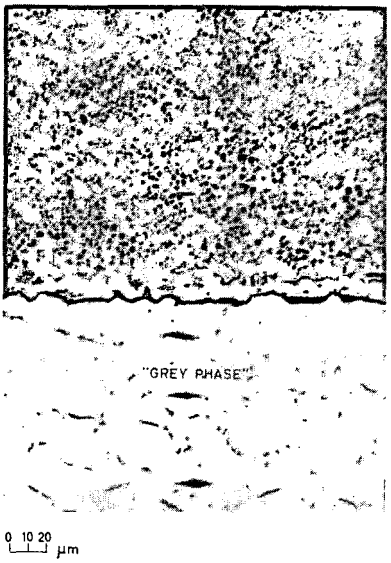


Fig. 39

Fuel-cladding interface between ZrO_2 - 34 wt. % UO_2 and Zircaloy cladding in sample 12D after 29.7×10^{20} fissions/cm^3

that the phase is formed during irradiation and that it increases in amount as irradiation continues. Although attempts to identify the layer by X-ray diffraction have been unsuccessful, it is assumed that ZrO_2 could form from the reaction of the cladding with the oxygen released from UO_2 during the fissioning of the uranium; also, this is consistent with the sub-stoichiometry assumed for the fuel above in conjunction with the development of the white spherical precipitates. Using the grey layer of sample 12D as an example, a calculation can be made to show that this explanation is a reasonable one.

The thickness of this layer for 12D (see Table XI) measures about 7.9 μm. A uniform layer of this thickness surrounding the entire fuel wafer would occupy 4.37×10^{-3} cm^3 corresponding to 24.4×10^{-3} g of ZrO_2. Assuming the reaction $Zr + O_2 \rightarrow ZrO_2$, a total of 1.2×10^{20} oxygen molecules would be required to produce this reaction. The fuel of 12D experienced 29.7×10^{20} fissions/cm^3, releasing 6.53×10^{20} molecules of oxygen within the compartment corresponding to the fuel volume of about 0.25 cm^3. Since 1.2×10^{20} molecules of oxygen are required to form the observed layer, only 18% of the total number of molecules released need react with the cladding to explain the amount of grey phase formed. A similar calculation for sample 11B with a layer thickness of 7.5 μm show that the percentage of oxygen required to form the grey layer amounts to 26%. Thus, from 4 to 5 times the necessary oxygen is made available by the fissioning process. For this reason, and because the gettering action of zirconium for oxygen gases is so effective, it is reasonable to identify this phase tentatively as ZrO_2. Knoop diamond-hardness impressions * were obtained on the grey layer using a 100-g load.

---

* Results quoted as Knoop Hardness Number (KHN)

TABLE XI

THICKNESS MEASUREMENTS OF GREY LAYER BETWEEN FUEL AND CLADDING

Element	Burn-up	GREY LAYER	
		Thickness	Nature
(No.)	(10^{20} fissions/cm^3)	(μm)	
BHB	5.8	<1.0	Discontinuous
14C	11.1	4.1	Discontinuous
JR-4	16.3	6.6	Continuous
BHK	17.2	5.4	Continuous
BFZ	19.7	5.8	Continuous
11B	19.9	7.5	Continuous
11C	21.2	7.6	Continuous
B91	25.0	7.1	Continuous
12D	29.7	7.9	Continuous

These yielded values ranging from 800 to 1100 KHN, which are not inconsistent with hardness values for ZrO_2. These results show that the grey phase increases with increasing burn-ups and that sufficient oxygen is present if released by fission events to account for the formation of ZrO_2. It is noteworthy in this connection that puncture tests of fuel compartments show by mass-spectrometry no liberated oxygen gas. Thus, the remainder of the oxygen must be contained within the fuel.

6. DISCUSSION OF RESULTS

The results of these investigations have shown that the oxide ceramic fuel materials considered herein, namely bulk UO_2, UO_2 dispersed in Al_2O_3 and BeO, and ZrO_2+ UO_2 solid solutions show vastly different dimensional changes in-pile, in unbonded plate elements. However, in the case of UO_2, ZrO_2+ UO_2, and BeO the specific differences between these fuel materials arises from the differences in their plasticity under irradiation. Al_2O_3, on the other hand, is not felt to be comparable to these oxide ceramics since some other phenomenon intervened and caused large volume changes at low exposures. Examination of the fission-gas release data and of the changes in the crystal structures of these materials enables a further evaluation of factors influencing their swelling behaviour to be made and provides an insight into the mechanisms operative in these fuels in-pile.

6.1. Fission-product mobility

The fraction of the theoretically produced fission gases which are released by the UO_2 is shown to be a function of burn-up (Fig. 13). Also, it may be seen that where excessive fuel temperatures occurred due to formation of an insulating gas-gap, then very large gas-release values were observed. Analysis of these results on the basis of volume diffusion theory utilized in bulk-UO_2 rods at relatively low exposures shows that the observed gas releases can be predicted if it is assumed that the logarithm of the diffusion rate (or of the factor D/a^2 in Eq. (1) of section 4) of the gases increases linearly with burn-up by about six orders of magnitude over a burn-up rate up to about 25×10^{20} fissions/cm^3. Thus, the calculational models developed for UO_2 fuel rods may be utilized up to exposures of about 40×10^{20} fissions/cm^3. These results are interpreted indicating a physical change in the UO_2 which reduces the effective diffusion path length and hence increases the release of the fission gases. This explanation is preferred to one involving structural changes in the UO_2 lattice since the X-ray diffraction examinations reported in section 5 would appear effectively to preclude property changes in the UO_2 so drastic as to cause an increase in diffusion rates by six order of magnitude.

Taking as a basis the observation in UO_2 of increased gas release with increased burn-up and the fragmentation to form sub-grain boundaries, an estimate can be made of the distribution of volatile fission products between those precipitated internally and those released from the fuel into the clad compartment. It has been shown that at temperatures below about 1800° F, the diffusion rate of fission gases in UO_2 has a constant value of about 10^{-18} cm^2/s [1]. Furthermore, in high-density fuel, the unit path length for volume diffusion is of the order of 10^{-2} cm. For times of interest in the irradiations given in this report (about 10^7 s) the diffusion path lengths are of the order of $\sqrt{Dt}$, or less than 10^{-5} cm. Thus, precipitation of fission gases will occur internally within the fuel body rather than be externally released. However, with the elevation of fuel temperatures into the neighbourhood of 3000°F and the attainment of diffusion rates of the order of 10^{-11} to 10^{-12} cm^2/s, diffusion path lengths of the order of 10^{-2} cm are realized and external release is favoured. Furthermore, with the formation of sub-grain boundaries and the consequent reduction of diffusion path length by three orders of magnitude to distances of the order of 10^{-5} cm, as discussed in section 5, external gas release becomes predominant even at temperatures slightly in excess of 1800°F. It was shown in section 5.1 that the electron microscopy results are consistent with migration of the fission products to the grain boundaries, or, at still higher exposures, to sub-grain boundaries. It is thus concluded that at low temperatures internal precipitation of gas occurs until sufficient structural fragmentation occurs (at burn-ups in excess of 20×10^{20} fissions/cm^3) to favour external release. At more elevated temperatures, reduction of diffusion path lengths need not progress so far as to cause an increase in external release rates and hence increased gas release into the compartment is attained at lower fission depletions of the fuel.

Based on the observations in $ZrO_2 + UO_2$ fuel materials of increased gas release with increased burn-up (Fig. 15), the unresolvable grain bound-

aries and the precipitated gas bubbles, similar estimates may be made on the relative distribution of the gases between those precipitated internally and those released from the fuel surface and these may be compared to UO_2 as shown in Fig. 16. CLAYTON [27] has shown that the diffusion coefficient for xenon in ZrO_2+ UO_2 is about two orders of magnitude higher than for the fission gases in bulk UO_2. Thus, it would be expected that the increased diffusion rate of the gases would be reflected in greater internal precipitation or else in greater external release than for bulk UO_2. Since the density of ZrO_2-base fuels increases to essentially 100% theoretical density after very short exposures (less than 5×10^{20} fissions/cm^3) and before appreciable quantities of gases are generated, the increased diffusivity of ZrO_2-base fuels is balanced by the increase in the unit path length for volume diffusion, which in this case would be the ratio of the fuel volume to the surface area, or about 4×10^{-2} cm : 1. Thus, for the irradiation times considered here and at low temperatures, the diffusion path lengths are of the order of $\sqrt{Dt}$, or less than 10^{-5} cm, and the fission gases will precipitate internally rather than be externally released. Also, since the ZrO_2-base fuels have a creep rate at least five times greater than UO_2 (see section 3.3), it seems reasonable to assume that the bubbles can precipitate more easily in this weaker material. Thus the precipitation of these bubbles removes additional gas from solution, leaving less to diffuse out. Therefore the behaviour of ZrO_2-based fuels (Fig. 16) when compared to UO_2, is consistent with these observations. At exposures below about 20×10^{20} fissions/cm^3, the ZrO_2-base fuels release more gas than UO_2, but not nearly the amount consistent with the differences in the diffusion coefficients in the materials. Similarly, at high exposures (above 24×10^{20} fissions/cm^3) the structural changes observed in the UO_2, described above, reduce the mean free path to a value which causes more gas release from UO_2 than from ZrO_2 + UO_2 fuels.

The gas releases from BeO and Al_2O_3 are compared to UO_2 and ZrO_2+ UO_2 in Fig. 16 and it may be seen that these materials also have excellent ability to retain the fission gases. These data do not permit a quantitative comparison of the performance of these two matrix oxides with the fissile materials in this respect, but it may be inferred that the BeO lattice has at least as good a gas-retention ability as UO_2 and ZrO_2+ UO_2.

The results presented here also indicate that the fission fragments accumulate at the grain and sub-grain boundaries, indicated by metallography in UO_2 and ZrO_2 + UO_2 and electron microscopy of UO_2 fuel (see section 5). Based on these results, the white spherical precipitates may be explained on the basis of the observations of MacEWAN [23] and LEWIS [24] in which they reported that unirradiated and very lightly irradiated UO_2, heated to temperatures of about 2000°C in a reducing atmosphere, precipitate uranium metal upon cooling. This was explained on the basis of the existence of a stable, oxygen-deficient, UO_2 lattice at high temperatures such that upon cooling back to temperatures at which $UO_{2.0}$ becomes stable, the insufficiency of oxygen caused the precipitation of uranium. Consider now the situation in highly burned-up UO_2 in the light of these results. Since the fission fragments are predominately cations and since there is experimental evidence of oxidation of the Zircaloy cladding as shown in section 5.4, it may be assumed that the fission fragments at the grain boundaries are highly sub-stoichiometric. When the UO_2 is raised to an elevated tempera-

ture the conditions for the existence of an oxygen-deficient phase are even more likely to occur than in unirradiated UO_2 (and it may be speculated that the temperature for such a phase is lower than for unirradiated material). Thus the sub-stoichiometric fission products at the grain boundaries contributed to the stabilization of the UO_{2-x} phase. It may be concluded that, upon cooling, uranium alloyed with mixed soluble products such as zirconium, niobium and molybdenium precipitates at the grain boundaries. These stabilized uranium precipitates would have a greatly decreased chemical activity compared with uranium and therefore could not be etched. Since ZrO_2-based fuel materials are more readily converted to an oxygen-deficient state than UO_2 in the unirradiated condition, the greater amount of precipitated white particles observed in $ZrO_2 + UO_2$ than in UO_2 is consistent with this premise.

6.2. Influence of crystal structure and temperature on swelling behaviour

The results of the dimensional and gravimetric density measurements on UO_2, ZrO_2-base fuels and BeO with increasing exposure (described in section 3) can be related to the variation of the fission-fragment induced plasticity of these materials in-pile. On this basis, the UO_2 and $ZrO_2 + UO_2$ fuel materials exhibit a linear swelling rate of about 0.7% ΔV per 10^{20} fissions/cm^3, and the BeO exhibited a swelling rate of 1% ΔV per 10^{20} fissions/cm^3. This difference in swelling rates may or may not be significant. The amount of swelling noted is almost minimal, if any reasonable values are to be ascribed to the fission-product nuclide volumes. If the differences are real, they are probably explainable by differences in effective fission-product volumes in BeO as compared with the fluorite lattice of UO_2 and $ZrO_2 + UO_2$. Al_2O_3 was shown to behave differently to these materials, probably because of the influence of an intervening, low-temperature phenomenon, which caused the very large increase in volume of about 19% after exposures as low as 0.9×10^{20} fissions/cm^3. For this reason, this material will not be considered in the following discussion.

The observed density increase of the low-density fuel materials described in section 3 results in apparent creep rates for fluorite-type cubic structure UO_2 of at least 40 times greater than unirradiated values. In addition to this greatly increased plasticity, the material may be assumed to have very little in-pile strength. A maximum value of the in-pile strength of UO_2 may be made by considering sample 8H2 containing 0.160-in thick fuel and 0.020-in thick cladding (see Table I). As pointed out in section 3.2, no significant changes in sample width occurred and the entire volume change was reflected in the thickness change. Since the transverse yield stress of Zircaloy at the temperature of the sample cladding in-pile is about 20 000 lb/in^2, the strength of the UO_2 in-pile must have some value less than 5000 lb/in^2. So low a value is not consistent with the hardness value of unirradiated UO_2, which is about 670 KHN [1]. The lower symmetry monoclinic-tetragonal $ZrO_2 + UO_2$ structures showed in-pile creep rates at least five times greater than that observed for UO_2 in-pile, and the hexagonal BeO evidenced an in-pile creep rate probably at least twice that of the UO_2. This behaviour is consistent with that noted by ROBERTS and COTTRELL [31] and by KONOBEEVSKY et al. [32] for uranium, in which the in-pile creep rate of alpha-uranium has been shown to increase by 50 to 100 times its

unirradiated value. Roberts and Cottrell explained their results on the basis of the continuous production of internal stresses between grains of the anisotropic uranium metal due to the "radiation growth" of this material. Konobeevsky et al. showed by stress relaxation experiments on body-centred-cubic U + 9 wt. % Mo alloy that even in the absence of anisotropic growth an enhancement of the creep rate of this material occurred in-pile; however, it was much smaller in magnitude than that observed in the highly anisotropic, orthorhombic alpha-uranium. On this basis, they concluded that the increased in-pile creep rate was due to irradiation annealing occurring within the fission spike causing stress relaxation. It thus appears that the enhanced plasticity of the anisotropic BeO + UO_2 and ZrO_2 + UO_2 result from operation of the Roberts-Cottrell mechanism, whereas the in-pile plasticity of cubic UO_2 or ZrO_2 + UO_2 results from the less effective mechanism proposed by KONOBEEVSKY [32].

Thus these results indicate that the swelling rate of oxide ceramic fuel materials up to exposures of about 40×10^{20} fissions/cm^3 is about 0.7 ΔV per 10^{20} fissions/cm^3. The dimensional changes noted on fuel samples, however, are influenced by the relative plasticity of the material in-pile. This in turn is related to the symmetry of the crystal lattice. UO_2 having the cubic crystal lattice exhibits the lowest creep rate in-pile while the tetragonal-monoclinic ZrO_2 + UO_2 and hexagonal BeO exhibit in-pile creep rates of two to five times that noted in UO_2.

Another factor which must influence the swelling behaviour of these oxide ceramic materials is the fuel temperature in-pile. X-ray diffraction studies of UO_2 and ZrO_2 + UO_2, shown in Tables VIII and IX, show that the fission products are not held in the crystal lattice and this was confirmed by the electron microscopy observations on UO_2 (section 5.1). In the case of the ZrO_2-base fuels, microstructurally observable gas bubbles were noted (Figs. 26, 27 and 28) and by consideration of the bubble volumes, the influence of temperature on the swelling rate may be calculated.

It will be assumed that the gas departs from ideality according to the data correlated by HOWLAND [33] for xenon. At pressures above 600 atm at 936°K, the factor N, equal to PV/RT, obeys the equation

$$N = 1.20 + 0.00050\,(P-650).$$

It is further assumed that all the volume increase generated by fuel swelling is available for the formation of gas bubbles. Taking P as the pressure (atm), V as the volume (cm^3) at the mean fuel-temperature T(°K), R as the gas constant and n as the number of moles of gas, the gas equation takes the form

$$\frac{PV}{RT} = nN, \text{ and substituting } \begin{cases} V = 7.0 \times 10^{-3}\ \text{cm}^3 \\ T = 936°\text{K} \\ R = 82.057\ \text{atm/mole} \\ n = 5.14 \times 10^{-5}\ \text{moles of gas} \\ \quad = \text{total gas generated} \\ \quad\quad \text{per } 10^{20}\ \text{fissions/cm}^3, \end{cases}$$

we obtain, on solving for P, the value P = 648 atm (9500 lb/in^2). This is

far higher than the confining pressure of the loop and the cladding of about 2500 lb/in^2. Only a very small proportion of this pressure can be accounted for by the additional restraint of surface tension. It was shown in section 5.3 that the typical bubble diameter in samples with a moderate irradiation temperature is 1 μm, with a radius therefore of 5×10^{-5} cm. The surface tension may be considered $P_T = 2\gamma/r$. GREENWOOD [34] used a value of 10^3 dyn/cm for γ, so that P_T is equal to 40 atm (600 lb/in^2). The initial assumption that all the gas is located in the gas bubbles cannot therefore be substantiated. Thus it may be assumed that most of the gas is lodged in solution in locations such as sub-grain boundaries or crystal structure defects, or in the form of bubbles whose diameter is less than that resolvable by light microscopy (about 0.1 μm) and hence stabilized by surface-tension forces. If as little as 30% of the gas finds its way to the visible gas bubbles, for which surface tension is negligible, then the external and internal pressures are balanced in the fuel.

If we assume that 30% of the gas is in these gas bubbles, that the pressure in the gas bubbles (neglecting surface tension) is 2500 lb/in^2 and that the gas bubbles are responsible for the observed swelling rate of 0.7% ΔV per 10^{20} fissions/cm^3 at 1800°F (see Fig. 11) then the swelling rate at temperatures other than 1800°F can be calculated. These calculations indicate that the swelling rate would vary from about 0.6 to 0.8% ΔV per 10^{20} fissions/cm^3 over the temperature range of 1200 to 2100°F fuel-centre temperature. This agrees well with the scatter observed in the data, which in general, represent irradiation history at varying temperatures. The results are thus consistent with the postulate that about 30% of the total fission gases reside in gas bubbles of significant size and that the swelling rate of ZrO_2-base fuel materials is not greatly affected by temperature in the range investigated here.

In the case of UO_2 and BeO, no gas bubbles are observed after exposures up to 30×10^{20} fissions/cm^3 as long as the fuel temperatures remain relatively low (below 1600°F). Since the X-ray diffraction data preclude the presence of the gases in the crystal lattice, it must be assumed that they also are located in solution at the grain boundaries, sub-grain boundaries and other lattice imperfections or that they exist as very small bubbles in which the surface-tension restraint, because of the very small size, is sufficiently high for them not to influence the swelling behaviour in the temperature range considered in these experiments.

8. CONCLUSIONS

The results of irradiation testing of oxide ceramic fuel materials of UO_2, $ZrO_2 + UO_2$ solid solutions and UO_2 dispersed in matrices of BeO and Al_2O_3 has permitted evaluation of the properties of these materials up to very high exposures and may be summarized as follows.

8.1. UO_2 exhibits an apparent volume change of 0.16% ΔV per 10^{20} fissions/cm^3 up to about 20×10^{20} fissions/cm^3 and at higher exposure swells at the rate of 0.7% ΔV per 10^{20} fissions/cm^3. ZrO_2-base fuel materials swell at the rate of 0.7% ΔV up to about 35×10^{20} fissions/cm^3 after undergoing a density increase to ~100% theoretical density (and consequently the volume de-

creases) at exposures below 6×10^{20} fissions/cm^3. BeO swells at the rate of about 1% ΔV per 10^{20} fissions/cm^3, based on closing of the open pores at low exposure. The variant behaviour of these materials, despite their similar swelling rates, is ascribed to differences in the fission-fragment-induced plasticity of these materials in-pile. The relative magnitude of the accelerated in-pile creep rate is shown to be related to the symmetry of the crystal lattice with the cubic UO_2 showing the least plastic behaviour.

Al_2O_3 was shown to be atypical of this class of fuel materials, because of an intervening, low-temperature phenomenon which caused a very large increase in volume of about 18% after exposures of less than 10^{20} fissions/cm^3.

8.2. The fraction of gas released from these fuel materials has been determined to be increased by (a) excessive operating temperatures and (b) accelerated release rates resulting from high fission depletions. The amount of gas released from UO_2 and $ZrO_2 + UO_2$ can be predicted using volume diffusion theory. All of these oxide ceramic fuel materials show excellent gas retention ability at the temperatures and exposures investigated.

8.3. UO_2 and $ZrO_2 + UO_2$ fuels exposed to high temperatures show precipitation of white spherical particles which are believed to contain non-volatile fission products.

8.4. Zircaloy cladding in contact with oxide ceramic fuel material shows evidence of oxidation which is believed to result from the oxygen released by fissioning of the fuel.

8.5. No evidence of large crystal-lattice dimension-change due to fission-product dissolution or extensive lattice damage by fission-fragment bombardment is noted in UO_2, by X-ray diffraction methods, after exposures up to 36×10^{20} fissions/cm^3. Inconclusive evidence, however, is presented which indicates the possibility of a slight dimunition of cell size in UO_2 due to oxygen freed by fissioning. This is felt to be consistent with 8.6 below.

8.6. ZrO_2-base fuel materials undergo a diffusionless transformation from the monoclinic to a system of higher symmetry at about 10^{16} fissions/cm^3. Two-phase tetragonal structures are homogenized into a single tetragonal phase having the composition corresponding to the bulk composition of the sample after exposures of the order of 10^{20} fissions/cm^3. Finally, the single tetragonal phase transforms into a metastable cubic phase after about 10×10^{20} fissions/cm^3. This is believed to be caused by suppression of the diffusionless transformation from the cubic to tetragonal phase in this binary system by liberated oxygen or by the fission products. The crystal lattice of this cubic phase is unaffected by exposure up to 33×10^{20} fissions/cm^3.

8.7. From optical and electron microscope evidence, it is inferred that in UO_2 fission products are segregated to the grain boundaries at fission depletions of about 13×10^{20} fissions/cm^3 and less. Such grain-boundary segregation is consistent with X-ray structural evidence, the appearance of pores at grain boundaries at elevated temperatures due to nucleation and growth of fission-gas bubbles, and the collection of the white spherical

particles referred to in 8.3 above, which precipitate at still higher temperatures with the fission-gas bubbles. At still higher depletions, sub-division of the original grains occurs to units approximately 0.5 μm in diameter; again it is inferred that fission-fragment segregation occurs at such sub-grain boundaries.

ZrO_2+ UO_2 differs from UO_2 in that optical microscope evidence for precipitation of fission-gas bubbles is noted even at low temperatures of irradiation and relatively low fission depletions. Again, at more elevated temperatures, precipitation of "white particles" is associated with the formation of fission-gas pores.

ACKNOWLEDGEMENTS

The authors wish to acknowledge the work of the many persons whose efforts made this report possible. Those primarily responsible for the various parts of the testing programme were: J. Belle, B. Schaner and L. Berrin, fuel fabrication; E. F. Losco and F. O. Bingman, fuel element fabrication; W. Schwartz, S. Lerner and D. J. Clark, nuclear and mechanical design; R. M. Lieberman, H. Clawson, F. P. Harries, test supervision at the reactor site; F. O. Von Plinsky and D. Gray, supervision of interim examinations at Expended Core Facility; and J. D. Eichenberg, supervision of Bettis Hot Laboratory. Aid in organizing the test data has been given by R. G. Daniel, G. Maskarinec, B. F. Rubin, H. B. Meieran, W. Yeniscavich, and R. G. Gray.

REFERENCES

[1] LUSTMAN, B., in Uranium Dioxide (BELLE, J., Ed.) Naval Reactors, Division of Reactor Development, USAEC (1961).

[2] ROBERTSON, J. A. L., BAIN, A. S., ALLISON, G. W. and STEVENS, W. H., Irradiation Behavior of UO_2 Fuel Elements, Nucl. Metallurgy, Amer. Inst. Mech. Engnrs, New York VI (1959) 45-70.

[3] BLEIBERG, M. L., YENISCAVICH, W. and GRAY, R. G., Effects of Burnup on Certain Ceramic Fuel Materials, USAEC Rpt. WAPD-T-1274 (April 1961).

[4] YENISCAVICH, W. and BLEIBERG, M. L., The Effects of Irradiation on BeO - UO_2, ThO_2 - UO_2 and ZrO_2 - UO_2, USAEC Rpt. WAPD-BT-20 (Sep. 1960).

[5] BERMAN, R. M., An X-Ray Diffraction Study of Irradiated Fluorite-Type Materials, USAEC Rpt. WAPD-BT-21 (1960) 33-42.

[6] SHERMAN, J., Design Description of the Second Core for the Shippingport Pressurized Water Reactor, USAEC Rpt. WAPD-254 (Sep. 1961).

[7] WOLFE, R. A., BINGMAN, F. O., FISCHER, R. L., LACERTE, R. C. and LOSCO, E. F., Eutectic-Diffusion-Bonding of Plate-Type Fuel Elements Containing Ceramic Fuel, USAEC Rpt. WAPD-211 (Oct. 1960).

[8] PAPROCKI, S. J. et al., Further Development of Gas-Pressure-Bonding of Zircaloy-Clad Uranium Dioxide Fuel Elements, USAEC Rpt. BMI-1436 (11 May 1960).

[9] COHEN, P. and WROUGHTON, D. M., Requirements and Techniques for Irradiation Testing of Reactor Materials for Pressurized Water Reactors, Proc. 2nd UN Int. Conf. PUAE 7 (1958) 499.

[10] BERMAN, R. M., BLEIBERG, M. L. and YENISCAVICH, W., Fission Fragment Damage to Crystal Structures, J. Nucl. Mat. 2 (1960) 129-140.

[11] DANIEL, R. C., BLEIBERG, M. L., MEIERAN, H. B. and YENISCAVICH, W., Effects of High Burnup on Zircaloy-Clad Bulk UO_2 Plate Fuel Element Samples, USAEC Rpt. WAPD-263 (Feb. 1962).

[12] RUBIN, B., BERMAN, R. M. and BLEIBERG, M. L., The Irradiation Behavior of ZrO_2 - UO_2 Fuels, USAEC Rpt. WAPD-264 (Feb. 1962).

[13] COHEN, I, LUSTMAN, B. and EICHENBERG, J. D., Measurement of the Thermal Conductivity of Metal-Clad Uranium Oxide Rods during Irradiation, USAEC Rpt. WAPD-228 (Aug. 1960).

[14] LOSCO, E. F., LIGGETT, R., LACERTE, R. C., BINGMAN, F. O. and WOODS, C. R., Pressure-Deflection and Fatigue Properties of Zircaloy Diaphragms, USAEC Rpt. WAPD-T-1228 (July 1958).

[15] DANIEL, R. C. and COHEN, I., In-Pile Effective Thermal Conductivity of Oxide Fuel Elements to High Fission Depletions, USAEC Rpt. WAPD-246, to be published.

[16] KITTEL, J. H. and PAINE, S. H., Effects of Irradiation on Fuel Materials, in Progress in Nuclear Energy, Series V, Pergamon Press, New York 3 (1961).

[17] HUGH, S. F., Radiation Damage in Fissile Materials, in Progress in Nuclear Energy, Series V, Pergamon Press, New York 1 (1961).

[18] WEBER, C. E., Progress on Dispersion Elements, in Progress in Nuclear Energy, Series V, Pergamon Press, New York 2 (1959).

[19] SCOTT, R., HALL, A. R. and WILLIAMS, J., The Plastic Deformation of Uranium Oxides above 800°C, J. Nucl. Mat. 1 1 (1959).

[20] BOOTH, A. H., A Method of Calculating Fission Gas Diffusion from UO_2 Fuel and Its Application to the X-2-f Loop Test, USAEC Rpt. CRDC-721 (Sep. 1957).

[21] CLAYTON, J. C., The Evaluation of Xenon-133 from Slightly-Irradiated Zirconia Urania Plates, USAEC Rpt. WAPD-TM-313 (1962).

[22] BELLE, J. et al., Iron Carbon and Nitrogen Impurities in PWR-2 Seed Fuel, USAEC Rpt. WAPD-251 (Dec. 1961).

[23] MacEWAN, J. R., Grain Growth in Sintered Uranium Dioxide, USAEC Rpt. AECL-1184 (Jan. 1961).

[24] LEWIS, W. D., Behavior of Fission Gases in UO_2 Fuel, USAEC Rpt. AECL-1402 (Nov. 1961).

[25] BRINKMAN, J. A., Fundamentals of Fission Damage, Nucl. Metallurgy, Amer. Inst. Mech. Engnrs, New York VI (1959).

[26] COHEN, I. and SCHANER, B. E., Metallographic X-Ray Study of UO_2 - ZrO_2 System, USAEC Rpt. WAPD-293 (March 1961).

[27] CLAYTON, J. C., Substoichiometry in Zirconia-Urania Solid Solutions, USAEC Rpt. WAPD-TM-299, to be published.

[28] WITTELS, M. C. and SHERRILL, F. A., Fission Fragment Damage in Zirconia, Phys. Rev. Letters, 3 (1959) 176.

[29] ADAM, J. and COX, B., The Irradiation-Induced Phase Transformation in Zirconia Solid Solutions, J. nucl. Energy, Pt A 2 (1959) 31-33.

[30] BLEIBERG, M. L., JONES, L. B. and LUSTMAN, B., Phase Changes in Pile-Irradiated Uranium-Base Alloys, J. appl. Phys. 27 (Nov. 1956) 1270-1283.

[31] ROBERTS, A. C. and COTTRELL, A. H., Creep of Alpha Uranium during Irradiation with Neutrons, Phil. Mag. 1 (1956) 595.

[32] KONOBEEVSKY, S. T., DUBROVIN, K. P., LEVITSKY, B. M., PANTELEEV, L. D. and PRAVOLYAK, N. F., Structural Changes Occurring in Fissile Materials during Irradiation, Prog. nucl. Energy, Series V, Pergamon Press, New York 3 (1961).

[33] HOWLAND, W., Bettis Atomic Power Laboratory, personal communication.

[34] GREENWOOD, G. W., The Effects of Neutron Irradiation on α-Uranium and Some Fissile Alloys of Cubic Crystal Structure, AERE Rpt. R-3468 (1960).

[35] GEBHARDT, E., SEGHEZZI, H. D. and DURRSCHNABEL, W., Investigations of the ZrO System II, J. nucl. Mat. 4 (1961) 255.

[36] SCHANER, B. E., Metallographic Determination of the UO_2 - U_4O_9 Phase Diagram, J. nucl. Mat. 2 2 (1960).

IRRADIATION ALTERATION OF URANIUM DIOXIDE

W. E. ROAKE
HANFORD LABORATORIES OPERATION, GENERAL ELECTRIC COMPANY,
RICHLAND, WASHINGTON

Abstract — Résumé — Аннотация — Resumen

IRRADIATION ALTERATION OF URANIUM DIOXIDE. Irradiation of nuclear fuel materials under conditions expected to be achieved in future power reactors produces many energy-associated changes that are reflected in the economic performance of the fuel. The causes and effects of those changes are being resolved by investigators at the Hanford Laboratories and at other sites through an integration of careful laboratory measurements with irradiation tests that demonstrate fuel performance at practical operating conditions.

Measurements of physical, chemical, and thermal properties of irradiated and non-irradiated ceramic nuclear fuel materials have been correlated with phenomena observed in a large number of test assemblies irradiated in the range 0 - 30 $\times 10^{20}$ fissions/cm^3 at fuel temperatures extending to the melting point. These phenomena include production of metastable states and modifications of fuel structure that effect order-of-magnitude changes in thermal and electrical properties of uranium dioxide.

Vaporization and condensation of nuclear fuels, studied ex-reactor, were shown to be associated with fuel densification, relocation, columnar grain growth, and the homogenizing of heterogeneous fuel mixtures during irradiation. Segregation of fission products and plutonium was measured, and correlated with vapour phase transfer and with solid-state diffusional processes.

Significant changes in the melting point of UO_2 were observed with specimens irradiated to a wide range of exposure. The observations demonstrate the remarkable effectiveness of extremely small concentrations of impurity (fission-fragment) atoms in stabilizing the UO_2 crystal lattice. The date, integrated with an extensive study of UO_2 melting and dissociation, suggest changes in the uranium-oxygen phase diagram in the region of the melting point of UO_2.

Rapid heating and cooling of microscopic fuel regions associated with individual fission events produce observed effects, at relatively low bulk fuel temperatures, effects that are measurable, outside a neutron field, only at temperatures several hundreds of degrees greater. Sintering of compacted uranium dioxide powder at only 300-400°C bulk fuel temperatures was revealed by fuel-temperature and thermal conductivity measurements during irradiation.

MODIFICATION DE L'OXYDE D'URANIUM SOUS IRRADIATION. L'irradiation des combustibles nucléaires dans les conditions qui, selon les prévisions, règneront dans les futurs réacteurs de puissance, donne lieu à un grand nombre de variations liées à l'énergie, qui se répercutent sur le rendement économique du combustible. Des chercheurs travaillent actuellement, aux laboratoires de Hanford et ailleurs, à la détermination des causes et des effets de ces variations, en coordonnant les résultats de mesures minutieuses en laboratoire et d'essais d'irradiation qui montrent comment se comporte le combustible dans des conditions de fonctionnement réel.

Ces chercheurs ont établi des corrélations entre des mesures de propriétés physiques, chimiques et thermiques des combustibles céramiques irradiés et non irradiés, et des phénomènes observés pour un grand nombre d'ensembles expérimentaux, où les taux de combustion étaient compris dans la gamme de 0 à 30 · 10^{20} fissions par cm^3, à des températures de combustion allant jusqu'au point de fusion. Ces phénomènes comprennent la production d'états métastables et des modifications de la structure du combustible qui entraînent des transformations d'un ordre de grandeur dans les propriétés thermiques et électriques de l'oxyde d'uranium.

Il a été démontré que la vaporisation et la condensation des combustibles nucléaires, étudiées hors réacteur, sont liées à la densification du combustible, à la relocation, à la croissance des grains en colonne et à l'homogénisation des mélanges hétérogènes de combustibles pendant l'irradiation. On a mesuré la ségrégation des produits de fission et du plutonium et établi une corrélation entre cette ségrégation et les processus de transfert en phase de vapeur et de diffusion dans l'état solide.

Dans des échantillon exposés à des rayonnements d'intensités très différentes, on a observé des variations importantes du point de fusion de l'UO_2. Ces observations montrent l'efficacité remarquable de certaines

concentrations extrêmement faibles des atomes d'impuretés (fragments de fission) pour la stabilisation du réseau cristallin de l'UO_2. Ces données, qui ont été intégrées dans une vaste étude sur la fusion et la dissociation de l'UO_2, suggèrent des modifications dans le diagramme uranium-oxygène, aux environs du point de fusion de l'UO_2.

Le chauffage et le refroidissement rapides de régions microscopiques du combustible, combinés avec les fissions, produisent les effets observés à des températures relativement peu élevées pour l'ensemble du combustible, effets qui, en dehors d'un champ neutronique, ne peuvent être mesurés qu'à des températures supérieures de plusieurs centaines de degrés. Des mesures de la température du combustible et de la conductivité thermique, effectuées pendant l'irradiation, ont permis de constater un frittage de la poudre comprimée d'oxyde d'uranium, lorsque les températures de l'ensemble du combustible ne dépassaient pas 300 ou 400°C.

ИЗМЕНЕНИЯ В UO_2, СВЯЗАННЫЕ С ОБЛУЧЕНИЕМ. Облучение материалов ядерного топлива в условиях, которые будут получены в будущих энергетических реакторах, вызывает многие изменения, связанные с энергией. Эти изменения отражаются на характеристике экономичности топлива. Причины и следствия этих изменений находятся исследователями в лабораториях Хэнфорда, а также посредством объединения тщательных лабораторных измерений в опытах по облучению, что наглядно показывает топливную характеристику в практических условиях эксплуатации.

Измерения физических, химических и тепловых свойств облученных и необлученных материалов керамического ядерного топлива соответствовали явлениям, наблюдавшимся в большом количестве испытательных сборок, подвергавшихся облучению в пределах от 0 до 30 · 10^{20} делений на 1 $см^3$ при температурах топлива, доходящего до точки плавления. Эти явления связаны с получением метастабильных состояний и видоизменениями структуры топлива, что ведет к изменениям величины тепловых и электрических свойств двуокиси урана.

Выпаривание и конденсация ядерного топлива, проводившиеся на экспериментальном реакторе, показали, что при этом происходит уплотнение топлива, перемещение, колоннообразное наращивание зерна и гомогенизация гетерогенных смесей топлива во время облучения. Было измерено разделение продуктов распада и плутония, которое соответствовало переходу в паровую фазу и диффузионным процессам в твердых телах.

Значительные изменения точки плавления UO_2 наблюдались по образцам, подвергавшимся облучению в широком диапазоне. Наблюдения показывают удивительную эффективность чрезвычайно малых концентраций атомов примесей (частицы деления) для стабилизации кристаллической решетки UO_2. Данные, полученные на основе обширного изучения плавления и распада UO_2, показывают проведение изменений в фазовой диаграмме уран-кислород в районе точки плавления UO_2.

Быстрое нагревание и охлаждение микроскопических районов топлива, связанное с отдельными случаями деления, дает наблюдаемые эффекты при сравнительно низких температурах массы топлива, т.е. эффекты, которые измеряются независимо от нейтронного поля только при температурах выше на несколько сот градусов. Спекание плотного порошка двуокиси урана было обнаружено лишь при температурах топливной массы 300 - 400° путем измерений температуры топлива и теплопроводности во время облучения.

CAMBIOS PRODUCIDOS EN EL UO_2 POR LA IRRADIACIÓN. La irradiación de los materiales combustibles nucleares, en las mismas condiciones en que se supone que han de utilizarse en los reactores de potencia del futuro, produce múltiples cambios dependientes del nivel energético, que se reflejan en el rendimiento económico del combustible. Los investigadores que trabajan en los laboratorios de Hanford y en otras instalaciones tratan de determinar las causas y efectos de esos cambios. combinando minuciosas mediciones efectuadas en el laboratorio con los resultados de pruebas de irradiación que permiten determinar el rendimiento del combustible en las condiciones efectivas de trabajo.

Los autores han comparado los resultados de las determinaciones de las propiedades físicas, químicas y térmicas de los materiales combustibles nucleares cerámicos irradiados y no irradiados con los fenómenos observados en una amplia serie de montajes de prueba irradiados con dosis comprendidas entre 0 y 30.10^{20} fisiones por centímetro cúbico y temperaturas del combustible que ascendían hasta el punto de fusión. Estos fenómenos comprenden la producción de estados metastables y de alteraciones de la estructura del combustible que modifican el orden de magnitud de las propiedades térmicas y eléctricas del dióxido de uranio.

Se demostró que la vaporización y condensación de los combustibles nucleares, estudiadas fuera del reactor, están relacionadas con la densificación del combustible, el cambio de posición, el crecimiento granu-

lar en columnas y la homogeneización de las mezclas de combustibles heterogéneas durante la irradiación. Los autores midieron la segregación de los productos de fisión y del plutonio, y determinaron su relación con la transmisión en fase vapor y con los processos de difusión en los sólidos.

Observaron cambios significativos en el punto de fusión del UO_2, en muestras expuestas a dosis de radiaciones muy favorables. Las observaciones demuestran que concentraciones sumamente pequeñas de átomos de impurezas (fragmentos de fisión) son capaces de estabilizar la red cristalina de UO_2. Estos datos, considerados conjuntamente con los resultados de un extenso estudio de las características de fusión y disociación del UO_2, aconsejan modificar el diagramma de las fases uranio-oxígeno, en la región correspondiente al punto de fusión del UO_2.

El calentamiento y enfriamiento rápidos de zonas microscópicas de combustible relacionados con fenómenos aislados de fisión producen efectos observables a temperaturas relativamente bajas del combustible, mientras que los mismos efectos sólo son susceptibles de medirse, fuera de un campo neutrónico, a temperaturas que superan a las anteriores en varios cientos de grados. La determinación de la temperatura del combustible y de la conductividad térmica durante la irradiación permitieron comprobar que ya se produce una sinterización del polvo compacto de dióxido de uranio a temperaturas del orden de 300 a 400°C.

1. INTRODUCTION

The altering of the properties and forms of nuclear fuel materials that occurs during neutron irradiation is not sufficiently understood to permit the straight-forward design of fuel elements for advanced reactors or, in fact, to explain entirely the performance of fuel materials in many of the currently operating reactors. The level of understanding of the phenomena is, however, improving at an accelerating pace. The rate of acquisition of technology and scientific comprehension is rapid by comparison with the time required to fix the design and construct a nuclear reactor. And that is as it should be.

Future applications of uranium oxide nuclear fuel will involve operating conditions more extreme than those ordinarily encountered in today's nuclear reactors. Core temperatures exceeding 1600°C and, in many cases, the melting point, will be common, as it now is in experimental elements. Thinner cladding, or cladding weakened by higher coolant temperature will demand greater internal support from the fuel. The function of the cladding may eventually evolve into simply maintaining the geometry of the fuel, allowing gaseous and soluble fission products to escape from the core.

As irradiation of a fuel element proceeds, the fuel becomes progressively more contaminated and the data obtained on pure components are, in many instances, no longer applicable. The characteristics of sintered UO_2 plates irradiated to beyond 20×10^{20} fissions/cm^3, as reported by BELLE et al. [1], is an example. The characteristics of recovered fuel, enhanced in plutonium content and only partially decontaminated from fission products and other impurities, are of perhaps greater interest to power-reactor fuel development engineers. Such a fuel material can now be produced by electrodeposition of UO_2 from fused salts in a form suitable for swaging or vibration-compacting. Already experiments have been performed at Hanford and other laboratories, and more are in progress, to determine what performance limits apply to "dirty" fuel systems. Simple, remote fabrication technology has been developed.

Effects of radiation on many properties of UO_2 are now relatively well defined in low to moderate temperature ranges. Intensive efforts in many laboratories have revealed the nature and extent of xenon release at and

below 1400°C from lightly irradiated UO_2 of several forms (porous, sintered, or crystalline). Reduction of thermal conductivity as well as partial recovery at high temperatures has been demonstrated with UO_2 irradiated at less than 100°C. Changes in hardness and in preferred mode of fracture have been demonstrated with UO_2 specimens irradiated to low exposures at 100°C or less. But these and other properties also depend on the structure of the material, the temperature and the chemical purity of the specimen. In our anticipated future fuel element, solid, liquid and gaseous UO_2 may co-exist; steep temperature gradients will extend from slightly above coolant temperature to beyond 2800°C and chemical composition will vary throughout the fuel as a result of dissociation at high temperatures and oxidation at lower temperatures, and because of migration of fission products and plutonium. Further, these conditions will be continuously varied, as is typical of operating nuclear reactors.

It is important to recognize that in practice, irradiation alteration is the result of a complex, dynamic interrelation of "radiation damage", thermal and chemical effects, many of which are beneficial.

2. EXPERIMENTS AND MEASUREMENTS

Hanford Laboratories personnel have studied irradiation alteration of UO_2 in three ways: exploratory irradiation and examination; specific irradiation tests; and out-of-reactor simulation experiments.

Exploratory irradiation tests are performed under conditions expected to be prototypic of future applications. Post-irradiation examinations of these test elements reveal the relative importance of the several phenomena that occur during irradiation, and dissection of the elements provides irradiated fuel specimens for physical and chemical measurements. Information gained from such measurements is difficult to correlate because of the wide variation of neutron flux, temperature, heat flux, chemical environment, mechanical restraint, etc., that occur. Consequently, small, carefully prepared and characterized fuel specimens are irradiated under controlled conditions to provide more accurate data on specific phenomena and to correlate these phenomena with a variety of irradiation conditions. Hypotheses developed from such data are tested in out-of-reactor experiments when no effect due to neutron field are indicated, or when such effects may be clarified by their absence.

The gross effects that occur during irradiation of a high-rated UO_2 fuel element are illustrated in Fig. 1, which is reduced from a photo-mosaic comprising many photomicrographs of a cut, polished and etched surface of an irradiated pellet. Several structural changes are apparent. The microstructure shown nearest the cladding is typical of the original pellet, with the exception that many hard lumps (appearing in the illustration as small, dark spots easily mistaken for pores) developed during irradiation. A region of small columnar grains is clearly defined, as is the change from small to large columnar grains. The outer limit of porosity in the large columnar grain region is distinct and regular and the circumscribed region reveals extensive sub-grain structure. The central portion of the specimen was not continuously molten during irradiation. Evidence of this would appear

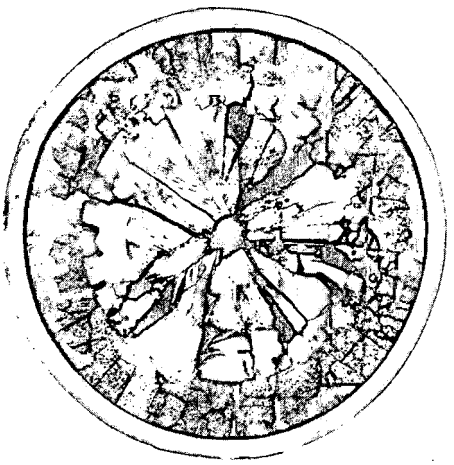


Fig. 1

Irradiated, sintered UO_2 pellet, cross-section, test GEH-14-189

Zircaloy-2 cladding, 0.505 in ID × 0.025 in wall
Diametral clearance, 0.004 $\{^{+0.000}_{-0.001}\}$ in at assembly
Polished, Linde A and Linde B abrasive, trace chromic acid
Etched, 60 ml 95% H_2SO_4 + 40 ml 30% H_2O_2
Large black areas indicate UO_2 fragments lost during grinding and polishing
Exposure 900 MWd/t (2.4×10^{19} fissions/cm^3)
Maximum heat rating, 31 kW/ft
Maximum surface heat flux, 230 W/cm^2 [730 000 BTU/(hr)(ft^2)]
Calculated UO_2 surface temperature, 450°C
Fission gas release, 41% of xenon and krypton
Pellet density, 10.3 g/cm^3 at assembly; sintered in 1700°C hydrogen
ground to 32 μin surface finish

in the microstructure as a spongy mass of large equiaxed grains occupying a portion of the central cavity.

The general configuration shown in Fig. 1 is developed by all high-rated UO_2 fuel elements, whether they be sintered pellets, swaged (Fig. 2), or vibrationally compacted UO_2 (Fig. 3), or admixtures containing other fuels such as ThO_2 (Fig. 4) or PuO_2 (Fig. 5). Porosity will vary with the original bulk fuel density and the uniformity of regional boundaries will be disturbed by large particles (Fig. 6) as in the case of vibrationally compacted fuel rods.

Irradiation alterations in UO_2 can conveniently be related to three broad, overlapping temperature ranges: below 1000°C (section 2.1), 500 to 1700°C (section 2.2) and above 1600°C (section 2.3). This discussion is continued on that basis.

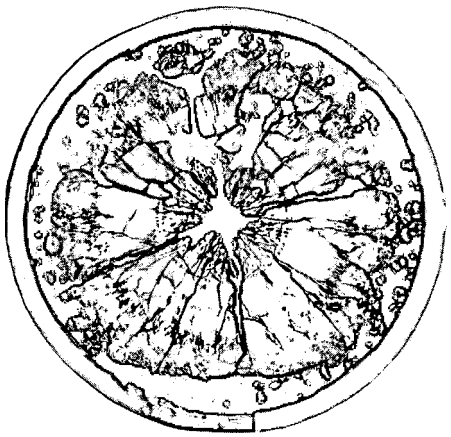


Fig. 2

Irradiated, swaged, arc-fused UO_2, cross-section, test GEH-14-190

Zircaloy-2 cladding, 0.505 in ID × 0.025 in wall
Polished, Linde A and Linde B abrasive, trace chromic acid
Etched, 60 ml 95% H_2SO_4 + 40 ml 30% H_2O_2
Large black areas indicate UO_2 fragments lost during grinding and polishing
Exposure, 750 MWd/t (1.85×10^{19} fissions/cm^3)
Maximum heat rating, 26 kW/ft
Maximum surface heat flux, 190 W/cm^2 [600 000 BTU/(hr)(ft^2)]
Calculated UO_2 surface temperature, 428°C
Bulk fuel density, 88% theoretical density at assembly
Particle density, 10.8 g/cm^3

2.1. The temperature range below 1000°C

Irradiation of UO_2 at bulk temperatures less than 1000°C causes gross effects such as cracking induced by thermal stress. Less obvious changes of thermal and electrical conductivity and hardness originate in the creation of defects and the obvious introduction of impurities such as fission fragments. Many other events that take place at relatively low bulk temperatures are, in fact, high-temperature phenomena.

Electron-micrographic examination of thin UO_2 films [2, 3] that were irradiated at bulk temperatures less than 100°C revealed primary effects of fission-fragment bombardment – the formation of tracks devoid of UO_2 by passage of recoiling fission fragments, and densification and crystal growth in the originally amorphous UO_2. These latter phenomena ordinarily require high bulk temperatures. They illustrate that many irradiation effects observed at low bulk temperature are cumulative effects resulting from the interaction of a great many microscopic regions of localized, transient, high temperatures that are caused by individual fission events. Beneficial effects of this form of "radiation damage" were observed during irradiation of test elements in the Plutonium Recycle Test Reactor (PRTR) at Hanford.

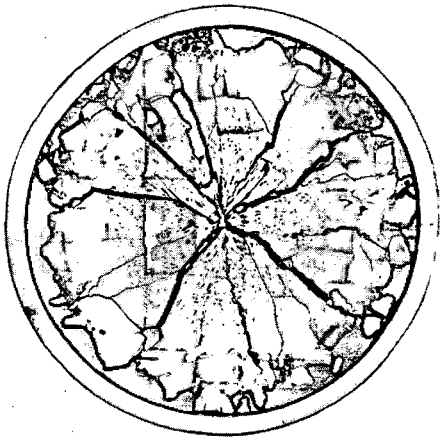


Fig. 3

Irradiated, vibrationally-compacted, arc-fused UO_2, cross-section, test GEH-14-188

Zircaloy-2 cladding, 0.505 in ID × 0.025 in wall
Polished, Linde A and Linde B abrasive, trace chromic acid
Etched, 60 ml 95% H_2SO_4 + 40 ml 30% H_2O_2
Large black areas indicate UO_2 fragments lost during grinding and polishing
Exposure, 1000 MWd/t (2.5×10^{19} fissions/cm^3)
Maximum heat rating, 39 kW/ft
Maximum surface heat flux, 290 W/cm^2 [920 000 BTU/(hr)(ft^2)]
Calculated UO_2 surface temperature, 474°C
Fission gas release, 55% xenon, 44% krypton
Bulk fuel density, 89% theoretical density at assembly
Particle Density, 10.8 g/cm^3

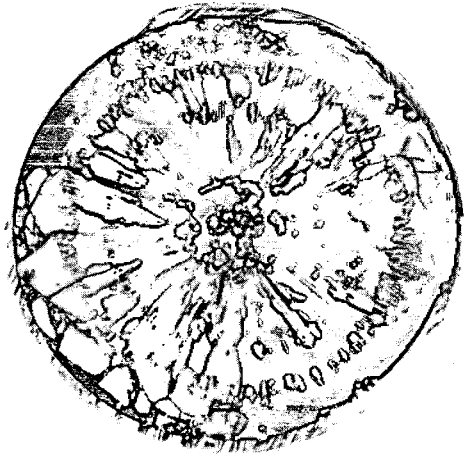


Fig. 4

Irradiated, vibrationally-compacted, sintered and crushed UO_2 - 10 wt. % ThO_2, cross-section, test GEH-4-61

Exposure, 390 MWd/t, 0.11×10^{20} fissions/cm^3
Maximum heat rating, 60 kW/ft
Maximum surface heat flux, 217 W/cm^2 [690 000 BTU/(hr)(ft^2)]
Stainless steel cladding (304L) 1.055 in ID × 0.030 in wall
Polished, 600 grit; not etched
Molten core during irradiation

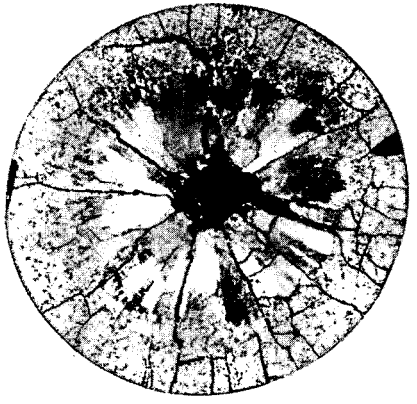


Fig. 5

Irradiated, sintered $(U, Pu)O_2$ pellet, cross-section

Fuel, (U-1.02 at.% Pu)O_2, sintered density, 10.2 g/cm^3, ground to 0.505-in diam.
Polished cross section, 600 grit

Exposure, 5500 MWd/t 1.66×10^{20} fissions/cm^3
Maximum heat rating, 19.2 kW/ft
Maximum surface heat flux, 140 W/cm^2 [441 000 BTU/(hr)(ft^2)]

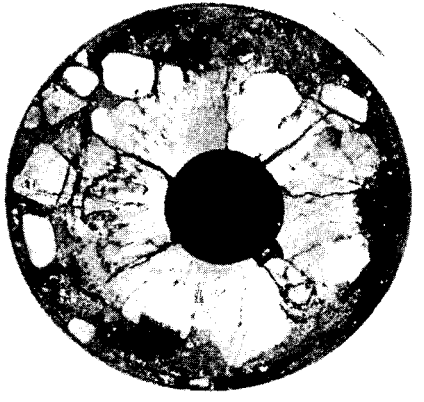


Fig. 6

Large pieces distort the outer limit of columnar grain growth in irradiated, vibrationally compacted UO_2

The majority of the fuel elements comprising the first core of the PRTR are 19-rod bundles of fused UO_2, crushed to pass through a 20-mesh Tyler screen and cold-swaged to 85% of theoretical density in Zircaloy sheaths. One fuel element was constructed with thermocouples located axially in six rods to measure maximum centre-line fuel temperatures. More than 10% improvement in bulk fuel thermal conductivity was observed during several hours' irradiation at constant heat generation rate at low reactor power. The phenomenon was observed several times at maximum centre-line fuel temperatures as low as 300°C. Sintering of stressed point contacts between particles because of localized, transient high temperature in the regions of individual fission events is believed to be the cause of the enhanced heat-transfer rate.

Of all the physical properties of UO_2, the thermal conductivity is perhaps the most far-reaching in its influence. Nearly all the properties are temperature-dependent; in turn, the temperature at any point in the fuel is determined largely by the thermal conductivity of the materials present, when a constant energy input is maintained. By constant interaction, the changes in properties, brought about by temperature changes, influence the thermal conductivity and modify the temperature. The result is an extremely complex relationship between thermal conductivity and many other properties.

Neutron irradiation introduces a still further complication, that of the effect of changes in crystal lattice. It has been recognized for some time that neutron irradiation reduces the thermal conductivity of UO_2. Recent co-operative investigations at the Hanford Laboratories and Battelle Memorial Institute shed light on the extent of the irradiation effect, the conditions under which it occurs and the cause of the observed thermal conductivity behaviour of irradiated UO_2. Nearly identical specimens of UO_2 were irradiated at less than 100°C to accumulated exposures between 0.014×10^{20} and 0.16×10^{20} fissions/cm^3. Thermal conductivity of the irradiated specimens was measured by an axial heat flow method. Data are compared, in Fig. 7, with those of non-irradiated control specimens. Several features of these curves are particularly noteworthy.

Irradiation to 10^{18} fissions/cm^3 or more reduced the room-temperature thermal conductivity of the irradiated UO_2 by at least 50%. No saturation of that damage was found at 0.16×10^{20} fissions/cm^3 in specimens irradiated at temperatures below 100°C. As the temperature of measurement was increased, the thermal conductivity decreased with increasing temperature in a normal manner until a point of inflection of the conductivity-temperature curve was reached at 150 to 200°C. At that point the conductivity abruptly increased by an amount independent of the irradiation exposure of the UO_2 (perhaps indicating saturation of one component of the over-all radiation damage effect). The rise occurred at lower temperatures with increasing exposures. A second region of increasing thermal conductivity, encountered at about 350°C, is not as marked as the first and appears proportional to the irradiation exposure of the UO_2. A third inflection point, at about 800°C, is suggested by the limited data from the specimen irradiated to 0.16×10^{20} fissions/cm^3. The occurrence of three stages of recovery of UO_2 from radiation damage is in substantial agreement with conclusions reached by ROSS [4], based on somewhat different evidence. There is also

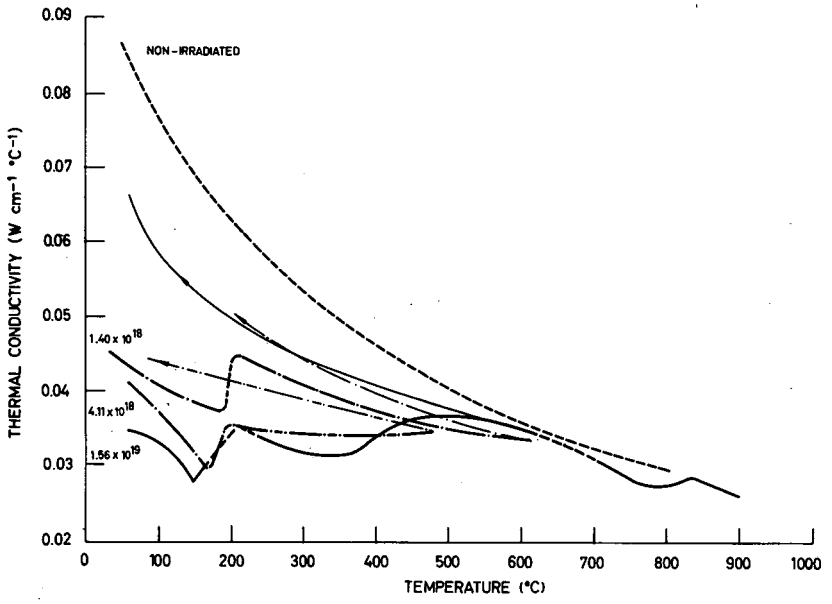


Fig. 7

Effect of irradiation on the thermal conductivity of sintered uranium dioxide

(Exposures shown are in fissions/cm^3)

good correlation with the annealing steps occurring in the recovery from irradiation-induced changes in UO_2 lattice dimensions, as measured by BLOCH [5].

If the specimen is cooled from any temperature reached during the initial rise, the thermal conductivity curve at all lower temperatures assumes the "normal" shape and slope, displaced downward to join the initial (irradiated) curve at the highest temperature previously reached. The extent of recovery from the non-annealed, irradiated, conductivity depends on the maximum temperature to which the material was subjected during or after irradiation and on the temperature of measurement.

The decrease in thermal conductivity during irradiation is much greater than would be caused by the relatively small increase observed in oxygen : uranium ratio. In addition, the irradiation-induced changes in lattice parameter are opposite to that which would be caused by oxidation. Fission product concentration, which is low at these irradiated levels, would not be expected to exert an appreciable influence. It seems evident, therefore, that the thermal conductivity changes are a result of lattice changes that occur during irradiation. The nature of the changes has not yet been determined.

By comparison, the effects of neutron irradiation on the electrical conductivity of UO_2 do not present as orderly a picture as the thermal effects. Relatively few electrical conductivity data are available, particularly for irradiated materials. Results to date on sintered, polycrystalline specimens are summarized in Fig. 8.

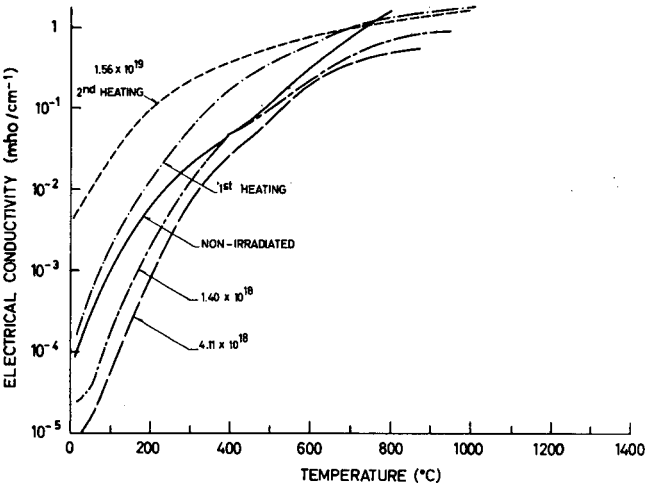


Fig. 8

Electrical conductivity of polycrystalline UO_2

(Exposures shown are in fissions/cm^3)

An initial decrease of electrical conductivity is followed by an increase as higher irradiation exposures are reached. That effect may be similar to that reported for some other semi-conductor materials, where the reversal coincides with a transition from n-type conductivity (lattice vacancies formed by increasing irradiation absorb electrons from the conduction band) to p-type (using electrons from the valency band). The data reported here for the most highly irradiated specimens (0.16×10^{20} fissions/cm^3) agree reasonably well with in-reactor measurements made under difficult conditions at Oak Ridge [6]. The temperature-dependent change of electrical conductivity of the irradiated specimens tends to decrease with increasing temperature, while that of the non-irradiated UO_2 remains, relatively, more constant. When the sample is heated, cooled and reheated, the low temperature portion of the second-cycle curve is shifted appreciably upward, although it retains approximately the same shape.

Perhaps the most impressive feature of the electrical-conductivity curves is their difference from the thermal-conductivity curves. Electrical conductivity shows no correlation with the annealing temperatures indicated by the thermal-conductivity data. The major effect of irradiation on the electrical conductivity may be interpreted as being indirect, being due to changes in physical state, density, porosity, oxidation states, and impurity contents.

Low-temperature irradiation of sintered UO_2 causes subtle changes in mechanical properties. An earlier Hanford study [7] showed that the predominant manner of fracture at room temperature of stressed polycrystalline specimens (87 to 94% of theoretical density) changed from transangular to intergranular after irradiation at bulk fuel temperatures less than 100°C, the effect terminating between 0.014×10^{20} and 0.16×10^{20} fissions/cm^3. Further, small holes (100 to 1000-Å diam.) and

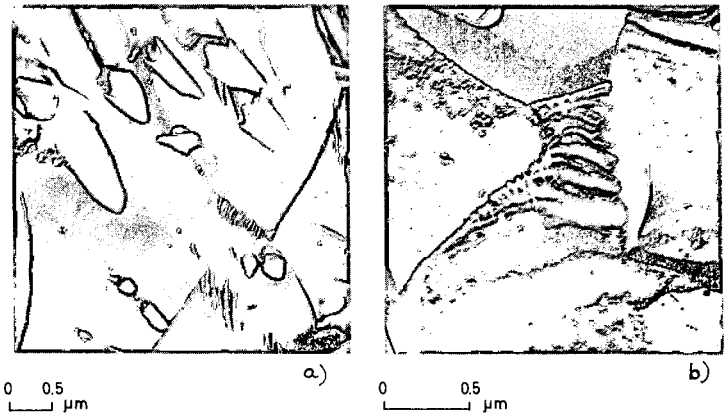


Fig. 9

Negative replicas showing change of UO_2 fracture characteristics by irradiation

(a) Non-irradiated (b) Irradiated at < 100°C to 0.014×10^{20} fissions/cm³

cracks were frequently found at grain boundaries in the irradiated specimens. Fig. 9 shows typical UO_2 fracture surfaces.

Insufficient observations have been made to permit an accurate description of the processes responsible for the change in preferred mode of fracture. Collection of voids at grain boundaries tends to weaken them and irradiation-induced hardening of the UO_2 within the grains tends also to make the grain boundaries relatively weaker than in the pre-irradiated specimens. The predominant intergranular fracture of irradiated polycrystalline UO_2 was used to advantage in the Westinghouse study [8, 9, 10, 11] of intragranular fission-fragment distribution in irradiated UO_2.

Micro-indentation hardness measurements are useful in precharacterizing the plastic deformability of UO_2 specimens and in measuring the significant increase in hardness induced by subsequent neutron irradiation.

Hardness measurements of several non-irradiated, arc-fused UO_2 single crystals and sintered specimens (Fig. 10) showed differences as great as 250 Knoop Hardness Numbers (KHN). Variation of hardness within each specimen was relatively small. Selection of 100 g as the standard load (maximum KHN values are observed in the 50 to 100-g load range) permitted reproducible measurements with minimum fracture of the specimen. Non-annealed uranium dioxide single crystals prepared by arc fusion often are slightly hypostoichiometric and contain small inclusions of uranium and uranium nitrides. Annealing in slightly moist hydrogen removes the inclusions, raises the atomic ratio to 2.00 and decreases the hardness as illustrated by data in Fig. 11. Crystals B and C, Fig. 10, were annealed 12 h in 1750°C hydrogen.

A polished single crystal of arc-fused UO_2 was irradiated to 1.44×10^{20} fissions/cm³ at a fission heat generation rate of 78 W/g. The centre-line and surface temperatures (calculated) were 400 and 325°C, respectively. Post-irradiation measurements showed that the Knoop Hardness

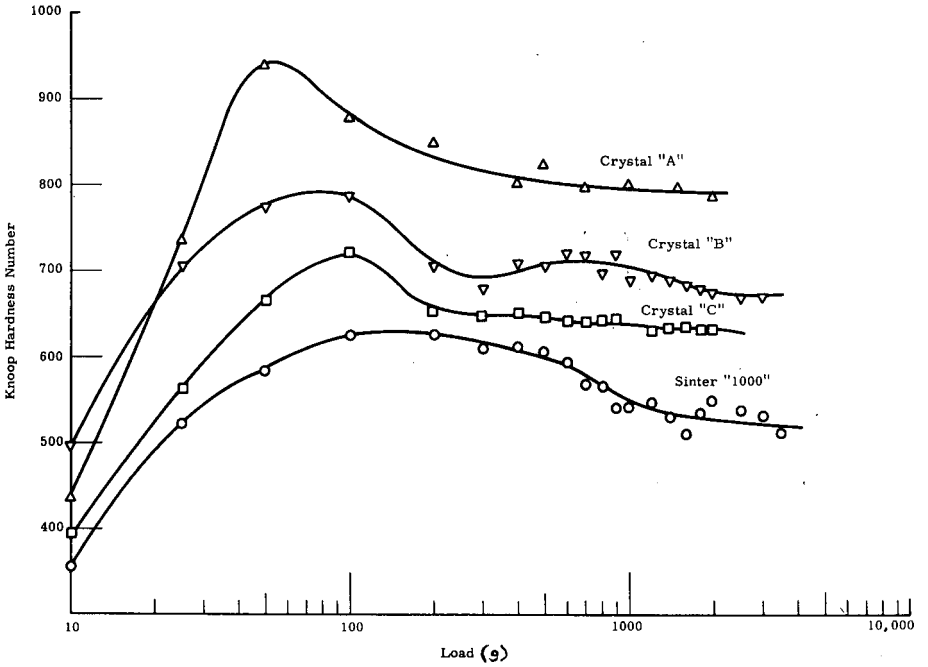


Fig. 10

Microhardness of uranium dioxide

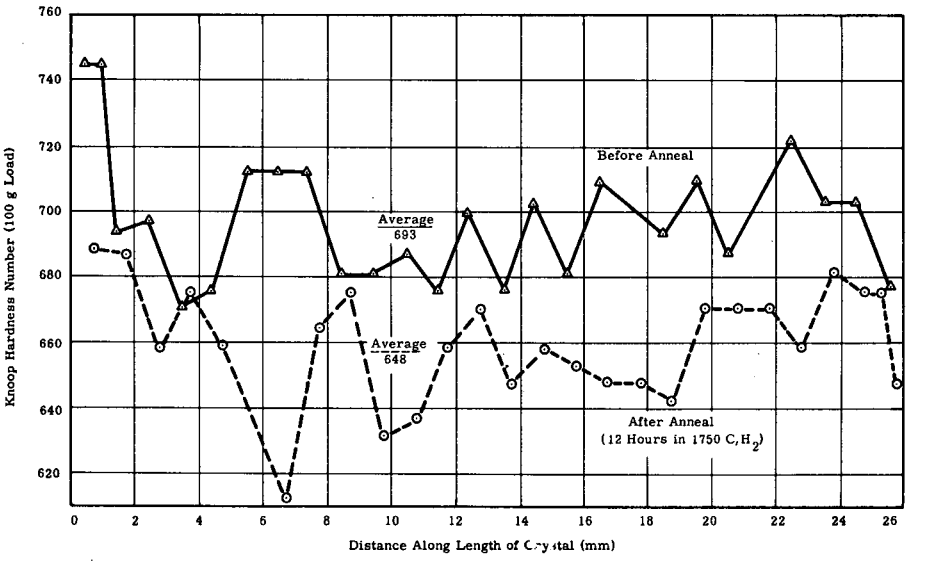


Fig. 11

Effect of annealing on microhardness of the UO_2 crystal

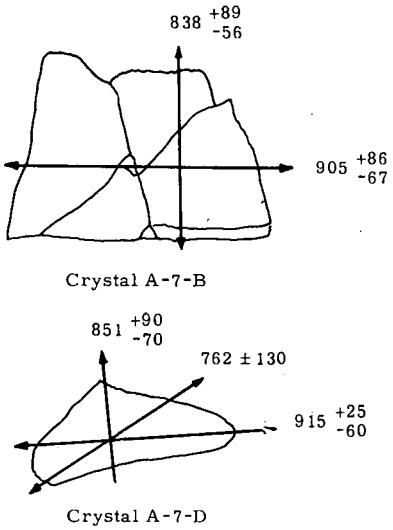


Fig. 12

Microhardness of irradiated UO_2 single crystals showing dependence on crystal orientation

Specimens irradiated to 1.44×10^{20} fissions/cm^3. Pre-irradiation hardness was 686 ± 12. Arrows indicate the direction of long axis of Knoop indenter.

Number increased from the pre-irradiation value (686 ± 12) and varied with the angular relation between the indenter axes and the crystal axes. Knoop Hardness Numbers measured on the irradiated crystal surface are shown in Fig. 12. The irradiated single crystals are stressed and brittle and are fractured more easily than non-irradiated slices of the same parent crystal. No detectable (less than 0.03%) fission-product xenon or krypton was released during irradiation.

Micro-indentation hardness was measured along a radius of the surface of the irradiated, sintered UO_2 pellet shown in Fig. 1. Although the pre-irradiation hardness of the pellet is unknown, KHN measured on similar specimens average 600. Hardness, after irradiation, was approximately 800 in the region in which no grain growth occurred, 770 in the region of small columnar grains and 700 near the central cavity. Measurements of the last value were complicated by the porosity outlining the sub-grain structure and only one radial set of measurements are reported.

2. 2. The temperature range between 500 and 1700°C

Much interest has been displayed in uranium dioxide operating in the range 500 to 1700°C and many investigations of irradiation-induced property changes have been completed. Extensive knowledge of sintering, grain growth, thermal expansion and fission-gas release from sintered or fused UO_2 can be applied safely in the design of fuel elements for moderately severe applications.

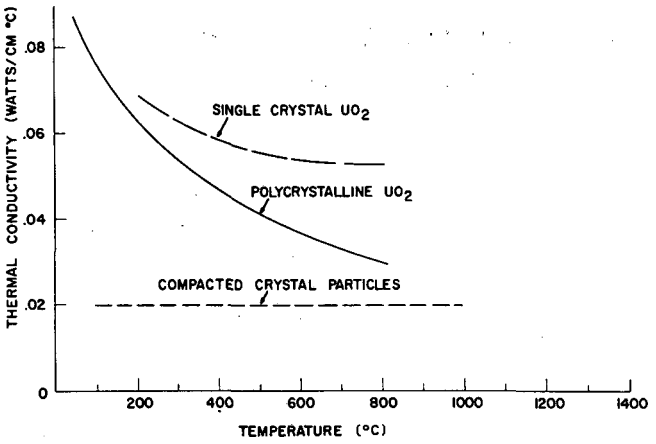


Fig. 13

Thermal conductivity of uranium dioxide

It is in this temperature range that the effect of irradiation damage on thermal conductivity becomes minimized. The predominant effects are caused by thermally induced changes of structure that occur during irradiation.

If the fuel element originally comprised a non-sintered compact of small single crystals the initial, bulk thermal conductivity would be low and constant over a broad temperature range (Fig. 13) and the limiting factor might be the interfacial resistance between particles, rather than the thermal conductivity of the UO_2. Sintering occurs (on both microscopic and macroscopic scale) during irradiation and the bulk conductivity increases and becomes temperature-dependent, subject to the low-temperature differences introduced, as discussed earlier, by radiation damage. A further substantial increase in bulk thermal conductivity is believed to occur if an appreciable portion of the fuel consists of large, single crystals, as in vibrationally compacted fuel rods. Data obtained to 800°C from a UO_2 single crystal (Fig. 13) strongly suggests a significant contribution by a radiant-energy transfer process. Work by BATES [12] based on interpretations of irradiated UO_2 micrographs and out-of-reactor simulation experiments leads to a prediction of increasing thermal conductivity above 1400°C.

Autoradiographs of sectioned uranium dioxide fuel elements irradiated to 10×10^{20} fissions/cm^3 reveal no gross segregation of fission fragments in regions not exhibiting in-reactor grain growth. Diffusion to grain boundaries occurs.

2.3. The temperature range above 1600°C

Extensive changes of the uranium dioxide structure occur in fuel elements irradiated to produce temperatures exceeding 1600°C. These changes are primarily associated with the net movement of the voids up the thermal gradient to coalesce eventually into a central cavity. It has been demonstrated [13, 14] that the end result of such movement of individual voids

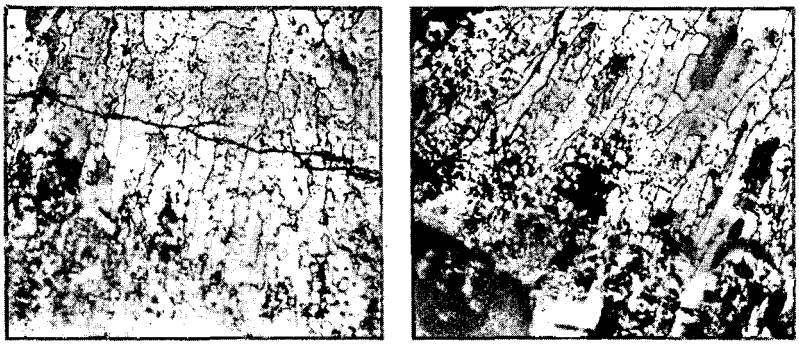


Fig. 14

Columnar grain growth is initiated at interparticle voids in irradiated, vibrationally compacted UO_2

is the formation of radially oriented, columnar grains of high-density uranium dioxide that exhibit properties quite different from those of the parent material. Columnar grain growth is initiated at residual porosity in sintered UO_2 and at interparticle voids in swaged or vibrationally compacted UO_2 (Fig. 14). A mechanically induced crack through a single crystal also will serve as a source of voids that produce columnar grains, as illustrated in Fig. 15. The formation of the columnar grain structure occurs rapidly during the initial heating of the fuel element, when steep temperature gradients exist in the unaltered fuel. After operating equilibrium is reached, each subsequent temperature rise or positive reactor transient starts a new wave of voids inward through the columnar grain structure.

The outer limit of columnar grain growth is thought to represent an isotherm of approximately 1700°C, this on the basis of a perhaps questionable assumption that the phenomenon occurs in-reactor at the same temperature as it is observed in experiments with non-irradiated UO_2. The expulsion of many atoms when a fission fragment passes through the surface of a void may effectively reduce the apparent temperature at which the phenomenon appears during irradiation. At a radius estimated to represent approximately 2100°C the structure changes from smaller columnar grains to relatively large grains that extend to the central cavity, or to the molten zone, if it exists. The characteristic advancing lenticular voids are often observed in the small columnar grains but not in the larger columnar grains, which exhibit exceptionally low porosity where the temperature is below approximately 2400°C. That temperature isotherm is marked by a well-defined ring of small spherical voids (clearly visible in Fig. 1) that do not decorate a grain boundary. That temperature perhaps represents the point at which increased plasticity of the fuel permits the surface tension to transform the moving lenticular voids into spheres. Examination of many photomicrographs of irradiated specimens suggests that spherical voids move much more slowly in a temperature gradient than do lenticular voids. Thus, the change of shape would cause a deceleration of void movement toward the central cavity and the observed increased concentration of voids.

Post-irradiation ceramography frequently reveals extensive sub-grain structure in columnar grains irradiated at temperatures greater than ap-

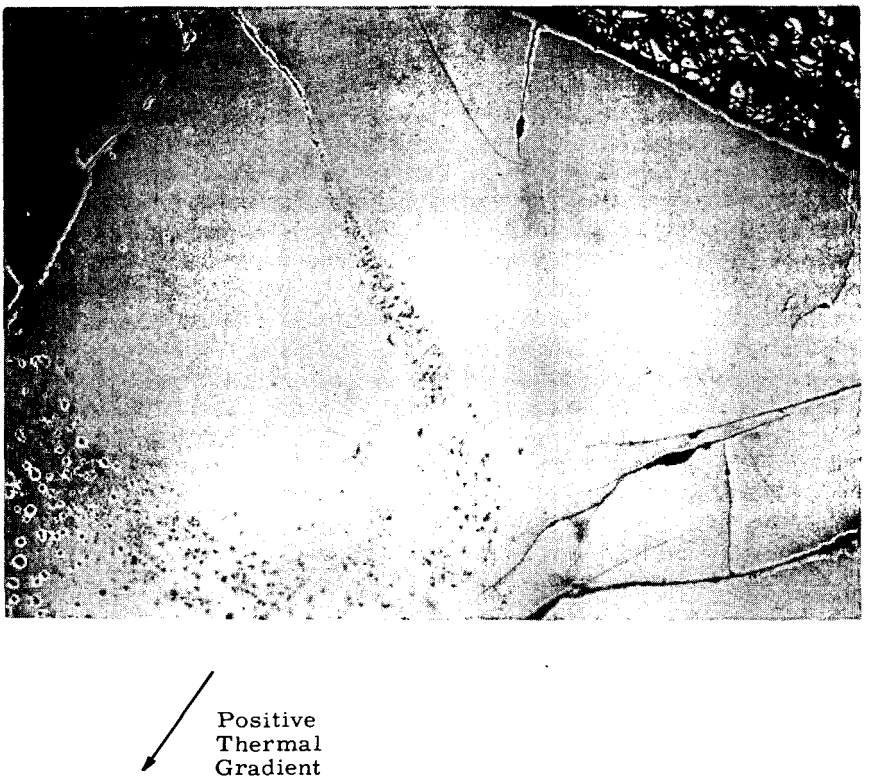


Fig. 15

A crack in an arc-fused UO_2 crystal serves as a source of voids that produce columnar grains

proximately 2400°C. The sub-grain structure is often emphasized by the porosity that has accumulated at the low angle boundaries, as in Figs. 1 and 16. In other test elements it is seen as a network of broad, diffuse boundaries revealed by chemical etching, as in Fig. 17. Accumulation of dislocations and fission fragments is a probable mechanism responsible for developing the sub-grain structure.

Other prominent large voids in the large columnar grain region represent ballooned accumulations of porosity at the low-angle boundaries, or at imperfectly healed radial cracks developed during earlier reactor shut-down operations.

A useful application of the columnar grain growth phenomenon is the homogenizing of mixtures of uranium dioxide particles having different enrichments, or mixtures of isomorphous crystals such as UO_2 and PuO_2, or UO_2 and ThO_2. For example, Fig. 18 shows a fuel mixture originally comprising 86 wt. % ThO_2 (−3+100 mesh, Tyler series) and the remainder UO_2 (−100 mesh, Tyler series, 10 wt. % U^{235} in total uranium). The autoradiograph clearly reveals the large particles of ThO_2 (in which relatively

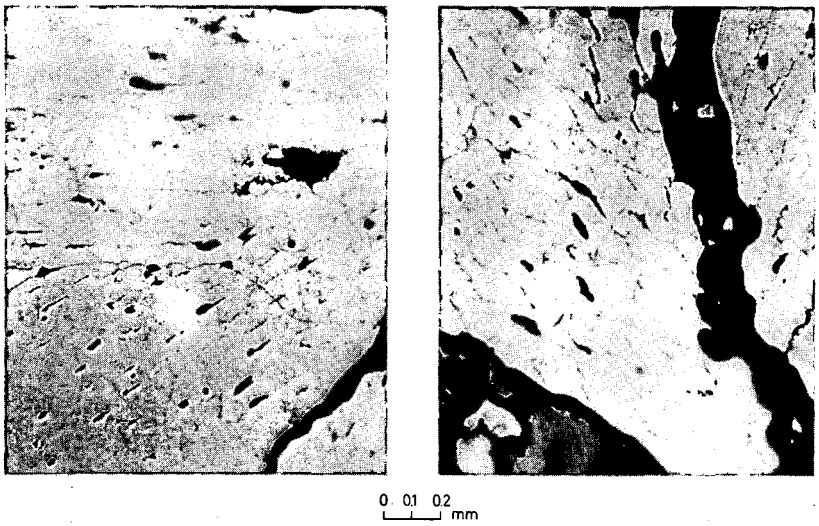


Fig. 16

Porosity accumulated at low-angle boundaries in large columnar-grain region of irradiated UO_2

(a) (b)

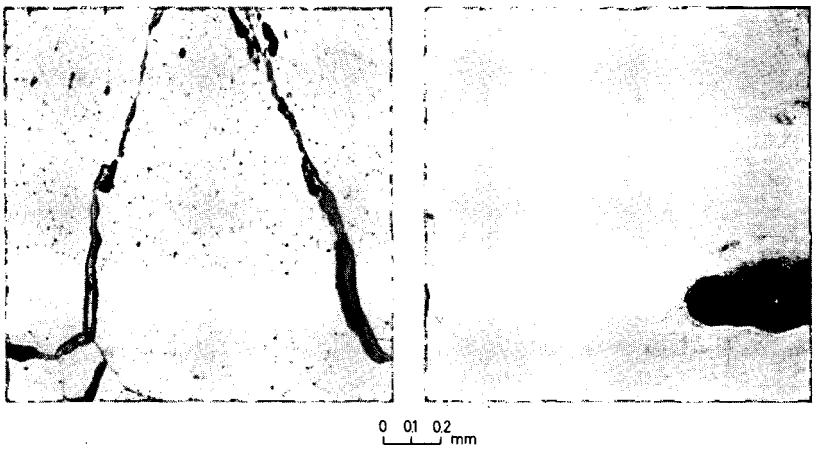


Fig. 17

Subgrain structure in large columnar-grain region of irradiated (a) UO_2 and (b) UO_2 - 10 wt. % ThO_2: revealed by chemical etching

(a) (b)

few fissions occurred) in the outer, colder regions. In the hot zone where large columnar grain growth occurred the distinction no longer exists, UO_2 and ThO_2 being uniformly distributed. Another element containing 10 wt. % ThO_2 and 90 wt. % UO_2 produced similar results when irradiated.

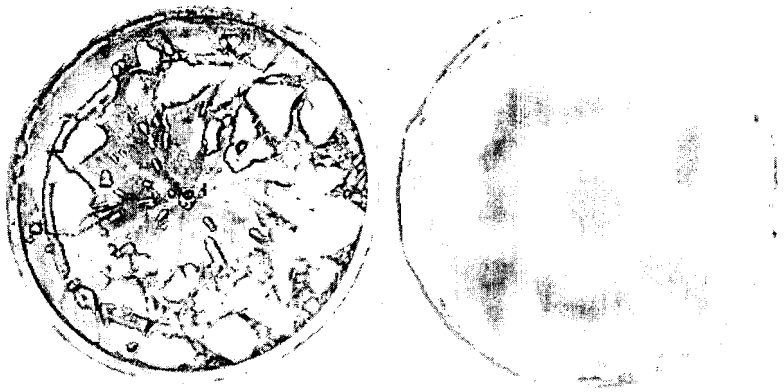


Fig. 18

Homogenizing of UO_2 - 86 wt. % ThO_2 by columnar grain growth

(b) is an autoradiograph

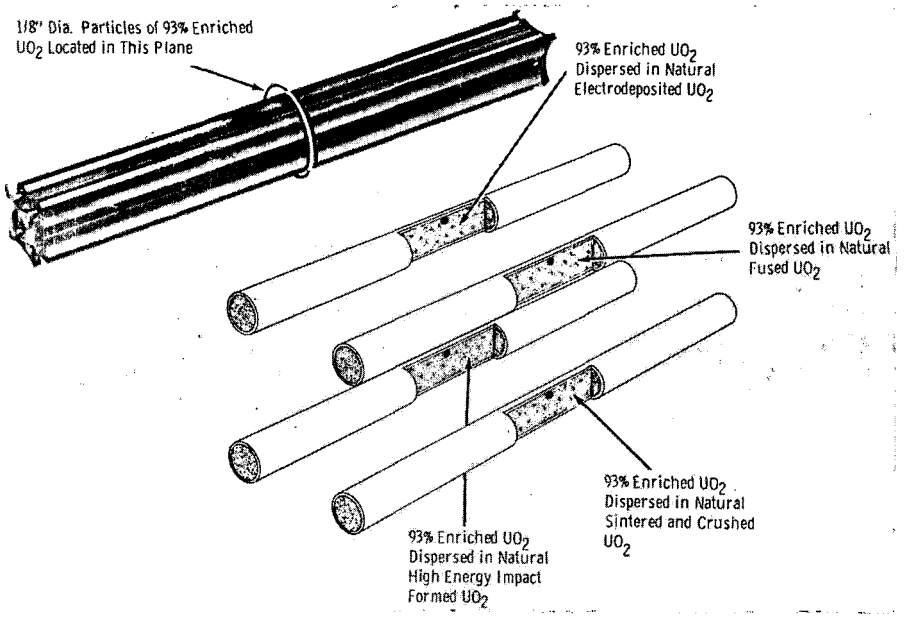


Fig. 19

Vibrationally compacted UO_2 fuel element for hot-spot test

Additional evidence of rapid homogenizing of UO_2 was obtained during post-irradiation examination of the test element shown in Fig. 19. Each vibrationally compacted fuel rod contained fused, naturally enriched UO_2 and sufficient fine particles of 93% enriched UO_2 to raise the average uranium

atom enrichment of the fuel to 1.6% U^{235}. A severe initial hot spot was created in each rod by placing a 3-mm diam. lump of 93% enriched UO_2 against the inner surface of the Zircaloy cladding. The calculated hot-spot surface heat flux was sufficient to cause boiling burn-out and melting of the cladding, but gross relocation of the U^{235} oxide (by the same sublimation-condensation mechanism responsible for columnar grain growth) occurred rapidly enough for the heat transfer to be spread over a safe area. Only small external discolorations marked the locations of the original hot spots.

A transverse section of one rod near the initial location of the 93% enriched UO_2 lump is shown in Fig. 20. A corresponding longitudinal section and its autoradiograph, Fig. 21, show continued presence of small, discrete particles of enriched UO_2 in the cooler, outer portion of the fuel. But the average concentration of U^{235} in the homogenized, columnar grain growth region is considerably greater than elsewhere, illustrating the net spreading of highly enriched UO_2 into that region.

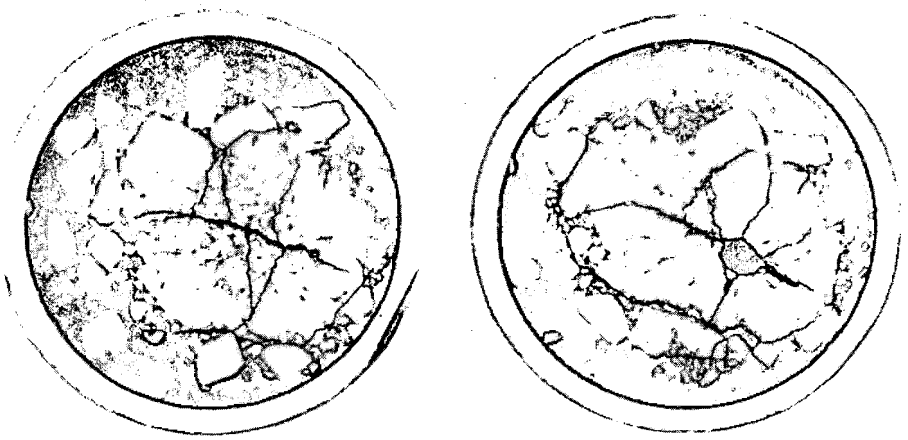


Fig. 20

Transverse sections of an irradiated, vibrationally compacted UO_2 fuel rod near the position of an initially severe hot-spot

(a) (b)

Radiant energy transfer assumes the major role in the columnar grain region. Additional data (Fig. 22) supporting that published earlier by BATES [12] include values obtained from analyses of swaged and vibrationally compacted UO_2 and also from sintered pellets. Recent out-of-reactor measurements by MURTHA and CHERNOCK [15] also show rising thermal conductivity between 1200 and 2200°C.

Evidence for the presence of molten uranium dioxide fuel during irradiation is revealed during post-irradiation examination by the presence of a mass of large, porous, equiaxed grains, centrally located and surrounded by the columnar grain region. It is established that the melting-point of uranium dioxide changes as a result of neutron irradiation, as dis-

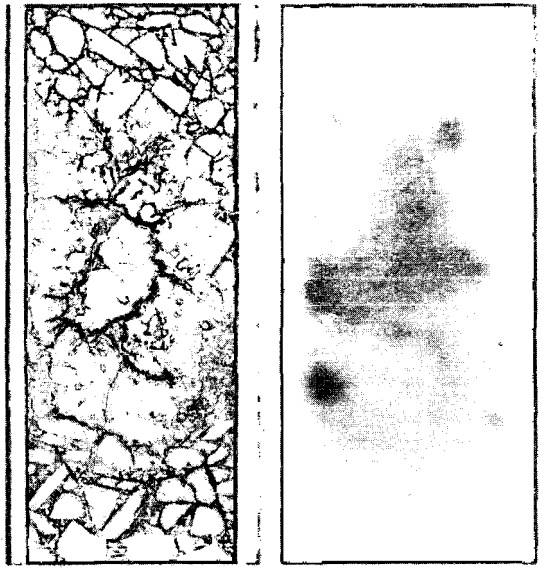


Fig. 21

Longitudinal section of an irradiated, vibrationally compacted UO_2 fuel rod near the position of an initially severe hot-spot

(a) As-polished, 600 grit (b) Autoradiograph

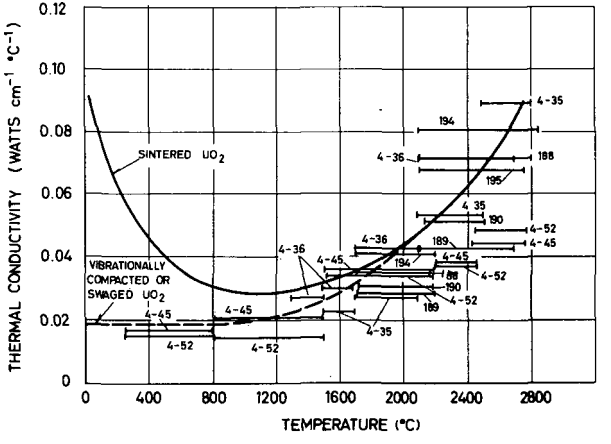
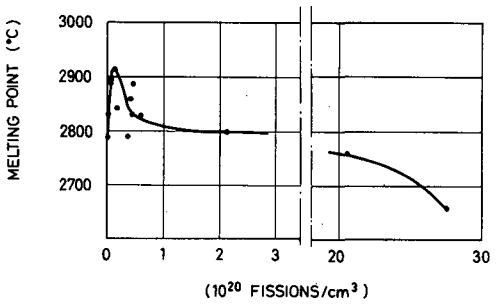


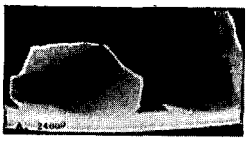
Fig. 22

Thermal conductivity of irradiated UO_2 based on analyses of test elements

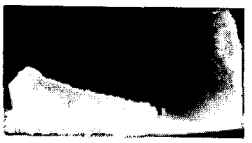
Swaged UO_2: 4 - 35, 190
Vibrationally compacted UO_2: 188, 195
Sintered UO_2: 4 - 36, 189, 194
Defected (water) swaged UO_2: 4 - 45, 4 - 52

(a) (b)

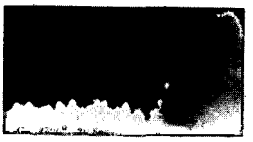




Both specimens unchanged at 2400°C



At 2790°C, non-irradiated specimen melts and vaporizes rapidly; about 60% vapourized after 10 s; irradiated specimen is little affected



After 20 s at 2790°C, non-irradiated specimen is nearly all vaporized; irradiated specimen shows some vaporization and recrystallization but is still nearly completely intact.

non-irradiated

5×10^{19} fissions/cm^3

Fig. 23

Effects of irradiation on the high-temperature properties of UO_2

(a) Melting temperature of irradiated UO_2
(b) Relative volatility of irradiated UO_2

cussed later, and it is recognized that subsequent grain growth might obscure evidence of central core melting during the initial stages of irradiation. However, gross axial flow of molten uranium dioxide would be expected in a vertically oriented fuel element. Laboratory tests demonstrated that the viscosity of molten, non-irradiated uranium dioxide was sufficiently low so that it flowed freely through holes and cracks as narrow as 0.15 mm under its own hydraulic head of a few millimetres.

A study of irradiation effects on melting revealed an unexpected increase of as much as 130°C in the melting point of UO_2 irradiated to 0.3×10^{20} fissions/cm^3 (Fig. 23). Volatility decreased in proportion to the increase in melting point. Irradiation beyond approximately 20×10^{20} fissions/cm^3 was required to suppress the melting-point appreciably below that of non-irradiated UO_2. Uranium dioxide irradiated to 31.5×10^{20} fissions/cm^3 melted at 2600°C.

The increase in melting point at low irradiation exposures suggests irradiation stabilization of hyperstoichiometric UO_2. In general, a compound that dissociates slightly at elevated temperatures, as does UO_2, exhibits a maximum in the liquidus at a non-stoichiometric composition. That dissociation may, in fact, have prevented accurate measurement of the melting temperature of non-irradiated $UO_{2.00}$. Stabilizing of oxygen concentrations in excess of those normally present at the melting point could result in a higher melting oxide. The mechanism by which irradiation would cause such stabilization is uncertain, but it may be associated with oxygen entrapment in anion vacancies surrounding less-than-quadrivalent fission fragments, or in vacancies formed by high-energy bombardment.

Heating rates greater than 1000°C/s were employed to melt non-irradiated, hyperstoichiometric uranium dioxide. A specimen having an initial atom ratio of 2.24 melted at 2400 ± 100°C, but the atom ratio decreased to 2.07 during the 4-s heating-cooling cycle.

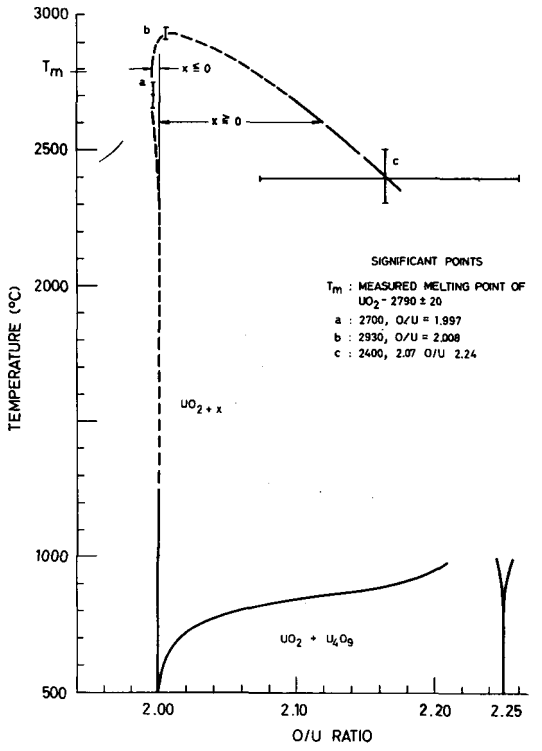


Fig. 24

Tentative $\overline{UO_2}$ phase diagram for temperatures above 2400°C

The melting observations were used to establish the tentative high-temperature phase diagram shown in Fig. 24.

The lattice parameter of uranium dioxide quenched from 2700°C to room temperature in less than 5 s indicated an atomic ratio of 1.997 ± 0.002 which is too near 2.000 to be considered conclusive evidence for retained UO_{2-x}.

These results agree with an expected limited solubility of uranium in uranium dioxide at temperatures near the melting point and with the recently observed evidence of precipitation of uranium near the centre of high-rated fuel cores during irradiation. Fig. 25 shows typical uranium inclusions

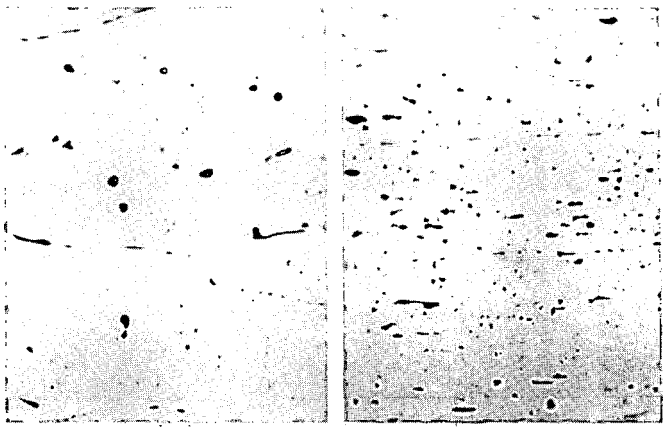


Fig. 25

Uranium inclusions in UO_2 columnar grains

Specimen details { swaged, fused UO_2 – irradiated to $\sim 16 \times 10^{20}$ fissions/cm^3
cut and polished – not etched

(a) Near thermal centre, estimated 2700°C during irradiation
(b) Small columnar-grain region, estimated 1800°C during irradiation

found throughout the columnar grain region. Their size increases with increasing irradiation temperature. Similarly appearing uranium inclusions reported [16] in non-irradiated UO_2 annealed above 2000°C were identified as alpha-uranium. ANDERSON reported [17] metastable beta-uranium inclusions that reverted to alpha-uranium when the sample was pulverized. Our irradiated inclusions were identified as beta-uranium by X-ray diffraction measurements at room temperature (Fig. 26). The diffraction patterns cannot be reconciled with alpha-uranium, higher oxides of uranium or uranium monoxide, and several lines are not identified, or are masked by high background. Aluminium contamination occurred during sectioning of the fuel rods. A general broadening of the UO_2 lines and possibly a shift to smaller 2θ values are apparent.

Significant movement of fission fragments and plutonium occurs in UO_2 during irradiation at temperatures above approximately 1700°C. Pronounced depletion was observed in the high-density region of the columnar grains (corresponding to an equilibrium temperature band roughly between 2100

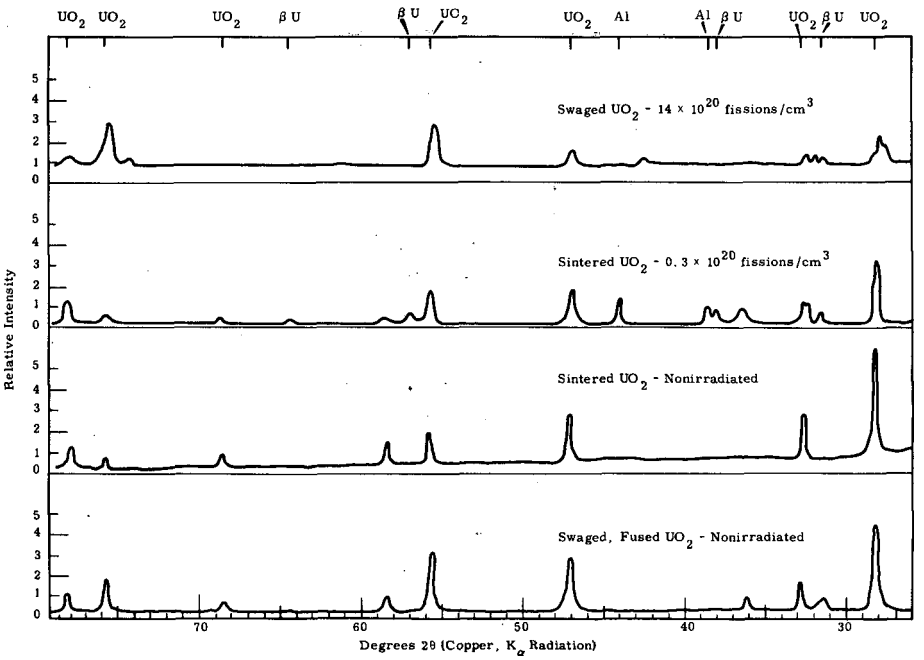


Fig. 26

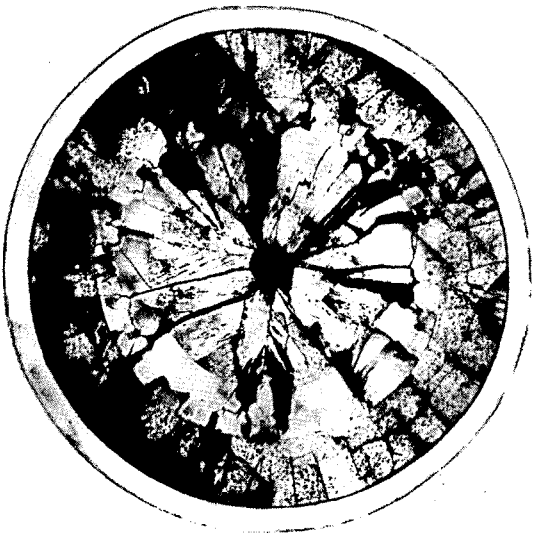
X-ray diffraction profiles of irradiated and non-irradiated UO_2

and 2500°C). Movement from the point at which the kinetic energy of fission is expended is presumably accomplished by diffusion, by void migration (a vapour-phase zone-refining process), or by vaporization of the fission fragment and redeposition in cooler portions of the fuel. These observations complement BLEIBERG's study [8, 9, 10, 11] of fission-fragment diffusion to grain boundaries in polycrystalline UO_2 irradiated a lower temperatures.

Preliminary evidence of extensive fission-fragment migration was obtained by autoradiography of polished cross-sections of uranium dioxide fuel rods irradiated to between 0.08×10^{20} and 16×10^{20} fissions/cm^3. Similar results were obtained from swaged, vibration-compacted and sintered UO_2 fuels. The migration revealed by the autoradiographs was better defined by micro-radiochemical analysis of the irradiated UO_2 [18].

Gross relocation of fission products in columnar grain-growth regions was observed to a varying degree in all test elements examined. Fig. 27 shows typical results obtained from the irradiated, sintered pellet illustrated in Fig. 1. Fig. 28 illustrates the migration of fission fragments and plutonium in vibrationally compacted, arc-fused uranium dioxide, irradiated to 0.08×10^{20} fissions/cm^3, at a heat rating of 36 kW/ft.

The concentration of caesium, which has a relatively low boiling-point and no stable high-temperature oxides, is highest in the coolest portion of the fuel. Zirconium, with its higher melting-point and a stable oxide, is most concentrated in the porous columnar grains near the thermal centre.



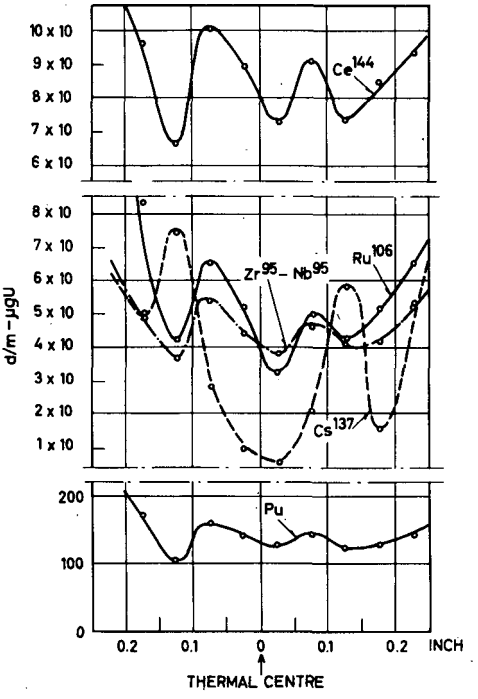


Fig. 27

Fission-fragment distribution in an irradiated, sintered UO_2 pellet, 0.563 in O. D.

*d/m - µg U : disintegration per minute per microgram of uranium

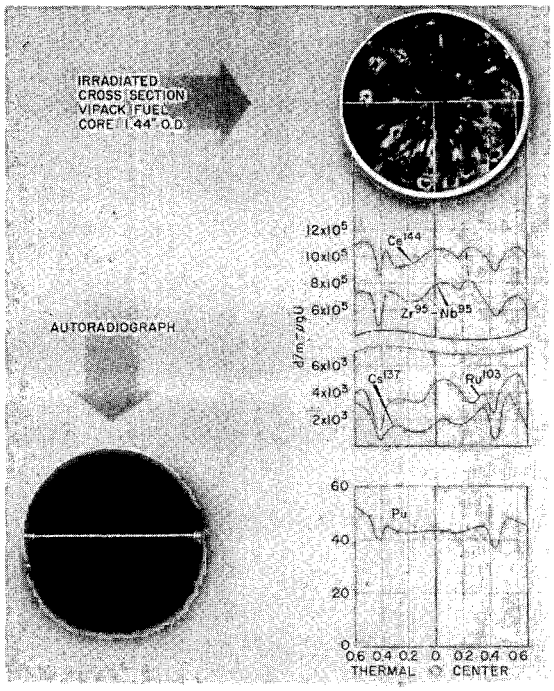


Fig. 28

Fission-fragment distribution in irradiated, vibrationally compacted, arc-fused UO_2

The difference between the positions of maximum concentration of caesium and zirconium may reflect differences in the refractory nature of these elements and their compounds.

Plutonium distribution is similar to that of fission fragments, but the deviation from the predicted distribution (assuming no migration) is less.

3. SUMMARY

The complex interrelation of thermal, chemical and radiation-damage effects that occur during neutron irradiation of uranium dioxide is revealed in the results of the exploratory experiments which have been described. Resolution of that interrelation is being achieved by study of the changes of properties of carefully prepared specimens that are then subjected to carefully controlled irradiation conditions, particularly at bulk temperatures lower than 500°C. Further understanding is being acquired by thorough micro-radiochemical analyses, property measurements and ceramographic examination of a large number of specimens irradiated at higher temperatures.

Thermal conductivity, relocation of fission fragments and plutonium, homogenizing of mixed fuels and the mechanical performance of high-rated fuel elements were shown to be dominated by the phenomenon of columnar grain growth where fuel temperatures exceed approximately 1800°C, as they do in fuel elements representing many advanced concepts.

Because nearly identical results were obtained from tests of fuel elements fabricated by sintering, swaging or vibrationally compacting UO_2, or UO_2 admixed with PuO_2 or ThO_2, fuel-element design engineers can now more confidently select from among a greater variety of fuel-element materials and fabrication processes to meet the increasingly demanding conditions expected in future nuclear reactors.

ACKNOWLEDGEMENTS

Members of Ceramic Fuels Development, Radiometallurgy Laboratory, and Photography Operations, Hanford Laboratories, General Electric Company, Richland, Washington, contributed extensively to the experimental studies and to the compiling of this report. Particular appreciation is expressed to Analytical Laboratories Operation personnel who developed and performed the micro-radiochemical analyses that provided data revealing fission-fragment migration in irradiated uranium dioxide. Fig. 5 and the associated data are presented through the courtesy of W.J. Bailey of Hanford's Plutonium Metallurgy Operation.

REFERENCES

[1] BELLE, J., Uranium Dioxide: Properties and Nuclear Applications, US Gov. Printing Office, Washington D.C. (1961) 557-585.

[2] BIERLEIN, T.K. and MASTEL, B., Damage in UO_2 Films and Particles During Reactor Irradiation, J. appl. Phys. 31 (1960) 2314-2315.

[3] NOGGLE, T.S. and STIEGLER, J.O., Electron Microscope Observations of Fission Fragment Tracks in Thin Films of UO_2, J. appl. Phys. 31 (1960) 2199-2208.

[4] ROSS, A.M., The Dependence of the Thermal Conductivity of Uranium Dioxide on Density, Microstructure, Stoichiometry, and Thermal Neutron Irradiation, USAEC Rpt. CRFD-817 (Sept. 1960).

[5] BLOCH, J., Restauration Thérmique Du Paramètre de l' UO_2 Faiblement Irradié, J. nucl. Mat. 3 (1961) 237-238.

[6] KARKHANAVALA, M.D. and CARROLL, R.M., In-Pile Measurement of the Electrical Resistivity and Thermoelectric Power of Sintered UO_2, USAEC Rpt. ORNL-3093 (2 May 1961).

[7] NEWKIRK, H.W., DANIEL, J.L. and MASTEL, B., Electron Microscope Studies of Damage in Irradiated Uranium Dioxide, J. nucl. Mat. 2 (1960) 269-273.

[8] BLEIBERG, M.L., Technical Progress Report, Pressurized Water Reactor Project for the Period December 24, 1960 to February 23, 1961, USAEC Rpt. WAPD-MRP-90 (April 1961) 50.

[9] BLEIBERG, M.L., Technical Progress Report, Pressurized Water Reactor Project for the Period April 24, 1961 to June 23, 1961, USAEC Rpt. WAPD-MRP-92 (23 June 1961) 53.

[10] BLEIBERG, M.L., Technical Progress Report, Pressurized Water Reactor Project for the Period August 24, 1961 to October 23, 1961, USAEC Rpt. WAPD-MRP-94 (23 October 1961) 61.

[11] BLEIBERG, M.L., Technical Progress Report, Pressurized Water Reactor Project for the Period October 24, 1961 to December 23, 1961, USAEC Rpt. WAPD-MRP-95 (23 December 1961) 43.

[12] BATES, J.L., Thermal Conductivity of UO_2 Improves at High Temperatures, Nucleonics 19 6 (1961) 83-86.

[13] NEWKIRK, H.W. and BATES, J.L., Photographic Observations of Thermal Effects in Unirradiated Uranium Dioxide Fuel Cores, USAEC Rpt. HW-60828 (22 June 1959).

[14] MacEWAN, J.R. and LAWSON, V.B., Grain Growth in Sintered Uranium Dioxide: II, Columnar Grain Growth, J. Amer. Ceram. Soc. 45 (1962) 42-46.

[15] MURTHA, B.E. and CHERNOCK, W.P., The Development and Testing of the UO_2 Fuel Element System, USAEC Rpt. CEND-141 (June 1961).

[16] MacEWAN, J.R., Grain Growth in Sintered Uranium Dioxide: I, Equiaxed Grain Growth, J. Amer. Ceram. Soc. 45 (1962) 37-41.

[17] ANDERSON, J. S. et al. Decomposition of Uranium Dioxide at Its Melting Point, Nature 185 (1960) 915-916.

[18] BATES, J. L., CHRISTENSEN, J. A. and ROAKE, W. E., Fission Products and Plutonium Migrate in Uranium-Dioxide Fuel, Nucleonics 20 2 (1962) 88-90.

IRRADIATION EXPERIMENTS WITH FUEL SUSPENSIONS

M.E.A. HERMANS AND H.S.G. SLOOTEN
REACTOR DEVELOPMENT GROUP, N.V. KEMA,
ARNHEM, NETHERLANDS
AND
R.G. SOWDEN
ATOMIC ENERGY RESEARCH ESTABLISHMENT
HARWELL, BERKS., ENGLAND

Abstract — Résumé — Аннотация — Resumen

IRRADIATION EXPERIMENTS WITH FUEL SUSPENSIONS. The effects of exposing dilute suspensions of fissile oxides to pile irradiation have been investigated. When the irradiation was carried out in an aqueous dispersing medium, breakdown of the original 5-μm particles into a colloid was observed. The results of experiments carried out to determine the influence of different variables on the rate of breakdown are presented. Possible mechanisms of the fragmentation process are discussed.

EXPÉRIENCES D'IRRADIATION DE COMBUSTIBLES EN SUSPENSION. L'auteur a étudié les conséquences de l'irradiation de suspensions diluées d'oxydes fissiles dans un réacteur. Il a constaté que lorsque l'irradiation a lieu dans un milieu dispersif aqueux, les particules initiales de 5 μm se décomposent en colloïdes. Il présente les résultats d'expériences effectuées en vue de déterminer l'influence des différents paramètres sur le taux de décomposition. Il discute quelques mécanismes pouvant expliquer le processus de fragmentation.

ОПЫТЫ ПО ОБЛУЧЕНИЮ ЯДЕРНОЙ ТОПЛИВНОЙ СУСПЕНЗИИ. Были исследованы результаты облучения в реакторе разбавленных суспензий окисей расщепляющихся материалов. При проведении облучения в водной дисперсионной среде наблюдается разложение первоначальных частиц (5 мк) с переходом их в коллоидальное состояние. Излагаются результаты опытов, направленных на определение влияния различных переменных величин на скорость разложения. Обсуждаются возможные способы процесса раздробления.

EXPERIMENTOS DE IRRADIACIÓN CON SUSPENSIONES DE COMBUSTIBLES. Se han investigado los efectos que ejerce sobre suspensiones diluidas de óxidos fisionables la exposición a las radiaciones en el reactor. Al proceder a la irradiación en un medio dispersante acuoso, se observó que las partículas originales (5) se disgregan hasta formar un coloide. El autor presentará los resultados de los experimentos efectuados con objeto de determinar la influencia de diversas variables sobre el índice de disgregación. Discutirá posibles mecanismos del proceso de fragmentación.

1. INTRODUCTION

One of the first nuclear reactor systems to be proposed, after the possibility of maintaining a neutronic chain-reaction had been established, was the aqueous slurry - or suspension - reactor. Since then development projects for reactor systems based on this concept have been carried out in different countries. Although much effort has been put into the study of the rheological, chemical and mechanical problems associated with suspension-systems, relatively little attention has been paid to the effect of the passage of fission fragments on the integrity of the particles. The re-

sults of a number of slurry-irradiation experiments supported [1, 2] the prevailing optimism with which this problem was treated.

The work described in this paper originated from experiments at Harwell on the irradiation of dilute suspensions of plutonium di-oxide [3] designed primarily to study the distribution of fission products between the solid surface and the aqueous phase. The formation of a green colloidal solution after quite short periods of irradiation revealed that radiation-induced fragmentation of the particles took place, and an extension of the work established that this effect persisted with high-fired material, and even with thoria-plutonia solid solutions in which the power density was reduced by a factor of thirty. At this stage the work became a collaborative venture between the Atomic Energy Research Establishment, Harwell, England and the Reactor Development Group at N.V. KEMA, Arnhem, Netherlands. This paper shows the progress made so far in attempts to define the factors which control radiation-induced fragmentation. It must be strongly emphasized that most of the work is still at an exploratory stage; the opinions advanced are of a tentative nature only and may well be modified in the light of further experience.

2. EXPERIMENTAL METHODS

The irradiations of the slurry-samples were carried out in the BEPO reactor at AERE, Harwell; the temperature varied during irradiation by ± 80°C and the thermal neutron-flux between (1.1 to 1.4) × 10^{12}n/cm^{2}s. The evacuated silica ampoules containing the slurry were encased in aluminium cans together with a neutron-dose monitor of cobalt wire. The dose-limiting factor was the build-up of pressure due to radiolytic gas within the ampoules, which was not to exceed 5 atm. After a cooling period of a few days the ampoules were opened and their contents investigated. The effects of the neutron irradiations were studied by three methods:

(1) α-counting of the supernate after centrifuging the ampoules. In this way, estimation of quantity of colloidal fragments was attempted.
(2) B. E. T. measurements on the above-mentioned centrifuged residue.
(3) Microscopic and electronmicroscopic investigation of the irradiated particles and the colloidal debris.

2.1. α-counting

The opened ampoules containing the slurry samples were centrifuged for 15 min at a nominal maximum of 1000 G using an MSE-laboratory centrifuge. Aliquots of the supernatant liquid containing the colloidal fragments were then transferred to aluminium trays which were dried and counted using an α-scintillation counter. Plateau determinations showed that it was possible to make an accurate assessment of the α-activity (± 5%) despite the fairly high $\beta\gamma$ background due to fission products. Blank experiments were performed to assess the amount of α-activity leached from the solid in the absence of radiation.

In some cases, particularly those where the irradiation was carried out under flocculating conditions, a further test for the presence of dispersible colloidal material was necessary. This was carried out by shaking

the dried powder for 2-3 d with a stabilizing solution, after which sampling and counting was performed as before.

2.2. B. E. T. measurements

Samples for B. E. T. measurements were taken by either transferring the centrifuged residue to the measuring-vessel of the adsorption-apparatus or by irradiating special samples in small silica vessels with standard ground cones. These vessels could be used directly as sample vessels for the B. E. T. apparatus thereby avoiding the handling of the irradiated powders. The gas used in the adsorption experiments was krypton.

2.3. Microscopic examinations

Two kinds of preparations were made for the electron microscope* work on the various samples. The colloidal material was mounted on the sample-holder by means of freeze-drying at -40°C to a vacuum of 10^{-4} mm Hg. The centrifuged residue mentioned in (1) was treated by means of a technique developed by Moscou for the investigation of silica-alumina-catalysts. In this the particles are partly embedded in a layer of lacquer after which a replica is prepared by means of the triafol-SiO-method.

The oxide samples used in the experiments are shown in Table I. The PuO_2 was prepared from the oxalate [4] and ThO_2-UO_2 by the "emulsion-gelation" technique [5].

3. RESULTS

3.1. α-activity measurements

The results of the α-activity measurements are summarized in Figs. 1-5. Particular attention has been paid to the effects of surface area of solid, irradiation time, power density and dispersion characteristics of the solid. In the light of information derived from microscopic and electron-microscopic plates the figures resulting from the α-activity measurement in particular for the ThO_2-UO_2 particles should be looked upon as relative figures. It is rather doubtful whether the real number of atoms evaporated per fission (N) has been determined here.

At higher levels of break-up, the appearance of the supernate after centrifuging at 1000 G was that of a clear solution, coloured bright green in the case of the PuO_2 experiments and yellow-brown in the case of the ThO_2-UO_2 experiments. The colloidal nature of these solutions was first established after centrifuging for 1 h with a high-speed centrifuge at a nominal maximum of 7000 G. Under these conditions, the supernatant liquid separated into a colourless aqueous layer and a solid deposit.

The variation of the fragmentation as a function of irradiation dose is described in Figs. 1, 2 and 3. In the case of material of higher surface

* This was carried out by Mr. L. Moscou of Koninklijke Zwavelzuurfabrieken v/h Ketjen N.V. with a Siemens Elmiskop I, at 80 kV.

Baird and Tatlock, Ltd.

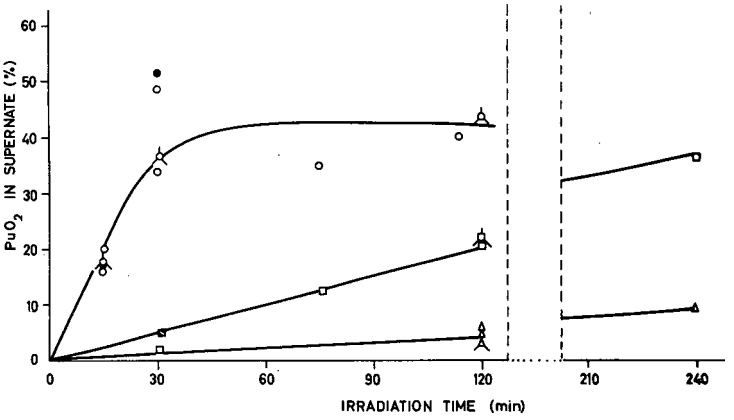


Fig. 1

Variation of PuO_2 in colloidal form with irradiation time and solid surface area

○ Material A (29 m^2/g) } Shading denotes 10^{-2} M HNO_3
□ Material B (3.0 m^2/g) } Spiked points (⅄) denote short cooling
△ Material C (< 0.3 m^2/g) } Period of 2 h before analysis

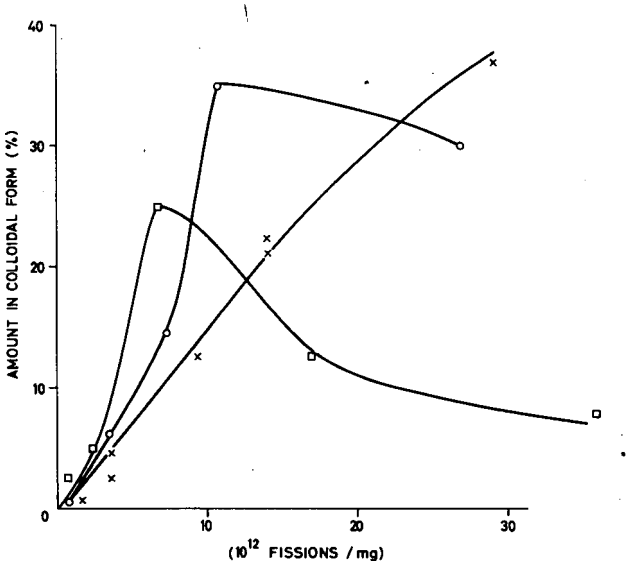


Fig. 2

Variation of metal atoms in colloidal form with total dose
(all solids 3 m^2/g)

× PuO_2
○ ThO_2 - 20% UO_2 (20% U^{235})
□ ThO_2 - 20% UO_2 (4% U^{235})

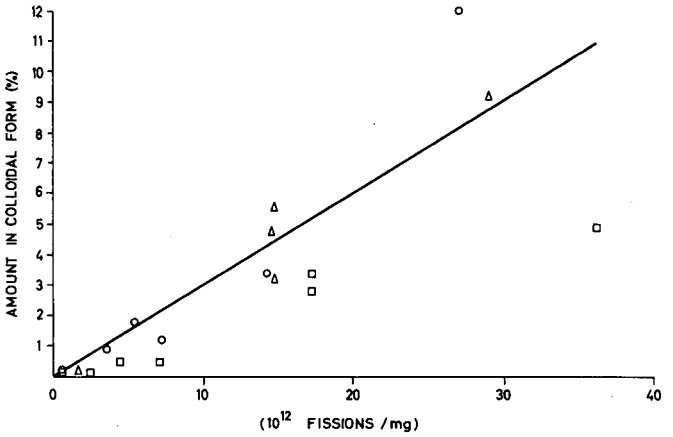


Fig. 3

Variation of metal atoms in colloidal form with total dose (all solids of low surface area)

△ PuO_2
○ ThO_2 - 20% UO_2 (20% U^{235}) } 0.3 m^2/g
□ ThO_2 - 20% UO_2 (4% U^{235}) } 0.2 m^2/g

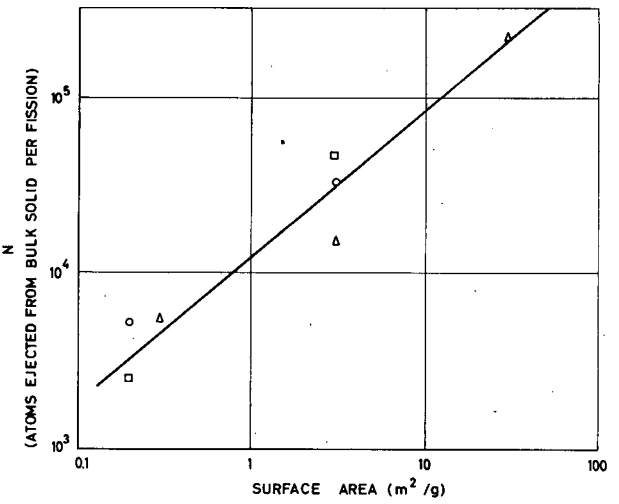


Fig. 4

Variation of initial rate of fragmentation with surface area of solid

△ PuO_2
○ ThO_2 - 20% UO_2 (20% U^{235})
□ ThO_2 - 20% UO_2 (4% U^{235})

area (29 m^2/g PuO_2 and 3 m^2/g) the effect seems to reach a maximum and then to suffer a decline.

The number of metal atoms (N) ejected from the bulk solid per fission event, calculated from the initial rate of fragmentation in all cases, is plotted against the surface area of the solid in Fig. 4: this would mean that the degree of fragmentation is unaffected by a 25-fold change in power density, but is in direct proportion to the surface area of the unirradiated solid.

All the data presented in Figs. 1-4 refer to results obtained when the oxides were irradiated in dispersing media (PuO_2 in H_2O or 10^{-2} M HNO_3; ThO_2-UO_2 in 10^{-2} M or 10^{-3} M KOH and in 10^{-3} M or 10^{-4} M $Th(NO_3)_4$ solution). The effect of dispersion was examined by carrying out similar experiments in flocculating media (PuO_2 in 10^{-1} M HNO_3; ThO_2, UO_2 in H_2O, NaCl and NaCl-KOH-solutions).

The results provide clear evidence that when irradiation is carried out under flocculating conditions, the degree of fragmentation is markedly reduced. The irradiation runs were supplemented by a large number of unirradiated control experiments: in cases where the α-activity in the supernates after irradiation was comparable with that of the control runs, the degree of fragmentation is recorded as zero.

The variation of fragmentation as a function of pH is shown on the graphs of Fig. 5 for one kind of oxide irradiated in pure water and in solutions of HNO_3 and KOH* . It is interesting to note that the centre of the region of low break-up for the 0.2 m^2/g material coincides with the point of zero charge for ThO_2 (pH 8.5 [6]).

In order to determine if in fact fragmentation was still taking place under flocculating conditions, but was being masked by a loose adhesion of colloidal fragments to the surface of the bulk solid, post-irradiation dispersing experiments were carried out. The irradiated solid was separated from the flocculating medium, dried and subjected to several days' agitation in 10^{-2}M KOH solution. The increase in α-activity of the supernate was in

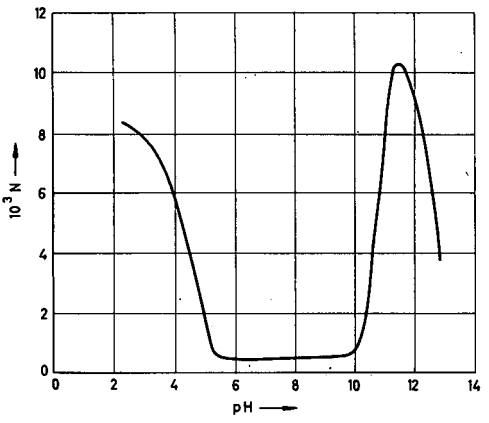


Fig. 5

Effect of pH of supernate on the fragmentation of ThO_2-20% UO_2 (20% U^{235}), fired at 1150°C

* Data obtained at acidities of pH 3 may be affected by dissolution of uranium. This was indicated by the fact that unusually high amounts of α-activity remained in the supernate after prolonged centrifuging at 7000 G.

most cases no greater than that obtained with unirradiated samples, and the situation was unaffected when the sample was not dried before adding the dispersing solution. Similarly, colloidal material from samples irradiated in the dry state or in benzene could not be dispersed. By contrast, a colloid-bulk solid mixture obtained after irradiation in 10^{-2} M KOH could be separated, dried and the colloid quantitatively redispersed.

3.2. B.E.T. measurements

The results of the relatively few B.E.T. measurements carried out can be summarized as follows:

Two samples of powder No. 8, irradiated under dispersing conditions, showed an increase in surface area from 0.2 m^2/g to 2 m^2/g after a dose of $5 \times 10^{16} n/cm^2$. Measurements on samples of the same powder irradiated to the same dose in the dry state and under flocculating conditions did not reveal an increase in surface area. Due to the small sample-size the accuracy of the measurements is rather low, though a three-fold increase in surface area would have been detected.

3.3. Microscopic evidence

The electron-microscopic work is represented by plates in the last section of this report. It should be pointed out that all electron-micrographs are concerned with powder No.8. The spherical form of the particles is clearly seen in Fig. 6, the size of the spheres being approximately 5 μm. Fig. 8 shows the unirradiated powder. The spheres appear to consist of rather smooth agglomerates of 0.1 - 0.5 μm crystallites with some residual porosity. The texture evident from this plate has been termed orange-structure.

Figs. 9 and 10 are pictures of the bulk centrifuged residue from a sample irradiated under dispersing conditions (10^{-2} M KOH), dose $2 \times 10^{16} n/cm^2$.

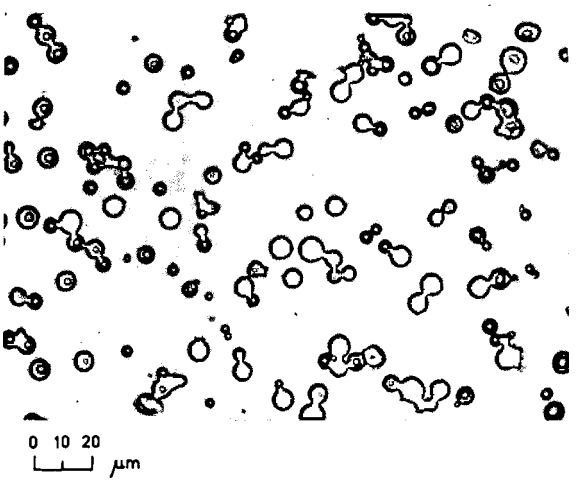


Fig. 6

UO_2-ThO_2 fuel before irradiation

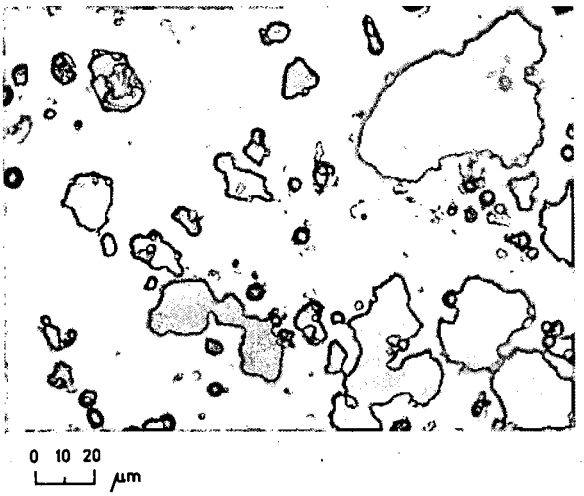


Fig. 7

UO_2 - ThO_2 fuel after irradiation



Fig. 8

K-0: 20% "$^{235}UO_2$ " - 80% ThO_2 (1150°C) unirradiated
(Triafol Replica)

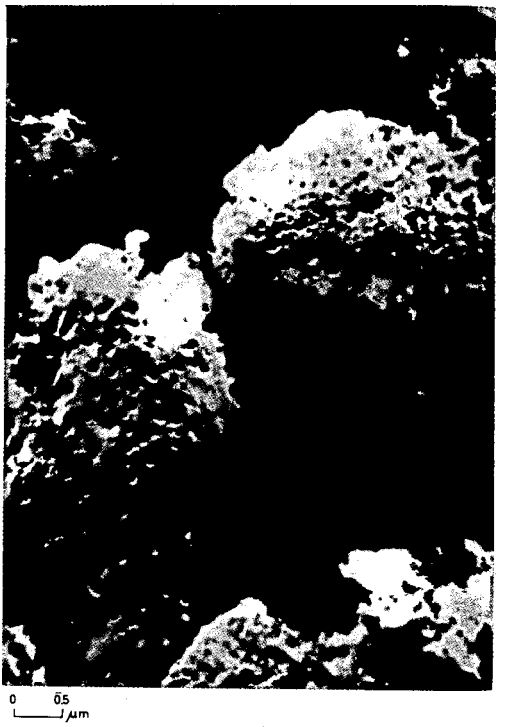


Fig. 9

K-1: 20% "$^{235}UO_2$" - 80% ThO_2 (1150°C)

Irradiated in 10^{-2} N KOH, Dose 2.0×10^{16} n/cm²
(Triafol Replica)

In Fig. 9 there is some evidence of the original form of the particles, whereas in Fig. 10 this is totally lost. As can be seen from Fig. 7, a microphotograph of the residue, the original spheres are surrounded by a large amount of plate-like material of a more or less crystalline nature. A large number of pores with diameter 500 - 1000 Å have come into existence.

Fig. 11 represents the colloidal debris from the above-mentioned sample. The size of the colloidal particles is smaller than 600 Å and there appears to be remarkably little variation in diameter. The electron diffraction pattern in Fig. 12 is evidence for the crystalline nature of this material. The cubic 111 and 113 reflections are clearly visible but rather wide, possibly indicating a variation in Th-U ratio or in U-valency.

For comparison an electron diffraction pattern of a Th-U-hydroxide sol* with the same composition is reproduced (Fig. 13). This pattern is rather different from the one exhibited by the colloidal debris.

Fig. 14 shows particles that have been irradiated under flocculating conditions (H_2O, dose 4×10^{16} n/cm²). The structure of the original particles

* First stage in the production process of the microspheres.

TABLE I

OXIDE SAMPLES USED IN THE EXPERIMENTS

Ref. (No.)	Oxide	Surface area (m^2/g)	Mean particle size (μm)	Calcination temperature in air (°C)
1	PuO_2	29	1-2	500
2	PuO_2	3	1-2	900
3	PuO_2	0.3	1-2	1600 (pellet crushed after sintering)
4	ThO_2-20% UO_2(4% U^{235})	3	5.5 (spheres)	950
5	ThO_2-20% UO_2(4% U^{235})	0.2	6 (")	1150
6	ThO_2-20% UO_2(4% U^{235})	0.2	6 (")	1300
7	ThO_2-20% UO_2(20% U^{235})	3	5.5 (")	950
8	ThO_2-20% UO_2(20% U^{235})	0.2	6 (")	1150

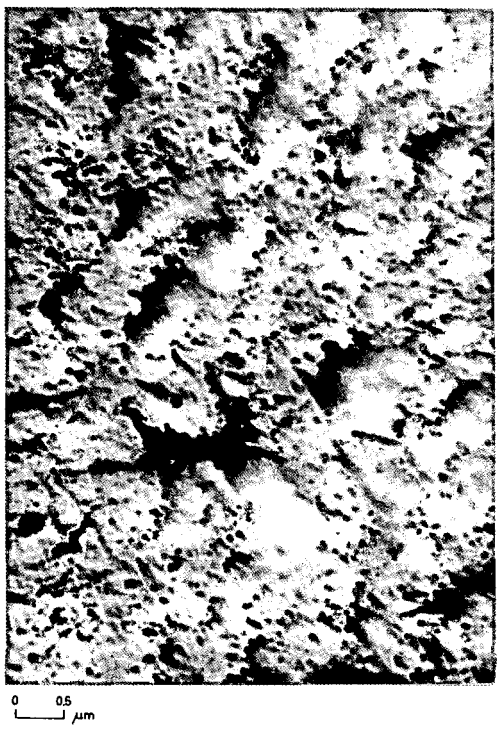


Fig.10

K-1: 20% "$^{235}UO_2$" - 80% ThO_2 (1150°C)
Irradiated in 10^{-2} N KOH, Dose 2.0×10^{16} n/cm²
(Triafol Replica)



Fig. 11

K-2: "Fines" 20% "$^{235}UO_2$"- 80% ThO_2 (K1)
Irradiated in 10^{-2} N KOH, Dose 2.0×10^{15} n/cm^2
(Direct photo)

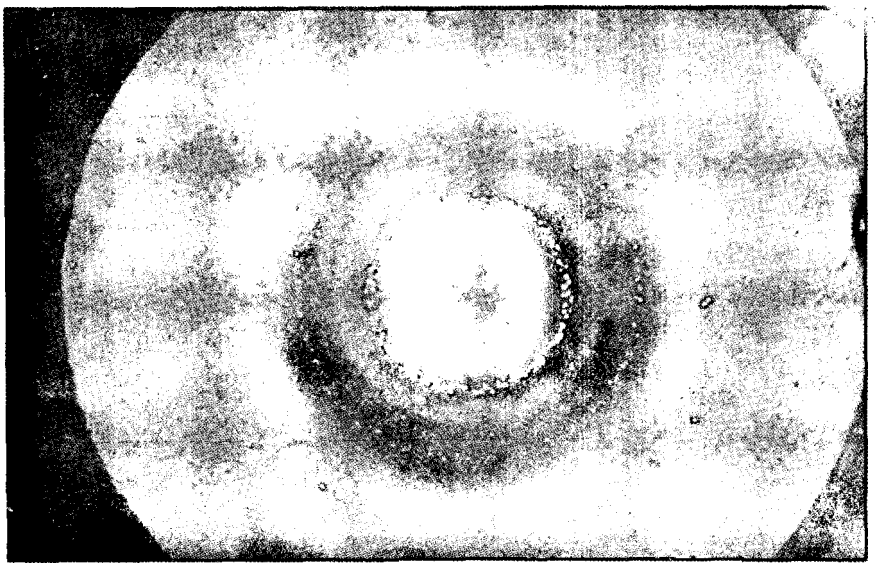


Fig. 12

"Fines" 20% "$^{235}UO_2$" - 80% ThO_2(1150°C)
Irradiated in 10^{-2} N KOH, Dose 2.0×10^{15} n/cm^2
Debye-Scherrer electron diffraction photograph.

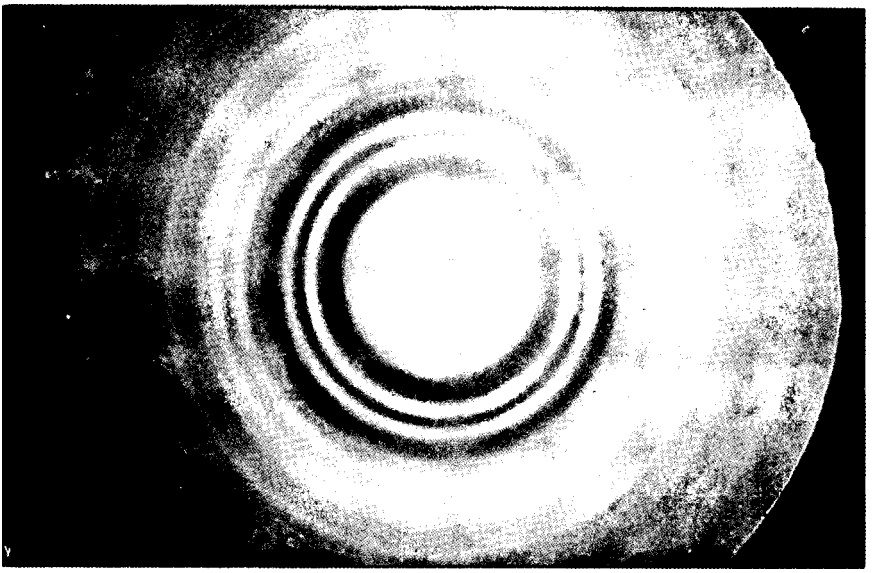


Fig. 13

Sol after freeze drying, 20% "UO_2" - 80% ThO_2
Debye-Scherrer electron diffraction photograph.



Fig. 14

K-3: 20% "$^{235}UO_2$" - 80% ThO_2 (1150°C)
Irradiated in water. Dose 4.0×10^{18} n/cm^2
(Triafol Replica)

appears to be well preserved. There is more porosity than in the unirradiated sample but the orange structure is still evident.

4. DISCUSSION

The investigation of the fragmentation effect is still in an early stage and all conclusions are therefore of a tentative nature. Above all it must be emphasized that the experiments carried out so far relate to burn-up values of not more than 20 MWd/t.

Before drawing conclusions it should be pointed out that the figures obtained by α-activity measurements and B. E. T. are of a relative nature only. Fig. 7 presents the reason for this qualification. It appears that rather large amounts of irradiation debris have recrystallized* to particles of microscopic size ("plates"). These plates naturally remain associated with the bulk solid on centrifuging, thereby decreasing the α-activity of the supernate, from which the disintegration rate is calculated. This does not, however, influence the qualitative value of the experiments because this effect has only lowered the N-value** in the cases where the break-up was large. It is reasonable to assume therefore that the break-up under dispersing conditions is even larger than found in this work, thus stressing even more the influence of colloid-chemical conditions. It is clear that this formation of large particles from debris presents an explanation for the "saturation" of the break-down after longer exposures (Fig. 2).

Although the crystalline nature of the irradiation debris (Fig. 12) seems to indicate that the particles are broken off the bulk solid as such, the difference in composition as concluded from the details of the diffraction-pattern would be hard to explain on this basis. Moreover the appearance of the fines (Fig. 11), especially their narrow size-range, would warrant the supposition of a condensation from solution.

Bearing these limitations in mind it is possible to make the following generalizations:

(1) Fragmentation of fissile-particles in a neutron flux is appreciable only if the solid is irradiated in a dispersing medium.

(2) The amount of break-up per fission in the early stages of fragmentation increases with increasing surface area of the unirradiated solid.

(3) The fragmentation rate is independent of dose-rate over a range of 2×10^9 fissions/mg sec to 3×10^7 fissions/mg sec. (PuO_2 in flux 1.2×10^{12}; ThO_2-UO_2(20% U^{235}) in flux 1.2×10^{11}).

On the basis of the results so far obtained, it is possible to make some suggestions regarding the mechanism of the break-up. In particular, some possibilities can be eliminated. Thus it seems unlikely that fragmentation is brought about solely by intercrystalline weakening followed by dispersion of the crystallites: electron-micrographs show that colloidal particles from an oxide with a surface area of 0.3 m^2/g have a mean diameter of 600 Å, which is several powers of ten lower than the crystallite size (equivalent

* Irradiation temperature was 80°C.

** Number of atoms "evaporated per fission".

spherical diameter) estimated from the surface area. However, work carried out by WAIT on single crystals [7] and by BLOCH [8] on polycrystalline UO_2 has established that no decrease in crystallite size takes place after burn-ups two powers of ten higher than those of the present investigation; it is most unlikely that a different situation will occur for PuO_2 and ThO_2-UO_2, and crystal fragmentation occurring in the bulk of the solid must therefore be ruled out.

At the moment the best available explanation for the disintegration phenomenon seems to be the supposition of some sort of dissolution or peptization. The dissolution or peptization takes place after the surface has been activated by the passage of a fission fragment.

The variation of the disintegration rate with specific surface area and colloid-chemical circumstances can be explained on the basis of this hyposthesis.

ACKNOWLEDGEMENT

We wish to thank Dr. J.K. Dawson of Harwell for stimulating discussions.

REFERENCES

[1] KROHN, N.A. and McBRIDE, J.P., Reactor irradiation of thorium and uranium oxide slurries, USAEC Rpt. ORNL-CF-57-1-119 (1957).

[2] DAWSON, J.K., ALCOCK, K., CHILTON, D.R. and JOHNSON, T., Unpublished work at AERE, Harwell (1956).

[3] HARDER, B.R. and SOWDEN, R.G., Irradiation experiments with aqueous suspensions of plutonium dioxide, U.K.A.E.A. Rpt. AERE-R-3537 (1960).

[4] FRANCIS, K.E. and SOWDEN, R.G., The microstructure of plutonium dioxide prepared by various methods, U.K.A.E.A. Rpt. AERE R-2939 (1959).

[5] HERMANS, M.E.A. and SLOOTEN, H.S.G., Preparation of UO_2 and ThO_2 powders with specific properties, E.A.E.S. Symp. on Reactor Materials, Sweden (1959).

[6] KALSHOVEN, J. and van der PLAS, Th., Unpublished work at KEMA, Arnhem (1960).

[7] WAIT, E., Unpublished work at AERE, Harwell (1959).

[8] BLOCH, J., Restauration thermique du paramètre d'UO_2 faiblement irradié, J. nucl. Mat. 3 (1961) 237.

C. RADIATION DAMAGE IN GRAPHITE

1. Review of papers and panel discussion

(Part of Session 6)

RECENT PROGRESS IN THE STUDY OF RADIATION DAMAGE IN GRAPHITE

J. H. W. SIMMONS
ATOMIC ENERGY RESEARCH ESTABLISHMENT, HARWELL, ENGLAND

1. INTRODUCTION

The effect of irradiation by reactor neutrons and by heavy and light charged particles on the properties of graphite has been studied extensively over the past 20 years, and there is now a very large body of experimental data recorded in the literature. No attempt to review this mass of data will be made in this paper. Instead, three topics are chosen for review. In each of these topics appreciable progress towards an understanding of atomic mechanisms has been made. The first topic concerns the production of irradiation damage by neutrons and heavy particles, and the effect of the rate at which the damage is produced. The second topic is mainly concerned with the annealing behaviour of graphite; this section contains a discussion of some of the important experimental data which have been obtained recently, as well as the theoretical models which are presented in papers given at this Symposium. The third topic is that of dimensional changes in graphite.

2. THE PRODUCTION OF RADIATION DAMAGE

In early days of work on radiation damage it was customary to calculate the number of displaced atoms by considering individual atomic collisions. In the case of radiation damage in metals this simple approach has had to be modified by introducing such concepts as thermal spikes, displacement spikes and focussing collisions. In graphite the situation is simpler mainly because the collision diameter of the carbon atom is small compared with the interatomic spacing in graphite. Furthermore, the diffusion of the interstitial atom, which is the mechanism whereby radiation damage anneals in graphite, takes place in two dimensions. For this reason the grouping of the displaced atoms that occurs in the initial displacement process is less important then it might otherwise be. It is therefore realistic in the case of graphite to think of individual collisions. WILLIS and PENNINCKX [1] have studied the effect of irradiating graphite with three types of bombarding particle: neutrons, which produce their effects through recoil carbon atoms; alpha particles, which are created by neutron reaction on boron; and fission fragments, which are created by a neutron reaction on U^{235}. The mass, charge and velocity of these three particles differ greatly. Willis and Penninckx measured the stored energy released, using a method which gives the energy released in the neighbourhood of the 200°C peak. They found that the annealing behaviour was similar whichever type of particle was used, although the rate at which the stored energy was accumulated during irradiation varied over a wide range. The 200°C peak is associated with interstitial defects. It is possible that more difference between the effects pro-

duced by the different particles would be found with measurements which are sensitive to the properties of vacancies, e.g. if a high-temperature, high-dose experiment were made. However, the result is consistent with the supposition that the damage in graphite can be regarded as individual displacements and that the grouping of the damage is not of the first order of importance. This conclusion is supported by other work on graphite; for example, after irradiation at liquid-nitrogen temperature, the annealing behaviour as observed by resistance changes is very similar whether irradiations are done with electrons or with reactor neutrons (AUSTERMAN and HOVE [2] and BLEWITT [3]). In a paper presented at another session of this Symposium, WRIGHT [4] has shown how it is possible to calculate the number of displaced atoms in various reactors from the calculated neutron spectra. He has compared his results with measurements of the relative rates of accumulation of damage (BELL et al.[5]), and found good agreement. The damaging power of a reactor neutron flux is represented by a single quantity which is proportional to the rate at which displaced atoms are produced. We call this quantity the damage flux (the damaging power of the flux would be a better term). The damage flux is given by

$$\phi_d = \int_0^\infty \psi [E] \rho (E) dE,$$

where $\psi(E)dE$ is the flux of neutrons with energies between E and $E+dE$ and $\rho(E)$ is a weighting factor. In irradiation experiments the flux is measured by activation of a foil or by other means, giving an experimental flux ϕ_e. By comparing the effects of irradiation in two reactors it is possible to determine the ratio $(\phi_d/\phi_e)_{\text{Reactor 1}}:(\phi_d/\phi_e)_{\text{Reactor 2}}$.

The first part of the paper by BRIDGE et al. [6] presented at this session concerns the measurement of the damaging power of the flux in the DR3 reactor and its comparison with the damaging power of the Bepo reactor at Harwell. Their result is compared with other similar observations in Table I.

TABLE I

RELATIVE DAMAGE FLUX IN DIFFERENT REACTORS

Position	Moderator	Ratio ϕ_d/ϕ_e
Bepo experimental hole	Graphite	1.00
Bepo hollow fuel element	"	0.43
Bepo empty fuel position	"	1.00
Pluto hollow fuel element	D_2O	0.49
Pluto replacement fuel position	D_2O	0.59
DR3 hollow fuel element	D_2O	0.49
Herald replacement fuel position	H_2O	0.39

In this work the experimental flux is determined by activation of nickel (appropriately corrected for decay and depletion by the (n, γ) reaction).

These results show that for a given dose as measured by activation of nickel the amount of damage may vary by as much as 2.5 : 1 from one reactor to another.

The second part of the paper by BRIDGE et al. [6] is concerned with the effect of the rate at which damage is produced. Consider two reactors operating at different power levels. Let us suppose the damaging power in the first reactor is ϕ_d and in the second reactor, $a\phi_d$. Let us suppose we irradiate for a time t in the first reactor and for a time t/a in the second reactor, so that the total accumulated dose is the same in each case. In the second reactor there will be less time for the annealing process to take place, and if these two irradiations are carried out at the same temperature the effects produced in the second reactor will be different from those in the first. However, if we compare two irradiations with the second reactor at a higher temperature than the first, with the temperature chosen so that the annealing processes in the second reactor are speeded up by a factor a, the sequence of configurations of displaced atoms will be the same in each case. The two irradiations are then equivalent, although the second one is taking place a times as fast as the first one. This introduces the concept of equivalent irradiation temperatures, which has been used to express the effect of flux-rate dependence. Bridge and his co-authors have shown that the effect of rate is considerable and that it is necessary to take it into account in applying the data from accelerated tests in high-flux reactors to practical problems in power reactors.

Table II shows the magnitude of the effect in several cases.

In the range 155 to 250°C, radiation damage varies very rapidly with the temperature of irradiation, so that the difference between irradiation temperature and equivalent temperature becomes very important. Bridge et al. showed that the equivalent temperature could be calculated using a single activation energy. Thus, for the two reactors referred to above, equivalent irradiations are obtained when the relation between the temperatures is

TABLE II

FLUX-LEVEL EFFECT

Irradiation temperature (°C)	Damage flux (arbitrary units)	Equivalent temperature (°C)
155	1	155
	10	125
	100	105
355	1	355
	10	295
	100	250

$$\frac{1}{T_1} - \frac{1}{T_2} = \frac{k}{U} \ln a,$$

where U is the activation energy, which Bridge et al. found to be 1.2 ± 0.1 eV. In view of the complex annealing behaviour which is known to occur in graphite, it may seem strange that such a wide range of data can be expressed by a single activation energy. This point is referred to again later.

3. ANNEALING MECHANISMS IN GRAPHITE

(a) Theory

The general features of annealing mechanisms in graphite can be conveniently introduced by considering the paper by IWATA and SUZUKI [7], in which a new model of irradiation damage in graphite is put forward. This model is generally based on the experimentally observed behaviour of graphite, but the details of the model are deduced by purely theoretical arguments. The paper starts with the observation that when graphite is irradiated, vacancies and interstitials are produced. The interstitial atoms migrate very easily at low temperatures, but vacancies have an activation energy of about 2.5 eV and do not migrate very much below 1000°C. The complex annealing behaviour of graphite below 1000°C is therefore attributed to various kinds of interstitial complexes. Details of the methods of calculation are given in the paper. The results are summarized in Table III.

Thus both C and C_2 should be mobile well below the temperature of liquid nitrogen. C_2 molecules cannot be formed at low temperatures because of the potential barrier. The authors consider that C_2 molecules can combine to form a cluster C_2-C_2 with a decomposition energy of about 1.3 eV. Alternatively, C_2 molecules can combine to form a large honeycomb structure. These require a large energy for dissociation, probably of the order of 7eV,

TABLE III

PROPERTIES OF INTERSTITIAL COMPLEXES

Species	Properties	
Single C	Energy required for formation:	2.5 eV
	Energy required for migration:	0.016 eV
Atomic Cluster C-C	Stable configuration with spacing of 10 Å	
Molecule C_2	Potential barrier for formation:	0.6 eV
	Energy required for decomposition:	7 eV
	Energy required for migration:	0.05 eV
Molecular Cluster C_2 - C_2	Energy required for decomposition:	1.3 eV
Honeycomb Structures $(C_2)_n$	Energy required for decomposition per molecule:	7 eV

and in fact they will be destroyed by vacancy migration rather than by dissociation. The authors do not attempt to compare their theory with experimental results in detail, except to say that they associate the 200°C annealing peak with decomposition of the molecular clusters and the high-temperature annealing with migration of vacancies, which destroy the honeycomb structures.

(b) Annealing at very low temperatures

Fig. 1 shows the effect of annealing graphite which has been irradiated in liquid helium (AUSTERMAN and HOVE [2]). Changes in the electrical resistivity were measured. There is no appreciable annealing until the

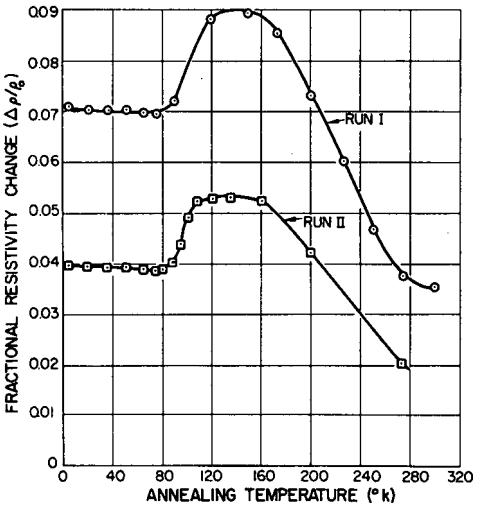


Fig. 1

Resistivity changes versus annealing temperature
(Courtesy of Physical Review).

temperature reaches nearly 100°K, at which point the resistivity increases and then falls off again. In order to understand the increase in electrical resistivity with annealing it is necessary to discriminate between the effect of irradiation on the scattering of the current carriers and the effect on the number of carriers due to the formation of electron traps. This has been done (Fig. 2) by REYNOLDS and GOGGIN [8], who measured resistivity changes, changes in Hall constant and changes in magneto-resistivity, all on the same specimen after irradiation at liquid-nitrogen temperature followed by annealing. They found that the anomalous increase in resistivity was accompanied by corresponding anomalies in the other two properties. Reynolds and Goggin attributed the 100°K peak to the dispersion of close vacancy-interstitial pairs. The dispersion enables the interstitial to capture an electron, thus increasing its scattering power and changing the number of current carriers. REYNOLDS and THROWER [9] consider that the dispersion

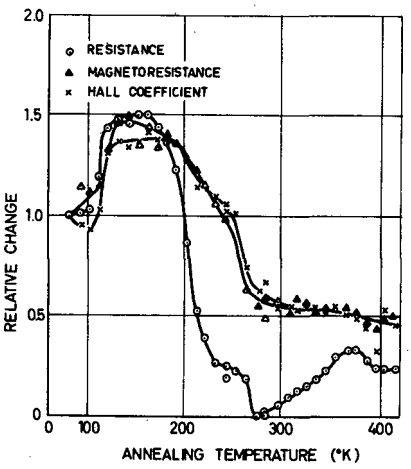


Fig. 2

Annealing of electrical resistance, Hall constant and magneto resistance
(Courtesy of Philosophical Magazine).

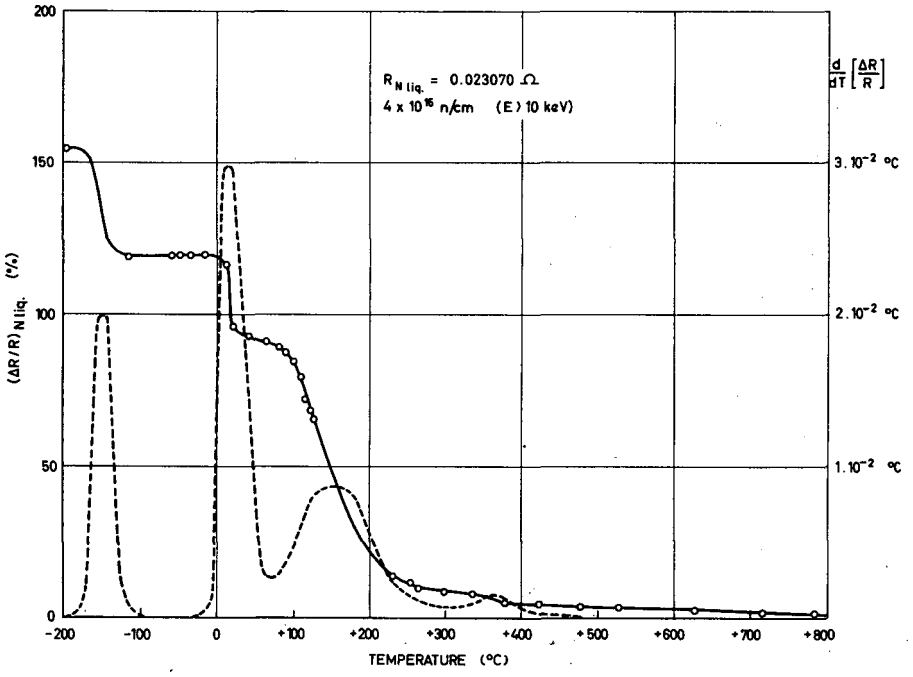


Fig. 3

Recovery of single crystal irradiated in liquid nitrogen

(From BLONS, J., PERRIOT, G. et TOURAND, G., «Étude comparative des effets des neutrons rapides sur le graphite monocristallin et le graphite nucléaire», these Proceedings, section C. 2)

is assisted by repulsion and that the true activation energy for migration of a free interstitial atom is about 0.4 eV.

Fig. 3 shows some data obtained by BLONS, PERRIOT and TOURAND [10]. The main purpose of their work was to compare the effect of irradiation on the resistivity of polycrystalline graphite and of single-crystal graphite. Their preliminary results substantiate an assumption which has been made by most workers in the past, namely that the effects in reactor graphite are due to lattice defects of the same type as would be produced in single crystals. The curve in Fig. 3 is of special interest because it shows, in addition to the 200°C peak and the peak at about 100°K, a new peak at about 20°C.

Fig. 4 shows the results of stored-energy measurements made by BOCHIROL et al. [11]. After irradiation at liquid-nitrogen temperature, the stored-energy release starts at about 100°K; there is a broad peak at 200°K and a further small peak at 20°C. The energy release above this appears to split into two peaks, one at about 200°C and the other a little below.

The effect of irradiation in liquid nitrogen followed by annealing on the lattice parameters of reactor graphite has been described by PLUCHERY

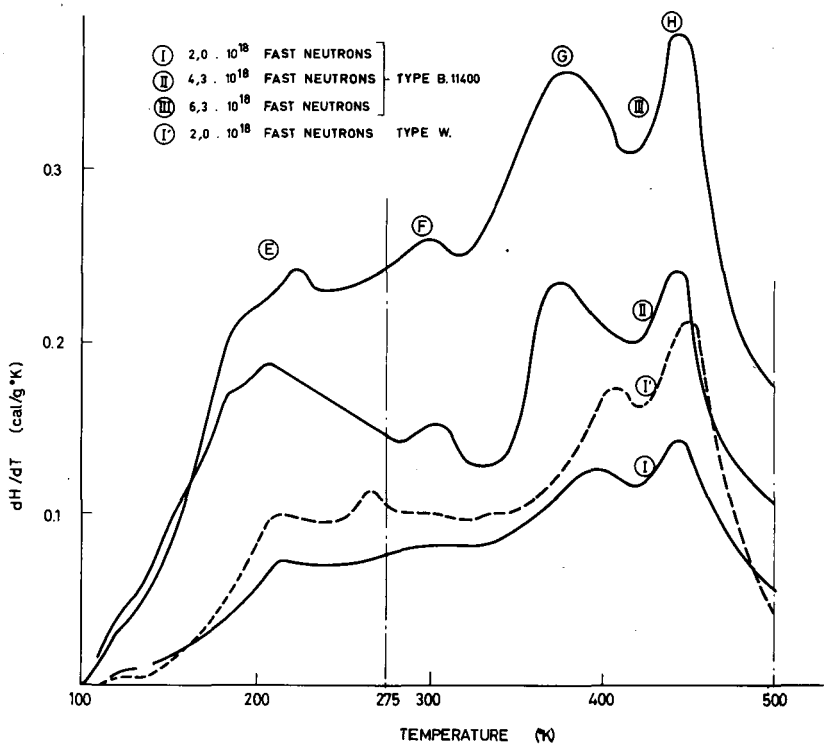


Fig. 4

Differential enthalpy

(From BOCHIROL, L., BONJOUR, E. et WEIL, L., «Irradiations neutroniques à 78°K de graphites polycristallins», these Proceedings, Section C.2)

[12]. Data for two annealing temperatures only are given, so that this work does not give information on the annealing peaks. The measurements are of particular interest because the defects responsible for the increase in c-spacing must be interstitials. The important conclusions from the experiments may be summarized as follows:

(i) The rate of increase of c-spacing at liquid-nitrogen temperature is about twice as great as that at room temperature;
(ii) The ratio $(\Delta a/a)/(\Delta c/c)$ is about 0.05, as compared with values rising from 0.08 at room temperature to 0.25 at 350°C; and
(iii) The amount of c-spacing change that can be removed by annealing below room temperature saturates after a small dose.

(c) Annealing at high temperatures

Many results have been obtained on the effect of irradiation and annealing at room temperature and above, e.g. WOODS, BUPP and FLETCHER [13], SIMMONS and REYNOLDS [14]. The main features of the annealing behaviour of graphite irradiated at room temperature are the annealing peaks at 200°C and 1200°C and the plateau that lies between them. The effect of irradiating at a higher temperature is to remove the annealing spectrum up to the irradiation temperature and to reduce the magnitude of the changes which can be annealed above that temperature.

Experiments reported by REYNOLDS and THROWER [9] have improved our understanding of the behaviour of the interstitial complexes at higher temperatures. Reynolds and Thrower used the electron microscope to study irradiation damage in graphite crystals which had been irradiated at temperatures in the range 150 to 650°C. At the lower end of this range the radiation damage consists of a very fine speckled pattern, barely resolvable. At higher temperatures the amount of damage appearing is much smaller, but the size of the spots is greater. Similar pictures of the radiation damage have been published before and have been seen by other workers. The new feature in this paper is the presentation of the results of a systematic survey of the number and size distribution of the defects. The results of this survey are summarized in Fig. 5. It will be seen that the spot size after irradiation is a linear function of the irradiation temperature. The effect of annealing is also shown. The smaller size spots obtained at low-temperature irradiations first of all increase with annealing, but the larger-size ones at first hardly change. The damage begins to disappear, more or less at the same temperature, irrespective of the irradiation temperature. Reynolds and Thrower have interpreted these experiments using a theory of homogeneous nucleation. They suppose that small defects, not visible in the electron microscope, are created at a constant rate uniformly through the graphite, and that these diffuse with two-dimensional motion to form the large visible defects. The large defects will occur if the conditions are such that the probability of two of the small defects forming a new nucleus is very small compared with the probability of a small defect condensing on an existing nucleus. By measuring the size of the defects, and the mean separation between them in the layer planes, it is possible to determine the activation energy for migration.

Fig. 6 shows a plot of the values of activation energy obtained by this analysis. It can be seen that in the range 150 - 350°C the activation energy

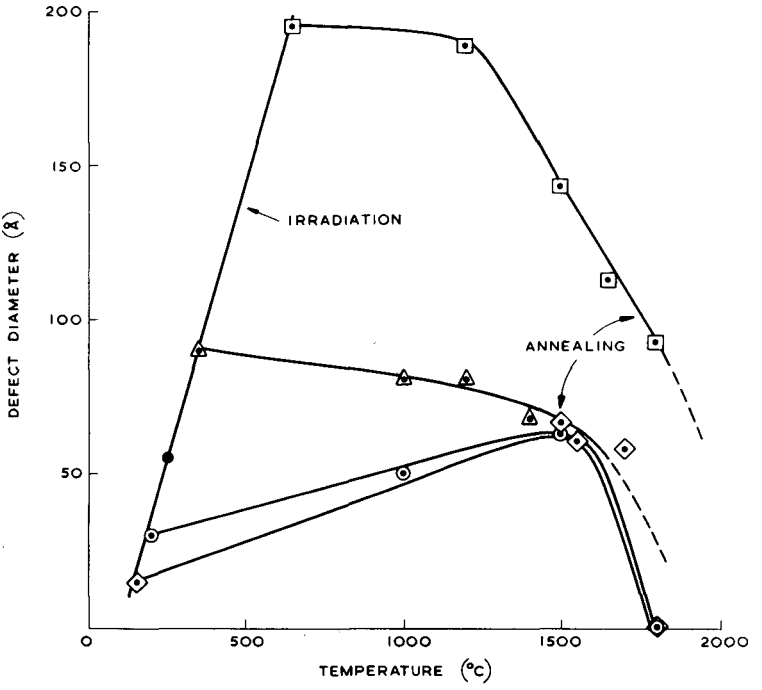


Fig 5

Mean defect diameter as a function of irradiation and annealing temperature

(From REYNOLDS, W. N. and THROWER, P.A., "Irradiation damage in graphite", these Proceedings, section C.2)

is about 1.25 eV. The diffusion of these small defects controls the rate of build-up of damage in this temperature range. The activation energy may therefore be identified with the activation energy measured by Bridge et al. in their studies of the effect of flux rate. A point is shown at 0.4 eV which is considered to be the value for the activation energy of migration of a single interstitial atom. The point at 2.5 eV was obtained from a second population of defects which appears at high doses in the high-temperature irradiations. This activation energy probably refers to the migration of single vacancies and the corresponding visible defects are probably vacancy clusters. The intermediate activation energies are attributed to interstitial complexes. The authors suggest that at 150°C the diffusion entity is probably C_4, and that at higher temperatures slightly more complex defects are involved.

The annealing of the radiation damage that is observed at about 1500°C may be reasonably attributed to the motion of vacancies. This is in agreement with the theoretical proposal if we identify the observed defects with the honeycomb structures described by Iwata and Suzuki. There is a large measure of agreement in the pictures put forward theoretically and the ones suggested by the experiments, but there are two important points of conflict. To make a simple interpretation of the low-temperature experiments one

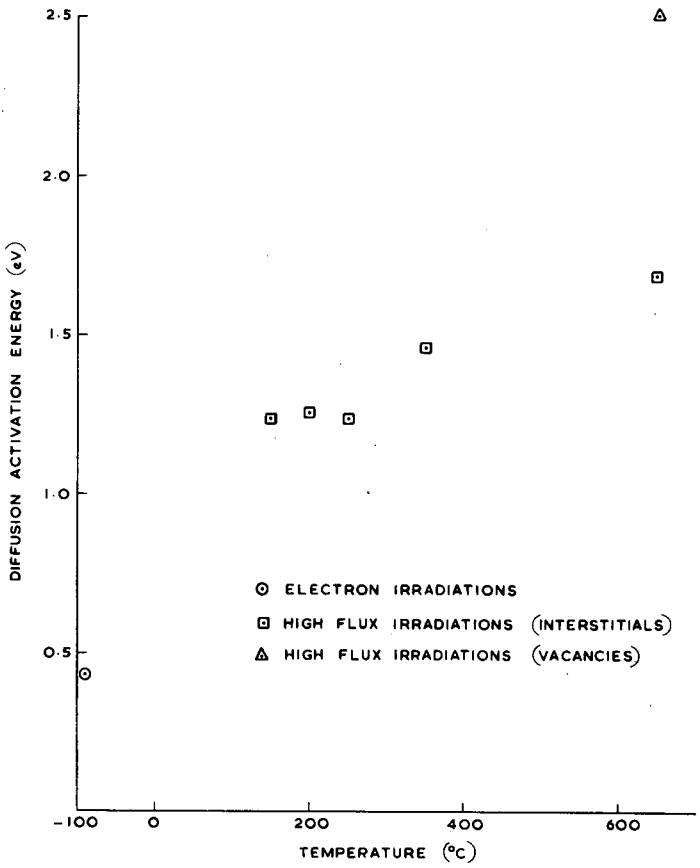


Fig. 6

Diffusion activation energies calculated from the theory for interstitials and vacancies

(From REYNOLDS, W.N. and THROWER, P.A., "Irradiation Damage in graphite", these Proceedings, section C. 2)

must suppose that the activation energies for motion of single and double interstitials is higher than that calculated. The other point is that the formation of the large defects observed at 150°C and above has been interpreted as being due to the motion of C_4 complexes, whereas Iwata and Suzuki have postulated that the annealing in this range is due to breaking up of the complexes.

4. DIMENSIONAL CHANGES

(a) Experimental results

Three papers presented at this meeting are concerned with the dimensional changes. YOSHIKAWA et al. [16] discuss dimensional changes in carbons and

graphites and part of the work reported in the papers by GAIN [17] and FITZER et al.[15] deal with dimensional changes.

Yoshikawa et al. first described the dimensional changes produced in various types of graphite by irradiation at 30°C. They show curves on which the irradiation dose has been extended to 10 000 MWd/t. The graphite grows in the direction perpendicular to extrusion and contracts in the direction parallel to extrusion. They report that apart from slight initial effects all graphites contract when irradiated at 300°C; the contraction varies linearly with dose up to at least 12 000 MWd/t. Some of their results at still higher temperatures are illustrated in Figs. 7 and 8. Fig. 9 shows the contractions of various graphites having different degrees of graphitization; poorly graphitized materials shrink very much more than well-graphitized materials. The effect of annealing on dimensional changes is also discussed. The contraction parallel to extrusion can be annealed almost completely on heating to the original graphitization temperature, but the contraction perpendicular to extrusion cannot be annealed.

The effect of irradiation in an intermediate range of temperature has been studied extensively in the United Kingdom. Figs. 10 and 11 show the dimensional changes inreactor graphite irradiated at temperatures between 150 and 650°C. At the lower temperatures the graphite expands in the

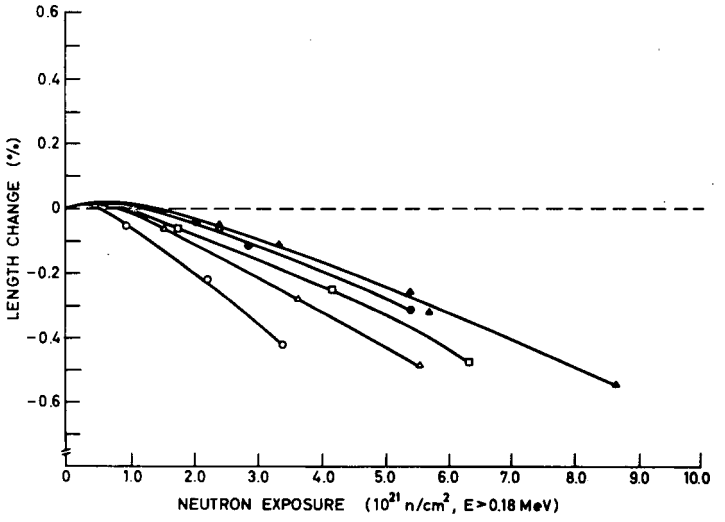


Fig. 7

Radiation-induced contraction of CSF (⊥) graphite

○ 475°C
△ 575°C
□ 625°C
● 725°C
▲ 800°C

(The last points on each curve are tentative, pending verification of exposure).

(From YOSHIKAWA, H.H., WOODRUFF, E.M., DAVIDSON, J.M., HELM, J W. and NIGHTINGALE, R.E., "Radiation effects in carbons and graphites", these Proceedings, section C.2)

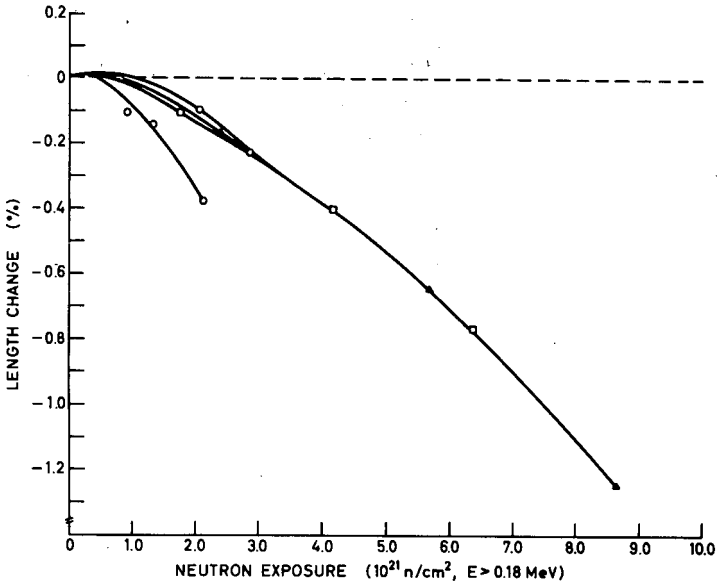


Fig. 8

Radiation-induced contraction of CSF(II) graphite

○ 475°C
△ 625°C
□ 625°C
● 725°C
▲ 800°C

(The last points on each curve are tentative, pending verification of exposure).

(From YOSHIKAWA, H.H., WOODRUFF, E.M., DAVIDSON, J.M., HELM, J.W. and NIGHTINGALE, R.E., "Radiation effects in carbons and graphites", these Proceedings, section C.2)

direction perpendicular to extrusion and contracts in the parallel direction. Above 300°C the graphite contracts in both directions except for a small initial effect. The results represent a transition between the low-temperature and high-temperature behaviour described in Yoshikawa et al. The dimensional changes are far from linear; both the contraction and expansion rate increase with irradiation dose.

GAIN [17] compares the dimensional changes for CSF graphite and bonded natural graphite. The main difference is due to the high degree of orientation in the bonded graphite. His high-temperature irradiations are not carried to a sufficiently high dose for concentrations to appear. FITZER et al. [15] give data on the dimensional changes at several temperatures of a number of different types of graphite. They report that the shape of the specimen affects the dimensional changes. It is possible that the effect may be due to internal stresses in the specimens. Such effects have been reported, for example by KINCHIN [19]. Yoshikawa et al. also report a size effect; they compare the changes in a full-size graphite block with those of small specimens, and arrive at the conclusion that the block shrinks twice as fast as the small specimens.

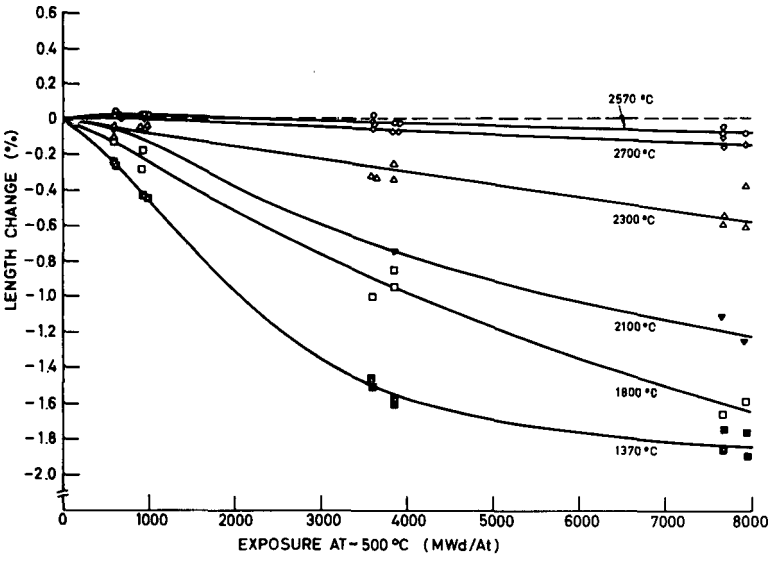


Fig 9

Radiation-induced dimensional changes at about 500°C as a function of heat-treatment temperature
All measurements transverse direction. 1 MWd/At = 1.3×10^{17} n/cm² E > 0.18 MeV.
Temperatures shown refer to heat treatment.

(From YOSHIKAWA, H.H., WOODRUFF, E.M., DAVIDSON, J.M., HELM, J.W. and NIGHTINGALE, R.E., "Radiation effects in carbons and graphites", these Proceedings, section C.2).

(b) Theory of dimensional changes

SIMMONS and REYNOLDS [18] have interpreted the dimensional changes in the range 150 to 650°C by assuming that the dimensional changes of polycrystalline graphite are entirely due to the dimensional changes of the crystals of which the graphite is composed, modified by the effect of orientation and porosity. By using measurements of thermal expansion to allow for orientation and porosity effects they were able to deduce the changes in the dimensions of the crystals, $\Delta X_c/X_c$ and $\Delta X_a/X_a$, from the measurements of dimensional changes of the polycrystalline graphite. The results are shown in Figs.12 and 13. The magnitude of the crystal changes is greater than the corresponding change in the crystal-lattice spacings. This is to be expected if we assume that the dimensional changes are due to the honeycomb structures described in the previous section. The porosity effect changes as irradiation proceeds. For small doses the volume change of the crystals is greater than the volume change of the bulk material, showing that some of the expansion is absorbed in the pores. The proportion of the volume change which is absorbed in the pore space diminishes as irradiation proceeds, indicating that the pore space is closing up. Closure of pore space in irradiated graphite has been observed in the electron microscope by THROWER and REYNOLDS [20] using replica methods.

YOSHIKAWA et al. [16] interpret the changes rather differently. They

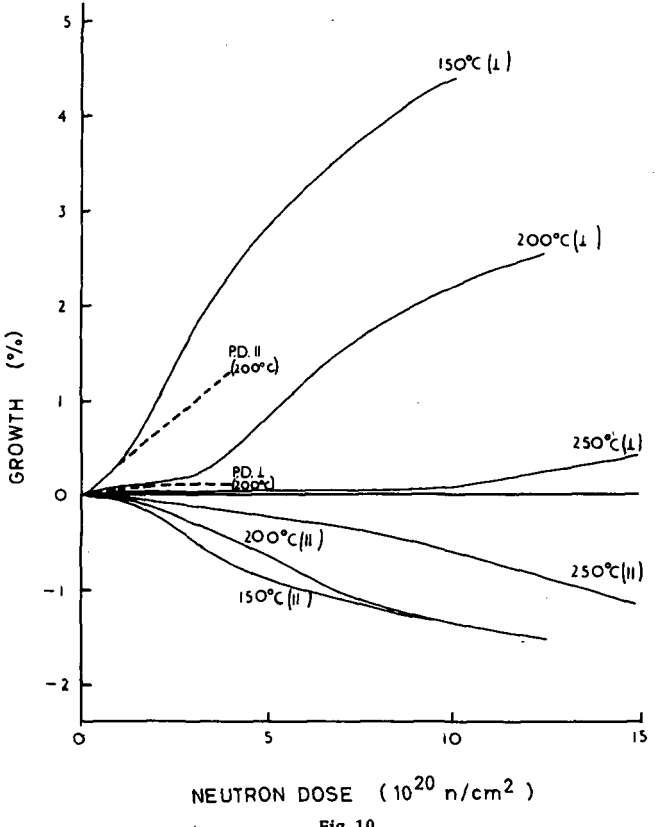


Fig. 10

Dimensional changes at 150° C, 200° C and 250° C
(Courtesy of Institute of Metals).

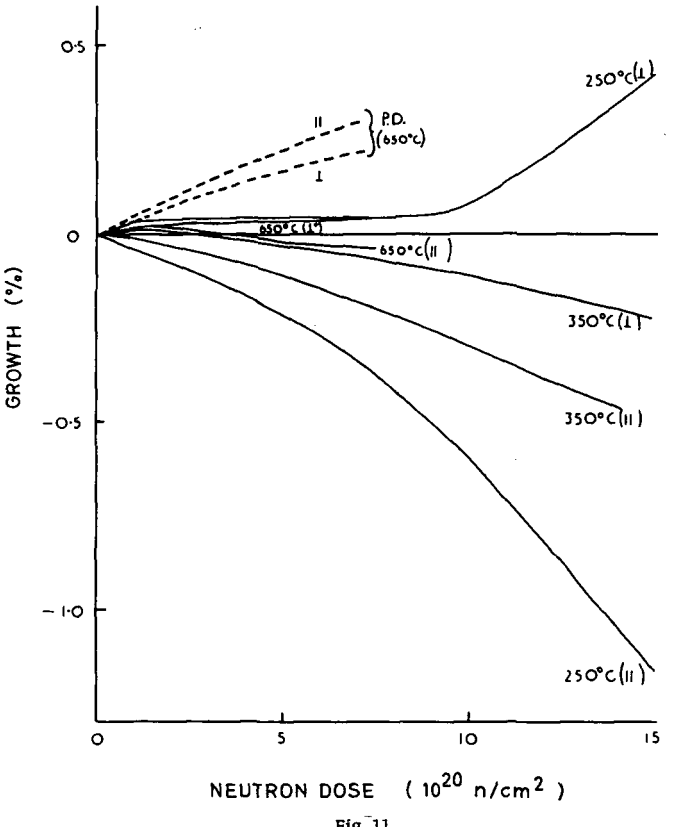


Fig. 11

Dimensional changes at 250° C, 350° C and 650° C
(Courtesy of Institute of Metals).

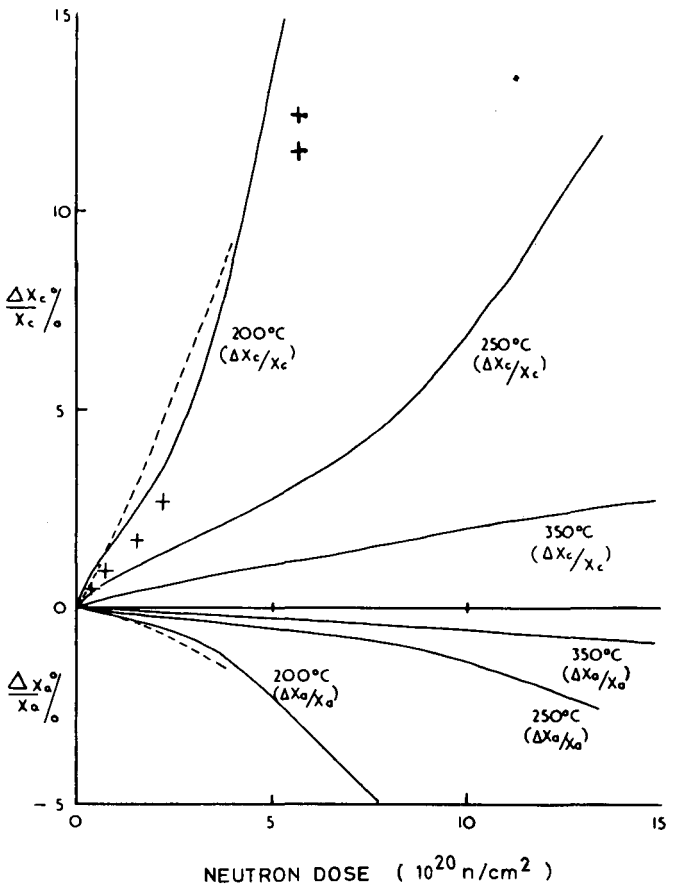


Fig. 12

Dimensional changes of crystals at 200°C, 250°C and 350°C
(Courtesy of Institute of Metals)

agree that there is a contribution from the expansion in the c-direction and the contraction in the a-direction of the crystals, appropriately modified by orientation and porosity, but they consider that an additional contraction must be postulated to explain the high-temperature behaviour. This contraction is substantially independent of temperature, but it varies with the degree of graphitization of the material, the contribution being greater in poorly graphitized material. The two main reasons for introducing this postulate are:

(a) The variation of contraction rate with degree of graphitization; and

(b) The presence of an unannealable component of contraction.

The additional contraction at high temperatures is attributed to radiation-induced processes similar in nature to those which occur during the process of graphitization. At the present time it is not possible to formulate detailed atomic models for these processes.

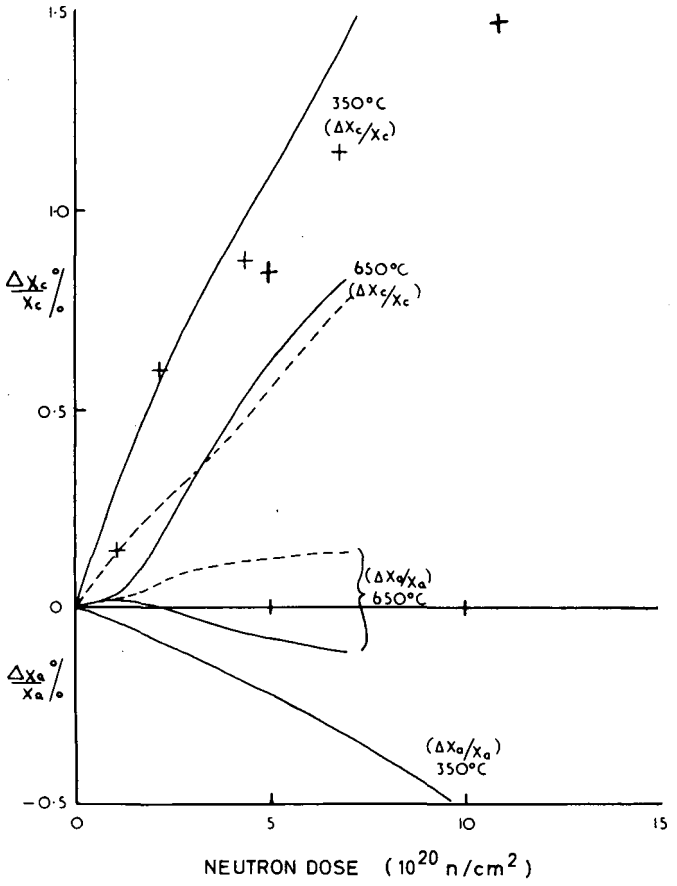


Fig. 13

Dimensional changes of crystals at 350°C and 650°C
(Courtesy of Institute of Metals).

5. CONCLUSIONS

Considerable progress has been made towards an understanding of the nature of the radiation defects in graphite, mainly as a consequence of a study of the behaviour at low temperatures and of the use of electron microscopy. Further work is required before details of the low-temperature processes can be established, but it appears fairly certain that these processes are associated with the migration of interstitial atoms and small groups of interstitial atoms which are formed during annealing. It seems most likely that the irradiation defects which are produced by irradiation in the range 150 to 650°C are large islands of displaced atoms between the layer planes, and that the high-temperature behaviour is governed by the migration of vacancies, although these conclusions are based rather on circumstantial evidence than upon crystallographic identification of the visible defects. The

behaviour in the intermediate temperature range, which includes the 200°C peak and such phenomena as l'effet précoce described by RAPPENEAU [21], appears to be somewhat complicated and there is still no quantitative theory covering this range.

Some progress has been made in the understanding of the effect of irradiation on the dimensional changes of graphite. The effect of irradiation on the electrical and thermal properties of graphite is reasonably well understood. The greatest weakness at the present time is undoubtedly in the understanding of the mechanical properties of graphite and the effect of irradiation on them.

REFERENCES

[1] WILLIS, A.H. and PENNINCKX, R., "The effect of heavy-particle bombardment on Wigner energy storage in graphite", these Proceedings, section C.2.

[2] AUSTERMAN, S.B. and HOVE, J.E., Phys.Rev. 100 (1955) 1214.

[3] KLABUNDE, C.E., BLEWITT, T.H. and COLTMAN, R.R., Bull.Amer.Phys.Soc. V.6, Series 2. March 20-23, 1961.

[4] WRIGHT, S.B., "The use of Monte Carlo calculations in the analysis of radiation damage experiments", Radiation Damage in Solids II, IAEA, Vienna (1962) 239-252.

[5] BELL, J.C., BRIDGE, H., COTTRELL, A.H., FRS., GREENOUGH, G.B., REYNOLDS, W.N. and SIMMONS, J.H.W., Phil.Trans.Roy.Soc. 254 (1962) 361.

[6] BRIDGE, H., GRAY, B.S. and KELLY, B.T., "An effect of flux level and flux spectrum on the accumulation of damage in reactor-irradiated graphites", these Proceedings, section C.2.

[7] IWATA, T. and SUZUKI, H., "A model of radiation damage in graphite", these Proceedings, section C.2.

[8] REYNOLDS, W.N. and GOGGIN, P.R., Phil. Mag., 8 (1960) 1049.

[9] REYNOLDS, W.N. and THROWER, P.A., "Irradiation damage in graphite", these Proceedings, section C.2.

[10] BLONS, J., PERRIOT, G. et TOURAND, G., «Etude comparative des effets des neutrons rapides sur le graphite monocristallin et le graphite nucléaire», these Proceedings, section C.2.

[11] BOCHIROL, L., BONJOUR, L. et WEIL, L., «Irradiations neutroniques à 78°K de graphites polycristallins», these Proceedings, section C.2.

[12] PLUCHERY, M., «Mesures de paramètres de graphite industriel irradié dans l'azote liquide», these Proceedings, section C.2.

[13] WOODS, W.K., BUPP, L.P. and FLETCHER, J.F., Proc. UN Int. Conf. Peaceful Uses of Atomic Energy, 7 (1960) 455.

[14] SIMMONS, J.H.W. and REYNOLDS, W.N., Proc. of the 5th Carbon Conf., 1961 (MROZOWSKI et al., Eds.) Pergamon Press, Oxford (1962).

[15] FITZER, E. and VOHLER, O., "The behaviour of various graphites under neutron irradiation", these Proceedings, section C.2.

[16] YOSHIKAWA, H.H., WOODRUFF, E.M., DAVISDON, J.M., HELM, J.W. and NIGHTINGALE, R.E., "Radiation effects in carbons and graphites", these Proceedings, section C.2.

[17] GAIN, R., "Comparison of irradiation damage in artificial and natural graphite at different irradiation temperatures", these Proceedings, section C.2.

[18] SIMMONS, J.H.W. and REYNOLDS, W.N., Proc. of Symposium on Uranium and Graphite. Institute of Metals, 1962. (In course of publication).

[19] KINCHIN, G.H., Report CRNE-539 (1953).

[20] REYNOLDS, W.N. and THROWER, P.A. (To be published).

[21] RAPPENEAU, J., FILLATRE, A., MICAUD, G. et QUETIER, M., «Evolution des propriétés physiques du graphite sous l'effet d'irradiations et de recuits successifs», these Proceedings, section C.2.

PANEL DISCUSSION

Chairman: W. KOSIBA

Moderator: J.H.W. SIMMONS

Presentation by J.H.W. Simmons of the foregoing survey paper.

Short presentations* by G. Perriot, L. Bochirol and M. Pluchery respectively of:

BLONS, J., PERRIOT. G. et TOURAND, G.: Étude comparative des effets des neutrons rapides sur le graphite monocristallin et le graphite nucléaire.

BOCHIROL, L., BONJOUR, E. et WEIL, L.; Irradiations neutroniques à 78°K de graphites polycristallins.

PLUCHERY, M.: Mesures de paramètres de graphite industriel irradié dans l'azote liquide.

B.G. CHILDS: I would like to ask Mr. Simmons whether he considers that the increasing understanding of the details of radiation damage mechanisms in graphite is leading to the possibility of controlling technologically important changes in the material.

J.H.W. SIMMONS: Yes, I think that there is a very strong possibility that it will be possible to control dimensional changes in this way. It is believed that the dimensional changes are closely related to the thermal expansion of graphite and I think that it may be possible to specify certain conditions for good behaviour as far as dimensional changes are concerned. In the case of other properties of graphite, for example the thermal conductivity and stored energy, I think it is rather unlikely that very much control can be obtained. Very little is known about the mechanical properties and there are no developments recently which would help us to any theoretical model when improving the chemical properties.

M.S. WECHSLER: Mr. Simmons mentioned the use of the nickel flux in correlating effects in various reactors of quite different natures - graphite-moderated, heavy-water and light-water-moderated reactors. I wish to ask if this approach is likely to lead to difficulties, inasmuch as the threshold energy for nickel is above 3 MeV and therefore the use of nickel yields no information concerning the population of neutrons below this energy.

J.H.W. SIMMONS: We have collected together some measurements of the rate at which damage occurs in these various reactors as compared with the rate at which nickel is activated, and we have tabulated the ratio of the damage rate to the nickel flux. The nickel flux does not give a direct indication of the damage; for example, for a given value of the nickel dose the damage rate in the heavy-water reactor is only half that in a graphite reactor and in the light-water reactor only 0.39. The point is that we now have a tabulation of these factors for practically the whole range of spectra which exists in reactors. With this tabulation we can use nickel as an indicator of damage.

---

* For full text, see section C.2.

Short presentations by B.S. Gray and W.N. Reynolds respectively of:*

BRIDGE, H., GRAY, B.S., KELLY, B.T. and SØRENSEN, H.: An effect of flux level and flux spectrum on the accumulation of damage in reactor-irradiated graphites.

REYNOLDS, W.N. and THROWER, P.A.: Irradiation damage in graphite.

E.W.J. MITCHELL: Dr. Reynolds mentioned that he had obtained the activation energy of 1.2 eV for the motion of a defect which leads to the build-up of the things seen in the electron microscope. If one accepts the view that single interstitials move with a much lower energy than 1.2 eV and single vacancies much higher, it is possible that the 1.2 eV corresponds to the motion of an interstitial carbon complex. It could also be the energy corresponding to the release of a single interstitial from an impurity trap. I am not clear how Dr. Reynolds has decided between these two possibilities.

I would also like to make a comment on Dr. Perriot's paper. We also have found that electron irradiation, with the rates of increase of resistivity of single crystals at liquid-nitrogen temperature, were greater than those of polycrystalline graphite. We are now irradiating at liquid-helium temperature but do not yet have any results to report.

W.N. REYNOLDS: It is quite true that we have not considered very much the impurities of our results, but I did emphasize that the results were taken from a large number of specimens and that the defects were observed uniformly distributed. This fact, together with the observed temperature-dependence, leads us to a homogeneous nucleation theory and what we have calculated is in fact the diffusion coefficient. We have interpreted this apparent diffusion coefficient in terms of an activation energy. The important point is that this activation energy is consistent over a wide range of conditions and agrees with the results obtained from microscopic effects on commercial graphites. We therefore think that it corresponds to the motion of some particular kind of defect. As we cannot identify this defect, either with a single interstitial or a single vacancy, and as it is generally supposed that defects are fairly simple in graphite, we suggest that it corresponds to the motion of a small group of interstitials.

A.T. CHURCHMAN: Dr. Reynolds said that his interpretation disagreed with that of Dr. Williamson. I should like to say that Dr. Williamson now takes the view that stored energy in graphite is due to much smaller defects than those observed in the electron microscope, and I would like to show a slide of some X-ray scattering taken by Dr. Eales of the Berkeley Laboratories which shows the change to low-angle scattering after irradiation to 2×10^{20} nvt (fast) at 150°C and shows the effects of annealing.

Dr. Eales interprets the change to low-angle scattering as due to interstitial groups of only 10-Å diameter. Even loops of this size do not contribute to the main stored energy peak as they do not disappear until vacancies move at greater than 1000°C; annealing at 860°C produces no change. The only change in low-angle scattering corresponding to the Wigner stored-energy peak at 200°C is a slight change in that part of the X-ray scattering corresponding to clusters of two or three atoms only. This is thus further support for the suggestion that the technological changes are due to the migration of clusters of two to four atoms.

* For full text, see section C.2

W.N. REYNOLDS: At the Berkeley conference* last year, Dr. Williamson reported two kinds of clusters - very large circular loops and small defects which correspond to the ones which we have shown today. He suggested that the smaller loops were vacancy clusters; we are saying that they must be interstitial clusters.

A.T. CHURCHMAN: I think Dr. Williamson would say now that the small visible defects could be vacancies or interstitials and that he could not prove which they were. I am suggesting that you cannot prove that they are interstitials either. The large loops were proved to be interstitials by contrasting effects inside the loops.

W.N. REYNOLDS: I would like to show another slide which is an electron micrograph with loops similar to those shown by Dr. Williamson. The difference is that we happen to have some Moiré fringes across the loops; the Moiré fringes are displaced as they move into the circle by exactly one fringe. We found it very difficult to square the interpretation of this with the interpretation suggested by Dr. Williamson that such loops are interstitial loops. We think that this is possibly a surface phenomenon.

At Berkeley last year, Dr. Williamson did suggest that the small defects must be vacancy loops; he was talking then about defects obtained by radiation in the 150 - 300°C range. Obviously, there is a lot more work to be done yet, but I really wanted to point out that our interpretation is different and, in some ways, in conflict with those which have been put forward elsewhere.

M.S. WECHSLER: I am compelled to raise the question again of the use of nickel as a flux monitor when comparisons are being made of effects in reactor locations where the flux spectra are quite different. As was mentioned earlier, the use of nickel yields information of the integral neutron flux above a threshold energy of about 3 MeV and thus, on the basis of the nickel measurements alone, nothing can be said about the damaging effect of neutrons below this energy.

I should also like to ask if consideration has been given to the burn-out of the Co^{58} which is produced by the $Ni^{58}(n, p)Co^{58}$ reaction due to the high neutron cross-section of Co^{58}. As has been pointed out by Passel and Heath, serious errors can result under appropriate circumstances if this factor is ignored.

J.H.W. SIMMONS: The damage flux measurements were carried out at low flux so that this correction is not important. When carrying out experiments at high flux, the correction is made, not by calculation, but by a careful series of calibrations. I think it would probably take us too far away from this discussion to go into this; I think it is dealt with a little more fully perhaps in other places.

The answer to the first question is that the nickel flux does not give you the damage because the rate of damage can vary from one reactor to another for a given nickel flux. Without the damage flux calibrations the nickel flux would be useless.

H. H. YOSHIKAWA: The procedure outlined by Mr. Simmons is prob-

---

* International Conference on Properties of Reactor Materials and the Effects of Radiation Damage, Berkeley, Glos., England, 1961 (Proceedings published by Butterworths, London, 1962)

ably quite satisfactory for existing reactors. How would he propose to apply it to reactors which are under construction or in the planning stage?

J.H.W. SIMMONS: The answer to this may be found in the paper to be presented by Dr. Wright+ . He has shown how to calculate the spectra in various reactor positions using a Monte Carlo method. For a future reactor we calculate a spectrum and use a weighting factor to calculate the damage flux. The form of the weighting factor has been justified experimentally as described in Dr. Wright's paper.

R. GAIN: There is reason to believe that most of the radiation damage in graphite is caused by neutrons having an energy above 0.1 MeV. Would it not be better to use a flux monitor with a lower threshold, for example U^{238} ?

S.B. WRIGHT: Our attitude to dose-monitoring experimental irradiations is to use the simplest technique available and to calculate or measure experimentally the correction required to give damage dose. The use of monitors with a lower threshold, such as the Rh(n, n') reaction, introduce a lot of experimental difficulties.

I would like to say in answer to a point raised earlier that the doses we obtain from the irradiation of nickel and the correction for the thermal burn-up of the Co^{58} and Co^{58m} agree very well with calculations of the nickel activation flux from measurements of thermal flux and subsequent calculation of the nickel flux from determinations of the fast-to-thermal flux ratios measured at a flux level for which the Co^{58} burn-up is negligible.

Short presentation* by H.H. Yoshikawa of:

YOSHIKAWA, H.H., WOODRUFF, E.M., DAVIDSON, J.M., HELM, J.W. and NIGHTINGALE, R.E.: Radiation effects in carbons and graphites.

W.N. Reynolds described results obtained for dimensional changes and showed electron micrographs of nuclear graphite taken by a replica method before and after irradiation. The micrographs showed the closure of cracks due to expansion of the crystallites. This closure is related to changes in thermal expansion and to some features of the dimensional changes.

Short presentations* by O. Vohler, R. Gain, J. Rappeneau and P. de Meester respectively of:

FITZER, E. and VOHLER, O.: The behaviour of various graphites under neutron irradiation.

GAIN, R.: Comparison of irradiation damage in artificial and natural graphite at different irradiation temperatures.

RAPPENEAU, J., FILLATRE, A., MICAUD, G. and QUETIER, M.: Évolution des propriétés physiques de graphite sous l'effet d'irradiations et de recuits successifs.

WILLIS, A.H. and PENNINCKX, R.: The effect of heavy-particle bombardment on Wigner-energy storage in graphite.

P. de MEESTER: In our laboratory we have observed, with irradiated and stressed graphite, that there is an inelastic effect recoverable by anneal-

---

+ WRIGHT, S.B., "The use of Monte Carlo calculations in the analysis of radiation damage experiments" Radiation Damage in Solids II, IAEA, Vienna (1962) 239-252.

* For full text, see section C.2.

ing at 300 -400°C. Can this be related to the curve of bend strength given in Dr. Gain's paper?

R. GAIN: We have not yet done annealing studies, so I cannot comment on this.

J.H.W. SIMMONS: L'effet précoce described by Dr. Rappeneau presents a problem of interpretation which will be a sensitive test of radiation damage theories.

I would also like to comment on the paper by Drs. Willis and Penninckx. It is interesting that the same type of damage is obtained with different types of particle. Perhaps at high temperatures, where vacancy migration becomes important, differences may be found.

C. RADIATION DAMAGE IN GRAPHITE

2. Full text of papers

ÉTUDE COMPARATIVE DES EFFETS DES NEUTRONS RAPIDES SUR LE GRAPHITE MONOCRISTALLIN ET LE GRAPHITE NUCLÉAIRE

J. BLONS, G. PERRIOT ET G. TOURAND
CENTRE D'ÉTUDES NUCLÉAIRES DE SACLAY,
GIF-SUR-YVETTE (S.& O.), FRANCE

Abstract — Résumé — Аннотация — Resumen

A COMPARATIVE STUDY OF THE EFFECTS OF FAST NEUTRONS ON MONOCRYSTALLINE AND ON NUCLEAR GRAPHITE. Samples of nuclear graphite and natural monocrystalline graphite were irradiated in the same position in a reactor and the changes in resistivity measured. By studying the elimination of this change in resistivity we were able to determine the contribution of the non-graphited part to the changes in the physical properties of nuclear graphite as observed in reactors.

ÉTUDE COMPARATIVE DES EFFETS DES NEUTRONS RAPIDES SUR LE GRAPHITE MONOCRISTALLIN ET LE GRAPHITE NUCLÉAIRE. On a irradié dans un même emplacement de pile des échantillons de graphite nucléaire et de graphite monocristallin naturel et l'on a mesuré les variations de résistivité obtenues. L'étude de la guérison de cette variation de résistivité a permis de déterminer quelle est la contribution de la partie non graphitée aux variations des propriétés physiques de graphite nucléaire observées dans les piles.

СРАВНИТЕЛЬНОЕ ИССЛЕДОВАНИЕ ВОЗДЕЙСТВИЯ БЫСТРЫХ НЕЙТРОНОВ НА МОНОКРИСТАЛЛИЧЕСКИЙ ГРАФИТ И ЯДЕРНЫЙ ГРАФИТ. В одном и том же месте реактора были облучены образцы ядерного графита и естественного монокристаллического графита и измерены изменения удельного сопротивления. Исследование изменения удельного сопротивления дало возможность определить, какое воздействие оказывает та часть реактора, где отсутствует графит, на наблюдаемые в реакторах изменения физических свойств ядерного графита.

ESTUDIO COMPARATIVO DE LOS EFECTOS DE LOS NEUTRONES RAPIDOS SOBRE EL GRAFITO MONOCRISTALINO Y SOBRE EL GRAFITO NUCLEAR. Los autores han irradiado en una misma posición del reactor, muestras de grafito nuclear y de grafito monocristalino natural y han medido las variaciones de la resistividad consiguientes. El estudio de la recuperación de estas variaciones ha permitido determinar la contribución de la parte no grafitada a las alteraciones de las propiedades físicas del grafito nuclear observadas en los reactores.

I. INTRODUCTION

Un problème de physique important et non dépourvu d'intérêt pour les neutroniciens est de savoir si les variations des propriétés physiques du graphite polycristallin observées sous l'effet du bombardement neutronique sont liées aux propriétés intrinsèques des grains cristallins ou dépendent des «caprices» des joints qui lient ces grains.

En 1949, BOWEN [1, 2] a affirmé que la conductivité du polycristal était due uniquement aux monocristaux présents et a calculé théoriquement la variation de résistivité d'un polycristal en fonction de la température. Pour cela, il a émis deux hypothèses.

La première est que la conduction d'un échantillon polycristallin se fait par les plans de clivage des monocristaux. Les différences de con-

ductivité ($\approx 10^4$) font qu'aucune conduction appréciable n'a lieu à travers les plans. Comme le courant doit suivre les plans cristallins et que ceux-ci ne coïncident pas en général avec la direction du champ éléctrique appliqué, il en résulte un accroissement de la résistivité du matériau polycristallin qui est alors égale à celle du monocristal dans le plan de clivage multipliée par un certain facteur géométrique. Ce facteur dépend des dimensions des cristaux et de leur orientation par rapport au champ.

La deuxième hypothèse de Bowen est que les ondes électroniques ne sont pas diffusées dans les joints des cristaux, c'est-à-dire qu'il n'y a pas de résistance de contact entre ces cristaux.

En partant de ces hypothèses, BOWEN a également expliqué le phénomène de saturation de l'accroissement de résistivité dû aux neutrons apparaissant aux doses élevées. Il a enfin prévu [3] que l'accroissement de résistivité des graphites mono et polycristallins avait un coefficient de température négatif dont la valeur absolue à une température donnée variait avec la dose de neutrons en passant par un minimum situé vers les faibles doses.

Les expériences que nous avons réalisées en irradiant des monocristaux de graphite et des échantillons polycristallins montrent l'identité des défauts créés dans les deux types de graphite et confirment l'existence, dans tous les cas, d'un coefficient de température négatif de l'accroissement de résistivité qui, d'autre part, décroît quand la dose augmente (très faibles doses).

Cette communication ne contient que les résultats préliminaires, non encore parfaitement élaborés, d'une étude entreprise très récemment. Ils ne sont évidemment que très fragmentaires et ne prétendent donc pas apporter de solution définitive aux problèmes physiques qu'ils ont soulevés.

II. TECHNIQUES EXPÉRIMENTALES

Les monocristaux étudiés ont été patiemment et méticuleusement découpés à la lame de rasoir dans des échantillons d'environ 1 cm^2 obtenus par clivage de blocs de graphite naturel incrustés dans une roche de quartz. Ils ont la forme représentée à la figure 1, à savoir deux arrivées de courant A et B et deux prises de tension C et D. Les contacts électriques sont pris aux quatre extrémités A, B, C, D à l'aide de fils de tungstène scellés sur le graphite à l'aide d'Aquadag (solution colloïdale de carbone). La résistance électrique mesurée est ainsi définie entre M et N dans le cristal lui-même. Le monocristal est fixé sur quatre supports de tungstène dans une ampoule en quartz à quatre passages étanches. Avant irradiation, le cristal est chauffé à haute température (~3000°C) sous vide dynamique ($\approx 5 \cdot 10^{-6}$ mm/Hg) par passage de courant. Quand le dégazage parfait de l'ampoule et de son contenu est réalisé, celle-ci est scellée sous le même vide que précédemment. La figure 1 montre une photo d'une ampoule contenant un monocristal.

La mesure de la résistance électrique est effectuée par comparaison à une résistance étalon, par une méthode d'opposition classique à l'aide d'un potentiomètre «Cambridge» du type «Microstep». La guérison après irradiation est effectuée par passage de courant en affichant, à l'aide d'un

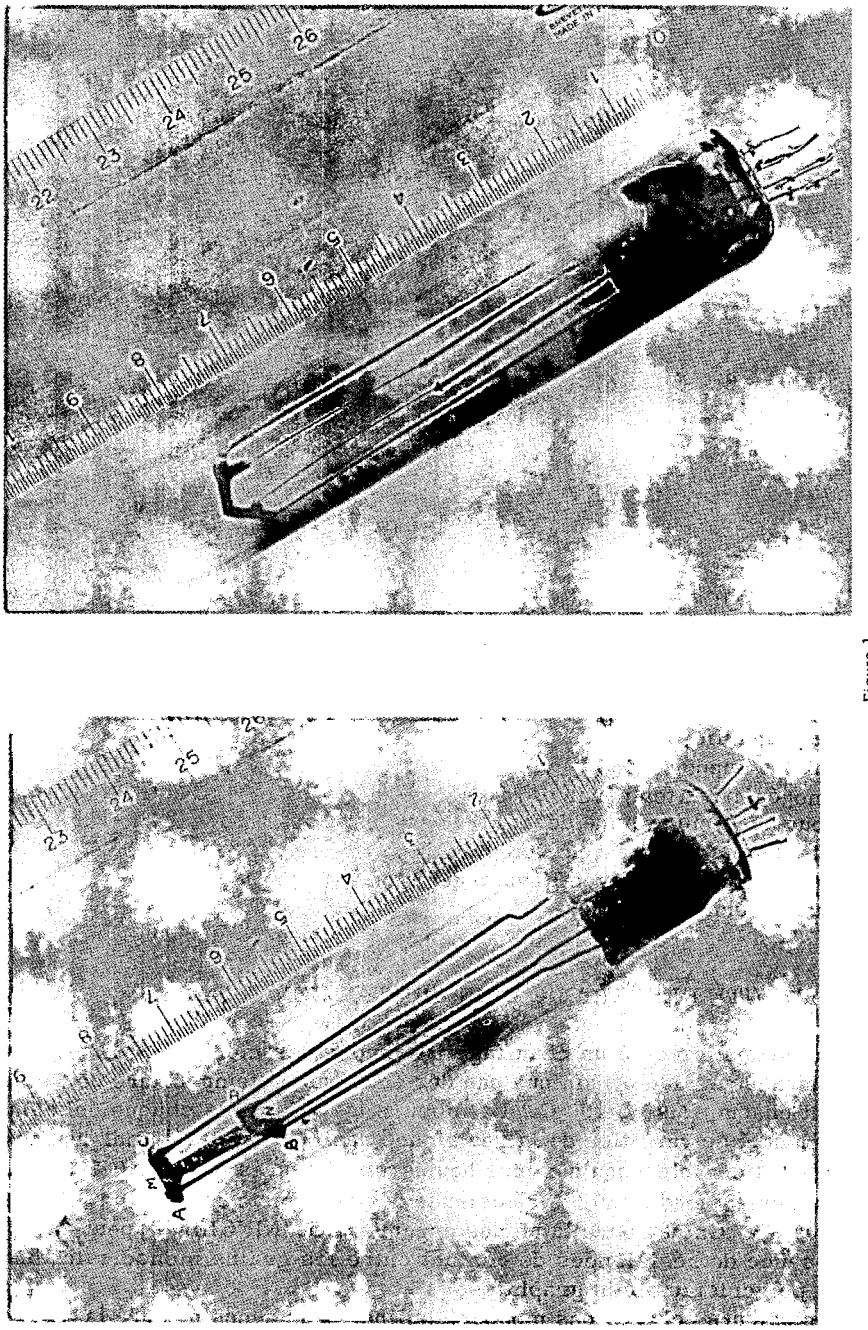


Figure 1

Ampoules contenant un monocristal.

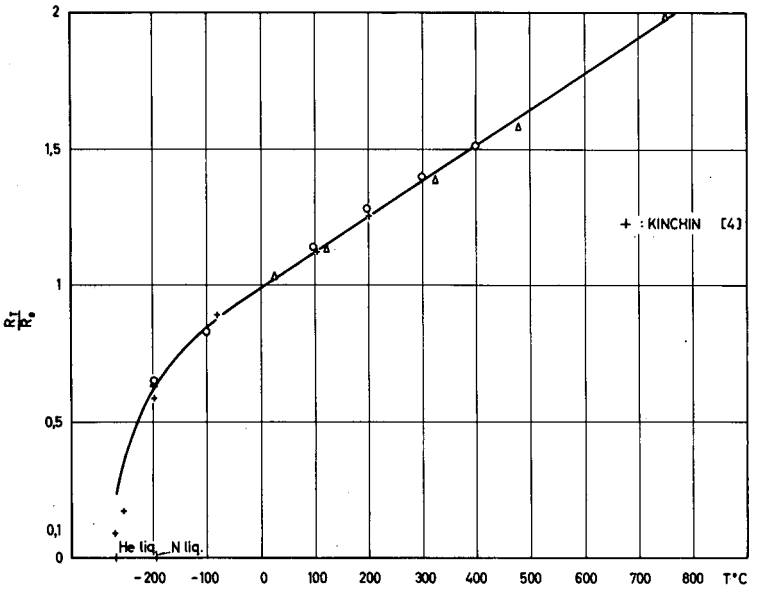


Figure 2

Résistivité du graphite monocristallin.

pont de Thomson, la résistance prévue à la température voulue. Le monocristal est chauffé, l'ampoule étant plongée dans l'azote liquide. Les dimensions des supports de tungstène sont adaptées à chaque échantillon pour que l'homogénéité de température le long du cristal soit parfaite. Les courants admis pour une température de 3000°C peuvent atteindre 15 A.

La technique adaptée aux polycristaux est exactement la même que celle des monocristaux, avec l'avantage qu'on peut les préparer industriellement sous la forme qu'on veut.

III. RÉSISTIVITÉ ÉLECTRIQUE D'UN CRISTAL NON IRRADIÉ

Nous avons effectué un chauffage isochrone des monocristaux et des polycristaux sous vide dynamique par des échelons de température de 5 min croissant chaque fois de 100°C. La mesure à 22°C après chaque échelon n'a pas montré de variation de la résistance des monocristaux malgré leur dégazage considérable jusqu'aux plus hautes températures obtenues (~2800°C). Dans les mêmes conditions, la résistance des polycristaux n'a jamais décru au-delà de 6%. On retrouve là un des arguments de KINCHIN [4] pour justifier l'absence de résistances de contact entre les grains monocristallins dans les polycristaux bien graphités.

Sur plusieurs échantillons monocristallins, nous avons mesuré la variation de résistance en fonction de la température. Nous avons porté la variation du rapport de la résistance à T°C à la résistance à 0°C sur la figure 2.

Sur cette même figure, nous avons porté les valeurs expérimentales obtenues par KINCHIN [4]. Nous constaterons seulement que les valeurs qu'il a obtenues aux basses températures sont plus faibles que les nôtres.

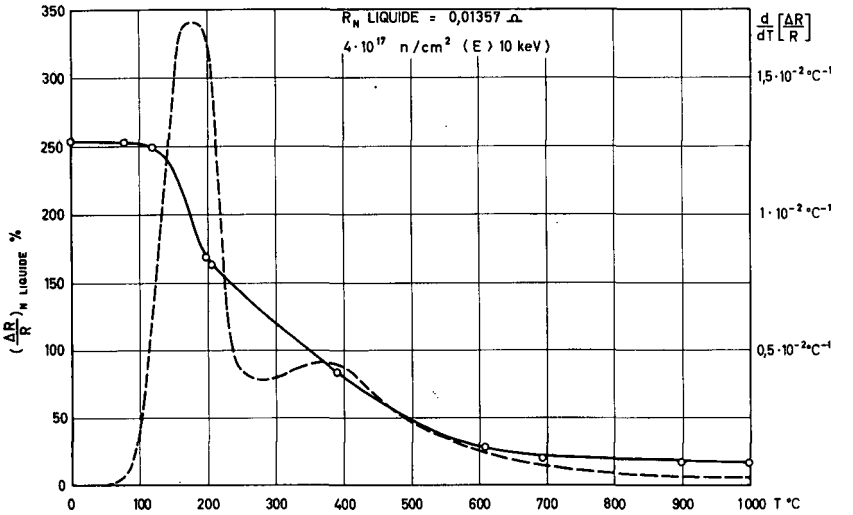


Figure 3

Guérison d'un monocristal irradié à -80°C.

IV. DÉFAUTS CRÉÉS DANS LE GRAPHITE IRRADIÉ

La figure 3 représente la courbe de guérison isochrone, et sa dérivée, d'un monocristal de graphite irradié vers 80°C à une dose voisine de $4 \cdot 10^{17}$ n/cm² (neutrons d'énergie E> 10 keV). L'accroissement global de résistivité $\Delta R/R$ est exprimé en % et égal à 252,25% mesuré à la température de l'azote liquide. Pendant la même irradiation et au même endroit, un échantillon polycristallin a donné une variation égale à 12,60% mesurée dans l'azote liquide. La vitesse de guérison était approximativement égale à 1°/min. Pratiquement, nous avons dû effectuer des corrections de température après chaque échelon, ceci étant dû au fait que nous ne connaissions pas bien au préalable la loi de variation de ΔR avec la température. On retrouve le pic de guérison bien connu du graphite polycristallin vers 170°C. Il semble également qu'il apparaisse un stade vers 360°C. Nous n'avons pu poursuivre la guérison de cet échantillon au-delà de 1000°C du fait de la rupture des supports.

La figure 4 représente la courbe de guérison isochrone, et sa dérivée, d'un monocristal irradié dans l'azote liquide à une dose voisine de $4 \cdot 10^{16}$n/cm² (neutrons d'énergie E > 10 keV). La variation globale $\Delta R/R$ mesurée dans l'azote liquide, égale à 154%, est donc relativement beaucoup plus importante que dans le cas d'une irradiation à 80°C. La vitesse de guérison est approximativement égale à 1°/min, mais nous avons encore dû effectuer

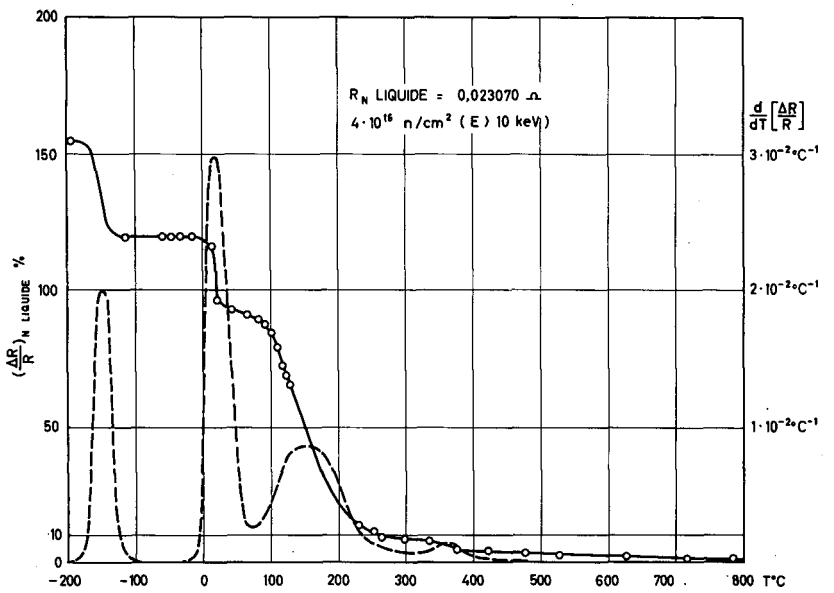


Figure 4

Guérison d'un monocristal irradié dans l'azote liquide.

des corrections de température après chaque échelon du fait de l'incertitude que nous avions sur la variation de ΔR avec la température. On reconnaît encore l'existence du pic classique de guérison vers 170°C; ce stade de guérison est d'ailleurs certainement réduit dans les irradiations aux températures de piles. Mais surtout, on retiendra l'existence d'un stade de guérison très important vers + 20°C qui n'apparaît évidemment jamais ordinairement. Enfin, il en existe un autre vers -150° C qui commence très certainement aux températures inférieures à -196°C.

La figure 5 contient, à une échelle plus dilatée pour les ordonnées, la suite de la guérison isochrone du même échantillon irradié dans l'azote liquide. On retrouve, entre 1100°C et 1400°C, l'accroissement de l'excès de résistivité ΔR trouvé par BOWEN [5] dans les différents types de graphite polycristallin. Ce nouveau type de défaut créé sous l'effet de l'augmentation de température est ensuite totalement guéri à 2400°C. Nous avons reproduit, sur la figure 6, une courbe de guérison d'un graphite polycristallin extraite du rapport de BOWEN [5] . On constatera ainsi la ressemblance existant entre les courbes de guérison respectives des graphites monocristallins et polycristallins.

Le peu de résultats expérimentaux que nous possédons ne nous permet pas de faire des hypothèses quant à la nature des défauts responsables des effets observés dans le graphite monocristallin. Nous rappellerons seulement que dans l'intervalle compris entre 100°C et 800°C, BOWEN [5] à calculé une réaction d'ordre 6 avec une énergie d'activation comprise entre 1,27 et 1,72 eV, dans l'intervalle compris entre 1100 et 1400°C une réaction d'ordre 1 avec une énergie d'activation de l'ordre de 2,5 eV et dans l'inter-

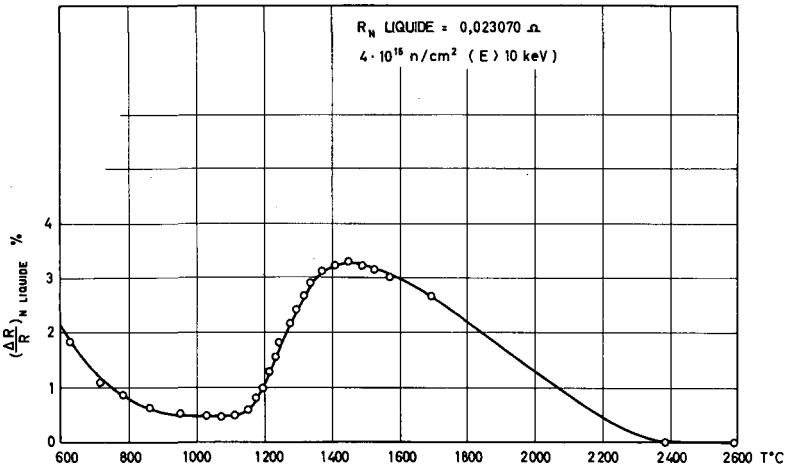


Figure 5

Guérison d'un monocristal irradié dans l'azote liquide.

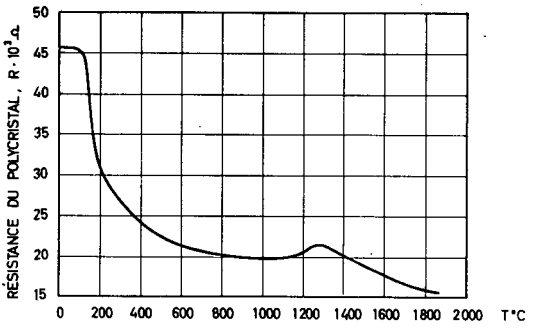


Figure 6

Guérison d'un polycristal irradié.

valle compris entre 1400 et 2400°C une réaction d'ordre 4 avec une énergie d'activation comprise entre 4,35 et 5,22 eV.

V. VARIATION DE LA RÉSISTIVITÉ DU GRAPHITE IRRADIÉ AVEC LA TEMPÉRATURE

Nous avons reporté sur la figure 7 les variations de l'excès de résistivité ΔR en fonction des températures inférieures à la température de début de guérison. En réalité, ΔR_T étant la variation à T°C et ΔR_0 étant celle à 0°C, nous avons tracé les courbes $\Delta R_T/\Delta R_0 = f(T)$.

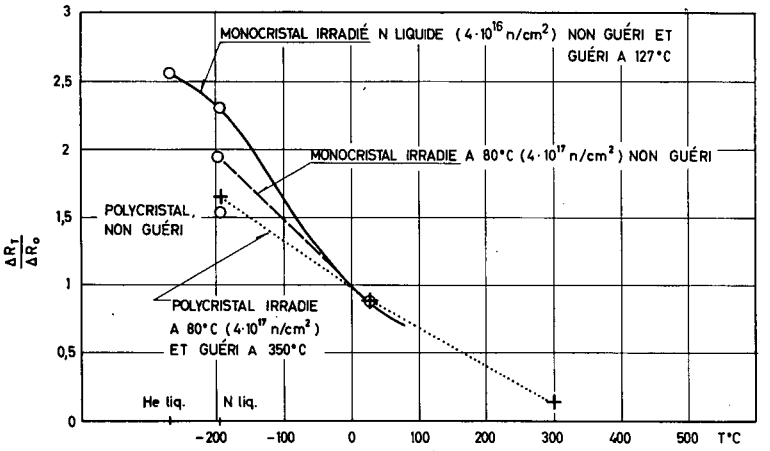


Figure 7

Variation de la résistivité avec la température.

La courbe en trait plein concerne le monocristal irradié dans l'azote liquide à une dose de $4 \cdot 10^{16} n/cm^2$. On a mesuré les rapports $\Delta R_{He}/\Delta R_N$ des variations dans l'hélium liquide et dans l'azote liquide avant toute guérison et après guérison à 100°C. Les deux rapports ont la même valeur (aux erreurs d'expérience près), ce qui semble indiquer que l'absence des deux premiers stades de guérison ne modifie pas la loi de variation. Après guérison à 100°C, nous avons effectué la mesure $\Delta R_T/\Delta R_0$ jusqu'à 27°C, ce qui nous a permis de tracer la courbe jusqu'à cette température. Nous n'avons pas couru le risque de détruire l'ampoule en effectuant des mesures à température plus élevée.

La courbe en traits interrompus concerne le monocristal irradié à la température de 80°C à une dose de $4 \cdot 10^{17} n/cm^2$. Nous n'avons effectué des mesures que de l'azote liquide à 27°C. On constate qu'à cette dose dix fois plus élevée, le coefficient de température est plus faible, confirmant les résultats de BOWEN [3] .

La courbe en pointillés concerne un échantillon de graphite polycristallin irradié à 80°C à une dose de $4 \cdot 10^{17} n/cm^2$ et guéri à 350°C. Le point (⊕) situé en dessous de celui qui correspond à l'azote liquide a été obtenu avant toute guérison. Il est donc difficile de conclure que la disparition d'un stade de guérison n'a pas perturbé la loi de variation avec la température.

VI. CONCLUSION

A la suite de ces expériences non encore parfaitement élaborées, nous nous contenterons de constater les analogies existant dans le comportement des défauts créés respectivement dans le graphite monocristallin et le graphite polycristallin. Ceci laisse donc présager que seuls les grains monocristallins sont à la base de nombreuses propriétés des graphites polycristallins irradiés ou non irradiés.

RÉFÉRENCES

[1] BOWEN, D., Theory of Electrical Resistivity of Polycrystalline Graphite, Phys. Rev. 76 12 (1949) 1875.
[2] BOWEN, D., The Electrical Conductivity of Irradiated Graphite, Part I, NAA – SR – 33 (1949).
[3] BOWEN, D., The Electrical Conductivity of Irradiated Graphite, Part II, NAA – SR – 39 (1950).
[4] KINCHIN, G. H., The Electrical Properties of Graphite, Proc. Ray. Soc. 217 A (1953) 9.
[5] BOWEN, D., On the Mechanism of Thermal Annealing of Irradiated Graphite, NAA – SR – 41 (1950).

IRRADIATIONS NEUTRONIQUES A 78°K DE GRAPHITES POLYCRISTALLINS

L. BOCHIROL, E. BONJOUR ET L. WEIL
CENTRE D'ÉTUDES NUCLÉAIRES DE GRENOBLE, FRANCE

Abstract — Résumé — Аннотация — Resumen

NEUTRON IRRADIATIONS OF POLYCRYSTALLINE GRAPHITE AT 78°K. Much experimental work has been devoted to the behaviour of graphite under irradiation, and a considerable amount of information is now available for reactor technology applications.

Relatively little is known, however, about the basic damage mechanisms, since most studies have been concerned with irradiation at laboratory temperature ranges, at which the defects occurring are very complicated.

To throw light on the basic processes, the graphite needs to be irradiated at low temperature, so that no incipient annealing can occur and only relatively simple defects are retained.

The authors accordingly irradiated crystalline graphite from various sources at the set temperature of 78°K in the MELUSINE reactor at the Grenoble Nuclear Research Centre.

The paper gives the first results.

IRRADIATIONS NEUTRONIQUES A 78°K DE GRAPHITES POLYCRISTALLINS. Le comportement du graphite soumis à l'irradiation a fait l'objet d'un grand nombre d'expériences. A l'heure actuelle, on dispose de nombreux renseignements susceptibles d'être utilisés en technologie des réacteurs.

Toutefois, les mécanismes fondamentaux de création des dommages sont relativement peu connus car la plupart des études a porté sur des irradiations réalisées à des températures voisines de celle du laboratoire, température à laquelle les défauts créés sont très complexes.

Pour saisir les processus de base, il y a intérêt à irradier le graphite à basse température de manière qu'aucun début de recuit ne puisse se produire et de ne conserver ainsi que des défauts relativement simples.

C'est dans ce but que les auteurs ont irradiés des graphites cristallins d'origines diverses, à la température fixe de 78°K, dans la pile MÉLUSINE du Centre d'études nucléaires de Grenoble.

Ils présentent les premiers résultats obtenus.

НЕЙТРОННОЕ ОБЛУЧЕНИЕ ПОЛИКРИСТАЛЛИЧЕСКОГО ГРАФИТА ПРИ ТЕМПЕРАТУРЕ 78°К. Свойства графита, подвергнутого облучению, являются предметом многочисленных экспериментов. В настоящее время имеется множество сведений о его использовании в технологии реактора.

Однако основные механизмы возникновения повреждений сравнительно мало известны, так как большая часть опытов касалась облучения, проведенного при температуре, близкой к лабораторной температуре, при которой созданные дефекты являются очень сложными.

Чтобы понять основные процессы, представляется интересным облучить графит при низкой температуре для того, чтобы не происходил никакой начальный отжиг и чтобы сохранить только относительно простые повреждения.

Именно в этих целях авторы облучили кристаллический графит различного происхождения при фиксированной температуре 78°К в реакторе MELUSINE. Исследовательского ядерного центра Гренобля.

Авторы показывают первые достигнутые результаты.

IRRADIACIÓN NEUTRÓNICA DE GRAFITOS POLICRISTALINOS A 78°K. Las alteraciones que la irradiación provoca en el grafito han sido objeto de gran número de trabajos experimentales y actualmente se dispone de numerosos datos de interés para la tecnología de los reactores.

No obstante, los mecanismos fundamentales de formación de los daños son relativamente poco conocidos, porque la mayor parte de los estudios se ha referido a irradiaciones realizadas a temperaturas próximas a las de laboratorio, a las cuales los daños que se producen son muy complejos.

Para comprender los procesos básicos, conviene irradiar el grafito a baja temperatura, a fin de evitar que se inicie el recocido y no se conserven más que defectos relativamente sencillos.

Con este fin, los autores han irradiado grafitos cristalinos de diversos orígenes a la temperatura fija de 78°K en el reactor MELUSINE del Centre d'études nucléaires de Grenoble.

La memoria presenta los primeros resultados obtenidos.

INTRODUCTION

Le nombre de travaux consacrés aux effets des rayonnements sur les graphites est considérable, et il n'est probablement pas de matériau qui ait été aussi largement étudié à ce point de vue.

L'utilisation des graphites, par milliers de tonnes, dans la construction des réacteurs comme modérateur ou réflecteur, et aussi les importantes modifications de propriétés physiques qu'ils subissent par irradiation, expliquent que l'on se soit efforcé de rassembler le plus possible de renseignements à ce sujet. On constate cependant que malgré l'énorme masse de données expérimentales dont on dispose, on connaît encore relativement peu de choses sur les mécanismes fondamentaux de création des dommages dans le graphite.

Parmi les raisons qui peuvent expliquer la difficulté de dégager des lois générales, il en est une qui tient à la nature même des matériaux étudiés : les graphites industriels sont très dissemblables les uns des autres suivant les matières de base et les techniques utilisées pour leur élaboration. D'autre part, la majorité des irradiations ont été effectuées à des températures susceptibles de donner des renseignements technologiques immédiatement utilisables, c'est-à-dire qu'elles concernent des températures plus ou moins supérieures à la température ambiante, où les défauts créés sont probablement plus complexes.

L'intérêt d'effectuer des irradiations à basse température n'avait bien entendu pas échappé : en se plaçant dans des conditions telles qu'aucun début de recuit ne puisse se produire en cours d'irradiation, on peut espérer ne conserver que des défauts primaires relativement simples, et saisir ainsi des mécanismes élémentaires d'endommagement. La publication de HOVE [1] résume des études effectuées dans cet esprit, en particulier par « Atomics International ». Il rappelle, entre autres, des expériences d'irradiations de graphites par des électrons, à 4°K, après lesquelles on a observé les variations de l'accroissement de résistivité résultant en fonction de la température; il est apparu que ces variations ne sont pas sensibles en-dessous de 80°K.

On peut donc penser que pour les graphites, le maintien de la température en cours d'irradiation au niveau de celle de l'azote liquide suffit pour conserver intégralement les défauts primaires et permet d'étudier ensuite leur cinétique de disparition ou d'évolution en fonction du réchauffement.

C'est dans cet esprit que des irradiations neutroniques avaient été effectuées à Brookhaven ; cependant, le dispositif cryogénique utilisé ne permettait pas d'éviter des fluctuations assez importantes (entre 78 et 125°K) de la température des échantillons qui intervenaient au cours même de l'irradiation et dans une zone de températures particulièrement critique comme on vient de le voir.

Nous disposons dans la pile « MELUSINE » du Centre d'études nucléaires de Grenoble d'installations cryogéniques [2], permettant à la fois des irradiations de longue durée à la température fixe de 78°K, et une récupération

aisée, sans réchauffage, des échantillons irradiés. Nous avons entrepris d'irradier dans ces conditions des graphites polycristallins d'origines diverses pour tenter de dégager quelques lois générales de comportement qu'il paraît moins difficile d'atteindre au cours d'irradiations à basse température. Cette communication présente les premiers résultats que nous avons obtenus.

I. GRAPHITES ÉTUDIÉS

Nos premières études ont pour objet deux catégories de matériaux : les graphites industriels classiques et les graphites naturels agglomérés.

1. Graphites industriels classiques

Ils ont été choisis comme représentant des graphites bien connus et largement utilisés par exemple dans la construction des réacteurs G2 et G3.

La matière de corps principale est pour tous du coke de pétrole ; la mise en forme a été effectuée par filage et il a été procédé à une imprégnation au brai entre cuisson et graphitation finale. Les différences entre eux portent sur l'origine du coke et l'addition, dans un des cas, de noir de carbone (10%) dans la pâte brai-coke.

Leurs caractéristiques d'identification sont :

- graphite «A» 16360 Coke «L» + noir de carbone, densité apparente typique 1, 78,
- graphite «B» 11400 Coke «L», densité apparente typique 1, 66,
- graphite «C» 11192 Coke «S», densité apparente typique 1, 72.

Les échantillons (cylindres: ϕ 4, 6 - longueur : 50 mm) ont été prélevés avec leur axe perpendiculaire à l'axe de filage des produits bruts.

2. Graphites naturels agglomérés

Ils représentent un matériau bien différent des précédents par la matière de corps principale et le procédé de mise en forme (pressage). Ces deux facteurs contribuent à leur donner une densité apparente élevée, mais aussi une anisotropie de propriétés considérable qui, dans un des cas, se rapproche sensiblement de celle du monocristal. Nous n'en connaissons pas les techniques de fabrication, mais il existe très probablement dans ces graphites une proportion de carbone, originaire du liant, beaucoup plus faible que dans les graphites à base de coke de pétrole, ce qui constitue une raison supplémentaire d'intérêt.

Leurs caractéristiques d'identification sont :

- graphite «K» KROPFMUHL KR 12, densité apparente typique 1, 95,
- graphite «W» WIRTZ, densité apparente typique 2, 08.

Les échantillons ont été prélevés avec leur axe parallèle à celui supposé pour la direction de pressage ; l'orientation de cette dernière a été confirmée par des mesures d'anisotropie (coefficient de dilatation thermique et résistivité électrique).

Nous exposons ici les résultats d'études concernant :
- les variations dimensionnelles macroscopiques mesurées à 78°K, et
- la libération entre 78 et 500°K de l'énergie emmagasinée,

après des irradiations neutroniques effectuées à 78°K, jusqu'à des doses atteignant $8,3 \cdot 10^{18}$ n/cm^2 (neutrons rapides d'énergie supérieure à 1 MeV)*.

Une étude des variations du paramètre cristallin c a été effectuée parallèlement [3].

II. VARIATIONS DIMENSIONNELLES

1. Dispositif expérimental

Les allongements macroscopiques ont été mesurés sur des éprouvettes cylindriques ayant les dimensions précitées, dont l'axe, compte tenu du mode de prélèvement choisi, est parallèle à la majorité des axes c des cristallites élémentaires constituant l'éprouvette.

Le dispositif de mesures également utilisé pour déterminer les coefficients de dilatation moyens α entre 77 et 293°K est représenté schématiquement à la figure 1.

L'échantillon étant immergé dans l'azote liquide, la position de son extrémité supérieure est repérée par une tige solidaire du noyau mobile d'un transformateur différentiel. Le support de l'échantillon et la tige guidée parallèlement à celui-ci sont en quartz fondu, ce qui rend les mesures insensibles aux fluctuations de niveau de l'azote liquide. Pour la détermination des coefficients de dilatation linéaires, on tient compte, bien entendu, de celui du quartz qui est très faible ($0,2 \cdot 10^{-6}$).

Le transformateur différentiel, alimenté sous 2 V, 1000 Hz, permet de définir la position du palpeur à ± 1 micron près. En fait, l'état de surface des éprouvettes limite la précision. Compte tenu de cela et des variations introduites par les légères différences de position de l'éprouvette au cours de mises en place successives, la reproductibilité des mesures est assurée à ± 4 microns pour des éprouvettes de 50 mm comme nous l'avons dit.

Les variations de dimensions dues à l'irradiation sont définies en établissant, pour chaque dose, la moyenne de quatre déterminations effectuées sur chacune des trois éprouvettes mesurées avant et après irradiation.

2. Résultats

La figure 2 représente, en fonction des doses reçues exprimées en neutrons rapides d'énergie supérieure à 1 MeV, les variations relatives de longueur $\Delta l/l$ mesurées à 78°K sur les différents types de graphites, comme il a été indiqué.

Les irradiations effectuées, qui ont duré au plus quelques semaines, ont cependant causé des expansions parfaitement mesurables ; on peut noter que leur ordre de grandeur correspond à des mois d'irradiation à la température

* Les doses ont été déterminées par la Section Pile CEN-G par comptage de détecteurs nickel.

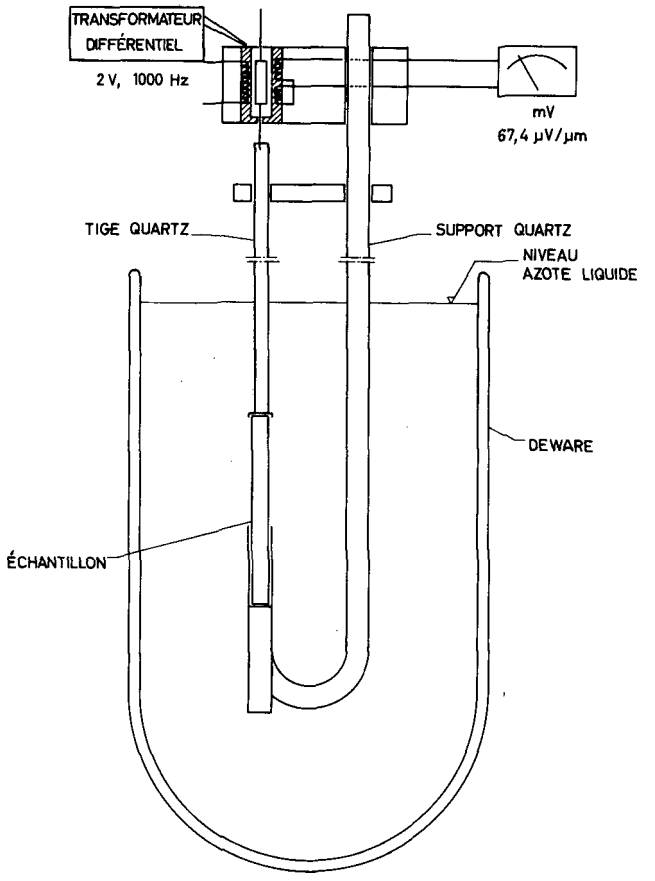


Figure 1

Dispositif de mesure des coefficients de dilatation et variations dimensionnelles.

ambiante dans un réacteur modéré au graphite. Les résultats obtenus sont nettement différenciés pour les deux grandes catégories de graphite étudiées :

a) Graphites industriels classiques («A», «B», «C»)

La majorité des déterminations concerne ces graphites dont nous avons rappelé par ailleurs les caractères essentiels. Ils se comportent de manière voisine, l'expansion linéaire ne dépassant pas 0, 2% pour la plus forte dose. La dispersion des mesures ne permet pas de distinguer nettement une différence de comportement entre eux.

Nous avons vérifié que cette dispersion n'est pas imputable à la méthode de mesure, mais à l'inhomogénéité du flux neutronique à l'intérieur même du cryostat d'irradiation dont le diamètre utile n'est pourtant que 40 mm.

Il semble bien, toutefois, que l'expansion cesse d'être linéaire lorsque la dose atteint $8 \cdot 10^{18}$ n/cm^2. Toutefois, un phénomène de ce genre n'ap-

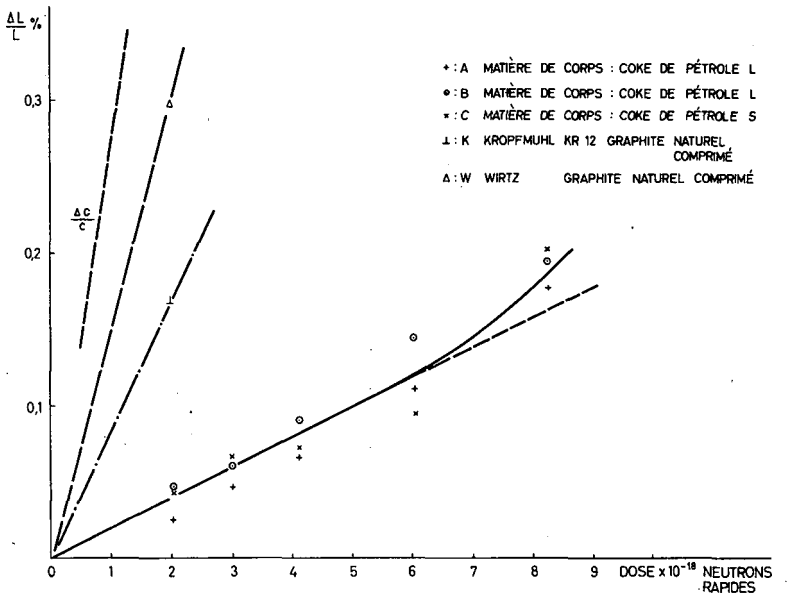


Figure 2

Expansion parallèle à l'axe c.
(Irradiations à 78°K)

paraît lors d'irradiations à la température ambiante que lorsque Δl/l est environ cinq fois supérieur.

b) Graphites naturels agglomérés («K» et «W»)

Nous n'avons encore qu'un nombre restreint de mesures sur ces matériaux; elles sont cependant en nombre suffisant pour mettre en évidence leur comportement très différent des précédentes.

En effet, pour une dose de $2 \cdot 10^{18}$ n/cm^2 on a mesuré des grandissements Δl/l de 0,3% et 0,17% respectivement pour les graphites «W» et «K», alors qu'ils ne dépassaient pas 0,04% pour «A», «B» ou «C».

On a calculé [4], dans le cas de certaines irradiations à la température ambiante, que les 4/5 de l'expansion volumique des cristallites sont absorbés par la porosité interne du graphite. On pourrait présenter ainsi une explication de la différence de comportement entre les graphites «A», «B» ou »C», dont les densités apparentes sont comprises entre 1,66 et 1,78 et les graphites «W» et «K», pour lesquels elles sont 1,95 et 2,08. Mais ces deux derniers chiffres montrent que le degré d'orientation des cristallites joue bien entendu un rôle prépondérant puisqu'on note pour les graphites «W» et «K» des allongements Δl/l dans un rapport voisin de 2, alors qu'ils présentent peu de différence de densité.

Nous montrons sur la même figure 2 la variation de Δc/c en fonction de la dose, qui a été mesurée parallèlement ailleurs [3]. On constate que, pour une dose de 10^{18} n/cm^2 par exemple, si Δl/l ne représente que 7 à 8%

de $\Delta c/c$ dans le cas de graphites industriels courants, ce grandissement en représente 60% pour le graphite «W» dont le comportement macroscopique se rapproche beaucoup de celui du monocristal. Il est intéressant de constater qu'il en est sensiblement de même pour le rapport des coefficients de dilatation linéaires ($22 \cdot 10^{-6}$ pour celui du cristal suivant l'axe c et $12,3 \cdot 10^{-6}$ pour le graphite «W»).

On sait que plusieurs auteurs ont recherché, comme il est rappelé dans l'étude précitée [4], une corrélation entre le coefficient de dilatation linéaire et l'expansion sous rayonnements. Elle concernait des graphites industriels ou de même type, dont les densités restaient modérées et dont les coefficients de dilatation ne dépassaient pas 5 ou $6 \cdot 10^{-6}$. Les corrélations montraient une dispersion de part et d'autre de la droite caractéristique du monocristal, qui était peut-être due en partie à des incertitudes sur les doses ou les températures d'irradiation.

Nous indiquons à la figure 3, en fonction des coefficients de dilatation linéaires moyens entre 78 et 273°K que nous avons mesurés sur les différents graphites, les expansions à 78°K pour une dose de 10^{18} n/cm^2; le point M représente les caractéristiques du monocristal.

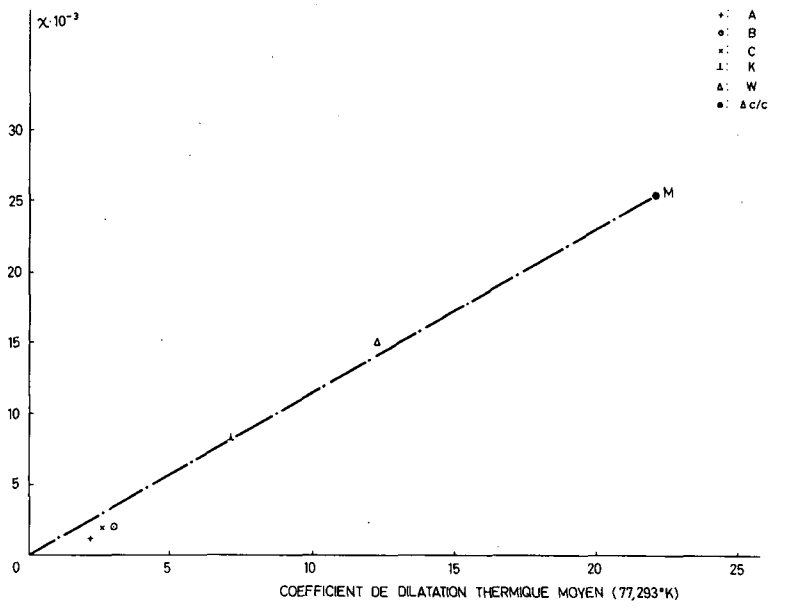


Figure 3

Expansion parallèle à l'axe c en ppm pour 10^{18} neutrons rapides : χ.
(Irradiations à 78°K)

Il semble que la liaison soit assez bonne dans cette gamme très étendue de coefficients de dilatation, bien que les points relatifs aux graphites industriels courants se situent sensiblement en-dessous de la droite. Peut-être la porosité encore voisine de 30% dans ces graphites joue-t-elle finalement un rôle différent vis-à-vis des expansions thermiques et sous rayonnements.

Il apparaît clairement, en tous cas, que si des matériaux à base de graphite naturel comprimé semblent intéressants pour des études systématiques par leur comportement qui se rapproche beaucoup de celui du monocristal, les variations dimensionnelles qu'ils subissent par irradiation les rendent peu appropriés à être utilisés dans des empilements de réacteurs, même lorsqu'on s'efforce, comme cela semble être le cas pour le graphite «K», de réduire leur anisotropie.

III. ÉNERGIES EMMAGASINÉES

Alors que d'innombrables mesures d'énergie Wigner ont été faites sur des graphites irradiés à des températures égales ou supérieures à la température ambiante, seul AUSTERMANN, à notre connaissance, en a effectué quelques-unes sur des échantillons irradiés à basse température [5].

1. Méthode de mesures

Nous avons repris une méthode connue d'analyse thermique différentielle, déjà utilisée par l'auteur précité, dont nous donnons par ailleurs des détails de réalisation et les améliorations apportées par l'un de nous [6].

Elle consiste essentiellement à mesurer la différence de température ΔT entre l'éprouvette et une enceinte dont la température augmente linéairement avec le temps, ainsi que la température Tc de l'échantillon lui-même, lors de deux recuits successifs entre 78 et 500°K. Au cours du premier, l'échantillon irradié libère son énergie, la seconde expérience sur l'éprouvette ainsi recuite servant de témoin pour la détermination des caractéristiques thermiques. Nous rappellerons seulement que les données expérimentales sont traitées en effectuant les bilans thermiques au cours de chacun des recuits.

Lors du premier recuit, l'augmentation instantanée de température dTe_1/dt de l'éprouvette de masse m est fonction :

- de l'énergie $h\Delta T_1$ qu'elle reçoit par conduction gazeuse,
- de l'enceinte avec laquelle elle a un écart de température ΔT_1, et aussi de l'énergie Wigner dH/dt qui se dégage en son sein, et enfin
- de sa chaleur spécifique c :

$$h\Delta T_1 + \frac{dH}{dt} = mc\frac{dTe_1}{dt} \tag{1}$$

que l'on peut finalement écrire

$$\frac{\Delta T_1}{dTe_1/dt} = \frac{m}{h}\left(c - \frac{1}{m}\,\frac{dH}{dTe_1}\right) \text{ ou } \frac{m}{h}\,c_a \tag{2}$$

en attribuant à la quantité entre paranthèses le rôle d'une chaleur spécifique apparente c_a.

Lors du second recuit, en l'absence de libération d'énergie, on a seulement

$$h\Delta T_2 = mc\frac{dTe_2}{dt} \quad \text{ou} \quad \frac{\Delta T_2}{dTe_2/dt} = \frac{m}{h}c. \tag{3}$$

On voit que $(1/m)(dH/dTe_1)$, quantité qui nous intéresse, est simplement égale à $c - c_a$ ou encore

$$\frac{1}{m}\frac{dH}{dTe_1} = c\left(1 - \frac{c_a}{c}\right). \qquad (4)$$

c_a/c est obtenu par le rapport de (2) et (3) en fonction des données expérimentales

$$\frac{\Delta T_1}{dTe_1/dt} \text{ et } \frac{\Delta T_2}{dTe_2/dt}.$$

On admet ainsi que h, coefficient d'échange, reste identique dans les deux recuits, ce qui est valable tant que le positionnement de l'éprouvette dans l'enceinte reste rigoureusement le même, et que les écarts de température ΔT restent faibles et du même ordre de grandeur.

L'augmentation relative de chaleur spécifique due à l'irradiation, peu importante [7], ne dépasse pas quelques pour cent dans notre cas. On peut négliger sa variation au cours du recuit et prendre pour c les valeurs connues [8].

La méthode est assez simple à mettre en œuvre. Elle permet, comme nous le verrons, de tracer avec fidélité et précision satisfaisantes, entre 78 et 500°K, les diagrammes de libération de l'énergie Wigner. Les résultats obtenus sont indépendants de la vitesse de réchauffement lorsque celle-ci reste comprise entre 1 et 3° par minute. Comme nous l'avons dit, elle n'est cependant pas rigoureuse et l'on doit noter qu'elle entraîne un travail considérable de dépouillement des mesures. Aussi, pour poursuivre une analyse plus fine des phénomènes, sommes-nous en train d'effectuer la mise au point d'une autre méthode connue [9] d'analyse thermique différentielle, de mise en œuvre plus délicate, mais ne souffrant pas des défauts précités : elle consiste essentiellement à mesurer directement l'énergie qu'il est nécessaire de fournir à un échantillon témoin pour lui faire suivre exactement l'évolution thermique de l'échantillon irradié au cours de son réchauffage.

2. Résultats

a) Energies globales libérées

Nous avons calculé, pour différentes doses et divers échantillons, les énergies globales libérées entre 100 et 273°K d'une part, et entre 100 et 500°K d'autre part. La figure 4 représente les résultats en fonction des doses reçues en neutrons rapides. Sur ce même diagramme, nous avons également reporté pour une dose de $8{,}2 \cdot 10^{18}$ n/cm^2 (points P et P') l'énergie libérée par deux échantillons, mesurée par vaporisation d'azote liquide, et qui peut être considérée comme l'énergie totale emmagasinée qui est libérable.

Nous avons, en effet, constaté que pour de fortes doses reçues les échantillons se trouvent dans un état d'extrême instabilité : un recuit spontané se déclenche alors sous l'effet d'une sollicitation mineure (choc, frottement) et, bien qu'il soit plongé dans l'azote liquide, on voit la température de l'échantillon monter à plusieurs centaines de degrés en un temps très bref. Il n'est alors pas question, bien entendu, de déterminer la courbe dH/dTe,

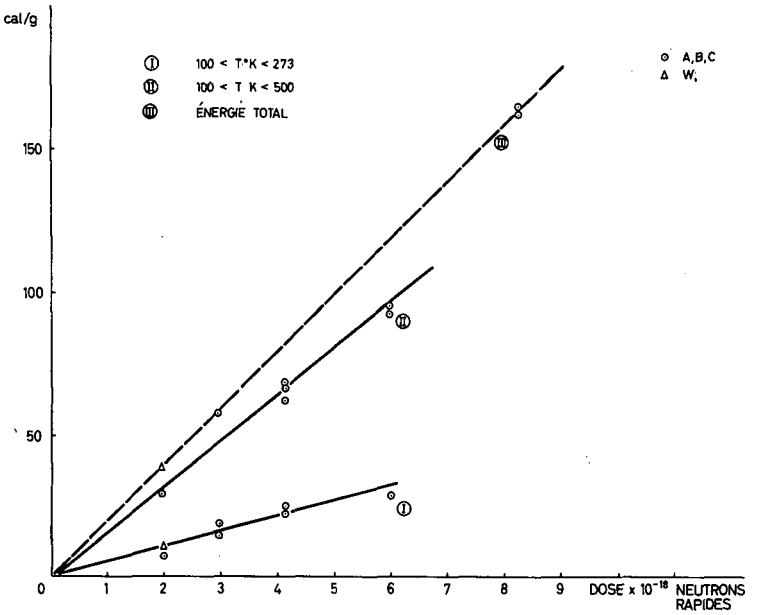


Figure 4

Energies globales libérées.
(Irradiations à 78° K)

mais nous avons pu évaluer l'énergie libérée par mesure de la quantité d'azote liquide vaporisé.

On peut admettre, comme nous l'avons représenté par la droite III, que l'énergie totale emmagasinée varie linéairement avec la dose. On constate qu'au fur et à mesure de l'augmentation de cette dernière l'écart grandit entre l'énergie totale et celle libérable entre 100 et 500°K : ceci s'explique par l'existence d'une quantité croissante de défauts guérissables à températures plus élevées.

Par ailleurs, on notera que jusqu'à $6 \cdot 10^{18}$ n/cm^2 environ, la fraction d'énergie libérée jusqu'à la température ambiante reste sensiblement constante et de l'ordre du quart de l'énergie totale emmagasinée, comme cela avait été noté antérieurement par AUSTERMANN [5].

b) Diagrammes d'enthalpie différentielle

La figure 5 représente les spectres d'énergie libérée par un même type «B» de graphite industriel, pour différentes doses reçues : 2, 0 - 4, 3 et $6,3 \cdot 10^{18}$ n/cm^2. Nous donnons également (courbe 1') le diagramme relatif, pour la plus faible de ces doses, à un graphite naturel type «W».

On notera d'abord que le début de libération d'énergie se situe à 100°K dans tous les cas, alors qu'il ne se manifestait que 25° plus haut dans les expériences précitées d'Austermann : ceci est attribuable aux fluctuations de température que subissent ces échantillons en cours d'irradiation, et qui occasionnaient un début de recuit.

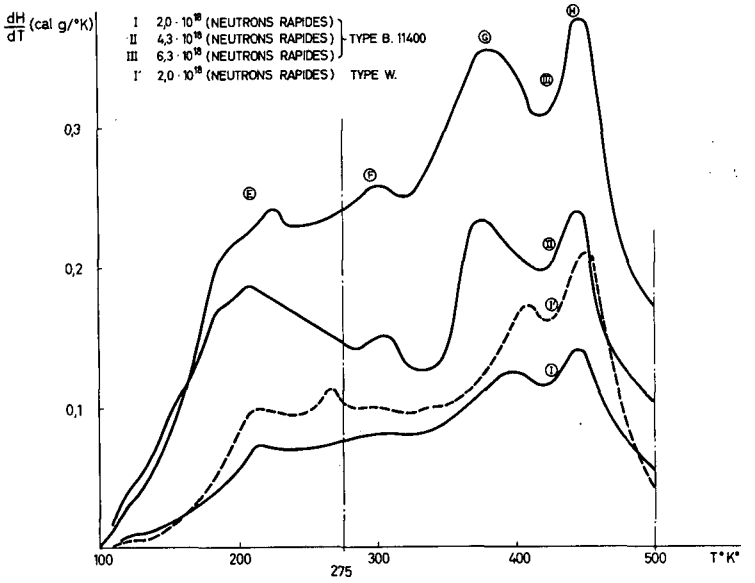


Figure 5

Enthalpie différentielle.
(Irradiations à 78°K)

On constate d'autre part l'existence de quatre maxima d'énergie bien définis aux fortes doses, et situés dans les plages de températures suivantes: 210/220° K (E), 300/310° K (F), 380/410°K (G) et 440/450°K (H).

Effet de la dose

La position de deux des pics reste à peu près fixe ; celle de « E», au voisinage de 200°K, antérieurement observée par Austermann et de «H», vers 450°K, qui correspond au pic bien connu, apparaissent au voisinage de 200°C lors d'irradiations à la température ambiante suivies d'un réchauffage avec vitesse de montée en température voisine de la nôtre. On sait que la position de ce dernier pic dépend de la température d'irradiation ; c'est ainsi que, situé dans notre cas à 445°K, il apparaît par exemple vers 445 et 470°K pour des températures d'irradiation de 60 et 80°C respectivement.

L'existence du pic «F», vers 300°K, avait été présumée par Austermann qui, toutefois, ne l'avait pas caractérisé nettement. On notera que ce pic disparaît pratiquement aux faibles doses (courbe I) ; ce peut être là une raison des difficultés rencontrées par l'auteur précité.

Nous trouvons enfin, comme nous l'avons signalé récemment [10], un quatrième pic, «G», situé dans la plage 380/410°K, qui jusqu'ici n'avait pas été observé. Il est cependant toujours bien marqué, et sa contribution à l'énergie globale apparaît importante aux fortes doses. Il est étonnant que ce maximum n'ait jamais été signalé - ne serait-ce que sous forme d'une inflexion avant le pic classique vers 200°C - dans le cas de graphites irradiés à la tempéra-

ture ambiante pour lesquels le début de libération d'énergie est toujours proche de 380°K. Il semblerait donc que ce pic «G» soit lié à la guérison ou à la recombinaison d'un type de défauts qui apparaît spécifiquement dans les irradiations à basse température. On notera enfin que pour les doses élevées, le maximum «G» se déplace de 25° environ vers les températures plus basses, montrant ainsi une nette dépendance vis-à-vis de la concentration en défauts.

Effet de la microstructure du graphite

On pouvait penser que dans un graphite naturel, dont les dimensions moyennes de cristallites sont beaucoup plus grandes que dans un graphite industriel, on observerait une modification importante des spectres d'énergie, liée par exemple à des modifications d'annihilation de défauts aux limites de cristallites. Il n'apparaît pas cependant de différences générales caractéristiques entre les courbes I (type «B» industriel) et I' (type «W» graphite naturel aggloméré).

L'énergie emmagasinée pour une même dose, libérable entre 100 et 500°K, est plus importante pour le type «W», laissant supposer une sensibilité plus grande de ce dernier aux dommages. Il est possible que ce soit, au moins en partie, dû à la présence dans le graphite industriel «B» d'une quantité non négligeable (au moins de l'ordre de 10%) de carbone originaire de la cokéfaction du liant. C'est par l'existence de ce carbone, à qui l'on a attribué une structure non graphitique désordonnée, que l'on a cherché à expliquer par exemple la déviation par rapport à la loi en T^2 de la conductibilité thermique à très basse température, qui se manifeste seulement pour les graphites de type industriel [11].

On note par ailleurs que le pic «G» est décalé d'une vingtaine de degrés vers les températures élevées, pour le graphite naturel «W». On peut voir là une influence de la taille des cristallites sur l'annihilation à leurs limites d'interstitiels ou de groupes d'interstitiels. L'explication est plus plausible dans cette gamme de température que vers 200°K où elle avait été proposée par Austermann. A cette dernière température, où les processus les plus probables sont des recombinaisons de paires interstitiels - lacunes proches, nous ne notons du reste pas un phénomène semblable. Par contre, l'apparition du pic à 265°K pour le graphite naturel «W» est plus difficilement explicable.

CONCLUSIONS

Ces premiers résultats d'irradiations neutroniques à 78°K de graphites polycristallins contribuent d'abord à une description plus complète des phénomènes. On a montré que la corrélation entre coefficients d'expansion thermique et sous irradiation reste valable pour des produits élaborés à partir de matières et par des méthodes très différentes. Par ailleurs, l'évolution thermique de la libération d'énergie Wigner a été précisée dans un large intervalle de températures, pour plusieurs doses, et des graphites bien différents.

Nous constatons que même dans les conditions particulières d'irradiation que nous avons choisies, la cinétique d'évolution thermique des défauts est complexe, puisqu'on en distingue quatre stades principaux. Dès le début de la guérison interviennent des mécanismes dépendant, au moins dans cer- large intervalle de températures, pour plusieurs doses, et des graphites bien différents.

Nous constatons que même dans les conditions particulières d'irradiation que nous avons choisies, la cinétique d'évolution thermique des défauts est complexe, puisqu'on en distingue quatre stades principaux. Dès le début de la guérison interviennent des mécanismes dépendant, au moins dans cer-taines limites, de la concentration initiale en défauts, comme le montrent vers leur origine les courbes relatives aux différentes doses.

D'autre part, il apparaît que le comportement de types divers de graphites n'est pas fondamentalement perturbé malgré les différences importantes de nature et de proportion de la matière de corps principale, des tailles des cristallites.

Les graphites naturels agglomérés nous apparaissent comme un matériau particulièrement intéressant pour la poursuite de ces études. Ils montrent pour certaines propriétés une variation après irradiation suffisamment importante à des doses faibles pour que son évolution par recuit soit facilement mesurable, et leur comportement est infiniment plus voisin de celui du monocristal que ne l'est celui de graphites industriels courants. C'est pourquoi nous comptons poursuivre ces travaux en nous attachant particulièrement à l'étude de tels matériaux, pensant pouvoir apporter ainsi une contribution à la connaissance des dommages élémentaires crées dans le graphite par irradiation neutronique.

RÉFÉRENCES

[1] HOVE, J.E., "Low temperature irradiation and annealing effects in graphite", Progress in Nuclear Energy, Series V, Metallurgy and Fuels 2 (1959) 551.

[2] BOCHIROL, L., DOULAT, J. et WEIL, L., Principe d'un dispositif d'irradiation à azote liquide et sa réalisation pour utilisation dans une pile piscine, Rapport CEA n° 1827 (1961).

[3] PLUCHERY, M., «Mesures de paramètres de graphite industriel irradié dans l'azote liquide», Voir ces Comptes rendus.

[4] HERING, H., «Effets des neutrons rapides sur le graphite», Génie atomique, B2 VI, PUF, Paris (1959-60).

[5] AUSTERMANN, S.B., MAA-SR-1564 (1956).

[6] BONJOUR, E. et FAIVRE, J., Dispositif pour la mesure de l'énergie Wigner dans des graphites irradiés à basse température, Note CEA (à l'impression).

[7] GOODMAN, B.B., MONPETIT, L. et WEIL, L., C.R. Acad. Sci. 248 (1959) 956.

[8] DE SORBO, W. and TYLER, W.H., J. chem. Phys. 21 (1953) 1660.

[9] COTTRELL, A.H. et al., «Théorie cinétique de la restauration appliquée à la libération d'énergie emmagasinée par le graphite irradié dans des piles refroidies par l'air», Actes 2e Conf. Genève 4 (1958) 580.

[10] BONJOUR, E., BOCHIROL, L. et WEIL, L., C.R. Acad. Sci. 254 (1962) 456.

[11] HOVE, J.E. et SMITH, A.W., Phys. Rev. 104, 4 (1956) 892-900.

MESURES DE PARAMÈTRES DE GRAPHITE INDUSTRIEL IRRADIÉ DANS L'AZOTE LIQUIDE

M. PLUCHERY
CENTRE D'ÉTUDES NUCLÉAIRES DE GRENOBLE, FRANCE

Abstract — Résumé — Аннотация — Resumen

PARAMETER MEASUREMENTS ON INDUSTRIAL GRAPHITE IRRADIATED IN LIQUID NITROGEN. Samples of graphite taken from rods intended for the G2 and G3 reactors at Marcoule were irradiated in a liquid-nitrogen loop. The doses given ranged from 0.15 to 1×10^{19} n/cm², these fluxes consisting of fast neutrons of energy greater than 1 MeV as measured on the sample. The temperature during irradiation did not exceed 78°K. An X-ray diffraction chamber was developed for measuring parameters at the temperature of liquid nitrogen without intermediate reheating. This chamber made it possible to obtain an accuracy of 0.001 Å for parameter a and 0.005 Å for c.

The variation in parameter c as a function of the dose is linear in the range indicated, the increase in $\Delta c/c$ being equal to 0.03 at 10^{19} n/cm².

The recovery of the parameter during annealing between 90°K and ambient temperature was briefly studied and compared with the measurements of liberated energy.

MESURES DE PARAMÈTRES DE GRAPHITE INDUSTRIEL IRRADIÉ DANS L'AZOTE LIQUIDE. Des échantillons de graphite prélevés sur des barres destinées aux réacteurs G2 et G3 de Marcoule ont été irradiés dans une boucle à azote liquide. Les doses recues s'échelonnent entre 0,15 et $1 \cdot 10^{19}$ n/cm². Ces flux s'entendent en neutrons rapides d'énergie supérieure à 1 MeV mesurée au niveau de l'échantillon. La température pendant l'irradiation n'a pas dépassé 78°K. Une chambre de diffraction de rayons X pour la mesure des paramètres à la température de l'azote liquide sans réchauffage intermédiaire a été mise au point. Elle permet d'atteindre une précision de 0,001 Å sur le paramètre a et de 0,005 Å sur c.

La variation du paramètre c observée en fonction de la dose est linéaire dans le domaine indiqué, la croissement de $\Delta c/c$ étant de 0,03 par 10^{19} n/cm².

La guérison du paramètre au cours du recuit entre 90°K et la température ambiante a été sommairement étudiée, et rapprochée des résultats des mesures d'énergie libérée.

ИЗМЕРЕНИЕ ПАРАМЕТРОВ ПРОМЫШЛЕННОГО ГРАФИТА, ОБЛУЧЕННОГО В ЖИДКОМ АЗОТЕ. Образцы графита, отобранные на стержнях и предназначенные для реакторов G-2 и G-3 в Маркуле, были облучены в контурах с жидким азотом. Полученные дозы колеблются в пределах 0,15 и $1 \cdot 10^{19}$ н/см². Само собой разумеется, что эти потоки состоят из быстрых нейтронов с энергией, превышающей 1 Мэв, измеряемой в месте нахождения образца. Температура во время облучения не превышала 78°К. Была разработана рентгеновская дифракционная камера для измерения параметров при температуре жидкого азота без промежуточного подогрева. Она позволяет достигнуть точности до 0,001 Å по параметру "a" и до 0,005 Å по параметру "c".

Изменение параметра "c", наблюдаемое в зависимости от дозы, является линейным в указанной области, причем увеличение $\Delta c/c$ составляет 0,03 на 10^{19} н/см².

Кратко было изучено восстановление параметра во время отжига между 90°К и комнатной температурой, и оно было сопоставлено с результатами измерения высвобождаемой энергии.

MEDICIÓN DE LOS PARÁMETROS DEL GRAFITO INDUSTRIAL IRRADIADO EN NITRÓGENO LÍQUIDO. Se han tomado muestras de grafito de las barras destinadas a los reactores G2 y G3 de Marcoule, para irradiarlas en un circuito de nitrógeno líquido. Las dosis recibidas varían entre 0,15 y $1 \cdot 10^{19}$ n/cm². Estos flujos se entienden constituidos por neutrones rápidos de energía superior a 1 MeV, medida al nivel de la muestra. La temperatura durante la irradiación no ha excedido de 78°K. Se ha construido una cámara de difracción de rayos X a fin de medir los parámetros a la temperatura del nitrógeno líquido sin calentamiento intermedio. Esta cámara permite alcanzar una precisión de 0,001 Å respecto del parámetro a y de 0,005 Å respecto del c.

La variación del parámetro c, observada en función de la dosis, es lineal en el intervalo indicado, siendo el crecimiento de $\Delta c/c = 0{,}03$ para $10^{19} n/cm^2$.

La recuperación del parámetro durante el recocido entre 90°K y la temperatura ambiente se ha estudiado someramente, y se relaciona con los resultados de las mediciones de la energía liberada.

I. GÉNÉRALITÉS

L'irradiation du graphite par les neutrons crée des interstitiels dont la présence entre les plans graphitiques, soit à l'état isolé, soit sous forme d'amas planaires, est responsable du grandissement de paramètre et des distorsions réticulaires. Ce modèle proposé dès les premières études d'irradiation de graphite [1, 2, 3] est maintenant généralement adopté. Par migration d'interstitiels ces amas peuvent se réarranger pour donner des défauts complexes: amas planaires isolés, systèmes d'amas planaires contenant des dipoles de dislocations ou limités par des boucles de dislocations, etc. Le type de défaut varie avec la température, le nombre d'atomes intéressés croissant en fonction de la température.

Mais entre le stade initial caractérisé par des interstitiels isolés et les stades de développement tels que la taille des défauts permette leur observation au microscope électronique [4, 5] ou leur mise en évidence par diffusion des rayons X aux petits angles (l'observation des amas est limitée à l'intervalle 5-30 Å; des amas plus petits donneraient une intensité diffusée trop faible, des amas plus gros donneraient une diffusion à des angles trop faibles) [6], les renseignements sur la nature des défauts sont rares; c'est ainsi que les processus de réarrangement correspondant aux pics d'énergie libérée ne sont, à notre connaissance, pas encore élucidés.

Au-dessous de 100°K la migration des interstitiels est négligeable et les défauts créés sont pratiquement figés. La diffraction des rayons X sur des échantillons irradiés à la température de l'azote liquide devait apporter des renseignements précieux sur le stade initial d'endommagement [7, 8]. L'observation d'échantillons partiellement restaurés par recuit à diverses températures doit permettre de préciser le type de défaut à chaque accident de la courbe de libération d'énergie emmagasinée [7, 9].

II. DISPOSITIF EXPÉRIMENTAL

Des échantillons de graphite nucléaire prélevés dans des barres destinées au réacteur G-2 ont été irradiés dans la boucle à azote liquide de la pile-piscine MÉLUSINE [10]. La température des échantillons restait celle de l'azote liquide à 1° près jusqu'à la fin des mesures aux rayons X. La dose de neutrons rapides était mesurée à l'aide de détecteurs au nickel munis d'écrans de cadmium; elle est exprimée en neutrons rapides d'énergie supérieure à 1 MeV sous le spectre de fission. Les dimensions du container (diamètre: 25 mm, hauteur: 80 mm) permettent de négliger les variations locales du flux.

La chambre de diffraction de rayons X utilisée et la méthode de mesure étant décrites ailleurs [13], nous nous bornerons ici à une description sommaire: l'échantillon émergeant de l'azote (dont le niveau est régulé à 1 mm

près) reçoit sur sa face supérieure le faisceau de rayons X issu d'un monochromateur (fig. 1). Les rayons diffractés en retour impressionnent le film. Les raies de diffraction sont localisées pour deux valeurs de l'angle de diffraction choisies à volonté. Les autres raies subissent un élargissement plus ou moins important suivant la disposition géométrique adoptée.

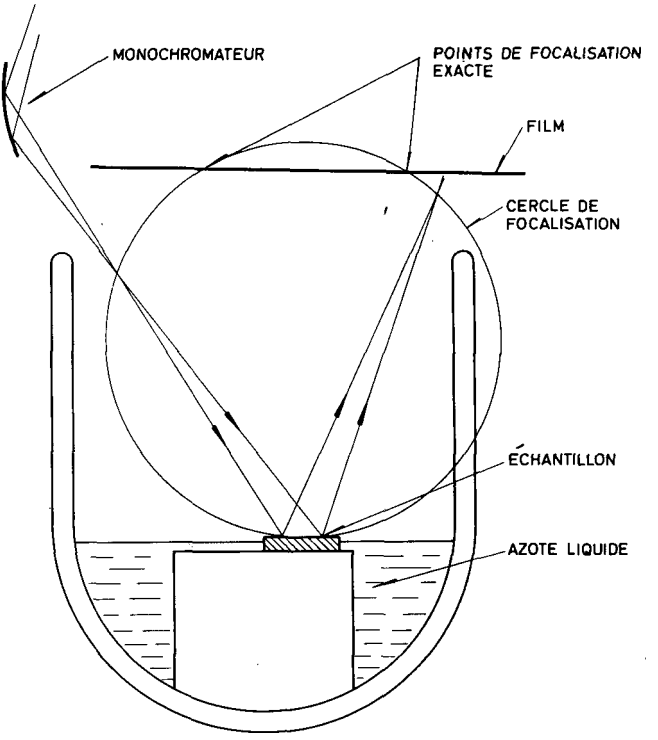


Figure 1

Schéma de la chambre de diffraction à azote liquide.

De la poudre de nickel déposée à la surface de l'échantillon jouait le rôle d'étalon. La mesure portait sur les raies 11.0, 11.2, 00.6, 20.0 et 20.1, en rayonnement strictement monochromatique ($K\alpha_1$ du fer).

La précision intrinsèque de la chambre est de $5 \cdot 10^{-5}$. Pour le graphite la précision est de $2 \cdot 10^{-4}$ ($5 \cdot 10^{-4}$ Å) sur le paramètre a, et $4 \cdot 10^{-4}$ ($3 \cdot 10^{-3}$ Å) sur c. La distance réticulaire des graphites irradiés n'a pas une valeur unique, mais est caractérisée par une distribution dont on peut définir la valeur moyenne (donnée en première approximation par le centre de gravité de la raie de diffraction) et la largeur intégrale. La précision indiquée ci-dessus se réfère à cette valeur moyenne; elle a été effectivement vérifiée par la dispersion des mesures répétées d'un même échantillon et par la cohérence des valeurs calculées à partir des différentes raies indiquées.

III. MESURES SUR LES ÉCHANTILLONS IRRADIÉS NON RECUITS

Pour des doses d'irradiation croissantes, on constate une augmentation pratiquement linéaire de c:

$$\frac{\Delta c}{D} = \frac{0{,}183\ \text{Å}}{10^{19}\ \text{nvt}}$$

et une diminution de a:

$$\frac{\Delta a}{D} = \frac{-0{,}0095\ \text{Å}}{10^{19}\ \text{nvt}}\ .$$

Pour la dose maximum observée, soit $0{,}83 \cdot 10^{19}$, l'écart à la linéarité est de 8%. Pour le paramètre a, l'effet de saturation semble plus marqué, mais la précision relative moins bonne ne nous permet qu'une définition assez vague du domaine de linéarité: les variations de a sont environ 25 fois plus faibles que celles de c.

L'étude sommaire du profil de la raie 00.6 montre que l'altération par rapport au profil avant irradiation se borne à un déplacement et à un élargissement; mais la symétrie de la raie et sa forme (courbe de Gauss) sont conservées. Il est à noter que pour une irradiation à la température ambiante donnant une variation de paramètre du même ordre [2], la symétrie de la raie 00.4 est déjà altérée: la raie semble résulter de la superposition d'une raie non déplacée mais élargie et d'une raie élargie et non déplacée, profil qui pourrait s'expliquer par la coexistence de domaines perturbés primaires et de domaines réarrangés avec formation de défauts complexes. On peut penser qu'après une irradiation à basse température les interstitiels sont encore disséminés dans la matrice ou tout au moins à un stade de rassemblement trop peu avancé pour donner un pic de diffraction distinct.

Pour la plus forte dose observée ($0{,}83 \cdot 10^{19}$ nvt), la largeur intégrale intrinsèque de la raie 00.6 est de 0,9° (θ) contre 0,5° avant irradiation. L'intensité totale de la raie est réduite à 55% de sa valeur initiale. On peut en déduire l'ordre de grandeur des fluctuations de l'espacement réticulaire, dans l'hypothèse où le dommage serait constitué principalement par ces fluctuations, le gauchissement des plans ne jouant qu'un rôle secondaire. Ce modèle proposé par COOPER [1] est certainement valable pour les irradiations à basse température, dans lesquelles les interstitiels isolés ne provoquent qu'un gauchissement négligeable. On trouve une fluctuation moyenne de 0,034 Å. Les résultats peuvent s'exprimer de la façon suivante: pour la dose maxima, la valeur moyenne de distances réticulaires c est augmentée de 2% par l'irradiation; la nouvelle distribution est sensiblement normale et présente une largeur intégrale égale à 0,5% de la valeur moyenne.

Dans les irradiations à la température ambiante, la même variation de la valeur moyenne (provoquée par une dose supérieure) s'accompagne d'une fluctuation moyenne de 1,7%, ainsi qu'on peut le calculer à partir des résultats de LOCH et al. [11]. Ces résultats sont à rapprocher de l'observation suivante: pour des doses supérieures à 10^{19} nvt les échantillons irradiés présentent une grande instabilité; un léger choc ou un frottement suffit parfois à déclencher au sein même de l'azote liquide une libération brutale d'énergie entraînant le recuit de l'échantillon à des températures de l'ordre

de 300°C. Du point de vue cristallographique, la mesure de paramètre serait encore possible pour des doses bien supérieures malgré l'élargissement considérable et la diminution d'intensité prévisibles. Mais il est à craindre que les tensions internes et l'énergie emmagasinée provoquent le recuit spontané, voire la destruction des échantillons. Ce phénomène intervient pour des grandissements inférieurs d'un facteur 4 au moins à ceux que l'on observe sur des échantillons irradiés à la température ambiante et qui ne manifestent ni instabilité mécanique, ni écart à la linéarité paramètre/dose.

IV. RECUITS A TEMPÉRATURE INFERIEURE A LA TEMPERATURE AMBIANTE

On a effectué des recuits linéaires à partir de la température de l'azote liquide avec la même vitesse de réchauffage que dans les mesures d'énergie libérée [12], soit 2°/min. Dès la température nominale atteinte, l'échantillon était ramené à la température de l'azote à laquelle avait lieu la mesure de paramètres. Grâce à un bon contact thermique entre échantillon et four, l'écart de température n'a pas dépassé 2°. Ceci est important en particulier aux températures de recuit proches de la température ambiante: sans précautions spéciales, l'élévation de température provoquée par la libération d'énergie emmagasinée peut en effet atteindre 300°C, et la restauration observée dans ce cas ne serait plus caractéristique du recuit à la température visée.

Les valeurs des paramètres après recuit à 220°K (premier accident de la courbe d'enthalpie différentielle [12]), à 145°K et à 295°K, sont portées sur les figures 2 et 3. La restauration du paramètre c est de 10% après recuit à 145°K et de 24% après recuit à 220°K pour une dose de $0{,}6 \cdot 10^{19}$ nvt. Pour des doses faibles de $0{,}083 \cdot 10^{19}$, le degré de restauration est sensiblement le même, ce qui suggère que le type de défauts susceptibles de guérison dans ce domaine de températures est indépendant de la dose, tout au moins jusqu'à $0{,}6 \cdot 10^{19}$ nvt. Ceci est en accord avec les mesures d'énergie libérée [12]: la quantité absolue d'énergie libérée au-dessous de 220°K est pratiquement proportionnelle à la dose jusqu'à $0{,}6 \cdot 10^{19}$ nvt; elle est par contre sensiblement constante au-dessus, ce qui semble indiquer une saturation en défauts de ce type.

V. RECUITS A LA TEMPÉRATURE AMBIANTE

Après recuit à la température ambiante le grandissement cristallin résiduel est de 53% de sa valeur initiale. Un recuit de durée inférieure à une minute (pulse annealing) suffit pour obtenir cette guérison; le maintien prolongé à la température ultérieure ne provoque pas de nouvelle évolution.

Après une irradiation à la température ambiante dont la dose n'était connue qu'approximativement, nous avions trouvé une variation de paramètre égale à la moitié de celle qui se serait produite pour la même dose d'irradiation à basse température. De même la courbe de grandissement de paramètre indiquée dans [11] montre que les doses nécessaires pour obtenir un grandissement de 0,17 Å sont de $1{,}42 \cdot 10^{19}$ alors que nous avons observé le même

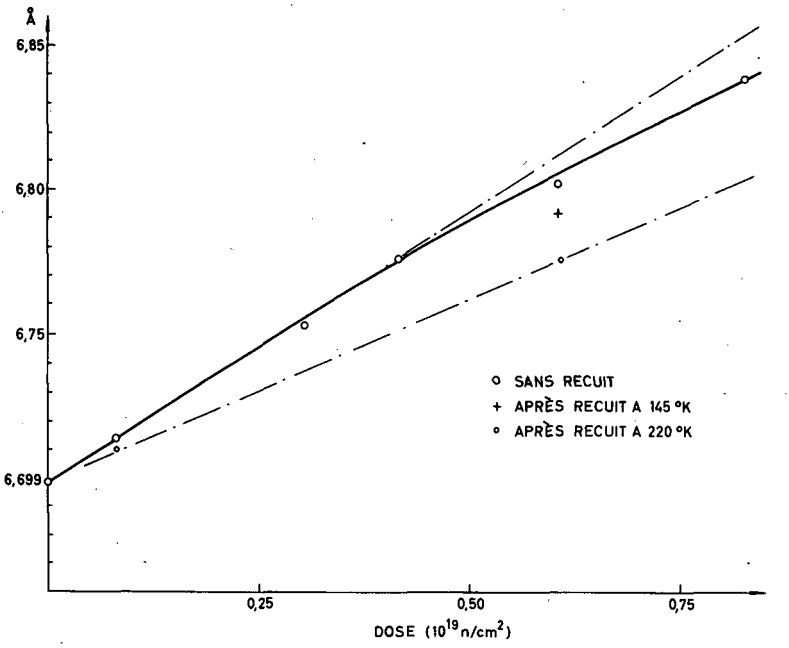


Figure 2

Variation de c en fonction de la dose.

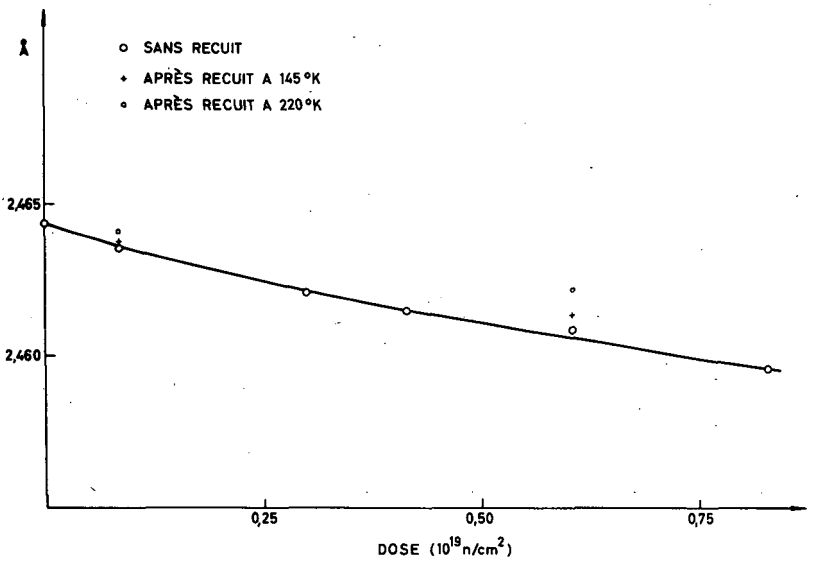


Figure 3

Variation de a en fonction de la dose.

grandissement pour une dose dans l'azote liquide de $0{,}83 \cdot 10^{19}$, soit un rapport de 0,58. L'irradiation à la température ambiante provoque donc sensiblement les mêmes dommages qu'une irradiation à basse température suivie d'un recuit à la température ambiante.

VI. CONCLUSION

Nous basant sur les résultats précédents et sur les mesures d'énergie libérée précitées [12], nous pouvons tirer les conclusions suivantes:

a) L'hypothèse selon laquelle les défauts constitueraient toute une gamme, chaque type étant caractérisé par une température minimum de guérison, se confirme.

b) La proportion des défauts guérissables à diverses températures inférieures à l'ambiante est indépendante de la dose reçue jusqu'à $0{,}6 \cdot 10^{19}$ nvt, ce qui suggère que dans ce domaine ces défauts ne sont pas sujets à saturation; ce domaine correspond à la partie linéaire de la courbe grandissement – dose.

Il pourrait par contre y avoir saturation pour des défauts guéris aux températures supérieures. Ces défauts complexes impliquent un réarrangement, la variation de paramètre qui les accompagne doit être plus faible: ceci pourrait expliquer l'écart à la linéarité observé pour les fortes doses.

Les résultats demanderaient à être précisés; la meilleure façon serait, à notre avis, d'étudier en détail la restauration du paramètre et l'évolution des profils de raies en fonction de la température de recuit.

RÉFÉRENCES

[1] COOPER, E. P., NAA-SR-135 (1951).
[2] WARREN, B. E. and CHIPMAN, D. R., KAPL – 938 (1953).
[3] CHIPMAN, D. R. and WARREN, B. E., KAPL – 1493 (1961).
[4] BOLLMANN, W., J. app. Phys. 32, 5 (1961) 869.
[5] BOLLMANN, W., "Dark field electron microscopy applied to radiation damage in graphite", Properties of Reactor Materials and the Effects of Radiation Damage, Butterworths, London (1962) 132.
[6] EELES, W. T. and SUTCLIFFE, J. M., "Further studies of small angle X-ray scattering by pile-irradiated graphite", Properties of Reactor Materials and the Effects of Radiation Damage, Butterworths, London (1962) 204
[7] AUSTERMANN, S. B., NAA-SR-2457 (1958).
[8] KEATING, D. T., Phys. Rev. 98, 6 (1955) 1859.
[9] AUSTERMANN, S. B., NAA-SR-1564 (1956).
[10] BOCHIROL, L., DOULAT, J. et WEIL, L., Rapport CEA n° 1827 (1961).
[11] LOCH, L. D., AUSTIN, A. E., HARRISON, R. J. and DUCKWORTH, W. H., BMI 1042 (1955).
[12] BOCHIROL, L., BONJOUR, E. et WEIL, L., «Irradiations neutroniques à 78 °K de graphites polycristallins», voir ces Comptes rendus.
[13] PLUCHERY, M. et DEBRENNE, P., Note CEA n° 337 (1961).

AN EFFECT OF FLUX LEVEL AND FLUX SPECTRUM ON THE ACCUMULATION OF DAMAGE IN REACTOR-IRRADIATED GRAPHITE

H. BRIDGE, B. S. GRAY AND B. T. KELLY
U.K.A.E.A. REACTOR MATERIALS LABORATORY,
CULCHETH, WARRINGTON, LANCS., ENGLAND
AND
H. SØRENSEN
RISØ RESEARCH ESTABLISHMENT, ROSKILDE, DENMARK

Abstract — Résumé — Аннотация — Resumen

AN EFFECT OF FLUX LEVEL AND FLUX SPECTRUM ON THE ACCUMULATION OF DAMAGE IN REACTOR-IRRADIATED GRAPHITE. The results of an experiment to measure the effect of flux level on the damage accumulated in reactor-quality graphite when it is irradiated to fast neutron doses of 4×10^{19} n/cm^2 are presented. An effect is clearly demonstrated from measurements of electrical and thermal resistivity, Young's modulus and dimensional changes, which can be interpreted in terms of a dominant process in the damaging mechanism with an activation energy for thermal annealing of 1.2 eV.

In addition, data are given comparing the changes in electrical resistivity occurring at low doses in an irradiation facility in a graphite-moderated reactor with those in a hollow fuel element facility in a heavy-water-moderated reactor. The variation with dose is shown to be of the same form in both cases, and is used to derive a relationship between the damaging powers of the neutron spectra in these facilities.

The irradiation temperatures used during the main experiment were in the range 150 - 225°C, while the flux levels chosen are typical of the rigs used in the United Kingdom for accelerated materials-testing programmes and of the core in current designs of graphite-moderated reactors. Thus, after consideration of the possible change in the effect with dose, the results of the two experiments are directly applicable to the problem of correcting the results of the accelerated tests in power reactor conditions. The use of an equivalent-temperature concept for this purpose is discussed in considerable detail.

EFFET DE L'INTENSITÉ DU FLUX ET DU SPECTRE NEUTRONIQUE SUR L'ACCUMULATION DES DOMMAGES CAUSÉS AU GRAPHITE IRRADIÉ DANS UN REACTEUR. Les auteurs présentent les résultats d'une expérience qui consiste à mesurer l'effet de l'intensité du flux sur l'accumulation des dommages dans du graphite pour réacteur, irradié à des doses de neutrons rapides de $4 \cdot 10^{19}$ n/cm^2. Les mesures de la résistivité thermique et électrique, du module de Young et des variations de dimensions montrent qu'il se produit un effet que l'on peut interpréter comme constituant le mécanisme dominant du processus d'altération, avec une énergie d'activation pour le recuit thermique de 1,2 eV.

En outre, les auteurs donnent des chiffres permettant de comparer les variations de résistivité électrique qui se manifestent, pour de faibles doses, dans les canaux d'irradiation d'un réacteur ralenti au graphite avec ceux qui apparaissent dans les canaux à cartouches de combustible d'un réacteur ralenti à l'eau lourde. Ils montrent que les variations selon la dose ont la même forme dans les deux cas; ils en dégagent une relation entre les pouvoirs d'altération des spectres neutroniques dans les canaux considérés.

Dans la principale expérience, les températures d'irradiation se situaient entre 150 et 225°C; les flux de neutrons choisis étaient typiques des dispositifs utilisés au Royaume-Uni pour les programmes d'essais accélérés de matériaux, et des cœurs de réacteurs de modèle courant ralentis au graphite. Il en résulte qu'après l'examen des variations possibles de l'effet en fonction de la dose, on peut directement appliquer les résultats de ces deux expériences pour ajuster ceux des tests accélérés aux conditions rencontrées dans un réacteur de puissance. Les auteurs examinent en détail l'avantage de recourir à une notion de température équivalente.

ВЛИЯНИЕ УРОВНЯ И СПЕКТРА ПОТОКА НА АККУМУЛИРОВАНИЕ ПОВРЕЖДЕНИЙ В ОБЛУЧЕННОМ В РЕАКТОРЕ ГРАФИТЕ. Приводятся результаты эксперимента по измерению влияния уровня потока на повреждение, аккумулированное в графите, пригодном для реактора, когда он облучен дозами быстрых нейтронов,

равными $4 \cdot 10^{19}$ н/см^2. Влияние ясно продемонстрировано измерением электрического и теплового сопротивления, модуля Юнга и изменений размеров, которые могут быть интерпретированы как доминирующий процесс в механизме повреждения с энергией активации для теплового отжига в 1,2 эв.

Кроме того, приводятся данные сравнения изменений в электрическом сопротивлении при малых дозах, получаемых в установке для облучения в реакторе с графитовым замедлителем, с изменениями, происходящими в установке с полными топливными элементами в реакторе с тяжеловодным замедлителем. Показано, что исследованные изменения в зависимости от дозы имеют одинаковый характер в обоих случаях и используются для выявления связи между силами повреждения нейтронного спектра этих установок.

Температуры при облучении, использованные во время основного эксперимента были в пределах 150 - 250°С, а выбранные уровни потока являются типичными для оборудования, используемого в Соединенном Королевстве для программ испытания материалов, используемых в ускорителях, и для активной зоны в современных конструкциях реакторов с графитовом замедлителем. Таким образом, после рассмотрения возможного изменения эффекта с изменением дозы, результаты двух экспериментов непосредственно применимы к проблеме корректировки результатов ускоренных испытаний для энергетических реакторов.

Концепция использования эквивалентной температуры для этой цели обсуждается достаточно подробно.

EFECTO DE LA INTENSIDAD Y DEL ESPECTRO DEL FLUJO SOBRE LA ACUMULACIÓN DE DAÑOS POR IRRADIACIÓN EN EL GRAFITO NUCLEAR. Los autores presentan los resultados de un experimento efectuado con el propósito de medir el efecto de la variación del flujo sobre los daños acumulados en el grafito de pureza nuclear cuando la irradiación se efectúa con neutrones rápidos en dosis hasta de $4 \cdot 10^{19}$ n/cm^2. La existencia del efecto queda claramente demostrada por las determinaciones de la resistividad eléctrica y térmica, del módulo de Young y de los cambios dimensionales, cuyos resultados pueden interpretarse admitiendo que el mecanismo del daño obedece a un proceso dominante con una energía de activación de 1,2 eV para el recocido térmico.

Además, aportan datos que permiten comparar los cambios de la resistividad eléctrica provocados por la exposición a dosis reducidas en la instalación de irradiación de un reactor moderado con grafito con los cambios originados al introducir las muestras en elementos combustibles huecos en un reactor moderado con agua pesada. Se comprueba que en ambos casos la variación en función de la dosis obedece a la misma ley, que los autores utilizan para establecer una relación entre la capacidad de los espectros neutrónicos para provocar daños en las dos instalaciones.

En los experimentos principales las temperaturas de irradiación estuvieron comprendidas entre 150° y 225°C, mientras que los valores de los flujos adoptados son típicos de las instalaciones usadas en el Reino Unido para los programas de ensayo acelerado de materiales y son también los adoptados para los cuerpos en los actuales diseños de reactores moderados con grafito. En esta forma, siempre que se tenga en cuenta el posible cambio del efecto en función de la dosis, los resultados de los dos experimentos pueden aplicarse directamente a resolver el problema que supone introducir en los resultados de los ensayos acelerados las correcciones necesarias para adaptarlos a las condiciones reales en un reactor de potencia. En la memoria se examina muy detalladamente la aplicación del concepto de "temperatura equivalente".

1. INTRODUCTION

For nearly twenty years the behaviour of materials under the influence of reactor irradiation has been studied extensively by an ever-increasing number of research groups using many different facilities. The dependence of the effects observed in any given irradiation facility on the temperature and duration of the irradiation is well known for many materials, but the correlation of the results from different facilities is often still in doubt.

This problem is of considerable practical importance because results obtained from tests in materials-testing reactors must often be used in the design of new power reactors, and before this can be done allowance must be made for differences in flux spectrum and flux intensity between the test

facility and the system to which the results are being applied. The methods used for this in the application of graphite-irradiation data to the design of graphite-moderated nuclear power stations in the United Kingdom have previously been described by BELL et al. [1]. The experiments described in the present paper were performed jointly by the Danish Atomic Energy Commission and the United Kingdom Atomic Energy Authority in the Danish Reactor DR3 to study these methods in more detail. The investigation of the flux-level effect required that a reactor should be operated at low power for several months, and the start-up period of operation of DR3 offered a rare opportunity for performing this type of work. Additionally, accelerated tests on graphite were also planned in DR3 and it was therefore necessary to set up a suitable dose scale for this reactor.

The first experiment described, to fulfil the latter requirement, involved a comparison of the changes of electrical resistivity of specimens irradiated in DR3 with the results reported for similar specimens irradiated in the BEPO reactor at Harwell. The second experiment on the effect of flux intensity involved a comparison of the property changes observed when the DR3 Reactor was operated at power levels differing by a factor of about ten.

An outline theory of the irradiation-damaging process for graphite

During the slowing-down of fast neutrons in graphite, carbon atoms are displaced from their normal lattice positions to form interstitial and vacancy defects which take up metastable arrangements. The rate of rearrangement of these defects due to thermal activation depends on the irradiation temperature.

BELL et al. [1] postulate that the damaging efficiency of a given reactor flux may be represented by a single parameter known as the "damage flux" ϕ_d which, with a knowledge of the irradiation temperature, is sufficient to define the irradiation conditions. The proven occurrence of annealing by irradiation may require that this concept be modified, but the close similarity of neutron spectra in graphite-moderated power reactors and in this type of materials-testing reactor over the important energy range suggests that it is not too surprising that the approximation holds in practice.

Neglecting the effects of electron and gamma irradiation, the parameter ϕ_d is defined by:

$$\phi_d = \int \psi(\epsilon)\ \phi(\epsilon)\ d\epsilon, \tag{1}$$

where $\phi(\epsilon)d\epsilon$ is the flux of neutrons with energies between ϵ and $\epsilon + d\epsilon$ and $\psi(\epsilon)$ is the factor which allows for the variable ability of neutrons of different energies to produce damage. Similarly the flux ϕ_m measured using the activation of suitable foils is defined by Eq. (2) in which σ_m is the differential activation cross-section, and $\bar{\sigma}$ is a constant.

$$\phi_m = \frac{1}{\bar{\sigma}} \int \sigma_m(\epsilon)\ \phi(\epsilon)\ d\epsilon. \tag{2}$$

For a particular spectrum, a ratio ϕ_d / ϕ_m may be defined using these

two equations and since interest is primarily in the comparison of facilities it is convenient to equate ϕ_d to ϕ_m in some standard facility. Thus a dose in any other facility may be expressed as an equivalent dose in the standard facility and this is referred to as the "integrated damage flux" or the damage dose.

It cannot, however, be assumed that the state of the graphite after a given integrated damage flux is independent of the magnitude of that flux. Thus, it is further postulated that displaced atoms are produced at a rate proportional to ϕ_d and pass through a sequence of configurations at a rate which is governed by a particular thermal process with an activation energy Q. Then at a temperature θ, the rate of accumulation of damage is a function of $\phi_d / \exp[-Q/k\theta]$, k being Boltzmann's constant. For two irradiations, characterized respectively by $((\phi_d)_1, \theta_1)$, $((\phi_d)_2, \theta_2)$, the damage accumulation per unit dose will be the same if

$$\frac{1}{\theta_1} - \frac{1}{\theta_2} = \frac{k}{Q} \ln \frac{(\phi_d)_2}{(\phi_d)_1}. \tag{3}$$

It is therefore possible on this theory to express the results of any experiment carried out under constant irradiation conditions in terms of a dose and a temperature for an irradiation at a standard flux. If $(\phi_d)_1$ is this standard flux, θ_1 is referred to as the equivalent irradiation temperature for an irradiation at θ_2 with damage flux $(\phi_d)_2$.

The first experiment is a test of the single-parameter theory applied to the calibration of high-flux, hollow fuel-elements in DR3 in terms of the vertical facility TE10 in BEPO, while the second is a test of Eq. (3) for a limited range of conditions.

BELL et al. determined a value of 1.58 eV for Q, but there was considerable scatter in the experimental results. Furthermore, only one physical property change, namely electrical resistivity, was investigated.

2. EXPERIMENTAL DETAILS

Irradiation facilities

Reference is made to irradiations in two reactors, BEPO and DR3, which have been fully described elsewhere [2, 3], but a few details are given here which are relevant to the present experiments. BEPO is an air-cooled, natural-uranium-fuelled and graphite-moderated research reactor with the fuel contained in horizontal channels. The results used here were obtained from specimens irradiated in thermostatically controlled rigs in the vertical facility TE10, where the maximum fast flux is less than 10^{11} n cm^{-2} s^{-1} at a normal reactor power of 6½ MW. In contrast DR3, heavy-water moderated and cooled, with fuel elements of highly-enriched uranium, is intended for use as an MTR with a maximum fast flux of 4×10^{13} n cm^{-2} s^{-1} at a power output of about 10 MW. The standard fuel element consists of ten fuel plates welded into a box with side plates but any of the 26 standard elements may be replaced by special 'hollow' fuel elements in which the fuel plates are arranged between two concentric tubes to provide a central space, some 6 cm in diameter, for experiments requiring a large fast-neutron flux.

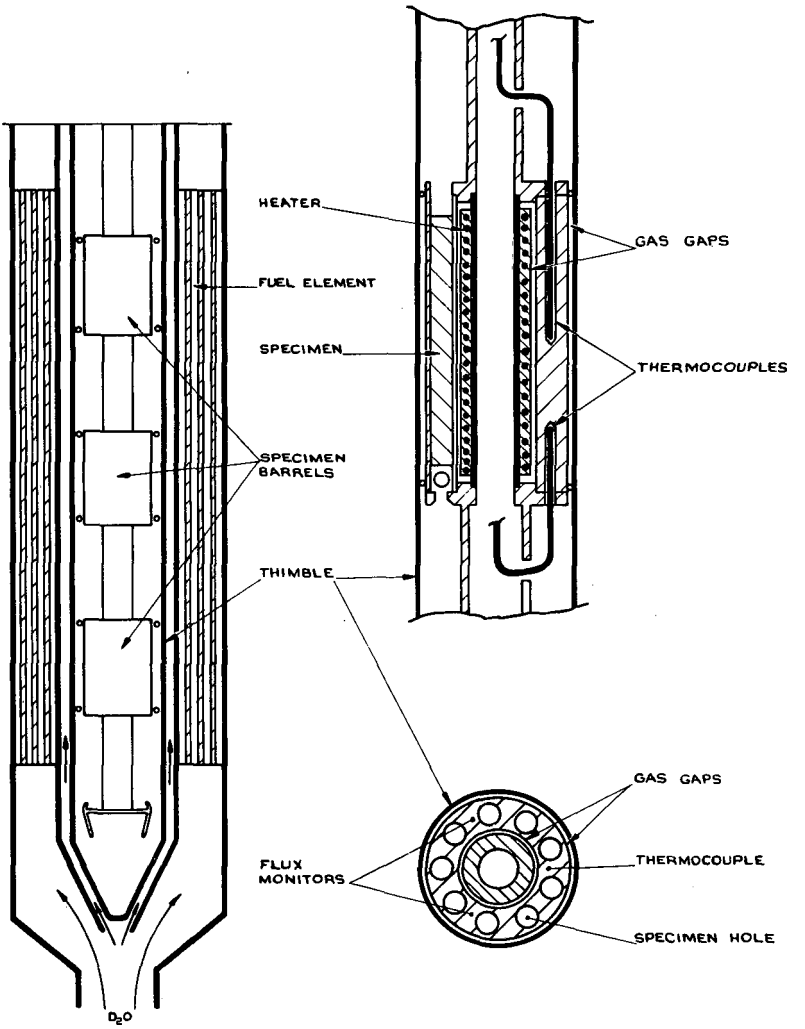


Fig. 1

Details of irradiation rig

The design of the rigs used for these facilities is shown schematically in Fig. 1. Three specimen magazines in the form of hollow cylinders of aluminium are suspended along the axis of a Zircaloy thimble. Temperature control is obtained by means of a central heater and careful choice of the gas gap between magazine and thimble. The gas used is either helium or a helium-neon mixture. Further details may be found in BELL et al. [1].

Measurements of irradiation doses by foil activation

The use of Eqs. (1) and (2) in the manner described requires that the ratio ϕ_d / ϕ_m remains constant for a given facility. In a reactor fuelled with

natural uranium like BEPO it is theoretically possible to use either fast or thermal detectors providing the absorber pattern of the reactor remains constant, since the variation of spectrum with the burn-up of U^{235} is negligible. In an enriched reactor like DR3 this is no longer true and the ratio of fast to thermal flux can vary by over 30% with burn-up. However, BELL et al. have shown that the ratio ϕ_d/ϕ_m is independent of fuel element burn-up if the reaction $Ni^{58}(n,p)Co^{oc}$ is used to determine ϕ_m. As the accurate measurement of doses by this method is difficult, particularly for long irradiations, an indirect method is used here which makes use of the thermal-neutron doses measured using cobalt foils, the ratio of the two fluxes being derived from Eq.(4) [1].

$$\phi_{Ni}/\phi_{Co} = 0.378 - 0.404\,b, \qquad (4)$$

where ϕ_{Ni} is the flux measured by nickel activation in DR3, ϕ_{Co} is that measured by cobalt activation in DR3 and b is the fraction of U^{235} in the fuel element burned up.

Eq.(4) was determined in irradiations of short duration at low thermal-flux levels. The cross-sections used in calculating the fluxes and in the derivation of Eq.(4) are the same as those in [1] and are shown in Table I.

TABLE I

SOME DATA ON THE REACTIONS USED FOR FLUX MEASUREMENT

Reaction	Cross-section (b)	Half-life of product nucleus
$Co^{59}(n,\gamma)Co^{60}$	38	5.25 yr
$Ni^{58}(n,p)Co^{58}$	0.107	72 d

It should be noted that the fuel elements in DR3, each containing 115 g U^{235} when new, were effectively unchanged in position during these irradiations, thus avoiding errors due to large variations in burn-up between adjacent elements.

The flux-measuring foils were not situated at the centre of the sample magazines and doses measured by the cobalt foils in each barrel were corrected to the level of the centre-line of the specimens, using the results of flux distributions measured in the core central position, before computation of the nickel doses.

Specimens and methods of measurement

According to the concepts of equivalent damage flux and equivalent temperature, the changes in different properties produced by an irradiation at a given temperature and flux must bear a unique relationship to one another and to the integrated-damage flux for a given graphite. Such a single relationship may only be used for several specimens if all the graphite has

been prepared from the same raw materials in an identical manner, which means in practice that for precise work one must at least use specimens cut from a single block of graphite. Even then, small corrections may be necessary to allow for inhomogeneities present. As a result of this requirement a selected block of graphite was used for the preparation of specimens for each of the experiments. These two blocks were of British extruded reactor-grade graphite, of the type denoted Grade A [4] and specimens for irradiation in DR3 had a nominal diameter of a quarter of an inch and lengths of 0.5 and 3.0 in.

The methods of analysis used are such that any systematic errors in the experimental measurements on specimens cannot affect the conclusions reached. Some data covering the effects of random errors are given later.

Electrical resistivities were determined using the potential probe method, while changes in Young's modulus were calculated from changes in the resonant frequencies for transverse oscillations; thermal-conductivity measurements were made using the Kohlrausch method. Length measurements were made using a block-gauge technique with an estimated accuracy (one standard deviation) of ± 10 ppm.

X-ray measurements were made using a Philips type P11050 wide-range goniometer and a PW1010/30 X-ray diffraction generator the values quoted; are taken from the (0002) reflection for c-spacing and (1120) for a-spacing, corrections being made for absorption, polarization, temperature and other factors.

The determination of the equivalent damage flux for DR3

Although in theory any change in the properties of graphite may be used for a comparison of damage fluxes in different facilities, in practice changes in electrical resistivity are usually chosen since such changes may be measured accurately and in addition, the variation with irradiation is very rapid during the initial period, thus allowing the use of short irradiations with the minimum variation in conditions.

Comparative data from TE10 in the range 25 to 180°C may be represented empirically by Eq. (5) [1], the accuracy of this equation for a temperature of 51°C being clearly demonstrated in Fig. 2 using data from SIMMONS [5].

$$\chi = (\rho/\rho_0) - 1 = 0.162\,(1 - 0.00514\,T)\,(\phi_{TE}\,t \times 10^{-16})^{0.75}, \qquad (5)$$

where T is the irradiation temperature (°C), ρ_0 is the resistivity before irradiation, ρ is the resistivity after irradiation, ϕ_{TE} is the nickel flux (measured directly in the experiment) in n $cm^{-2}s^{-1}$ and t is the duration of the irradiation in seconds.

Material from the same block of graphite from which these specimens were machined was made available for the calibration of DR3 and twelve sets of six specimens were irradiated in hollow fuel element positions, each set being chosen to have approximately the same mean unirradiated electrical resistivity. The initial irradiations were carried out for 48 h and 24 h respectively in each of two pairs of central positions, while the core contained new fuel elements. Subsequently some of the specimens were twice re-

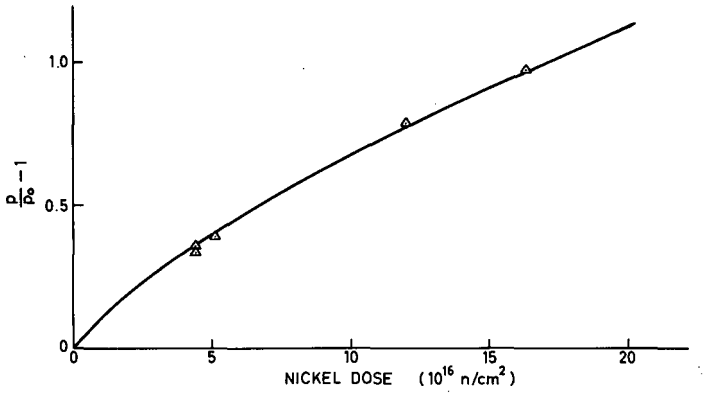


Fig. 2

Fractional change of resistivity for specimens in TE10 BEPO (at 51°C)

△: Experimental values [5]
—: $(\phi_t)^{0.75}(1 - 0.00514\ T)\ 0.162 = P/P_0 - 1$

irradiated for periods of 36 h, when the fuel burn-up corresponded to a change of not more than 4% in the ratio of fast to thermal flux.

The reactor power was 300 kW for these irradiations while nominal temperatures of 50°C were maintained for each barrel. The temperatures indicated on an associated strip-chart recorder were stable to ± 1°C in most cases, while at least once during each irradiation a potentiometer was used to measure the output of the control thermocouple and in some cases the outputs of the other two thermocouples. The maximum temperature difference corresponding to the three thermocouple readings within a single barrel was 6°C. Some details of the irradiations are given in Table II, together with the average value of the fractional change in resistivity after each irradiation.

The values of $(\phi_{TE}t)$ calculated from Eq. (5), using the measured resistivity changes in the rig and putting T equal to the observed irradiation temperatures, are also given in the table. Fig. 3 is a graphical comparison of the calculated values $(\phi_{TE}t)$ with the nickel doses in the rigs; the linearity of this relationship demonstrates the applicability of the equivalent damage flux concept. In the absence of an effect of flux level the slope of the line would give the conversion factor from ϕ_{Ni} to ϕ_d (now defined using TE10 as the standard facility). If the flux spectrum varied with position a single line could only have been obtained from successive irradiations in a single barrel. It is important to note, therefore, that the calibration factors are the same for each position examined within the limits of accuracy of the experiment.

The analysis of the main experiment described later yields a value of 1.2 eV for Q and Eq. (3) can then be applied to determine the true conversion factor to ϕ_d using an iterative process. Thus from the values of $(\phi_{TE}t)$ and the irradiation time in Table II, values of ϕ_{TE} may be calculated and used as a first approximation to $(\phi_d)_2$ in Eq. (3), with $(\phi_d)_1$ equal to the nickel flux in TE10, i.e. 0.9×10^{11} n cm^{-2} s^{-1}. Thus, approximate values of the

TABLE II

THE CALCULATION OF DAMAGE FLUXES FOR THE EQUIVALENT-FLUX EXPERIMENT

Specimen set number	Barrel*	Position in reactor	Irr. temp. (°C)	Irr. time (10^4 s)	Period nickel dose (10^{17} n/cm^2)	Total nickel dose (10^{17} n/cm^2)	Average Value of $\rho/(\rho_0-1)$	$\phi_{TE}t$ (10^{16} n/cm^2)	θ (°C)	ϕ_{dt} (10^{16} n^2/cm)
1	T	B2	49	17.09	1.22	1.22	0.499	6.51	39	6.04
2	M	B2	53	17.09	2.02	2.02	0.689	10.5	40	9.37
3	B	B2	56	17.09	2.00	2.00	0.707	11.2	42	9.87
4	T	B4	53	17.09	1.45	1.45	0.569	8.15	41	7.31
		D3	52	12.97	1.09	2.54	0.893	14.8	41	13.3
		D3	53	12.65	1.09	3.63	1.158	21.0	41	18.9
5	M	B4	52	17.09	2.25	2.25	0.788	12.5	38	11.0
6	B	B4	49	17.09	2.34	2.34	0.837	13.1	35	11.6
7	T	D5	51	8.64	0.63	0.63	0.291	3.27	41	2.99
8	M	D5	52	8.64	1.04	1.04	0.420	5.39	39	4.80
9	B	D5	53	8.64	1.04	1.04	0.430	5.61	39	4.95
10	T	D3	53	8.64	0.74	0.74	0.329	3.93	42	3.56
11	M	D3	52	8.64	1.16	1.16	0.483	6.49	38	5.73
		D3	53	12.97	1.72	2.88	0.966	16.5	39	14.5
		D3	54	12.65	1.63	4.51	1.312	24.8	39	21.9
12	B	D3	53	8.64	1.24	1.24	0.495	6.77	38	5.93
		D3	51	12.97	1.90	3.14	0.999	17.1	37	15.0
		D3	52	12.65	1.72	4.86	1.349	25.6	37	22.4

* T = Top barrel
M = Middle barrel
B = Bottom barrel

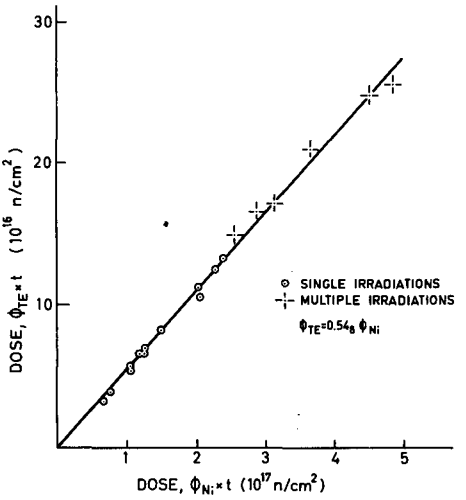


Fig. 3

Comparison of $\phi_{TE}t$ with the measured dose

equivalent temperature θ_1 are derived and are used to compute new values of $(\phi_{TE}t)$ using Eq.(5). This is repeated until no change is produced in the values obtained for θ_1. The final values of θ_1 and $(\phi_{TE}t)$ [= $\phi_d t$] are given in Table II.

The values of $(\phi_d t)$ and $(\phi_{Ni}t)$ are compared in Fig. 4 and the required calibration factor, ϕ_d/ϕ_{Ni} is determined by the slope of the best line. This was calculated using only data from the initial single irradiations, to reduce errors due to the small variations in temperature between successive periods of the multiple irradiations and also because Eq.(5) must be ex-

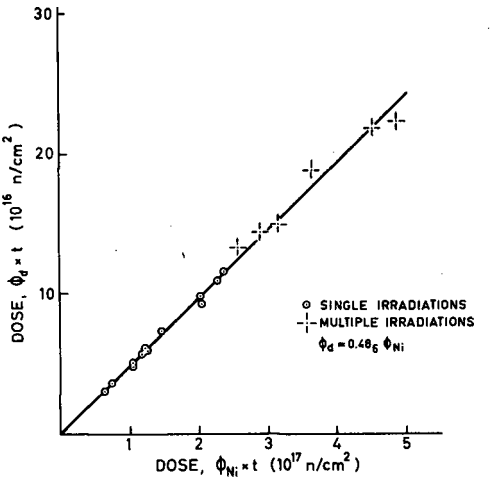


Fig. 4

Comparison of the integrated damage flux $\phi_d t$ with the measured dose

trapolated beyond the experimental data in order to determine ϕ_d from values of $(\rho/\rho_0)^{-1}$ for some of the multi-irradiated specimens. These experiments clearly demonstrate that measurements of nickel flux in any of the irradiation facilities examined in DR3 are directly related to ϕ_d and thus nickel flux measurements alone may be used in later experiments.

The flux-level experiment

In this experiment specimens taken from one block of graphite were irradiated in one hollow fuel element position in DR3 with the reactor operating at nominal powers of 1 and 10 MW. The results for specimens irradiated in a second position during the 1 MW run were also used in the analysis. Nominal irradiation temperatures were chosen to give comparisons for the same actual and equivalent irradiation temperatures assuming that Eq.(3) applied with Q equal to 1.2 eV, a value originally chosen on the basis of the annealing of resistivity changes as reported by KINCHIN[6]. These temperatures are given in Table III together with those actually measured for each period of irradiation, the irradiation times and a representative set of doses. The actual doses varied from specimen to specimen because of the variations of position in the rig of specimens with different sizes. The quoted temperatures assume a difference of 5°C between specimens and barrel when the reactor is operating at 10 MW [1].

The changes in Young's modulus and in electrical and thermal resistivity were studied on specimens cut parallel to the extrusion axis, while both parallel and perpendicular-cut specimens were irradiated for the study of dimensional changes. The measured changes are summarized in Figs. 5-12 in a form which clearly shows the effect of flux level. Both in these figures and in the subsequent discussion, a standard flux level of 4.4×10^{12} n cm^{-2} s^{-1} is used as the basis for the equivalent temperatures, this being approximately the nickel flux in the middle and bottom barrels of the rigs with the reactor operating at 1 MW. In the method of analysis adopted it is assumed that the effect of flux level is described by Eq.(3) and the appropriate value of Q is 1.2 eV. The assumption is then tested by plotting property changes against the equivalent temperatures calculated from Eq.(3).

The variation with equivalent temperature of the change in Young's modulus for a dose of 2.0×10^{19} n/cm^2 obtained from the experimental results by interpolation is shown first in Fig.5. The error limits on the modulus changes are the standard errors of the means of the results from the groups, each initially of six specimens. The limits on the temperature show the effect of a change of 0.1 eV in the value assumed for Q. In addition, there is a random uncertainty of two to three degrees in the temperatures for experimental reasons. It may be seen from the graph that the application of the equivalent-temperature concept results in agreement between points from irradiations under 'equivalent' conditions. An exact numerical value for Q cannot be derived without an assumption as to the temperature dependence of the property change, but the existence of a flux-level effect is clearly demonstrated and furthermore the equivalent-temperature correction with 1.2 eV for Q represents it quite adequately.

Electrical resistivity changes at two doses are similarly displayed in Fig.6 and the same conclusions apply. A variation in temperature de-

TABLE III

SOME IRRADIATION DETAILS FOR THE FLUX-LEVEL EXPERIMENT

Reactor position code of rig		B4			B4+			D3		
Reactor power (MW)		1			10			1		
Irradiation time (10^5 s)	Period 1	27.6			(0.537+2.11)			27.6		
	Period 2	21.4			3.62			21.4		
	Period 3	20.1			4.16			20.1		
Barrel		T (Top)	M (Middle)	B (Bottom)	T	M	B	T	M	B
Nominal specimen temperatures (°C)		182	182	150	219	219	182	210	210	210
Observed specimen temperatures (°C)	Period 1	186	184	152	{216 / 218}	{219 / 220}	{174 / 185}	214	213	210
	Period 2	186	186	151	218	220	186	214	216	211
	Period 3	186	186	151	218	219	183	214	215	211
Typical nickel doses (10^{18} n/cm^2)	Period 1	8.50	12.0	12.7	1.35 6.46	2.06 8.50	2.14 8.76	8.31	11.7	12.6
	Period 2	6.47	9.09	9.42	10.5	14.7	14.4	6.44	9.16	9.50
	Period 3	6.22	8.98	8.68	12.4	15.9	16.4	6.14	8.98	9.05

+ First irradiation period at 10 MW in two parts owing to enforced change of rig.

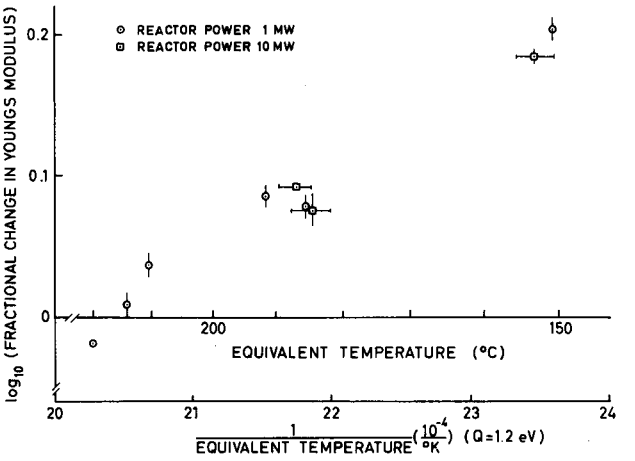


Fig. 5

The variation of the change of Young's modulus with temperature at a dose of 2.0×10^{19} n cm^{-2}

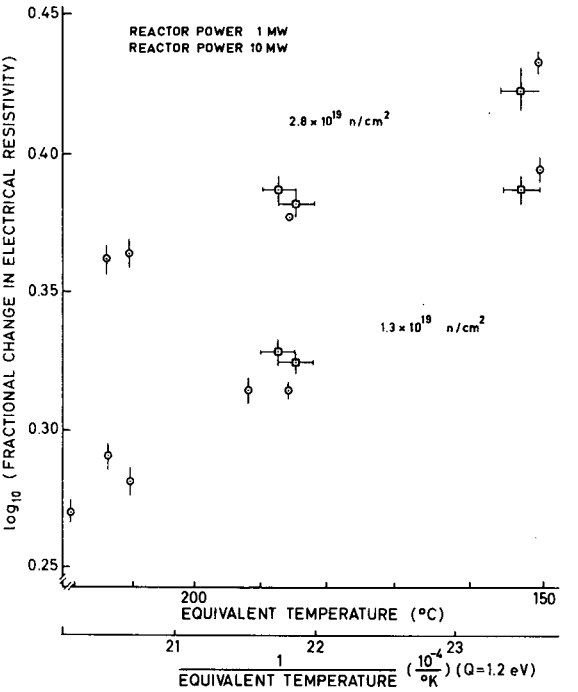


Fig. 6

The variation of the change of electrical resistivity with temperature

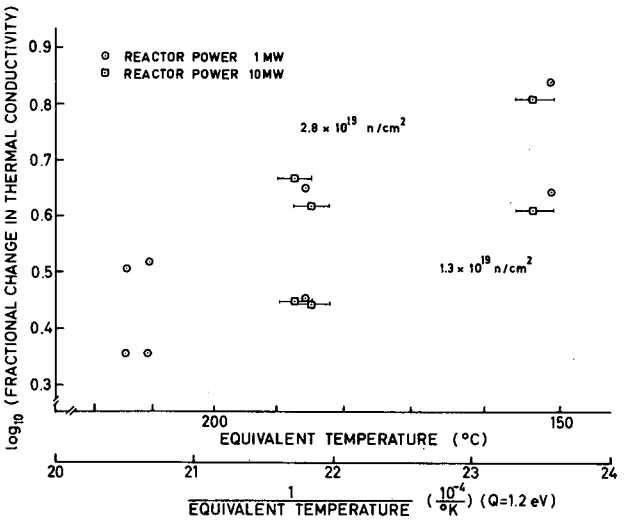


Fig. 7

The variation of the change of thermal conductivity with temperature

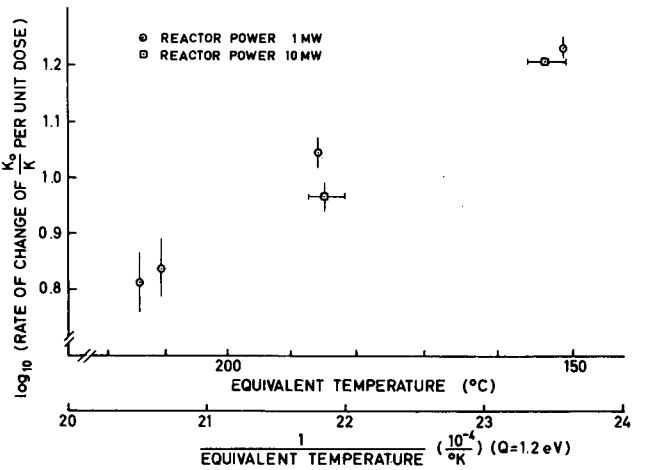


Fig. 8

The variation of the change of thermal conductivity per unit dose with temperature

pendence with dose is clearly shown. Fig. 7 is the corresponding graph for thermal-conductivity changes, while Fig. 8 shows the temperature variation of the change of thermal conductivity per unit dose. Again a flux-level correction is confirmed with a value of 1.2 eV for Q.

The temperature variation of the length changes and of the final rate of change per unit dose for specimens cut perpendicular to the extrusion direction are given in Figs. 9 and 10, with each point representing a single specimen. Fig. 11 shows the variation of length with dose for parallel-cut

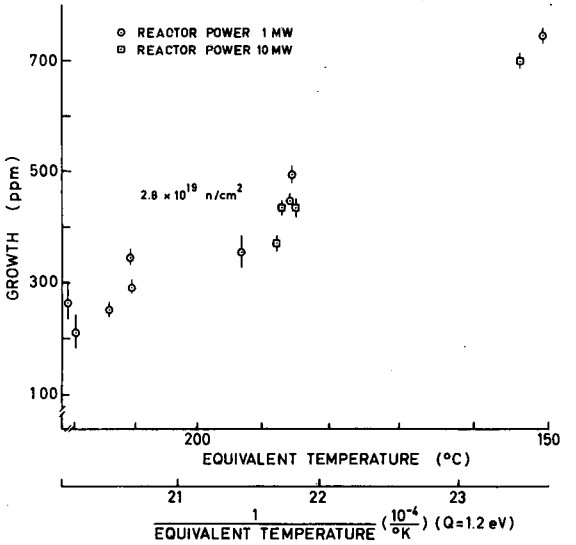


Fig. 9

The variation of the growth of perpendicular cut specimens with temperature

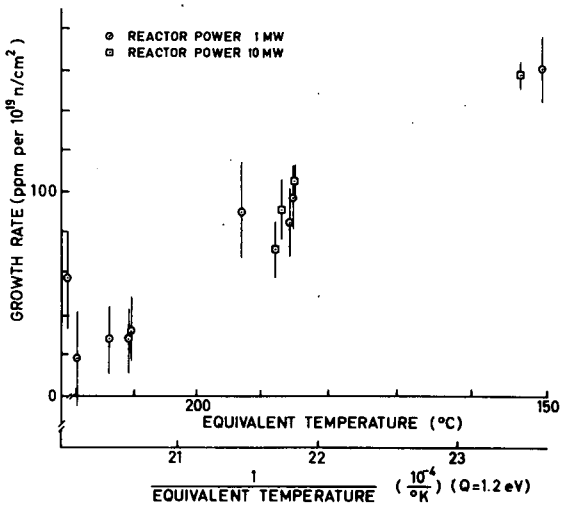


Fig. 10

The variation of the growth rate per unit dose with temperature for perpendicular cut specimens

specimens and besides showing the lack of a strong temperature dependence indicates the precision of the measurements.

Theoretically, differences in the co-efficient of thermal expansion between specimens of graphite also correspond to differences in the rates of dimension-changes with dose at a given irradiation temperature [7]. Differences between specimens cannot be corrected for in the case of the small

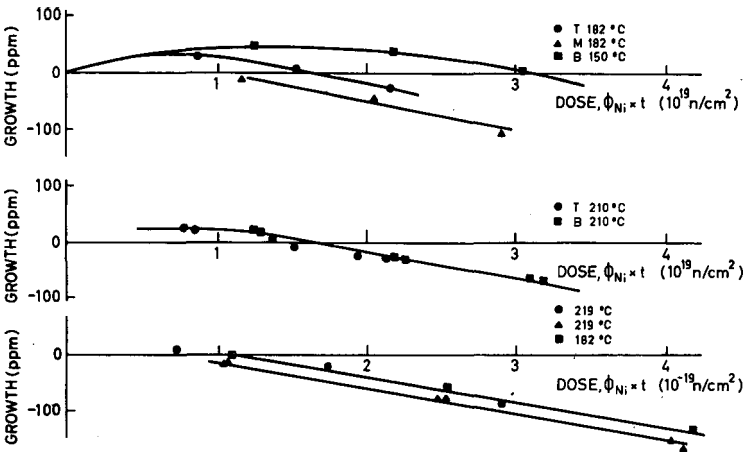


Fig. 11

The growth of parallel cut specimens with dose

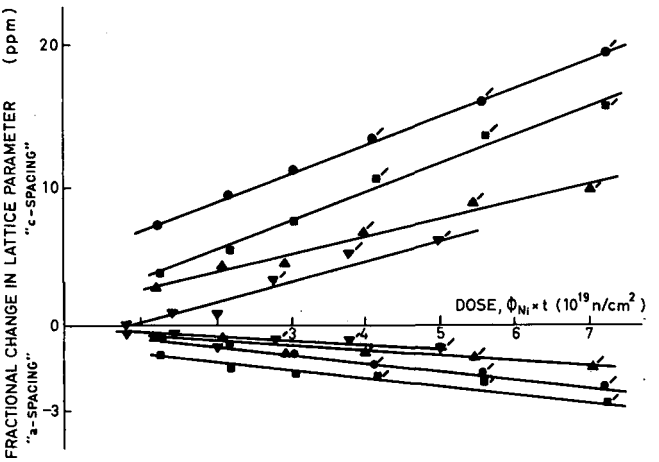


Fig. 12

The variation of the lattice parameters with dose

specimens used here. This does not, however, affect the conclusion from Figs. 9 and 10 that a flux-level effect exists for the perpendicular-cut specimens, although such an effect is undetectable in Fig. 11 for parallel-cut specimens owing to the lack of temperature dependence. Fig. 12 shows the changes of crystal-lattice parameters obtained by X-ray measurements for specimens irradiated successively at the two flux levels but with only small changes in equivalent temperature. The absence of any abrupt changes in slope when the irradiation temperatures were raised 30°C in conjunction with the increase in flux intensity again confirms the existence of a flux-level effect of about the predicted magnitude; since these changes are res-

ponsible for a large part of the bulk dimension-changes, this is additional evidence in favour of 1.2 eV for Q for the latter changes.

3. DISCUSSION

The experimental results are consistent with a single parameter representation of the damaging efficiency of a reactor flux with respect to graphite, with a ratio of ϕ_d / ϕ_{Ni} which is the same for all the hollow fuel element facilities tested in DR3. Moreover, the value of this ratio is comparable with previous values measured in similar facilities in DIDO and PLUTO at Harwell [1]. Further, they show that, within the limits of experimental error, an accurate allowance for the effect of the magnitude of ϕ_d on the changes in physical properties produced by a given integrated damage-flux may be made using Eq.(3) with a value of 1.2 eV for Q over the range of irradiation flux, dose, and temperature considered.

Any prediction of the behaviour of graphite under irradiation, which made direct use of the results of these experiments, could be in error both because of experimental error and due to the breakdown of the theories of equivalent flux and temperature.

Considering the former source of errors first, these may arise in the estimation of the doses and temperatures and the measurements of the property changes. In the calibration experiment the latter error was negligible, doses were measured to within 1% and under the conditions of low-power operation of DR3 irradiation temperatures could be determined to within 2°C. Thus, making due allowances for variations of flux level within the rigs, the calibration factor to TE10 may be estimated to within 2% while tne relative values of ϕ_d / ϕ_{Ni} within different hollow fuel element facilities in DR3 are known to ± 1%.

In the flux-level experiment, an additional source of error is present in calculating the doses owing to the use of Eq.(4), but because of the small variation in core conditions during the experiment, it is insignificant. The possible effect on the value for Q of an error in any of the physical-property measurements may be deduced from an examination of the various graphs, and it may be seen that in general only the confidence limits are affected. The possible error in the determination of the irradiation temperature is of greater importance since the difference between the specimen magazine and the specimen is dependent on the power level of the reactor. The difference is small for low-power runs but it has been shown [1] that 5°C (equivalent to a charge of 0.1 eV in Q) is likely during operation at 10 MW. Since this calculated difference has been allowed for, the expected error in Q due to this cause is less than 0.1 eV. Consideration of all the graphs referring to the temperature dependence of the physical-property changes shows that an alteration of 0.1 eV in the value used for Q would clearly lessen the agreement in a majority of cases and we may write $Q = 1.2 \pm 0.1$ eV. The standard sources for the dose measurements have been compared with those used by Bell et al., but the results were not available in time to correct the figures in this paper to the same dose scale (difference less than 4%).

Before proceeding to a discussion of the theoretical interpretation of the experimental results and the extrapolation to other conditions, it is worth emphasizing the practical importance of an effect of flux level.

TABLE IV

THE VARIATION OF EQUIVALENT TEMPERATURE WITH FLUX LEVEL FOR SOME TYPICAL TEST-RIG TEMPERATURES (Q = 1.2 eV)

Irradiation temperature (°C)	Damage flux, (Arbitrary units)	Equivalent irradiation temperature at unit flux (°C)
155	1	155
	10	125
	100	105
355	1	355
	10	295
	100	250
655	1	655
	10	540
	100	440

Table IV gives the computed equivalent temperatures at unit flux for specimens irradiated at 155, 355 and 655°C in rigs giving ten and hundred-fold reduction in irradiation time. It is clear from a consideration of the known temperature dependence of the damage to graphite that major design errors are possible if incorrect allowance is made for the flux level when applying data from MTR tests to power-reactor conditions. For this purpose, the correction required is for doses as much as fifty times greater than in these irradiations since, using the data of BELL et al. [1], they correspond to less than six months' irradiation of the core of graphite-moderated reactors of current design. Although undesirable, the use of the equivalent-temperature correction could be separated from any explanation since it may be shown that the damage flux during the low-power (1-MW) runs corresponds approximately to these reactors and during the high-power runs to conditions in a standard test rig.

The hypotheses on which these experiments were based are the simplest possible if the existence of a temperature dependence for graphite irradiation damage is to be taken into account.

Irradiation annealing will not affect the single-parameter representation of the flux as long as $\psi(\epsilon)$ represents a net effect on the state of the graphite due to processes whose nature is independent of the neutron energy, only their frequency of occurrence being affected by the latter. Perhaps it is significant that considerable success has been achieved [8] in calculating relative values of ϕ_d/ϕ_m for different spectra by assuming that $\psi(\epsilon)$ is proportional to the average number of carbon atoms displaced per collision by a neutron of energy ϵ.

While the postulates used lead to a convenient way of allowing for flux level which satisfies the present experimental results, it can only be an

approximation to state that the sequence of configurations of all newly displaced atoms is the same after a given dose under equivalent conditions, as defined by Eq.(3). For example, the lowest activation energy for which measurable defects are present after irradiation is determined by thermal annealing. However, the annealing rate is insignificant for the majority of defects and the approximation is valid provided that the flux ratio is not too great, or the damage level too small. The "state of the graphite" after a given irradiation must, in general, be inferred from observed property changes and while the state of the material uniquely defines the property change, the converse is not true and similar changes in one or more properties could result from different damage configurations. In addition, recent work by REYNOLDS et al. [9] supports the hypothesis that the damage observed is due to interstitial clusters, the sizes of which possibly depend on the irradiation conditions, and to single vacancies which may cluster at high irradiation temperatures and/or high levels of exposure.

However, what may be termed the importance factor [10] relating defects to the property changes which they produce is unlikely to vary significantly for small changes in conditions. Any rapid variation in the importance factor in these experiments would have caused the value of Q to vary with the property considered. In fact, such variations as occurred are within the experimental error but variations are likely to be significant if attempts are made to use the results for conditions far removed from those of the experiment.

A more serious criticism of Eq.(3) is that the formation of many complex defects and the associated distortion of the lattice must modify the diffusion of single and low-order primary groups and this may modify the equivalent-temperature concept, the present form being applicable only to low-damage levels.

The results of a thermal-annealing experiment were used to make the original estimate of Q and using more recent studies, limits may be placed on the likely range of values. Thus, while, as mentioned above, most of the final defects do not anneal thermally at the irradiation temperature, the observed damage is strongly dependent on this temperature and hence the damage accumulation must be controlled by some thermal process or processes. This is basic to the equivalent-temperature concept. From the results of this experiment and the data given by BRIDGE et al. [10], it is probable that the activation energies for such processes are less than 1.5 eV while the temperature dependence of property changes may frequently be associated with an activation energy which is nearer 0.3 eV. It may be that any difference between Q and this latter value is to be associated with the order of reaction of the postulated dominant process which, according to present experiments, must be about four. On this basis, it is possibly incorrect to assume that Eq.(3) with Q equal to 1.2 eV can be applied for irradiations at 50°C and this would alter the numerical value obtained for ϕ_d/ϕ_m. A simple check would be to repeat the calibration, but at a reactor power of about 100 kW.

Different flux-conversion factors for different properties appear to be empirically possible, but are, in fact, incompatible with any universal equivalent-temperature concept, since it would not be possible for the equiva-

lent temperatures to be the same for two properties at all flux levels in more than one facility.

Although probably connected with irradiation annealing (which is beyond the scope of this paper) it is worth pointing out that the dominant process may be merely the process with the highest activation energy that is significantly affected by thermal annealing. Thus the process concerned would be dependent on irradiation temperature. As it is essential, however, for the major production term for such defects to be flux-dependent, an assessment of this process requires a more detailed knowledge than is now in existence of the damage mechanism particularly with regard to a successive-reaction model. Such a mechanism might reduce the effect of flux level as the temperature was raised due to the increasing value of Q. The differing behaviour of interstitials and vacancies is of considerable interest in this respect.

4. CONCLUSION

The experiments have demonstrated that the flux determined by nickel activation in core position in DR3 is an excellent measure of the defined damage-flux. The experiments also clearly show that the rate of build-up of damage is dependent on flux intensity and that this effect can be represented by the concept of equivalent temperature through the equation

$$\frac{1}{\theta_1} - \frac{1}{\theta_2} = \frac{k}{Q} \ln \frac{(\phi_d)_2}{(\phi_d)_1} \qquad (3)$$

with Q = 1.2 eV. In many materials the mechanism of irradiation damage is related basically to that in graphite and it is to be expected that an effect of flux level is more general than has been acknowledged in the past.

ACKNOWLEDGEMENTS

The experiments described in this report required the co-operation of many people. These included J.H. Kramers who carried out the X-ray measurements, J. Olsen who carried out the flux measurements, the staff of DR3 who were very helpful during the extended period when they were running their reactor and the rigs in accordance with the strict requirement of these experiments, and not least, J.H.W. Simmons of Harwell who took part in many helpful discussions and provided the standard graphite. One of the authors (B.S. Gray) would like to thank the staff at Risø for their hospitality while the experimental programme was being performed.

The permission of the Executive Committee of the Danish Atomic Energy Commission and the Managing Director of the Reactor Group of the United Kingdom Atomic Energy Authority to publish this paper is gratefully acknowledged.

REFERENCES

[1] BELL, J.C., BRIDGE, H., COTTRELL, A.H., GREENOUGH, G.B., REYNOLDS, W.N. and SIMMONS, J.H.W., Stored Energy in the Graphite of power-producing reactors. Phil. Trans. Roy. Soc. (London) Series A 254 Sect. 1043 (1962) 361-395.

[2] Directory of Nuclear Reactors, IAEA, Vienna, II (1959) 323.
[3] Directory of Nuclear Reactors, IAEA, Vienna, II (1959) 293.
[4] O'DRISCOLL, W. G. and BELL, J. C., Materials for Nuclear Engineering, Ch. 7, Graphite, Temple Press Books, London (1960).
[5] SIMMONS, J. H. W., Metallurgy Division, AERE, private communication.
[6] KINCHIN, G. H., The effects of irradiation on graphite, Proc. UN. Int. Conf. PUAE 7 (1956) 472.
[7] SIMMONS, J. H. W., The effects of irradiation on the mechanical properties of graphite, Proc. Third Conf. on Carbon, Pergamon Press (1958) 554.
[8] WRIGHT, S. B., The use of Monte-Carlo calculations in the analysis of radiation damage experiments, Radiation damage in solids, IAEA, Vienna, II (1962) 239.
[9] REYNOLDS, W. N., THROWER, P. A. and SHELDON, B. E., Nature 189 (1961) 824.
[10] BRIDGE, H., KELLY, B. T. and GRAY, B. S., Stored Energy and dimensional changes in reactor graphite, Proc. Fifth Conf. on Carbon, Pergamon Press, Oxford (1962).

IRRADIATION DAMAGE IN GRAPHITE

W. N. REYNOLDS AND P. A. THROWER
ATOMIC ENERGY RESEARCH ESTABLISHMENT,
HARWELL, BERKS., ENGLAND

Abstract — Résumé — Аннотация — Resumen

IRRADIATION DAMAGE IN GRAPHITE. A wide study of defect clusters formed in graphite by high-flux neutron irradiation at temperatures up to 650°C has been made, using the techniques of transmission electron microscopy. A linear relationship exists between cluster size and irradiation temperature, and the subsequent annealing behaviour of the defects is consistent with the hypothesis that the visible defects are all of one kind, probably interstitial. The difficulty of measuring film thicknesses has so far prevented an accurate comparison of defect behaviour with that of macriscopic properties, but there is sufficient evidence to show that other defects than those visible must be involved. Some observations at the highest temperatures and doses suggest that vacancy clusters may also become identifiable.

DOMMAGES CAUSÉS PAR L'IRRADIATION AU GRAPHITE. Les auteurs ont procédé à une vaste étude des défauts qui s'accumulent dans le graphite à la suite d'une irradiation par un flux de neutrons dense à des températures atteignant 650°C, en recourant aux méthodes de transmissions au microscope électronique. Il existe une relation linéaire entre la dimension de l'amas et la température d'irradiation; en outre, le comportement des défauts pendant le recuit confirme l'hypothèse d'après laquelle les dommages visibles sont tous de même espèce et qu'ils sont probablement interstitiels. La difficulté de mesurer l'épaisseur de la coupe mince a jusqu'ici empêché de comparer avec précision le comportement du défaut avec celui des propriétés macroscopiques, mais on possède suffisamment d'éléments prouvant qu'il doit y avoir d'autres défauts que ceux qui sont visibles. Certaines observations aux températures les plus élevées et avec les doses les plus intenses laissent présager la possibilité d'identifier aussi des amas de lacunes.

РАДИАЦИОННОЕ ПОВРЕЖДЕНИЕ В ГРАФИТЕ. Методом трансмиссионной электронной микроскопии проводилось широкое исследование скоплений дефектов, образовавшихся в графите в результате облучения его потоком нейтронов большой плотности при температуре 650°С. В результате исследования установлено наличие линейной связи между размером скопления и температурой облучения, а последующее поведение дефектов при отжиге соответствовало предположению о том, что видимые дефекты имеют один и тот же характер, т.е. по-видимому, междоузельный. Трудность измерения толщины пленки пока не позволила дать сравнение поведения дефекта с макроскопическими свойствами, но имеется достаточно доказательств для подтверждения того, что сюда вовлечены другие деффекты, кроме видимых. Некоторые наблюдения при самых высоких температурах и дозах говорят о том, что скопления вакансий могут оказаться также доступными для опознавания.

DAÑOS CAUSADOS POR LA IRRADIACIÓN EN EL GRAFITO. Aplicando las técnicas de microscopía electrónica de transmisión, los autores hicieron un estudio general de los racimos de defectos formados en el grafito por exposición a un elevado flujo neutrónico a temperaturas hasta 650°C. Comprobaron que el tamaño de los racimos es función lineal de la temperatura de irradiación y que el ulterior comportamiento de los defectos, cuando el material se somete a un recocido, es compatible con la hipótesis de que los defectos visibles corresponden todos a un tipo único, probablemente intersticial. La dificultad de medir los espesores de las películas ha impedido hasta ahora que se establezca una comparación precisa entre el comportamiento de los defectos y las propiedades macroscópicas, pero existen suficientes pruebas de que intervienen otros defectos, además de los visibles. Ciertas observaciones realizadas a temperaturas y dosis más elevadas sugieren que es posible que también sean susceptibles de identificarse los racimos de vacantes.

1. INTRODUCTION

In 1960, BOLLMANN [1] described point defects he found by the transmission electron microscopy of neutron-irradiated graphite. Defects simi-

lar to those he saw have also been reported by WILLIAMSON and BAKER [2], BACON and SPRAGUE [3] and IZUI and FUJITA [4] working on various kinds of graphite and in a variety of irradiation conditions. The present authors have already published a preliminary account of the effects of different irradiation and annealing temperatures on the behaviour of the defects [5]. The most detailed interpretations of the nature of the defects so far given are those of WILLIAMSON [6] and BOLLMANN [7, 8, 9]. The extension of our work, however, has led to the conclusion that the behaviour of all true radiation defects can be described in terms of a simple homogeneous nucleation theory with some features peculiar to graphite. Our identification of the defects arises from correlation with well-established data on macroscopic behaviour rather than from pure microscopy, and reasons will be given to show that identifications of vacancy and interstitial loops and other defects proposed elsewhere are not well founded.

2. EXPERIMENTAL RESULTS

The bulk of the work to be described was performed on natural crystals of graphite showing regions of high perfection, irradiated in a hollow fuel element in one of the heavy-water-moderated research reactors DIDO[1] or PLUTO[2] for 3-4 weeks to nickel activation[3] doses of $(0.5 - 1) \times 10^{20}$ n/cm^2. The crystals were obtained from Ticonderoga calcite and were purified by vacuum heat-treatment at 1500°C. A few observations were also made on grade 'A' pile graphite, as used in British power reactors.

The general features of the damage have been outlined in a previous publication [5]. It is visible as a dense fine speckling in material irradiated at 150°C, and increases in size and separation at higher irradiation temperatures. On thermal annealing after irradiation, the smaller defects aggregate into larger clusters and all defects finally disappear between 1650 and 2150°C. The contrast of the defects may be light or dark, depending on their depth in the specimen and their proximity to neighbouring extinction contours, and may also be enhanced in dark field. Some examples are given in Fig. 1.

Fig. 2 shows the quantitative relationships which have now been established between mean defect diameters and irradiation and annealing temperatures for specimens having roughly the same doses. The most striking feature is the high degree of linearity of the spot-size increase with irradiation temperature. Fig. 3 shows some typical size distribution curves from which Fig. 2 was constructed. In general the spots show a distribution of $\sim \pm 30\%$ about the mean value. On annealing, the smaller defects tend to coalesce, if on the same plane, or to take up adjacent positions if they are on different planes. At temperatures above 1200°C the total amount of damage begins to decrease.

A number of observations have been made on specimens with higher irradiation doses. For the lower irradiation temperatures it was impossible to see individual defects as the whole field became too distorted. At 650°C,

---

1 Dido reactor, AERE, Harwell, England.

2 Pluto reactor, AERE, Harwell, England.

3 For a complete discussion of the dose scale used, see BELL et al. [10]. A brief account has also been given by SIMMONS and REYNOLDS [11].

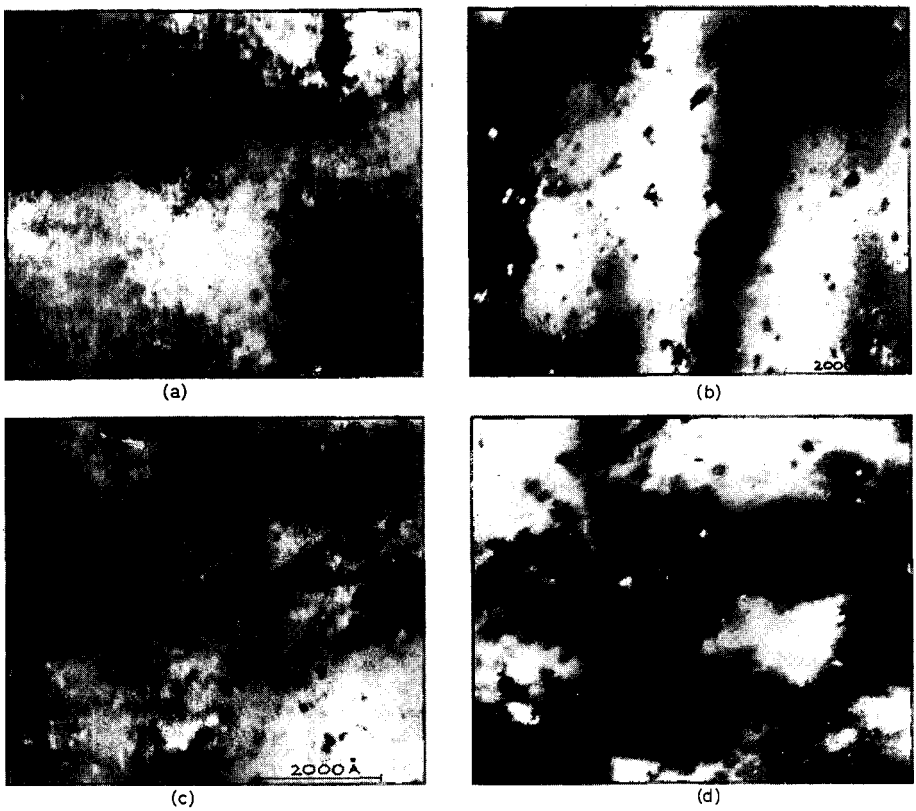


Fig. 1

Examples of damage clusters for various irradiation and annealing conditions

(a) Irradiated at 150°C.
(b) Irradiated at 150°C; annealed at 1500°C
(c) Irradiated at 350°C; annealed at 1500°C
(d) Irradiated at 650°C; annealed at 1200°C

as shown in Fig. 4, the defects increased in size but not in density, and at a dose of $\sim 5 \times 10^{20}$ n/cm^2 a new population of uniformly distributed fine damage began to appear. The new defects were similar to those characteristic of 150°C irradiation, and coarsened on annealing at 1200°C.

The other measureable quantity required from the micrographs, viz. the density or separation of the sites, is more difficult to obtain because of the unknown thickness of the specimens. Several estimates have, however, been made by various methods and it appears that the single crystals are about 1000 Å or 300 layer planes thick, although transparent polycrystalline samples are probably a good deal thinner. We have therefore estimated defect densities by dividing the apparent density on the plate by 300 to obtain the density on the basal plane.

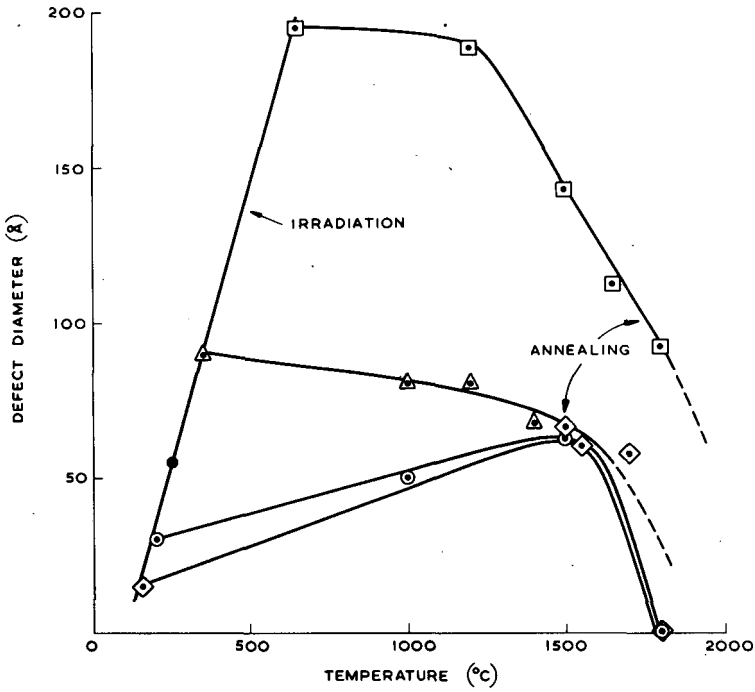


Fig. 2

Mean defect diameter as a function of irradiation and annealing temperature

3. THEORY

We shall assume that the phenomena summarized in Fig. 2 all refer to the same kind of defeet and that this defect is free to move only in the two dimensions of the basal planes. A homogeneous nucleation theory may then be formulated on the lines of that used to discuss gas-bubble formation in irradiated fissile materials by GREENWOOD et al. [12], except that the equations refer to two dimensions instead of three.

Let G be the rate of defect formation per atomic site per second, D the diffusion co-efficient and c the atomic concentration of the defects. Then the steady-state diffusion equation is

$$D\,\nabla^2 c = -G. \tag{1}$$

Suppose also that the defects have a net attraction for each other so that stable groups are formed by chance encounters. Then after some time t there will be complexes present of diameter $2r_0$, say, at a mean spacing of $2r_1$, and if we insert into the solution of Eq. (1) the boundary conditions $c = 0$ at $r = r_0$ and $dc/dr = 0$ at $r = r_1$, we obtain

$$c = \frac{G}{D}\left[\frac{r_0^2 - r^2}{4} + \frac{r_1^2}{2}\ln\frac{r}{r_0}\right]. \tag{2}$$

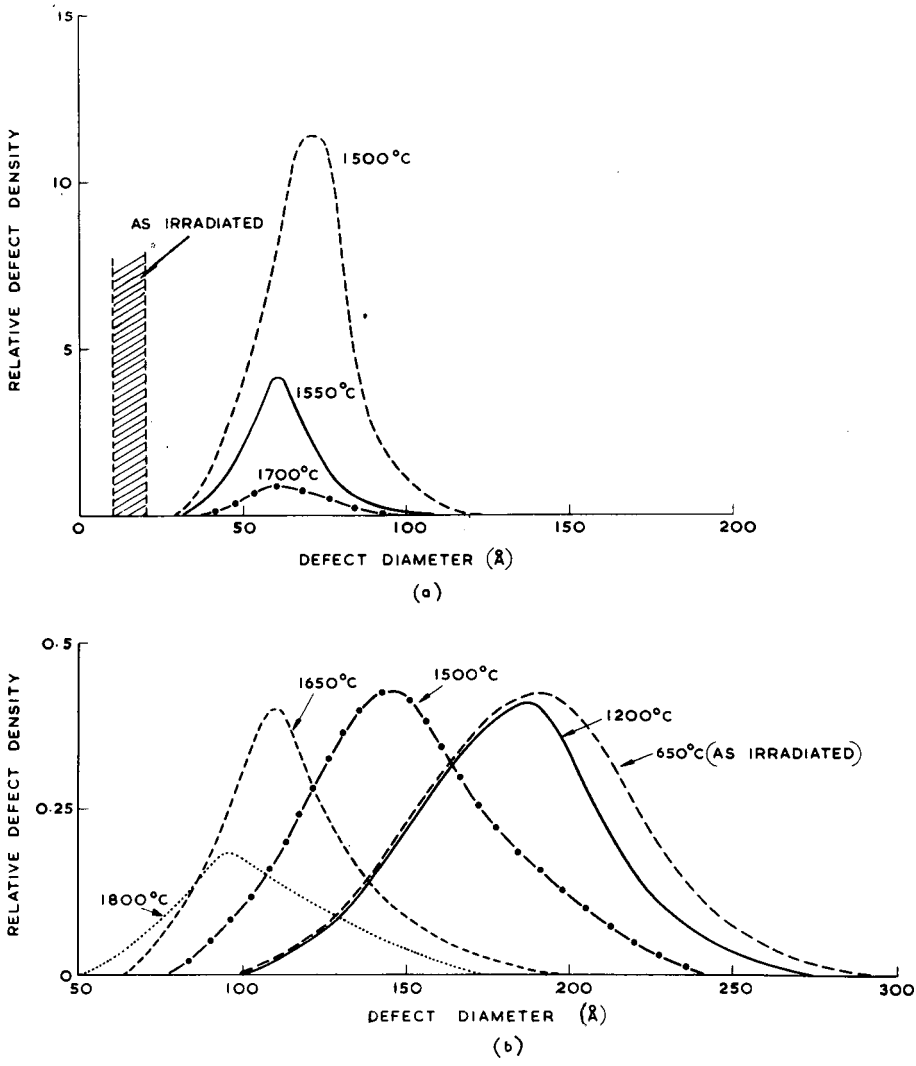


Fig. 3

Distribution of defect diameters for a specimen irradiated at (a) 150° C or (b) 650° C and annealed at various temperatures

Since we are only interested in cases where $r_0 \ll r_1$, this becomes

$$c_1 = c(r_1) = \frac{Gr_1^2}{2D} \ln \frac{r_1}{r_0} \qquad (3)$$

at $r = r_1$, i.e. at points in the lattice well away from complexes.

From this it follows that the mean number (n) of defect jumps required

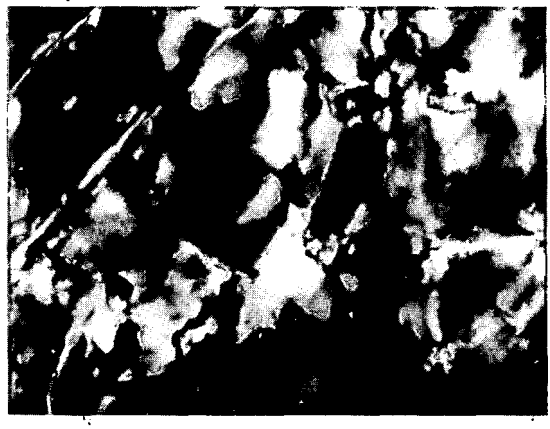


Fig. 4

Defects observed at ~5 x 10^{20} n/cm^2 dose for 650°C irradiation

for a newly created defect to reach a nucleus is

$$n = \frac{3r_1^2}{2a^2} \ln \frac{r_1}{r_0}, \tag{4}$$

where a is the interatomic spacing in the basal plane and the jump frequency is taken as $3D/a^2$.

Again, the average number of jumps made by a new defect before it meets another one is

$$n_d = \frac{1}{Zc_1} = \frac{2D}{ZG{r_1}^2 \ln(r_1/r_0)}, \tag{5}$$

where z (≒ 2) is the number of new sites explored per jump.

Then when $n_d > n$, new complexes will be unlikely to form, i.e.

$$\frac{D}{Gr_1^2 \ln (r_1/r_0)} > \frac{3r_1^2}{2a^2} \ln \frac{r_1}{r_0}, \tag{6}$$

and the homogeneous nucleation separation $2r_1$ is given by

$$r_1{}^4 \left[\ln \frac{r_1}{r_0} \right]^2 = \frac{2Da^2}{3G} \tag{7}$$

In the following we shall put

$$D = D_0 \exp(-E/kT), \tag{8}$$

where D_0 is a constant of order unity (cf. work on diffusion in graphite by

KANTER [13]) and E is an activation energy. We also have, to a good approximation,

$$G = \frac{1}{t}\left[\frac{r_0}{r_1}\right]^2, \tag{9}$$

so that measurements of r_0 and r_1 and a knowledge of T, the absolute temperature, are sufficient to determine E.

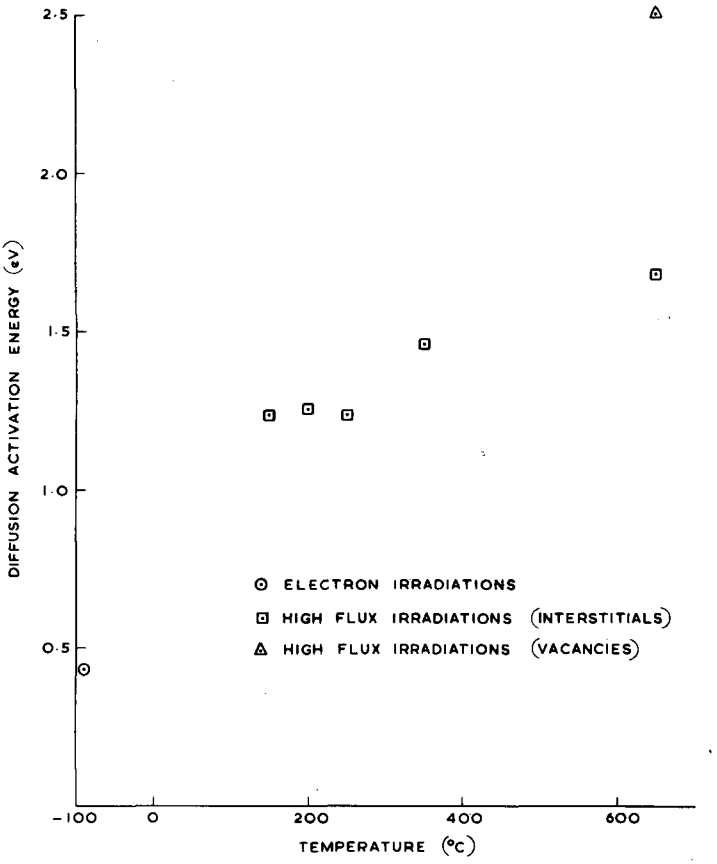


Fig. 5

Diffusion activation energies calculated from the theory for interstitials and vacancies

4. RESULTS AND DISCUSSION

A separate value of E has been obtained for each irradiation temperature and the results are shown in Fig. 5. They indicate a constant value of about 1.25 eV in the range 150 - 250°C, with a slow rise at higher temperatures. This result may be compared with the activation energy commonly used in

the 'equivalent-temperature correction'. This is a correction which must be applied when radiation damage rates at various temperatures and fluxes are compared, and has been fully described by BELL et al. [10], who give a value of 1.58 eV for this temperature range. However, more recent work by Bridge et al.* suggests that the proper value should be somewhat lower. We suggest that the diffusion process we have described is the chief source of the macroscopic effect.

As regards the identification of the migrating defects, we may note that the activation energies for the migration of single interstitials and single vacancies are now well established. Studies of the annealing of low-temperature electron-beam damage by REYNOLDS and GOGGIN [14] and GOGGIN (in preparation) indicate that single interstitials become freely mobile at ~ 181°K, with an activation energy of 0.43 eV. On the other hand BAKER and KELLY [15] have obtained the activation energy for the free motion of a single vacancy from quenching studies and report values in the range 2.6 - 3.7 eV. The migrating defects in our experiments are therefore neither single interstitials nor single vacancies and it is difficult to avoid the conclusion that they must consist of small groups of interstitials. It is conceivable that these small groups are doubles, but they could also be fours or even larger. The observation that such a group has an activation energy of motion of 1.25 eV gives a simple physical basis to the well-known 200°C peak (see, e.g. KINCHIN [16]) in the stored-energy release curve of graphite irradiated at room temperature.

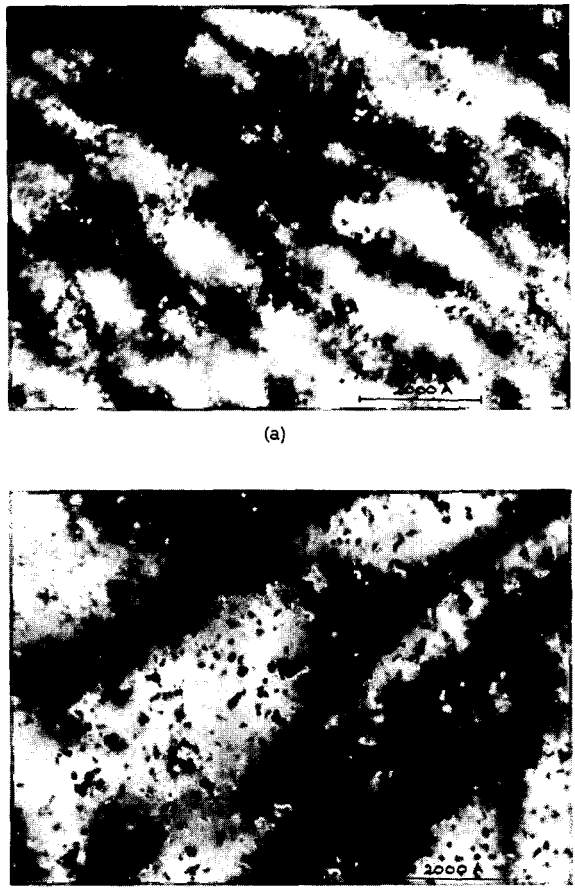
Another problem of long standing in the theory of stored energy is the fact that activation energies obtained by annealing experiments are higher than those obtained by damage-rate experiments in the 150 - 300°C temperature range. We may now ascribe the annealing effects to the motion of the large clusters visible in the microscope, as in Fig. 6, where large defects move a small distance in 2 h at 1200°C, with an activation energy of ~3 eV. It appears that the visible clusters are mobile, the activation energy increasing with the size.

Eq. (7) may now be applied to vacancies with an activation energy for D of 3 eV. This leads to the prediction that they are to all intents and purposes stationary and single at irradiation temperatures up to 350°C, but that they will begin to nucleate on a fine scale at 650°C. This is the explanation of the second damage population found at higher doses at this temperature. At annealing temperatures above 1200°C the increasing mobility of vacancies enables them to attack the interstitial groups, which therefore being to decrease in size and eventually disappear rapidly as shown at the high-temperature end of Fig. 2.

It is worth noting that, for example, the application of the theory in section 3 to the defects said by WILLIAMSON [3] to be interstitial loops leads to an activation energy of 0.23 eV for a 300°C irradiation, which is much too low even for single interstitials.

Some results obtained on pile graphite may also be fitted into the theory. They are illustrated in Fig. 7. In the 650°C irradiation the value of r_1 is comparable with the crystallite size and the defects are smaller than those

* BRIDGE, H., GRAY, B. S., KELLY, B. T. and SØRENSEN, H., An effect of flux level and flux spectrum on the accumulation of damage in reactor-irradiated graphite, these Proceedings.



(a)

(b)

Fig. 6

Defects observed after (a) irradiation at 250° C or (b) irradiation at 250° C and annealing at 1200° C

in a single crystal at the same dose because the crystallite boundaries act as sinks. In the 1200°C irradiation r_1 is very much larger than the crystallite size and no interstitials are found. The defects are all vacancy loops.

In fact vacancy and interstitial loops are not readily distinguished in the microscope. The idea that they could be has arisen from the supposition that a single c-plane in an abab stacking sequence is merely a dislocation loop with Burgers vector confined to the c-axis. This is not the case, because interstitial loops reduce their energy by shear in the basal plane (READ [18]) and the interstitial and vacancy loop cases, though not identical, are very similar.

The theory outlined can also be shown to explain the main features of the complex growth and shrinkage effects observed in irradiated graphite (see SIMMONS and REYNOLDS [11]) and it is now possible to apply it in detail

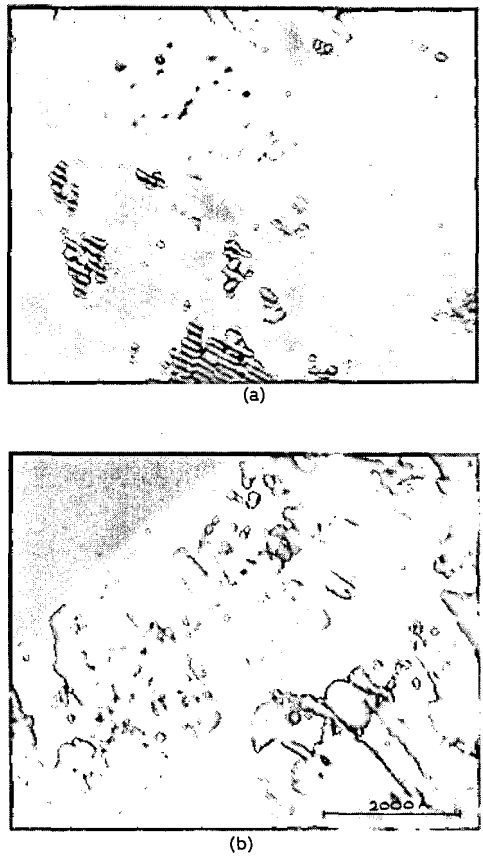


Fig. 7

Pile graphite irradiated to high dose at (a) 650°C or (b) 1200°C

to changes such as those in thermal conductivity and Young's modulus (see REYNOLDS and SIMMONS [17]).

5. SUMMARY AND CONCLUSIONS

A simple model of homogeneous nucleation has been shown to explain qualitatively some aspects of irradiation damage in graphite with some good quantitative agreement. Two features appear to be peculiar to graphite, viz. (i) the difference of an order of magnitude in activation energy of motion of interstitials and vacancies and (ii) the function of small highly-mobile interstitial groups which control the damage rate at intermediate temperatures. As regards the electron microscopy, we wish to emphasize that all our reported results relate to features found on many occasions to be uniformly distributed throughout the samples. We feel that other workers had

often been misled by spurious defects which are commonly found in all kinds of graphite.

ACKNOWLEDGEMENTS

We wish to thank Dr. G.W. Greenwood of the CEGB Laboratories, Berkeley, for a most stimulating discussion of condensation theories, and Dr. T.Eeles of the same establishment for supplying a small sample of material irradiated at 1200°C.

REFERENCES

[1] BOLLMANN, W., Phil Mag. 5 (1960) 621.
[2] WILLIAMSON, G.K. and BAKER, C., Phil. Mag. 6 (1961) 313.
[3] BACON, R. and SPRAGUE, R., Fifth Biennial Conf. Carbon, Pennsylvania (1961).
[4] IZUI, K. and FUJITA, F.E., J. Phys. Soc. Jap. 16 (1961) 1032.
[5] REYNOLDS, W.N., THROWER, P.A. and SHELDON, B.E., Nature 189 (1961) 824.
[6] WILLIAMSON, G.K., Int. Conf. Reactor Materials and Irradiation Damage, Berkeley (1961).
[7] BOLLMANN, W., Proc. Eur. Reg. Conf. on Electron Microscopy, Delft (1960).
[8] BOLLMANN, W., J. app. Phys. 32 (1961) 869.
[9] BOLLMANN, W., Int. Conf. Reactor Materials and Irradiation Damage, Berkeley (1961).
[10] BELL, J.C. et.al., Phil. Trans. Roy. Soc. 254 (1962) 361.
[11] SIMMONS, J.H.W. and REYNOLDS, W.N., Proc. Conf. on Uranium and Graphite, Institute of Metals, London (1962).
[12] GREENWOOD, G.W., FOREMAN, A.J.E. and RIMMER, D.E., J. nucl. Mat. 4 (1959) 305.
[13] KANTER, M.A., Phys. Rev. 107 (1957) 655.
[14] REYNOLDS, W.N. and GOGGIN, P.R., Phil Mag. 5 (1960) 1049.
[15] BAKER, C. and KELLY, A., Nature 193 (1962) 235.
[16] KINCHIN, G.H., Proc. UN. Int. Conf. PUAE 7 (1958) 472.
[17] REYNOLDS, W.N. and SIMMONS, J.H.W., Fifth Biennal Conf. Carbon, Pennsylvania (1961).
[18] READ, W.T., Dislocations in crystals, McGraw-Hill (1953).

A MODEL OF RADIATION DAMAGE IN GRAPHITE

T. IWATA AND H. SUZUKI
JAPAN ATOMIC ENERGY RESEARCH INSTITUTE,
TOKAI-MURA, IBARAKI-KEN, JAPAN

Abstract — Résumé — Аннотация — Resumen

A MODEL OF RADIATION DAMAGE IN GRAPHITE. Hennig and Hove proposed a model of radiation damage to graphite at the first Geneva Conference and attributed the so-called Wigner-energy release around 200°C to the reaction of single interstitials forming C_2 molecules.

We propose a new model as follows:

(1) Single interstitial atoms migrate easily far below liquid-nitrogen temperature. They gather to make clusters (atomic clusters) where each atom has about a 10-Å separation. This distance is shown to be elastically stable.

(2) C_2 molecules (partially C_3 molecules) are formed from atomic clusters between 80°K and 110°K. The reverse annealing of electrical resistivity in this temperature range is explained with the aid of electronic band structure.

(3) C_2 molecules migrate and form the clusters consisting of molecules (molecular clusters) above 160°K. Larger clusters are made at higher temperatures. Each molecule in the clusters is held together by bonds which are much weaker than ordinary covalent bonds and by the elastic forces due to strained layers.

(4) Molecular clusters may decompose to constituent molecules around 200°C and above. C_2 molecules then recombine with vacancies or escape to surfaces, causing energy release. The striking energy release around 200°C is caused by the disappearance of C_2-C_2 molecular clusters. As the temperature is raised, these clusters are further decomposed. Its decomposition is completed below 1000°C.

(5) When molecular clusters become large (the number of constituent atoms > about 10), they can be transformed co-operatively to hexagonal covalent-bonded clusters as graphite layers by externally supplied energy. Further, at the region heavily strained by large clusters, some intra-layer covalent bonds are cut by energetic particles and the new covalent bonds are formed between the clusters and the unpaired atoms in the layers. This coupling explains the sudden broadening of X-ray line profiles and the abrupt change in stored-energy release and electrical resistivity recovery found above doses of 6×10^{20} n/cm^2.

(6) The hexagonal covalent-bonded clusters do not disappear until irradiation-induced vacancies begin to migrate and recombine with them. The disappearance probably starts above 1000°C.

MÉCANISME D'ALTÉRATION DU GRAPHITE SOUS L'ACTION DES RAYONNEMENTS. A la première Conférence de Genève, Hennig et Hove avaient envisagé un mécanisme d'altération du graphite sous l'action des rayonnements et avaient attribué la libération d'énergie de Wigner, qui se produit aux environs de 200°C, à la réaction d'atomes interstitiels simples donnant lieu à la formation de molécules C_2.

Les auteurs proposent le nouveau mécanisme suivant:

1. Les atomes interstitiels simples se déplacent sans difficulté, à une température sensiblement inférieure à celle de l'azote liquide. Ils s'assemblent pour former des amas (amas atomiques), où chaque atome est séparé du suivant par un écart d'environ 10 Å. La stabilité élastique de cette distance est démontrée.

2. Entre 80 et 110°K, les amas d'atomes donnent lieu à la formation de molécules C_2 (et, en partie, des molécules C_3). Le retour de la résistivité électrique à la normale dans cette gamme de températures s'explique par la structure de bande électronique.

3. Les molécules C_2 se déplacent et forment des amas de molécules au-dessus de 160°K. A des températures plus élevées, il se forme des amas plus importants. Dans chaque molécule d'un amas, les liaisons entre les atomes sont beaucoup plus faibles que les liaisons de covalence ordinaires; les atomes sont aussi liés par des forces élastiques résultant de la déformation de couches.

4. Il se peut que les amas de molécules se décomposent aux environs de 200°C et au-delà. Les molécules constitutives C_2 se recombinent alors avec les lacunes ou s'échappent vers les surfaces, donnant ainsi lieu à une libération d'énergie. La libération d'énergie remarquable qui se produit aux environs de 200°C est due à la disparition des amas de molécules C_2-C_2. A mesure que la température augmente, la décomposition des amas se poursuit pour s'achever en peu en dessous de 1000°C.

5. Lorsque les amas de molécules atteignent de grandes dimensions (le nombre des atomes constitutifs étant supérieur à la dizaine), on peut les transformer en amas hexagonaux dans lesquels les liaisons sont des liaisons de covalence semblables à celles qui existent dans les couches de graphite, en leur fournissant de l'énergie de source extérieure. De plus, dans la zone fortement déformée par des amas de grande dimensions, certaines liaisons de covalence à l'intérieur des couches sont rompues par des particules énergétiques; de nouvelles liaisons de covalence se forment entre les amas et les atomes isolés dans les couches. Ce couplage explique l'élargissement brusque des raies du spectre des rayons X, de même que la variation brusque dans la libération d'énergie accumulée et le retour à la normale de la résistivité électrique que l'on observe pour des doses supérieures à $6 \cdot 10^{20}$ nvt.

6. Les amas hexagonaux à liaisons de covalence ne disparaissent pas avant que les lacunes radioinduites ne commencent à se déplacer et à se recombiner avec des molécules. Il est probable que la disparition commence au-dessus de 1000°C.

МОДЕЛЬ РАДИАЦИОННОГО ПОВРЕЖДЕНИЯ ГРАФИТА. На первой Женевской конференции Хенниг и Хов предложили модель радиационного повреждения графита и связали высвобождение т.н. энергии Вигнера при температуре около 200°C с взаимодействиями между отдельными внедренными атомами, образующими молекулы C_2.

Мы предлагаем слудующую новую модель:

1. Отдельные внедренные атомы с легкостью мигрируют при температурах много ниже температуры жидкого азота. Они группируются и образуют скопления (атомные скопления), в которых атомы отстоят друг от друга приблизительно на расстоянии в 10 Å. Было доказано, что это расстояние соответствует упруго-устойчивому состоянию.

2. Молекулы C_2 (и, частично, молекулы C_3) образуются из атомных скоплений при температурах между 80°K и 110°K. Обратный отжиг электрического сопротивления в этом интервале температур объясняется структурой электронных полос.

3. Молекулы C_2 мигрируют и при температуре свыше 160°K образуют скопления, состоящие из молекул (молекулярные скопления). При более высоких температурах образуются более крупные скопления. Каждая из молекул такого скопления связана с другими молекулами-связями, которые гораздо слабее, чем обычные ковалентные связи, а также силами упругости, образованными напряженными слоями.

4. Молекулярные скопления могут распадаться на отдельные составляющие молекулы при температуре около 200°C и выше. Затем молекулы C_2 воссоединяются с вакансиями или же выскальзывают на поверхность, что ведет к высвобождению энергии. Это удивительное высвобождение энергии при температуре около 200°C объясняется исчезновением молекулярных скоплений $C_2 - C_2$. По мере поднятия температуры эти скопления распадаются еще дальше. Распад становится полным при температуре ниже 1000°C.

5. При укрупнении молекулярных скоплений (когда число составляющих атомов превышает приблизительно 10) они могут превращаться совместно в гексагональные ковалентно-связанные скопления, как, например, слой графита под влиянием полученной извне энергии. Более того, в зонах, сильно напряженных в результате крупных скоплений, некоторые ковалентные связи между слоями разрываются энергетическими частицами, и между скоплениями и неспаренными атомами в этих слоях образуются новые ковалентные связи. Это спаривание объясняет внезапное расширение рентгеновской полосы в спектре и быстрое изменение в высвобождении латентной энергии, а также восстановление электрического сопротивления, наблюдаемое при дозах свыше $6 \cdot 10^{20}$ nvt.

6. Гексагональные ковалентно-связанные скопления не исчезают до тех пор, пока наведенные обучением вакансии не начнут мигрировать и воссоединяться с ними. Это исчезновение начинается, вероятно, при температуре свыше 1000°C.

MODELO EXPLICATIVO DEL DAÑO CAUSADO AL GRAFITO POR LAS RADIACIONES. En la Primera conferencia de Ginebra, Hennig y Hove propusieron un modelo para explicar los daños que las radiaciones causan en el grafito y atribuyeron el fenómeno llamado desprendimiento de energía de Wigner, que se manifiesta alrededor de los 200°C, a la reacción entre átomos intersticiales simples para formar moléculas de C_2.

Por su parte, los autores proponen un nuevo modelo que se describe a continuación:

1. A una temperatura muy inferior a la del nitrógeno líquido, los átomos intersticiales simples pueden migrar fácilmente. Se reúnen formando racimos (racimos atómicos) en los cuales la distancia interatómica es de unos 10 Å. Se demuestra que esta distancia es elásticamente estable.

2. Entre 80°K y 110°K, se forman moléculas de C_2 (en parte, también moléculas de C_3) a partir de esos racimos atómicos. El efecto inverso de recocido de la resistividad eléctrica, en este intervalo de temperatura, se explica mediante la hipótesis de la estructura electrónica en bandas.

3. Por encima de los 160°K, las moléculas de C_2 migran y forman a su vez racimos moleculares. Los racimos son más grandes cuanto mayor es la temperatura. Los componentes de cada molécula del racimo están unidos entre sí por enlaces mucho más débiles que los enlaces covalentes ordinarios y por las fuerzas elásticas que se originan por la acción de las capas en tensión.

4. A 200°C o a temperaturas más elevadas, los racimos moleculares pueden descomponerse en sus moléculas constituyentes. Las moléculas de C_2 se recombinan entonces con huecos o escapan a las superficies, dando lugar a un desprendimiento de energía. El notable desprendimiento de energía registrado a una temperatura del orden de los 200°C, es provocado por la desaparición de los racimos moleculares C_2-C_2. Al aumentar la temperatura prosigue la descomposición de los racimos. La misma es cuantitativa antes de alcanzar los 1000°C.

5. Al crecer el tamaño de los racimos moleculares (cuando el número de átomos constituyentes excede de 10), puede ocurrir que se transformen cooperativamente en estructuras exagonales de enlace covalente, constituyendo capas de grafito por acción de una energía procedente de una fuente exterior. Además, en la zona sometida a una elevada tensión por la presencia de esos racimos de gran tamaño, algunos enlaces covalentes entre capas son rotos por partículas energéticas y se forman nuevos enlaces covalentes entre los racimos y los átomos no aparcados en las capas. Esta unión explica el repentino ensanchamiento del perfil de las líneas de rayos X y la brusca variación de la cantidad de energía almacenada que se desprende así como la recuperación de la resistividad eléctrica que se registran cuando las dosis superan los $6 \cdot 10^{20}$ nvt.

6. Los racimos exagonales de enlace covalente sólo desaparecen cuando los huecos inducidos por las radiaciones comienzan a migrar y a recombinarse con ellos. Este proceso comienza a una temperatura superior a los 1000°C.

1. INTRODUCTION

Graphite has been extensively used in nuclear reactors as a moderator and a structural material because of its excellent nuclear properties. Since WIGNER [1] first predicted in 1942 that significant changes in the physical properties of graphite are caused by fission neutrons, the effects of radiation on graphite has been studied by many workers. An understanding of these effects on an atomic model seems to be important and in particular the effect known as Wigner-energy storage and its release.

HENNING and HOVE [2] proposed a radiation-damage model, based mainly on the spin-resonance measurement of neutron-irradiated polycrystalline material at the Geneva Conference in 1955. They attributed the Wigner-energy release around 200°C to the reaction of single interstitial atoms forming C_2 molecules. On the other hand, a similar experiment recently conducted by MÜLLER [3] on a single crystal of graphite did not show any line other than the conduction-carrier resonance line. It seems to be difficult (with a few exceptions [4]) to explain the origin of the observed electro-spin resonance satisfactorily.

The graphite crystal consists of superimposed, hexagonal-pattern atomic layers held together only by a weak van der Waals force, the interlayer distance being 3.35 Å. The atoms within the layers are held together by very strong covalent bonds corresponding to an interatomic distance of 1.42 Å. Because of the large interlayer space and the localized nature of electrons in each atomic layer, the electronic structure of an interstitital atom or molecule in a graphite crystal may be similar to that found in free space. The behaviour of interstitial atoms, molecules and clusters in graphite is, therefore, considerably different from that in metals, where

the behaviour of interstitial atoms is determined by the strong influence of the surrounding lattice. In this paper a new model of radiation damage and its recovery is proposed on the basis of energy calculations of interstitial atoms, molecules and their clusters and also from inferences drawn from the behaviour of carbon atoms and molecules in free space.

2. DESCRIPTION OF THE PROPOSED MODEL

This section describes the proposed model in outline. The detailed discussions and the basis of our proposal will be given in the following sections. The model is as follows:

(1) As graphite crystals are irradiated vacancies, interstitials and their complexes are produced.

(2) Single interstitial atoms migrate easily below liquid-nitrogen temperature. They gather to make clusters where atom separation is about 10 Å. This distance is shown to be elastically stable. We will refer here to this kind of cluster of carbon atoms as the 'atomic cluster'.

(3) C_2 molecules (and some C_3 molecules) are formed from atomic clusters at temperatures between liquid-nitrogen temperature and room temperature. Then C_2 molecules migrate and form clusters of molecules. We will call a cluster of C_2 molecules the 'molecular cluster'. Each molecule in the molecular cluster is held together by a bond (which is much weaker than the ordinary covalent bond) and the elastic interaction between molecules.

(4) Molecular clusters may decompose to constituent C_2 molecules at around and above 200°C. C_2 molecules are then absorbed into larger molecular clusters and honeycomb clusters, escape to surfaces or recombine with vacancies. Here 'honeycomb cluster' means a cluster with a hexagonal pattern such as a graphite layer. The striking energy release around 200°C is caused by the disappearance of small molecular clusters. As the temperature is raised, further decomposition takes place in larger molecular clusters.

(5) When a molecular cluster has grown larger than a certain size, it can be transformed co-operatively into a honeycomb cluster by passing through some excited state.

(6) Honeycomb clusters do not disappear until vacancies begin to migrate and recombine with them. This process takes place above 1000°C.

(7) If the density of vacancies is comparatively high, they may coagulate into clusters rather than disappear by escaping to the surface or recombining with honeycomb clusters. The migration of a vacancy-doublet requires a higher activation energy than single vacancies, in contrast to the case in metals. Extremely large vacancy clusters can disappear only through the process of self-diffusion.

3. SINGLE INTERSTITIAL ATOMS

In this section the method of calculation of self- and migration-energy of an interstitial atom is summarized. This method is also applicable to

the calculation of energies of the interstitial C_2 molecules and atomic or molecular clusters. The details of the method have been given by IWATA et al. [5].

To calculate the strain field around an interstitial atom, the graphite lattice is assumed to be a system of parallel, thin, elastic plates placed at a constant separation and which are held together by weak interaction forces. The self-energy of an interstitial atom, therefore, consists of two parts: (1) the elastic strain energy in the plates under strain around the interstitial, and (2) the electronic interaction energy between the interstitial and all the atoms in the lattice.

Since the strain in each elastic plate has radial symmetry around the axis perpendicular to the plate and passing through the interstitial, the elastic energy increase is given by the expression

$$V = \sum_{m=-\infty}^{\infty} \int_0^{\infty} [\tfrac{1}{2} c\rho\kappa^2 \{\nabla^2 w_m(r)\}^2 + \tfrac{1}{2} c\rho\mu^2 \{w_{m+1}(r) - w_m(r)\}^2] 2\pi r\, dr . \quad (1)$$

Here $w_m(r)$ represents the transverse displacement of the m-th plate at a radius r, the displacement parallel to the plate being neglected. c is the distance between the adjacent plates and ρ the volume density. κ^2 and μ^2, each multiplied by $c\rho$, are the bending elastic constant and the Hooke's force constant between the neighbouring plates, respectively.

In order to determine the strain of the n-th plate, electronic interaction forces to bend the atomic layers are replaced by the elastic distributed load $c\rho F_n(r)$. Then $w_n(r)$ is the solution of the equation

$$-\kappa^2\nabla^4 w_n(r) + \mu^2\{w_{n+1}(r) + w_{n-1}(r) - 2\, w_n(r)\} = -F_n(r) . \quad (2)$$

The interstitial atom is assumed to be between the n-th plate and the (n-1)-th plate, and also the following relations are assumed

$$w_{n-1-i}(r) = w_{n+i}(r),$$
$$w_{n\pm(1+i)}(r) = \alpha\, w_{n\pm i}(r)$$

$$F_n(r) \begin{cases} = \text{const.} & : (0 \le r \le r_c) \\ = 0 & : (r_c \le r), \end{cases} \quad (3)$$

where α is a constant and i is zero or positive integer. Then we have

$$\text{for } (0 \leqslant r \leqslant r_c), \quad \frac{w_n(r)}{w_n(0)} = \frac{1}{c_n} \Big\{ 1 + \tfrac{1}{2} \frac{\pi i}{2} \sqrt{i}\, hr_c \cdot H_0^{(1)'}(\sqrt{i}\, hr_c) \cdot J_0(\sqrt{i}\, hr)$$
$$+ \tfrac{1}{2} \frac{\pi i}{2} \sqrt{-i}\, hr_c \cdot H_0^{(1)'}(\sqrt{-i} hr_c) \cdot J_0(\sqrt{i} hr) \Big\}, \quad (4)$$

$$\text{for } (r_c \leqslant r), \quad \frac{w_n(r)}{w_n(0)} = \frac{1}{c_n}\left\{ \tfrac{1}{2}\sqrt{i}\, hr_c \cdot J_0'(\sqrt{i}\, hr_c) \cdot \frac{\pi i}{2} H_0^{(1)}(\sqrt{i}\, hr) + \tfrac{1}{2}\sqrt{-i}\, hr_c \cdot J_0'(\sqrt{-i}\, hr_c) \cdot \frac{\pi i}{2} H_0^{(1)}(\sqrt{-i}\, hr) \right\},$$

$$\text{where} \quad c_n = R\left\{ 1 + \frac{\pi i}{2} \sqrt{i}\, hr_c \cdot H_0^{(1)'}(\sqrt{i}\, hr_c) \right\}$$

and $h = (3-\alpha)^{\frac{1}{4}} \cdot (\mu/\kappa)^{\frac{1}{2}}$.

Also $w_n(0)$ is the displacement at $r = 0$ of the n-th plate, which is the maximum value of $w_n(r)$, and h is nearly constant, J_0 and $H_0^{(1)}$ are the first and the third kind of Bessel function, respectively. The primes refer to the first differential.

In the case of an interstitial molecule or cluster, the strain of plates is no longer radially symmetrical. The above treatment, however, is still applicable to that case, if the elastic load over the plates is assumed to be elliptically distributed.

The strain form, $w_n(r)$, is determined by Eq. (4) for given values of parameters, $w_n(0)$ and r_c. We can obtain the electronic interaction energy between the interstitial atom and all atoms in the lattice by the following potentials

$$\varphi(r)\begin{cases} = \exp(1.652 - 1.386\, r) & : r \leqslant 5.56\ \text{Å} \\ = -\dfrac{309.3}{r^6} + 0.5153 \exp(-0.2223\, r - 0.07951\, r^2) & : r \leqslant 5.56\ \text{Å} \end{cases} \quad (5)$$

The potential for small distances was determined by taking into account the energies of single, double and benzene bonds of carbon atoms. Meanwhile, the potential for large distances was taken from the quantum-mechanical calculation by KOMATSU [6].

The self-energy of an interstitial atom is obtained as the minimum value of the total energy increase for the variation of $w_n(0)$ and r_c. It was 2.5 eV and the corresponding values of parameters were $w_n(0) = 0.48$ Å and $r_c = 2.29$ Å.

The migration energy of an interstitial atom was estimated as the difference between the energies for the configurations of Figs. 1a and 1b. The migration energy was 0.016 eV. The elastic-plate approximation employed in the above calculation may underestimate the migration energy. This error, however, does not seem to change the order of magnitude. An interstitial atom in graphite, therefore, seems to be able to migrate at below liquid-nitrogen temperature.

4. FORMATION OF THE C_2 MOLECULE

4.1. Interaction between two interstitial atoms

When two interstitial atoms approach to a distance less than several tens of Angstroms, the overlap of spread-clouds of anti-parallel 2p electrons

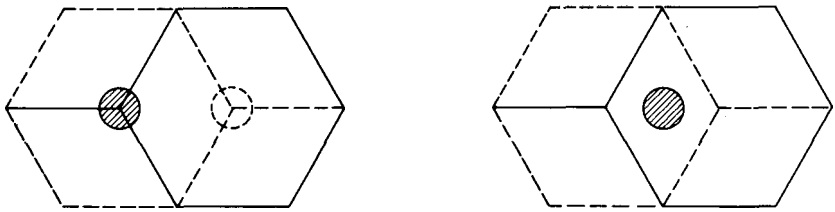


Fig.1

Migration of a single interstitial atom
(a) Equilibrium (b) Saddle point.

may take place, and a weak covalent bond may be formed. The covalent bond becomes stronger as the distance between interstitials decreases. The electronic interaction between interstitial atoms is, therefore, always one of attraction.

There is another interaction between two interstitial atoms through the elastic strain around them and this interaction should be added to the electronic interaction. Since we have employed the linear elasticity, the strain at any point C in Fig. 2 is given by the superposition of the strains

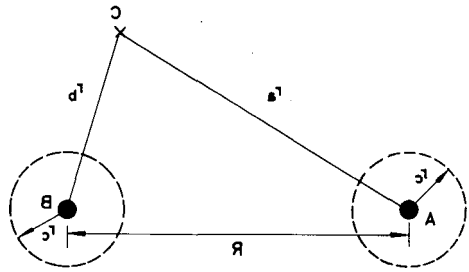


Fig.2

Interaction of two interstitial atoms

due to two interstitial atoms at A and B. The elastic interaction energy is then given by the expression

$$V' = \sum_{m=-\infty}^{\infty} \int [\, c\rho\kappa^2 \{ \nabla^2 w_m(r_a) \cdot \nabla^2 w_m(r_b) \} + c\rho\mu^2 \{ w_{m+1}(r_a) - w_m(r_a) \} \cdot \{ w_{m+1}(r_b) - w_m(r_b) \} \,]\, dS \qquad (6)$$

by means of Eq. (1). Here $w_m(r)$ is given in Eq. (4) and dS is the surface element of elastic plates.

$w_m(r)$ and $\nabla^2 w_m(r)$ in the integration (6) are rather large when $r < 2r_c$, but decrease rapidly as r increase beyond $2r_c$. The integration (6) may be, therefore, approximated by the integration over the region within $2r_c$ from

each interstitial atom. Further, we assume that the strain and its derivative due to the interstitial atom A have the constant values $w_m(R)$ and $\nabla^2 w_m(R)$ respectively in the region within $2r_c$ from the point B, and vice versa. Then we have

$$V' = 2 \sum_{m=-\infty}^{\infty} [\, c\rho\kappa^2 \cdot \nabla^2 w_m(R) \cdot \int_0^{2r_c} \nabla^2 w_m(r) \cdot 2\pi r\, dr + c\rho\mu^2 \{w_{m+1}(R) - w_m(R)\} \cdot \int_0^{2r_c} \{w_{m+1}(r) - w_m(r)\}\, 2\pi r\, dr \,]. \quad (7)$$

Substituting appropriate values into Eq. (7), the elastic interaction energy is obtained as a function of interatomic distance. The result is represented by the full line in Fig. 3.

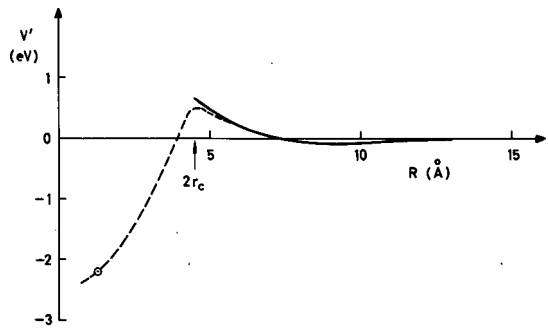


Fig. 3

Elastic interaction energy between interstitial atoms

The above calculation holds when the interatomic distance R is larger then $2r_c$. In the region of $R \leq 2r_c$, the interaction energy is expected to decrease with decreasing distance as shown by dotted line in the figure. The point in the left side was obtained from the calculation of elastic energy accompanied with an interstitial C_2 molecule.

It is worthwhile to note that there is a stable configuration for two interstitial atoms with interatomic distance of about 10 Å, as expected from Fig. 3. Interstitial atoms, therefore, may gather and form atomic clusters in which the atomic distance is about 10 Å, at very low temperatures.

It must also be mentioned that there is a potential barrier of about 0.6 eV at the most. The elastic repulsion is partially cancelled by the electronic attraction. It may be reasonable to conclude that the interstitial C_2 molecule is formed at below room temperature and perhaps near or above the liquid-nitrogen temperature.

4.2. *State of C_2 and C_3 molecules*

The electronic structure of the C_2 molecule in free space is rather well known. The ground state is $KK(\sigma_g 2s)^2 (\sigma_u 2s)^2 (\pi_u 2p)^3 \sigma_g 2p$, $^3\prod_u$ [7], the interatomic distance 1.31 Å [7] and the dissociation energy 4.95 eV [8]. The electronic structure of the interstitial C_2 molecule in graphite, though having a spread electron cloud, may be considered as similar to that found in free space.

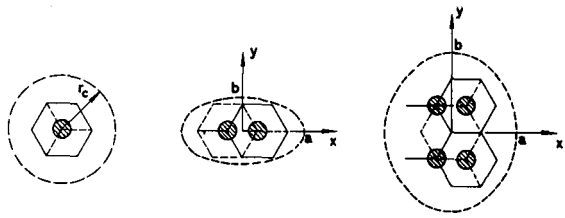


Fig.4

Assumed equilibrium states
(a) interstitial atoms (b) C_2 molecule (c) $(C_2)_2$ cluster
Two superimposed hexagonal networks above and below interstitials are shown as full and broken lines

The self-energy of an interstitial C_2 molecule can be calculated by the method described in section 3, provided that the load is assumed to be uniformly distributed over the elastic plates in the region $x^2/a^2 + y^2/b^2 \leq 1$ (Fig.4b). After computation we obtain the self-energy as 2.85 eV, when $w_n(0) = 0.85$ Å, $a = 2.65$ Å and $b/a = 0.5$. The energy release by the formation of an interstitial C_2 molecule from two single interstitial atoms is about 7 eV.

When an interstitial atom and an interstitial C_2 molecule are placed a small distance apart, a linear C_3 molecule will be formed by an interaction similar to that described in section 4.1. In the case of a linear C_3 molecule the intermediate atom is in the sp hybrid state. The formation of a C_3 molecule should take place at a higher temperature than a C_2 molecule, although still below room temperature. The C_3 molecule in free space [9] is also well known spectroscopically and, according to WALSH's notation [10], has the configuration $(s_1)^2 (s_2)^2 (\sigma_g)^2 (\sigma_u)^2 (\pi_u)^4$, $^1\Sigma_g^+$. The interatomic distance is 1.28 Å.

The formation of a C_4 molecule [11] might be considered, but two C_2 molecules arranged as in Fig.4c are more stable in graphite because of the smaller elastic energy.

5. MIGRATION AND COAGULATION OF C_2 MOLECULES

There may be two possibilities for the path of migration of a C_2 molecule as shown in Fig.5. The estimation according to the procedure in section 3, gave migration energies of about 0.05 eV for both the paths (A) and (B).

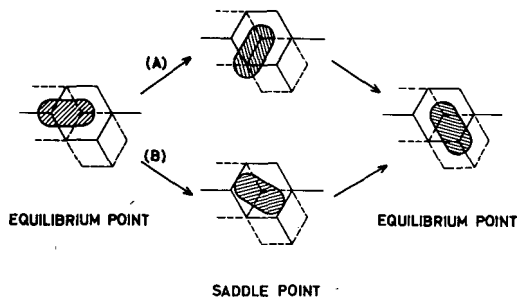


Fig. 5

The migration of an interstitial C_2 molecule

The plate approximation may underestimate the energy in this case, too. The interstitial C_2 molecule, however, seems to migrate at below room temperature.

The interaction between C_2 molecules is almost all due to elastic strain energy and the electronic attraction is very weak, as discussed in the next section. Clusters of C_2 molecules may be formed at below and near room temperature. The larger clusters are formed at the higher temperatures, because the formation of the larger cluster is accompanied by a larger elastic repulsion.

Since there are few experiments on the annealing stages below room temperature, there is no detailed discussion of these here.

6. STABILITY OF A MOLECULAR CLUSTER AND ITS TRANSFORMATION

6.1. The nature of cohesion within a molecular cluster

The stability of a molecular cluster depends strongly upon the nature of cohesion within it. If each atom in the cluster is arranged in hexagonal pattern and connected with its three nearest neighbours by strong covalent bonds as in a graphite crystal, the decomposition of the interstitial cluster requires an activation energy of about 7.5 eV, which is equal to the energy of sublimation [12], provided that vacancies do not exist. On the other hand, the migration of vacancies takes place only above 1000°C. Therefore such a cluster, connected by covalent bonds, cannot decompose below 1000°C. Meanwhile, there is evidence to support the fact that interstitial clusters do decompose at around 200°C.

The most significant recovery of irradiated graphite takes place around 200°C, where release of stored energy, recovery of c-axis expansion, recovery of elastic constant etc. take place over a relatively wide temperature range [13-15]. The recovery process is characterized by a spectrum of activation energies of about 3 eV [16], considerably less than that of vacancy migration. The recovery of c-axis expansion suggests that interstitial clusters disappear in this temperature range. Other evidence to support the decomposition of the interstitial cluster is the electron-microscope observation by BOLLMAN [17], who observed dark and light dots with

dimensions of up to 60 Å in diameter in a sample irradiated to 10^{20} n/cm^2 at 30°C. He also observed that the light dots disappeared after heating for 3 h to 400°C. According to his interpretation the light dots are clusters of interstitial atoms.

As already mentioned in previous sections, the C_2 molecules are formed at below room temperature. Therefore, the interstitial clusters, which disappear below 1000°C, are composed of C_2 molecules which interact weakly with each other.

The interstitial cluster composed of carbon atoms which are connected to each other by strong covalent bonds (the honeycomb cluster) is obviously more stable than the cluster of C_2 molecules (the molecular cluster). A molecular cluster, however, should pass through an excited state in order to transform into a honeycomb cluster.

The electronic interaction energy between C_2 molecules in a molecular cluster may be estimated from the electronic configuration. Since C_2 molecules have the unsaturated bonding orbitals, it is possible to make covalent bonds between them; C_3 molecules do not have the unsaturated bonding orbitals. The electronic configuration of C_2 molecules for the maximum bond strength would be on the ground states rather than the excited states. The ground states have two unpaired electrons ($\pi_u 2p$) ($\sigma_g 2p$), where the ($\pi_u 2p$) electron contributes most to the bond between molecules. In the simple case of $(C_2)_2$ molecular cluster the bond energy may be estimated from that of the $(O_2)_2$ cluster which exists in air at a very low concentration. The $(O_2)_2$ cluster is known to consist of two O_2 molecules, with nearly the same configuration and structure as usual O_2 molecules [18]. The electronic configuration of O_2 is $KK(\sigma_g 2s)^2 (\sigma_u 2s)^2 (\sigma_g 2p)^2 (\pi_u 2p)^4 (\pi_g 2p)^2\ ^3\Sigma_g^-$ [19]. Two unpaired electrons $(\pi_g 2p)^2$, although antibonding in an O_2 molecule, may cause a weak covalent bond between two O_2 molecules. The bond energy is known to be 0.16 kcal/mol, which is less than 0.01 eV. It seems to be reasonable, therefore, to suppose that the bond energy between C_2 molecules in the molecular cluster is of the same order of magnitude, namely less than 0.1 eV.

6.2. Decomposition of molecular clusters to constituent molecules

We shall next examine the stability of a molecular cluster at elevated temperatures. The attractive force between molecules in the cluster mainly comes from the elastic interaction; the electronic interaction becomes appreciable only at a small spacing. We will assume that the electronic interaction potential between a molecule and all atoms in the crystal lattice is given by Eq. (5), where the weak covalent bonds have been neglected.

The self-energy of $(C_2)_2$ cluster was calculated for the configuration shown in Fig. 4c, and it was estimated as 4.8 eV when $w_n(0) = 0.90$ Å, $a = 2.95$ Å, and $b/a = 1.2$. The difference of the self-energy between two independent C_2 molecules and a $(C_2)_2$ cluster (about 0.9 eV) is released when the latter is formed from the former. On the other hand, the energy required to decompose a $(C_2)_2$ cluster to two independent C_2 molecules is the sum of the above difference, the migration energy of C_2 molecule and the energy to surmount the barrier of elastic interaction (shown in Fig. 3) and is estimated to be about 1.3 eV.

WOOD et al. [14] have shown that below 200°C the activation energy for resistivity-recovery is relatively constant at about 1.2 eV for low-dose irradiation by neutrons. BURTON and NEUBERT [13] have estimated, from their annealing experiment, the activation energy for the recovery around 200°C to be about 1.3 eV. More precise measurements on the isothermal annealing of electrical resistivity of artificial graphite irradiated to 5.8×10^{20}n/cm^2 at 30°C are now proceeding in our laboratory. The measurements indicate that the activation energy is about 1.3 eV between 80 and 150°C and about 1.8 eV between 160 and 200°C [20].

These results seem to show that the recovery with the activation energy of 1.2 or 1.3 eV is due to the decomposition of $(C_2)_2$ molecular clusters. The energy required to decompose a molecular cluster increases with increasing number of constituent molecules, as is easily seen from the calculation of elastic energy. The greatest activation energy for the decomposition should be equal to the sum of the self-energy of a C_2 molecule, its migration energy and the energy to surmount the barrier of elastic interaction. This sum is estimated to be 3.5 eV. The recovery with the activation energy of 1.8 eV may be due to decomposition of $(C_2)_3$ molecular clusters.

The stored energy release in irradiated graphite was measured above room temperature by BURTON and NEUBERT [13] and by WOOD, BUPP and FLETCHER [14]. At low doses the stored energy appears to be completely released below 400°C. This result indicates that the decomposed C_2 molecules are probably annihilated by escaping to free surface and or recombining with vacancies. A considerable part of the radiation-induced vacancies are left in the crystal and annihilate only above 1000°C. The electrical resistivity measurement indicates that the recovery only takes place at such high temperatures in a sample irradiated to 10^{18}n/cm^2 [13]. At high doses the energy releases take place over a wider temperature range. This tendency may be explained by the formation of the larger cluster with increasing dose. A large cluster requires higher activation energy for decomposition than a small cluster. The chances of the capture of a decomposed C_2 molecule by the larger clusters increases with the increasing dose.

6.3. Transformation into honeycomb clusters

The molecular cluster in graphite is obviously in a metastable state and is able to transform into the more stable honeycomb cluster, provided that a sufficient amount of energy is given to the molecular cluster. As the size of the molecular cluster increases, its stability, which resists the transformation, decreases. At high doses the possibility of the formation of a honeycomb cluster may increase appreciably.

The formation of a honeycomb cluster will be much easier if the following process take place. Take two molecular clusters formed in the two adjacent interlayer positions as shown in Fig. 6. These two molecular clusters bend the atomic layer b strongly. If inter-layer covalent bonds in the vicinity of P are cut by an energetic particle, new covalent bonds may be formed between the molecules in the clusters and the atoms with broken bonds within the layer b. After such a row of broken bonds is formed, other C_2 molecules are absorbed at the edge of the atomic layer with the broken bonds.

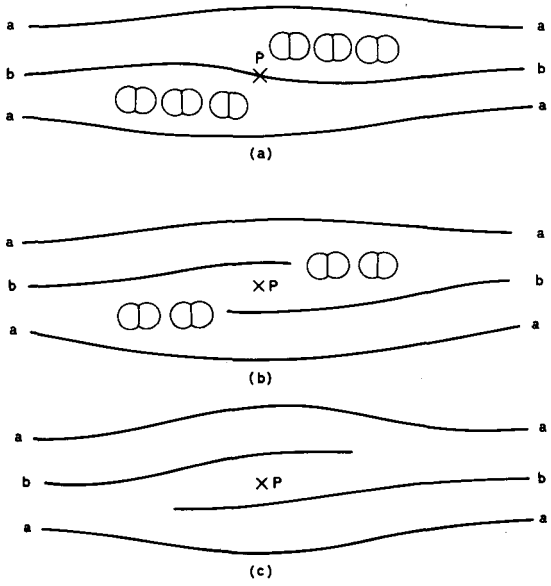


Fig. 6

Transformation from molecular cluster to honeycomb cluster

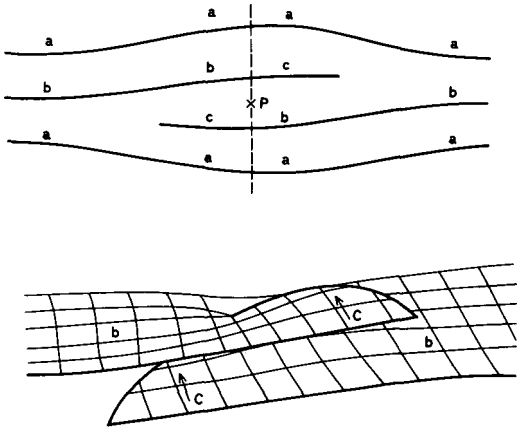


Fig. 7

Tongue dipole

(a) Stacking order of atomic layers (b) Displacement in tongue dipole

We will call this type of cluster a 'tongue dipole' as two honeycomb clusters grow each in the shape of a tongue (see Fig. 6), and the stacking of atomic layers are symmetrical with respect to the point P.

There is a strain field tending to shear the atomic layers in the area of each tongue in opposite directions to each other, as shown in Fig. 7. This

type of strain field gives the same contrast with the dislocation dipole as that proposed by BOLLMAN [17] in the dark-field electron transmission-microscope image.

X-ray measurements [14] show that the profile of the (0002) line becomes suddenly broad, due to the drastic lattice distortion above a dose of 6×10^{20} n/cm^2. These results are explained by the strong bending of atomic layers around the tongue dipoles.

7. DISAPPEARANCE OF HONEYCOMB CLUSTERS

The decomposition of a honeycomb cluster into independent atoms requires nearly the same amount of energy as the sublimation energy of graphite (171.7 kcal/mol). AMELINCKX and DELAVIGNETTE [21] observed by electron microscopy that quenched-in vacancies migrate and coagulate to form vacancy clusters at about 1200°C. The migration energy of single vacancies was estimated to be 3.0 eV [16]. The honeycomb cluster may, therefore, disappear by absorbing migrating vacancies.

At high doses vacancies may form vacancy doublets or coagulate to form vacancy clusters. The migration energy of the vacancy doublets seems to be greater than that of single vacancies, in contrast to the case in metals, because a longer path of atom migration is required in the case of a vacancy doublet than in the case of a single vacancy (see Fig. 8). The radiation-

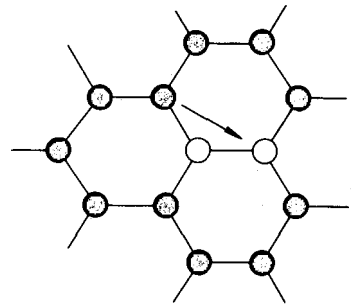


Fig. 8

Migration of a vacancy doublet

induced vacancies may be exhausted before the honeycomb clusters are completely removed and then the recovery takes place through the migration of thermally formed vacancies. The recovery is then controlled by the activation energy of the self-diffusion. The disappearance of honeycomb clusters may occur over a relatively wide range of temperatures.

8. CONCLUSION

The behaviours of interstitial atoms, molecules and their clusters are discussed in some detail and a model was proposed to interpret the radiation damage and the recovery process in graphite on the basis of these considerations. A few typical experimental results at temperatures above room

temperature, on some relatively straightforward physical quantities, such as the release of stored energy, were tentatively explained by means of the model.

The recovery of the electrical resistivity depends greatly on the electronic band structure [22, 23], the energy level of lattice defects, the carrier scattering ability of defects and so on. Since there are few experiments which clarify the structure pattern, it is difficult to give a consistent explanation for its recovery. Therefore the relation of the proposed model to the recovery of the electrical resistivity was not discussed here.

It is unfortunate that there are few experiments at low temperatures [2, 24]. No attempt was made to link the proposed behaviour of interstitials to the experiments and further work at low temperatures will have to test the propositions.

ACKNOWLEDGEMENTS

The authors express their thanks to Dr. Y. Takagi for his interest and encouragement during the course of this work, Dr. F. E. Fujita for his co-operation at the initial stage of this work and Dr. Y. Sato for his discussions on the electronic structures of molecules.

REFERENCES

[1] WIGNER, E.P., USAEC Rpt. CP-387 (1942) 4.
[2] HENNING, G.R. and HOVE, J.E., Proc. UN Int. Conf. PUAE 7 (1956) 666.
[3] MÜLLER, K.A., Phys. Rev. 123 (1961) 1550.
[4] WAGONER, G., Phys. Rev. 118 (1960) 647.
[5] IWATA, T., FUJITA, F.E. and SUZUKI, H., J. Phys. Soc. Japan 16 (1961) 197.
[6] KOMATSU, K., J. Phys. Soc. Japan 10 (1955) 346.
[7] HERZBERG, G., Spectra of Diatomic Molecules, 2nd Ed., Van Nostrand (1950) 344, 454, 513.
[8] BREWER, L., GILLES, P.W. and JENKINS, F.A., J. Chem. Phys. 16 (1948) 797.
[9] RAMSAY, D.A., Advance in Spectroscopy, (THOMPSON, H.W., ed.) Interscience 1 (1959) 1.
[10] WALSH, A.D., J. Chem. Soc. (1953) 2260.
[11] CLEMENTI, E., J. Amer. Chem. Soc. 83 (1961) 4501.
[12] PAULING, L., The Nature of the Chemical Bond, 3rd Ed., Cornell University (1960) 86.
[13] BURTON, M. and NEUBERT, T.J., J. Appl. Phys. 27 (1956) 557.
[14] WOODS, W.K., BUPP, L.P. and FLETCHER, J.F., Proc. UN Int. Conf. PUAE 7 (1956) 455.
[15] KINCHIN, G.H., Proc. UN Int. Conf. PUAE 7 (1956) 472.
[16] COTTRELL, A.H., Lecture at Tokyo (1961).
[17] BOLLMANN, W., J. Appl. Phys. 32 (1961) 869.
[18] PAULING, L., The Nature of the Chemical Bond, 3rd Ed., Cornell University (1960) 353.
[19] HERZBERG, G., Spectra of Diatomic of Members, 2nd Ed., Van Nostrand (1950) 343.
[20] KIMURA, O. and SUZUKI, H., private communication.
[21] AMELINCKX, S. and DELAVIGNETTE, P., Phys. Rev. Letters 5 (1960) 50.
[22] SLONCZEWSKI, J.C. and WEISS, P.R., Phys. Rev. 109 (1958) 272.
[23] NOZIÈRES, P., Phys. Rev. 109 (1958) 1510.

RADIATION EFFECTS IN CARBONS AND GRAPHITES*

H.H. YOSHIKAWA, E.M. WOODRUFF, J.M. DAVIDSON,
J.W. HELM AND R.E. NIGHTINGALE
HANFORD LABORATORIES OPERATION, GENERAL ELECTRIC COMPANY,
RICHLAND, WASHINGTON

Abstract — Résumé — Аннотация — Resumen

RADIATION EFFECTS IN CARBONS AND GRAPHITES. The radiation effects produced in graphites and carbons by neutron irradiation are influenced both by the irradiation conditions and by the structure of the carbons. Of the property changes that occur at high temperatures, the dimensional changes are of current interest since high-temperature radiation-induced contraction is an important factor in the design of graphite-moderated reactors.

Dimensional changes transverse to the extrusion axis depend in a complex way upon the irradiation temperature. Below 300°C expansion occurs and above this temperature contraction occurs. There appears to be a local maximum in the rate of contraction at approximately 500°C. Parallel to the extrusion axis the contraction rate is greater. The effect of irradiation temperature between 475 and 800°C has been determined to a maximum neutron exposure of $8.6 \times 10^{21} n/cm^2$ ($E > 0.18$ MeV).

The effect of structural parameters on radiation effects has been investigated in graphites and carbons having a wide range of structural development. Graphites made from a variety of graphitizing and non-graphitizing base materials and heat-treated to various temperatures have been studied. The radiation-induced contraction rates of both carbons and graphites decrease as the heat-treatment temperature is increased. Contraction rates are also lower in material produced from well-graphitizing cokes and in graphites whose crystallinity has been improved by the addition of graphitizing aids to the raw materials. These results indicate that crystalline perfection is a major factor in determining contraction rates during high-temperature irradiation.

Certain carbonaceous impregnants, which are decomposed in the pores of graphite to reduce permeability, appear to increase the rate of contraction.

The foregoing results have been incorporated in a phenomenological theory which attributes contraction in polycrystalline graphites primarily to a radiation-induced densification of disordered regions. These disordered regions appear to occur at crystallite and particle boundaries. The annealing characteristics of high-temperature radiation-induced changes are presented to support possible atomic mechanisms causing the densification.

EFFETS DES RAYONNEMENTS DANS LES CARBONES ET LES GRAPHITES. Les effets que l'irradiation par les neutrons exerce sur les graphites et les carbones dépendent à la fois des conditions d'irradiation et de la structure des carbones. Parmi les diverses modifications de propriétés qui interviennent à des températures élevées, ce sont les variations dimensionnelles qui présentent l'intérêt le plus immédiat, du fait que la contraction radioinduite à haute température constitue un facteur important dans les études des réacteurs ralentis au graphite.

Les variations dimensionnelles perpendiculaires à l'axe d'extrudage dépendent de la température d'irradiation, selon une formule assez complexe. Au-dessous de 300°C, on observe une dilatation; au-dessus de cette température, il se produit une contraction. Le taux de contraction semble atteindre un maximum local aux environs de 500°C. Pour les variations parallèles à l'axe d'extrudage, le taux de contraction est plus élevé. L'effet de la température d'irradiation pour des valeurs comprises entre 475 et 800°C a été déterminé pour des doses allant jusqu'à $8,6 \cdot 10^{21}$ nvt ($E > 0,18$ MeV).

L'influence des paramètres structuraux sur les effets des rayonnements a été étudiée dans des graphites et des carbones de structures très diverses. Ces études ont porté sur des graphites fabriqués à partir de différentes matières premières susceptibles ou non de graphitisation, qui ont été soumis à un traitement thermique à diverses températures. Les taux de contraction radioinduite des carbones et des graphites diminuent à mesure qu'augmente la température de traitement. On relève aussi des taux de contraction plus faibles lorsque la matière

* This work was sponsored by the United States Atomic Energy Commission under contract AT-(4501)-1350.

première est du coke bien graphitisable ainsi que pour les graphites dont on a amélioré la structure cristalline par l'addition de graphitiseurs aux matières premières. Il ressort de ces résultats que la perfection cristalline est un facteur essentiel pour déterminer les taux de contraction pendant l'irradiation à haute température.

Certaines substances d'imprégnation carbonnées, que l'on introduit dans les pores du graphite pour réduire sa perméabilité, semblent accroître le taux de contraction.

Il est fait état des résultats ci-dessus dans une étude phénoménologique qui attribue la contraction des graphites polycristallins essentiellement à une densification radioinduite des régions désordonnées. Ces dernières semblent se manifester aux limites de la cristallité et des grains. Les caractéristiques de recuit des variations radioinduites à haute température sont présentées à l'appui d'hypothèses concernant les processus atomiques qui produisent la densification.

ВЛИЯНИЕ РАДИАЦИИ НА УГЛЕРОДЫ И ГРАФИТЫ. На изменения, вызываемые в графитах и углеродах нейтронным облучением, оказывают влияние как условия облучения, так и структура углеродов. Из изменений свойств, которые возникают при высоких температурах сейчас представляют интерес изменения размеров, поскольку вызываемое высокотемпературной радиацией сжатие является фактором, играющим важную роль в конструкции реакторов с графитовым замедлителем.

Между изменениями в размерах, поперечными к оси выдавливания, и температурой облучения существует сложная зависимость. До 300°С происходит расширение, выше этой температуры - сжатие. Местный максимум величины сжатия достигается, по-видимому, приблизительно при 500°С. Величина сжатия больше в направлении, параллельном оси выдавливания. Влияние температуры облучения между 475° и 800°С было определено при максимальном интегральном нейтронном потоке $8,6 \cdot 10^{21}$ (E > 0,18 Мэв).

Влияние струтурных параметров на радиационные изменения было исследовано в графитах и углеродах, имеющих широкий диапазон конструкционных применений. Были изучены графиты, изготовленные из различных материалов с графитизирующей и неграфитизирующей основой и обработанные теплом при различных температурах. Величина вызываемого радиацией сжатия как углеродов, так и графитов уменьшается по мере того, как увеличивается температура тепловой обработки. Величина сжатия также меньше у материалов, изготовленных из хорошо графитизирующихся коксов, и у графитов, степень кристаллизации которых повышалась за счет добавления к исходным материалам графитизирующих веществ. Эти результаты указывают на то, что улучшение кристаллического состояния является важным фактором для определения величины сжатия при высокой температуре облучения.

Некоторые пропитывающие составы, которые содержат углерод и подвергаются разложению в порах графита для уменьшения его проницаемости, по-видимому, увеличивают величину сжатия.

Представленные результаты были включены в феноменологическую теорию, которая объясняет сжатие происходящее в поликристаллических графитах, в первую очередь вызванным радиацией уплотнением разупорядоченных районов. Эти разупорядоченные районы возникают, по-видимому, на границах кристаллов и частиц. Характеристики отжига тех изменений, которые вызываются высокотемпературной радиацией, приводятся в поддержку возможных атомных механизмов, вызывающих уплотнение.

EFECTOS DE LA RADIACIÓN SOBRE LOS CARBONES Y GRAFITOS. Los efectos causados en los grafitos y carbones por la irradiación neutrónica dependen tanto de las condiciones en que se efectúa esta última como de la estructura de los carbones. Entre las alteraciones que se manifiestan a temperaturas elevadas, las que más interesan actualmente son las dimensionales, dado que la contracción radioinducida a altas temperaturas constituye un factor importante en el diseño de los reactores moderados con grafito.

Entre los cambios dimensionales en dirección transversal con respecto al eje de extrusión y la temperatura de irradiación existe una compleja relación de dependencia. Por debajo de los 300°C, se observa una dilatación y sobrepasando dicha temperatura, una contracción. A unos 500°C, el coeficiente de contracción pasa, aparentemente, por un máximo local. En dirección paralela al eje de extrusión, el coeficiente de contracción es mayor. Los autores determinaron el efecto de la variación de la temperatura de irradiación entre 475 y 800°C, llevando la exposición neutrónica hasta un máximo de $8,6 \cdot 10^{21}$ nvt (E > 0,18 MeV).

También estudiaron la influencia de los parámetros estructurales sobre los efectos de la radiación en una extensa serie de grafitos y carbones. Examinaron grafitos preparados con una variedad de materiales básicos grafitizantes y no grafitizantes sometidos a tratamiento térmico a diversas temperaturas. Comprobaron que los coeficientes de la contracción radioinducida en los carbones y en los grafitos disminuye a medida que se eleva la temperatura del tratamiento térmico. Los coeficientes de contracción son asimismo menores en los materiales producidos a partir de coques con buenas características de grafitización y en los grafitos cuya cristalinidad se ha mejorado mediante el agregado de sustancias grafitizadoras a las materias primas. Estos

resultados indican que la perfección de la estructura cristalina es un factor decisivo en la determinación de los coeficientes de contracción durante la irradiación a alta temperatura.

Ciertas sustancias carbonosas impregnantes, que se descomponen en los poros del grafito para reducir su permeabilidad provocan, al parecer, un aumento del coeficiente de contracción.

Los resultados precedentes se han tenido en cuenta al elaborar una teoría fenomenológica que presume que la causa principal de la contracción en los grafitos policristalinos es una densificación radioinducida de las regiones estructuralmente desordenadas. Estas regiones se presentan en la superficie de contacto entre los cristalitos y las partículas. En apoyo de la teoría de que determinados mecanismos atómicos pueden ser la causa de la densificación, los autores exponen las características de recocido de los cambios radioinducidos a temperaturas elevadas.

1. INTRODUCTION

The results of both low- and high-temperature irradiations on graphite were presented in previous papers [1-5]. In this paper, radiation effects up to a maximum exposure of 8.6×10^{21} n/cm^2 (E> 0.18 MeV), and up to a maximum temperature of 1200°C are presented. The data include high-temperature radiation effects on a variety of carbons and graphites. Based on these data, a phenomenological theory for high-temperature radiation effects in graphite has been developed.

The high-temperature radiation-induced contraction in graphite is of concern in the design and operation of high-temperature graphite-moderated reactors. This dimensional instability can affect the alignment of reactor components and cause operational problems. Another potential hazard is the cracking of graphite in regions with appreciable flux gradients because of the differential contraction in portions of a graphite bar.

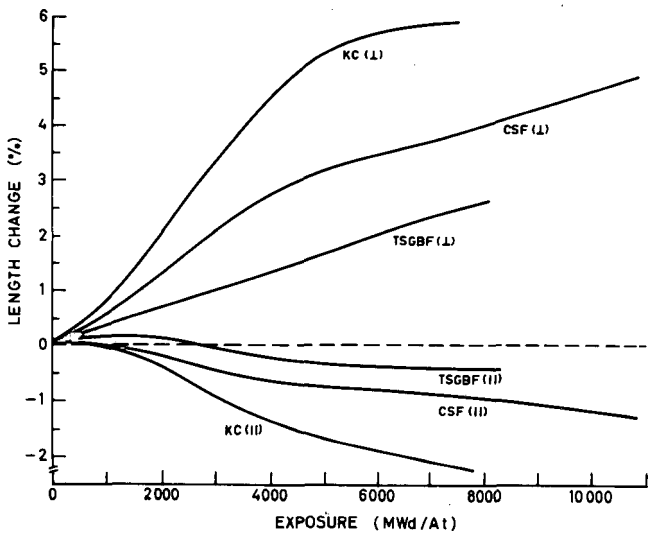


Fig. 1

Radiation-induced dimension-changes in nuclear graphite at 30°C
(1 MWd/At = 1.3×10^{17} n/cm^2 E>0.18 MeV)

2. DIMENSIONAL CHANGES IN NUCLEAR GRAPHITES

Irradiations at 30°C produced the dimensional changes shown in Fig. 1. These results are an extension of previously published work [3] and involve higher exposures. The transverse expansion of KC graphite[1] appears to approach saturation near 6%, but no apparent trend toward saturation of parallel contraction is observed. Transverse expansion is caused by the accumulation of interstitials within the lattice which forces the graphite layers apart. It has been suggested that parallel contraction is caused by buckling of the planes around the interstitials and by relaxation of the lattice around vacancies.

When graphite is irradiated at above 300°C, the relation between length change and exposure is complex. In the transverse direction, an initial expansion is generally observed to an exposure[2] of at least 2000 MWd/At.[3] At higher exposures a contraction is observed (see Fig. 2). In the parallel direction, a small initial expansion is observed below 2000 MWd/At. Contraction is observed at higher exposures. The contraction in both directions is linear to an exposure of at least 12 000 MWd/At, the maximum exposure for these samples.

Maximum exposures of approximately 8.7×10^{21} n/cm^2 ($\simeq$ 58 000 MWd/At) have been achieved during high-temperature irradiations in the GETR.[4] CSF and EGCR[5] graphites were included in these tests. During these irradiations at 475 to 800°C, the graphites contracted at approximately a linear rate (see Figs. 3 to 6).

The above results, in conjunction with data [4] obtained to a maximum exposure of 3.2×10^{21} n/cm^2 at 800 to 1200°C, indicate a minimum in the contraction rate near 800°C. At 800°C the contraction, after the maximum exposure of 8.7×10^{21} n/cm^2, was 0.55% transversely to the extrusion axis of the graphite bar and 1.2% parallel to the extrusion axis for CSF graphite, and 0.30% transversely and 1.2% parallel for EGCR graphite.

The length changes in Figs. 1 to 6 were obtained on samples with a cross-sectional area of ≤ 0.14 in^2 and a length of 4 in. Measurements have also been made of radiation-induced dimensional changes of bars 4 in × 4 in × 24 in, which are the full cross-section but half the length of Hanford moderator-bars. The concentration of the bars at 18 600 MWd/At is more than twice that predicted from small-sample results. Extrapolation of the transverse CSGBF data in Fig. 2 to 18 600 MWd/At shows a concentration of 0.21%, whereas the observed contraction is 0.57% for the full bar. The reason for this difference is not known. The comparatively low value for the small samples could be caused by the absence of stresses which may accumulate in large bars during irradiation. More data are needed to test this possibility.

---

1 Transverse and parallel orientation refer to directions transverse and parallel to the predominant layer-plane orientation. The properties of KC graphite and other graphite grades are given in [3].

2 One MWd/At for these irradiations is equal to 1.3×10^{17} n/cm^2. Neutron exposures given in this paper are for neutrons with energy greater than 0.18 MeV.

3 MWd/At: Megawatt-days per American ton (2000 lb).

4 GETR: General Electric Test Reactor, Pleasanton, Calif.

5 EGCR: Experimental Gas Cooled Reactor, Oak Ridge, Tenn.

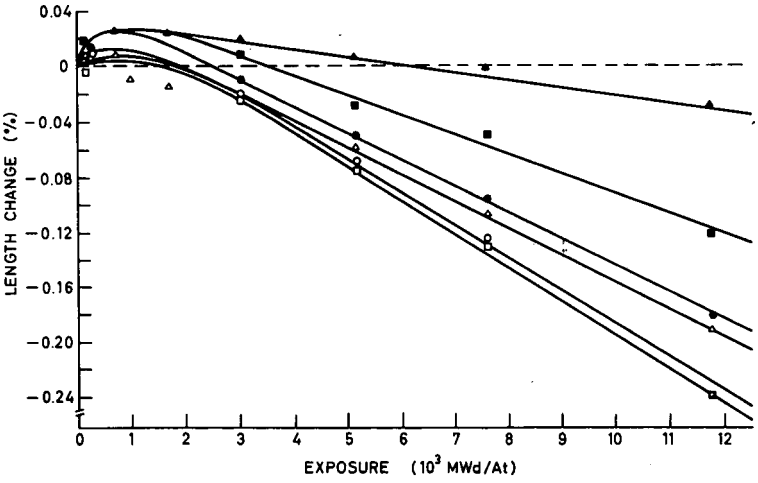


Fig. 2

Radiation-induced dimension-changes in nuclear graphite at 500°C
(1 MWd/At = 2.3×10^{17} n/cm^2 E >1 MeV)

▲ KC (⊥)
■ CSGBF (⊥)
● SGBF (⊥)

△ KC (∥)
□ CSGBF (∥)
○ SGBF (∥)

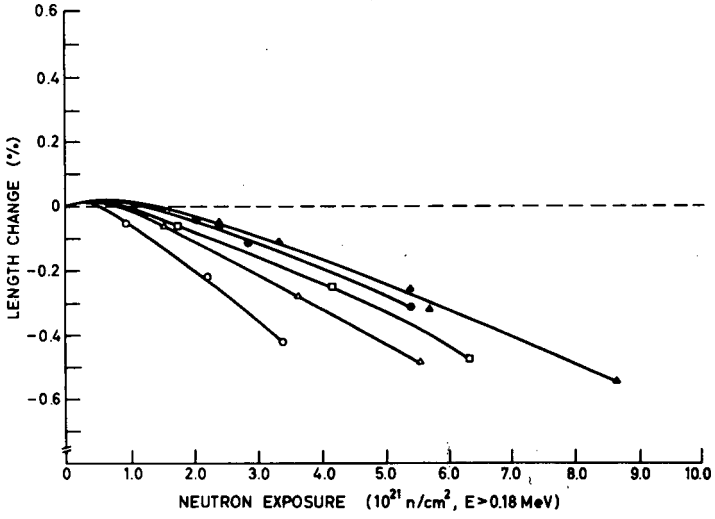


Fig. 3

Radiation-induced contraction of CSF (⊥) graphite
Last points on each curve are tentative, pending verification of exposure

○ 475°C ● 725°C
△ 575°C ▲ 800°C
□ 625°C

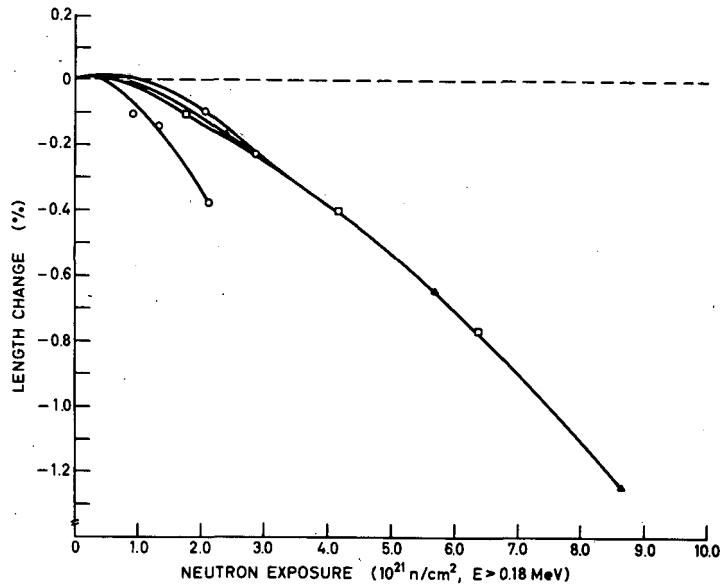


Fig. 4

Radiation-induced contraction of CSF (‖) graphite
Last points on each curve are tentative, pending verification of exposure

○ 475°C ● 725°C
△ 575°C ▲ 800°C
□ 625°C

3. RADIATION EFFECTS IN EXPERIMENTAL GRAPHITES

The concentration rate of graphite in the transverse direction depends upon the graphitization temperature, the graphitizability of the coke, the extent of grain orientation and probably upon other factors which have not been investigated. Some of the factors responsible for the different contraction rates are shown in Fig. 2. For example, KC graphite, which has the lowest transverse-contraction rate, was manufactured from a well-graphitizing coke and has a high degree of preferred orientation. The SGBF and CSGBF materials were not fully graphitized and are not as highly oriented as KC.

A number of experimental graphites are being tested at Hanford in an attempt to identify the factors responsible for radiation-induced contraction at high temperatures. The effect of graphitization temperature on the contraction rate is shown in Fig. 7. The results on this series of graphites for exposures to 4000 MWd/At have been published previously [5]. It will be noted that at the high exposures the graphites that were processed at the lower temperatures are now contracting at a significantly lower rate. This appears to be the first indication of a 'saturation of contraction' in carbons which have undergone irradiation at high-temperature.

Additional evidence that carbons heat-treated below graphitization temperatures have high contraction rates comes from the irradiation of a

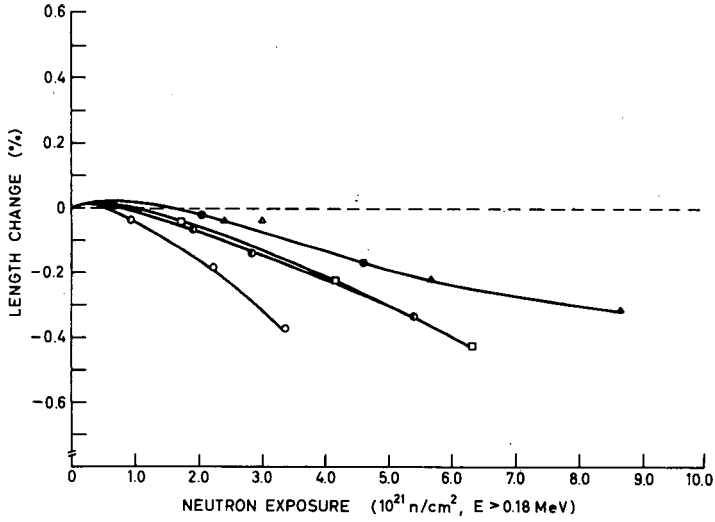


Fig. 5

Radiation-induced contraction of EGCR (⊥) graphite
Last points on each curve are tentative pending verification of exposure

EGCR graphite NC7	EGCR graphite NC8
○ 475°C	
□ 625°C	
● 725°C	◐ 725°C
▲ 800°C	▲ 800°C

lampblack-binder mixture heat-treated to 1400°C. After an exposure of 1370 MWd/At at 600°C, this material contracted 0.6%. Similar samples heat-treated to 3000°C contracted only 0.2%. In an effort to trace the cause of this difference, samples of unirradiated lampblack that had been heat-treated to 1400°C were heated to 3000°C. An average length change of -1.7% was observed. It therefore appears that the higher contraction of the 1400°C lampblack may be partially due to radiation activation of processes which are normally thermally activated between 1400 and 3000°C.

Lampblack heat-treated to 1400°C has been irradiated to higher equivalent exposures in the ETR[6] at a temperature estimated to be between 600 and 800°C. After an exposure equivalent to approximately 6000 MWd/At, the sample had contracted 2.2% in the transverse direction and 2.7% in the parallel direction. This is equivalent to a volume contraction of 7%, roughly a quarter of the volume contraction necessary to attain 100% theoretical density.

The radiation-induced contraction of several low-permeability graphites has been compared with CSF graphite. Table I gives the data from these tests. The irradiations were performed in non-instrumented capsules in the MTR[7] at a temperature estimated to be between 600 and 800°C.

---

6 ETR: Engineering Test Reactor, Idaho Falls, Idaho.

7 MTR: Materials Testing Reactor, Idaho Falls, Idaho.

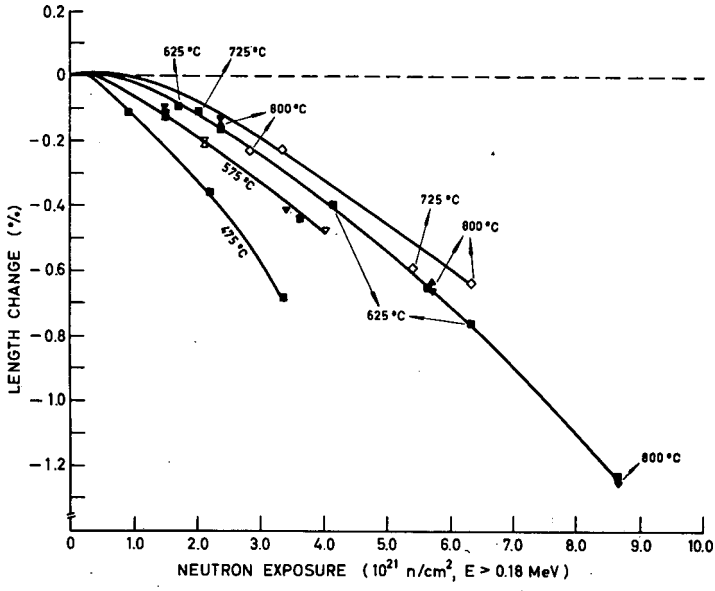


Fig. 6

Radiation-induced contraction of EGCR (||) graphite
Last points on each curve are tentative, pending verification of exposure

E > 0.18 MeV

■ EGCR graphite NC7 N1
▼ EGCR graphite NC7 N2
▲ EGCR graphite NC7 N3
◇ EGCR graphite NC8 P1
▽ EGCR graphite NC8 P2
△ EGCR graphite NC8 P3

B-10 and B-12 were both manufactured with lampblack added to the original mix. It is interesting to note that the ratio of concentration of these two graphites (0.75) is nearly equal to the ratio of lampblack content (0.7). The greater contraction noted in B-60 is attributed mainly to the low graphitization temperature of 2300°C compared to 2700°C for the other grades.

4. ANNEALING OF HIGH-TEMPERATURE DAMAGE

During the annealing of irradiated nuclear graphites, it was noted [5] that the transverse contraction did not anneal but that the parallel contraction annealed almost completely upon heating the samples to their original graphitization temperature of 2800°C. Therefore, it was surmised that there exist two separate components in high-temperature contraction. It has also been observed that lampblack samples which had been heat-treated to 3000°C and irradiated at 600°C recovered approximately 20% of the contraction when reheated to 3000°C (see Table II). This observation tends to confirm the surmise that there exists an annealable and an unannealable component in high-temperature contraction.

TABLE I

HIGH-TEMPERATURE RADIATION-INDUCED LENGTH CHANGES IN LOW-PERMEABILITY GRAPHITES

Graphite	Transverse change		Parallel change	
	[Dose 0.79×10^{21} n/cm^2] (%)	[Dose 1.50×10^{21} n/cm^2] (%)	[Dose 1.50×10^{21} n/cm^2] (%)	[Dose 2.20×10^{21} n/cm^2] (%)
CSF	-0.064	-0.233	-0.233	-0.623
B-10	-0.127	-0.311	-0.327	-0.730
B-12	-0.171	-0.429	-0.436	-0.942
B-60	-0.397	-0.711	-0.645	-1.270

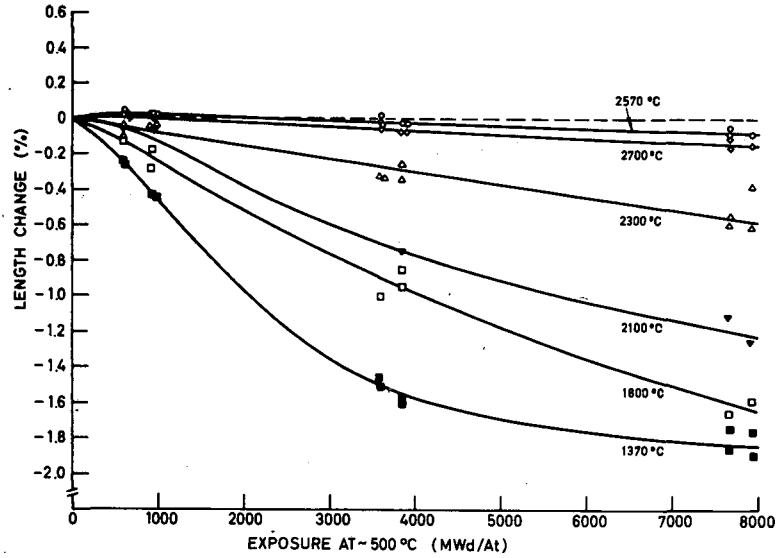


Fig. 7

Radiation-induced dimensional changes at about 500°C as a function of heat-treatment temperature all measurements transverse direction
{1 MWd/At = 1.3×10^{17} n/cm^2 E > 0.18 MeV
Temperatures shown refer to heat treatment}.

TABLE II

ANNEALING OF LENGTH CHANGES IN LAMPBLACK-GRAPHITE IRRADIATED AT 600°C

Sample	Exposure, (10^{20} n/cm^2)	Length change induced by radiation (in)	Length change on annealing to 3000°C (in)	Recovery (%)
2	0.64	-0.068	0.012	18
4	1.2	-0.094	0.021	21
6	1.6	-0.128	0.029	23

5. DISCUSSION

In nuclear graphites an increase in c-lattice spacing is generally noted even after high-temperature irradiation. This crystallite expansion implies that even during high-temperature irradiation there exists a vestige of low-temperature damage which is annealable. As in the case of low-temperature damage, this annealable component of damage causes a slight expansion in the transverse direction and a contraction in the parallel direction.

A clue as to the origin of the unannealable component of damage is obtained from the annealing results on the lampblack-based graphites. Lampblack does not graphitize fully even when heated to 3000°C. As previously noted, 80% of the contraction does not anneal upon re-heating to 3000°C. Therefore, non-graphitic carbon could be the principal source of the unannealable contraction. The effect of processing temperature can be explained, for non-graphitic carbon would be more prevalent at lower processing temperatures and hence a higher contraction rate would be expected.

The binder, coke filler and impregnant all probably contribute to the total of non-graphitic material in artificial graphite. The binder and impregnant are prevented from more complete graphitization during high-temperature treatment by the presence of excessive nucleation sites on the surface of the filler particles, and/or by the high degree of mismatch in the layer plane orientation between the filler and the binder. The filler particles also contribute to the amount of non-graphitic material, as indicated by the sensitivity of contraction to the type of coke. Since the coke particles are not single crystals of graphite, they contain many grain-boundary regions where the carbon is poorly ordered.

The unannealable contraction acts primarily in the transverse direction for two reasons. Firstly, the filler particles are oriented so that a larger number of binder layers occur in the transverse direction. In addition, there is an internal orientation within the coke particles which causes a larger number of grain boundaries to occur in the c-crystallite direction.

On the atomic level, there is little direct evidence of the mechanism by which radiation could cause poorly ordered regions of carbon atoms to densify. However, it is known that graphitization will cause an increase in the density of carbon and it seems reasonable that radiation causes an atomic re-arrangement in poorly ordered regions with an increase in density analogous to that resulting from graphitization. Thermal and displacement spikes caused by radiation may supply the necessary activation energy for a graphitization-like process [2]. If this is the case, the non-annealable contraction should be relatively independent of temperature. It is interesting that graphites produced from poorly graphitizing sugar-coke have been observed [6] to contract during irradiation at 30°C.

Other mechanisms may be of significance at the atomic level. Because of the anisotropy of the a-axis and c-axis co-efficients of thermal expansion, internal stresses accumulate in graphite during cooling from the graphitization temperature. Microscopic stress fields would be more numerous in disordered regions. The stress could be relaxed during high-temperature irradiation by the migration of interstitials and vacancies. Such processes will cause local migration of mass.

Stacking-fault loops, resulting from the collapse around vacancy agglomerates, have been detected in graphite by electron microscopy [7]. There is evidence for preferential condensation of these 'vacancy loops' at dislocations [8]. If such processes occur in disordered regions during irradiation, a non-annealable dimensional change would result.

6. SUMMARY AND CONCLUSIONS

Two simultaneous effects occur during the irradiation of polycrystalline graphite which account for the observed dimensional instability. The first is a disordering of the crystallites which results in an expansion parallel to the c-axis and a contraction parallel to the a-axis. This process is highly temperature-dependent and at room temperature is the principal effect. The second effect is a non-annealable contraction, which acts primarily in the transverse direction in anisotropic nuclear graphite, and seems to occur primarily in the non-graphitic part of the polycrystalline structure.

REFERENCES

[1] WOODS, W.K. et al., Irradiation Damage in Artificial Graphite, Proc. UN Int. Conf. PUAE 7 (1956) 307-314.

[2] NIGHTINGALE, R.E. et al., Damage to Graphite Irradiated up to 1000°C, Proc. 2nd UN Int. Conf. PUAE 7 (1958) 295-300.

[3] DAVIDSON, J.M. et al., High Temperature Radiation-Induced Contraction in Graphite, Proc. Fourth Conf. on Carbon, Pergamon Press, New York (1960) 599-605.

[4] DAVIDSON, J.M. and HELM, J.W., Effect of Temperature on Radiation-Induced Contraction of Reactor Graphite, Proc. Fifth Conf. on Carbon, in press.

[5] de HALAS, D.R. and YOSHIKAWA, H.H., Mechanism of Radiation Damage to Graphite at High Temperature, Proc. Fifth Conf. on Carbon, in press.

[6] LOCH, L.D. et al., Effect of Constitution of Graphites on Their Stability Under Low-Temperature Irradiations, USAEC Rpt. BMI-1042-Del (1955).

[7] AMELINCKX, S. and DELAVIGNETTE, P., Phys. Rev. Letters, 5 (1960) 50-51.

[8] DELAVIGNETTE, P. and AMELINCKX, S., J. appl. Phys. 32 (1961) 554.

THE BEHAVIOUR OF VARIOUS GRAPHITES UNDER NEUTRON IRRADIATION

E. FITZER AND O. VOHLER
SIEMENS-PLANIAWERKE AG FÜR KOHLEFABRIKATE,
MEITINGEN BEI AUGSBURG, FEDERAL REPUBLIC OF GERMANY

Abstract — Résumé — Аннотация — Resumen

THE BEHAVIOUR OF VARIOUS GRAPHITES UNDER NEUTRON IRRADIATION. The change of graphite properties under neutron irradiation, which is quite important for reactor designers, has been investigated closely for several years, and results have been reported in detail by several authors. The goal of these irradiation experiments was the quantitative determination of property changes as a function of irradiation dose and temperature. The concern of our own irradiation programme, which is sponsored by the Ministry of Atomic Affairs of the Federal Republic of Germany, was to study the behaviour of a wide range of reactor-grade graphites under controlled irradiation conditions.

In the first part of the paper, radiation damage as a function of different types of artificial graphite is dealt with. The graphite types differed only by their degree of crystalline order, even though they were produced under the same graphitizing conditions. The differences are caused by the different graphitizabilities of the raw materials. The dependence of the radiation damage on the graphite type seems to be of fundamental importance for the development of reactor-grade graphites with respect to various applications.

Within one group the physical properties are changed in different ways for different graphite types. The differences of the unirradiated samples remain largely unchanged or are even more pronounced after irradiation. Mechanical properties, such as strength, Young's Modulus and thermal expansion, fall into this group. The well-known Wigner growth of various graphites under irradiation was studied systematically. Furthermore, such properties are reported which are levelled out to a final value under the same irradiation conditions even when the raw materials are different. This is true for the thermal and electrical conductivity, the magnetic susceptibility and to some extent for the lattice dimensions of the graphites. Finally, the effect of irradiation on the pore distribution of the various graphites is discussed.

The second section of the paper is concerned with the correlation between the Wigner growth and the shape of the sample. The results presented here are compared with those reported in the literature, and it is shown that the absolute value of the Wigner growth depends on the shape of the irradiated graphite sample in such a manner that the specimens with the greatest length-to-width ratio show the greatest relative change in length after irradiation.

In the last section the results of irradiations of the same graphite types in three different reactors, FRM, EL.3 and GETR, are compared. The reactors differ very much in the neutron spectrum of their irradiation channels, and on the basis of the measured radiation damages the neutron doses can be estimated. It was found that in a test hole in the FRM the same irradiation damage is caused by a dose of 1×10^{19} n/cm² as in the core of the GETR at 1×10^{21} n/cm². In the EL.3, the equivalent degree of damage could not be achieved because of the low neutron energy at the irradiation channel.

COMPORTEMENT DE DIVERS GRAPHITES SOUS L'EFFET DE L'IRRADIATION NEUTRONIQUE. Depuis un certain nombre d'années, la modification des propriétés du graphite sous l'effet de l'irradiation neutronique - question très importante dans les études de réacteurs - fait l'objet de recherches approfondies, dont les résultats ont été exposés en détail par plusieurs auteurs. Ces expériences sur l'irradiation visaient à déterminer quantitativement les modifications des propriétés en fonction du nombre de neutrons par cm² et de la température. Le programme de recherche sur l'irradiation, entrepris à l'initiative du Ministère des affaires atomiques de la République fédérale d'Allemagne, avait pour objet d'étudier le comportement de toute une gamme de graphites pour réacteurs sous irradiation contrôlée.

Dans la première partie du mémoire, les auteurs indiquent quels ont été les dommages causés par les rayonnements, selon le type de graphite artificiel. Les types de graphite ne diffèrent que par le degré de cristallisation, même s'ils sont produits dans les mêmes conditions de graphitisation. Les différences s'expliquent par les diverses possibilités de graphitisation de la matière première. L'influence du type de graphite

sur l'étendue des dommages causés par les rayonnements semble avoir une grande importance pour la recherche des qualités de graphite pour réacteurs destinés à différents usages.

Dans les divers types de graphite, les propriétés physiques d'un même groupe se modifient de différentes façons. Les différences entre échantillons non irradiés subsistent en grande partie ou sont même encore plus marquées après irradiation. Les propriétés mécaniques, telles que la résistance, le module de Young et la dilatation thermique appartiennent à ce groupe. Les auteurs ont étudié systématiquement la croissance de Wigner des divers graphites sous l'effet de l'irradiation. Ils signalent en outre certaines propriétés qui, dans les mêmes conditions d'irradiation, tendent vers une même valeur finale, même si les matières premières sont différentes. Il en est ainsi pour la conductivité thermique et électrique, la susceptibilité magnétique et, dans une certaine mesure, les dimensions du réseau des graphites. Les auteurs examinent ensuite l'effet de l'irradiation sur la distribution des pores dans les différents graphites.

Dans la deuxième partie du mémoire, les auteurs s'occupent de la corrélation entre la croissance de Wigner et la forme de l'échantillon. Les auteurs comparent les résultats qu'ils ont obtenus à ceux qui ont été publiés, et montrent que la valeur absolue de la croissance de Wigner est fonction de la forme de l'échantillon de graphite irradié et que les échantillons pour lesquels le rapport entre la longueur et la largeur est le plus élevé accusent la plus forte variation de longueur relative après irradiation.

Enfin, les auteurs comparent les résultats obtenus pour les mêmes types de graphite à la suite de leur irradiation dans trois réacteurs différents: le réacteur FRM, EL.3 et GETR. Dans ces réacteurs, les spectres des neutrons des canaux d'irradiation sont très différents et on peut estimer les quantités de neutrons par cm^2 d'après les dommages causés par les rayonnements. On a constaté qu'un même dommage était dû à $1 \cdot 10^{19}$ nvt dans un canal d'expérimentation du FRM et à $1 \cdot 10^{21}$ nvt dans le cœur du GETR. Pour ce qui est du réacteur EL.3, il n'a pas été possible d'obtenir un dommage équivalent en raison de la faible énergie de neutrons dans le canal d'irradiation.

ПОВЕДЕНИЕ РАЗЛИЧНЫХ ГРАФИТОВ ПОД ДЕЙСТВИЕМ НЕЙТРОННОГО ОБЛУЧЕНИЯ. Изменение свойства графита под действием нейтронного облучения, имеющее весьма большое значение для конструкторов реакторов, тщательно исследовалось в течение многих лет, и результаты докладывались подробно рядом авторов. Целью этих опытов по облучению было количественное определение изменений свойств в зависимости от дозы облучения и температуры. Задачей нашей собственной программы облучения, проводимой по поручению Министерства атомной промышленности Федеративной Республики Германии, было изучение поведения различных графитов реакторных сортов в условиях контролируемого облучения.

В первой части доклада приводятся данные относительно радиационного повреждения в зависимости от различных сортов искуственных графитов. Сорта графитов отличаются друг от друга только по степени своего кристаллического порядка, хотя все они были изготовлены в одинаковых условиях графитизации. Различие возникает из-за неодинаковой способности к графитизации исходного сырья. Зависимость радиационного повреждения от сорта графита имеет, по-видимому, большое значение для выработки графитов реакторных сортов в зависимости от назначения.

В одной и той же группе физические свойства изменяются не одинаково для графитов разных сортов. Разница, существовавшая между необлученными образцами, остается в основном неизменной или даже усиливается после облучения. Сюда относятся механические свойства, например прочность материала, модуль Юнга, а также коэффициент термического расширения. Систематически излучался хорошо известный вигнеровский рост различных графитов под влиянием облучени Далее, сообщается о таких свойствах, которые выравниваются до определенной величины в одинаковых условиях облучения даже в случае, если исходное сырье различно. Это имеет место для теплопроводности и электропроводимости, магнитной восприимчивости и, в некоторой мере, для размеров решетки графитов. Наконец, обсуждается воздействие облучения на распределение пор в различных графитах.

Вторая часть доклада посвящена изучению связи между вигнеровским ростом и формой образца. Представляемые в настоящем докладе разультаты сравниваются с другими данными, о которых сообщалось в технической литературе, причем показано, что абсолютная величина вигнеровского роста зависит от формы облучаемого образца графита, так что образцы с наибольшим соотношением между длиной и шириной испытывают в результате облучения наибольшее относительное изменение длины.

В последней главе сравниваются результаты облучения графитов одного и того же типа в трех различных реакторах, а именно в реакторе FR в Мюнхене, в реакторе EL.3 в Сакле и в реакторе GETR в Валлеситосе. Эти реакторы сильно отличаются друг от друга по нейтронному спектру в каналах для облучения; исходя из измерения радиационных поражений, представляется возможным определять дозы нейтронов. Было найдено, что в экспериментальном канале реактора FR в Мюнхене доза в

$1 \cdot 10^{19}$ nvt наносит такое же радиационное повреждение, как доза в $1 \cdot 10^{21}$ nvt в активной зоне реактора GETR. В реакторе EL.3 в Сакле, ввиду малой энергии нейтронов в канале облучения, равноценного вреждения достичь не удалось.

EFECTOS DE LA IRRADIACIÓN NEUTRÓNICA SOBRE DIVERSOS TIPOS DE GRAFITOS. Por el interés que presentan para la construcción de reactores, las modificaciones que la irradiación neutrónica introduce en las propiedades del grafito, se vienen estudiando desde hace varios años, y diversos autores han publicado los resultados obtenidos. La finalidad de aquellos experimentos de irradiación era determinar cuantitativamente los cambios sufridos por las propiedades del mencionado material en función de la dosis de irradiación y de la temperatura. El objeto perseguido por los autores con su presente programa de irradiación, que ha sido patrocinado por el Ministerio de Asuntos Atómicos de la República Federal de Alemania, fue estudiar el comportamiento de un gran número de variedades de grafito de pureza nuclear en condiciones de irradiación controladas.

En la primera parte de la memoria se indican los daños que las radiaciones producen en diversos tipos de grafitos artificiales, que se diferencian solamente por sus respectivos grados de orden de cristalización, a pesar de haber sido obtenidos todos en las mismas condiciones de grafitización. Las diferencias se deben a la capacidad de transformarse en grafito, que varía según las materias primas. Al parecer, la manera en que los daños sufridos por irradiación dependen del tipo de grafito es de fundamental importancia en la obtención de grafitos adecuados para las diversas aplicaciones que este material encuentra en los reactores.

Dentro de un mismo grupo, las propiedades físicas cambian de modo distinto para los diferentes tipos de grafito. Las diferencias que existen entre las muestras no irradiadas se conservan en gran parte o incluso se acentúan con la irradiación. En este grupo se cuentan las propiedades mecánicas tales como la resistencia, el módulo de Young y la dilatación térmica. Los autores estudiaron sistemáticamente el conocido efecto de crecimiento de Wigner en diversos tipos de grafito sometidos a la irradiación.

Además, la memoria informa sobre aquellas propiedades que, en las mismas condiciones de irradiación, tienden hacia un mismo valor final aunque las materias primas sean distintas. Esto sucede en el caso de la conductividad térmica y eléctrica, de la susceptibilidad magnética y, hasta cierto punto, de las dimensiones de la red cristalina de los grafitos.

Por último, los autores analizan el efecto de la irradiación sobre la distribución de los poros en los diversos tipos de grafitos.

La segunda parte de la memoria se ocupa de la correlación existente entre el crecimiento de Wigner y la forma de la muestra. Los resultados que se citan en la memoria son comparados con los que figuran en la bibliografía y se demuestra que el valor absoluto del crecimiento de Wigner depende de la forma de la muestra de grafito irradiada, observándose que la longitud de las muestras en las que la razón longitud : ancho es más elevada sufre un cambio relativo mayor a raíz de la irradiación.

En el último capítulo se comparan los resultados obtenidos al irradiar los mismos tipos de grafito en tres reactores diferentes, a saber, el FRM, el EL.3 y el GETR. Los espectros neutrónicos en los canales de irradiación de esos tres reactores son muy diferentes y la medición de los daños ocasionados por las radiaciones puede servir de base para calcular las dosis neutrónicas. Se encontró que una dosis de $1 \cdot 10^{19}$ nvt en el orificio de exploración del reactor FRM causa los mismos daños que una dosis de $1 \cdot 10^{21}$ nvt en el cuerpo del reactor GETR. No fue posible alcanzar daños de un grado equivalente en el reactor EL.3, por ser demasiado baja la energía de los neutrones en el canal de irradiación.

1. INTRODUCTION

Graphite was one of the first materials used in the advancement of reactor techniques. Today graphite is becoming more and more important in the many special fields of nuclear technology. The nuclear physicist considers graphite as the 'light element' carbon with excellent neutron-physical properties and he demands the utmost purity and absence of neutron absorbers. The reactor designer welcomes the fact that this pure carbon demanded by the nuclear physicist represents a solid with outstanding properties. In the beginning of reactor technology the quality of reactor-grade graphites was governed by the possibility of producing the purest graphite carbon from

a chemical standpoint and not by demands for specific mechanical or thermal qualities.

A typical example is the British reactor-grade graphite which is based on raw material and procedures guaranteeing high purity. This has necessarily led to a special graphite material with typical well-known properties. such as extremely high conductivity, low hardness and increased anisotropy. In the view of the expert this grade of graphite is only one of a large number of possible types. Such properties of graphite as the electrical and thermal conductivities, thermal expansion, strength, Young's modulus etc. can be varied over a large range by using different raw materials, granulometry, manufacturing procedures and degree of graphitization [1, 2]. Since purification is possible, the graphite manufacturer is largely independent of the purity of his raw material, and in principle it is possible to synthesize reactor-grade graphites of specific qualities different from the usual ones.

For instance, the raw material was varied by the French in the development of a reduced-anisotropic reactor-grade graphite for use in the Marcoule reactors [3]. This change of the material's properties was made in an attempt to influence the well-known anisotropic Wigner growth for moderators exposed to neutron irradiation at relatively low temperatures. As a further example the application of graphite in high-temperature reactors can be mentioned; here the material must have specific thermal qualities and strength, and must serve partly as a sealer [4, 5, 6].

The aim of our work was to study the behaviour of various graphites under neutron irradiation, principally to enable the graphite manufacturer to develop optimum graphite qualities for specific reactor applications. It is difficult to press the wide range of varieties obtained from different raw materials and manufacturing procedures into a generally valid scheme. We believe the best way is to characterize the various graphites by their crystal order, because the neutron irradiation influences or disturbs primarily this type of microcrystalline order.

A criterion for the crystalline order is the so-called degree of graphitization. This is governed by the graphitization process which continues by itself once the kinetic barrier is removed by operation at high temperature. Depending on the level of crystalline distortion, one reaches a final state of a more or less high degree of order under extreme conditions, for instance at temperatures of about 3000°C. The degree of graphitization obtained therefore depends on the raw material as well as on the treatment. The influence of graphitization treatment on the extent of radiation damage has already been reported [7]. In the present paper only "completely graphitized" graphites of different degrees of graphitization are examined for their behaviour under irradiation. This different degree of graphitization of the samples was not obtained by different heat treatments; it was due only to the different behaviour of the raw materials graphitized at temperatures of more than 3000°C. Some preliminary results of these investigations have already been reported at the 5th Conference on Carbon in 1961 [8]. The literature does not contain reports of such investigations of systematically varied graphite types and their behaviour under irradiation. Only one United States research group has studied a similar problem. This was the influence of the filler on the radiation behaviour of graphite samples using Kendall, Texas and Cleeves cokes [11]. These published data, however, give no

details about the specific properties of the irradiated specimens, whereas the influence of the anisotropy can be clearly seen from these results.

For this reason some fundamental remarks on the anisotropy of graphite bodies concerning the different degree of graphitization obtained in the raw material under the same conditions of graphitization seem to be applicable.

The coherent regions of an easily graphitizing coke are very anisotropic because of their largely ideal layer-lattice structure. Thus the anisotropy is formed by the micro- or inner-crystalline structure. However, should the single coke grains be distributed statistically an isotropic body would result.

In practice strong deviations from these statistical distributions can be found for the following reasons:

(a) The form of the coke grain

Regarding good graphitizing materials (i. e. raw materials with large regions of the same anisotropy: this can be recognized very well by means of polarized light), the grain is split along the layer planes which are largely oriented in the same direction. This results in long, plate-like grains, as shown on the left-hand side of Fig. 1. For these types of coke the term

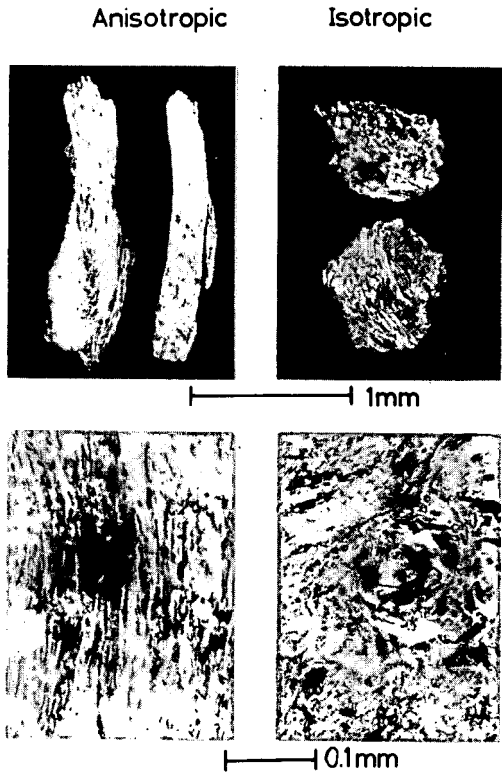


Fig. 1

Different forms of coke

"needle-like coke" has been used in the patent literature [9] and found its way into technical language. Of the above-mentioned raw materials for reactor-grade graphites described in the literature, the Kendall coke would correspond best to this type.

In contrast to this, on the right-hand side of Fig. 1, another type of coke can be seen which yields sphere-like grains on grinding. Generally, all poorly graphitizing raw materials tend to this grain structure, which is caused by the poorer orientation of the single-crystal regions within the coke. In this sense there is indeed a rough correlation between the degree of graphitization obtainable and the anisotropy of grain which results in the anisotropy of shaped bodies by corresponding arrangement (Fig. 2).

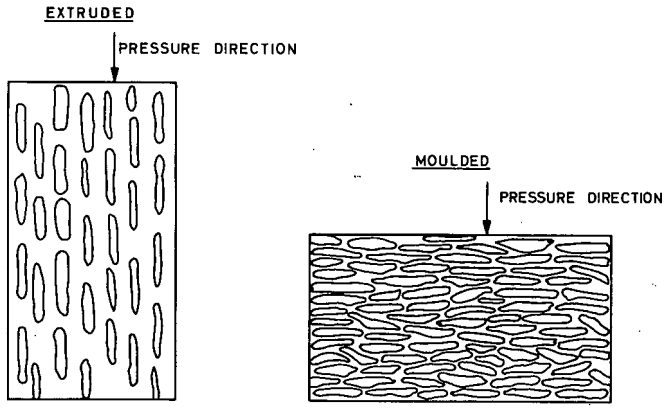


Fig. 2

Structure anisotropy of graphite bodies

(b) Anisotropy caused by the manufacturing procedure

The smaller the coke grains the more obvious is the advantage that these should be cleavable along layer planes. This is reported on in more detail in an earlier paper [10]. Thus the grain size can intensify or diminish the effect discussed in 'a' above.

(c) Bulk anisotropy

The bulk anisotropy is also dependent on relative packing density of the filler and the binder component of the shaped body. The binder is always more isotropic than the filler. In Fig. 2 the variation of the packing density in different directions resulting from the manufacturing procedure is indicated for moulded and extruded pieces.

On the basis of these considerations, it can be concluded that the anisotropy of shaped bodies is dependent on different factors. One of these, the grain-shape anisotropy, is related to the degree of graphitization; however, this is not true of the grain-orientation-dependent anisotropy resulting from the packing occurring in manufacture. Irradiation will influence each factor differently.

2. LITERATURE ON RADIATION DAMAGE IN GRAPHITE

It is impossible to cite all papers concerned with irradiation damage of graphite. As an introduction to our results some fundamental findings of the literature are given in Figs. 3 - 6. Fig. 3* presents in a simplified

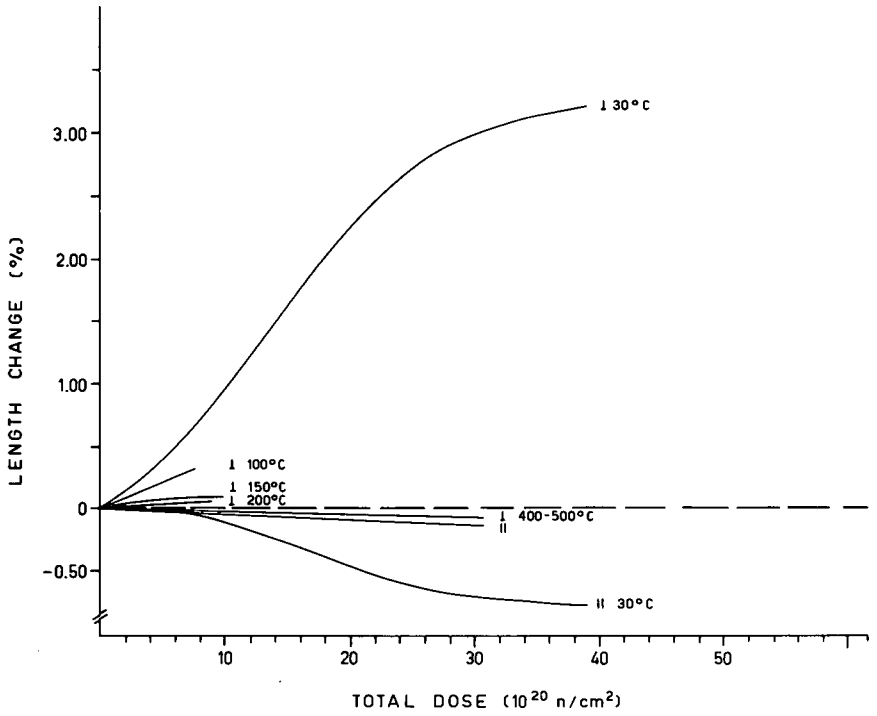


Fig. 3*

Dimension changes of CSF graphite with neutron irradiation [11, 12, 13]

picture a summary of the dimensional changes of graphites irradiated at different temperatures. In this graph only corresponding data are given to avoid an unnecessarily complicated figure. The difficulties met in comparing different irradiation results will be mentioned later. Fig. 4 shows the dependence of the dimensional changes of different graphites under the same irradiation conditions: the needle-like-coke component, KC, and its high anisotropy will be discussed in detail. The change of the c-spacing is also plotted to demonstrate the difference between bulk expansion and the increase of lattice distance

As indicated in Fig. 3 the Wigner-growth falls rapidly with increasing irradiation temperatures and finally changes to a shrinkage. Fig. 5 gives the fundamental results obtained by de HALAS and YOSHIKAWA [14] for irradiation at 400-500°C. They have clearly shown the interesting effect

---

* In all the following figures { ⊥ will indicate results across the grain; ∥ will indicate results with the grain }

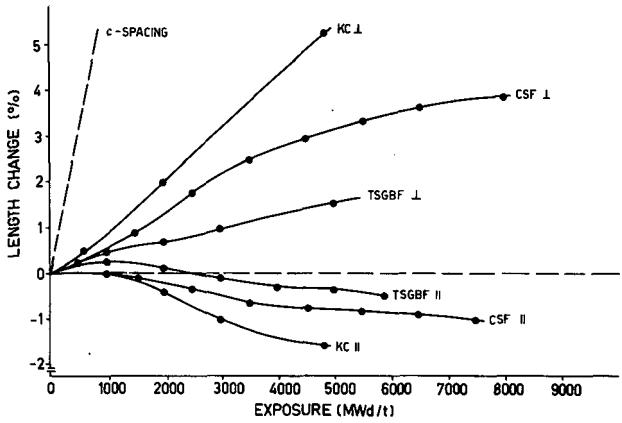


Fig. 4

Dimension changes of various reactor-grade graphites with neutron irradiation [15]

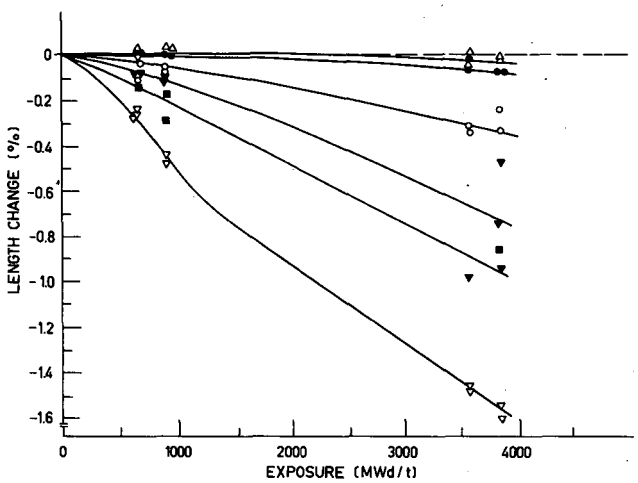


Fig. 5

Dimension changes of reactor grade graphite with neutron irradiation [14]

Key to heat treatment temperature

▽ 1370°C	○ 2300°C
■ 1800°C	● 2700°C
▼ 2100°C	△ 2570°C

(Fig. 6) of transition from growth to shrinkage in a dimension perpendicular to the grain direction (i. e. at high bulk anisotropy, mainly in direction of the crystallographic c-axis).

It seems important to note that for irradiation in the low and medium temperature ranges (below 200°C), the greatest anisotropic dimension-changes occur in the most anisotropic (i. e. the best graphitized) cokes.

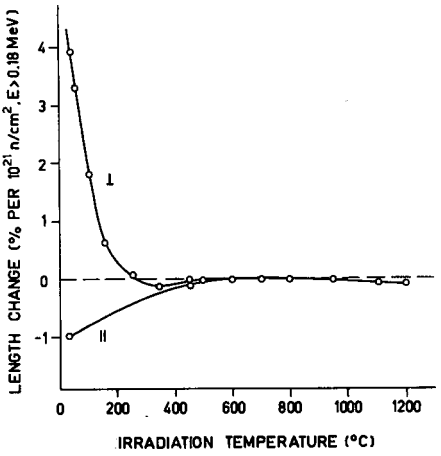


Fig. 6

Dimension changes of reactor-grade graphite with neutron irradiation [14]

Systematic data are not available on the dependence of dimension changes on the graphitizability of different fillers under high-temperature irradiation (above 300°C) where a shrinking effect is observed despite lattice growth; only the influence of graphitization temperature is known. The sample graphitized at the lowest temperature shows the highest shrinkage. In a certain sense this is exactly the reverse of the conditions found for low-temperature irradiation.

3. AUTHORS' IRRADIATION EXPERIMENTS

Because of this lack of exact data on the irradiation behaviour at different temperatures as a function of the type of graphite, we carried out some systematic experiments in this field. Our investigations can be divided into two parts:

(a) Irradiation at temperatures below 200°C
These experiments are largely finished and their results will be given below.

(b) Irradiation at higher temperatures
Here only data on irradiations to 10^{20} n/cm² (E > 0.17 eV) at up to 610°C are on hand. Under these irradiation conditions the characteristic shrinking effects were not yet observed. The results of this part of our experiments will be published later.

3.1. Irradiated graphite-types

As already mentioned, the types of graphite used for irradiation studies were chosen according to their degree of graphitization. As a measure of the degree of graphitization the so-called I. V. value [8], deter-

mined from X-ray measurements, was chosen. Since there are easily and poorly graphitizing portions in commercial carbon products, certain difficulties arise from the determination of an average lattice spacing or crystallite size. If one attempts to use the diffraction peak as a measure for lattice spacing, the well-crystallized portions are found merely to have a more pronounced pattern than the disordered regions. The lattice spacing therefore gives no differentiation between the easily graphitizing cokes, because changing portions of poorly graphitizing areas only effect a broadening or rising of the flank of the diffraction line at low scattering angles.

In order to get an X-ray criterion comprising also the poorly graphitizing regions the slopes of at least two (001) lines must be considered. Supposing that the graphite crystallites consist only of regions with two defined lattice spacings, namely the ordered state with 3.354 A and the disordered state with 3.44 Å, FRANKLIN[16], an X-ray method can be used for determining quickly the degree of graphitization even of highly heterogeneous products. For this purpose the (002) line is divided into two theoretical curves, one for the ordered and one for the disordered state. The ratio of the two areas represents a relative criterion for the degree of graphitization.

But it is sufficient to take only the ratio of the intensities of the two theoretical peaks. The intensities are therefore determined for the scattering angle belonging to the easily graphitizing areas (i.e. in easily graphitizing materials the maximum of the (002)-line) as well as for the angle of the lattice distance of the disordered state, 3.44 Å. The ratio of these two intensities is defined as the I. V. value. According to our results this represents a good measure for the average degree of order of a graphite material.

For several decades another technique has been used for characterizing the quality of graphites: the real density [17]. This is the density of the finely powdered "completely graphitized" carbon material. Easily graphitizing cokes show a small c-spacing, large crystallites and a good orientation of the single coherent regions, which means a very dense packing of the carbon atoms and must therefore result in high density. In poorly graphitizing materials, however, the real density is diminished by lattice distortion and inaccessible micropores caused by a low degree of orientation of the single crystallites. Since the two criteria, the I.V. value and the real density, complement each other in their definition of cyrstalline order, both were used for characterizing the graphite types. Both the I.V. region and the region of the real density were divided into five groups and the various graphites were classified accordingly. The samples were marked with a two-digit number, the first figure signifying the I.V. group, the second the real density group. The numbering begins with the easily graphitizing types, i.e. at high characteristic numbers, and ends at group 5 with the lowest characteristic numbers, i.e. type 11 = best graphitizing, type 55 = most poorly graphitizing (c.f. Figs. 7 and 8, top left).

Samples 11, 23, 34 and 44 are types produced by the same manufacturing technique, using the same binder and the same grain size distribution. They differ only in the filler quality. Type 55 had to be manufactured by a special forming procedure because of the extremely poor graphitizability of the raw material. Types 54 and 22, especially the latter, show very strong bonding of the grains; in addition to that 54 and 43 are sealed

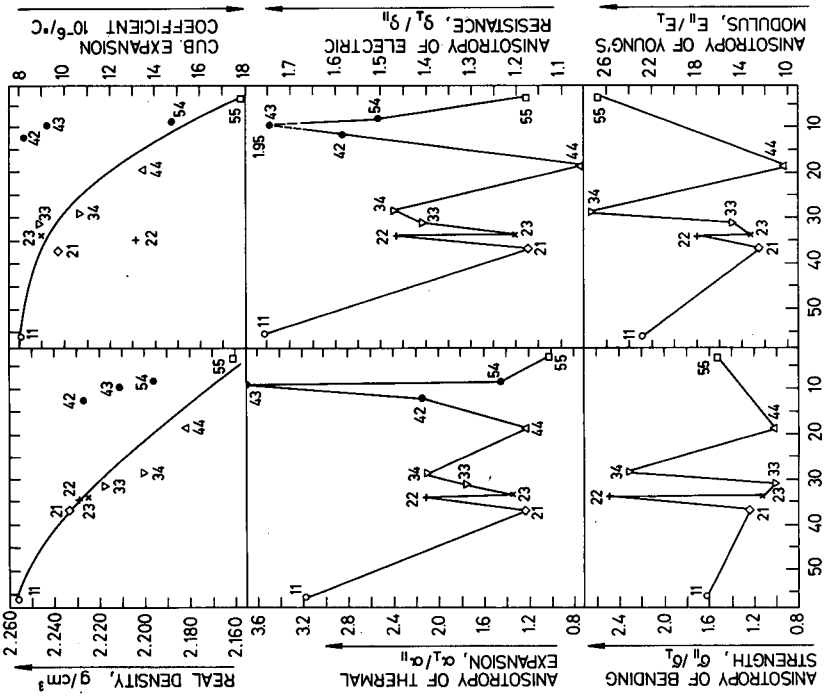


Fig. 8

Physical properties of the unirradiated graphite-types

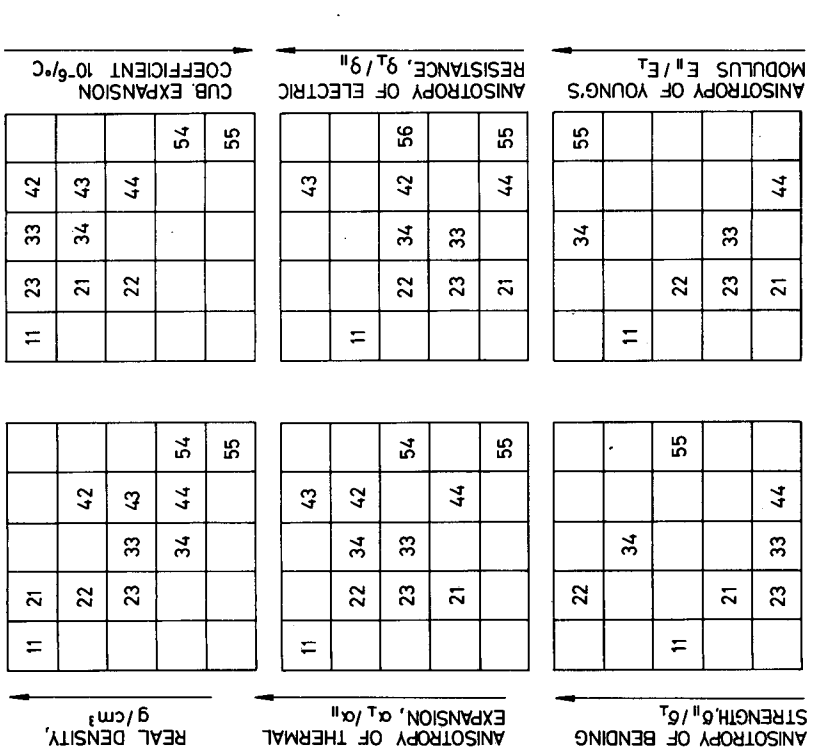


Fig. 7

Classification of graphite types based on I. V. value and real density

by deposits of poorly ordered secondary carbon. Furthermore Type 43, in the unsealed state compared with Type 11, is an excellent example for the above-mentioned increase of anisotropy obtained by finer grinding. Types 21, 33 and 42 represent commercial reactor-grade graphites which fit very well into this scheme, although their grain size is somewhat larger and they differ somewhat from each other because of different binders.

The other diagrams and chess-board representations of Figs. 7 and 8 show that the dependence of anisotropy on the degree of graphitization represented by the I.V. value becomes smaller and smaller, when properties connected with the grain anisotropy and bulk anisotropy are considered. Though there is a rough connection between the degree of graphitization and the thermal, electrical and mechanical properties [17] it can be seen very clearly that a change of other variables such as granule size, binder, coke distribution etc., affect the properties of the end-product greatly. A further aim of the present paper is to report the changes in the influence of these variables after irradiation.

3.2. Irradiation conditions

Samples of 5×5×45 mm of various graphite types were irradiated in the reactors GETR at Pleasanton, California, FRM at Munich and EL. 3 at Saclay. The positions of the irradiation capsules are plotted in the cross-sections of the reactor cores of Fig. 9. The different reactor types will be described later, in the discussion of the irradiation results.

The details of the capsules and their installation in GETR can be found from GAIN [18] who has carried out these irradiations for us. The irradiations from 45 to 70°C ranged up to a dose of 8.5×10^{19} n/cm² (E >0.18 MeV). The temperature of the capsules with a higher dose (2.84×10^{21} n/cm², E >0.18 MeV max.) reached 120 to 220°C. Irradiations at 345 - 425°C and 460 - 610°C respectively were carried out up to a maximum dose of about 7×10^{19} n/cm², E >0.18 MeV.

For irradiations in FRM, the samples were put into aluminium capsules where they were pressed to the wall by aluminium springs to allow of better heat transfer. The temperature was measured by monitors and was about 120°C. The capsules were fitted in special fuel elements with a neutron flux of 1.8×10^{13} n cm^{-2} s^{-1}, E >0.1 MeV (Fig. 10). In the following, irradiations with a maximum dose of 1.6×10^{19} n/cm² are reported. Besides the usual sample size of 5×5×45 mm, samples of 15×15×45 mm were also used, this for studying the influence of sample size.

For the irradiations in EL.3, the graphite samples were placed in aluminium capsules (23 mm I. D. ×75 mm) with a screw cap. The spaces between the samples and the capsule-wall were filled-up with aluminium shavings. The aluminium capsules were placed in the bore holes of a graphite bar which was put into the central canal of EL.3. The flux present is shown in Fig.10. The irradiation ranged up to a dose of 6×10^{18} n/cm², E >1.0 MeV. For temperature measurements during irradiation, two thermocouples were placed between the outside of the capsule wall and the graphite bar. The flux was measured with thorium monitors.

The dose data given in the following are referred to neutron energies

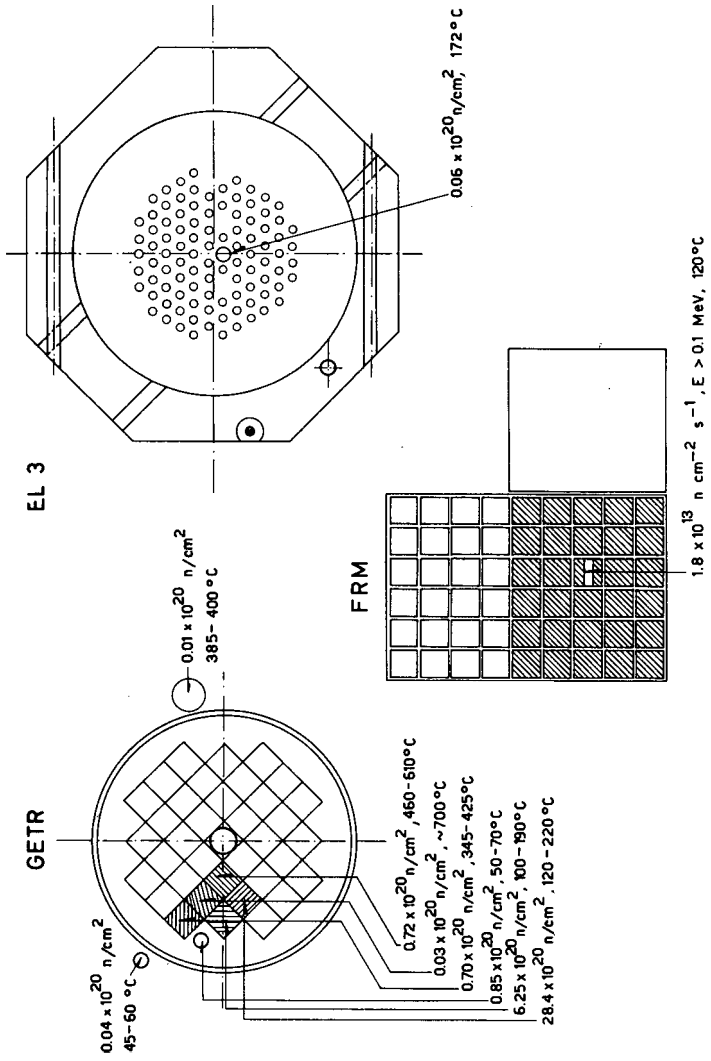


Fig. 9
Irradiation facilities of GETR, FRM and EL 3 reactors

Reactor	Neutron flux $n\ cm^{-2}\ s^{-1}$	
GETR	5×10^{12} - 3×10^{14}	> 0.17 eV
	43-50% therefrom	> 0.18 MeV
EL3	5.8×10^{13}	< 0.04 eV
	3.3×10^{13}	> 0.04 eV
	1.1×10^{12}	> 1.00 MeV
FRM	2.2×10^{13}	> 0.01 MeV
	1.8×10^{13}	> 0.1 MeV

Fig. 10

Neutron flux at the irradiation facilities

of E > 0.18 MeV for GETR irradiations, of E > 0.1 MeV for FRM irradiations and of E > 1.0 MeV for EL.3 data.

4. IRRADIATION RESULTS

For the present the irradiation - induced changes of the graphite properties will be divided roughly into those concerning bulk properties and others concerning microproperties. The changes of the pore volume will be discussed separately. Furthermore, the influence of the size of the graphite samples on the property - changes and the influence of the neutron spectrum of different reactors will be reported on in a separate section.

4.1. Bulk properties

The bulk properties of the graphite samples, such as thermal and electrical conductivity and mechanical properties are determined not only by the intracrystalline order but also by the bulk binding structure between the grains.

We have found that two different groups of irradiation damage can be recognized. The properties of the first group are levelled out in the various graphite types, whereas in the other group relative differences are preserved or become even more pronounced after irradiation.

4.1.1. Properties levelled out by irradiation

According to our results, the properties levelled out by irradiation are thermal conductivity, in part electrical conductivity and also the magnetic susceptibility. These properties depend on the carrier population, the mobility of the electrons and the carbon atoms, but not on bulk strength or bulk anisotropy.

It is well known that Frenkel defects are built up by neutron irradiation, whereas interstitial atoms are formed between the a-b-planes. Beside the interesting considerations regarding the dependence of electrical and magnetic properties on the increase in the c-spacing, the effective concentration of free electrons, for instance, is changed because electrons are trapped at the lattice vacancies within the a - b planes [19]. We shall consider the effects in detail.

4.1.1.1. Magnetic susceptibility. The magnetic susceptibility is a criterion for the carrier population and their spatial distribution. The high magnetic susceptibility of graphite can be supposed to be due to the motion of the electrons within the layer planes. The interaction with neighbouring planes, however, is very low. Thus the susceptibility is a certain criterion for the expansion of the ordered areas in the a - b direction. For the experimental determination of the magnetic susceptibility the force of an inhomogeneous magnetic field of 10 000 to 12 000 Oe acting on the sample rods was used. The samples were suspended with aluminium wires of 0.05 - mm diam. from a pendulum beam. The deflection of the pendulum, due to the magnetic-field force acting on the sample, zero position was measured optically. The measurement of specimens cut with the grain yield only an across-grain value. Samples cut perpendicular to the grain may be positioned so as to give either an across-grain value or a with-grain value.

As Fig. 11 shows, the magnetic susceptibility is greatly decreased after relatively low irradiation doses at temperatures up to 200°C and reaches the final value for all samples at 6×10^{20} n/cm^2, E >0.18 MeV. By this means the diminution of the carriers in the π - electron band is demonstrated. This is caused by the trapping of electrons at lattice distortions built up by the irradiation. Irradiations at higher temperatures (400 - 610°C) show that a smaller decrease of the susceptibility due to less damage in the microcrystalline region (Fig.12). At doses of 7×10^{19} n/cm^2 there appears to be no tendency to level-out.

In order to illustrate the variation of the dependence of irradiation on the degree of graphitization, a special form of graphic presentation was chosen with the I. V. value (representing the degree of graphitization) as abscissae for the arrangement of the graphite types. The ordinates represent the property under consideration. Of this form, the graph in Fig.13 shows the variation of magnetic susceptibility with irradiation.

The sharp decrease and the levelling - out effect of the magnetic susceptibility at high doses can be clearly seen. Thus the magnetic susceptibility reaches a final value which is nearly the same for all graphite types. Since the susceptibility responds mainly to the two-dimensional spread of the coherent areas, the levelling-out suggests that all graphite types are disturbed in the a - b direction of the lattice in about the same fashion.

4.1.1.2. Thermal conductivity. In graphite, thermal energy is mainly conducted by lattice vibrations, i.e. as opposed to the case for metals, the free electrons participate to only a small extent in heat transport [20]. This fact is expressed especially in the high value of the Wiedemann - Franz ratio, determined experimentally for about room temperature. Like the

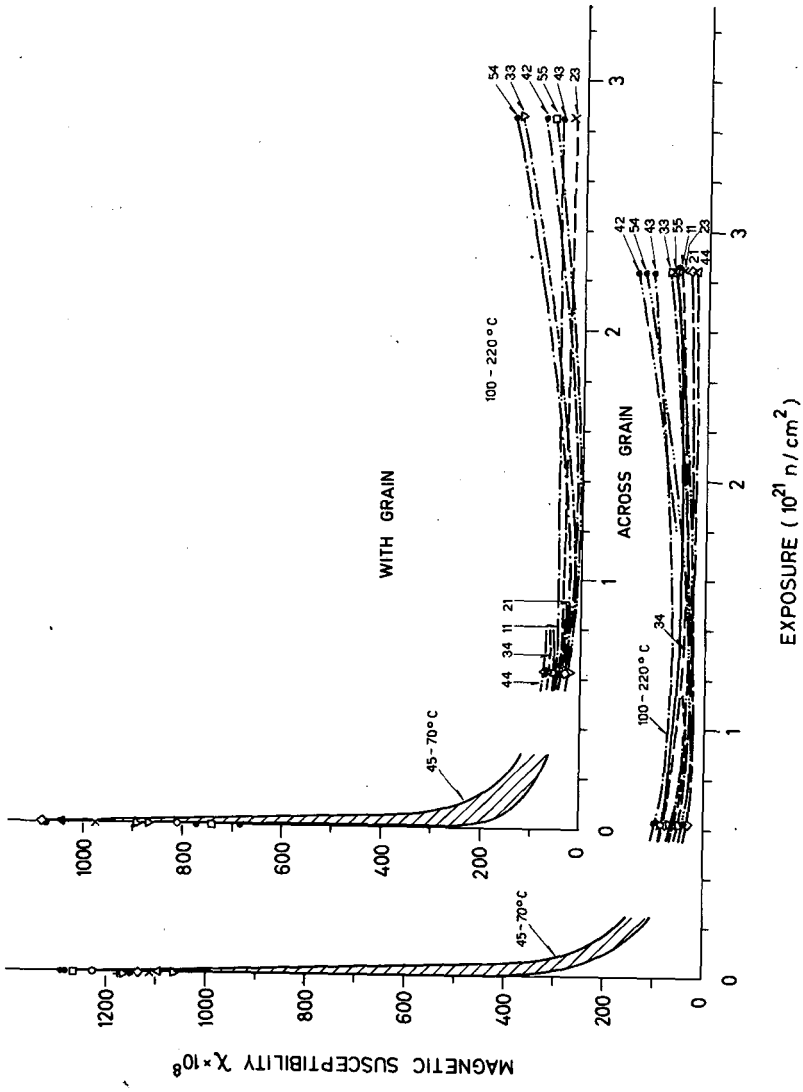


Fig. 11

Variation of magnetic susceptibility with neutron irradiation at 45 - 220°C

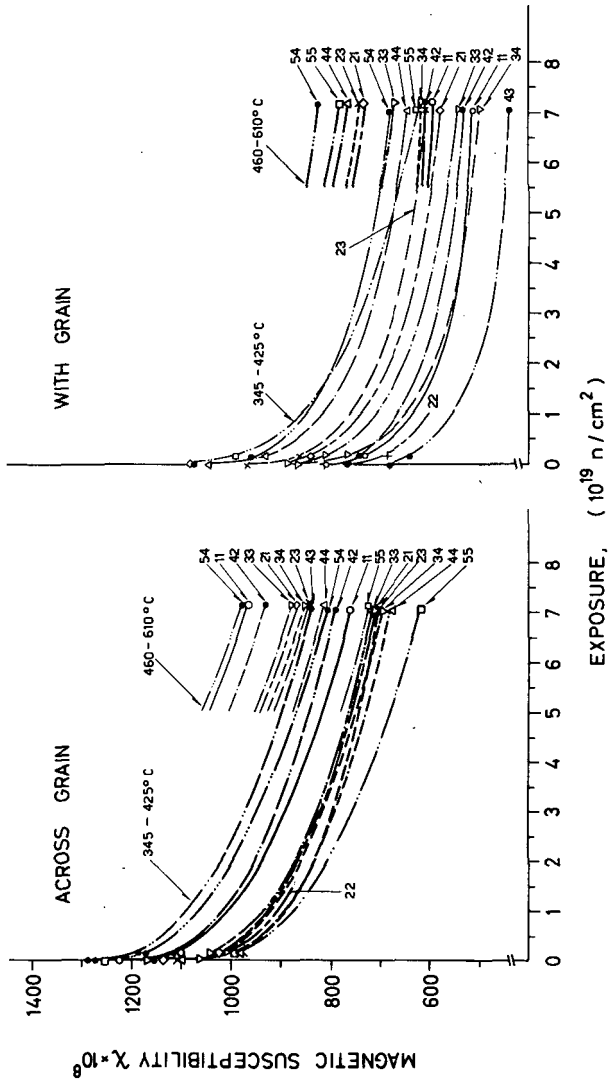


Fig. 12

Variation of magnetic susceptibility with neutron irradiation at 345 - 610°C

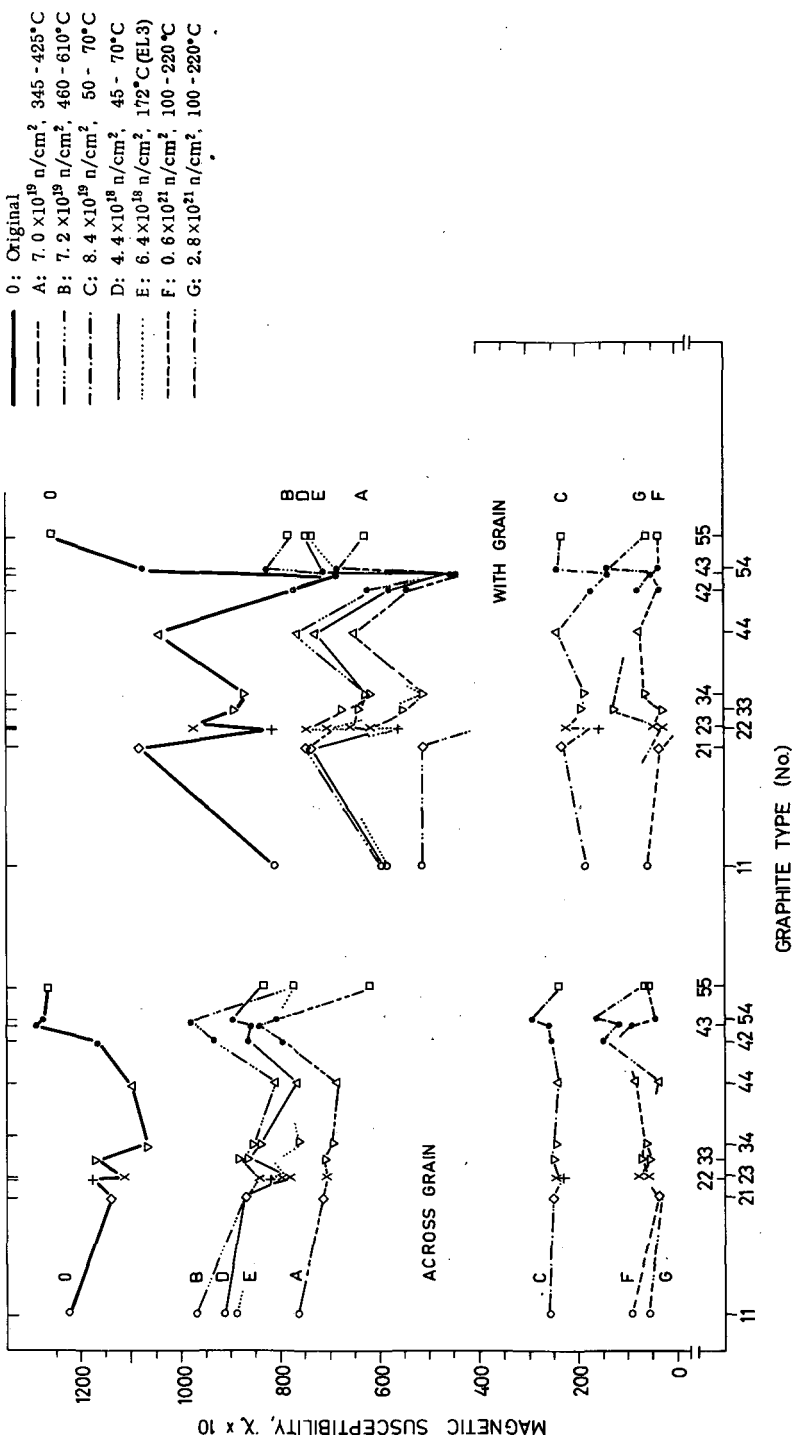


Fig. 13
Variation of magnetic susceptibility with neutron irradiation

magnetic susceptibility, the bulk thermal conductivity is also essentially determined by the microcrystalline order. Since the mean free path of elastic lattice vibrations within the intra-crystalline region is dependent on the extension of these regions and since this extension is diminished to a final state which is independent of the original state and which is the same for all graphite types (as the magnetic susceptibility shows) the thermal conductivity should also be decreased to a final value by irradiation. In fact the thermal conductivity is decreased much more quickly than the magnetic susceptibility. As is shown in Fig.14, the final value is almost reached by

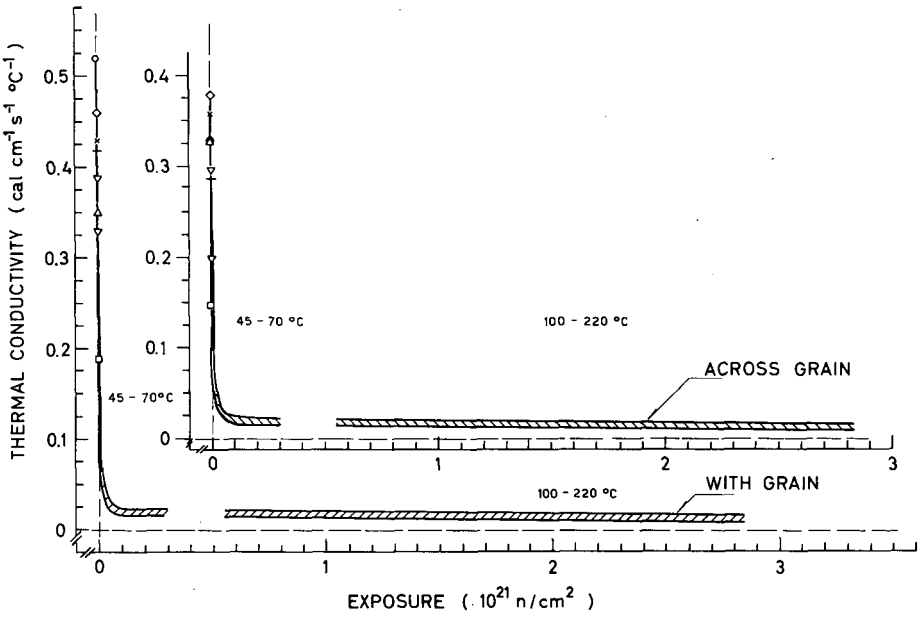


Fig. 14

Variation of thermal conductivity with neutron irradiation at 45 - 220°C

(1 to 2) $\times 10^{20}$ n/cm^2, E > 0.18 MeV. Very striking is the extremely pronounced levelling - out. The conductivity, both with and across the grain, is nearly the same in the saturation state, so that the anisotropy is diminished too (Fig.15). These low conductivity values of the final state, however, are not very accurate since they were determined by comparative measurement (see WILD [21]); some of the deviations may therefore have to be attributed to measurement errors.

Irradiations at higher temperatures also yield a relatively marked decrease of thermal conductivity with already a surprising tendency to level-out at 7×10^{19} n/cm^2 (Fig.16). Furthermore, the results of the EL.3 irradiations fit well into this picture when allowance is made for the actual irradiation temperature. The graphical representation of the variation of the thermal behaviour with the degree of graphitization (Fig.17) demonstrates the saturation and levelling-out effects very clearly. Whereas in the unirradi-

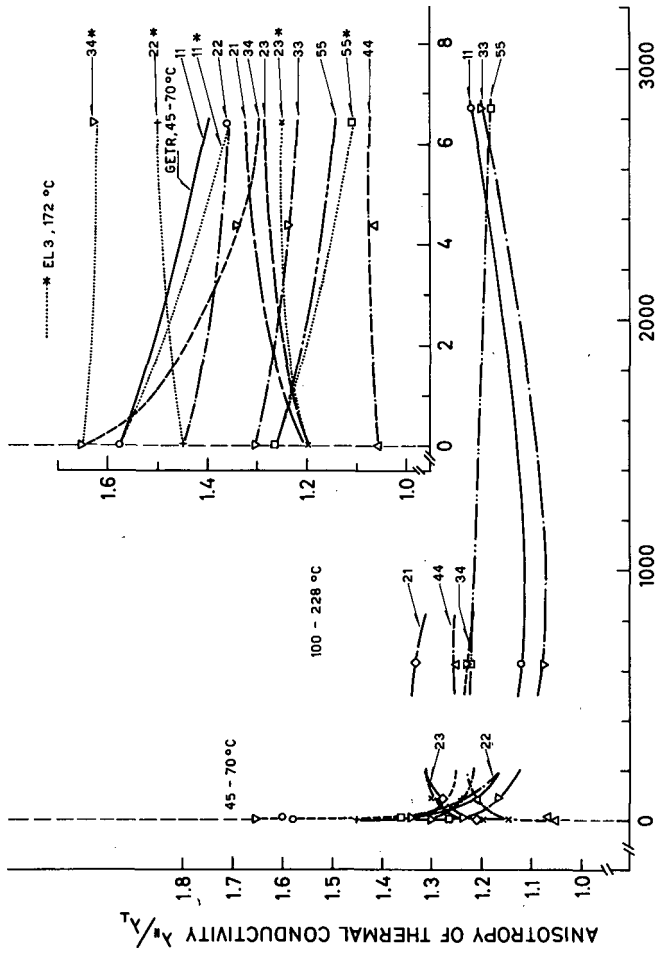


Fig. 15

Variation of anisotropy of thermal conductivity with neutron irradiation at 45 - 220°C

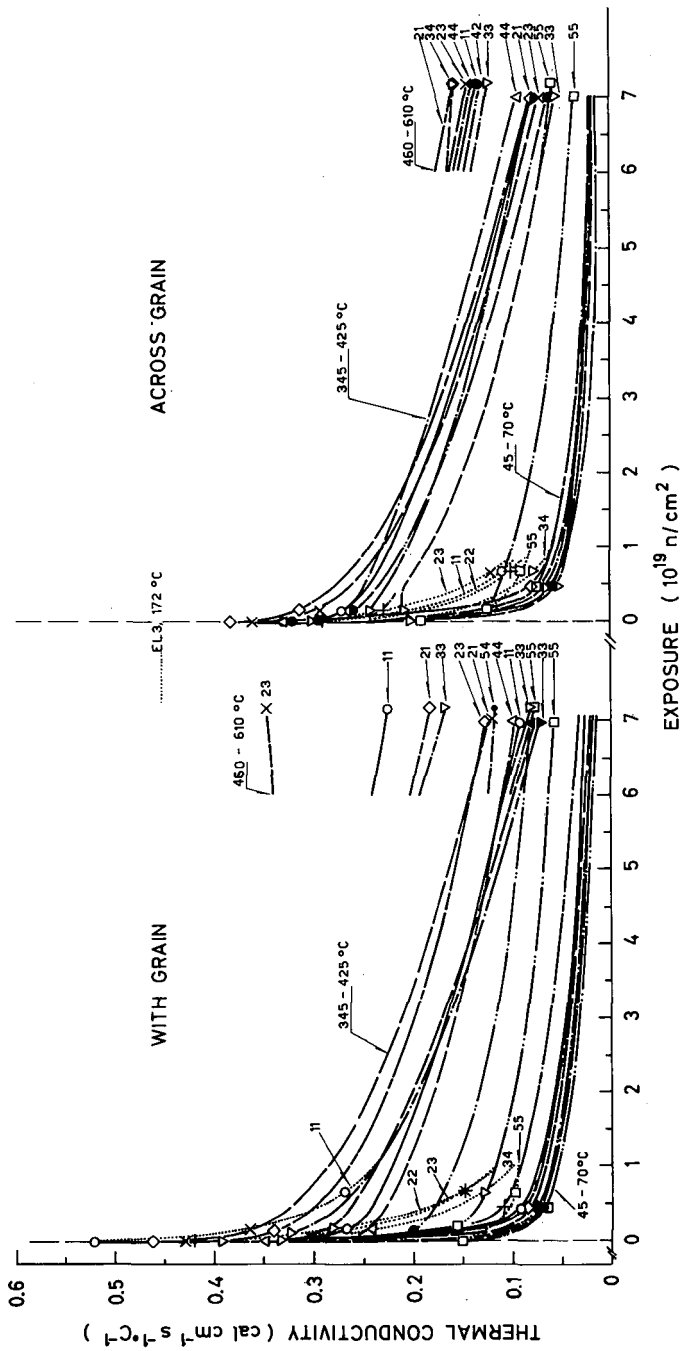


Fig. 16

Variation of thermal conductivity with neutron irradiation at 45 - 610°C

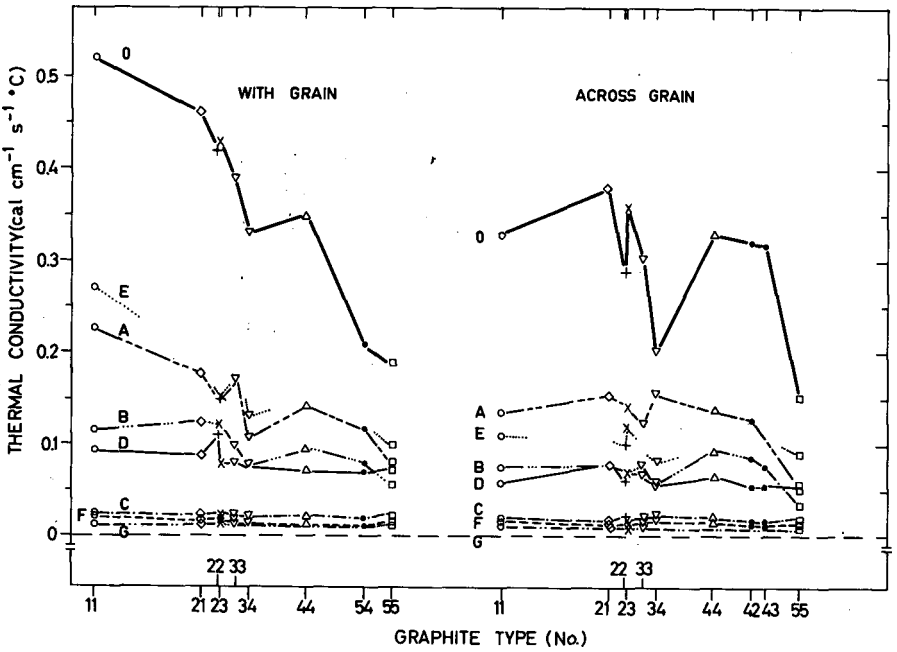


Fig. 17

Variation of thermal conductivity with neutron irradiation

0: Original
A: 7.0×10^{19} n/cm², 345 - 425°C
B: 7.2×10^{19} n/cm², 460 - 610°C
C: 8.4×10^{19} n/cm², 50 - 70°C
D: 4.4×10^{18} n/cm², 45 - 70°C
E: 6.4×10^{18} n/cm², 172°C (EL3)
F: 0.6×10^{21} n/cm², 100 - 220°C
G: 2.8×10^{21} n/cm², 100 - 220°C

ated state the thermal conductivity in the grain direction is decreased continously with the degree of graphitization, the influence of the intra-crystalline order of the original state becomes smaller and smaller with increasing radiation damage and finally vanishes entirely.

It is remarkable that the thermal conductivity levels-out more quickly than the magnetic susceptibility. This could be because the mobility of the free carriers, on which the magnetic susceptibility depends, is reduced less quickly than the mobility of the carbon atoms which effect the heat transport.

4.1.1.3. Electrical resistance. Whereas the thermal conductivity of graphite is due to the thermal vibrations of the carbon atoms, the electrical conductivity is an electron-dependent effect similar to that in metals. The conductance band is markedly disturbed by neutron irradiation. Thus, at first, one might expect that the electron conductivity within coherent regions would be perturbed more by lattice vacancies than the thermal conductivity caused by lattice vibrations. In fact, at the beginning, the electrical resistance is increased greatly and a saturation level is reached already at $\sim1\times10^{20}$ n/cm², $E>0.18$ MeV, (Fig. 18). This pattern resembles that of the

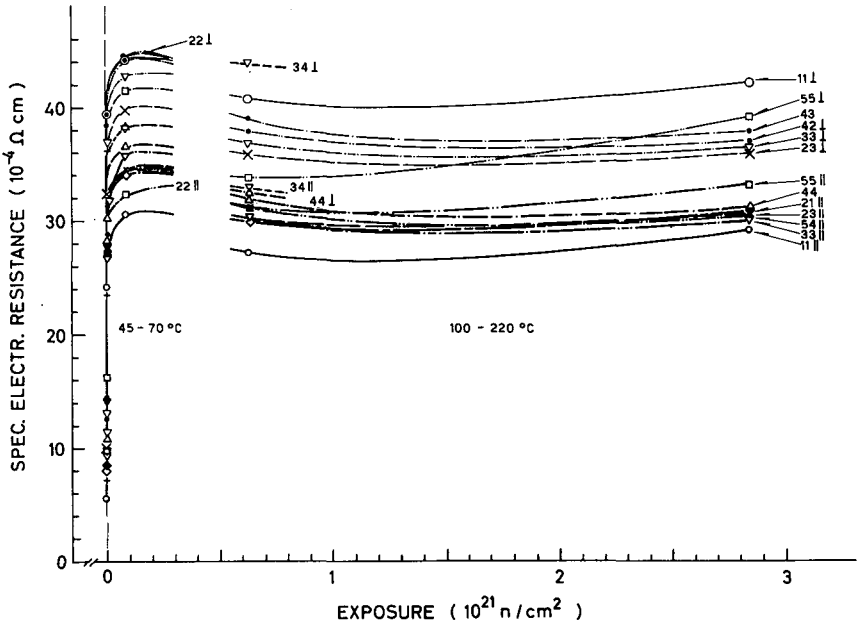


Fig. 18

Variation of specific electrical resistance with neutron irradiation

thermal conductivity except that the change is not as large as that of the thermal conductivity, as can be seen clearly in Fig. 19. Furthermore, only an insignificant levelling-out is observable. Nevertheless the differences between the parallel and the cross-grain directions, especially in the most anisotropic types, are diminshed (Fig.20) in a way similar to that of the corresponding values of the thermal conductivity. The irradiations at higher temperatures show smaller variations because of the lower irradiation damage (Fig. 21). The somewhat different results in the various reactors (Fig. 22) are explained more closely in section 4.-5 .

The relatively small decrease of the electrical conductivity and the fact that there is, in contrast to the above-mentioned behaviour of the magnetic susceptibility and the thermal conductivity, only slight levelling-out for the various graphites show that the electrical conductivity is determined not only by the electrical behaviour within the coherent regions or within the grains, but also by charge-movement (transition) between the single crystallites and the grain boundaries. Obviously the bulk of the resistance is attributable to the transition resistance between the single regions and grains and the resistance in the poorly graphitized binder bridges. Although the irradiation creates new, greater transition resistances, which lead to the initial steep increase of the electrical resistance by the destruction of crystallites in the microcrystalline region, a levelling-out effect cannot be observed because the electron traps at the boundaries of the intercrystalline regions remain relatively unchanged.

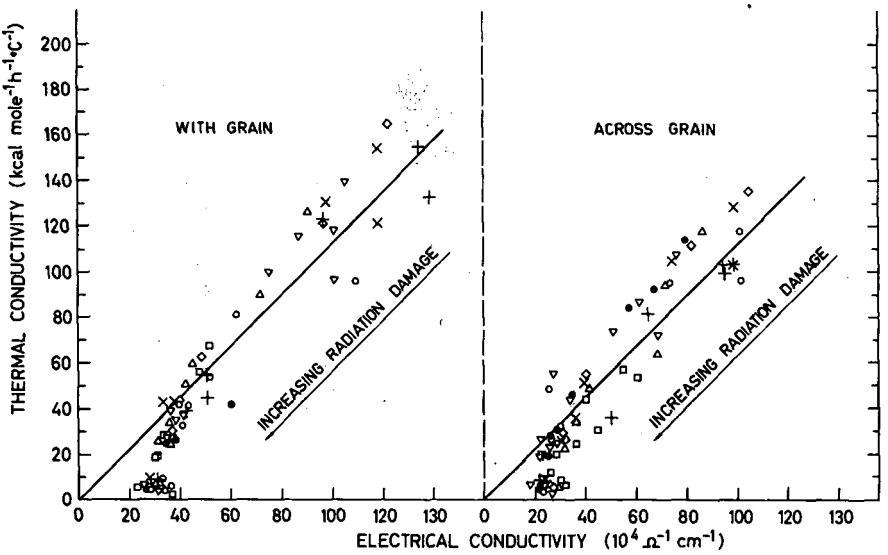


Fig. 19

Relations between thermal and electrical conductivity

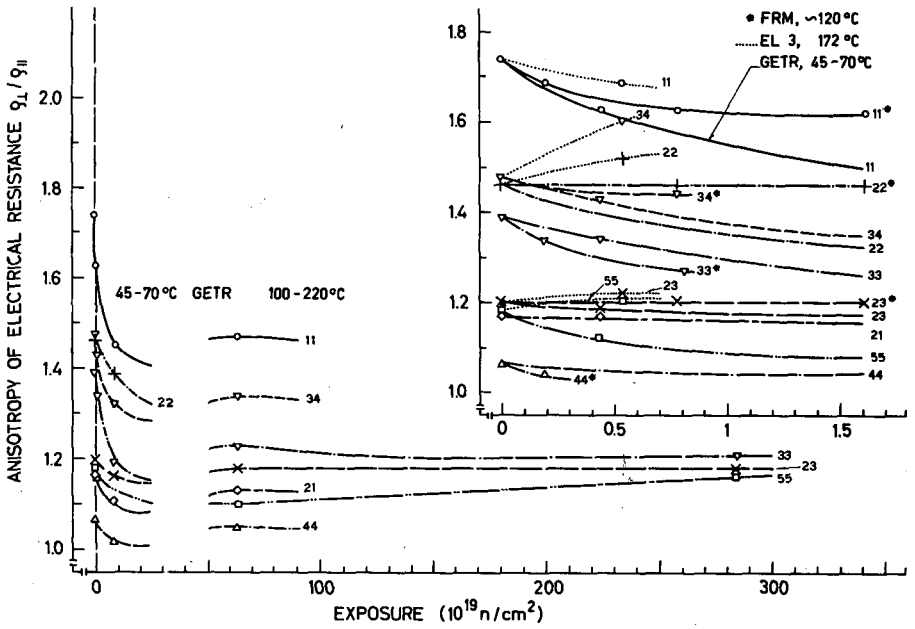


Fig. 20

Anisotropy of electrical resistance

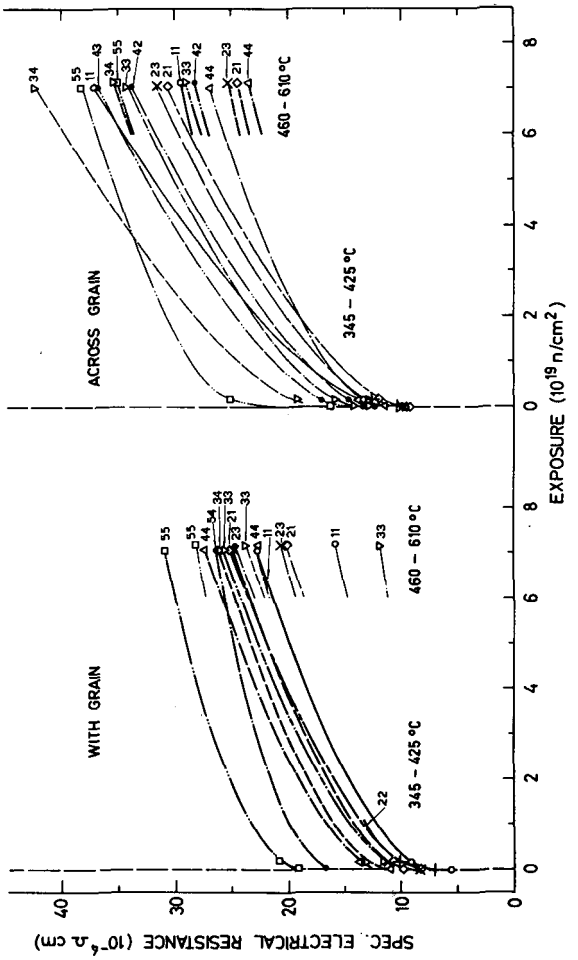


Fig. 21
Variation of specific electrical resistance with neutron irradiation for temperatures between 345 and 610°C

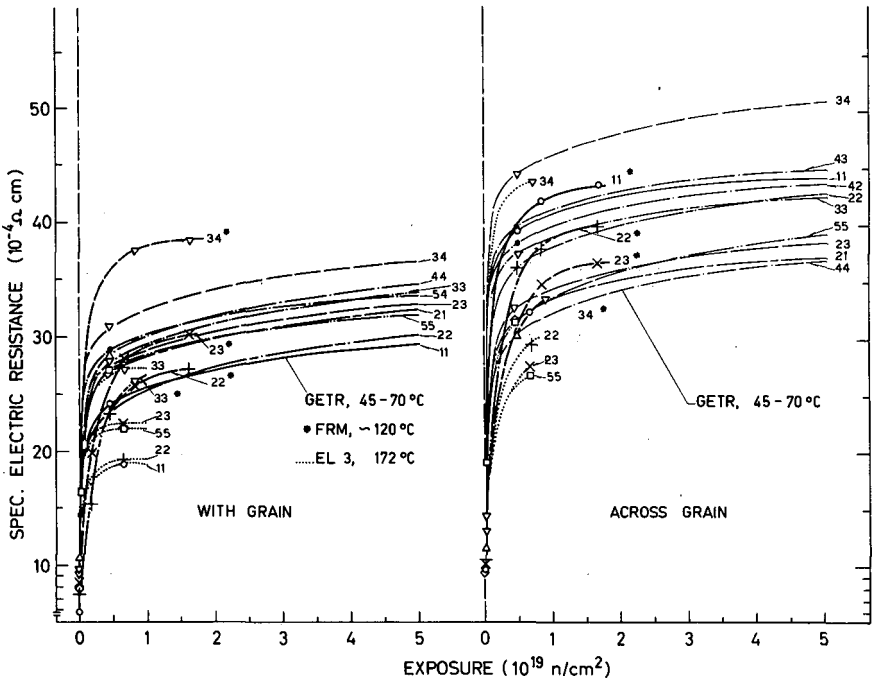


Fig. 22

Variation of specific electrical resistance with neutron irradiation for temperatures between 45 and 172°C

As will be shown later on the basis of the mechanical properties (especially of bending strength and Young's modulus) the relative behaviour of binding properties is changed only slightly by neutron irradiation. The remaining differences of the electrical resistance, at least to some extent, could be referred to these differences in the quality of the bulk binding properties. In these circumstances no levelling-out is to be expected. The relationships do not, however, remain unchanged as for the mechanical properties.

4.1.2. Properties not levelled out by irradiation

This group comprises all those bulk properties which, even after irradiation, still depend on the graphite type, i.e. the mechanical properties. Because of their relation to the pore structure, the macroscopic dimension changes are discussed in a special section.

Brittle materials which show relatively high compressive strength and low tensile strength are better characterized by their bending than by their tensile strengths. Thus, for artificial carbon bodies in general, compressive and bending strengths as well as Young's modulus are characteristic criteria for the mechanical properties. It was found that Young's modulus, determined by elastic vibrations, can be brought into a valid re-

lationship with the bending strength of the different artificial carbon bodies. Thus, bending strength and Young's modulus represent a valid measure for the binding between the grains, whereas the compressive strength is referred mainly to the different compressibility of the single grains building up the graphite body.

4.1.2.1. Compressive strength. By low-temperature irradiation, the compressive strength is increased for all samples and the relative differences of the compressive strength of the various graphite types in their original state are even more pronounced after irradiation (Fig. 23). Furthermore there is another typical result, namely that graphites produced from the best graphitizing cokes yield the lowest relative increase of compressive strength. When the compressive strength increase is compared with the compressibility of a single grain, we obtain the following result. Samples with a high degree of graphitization usually consist of lamellar, fan-shaped cokes of high compressibility (see Fig. 49 and 50). The radiation damage, i.e. the barrier of the slip planes caused by Frenkel defects, is not able to change the bulk structure of the single coke grain to any great degree and therefore to diminish the compressibility very much. Poorly graphitizing cokes, however, generally represent the more isotropic cokes which have a more compact grain structure, the inner pores and cavities being supported by isotropic bridges and walls. Thus the obstruction to sliding within

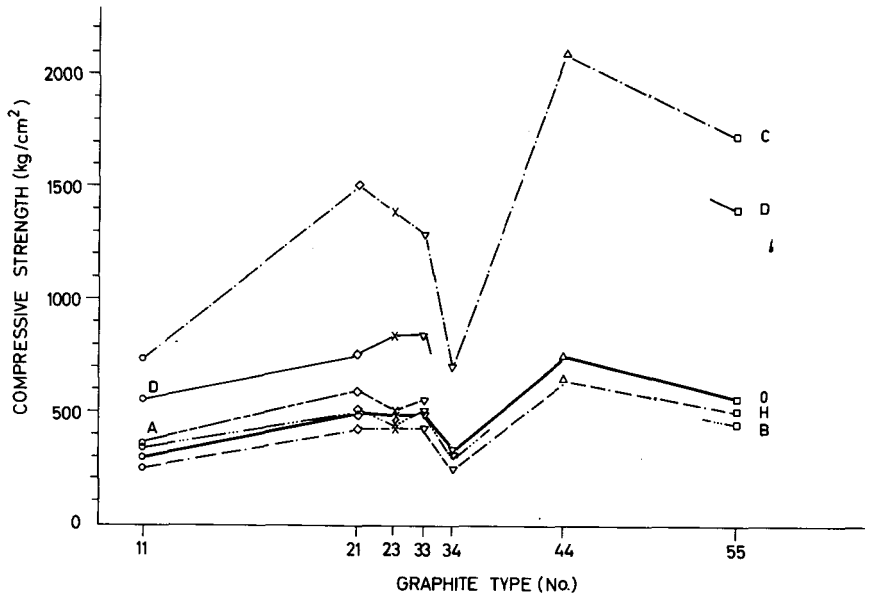


Fig. 23

Variation of compressive strength with neutron irradiation

0: Original
A: 7.0×10^{19} n/cm², 345 - 425°C
B: 7.2×10^{19} n/cm², 460 - 610°C
C: 8.4×10^{19} n/cm², 50 - 70°C
D: 4.4×10^{18} n/cm², 45 - 70°C
H: 1.5×10^{18} n/cm², 385 - 400°C

the single planes cannot be absorbed by the single lamellae within the coke grain.

Type 34 graphite, for instance, represents a graphite from a compact coke, but with low bulk strength. This bulk strength affects also the compressive strength to some extent. After irradiation, this graphite-34 shows the lowest compressive strength. As expected, the incompressible grain escapes when under compression, into the regions of weak spots in the binding matrix. In sum, it can be stated that the variation of the compressive strength really depends on the degree of graphitization of the raw material. Thus, the increase of compressive strength of a poorly graphitizing coke is greater for the same binding strength.

4.1.2.2. Bending strength. The bending strength is also increased by irradiation (Fig. 24). The amount of the increase, however, leaves differences of the same order of magnitude as the original differences of the strength values. This is valid for the bending strength to an even greater extent than for the compressive strength. As can be seen from Fig. 25, it is quite certain that there is no dependence of increase of bending strength on the degree of graphitization. The only factor prevailing seems to be the original bulk strength. It can be clearly seen that graphites having low bending strength show less strength increase than those with extremely good binding properties. We refer here especially to Types 22 and 54, which are graphites where the grains show a weld-like bond and exhibit not only maximum relative strength, but also the greatest increase with irradiation.

The inter-relation of the bulk properties of the various graphites, which properties were fixed by the original manufacturing process, are not changed by irradiation.

We will come back to Fig. 26 when comparing the various reactors. Fig. 27 shows the results at irradiation temperatures between 345 and 610°C. In general the bending strength is also increased at these irradiation conditions; the changes, however, are not definite for all types. Thus further investigation seems to be necessary to clarifying this behaviour.

4.1.2.3. Young's Modulus. We succeeded in determining the Young's modulus of the relatively small samples used for irradiation in a very exact manner by measuring the resonance frequency. When this method is used, the specimens are excited by means of piezo-electric crystals using plastic fibre loops to support the samples (Fig.28)*. This exact (± 0.5%) measurement of Young's modulus gives more precise and valuable results than other mechanical methods such as determinations of bending strength etc.

The Young's modulus is also increased very markedly by neutron irradiation. As Fig. 29 indicates, irradiation at below 200°C brings the Young's modulus, also after about 2×10^{20} n/cm^2 E >0.18 MeV, up to a saturation level which is characteristic of the graphite type. Just as in the case of bending strength, the Young's modulus shows no relation between radiation damage and degree of graphitization (Fig.30). The relative differences are even more pronounced after than before irradiation. Thus

* For the elaboration of this method we are obliged to Dr. Beutell (Miss) and to the Company, Messrs. Dr. Förster, Reutlingen.

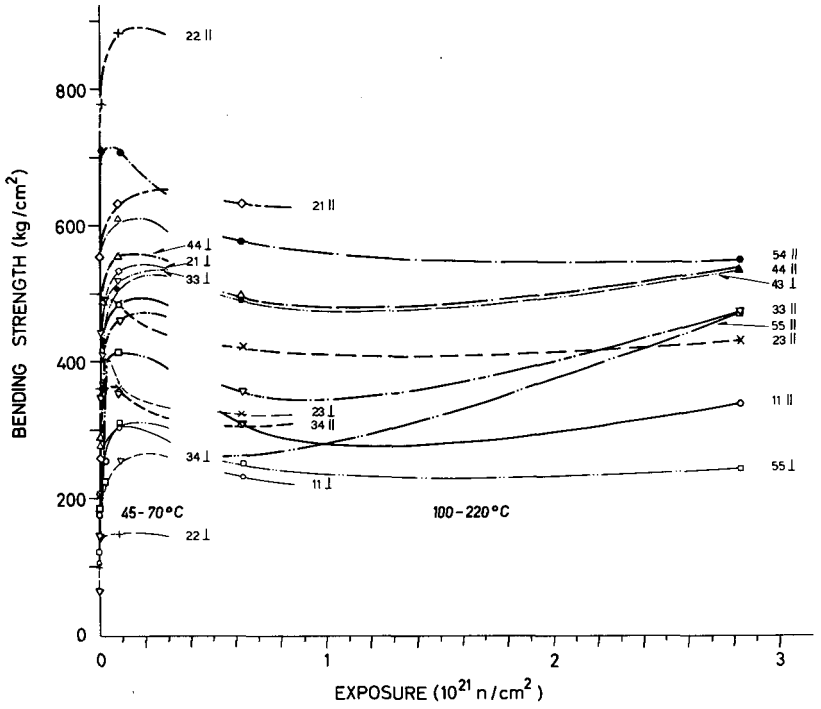


Fig. 24

Variation of bending strength with neutron irradiation for temperatures between 45 and 220°C

graphites with the higher, pre-irradiation values of Young's modulus exhibit the highest post-irradiation values.

For comparison with the increased values of Young's modulus obtained in the GETR, in Fig. 31 are plotted the results of the irradiation experiments carried out in the facilities of the EL. 3 and the FRM. To these we will refer once more later on. The increase of Young's modulus at irradiation temperatures between 345 and 610°C are shown in Fig. 32.

The relation between Young's modulus and bending strength of artificial carbon products as given at the beginning can be extended in general to irradiated graphites, too. Both properties have the same basic meaning, because they are both criteria for the bulk strength. They indicate that the originally good binding properties were increased by irradiation: this is in contrast to the compressive strength, the variation of which is influenced by the degree of graphitization of the grain.

4.2. Micro-properties

The micro-properties represent properties which are not influenced by bulk structure, i.e. data given by X-ray diffraction. On the other hand we have already discussed the magnetic susceptibility because of its better

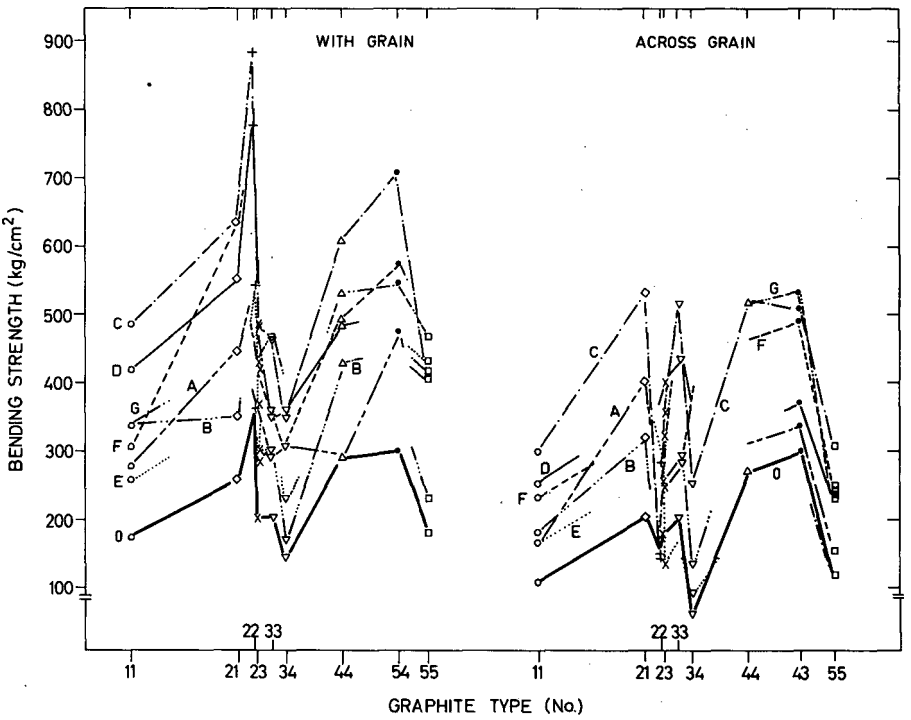


Fig. 25

Variation of bending strength with neutron irradiation

0: Original
A: 7.0×10^{19} n/cm², 345 - 425°C
B: 7.2×10^{19} n/cm², 460 - 610°C
C: 8.4×10^{19} n/cm², 50 - 70°C
D: 4.4×10^{18} n/cm², 45 - 70°C
E: 6.4×10^{18} n/cm², 172°C (EL3)
F: 0.6×10^{21} n/cm², 100 - 220°C
G: 2.8×10^{21} n/cm², 100 - 220°C

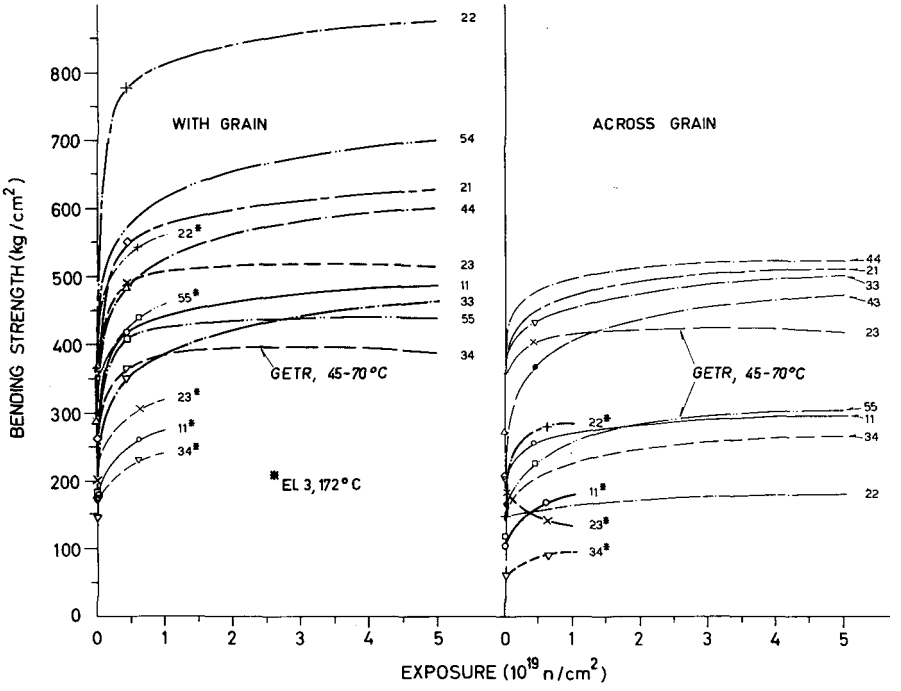


Fig. 26

Variation of bending strength with neutron irradiation
for temperatures between 45 - 172°C

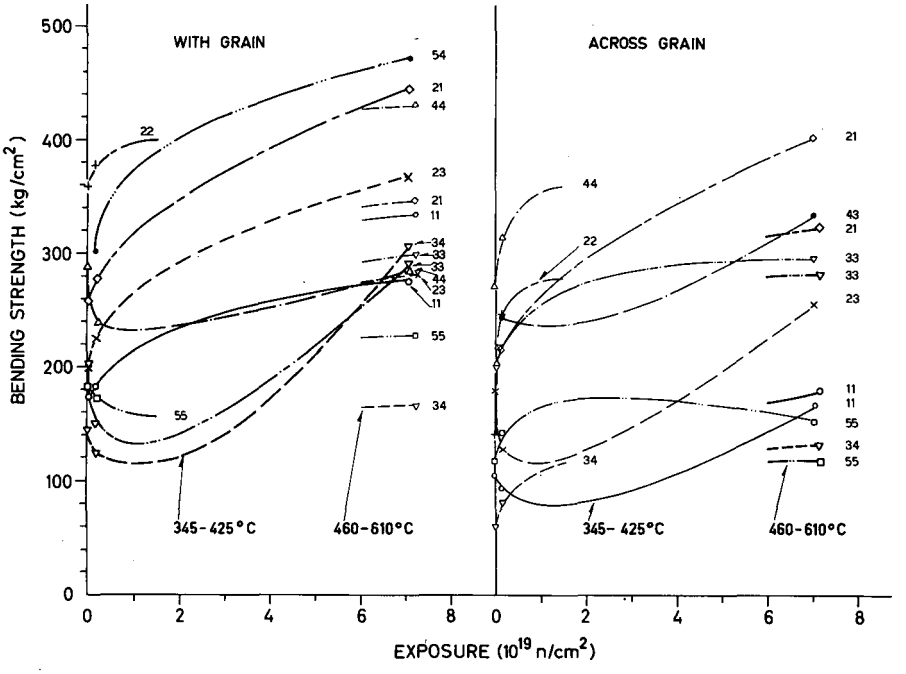


Fig. 27

Variation of bending strength with neutron irradiation

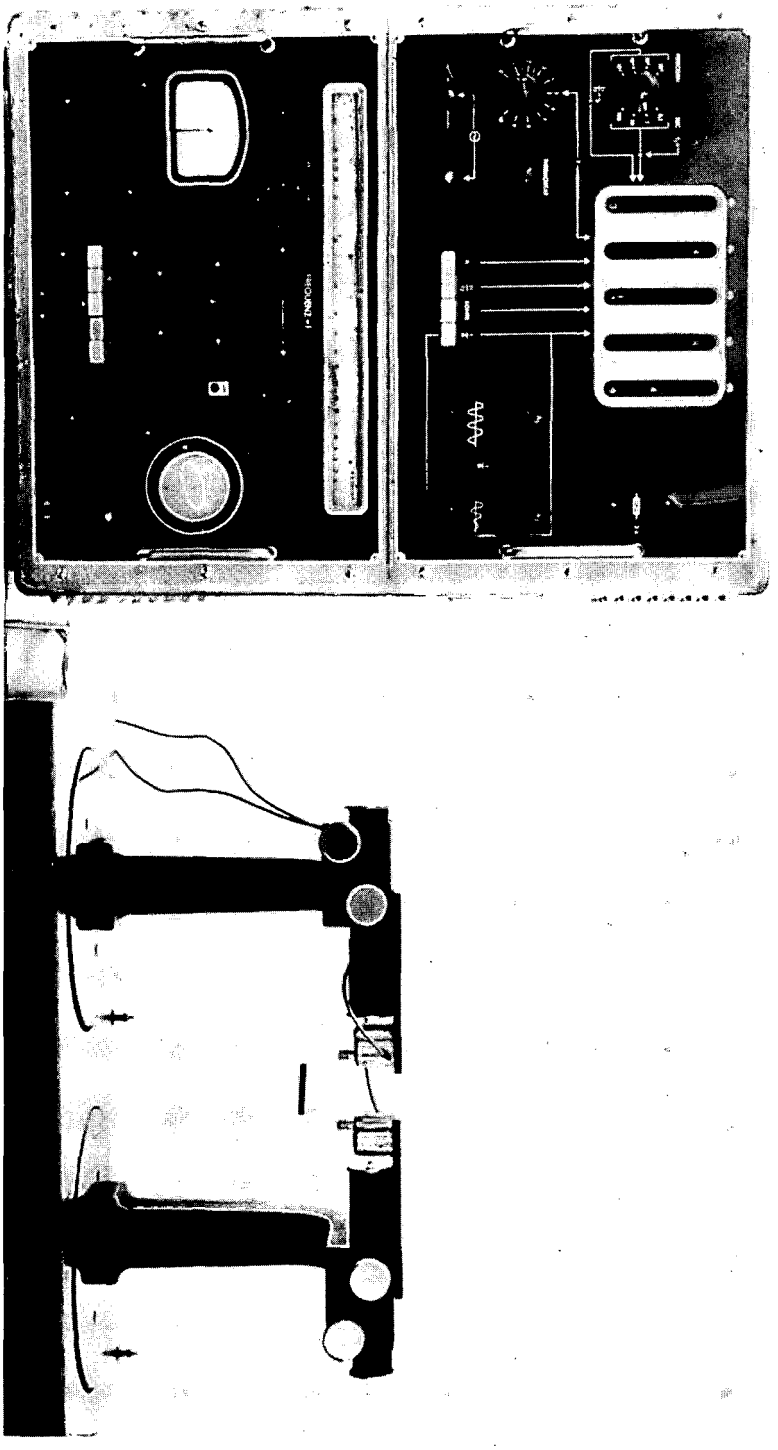


Fig. 28
Apparatus for the measurement of Young's modulus

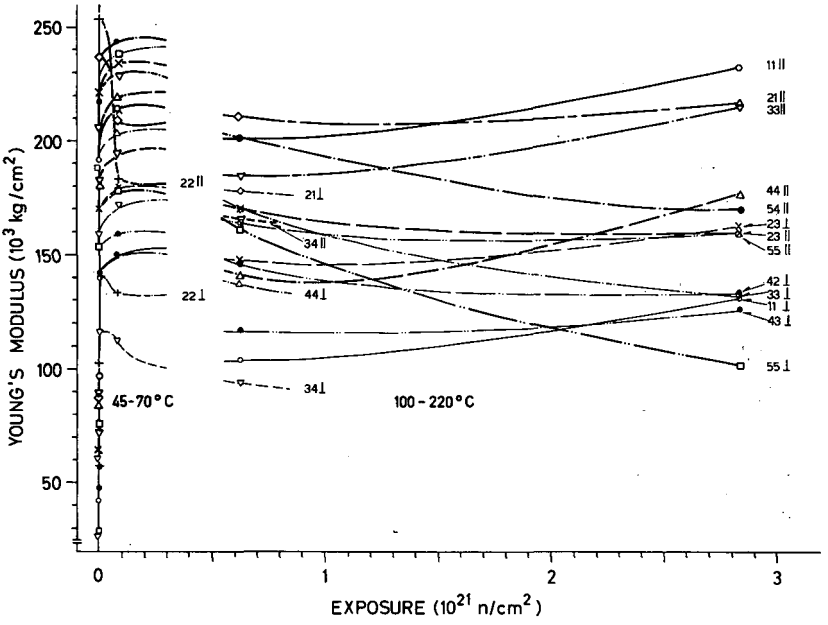


Fig. 29

Variation of Young's modulus with neutron irradiation

correlation with thermal conductivity. In the following therefore we only deal with the results and conclusions obtained by X-ray diffraction data.

4.2.1. C-spacing

The dislocation of the carbon atoms by irradiation from their potential wells within the a-b planes to interstitial places with higher energy levels between the planes causes growth of c-spacing on the one hand and reduces the coherent regions on the other. For example, Fig. 33 shows the respective shifting and broadening of the (002)-line of the well-graphitized Type 11 graphite. The lattice distance in the unirradiated state indicates a certain dependence on the degree of graphitization in such a way that, in general, uniformly but poorly ordered graphites show a greater c-spacing than uniformly well-graphitized ones. If the samples contain poorly graphitizing regions as well as easily graphitizing ones, e.g. Types 42, 43 and 54, then the peak of the diffraction line suggests a smaller lattice distance than would correspond to the average degree of graphitization (I. V. value); thus a better degree of order is simulated. The tendency for lattice distance to increase with decreasing degree of graphitization is not very marked, but persists after irradiation, when a saturation value is reached. For intense radiation damage, the accuracy of lattice-distance measurements becomes very poor, i.e. the values are very scattered as a consequence of the broadening of the diffraction lines (see Fig. 34 and also Fig. 33).

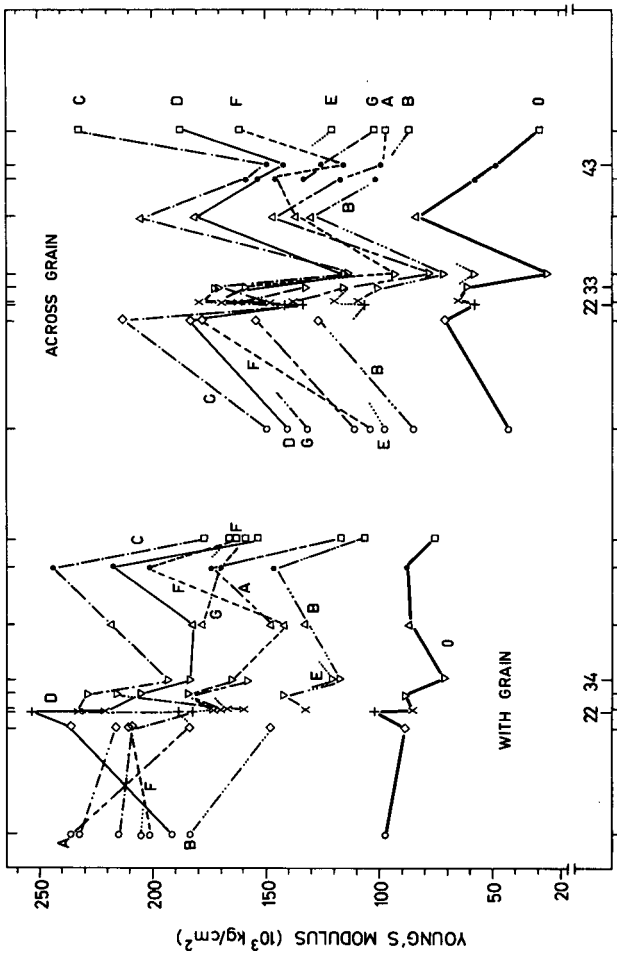


Fig. 30

Variation of Young's modulus with neutron irradiation

0: Original
A: 7.0×10^{19} n/cm^2, 345 - 425°C
B: 7.2×10^{19} n/cm^2, 460 - 610°C
C: 8.4×10^{19} n/cm^2, 50 - 70°C
D: 4.4×10^{18} n/cm^2, 45 - 70°C
E: 6.4×10^{18} n/cm^2, 172°C (EL3)
F: 0.6×10^{21} n/cm^2, 100 - 220°C
G: 2.8×10^{21} n/cm^2, 100 - 220°C

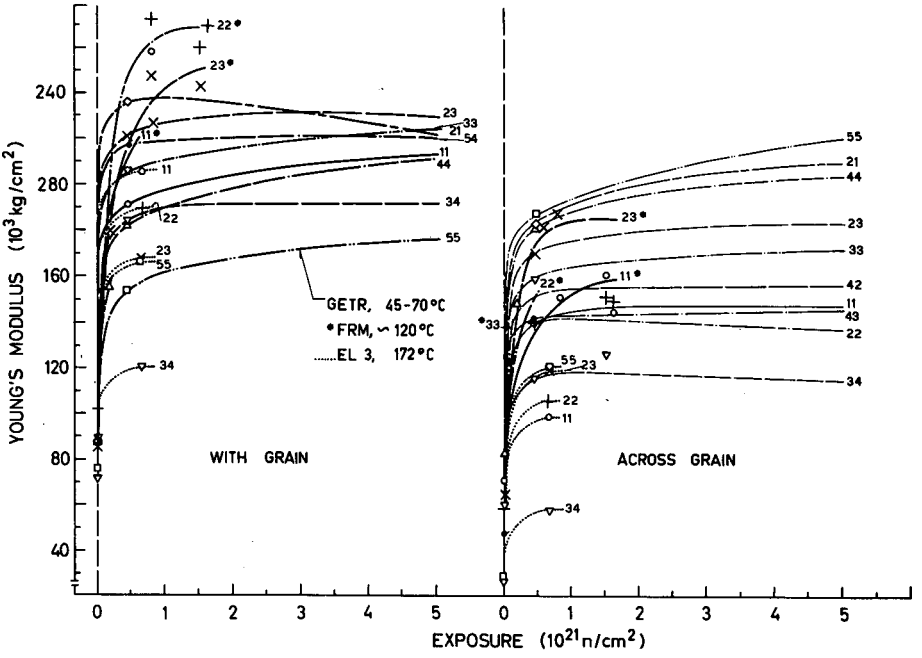


Fig. 31

Variation of Young's modulus with neutron irradiation

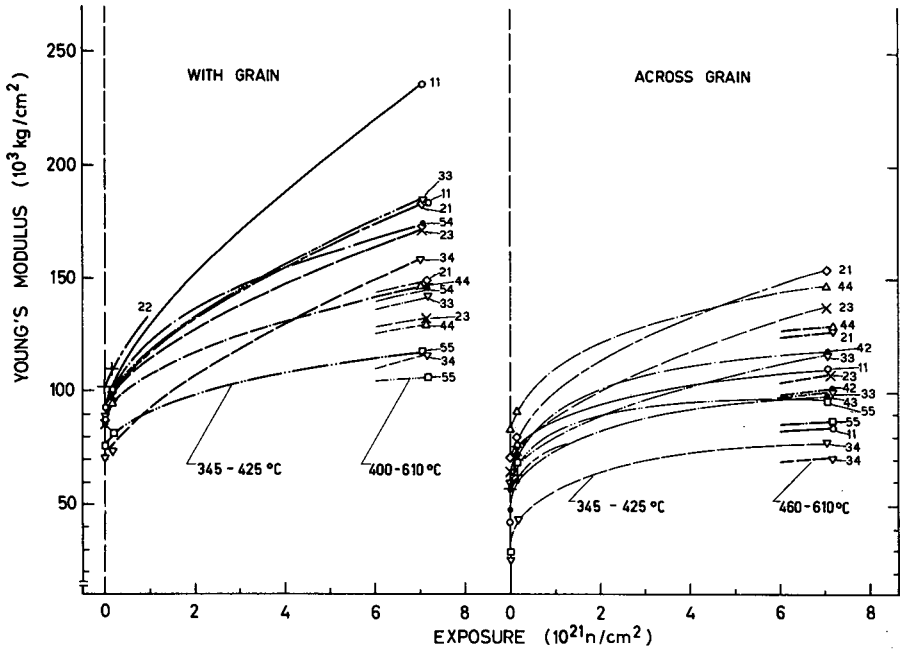


Fig. 32

Variation of Young's modulus with neutron irradiation

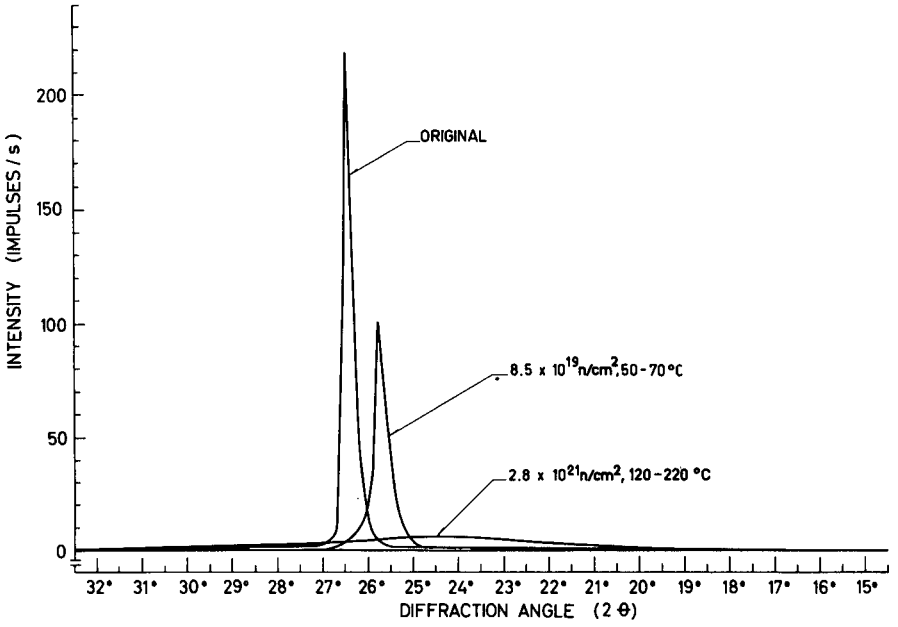


Fig. 33

Variation of the (002)-line of Type 11 graphite with neutron irradiation

4.2.2. I. V.value

It should be noted that already after about 9×10^{19} n/cm^2, E >0.18 MeV (at 50-70°C), the identity distance of the disordered state (6.88 A) is exceeded. Thus the I. V. value looses its meaning, because the reference, the lattice distance of the disordered state, is no longer representative of the newly generated state which has a degree of order even smaller than that of the disordered state. As expected, the I. V. value decreases very rapidly (see Fig. 35) and owing to the growth of the c-spacing it, by definition, approaches the value zero.

4.2.3. (002) Half-maximum breadth

With uniform graphites, the half-maximum breadth of the basal interference lines can, with some caution, also be taken as a criterion for the degree of crystalline order. As is well-known, the broadening of an X-ray line is caused by small crystallite dimensions and lattice defects, apart from considerations of the X-ray apparatus itself. Its readings therefore will be ambiguous even for uniform graphites. If graphites, which consist of a mixture of well and poorly graphitized regions, are investigated, the half-maximum breadth is naturally largely determined by the well-ordered parts.

Figs.36,37 and 38 show the variation of the half-maximum breadth of the (002)-line after irradiation. Its relatively small increase at the beginning

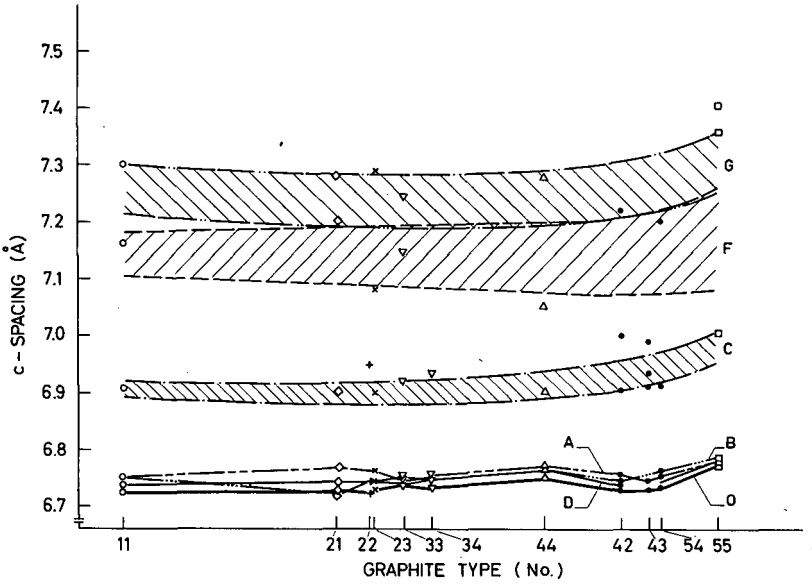


Fig. 34

Growth of c-spacing with neutron irradiation

0: Original
A: 7.0×10^{19} n/cm², 345 - 425°C
B: 7.2×10^{19} n/cm², 460 - 610°C
C: 8.4×10^{19} n/cm², 50 - 70°C
D: 4.4×10^{18} n/cm², 45 - 70°C
E: 6.4×10^{18} n/cm², 172°C (EL3)
F: 0.6×10^{21} n/cm², 100 - 220°C
G: 2.8×10^{21} n/cm², 100 - 220°C

(Fig. 36) is caused by the fact that there are still larger coherent regions simulating a less damaged state. The half-maximum breadths of the diffraction lines of graphites intensively damaged by irradiation are of no great accuracy for the reasons already mentioned in section 4. 2. 1.

The slightly increasing values with decreasing degree of graphitization (Fig. 38) for the original state is no longer apparent after an irradiation of 6×10^{20} to 2.8×10^{21} n/cm² (E > 0.18 MeV) at 100 to 220°C respectively. It rather seems that the reverse is the case, i. e. after irradiation the best graphitizing types exhibit a greater disorder than poorly graphitizing ones. These findings are reported; a valid explanation of these measurements, however, cannot yet be offered.

4. 3. Dimensional changes and pore volume

Only a fraction of the variations with irradiation determined in the microcrystalline region are reflected in the macroscopic dimensional changes of the graphite body, because the bulk system with its pores is able to absorb a part of the changes. With regard to the macroscopic dimension changes of graphite bodies across the grain under irradiation we must distinguish between Wigner growth, caused by low-temperature irradiations, and the shrinkage reported in the literature as occurring during higher-

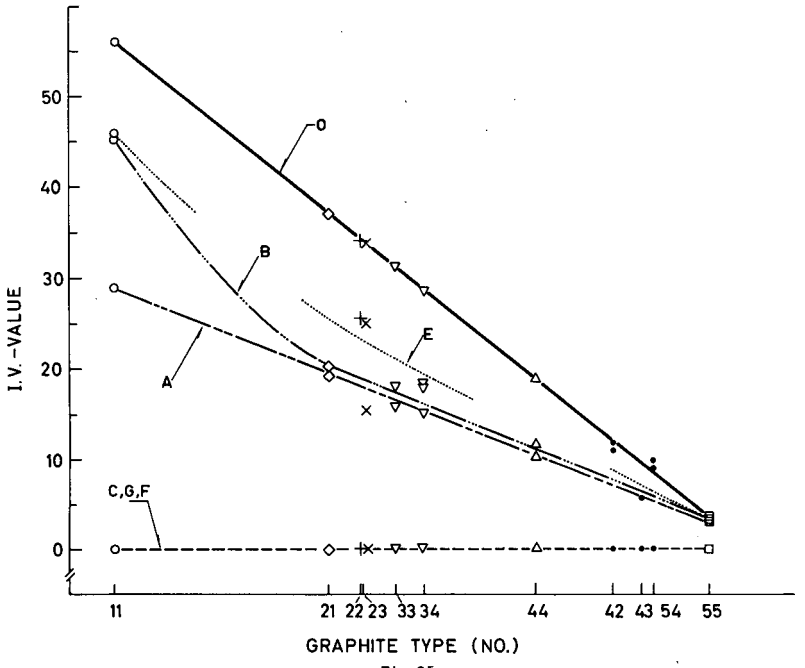


Fig. 35

Decrease of I. V. value with neutron irradiation

0: Original
A: 7.0×10^{19} n/cm^2, 345 - 425°C
B: 7.2×10^{19} n/cm^2, 460 - 610°C
E: 6.4×10^{18} n/cm^2, 172°C (EL 3)
C: 8.4×10^{19} n/cm^2, 50 - 70°C
F: 0.6×10^{21} n/cm^2, 100 - 220°C
G: 2.8×10^{21} n/cm^2, 100 - 220°C

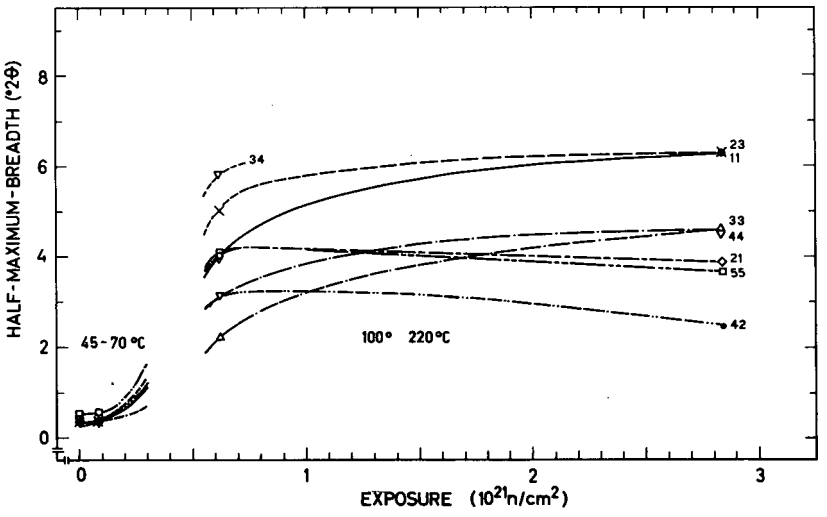


Fig. 36

Variation of the (002)-half-maximum breadth with neutron irradiation

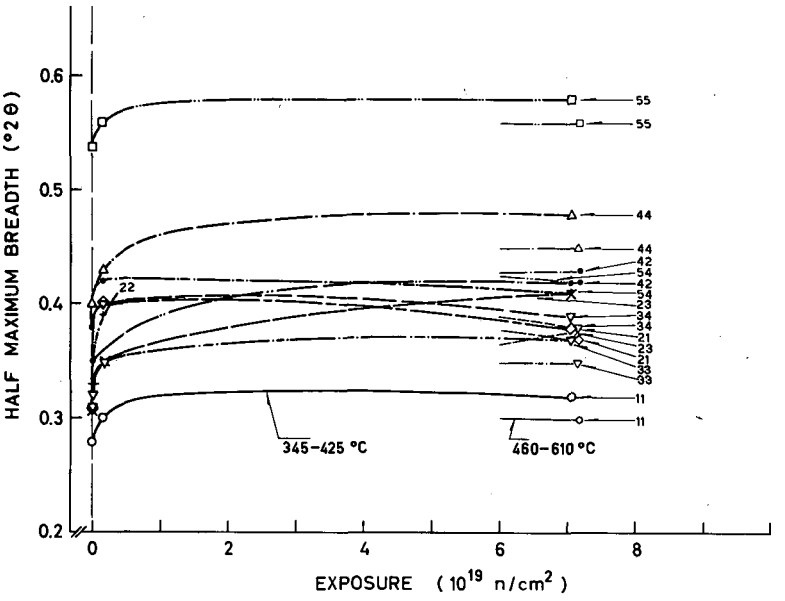


Fig. 37

Variation of the (002)-half-maximum breadth with neutron irradiation

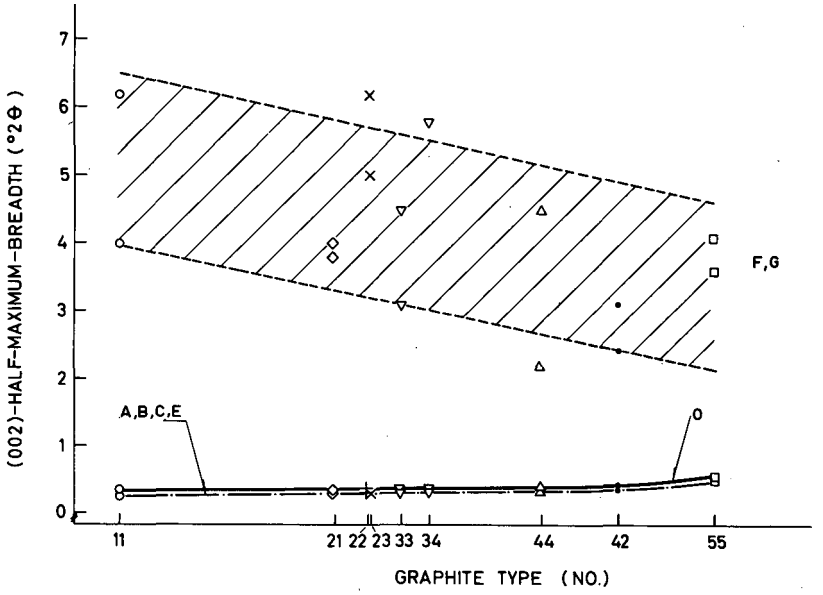


Fig. 38

Increase of (002)-half-maximum breadth with neutron irradiation

0: Original

F: 0.6×10^{21} n/cm², 100 - 220°C

G: 2.8×10^{21} n/cm², 100 - 220°C

A: 7.0×10^{19} n/cm², 345 - 425°C

B: 7.2×10^{19} n/cm², 460 - 610°C

C: 8.4×10^{19} n/cm², 50 - 70°C

E: 6.4×10^{18} n/cm², 172°C (EL3)

temperature irradiations. The latter is caused by irreversible changes within the bulk structure, i.e. within the binder bridges and within the crystalline regions. This leads to a dimension shrinkage in spite of the growth of the c-spacing as a result of the build-up of Frenkel defects. This shrinkage is a typical effect of the bulk binding properties within the graphite body which mask the variations within the intracrystalline regions.

4.3.1. Linear Wigner growth

From our irradiation results obtained so far, the only conclusions that can be made concern the first group of dimension changes. These low-temperature irradiations, especially in the anisotropic types, indicate effects which may confirm a picture of the high-temperature shrinkage discussed in the literature [14]. The dimension changes shown in Fig. 39 largely confirm the known picture and complete it: samples manufactured from easily graphitizing cokes shrink in the parallel direction and grow across the grain, c.f. Type-11, the best graphitized sample with the largest anisotropy. Poorly graphitizing types, such as Types 44 and 55, show about the same expansion in both directions, and here the Δl-values of Type 55, the specimen with the lowest degree of graphitization, are larger than those of Type 44.

With irradiation at temperatures between 345 and 610°C, a greater Wigner-growth was found than is generally described in the literature. Also

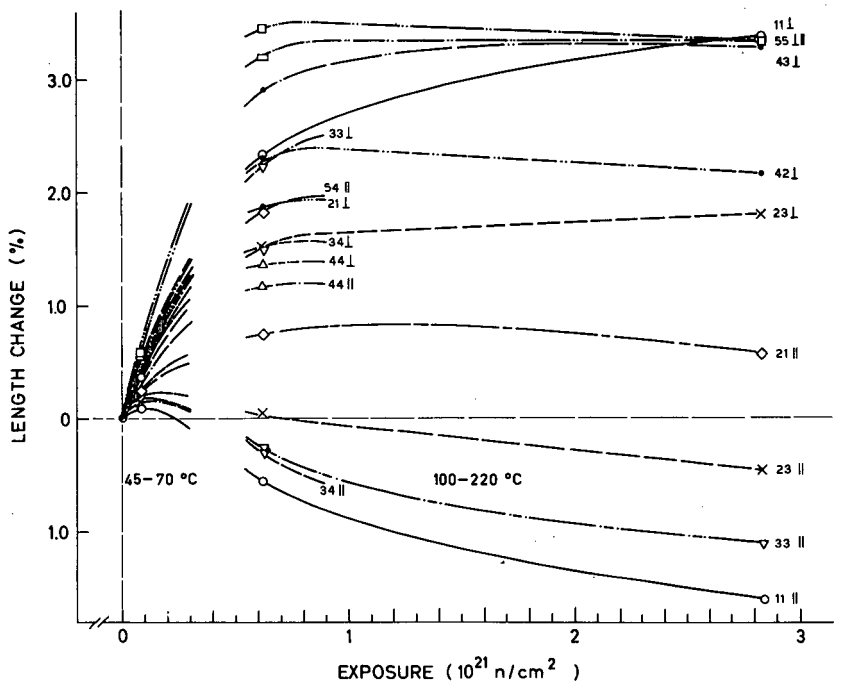


Fig. 39

Dimension changes of various graphites with neutron irradiation

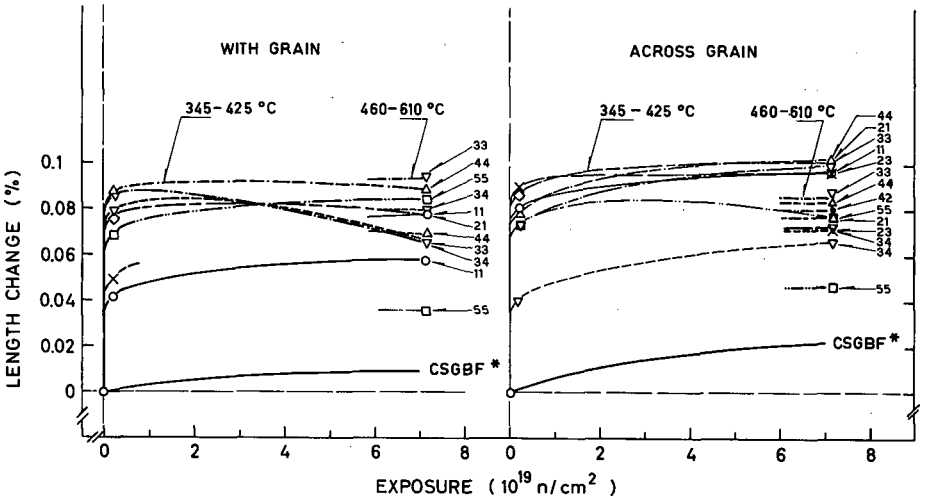


Fig. 40

Dimension changes of various graphites with neutron irradiation
*ref. [11]

in Fig. 40 values are plotted which can be found in the literature [11] for CSGBF graphite at temperatures of between 400 and 500°C. As will be discussed later and in more detail, this discrepancy is obviously caused by the high length-to-width ratio of the specimens irradiated in our programme.

4.3.2. Volume growth

Since the dimension changes are more or less anisotropic, a consideration of these linear changes in the form of a volume growth seems to give a clearer picture. Just as the coefficient of cubic thermal expansion (β) can be evaluated from the respective linear coefficients according to

$$\beta = \alpha_{\parallel} + 2\alpha_{\perp},$$

the Wigner volume growth consists of

$$\Delta V = \Delta l_{\parallel} + 2\,\Delta l_{\perp}.$$

The ΔV-values on which the following considerations are based have been evaluated according to this equation and, according to this, the volume of all irradiated specimens has increased. The relative differences in volume growth show a distinct minimum of volume growth for the averagely graphitized bodies and an equally definite maximum at an extremely low degree of graphitization (see Fig. 41).

It is surprising that extremely well graphitized bodies give a higher volume growth than the averagely graphitized types. As is well-known, WOODS [7] has given a relation for the evaluation of the Wigner growth from the behaviour of thermal expansion before irradiation. This evaluation is

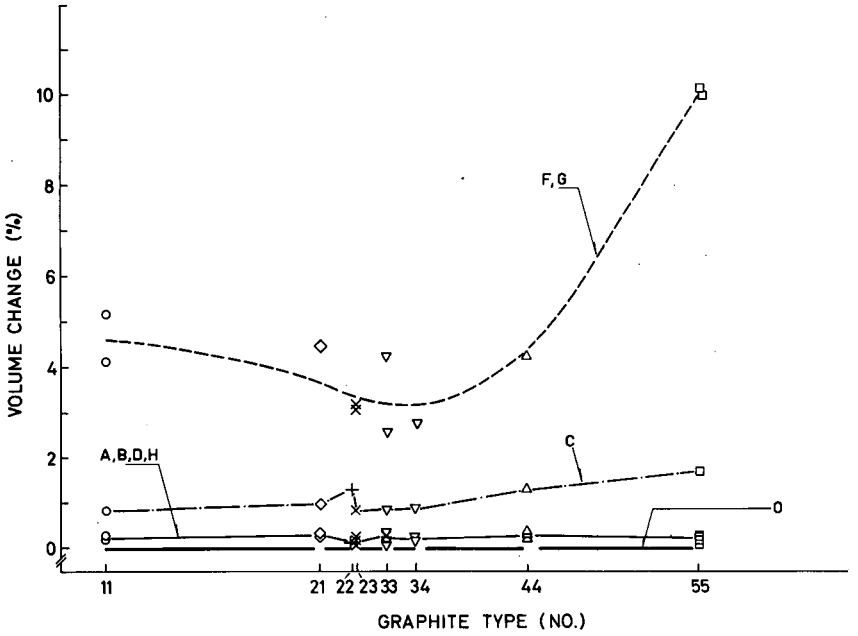


Fig. 41

Volume growth with neutron irradiation

0: Original

F: 0.6×10^{21} n/cm², 100 - 220°C

G: 2.8×10^{21} n/cm², 100 - 220°C

A: 7.0×10^{19} n/cm², 345 - 425°C

B: 7.2×10^{19} n/cm², 460 - 610°C

D: 4.4×10^{18} n/cm², 45 - 70°C

H: 1.5×10^{18} n/cm², 385 - 400°C

based on the observation of a linear relation between both coefficients of expansion. According to our results this is no longer completely valid for the volume expansion. For a better understanding of this, in Fig. 42 are plotted the Wigner volume growth and the cubic thermal expansion coefficient as a function of the degree of graphitization. As is clearly seen, mainly the extremely well graphitized bodies, especially, show a somewhat reverse slope for the cubic Wigner growth. Later it will be shown that this deviation of the Wigner growth from the thermal expansion of the unirradiated sample is only observable when specimens with a high length-to-diameter ratio are irradiated. We suppose that this is the reason why this deviation has not yet been reported in the literature. Since, however, our samples for the measurement of the thermal expansion have the same length-to-diameter ratio as those used for irradiation, it seems justified to call special attention to this difference in behaviour. Thermal delatation is, however, independent of the length-to-diameter ratio of the samples.

4.3.3. Thermal expansion

Both dilatations, the Wigner growth and the thermal expansion across the grain are based on the growth of the c-spacing, but they show only a fraction of the lattice dilatation indicated by X-ray diffraction.

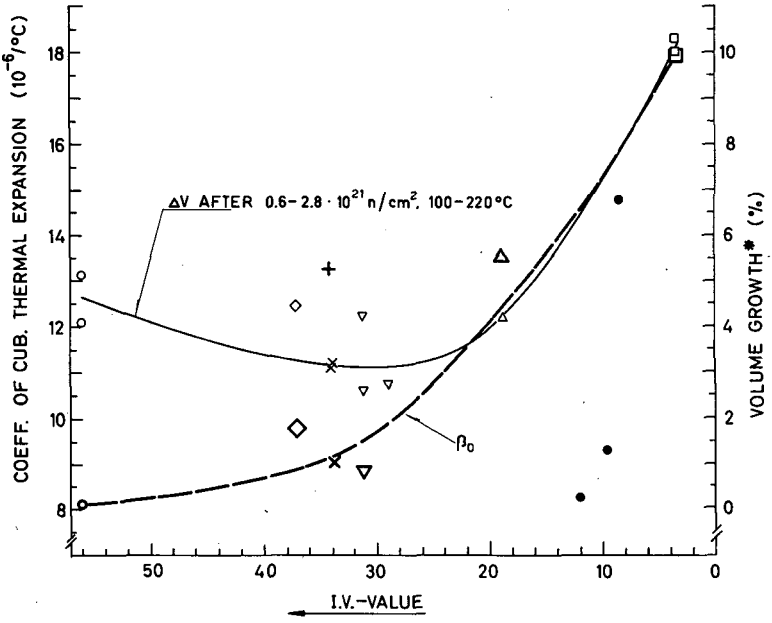


Fig. 42

Coefficient of cubic thermal expansion and Wigner growth as a function of the I.V. value

* after 2.84×10^{21} n/cm², E > 0.18 MeV, 120 - 220°C

If we consider the volume behaviour once more, it emerges that a smaller part of the lattice dilatation appears macroscopically as cubic thermal expansion than that part of lattice growth appearing as Wigner volume growth. It may be concluded that the enlarged lattice distance in the c-direction can be more easily compensated for by a sliding of the layer planes and crystallites respectively against each other thus diminishing the pore size in the unirradiated state. It seems reasonable to surmise that for the irradiated samples this sliding is blocked by interstitial atoms. The same barrier, however, should be expected for the compensation of the thermal expansion in the irradiated state. For this reason the coefficient of thermal expansion was determined on irradiated samples also. Naturally these measurements were carried out only at temperatures below the irradiation temperature, in order to avoid annealing effects. As shown in Figs. 43, 44 and 45, the coefficient of thermal expansion is hardly changed with irradiation and the individuality of thermal expansion of the various graphite types remains unchanged. It is therefore not possible to explain the volume effects by means of such simplified pictures. Furthermore the unchanged thermal expansion coefficient rather points to a compensation of the lattice dilatation by an intercrystalline sliding than to a sliding between the single layer planes within the crystallites.

Systematic investigations on a possible cancellation of Wigner growth by thermal annealing of the irradiated specimens are in progress and the results of these investigations are not yet available. We have in view, es-

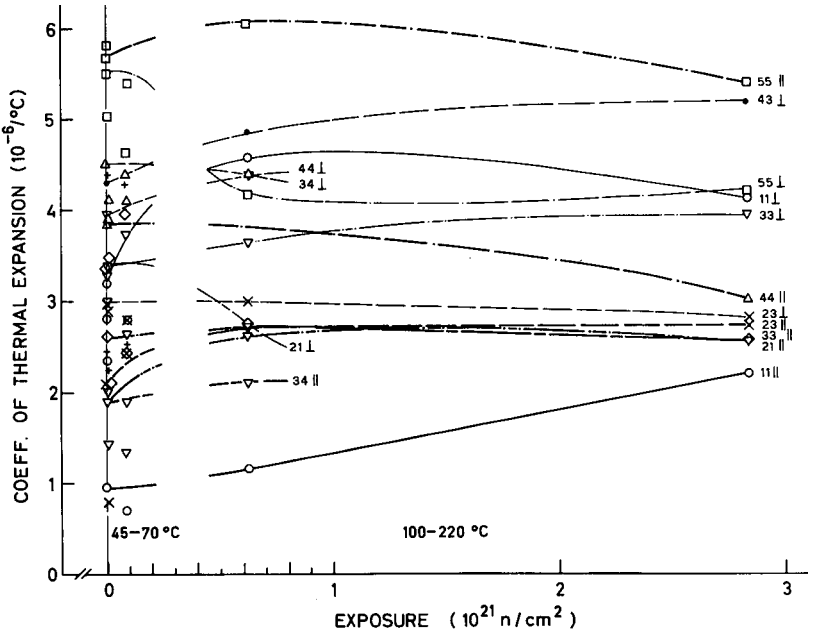


Fig. 43

Variation of thermal expansion coefficient with neutron irradiation

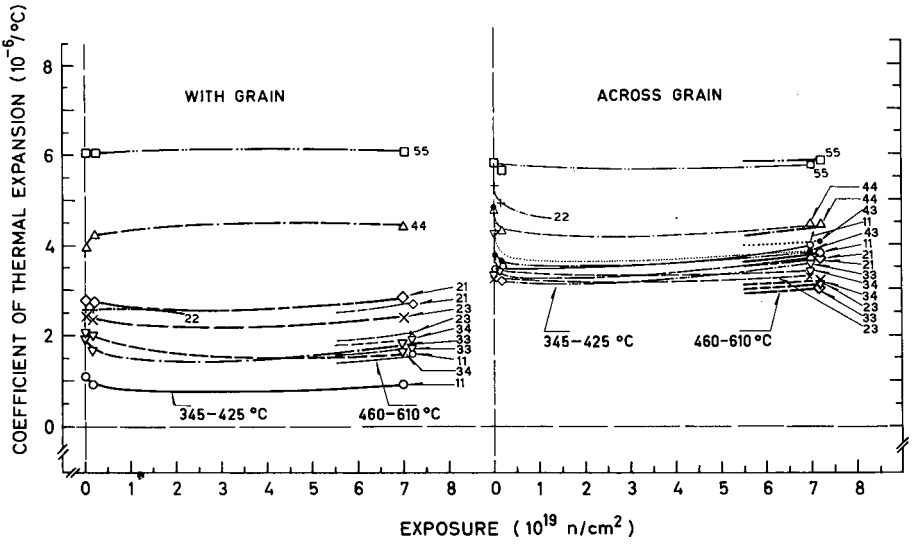


Fig. 44

Variation of thermal expansion coefficient by neutron irradiation

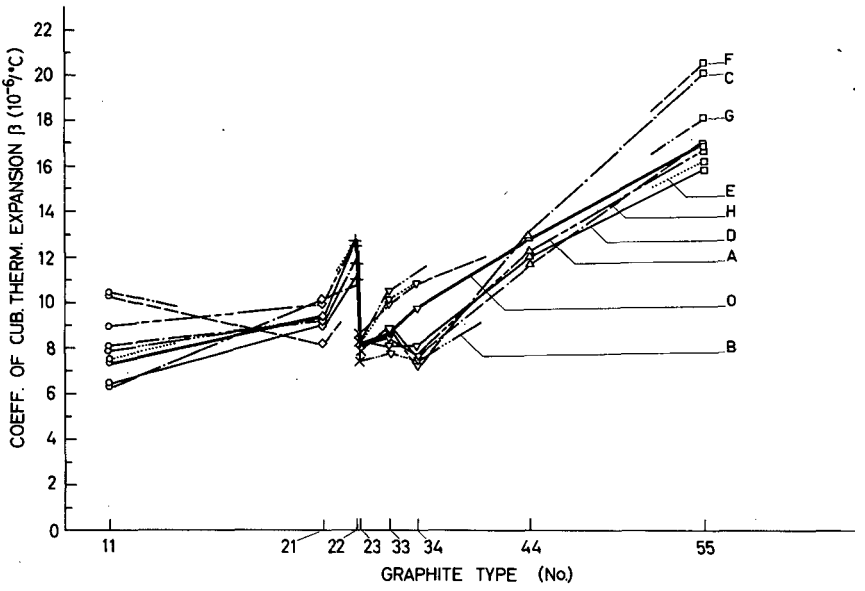


Fig. 45

Variation of cubic thermal expansion (β) with neutron irradiation

0: Original
A: 7.0×10^{19} n/cm², 345 - 425°C
B: 7.2×10^{19} n/cm², 460 - 610°C
C: 8.4×10^{19} n/cm², 50 - 70°C
D: 4.4×10^{18} n/cm², 45 - 70°C
E: 6.4×10^{18} n/cm², 172°C (EL3)
F: 0.6×10^{21} n/cm², 100 - 220°C
G: 2.8×10^{21} n/cm², 100 - 220°C
H: 1.5×10^{18} n/cm², 385 - 400°C

pecially, a different behaviour among the various graphite-types in order to obtain a key for the different Wigner volume growth of the best graphitized samples.

Even more complicated is the behaviour of highly heterogeneous artificial graphite products such as Type 43, which consists of the same filler as Type 11 but is subsequently impregnated and sealed with a poorly graphitizing coke. This subsequent filling with an isotropic coke component cannot influence the Wigner growth behaviour, which is typical for the unsealed body (Fig. 39).

4.3.4. Bulk density

The bulk density of the shaped body is decreased by means of the above-mentioned Wigner volume growth. The so-called real density, however, determined by helium or xylene displacement on finely powdered samples, is decreased to a greater extent (see Fig. 46). This means that the "bulk pore volume" (volume of accessible macropores), as evaluated from the difference of bulk density and real density, is decreased too. In carbon technology this bulk pore volume is generally called the "pore volume" of a shaped body. As already reported in our preliminary paper [8] this bulk pore volume obviously cannot be equal to the total pore volume, because

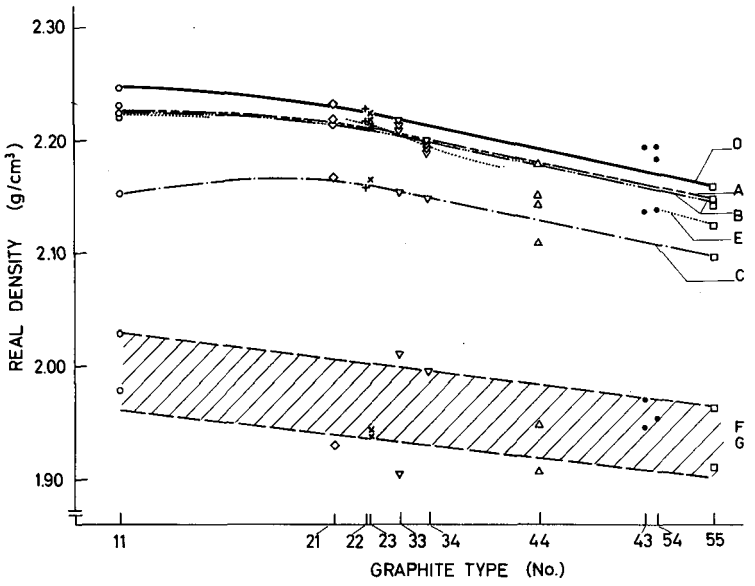


Fig. 46

Variation of real density with neutron irradiation

0: Original
A: 7.0×10^{19} n/cm², 345 - 425°C
B: 7.2×10^{19} n/cm², 460 - 610°C
C: 8.4×10^{19} n/cm², 50 - 70°C
E: 6.4×10^{18} n/cm², 172°C (EL3)
F: 0.6×10^{21} n/cm², 100 - 220°C
G: 2.8×10^{21} n/cm², 100 - 220°C

even in the powdered state graphite samples contain micropores, which are inaccessible to liquids and gases, as well as lattice defects representing a part of the total pore volume too, i. e. a space not filled with carbon atoms.

From X-ray data it is known that a perfect graphite single - crystal shows a density of 2.266 g/cm³. Conversely, on the basis of measurements of the lattice distances of various irradiated and unirradiated graphites their actual X-ray density can be determined. The difference between the theoretical lattice density and the X-ray density enables us to determine the extent of the lattice defects quantitatively. This difference is caused by imperfections in the lattice from the perfect spacing of 3.354 Å and by spaces between the crystallites caused by dislocations, distortions or interstitial atoms in the lattice. The real density, experimentally determined by helium or xylene displacement, differs from the X-ray density by the volume of the micropores which are inaccessible to liquids and gases. According, then, to this definition, the total pore volume is built up of the sum of the bulk pore volume + the volume of inaccessible micropores + the volume of lattice defects.

Fig. 47 demonstrates the average behaviour with irradiations at temperatures of up to 220°C: whereas the total pore volume is slightly increased, the bulk pore volume is decreased. The volume of inaccessible micropores and that of lattice defects are increased. Fig. 48 shows these

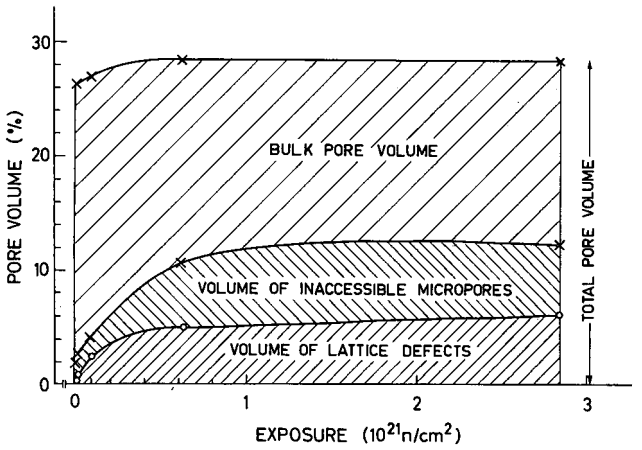


Fig. 47

Variation of pore volume with neutron irradiation

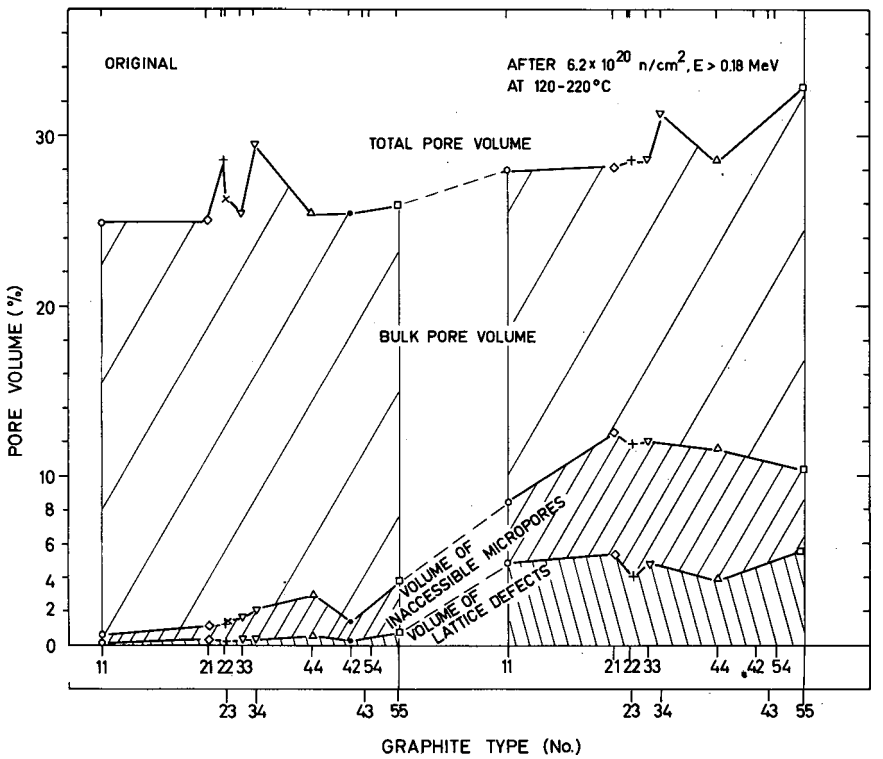


Fig. 48

Variation of pore volume by neutron irradiation

relations in more detailed form, for the unirradiated state and after 6.2×10^{20} n/cm^2 (at 120 - 220°C) and as a function of the degree of order.

A discussion of the relations shown in Fig. 48 would be very interesting because technical conclusions could be drawn from this for the use of reactor-grade graphite. In our experiments the number of samples was somewhat too small, so that the simplified conclusions are only preliminary.

The lattice defects are largely levelled out, because they exceed the differences between the individual samples of all graphites.

The volume of inaccessible micropores is increased, but the dependence on the degree of graphitization seen in the unirradiated state can no longer be recognized.

The volume of accessible macropores (bulk pore volume) is clearly decreased. This decrease seems to be somewhat related to the degree of graphitization in such a way that the highest reduction can be seen for the average graphitized types and the lowest decrease with the poorly graphitized ones. Only the well - graphitized types are an exception.

These results are of interest for the irradiation behaviour of impermeable graphite types, where it is important that the accessible pore-volume is diminished and inaccessible volume increased. According to the results the types with average degree of graphitization may come close to this tendency when irradiated. For preliminary results of the irradiation of impermeable graphite types we refer to another of our papers [22].

4.3.5. Microphotographs

On the strength of the above-mentioned findings it seemed a promising approach to see whether the variations of pore structure could be determined under the microscope. In Fig. 49, microphotographs are given of some graphite types in their original state and after an intensive irradiation with 2.8×10^{21} n/cm^2 at 120 - 220°C. Looking at polished, unirradiated sections under polarized light showed regions of the same optical anisotropy, i.e. regions with nearly the same alignment of the different crystallites. The sequence according to degree can be seen clearly, because the regions with the same optical anisotropy become smaller with decreasing degree of graphitization until they cannot be resolved any more. These regions of the same anisotropy remain, as the higher magnification of Fig. 50 shows, even after an intensive irradiation. This is not astonishing, because the crystalline pre-orientation cannot be changed by irradiation. In the same way there is no difference in the extinction regions for the same crystal alignments before graphitization and after it. The process of ordering, an intracrystalline process, and the reverse process caused by irradiation cannot be microscopically recognized.

What is rather surprising, on the other hand, is the increase of pores of a few microns in diameter in all samples. This would not have been expected from the results showing a decrease of macropores as evaluated from the densities (Fig. 48). Annealing experiments at 550°C did not change this pore structure; even after renewed abrasion and polishing the microscopic picture remained unchanged. Only after the samples had been graphitized again at about 3000°C was a picture obtained similar to that of the original state (Fig. 50). There may be a few, but negligible deviations in the band

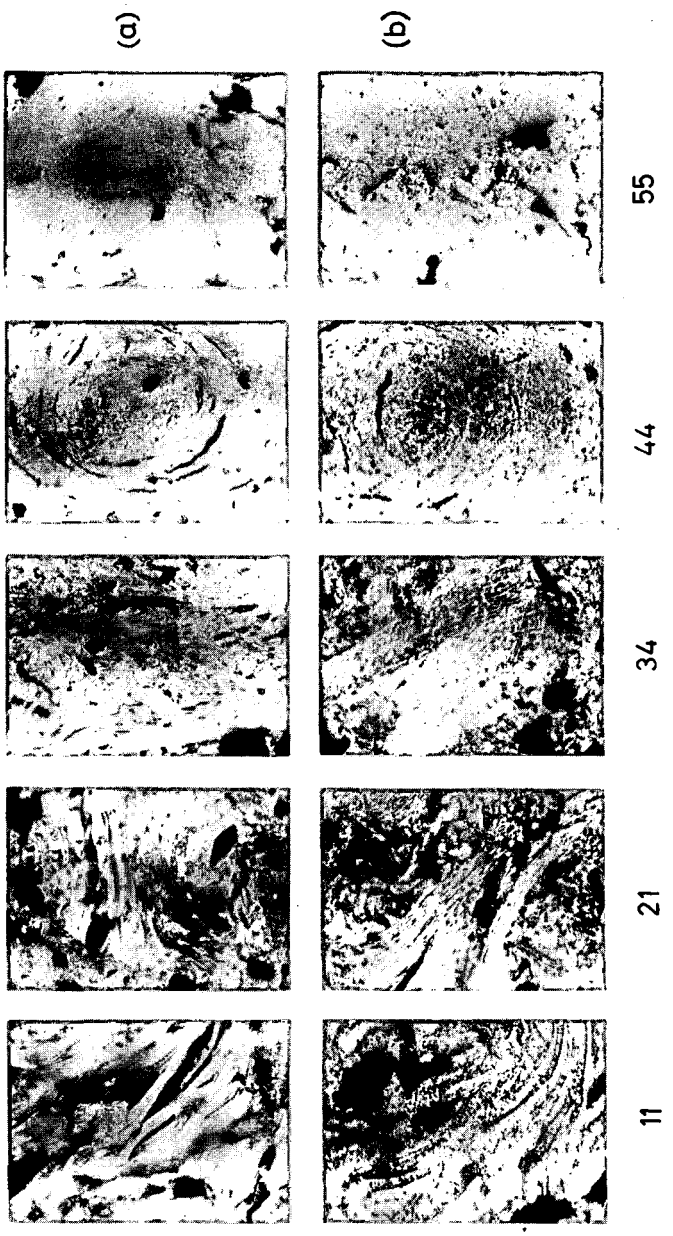


Fig. 49
Microphotographs of various graphite types
(a) original (b) irradiated to 2.8×10^{21} n/cm^2, 120 - 220°C

structure for regions with equal anisotropy. We guess that the apparent increase in porosity after irradiation is due to the enormous brittleness of the irradiated graphite causing many breaks during the mechanical abrasion of the sample. This question, however, has not been cleared completely and it will be investigated more closely after the annealing experiments which still have to be carried out.

4.4. The influence of the shape of sample on Wigner growth

In the preceding chapters the aim of this irradiation programme, i.e. to enable us to become acquainted with the relative differences of the irradiation behaviour of various graphite types under the same irradiation conditions, was discussed in detail. Now the question arises how well these results are qualified to act as an absolute measure for the prospective evaluation of irradiation damages for graphite bars of different size and quality as well as for comparison with irradiation results of other authors. The possibilities of evaluation are narrowed down by two limitations:

(a) There are different methods of representating data on neutron flux and of neutron spectrum: this makes a comparison with data given in the literature quite difficult. We shall come back to this question again in the next section 5.

(b) The different shape of samples used in different irradiation experiments may influence the extent of the radiation damage. This point is discussed below.

During the comparison of the volume change and the extent of lattice growth (see Figs. 4, 34 and 41) the fact that the volume growth of the coherent regions is, for the most part, intercepted by the bulk structure of the graphite body was referred to. These relations differ from those of the thermal expansion in that the latter causes a relatively smaller volume dilatation in the sample than the observed Wigner growth. The ability of the bulk structure to absorb crystallite dilatations is not only a peculiarity of the different graphite types but is also dependent on the kind of lattice growth.

It is also possible that the shape of the specimens used for the measurement of the volume dilatation influences the results. Some of this was given, for instance, by the growth under the high-temperature irradiations, which is extremely high for our samples as compared with data given in the literature (Fig. 40). Attention may be drawn to Type - 42 representing the graphite whose small expansion is described in the literature.

Discussions with authors regarding former irradiation experiments have shown that the specimens with the extremely high length-to-diameter ratio chosen by us were not tested by other experimenters. Nightingale, for example, used cylindrical samples with the same diameter as height. The shape of our specimens has been proposed by Gain, and was used to enable us to place as many different and parallel samples as possible in a capsule and get data as exactly as possible by simple measurements [8]. For these reasons the influence of the length-to-diameter ration on volume change with irradiation had to be investigated. Samples with different shapes were placed in the same irradiation canal of FRM. In order to get the same accuracy of the length measurement for the different samples, the same length

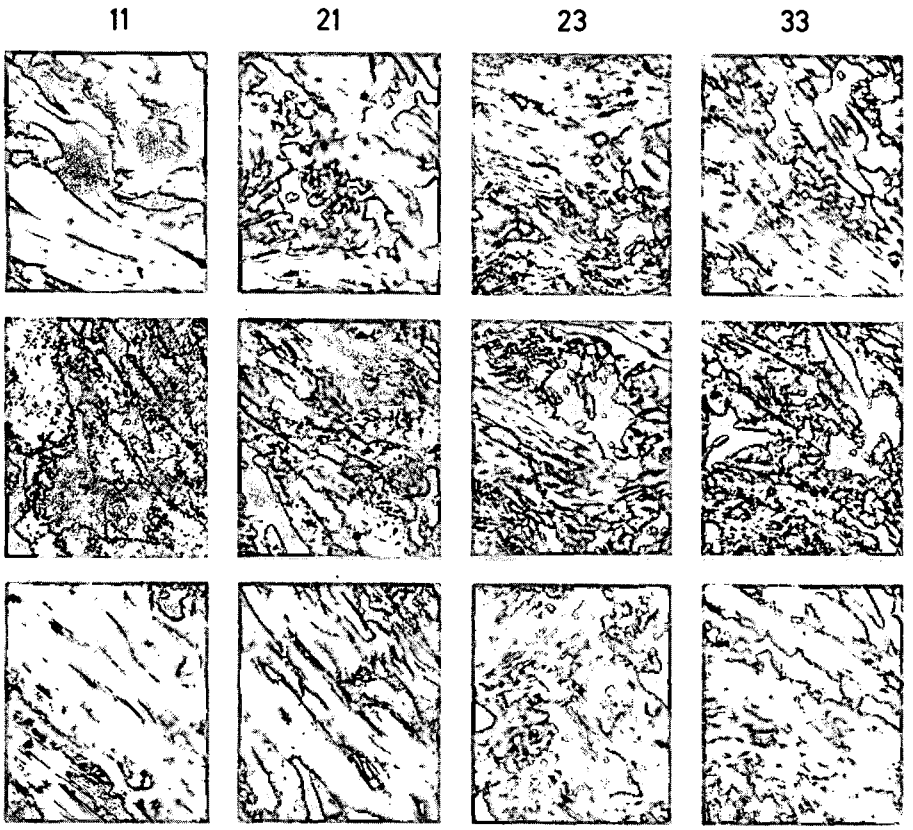


Fig. 50

Microphotographs of various graphite types

(a) original (b) irradiated to 2.8×10^{21} n/cm^2, 120 - 220°C (c) annealed at 3000°C

was chosen for all specimens, i. e. 45 mm. The cross-section was chosen to be 5 mm × 5 mm or 15 mm × 15 mm; thus a ratio of cross-section areas of 1 : 9 was obtained. Because of their higher Wigner growth mainly cross-grain samples have been compared.

Table I shows the results obtained with the unsealed material of Type 43 after an irradiation of 1.6×10^{19} n/cm^2, E > 0.1 MeV at about 120°C. It is surprising that there is such a great difference of the Wigner growth for those two sample shapes. At present the reproducibility of this result is being checked for the same and for other graphite types. For example, the specific electrical resistance of the specimens was also determined. As can be seen from the table, the variation of the electrical resistance is entirely independent of the length-to-diameter ratio of the samples. This seems to prove that at least for short-time irradiations the absolute value of Wigner growth may be influenced by the shape of the specimens. Obviously a specimen having a length-to-diameter ratio of about unity is better able to intercept or to moderate the anisotropic growth than a very slender specimen. (Per-

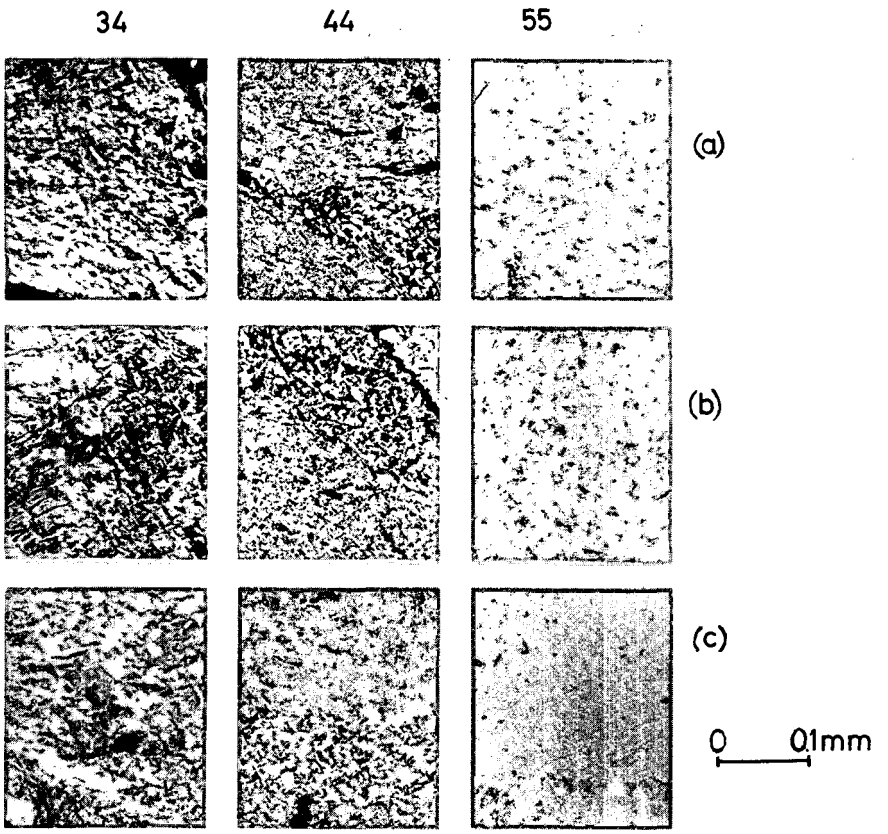


Fig. 50

Microphotographs of various graphite types

(a) original (b) irradiated to 2.8×10^{21} n/cm^2, 120 - 220°C (c) annealed at 3000°C

haps this behaviour is similar to the growth of rod-shaped uranium bodies with alternating stress under irradiation.) The relative length change measured on the small, slender samples cannot be used immediately as an absolute value for the evaluation of behaviour of big bars.

Somewhat different are the relationships concerning the Wigner growth after high irradiation doses; these are only very slightly dependent on the dose and seem to approach a saturation value. These high-dose irradiations have so far been performed only at temperatures below 200°C, and their results agree very well in their final values with the values measured on cylindrical samples reported in the literature. It is evident, therefore, that the influence of the sample-shape is mainly effective at relatively low doses, i. e. at the beginning of the irradiation.

4. 5. Influence of neutron spectrum

It is generally known that it is difficult to compare the irradiation results of various authors. We wanted to make it clear how far it is at all

Size (mm)	Direction	Wigner-growth, (%)*	Specific electrical resistance, (10^{-4} Ωcm)	
			original	irradiated*
5× 5× 45	with grain	+0.032	5.1	23.4
5× 5× 45	across grain	+0.100	10.5	42.1
15× 15× 45	across grain	+0.002	10.9	42.5

* After 1.6×10^{19} n/cm², E > 0.1 MeV at ~ 120°C (FRM)

Fig. 51

Influence of sample shape on Wigner growth of Type 43' graphite

possible to use the dose-figures which were experimentally determined or evaluated as a reference for radiation damage. For this reason samples were cut from neighbouring parts of the shaped body and in parallel experiments were irradiated in the reactors mentioned in section 3.2.

GETR is a highly enriched, water-cooled testing reactor. The large water-filled pool contains the aluminium tank with the core. The different irradiations were carried out in facilities in the core and on its outer shell (see Fig. 9). As shown in Fig. 10, there is a neutron flux in the irradiation facilities of between 5×10^{12} and 3×10^{14} n cm^{-2} sec^{-1} with an energy greater than 0.17 eV, and 43 - 50% of this is greater than 0.18 MeV.

EL. 3 is a heavy - water - moderated testing reactor, with hollow, cylindrical fuel elements containing enriched uranium (1.5% U^{235}). The irradiation capsules were placed within the holes of a graphite bar which was suspended in the central channel at the point of highest neutron flux (see Fig. 9). The spectrum of the neutron flux can be seen in Fig. 10. It shows a relatively low energy.

FRM (like GETR) is a water - cooled testing reactor working with highly enriched uranium (a "swimming-pool" reactor). The irradiation capsules were inserted into a special fuel alignment consisting of one irradiation channel with four capsules and six fuel plates (see Fig. 9). In the energy spectrum of these irradiation facilities, neutrons with energies less than 10 keV are nearly completely absent. As Fig. 10 shows, the spectrum shows very high energy: an extremely high fraction of the neutrons have an energy greater than 0.1 MeV. On the strength of extremely different energy distributions at the irradiation facilities, the results of irradiations in these three different reactors can be accepted for a comparison of the influence of the neutron spectrum on the radiation damage. The results of parallel measurements have been plotted in the foregoing Figs. 13, 15, 16, 17, 20, 22, 25, 26, 30, 31, 35, 38, 45 and 46, where the different testing reactors are specially marked.

The first difficulty for comparison arises already with the neutron doses of the different reactors. In the diagrams the dose of GETR is referred to neutrons with energies > 0.18 MeV, in EL.3 to neutron energies > 1 MeV and for FRM to neutrons having energies > 0.1 MeV.

The irradiation facility in the Munich reactor shows the spectrum with the highest energy, whereas the facility used in the French reactor EL.3 possesses without question the lowest energy. It might be added in connection with this (see Fig.9) that the results of all irradiations compared here, at least all irradiations at FRM and EL.3 and most of the GETR irradiations, were carried out inside the core of the testing reactors. The above - mentioned energy distribution of the irradiation facilities is therefore generally valid for these testing reactors.

As the results show, the irradiations at EL.3 fit very well into the corresponding picture of the property variations in the GETR under the above-mentioned dose or energy limitations, if it is borne in mind that the temperature of the EL.3 irradiations is about 172°C. That means the energy limitations for GETR (E >0.18 MeV) and EL.3 (E >1 MeV) represent practically disadvantageous limits, because the dose data referred to those limiting energies yield results which are practically comparable. The dose data at Munich FRM cannot be compared in such a simple way. The dose referred to neutrons with energies greater than 0.1 MeV, as given by the reactor station, is not comparable with the GETR dose E >0.18 MeV. The FRM dose represents a more effective dose when referred to the radiation damage. This fact is shown especially in Figs. 22 and 31 by the steep ascent of the electrical resistance and Young's modulus. This effect is still more pronounced, if one takes into consideration that the irradiation temperature was higher in the FRM facility than for the corresponding GETR irradiations.

To summarize, it can be stated that, in spite of a somewhat higher irradiation temperature and a rather lower energy limit for the neutrons under consideration, the damage caused by irradiation in the FRM is greater than in the GETR. Despite the higher energy limit of the related neutron dose at EL.3, the irradiations at this facility result in lower damage. The somewhat higher irradiation temperature cannot be responsible for differences of such extent.

5. CONCLUSIONS

The aim of these investigations was to determine whether the irradiation behaviour of graphite as a reactor material can be influenced from the manufacturing side. If so, it must be possible to develop optimum graphite types for certain applications in reactor construction. To solve this problem, the behaviour of various graphites of different degrees of graphitization was investigated under the same irradiation conditions. This idea arose from the consideration that the bulk properties of a graphite body are largely influenced by its degree of graphitization. The degree of crystalline order obtainable under technical conditions is already fixed by the raw material. Therefore graphites with different fillers were studied. From these investigations the following detailed questions arose: -

(a) Do artificial graphite bodies with different filler material all show the same behaviour after intensive irradiation, i. e. is the neutron irradiation able to level-out differences in the degree of order by the lattice damage which then exceeds the original extent of disorientation in the non-graphitized, amorphous-carbon body?

(b) Do the differences between the various graphite types remain unchanged even after intensive neutron irradiation?

According to our investigations the following answer can be given. Only one technically interesting bulk property is completely levelled out after intensive irradiation for all graphite types, no matter what raw materials are used or what binding properties are shown, the thermal conductivity. The thermal conductivity definitely reaches a saturation state which is about 0.01 cal $cm^{-1} sec^{-1} °C^{-1}$ for irradiations at 45 - 220°C. This is less than 5% of the thermal conductivity of the original state.

All other technically interesting bulk properties of graphites remain more or less unchanged in proportion to each other, or these differences are made even more pronounced by irradiation. This is valid, first of all, for mechanical strength and Young's modulus. To a certain degree this can be said for the electrical resistance after irradiation, too.

The compressive strength represents the strength property which is influenced also by the degree of graphitization; its increase with irradiation depends definitely on the degree of graphitization.

The properties of graphite bodies which are exclusively dependent upon the bulk binding structure, such as Young's modulus and bending strength, are independent of the degree of graphitization even after irradiation.

For a material such as graphite, the coefficient of thermal expansion is a very important property especially in its application at the higher temperatures. It remains nearly unchanged after irradiation. Thus, the dependence of the thermal-expansion coefficient on the degree of graphitization is not affected by the irradiation.

With regard to the fundamental question of our irradiation programme, the possibility of developing special-purpose reactor-grade graphites can be affirmed. In the choice of distinct graphite types for reactor design, nearly the same points of view are valid as are used for conventional uses of artificial graphite. This conventional usage is mainly determined by the thermal stress resistance given by the simplified expression:

$$\frac{\text{strength} \times \text{thermal conductivity}}{\text{Young's modulus} \times \text{thermal-expansion coefficient}}$$

Of these properties, only the thermal conductivity remains constant after irradiation. It is well known that the thermal stress resistance is influenced to a great degree by the thermal-expansion coefficient; there is a large enough range to select from irradiated graphites a certain type chosen with regard to thermal stress resistance.

An additional property of graphite bodies undergoing irradiation is represented by the Wigner growth. This property can also be influenced by the graphite manufacturer, because the changes in length of the various graphites under low-temperature irradiations are different and special types

can be developed exhibiting a growth in one direction or others, by growing more isotropically, having a low volume expansion. The latter represent medium-graphitized types, whereas the first ones are extremely well graphitized ones. The poorly graphitized types show the highest Wigner volume growth.

Leaving the results concerning technological properties, let us now turn to the fundamental question of the influence of the crystalline order on irradiation behaviour. From the present results the following picture is obtained.

The bulk properties of a graphite body in the unirradiated state are determined by the degree of order and the binding properties. The degree of order can be divided into three parts:

(a) The region of intracrystalline order (within the crystallites),
(b) The region of intercrystalline order (between the crystallites),
(c) The order of the grains within the matrix (between the grains).

(a) Intracrystalline order

The intracrystalline order as an ordering scheme is lost after neutron irradiation so that the disorientation of the raw material in the non-graphitized state is very much exceeded. To describe this intracrystalline degree of graphitization, microcrystalline properties such as magnetic susceptibility and X-ray data can be used. All properties of different graphite types determined by this intracrystalline order must be levelled out by irradiation.

(b) Intercrystalline order

For describing the intercrystalline order no criterion is available as yet. The extraordinarily low change in the thermal expansion coefficient indicates that this property is mainly influenced by the mutual positions of the crystallites and the sliding between the crystallites respectively. Taking the coefficient of thermal expansion as the criterion for the degree of intercrystalline order, we can conclude that the intercrystalline order is not essentially changed by irradiation.

(c) Grain order

There is no doubt that this order of the grains within the matrix is expressed by Young's modulus and bending strength. According to the results of these investigations the relative order between the grains remains almost unchanged after irradiation.

There is another criterion for the degree of graphitization, the real density. Since it is not completely levelled-out it must be influenced besides by the considerations put forward in (a) and (b) above as well.

One interesting result is that these three groups of order show different degrees of influence on the physical bulk properties, depending on the degree of radiation damage. The change of intracrystalline order is expressed predominantly in the thermal conductivity.

ACKNOWLEDGEMENTS

The irradiation programme referred to in this paper was sponsored by the Ministry of Atomic Affairs of the Federal Republic of Germany. The authors are indebted to the Ministry for the financial support given and for making possible this publication. Irradiations in GETR were carried out by Dr. Gain (of the Reactor Materials Institute of the Julich Nuclear Research Establishment) and by the reactor staff of the United States General Electric Company. The EL.3 were carried out by S.E.R.A.I., Brussels under the direction of Dr. Rappeneau. We are very obliged to both institutes for their assistance. Our thanks are also due to the FRM team at Munich, under the direction of Professor Meier-Leibnitz, for their intensive co-operation over the last few years.

The measurements of the property changes were carried out at the Reactor Materials Institute of the Jülich Nuclear Research Establishment, at S.E.R.A.I. Brussels, within the GFKF at the institute of Professor Knappwost, Tübingen, and in our own laboratories, where Dr. Beutell (Miss), Dr. Semmler, Mr. Reinhard, Miss Nega, Mr. Schmid and Mr. Stohl have provided the bulk of the assistance.

Finally we are very obliged to all co-workers who have assisted in carrying out this irradiation programme.

REFERENCES

[1] CURRIE, L. M., HAMISTER, V. C. and MacPHERSON, H. G., Proc. UN Int. Conf. PUAE 8 (1956) 451.
[2] FITZER, E. and ETZEL, K. W. F., Atom u. Strom 10 (1960) 87.
[3] BERGOGNON, P., Dragon Symposium, Bournemouth (1959) paper 17.
[4] BOETTCHER, A., SCHULTEN, R., and WIRTHS, G., Proc. 2nd UN Int. Conf. PUAE 7 (1958) 748.
[5] DRAGON Sumposium of OEEC, Bournemouth (1959).
[6] For example HTGR Quart. Rpt Series GA-1235, 1378, 1640, 1774.
[7] WOODS, W. K., BUPP, L. P. and FLETCHER J. F., Proc. UN Int. Conf. PUAE 7 (1956) 455.
[8] BEUTELL, M., FITZER, E., GAIN, R. and VOHLER, O., Proc. Fifth Carbon Conf. Pergamon Press, Oxford (1962).
[9] United States of America Patent 2 775 549 (25 Dec. 1956).
[10] ALI, D., FITZER, E. and RAGOSS, A., Proc. Soc. Chem. Ind., London (1958) 135.
[11] DAVIDSON, J. M., WOODRUFF, E. M. and YOSHIKAWA, H. H., Proc. Fourth Carbon Conf. (1959) 599.
[12] NIGHTINGALE, R. E. and FLETCHER, J. F., USAEC Rpt. HW-47776 REV (26 Sep. 1957).
[13] NIGHTINGALE, R. E., DAVIDSON, J. M. and SNYDER, W. A., Proc. 2nd UN Int. Conf. PUAE 7 (1958) 295.
[14] HALAS, D. R. and YOSHIKAWA, H. H., Proc. Fifth Carbon Conf. Pergamon Press, Oxford (1962).
[15] DAVIDSON, J. M. and HELM, J. W., Proc. Fifth Carbon Conf. Pergamon Press, Oxford (1962).
[16] FRANKLIN, R. E., Acta Cryst. 4 (1951) 253.
[17] RAGOSS, A., Arch. Eisenhüttenw. 27 (1956) 681.
[18] GAIN, R. these Proceedings, section C. 2
[19] EATHERLY, W. P., Phys. Rev. 98 (1955) 1531.
[20] TYLER, W. W. and WILSON, A. C. Jr., Phys. Rev. 89 (1953) 870.
[21] WILD, D., 2. Ver. dtsch. Ing. 100 (1958) 95.
[22] FITZER, E., ETZEL, K. W. F., PELZ, A. and VOHLER, O., in Fuel Element Fabrication, 1, Academic Press, London - New York (1961) 189.

COMPARISON OF IRRADIATION DAMAGE IN ARTIFICIAL AND NATURAL GRAPHITE AT DIFFERENT IRRADIATION TEMPERATURES

R. GAIN
REACTOR MATERIALS INSTITUTE,
JÜLICH NUCLEAR RESEARCH ESTABLISHMENT,
JÜLICH, FEDERAL REPUBLIC OF GERMANY

Abstract — Résumé — Аннотация — Resumen

COMPARISON OF IRRADIATION DAMAGE IN ARTIFICIAL AND NATURAL GRAPHITE AT DIFFERENT IRRADIATION TEMPERATURES. Results of irradiation experiments on artificial and natural graphite in the three temperature ranges 70 - 150°C, 300 - 400°C and 550 - 650°C are compared. These irradiation experiments were carried out in core or pool positions of the GETR, Vallecitos. The samples investigated received neutron doses up to 5×10^{21} nvt with E > 0.17 eV, which is approximately 3×10^{21} nvt with E > 0.18 MeV. Changes in the lattice parameters, the electric and thermal conductivity, the macroscopic dimensions and the bending strength are discussed. The natural graphite samples investigated were manufactured partly with, partly without a binding material. The results obtained during these investigations indicate, in addition to the dependence on the irradiation temperature and the neutron dose, a strong influence exerted by the basic materials, the treatment during production and the density. Strong anisotropic effects in natural graphite at lower irradiation temperatures, resulting from the treatment during production, level out at higher irradiation temperatures.

COMPARAISON DES DOMMAGES SUBIS PAR DES GRAPHITES ARTIFICIELS ET NATURELS IRRADIÉS A DES TEMPÉRATURES DIFFÉRENTES. L'auteur compare les résultats d'expériences consistant à exposer du graphite artificiel et naturel à un flux de neutrons, à des températures comprises dans les trois gammes suivantes: 70 - 150°C, 300 - 400°C et 550 - 650°C. Ces expériences ont eu lieu tant à l'intérieur qu'à l'extérieur du cœur du réacteur GETR de Vallecitos. Les échantillons étudiés ont reçu des doses allant jusqu'à $5\cdot10^{21}$ nvt avec une énergie de E > 0,17 eV, ce qui correspond à environ $3\cdot10^{21}$ nvt avec E > 0,18 MeV. L'auteur discute les modifications observées dans les paramètres de réseau, la conductivité électrique et thermique, les dimensions macroscopiques et la flexibilité. Les échantillons de graphite naturel considérés avaient été fabriqués en partie à l'aide d'une substance liante et en partie sans une telle substance. Il ressort de ces expériences que les résultats varient non seulement avec la température d'irradiation et la dose de neutrons mais qu'ils sont déterminés dans une forte mesure par les matériaux de base, le traitement au cours de la fabrication et la densité. Les effets anisotropiques considérables qu'on observe dans le graphite naturel à des températures d'irradiation relativement peu élevées et qui résultent du traitement au cours de la fabrication, s'atténuent graduellement lorsque la température d'irradiation augmente.

СРАВНЕНИЕ РАДИАЦИОННЫХ ПОВРЕЖДЕНИЙ В ИСКУСТВЕННОМ И ПРИРОДНОМ ГРАФИТЕ ПРИ РАЗЛИЧНЫХ ТЕМПЕРАТУРАХ ВО ВРЕМЯ ОБЛУЧЕНИЯ. Сравниваются результаты опытов облучения искуственного и природного графита при температурах в пределах от 70 до 150°C, от 300 до 400°C и от 550 до 650°C. Опыты производились в активной зоне или в бассейне реактора GETR в Вальлеситосе. Обследованные образцы были подвергнуты воздействию доз нейтронов до $5\cdot10^{21}$ nvt при E > 0,17 Мэв, что соответствует приблизительно $3\cdot10^{21}$ nvt при E > 0,18 Мэв. Обсуждаются изменения параметров решетки, электропроводимости и теплопроводности, микроскопических размеров и сопротивления на изгиб. Изученные образцы природного графита были изготовлены частью со связующим материалом, а частью без него. Полученные при этих исследованиях результаты показывают, что, помимо зависимости от температуры при облучении и от дозы нейтронов, имеет место также сильная зависимость от исходных материалов, обработки во время изготовления и плотности. Сильное анизотропное воздействие в природном гра-

фите при более низких температурах во время облучения, возникающее в результате обработки в процессе производства, выравнивается при облучении при более высоких температурах.

COMPARACIÓN ENTRE LOS DAÑOS CAUSADOS POR LAS RADIACIONES EN GRAFITOS ARTIFICIALES Y NATURALES POR IRRADIACION A DIVERSAS TEMPERATURAS. La memoria compara los resultados de experimentos de irradiación de grafito artificial y natural en tres intervalos de temperatura que abarcan de 70 - 150°C, de 300 - 400°C y de 550 - 650°C, respectivamente. Los experimentos se efectuaron en el cuerpo o en el tanque del reactor GETR de Vallecitos. Las muestras investigadas recibieron dosis neutrónicas de hasta $5 \cdot 10^{21}$ nvt, con E > 0,17 eV, lo que corresponde aproximadamente a $3 \cdot 10^{21}$ nvt, con E > 0,18 MeV. La memoria discute las alteraciones sufridas por los parámetros de la red cristalina, la conductividad eléctrica y térmica, las dimensiones macroscopicas y la resistencia a la flexion. Las muestras de grafito natural investigadas fueron preparadas en parte con material aglomerante y en parte sin él. Los resultados obtenidos durante estas investigaciones indican que, además de la temperatura de irradiación y de la dosis neutrónica, las materias primas, el tratamiento recibido durante la elaboración y la densidad ejercen una influencia muy marcada. Los fuertes efectos anisotrópicos que aparecen en el grafito natural a reducidas temperaturas de irradiación, y que son resultado del tratamiento durante la elaboración, quedan compensados al irradiar a temperaturas más elevadas.

1. INTRODUCTION

Graphite is used extensively in nuclear reactors both as a moderator and as a structural material and it also plays a particularly important part in the design of high-temperature reactors. Apart from acting as a moderator or reflector, it is used as a canning material and in most cases replaces the normal metallic canning for fuel elements.

Apart from the nuclear purity and the fulfilment of the physical and technical properties required at normal operating temperatures, there are additional demands for a very low permeability in order to keep the diffusion rate of gaseous fission products low.

As early as 1955 it was pointed out [1] that, because of its high density, natural graphite could have considerable advantages in reactor-construction applications. While the apparent density of artificial graphite is normally between 1.6 g/cm^3 and 1.7 g/cm^3 and much higher densities can only be achieved by expensive impregnation processes, apparent densities of more than 2.0 g/cm^3 are easily obtained with natural graphite: because of the higher density and the resultant better neutron moderation, savings in core volume and construction costs could be expected.

Unfortunately, at that time, the mechanical properties of moulded natural-graphite blocks without any binding material were not sufficient to justify its use in reactor construction, especially at normal operating temperatures. Moreover, because of the high density and considerable anisotropy of the die-moulded blocks, larger amounts of irradiation damage were expected at ambient temperatures. Hence this material has had only limited use, e.g. for thermal columns in research reactors.

Since that time the properties of natural graphite have been improved by the use of appropriate binding materials [2] and the possibility of using this material in high-temperature reactors and as a canning material has, as a result, become more interesting. As the apparent density is close to 2.0 g/cm^3, this graphite has, because of its dense texture, a primary permeability of about 10^{-3} cm^2/sec. This can be brought to a permeability of better than 10^{-7} cm^2/sec by a simple and economical procedure.

The investigation described below was carried out in order to obtain information on the behaviour of natural-graphite samples under reactor irradiation at different temperatures.

2. INVESTIGATION OF GRAPHITE GRADES

Two grades of natural graphite were irradiated. Both were die-moulded into blocks, grade A without any binder, grade B using formaldehyde resins as a binder. Because of the disc form of the crystallites, they become preferentially orientated during the moulding with the c-axis parallel to the direction of pressure.

In order to compare the results of these experiments with the damage induced in a representative artificial graphite, samples of CSF graphite were also irradiated. This grade and its property changes under neutron irradiation have been extensively investigated by many authors, e.g. [3-10].

Artificial graphite generally will be extruded during production. In such a case, therefore, the c-axis of the crystallites is preferentially orientated perpendicular to the direction of pressure. Samples with their axes in some cases perpendicular and in others parallel to the direction of pressure were cut out of the moulded blocks. Because of the different method of manufacture parallel ($\parallel$) samples of this natural graphite correspond to the perpendicular ($\perp$) samples of CSF graphite and vice versa.

Table I lists the properties of the samples investigated before irradiation. Irradiations were carried out in pool or core positions of the GETR* reactor. The fast-neutron dose-value was obtained using sulphur monitors and theoretical calculations, applying the three-group treatment. As the group with the highest energy lay above 0.18 MeV, we used this group to measure the neutron dose. There is reason to believe that irradiation damage in graphite will be induced mainly by neutrons having a threshold energy of at least 0.1 MeV.

Discrepancies between the calculated and measured neutron dose are of minor importance in this case, as the samples compared with each other at the same temperature were always placed in the same capsule. During irradiation the recorded temperature showed some oscillations introduced by fluctuations in reactor operation. The data given in the figures are best averages, the temperature dependence of irradiation damage being taken into account.

3. CRYSTALLITE PROPERTIES

The crystallite changes in the c- and a-spacing induced in graphite by irradiation were studied by X-ray diffraction techniques using the (002) and (110) reflections. While there is no noticeable difference in the a_0-spacing of the three grades investigated before irradiation (Table I), the c_0-spacing shows the expected variations. Samples containing more perfect crystallites (natural graphite) have a smaller lattice spacing. In Figs. 1 and 2, changes of the lattice parameters are plotted against the irradiation temperature

* GETR: General Electric Test Reactor, Vallecitos Atomic Laboratory, California.

TABLE I

PROPERTIES OF GRAPHITE
(Average, unirradiated)

Type	CSF	A	B
	Artificial graphite Petrol-coke, extruded	Natural graphite moulded blocks	Natural graphite moulded blocks
Binder	coal tar pitch	none	phenol-formaldehyde resins
Apparent density (g/cm^3)	1.66	2.07	1.97
Thermal conductivity ($cal\ cm^{-1}\ sec^{-1}\ °C^{-1}$)	0.32 ⊥ 0	0.55 ⊥ 0.08 ∥	0.30 ⊥ 0.09 ∥
Electrical resistivity ($\Omega mm^2\ m^{-1}$)	12 ⊥	5.2 ⊥ 45 ∥	9.1 ⊥ 32 ∥
c_0 spacing (Å)	6.732	6.715	6.715
a_0 spacing (Å)	2.461	2.461	2.461

for neutron doses of 7.5×10^{19} and $4.5 \times 10^{20} n/cm^2$, $E > 0.18$ MeV, respectively. The strong increase of the c-spacing at ambient temperatures is much less marked for exposure at higher temperatures. At 500°C the change of this lattice parameter has already decreased to only 0.1 to 0.2%. Within the accuracy of measurement, all graphite grades investigated show the same relative changes.

This small increase in the c-spacing indicates that no single interstitial is stable under these conditions. Because of the high thermal energy, their mobility is high enough to effect recombination with vacancies. The measured increase in the c-spacing should therefore, as assumed by HENNIG and HOVE [11], result from complexes or clusters of carbon atoms or from molecules.

There is also a relatively high contraction in the direction of the a-axes, which is the same for all investigated grades. Though it is difficult to give

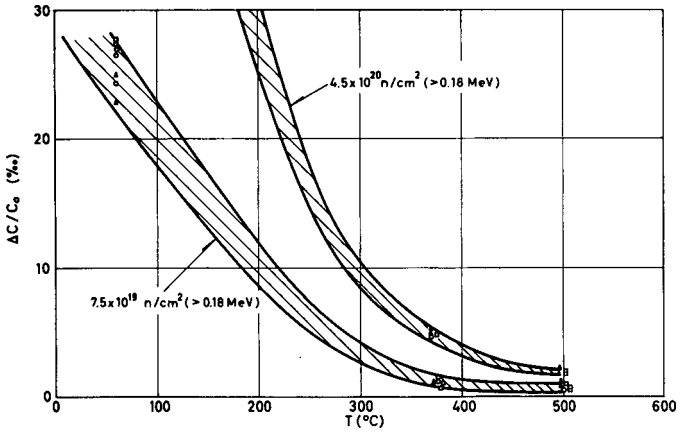


Fig. 1

Variation of c_0-spacing with exposure temperature

○ CSF ⊥ ▲ A ∥
△ A ⊥ ■ B ∥
□ B ⊥

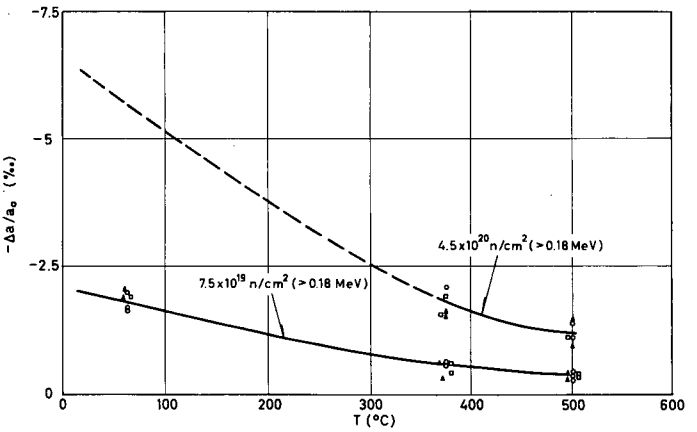


Fig. 2

Variation of a_0-spacing with exposure temperature

○ CSF ⊥ ▲ A ∥
△ A ⊥ ■ B ∥
□ B ⊥

quantitative statements, it is believed that this high amount cannot only be attributed to buckling of the planes. Also the assumed production of dislocations [11], most likely formed when displaced atoms try to re-integrate into the lattice, must contribute to this effect.

4. DIMENSIONAL CHANGES

Because of the strong anisotropy of the graphite bodies, the samples cut out in the two main directions also show very different changes in length (Figs. 3 and 4). The increase of the c-spacing is essentially responsible for this; a smaller or larger proportion of the crystallite expansion takes place parallel to the sample axis, depending on the degree of anisotropy. At 500°C this increase is not yet compensated by the crystallite contractions in the direction of the a-axis.

The higher the density of a graphite grade, the more the crystallite growth contributes to the macroscopic length changes, as less pore volume is available for filling out by the expanding crystallites.

At 500°C the bound natural graphite (grade B) shows the same length change as the CSF graphite. By a comparison of Figs. 1 to 4, one can see that the macroscopic length changes of grade A (without binders) are in some cases larger than the increases in the crystallite dimensions. We attribute this to irreversible processes produced by thermal cycling during irradiation which cause a loosening of the texture.

5. ELECTRICAL RESISTIVITY

It is well known from the literature that the electrical resistivity of irradiated graphite approaches a saturation value at a relatively low neutron dose. This fact is also indicated by Figs. 5 and 6. Though the neutron dose in Fig. 5 is higher by a factor of six than in Fig. 6, there is only little difference in the resistivity changes of the same samples. But there is a linear decrease in the resistivity change with increasing temperature at a certain neutron dose.

In this case the relative changes ρ/ρ_0 for the grades A and B seem to be more favourable than for CSF. As these are only relative values (referred to the resistivity of each grade and cut before irradiation), one has to apply the original data given in Table I in order to obtain absolute values.

6. THERMAL CONDUCTIVITY

The behaviour of the thermal conductivity of graphite under neutron irradiation plays an important part in reactor design. In this case also, the curves of the graphite grades investigated converge strongly at 500°C (Figs. 7 and 8). The relative values λ/λ_0 are again below those of CSF graphite at this point. In order to get the absolute values of the thermal conductivity, one again has to use the original data before irradiation, given in Table I.

7. BENDING STRENGTH

The variation of the bending strength (transverse breaking strength) is plotted in Figs. 9 and 10 against the irradiation temperature for neutron doses of 7.5×10^{19} and 4.5×10^{20} n/cm², $E > 0.18$ MeV, respectively. The graphite samples, which were of 5-mm square cross-section, were laid on blunt edges 40 mm apart. The load was applied in the middle of the

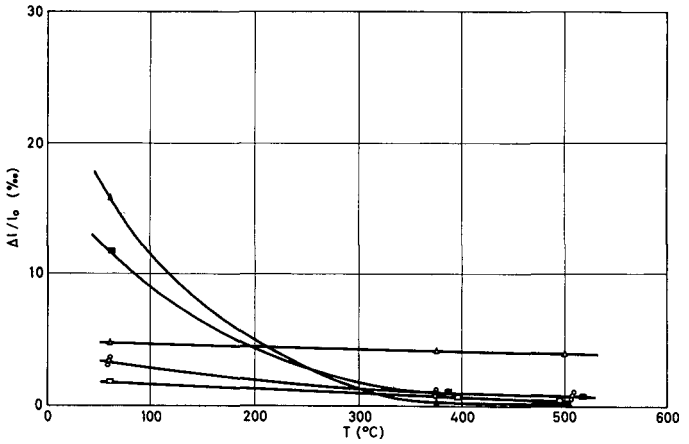


Fig. 3

Effects of temperature on physical expansion
(Exposure to 7.5×10^{19} n/cm² with energies > 0.18 MeV)

○ CSF ⊥ ▲ A ∥
△ A ⊥ ■ B ∥
□ B ⊥

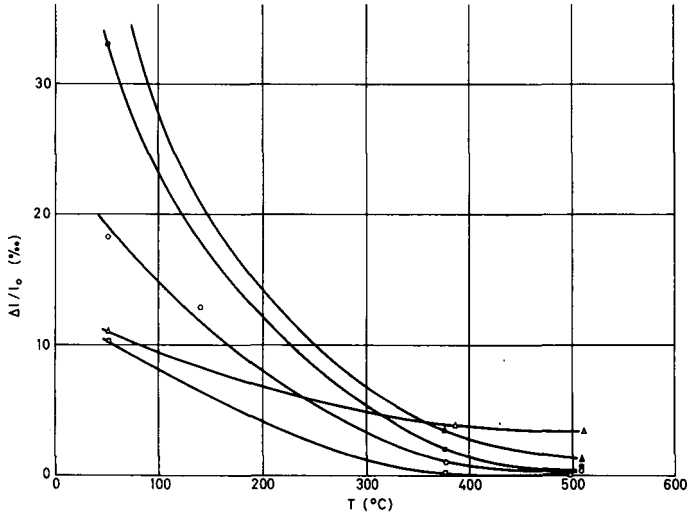


Fig. 4

Effects of temperature on physical expansion
(Exposure to 4.5×10^{20} n/cm² with energies > 0.18 MeV)

○ CSF ⊥ ▲ A ∥
△ A ⊥ ■ B ∥
□ B ⊥

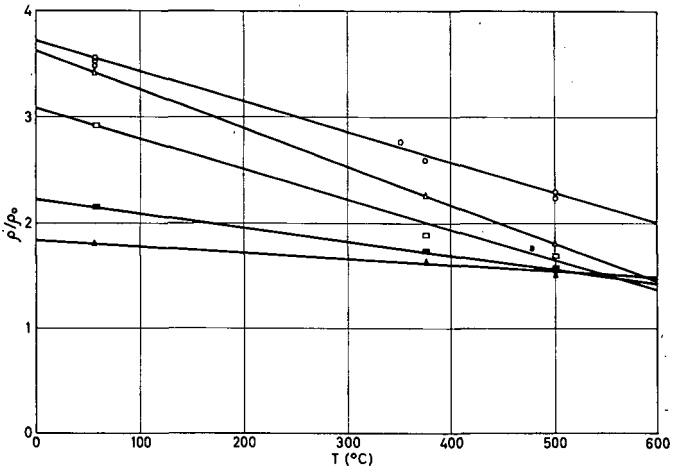


Fig. 5

Variation in electrical resistivity with irradiation temperature
(Exposure 7.5 × 10^{19} n/cm² with energies > 0.18 MeV)

○ CSF ⊥ ▲ A ∥
△ A ⊥ ■ B ∥
□ B ⊥

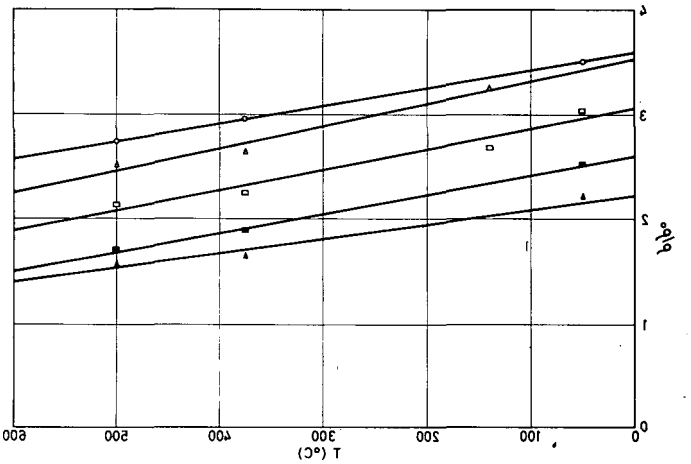


Fig. 6

Variation in electrical resistivity with irradiation temperature
(Exposure 4.5 × 10^{20} n/cm² with energies > 0.18 MeV)

○ CSF ⊥ ▲ A ∥
△ A ⊥ ■ B ∥
□ B ⊥

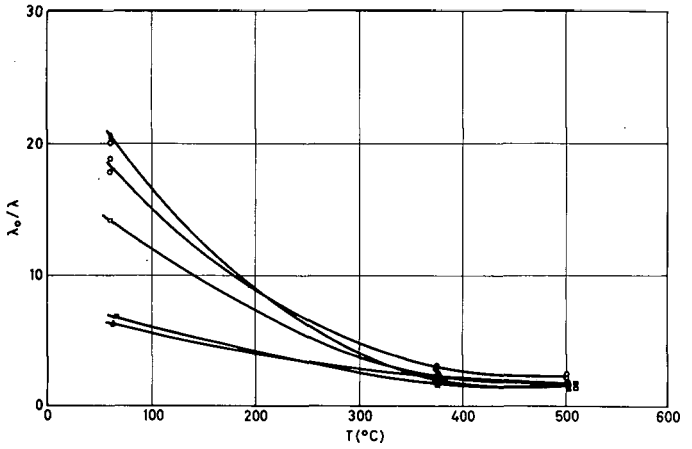


Fig. 7

Variation in thermal conductivity with irradiation temperature
(Exposure 7.5×10^{19} n/cm² with energies > 0.18 MeV)

○ CSF ⊥ ▲ A ∥
△ A ⊥ ■ B ∥
□ B ⊥

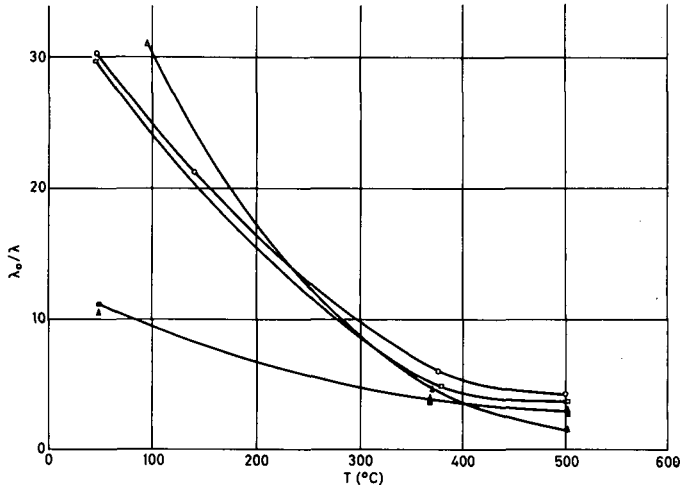


Fig. 8

Variation in thermal conductivity with irradiation temperature
(Exposure 4.5×10^{20} n/cm² with energies > 0.18 MeV)

○ CSF ⊥ ▲ A ∥
△ A ⊥ ■ B ∥
□ B ⊥

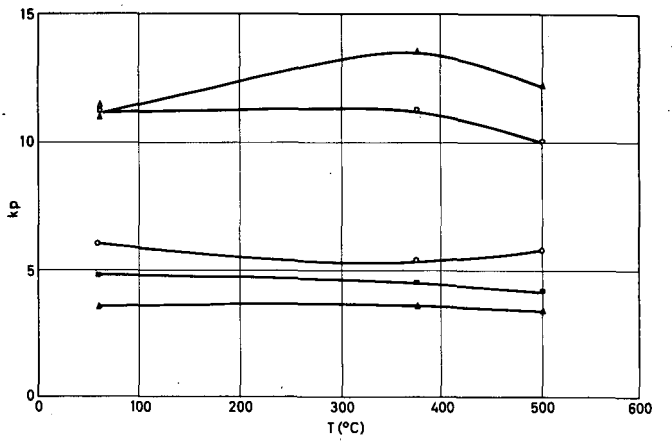


Fig. 9

Changes in bending strength with irradiation temperature
(Exposure 7.5 × 10^{19} n/cm² with energies > 0.18 MeV, 5mm square sample)

○ CSF ⊥ ▲ A ∥
△ A ⊥ ■ B ∥
□ B ⊥

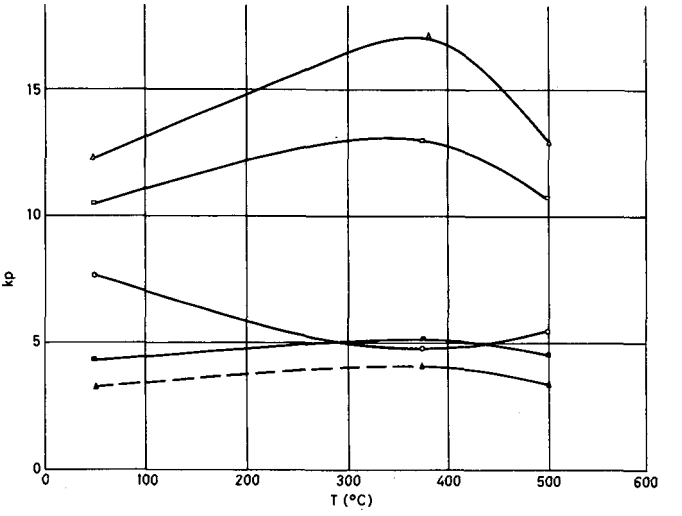


Fig. 10

Changes in bending strength with irradiation temperature
(Exposure 4.5 × 10^{20} n/cm² with energies > 0.18 MeV, 5-mm square sample)

○ CSF ⊥ ▲ A ∥
△ A ⊥ ■ B ∥
□ B ⊥

sample through a 10-mm radius, cylindrical section. Because of inevitable notch effects resulting from small cracks or larger pores, the values obtained cannot be converted to the commonly used unit kp*/cm². Much smaller values are found in 5-mm square samples as compared with those resulting from 10-mm square samples. Therefore the numbers on the ordinates of the graphs give only a relative measure.

Again these figures indicate the considerable difference in the bending strength in both directions, caused by the strong anisotropy. While both perpendicular-cut natural graphite samples have a very high bending strength, the values of the A(||) and B(||) samples are a little below those of CSF.

The nature of the bending strength against irradiation temperature curve is very interesting. Whereas all natural graphite curves are convex, those of CSF graphite are concave. Two competing effects seem to overlap. It is assumed that at first (lower-temperature condition) there is an increase in strength due to the formation of bridges between neighbouring grains. The easily-mobile groups of interstitials must be responsible for this effect, some of which migrate to the grain boundaries and form the connexion. At higher temperatures the rate of production of groups of interstitials becomes less and less because of the high rate of recombination. This may explain the falling portion of the bending-strength curve. The diffusion of vacancies to the grain boundary, where they are able to form small pores and thus loosen the texture, must be of minor importance in this temperature range. As the average crystallite or grain size is much higher in natural graphite than in artificial graphite, this initial increase and subsequent decrease in bending strength should occur strongly here, the more so since there is very little pore volume at the beginning. This effect is greater in natural graphite without binder, as would be expected.

8. CONCLUSIONS

The investigations carried out on these graphite grades show clearly the limitations and possibilities of moulded natural graphite in reactor construction.

At ambient irradiation temperatures, due to the strong anisotropy of the moulded blocks and because of their high density, dimension changes are already so considerable that even a relatively low neutron dose of about 10^{19}n/cm², E > 0.18 MeV is not tolerable.

These high damage rates increasingly disappear with rising irradiation temperature. By about 500°C all property changes investigated are of the same magnitude as those of CSF graphite. There is also very little difference in the strength factors. Therefore in this temperature region the use of natural-graphite grades in reactor construction should be possible at the present stage of development. Compared with the commonly used artificial graphite, the higher density and lower permeability should also be advantageous.

---

* kp: kilo-pond or kilogram weight.

REFERENCES

[1] WIRTZ, K., Prof. UN Int. Conf. PUAE 8 (1956) 496.
[2] LIPSDORF, K., SCHAFER, R., SPENCER, G. and WEGE, E., Fuel Element Fabrication, Academic Press (1961) 179.
[3] WOODS, W.K., BUPP, L.P. and FLETCHER, I.F., Proc. UN Int. Conf. PUAE 7 (1956) 455.
[4] NIGHTINGALE, R.E. and SNYDER, W.A., Third Conf. Carbon (1957) 575.
[5] SPALARIS, C.N., Third Conf. Carbon (1957) 575.
[6] NIGHTINGALE, R.E., DAVIDSON, J.M. and SNYDER, W.A., Proc. 2nd UN Int. Conf. PUAE 7 (1958) 295.
[7] DAVIDSON, J.M. and HELM, J.W., Fourth Conf. Carbon (1959) 599.
[8] DAVIDSON, J.M. and HELM, J.W., Fifth Conf. Carbon (1961).
[9] NIGHTINGALE, R.E. and FLETCHER, J.F., USAEC Rpt. HW - 47776 (26 Sept. 1957).
[10] DURAND, R.E. and KLEIN, D.J., USAEC Rpt. NAA - SR - 1520 (15 July 1956).
[11] HENNIG, G.R. and HOVE, L.E., Proc. UN Int. Conf. PUAE 7 (1956) 666.

ÉVOLUTION DES PROPRIÉTÉS PHYSIQUES DE GRAPHITE SOUS L'EFFET D'IRRADIATIONS ET DE RECUITS SUCCESSIFS

J. RAPPENEAU, A. FILLATRE, G. MICAUD ET M. QUETIER
CENTRE D'ÉTUDES NUCLÉAIRES DE SACLAY,
GIF-SUR-YVETTE (S. & O.), FRANCE

Abstract — Résumé — Аннотация — Resumen

CHANGES IN THE PHYSICAL PROPERTIES OF GRAPHITE DUE TO REPEATED IRRADIATION AND ANNEALING. Under the effect of neutron irradiation at fairly low temperatures (40 - 150°C) graphite stores energy and the initial physical properties, such as thermal conductivity, crystal parameters, etc. are quickly altered. The graphite moderator of reactors operating at these temperatures must therefore be annealed fairly frequently. This is the case with the G.1 reactor at Marcoule, which has undergone three annealing operations – in 1958, 1959 and 1961.

Measuring methods have been developed for observing trends in the increase in internal energy or in the changes in thermal conductivity and crystal parameters.

After a brief reference to these methods, it is shown that with irradiated graphite the amount of energy liberated and the change $\Delta c/c$ in the parameter c increase linearly with dose at a given irradiation temperature. These relationships were established in respect of graphite which had never undergone previous annealing and of relatively weak radiation doses (of the order of 10^{20} n/cm²).

The annealing operations performed on the moderator of the G.1 reactor leave a rather low residual energy in the graphite, at least at temperatures below 400°C, but the radiation damage to the graphite does not by any means completely disappear; the recovery of the crystal parameters is therefore relatively slight.

Re-irradiation of the annealed graphite gives rise to effects which differ from those observed in graphite never having been previously annealed. Thus, before the second, third and fourth annealings of the G.1 reactor moderator, an "early effect" was observed: the energy accumulates very rapidly at the beginning of re-irradiation, irrespective of the irradiation temperature. This "early effect" disappears with fairly low irradiation doses (approximately 0.3×10^{20} n/cm²), and then the energy, at a given irradiation temperature, again increases linearly with dose, the rate of increase being approximately that observed before the first annealing of the moderator.

A study of the changes in thermal conductivity and crystal parameters seems to indicate that there is an "early effect" similar to that observed for the internal energy.

ÉVOLUTION DES PROPRIÉTÉS PHYSIQUES DU GRAPHITE SOUS L'EFFET D'IRRADIATIONS ET DE RECUITS SUCCESSIFS. Sous l'effet des rayonnements neutroniques et à des températures d'irradiation peu élevées (40 - 150°C), le graphite emmagasine de l'énergie et les propriétés physiques initiales comme la conductibilité thermique, les paramètres cristallins, etc. sont rapidement modifiées. Aussi le recuit du ralentisseur en graphite des réacteurs fonctionnant à ces températures doit-il être effectué assez fréquemment. Il en est ainsi pour la pile G.1 (Marcoule), qui a subi successivement trois opérations de recuit en 1958, 1959 et 1961.

Des méthodes de mesure ont été mises au point pour suivre, en fonction du temps, la croissance de l'énergie interne ou les modifications de la conductibilité thermique et des paramètres cristallins.

Après avoir rappelé brièvement ces méthodes, on montre que, pour du graphite irradié, la quantité d'énergie libérée et la variation $\Delta c/c$ du paramètre c augmentent linéairement avec la dose à une température d'irradiation donnée. Ces relations ont été établies pour du graphite n'ayant jamais subi de recuits antérieurs et pour des doses d'irradiation relativement faibles (de l'ordre de 10^{20} n/cm²).

Les opérations de recuit pratiquées sur le ralentisseur de la pile G.1 laissent subsister dans le graphite une énergie résiduelle assez faible, tout au moins à des températures inférieures à 400°C, mais la disparition des dommages causés au graphite par les rayonnements est très incomplète; ainsi, la guérison des paramètres cristallins est relativement faible.

La re-irradiation du graphite recuit conduit à des effets différents de ceux observés pour du graphite n'ayant jamais été recuit précédemment. Ainsi, avant les deuxième, troisième et quatrième recuits du ralen-

tisseur de la pile G.1, un «effet précoce» a été mis en évidence: l'énergie s'accumule très rapidement au début de la re-irradiation, quelle que soit la température d'irradiation. Cet «effet précoce» disparaît pour des doses d'irradiation assez faibles ($\simeq 0,3 \cdot 10^{20}$ n/cm^2), puis l'énergie, à une température d'irradiation donnée, croît à nouveau linéairement avec la dose, la vitesse de croissance étant voisine de celle observée avant le premier recuit du ralentisseur.

L'étude de l'évolution de la conductibilité thermique et des paramètres cristallins semble montrer l'existence d'un «effet précoce» analogue à celui observé pour l'énergie interne.

ИЗМЕНЕНИЕ ФИЗИЧЕСКИХ СВОЙСТВ ГРАФИТА ПОД ДЕЙСТВИЕМ ОБЛУЧЕНИЯ И ПОСЛЕДУЮЩЕГО МНОГОКРАТНОГО ОТЖИГА. Под действием нейтронного облучения при невысоких температурах (40 - 150°C) графит накапливает энергию, и его первоначальные физические свойства, например теплопроводность, кристаллические параметры и т.д., быстро изменяются. Поэтому отжиг графитовых замедлителей в реакторах, работающих при этих температурах, должен производиться довольно часто. Так обстоит дело с реактором G.1 (в Маркуле), в котором было произведено три последовательных операции отжига соответственно в 1958, 1959 и 1961 годах.

Для наблюдения за ростом внутренней энергии, в зависимости от времени или за изменениями теплопроводности и кристаллических параметров, были выработаны соответствующие методы измерений.

После краткого обзора этих методов указывается, что для облученного графита количество высвобожденной энергии и изменение $\Delta c/c$ параметра "c" возрастают пропорционально дозе при данной температуре облучения. Эти соотношения были установлены для графита, ни разу не подвергавшегося ранее предварительному отжигу, и для относительно слабых доз облучения (порядка 10^{20} н/см^2).

В результате отжига замедлителя реактора G.1 графит содержит довольно незначительную остаточную энергию, во всяком случае при температурах ниже 400°C; однако исчезновение повреждений, вызванных облучением графита, далеко не полно; поэтому восстановление кристаллических параметров происходит относительно слабо.

Повторное облучение отожженного графита приводит к результатам, отличающимся от результатов,

Повторное облучение отожженного графита приводит к результатам, отличающимся от результатов,

полученных для не отожженного ранее графита. Так, например, перед вторым, третьим и четвертым отжигами замедлителя реактора G.1 было выявлено "раннее воздействие"; энергия накапливается очень быстро в начале повторного облучения, независимо от температуры облучения. Это "раннее воздействие" исчезает при довольно слабых дозах облучения ($\simeq 0,3 \cdot 10^{20}$ н/см^2), после чего, при данной температуре облучения, энергия снова возрастает прямо пропорционально дозе. При этом скорость возрастания мало отличается от скорости, наблюдавшейся при первом отжиге замедлителя.

Изучение изменений теплопроводности и кристаллических параметров указывает на вероятность наличия "раннего воздействия", аналогичного тому, которое наблюдается для внутренней энергии.

EVOLUCIÓN DE LAS PROPIEDADES FÍSICAS DEL GRAFITO BAJO EL EFECTO DE IRRADIACIONES Y RECOCIDOS SUCESIVOS. El grafito sometido a irradiación neutrónica a temperaturas poco elevadas (de 40 - 150°C) acumula energía y los valores iniciales de sus propiedades físicas, como la conductibilidad térmica, los parámetros cristalinos, etc., sufren rápidas modificaciones. Por ello, debe procederse con frecuencia a recocer el moderador de grafito de los reactores que funcionan a esas temperaturas. Tal es el caso del reactor G.1 (Marcoule) que se ha sometido a tres operaciones de recocido en 1958, 1959 y 1961.

Se han elaborado métodos de medición para observar, en función del tiempo, el aumento de la energía interna o las modificaciones provocadas en la conductibilidad térmica y en los parámetros cristalinos.

Después de describir brevemente estos métodos, en la memoria se muestra que, en el caso del grafito irradiado, la cantidad de energía liberada y la variación $\Delta c/c$ del parámetro c aumenta proporcionalmente a la dosis para una temperatura de irradiación dada. Estas relaciones se han establecido para grafito que nunca había sufrido recocidos y para dosis de irradiación relativamente bajas (unos 10^{20} n/cm^2).

Las operaciones de recocido practicadas con el moderador del reactor G.1 dejan subsistir en el grafito una energía residual bastante pequeña, al menos a temperaturas inferiores a 400°C, pero la desaparición de los daños causados al grafito por las radiaciones dista de ser completa, por lo que la recuperación de los parámetros cristalinos es relativamente escasa.

La reirradiación del grafito recocido da lugar a efectos diferentes de los observados en el caso del grafito que no ha sufrido recocido alguno. Así, antes del recocido segundo, tercero y cuarto del moderador del reactor G.1, se ha puesto de manifiesto un «efecto precoz» : la energía se acumula muy rápidamente al principio de la reirradiación, sea cual fuere la temperatura a la cual se lleve a cabo esta operación. Este

«efecto precoz» desaparece para dosis de irradiación bastante bajas ($\simeq 0,3 \cdot 10^{20}$ n/cm^2) y después, a una temperatura de irradiación dada, la energía aumenta de nuevo proporcionalmente a la dosis, siendo la velocidad de aumento comparable a la observada antes del primer recocido del moderador.

El estudio de la evolución de la conductibilidad térmica y de los parámetros cristalinos parece mostrar la existencia de un «efecto precoz» análogo al observado en el caso de la energía interna.

INTRODUCTION

On sait que le bombardement du graphite par des neutrons rapides provoque le déplacement des atomes de carbone hors de leur position normale dans le réseau cristallin. Les atomes éjectés de leur position d'équilibre créent des lacunes et occupent, après ralentissement, des positions interstitielles. Il en résulte en fonction des conditions d'irradiation un ensemble de défauts complexes et le graphite irradié est dans un état métastable.

Par élévation de température, les défauts créés par l'irradiation peuvent être guéris à condition que la température soit assez élevée pour que la mobilité des défauts soit suffisamment grande. Cette recombinaison des défauts dont le mécanisme n'est pas simple, s'accompagne d'un dégagement de chaleur et l'énergie libérée par élévation de température peut, dans certains cas, être importante. Ainsi, il est bien connu que pour des températures d'irradiation comprises entre l'ambiante et 100°C, l'énergie H s'accumule rapidement et l'enthalpie différentielle $dH/d\theta$ présente un «pic» situé à la température de 200°C qui peut dépasser, dans certains cas, la chaleur spécifique du graphite non irradié. Le réchauffage d'un graphite irradié dans ces conditions provoque un dégagement de chaleur spontané lorsque le matériau atteint une température appelée «température de déclenchement» (voir par. III,1).

Ainsi, on conçoit que le modérateur de graphite d'un réacteur fonctionnant à des températures relativement basses, emmagasine rapidement de l'énergie. Un faible échauffement du modérateur peut conduire, dans certains cas, à une élévation brutale de température qui peut endommager le réacteur. Pour éviter de tels incidents, on procède périodiquement au recuit des empilements de graphite. Toutefois, sous l'effet des rayonnements, le graphite emmagasine non seulement de l'énergie mais subit une altération de toutes ses propriétés physiques. Après un certain temps d'irradiation, on observe des variations de la conductibilité thermique, des caractéristiques mécaniques, des dimensions géométriques et des paramètres cristallins. Par suite, suivant la conception du réacteur considéré, le recuit peut être imposé par la quantité d'énergie emmagasinée ou par la variation des dimensions géométriques. La fréquence des recuits dépend évidemment des dommages créés en fonction du temps et plusieurs réacteurs tels le réacteur de Brookhaven (USA), le réacteur BEPO (Grande-Bretagne) et le réacteur G1 (Marcoule, France) subissent périodiquement des recuits.

Le réacteur G1, installé à Marcoule, fonctionne depuis 1956 et les températures d'irradiation du graphite comprises entre 40 et 150°C sont suffisamment basses pour nécessiter le recuit fréquent du modérateur. Nous avons été amenés à suivre la croissance de l'énergie dans le graphite du réacteur G1 ainsi que les dommages causés à la conductibilité thermique et aux paramètres cristallins, avant les opérations de recuit pratiquées en 1958, 1959 et 1961 et à étudier l'efficacité de ces recuits. Les résultats

obtenus seront exposés après avoir rappelé brièvement les méthodes de mesure utilisées pour étudier les dommages créés au graphite par l'irradiation.

I. MÉTHODES EXPÉRIMENTALES

1. Energie emmagasinée

Plusieurs méthodes ont été développées pour mesurer l'énergie emmagasinée par le graphite irradié; d'une part, le recuit à température constante (RTC) où le recuit semi-adiabatique (RSA) qui fournissent la quantité globale d'énergie libérée dans un intervalle de température donné; d'autre part, l'analyse thermique différentielle (ATD) qui donne l'évolution de l'enthalpie différentielle $dH/d\theta$ en fonction de la température.

Le recuit à température constante* consiste à plonger l'échantillon de graphite irradié étudié dans une enceinte à température constante θ_0. Cet échantillon contenant de l'énergie s'échauffe rapidement et sa température, en fonction du temps, suit une loi $\theta(t)$; dans certains cas, la température de l'échantillon peut atteindre une valeur θ_m supérieure à celle θ_0 de l'enceinte. Puis l'échantillon est extrait de l'enceinte, refroidi et à nouveau plongé dans l'enceinte. Ne contenant pas d'énergie libérable aux températures d'expérimentation, l'échantillon s'échauffe en fonction du temps suivant une loi $\theta'(t)$ différente. L'aire comprise entre les deux courbes $\theta(t)$ et $\theta'(t)$ permet de calculer la valeur de l'énergie libérée entre la température ambiante et la température θ_m. Les valeurs de θ_m dépendent de la quantité d'énergie accumulée, c'est-à-dire des conditions d'irradiation (doses et températures). En élevant la température de l'enceinte à une valeur suffisante, par exemple 400°C, on évite que la température de l'échantillon ne dépasse celle de l'enceinte, la plus grande partie de l'énergie libérable se trouvant concentrée dans le «pic» situé à 200°C. Dans ces conditions, l'énergie mesurée sur un échantillon de graphite représente la quantité globale libérée entre la température ambiante et 400°C. Cette méthode très rapide, antérieurement décrite [1, 2], permet d'étudier de nombreux échantillons et a été utilisée par d'autres expérimentateurs [3]; elle est très utile pour déterminer la répartition de l'énergie dans l'empilement de graphite d'un réacteur avant de procéder au recuit de cet empilement.

Le recuit semi-adiabatique** consiste à plonger l'échantillon dans une enceinte dont la température croît en fonction de la distance de plongée [4, 5]. Le graphite commence à libérer de l'énergie à partir d'une «température de démarrage» θ'_s et un dispositif à thermocouples permet à tout instant de maintenir l'échantillon à la même température que l'enceinte en le plongeant progressivement dans celle-ci. Ainsi, les pertes calorifiques sont réduites au minimum et la température de l'échantillon s'élève plus ou moins rapidement jusqu'à une valeur θ_a assez proche de la température adiabatique. La vitesse de montée en température dépend évidemment de la quantité d'énergie emmagasinée par le graphite et une contre-

* Cette méthode a été développée en collaboration avec A. HERPIN, CEN, Saclay (France).

** Cette méthode a été mise au point en collaboration avec P. GELIN, CEN, Saclay (France).

épreuve de chauffage donne la possibilité de déterminer la valeur de la température de démarrage θ'_s. Les courbes obtenues permettent de calculer la quantité d'énergie libérée entre les températures θ'_s et θ_a.

Cette méthode de mesure, dérivée de la méthode de recuit à température constante, est assez simple pour permettre l'obtention rapide de nombreux résultats.

L'analyse thermique différentielle consiste à chauffer à vitesse constante deux échantillons de graphite, l'un irradié, l'autre non irradié. Une enceinte métallique placée dans un four contient les deux échantillons de graphite. Elle peut être vidée d'air puis remplie d'hélium. En fonction du temps, on enregistre simultanément la différence de température entre l'échantillon irradié et l'enceinte, la différence de température entre l'échantillon non irradié et l'enceinte, et la température de l'enceinte qui varie depuis l'ambiante jusqu'à 900°C. En effectuant une épreuve, puis une contre-épreuve de chauffage, l'enthalpie différentielle $dH/d\theta$ de l'échantillon irradié peut être déterminée en fonction de la température à condition de connaître les échanges thermiques entre l'enceinte et les échantillons de graphite. L'appareil mis au point a déjà été décrit [2,5]; il est dérivé de celui de SYKES [6] qui a été employé par divers expérimentateurs [7, 8].

La mesure de l'énergie emmagasinée par le graphite irradié est difficile. Aussi, la comparaison des résultats fournis par les différentes méthodes mises en œuvre est nécessaire. Les quantités d'énergie mesurées par recuit à température constante entre la température ambiante et 400°C se sont révélées en bon accord avec les quantités d'énergie obtenues par intégration jusqu'à 400°C des spectres d'énergie déterminés par analyse thermique différentielle. La comparaison de ces deux méthodes a été faite en utilisant des échantillons de graphite irradiés dans des conditions analogues. Toutefois, des expériences récentes ont montré que la validité de la méthode de recuit à température constante pouvait être discutée pour des échantillons de graphite recuits et irradiés à nouveau. L'emploi de cette méthode de mesure est donc limité. Jusqu'à présent, les résultats obtenus par recuit semi-adiabatique et par analyse thermique différentielle se sont montrés en bon accord même pour des échantillons de graphite irradiés qui avaient subi antérieurement plusieurs recuits et plusieurs irradiations [5]. De plus, un bon accord a été observé entre les résultats obtenus au CEA et ceux publiés par différents expérimentateurs, notamment SIMMONS [9], NEUBERT, LEES [7] et NIGHTINGALE [10, 11]. L'examen des résultats obtenus par les différents expérimentateurs pour des échantillons de graphite irradiés dans des conditions voisines, a fait l'objet d'une publication antérieure [5].

2. Conductibilité thermique

Le coefficient de conductibilité thermique K est mesuré au voisinage de la température ambiante en utilisant la méthode du «transfert de chaleur». L'échantillon de graphite étudié est placé sous vide entre une source chaude et une source froide qui créent en régime permanent, un gradient de température $\Delta\theta/\Delta x$. La quantité de chaleur transférée Q est déduite de la puissance électrique et dissipée dans la source chaude en déduisant les pertes

thermiques. Le coefficient de conductibilité thermique est défini par

$$K = \frac{Q}{S} \frac{\Delta\theta}{\Delta x}$$

en désignant par S la surface de la section de l'échantillon. En effectuant deux opérations successives: d'une part, mesure de la puissance calorifique dissipée dans la source chaude en présence de l'échantillon et, d'autre part, mesure de la puissance calorifique dissipée, l'échantillon étant absent, en maintenant la source chaude à la même température que dans la 1re opération, on détermine les pertes thermiques et la quantité de chaleur Q qui a été dissipée dans l'échantillon. Cette méthode de mesure [12] fournit une précision de l'ordre de ± 3% environ sur les valeurs du coefficient de conductibilité thermique.

3. Paramètres cristallins

Les paramètres cristallins a et c du graphite sont mesurés par diffraction des rayons X en utilisant la méthode Debye-Scherrer. Sous l'effet des rayonnements, la création de lacunes et d'interstitiels dans le graphite produit un accroissement du paramètre c et une très légère contraction du paramètre a. L'accroissement $\Delta c/c$ du paramètre c est d'autant plus important que la dose est élevée et la température d'irradiation faible. Toutefois, l'irradiation produit un étalement des raies qui exige très rapidement l'utilisation d'un spectrogoniomètre. Dans ces conditions, les variations $\Delta c/c$ du paramètre c sont mesurées par déplacement des centres de gravité des raies (004) à partir de la position correspondant à l'échantillon témoin. Pour le graphite que nous étudierons dans la suite, la valeur du paramètre c_0 du produit non irradié est

$$c_0 = 6{,}717 \pm 0{,}003 \text{ Å}.$$

II. EFFETS DE L'IRRADIATION SUR LE GRAPHITE DU RÉACTEUR G1

L'empilement de graphite du réacteur G1 est consitué de deux «blocs» séparés par une fente centrale. Cette fente assure l'admission de l'air de refroidissement qui traverse les canaux horizontaux du réacteur situés de part et d'autre de la fente. Le flux est maximum au voisinage de la fente du réacteur où la température du graphite est la plus basse [13]. Aussi, les «dommages» subis par le graphite sont importants dans la région proche de la fente. A cet égard, la distribution des énergies libérées jusqu'à 400°C (RTC) des doses et des températures d'irradiation en fonction de la distance à la fente pour un canal situé dans la région centrale du réacteur, est significative (fig. 1).

Avant le 1er recuit du réacteur G1 (1958), nous nous sommes limités à l'étude de l'énergie interne accumulée et des paramètres cristallins.

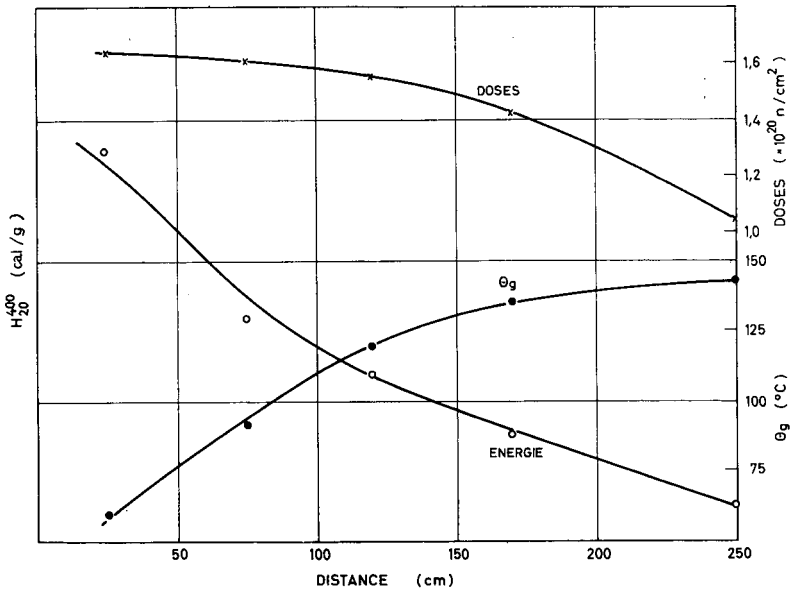


Figure 1

Energies libérées, doses et températures d'irradiation en fonction de la distance à la fente.

1. Energie interne

Les spectres d'énergie obtenus par analyse thermique différentielle pour des échantillons extraits d'un même canal, montrent la décroissance rapide de l'énergie emmagasinée lorsque la distance à la fente augmente (fig. 2). Dans différents canaux du réacteur G1, la répartition des énergies emmagasinées par le graphite en fonction des doses et des températures

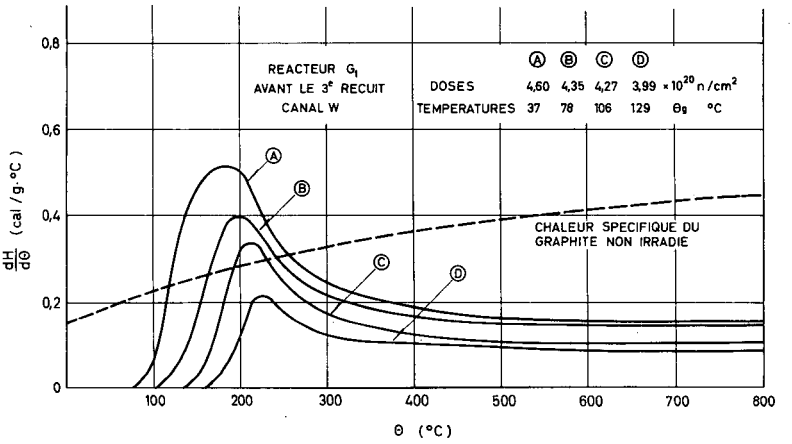


Figure 2

Energie libérée par des échantillons de graphite irradiés (non recuits).

d'irradiation a été étudiée. En prenant en considération les résultats relatifs à différents canaux, l'énergie étant mesurée soit par RTC, soit par ATD, il a été établi que la quantité d'énergie augmente linéairement avec la dose d'irradiation à une température d'irradiation donnée [2]. Cette relation linéaire (fig. 3) n'est évidemment valable que pour les faibles doses

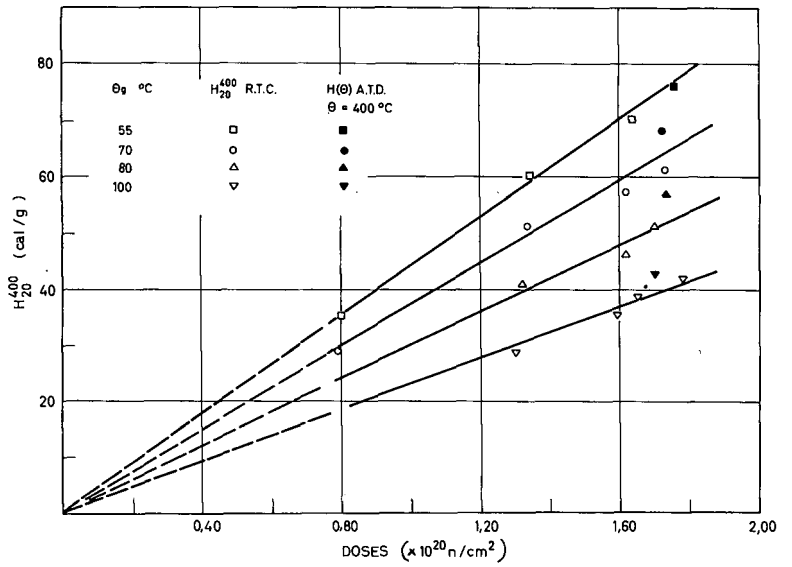


Figure 3

Croissance de l'énergie en fonction de la dose à différentes températures d'irradiation.

d'irradiation obtenues dans le réacteur. De plus, les températures d'irradiation, comprises entre 40 et 150°C, conduisent à l'accumulation de la majeure partie de l'énergie au voisinage du «pic» de 200°C. Les vitesses d'accumulation de l'énergie à une température d'irradiation donnée sont fournies par les pentes des droites représentant la croissance de l'énergie en fonction de la dose d'irradiation. Cette connaissance des vitesses d'accumulation de l'énergie permet de prévoir en fonction de la marche du réacteur, le moment où la quantité d'énergie atteindra la valeur maximum fixée pour le recuit du réacteur et par conséquent de prévoir avec une bonne approximation la date de l'opération de recuit.

2. Effets sur les paramètres cristallins

Les variations $\Delta c/c$ du paramètre c ont été mesurées sur de nombreux échantillons provenant de différents canaux. A la dose maximum d'irradiation atteinte avant le 1er recuit du réacteur ($\simeq$ de $1{,}7 \cdot 10^{20}$ n/cm^2) et pour une température d'irradiation de 60°C, les valeurs de $\Delta c/c$ sont de l'ordre de 2‰*. L'effet de l'irradiation est donc important et, en regroupant les résultats, il a été établi que l'accroissement $\Delta c/c$ du paramètre c aug-

* G. Jehanno, CEN, Saclay (France). Travail non publié.

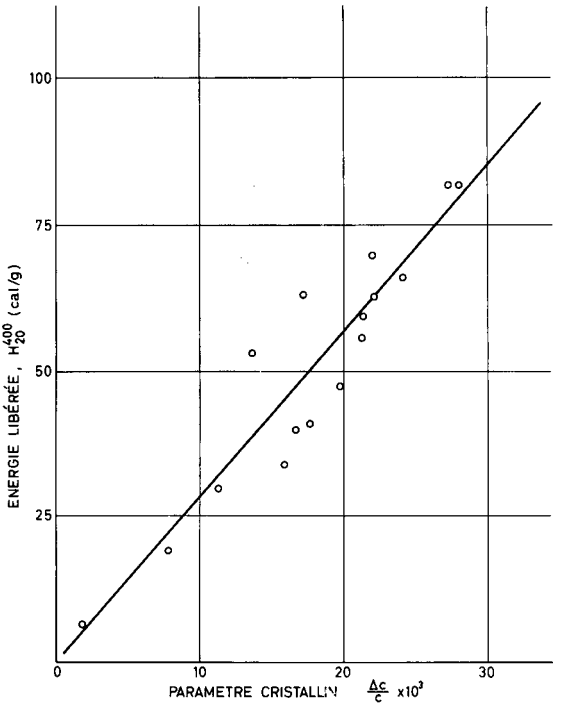


Figure 4

Energie libérée par différents graphites irradiés en fonction de la variation Δc/c du paramètre cristallin c.

mentait linéairement avec la dose à une température d'irradiation déterminée. Cette relation linéaire n'est évidemment valable que pour certaines conditions d'irradiation, c'est-à-dire que les restrictions faites précédemment au paragraphe II, 1 pour l'énergie interne, sont applicables aux variations de paramètre. Par suite, il existe une relation linéaire entre les énergies libérées jusqu'à 400°C par les échantillons de graphite irradié étudiés et les variations correspondantes Δc/c du paramètre c (fig. 4). Sans aucun doute cette relation, limitée à des doses pas trop élevées, peut permettre de compléter les données acquises sur l'énergie interne.

3. 1er recuit du réacteur G1

Lorsque l'énergie interne libérable entre la température ambiante et 400°C a atteint 75 cal/g environ au voisinage de la fente du réacteur G1, la 1re opération de recuit de l'empilement de graphite a été effectuée. Cette opération pratiquée en septembre 1958 n'a laissé subsister qu'une faible fraction d'énergie libérable à basse température. L'efficacité de la guérison définie par

$$g\,\% = 100\,\frac{H_i - H_r}{H_i}$$

en désignant par H_i et H_r les énergies initiales et résiduelles libérables entre

la température ambiante et 400°C a été satisfaisante. La majeure partie de l'énergie localisée dans le «pic» situé vers 200°C a été éliminée [2] et les mesures effectuées avant et après le recuit de l'empilement de graphite ont montré que les valeurs de g étaient de l'ordre de 85% au voisinage de la fente du réacteur. Par contre, les paramètres cristallins ont subi une guérison très partielle et beaucoup plus faible que celle de l'énergie emmagasinée. Elle atteint au maximum 30% au voisinage de la fente du réacteur et pour tenter d'expliquer ce résultat, une étude de la guérison du paramètre a été faite par Jehanno sur des échantillons de graphite irradié qui ont subi divers recuits thermiques en laboratoire dans des conditions bien définies. Le processus de guérison du paramètre cristallin a été déterminé, la courbe de variation de la quantité $d(c)/d\theta$ en fonction de θ présente un «pic» situé à la température de 500°C [14]. Aussi, la guérison du paramètre ne peut être que faible par rapport à celle de l'énergie interne, les deux pics étant situés à des températures très différentes et les températures maximales atteintes lors de l'opération de recuit ne dépassant pas 300°C, cette valeur étant limitée par la sécurité de certains éléments du réacteur.

III. EFFETS DE L'IRRADIATION SUR LE GRAPHITE RECUIT

Le traitement du graphite irradié dans les conditions de recuit du réacteur élimine la majeure partie de l'énergie concentrée dans le «pic» situé vers 200°C, mais les propriétés physiques initiales du matériau ne sont que très partiellement rétablies. Il en est ainsi pour les paramètres cristallins (par. II, 3) et pour les caractéristiques mécaniques [15] ou dimensionnelles du graphite. De plus, l'énergie accumulée à des températures supérieures à celles atteintes pendant l'opération de recuit subsiste dans le graphite.

La re-irradiation du graphite recuit peut conduire, du fait des dommages subsistant dans le matériau, à des effets différents de ceux observés pour le graphite non recuit.

Les effets suivants des rayonnements sur le graphite constituant l'empilement du réacteur G1 ont été étudiés:

1. Avant le 2^{e} recuit, en mesurant les quantités d'énergie interne; la deuxième opération de recuit a été pratiquée en novembre 1959.
2. Avant le 3^{e} recuit, en mesurant non seulement les quantités d'énergie accumulée mais aussi les conductibilités thermiques et les paramètres cristallins; le 3^{e} recuit a été pratiqué en Juin 1961.
3 Avant le 4^{e} recuit en suivant les mêmes propriétés qu'avant le 3^{e} recuit; actuellement, le réacteur G1 est en fonctionnement et la 4^{e} opération de recuit sera pratiquée ultérieurement.

Les effets des recuits et des re-irradiations successives sur la croissance de l'énergie interne, les conductibilités thermiques et les paramètres cristallins seront examinés successivement.

1. Energie interne

Les prélèvements de graphite effectués dans plusieurs canaux du réacteur G1 à différentes époques ont permis d'étudier la croissance de l'énergie

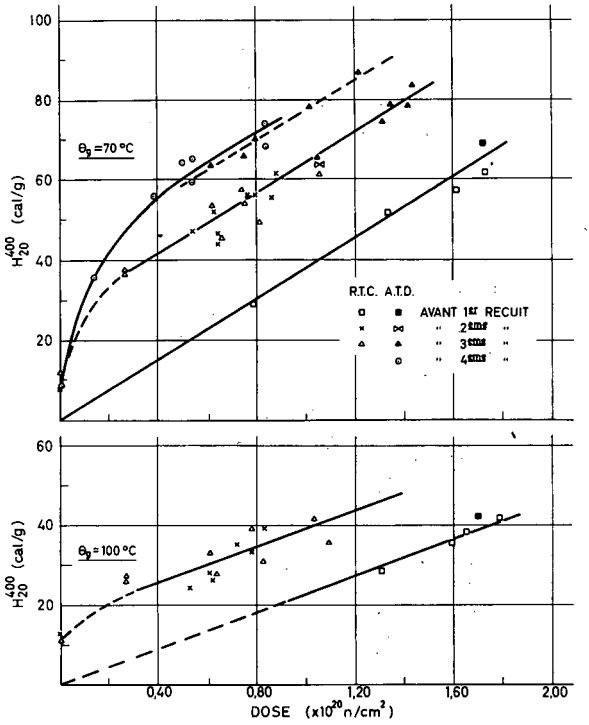


Figure 5a

Croissance de l'énergie en fonction de la dose à différentes températures d'irradiation (55 et 60°C).

en fonction du temps d'irradiation avant les 2e, 3e et 4e recuits. Au début de la re-irradiation du graphite, une croissance rapide de l'énergie a été observée en fonction de la dose quelle que soit la température d'irradiation (fig. 5a et 5b). Lorsque la dose d'irradiation atteint 0,3 à 0,4 . 10^{20} n/cm^2, l'énergie croît plus lentement et à une vitesse sensiblement analogue à celle observée pour du graphite non recuit. Cette croissance rapide de l'énergie au début de la re-irradiation du graphite a été constatée avant les 2e et 3e recuits du réacteur G1 mais,pour préciser la forme des courbes de croissance de l'énergie, des prélèvements ont été faits à des doses d'irradiation faible (inférieures à $0,3 \cdot 10^{20}$ n/cm^2) avant le 4e recuit. On constate que l'énergie augmente très rapidement dès le début de la re-irradiation du graphite (fig. 5a et 5b). On remarquera, compte-tenu des incertitudes sur les doses et les températures d'irradiation, que les valeurs de l'énergie libérable jusqu'à 400°C mesurées avant le 2e recuit sont du même ordre de grandeur pour une même dose et une même température d'irradiation que celles mesurées avant le 3e recuit. L'énergie croît linéairement en fonction de la dose lorsque celle-ci est supérieure à $0,3 \cdot 10^{20}$ n/cm^2 et la plupart des points expérimentaux se groupent autour d'une même «droite moyenne». Cependant, certains points obtenus avant le 3e recuit ne sont pas situés sur cette «droite moyenne» mais sur une droite parallèle. Ils correspondent à des échantillons de graphite issus de canaux peu recuits au cours des précédentes

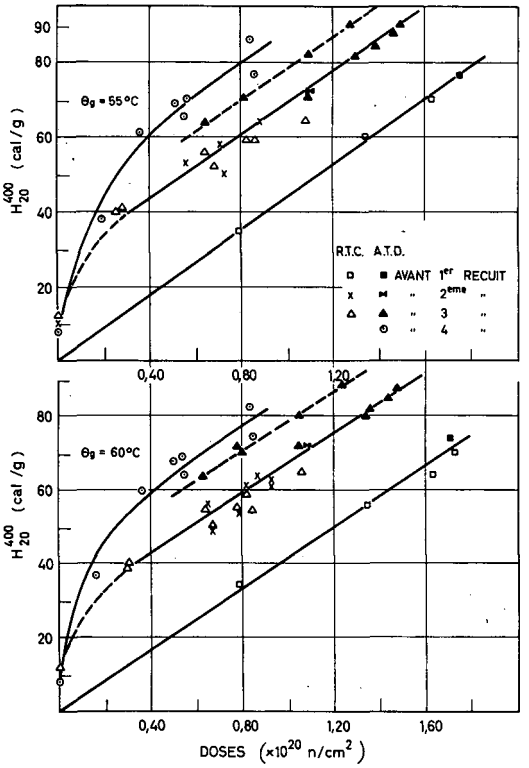


Figure 5b

Croissance de l'énergie en fonction de la dose à différentes températures d'irradiation (70 et 100°C).

opérations de recuit du réacteur G1. L'énergie emmagasinée à une température et à une dose d'irradiation déterminée dans ces canaux particuliers est plus élevée que dans l'ensemble des canaux étudiés, mais la vitesse d'accumulation de l'énergie demeure la même. Après le 3e recuit, l'énergie a crû très rapidement au début de la re-irradiation du graphite et il semble que la «droite moyenne» obtenue à partir des mesures faites sur des échantillons issus de différents canaux se situe à un niveau plus élevé. Si un tel phénomène devait se confirmer, il aurait pour conséquence l'augmentation de la fréquence des recuits si ceux-ci sont toujours effectués à la même énergie maximum.

L'accroissement rapide de l'énergie au début de la re-irradiation du graphite peut être interprété comme un «effet précoce» dû à la «fragilisation» de certains atomes de carbone. Le recuit du graphite ne rétablit que très partiellement les propriétés initiales du matériau et certains atomes de carbone peuvent être amenés à nouveau dans un état métastable par des neutrons animés d'une énergie moins grande que s'il s'agissait de graphite non recuit. Pour bien vérifier l'existence de cet «effet précoce», des échantillons de graphite irradié prélevés avant le 2e recuit, ont été recuits en laboratoire jusqu'à 400°C et l'énergie libérée a été mesurée (tableau I). Ces échantillons recuits ont été placés dans une cartouche d'irradiation

TABLEAU I

ÉNERGIE LIBERÉE PAR DES ÉCHANTILLONS DE GRAPHITE IRRADIÉ PRÉLEVÉS DANS LE RÉACTEUR G1 AVANT LE 2e RECUIT

Echantillons	Température d'irradiation (θ_g°C)	Doses ($\times 10^{20}$ n/cm^2)	H(θ)400 (cal/g)
a	53	1,24	67
b	65	1,20	64
c	72	1,17	59
d	86	1,16	48
e	101	1,15	32
f	125	1,07	18

avec des échantillons de graphite n'ayant jamais été irradiés. Après irradiation de l'ensemble de ces échantillons à une dose de $1{,}11 \cdot 10^{20}$ n/cm^2 et à une température de 130°C environ, l'énergie de ces différents échantillons a été à nouveau mesurée. On a constaté que tous les échantillons de graphite n'ayant jamais été irradiés avaient libéré la même quantité d'énergie jusqu'à 400°C. Par contre, les échantillons de graphite recuits, puis re-irradiés, libéraient des quantités d'énergie supérieures à celles mesurées sur les échantillons irradiés et non recuits (tableau II). Celles-ci étaient d'autant plus importantes que les «dommages» créés avant le recuit de ces échantillons étaient grands (tableau I). Ces résultats vérifient bien l'existence de «l'effet précoce» observé sur les échantillons prélevés directement dans les canaux du réacteur G1 en fonction du temps.

Par ailleurs, la re-irradiation du graphite recuit provoque simultanément la modification du spectre d'énergie. En fonction des recuits successifs pratiqués sur l'empilement de graphite du réacteur G1 le «pic» d'énergie s'élargit et l'ordonnée $(dH/d\theta)_m$ du maximum du «pic» diminue en accord avec les résultats publiés par d'autres auteurs [16]; enfin, l'énergie accumulée entre 400°C et 800°C sur laquelle les opérations de recuit n'ont pas d'influence, augmente. L'évolution des spectres d'énergie avant les 1er, 2e et 3e recuits apparaît nettement [2] (fig. 2 et 6) et ne semble pas liée à l'efficacité de la guérison de l'empilement qui était à peu près la même pour les 3 opérations de recuit dans la région proche de la fente du réacteur. Il semble plutôt que l'évolution du spectre d'énergie soit liée à la création de défauts de plus en plus complexes et à l'apparition au début de la re-irradiation de «l'effet précoce». Toutefois, si les recuits du graphite suivis d'irradiation provoquent une modification de la forme du spectre d'énergie, les températures caractéristiques du spectre (température de seuil θ_s, température de déclenchement θ_d, et température du maximum du «pic» d'énergie θ_m) paraissent ne pas évoluer en fonction des recuits tout au moins

TABLEAU II

ÉNERGIE LIBÉRÉE PAR DES ÉCHANTILLONS DE GRAPHITE «RECUITS» ET «NON RECUITS» IRRADIÉS SIMULTANÉMENT*

Echantillons recuits a 400°C et re-irradiés				Echantillons irradiés (1re irradiation)		
N°	H(θ)400 (cal/g)	H(θ)800 (cal/g)		N°	H(θ)400 (cal/g)	H(θ)800 (cal/g)
a	26	65		a1	15	27
b	26	66		a2	14	25
c	25	65		a3	14	26
d	21	58				
e	19	53				
f	19	48				

* Conditions d'irradiation: Dose: $1{,}11 \cdot 10^{20}$ n/cm²
Température: 134°C

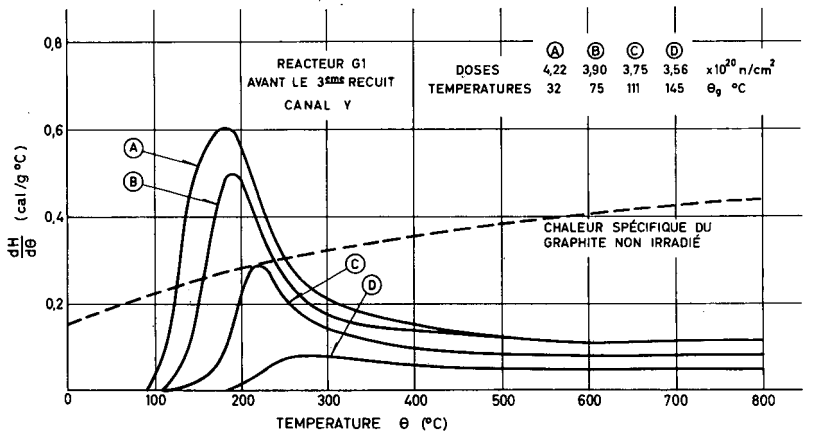


Figure 6

Energies libérées par des échantillons de graphite après deux recuits intermédiaires (canal W).

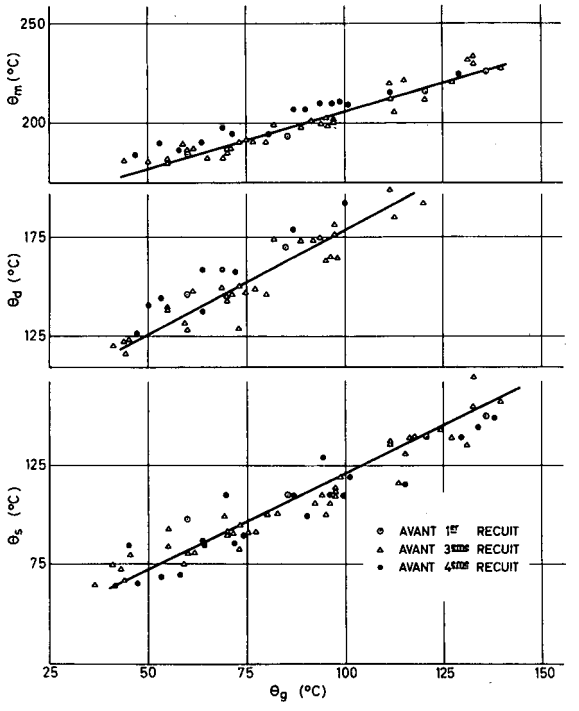


Figure 7

Evolution des « températures caractéristiques » du pic d'énergie en fonction de la température d'irradiation du graphite.

jusqu'à présent. En effet, les valeurs des températures θ_s, θ_d, et θ_m, déterminées sur des échantillons de graphite prélevés dans l'empilement du réacteur G1 avant les différents recuits, sont en bon accord et dépendent essentiellement de la température d'irradiation θ_g du graphite (fig. 7). La corrélation $\theta_d = f(\theta_g)$ est cependant moins satisfaisante que celle obtenue à partir des températures θ_s et θ_m. Les points expérimentaux présentent une certaine dispersion qui peut être attribuée au fait que la température de déclenchement θ_d dépend, non seulement de la température d'irradiation θ_g du graphite, mais aussi de la dose d'irradiation. Par suite, la corrélation $\theta_d = f(\theta_g)$ est plus satisfaisante pour des échantillons ayant reçus des doses d'irradiation voisines, ce qui n'est pas le cas pour tous les points relatifs aux températures de déclenchement représentées sur la figure 7. On remarquera que la relation étroite existant entre la température θ_s et la température d'irradiation θ_g du graphite avait été observée antérieurement par d'autres auteurs [17].

Ces résultats paraissent mettre en évidence l'existence de «niveaux de dommages» différents, les «défauts complexes» créés par irradiation pouvant être remplacés par des «défauts encore plus complexes» dus aux processus de guérison antérieurs. Chaque canal ou chaque groupe de canaux semble étroitement lié à son histoire antérieure et, à un moment donné, pour des quantités d'énergie égales (libérables jusqu'à 400°C), les spectres d'énergie peuvent être plus ou moins modifiés, ce qui correspondrait à des niveaux de dommages variables. Les spectres d'énergie obtenus avant le 3e recuit de l'empilement du réacteur G1 à partir d'échantillons prélevés dans deux canaux (W et Y) irradiés dans des conditions sensiblement analogues sont, à cet égard, significatifs (fig. 6 et 8). Comme nous le verrons dans la suite, il ne s'agit pas de dommages propres à l'énergie interne et les mesures de conductibilité thermique et des variations $\Delta c/c$ du paramètre cristallin c conduisent à des interprétations semblables.

2. Conductibilité thermique

Malgré les opérations de recuit intermédiaires, l'irradiation a conduit à une détérioration sensible de la conductibilité thermique du graphite de l'empilement du réacteur G1. Aussi, avant la 3e opération de recuit, la conductibilité thermique du graphite irradié K_i mesurée à la température ambiante est environ 25 à 35 fois plus faible que la conductiblité thermique initiale K_0. Evidemment, au voisinage de la fente du réacteur, les dommages sont plus importants, les valeurs du rapport $[(K_0/K_i) - 1]$ atteignant au maximum 39.

On sait que pour du graphite irradié n'ayant jamais subi de recuits antérieurs, l'énergie totale libérée H_t peut être reliée à la conductibilité thermique par une relation de la forme $H_t = a[(K_0/K_i) - 1]$. Cette relation est à peu près linéaire pour des doses d'irradiation pas trop élevées. A des doses d'irradiation faible, on peut admettre que l'énergie H_t est suffisamment proche de la quantité $H(\theta)$ 800 déterminée par intégration du spectre d'énergie (ATD) pour tenter d'appliquer cette relation aux résultats obtenus avant le 3e recuit. A partir des échantillons issus des deux canaux précédemment étudiés en énergie interne, on obtient alors deux droites distinctes (fig. 9). Pour une même énergie $H(\theta)$ 800, les dommages causés

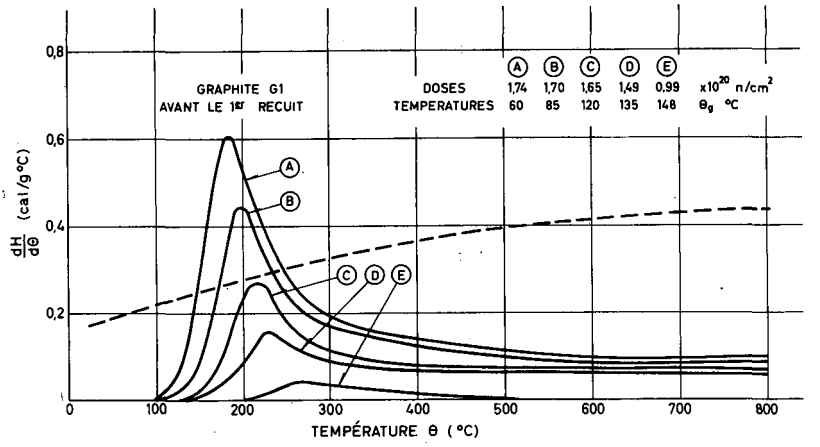


Figure 8

Energies libérées par des échantillons de graphite après deux recuits intermédiaires (canal Y).

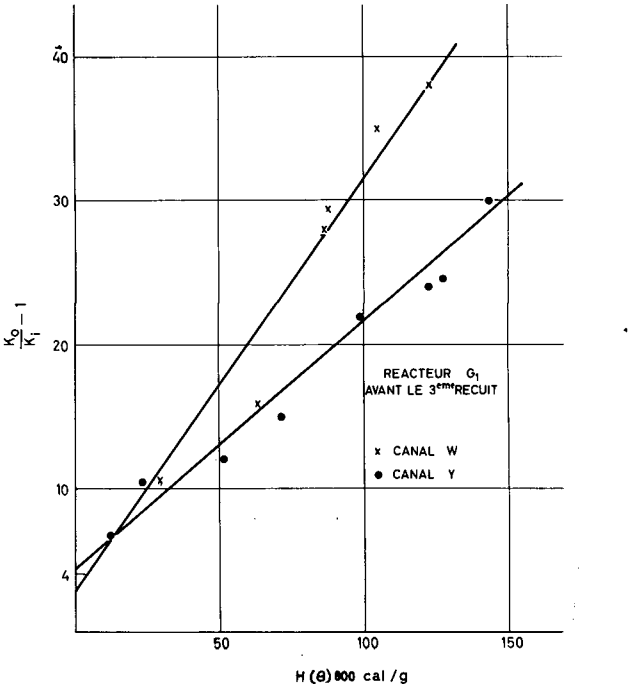


Figure 9

Relation énergie libérée-conductibilité thermique.

à la conductibilité thermique du graphite sont plus importants pour les échantillons issus du canal où le spectre d'énergie est le plus déformé (aplatissement du spectre). Les «dommages» peuvent donc être très différents d'un canal à l'autre pour une même quantité d'énergie libérée.

Après le 3e recuit, le réacteur G1 a été remis en marche et de la même manière que la croissance de l'énergie a été suivie, les dommages causés à la conductibilité thermique ont été étudiés. En fonction de la dose d'irradiation on a observé comme pour l'énergie interne l'existence d'un «effet précoce» quelle que soit la température d'irradiation (fig. 10). La conduc-

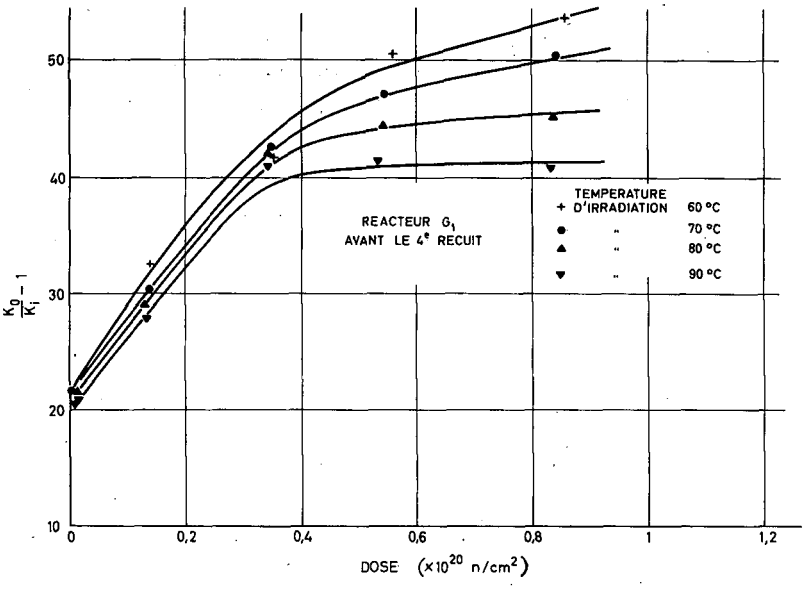


Figure 10

Croissance des dommages créés à la conductibilité thermique en fonction de la dose à différentes températures d'irradiation.

tibilité thermique diminue très rapidement au début de la re-irradiation du graphite jusqu'à des doses de l'ordre de $0,3 \cdot 10^{20}$ n/cm^2, puis plus lentement pour des doses d'irradiation supérieures.

Les résultats obtenus à partir des mesures de la conductibilité thermique du graphite recuit puis re-irradié sont donc en bon accord avec les résultats relatifs à l'énergie interne.

3. Paramètres cristallins

L'accroissement $\Delta c/c$ du paramètre cristallin c sous l'effet des rayonnements a été peu guéri au cours des opérations de recuits pratiquées sur l'empilement de graphite du réacteur G1 (par. II, 3). Avant le 3e recuit de l'empilement, les valeurs $\Delta c/c$ obtenues au voisinage de la fente, de l'ordre de 2,5%, montraient que l'accroissement du paramètre était important. Avant le 1er recuit de l'empilement une relation linéaire entre

l'énergie interne H(θ)400 et la variation Δc/c du paramètre c avait été mise en évidence (fig. 4). Les mesures de Δc/c faites avant le 3e recuit sur les échantillons issus des deux canaux précédemment étudiés montrent que l'on obtient en fonction de l'énergie H(θ)400 deux droites distinctes qui présentent toutes deux une abcisse à l'origine (fig. 11). Pour une même énergie H(θ)400, l'accroissement Δc/c du paramètre c est moindre pour les échantillons de graphite issus du canal qui présentent des spectres d'énergie moins déformés. Il y a donc une excellente corrélation entre les mesures d'énergie interne, de conductibilité thermique et de paramètres cristallins et la notion de «niveaux de dommages» précédemment suggérée semble valable.

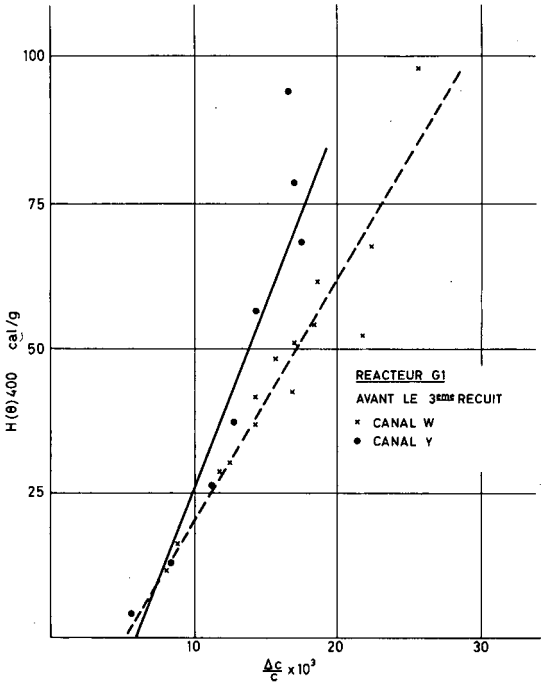


Figure 11

Relation énergie libérée-accroissement Δc/c du paramètre c.

Après le 3e recuit, l'accroissement Δc/c du paramètre c a été suivi en fonction de la dose d'irradiation de la même manière que pour la conductibilité thermique et l'énergie interne. Au début de la re-irradiation les valeurs de Δc/c augmentent très rapidement jusqu'à une dose de l'ordre de $0{,}3 \cdot 10^{20}$ n/cm² puis ensuite plus lentement mettant ainsi en évidence l'existence d'un «effet précoce» (fig. 12). Cet «effet précoce» relatif au paramètre cristallin est en relation étroite avec celui observé pour la conductibilité thermique et l'énergie interne.

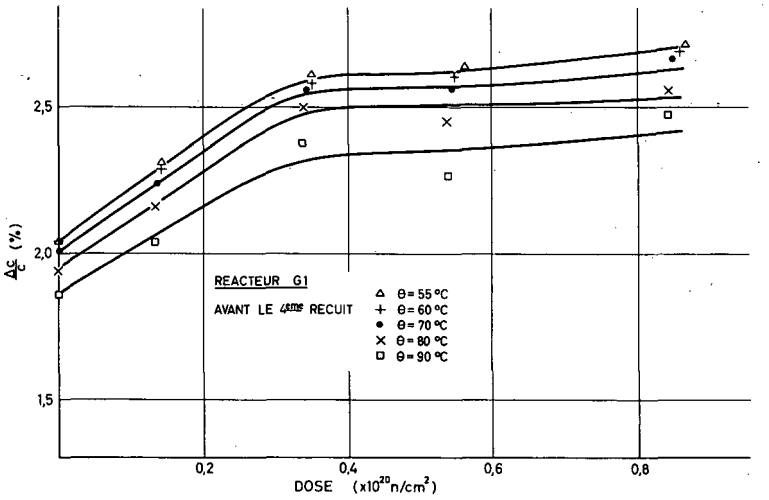


Figure 12

Variation Δc/c du paramètre c en fonction de la dose à différentes températures d'irradiation.

IV. CONCLUSION

En définitive, l'étude des échantillons de graphite prélevés dans le réacteur G1 avant les différents recuits montre que sous l'effet des rayonnements le comportement du graphite recuit est différent de celui n'ayant jamais subi de recuits antérieurs. Au début de la re-irradiation du graphite un «effet précoce» qui semble intéresser toutes les propriétés physiques du graphite a été mis en évidence. Les «dommages» augmentent très rapidement au début de la re-irradiation.

Sous l'influence des recuits les «dommages » peuvent être différents d'un canal du réacteur à un autre canal, irradié dans des conditions analogues. A une même quantité d'énergie intégrée libérable peuvent correspondre deux spectres d'énergie, l'un très aplati et l'autre beaucoup moins. Aux spectres d'énergie très aplatis correspondent des conductibilités thermiques plus faibles et des variations Δc/c plus grandes que pour des spectres d'énergie moins modifiés présentant la même énergie libérable. Les «niveaux de dommages» peuvent donc être différents et les «défauts complexes» créés par irradiation remplacés par des «défauts encore plus complexes» dus aux processus de guérison antérieurs.

Sur le plan pratique, l'existence de «l'effet précoce» et des défauts de plus en plus complexes peut conduire à une accumulation plus rapide des dommages. Celle-ci aurait pour conséquence un accroissement de la fréquence des opérations de recuits en admettant que les recuits soient toujours effectués à la même énergie maximum.

De ce fait, il pourrait en résulter une durée de vie limitée pour les réacteurs du type G1.

RÉFÉRENCES

[1] RAPPENEAU, J., Bull. inform. Scient. et Tech. du CEA n° 48 (1961) 27.

[2] QUETIER, M. and RAPPENEAU, J., Properties of reactor materials and the effects of radiation damage, Butterworths, London (1962) 208-18.

[3] BELL, J.C. and SIMMONS, J.H.W., US/UK Graphite Conference (London) (1957) 82.

[4] GELIN, P., RAPPENEAU, J., BRUNETON, C. et QUETIER, M., Rapport CEA n° 2 241, CEN, Saclay (Mai 1962).

[5] RAPPENEAU, J., J. nucl. Mater. 6 (1962) 107.

[6] SYKES, C., Proc. Roy. Soc. (London) A. 148 (1935) 422.

[7] NEUBERT, T.J. and LEES, R.B., Nucl. Sci. Engng 2 (1957) 748-767.

[8] NEUBERT, T.J., BURTON, M. et al., ANL-Report 5472 (1956) 126.

[9] SIMMONS, J.H.W., US/UK Graphite Conference (London) (1957) 91.

[10] NIGHTINGALE, R.E. and FLETCHER, J.F., Rapport H.W. 47776 EV. - Gen. Electric (Hanford) (1957).

[11] NIGHTINGALE, R.E., DAVIDSON, J.H. and SNYDER, W.A., «Dommages causés au graphite irradié jusqu'à 1000°C», 2e Conf. int. ONU util. EAFP, 4 (1958) 574.

[12] BOCQUET, M. et MICAUD, G., Rapport CEA n° 2 242, CEN Saclay (Avril 1962).

[13] BUSSAC, J., LEDUC, C. et ZALESKI, C.P., Rapport CEA n° 670 A (1957).

[14] Bull. Inf. Scient. et Tech. du CEA n° 31 (1959) 91.

[15] JOUQUET, G. and RAPPENEAU, J., Properties of reactor materials and the effects of radiation damage, Butterworths, London (1962) 276-86.

[16] BELL, J.C. and GREENOUGH, G.B., US/UK Graphite Conference (London) (1957) 102.

[17] DICKSON, J.L., KINCHIN, G.H., JACKSON, R.F., LOMER, W.A. and SIMMONS, J.H.W., «Libération d'énergie Wigner dans BEPO», 2e Conf. int. ONU util. EAFP, 4 (1958) 539.

THE EFFECT OF HEAVY-PARTICLE BOMBARDMENT ON WIGNER-ENERGY STORAGE IN GRAPHITE

A. WILLIS AND R. PENNINCKX
CENTRE D'ÉTUDE DE L'ÉNERGIE NUCLÉAIRE,
MOL-DONK, BELGIUM

Abstract — Résumé — Аннотация — Resumen

THE EFFECT OF HEAVY-PARTICLE BOMBARDMENT ON WIGNER-ENERGY STORAGE IN GRAPHITE. The rate of Wigner energy storage can be accelerated, relative to neutron-bombarded graphite, if this base material is bombarded by suitable quantities of heavy particles. This has been shown by irradiation of porous graphite samples that were solution impregnated with uranium and boron. The particle size in these samples was so small that the heterogeneous mixture is homogeneously damaged.

The uranium and boron reaction products have large differences in mass, initial charge and reaction energy, and they give rise to different rates of energy storage. The energy storage is nearly proportional to the total kinetic energy dissipated in the graphite. Interpretation of these data provides the basis for this report.

ACTION DU BOMBARDEMENT PAR DES PARTICULES LOURDES SUR L'EMMAGASINAGE D'ÉNERGIE PAR EFFET WIGNER DANS LE GRAPHITE. On peut accélérer l'emmagasinage d'énergie par effet Wigner dans le graphite bombardé par des neutrons si cette matière est soumise au bombardement de quantités appropriées de particules lourdes. Les auteurs l'ont démontré en irradiant des échantillons de graphite poreux, imprégnés par une solution d'uranium et de bore. Dans ces échantillons, les particules étaient si petites que le mélange hétérogène a été altéré d'une manière uniforme.

Les produits de réaction de l'uranium et du bore accusent de fortes différences quant à leur masse, leur charge initiale et leur énergie de réaction, et donnent lieu à des différents taux de stockage d'énergie. L'énergie emmagasinée est presque proportionnelle à l'énergie cinétique totale dissipée dans le graphite. Le mémoire porte essentiellement sur l'interprétation de ces résultats.

ВЛИЯНИЕ БОМБАРДИРОВКИ ТЯЖЕЛЫМИ ЧАСТИЦАМИ НА АККУМУЛИРОВАНИЕ ЭНЕРГИИ ВИГНЕРА В ГРАФИТЕ. Скорость аккумулирования энергии Вигнера может быть увеличена бомбардировкой графита нейтронами при достаточном количестве тяжелых частиц. Это показывается путем облучения образцов пористого графита, которые пропитаны раствором урана и бора. Размеры частиц в этих образцах настолько малы, что гетерогенная смесь повреждается равномерно.

Урановые и боровые продукты реакции имеют большое различие в массе, первоначальной нагрузке и энергии реакции, и они вызывают различные скорости аккумулирования энергии. Аккумулирование энергии почти пропорционально общей кинетической энергии, рассеянной в графите. Интерпретация этих данных обеспечивает основу для данного доклада.

EFECTOS DEL BOMBARDEO CON PARTÍCULAS PESADAS SOBRE LA ACUMULACIÓN DE ENERGÍA DE WIGNER EN EL GRAFITO. La irradiación del grafito con cantidades adecuadas de partículas pesadas permite alcanzar un índice de acumulación de energía de Wigner más elevado que el obtenido al bombardear el mismo material con neutrones. Los autores demostraron este hecho irradiando muestras de grafito poroso impregnadas con soluciones de uranio y boro. El tamaño de las partículas de estas muestras es tan pequeño que el daño se distribuye en forma homogénea en la mezcla heterogénea.

Los productos de reacción del uranio y del boro se diferencian grandemente por su masa, su carga inicial y su energía de reacción, y dan lugar a diferentes velocidades de acumulación de energía. La acumulación de energía es prácticamente proporcional a la energía cinética total disipada en el grafito. La interpretación de estos datos constituye la base de la presente memoria.

1. INTRODUCTION

Even if Wigner energy storage in graphite did not pose an operational problem for low-temperature graphite-moderated reactors, it would still be a technically interesting phenomenon. Not many materials store such large amounts of internal energy as a result of irradiation. Our observation that heavy-particle bombardment causes acceleration of the energy storage is potentially important in identifying the characteristics of a fission spike. It couples variations in the type or nature of the damage with a material that is sensitive to damage.

In contrast to the time when this programme was started, there may be little question concerning whether uranium or boron reaction products should cause Wigner energy storage in graphite. In-pile growth is no longer considered to be a unique attribute of uranium [1, 2]. In addition, point defect models for a fission spike are currently popular. The same basic driving forces should cause Wigner energy storage. Nevertheless, the basic energy-storage process has not yet been identified.

The nuclear reaction products that are being discussed here are quite different in nuclear mass, initial charge and kinetic energy. They are compared in Table I.

TABLE I

CHARACTERISTICS OF PARTICLES WHICH CAN CAUSE WIGNER ENERGY STORAGE

Reacting particles	Reaction cross-section (b)	Reaction products		
		Mass	Initial charge	Recoil energy (MeV)
n-C	4.5 (scattering)	12	?	0.1-2
n-U^{235}	580	85; 145	+20	180
n-B^{10}	4010	4; 7	+2; +3	2.5

These particles might be expected to cause different types of damage. The neutron mean free path is quite long and the damage density will accordingly be low. The displaced carbon atoms will be similar to heavier particles of course. Fission fragments dissipate a considerably larger amount of energy in quite a small volume and, with their heavy masses, they are capable of producing large numbers of displaced carbon atoms in each collision. The boron reaction products have not only lower energy and smaller mass, but also have a smaller initial charge.

2. EXPERIMENTAL OBSERVATIONS

(1) Our first experiment in this field has already been reported [3, 4]. About a forty-fold increase in the rate of Wigner energy storage was obtained when a sample containing only 0.0332 g of uranium-235 per cubic centimetre of graphite was irradiated to 1.3×10^{18} n/cm^2 (thermal). No thermal conductivity change was apparent, based on the measured centre-temperature of the sample.

(2) A second sample containing 0.029 g of boric acid ($B_2^{11}O_3$) per gram of graphite was irradiated to 1×10^{18} n/cm^2 in the BR-1* reactor, at a temperature of 30-35°C. Annealing in a furnace calorimeter at 156 and 400°C caused the release of 3.2 ± 1 cal/g of stored energy. The measured neutron flux and the analysis of lithium content in the irradiated sample were in close agreement.

(3) Several additional boron-containing samples were irradiated for four cycles of BR-1 operation and annealed using a 200°C furnace temperature. The results are shown in Table II.

TABLE II

RELEASE OF STORED ENERGY FOR SOME BORON-CONTAINING SAMPLES

Sample (Na)	Boron content (mg B_2O_3 per g/C)	Stored energy (cal/g)
-	0	4.09
-	0	4.24
-	0	3.94
14	65.6	6.54
20	77	8.73
10	106	10.33
26	134	9.07
27	155	9.88
13	189	9.02
29	208	9.40
23	291	11.88

The measured neutron dose at the centre of sample 26 was 2.4×10^{18} n/cm^2 (thermal). The higher-than-normal energy storage in sample 10 probably arises from its relatively advantageous position in the capsule with respect

* Belgian Reactor BR-1, Centre d'Etude de l'Energie Nucléaire, Mol, Belgium.

to self-shielding. Water absorbed by the boric acid after irradiation is the major source of scatter among these results.

Graphite single crystals were irradiated between sheets of boric oxide and were examined using an electron microscope. No positive results were obtained. No unusual effects were noted.

(4) Graphite, initially containing 35 cal/g of stored energy, was impregnated with boric acid and re-irradiated. An increase of 2-5 cal/g of Wigner energy storage was obtained. A different impregnation cycle had to be used for these samples to prevent energy release during fabrication, and direct comparison with other samples is probably difficult.

3. DISCUSSION

The Wigner-energy storage caused by neutrons, fission products and boron reactions appears to be quite similar, at least over the range of exposures that have been investigated here. The shapes of the annealing curves are quite the same. The energy release starts when the sample reaches a temperature 50-60°C higher than the irradiation temperature. The peak energy release occurs at 180-200°C and little additional energy is released upon heating to 400°C.

One can infer from these experiments that the Wigner-energy storage depends most heavily upon the quantity of energy released and large differences in mass and charge of the reaction products seem unimportant. For example, the energy release for the uranium reaction is nearly 70 times greater than it is for the boron reaction. Because of the higher loading and the higher reaction cross-section, the single boron sample described as experiment 2 had a fission density that was nearly eight times higher. The energy storage is approximately one ninth as large.

The highly localized damage which is normally attributed to these heavy particles appears to be spread out in graphite. At least no strong rate-dependence of energy storage is apparent. The characteristics of the energy release for the different sources of damage are so similar that it is probable that recoiling graphite atoms are the source of energy storage.

No phenomenon similar to the "hot spikes", that have been proposed [5] to interpret in-pile annealing effects in neutron-bombarded graphite, were observed in the re-irradiated boron-containing samples. This also implies that the various types of damage that have been studied here are similar in nature in spite of the expected variations in damage density.

4. SUMMARY

Heavy-particle bombardment produces large Wigner-energy storage in graphite and the nature of this damage is quite similar to the damage caused by neutron bombardment.

REFERENCES

[1] WILLIS, A.H. and BIBB, A.E., The dimensional instability of Zr-U-alloys, USAEC Rpt. KAPL-2000-9.

[2] HORAK, J.A. and RHUDE, H.V., Letter to the editor, Irradiation growth of zirconium-plutonium alloys, J. nucl. Mat. 3 (1961) 1.

[3] WILLIS, A.H., Letter to the editor, Wigner energy storage in fission product damaged graphite, J. appl. Phys. 32 (1961) 8.

[4] WILLIS, A.H., BAUGNET, J.M. and DE BEUKELAER, R.C., Wigner energy storage in fission product damaged graphite, J. appl. Phys. 32 (1961) 1622.

[5] NIGHTINGALE, R.E., DAVIDSON, J.M. and SNYDER, W.A., Damage to graphite irradiated up to 1000°C, Proc. 2nd UN Int. Conf. PUAE 1 (1958) 295.

D. RADIATION DAMAGE IN BERYLLIUM OXIDE

(Part of Session 6)

RADIATION DAMAGE IN BeO

G. W. KEILHOLTZ, J. E. LEE, JR., R. P. SHIELDS AND W. E. BROWNING, JR.
REACTOR CHEMISTRY DIVISION, OAK RIDGE NATIONAL LABORATORY,
OAK RIDGE, TENNESSEE

Abstract — Résumé — Аннотация — Resumen

RADIATION DAMAGE IN BeO. The stability of BeO bodies under irradiation is under examination at the Oak Ridge National Laboratory. Cylindrical specimens, encapsulated in stainless steel and installed within an annulus through which a mixture of argon and helium is circulated to achieve temperature control, have been irradiated in the Engineering Test Reactor, Arco, Idaho. Specimens have been exposed to total fast (> 1 MeV) neutron dosages from 10^{20} to 2.6×10^{21} n/cm² at temperatures over the range 100 - 1100°C. In addition to observation of gross changes, specimens were examined by the techniques of X-ray diffraction, optical microscopy, metallography and electron microscopy; some specimens were dissolved for determination of their contained tritium and helium.

The greatest damage appears in bodies irradiated to high neutron dosages at low temperatures. Specimens receiving as much as 1.5×10^{21} n/cm² at about 110°C disintegrated to powder. Fractures were observed in specimens irradiated to 2.6×10^{21} n/cm² at 800 - 950°C. Some specimens exposed to intermediate dosages at intermediate temperatures have survived intact.

Significant structural differences which depend on irradiation temperature and on fabrication technique have been observed on examination of the bodies by X-ray diffraction. Diffraction patterns of both hot- and cold-pressed irradiated BeO indicate anisotropic lattice expansion ratios $(\Delta c/c_0) \div (\Delta a/a_0)$ of approximately 9.

X-ray patterns of BeO irradiated at 100°C resemble those reported for irradiated graphite. The data may be interpreted as showing, in addition to isolated point defects, the presence of small (10 - 20 atom) discs of interstitial atoms (such as Be, He, O) in semi-regular array between closely-packed planes. Strain energy in such a lattice should be high. Annealing of radiation damage effects has been observed at sufficiently high temperatures.

Helium found in the specimens increases directly with exposure to about 1.6×10^{21} n/cm² and appears to level, with higher dosages, at about 400 µl per gram of BeO; neither irradiation temperature nor extent of specimen fracture markedly affect retention of He. Tritium content is very low in specimens irradiated at temperatures above 450°C but is proportional to the square of the neutron dosage for irradiations at lower temperatures.

Thermal conductivity of the BeO was decreased on irradiation as indicated by changes in the temperature gradient across specimens as the exposure progressed. However, since no sudden discontinuities in the temperature gradient were observed, and since more than 25 samples survived the thermal cycling without cracking, thermal stress seems unlikely as the sole cause of failure. Atomic displacements or build-up of gas within the crystal or a combination of these appear to be the primary cause of failure of the bodies. Further experiments designed to permit a better separation of the several experimental variables are in progress.

ALTERATIONS DE L'OXYDE DE BÉRYLLIUM SOUS L'EFFET DES RAYONNEMENTS. Le Laboratoire national d'Oak Ridge procède actuellement à une étude sur la stabilité de pièces en BeO soumises à l'action des rayonnements. Dans le réacteur d'essai de matériaux installé à Arco (Idaho), on a irradié des échantillons cylindriques en capsules d'acier inoxydable, placés à l'intérieur d'un circuit annulaire dans lequel on a fait circuler un mélange d'argon et d'hélium pour régler la température. Les échantillons ont été exposés à des doses totales de neutrons rapides (> 1 MeV) allant de 10^{20} à $2{,}6 \cdot 10^{21}$ n/cm², à des températures comprises entre 100 et 1100°C. Après un examen sommaire des modifications grossières, on a soumis les échantillons à un examen rigoureux par les méthodes de la diffraction des rayons X, de la microscopie optique, de la métallographie et la microscopie électronique; on a dissous plusieurs de ces échantillons pour en déterminer la teneur en tritium et en hélium.

Les altérations les plus profondes apparaissent dans des pièces exposées, à basse température, à de fortes doses de neutrons. Les échantillons qui avaient reçu une dose allant jusqu'a $1{,}5 \cdot 10^{21}$ n/cm², à une température d'environ 110°C, ont été reduits en poudre. Des fractures ont été observées dans des échantillons exposés

à des doses atteignant $2,6 \cdot 10^{21}$ n/cm², entre 800 et 950°C. Quelques échantillons exposés à des doses et à des températures intermédiaires sont restés intacts.

L'examen des pièces en question par la méthode de la diffraction des rayons X a révélé d'importantes différences de structure qui dépendent de la température d'irradiation et du procédé de fabrication. Les diagrammes de diffraction du BeO aggloméré à chaud ou à froid et irradié donnent des rapports de dilatation du réseau anisotropique $(\Delta c/c_0) \div (\Delta a/a_0)$ d'environ 9.

Les diagrammes radiographiques du BeO irradié à 100°C ressemblent aux diagrammes obtenus pour le graphite irradié. On peut interpréter les données comme indiquant la présence, non seulement de défauts ponctuels isolés, mais aussi de petits disques (de 10 à 20 atomes) d'atomes interstitiels (tels que Be, He, O), disposés de façon semi-régulière entre des plans très serrés. Dans un tel réseau, l'énergie de déformation devrait être assez élevée. On a observé un processus de « guérison » des altérations dues aux rayonnements, à des températures suffisamment élevées.

La quantité d'hélium décelée dans les échantillons augmente proportionnellement à la dose d'exposition jusqu'à environ $1,6 \cdot 10^{21}$ n/cm²; à des doses plus élevées, elle atteint un palier d'environ 400 µl par gramme de BeO; ni la température d'irradiation, ni l'étendue de la fracture de l'échantillon n'ont d'influence marquée sur la rétention de He. Dans les échantillons irradiés à des températures supérieures à 450°C, la teneur en tritium est très faible; en revanche, pour les irradiations à température plus basse, elle est proportionnelle au carré de la dose neutronique.

La conductivité thermique du BeO a été réduite par irradiation, comme l'ont indiqué les variations du gradient de température constatées dans des sections d'échantillons à mesure que l'exposition se poursuivait. Cependant, on n'a observé aucune discontinuité brusque de gradient de température et plus de 25 échantillons ont résisté au traitement thermique sans qu'il se produise du criques; il n'est donc guère probable que l'effort thermique soit la seule cause des défaillances. Il semble au contraire que ce soit le déplacement d'atomes ou l'accumulation de gaz à l'intérieur du cristal, ou encore une combinaison de ces deux phénomènes, qui soit la cause principale des défaillances des pièces. On tait à l'heure actuelle de nouvelles expériences pour mieux séparer plusieurs variables expérimentales.

РАДИАЦИОННОЕ ПОВРЕЖДЕНИЕ В BeO. В национальной лаборатории Окридж изучается стабильность основной массы BeO при облучении. Цилиндрические образцы, заделанные в капсулы из нержавеющей стали и помещенные внутрь кольцевого канала, через который проходит смесь аргона и гелия для регулирования температуры, были облучены в реакторе для технических испытаний, Арко, Айдахо. Образцы были подвергнуты облучению быстрыми (> 1 Мэв) нейтронами от 10^{20} до $2,6 \cdot 10^{21}$ н/см² при температурах в пределах 100 - 1100°C. В дополнение к наблюдениям за большими изменениями образцы изучались с помощью технических приемов рентгеновской дифракции, оптической микроскопии, металлографии и электронной микроскопии; некоторые образцы умышленно растворялись с целью определения содержания в них трития и гелия.

Наибольшие повреждения обнаружились в слитках, облученных высокими дозами нейтронов при малых температурах. Образцы, облученные дозами $1,5 \cdot 10^{21}$ н/см² при температуре 110°C, превращались в порошок. Раздробления в образцах наблюдались при облучении до $2,6 \cdot 10^{21}$ н/см² при температуре от 800 до 950°C. Некоторые образцы, облученные при средних дозах и при средних температурах, оставались неповрежденными.

Значительные структурные различия, которые зависят от температуры облучения и от технических приемов изготовления, наблюдались при изучении основных частей с помощью рентгенограммы. Дифракционная картина облученного BeO, полученного при прессовке как в холодном, так и в горячем состоянии, показывает приблизительно 9 степеней расширения анизотропной решетки $(\Delta C/C_0) + (\Delta a/a_0)$.

Рентгенограммы BeO, облученного при 120°C, схожи с рентгенограммами облученного графита. Данные могут интерпретироваться как показывающие в дополнение к отдельным точечным дефектам наличие небольших дисков (в 10 - 20 атомов), внедренных атомов (таких веществ, как Be,He,O) в полуправильной системе между плотноупакованными плоскостями. Энергия напряжений в такой решетки должна быть высокой. Отжиг последствий радиационного повреждения наблюдался при достаточно высоких температурах.

Рентгенограммы BeO, облученного при 120°C, схожи с рентгенограммами облученного графита. Данные могут интерпретироваться как показывающие в дополнение к отдельным точечным дефектам наличие небольших дисков (в 10 - 20 атомов), внедренных атомов (таких веществ, как Be,He,O) в полуправильной системе между плотноупакованными плоскостями. Энергия напряжений в такой решетки

должна быть высокой. Отжиг последствий радиационного повреждения наблюдался при достаточно высоких температурах.

Гелий, обнаруженный в образцах, увеличивается непосредственно при облучении около $1,6 \cdot 10^{21}$ н/см² и приближается к уровню с наивысшей дозировкой около 400 мкл из расчета на 1 BeO; ни температура облучения, ни степень раздробления образца не оказывают существенного влияния на содержание He. *Содержание трития в образцах, облученных при температуре выше 450°C,* очень низкое, однако оно пропорционально квадрату нейтронной дозы облучения при низких температурах.

Теплопроводность BeO уменьшалась во время облучения, как это видно на основе изменений в температурном градиенте *всех образцов по мере их облучения.* Тем не менее, поскольку не наблюдалось неожиданного перерыва в температурном градиенте и поскольку более 25 образцов выдержали тепловой цикл без образования трещин, тепловое напряжение представляется маловероятной причиной для аварии. Смещение атомов в кристаллической решетке, *или накопление газа внутри кристалла,* или сочетание того и другого, представляется главной причиной отказа в работе основных частей. Ведутся дальнейшие эксперименты, имеющие целью еще лучше исследовать отдельные причины.

DAÑOS CAUSADOS POR LA RADIACIÓN AL ÓXIDO DE BERILIO. En el Oak Ridge National Laboratory se está estudiando actualmente la estabilidad de las piezas de BeO sometidas a irradiación. En el Engineering Test Reactor, de Arco, Idaho, se han irradiado probetas cilíndricas contenidas en cápsulas de acero inoxidable, y colocadas dentro de un conducto anular por el que circula una mezcla de argón y helio para permitir la regulación de la temperatura. Las muestras se expusieron a la acción de neutrones rápidos (> 1 MeV) en dosis totales comprendidas entre 10^{20} y $2,6 \cdot 10^{21}$ n/cm² y temperaturas entre 100° y 1100°C. Se observaron las alteraciones macroscópicas consiguientes y además, las muestras se examinaron mediante las técnicas de difracción de rayos X, microscopía óptica, metalografía y microscopía electrónica. Por otra parte, algunas de las muestras se disolvieron a fin de determinar su contenido de tritio y helio.

Los daños mayores se registraron en las piezas irradiadas con elevadas dosis neutrónicas a bajas temperaturas. Las muestras sometidas a $1,5 \cdot 10^{21}$ n/cm², a unos 110°C quedaron pulverizadas. En las muestras irradiadas con $2,6 \cdot 10^{21}$ n/cm², entre 800° y 950°C, se observaron fracturas. Algunas muestras expuestas a dosis y temperaturas intermedias no sufrieron alteraciones.

La difracción de rayos X, permitió comprobar la existencia de diferencias estructurales significativas que dependen de la temperatura de irradiación y de la técnica aplicada en la elaboración. De los diagramas de difracción de las piezas de BeO irradiadas, prensadas en caliente y en frío, se deduce que los coeficientes de dilatación anisotrópica del reticulado $(\Delta c/c_0) \div (\Delta a/a_0)$ son del orden de 9.

Los diagramas de rayos X de las piezas de BeO irradiadas a 100°C se asemejan a los obtenidos en el caso del grafito irradiado. Los datos pueden interpretarse como prueba de que, además de los defectos puntiformes aislados, existen pequeños discos de átomos intersticiales (10 a 20 átomos, de elementos tales como Be, He, O) dispuestos en forma semiregular entre planos densamente poblados. En un reticulado de este tipo, la energía de tension deberia ser elevada. A temperaturas suficientemente altas, se produce un recocido de los efectos de los daños causados por la radiación.

El contenido de helio de las muestras es directamente proporcional a la exposición, al aumentar la dosis hasta $1,6 \cdot 10^{21}$ n/cm² y luego parece estacionarse, aunque siga aumentando la dosis, en unos 400 µl por gramo de BeO; en la retención del helio no influye la temperatura de irradiación ni el grado de resquebrajamiento de la muestra. El contenido de tritio es muy pequeño en las muestras irradiadas a temperaturas superiores a los 450°C, mientras que a temperaturas más bajas, es proporcional al cuadrado de la dosis neutrónica.

La irradiacion produce una disminución de la conductividad térmica del BeO, según se comprueba por las modificaciones del gradiente de temperatura a través de las muestras, al proseguir la exposición. No obstante, como no se observaron discontinuidades bruscas en el gradiente de temperatura y dado que más de 25 muestras resistieron el ciclado térmico sin agrietarse, no parece probable que las tensiones térmicas sean la causa exclusiva de las fallas. Estas se deberían más bien a los desplazamientos atómicos, a la acumulación de gases en los cristales o a una combinación de ambos factores. Se están efectuando nuevos experimentos con el objeto de poder establecer una diferenciación más neta entre las variables que intervienen en estos fenómenos.

The attractive nuclear properties of beryllium oxide and its general excellence as a high-temperature ceramic recommend its consideration as a moderator or reflector for a variety of power reactors in the United States

of America and in other countries. The satisfactory and economical usage of BeO requires that the material withstand very high integrated neutron doses. Damage to BeO by fast neutrons has been detected by several investigators [1-11]. Experiments are now in progress to determine specific mechanisms of the observed damages and to establish optimum parameters for fabrication and successful operation of BeO-moderated reactors.

Fifty-seven cylindrical BeO specimens were irradiated in the Experimental Test Reactor at Arco, Idaho, with integrated doses from 1×10^{20} to 2.6×10^{21} n/cm^2 (E > 1 MeV) over the range 100-1025°C. The conditions are summarized in Table I. Two types were used: hot-pressed specimens; and cold-pressed specimens sintered at 1650°C (made from Brush UOX grade BeO). Spectrographic analyses of both types are given in Table II. The specimens were encapsulated in stainless steel. In the reactor, each capsule was surrounded by an annulus through which an argon-helium mixture was circulated to control the temperature. Internal heat generation was provided by absorption of gamma radiation at a peak rate of approximately 25 W/g. A typical capsule is shown in Fig. 1. The BeO specimens are inserted with a press fit; the capsule is then welded and machined to size.

After irradiation, the specimens were observed for gross changes and examined by X-ray diffraction, petrographic microscopy, electron microscopy and metallography; some specimens were dissolved for determination of helium and tritium. The greatest damage occurred to specimens irradiated to high fast-neutron doses at low temperatures. Fig. 2 shows twelve specimens irradiated over the range (1.8 to 2.6) $\times 10^{21}$n/cm^2 at 120°C in Experiment 4. Eleven of these cracked or powdered. Deterioration was in proportion to the fast-neutron dose, which increases from left to right in Fig. 2.

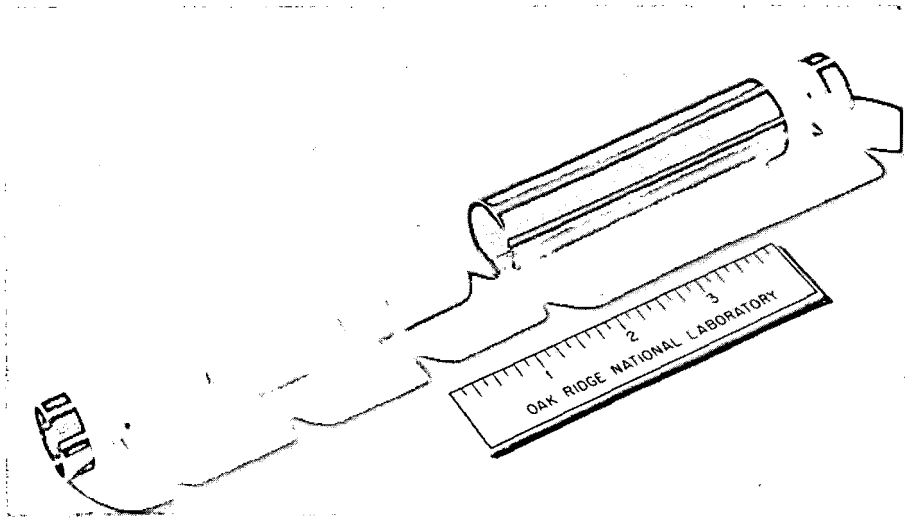


Fig. 1

Exploded view of ORNL-41 BeO-moderator capsule
(Scale is in inches)

TABLE I

CONDITIONS OF BERYLLIUM OXIDE IRRADIATION TESTS
Length of each specimen: 1.000 in

Experiment number	Number of specimens	Type of material	Diameter (in)	Density (g/cm^3)	Exposure ($10^{21} n/cm^2$)	Temperature (°C)
1	3	Hot pressed	0.636	2.9	0.14	722
2	9	Hot pressed	0.636	2.9	0.11-0.35	219-500
3	3	Hot pressed	0.428	2.9	0.11-0.45	458
	3	Hot pressed	0.636	2.9	0.11-0.45	858
	6	Hot pressed	0.800	2.9	0.11-0.45	120-1025
4	12	Cold pressed and sintered	0.800	2.65-2.70	1.8-2.6	120
5	21	Cold pressed and sintered	0.800	2.65-2.70	1.1-2.6	110-950

TABLE II

SPECTROGRAPHIC ANALYSIS OF BERYLLIUM OXIDE SPECIMENS*

Element	Concentration	
	Hot pressed (ppm)	Cold pressed and sintered (ppm)
Al	< 500	100
Si	6000	110
Ca	< 800	50
K		100
Fe	1000	20
Cr	< 500	20
Mg		< 70
Mo		< 50
Mn		< 20
Ni	< 800	< 20
Cu	< 500	
Pb	< 500	

* J.A. Norris et al., Analytical Chemistry Division, Oak Ridge National Laboratory, USA.

Fig. 3 shows radial separation after an exposure of $2.5 \times 10^{21} n/cm^2$ at 825°C in Experiment 5. In this specimen a thermocouple well is in the centre. Cracks were observed in twelve specimens irradiated to $(2.1 \text{ to } 2.6) \times 10^{21} n/cm^2$ at 825-950°C. Fig. 4 shows cracking in three specimens after an exposure of $2.5 \times 10^{21} n/cm^2$ at 950°C. Specimens exposed to $1.1 \times 10^{21} n/cm^2$ at 445°C survived without any apparent gross damage (Fig. 5).

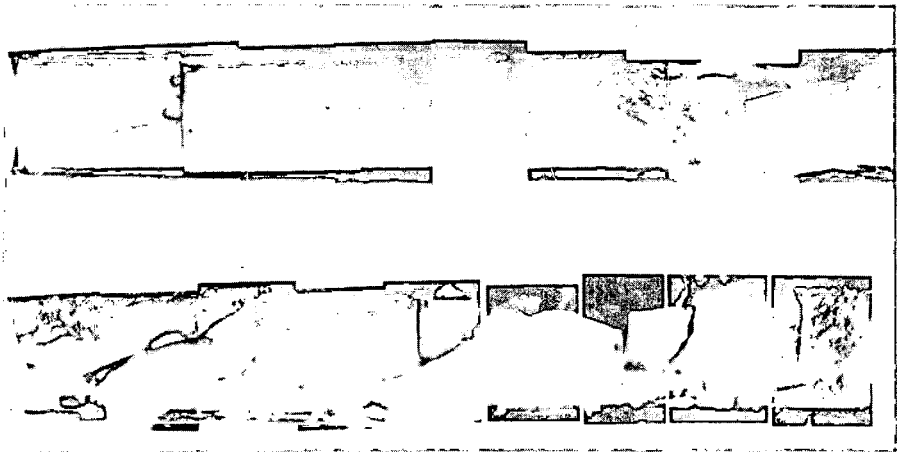


Fig.2

BeO experiment 4
Twelve specimens irradiated to (1.8-2.6) 10^{21} n/cm^2(E > 1MeV) at 120°C.



Fig.3

BeO experiment 5
Specimen irradiated to 2.5×10^{21} n/cm^2(E > 1MeV) at 825°C.

Increases in linear dimensions of irradiated samples from 0.5% to 4% were observed. This effect increased with neutron dose and decreased with temperature.

X-ray diffraction examinations [12] of both types of specimens after irradiation show anisotropic lattice expansion ratios $(\Delta c/c_0)/(\Delta a/a_0) \simeq 9$. X-ray patterns of BeO irradiated at 120°C show points of similarity to those of irradiated graphite. The data may be interpreted as showing, in addition



Fig.4

BeO experiment 5
Three specimens irradiated to 2.5×10^{21} n/cm^2(E > 1MeV) at 950°C.

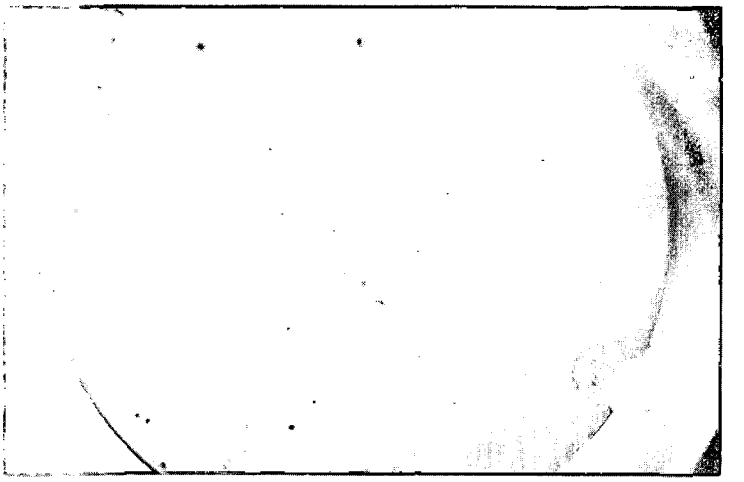


Fig.5

BeO experiment 5
Specimen irradiated to 1.1×10^{21} n/cm^2(E > 1MeV) at 445°C.

to isolated point defects, the presence of small discs of 10 to 20 interstitial atoms (such as Be, He, or 0) in semi-regular array between closely packed planes. The strain energy in such a lattice should be high.

Petrographic examinations [13] of the irradiated specimens showed a decrease in the refractive index corresponding to the decrease in density. Specimens irradiated in the 10^{21}n/cm^2 range, with a refractive index of 1.70, began to anneal at 700°C, with complete annealing to the standard index of 1.72 at 1050°C.

Extensive intergranular fracture after irradiation in the 10^{21}n/cm^2 range was revealed by observations of excessive pull-out of material during polishing of metallographic specimens.

Electron microscopic examinations of irradiated BeO showed that voids 0.1 to 0.3 μm in diameter were present in the interior of the grains and at

grain boundaries, whereas they were not present in the original material. These voids were sometimes found in parallel alignment, suggesting a crystallographic relationship to the sites of void formation. Heat treatment caused the voids to coalesce and form blisters.

The thermal conductivity of the samples decreased substantially as exposure progressed; this was indicated by 50 to 100% increases in the radial temperature differences, which result from internal generation of heat by absorption of gamma radiation. However, since there were no sudden changes in the temperature gradient and since more than 25 samples survived thermal cycling without cracking, thermal stress seems unlikely to be the sole cause of failure.

Gas analyses [14] of irradiated BeO show that internally generated helium is retained even at high temperatures up to a fast-neutron dose of 1.6×10^{21} n/cm^2, as shown in Fig. 6. The scatter of the points above this dose could be caused by the release of helium by fracture of the specimens.

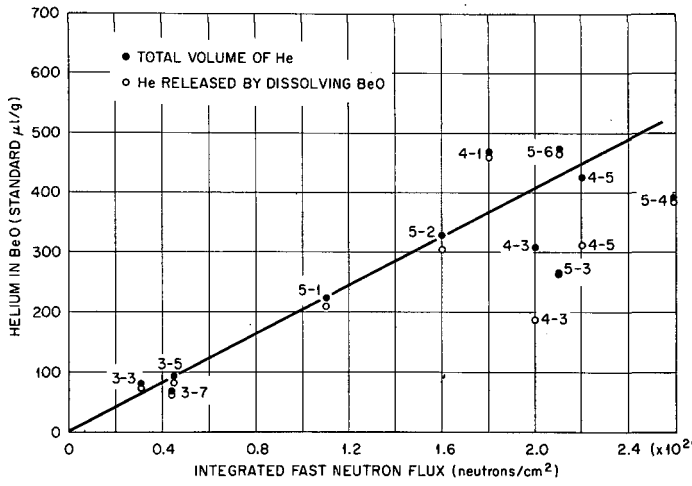


Fig. 6

Helium concentration in irradiated BeO plotted against the integrated fast-neutron flux with E > 1MeV

Helium is produced through two nuclear reactions: the (n, 2n) reaction, in which the yield is proportional to the total dose; and the (n, α) reaction, in which the yield is approximately proportional to the square of the total dose. The linear relationship in the plot indicates that the (n, 2n) reaction predominates over the (n, α) reaction, as expected from the known cross-section values [15]. The slope of the line in Fig. 6 gives a yield of 205 μl of He per gram of BeO per 10^{21}n/cm^2, which is somewhat less than the range 250 to 269 μl/g per 10^{21}n/cm^2 based on the data of RICH and WALTERS [16] for metallic beryllium. Data reported by ELLS [17] are equivalent to a yield of 460 μl/g per 10^{21}n/cm^2.

Since tritium is generated entirely through the (n,α) reaction, the yield should be approximately proportional to the square of the dose for the conditions of this experiment. Gas analyses of tritium content plotted in Fig. 7

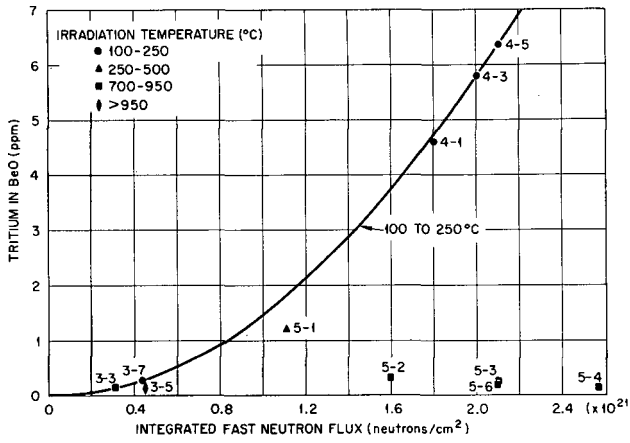


Fig. 7

Tritium concentration in irradiated BeO plotted against the integrated fast-neutron flux with E > 1MeV

agree with the theoretical expectation at 120°C, but show that tritium is lost to an increasing degree at higher temperatures. Tritium content is very low in specimens irradiated at temperatures above 450°C.

Two processes which have been proposed to explain the failure of specimens under irradiation are: (1) displacements of beryllium and oxygen atoms within the crystals (based on X-ray data indicating the existence of interstitial atoms between planes in the lattice); (2) gas generation and formation of voids. Experiments now in progress are designed to permit a better separation of variables in order to determine the relative importance of these and other possible processes. An irradiation experiment contains samples exposed to higher neutron dose at lower temperatures and lower dose at higher temperatures, thus separating the competing dose and temperature factors. Experiments in preparation are statistically designed to provide information on the following variables: exposure time, flux, temperature, specimen size, density and grain size. Information on the effect of density on irradiation damage, for example, may help to establish the importance of gas generation. Diffusion of the generated gases from low-density specimens may possibly be so rapid that there will be little or no retention and void formation. Under consideration is a study of the effect of sample purity, in which irradiated specimens made from commercial BeO would be statistically compared with those made from ultra-pure BeO, with sintering temperature as one of the variables.

REFERENCES

[1] GILBREATH, J.R. and SIMPSON, O.C., Proc. 2nd UN Int. Conf. PUAE 5 (1958) 367-374.
[2] MANNING, W.M., USAEC Rpt. ANL-4204 (Dec. 1948).
[3] McGILL, R.C. and SMITH, J.A.G., U.K.A.E.A. Rpt. AERE-R-3019 (1959).
[4] GHOSH, T.K. and CLARKE, F.J.P., U.K.A.E.A. Rpt. AERE-R-2889 (1959).

[5] CLARKE, F.J.P. and WILLIAMS, J., U.K.A.E.A. Rpt. AERE-M/M-229 (1959).
[6] CLARKE, F.J.P. and TAPPIN, G., U.K.A.E.A. Rpt. AERE-R-3164 (1960).
[7] ELSTON, J., GeWISS, C. and LABBE, C., Compt. Rend. 249 (Oct. 1959) 1635-1637.
[8] ELSTON, J. and CAILLAT, R., Proc. 2nd UN Int. Conf. PUAE 5 (1958) 345-366.
[9] FRISBIE, H., BISSON, A. and CAILLAT, R., J. nucl. Mat. 1 (1959) 106-108.
[10] SHIELDS, R.P., LEE, J.E. Jr. and BROWNING, W.E. ,Jr., USAEC Rpt. ORNL-3164 (7 June 1961).
[11] SHIELDS, R.P., LEE, J.E., Jr. and BROWNING, W.E., Jr., Trans Amer. Nucl. Soc. 4 2 (Nov. 1961) 338.
[12] YAKEL, H.L., Metallurgy Division, Oak Ridge National Laboratory, personal communication.
[13] McVAY, T.N., THOMA, R.E., INSLEY, H., FRIEDMAN, H.A. and WEAVER, C.F., J. Amer. Ceram. Soc. 45 (1962) 48.
[14] WHITE, J.C., MEYER, A.S., Jr. and RUBIN, I.B., Proc. 4th Conf. Analytical Chemistry in Nuclear Reactor Technology, USAEC Rpt. TID-7606 (1960) 158-63.
[15] EVANS, J.E., USAEC Rpt. IDO-16364 (Sep. 1956).
[16] RICH, J.B. and WALTERS, G.P., U.K.A.E.A. Rpt. AERE-R-3684 (1961).
[17] ELLS, C.E., AECL CRMet-809 (1958).

DISCUSSION

J.R. BEELER: There are four questions I want to ask regarding the discs of interstitial atoms mentioned by Dr. Keilholtz in his paper:

(1) Are the discs composed primarily of one type of atom?; (2) Are the discs regular in shape or are they elongated?; (3) Did there appear to be a distribution of disc sizes or was the 20-interstitial size mentioned pertinent to all discs for the irradiation time concerned?; (4) Have experiments been done wherein a series of successively longer short-time irradiations were employed? This type of experiment might indicate whether the discs are formed primarily as the result of interstitial diffusion or as the result of the pile-up of energetic knock-on atoms against an atom previously absorbed at an interstitial position.

G.W. KEILHOLTZ: The work on the interstitials and the X-ray work was done by H. L. Yakel of Oak Ridge National Laboratory and he did not specify whether his X-ray data referred to beryllium oxygen or helium. He developed a model to explain the line-broadening which I have mentioned, and he suggested that the 15-20 atoms will explain the line-broadening that he observed in the X-ray data. He also pointed out that several other models could be used equally well for this purpose. He thinks that in nine cases out of ten the interstitials account for the effects that he observed. In reply to the third and fourth questions I should like to mention that Mr. Yakel indicated that there are point defects at low irradiation times, and that we observe these clusters at the high irradiation times and at the low temperature.

COMPORTEMENT DE L'OXYDE DE BÉRYLLIUM FRITTÉ IRRADIÉ PAR DES NEUTRONS

J. ELSTON
CENTRE D'ÉTUDES NUCLÉAIRES DE SACLAY
GIF-SUR-YVETTE (S. & O.), FRANCE

Abstract — Résumé — Аннотация — Resumen

THE BEHAVIOUR OF SINTERED BERYLLIUM OXIDE UNDER NEUTRON IRRADIATION. The effects of irradiation on the properties of beryllium oxide were studied as a function of the fast integrated flux (neutrons of energy greater than 1 MeV), the irradiation temperature, and the density of the oxide.

The disintegration of beryllium oxide sinters irradiated by doses of 2×10^{20} n_f/cm^2 or higher at temperatures below 100°C is attributed to the fact that the increase of parameter c is much greater than that of parameter a. A micrograph of a sample irradiated with 9×10^{19} n_f/cm^2 (T_{ir} < 100°C) shows how intergranular dissociation occurs in the sinters.

The effect of annealing the irradiated beryllium oxide samples at different temperatures on the variation in the crystal parameters and the dimensions of the test pieces was ascertained.

Some results are given relating to the production of helium by nuclear reactions after heat treatment of the irradiated beryllium oxide samples.

In addition, a comparison is made between the influence of the irradiation temperature on the resistance to compression at 20, 400 and 1000°C, in annealed and non-annealed beryllium oxide test pieces and in magnesium oxide samples irradiated at a temperature in the neighbourhood of 400°C.

COMPORTEMENT DE L'OXYDE DE BÉRYLLIUM FRITTÉ IRRADIÉ PAR LES NEUTRONS. Les effets de l'irradiation sur les propriétés de l'oxyde de béryllium ont été étudiés en fonction du flux rapide intégré (neutrons d'énergie supérieure à 1 MeV), de la température d'irradiation et de la densité de ce réfractaire.

La désagrégation des frittés d'oxyde de béryllium irradiés à une dose supérieure ou égale à $2\cdot10^{20}$ n_r/cm^2 et à une température intérieure à 100°C est attribuée à l'augmentation du paramètre c, beaucoup plus importante que celle du paramètre a. Une micrographie d'un échantillon irradié à $9\cdot10^{19}$ n_r/cm^2 (T_{Ir} < 100°C) montre comment se produit la décohésion intergranulaire des frittés.

On a déterminé l'influence des recuits, à différentes températures, des échantillons d'oxyde de béryllium irradiés sur la variation des paramètres cristallins et des dimensions des éprouvettes.

Le mémoire donne quelques résultats concernant l'évolution de l'hélium produit par les réactions nucléaires après traitements thermiques des échantillons d'oxyde de béryllium irradiés.

On compare, d'autre part, l'influence de la température d'irradiation sur la résistance à la compression à 20, 400 et 1000°C d'éprouvettes d'oxyde de béryllium recuites et non recuites et d'échantillons d'oxyde de magnésium irradiés à une température voisine de 400°C.

ПОВЕДЕНИЕ СПЕЧЕННОЙ ОКИСИ БЕРИЛЛИЯ ПОД ДЕЙСТВИЕМ НЕЙТРОННОГО ОБЛУЧЕНИЯ. Действие облучения на свойства окиси бериллия были изучены в зависимости от общего потока быстрых нейтронов (с энергией свыше 1 Мэв) от температуры облучения и от плотности этого огнеупорного материала.

Распадение спеченных окисей бериллия под действием дозы облучения, равной $2\cdot10^{20}$ $n_r/см^2$ или большей при температуре ниже 100°C, приписывается значительно большему увеличению параметра "c", чем параметра "a". Микрофотография образца, облученного дозой в 9×10^{19} $n_r/см^2$ (T_{Ir} < 100°C) показывает, каким образом происходит распад между зернами спеченного материала.

Было определено влияние отжига при различных температурах облученных образцов окиси бериллия на изменение кристаллических параметров и на размеры образцов.

Даются некоторые результаты относительно гелия, образуемого ядерными реакциями, после термической обработки облученных образцов окиси бериллия.

Кроме того, сравнивается влияние температуры облучения на сопротивление сжатию отожженных и неотожженных образцов окиси бериллия при температурах 20, 400 и 1000°С, а также образцов окиси магния, облученных при температуре приблизительно 400°С.

COMPORTAMIENTO DEL ÓXIDO DE BERILIO SINTERIZADO IRRADIADO CON NEUTRONES. El autor ha estudiado los efectos de la irradiación sobre las propiedades del óxido de berilio, en función del flujo rápido integrado (neutrones de energía superior a 1 MeV), de la temperatura de irradiación y de la densidad del material refractario.

La disgregación del óxido de berilio sinterizado sometido a una dosis superior o igual a $2 \cdot 10^{20}$ n_r/cm^2 y a una temperatura inferior a 100°C se atribuye al aumento del parámetro c, que es mucho más considerable que el del parámetro a. La micrografía de una muestra expuesta a una dosis de $9 \cdot 10^{19}$ n_r/cm^2 ($T_{Ir} < 100°C$) revela cómo desaparece la cohesión intergranular del material sinterizado.

El autor ha determinado la influencia que el recocido, a temperaturas diferentes, ejerce sobre la variación de los parámetros cristalinos y de las dimensiones de las probetas de óxido de berilio irradiadas.

Expone algunos resultados referentes al desprendimiento del helio formado en virtud de reacciones nucleares después del tratamiento térmico de las muestras de óxido de berilio irradiadas.

Compara, por otra parte, la influencia de la temperatura de irradiación sobre la resistencia a la compresión, a 20, 400 y 1000°C, de probetas de óxido de berilio recocidas y no recocidas, y de muestras de óxido de magnesio irradiadas a una temperatura del orden de los 400°C.

Les résultats rapportés dans de précédentes communications [1, 2] sur le comportement de l'oxyde de béryllium irradié dans un réacteur nucléaire ont mis en évidence le rôle important de la température d'irradiation, de la densité des frittés, de la structure cristalline de ce composé et de l'hélium formé sous irradiation.

Dans cet exposé les points suivants sont présentés puis discutés:

- les effets d'irradiations effectuées à une température inférieure à 100°C sur l'oxyde de béryllium,
- le comportement de ce matériau sous flux de neutrons à une température de l'ordre de 400°C,
- l'évolution de l'hélium formé par irradiation dans l'oxyde de béryllium,
- les effets de l'irradiation sur l'oxyde de magnésium de structure cubique comparés aux résultats précédents obtenus avec l'oxyde de béryllium de structure hexagonale.

1. COMPORTEMENT DE L'OXYDE DE BÉRYLLIUM FRITTÉ SOUS CHARGE IRRADIÉ A UNE TEMPÉRATURE INFÉRIEURE A 100°C

L'irradiation par les neutrons d'un réacteur produit un accroissement des paramètres cristallins de l'oxyde de béryllium. Pour ce composé de structure type wurtzite, la dilatation des cristallites a un caractère nettement anisotrope, comme le montre le tableau I. Les déformations sont beaucoup plus grandes suivant l'axe c que suivant les directions a.

Cette déformation anisotrope des cristallites entraîne l'apparition de tensions importantes entre les grains des frittés d'oxyde de béryllium soumis à l'irradiation et a pour conséquence une diminution très notable des caractéristiques mécaniques du matériau [2].

Le tableau I montre comment évolue la résistance à la compression R_E des frittés sous charge de forte densité. Quand l'irradiation atteint

TABLEAU I

VARIATION DES PARAMÈTRES CRISTALLINS ET DE LA RÉSISTANCE A LA COMPRESSION DES FRITTÉS SOUS CHARGE DE DENSITÉ 2,97 - 3,00 APRÈS IRRADIATION

ϕ_r (n_r/cm^2)	T_{Ir} (°C)	$\frac{\Delta a}{a}\ 10^{-3}$	$\frac{\Delta c}{c}\ 10^{-3}$	R_E à 20°C (t/cm²)	Dispersion (t/cm²)
Avant irradiation	-	0	0	20	± 2
$2,5 \cdot 10^{19}$	< 100	0,11	0,95	15,3	± 3
$6,0 \cdot 10^{19}$	< 100	0,36	3,1	4,5	± 0,2
$9,0 \cdot 10^{19}$	< 100	0,37	5,2	1,4	± 0,1
$2,0 \cdot 10^{20}$	< 100	1,0	non mesurable	poudre	-

des flux rapides intégrés égaux ou supérieurs à $2 \cdot 10^{20}\ n_r/cm^2$, les tensions introduites entre les grains des frittés sont suffisantes pour provoquer la désagrégation totale des échantillons : ceux-ci sont retrouvés sous forme de poudre [3].

Un calcul — très approximatif, il est vrai — permet néanmoins de fixer les ordres de grandeurs des contraintes et de comprendre ces phénomènes de fragilisation ou de désagrégation des frittés d'oxyde de béryllium sous irradiation. En effet, déjà pour un flux de $6 \cdot 10^{19}\ n_r/cm^2$ la dilatation du réseau cristallin produit dans un fritté supposé statistiquement isotrope une extension moyenne $\frac{\Delta l}{l}$ égale à:

$$\frac{\Delta l}{l} = \frac{3,1 \cdot 10^{-3} + 2 \cdot 0,36 \cdot 10^{-3}}{3} \simeq 1,3 \cdot 10^{-3}.$$

A cette dilatation correspond une contrainte bien supérieure à la valeur limite ϵ supportable sans rupture par BeO. En effet, si le module d'élasticité E de l'oxyde de béryllium a pour valeur 30 000 kg/mm² et la contrainte de rupture σ 10 kg/mm², on a

$$\epsilon = \frac{\sigma}{E} = 0,3 \cdot 10^{-3}.$$

Il n'est donc pas surprenant que l'irradiation puisse désagréger ces frittés.

La décohésion entre les grains des frittés denses est d'ailleurs bien visible par examen micrographique. La figure 1 représente un échantillon d'oxyde de béryllium fritté sous charge de densité 3,00, irradié à la dose de $9 \cdot 10^{19}\ n_r/cm^2$, puis poli à la poudre de diamant, sans attaque chimique. Sur cette micrographie les joints entre les grains sont très apparents et très larges. Avant l'irradiation, par contre, les joints de grains sont très

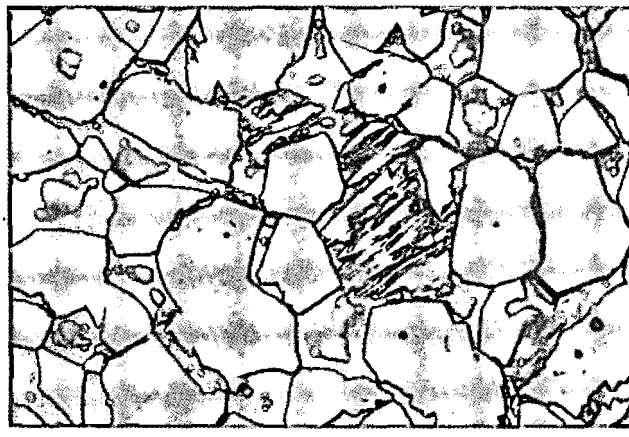


Figure 1

Décohésion des grains de l'oxyde de béryllium fritté sous charge après une irradiation de $9 \cdot 10^{19}$ n_r/cm^2 (T_{Ir} < 100°C).

minces et ne sont révélés qu'après attaque chimique par l'acide fluorhydrique [19].

L'attaque chimique de l'échantillon irradié ne révèle pas d'autres limites entre les grains que celles mises en évidence par le polissage seul. On en conclut que les zones intergranulaires ont été particulièrement perturbées par l'irradiation. Ce phénomène de décohésion entre les grains rend bien compte de la diminution des caractéristiques mécaniques des frittés de BeO irradié. De plus, une fragilité semble se manifester plus particulièrement dans certaines directions cristallines, comme le montre le parallélisme des arrachements que l'on peut remarquer sur certains grains de la figure 1.

On observe qualitativement que les frittés d'oxyde de béryllium peu denses sont moins fragiles après irradiation que les échantillons très denses. Le tableau II donne la résistance à l'écrasement des éprouvettes de densité relativement faible pour de fortes irradiations effectuées à température inférieure à 100°C.

Il est vraisemblable d'admettre que dans les frittés peu denses les tensions dues à la déformation anisotrope des cristallites sont moins intenses par suite d'une plus grande possibilité d'accommodation que dans l'oxyde de béryllium très dense.

2. COMPORTEMENT DE L'OXYDE DE BERYLLIUM FRITTÉ SOUS CHARGE APRÈS IRRADIATION A UNE TEMPÉRATURE VOISINE DE 400°C

La température d'irradiation est un facteur prépondérant pour le comportement de l'oxyde de béryllium sous flux de neutrons. Ainsi les variations des paramètres cristallins et par suite la diminution des caractéristi-

TABLEAU II

DIMINUTION DE LA RÉSISTANCE A LA COMPRESSION DES FRITTÉS SOUS CHARGE DE FAIBLE DENSITÉ APRÈS IRRADIATION ($T_{Ir} < 100°C$)

ϕ_r [$(n_r/cm^2)\ 10^{20}$]	Densité (g/cm^3)	R_E (t/cm^2)	R_E témoin (t/cm^2)
2	2,80	0,36	15
2	2,74	1,00	15
2	2,52	0,51	10
3	2,53	0,28	10

ques mécaniques d'éprouvettes irradiées à une température voisine de 400°C sont moins importantes que si l'irradiation avait été effectuée à une température inférieure à 100°C. Le tableau III donne les valeurs des paramètres cristallins mesurés sur trois aiguilles de densité 3,00, 2,65 et 2,67 avant irradiation, après une irradiation de $2,2 \cdot 10^{20}\ n_r/cm^2$ à 400°C environ et après des recuits successifs à différentes températures [4].

On constate que cette irradiation produit des variations relatives des paramètres cristallins respectivement égales à $0,37\text{-}0,40 \cdot 10^{-3}$ pour $\Delta a/a$ et $2,68\text{-}2,78 \cdot 10^{-3}$ pour $\Delta c/c$. Des éprouvettes de densité 2,98 irradiées dans les mêmes conditions que ces trois aiguilles ont été utilisées pour des mesures de résistance à l'écrasement. Les paramètres cristallins déterminés sur la poudre obtenue après ces essais ont subi les augmentations relatives suivantes du fait de l'irradiation:

$$\frac{\Delta a}{a} = 0,4 \cdot 10^{-3},\ \frac{\Delta c}{c} = 3,0 \cdot 10^{-3}.$$

Les traitements thermiques des aiguilles irradiées ont une action sensible sur la valeur du paramètre a à partir de 600°C, tandis que la guérison du paramètre c ne se produit pratiquement qu'au-dessus de 800°C. Les recuits à 1100°C permettent au paramètre a de retrouver sa valeur d'avant irradiation. Par contre, même après 86 h à cette température, le paramètre c n'a pas encore retrouvé sa valeur initiale (guérison 93% environ).

L'irradiation de $2,2 \cdot 10^{20}\ n_r/cm^2$ à une température voisine de 400°C produit une déformation anisotrope très sensible des cristallites de BeO. La résistance à la compression d'éprouvettes d'oxyde de béryllium fritté sous charge déterminée à 20°C doit donc être affectée par cette irradiation. Le tableau IV donne les résultats des mesures de résistance à l'écrasement à 20, 400 et 1000°C avant et après irradiation [5]. On constate, en comparant ces résultats à ceux présentés dans les tablaux I et II, que dans le

TABLEAU III

ÉFFET DE L'IRRADIATION ($T_{ir} \simeq 400°C$) ET DES RECUITS SUR LES PARAMÈTRES CRISTALLINS DE L'OXYDE DE BÉRYLLIUM FRITTÉ SOUS CHARGE

Caractéristiques des aiguilles		Densité 3,00 Grosseur moyenne des grains 25 μ		Densité 2,65 Grosseur moyenne des grains 15 μ		Densité 2,67 Grosseur moyenne des grains 13 μ	
Paramètres cristallins		a en Å	c en Å	a en Å	c en Å	a en Å	c en Å
Avant irradiation		2,6980	4,3762	2,6980	4,3761	2,6981	4,3766
Après irradiation		2,6990	4,3883	2,6991	4,3883	2,6991	4,3883
T du recuit (°C)	Durée (h)						
350	112			2,6990	4,3881		
450	50			2,6990	4,3877		
	100			2,6989	4,3882		
500	1/4			2,6988	4,3874		
	1/2	2,6990	4,3876	2,6988	4,3884		
	1	2,6989	4,3882	2,6988	4,3884		
	2			2,6988	4,3885		
	4			2,6986	4,3884		
	8			2,6988	4,3879		

600	1/4	2,6987	4,3879	2,6989	4,3883		
	1/2	2,6988	4,3879	2,6988	4,3883		
	1	2,6988	4,3882	2,6989	4,3881		
	2	2,6989	4,3878	2,6988	4,3882		
	4	2,6989	4,3878	2,6988	4,3881		
	8	2,6988	4,3880				
700	1/4	2,6987	4,3883	2,6988	4,3881		
	1/2	2,6987	4,3877	2,6987	4,3886		
	1	2,6988	4,3881	2,6987	4,3883		
	2	2,6987	4,3878	2,6986	4,3885		
	4	2,6986	4,3878	2,6987	4,3881		
	8	2,6987	4,3880	2,6987	4,3881		
800	1/4	2,6986	4,3885	2,6985	4,3881		
	1/2	2,6987	4,3878	2,6986	4,3877		
	1	2,6986	4,3882	2,6986	4,3877		
	2	2,6987	4,3880	2,6985	4,3880		
	4	2,6986	4,3883				
	8	2,6986	4,3880				
820	1/4					2,6988	4,3874
	2			2,6986	4,3883		
	4			2,6985	4,3883		
	8			2,6985	4,3885		

TABLEAU III (suite)

Caractéristiques des aiguilles		Densité 3,00 Grosseur moyenne des grains 25 μ		Densité 2,65 Grosseur moyenne des grains 15 μ		Densité 2,67 Grosseur moyenne des grains 13 μ	
Paramètres cristallins		a en Å	c en Å	a en Å	c en Å	a en Å	c en Å
Avant irradiation		2,6980	4,3762	2,6980	4,3761	2,6981	4,3766
Après irradiation		2,6990	4,3883	2,6991	4,3883	2,6991	4,3883
T du recuit (°C)	Durée (h)						
820 (suite)	50					2,6985	4,3872
	100					2,6985	4,3871
875	1/4					2,6984	4,3875
	1/2					2,6986	4,3871
	1					2,6985	4,3869
	2					2,6984	4,3871
	4					2,6987	4,3869
	8					2,6987	4,3872
900	1/4	2,6986	4,3880	2,6985	4,3885		
	1/2	2,6986	4,3879	2,6985	4,3884		
	3/4			2,6985	4,3880		

	1	2,6987	4,3878				
	1½			2,6985	4,3880		
	2	2,6986	4,3879				
	3			2,6985	4,3879		
	4	2,6986	4,3875				
	6			2,6985	4,3878		
	12			2,6985	4,3875		
1000	1/4					2,6985	4,3873
	1/2					2,6984	4,3863
	1					2,6985	4,3865
	2					2,6984	4,3862
	4					2,6984	4,3859
	8					2,6983	4,3857
1100	1/4					2,6984	4,3847
	1/2					2,6983	4,3846
	1					2,6983	4,3839
	2					2,6981	4,3831
	4					2,6981	4,3822
	8					2,6981	4,3811
	16					2,6982	4,3793
	24					2,6980	4,3779
	32					2,6982	4,3778

TABLEAU III (suite)

Caractéristiques des aiguilles		Densité 3,00 Grosseur moyenne des grains 25 μ		Densité 2,65 Grosseur moyenne des grains 15 μ		Densité 2,67 Grosseur moyenne des grains 13 μ	
Paramètres cristallins		a en Å	c en Å	a en Å	c en Å	a en Å	c en Å
Avant irradiation		2,6980	4,3762	2,6980	4,3761	2,6981	4,3766
Après irradiation		2,6990	4,3883	2,6991	4,3883	2,6991	4,3883
T du recuit (°C)	Durée (h)						
1100 (suite)	40					2,6982	4,3779
	55					2,6982	4,3779
	70					2,6982	4,3777
	86					2,6981	4,3774

Les valeurs de «a» sont déterminées à ±0,0002 Å et de «c» à ±0,0005 Å

TABLEAU IV

RÉSISTANCE A L'ÉCRASEMENT DÉTERMINÉE A 20, 400 ET 1000°C APRÈS UNE IRRADIATION DE $2,2 \cdot 10^{20}$ n_r/cm^2 ($T_{Ir} \simeq 400°C$)

Densité des éprouvettes (g/cm^3)	Recuit	Température de la mesure (°C)	R_{ET} moyenne des témoins (t/cm^2)	R_{EI} de l'éprouvette irradiée (t/cm^2)	$\frac{R_{EI}}{R_{ET}}$
2,96	sans	20	19,0	7,05	0,37
2,97	"	20	20,8	5,0	0,24
2,98	"	20	20,6	5,44	0,26
2,99	"	20	20,6	5,40	0,26
2,79	"	400	12,6	10,3	0,82
2,83	"	400	13,3	7,5	0,57
2,97	"	400	14,4	5,2	0,36
2,98	"	400	14,2	8,6	0,61
2,99	"	400	13,9	5,4	0,39
2,99	"	400	14,1	3,8	0,27
2,99	"	400	14,9	4,2	0,28
2,70	24 h - 400°C	400	10,7	10,5	0,98
2,67	"	400	10,0	9,5	0,95
2,54	"	400	8,7	6,2	0,71
2,89	"	400	12,6	10,2	0,81
2,54	"	400	8,5	7,5	0,88
2,96	sans	1000	6,1	7,2	1,18
2,97	"	1000	5,1	5,3	1,04
2,99	"	1000	6,1	6,1	1,00
2,99	"	1000	6,3	6,6	1,05
2,99	"	1000	5,7	5,5	0,97
2,99	"	1000	5,9	6,5	1,10

cas de l'irradiation à 400°C la diminution de cette caractéristique mécanique est moins importante que si l'éprouvette avait reçu la même dose de neutrons à une température inférieure à 100°C.

Une série d'éprouvettes a été recuite 24 h à 400°C avant d'être soumise à la mesure de résistance à la compression. Il est peu probable que ce traitement thermique ait une grande influence sur les propriétés de BeO,

puisque l'irradiation a été elle-même effectuée entre 350 et 400°C. Les résultats du tableau IV montrent que dans ces conditions le comportement sous irradiation à 400°C des frittés peu denses est satisfaisant.

Ces résultats encourageants ne sont toutefois pas confirmés par les mesures de la résistance à la traction d'éprouvettes de BeO irradiées dans les mêmes conditions que précédemment. Le tableau V indique une diminution très importante de cette caractéristique mécanique, même dans le cas des éprouvettes de faible densité [5].

Pour essayer de déterminer l'énergie emmagasinée dans l'oxyde de béryllium du fait de l'irradiation, un microcalorimètre déjà décrit et utilisé pour des mesures aux basses températures [6] a été adapté et mis au point pour fonctionner à 1150°C (Laboratoire du Professeur Eyraud, INSA, Lyon).

TABLEAU V

RÉSISTANCE A LA TRACTION DE L'OXYDE DE BÉRYLLIUM FRITTÉ SOUS CHARGE IRRADIÉ A 350 - 400°C ($2,2 \cdot 10^{20}$ n_r/cm^2)

Densité des éprouvettes	Température de la mesure (°C)	R_{tT} (t/cm²)	R_{tI} (t/cm²)	$\frac{R_{tI}}{R_{tT}}$
2,85	400	0,93	0,11	0,12
2,74	400	1,04	0,21	0,20
2,80	400	1,50	0,11	0,07
2,67	400	1,04	0,14	0,13

Le principe de la mesure consiste en une plongée rapide le l'échantillon irradié dans une cellule de mesure du calorimètre dont on enregistre la différence de température avec celle d'une cellule contenant un échantillon témoin fixe. L'échantillon irradié est placé par mesure de sécurité dans une nacelle de platine de 1/10 mm d'épaisseur. A chaque plongée, la température de l'équipage nacelle plus échantillon passe très rapidement de la température ambiante à la température initiale du calorimètre (1150°C environ). La force électromotrice différentielle entre les couples de la cellule de mesure et ceux de la cellule témoin est enregistrée à l'aide d'un suiveur de spot SEFRAM. L'enregistrement est terminé quand cette force électromotrice différentielle est nulle. L'aire du thermogramme qui s'étend pour une mesure sur une durée de l'ordre de quinze minutes est proportionnelle à l'énergie totale S_{ml} effectivement absorbée par l'échantillon et la nacelle de platine.

Cette énergie S_{ml} est égale à la différence entre l'énergie absorbée S_a nécessaire pour élever la température de l'équipage et l'énergie libérée S_l

par l'échantillon durant la plongée:

$$S_{m1} = S_a - |S_1|.$$

L'énergie emmagasinée dans l'échantillon et libérée durant le recuit d'environ quinze minutes à 1150°C est

$$|S_1| = S_a - S_{m1}.$$

Après plusieurs essais successifs avec le même échantillon irradié, l'aire mesurée S_{mn} correspondant à la $n^{ième}$ plongée reste constante et égale à l'aire S_a, ce qui signifie qu'aux erreurs expérimentales près, l'échantillon ne cède plus d'énergie.

Dans le cas d'un échantillon d'oxyde de béryllium de 0,7567 g de densité 2,86, irradié à une dose de $2{,}2 \cdot 10^{20}\ n_r/cm^2$ à 400°C environ, l'énergie libérée au cours de la deuxième plongée est inférieure au 1/10 de l'énergie libérée durant la première plongée. Dans ces conditions et après étalonnage de l'appareil avec de petites masses de nickel, on estime que l'énergie «Wigner» libérée à 1132°C par cet échantillon irradié est comprise entre 14 et 27 calories par gramme de BeO.

Avec un échantillon de 0,7033 g ayant subi la même irradiation que l'échantillon précédent, mais de densité 2,97, aucune libération significative d'énergie n'a pu être mise en évidence.

Comme cet échantillon dense était extrêmement friable après irradiation, alors que la tenue mécanique du fritté de densité 2,86 était plus satisfaisante (tableau IV), il paraît possible d'avancer deux hypothèses:

a) Avec l'échantillon dense, très friable, les échanges thermiques sont mauvais et l'énergie libérée durant la mesure devient plus difficilement décelable que dans le cas des frittés ayant conservé une certaine cohésion après irradiation.

b) L'énergie élastique correspondant aux tensions intergranulaires apparues sous rayonnement est une partie importante de l'énergie «Wigner» dans les frittés d'oxyde de béryllium irradié. Dans l'échantillon très dense irradié, les tensions se sont relâchées par suite de la décohésion des grains et l'énergie emmagasinée libérable à 1130°C est de l'ordre de grandeur des erreurs de mesure.

3. ÉVOLUTION DE L'HÉLIUM FORMÉ SOUS IRRADIATION DANS L'OXYDE DE BÉRYLLIUM

Le bombardement de l'oxyde de béryllium par les neutrons produit un déplacement des ions dans le réseau cristallin, d'où apparition d'un certain nombre de défauts. Ces perturbations dans le réseau peuvent être éliminées, en principe, par des traitements thermiques appropriés de l'oxyde irradié.

De plus, les neutrons possédant une énergie suffisante provoquent des réactions (n, 2n) et (n, α) avec les noyaux ^9Be, d'où formation d'hélium et de tritium dans les frittés d'oxyde de béryllium [2]. Si l'échantillon est irradié à basse température, on peut penser que les noyaux d'hélium et de

tritium sont dispersés dans le réseau cristallin et contribuent à sa déformation au même titre que les autres défauts introduits par l'irradiation.

Pour des concentrations en hélium et en tritium suffisantes, ces gaz tendent à se rassembler dans les frittés quand on élève la température de l'échantillon irradié.

Ainsi on observe par fractographie [7] un rassemblement de bulles aux joints de grains dans les frittés sous charge d'oxyde de béryllium de densité supérieure à 2,87 après une irradiation de l'ordre de $5,5 \cdot 10^{19} n_r/cm^2$, à une temperature inférieure à 100°C, suivie d'un traitement thermique à 1000°C. Il n'a pas été possible de mettre en évidence de telles bulles au microscope électronique sur des échantillons de même densité, irradiés, non recuits ou recuits seulement à 800°C.

Le rassemblement de l'hélium a pu être suivi directement, au laboratoire du Professeur Weil à Grenoble, en mesurant entre 1,3 et 3,5°K la chaleur spécifique d'un fritté d'oxyde de béryllium avant et après irradiation. Cette méthode, particulièrement sensible au voisinage du point λ de l'hélium du fait de la faible valeur de la chaleur spécifique propre de BeO, est spécifique de l'hélium sous forme de molécules rassemblées [8].

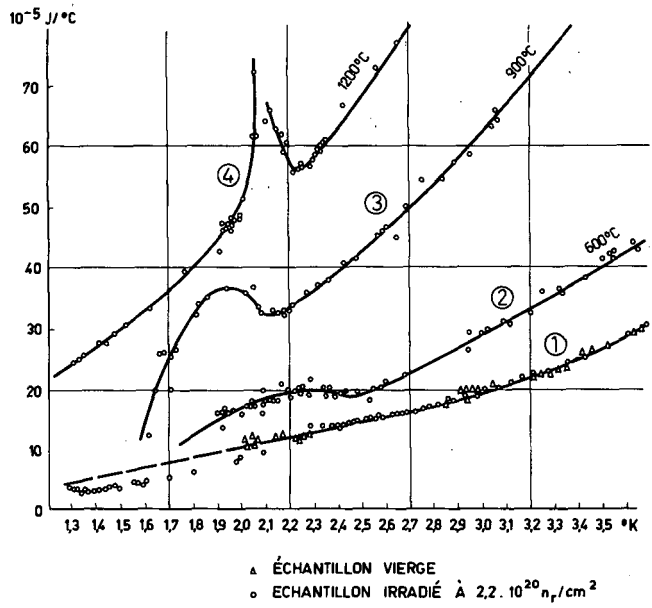


Figure 2

Variation de la chaleur spécifique en fonction de la température.

Sur la figure 2, les points indiqués par des triangles autour de la courbe 1 représentent la variation de la chaleur spécifique d'un échantillon de BeO non irradié de densité 2,95.

Après une irradiation de l'ordre de $2,2 \cdot 10^{20} n_r/cm^2$ à une température voisine de 400°C, la courbe des chaleurs spécifiques dans le domaine de

température étudié (points représentés par des cercles) reste identique à celle obtenue avant l'irradiation.

Des traitements thermiques sous vide ont été effectués sur cet échantillon irradié à 600, 900 et 1200°C durant 24 h chaque fois. La chaleur spécifique évolue respectivement après chacun des recuits, suivant les courbes 2, 3 et 4 de la figure 2.

Ainsi, après cette irradiation effectuée au voisinage de 400°C, les noyaux d'hélium sont suffisamment dispersés dans le réseau cristallin pour que les propriétés de l'hélium rassemblé ne soient pas décelables par la méthode utilisée.

Par contre, dès le recuit à 600°C, une anomalie de chaleur spécifique apparaît au voisinage de 2°K. Cet accident devient plus prononcé après traitement à 900°C et prend après le recuit à 1200°C l'allure caractéristique reconnue pour le point λ qui se trouve au voisinage de 2,14°K.

Si l'hélium se rassemble à 1200°C dans un fritté d'oxyde de béryllium irradié, c'est donc qu'à cette température ce gaz ne s'échappe pas ou tout au moins diffuse peu en dehors de l'échantillon.

Pour étudier l'extraction de l'hélium de l'oxyde de béryllium irradié, on a utilisé la poudre obtenue après irradiation à température inférieure à 100°C de frittés d'oxyde de béryllium de densités supérieures à 2,9. La dose reçue par ces échantillons était de l'ordre de $2{,}5 \cdot 10^{20}\ n_r/cm^2$; à ce flux devrait correspondre approximativement une formation d'hélium dans les frittés d'environ 100 mm^3 par gramme de BeO. Le calcul de la quantité de gaz formé est en fait très difficile à effectuer. En effet, la variation de la section de capture des réactions (n, 2n) et (n, α) en fonction de l'énergie des neutrons est rapide. De plus, le spectre des neutrons dans le flux utilisé est très mal connu.

Expérimentalement, la quantitié d'hélium déterminée par dissolution de la poudre irradiée dans la cryolithe à 1050°C est de 240 mm^3 par gramme de BeO.

Une autre prise d'essai de la même poudre chauffée sous vide à 1100°C durant trois heures ne laisse échapper que 0,5 à 1,5% de l'hélium contenu dans l'échantillon irradié. En prolongeant le recuit de cette poudre à la même température et en effectuant l'analyse des gaz par chromatographie, il n'a pas été possible de mettre en évidence un nouveau départ d'hélium[9]. La quantité minimum d'hélium détectable par cette méthode est de 1/10 de mm^3.

Par contre, on constate que l'hélium s'échappe beaucoup plus facilement de la même poudre d'oxyde de béryllium irradié traitée sous vide à 1500°C [10]. La courbe de la figure 3 donne le pourcentage du volume d'hélium extrait par rapport à la quantité totale contenue dans l'échantillon irradié, en fonction de la durée du chauffage à 1500°C. Dans ces conditions, il est possible d'extraire plus de 50% de ce gaz en moins de 15 h. La courbe de la figure 4 représente la vitesse d'extraction en fonction du temps. Dans ce cas, on remarque l'existence d'un net maximum de la vitesse d'extraction de l'hélium vers la deuxième heure de chauffage.

Des essais plus qualitatifs effectués à 1400°C montrent que les vitesses de dégazage de l'hélium sont alors au moins deux fois plus faibles qu'à 1500°C.

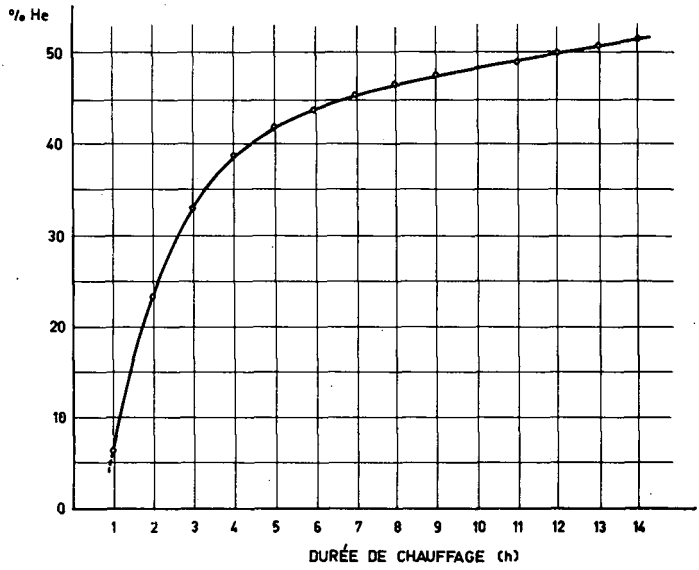


Figure 3

Pourcentage d'hélium extrait à 1500°C en fonction du temps.
BeO (poudre) irradié à $2,5 \cdot 10^{20}$ n_r/cm^2 ($T_{Ir} < 100°C$).

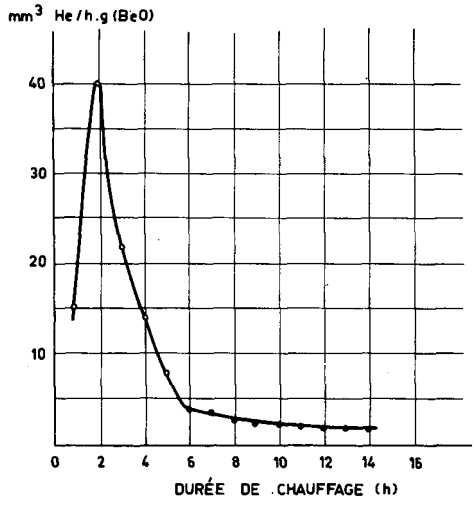


Figure 4

Vitesse d'extraction de l'hélium à 1500°C.
BeO (poudre) irradié à $2,5 \cdot 10^{20}$ n_r/cm^2 ($T_{Ir} < 100°C$).

4. EFFETS DE L'IRRADIATION SUR L'OXYDE DE MAGNÉSIUM

Puisque les neutrons produisent une déformation anisotrope des cristallites d'oxyde de béryllium, il peut être intéressant de comparer les résultats exposés plus haut à ceux obtenus avec l'oxyde de magnésium qui possède une structure cubique à face centrée.

Deux qualités de magnésie (A et B) ont été soumises à une irradiation de l'ordre de $2{,}2 \cdot 10^{20}$ n_r/cm^2, effectuée à une température voisine de 400°C. Dans les deux cas, les échantillons irradiés sont des pastilles de 12 mm de diamètre et de 12 mm de hauteur.

Magnésie A

Les pastilles sont frittées 10 h à 1700°C, en atmosphère ammoniac craqué à partir de la poudre «MgO RP.» [11]. La densité est de 95% de la valeur théorique; la porosité totale 4,5% et la porosité ouverte 0,05% du volume spécifique.

Magnésie B

L'oxyde de magnésium électro-fondu est fritté 2 h à 1850°C dans un four à gaz aux Etablissements Desmarquest. La densité moyenne est de 83% de la valeur théorique avec une porosité totale de 17,0% et une porosité ouverte de 16,1% du volume spécifique.

Après irradiation, la couleur des éprouvettes de la qualité A est devenue violet-noire, celle correspondant à la qualité B gris-noire. Le paramètre cristallin de MgO est déterminé à partir d'un diagramme de Debye et Scherrer sur la poudre obtenue après le test d'écrasement d'une pastille de qualité A. La valeur obtenue par extrapolation est égale à $4{,}2150 \pm 0{,}0008$ Å. Le paramètre du témoin est de $4{,}2115 \pm 0{,}0008$ Å.

La variation relative du paramètre est de l'ordre de $0{,}85 \cdot 10^{-3}$.

Les résistances à l'écrasement des pastilles de MgO ont été mesurées à 20°C (tableau VI) [12] et à 400°C (tableau VII) [13]. Ces déterminations ont été effectuées sur des témoins, sur des échantillons irradiés et sur des échantillons irradiés et recuits 24 h à 800°C. Les résultats montrent que l'irradiation produit une augmentation de la résistance à la compression, particulièrement sensible dans le cas de la qualité A, magnésie dense.

Malgré l'augmentation de cette caractéristique mécanique, l'étude au microscope électronique indique que la fracture des échantillons surtout transgranulaire avant irradiation évolue après irradiation vers une rupture où la proportion des décohésions est plus importante.

5. DISCUSSION DES RÉSULTATS

Il semble bien établi que l'irradiation des frittés sous charge d'oxyde de béryllium produit une déformation anisotrope du réseau cristallin qui provoque l'apparition de tensions entre les grains constituant le matériau.

TABLEAU VI

RÉSISTANCES A L'ÉCRASEMENT DE MgO A 20°C

Matériau	Traitements	Nombre d'éprouvettes	Résistance à l'écrasement (t/cm²)		$\frac{R_{EI}}{R_{Em}}$
			R_{Em}	e	
A	Non irradié	7	4,75	±4,8	1
	Irradié	3	9,64	6,6	2,01
	Irradié et recuit	4	10,46	3,9	2,20
B	Non irradié	7	3,00	4,5	1
	Irradié	3	3,52	3,4	1,17
	Irradié et recuit	4	3,10	1,6	1,03

R_{Em} : charge de rupture moyenne à 20°C

e : écart moyen des charges de rupture, en % de R_{Em}

R_{EI} : résistance à l'écrasement des éprouvettes irradiées / résistance à l'écrasement des éprouvettes irradiées et recuites

Ce phénomène entraîne la fragilisation et même la complète désagrégation des échantillons denses, quand la dose reçue atteint $2 \cdot 10^{20} n_r/cm^2$, à une température inférieure à 100°C.

Une intéressante comparaison peut être faite en rapprochant les résultats obtenus avec MgO et BeO pour deux irradiations effectuées dans les mêmes conditions: flux rapide $2{,}2 \cdot 10^{20} n_r/cm^2$, à une température voisine de 400°C. Les variations de volume de la maille cristalline des deux oxydes sont assez voisines de l'ordre de $3 \cdot 10^{-3}$, mais, alors que la dilatation est isotrope dans MgO, l'extension relative observée sur l'axe c de BeO est sept fois plus grande que la variation $\Delta a/a$. Parallèlement, alors que la résistance à la compression de BeO déterminée à 20 ou 400°C diminue après cette irradiation, cette caractéristique mécanique se conserve ou s'améliore dans le cas de l'oxyde de magnésium. La raison de l'augmentation de la résistance à l'écrasement de MgO après irradiation n'a pas été établie de façon certaine.

La formation de l'hélium dans BeO et de néon dans MgO ne semble pas avoir d'influence directe sur les caractéristiques mécaniques de ces frittés,

TABLEAU VII

RÉSISTANCES A L'ÉCRASEMENT DE MgO A 400°C

Matériau	Traitements	Nombre d'éprouvettes	Résistance à l'écrasement (t/cm²)		$\frac{R_{EI}}{R_{Em'}}$
			$R_{Em'}$	e	
A	Non irradié	6	4,55	±1,2	1
	Irradié	3	10,0	18	2,2
	Irradié et recuit	4	9,50	10	2,1
B	Non irradié	7	3,02	2,7	1
	Irradié	2	3,88	1,3	1,29
	Irradié et recuit	4	3,12	5,8	1,03

$R_{Em'}$: charge de rupture moyenne à 400°C

si ni la température d'irradiation ni les traitements thermiques effectués sur les échantillons après irradiation ne dépassent 400°C. Les mesures de chaleur spécifique montrent que le rassemblement de l'hélium sous forme de bulles n'est qu'à peine amorcé après des recuits à 600°C. Si des bulles ont été mises en évidence par fractographie après recuit des échantillons à 1000°C, elles n'ont une influence vraiment néfaste sur les propriétés mécaniques de BeO qu'après des traitements thermiques au-dessus de 1200°C [2].

L'apparition de tensions dans les frittés d'oxyde de béryllium sous irradiations, en particulier celles effectuées à basse température, nous conduit à une certaine prudence dans l'interprétation des diagrammes de rayons X de BeO irradié.

Les variations des paramètres cristallins et l'évolution du profil des raies dépendent en partie de l'état physique sous lequel se trouve l'échantillon de BeO. Ainsi, pour une même irradiation (flux intégré et température identiques), les résultats pourront être sensiblement différents suivant que l'oxyde est sous forme de poudre, formée de grains monocristallins, d'un fritté peu dense ou d'un fritté très dense. Avec ces derniers, les contraintes entre les grains empêchent la libre expansion du réseau cristallin due à l'effet des neutrons. Ces tensions auront une influence non seulement sur les valeurs des paramètres cristallins [18], mais aussi sur le profil des

raies. Dans les échantillons peu denses existe une plus grande possibilité d'accommodation des dilatations et des tensions que dans les frittés d'oxyde de béryllium de densité voisine de 3,0.

Au cas où les échantillons conservent une cohésion après irradiation, il n'est pas indiqué de les réduire en poudre pour entreprendre une étude cristallographique précise. En effet, il est à craindre que les résultats obtenus avec cette poudre ne correspondraient pas aux propriétés du fritté irradié.

Les résultats du tableau III ont été obtenus à partir d'aiguilles de BeO; la pointe utilisée pour l'étude aux rayons X n'a que de 0,5 mm ± 0,3 mm. Le diamètre des grains des frittés étudiés étant environ de 10 à 50 μ, le nombre des cristallites dans la pointe de l'aiguille n'est que de quelques dizaines. Dans ces conditions, après l'irradiation à $2,2 \cdot 10^{20}$ n_r/cm^2 effectuée à une température voisine de 400°C, on n'observe pratiquement pas de différence entre les valeurs des paramètres déterminés à partir d'aiguilles de densité comprise entre 2,65 et 3,00. De plus, l'étude de la restauration des paramètres cristallins de ces deux aiguilles par traitements thermiques montre que les résultats sont très voisins pour les deux densités. Par contre, on a remarqué lors d'une étude [15] de la guérison des paramètres cristallins d'aiguilles irradiées ($3 \cdot 10^{19}$ n_r/cm^2, $T_{Ir} < 100°C$), que $\Delta c/c$ diminuait plus rapidement dans le cas de l'oxyde de béryllium de densité 3,0 que dans celui d'un fritté de densité 2,6. D'autre part, il semble bien qu'après l'irradiation à 400°C, la valeur de $\Delta c/c$ soit plus petite pour les aiguilles que pour une poudre obtenue après la mesure de la résistance à l'écrasement d'une éprouvette de densité 2,98.

Des résultats préliminaires de la détermination à 1130°C de l'énergie emmagasinée dans l'oxyde de béryllium irradié par une méthode calorimétrique indiquent qu'il convient de tenir compte de l'énergie élastique correspondant aux tensions apparues dans les frittés sous irradiation. Ces mesures sont très délicates et des résultats antérieurs [16] ont indiqué que l'énergie libérée entre 100 et 500°C était très faible.

Enfin, un autre point important pour le comportement de l'oxyde de béryllium sous irradiation est l'évolution de l'hélium dans le fritté, puis hors du solide en fonction de la température. Ce gaz s'échappe relativement facilement de l'oxyde de béryllium à 1500°C; son extraction paraît encore possible à 1400°C. Par contre, à 1100°C, il est très difficile de sortir plus de 1,5% de la quantité emmagasinée dans un fritté, tombé en poudre, ayant reçu $2,5 \cdot 10^{20}$ n_r/cm^2 à une température inférieure à 100°C.

D'autre part, l'étude par fractographie des échantillons irradiés a montré qu'avant de sortir du fritté, l'hélium se rassemble sous forme de bulles situées de préférence aux joints de grains. L'étude de l'oxyde de béryllium irradié par une méthode consistant en des déterminations de la chaleur spécifique de l'échantillon au voisinage de 2,1°K, température correspondant au point λ de l'hélium, a permis de prouver la présence de l'hélium dans ces bulles et la mobilité de ce gaz dans le solide à 600°C.

CONCLUSION

Cette étude a mis en évidence l'importance des tensions apparues dans les frittés sous charge d'oxyde de béryllium irradié. Ces tensions dues à

la déformation anisotrope des cristallites sous l'effet des neutrons sont la cause de la fragilisation des échantillons, de leur fragmentation et de leur décohésion. L'énergie élastique contenue après irradiation dans les frittés conservant une certaine cohésion semble être une partie non négligeable de l'énergie «Wigner».

D'autre part, l'hélium ne semble s'éliminer que très difficilement de l'oxyde de béryllium irradié au-dessous de [17] 1100°C. Ce résultat indique deux voies dans les possibilités d'utilisation des frittés d'oxyde de béryllium comme modérateur dans un réacteur.

a) Piles dans lesquelles le modérateur est à une température comprise entre 600 et 900°C. La température est suffisamment élevée pour que les dégâts dus à l'irradiation soient limités [17], mais ne permet pas à l'hélium de s'échapper de l'oxyde de béryllium. Dans ces conditions, pour un fonctionnement d'une dizaine d'années, le flux rapide ne devra vraisemblablement pas dépasser $10^{13} n_r/cm^2 \cdot s$.

b) Piles où le flux rapide dans le modérateur est de l'ordre de $10^{14} n_r/cm^2 \cdot s$. Dans ces conditions, la formation de gaz devient importante pour des fonctionnements de longue durée. La température du modérateur doit alors être au moins de 1200°C et les frittés convenablement choisis pour permettre à l'hélium de s'échapper. A ces températures, l'accumulation de ce gaz dans BeO pourrait être dangereuse pour la tenue mécanique du matériau. Le tritium s'éliminerait beaucoup plus facilement que l'hélium [17] et ne serait donc pas à redouter.

REMERCIEMENTS

Je suis reconnaissant à MM. Salesse et Caillat de l'intérêt qu'ils ont porté à ce travail et à mes collaborateurs de la Section d'étude des réfractaires de leur précieux concours dans ces recherches.

Je remercie particulièrement M. le Professeur L. Weil et M. le Professeur C. Eyraud de l'importante contribution que les expériences effectuées dans leur laboratoire ont apportée à cette étude.

RÉFÉRENCES

[1] ELSTON, J. et CAILLAT, R., Actes 2e Conf. Genève 3 (1958) 715.
[2] ELSTON, J. et LABBE, C., J. nucl. Mater. 4, 2 (1961) 143.
[3] ELSTON, J., GEWISS, C. et LABBE, C., C.R. Acad. Sci. 249 (1959) 1635.
[4] SIMBOZEL, M., DM/CS/ER/1513.
[5] LABBE, C., DM/CS/ER/1142.
[6] EYRAUD, L, SICARD, L. et PETIT, J.L., C.R. Acad. Sci. 252 (1961) 1740.
[7] FRISBY, H., BISSON, A. et CAILLAT, R., C.R. Acad. Sci. 248 (1959) 672; J. nucl. Mat. 1 (1959) 106.
[8] ASLANIAN, J., CAILLAT, R., SALESSE, M. et WEIL, L., C.R. Acad. Sci. 253 (1961) 1032.
[9] CARTERET, Y., DM/CS/ER/1046.
[10] CARTERET, Y. et BESSON, M., DM/CS/ER/1514.
[11] ROGER, J., MCA/22/4346.
[12] LABBE, C., DM/CS/ER/996.
[13] LABBE, C. et THOUMY, J., DM/CS/ER/1408.
[14] FRISBY, H., DM/CS/ER/996.
[15] BELBEOCH, B. et LAIGLE, MC., DM/CS/ER/549.

[16] CLARKE, F. J. P. et WILLIAMS, J., AERE M/M 229 (1959).
[17] KEILHOLTZ, G. W. et LEE, J. E., ORNL 3210 (Sept. 1961).
[18] HICKMAN, B. S., SABINE, T. M. et COYLE, R. A., Communication personnelle.
[19] MORIZE, P. et TOURNIER, A., DM/CS/ER/1091.

RADIATION EFFECTS IN SINTERED BeO BODIES OF SEVERAL COMPOSITIONS*

C.G. COLLINS
NUCLEAR MATERIALS AND PROPULSION OPERATION,
GENERAL ELECTRIC COMPANY, CINCINNATI, OHIO

Abstract — Résumé — Аннотация — Resumen

RADIATION EFFECTS IN SINTERED BeO BODIES OF SEVERAL COMPOSITIONS. Results are presented from a programme in progress to define radiation effects in BeO in terms of purity, density, grain size, porosity, and irradiation dosage and temperature. The initial data reported cover five BeO compositions prepared by extrusion and sintering of three commercially available grades of BeO of different purities and of one high-purity grade with MgO and ZrO_2 as additives. Specimens were of density 2.90 - 2.95 g/cm^3 and of 15 - 20 μm grain size, with the exception of one group of specimens of 50-μm grain size. Measurements were performed following irradiation at ~ 100°C to dosages up to ~4×10^{20} n/cm^2 (≥ 1 MeV) and include lattice constants, dimensions, density, elastic constants, modulus of rupture, thermal expansion, thermal conductivity, and thermal annealing.

Changes produced by irradiation were, in general, of the types and amounts observed previously but differed for the various compositions. Gross expansion of the specimens amounted to ~ 1% at the maximum dosage. Non-uniform growth in the diameter as compared to the length of the specimens of some compositions was attributed to grain orientation. Lattice expansion could be followed in powder-diffraction patterns up to a dosage of ~ 1.9×10^{20} n/cm^2; at higher dosages patterns were too diffuse for measurement. Young's modulus (dynamic) was increased about 1%. The modulus of rupture decreased to about 10% of the non-irradiated value and was more pronounced in the specimens of the less pure compositions.

Thermal annealing measurements indicated that annealing was dependent on the amount of radiation-induced expansion, i.e., on the dosage. In specimens irradiated to greater than ~ 10^{20} n/cm^2, annealing of the gross expansion at temperatures up to 800°C was less than 20% in time periods up to 1000 h. Essentially complete annealing occurred in ~ 40 h at 1000°C and ~ 1 h at 1100°C. Detailed annealing data and kinetics are discussed together with data on recovery of properties following annealing.

INFLUENCE DES RAYONNEMENTS SUR DIVERS OXYDES DE BÉRYLLIUM FRITTÉS. L'auteur présente les résultats de travaux entrepris pour déterminer les effets des rayonnements dans l'oxyde de béryllium en fonction de la pureté, de la densité, de la porosité, de la dimension des grains, des doses et de la température d'irradiation. Les premiers résultats portent sur cinq compositions de BeO, préparées par extrusion et frittage : trois d'oxydes de qualités commerciales différentes et de degrés de pureté différents, et deux d'oxyde très pur avec addition de MgO et ZrO_2. La densité des échantillons était de l'ordre de 2,90 - 2,95 g/cm^3, tandis que le diamètre des grains variait entre 15 et 20 μ, sauf pour un groupe où il était de 50 μ. Des mesures des constantes du réseau cristallin, des dimensions, de la densité, des constantes élastiques, du module de rupture, de la dilatation thermique, de la conductivité thermique et du recuit thermique ont été faites à la suite d'irradiations à des doses allant jusqu'à $4 \cdot 10^{20}$ n/cm^2 (≥1 MeV), à la température de 100°C.

En général, les modifications provoquées par l'irradiation sont conformes, qualitativement et quantitativement, aux observations antérieures, mais elles présentent certaines différences suivant les diverses compositions. La dilatation brute des échantillons est de l'ordre de ~ 1% à la dose d'irradiation maximum. La non-uniformité de l'accroissement relatif du diamètre par rapport à la longueur des échantillons de certaines compositions est attribuée à l'orientation des grains. Des mesures de la dilatation du réseau ont pu être faites grâce aux diagrammes de diffraction sur poudre jusqu'à une dose de ~$1,9 \cdot 10^{20}$ n/cm^2; aux doses supérieures, les diagrammes étaient trop diffus pour permettre des mesures. Le module de Young (dynamique) augmente de 1% environ. Le module de rupture décroît d'environ 10% et il est plus accentué dans les compositions moins pures.

Les mesures de recuit thermique montrent que le recuit dépend de la dilatation radioinduite, c'est-à-dire de la dose d'irradiation. Dans des échantillons irradiés par des flux supérieurs à ~10^{20} n/cm^2, la guérison de

* Work performed under the auspices of the United States Atomic Energy Commission.

la dilatation brute, à des températures allant jusqu'à 800°C, n'atteignait pas 20% pour des durées atteignant 1000 h. Une guérison complète est obtenue en ~40 h à 1000°C et en ~1 h à 1100°C. L'auteur examine les données détaillées et la cinétique du recuit ainsi que les données sur la guérison consécutive au recuit.

ДЕЙСТВИЕ ИЗЛУЧЕНИЯ НА НЕКОТОРЫЕ ШЛАКООБРАЗНЫЕ СОЕДИНЕНИЯ BeO. На основе осуществляемой программы по определению действия излучения в BeO были получены результаты с точки зрения чистоты, плотности, размера зерен, пористости, дозы излучения и температуры. Первоначальные данные, которые сообщались, относятся к пяти составам BeO, подготовленных с помощью экструзии и отшлаковывания трех коммерческих сортов BeO различной чистоты и одного сорта высокой чистоты MgO и ZrO_2 как аддитивных. Образцы имели плотность 2,90 - 2,95 г/см³ и размер зерна 15 - 20 микрон, за исключением одной группы образцов, которая имела размер зерна 50 микрон. Измерения проводились после облучения при ~100°C при дозах ~4 · 10^{20} н/см² (≥ 1 Мэв) и включали в себя определение постоянных решетки, размеры, плотность, упругие константы, модуль разрыва, тепловое расширение, теплопроводность и тепловой отжиг.

Изменения, вызванные облучением, оказались в общем таких же типов и в таких же количествах, которые наблюдались ранее, но были разными для различных составов. Большое расширение образцов достигало приблизительно 1% при максимальной дозе. Неравномерное увеличение в диаметре по сравнению с длиной образцов некоторых соединений получалось за счет ориентации зерна. Расширение решетки могло бы произойти в образцах порошковой дифракции при дозе ~1,9 · 10^{20} н/см²; при более высоких дозах образцы были слишком диффузными, чтобы их можно было измерить. Модуль Юнга (динамический) увеличился почти на 1%. Модуль разрыва уменьшился почти до 10% необлученной величины и был более значителен в образцах менее чистых соединений.

Измерения теплового отжига показали, что отжиг зависит от количества излучения, вызывающего расширение, то-есть от дозы. В образцах, облучавшихся дозой более ~ 10^{20} н/см², отжиг, в течение около 1000 часов, при температуре до 800°C приводил к уменьшению расширения на 20%. Почти полный отжиг имел место при ~40 часах и при 1000°C и приблизительно 1 час при той же температуре. Обсуждаются подробные данные отжига и динамики вместе с данными по восстановлению свойств после отжига.

EFECTOS DE LAS RADIACIONES EN PIEZAS DE BeO SINTERIZADAS DE DISTINTAS COMPOSICIONES. El autor expone los resultados de un programa experimental que se está ejecutando para determinar los efectos de las radiaciones en el BeO, en función de la pureza, densidad, tamaño de grano, porosidad, dosis de irradiación y temperatura. Los datos iniciales se refieren a cinco compuestos de BeO, preparados por extrusión y sinterización de tres variedades comerciales de BeO de pureza diferente y de una variedad de elevada pureza, con MgO y ZrO_2 como aditivos. La densidad de las muestras utilizadas fue de 2,90 - 2,95 g/cm³, y el tamaño de grano de 15 - 20 μ, a excepción de un grupo de muestras cuyo tamaño de grano es de 50 μ. Después de irradiar las probetas a unos 100°C, con flujos de hasta 4 · 10^{20} n/cm² (≥ 1 MeV) se midieron los siguientes parámetros: constantes reticulares, dimensiones, densidad, constantes elásticas, módulo de rotura, dilatación térmica, conductividad térmica y recocido térmico.

En general, las modificaciones causadas por la irradiación son, desde el punto de vista cualitativo y cuantitativo, análogas a las observadas anteriormente, pero difieren para las diferentes composiciones. La macrodilatación de las muestras asciende a ~1%, para el flujo máximo. El aumento no uniforme del diámetro, en relación con la longitud de las muestras de determinadas composiciones, se atribuye a la orientación del grano. La dilatación reticular se ha podido observar en diagramas de difracción de polvos hasta un flujo de ~1,9 · 10^{20} n/cm²; cuando el flujo es superior, los diagramas resultan demasiado difusos para efectuar mediciones. El módulo de Young (dinámico) aumenta en un 1%, aproximadamente. El módulo de rotura disminuye hasta cerca del 10% del valor correspondiente a la muestra sin irradiar y es más acusado en las probetas menos puras.

Las mediciones referentes al recocido térmico muestran que la recuperación por recocido depende del grado de dilatación provocado por las radiaciones, y por tanto, de la dosis. En las muestras irradiadas con flujos superiores a ~10^{20} n/cm², la recuperación por recocido de la macrodilatación a temperaturas de hasta 800°C es inferior al 20%, en un período de hasta 1000 h. Se ha obtenido una recuperación prácticamente completa en unas 40 h a 1000°C y en ~1 h a 1100°C. El autor examina con detalle los resultados relativos al recocido, los fenómenos cinéticos y los datos referentes a la recuperación de las propiedades a raíz del recocido.

1. INTRODUCTION

The expansion behaviour of BeO in low-temperature neutron irradiations has been fairly well defined in previous investigations. The causative processes, anisotropic expansion of the lattice and production of helium and tritium gases by transmutations, lead to macroscopic expansion of sintered bodies which extends to disintegration. A recent review and summary of the data and expansion mechanisms has been completed by CLARKE [1]. Some of the details of the expansion processes remain conjectural, however, as a result of differences in the specimens, dosages, and other variables studied. The results of the present investigation relate to the expansion behaviour leading up to disintegration and provide some further details of the process involved.

The data were obtained in a programme directed to determination of the influence of specimen composition on radiation effects. Studies of two of the six compositions under investigation were relatively complete and are presented together with the limited data on the remaining compositions. Some of the compositions contained a degree of preferred crystal orientation and it was possible to examine the expansion and thermal annealing behaviour of specimens of both random and preferred orientations

The experimental programme consisted essentially of irradiation, at a temperature of 100°C, of the six BeO compositions over a range of dosages. Dimension, volume, strength, and thermal-annealing measurements were completed after irradiation.

2. PROCEDURES

The six compositions studied are defined in Table I in terms of the grade designation of the powder material used in their preparation; the notation listed in the first column will be followed in the remainder of this report. The three grades of BeO powder used may be briefly described as follows:

TABLE I

DEFINITION OF THE SIX BeO COMPOSITIONS STUDIED

Notation used	Composition	Powder raw-material
AOX	AOX	AOX
UOX	UOX	UOX
UOX-MgO	UOX - 0.5 wt.% MgO	UOX
UOX-ZrO_2	UOX - 3.0 wt.% ZrO_2	UOX
HPA	HPA	HPA
HPA-MgO	HPA - 0.5 wt.% MgO	HPA

(1) The AOX-grade BeO is supplied by Brush Beryllium Company. It is a relatively low-purity material averaging about 1500 to 2000 ppm total impurities. The principal impurity elements (those present in concentrations of 100 ppm or higher) are fluorine, sodium, silicon, carbon, and manganese. The size of the crystallites is about 400 Å by X-ray analysis.

(2) The UOX-grade BeO is also supplied by the Brush Beryllium Company. Although the production process has not been described by the manufacturer, UOX is generally considered to be derived from the sulphate. The principal impurity elements are sulphur (400 to 1000 ppm), calcium (~100 ppm) and carbon (~100 ppm); the total impurity concentration ranges from 800 to 1500 ppm. The crystallite sizes ranges from 600 to 1000 Å.

(3) HPA is our laboratory's designation for high-purity BeO derived from the basic acetate process. The material used in this programme is obtained from the Mineral Concentrates and Chemical Company as beryllium hydroxide. After being calcined to BeO at 950°C, the material contains a total of 100 to 150 ppm of impurities and is comprised of crystallites of about 1000Å diameter.

Many of the impurities are removed during sintering and, as indicated by the specimen analyses listed in Table II, the difference in chemical composition of the actual specimens appears slight. Differences in the properties of the specimens, other than those due to crystal orientation, were nevertheless apparent.

Specimens were solid right cylinders 0.238-in diam. by 3.5-in long and were of a common grain size and fraction of theoretical density. Grain sizes ranged from 15 to 22 μm by lineal analysis[1], the most common value being about 17 μm. All specimens were of density 2.90 to 2.95 g/cm^3 except those of the UOX-ZrO_2 composition which were made 2.94 to 2.98 g/cm^3 in order to maintain the same fraction of theoretical density (0.96 to 0.98). UOX-ZrO_2 was the only composition that did not exhibit a single-phase microstructure; at least some of the zirconia appeared as a separate grain-boundary phase. A few data are included on AOX specimens of 50-μm grain size and 2.90 to 2.95 g/cm^3.

The specimens were prepared by extrusion and sintering. The powder materials were combined with an aqueous organic plasticizer[2] and extruded at 6000 lb/in^2 with a 4-in diam. ram, the extruded size being 0.352 in diam. The extruded pieces were then dried at 110°C (by step-wise reduction of humidity) pre-fired in air at 810°C and finally sintered in dry hydrogen at 1500 to 1700°C. Typical sintering conditions are listed in Table III. Final specimen dimensions were obtained by centreless grinding, following which the rods were inspected by Zyglo, X-ray and ultrasonic techniques. All specimens received a final heat treatment of 1 h at 425°C to remove traces of the fluids used in inspection.

---

[1] ASTM Method E 112. The average intercept is determined by measuring the total length of 100 grains in several random parts of a polished section. Grain diameter is then calculated as $4/\pi$ times the average intercept.

[2] A hydroxy-ethyl ether derivative of starch.

TABLE II

IMPURITY LEVELS AFTER SINTERING IN BeO RODS OF SIX COMPOSITIONS

Impurity element	AOX 2*	UOX 4*	UOX-MgO 2*	UOX-ZrO_2 4*	HPA 2*	HPA-MgO 2*
	(ppm impurities)					
C	115	160	125	186	145	86
F		20	20	10	15	20
P		27	23	16	25	22
S	15	23	60	26	35	30
Al	25	50	45	50	30	83
B	<3	<3	<3	<3	<3	<3
Ca	80	130	150	125	25	28
Cr	10	24	35	20	18	45
Fe	103	240	215	140	118	205
Li	<1	<1	<1	<1	<1	<1
Mg	110	80		72	85	
Mn		<10	20	<10	<10	<10
Na	25	17	10	15	25	12
Ni	33	35	33	30	<10	50
Si	83	90	95	113	125	180
Sr		<10	<10	<10	<10	<10
Zn		<20	<20	<20	<20	<20

* Number of determinations.

For the irradiations, the specimens were sealed in air in aluminium capsules which were exposed directly to the reactor coolant water in the Engineering Test Reactor[3]. Thermocouples indicated the maximum specimen temperature to be 100 to 110°C. Exposures ranged up to a dosage of 8×10^{20} n/cm^2 (≥ 1 MeV) as determined by Ni-Co^{58} and Fe-Mn^{54} dosimeters. The "reactor" thermal flux measured with unshielded cobalt, was approximately equal to the flux ≥ 1 MeV.

3. PREFERRED ORIENTATION

One of the most interesting differences in the specimens was preferred orientation in the compositions made from the UOX grade of material. The AOX and HPA compositions appeared to be very close to a random orien-

[3] Engineering Test Reactor (ETR); Idaho Falls, Idaho.

tation. Preferred orientation in the UOX compositions consisted of a degree of alignment of the crystallographic c-axis with the longitudinal, or extrusion, axis of the specimens[4]. Measurements indicated that about four times as many crystals were oriented with their c-axes within 10 to 15° of the longitudinal axis of the specimen as would occur in a random distribution.

The influence of the preferred orientation on the physical properties is being studied at present. The effect on Young's modulus has been clearly established by examination of UOX-MgO specimens of both preferred and random orientation. The latter specimens were prepared by isostatic pressing and the random orientation verified by X-ray analysis. The oriented specimens possessed a Young's modulus 9% greater than the randomly oriented ones.

This comparison is shown in Fig. 1 together with the curves of the variation of the modulus of the six compositions over a range of porosity. The

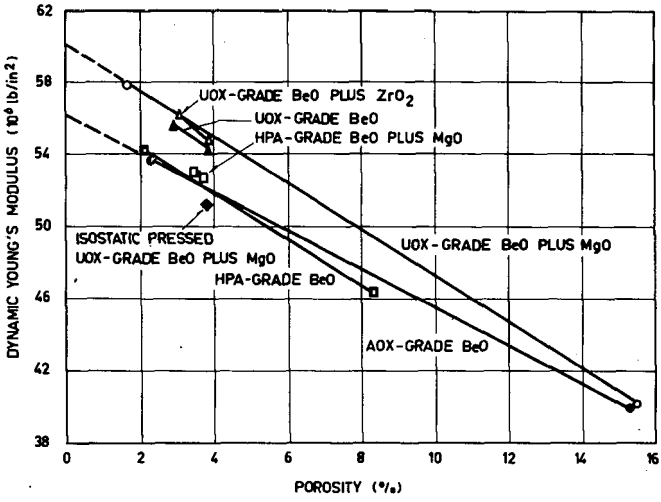


Fig. 1

Dynamic Young's modulus against percentage porosity for six compositions of BeO at 20°C

points on the curves represent the extremes of the porosity range examined[5]. The value for the randomly oriented UOX-MgO lies close to the curves for the other randomly oriented compositions – AOX, HPA, and HPA-MgO. The moduli of the three preferentially oriented UOX compositions form a second, separate grouping. As indicated in Figs. 2 and 3, similar separation of modulus-of-rupture data and of creep data into groups corresponding to oriented and random specimen types is indicative of an orientation effect on these properties; in these instances, however, there remains the possibility that the differences are due to compositional variations. The creep data are recorded in Table IV.

[4] It is in this sense that the term preferred orientation will be used in this report.

[5] Correlation co-efficients for UOX-MgO and AOX were 0.974 and 0.987 respectively, indicating that 90 and 97.5% of the variation in E was due to porosity.

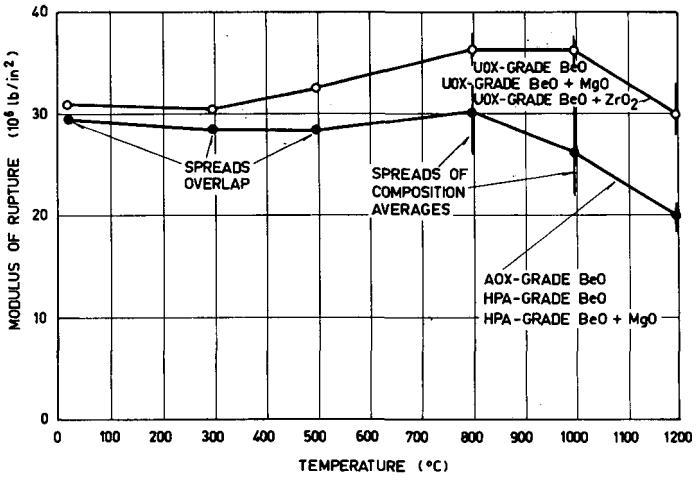


Fig. 2

Modulus of rupture against temperature for BeO
All samples had a density of 2.90 g/cm^3 and a size of 20 μm.

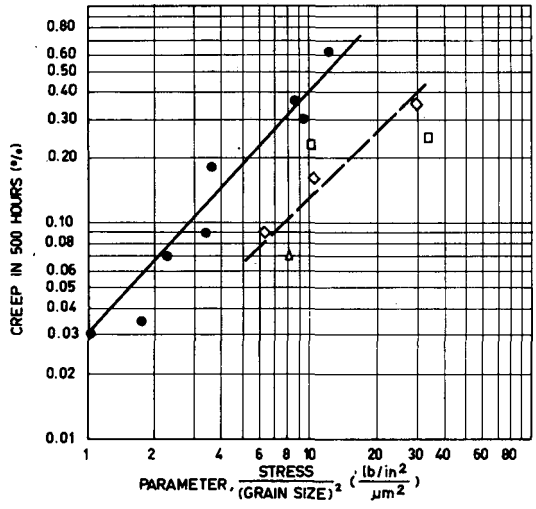


Fig. 3

Percentage creep in 500 h as a function of stress and grain size

- ● AOX-gradė BeO
- □ UOX-grade BeO plus MgO
- ◇ UOX-grade BeO
- △ UOX-grade BeO plus ZrO_2

TABLE III

SINTERING CONDITIONS FOR BeO COMPOSITIONS STUDIED

Composition*	Density range (g/cm^3)	Sintering time (h)	Sintering temperature (°C)
UOX	2.90-2.95	1	1700
UOX-MgO	2.90-2.95	2	1480
UOX-ZrO_2	2.94-2.98	1	1700
AOX	2.90-2.95	3	1540
HPA	2.90-2.95	4	1700
HPA-MgO	2.90-2.95	2	1540

* All compositions of 15 to 22 μm grain size.

4. RESULTS

Volume and dimensional expansion following irradiation are summarized in Table V. The volume-expansion behaviour, illustrated in Figure 4, consisted of two regions in which the rate of expansion appeared to vary linearly with dosage. The initial expansion rate of 0.6% per 10^{20} n/cm^2 applied up to a dosage of about $(1.5-2) \times 10^{20}$ n/cm^2 ($E \geq 1$ MeV). This rate of expansion was obtained from the more numerous low-dosage results reported by CLARKE and WILLIAMS [2] and ELSTON and LABBE [3]. Extrapolation of their results gives good agreement with the volume expansion of the randomly oriented AOX specimens. At higher dosages the rate of expansion increased to 1.4% per 10^{20} n/cm^2 and continued at this rate to at least the 4×10^{20} dosage. The expansion of the different compositions, while generally similar, showed some variation. The two curves shown in Fig. 1 are drawn through the data for the UOX-MgO and AOX compositions, the separation in the curves at 4×10^{20} n/cm^2 being considered real since these particular specimens were irradiated in the same capsule. All of the compositions based on the UOX grade of BeO fall on one curve. The HPA data fall on both curves, presumably because of some uncertainty in the dosage.

The maximum volume expansion measured, about 6.1%, occurred at a dosage of 6×10^{20} n/cm^2 in the UOX specimen. This measurement was made on a fragment of a specimen that received the lowest dosage in an irradiation cartridge in which the dosage ranged up to 8×10^{20} n/cm^2. With the exception of the two HPA compositions, the other compositions were intact but too fragile for density and dimension measurements. Both of the HPA compositions had disintegrated into powder at dosage of $\sim 7 \times 10^{20}$ n/cm^2. These observations indicate that the limiting dosage for these irradiation conditions is $(6-8) \times 10^{20}$ n/cm^2 and that the volume expansion corresponding to disintegration is of the order of 6 to 8%.

Dimensional expansion of the specimens followed the two-stage pattern of the volume changes and ranged up to a maximum measured value of about

TABLE IV

COMPRESSIVE CREEP OF BeO SPECIMENS AT 1200°C

Material	Grain size [a] (μm)	Density (g/cm^3)	Porosity (%)	Stress (lb/in^2)	Creep [b] in 500h (%)
AOX	15	2.87	4.8	3000	0.62
	16	2.88	4.4	1000	0.18
	17	2.79	7.3	3000	0.30
	(19)	2.76	8.4	3000	0.37
	(36)	2.90	3.6	3000	0.07
	42	2.91	3.5	6000	0.09
	41	2.97	1.4	3000	0.03
	46	2.97	1.4	2000	0.03
HPA	8	2.90	3.7	3000	0.18
	(12)	2.83	6.0	3000	0.67
	17	2.89	3.9	6000	0.21
HPA-MgO	18	2.94	2.5	3000	0.14
	18	2.94	2.3	3000	0.18
	(18)	2.94	2.4	6000	0.58
UOX-MgO	13	2.94	2.5	6000	0.25
	17	2.90	3.8	3000	0.23
UOX	(18)	2.87	4.7	10000	0.35
	22	2.90	3.6	3000	0.09
	24	2.89	4.1	6000	0.16
UOX-ZrO_2	19	2.94	3.3	3000	0.07

[a] Measured on actual pieces tested, except values in parentheses which are from other rods in the same sintering batch.

[b] Column loading or specimens 1-in long by 0.238-in diameter, Tested in dry air.

2%. Differences were apparent in the expansion behaviour of the various compositions. On a percentage basis, diameter expansion in the AOX specimens was greater than length expansion (see Fig. 5). The ratio of the percentage changes in length versus diameter was about 0.6 to 0.8. (Some comment should be made regarding the difference in the length and diameter expansion of the AOX specimens. For a randomly oriented material, of course, equal expansion of the two dimensions would be expected. Since orientation measurements indicate that the material is random, the reason for the difference in the expansion in the two dimensions is not readily apparent. The possibility of measurement error because of the small diametral dimension would seem to be minimized, if not eliminated, by the magnitude of the changes at the higher dosages. A more likely possibility is that, since the contribution of the grain-boundary separation to the expansion is proportional to the dimension, there is an inherent bias in measurements where the specimen dimensions differ appreciably.) The

TABLE V

DIMENSIONAL AND VOLUME CHANGES IN BeO IRRADIATED AT 100°C

Specimen composition[a]	Dosage (E ≥ 1 MeV), (10^{20} n/cm^2)	Dimensional expansion		Decrease in bulk density (%)	Increase in volume (%)
		Length (%)	Diameter (%)		
AOX	0.086	0.03	<0.08	<0.1	-
	1.2	0.16	0.23	0.7	0.7
	1.6	0.21	0.29	1.0	1.1
	1.8	0.30	0.40	1.2	1.3
	2.0	0.36	0.47	1.3	1.3
	2.0	0.41	0.51	1.6	1.6
	2-1	0.44	0.59	1.5	1.6
	3.7	1.14	1.4	3.4	4.0
	3.9	1.41	1.7	3.8	4.1
	4.0	1.45	1.7	4.2	4.4
	8.1	Intact, disintegrated on handling			
UOX-MgO	0.088	0.03	<0.08	<0.1	-
	1.3	0.23	0.14	0.7	0.7
	1.8	0.36	0.23	1.0	1.0
	1.8	0.40	0.30	0.9	1.0
	2.1	0.50	0.35	1.1	1.2
	2.2	0.53	0.36	1.1	1.2
	2.3	0.55	0.43	1.3	1.4
	3.2	-	-	-	-
	3.6	-	-	-	-
	4.0	1.8	1.4	3.9	3.7
	8.1	Intact, disintegrated on handling			
HPA	0.082	0.02	<0.08	<0.1	-
	3.6	1.62	1.0	3.6	3.8
	4.5	-	1.4	4.6	4.8
	7.8	Powder			
HPA-MgO	0.074	<0.006	<0.08	<0.1	-
	7.4	Powder			
UOX	0.061	0.02	<0.08	<0.1	-
	3.8	1.8	1.3	4.2	4.5
	6.0	Not measurable	2.1	5.8[b]	6.3
UOX-ZrO_2	0.074	<0.006	<0.08	-	-
	5.4	2.1	1.7	5.4	5.8
	7.4	Intact, disintegrated on handling			

[a] All specimens 15 to 20 μm grain size and density of 2.90 to 2.95 g/cm^3 except UOX-ZrO_2 2.94 to 2.98 g/cm^3.

[b] Data from single measurement; all other values quoted are average of six specimens.

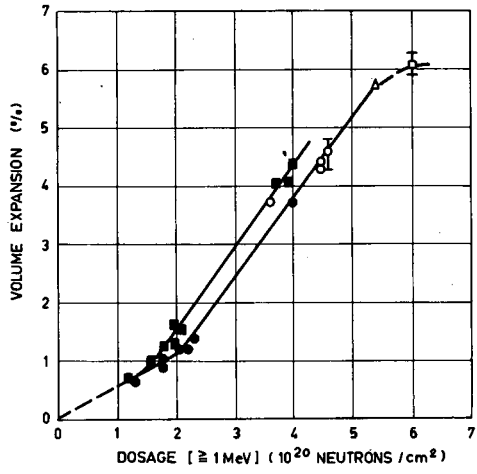


Fig. 4

Volume expansion in BeO compositions irradiated at 100°C as a function of dosage

■ AOX-grade BeO
○ UOX-grade BeO plus MgO
□ UOX-grade BeO
△ UOX-grade BeO plus ZrO_2
● HPA-grade BeO

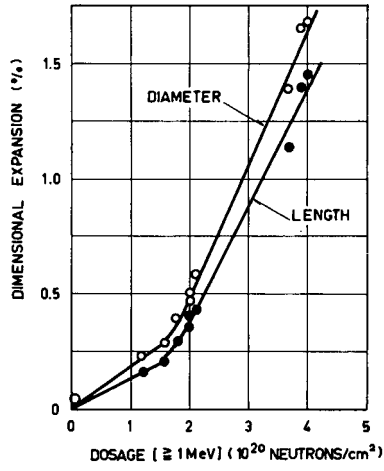


Fig. 5

Dimensional changes in AOX-grade BeO irradiated at 100°C

reverse of this behaviour occurred in the remaining compositions; the ratio of percentage changes (length versus diameter) being about 1.6. Fig.6 shows the expansion curves for the UOX-MgO composition and includes points for the UOX, UOX-ZrO_2 and HPA compositions. In contrast to the volume ex-

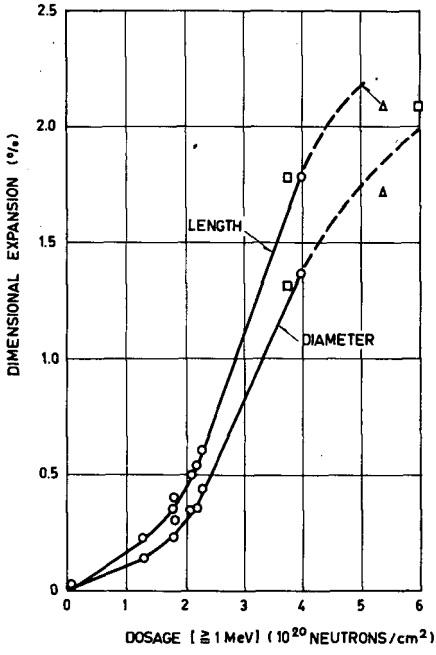


Fig. 6

Dimensional changes in UOX compositions irradiated at 100°C

○ UOX-grade BeO plus MgO
□ UOX-grade BeO
△ UOX-grade BeO plus ZrO_2

pansion data, the dimensional changes in the three compositions based on UOX material did not fall on the same curve; it has not been established whether this difference represents a true difference in the specimens or is simply due to uncertainties in the dosages.

The lattice expansion data, summarized in Table VI, were in general agreement with extrapolations of previous data. Measurements were obtained by Debye-Scherrer photographs on powder made by pulverizing the specimens following their irradiation. With this technique, the c-axis expansion could be measured only at dosages up to about 2×10^{20} n/cm^2; at this point, the expansion was approximately 0.52% and was 7 to 8 times that in the a-axis. The a-axis was measurable at higher dosages, the maximum observed value amounting to 0.16% in a specimen irradiated to 5.4×10^{20} n/cm^2. Since the lattice expansion is not expected to differ appreciably in different compositions, comparison of the Δa values should be possible; on this basis the expansion of the a-axis was not saturated at less than 5×10^{20} n/cm^2. However, the change per unit dosage indicated that the onset of saturation occurred between 3.5×10^{20} and 5×10^{2} n/cm^2.

Elastic constants could be measured by the resonant frequency method only at the lowest dosage of 8×10^{18} n/cm^2. The measurements at this dosage showed an increase in both the Young's and shear moduli of about 1%. The trend

TABLE VI

LATTICE PARAMETER MEASUREMENTS IN BeO IRRADIATED AT 100°C

BeO Grade	Dosage (E ≧ 1 MeV) (n/cm^2)	Lattice parameters							
		a-Axis (Å)	Δa (Å)	c-Axis (Å)	Δc (Å)	Δa %	Δc %	%Δc / %Δa	ΔV[a] %
AOX	none	2.6980	-	4.3780	-	-	-	-	-
AOX	1.8×10^{20}	2.6998	0.0018	4.4000	0.0220	0.0667	0.503	7.54	0.637
AOX	2.1×10^{20}	2.6998	0.0018	4.4011	0.0231	0.0667	0.528	7.92	0.662
UOX-MgO	none	2.6982	-	4.3780	-	-	-	-	-
UOX-MgO	2.05×10^{20}	2.7002	0.0020	4.4007	0.0227	0.0941	0.519	7.00	0.667
UOX-MgO	2.2×10^{20}	2.7004	0.0022	4.4031	0.0251	0.015	0.573	7.03	0.738
HPA	none	2.6979	-	4.3777	-	-	-	-	-
HPA	$\sim 3.6 \times 10^{20}$	2.7013	0.0034	-[b]	-	0.1260	-	-	-
UOX-ZrO_2	none	2.6980	-	4.3780	-	-	-	-	-
UOX-ZrO_2	$\sim 5.4 \times 10^{20}$	2.7024	0.0044	-[b]	-	0.1631	-	-	-

[a] V = volume.

[b] Lines on Debye-Scherrer photographs were too diffuse for measurement.

of the results in this dosage range was thus the same as that noted by CLARKE and WILLIAMS [2]. At the higher dosages investigated, the resonant frequency was reduced in amplitude to the level of some of the background peaks and could not be detected with certainty. By analysis of the observed frequency peaks for a harmonic sequence, a value of 19.2×10^6 lb/in^2 was obtained for the Young's modulus of the UOX-MgO material at the 2×10^{20} dosage. This value is 37% of the pre-irradiation value.

The strength of the irradiated specimens increased at the lowest dosage investigated and decreased markedly at the higher dosages. As indicated in Table VII, the modulus of rupture of the six compositions ranged from 2 to 14% higher than the pre-irradiation value at the 8×10^{18} dosage. The increase in most compositions was within the standard deviation of the pre-irradiation measurements and was not statistically significant; some importance, may be attached to the fact that all six of the compositions exhibited an increase. Similar increases were noted by CLARKE and WILLIAMS [2] in this range of dosage. At approximately 2×10^{20} n/cm^2, the modulus of rupture ranged from 15 to 37% of the non-irradiated value, and by 4×10^{20} n/cm^2 had decrease to less than 5%.

Microscopic examination disclosed separation of the grains at boundaries. Fig. 7 is a more or less typical illustration of this effect at the 2×10^{20} n/cm^2 dosage. Further qualitative evidence of grain-boundary separation was apparent as a marked increase in the "pull-out" of grains during polishing operations.

5. DISCUSSION OF RESULTS

The most important aspect of the expansion measurements is the change in slope of the expansion-versus-dosage curves. This behaviour can be a consequence of either continued anisotropic expansion of the lattice or of agglomeration of the helium and tritium gases produced by transmutation. The indications of the present data are that the anisotropic expansion is the direct cause and that the gases contribute to the expansion indirectly through their effect on lattice distortion rather than directly by agglomeration.

Two rates of volume or macroscopic expansion can be predicted from anisotropic expansion of the grains. The first of these occurs at low dosages in which the amount of expansion is within the elastic limits of the material. In this region, the expansion corresponds to that calculable from the lattice expansion. For a material of theoretical density, the volume expansion is closely approximated by

$$\Delta V/V = (2\Delta a/a) + (\Delta c/c). \quad (1)$$

In general, the existing data up to about 10^{20} n/cm^2 tend to approximate this value; however, some complications have been noted. CLARKE and WILLIAMS [2] and ELSTON et al. [3] found that expansion in high-density (2.9 g/cm^3) samples exceeded the calculated value while the reverse was true in low-density samples (2.8 g/cm^3). However, since the expansion for specimens of each of these densities tended to parallel the calculated expansion curve, this effect does not alter the rate of expansion.

TABLE VII

MODULUS OF RUPTURE OF IRRADIATED BeO

Type of BeO	Nominal grain size (μm)	Nominal density (g/cm^3)	Modulus of rupture[b]			
			Dosage[a] ($E \geq 1$ MeV) (n/cm^2)	Pre-irradiation average (lb/in^2)	Post-irradiation average (lb/in^2)	Post-irradiation average (% of pre-irr. average)
UOX-MgO	20	2.90	8.8×10^{18}	31 700	32 400	102.2
	20	2.90	2.1×10^{20}	31 700	11 800	37.2
	20	2.90	3.6×10^{20}	31 700	-	-
AOX	20	2.90	8.6×10^{18}	34 800	38 800	111.5
	20	2.90	2.0×10^{20}	34 800	7800	22.1
	20	2.90	3.9×10^{20}	34 800	900	2.6
	50	2.90	1.8×10^{20}	19 500	3000	15.4
HPA	20	2.90	8.2×10^{18}	25 000	26 800	107.2
	20	2.90	3.6×10^{20}	25 000	1700	6.8
HPA-MgO	20	2.90	7.4×10^{18}	29 800	30 700	103.0
UOX	20	2.90	6.1×10^{18}	30 300	32 500	107.3
	20	2.90	3.8×10^{20}	30 300	700	2.3
UOX-ZrO_2	20	2.94	7.4×10^{18}	30 300	34 700	114.5
	20	2.94	5.4×10^{20}	30 300	1000	3.3

[a] Irradiated at 100°C.

[b] Pre-irradiation values are average of 30 specimens.
Post-irradiation values are average of 6 to 12 specimens.
Measured with 4-point loading on 3-in span at 0.06-in-per-minute load rate.

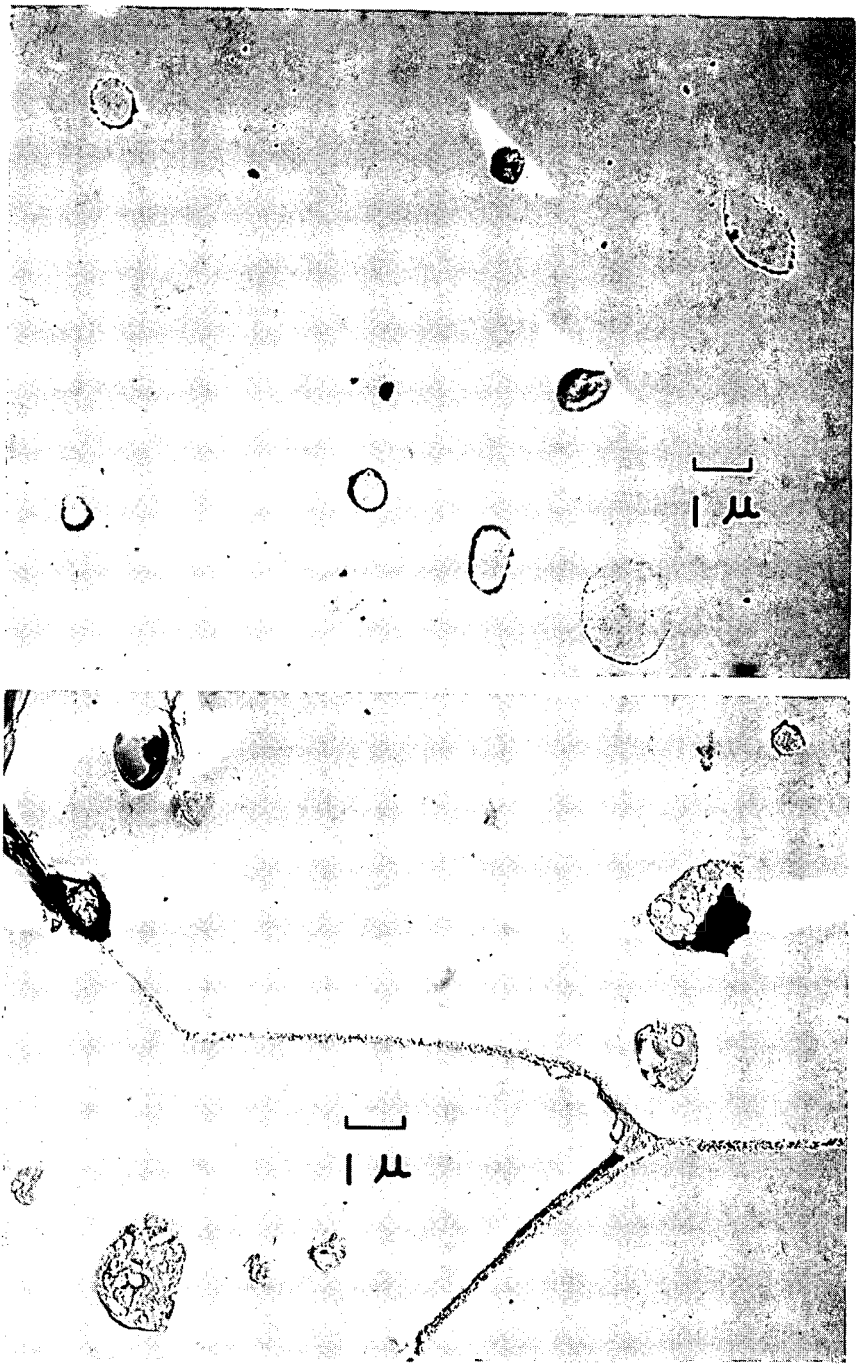


Fig. 7

Electron micrographs of AOX-grade BeO before and after irradiation (As-polished)
(a) Unirradiated (b) Irradiated

The second expansion rate predictable on the basis of anisotropic lattice expansion is that the volume expansion of a polycrystalline body must approach the value $3\Delta c/c$. This point is evident from an examination of the volume expansion of a spherical representation of randomly oriented crystals. In the model, the radii correspond to the c axes and describe all possible orientation angles; the equal length of the radii is representative of equal concentrations of crystals at each angle. The c axis now represents the radius of the sphere and the volume after an expansion of $\Delta c/c$ becomes $4\pi(r+\Delta r)/3$; where $(r+\Delta r) = (c+\Delta c/c)$, whence

$$\Delta v/V = 3\Delta c/c \ . \qquad (2)$$

Thus as a consequence of continued anisotropic expansion in the grains, the expansion of the body increases from $(2\Delta a/a)+(\Delta c/c)$ to $3\Delta c/c$ and is accompanied by the formation of voids or cracks. This behaviour results from purely geometrical considerations of anisotropic expansion and is independent of the material (assuming limited elasticity); however the crack location and the amount of expansion at which cracking occurs are dependent on the material. HICKMAN et al. [4] and CARNIGLIA [5] have shown that the stress in BeO is concentrated at the boundaries between grains of unlike orientation. Hence, the cracks should occur at this location. Variation of the stress with the orientation angle between grains permits a gradual transition of the expansion from the lower to the higher expansion rate.

The essential requirement for such macroscopic expansion behaviour is continued anisotropic expansion of the lattice. The expansion in the a-axis noted in this study indicates that saturation has not occurred at a dosage less than 5×10^{20} n/cm^2 and possibly higher, and the volume expansion data suggest that the same is true of the c-axis. Continued expansion of the parameters up to this dosage would not be surprising except that measurements at $(2-2.8)\times 10^{21}$ n/cm^2, reported by SHIELDS, LEE and BROWNING [6], led to inferences that saturation occurred at a lower level of expansion. It is entirely possible that no discrepancy exists. A "crystalline to amorphous to crystalline" pattern of lattice change with increasing dosage has been observed in LiF [7] and UO_2 [8]; it is not inconceivable that such a pattern may occur in BeO.

The data for the randomly oriented AOX specimens are in good agreement (Table VIII) with the expansion behaviour discussed. The data appear to be (1) an extension of the expansion curve presented by CLARKE [1] in his summary of BeO results, together with (2) sufficient evidence of continued anisotropic expansion of the lattice to account for the second, higher rate of expansion.

6. EFFECT OF PREFERRED ORIENTATION

Differences in the irradiation behaviour in UOX-MgO as compared to AOX can be attributed to preferred orientation. Preferential alignment of crystals in UOX-MgO caused some of anisotropic expansion of the lattice to appear as anisotropic expansion of the specimen itself. Consequently,

TABLE VIII

COMPARISON OF COMPUTED AND OBSERVED EXPANSION BEHAVIOUR OF AOX-GRADE BeO

Parameter	Calculated from lattice expansion		Observed in AOX grade BeO (20-μm grains, 2.9 g/cm^3)
	Relationship	Computed value	
Number of expansion rates as function of dosage.	2		2
Initial expansion rate per 10^{20} n/cm^2 ($E \geq 1$ MeV).	$\frac{2\Delta a/a + \Delta c/c}{\text{(dosage)}}$	0.6%	0.6%
Final expansion rate per 10^{20} n/cm^2 ($E \geq 1$ MeV).	$\frac{3\Delta c/c}{\text{(dosage)}}$	-	1.41%
Expansion at point in final expansion rate region.	$3\Delta c/c$	1.51 [a] 1.58 [b]	1.2 [a] 1.6 [b]
Ratio of final to initial expansion rate.	$\frac{(3\Delta c/c)}{(2\Delta a/a + \Delta c/c)}$	2.37 [a] 2.40 [b]	2.35

[a] Dosage 1.8×10^{20} n/cm^2 ($E \geq 1$ MeV).

[b] Dosage 2.1×10^{20} n/cm^2 ($E \geq 1$ MeV).

TABLE IX

THERMAL ANNEALING OF RADIATION INDUCED EXPANSION IN BeO

Specimen composition	Dosage [a] ($E \geq 1$ MeV) (10^{20} n/cm^2)	Nominal length expansion (in)	Maximum annealing [b] 600°C (%)	800°C (%)	900°C (%)	1000°C (%)	1050°C (%)	1100°C (%)
AOX	1.2	0.0056	33	(54)	-	90	-	105
	2.0	0.0144	13	(44)	(60)	78	82	82
	4.0	0.0508	-		(55)	65	65	
UOX-MgO	1.3	0.0077	40	76	-	100	100	105
	2.2	0.0195	19	(60)	91	93	97	98
	4.0	0.0630	-	-	89	89	89	-

[a] Irradiated at 100°C.

[b] Values listed in parentheses indicate continuing annealing after several hundred hours.

the changes in volume, dimensions and strength differed from those in randomly oriented specimens. At 2×10^{20} n/cm^2, the changes in UOX-MgO relative to those in AOX included: volume increase – 20% smaller; length increase – 10% larger; diameter increase – 25% smaller; and strength – 50% greater. In addition, thermal-annealing measurements show that the maximum recovery (Table IX) and the rate of recovery of dimensions (Figs. 8 and 9) exceed those of a random material.

The significance of these few data is the confirmation of the expected improvement in the radiation stability of a polycrystalline body containing preferred orientation. The use of such BeO is one means of coping with the expansion problem in reactor applications. By concentrating much of the expansion in one dimension, material with a high degree of preferred orientation should permit greater freedom in design. The data for the UOX-MgO composition demonstrate some of the gain possible; concentrations of preferred orientation considerably higher than that contained in this material are theoretically possible.

7. FUTURE WORK PLANNED

The data presented represent the initial results of a programme which is expected to include irradiations of various compositions at temperatures up to 1200°C and studies of three of the compositions over a range of grain sizes and densities. The ultimate objectives of the programme are determination of the micro-structural characteristics of the BeO material that exhibits the best stability to irradiation and definition of the properties over the useful range of dosage.

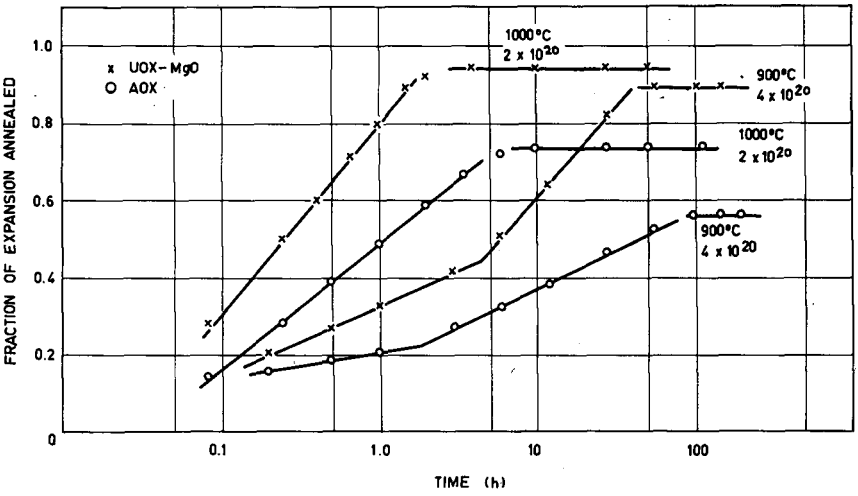


Fig. 8

Thermal annealing of irradiated BeO

x UOX-MgO
O AOX

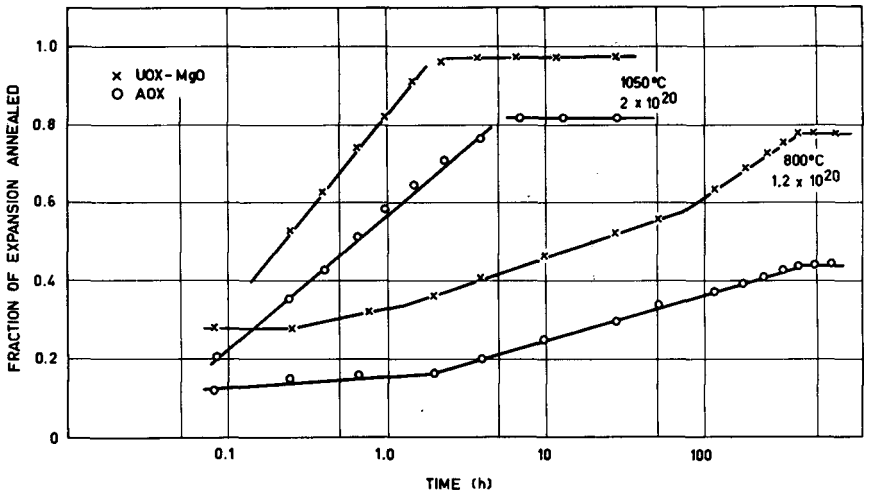


Fig. 9

Thermal annealing of irradiated BeO

× UOX-MgO
O AOX

ACKNOWLEDGEMENTS

This investigation involves the combined efforts of a number of personnel. The writer wishes to acknowledge particularly the contributions of J.F. White, E.C. Duderstadt, A.L. Clavel and L.J. Sjodahl in the preparation of specimens; of B.A. Chandler and R.E. Fryxell in property measurements; and of S.F. Bartram, G.A. Chase and R.C. Rau in X-ray and micro-structural examinations.

REFERENCES

[1] CLARKE, F.J.P., U.K.A.E.A. Rpt. AERE-R 3971 (1962).
[2] CLARKE, F.J.P. and WILLIAMS, J., U.K.A.E.A. Rpt. AERE M/M 229(1959); J. nucl. Mat. 4 (1961) 121.
[3] ELSTON, J. and LABBE, C., J. nucl. Mat. 4 (1961) 143.
[4] HICKMAN, B.S., SABINE, T.M. and COYLE, R.A., J. nucl. Mat. 6 (1962) 190.
[5] CARNIGLIA, S.C., J. nucl. Mat. 6 (1962) 330.
[6] SHIELDS, R.P., LEE, J.E. and BROWNING, W.E., USAEC Rpt. ORNL-3164 (1961).
[7] GILMAN, J.J. and JOHNSTON, W.G., J. app. Phys. 29 (1958) 877.
[8] BIERLEIN, T.K. and MASTEL, B., USAEC Rpt. HW-61656 (1959).

SYMPOSIUM ON RADIATION DAMAGE IN SOLIDS AND REACTOR MATERIALS

HELD AT VENICE, 7-11 MAY 1962

CHAIRMEN OF SESSIONS

Session 1	A. SEEGER	Max-Planck-Institut für Metallforschung, Stuttgart
Session 2	H. G. van BUEREN	N. V. Philips, Eindhoven
Session 3	S. V. STARODUBTSEV	Academy of Sciences of the USSR, Tashkent
Session 4	E. W. J. MITCHELL	J. J. Thomson Physical Laboratory, Reading
Session 5	E. NAGY	Central Research Institute for Physics, Budapest
Session 6	W. KOSIBA	European Atomic Energy Community, Brussels
Session 7	K. ALEXOPOULOS	University of Athens
Session 8	L. GIULOTTO	University of Pavia

SECRETARIAT OF THE SYMPOSIUM

Scientific Secretaries:	A. W. McREYNOLDS	Division of Research and Laboratories, IAEA
	B. BURAS	Consultant to the IAEA
	C. ERGINSOY	Division of Reactors, IAEA
Assistant Scientific Secretaries:	S. RODOVNICHENKO	Division of Scientific and Technical Information, IAEA
	B. TORKI	Division of Research and Laboratories, IAEA
Technical Secretary:	I. DRUTMAN	Division of Research and Laboratories, IAEA
Editor:	R. L. READING	Division of Scientific and Technical Information, IAEA
Records Officer:	T. B. DUNNE	Division of Languages, IAEA
Administrative Secretary:	R. de MAZANCOURT	Division of Scientific and Technical Information, IAEA

LIST OF PARTICIPANTS

Name	Institution	Nominating State or Organization
S. Aas	Institutt for Atomenergi, Lillestrøm	Norway
A. Abbate	Nuclear Energy Division, Ministry of Industry, Rome	Italy
K. Alexopoulos	Dept. of Physics, University of Athens	Greece
Miss C. de d'Amato	L. R. S. R., S. Donato Milanese, Milan	Italy
E. *Andronikashvili*	*Institute of Physics*, Academy of Sciences of the Georgian SSR, Tiflis	Union of Socialist Republics
J. J. Antal	Materials Research Laboratory, U. S. Army Ordnance Materials Research Office, Watertown, Mass.	United States of America
Moeller-Arnsberg	(See under "Moeller")	
A. Ascoli	C. L. S. E. Laboratories, Milan	Italy
H. F. Atkins	Vickers Nuclear Engineering, London	United Kingdom
M. Balkanski	Physics Laboratory, École Normale Supérieure, Paris	France
J. G. Ball	Metallurgy Dept., Imperial College, London	United Kingdom
R. W. Balluffi	Dept. of Metallurgical Engineering, University of Illinois, Urbana, Ill.	United States of America
P. Baruch	École Normale Supérieure, Paris	France
Miss M. R. Bastelli	L. R. S. R., S. Donato Milanese, Milan	Italy
R. Bäuerlein	Research Laboratory, Siemens-Schuckert-Werke, Erlangen	Federal Republic of Germany
J. *Beeler*	*General Electric Company*, Nuclear Materials and Propulsion Operation, Cincinnati, Ohio	United States of America
E. L. F. Vanden Bemden	Belgonucléaire, Brussels	Belgium
U. Bergenlid	AB Atomenergi, Tystberga	Sweden
M. Bleiberg	Bettis Atomic Power Laboratory, Westinghouse Electric Corporation, Pittsburgh, Pa.	United States of America
R. Blinc	J. Stefan Nuclear Institute, Ljubljana	Yugoslavia
R. Blöch	Research Dept. Gebr. Böhler & Co., Kapfenberg, Styria	Austria
B. Bochenek	Institute of Nuclear Research of the Polish Academy of Sciences, Warsaw	Poland
L. Bochirol	Centre d'Études Nucléaires de Grenoble, Grenoble (Isère)	France

Name	Institution	Nominating State or Organization
M. Bogaïevsky	Bureau Véritas, Paris	France
Miss S. de Bonnery	St. Gobain Nucléaire, Courbevoie (Seine)	France
G. Brogren	Chalmers Technological University, Gothenburg	Sweden
A. Brown	Natural Philosophy Dept., University of Edinburgh	United Kingdom
H. G. van Bueren	N. V. Philips Research Laboratories, Eindhoven, and Technological University of Delft	Netherlands
H. Bumm	Kernreaktor- Bau- u. Betriebsges. m. b. H., Karlsruhe	Federal Republic of Germany
R. Cananzi	Società Adriatica d'Elettricità, Venice	Italy
J. Červašek	Institute of Nuclear Research of the Czechoslovak Academy of Sciences, Řež-Praga	Czechoslovak Socialist Republic
B. G. Childs	Dounreay Experimental Reactor Establishment, Thurso, Caithness	United Kingdom
J. G. Y. Chow	Brookhaven National Laboratory, Upton, N. Y.	United States of America
A. T. Churchman	Central Electricity Generating Board, Berkeley Nuclear Laboratories, Berkeley, Glos.	United Kingdom
C. D. Clark	University of Reading	United Kingdom
C. G. Collins	General Electric Company, Nuclear Materials and Propulsion Operation, Cincinnati, Ohio	United States of America
R. Colombo	Nuclear Energy Dept., FIAT, Turin	Italy
R. R. Coltman	Oak Ridge National Laboratory, Oak Ridge, Tenn.	United States of America
Mrs. E. Cremer	Institute of Physical Chemistry, University of Innsbruck	Austria
G. Crocenzi	Comitato Nazionale per l'Energia Nucleare, Rome	Italy
A. Czachor	Institute of Nuclear Research of the Polish Academy of Sciences, Warsaw	Poland
A. D. Damask	Brookhaven National Laboratory, Upton, N. Y.	United States of America
J. Damm	Department of Structural Research of the Polish Academy of Sciences, Wrocław	Poland
U. Däunert	Karlsruhe Nuclear Research Centre, Karlsruhe	Federal Republic of Germany
D. Dautreppe	Centre d'Études Nucléaires de Grenoble, Grenoble (Isère)	France

Name	Institution	Nominating State or Organization
J. Diaz Diaz	Metallurgy Division, Nuclear Energy Board, Madrid	Spain
J. Diehl	Max-Planck-Institut für Metallforschung, Stuttgart	Federal Republic of Germany
V. Dimitriu	Romanian Legation in Vienna	Romania
B. Dunnington	Battelle Institute, Columbus, Ohio	United States of America
G. Edling	Steam-boiler Users' Association, Stockholm	Sweden
H. Ehringer	European Atomic Energy Community, Brussels, Belgium	European Atomic Energy Community
R. O. Elliott	Los Alamos Scientific Laboratory, Los Alamos, N. Mex.	United States of America
H. van Elst	TNO Metal Research Institute, Delft	Netherlands
J. Elston	Centre d'Études Nucléaires de Saclay, Gif-sur-Yvette (S. et O.)	France
M. Englander	Centre d'Études Nucléaires de Saclay, Gif-sur-Yvette (S. et O.)	France
R. Eriksson	Chalmers Technological University, Gothenburg	Sweden
K. Etzel	Farbwerke Höchst, Frankfurt a. M.	Federal Republic of Germany
P. Fernet	European Atomic Energy Community, Brussels, Belgium	European Atomic Energy Community
S. Ferrari	Comitato Nazionale per l'Energia Nucleare, Rome	Italy
J. Fischer	Allgemeine Elektricitäts-Gesellschaft, Munich	Federal Republic of Germany
P. Frank	American General Electric Company, European Office, Zürich, Switzerland	United States of America
C. Fréjacques	Centre d'Études Nucléaires de Saclay, Gif-sur-Yvette (S. et O.)	France
R. Frère	Solid-state Physics Dept., C. E. N. /S. C. K., Mol-Donk	Belgium
B. Frost	Metallurgy Division, Atomic Energy Research Establishment, Harwell, Berks.	United Kingdom
R. Gain	Jülich Nuclear Research Establishment, Jülich	Federal Republic of Germany
D. Gelli	Light Metals Experimental Institute, Novara	Italy
L. Gentilini	Reactor Engineering Laboratory, Comitato Nazionale per l'Energia Nucleare, Rome	Italy

Name	Institution	Nominating State or Organization
A. Gerosa	Reactor Engineering and Servomechanisms Laboratory, Centro di Studi Nucleari della Casaccia, Rome	Italy
J. Gittus	UKAEA Reactor Fuel Element Laboratory, Springfields, Lancs.	United Kingdom
L. Guilotto	Physics Institute, University of Pavia	Italy
V. Goldansky	Institute of Chemical Physics of the Academy of Sciences of the USSR	Union of Soviet Socialist Republics
S. Golyanov	Institute of Atomic Energy of the Academy of Sciences of the USSR, Moscow	Union of Soviet Socialist Republics
S. Granata	L. R. S. R., S. Donato Milanese, Milan	Italy
B. S. Gray	UKAEA Reactor Group, Reactor Materials Laboratory, Warrington, Lancs.	United Kingdom
N. Hansen	Risø Research Establishment, Roskilde	Denmark
Kofoed-Hansen	(See under "Kofoed")	
B. Henriksson	Chalmers Technological University, Gothenburg	Sweden
Miss M. E. A. Hermans	N. V. KEMA, Arnhem	Netherlands
K. Herne	Farbenfabriken Bayer, Leverkusen	Federal Republic of Germany
A. Herpin	Centre d'Études Nucléaires de Saclay, Gif-sur-Yvette (S. et O.)	France
D. K. Holmes	Oak Ridge National Laboratory, Oak Ridge, Tenn.	United States of America
E. Hörl	Österreichische Studiengesellschaft für Atomenergie, Seibersdorf, Lower Austria	Austria
L. M. Howe	Atomic Energy of Canada Ltd., Chalk River, Ont.	Canada
E. Hyam	UKAEA Reactor Group, Windscale Works, Seascale, Cumberland	United Kingdom
W. Jahns	Deutsche Babcock & Wilcox Dampfkesselwerke AG, Oberhausen	Federal Republic of Germany
E. Jensen	Reactor Centrum Nederland, Petten, North Holland	Norway
A. A. Johnson	Metallurgy Dept., Imperial College, London	United Kingdom
C. Kaplan	Électricité de France, Clamart (Seine)	France
G. W. Keilholtz	Oak Ridge National Laboratory, Oak Ridge, Tenn.	United States of America
R. Kiessling	Swedish Metal Research Institute, Stockholm	Sweden

Name	Institution	Nominating State or Organization
P. Kirsch	Army Technical Branch, Paris	France
B. Kit	Library of Congress, Washington, D.C.	United States of America
G. Klar	Grafitbergbau Kaisersberg Franz Mayr-Melnhof AG, Vienna	Austria
R. Klersy	Metallurgy and Ceramics Dept., EURATOM Joint Research Centre, Ispra (Varese), Italy	European Atomic Energy Community
B. Knook	Kamerlingh Onnes Laboratory, Leyden	Netherlands
O. M. Kofoed-Hansen	Physics Dept., Risø Research Establishment, Roskilde	Denmark
W. Kosiba	European Atomic Energy Community, Brussels, Belgium	European Atomic Energy Community
P. Koss	Österreichische Studiengesellschaft für Atomenergie, Vienna	Austria
P. Kruys	European Atomic Energy Community, Brussels, Belgium	European Atomic Energy Community
W. Kunz	Verbundgesellschaft, Vienna	Austria
R. A. van der Laken	Reactor Centrum Nederland, The Hague	Netherlands
Mrs. M. Lambert	Centre d'Études Nucléaires de Saclay, Gif-sur-Yvette (S. et O.)	France
G. Lautz	Institute of Pure and Applied Nuclear Physics, University of Kiel	Federal Republic of Germany
T. Leardini	Società Adriatica d'Elettricità, Venice	Italy
J. M. Leblanc	Belgonucléaire, Mol-Donk	Belgium
J.-P. Lecocq	EURATOM Joint Research Centre, Ispra (Varese), Italy	European Atomic Energy Community
J. Lemaire	Centre d'Études Nucléaires de Saclay, Gif-sur-Yvette (S. et O.)	France
Mrs. J. Lehmann	Centre d'Études Nucléaires de Saclay, Gif-sur-Yvette (S. et O.)	France
F. Letournay	Électricité de France, Clamart (Seine)	France
P. Lévêque	Centre d'Études Nucléaires de Saclay, Gif-sur-Yvette (S. et O.)	France
F. Levi	Physics Institute, University of Perugia	Italy
Miss V. Lévy	Centre d'Études Nucléaires de Saclay, Gif-sur-Yvette (S. et O.)	France
D. S. Lieberman	United States Office of Naval Research, London, England	United States of America

Name	Institution	Nominating State or Organization
B. Liebmann	"Nukem", Hanau a. M.	Federal Republic of Germany
J. Lindhard	Institute of Physics, University of Aarhus	Denmark
R. Lindner	EURATOM Joint Research Centre, Ispra (Varese), Italy	European Atomic Energy Community
Miss J. N. Lomer	J. J. Thomson Physical Laboratory, University of Reading	United Kingdom
B. Loomis	Argonne National Laboratory, Argonne, Ill.	United States of America
P. Lucasson	Physical Chemistry Laboratory, Faculté des Sciences, Orsay (S. et O.)	France
J. MacKay	Physics Dept., Purdue University, Lafayette, Ind.	United States of America
J. H. McMillen	National Science Foundation, Washington, D. C. Washington, D. C.	United States of Ameria
G. Marangio	Safety Division, Comitato Nazionale per l'Energia Nucleare, Rome	Italy
V. Marinković	J. Stefan Nuclear Institute, Ljubljana	Yugoslavia
F. Marques Videira	Nuclear Energy Board, Lisbon	Portugal
D. Martin	Centre d'Études Nucléaires de Marcoule, Marcoule (Gard)	France
M. Martini	Reactor Engineering and Servomechanisms Laboratory, Centro di Studi Nucleari della Casaccia, Rome	Italy
H. Matzke	Technische Hochschule Braunschweig, Brunswick, Federal Republic of Germany	European Atomic Energy Community
S. Mayerhofer	Schoeller-Bleckmann Stahlwerke AG, Ternitz, Lower Austria	Austria
J. Medema	Reactor Institute, Technological University of Delft	Netherlands
C. J. Meechan	Atomics International Division of North American Aviation, Inc., Canoga Park, Calif.	United States of America
P. de Meester	C. E. N. /S. C. K., Mol-Donk	Belgium
R. di Menza	Comitato Nazionale per l'Energia Nucleare, Rome	Italy
A. Merlini	Solid-State Physics Dept., EURATOM Joint Research Centre, Ispra (Varese), Italy	European Atomic Energy Community
N. Milašin	Boris Kidrič Institute of Nuclear Science, Belgrade	Yugoslavia

Name	Institution	Nominating State or Organization
E. W. J. Mitchell	J. J. Thomson Physical Laboratory, University of Reading	United Kingdom
O. Moeller-Arnsberg	Munich	Federal Republic of Germany
C. Moranville	Metallurgy and Ceramics Dept., EURATOM Joint Research Centre, Ispra (Varese), Italy	European Atomic Energy Community
P. Moser	Centre d'Études Nucléaires de Grenoble, Grenoble (Isère)	France
J. Moteff	General Electric Company, Nuclear Materials and Propulsion Operation, Cincinnati, Ohio	United States of America
H. Müller	Chemical Laboratory, University of Freiburg, Freiburg i. Br.	Federal Republic of Germany
J. P. Mustelier	Centre d'Études Nucléaires de Saclay, Gif-sur-Yvette (S. et O.)	France
P. Myers	AB Atomenergi, Tystberga	Sweden
E. Nagy	Central Research Institute of Physics, Budapest	Hungary
G. F. Nardelli	Physics Institute, University of Pavia	Italy
J. Nihoul	C. E. N. /S. C. K., Mol-Donk	Belgium
A. J. O'Donnell	United States Mission to the IAEA, Vienna, Austria	United States of America
G. Palladino	C. I. S. E., Milan	Italy
M. Patané	C. E. N. /S. C. K., Mol-Donk, Belgium	European Atomic Energy Community
J. Paulevé	Centre d'Études Nucléaires de Grenoble, Grenoble (Isère)	France
U. Pepi	AGIP Nucleare, S. Donato Milanese, Milan	Italy
G. Perriot	Centre d'Études Nucléaires de Saclay, Gif-sur-Yvette (S. et O.)	France
J. C. Pfister	École Normale Supérieure, Paris	France
M. Pluchery	Centre d'Études Nucléaires de Grenoble, Grenoble (Isère)	France
G. Poletti	C. I. S. E., Milan	Italy
J. Rappeneau	Centre d'Études Nucléaires de Saclay, Gif-sur-Yvette (S. et O.)	France
W. N. Reynolds	Atomic Energy Research Establishment, Harwell, Berks.	United Kingdom
W. E. Roake	General Electric Company, Hanford Laboratories Operation, Richland, Wash.	United States of America

Name	Institution	Nominating State or Organization
A. Rocchi	Società Elettronucleare Nazionale, Rome	Italy
F. Roncaglia	Reactor Engineering and Servomechanisms Laboratory, Centro di Studi Nucleari della Casaccia, Rome	Italy
F. Rossi	Nuclear Research Centre of the Società per le Ricerche ed Impianti Nucleari, Saluggia (Vercelli)	Italy
E. Ruedl	Solid-State Physics Dept., C.E.N./S.C.K., Mol-Donk, Belgium	European Atomic Energy Community
H.-G. Rumpf	Technischer Überwachungsverein Bayern, Munich	Federal Republic of Germany
P. Salvi	Nuclear Energy Division, Ministry of Industry, Rome	Italy
F. Saraceno	L.R.S.R., S. Donato Milanese, Milan	Italy
G.B. Schmidt	Institute of Nuclear Chemistry, University of Cologne	Federal Republic of Germany
W. in der Schmitten	"Nukem", Hanau a. M.	Federal Republic of Germany
R. Schuttler	Centre d'Études Nucléaires de Fontenay-aux-Roses, Fontenay-aux-Roses (Seine)	France
R. Schwarzwälder	Allgemeine Elektricitäts-Gesellschaft, Frankfurt a. M.	Federal Republic of Germany
G.B. Scuricini	Comitato Nazionale per l'Energia Nucleare, Rome	Italy
F. Sebilleau	Centre d'Études Nucléaires de Fontenay-aux-Roses, Fontenay-aux-Roses (Seine)	France
B. Secretan	École Polytechnique de l'Université de Lausanne	Switzerland
A. Séeger	Max-Planck-Institut für Metallforschung, Stuttgart	Federal Republic of Germany
P. Sens	Reactor Centrum Nederland, Petten, North Holland	Netherlands
W. Sheely	Division of Research, United States Atomic Energy Commission, Washington, D.C.	United States of America
A. Shoudy	Atomic Power Development Associates, Inc., Detroit, Mich.	United States of America
J. Siejka	Institute of Nuclear Research of the Polish Academy of Sciences, Warsaw	Poland
Č. Šimáně	Division of Technical Supplies, IAEA, Vienna	International Atomic Energy Agency
J. Simmons	United States Atomic Energy Commission, Washington, D.C.	United States of America

Name	Institution	Nominating State or Organization
J. H. W. Simmons	Atomic Energy Research Establishment, Harwell, Berks.	United Kingdom
D. Sinizer	Atomics International Division of North American Aviation, Inc., Canoga Park, Calif.	United States of America
R. Sizmann	Technische Hochschule München, Munich	Federal Republic of Germany
H. S. G. Slooten	N. V. KEMA, Arnhem	Netherlands
G. P. Soardo	Istituto Elettrotechnico Nazionale Galileo Ferraris, Turin	Italy
M. Sole	South African Atomic Energy Board	South Africa
H. Sørensen	Risø Research Establishment, Roskilde	Denmark
A. Sosin	Atomics International Division of North American Aviation, Inc., Canoga Park, Calif.	United States of America
W. Spalthoff	Gesellschaft für Kernenergieverwertung in Schiffbau und Schiffahrt, Hamburg	Federal Republic of Germany
H. Spatzek	Grafitbergbau Kaisersberg Franz Mayr-Melnhof AG, St. Stefan o. L., Styria	Austria
W. Špeťko	Ministry of Fuel and Power, Prague	Czechoslovak Socialist Republic
E. Stampone	Comitato Nazionale per l'Energia Nucleare, Rome	Italy
S. V. Starodubtsev	Academy of Sciences of the USSR, Tashkend	Union of Soviet Socialist Republics
W. Staubwasser	Interatom, Cologne	Federal Republic of Germany
B. Stebler	Chalmers Technological University, Gothenburg	Sweden
L. E. Steele	Metallurgy Division, U. S. Naval Research Laboratory, Washington, D. C.	United States of America
J. Suwalski	Institute of Nuclear Research of the Polish Academy of Sciences, Warsaw	Poland
G. Swenson	Chalmers Technological University, Gothenburg	Sweden
M. Terada	Mitsubishi Atomic Power Industries, Inc., Omya City, Saitama	Japan
M. Ternault	Commissariat à l'Énergie Atomique, Paris	France
S. Teruggi	AGIP Nucleare, S. Donato Milanese, Milan	Italy
A. Terzano	Società Elettronucleare Nazionale, Rome	Italy

THERMODYNAMICS OF NUCLEAR MATERIALS

Proceedings of an IAEA symposium held in Vienna, May 1962, with more than 100 participants from 16 countries and two international organizations. The purpose was to present and appraise current work, to assess the reliability of nuclear materials and to discuss application of such information to current problems in nuclear technology. Emphasis was on thermodynamics of actinides and vaporization processes.

Contents: Actinides in general (4 papers), Applications of theory (4 papers), Experimental techniques (4 papers), Alloy systems (9 papers), Vaporization processes (10 papers), Condensed phases other than alloys (15 papers).

Papers are in their original languages (40 English, 1 French and 5 Russian). Each is preceded by an abstract in English, French, Russian and Spanish. Discussions are in English.

808 pp, 16 x 24 cm, cloth-bound, 227 figures, tables

(1962) In North America US $ 11.00; Elsewhere S 231.- (66s.stg., NF 44.-, DM 38.50)

REVIEW SERIES

No.26: ANALYTIC CRITICALITY STUDIES ASSOCIATED WITH NEUTRON DIFFUSION THEORY

(Henry L. Garabedian,
Research Laboratories,
General Motors Corporation,
Warren, Michigan)

A review devoted to diffusion-theory methods in reactor criticality and primarily concerned with history and development of basic researches in the field.

The essay in English is preceded by an abstract in English, French, Russian and Spanish.

57 pp, 14.8 x 21 cm, paper-bound, 9 figures, 2 tables

(1962) In North America US $ 1.00; Elsewhere S 21.- (6s.stg., NF 4.-, DM 3.20)

No.25: FABRICATION OF FUEL ELEMENTS

(G. Matz,
Nuclear-Chemie und Metallurgie GmbH
Hanau am Main
Federal Republic of Germany)

A survey of the production of those elements that are now manufactured on a large scale: elements of uranium metal, uranium oxide, uranium dispersions, cermets, carbides. As a representative example, the method proposed for making plutonium elements for EBR-II is described.

80 pp, 14.8 x 21 cm, paper-bound, 36 figures

(1962) In North America US $ 1.00; Elsewhere S 21.- (6s.stg., NF 4.-, DM 3.20)

No.11: POWDER METALLURGY IN NUCLEAR REACTOR CONSTRUCTION

(H.H. Hausner,
Polytechnic Institute of Brooklyn,
New York, New York)

A review of general principles, basic variables in technique, fabrication methods and safe handling. Included are data on fibre-powder combinations, sinter-welding and sintering with irradiation.

Subjects: general principles, powder fabrication for nuclear engineering, fuel materials, control materials, beryllium, zirconium, thermoelectric materials, safe handling.

The review is in English; the preceding abstract is in English, French, Russian and Spanish.

72 pp, 14.8 x 21 cm, paper-bound, 24 figures, 23 tables

(1961) In North America US $ 1.00; Elsewhere S 21.- (6s.stg., NF 4.-, DM 3.20)

No. 6: THE BEHAVIOUR OF REACTOR COMPONENTS UNDER IRRADIATION

(L. Grainger,
Atomic Energy Research Establishment,
Harwell, England)

A discussion of radiation effects on such materials and components as uranium metal, uranium compounds, structural materials, fuel elements and pressure vessels.

The review in English is preceded by an abstract in English, French, Russian and Spanish.

64 pp, 14.8 x 21 cm, paper-bound, 19 figures

(1960) In North America US $ 1.00; Elsewhere S 21.- (6s.stg., NF 4.-, DM 3.20)

TECHNICAL REPORTS SERIES

No. 12: LIGHT WATER LATTICES

The report of a panel that met in Vienna, May-June 1962, as part of a continuing IAEA programme of reactor-physics panels. The members were five experts from France, two from the United Kingdom and six from the United States.

Contents of the volume consist of a general summary by H. Kouts (Brookhaven National Laboratory, USA), three status reports, one from each of the participating countries, four summaries of discussions (Criticality predictions, Thermal-neutron cell distributions, Resonance absorption, Plutonium-fuelled systems) and 13 papers prepared as supporting material in preparation for the panel meeting.

General summary, status reports and discussion summaries are in English. Supporting papers are in their original languages (10 English, 3 French).

363 pp, paper-bound, 16 x 24 cm. 117 figures, tables

(1962) In North America US $ 7.00; Elsewhere S 147.- (42s.stg., NF 28.-, DM 24.50)

IN PRESS (further details and prices on application)

TECHNICAL REPORTS SERIES

HEAVY WATER LATTICES

Proceedings, with summaries, of a panel held at IAEA Headquarters, Vienna, in 1963.

PROCEEDINGS SERIES

NEW NUCLEAR MATERIALS TECHNOLOGY

Complete proceedings of an IAEA Symposium held at Prague in July 1963.

OTHER IAEA PUBLICATIONS
PROCEEDINGS SERIES

	STI/PUB/
L'électronique nucléaire - Nuclear Electronics (1959) (2 Vols.)	2
Medical Radioisotope Scanning	3
Large Radiation Sources in Industry (2 Vols.)	12
Metrology of Radionuclides	6
Disposal of Radioactive Wastes (2 Vols.)	18
Codes for Reactor Computations	24
Selected Topics in Radiation Dosimetry	25
Effects of Ionizing Radiations on Seeds	13
Small and Medium Power Reactors (2 Vols.)	30
Radioisotopes in the Physical Sciences and Industry (3 Vols.)	20
Inelastic Scattering of Neutrons in Solids and Liquids (1961)	35
Pile Neutron Research in Physics	36
Chemical Effects of Nuclear Transformations (2 Vols.)	34
Nuclear Ship Propulsion	37
Radioisotopes and Radiation in Entomology	38
Radioisotopes in Tropical Medicine	31
Tritium in the Physical and Biological Science (2 Vols.)	39
Nuclear Electronics (3 Vols.) (1961)	42
Effects of Ionizing Radiation on the Nervous System	46
Whole-Body Counting	47
Physics of Fast and Intermediate Reactors (3 Vols.)	49
Plasma Physics and Controlled Nuclear Fusion Research (3 Parts)	50
Power Reactor Experiments (2 Vols.)	51
Radiation Damage in Solids (3 Vols.)	56
Radioisotopes in Soil-Plant Nutrition Studies	55
Reactor Safety and Hazards Evaluation Techniques (2 Vols.)	57
Thermodynamics of Nuclear Materials	58
Corrosion of Reactor Materials (2 Vols.)	59
Biological Effects of Ionizing Radiation at the Molecular Level	60
Inelastic Scattering of Neutrons in Solids and Liquids (1963) (2 Vols.)	62
Selected Topics in Nuclear Theory	67
Theoretical Physics	61
Treatment and Storage of High-Level Radioactive Wastes	63
Diagnosis and Treatment of Radioactive Poisoning	65
Radioactive Dating	68
Neutron Dosimetry (2 Vols.)	69
Radioisotopes in Hydrology	71
Siting of Reactors and Nuclear Research Centres	72

IN PRESS

Radiation and Radioisotopes applied to Insects of Agricultural Importance
Industrial Uses of Large Radiation Sources
Operating Experience with Power Reactors
New Nuclear Materials Technology
Radiological Health and Safety in Nuclear Materials Milling and Mining

A complete Catalogue of all Agency publications will be gladly supplied by any of the Sales Agents or directly by the Editorial and Publications Section, International Atomic Energy Agency, Kärntner Ring, Vienna I, Austria.

IAEA SALES AGENTS

ARGENTINA
Editorial Sudamericana, S.A.
Alsina 500
Buenos Aires

AUSTRALIA
R.W. Barclay
90, Queen Street
Melbourne

AUSTRIA
Georg Fromme & Co.
Spengergasse 39
Vienna V

BELGIUM
Office International de Librairie
30, avenue Marnix
Brussels 5

BRAZIL
Livraria Kosmos Editora
Rua do Rosario, 135-137
Rio de Janeiro
Agencia Expoente Oscar M. Silva
Rua Xavier de Toledo, 140-1° Andar
(Caixa Postal N° 5.614)
São Paulo

BURMA
See under India

BYELORUSSIAN SOVIET SOCIALIST REPUBLIC
See under USSR

CANADA
The Queen's Printer
Ottawa

CEYLON
See under India

CHINA (Taiwan)
Books and Scientific Supplies
Service, Ltd.,
P.O. Box 83
Taipei

DENMARK
Ejnar Munksgaard Ltd.
6 Nörregade
Copenhagen K

ETHIOPIA
G.P. Giannopoulos
International Press Agency
P.O. Box 120
Addis Ababa

FINLAND
Akateeminen Kirjakauppa
Keskuskatu 2
Helsinki

FRANCE and FRENCH UNION
Office International de
Documentation et Librairie
48, Rue Gay-Lussac
Paris, 5e

GERMANY, Federal Republic of
R. Oldenbourg
Rosenheimer Strasse 145
Munich 8

ICELAND
Halldór Jónsson
Mjóstræti 2
Reykjavík

INDIA
Orient Longmans Ltd.
17, Chittaranjan Ave.
Calcutta 13

ISRAEL
Heiliger and Co.
3 Nathan Strauss Street
Jerusalem

ITALY
Agenzia Editoriale Internazionale
Organizzazioni Universali
(A.E.I.O.U.)
Via Meravigli 16
Milan

JAPAN
Maruzen Company Ltd.
6, Tori Nichome
Nihonbashi
P.O. Box 605
Tokyo Central

KOREA, Republic of
The Eul-Yoo Publishing Co.
5,2-ka Chong-ro
Seoul

MEXICO
Librería Internacional
Av. Sonora 206
Mexico 11, D.F.

MONACO
The British Library
30, bd des Moulins
Monte Carlo

MOROCCO
Centre de diffusion documentaire
du B.E.P.I.
8, rue Michaux-Bellaire
(B.P. N° 211)
Rabat

NEPAL
See under India

NETHERLANDS
N.V. Martinus Nijhoff
Lange Voorhout 9
The Hague

NEW ZEALAND
Whitcombe & Tombs, Ltd.
G.P.O. Box 1894
Wellington, C.1

NORWAY
Johan Grundt Tanum
Karl Johans gate 43
Oslo

PAKISTAN
Karachi Education Society
Haroon Chambers
South Napier Road
P.O. Box No. 4866
Karachi, 2

PARAGUAY
Agencia de Librerías
de Salvador Nizza
Calle Pte. Franco No. 39-43
Assunción

PERU
Livrería Internacional de Perú S. A.
Boza 879
(Casilla 1417)
Lima

PHILIPPINES
The Modern Book Company
508 Rizal Avenue
Manila

POLAND
Ośrodek Rozpowszechniana
Wydawnistw Naukowych
Polska Akademia Nauk
Palac Kultury i Nauki
Warsaw

PORTUGAL
Livraria Rodrigues
186, Rua do Ouro, 188
Lisbon 2

SOUTH AFRICA
Van Schaik's Bookstore (Pty) Ltd.
Libri Building
Church St.
(P.O. Box 724)
Pretoria

SPAIN
Librería Bosch
Ronda Universidad, 11
Barcelona

SWEDEN
C.E. Fritzes Kungl. Hovbokhandel
Fredsgatan 2
Stockholm 16

SWITZERLAND
Librairie Payot
40, rue du Marché
Geneva

SYRIA
Georges N. Coussa
Imm. Chanan
rue Khan el-Harir
(B.P. 779)
Aleppo

TURKEY
Librairie Hachette
469, Istiklal Caddesi
Beyoğlu, Istanbul

UKRAINIAN SOVIET SOCIALIST REPUBLIC
See under USSR

UNION OF SOVIET SOCIALIST REPUBLICS
Mezhdunarodnaya Kniga
Smolenskaya-Sennaya 32-34
Moscow G-200

UNITED KINGDOM OF GREAT BRITAIN AND NORTHERN IRELAND
Her Majesty's Stationery Office
P.O. Box 569
London, S.E.1

UNITED STATES OF AMERICA
National Agency for
International Publications, Inc.
317-23 East 34th St
New York 16, N.Y.

VENEZUELA
Sr. Braulio Gabriel Chacares
Gobernador a Candilito 37
Santa Rosalia
Apartado Postal 8092
Caracas D.F.

YUGOSLAVIA
Jugoslovenska Knjiga
Terazije 27
Belgrade

IAEA publications can also be purchased retail at the United Nations Bookshop at United Nations Headquarters, New York, at the news-stand at the Agency's Headquarters, Vienna, and at most conferences, symposia and seminars organized by the Agency.

Orders and inquiries from countries where sales agents have not yet been appointed may be sent to:

Distribution and Sales Unit, International Atomic Energy Agency,
Kärntner Ring, Vienna I, Austria